DTIC FILE COPY

MARINE PHYSICAL LABORATORY

SCRIPPS INSTITUTION OF OCEANOGRAPHY

San Diego, California 92152

AD-A206 968

FREELY DRIFTING SWALLOW FLOAT ARRAY: AUGUST 1988 TRIP REPORT

G.L. D'Spain, R.L. Culver, W.S. Hodgkiss, and G.L. Edmonds

DTIC
ELECTE
APR 19 1989
S E D

MPL TECHNICAL MEMORANDUM 407

MPL-U-02/89
January 1989

Approved for public release; distribution unlimited.

89 4 19 035

ADA208968

SECURITY CLASSIFICATION OF THIS PAGE

REPORT DOCUMENTATION PAGE

1a. REPORT SECURITY CLASSIFICATION UNCLASSIFIED	1b. RESTRICTIVE MARKINGS
2a. SECURITY CLASSIFICATION AUTHORITY	3. DISTRIBUTION / AVAILABILITY OF REPORT Approved for public release; distribution unlimited.
2b. DECLASSIFICATION / DOWNGRADING SCHEDULE	
4. PERFORMING ORGANIZATION REPORT NUMBER(S) MPL TECHNICAL MEMORANDUM 407 [MPL-U-02/89]	5. MONITORING ORGANIZATION REPORT NUMBER(S)
6a. NAME OF PERFORMING ORGANIZATION Marine Physical Laboratory 6b. OFFICE SYMBOL (If applicable) MPL	7a. NAME OF MONITORING ORGANIZATION Office of Naval Research Department of the Navy
6c. ADDRESS (City, State, and ZIP Code) University of California, San Diego Scripps Institution of Oceanography San Diego, CA 92152	7b. ADDRESS (City, State, and ZIP Code) 800 North Quincy Street Arlington, VA 22217-5000
8a. NAME OF FUNDING / SPONSORING ORGANIZATION Office of Naval Research 8b. OFFICE SYMBOL (If applicable) ONR	9. PROCUREMENT INSTRUMENT IDENTIFICATION NUMBER N00014-87-C-0127
8c. ADDRESS (City, State, and ZIP Code) Department of the Navy 800 North Quincy Street Arlington, VA 22217-5000	10. SOURCE OF FUNDING NUMBERS PROGRAM ELEMENT NO. / PROJECT NO. / TASK NO. / WORK UNIT ACCESSION N
11. TITLE (Include Security Classification) FREELY DRIFTING SWALLOW FLOAT ARRAY: AUGUST 1988 TRIP REPORT	
12. PERSONAL AUTHOR(S) G.L. D'Spain, R.L. Culver, W.S. Hodgkiss, and G.L. Edmonds	
13a. TYPE OF REPORT tech memo 13b. TIME COVERED FROM _____ TO _____ 14. DATE OF REPORT (Year, Month, Day) January 1989 15. PAGE COUNT	
16. SUPPLEMENTARY NOTATION	

17. COSATI CODES		
FIELD	GROUP	SUB-GROUP

18. SUBJECT TERMS (Continue on reverse if necessary and identify by block number)
Swallow floats, Patton Escarpment

19. ABSTRACT (Continue on reverse if necessary and identify by block number)

This report presents Representative data from the 30-31 August, 1988 deployment of the Marine Physical Laboratory's (MPL) set of 12 Swallow floats, ~~are presented in this report.~~ The deployment location was about 20 km to the west of the Patton Escarpment, near deep sea drilling project hole 469, at 32.5° N, 120.5° W. The midwater floats were ballasted to depths starting at 350 meters and spaced every 150 meters, to 1400 meters, except for one float which equilibrated at 3360 meters. Thirteen ship-launched and two air-launched sonobuoys of various design from the Naval Air Development Center (NADC) and four Prototype Array Element Localization (PAEL) buoys from the Naval Ocean Systems Center (NOSC) were concurrently deployed at depths between 120 and 150 meters. This report presents the instrument deployment locations, the positions and characteristics of known signal sources, expendable bathythermograph (XBT) and anemometer data, and representative Swallow float data from the experiment. The Swal-

20. DISTRIBUTION / AVAILABILITY OF ABSTRACT ☐ UNCLASSIFIED/UNLIMITED ☒ SAME AS RPT. ☐ DTIC USERS	21. ABSTRACT SECURITY CLASSIFICATION UNCLASSIFIED
22a. NAME OF RESPONSIBLE INDIVIDUAL W. S. Hodgkiss	22b. TELEPHONE (Include Area Code) (619) 534-1798 22c. OFFICE SYMBOL MPL

DD FORM 1473, 84 MAR 83 APR edition may be used until exhausted. All other editions are obsolete

SECURITY CLASSIFICATION OF THIS PAGE

★ U.S. Government Printing Office: 1986

low float data include battery voltage, compass heading, and automatic gain control (AGC) measurements, the 8 kHz acoustic localization ping arrivals, and the VLF pressure and particle velocity data. Data collected by the sonobuoys and the PAEL buoys will be presented at a later time.

All 12 Swallow floats operated nearly flawlessly, resulting in a 99.7 % full data set. A number of conclusions can be drawn from a preliminary look at these data. First, throughout the experiment, an unknown source, or sources, generated acoustic energy centered at about 18 Hz and as much as 40 dB above background noise levels. The characteristics of the arrivals varied in time in an apparently deterministic way, suggesting a man-made sound source. This contamination will make it difficult to obtain useful information from a preliminary study of the coupling of noise by the Patton Escarpment into the deep sound channel conducted in this deployment. Second, the calibrated pressure spectral levels estimated directly from data collected by newly-installed VLF hydrophones agree with those derived from the geophone data except near frequencies corresponding to float rocking resonances and at times when signal clipping or overloading was present. Third, a 20 Hz line generated by the Sproul (apparently by the ship's generator) was at times audible to the floats, allowing for future efforts at beamforming the Swallow float data on a known source. Fourth, this experiment revealed that the Swallow floats can successfully operate when two, rather than one, of the floats issue range pings in a record, thus doubling the float localization sampling rate. Fifth, by varying the number of guy wires attached to each of the floats' radio beacon antennae, it was determined that motion of the antennae somehow cause a 4 Hz contamination and that the antennae should somehow be supported in future deployments. Finally, in situ measurements of the floats' clock drifts were obtained; the absolute drifts were on the order of one part in 10^5 and the relative clock drifts were approximately equal to those measured previously.

Keywords: Background noise sources; Radiated noise contamination; Underwater acoustics; Deep sound channels. Underwater acoustics data. Oceanographic data; North Pacific Ocean. Ship noise; Beamforming pingers; Rocking, radio beacon antennae. Floating acoustic arrays. (edc)

DTIC
COPY
INSPECTED
4

Accession For
NTIS GRA&I
DTIC TAB
Unannounced
Justification
By
Distribution/
Availability Codes
Dist | Avail and/or Special
A-1

Freely Drifting Swallow Float Array: August 1988 Trip Report

G. L. D'Spain, R. L. Culver, W. S. Hodgkiss, and G. L. Edmonds

Marine Physical Laboratory
Scripps Institution of Oceanography
San Diego, CA 92152

ABSTRACT

Representative data from the 30-31 August, 1988 deployment of the Marine Physical Laboratory's (MPL) set of 12 Swallow floats are presented in this report. The deployment location was about 20 km to the west of the Patton Escarpment, near deep sea drilling project hole 469, at 32.5° N, 120.5° W. The midwater floats were ballasted to depths starting at 350 meters and spaced every 150 meters, to 1400 meters, except for one float which equilibrated at 3360 meters. Thirteen ship-launched and two air-launched sonobuoys of various design from the Naval Air Development Center (NADC) and four Prototype Array Element Localization (PAEL) buoys from the Naval Ocean Systems Center (NOSC) were concurrently deployed at depths between 120 and 150 meters. This report presents the instrument deployment locations, the positions and characteristics of known signal sources, expendable bathythermograph (XBT) and anemometer data, and representative Swallow float data from the experiment. The Swallow float data include battery voltage, compass heading, and automatic gain control (AGC) measurements, the 8 kHz acoustic localization ping arrivals, and the VLF pressure and particle velocity data. Data collected by the sonobuoys and the PAEL buoys will be presented at a later time.

All 12 Swallow floats operated nearly flawlessly, resulting in a 99.7 % full data set. A number of conclusions can be drawn from a preliminary look at these data. First, throughout the experiment, an unknown source, or sources, generated acoustic energy centered at about 18 Hz and as much as 40 dB above background noise levels. The characteristics of the arrivals varied in time in an apparently deterministic way, suggesting a man-made sound source. This contamination will make it difficult to obtain useful information from a preliminary study of the coupling of noise by the Patton Escarpment into the deep sound channel conducted in this deployment. Second, the calibrated pressure spectral levels estimated directly from data collected by newly-installed VLF hydrophones agree with those derived from the geophone data except near frequencies corresponding to float rocking resonances and at times when signal clipping or overloading was present. Third, a 20 Hz line generated by the Sproul (apparently by the ship's generator) was at times audible to the floats, allowing for future efforts at beamforming the Swallow float data on a known source. Fourth, this experiment revealed that the Swallow floats can successfully operate when two, rather than one, of the floats issue range pings in a record, thus doubling the float localization sampling rate. Fifth, by varying the number of guy wires attached to each of the floats' radio beacon antennae, it was determined that motion of the antennae somehow cause a 4 Hz contamination and that the antennae should somehow be supported in future deployments. Finally, in situ measurements of the floats' clock drifts were obtained; the absolute drifts were on the order of one part in 10^5 and the relative clock drifts were approximately equal to those measured previously.

Table of Contents

Introduction

I. Deployment Geometry
- a) Swallow Float Deployment and Retrieval
- b) Sonobuoy and PAEL Buoy Deployment
- c) Deployment Depths

II. Known Sound Sources
- a) R/V R. G. Sproul Ship Tracks
- b) R/V R. G. Sproul Radiated Noise Characteristics
- c) Ship Sitings
- d) Seal Bombs and Light Bulb
- e) Acoustic Transmission Test
- f) PAEL Buoy Transmissions

III. Swallow Float Log Summary

IV. Environmental Data
- a) XBT Measurements
- b) Anemometer Readings
- c) Additional Environmental Information

V. Swallow Float Data - General Indication of Data Integrity

VI. Swallow Float Time Base Measurements

VII. Battery Voltage, Float Heading, and AGC Level
- a) Battery Voltage
- b) Float Heading
- c) AGC Level

VIII. The 8 kHz Surface and Bottom Bounce Data

IX. The 8 kHz Interelement Range Data

X. RMS Pressure and Velocity
- a) VLF-Hydrophone-Equipped Swallow Floats
- b) Midwater Swallow Float Data
- c) Bottom-Mounted Swallow Float Data

XI. Geophone and Hydrophone Time Series
- a) Comparison of Hydrophone and Geophone Time Series
- b) Unknown Source Contamination
- c) Floodlight Bulb and Seal Bomb Arrivals
- d) Tape Recorder Contamination
- e) Tether Contamination
- f) Sproul Generated Signals
- g) Other Unknown Signals in the Time Series
- h) Geophone Time Series Recorded on the Sproul's Deck

XII. Velocity and Pressure Power Spectra
- a) Comparison of Hydrophone and Geophone Pressure Spectra
- b) Contaminating Noise
- c) Sproul-Generated Noise

Acknowledgements

References

Appendix 1 - Swallow Float VLF Data Acquisition System

Appendix 2 - Loran-C Position Fixes

Appendix 3 - Initial Results from a VLF-II Sonobuoy

Figures

Introduction

The Marine Physical Laboratory's (MPL) set of 12 Swallow floats were deployed for a 24-hour period on 30-31 August 1988, near deep sea drilling project hole 469, 32.5° N, 120.5° W. All 12 floats operated nearly flawlessly. Thirteen ship-launched and two air-launched sonobuoys of various design from the Naval Air Development Center (NADC) and four Prototype Array Element Localization (PAEL) buoys from the Naval Ocean Systems Center (NOSC) were concurrently deployed. This report presents the instrument deployment locations, the positions and characteristics of known signal sources, expendable bathythermograph (XBT) and anemometer data, and representative Swallow float data from the experiment. The Swallow float data include battery voltage, compass heading, and automatic gain control (AGC) measurements, the 8 kHz acoustic localization ping arrivals, and the VLF pressure and particle velocity data. Data collected by the sonobuoys and the PAEL buoys, except for the initial results from a VLF-II sonobuoy given in Appendix 3, will be presented at a later time.

Two previous Swallow float deployments were made in 1987 at this study site [1,2]. However, a number of aspects of this experiment with the Swallow floats were unique. First, the Swallow floats were deployed in a vertical, freely drifting, array (this deployment geometry was also used in the September, 1987 Swallow float experiment [3]) rather than a horizontal planar array, and a preliminary study of ship-generated noise coupled into the deep sound channel by the Patton escarpment was conducted. To supplement the noise-coupling study, a set of five seal charges and three expendable bathythermographs (XBT) were deployed at selected positions over the escarpment. Second, four of the Swallow floats were equipped with Ocean and Atmospheric Science (OAS) model E-4SD hydrophones, in addition to the Geo Space three-component geophones which are installed on all of the floats, so that the calibrated acoustic spectral levels heard by the two types of sensors could be compared (re Section XII). Third, this was the first time that the Swallow floats' clock drifts were measured in situ; the results are presented in Section VI. Fourth, two changes were made in order to improve the understanding of the localization data. The first change was that two of the floats, floats 10 and 11, were programmed to generate their 8 kHz localization pings 20 seconds after the beginning of the record in which two other floats, floats 5 and 6, respectively, were issuing pings 10 seconds into the record. The success of this test will allow the sampling frequency of the inter-float ranges to be increased to twice every 45 seconds rather than once every 45 seconds. Also, the length of the three bottom-mounted floats' tethers were increased from 4.57 meters (this was their length in the May and September 1987 deployments; in April, they were 3.05 meters) to 17.98 meters in an attempt to distinguish the surface-bounce arrival from the surface-to-bottom-to-float arrival. Finally, fifth, a set of high-frequency acoustic transmission tests were made. Three types of signals were broadcast from the research vessel R. G. Sproul in order to study the feasibility of real-time acoustic transmission of Swallow float data. In addition, the PAEL buoys generated a frequency-modulated chirp which may allow the sonobuoy array to be localized. These high-frequency transmissions were only recorded by the sonobuoys; these data will be examined later.

The people on board the Sproul involved in the deployment of the Swallow floats were Bill Hodgkiss, Greg Edmonds, Marvin Darling, Lee Culver, and Gerald D'Spain from MPL and resident technician Gene Pillard from the Nimitz Marine Facility. Mary Beth Dormuth, from the Naval Air Development Center in Pennsylvania, was on board the Sproul to deploy the sonobuoys. Jim McEachern, also from the Naval Air Development Center, was aboard the P-3 aircraft, monitoring the recording of the sonobuoy and PAEL buoy data.

Note that all times given in this report are in local Pacific Daylight Time. To get Greenwich Mean Time, add seven hours.

I. Deployment Geometry

a) Swallow Float Deployment and Retrieval

Figure I.1 shows the deployment and retrieval positions of all 12 Swallow floats. The symbols used for plotting the float positions are the float identification numbers (not the float serial numbers) in hexadecimal notation, i.e. float 10 is plotted as an "A" and float 11 is plotted as a "B". In addition, the locations of DSDP hole 469 and of four of the XBT measurements (three other XBTs were taken over the Patton escarpment) are also plotted. The axes used in the plot are identical to those in the deployment geometry plots for the April and May, 1987 experiments [1,2].

The three bottom-mounted floats, floats 7, 8, and 9, formed a triangle about 6.3 km on a side. The midwater floats were deployed in the approximate center of the triangle at various depths (see Figure I.3). They drifted generally to the east during the deployment period, dispersing more than in April or May probably since they were at different depths. Note that both bottom floats 8 and 9 were retrieved several kilometers southeast of their deployment positions. They drifted on the surface for some undetermined number of hours before being retrieved since their galvanic time release (GTR) pins corroded and broke (thereby dropping the floats' anchors) sooner than expected.

b) Sonobuoy and PAEL Buoy Deployment

The plan view of the ship-launched sonobuoy and PAEL buoy deployment positions, referenced to the bottom-mounted Swallow float triangle, is shown in Figure I.2. Their locations were generally outside the triangle, in the vicinity of the estimated positions of the midwater Swallow floats. The 13 sonobuoys were deployed, typically two at a time, from the port and starboard stern, in a seven-minute period (from 21:41, 30 August, to 21:48) as the Sproul traveled at about 3 knots (1.5 m/sec) to the southeast. Their deployment positions are therefore plotted as a straight line in the figure.

The sonobuoys were not all of identical design. The following table lists, in the order in which the sonobuoys were deployed from the Sproul, the sonobuoy type (using the abbreviations in [8]) and the radio frequency channel over which the data were broadcast;

RF Channel	Sonobuoy Type
30	EARS2B-A
14	VLF-II
17	VLF-II
27	EARS2B-A
18	VLF-II
19	VLF-II
20	VLF-II
22	VLF-II
28	EARS2B-A
6	VLF-IIa
8	VLF-IIa
12	VLF-II (translate)
16	VLF-II (no audio)

Note that the VLF-II sonobuoy which was scheduled to broadcast over RF channel 2, as well as a wave buoy, did not arrive from the Naval Air Development Center (NADC) before the Sproul left port.

The VLF-II sonobuoys were designed by NADC to lower the effective range of the sensors into the infrasonic frequency band (refer to [10] for a discussion of the comparison between Swallow float, ocean bottom seismometer, and sonobuoy data in the VLF band). The VLF-IIa sonobuoys have been modified by NADC to have a somewhat different frequency response than the VLF-II sonobuoys. The three EARS2B-A (with a manufacturer model number of X17701A) sonobuoys were designed and manufactured in Great

Britain.

The deployment locations of the two air-launched sonobuoys, an SSQ-53B sonobuoy and an SSQ-77 sonobuoy, are not plotted in Figure I.2. They transmitted their data over RF channels 13 and 25.

The PAEL buoys were deployed, starting at 22:12, 30 August with the northern-most buoy and continuing in a counter-clockwise direction. The order, position, and time of deployment for each of the PAEL buoys, identified by the RF channel over which they broadcast their data, is given in the following table;

RF Channel	Position (32° N, 120° W)	Time (30 August)
11	36.78 31.40	22:12
29	36.20 32(3).55?	22:27
21	35.59 31.56	22:42
23	36.23 30.37	22:53

The deployment position for channel 29 is uncertain at present; the navigation chart on which positions were plotted during the experiment shows the deployment position was longitude 120° 32.55′ W, whereas the log entry indicates the longitude as 120° 33.55′ W. These two positions are marked by question marks in the plot. The uncertainty will probably be resolved once the sonobuoy data are analyzed. In either case, the PAEL buoy locations formed a diamond-shaped polygon encompassing the sonobuoy positions; the size of the polygon was determined in order to optimize, without overloading, the sonobuoy reception of the PAEL buoys' FM chirps.

The VLF-II and VLF-IIa sonobuoys were set for long life (8 hours) and 430 ft (131 m). The EARS2B-A sonobuoys also transmitted data for 8 hours, but were deployed at 150 meters. The PAEL buoys were deployed at 400 ft (122 m) and were set to scuttle after 3 hours. This allowed the sonobuoys to collect some data uncontaminated by the PAEL buoy localization chirps.

c) Deployment Depths

The deployment depths of the Swallow floats, the sonobuoys, and the PAEL buoys are shown in Figure I.3. The four PAEL buoys, plotted as four "*"s in the figure, were connected to their surface RF transmitters by 400-ft-long (122 meters) tethers. The 10 sonobuoys of the VLF-II and VLF-IIa design had 430-ft-long (131 meters) tethers; they are plotted as upward-pointing arrows connected by a straight line. The three EARS2B-A sensors were deployed to 150 meters and are plotted using three "e"s. The set of horizontal dotted lines, starting at about 425 meters depth, indicate the depths at which the Swallow floats stabilized. The floats, in order of increasing depth (re Table VIII.2 in Section VIII), were float 10 (425 meters), float 3 (*estimated* at 550 meters since its 8 kHz hydrophone did not generate sound during the deployment), floats 5 and 0 (700 meters), float 1 (825 meters), float 2 (975 meters), float 4 (1250 meters), and float 6 (1375 meters). Float 11 initially went to the ocean bottom and then released some ballast and drifted up to around 3360 meters depth. Finally, floats 7, 8, and 9 were anchored on the ocean bottom at about 3750 meters depth. The three shallowest floats, 10, 3, and 5, were equipped with VLF hydrophones (in addition to the VLF geophones installed on all the floats), as was float 11. These four floats reached their equilibrium depths faster than all other freely drifting floats; since the VLF-hydrophone-equipped floats have a recording capacity of only about 19 hours, which is 6 hours shorter than the 25-hour capacity of the VLF-geophone-only floats, it was important that they stabilized quickly.

The horizontal line of dots for each float is the output from a program which finds the time (converted to depth by using a speed of sound of 1500 m/sec) of the first detection by the 8 kHz localization circuit of a surface-bounce arrival. Note that float 3, whose localization hydrophone did not generate sound during the experiment, is plotted as a straight line at a depth about half-way between float 10 and float 5. A discussion of the 8 kHz localization data is given in Section VIII. The plots presented in that section show *all* 8 kHz detections within a specified time window (which is converted to depth) for data records in which a float was listening to its own localization ping. Table VIII.1 in Section VIII lists the deployment depths of the floats, as well as the floats' planned deployment depths (the vertical array was designed to have an

inter-element spacing equal to the wavelength of sound at 10 Hz). Also included in that section is Table VIII.2 which provides a estimates of the time it took each float to reach its equilibrium depth.

The lower horizontal axis of Figure I.3 gives the record number in which the surface bounce detection was made. This axis is actually a measure of time elapsed since the synchronization of the floats at 09:31, 30 August. To convert from record number to minutes, multiply the record number by 0.75 (since each record is 45 seconds long). Each float was programmed to ping every 10 records; the spacing between each of the dots in a given line is 10 records. The waviness of the midwater floats' dotted lines, due to their depths changing as a function of time, is indicative of the presence of internal waves. Note that while float 11 was on the bottom, before record 400, it appears to be slightly deeper than bottom-mounted floats 7, 8, and 9. Float 11 had a 4.6-meter-long tether while the other three bottom floats had 18.0-meter tethers.

The final piece of information added to Figure I.3 is the sound velocity profile based upon historical salinity and temperature data [6] and an equation relating salinity, temperature, and depth to sound velocity [7]. The upper horizontal axis of the plot gives the sound velocity in meters/sec.

II. Known Sound Sources

a) R/V R. G. Sproul Ship Tracks

Loran-C position fixes of the research vessel used in this experiment, the R. G. Sproul, were recorded intermittently in the Swallow float log while the experiment was being conducted. All position fixes, indicated by "+"'s, are plotted in Figure II.1. The axes of the plot are identical to the axes in the Scorpius-track plot in the May 1987 trip report [2]. Also plotted on the figure using small boxes are the locations of DSDP hole 469, in the center of the bottom-Swallow-float triangle, and DSDP hole 468, on top of the Patton escarpment to the east.

The ship track began in the middle of the triangle, where the midwater floats were deployed. It then traced out the triangle as the bottom-mounted floats were put in the water. From there, various courses near the array were followed as surveys of the ranges to the floats, spectral measurements of the Sproul-generated noise, and float clock-drift measurements were made. At 18:50, 30 August, the Sproul increased its speed to 7 knots (3.5 m/sec) and headed to the southwest away from the array; the ship track approaches the origin of the plot at this time. This was done so that Sproul-uncontaminated ambient noise could be collected. An hour-and-a-half later, the Sproul turned back to the array. After arriving, a range survey was made to determine the approximate locations of the midwater Swallow floats; the sonobuoys, and then the PAEL buoys, were deployed on the eastern side of the triangle. After waiting 1.5 hours for the P-3 aircraft on the eastern side of the triangle, and then conducting the acoustic transmission tests once the plane was on station, the ship then commenced to traverse a predetermined path at about 3 knots (1.5 m/sec) so that it could be used as a source in future beamforming efforts. The positions of the ship during these maneuvers, as well as its continuation over the Patton escarpment for the remainder of the night of 30-31 August, are plotted in Figure II.2. At 07:55 in the morning of 31 August, the Sproul returned to the array, deploying seal bombs and XBTs along the way over the Patton escarpment (re Figure II.7 and II.8) for the ship-noise-coupled-into-the-sound-channel study. The process of retrieval of the floats then began after a set of float clock-drift measurements were made; the track to the south-southeast of the array was followed in chasing float 9.

b) R/V R. G. Sproul Radiated Noise Characteristics

Plots were made of a set of spectral measurements of Sproul-generated noise at ship speeds of idle, 0.5 knots, 1.3 knots, 2.0 knots, and 3.0 knots; these are given in Figures II.3a through II.3h. Information pertaining to each of the figures is given in the following table;

Information on the Sproul Radiated Noise Spectral Plots

Time of Measurement	Ship Speed (knots)	Engine rpm starboard/port	Receiver Location	Major Spectral Peaks (Hz, dBV)
Figure II.3a				
14:26, 30 Aug	0.0 props stopped	500/500	starboard side	(20.0, -23.7) (23.0, -33.0) (31.6, -42.6) (38.0, -40.2) (39.4, -40.0) (45.6, -34.9) (47.2, -29.8)
Figure II.3b				
14:35, 30 Aug	0.0 props stopped	500/500	starboard stern	(20.0, -27.8) (23.0, -39.2) (45.6, -40.1) (47.2, -39.6)
Figure II.3c				
15:51, 30 Aug	0.5	0/470	starboard stern	(6.0, -24.6) (20.0, -31.1) (36.2, -48.5) (40.2, -47.6) (43.4, -32.1)
Figure II.3d				
14:48, 30 Aug	1.3	500/500	starboard stern	(8.0, -4.8) (43.8, -36.1)
Figure II.3e				
16:12, 30 Aug	2.0	525/525	starboard stern	(10.2, -11.3)
Figure II.3f				
14:58, 30 Aug	2.0	675/725	starboard stern	(15.8, -7.9) (33.2, -11.6) (35.4, -11.4)
Figure II.3g				
15:17, 30 Aug	3.0	700/825	starboard stern	(18.2, -3.0) (36.8, -8.6)
Figure II.3h				
15:29, 30 Aug	3.0	700/825	starboard stern	(18.6, +2.8) (21.0, -3.1)

Note that the tachometer reading for the starboard and port engines was gotten from the engine room; the accuracy of this reading was about ±50 rpm and was considered to be much more accurate than the

tachometer reading on the bridge. Also note that each spectral estimate was gotten by averaging 16 individual spectra.

The measurements were made using a Clevite hydrophone, whose sensitivity was -146 dBV re 1 μPa, and a Hewlett Packard spectrum analyzer. The Clevite hydrophone was attached to a cable, which had a streamlined weight on its end, about 6 to 9 meters below the surface of the water. It was deployed off either the starboard side or the starboard stern of the ship; the hydrophone location is given in the table above.

With the props engaged and the engines turning at 470 rpm, the predicted *diesel* shaft rate is 7.8 Hz, the predicted shaft rate is 1.5 Hz since the reduction gear ratio is 5.17-to-1, and the predicted blade rate is 6.1 Hz since the prop has four fixed blades. The peak at 6.0 Hz in Figure II.3c is therefore believed to correspond to the blade pass rate for the port prop. For the other ship speeds, the engine rpm, the predicted blade rate (the blade pass rate is usually the dominant line in a surface ship's source spectrum in the VLF band at these ship speeds [13]), and the frequency of the peak in the corresponding spectrum are;

Ship Speed (knots)	Engine rpm starboard/port	Predicted Blade Rate (Hz)	Frequency of Peak (Hz)
0.5	0/470	0/6.1	6.0
1.3	500/500	6.5/6.5	8.0
2.0	675/725	8.7/9.3	15.8
2.0	525/525	6.8/6.8	10.2
3.0	700/825	9.0/10.6	18.2/18.6

The frequency of the spectral peak may be higher than the predicted blade rate because of inaccuracies in measuring the engine rotation rate. Evidence for this comes from the two sets of measurements at 2.0 knots. In addition, the spectra at the higher ship speeds were not very reproducible. This was probably because the Clevite hydrophone was affected by flow noise.

The 20 Hz peak in Figures II.3a through II.3c is believed to be caused by the ship's generator.

c) Ship Sightings

The Sproul's radar was continuously monitored by the ship's crew during the course of the experiment for possible ship sightings. The radar has a maximum range of about 20 nautical miles (37 km). In Figure II.4, the tracks of the two contacts which were made during the experiment, both occurring around 08:30, 31 August during the Sproul's return to the array from the Patton escarpment, are plotted with reference to the Swallow float bottom-float triangle. Both sightings were located near the coastal lanes used by commercial shipping. Again plotted on the figure are the locations of DSDP holes 468 and 469.

Another ship, the research vessel New Horizon, which is also operated by the Scripps Institution of Oceanography, was sighted upon the return of the Sproul to the array. The scientific log from the New Horizon was obtained and the ship's locations on the morning of 31 August, from 01:26 to 10:40, are plotted in Figure II.5. (Before 01:26, 31 August, the ship was at least 20 km to the west of the westernmost New Horizon position plotted in the figure). The ship, whose chief scientist during this cruise was Dr. Venrick of Scripps, was involved in making net tows, Doppler current profiler measurements, and conductivity-temperature-depth (CTD) measurements. The deployment locations of three CTD casts, each about a thousand meters in depth, are plotted as stars in Figure II.5; these data will probably be obtained in late November from Dr. Venrick so that sound velocity profiles can be calculated.

d) Seal Bombs and Light Bulb

To provide a broadband sound source, seal bombs were thrown overboard from the Sproul. These charges are commonly used by commercial fishermen and have been determined in previous experiments [4] to be audible by the Swallow floats. The deployment positions of the two seal bombs thrown overboard

while the sonobuoys were still collecting data, at 01:35 and 01:36, 31 August, are indicated in Figure II.6 as exclamation marks. Also shown on the figure, as a pound sign, was the ship's position when a floodlight light bulb attached to an anchor was deployed at 01:25, 31 August. The straight line drawn on the plot to the east of the triangle indicates the track of the Sproul while some acoustic transmission tests were being conducted. These tests are discussed further in part e of this section.

The implosion of a floodlight was thought to potentially provide a cheap, safe, impulsive sound source. However, as discussed in Section XI, an arrival due to the floodlight implosion cannot be seen in the Swallow float time series. (It is audible on the analog magnetic tapes of sonobuoy data given to us by NADC). The seal bomb explosions, on the other hand, are discernible in the data (re Section XI). The arrival times of the seal bomb detonations, if they are audible on the sonobuoys and the PAEL buoys, will allow the time bases of the Swallow floats, the sonobuoys, and the PAEL buoys to be approximately aligned.

In order to aid in the study of ship generated noise coupled into the deep sound channel, seal bombs were deployed from the Sproul as the ship passed over the Patton escarpment on its way back to the array during the mid-morning of 31 August. The deployment positions of the bombs, as well as the deployment positions of three XBTs, are plotted in Figure II.7. The seal bomb deployment positions, referenced to the DSDP holes 468 and 469 and the bottom Swallow float triangle, are also plotted on a bathymetric chart in Figure II.8 in order to show their relationship to the Patton Escarpment. In addition, the positions are listed in the following table, along with their times of deployment (they were deployed in sequential order, with number 1 being the farthest east);

Seal Bomb Number	Position (32° N, 120° W)	Time (31 August)
1	44.83 09.86	08:18
2	44.05 12.52	08:48
3	43.02 15.04	09:04
4	41.93 17.59	09:27
5	40.93 19.87	09:41

A seal bomb was thrown overboard just before # 3, at 09:03. Its detonation was not heard on board the Sproul and was believed to have failed to explode. However, Sproul-generated noise may have drowned out its arrival. The recorded arrivals of the seal bomb detonations are discussed in Section XI.

The positions and times of the XBT deployments plotted in Figure II.7, as well as the other XBT deployments plotted in Figure I.1, are listed in a table in Section IV, the section in which these data are presented.

e) Acoustic Transmission Test

Once the P-3 aircraft was on station and recording the sonobuoy and PAEL buoy data, an acoustic transmission test was conducted from the Sproul, starting at 00:53 and ending at 01:22, 31 August. The Sproul's track during the test is plotted as a straight line in Figure II.6. The purpose of the test was to examine the time-evolving impulse response of the ocean communication channel for the possible future implementation of real-time acoustic transmission of Swallow float data. The test was also designed to determine the maximum rate at which Swallow float data could be successfully transmitted in the ocean channel.

The three signal sequences were broadcast for ten minutes each at a source level of 171 dB (re 1 μPa at 1 meter) from the Clevite hydrophone, which was lowered into the water about 130 ft (39.6 meters). The characteristics of the three sequences are summarized in the following table and are described below;

Sequence # 1	
	ping sequence mode
	2 msec pulse length
	16 frequencies, from 9 to 16.5 kHz, in 0.5 kHz steps
	ping interval of 1 second
Sequence # 2	
	ping sequence mode
	0.25 msec pulse length
	16 frequencies, from 9 to 16.5 kHz, in 0.5 kHz steps
	ping interval of 1 second
Sequence # 3	
	PRNG-FSK mode
	12 to 13 kHz FSK
	new bit rates start every 20 seconds

For sequence # 3;

Bit Period (msec/bit)	Sequence Length (bits)	Sequence Length (sec)
1	8191	8.2
2	4095	8.2
5	2047	10.2
10	1023	10.2
20	511	10.2
50	255	12.8
100	127	12.7

The first two sequences were both composed of sixteen harmonic pings; the frequency of the first ping of each sequence was 9 kHz, the next ping frequency was 9.5 kHz, and so on, in steps of 0.5 kHz, up to 16.5 kHz (the ping sequence mode). The beginnings of the pings in both sequences were separated by 1 second. The 16-second total duration of the sequences allowed for the arrival of all detectable multipath phases at a given frequency before the next ping of that frequency was generated. The difference between the two sequences was the duration of the pings; this was varied in order to examine the bandwidth of the channel (ping duration is inversely proportional to the bandwidth).

The third sequence used a pseudo-random noise generator with frequency shift keying (the PRNG-FSK mode). That is, the pseudo-random noise generator (PRNG) created a string of ones and zeros; a zero caused a 12 kHz tone to be broadcast from the Clevite hydrophone and a one caused a 13 kHz tone to be issued. The rate at which a one or zero was created by the PRNG, which determined the duration of the resulting tones, was varied from 1 bit/msec (bit period of 1 msec/bit) to 0.01 bit/msec (100 msec/bit period). This allowed for the effect of bit rate on the acoustic transmissions to be investigated.

These acoustic transmissions were recorded only by the sonobuoys and the PAEL buoys; these data will be presented at a later date.

f) PAEL Buoy Transmissions

Each of the four Prototype Array Element Localization (PAEL) buoys transmitted a frequency-modulated chirp, centered at 1.875 kHz. The inter-chirp time period was determined by the buoys at random from the interval between 25 and 35 seconds. A plot of the spectrum of a model PAEL buoy chirp is given in Figure II.9. The chirp time series from which the spectrum was derived was windowed using a triangular window with a DC offset in order to model the amplitude taper seen in Figure 7 of the "STRAP Data Collection Quick-Look Report" [5]. As with the acoustic transmission test signals, the PAEL buoy localization chirps were recorded only by the sonobuoys and the PAEL buoys; their source power level, about 100 dB re 1 μ Pa at 1 meter at 8 kHz, was too low for the signal to be detected by the Swallow floats' localization circuit.

III. Swallow Float Log Summary

Note: All times are in local Pacific Daylight Time. To obtain standard Greenwich Mean Time, add 7 hours.

30 August 1988

08:45 Arrive on station at DSDP hole 469. Begin preparations for Swallow float synchronization.

09:25 Conduct 8 kHz transponder tests. All floats check out normally.

09:31 Synchronize floats using GOES clock pulse.

09:39 Begin initial Swallow float clock drift measurements using the GOES clock.

10:42 Deploy float 11. One of the antenna guy wires is broken in deployment. Ship's position is 32° 36.93′ N, 120° 32.81′ W.

10:44 Deploy float 6. Ship location is 32° 36.83′ N, 120° 32.84′ W.

10:46 Deploy float 4. Localization hydrophone hits the side of the ship hard during deployment. Ship location is 32° 36.74′ N, 120° 32.85′ W.

10:48 Deploy float 2. Ship location is 32° 36.83′ N, 120° 32.77′ W.

10:50 Deploy float 1. Both antenna guy wires are broken in deployment. Ship location is 32° 36.80′ N, 120° 32.75′ W.

10:51 Deploy float 0. One of the antenna guy wires is broken in deployment. Ship location is 32° 36.97′ N, 120° 32.63′ W.

10:54 Deploy float 5. No antenna guy wires were installed on this float. Ship location is 32° 37.03′ N, 120° 32.56′ W.

10:58 Deploy float 3. Float is shaken badly and is tilted briefly during deployment, possibly causing one data record to not be recorded. Ship location is 32° 36.93′ N, 120° 32.54′ W.

10:59 Float 10's ballast breaks off during first attempt to deploy it. Repairs are begun to reattach the ballast.

11:09 Deploy float 10. One of the antenna guy wires is broken in deployment. Ship location is 32° 36.95′ N, 120° 32.79′ W.

11:14 Underway to deployment position for float 7. Deployment crane is refitted with a pelican hook.

11:51 Deploy float 7. During initial attempt at deployment, the pelican hook is accidentally released, causing the float to drop about 10 ft into the water. The damage to the float are broken localization hydrophone nylon support wires and a broken flasher support, resulting in the loss of the flasher overboard. Repairs are made. Ship location is 32° 38.04′ N, 120° 30.89′ W.

12:26 Deploy float 8. Ship location is 32° 38.03′ N, 120° 34.92′ W.

12:58 Deploy float 9. Ship location is 32° 34.93′ N, 120° 32.97′ W.

13:13 Unable to survey float ranges using the "poleducer" (a hydrophone attached to the end of an aluminum pole which is bolted to the side of the Sproul). Underway for center of the array since float ranges cannot be determined.

13:53 XBT 1 is taken near center of the float array. Ship location is 32° 37.04′ N, 120° 32.81′ W.

14:01 Begin float range survey. The range pings from all floats except float 3 are heard.

14:26 Begin spectral measurements of Sproul-generated noise (re Section IIb).

15:25 Continuing spectral measurements of Sproul-generated noise. Ship's position is 32° 38.19′ N, 120° 31.77′ W.

16:07 Continuing spectral measurements of Sproul-generated noise. Starboard engine is turned off at 15:33 and turned back on at 16:02. Ship's position is 32° 39.03′ N, 120° 31.88′ W.

16:30 Begin in situ measurement of the floats' clock drifts using the GOES clock.

16:37 Ship location is 32° 37.65′ N, 120° 31.57′ W.

17:08 Finished in situ measurement of the floats' clock drifts using the GOES clock. Ship location is 32° 36.12′ N, 120° 30.86′ W.

18:32 Begin another float survey. Ship location is 32° 35.78′ N, 120° 33.58′ W.

18:50 Increase ship speed to 7 knots and head to the southwest, away from the float array so that Sproul-uncontaminated noise can be measured.

20:28 Increase ship speed to 8 knots and head back to the array to deploy the sonobuoys and the PAEL buoys. Ship location is 32° 31.94′ N, 120° 38.01′ W.

21:33 End of float range survey to determine the approximate position of the Swallow float array. Ship location is 32° 36.32′ N, 120° 32.03′ W.

21:39 Ship traveling at 3 knots to the east. Prepare for sonobuoy deployment. Ship's position is 32° 36.33′ N, 120° 31.54′ W.

21:41 Begin deployment of 13 ship-launched sonobuoys (re Section Ib).

21:45 XBT 2 is taken.

21:48 Finish deploying sonobuoys.

21:49 Underway to deploy the four PAEL buoys. Ship's position is 32° 36.13′ N, 120° 31.03′ W.

22:12 Deploy PAEL buoy channel 11. Ship's position is 32° 36.78′ N, 120° 31.40′ W.

22:27 Deploy PAEL buoy channel 29. Ship's position is 32° 36.20′ N, 120° 32(3).55′ W?

22:42 Deploy PAEL buoy channel 21. Ship's position is 32° 35.59′ N, 120° 31.56′ W.

22:53 Deploy PAEL buoy channel 23. Ship's position is 32° 36.23′ N, 120° 30.37′ W.

23:54 Ship headed into the weather, waiting for the P-3 aircraft. Ship's position is 32° 37.17′ N, 120° 30.89′ W.

31 August 1988

00:13 A buoy is spotted near the ship. It is probably the eastern-most PAEL buoy, channel 23. Ship's position is 32° 36.47′ N, 120° 30.56′ W.

00:35 P-3 aircraft is (finally) on station.

00:38 XBT 3 is taken. The data are nonsensical possibly because the XBT wire may have had its insulation scraped off by the launcher.

00:46 From communication with the P-3 personnel, data from all sonobuoy channels check out properly. They are preparing to deploy some air-launched buoys. Ship's position is 32° 36.67′ N, 120° 30.59′ W.

00:53 Start of acoustic transmission tests; transmitting sequence 1. Ship speed is 1.2 knots and present position is 32° 36.68′ N, 120° 30.72′ W.

01:02 Start transmitting sequence 2.

01:12 Start transmitting sequence 3.

01:22 End of acoustic transmission tests. Ship's position is 32° 37.33′ N, 120° 30.92′ W.

01:25 Floodlight light bulb is deployed.

01:29 From communication with the P-3 aircraft, PAEL buoy channel 11 is no longer transmitting data. XBT 4 is deployed.

01:35 The first seal bomb is deployed.

01:36 The second seal bomb is deployed.

01:38 Ship's position is 32° 37.62′ N, 120° 31.11′ W.

02:05 Begin leg 1 of Sproul maneuvers which will provide a known source for future beamforming efforts. Ship's speed is 2.9 knots and ship's heading is due east; present position is 32° 37.33′

N, 120° 30.92′ W. The starboard engine is rotating at 650 rpm, the port engine is rotating at 700 rpm.

02:20 Personnel on the P-3 are given a mark at 02:20:00 as read from the GOES clock. The sonobuoy time code generator reads 02:20:06 at this time.

02:25 End of leg 1 of Sproul maneuvers. Ship's position is 32° 37.05′ N, 120° 29.92′ W.

02:26 Start of leg 2 of Sproul maneuvers. Ship's position is 32° 37.16′ N, 120° 29.73′ W.

02:30 Sproul maneuvers continue. Scientific party retires for the night. The personnel on the bridge will continue to record the ship's position, speed, and other ship sightings throughout the night.

03:45 End of leg 2 of Sproul maneuvers. Ship's position is 32° 40.10′ N, 120° 30.90′ W.

03:50 Start of leg 3 of Sproul maneuvers. Ship's position is 32° 40.16′ N, 120° 31.07′ W.

04:17 End of leg 3 of Sproul maneuvers. Start transit to Patton escarpment. Ship's position is 32° 39.93′ N, 120° 28.95′ W.

05:36 Start of leg 4 of Sproul maneuvers. Ship's position is 32° 39.99′ N, 120° 15.03′ W.

06:22 P-3 aircraft departs study area.

07:55 End of leg 4 of Sproul maneuvers. Scientific party is awake and in the ship's lab. Begin to return to the Swallow float array. Ship's position is 32° 45.00′ N, 120° 08.03′ W.

08:17 The first ship is sighted (re Section IIc). Track the ship for the next 36 minutes.

08:18 Seal bomb number 3 is deployed. Ship's position is 32° 44.83′ N, 120° 09.86′ W.

08:20 XBT 5 is taken.

08:27 Make second ship sighting. Track the ship for the next 26 minutes.

08:39 Ship speed is 5.9 knots and heading is 245° magnetic.

08:48 Seal bomb 4 is deployed. Ship's position is 32° 44.05′ N, 120° 12.52′ W.

08:50 Ship speed is increasing from 8.5 knots to 9.3 knots.

09:03 Seal bomb 5 is deployed; probably does not detonate.

09:04 Seal bomb 6 is deployed. Ship's position is 32° 43.02′ N, 120° 15.04′ W.

09:12 XBT 6 is taken. Ship's position is 32° 42.92′ N, 120° 15.29′ W. Ship will continue underway at 9.1 knots as the final seal bombs and XBTs are taken.

09:27 Seal bomb 7 is deployed. Ship's position is 32° 41.93′ N, 120° 17.59′ W.

09:41 Seal bomb 8 is deployed. Ship's position is 32° 40.93′ N, 120° 19.87′ W.

09:44 Launch old XBT. It was defective and its data were not recorded.

09:51 Deploy XBT 7. Ship's position is 32° 40.54′ N, 120° 20.38′ W.

10:23 All Swallow floats without VLF hydrophones will have stopped recording data in about 10 minutes or so. Ship's position is 32° 38.26′ N, 120° 26.31′ W, and speed and heading are 9.2 knots and 245°.

10:43 New Horizon is spotted at range 3.7 nautical miles and bearing 227°. From the Scripps Institution of Oceanography Log for the week of 26 August to 2 September, the New Horizon will return to port on 24 September, the chief scientist is Eliza Venrick, and the captain is Robert Haines.

10:44 Ship's position is 32° 36.80′ N, 120° 29.76′ W.

10:49 New Horizon is slowly moving to the south of the estimated Swallow float positions. It will be about 6 nautical miles south of the array.

10:54 XBT 8 is taken. An error in recording the data on cassette tape occurs. Ship's position is 32° 36.12′ N, 120° 30.94′ W.

11:01 Begin to conduct Swallow float range survey.

11:50 A Swallow float is detected on the surface by the ship's radio.

11:57 Recover float 10. The float had somehow been acoustically recalled. Its galvanic time release (GTR) was not broken, but it was not intentionally recalled from the Sproul. Float 10 is the float whose ballast fell off during the initial attempt to deploy it. Its microprocessor program is still running. Ship's position is 32° 36.45′ N, 120° 30.45′ W.

12:13 Make clock drift measurement for float 10 on the deck of the ship using the GOES clock. Note that the first ping issued from float 10 after it was recovered was a long release-type ping; the second ping was short.

12:19 Begin in situ measurements of the floats' clock drifts using the GOES clock for all floats except floats 3 and 10.

12:35 Recall float 5.

13:59 Recover float 5. Its microprocessor program is still running. Ship's position is 32° 37.27′ N, 120° 31.27′ W.

14:05 Make clock drift measurement for float 5 on the ship's deck.

14:08 Recall float 0.

15:03 A float is detected on the surface.

15:16 Recover float 0. Its microprocessor program is still running. Ship's position is 32° 37.14′ N, 120° 31.98′ W.

15:24 Make clock drift measurement for float 0 on the ship's deck.

15:29 Recall float 1. It may have already started to ascend to the surface because of a GTR release.

15:40 A float is detected on the surface. It may be float 3, whose 8 kHz hydrophone did not generate sound during the deployment. An attempt at locating the float on the surface using the direction information provided by the RF direction finder is started.

16:20 Float 3 is recovered! Its GTR pin had corroded and its microprocessor program is still running. Ship's position is 32° 36.77′ N, 120° 31.29′ W.

16:43 Recall float 2.

16:57 Recover float 1. Its microprocessor program is still running. Ship's position is 32° 37.00′ N, 120° 31.37′ W.

17:00 Another float is detected on the surface.

17:02 Make clock drift measurement for float 1 on the ship's deck.

17:32 Recover float 6. Its GTR is broken. Its microprocessor program is still running. Ship's position is 32° 36.77′ N, 120° 29.98′ W.

17:35 Make clock drift measurement for float 6 on the ship's deck.

18:08 Recall float 4.

18:13 Recall float 11.

18:49 Recover float 4. Its microprocessor program is still running. Ship's position is 32° 37.45′ N, 120° 31.63′ W.

18:56 Make clock drift measurement for float 4 on the ship's deck.

19:08 Recover float 2. Its microprocessor program is still running. Ship's position is 32° 37.01′ N, 120° 31.00′ W.

19:10 Make clock drift measurement for float 2 on the ship's deck.

19:19 Recall float 7.

20:23 Recall float 9. From a range survey, it appears to have already started ascending to the surface.

21:12 Recall float 8.

21:42 Recover float 11. Its flasher suddenly quit working while the Sproul was maneuvering into position to retrieve the float. Its microprocessor program is still running. Ship's position is 32° 35.88′ N, 120° 31.12′ W.

21:43 Make clock drift measurement for float 11 on the ship's deck.

23:17 Near float 7's estimated retrieval position. The float appears to not have reached the surface yet, although the radio direction finder indicates that some float is presently on the surface.

23:52 Float 7's flasher is finally seen on the surface.

1 September 1988

00:00 Recover float 7. Its microprocessor program is still running. Ship's position is 32° 37.89′ N, 120° 30.63′ W.

00:06 Make clock drift measurement for float 7 on the ship's deck. Underway to float 9's estimated retrieval position. The direction finder indicates that float 8 may be on the surface.

00:51 Ship's position is 32° 34.90′ N, 120° 32.96′ W, near float 9's deployment position.

00:58 Range from float 9 is about 4900 meters! It must have been on the surface for a few hours and drifted to the southeast. Float 8 is probably also on the surface and drifting to the southeast. Float 9 will be recovered first.

01:46 Recover float 9. Its microprocessor program is still running. Ship's position is 32° 32.14′ N, 120° 30.17′ W.

01:53 Make clock drift measurement for float 9 on the ship's deck.

03:00 Recover float 8. Its microprocessor program is still running. A problem with attaching the magnet to the float in order to turn off its microprocessor program is resolved. Ship's position is 32° 36.17′ N, 120° 32.24′ W.

03:07 Make clock drift measurement for float 8 on the ship's deck. Begin to make preparations to get underway for San Diego.

IV. Environmental Data

a) XBT Measurements

Expendable bathythermograph (XBT) measurements were made from the Sproul at various times during the experiment. Sippican model T-7 XBTs, which have a maximum depth of 760 meters, were used. These temperature measurements, along with historical salinity data archived by the National Oceanographic Data Center [6] and an equation relating temperature, salinity, and depth to sound speed [7], were used to derive sound velocity profiles. Shown in Figure IV.1 are the sound velocity profiles derived from XBTs 1, 2, and 4, which were taken near the Swallow float array. For comparison, a sound speed profile based upon historical temperature data [6] is also plotted on the figure. Figure IV.2 shows the profiles derived from XBTs 5, 6, and 7, which were taken over the Patton escarpment, along with the historical-data-derived profile.

The sound speed profiles derived from the XBTs 1, 2, and 4 are quite similar to each other and they deviate only slightly from the historical profile. Other than showing more structure than the historical profile (the historical data are averaged and are reported only at standard oceanographic depths), the XBT-derived profiles in Figure IV.1 indicate a somewhat higher sound velocity very near the surface, a lower sound speed between 400 and 500 meters, and possibly a higher sound speed near the deep sound channel axis than the historical profile. The profiles derived from XBTs 5, 6, and 7 in Figure IV.2 show a smaller sound velocity than in the historical profile throughout the upper 500 meters except very near surface. Note that a horizontal spike appears at about 600 meters; this spike occurs in XBT 5's data and its data below this depth are contaminated. Also note that the sound velocity derived from XBT 7's temperature profile differs significantly from the other XBT-derived profiles between 150 and 570 meters.

The locations of the measurements are shown in Figures I.1 and II.6. Below is a listing of the times, in addition to the locations, at which the measurements were taken;

XBT Number	Position (32° N, 120° W)	Time (Date)
1	37.04 32.81	13:53 (30 Aug)
2	36.33 31.54	21:45 (30 Aug)
4	37.33 30.92	01:29 (31 Aug)
5	44.83 09.86	08:17 (31 Aug)
6	42.92 15.29	09:12 (31 Aug)
7	40.54 20.38	09:51 (31 Aug)
8	36.12 30.94	10:54 (31 Aug)

XBT 3 did not provide useful information due to inexperienced operator error and XBT 8 was not recorded onto the cassette data tape due to a tape error.

b) Anemometer Readings

Anemometer readings taken from the bridge are recorded every two hours in the ship's log as standard practice. A plot of these wind velocity vectors for the 48-hour period of 30, 31 August is given in Figure IV.3. The vectors, starting at the dashed line, point in the direction the wind was blowing *from*; the lengths of the vectors, when measured against the plot's y axis, determine the wind speed. This plot is quite similar to the wind velocity plots for the April and May, 1987 experiments [Figures IV.2 and IV.3 of reference 1, and Figure IV.1 of reference 2]. The weather in this part of the ocean typically comes from the northwest and the wind speed is usually around 10 to 15 knots. One possible difference is that the wind appears to have been blowing slightly harder in this experiment than in either the April or, especially, the May, 1987 experiments.

c) Additional Environmental Information

Also recorded in the Sproul's ship log every two hours are the sea state, the estimated wave swell height and direction, the temperature, barometric pressure, and cloud observations. During the experiment, the swell was observed to be 5 to 7 feet (1.5 to 2 meters) in height, coming from 300° magnetic. The temperature was in the mid sixties (in degrees Farenheit) and the barometric pressure varied very slightly about 29.8 inches.

Other pertinent environmental information relating to the experiment may be gathered in the future. The data from three CTD casts collected from the New Horizon, another Scripps ship which was involved in an unrelated research project near our study site during the time of the Swallow float deployment, will probably be obtained in late November. Additional potential sources of information are the Fleet Numerical Oceanography Center, which provides ocean wave spectra hindcasts and shipping density information, California Cooperative Oceanic Fisheries Investigations data reports which provide hydrocast data, and the ship's log from the New Horizon. Note that a wave buoy which was to be deployed from the Sproul did not arrive from NADC before the ship left port.

V. Swallow Float Data - General Indication of Data Integrity

After being synchronously started (and spending about a half second in performing an initialization), each float begins to accumulate data into a temporary buffer. Once 44 seconds of data have been accumulated, they are written to cassette tape during a one-second period in which no data are gathered by the float. This 45-second cycle, called a record, is repeated until the cassette tape is filled. For those floats equipped only with a geophone, each record is composed of 7646 bytes; for those floats equipped with a VLF hydrophone as well as a geophone, a record is 9766 bytes long. Appendix 1 contains a description of the format of each record type. Due to their larger record size, the VLF-hydrophone-equipped floats, floats 3, 5, 10, and 11 in this deployment, were only able to store up to 1600 records, or 20 hours of data, on cassette tape as opposed to 2100 records (26 hours of data) for the geophone-equipped-only floats.

The first step in the data analysis of the Swallow floats is to scan all the floats' cassette tapes with a general screening program. This program checks each record for the proper location of resynchronization characters and the proper sum of byte values in a group prior to a checksum. The output from the screening program is given in Figure V.1. Note that the cassette-tape-reading program attaches a zero-byte record with the same internal record number as the last record on the cassette tape onto the end of each float's data file; this allows the number of internal records to be determined. For example, float 0's last-written record was internal record number 1982. (The record number listed in the left-most column is assigned by the screening program itself). Since the internal record number begins with record 0, float 0 wrote 1983 records onto tape.

The number of errors detected by the screening program is typical of that in other Swallow float deployments. However, a few special observations can be made of the types of errors. First, almost all the records which did not pass the screening tests for those floats with a VLF hydrophone contain the same type of error. That is, the bad records have the correct number of bytes, but have one failed checksum in the acoustic data. Further investigation has shown that the failed checksum always occurs in the 81st block of the set of 88 half-second blocks of acoustic data. (Each float record is comprised of 88 half-second blocks of VLF acoustic data. Each half-second block contains 100 bytes of VLF data which are prepended with a 3-byte resynchronization character and appended with a 2-byte checksum). In addition, the reason for the failed checksum is due to a set of four erroneous bytes, the same four bytes in every case, occurring in the 34th through 37th places in the block. However, the number and identity of the records in which this error occurs varies from one transcibing of the same cassette data tape to the next. A direct examination of the data byte values on the cassette tape by another method indicates that the checksum equals the sum of the byte values on the cassette tape; therefore, the contaminating four bytes somehow replace the correct data bytes in the postprocessing of the Swallow float cassette tapes. The problem is believed to be located in the Swallow-float-cassette-tape-to-magnetic-tape transcribing hardware. It is currently under investigation.

A second observation is that although float 5's data appear to have a greater-than-normal number of errors, most of the bad records occur after record 1567 (which is internal record number 1564) and they all have 88 failed acoustic checksums, the maximum number possible. These bad records are believed to be due to erroneous bytes attached to the end of float 5's data by the cassette-tape-to-magnetic-tape transcriber program and/or hardware. Note that this appended erroneous information is also the cause of the straight-line appearance of the plot of float 5's automatic gain control (AGC) setting after record 1564 (re Figure VII.3 and Section VII). Float 5's cassette data tape was transcribed a second time and the appended bytes were not present.

The greatest source of lost data in past deployments [1,2,4] was due to floats which quit recording prematurely or which could not be synchronously started properly. In this deployment, *all* 12 floats which were taken on the trip were deployed and all recorded full data tapes! Therefore, 99.7 % of the potential number of records which could have been recorded by 12 properly functioning floats were recorded and passed the screening test.

VI. Swallow Float Time Base Measurements

Each Swallow float contains its own quartz-crystal clock for timing. The clocks are not temperature-compensated; temperature-stabilized clocks are more expensive in terms of cost and power requirements. A unique aspect of this deployment was the attempt to measure the absolute drift of the individual float clocks in situ. The time standard used in the experiment was a Model 468-DC satellite-synchronized clock. This clock, when possible, phase-locks to one of two Geostationary Operational Environmental Satellites (GOES); when neither of the satellites is visible, the clock operates on its own internal crystal clock. It has an accuracy of ± 1.0 msec.

The individual float clock drifts were determined from the 8 kHz localization pulses. Once synchronized, the floats take turns pinging in sequence; one float pings approximately 10 seconds after the beginning of each record. (In this deployment, float 10 pinged 20 seconds after the beginning of those records in which float 5 pinged and float 11 pinged 20 seconds after the beginning of those records in which float 6 pinged; refer to Sections VIII and IX). The exact time that each float issues a localization ping is determined by its internal clock. Therefore, the times of localization pulse generation, as measured by an accurate time standard, can then be used to determine the drift of the floats' clocks.

The GOES clock was used to synchronously start the floats; synchronization occurred at 09:31:00, 30 August. After synchronization and before deployment, each float's 8 kHz localization pulse was used to trigger an oscilloscope which used the GOES clock as a time base. The time of the pulse arrival read from the oscilloscope was recorded. The floats were then deployed and, after sufficient time had elapsed in order for them to stabilize at depth, their localization pings (except for float 3, whose 8 kHz hydrophone did not generate sound after being deployed; refer to Section VIII) were again used to trigger the oscilloscope in order to determine the time of ping arrival. Immediately upon hearing a given float's range ping, the float was acoustically requested to send a second range ping. This allowed the arrival time of the first range ping to be corrected for the travel time from the float to the ship. This procedure was repeated the next day after the floats had completed recording data and before they were recalled to the surface. A final measurement of each float's pulse generation time was made once the float was recovered on board ship.

The following table lists the floats in the order in which they pinged and the travel-time-corrected times, according to the GOES clock, of their localization ping generation;

Time of Localization Ping Generation				
Float Number	Before Deployment	After Stabilizing on 30 August	Before Recall on 31 August	After Recovery
0	10:08:40.566	16:46:10.428	12:23:40.034	15:23:41.000
1	10:09:25.573	* 16:31:56.464 * 16:39:25.457	12:24:25.240	17:01:55.208
2	10:10:10.571	16:32:40.301 16:40:10.301	12:25:09.489	19:10:09.252
3	10:10:55.621	-	-	-
4	10:11:40.596	16:34:10.368 16:41:40.363 16:49:10.348	12:19:09.526 12:26:39.520	18:56:39.272
5	10:12:25.614	16:34:55.540 * 16:49:56.527 *	12:27:25.231	14:04:55.220
10	* 10:12:36.589 *	16:42:35.661	-	12:12:35.640
6	10:13:10.571	16:43:10.424	* 12:20:39.784 *	17:35:39.612
11	10:13:20.611	# 16:50:49.129 # 16:58:20.643	12:28:20.684	21:43:20.740
7	10:13:55.581	16:43:55.445 16:58:55.282	12:21:24.337	24:06:23.804
8	10:14:40.608	* 16:37:11.537 *	12:22:10.047 12:29:40.048	27:07:09.800
9	10:15:25.583	16:30:25.434 * 16:37:56.399 * 16:45:25.396	12:30:24.570	25:52:54.124

(*) These times probably contain a one second error due to the uncertainty in reading the seconds place from the GOES clock.

(#) This appears to be an erroneous reading.

Since the floats each ping every 7.5 minutes, then, according to the floats, the difference between the times listed in the columns of the table above should be an integral multiple of 7.5 minutes. The following table lists the integral number of ping rotations which have elapsed since the first set of ping generation measurements were made on board ship (column 2 of the table above), the difference between the time measured by the floats and the time measured by the GOES clock, and the dimensionless float clock drift;

Difference between Float Time and GOES Clock Time and the Clock Drift

Float Number	After Stabilizing on Aug 30			Before Recall on Aug 31		
	Ping Rotations	Difference (sec)	Clock Drift ($X\ 10^{-6}$)	Ping Rotations	Difference (sec)	Clock Drift ($X\ 10^{-6}$)
0	53	+ 0.138	+ 5.79	210	+ 0.532	+ 5.63
1	51	+ 0.109	+ 4.75	210	+ 0.333	+ 3.52
	52	+ 0.116	+ 4.96			
2	51	+ 0.270	+ 11.76	210	+ 1.082	+ 11.45
	52	+ 0.270	+ 11.54			
3	-	-	-	-	-	-
4	51	+ 0.288	+ 9.93	209	+ 1.070	+ 11.38
	52	+ 0.233	+ 9.96	210	+ 1.076	+ 11.39
	53	+ 0.248	+ 10.40			
5	51	+ 0.074	+ 3.22	210	+ 0.383	+ 4.05
	53	+ 0.087	+ 3.65			
10	52	- 0.072	- 3.08	* 208 *	- 0.051	- 0.54
6	52	+ 0.147	+ 6.28	209	+ 0.787	+ 8.37
11	53	+ 1.482	# + 62.14 #	210	- 0.073	- 0.77
	54	- 0.032	- 1.32			
7	52	+ 0.136	+ 5.81	209	+ 1.244	+ 13.16
	54	+ 0.299	+ 12.30			
8	51	+ 0.071	+ 3.09	209	+ 0.561	+ 5.96
				210	+ 0.560	+ 5.93
9	50	+ 0.149	+ 6.62			
	51	+ 0.184	+ 8.02	210	+ 1.013	+ 10.72
	52	+ 0.187	+ 7.99			

(*) A measurement of float 10's localization ping arrival time could not be made before the float was recalled since it returned to the surface prematurely. The measurement listed in the table was made after the float was recovered.

(#) This appears to be due to an erroneous reading.

The float clock drift is defined as float elapsed time minus true elapsed time, normalized by the true elapsed time. The float clock *rate* is the ratio of float elapsed time to the true elapsed time so that float clock drift plus one equals the float clock rate (re [9]). Therefore, a positive clock drift in the table above indicates that a float's clock is fast, so that the float thinks it is later than it really is. The floats' clocks are expected to be fast; since the dimensions and elastic properties of a quartz crystal are used to determine time and since the crystal shrinks and becomes more "rigid" (its shear modulus increases) with decreasing temperature, then it will vibrate at a greater rate with decreasing temperature and keep faster time. It is surprising that the two floats whose clocks are slow, floats 10 and 11, are the two floats which pinged 20 seconds, rather than 10 seconds, after the beginning of the record. It is possible that these two floats were coincidentally equipped with clocks which keep especially slow time at room temperature.

The relative inter-float clock drifts calculated from the the absolute clock drift measurements in the table above agree quite well with the relative clock drifts estimated from the 8 kHz interelement range data from the April, 1987 data. (Refer to [9] for a description of the method of calculating relative float clock drifts by taking differences in the reciprocal inter-float travel times). The following table presents a comparison of the relative clock drifts measured in this experiment and in the April, 1987 experiment for those floats which operated properly in both deployments;

Comparison of Relative Float Clock Drift Measurements

Float j minus Float i	Aug, 1988 Experiment Using the GOES Clock	April, 1987 Experiment Using the 8 kHz Interelement Travel Times
9 - 8	+ 4.54	+ 4.76
9 - 0	+ 5.97	+ 5.09
9 - 1	+ 7.32	+ 7.20
9 - 2	- 1.01	- 0.73
8 - 0	+ 1.60	+ 0.33
8 - 1	+ 2.87	+ 2.44
8 - 2	- 5.51	- 5.49
0 1	+ 1.27	+ 2.11
0 - 2	- 7.07	- 5.82
1 - 2	- 8.41	- 7.93

The consistency of these two independent sets of measurements supports the two methods of estimating float clock drifts.

From the attempt to analyze the data from this initial clock drift experiment, a few recommendations for future tests can be made. First, at least two, and preferably three or more, measurements of each float's ping generation time should be made when a set of measurements are taken. While the in situ measurements are being made, the ship should remain dead in the water rather than being underway. The float-to-ship travel time would then remain relatively constant, and the multiple measurements for each float could be averaged and an estimate of the noise (from the variance) in the measurements could be made. In addition, the one second errors in reading the GOES clock could be more readily identified. Also, there appears to be no need in measuring the ping generation times once the floats are recovered; variations in the amount of time each float stays on the surface before being recovered contaminate the clock drift measurements. Finally, over an hour was spent (re Section III) after the floats were synchronized in making the initial clock drift measurements on the ship's deck. In the future, the floats should probably be deployed immediately after they start recording data; from the analysis of this data set, it appears possible to make accurate *in situ* float clock drift measurements.

In order to measure the time base offset between the Swallow floats and the sonobuoys, the GOES clock's time was compared to that reported by the time code generator on board the P-3 aircraft. The time code generator served as a time base for all recorded sonobuoy data. When the GOES clock reported the time as 02:20:00, 31 August, the time code generator read 02:20:06; thus sonobuoy time is 6 seconds later than Swallow float time.

VII. Battery Voltage, Float Heading, and AGC Level

The battery voltage, the compass reading, and the automatic gain control (AGC) level, measured once during each 45-second record, are plotted in Figures VII.1 through VII.12 for all Swallow floats. The plots are ordered according to the floats' deployment depths, from the shallowest (float 10) to the deepest (bottom floats 7, 8, and 9). This ordering scheme for the figures will be followed in all subsequent sections.

a) Battery Voltage

The battery level for all floats remained constant at slightly more than 6 volts. The duration of the floats' deployment is therefore determined not by their power supply requirements, but by their recording capacity. This situation will change if real-time transmission of the Swallow float data is implemented.

b) Float Heading

Installed on the inside of each of the Swallow float glass spheres, at the sphere's south pole, is a compass for determining the orientation of the sphere, and thus, the orientation of the horizontal components of the float's geophone with respect to magnetic north. The compass heading during each 45-second record is shown in the middle plot of Figures VII.1 through VII.12. After being put into the water, the floats typically underwent rapid rotations as they descended. Once the midwater floats stabilized at depth, they twisted back and forth at a characteristic period of between 25 minutes to an hour. The twisting is believed to be caused by internal waves. Note that the twisting of float 11 after it had stabilized at 3360 meters (after record 700) was small in amplitude compared to the shallower midwider floats. As observed in previous deployments, the midwater floats' headings appeared to stabilize at about 300° near the end of the experiment (float 11's heading is a possible exception). The force responsible for this asymptotic approach to 300° magnetic is believed to be due to the interaction of a small, intrinsic magnetic field of the float (possibly due to the permanent magnets inside the geophone's components) with the earth's magnetic field.

The three bottom-mounted floats, floats 7, 8, and 9, were tethered to the bottom by 18.0-meter cotton lines; their compass headings usually remained approximately constant or varied slowly due to the constraining effects of the tether and the prevailing ocean current. However, at certain times, around record 880 for float 7 and records 890, 940, 1200, 1447, and 1928 for float 9, the heading changed significantly over a short period of time. Concurrently, the AGC level shown in the lower plot (and discussed in the next part of this section) increased to non-zero values. These periods of large changes in the bottom floats' heading, with associated increases in the AGC level, are thought to be caused by changes in the prevailing ocean current, with a resulting decrease in tether contamination.

c) AGC Level

The AGC is a variable gain amplifier, with a range of 0 to 25 dB gain, which allows the full dynamic range of the eight-bit A/D converter to be used. (The range can be increased to be from 0 dB to 48 dB gain by changing internal firmware; this change may be implemented in the future). The AGC gain always changes by a 0.5 dB step between records. After a five-second delay in the record, if more than 1 % of the points sampled on all components (three components for geophone-only floats and four components for floats with a VLF hydrophone) are clipped, then the AGC decreases by 0.5 dB. Otherwise, it increases. Because of the slow adjustment time of the AGC gain, amplitude information for large impulsive arrivals cannot be obtained.

The bottom plot in each figure shows the automatic gain control (AGC) level during every 45-second record. The first point of note is that the AGC levels were 5 to 15 dB lower during this deployment than in the two previous Swallow float deployments at this study site [1,2]. The levels appear to increase with

increasing depth of the float (ignoring bottom floats 7, 8, and 9 since their AGC level is dominated by tether effects), except for float 11. However, this is probably not mainly due to a depth dependence of the noise levels, but rather because the three shallowest floats, floats 10, 3, and 5, as well as float 11, were equipped with VLF hydrophones. The hydrophone circuits' fixed gain was set 4 dB higher relative to the geophone circuits' fixed gain so that the hydrophone channel would dominate the AGC level.

Float 11's AGC level after the float was freely drifting at about 3360 meters depth (after record 700) was lower than the levels on the bottom floats at certain periods of time (i.e. between records 800 and 950 for float 7 and between records 1200 and 1350 for float 9) even after taking into account the fixed gain offset mentioned in the previous paragraph. The unknown noise source(s) responsible for the low AGC gains in this experiment somehow was heard more effectively by float 11 than by the other floats. However, an exception to this may have occurred during the period between records 900 and 1000, when the non-zero AGC levels on float 9 are low apparently because of the unknown source(s) rather than tether contamination (re Section X and XI).

The AGC gains also appear to gradually increase over the duration of the experiment. A "jump" in levels occurs between records 1100 and 1200 for floats 2, 4, and 6. A trough in the curves for floats 3 and 5 at around record 900 is probably due to the change in Sproul noise as the ship returned at 8 knots to the array from the southwest (re Section III).

The AGC level on float 9 started to increase to the maximum level around record 12 (09:40, 30 August) and remained there until record 235 (12:27, 30 August). The cause of this anomalous AGC behavior is believed to be due to a temporary loss of power to float 9's geophone circuit board.

VIII. The 8 kHz Surface and Bottom Bounce Data

Each Swallow float possesses an 8 kHz hydrophone suspended 1.83 m below its glass sphere (see Figure 1). The source strength of the hydrophone is 192 dB (re 1 μPa at 1 meter). The floats periodically transmit and receive 10 msec acoustic pulses in order to measure interfloat and float-to-surface acoustic travel times. Normally one float transmits 10 seconds into each 45 second period. In this experiment, floats 0 through 9 were thus programmed, but floats 10 and 11 transmitted 20 seconds into records when floats 5 and 6 transmitted, respectively. The impact of having two floats transmit during one record is discussed below. In general, though, each float transmitted every 7.5 minutes, except that float 3 did not transmit at all as the result of a circuit board being jarred loose while the float was being lowered into the water.

Figures VIII.1 through VIII.12 show each float's record of receiving reflections of its own pulses. Reflections are received primarily from the ocean surface and bottom, and secondarily from their own (and occasionally another float's) glass sphere. The spheres may be excited and re-radiate sound at or near 8 kHz [11] The floats may also receive reverberation returns from the surface, bottom, and volume surrounding them.

The vertical axes in the figures have been scaled from travel time to distance (using 1500 m/s for the speed of sound in water) so that float depth is indicated by the leading edge of pulses propagated from the float to the ocean surface and back. The horizontal axes are record number, but may be converted to elapsed experiment time using 80 records per hour. A line of 16 very faint dots descending from 0 range are discernible on some of the plots. They are an artifact and should be ignored.

The experiment test plan called for 8 floats to be deployed in a vertical string extending from 350 to 1400 meters in depth, spaced at 150 meter intervals. Figures VIII.1 through VIII.8 contain data for these eight floats. Note that float 3 transmitted only briefly. The band of lines of varying length whose upper edge remains at approximately range 0 correspond to the outgoing acoustic pulse. The length of the lines after the floats reached equilibrium varies among the floats from essentially the length of the pulse (10 msec scaled to 15 meters) in float 1 to about 500 msec in float 10. The long outgoing pulse return seen in float 10 has been seen in other experiments when a float was deployed shallower than 500 meters. It may be caused by scatters in the water volume [1,12] or by temperature-dependent resonance of the glass sphere excited by the 8 kHz acoustic pulse [11]. Factors which must be considered include a possible depth-dependent ambient ocean noise level (the range pulse detector circuit compares the signal level in a narrow band centered at 8 kHz to that in a broader band) and variations among the electronic components in each float's range pulse detection circuit (thus influencing the threshold).

Data for float 11 is shown in Figure VIII.9. This float was intended to descend to the ocean bottom, remain there briefly, and then ascend to about 100 meters off the bottom. Part of its release ballast was attached with a corrodible link which was supposed to separate about 7 hours after entering the water. The remaining release ballast was adjusted so that the float would be neutrally buoyant at approximately 3700 meters depth. In Figure VIII.9, the returns due to the outgoing pulse are quite short as the float descends, longer while the float sat on the ocean bottom, and only faintly visible once the float leaves the bottom and begins to drift freely. The longer returns which occur at about 400 meters "depth" after the float stabilized for the second time (after record 700) are the bottom reflection, and their extended length is due to scattering by the bottom.

Figures VIII.10 through VIII.12 pertain to floats 7, 8 and 9, which were deployed to the ocean bottom using a large weight and 18 meter tether to provide a fixed coordinate system for the experiment. The longer outgoing pulse return is due to scattering by the bottom. In floats 7 and 8 it is possible to distinguish between the outgoing pulse and the bottom reflection (See discussion of tether length below).

The surface echoes in Figures VIII.1 through VIII.8 are marked by a band of vertical lines whose upper edge descends from the left side of the plots beginning approximately 100 to 300 records after the floats were synchronously started. The upper end of these lines marks the leading edge of the surface echo pulse. The lines are much longer than the 10 msec pulse length due to scattering by the ocean surface. However, as with the outgoing pulse, the length of the return varies among the floats. It apparently does not depend exclusively upon float depth, but may depend upon the other factors discussed above regarding

the length of the outgoing pulse return. The floats stabilize in depth between records 250 and 700. Quasi-periodic depth variation thereafter reflects the effect of internal waves.

Planned and actual deployment depths are shown in Table VIII-1 and plotted in Figure II.1. Floats 0 through 6 and 10 deployed to approximately their intended depths. The shallow floats with external VLF hydrophones, indicated by the (h) in Table VIII-1, all deployed slightly deeper than desired. Float 3's depth is unknown because it did not transmit. Float 3 was tilted briefly while being lowered into the water, however the float did not omit recording any records as occurred in the April 1987 experiment (re addendum to [1]).

Table VIII-1: Planned and Actual Deployments Depths, August 1988 Experiment

Float	Deployment Depth, m.	
	Planned	Achieved
10 (h)	350	425
3 (h)	500	unknown
5 (h)	650	700
0	800	700
1	950	825
2	1100	975
4	1250	1250
6	1400	1375
11 (h)	3700	3360
7	bottom	3750 (bottom)
8	bottom	3750 (bottom)
9	bottom	3750 (bottom)

The equilibrium depths of freely drifting floats are controlled by the weight of the float release ballast, which must be carefully determined for each float prior to each experiment. Equilibrium depth is an extremely sensitive function of ballast weight, with a 1 gram change in ballast corresponding to approximately 10 meters change in equilibrium depth. All of the float components are compressible to some degree, which must be accounted for as the floats descend. Also, it is difficult to predict the exact density versus depth distribution for a particular experiment location.

Referring to Figure VIII.9, the surface echoes for float 11 are marked by a band of vertical lines whose upper edge descends sharply from the left side of the plot, stabilizes briefly at approximately 3800 meters depth, then ascends and finally stabilizes at approximately 3360 meters depth. The surface echo lines are quite short because the distance to the surface is great. This float required about 2 hours to descend, remained on the bottom for about 2 more hours before the corrodible link severed, and stabilized at 3360 meters depth some 4 hours later. It is difficult to estimate when the corrodible links will release. The devices are not designed for precisely repeatable performance, and in-house calibration efforts show considerable variation from the manufacturer's curves.

The surface echoes for the bottomed floats, seen in Figures VIII.10 through VIII.12, are marked by a band of vertical lines whose upper edge descends sharply from the left side of the plots and stabilizes at approximately 3800 meters depth. The float depths are constant once their weights are resting on the bottom, although small-scale depth variations are apparent. These depth variations decrease the accuracy in estimating the positions of the floats as a prelude to beamforming the float acoustic data. Prior to this experiment, its cause was thought to be interference between the surface bounce and the surface-bottom bounce arrivals. Therefore, for this experiment, bottomed float tethers were lengthened from

approximately 4 to 18 meters so that the surface bounce and surface-bottom bounce paths would differ by more that the pulse length (10 msec = 15 m). However, the figures show that the surface-bottom bounce arrivals still cannot be distinguished. It now appears that the problem is caused by interference between multiple, scattered surface returns. Future effort should be directed toward solving this problem.

Table VIII-2 shows the approximate descent times for the floats. The second entry for float 11 pertains to its rise from the bottom. All freely drifting floats, including float 11, had reached equilibrium depth by record 735. Float 11 descended more quickly than the three bottomed floats because it had heavier ballast. In addition to the same large weight (approximately 5 kg) as carried by the bottomed floats, float 11 had another weight (approximately 1.5 kg) to keep it at 3360 meters depth once the large weight was dropped.

Table VIII-2: Float Descent Times, August 1988 Experiment

Float	Deployed at:		Arrived at depth at:	Descent Time		Deployment
	Time	Record	Record	Records	HH:MM	Depth, m.
10 (h)	1109	131	390	159	1:59	425
3 (h)	1058	116	-	-	-	-
5 (h)	1054	111	480	369	4:36	700
0	1051	107	470	363	4:32	700
1	1050	105	600	495	6:11	825
2	1048	103	630	527	6:35	975
4	1046	100	710	610	7:37	1250
6	1044	97	720	623	7:47	1375
11 (h)	1042	95	250	155	2:00	3750 (bottom)
11 (h)		390	735	345	4:18	3360
7	1151	187	390	203	2:32	3750 (bottom)
8	1226	233	420	187	2:20	3750 (bottom)
9	1259	277	465	188	2:21	3750 (bottom)

The seemingly random vertical lines appearing on the plots near record 360 are indicative of the floats being acoustically requested from the ship to transmit an 8 kHz pulse. This is done to survey floats' positions. Known possible causes of spurious lines, taken from the experiment log, are tabulated in Table VIII-3. The source of several long lines seen near record 1000 is unknown, however it may be a range survey (refer to the Log Summary) which was not recorded. Other randomly distributed dots represent noise in the acoustic localization system.

As was mentioned in the opening paragraph, this is the first experiment in which two floats transmitted during one record. The range buffers of all floats were examined to determine the effect of this change upon the number of range returns recorded (during each record, the floats can record a maximum of 85 returns in each of two range buffers). It was found that:

- Float 10, the shallowest float, recorded an average of 129 returns during records when it and float 5 transmitted. During these records, its range buffers were 76% full. Float 5, which was 275 meters deeper, recorded an average of 87 returns (51% full) during these same records.
- Floats 6 and 11, which transmitted during the same record, recorded an average of 45 returns (27%) and 85 returns (50%), respectively, during those records.
- The nine freely drifting float (0 through 6 and 11) averaged 33 returns (19%) during records when only one freely drifting float transmitted. The five freely drifting floats other than 5, 10, 6 and 11,

Table VIII-3: Known Possible Sources of 8 kHz Noise

Time	Record	Event
1401	360	position survey
1630-1700	560-600	GOES clock tests
1830	720	position survey
2212-0153	1015-1309	PAEL buoys active
0052-0122	1228-1268	acoustic transmission tests

averaged 55 returns (32%) during records when two floats transmitted.

- The bottomed floats averaged 25 returns (15%) during records when only one freely drifting float transmitted, 45 returns (26%) during records when two (freely drifting) float transmitted, and 57 returns (34%) during records when they themselves transmitted.

From these results we conclude that two floats can transmit during the same record without causing the range buffers to be overfilled as long as only one of them is deployed to depths less than about 600 meters.

IX. The 8 kHz Interelement Range Data

Figures IX.1 through IX.12 contain the record of pulses transmitted by one float and received by another. As in Figure VIII.1 through VIII.12, the vertical axes have been scaled from travel time to range using 1500 m/s for the speed of sound, and the horizontal axes are record number.

The short band of lines at the extreme left of each plot were recorded when the floats were side by side aboard ship. The upper edges of the lines are generally not horizontal, and indicate small differences in clock rates [9]. Clock rate measurements relative to a satellite receiver standard are discussed in Section VI.

Figures IX.1a - g through IX.8a - g contain travel times between freely drifting floats other than float 11. Except for the plots involving float 3 as the transmitter, which contain only the on-deck arrivals, these plots include a strong direct path pulse arrival followed by a strong surface bounce pulse arrival, followed by much weaker multiple bounce pulse arrivals. The direct path arrivals are generally short, approximately the length of the pulse (10 msec). The surface bounce arrivals are much longer due to scattering by the ocean surface.

Both the direct path and surface bounce arrivals are longer early in the experiment. The period during which the arrivals are long appears to decrease with increasing float separation and float depth. Another interesting observation is that the duration of the longer returns is identical in reciprocal path plots. However, these observations do not permit us to discriminate between scatterers in the water and re-radiation by the glass spheres (discussed in Section VIII) as the cause of the longer returns.

Figures IX.1i - k through IX.8i - k, and Figures IX.10a - g, IX.11a - g, and IX.12a - g contain travel times between freely drifting floats (other than 11) and the bottomed floats, 7, 8 and 9. These plots are also characterized by a strong, short direct path arrival followed by a strong surface bounce arrival and weaker multiple bounce arrivals. Upon closer inspection, the direct path often shows a second distinct arrival which is the bottom bounce. It comes in close behind the direct path because the bottom floats are only about 18 meters above the bottom. Also, on some plots, the bottom bounce can be seen to rise from the left as the float descends and merge with the direct path arrival when the float reaches the bottom.

Figures IX.11i - k, IX.12i - k, and IX.13i - k contain the travel times between bottomed floats. The direct path, surface bounce and bottom bounce arrivals are visible as the floats descend, but once the floats reach the bottom, only the surface bounce arrival remains. The direct path pulse is bent upward by the sound speed gradient as sound travels between the floats, so that it is too weak to be detected by another bottomed float approximately 6.3 km away. In order for the direct path between two bottomed floats to be audible, the tethers must be at least 70 meters long based upon the velocity profile in this area. Once the floats are bottomed, the leading edge of the band of surface bounce arrivals varies linearly with time. Since the floats are tethered to the bottom, their surface bounce travel time would be constant were it not for their clock rate differences. Random variations in surface bounce travel time are thought to be due to interference between multiple, scattered surface returns.

Figure IX.10a - h and Figures IX.1h through IX.9h contain travel times between float 11 and the other freely drifting floats. These plots show a direct path and surface and bottom bounce paths as the floats descended, and a direct and surface bounce path while float 11 remained on the bottom (approximately until record 390). After that, the direct path, surface and bottom bounce paths are again visible, along with some multiple bounce paths. The direct path return is short and the surface bounce return is much longer due to surface scattering.

Figures IX.10i, IX.10j, and IX.10k, and Figures IX.11h, IX.12h, and IX.13h contain the travel times between float 11 and the bottomed floats. These plots contain the direct path and the surface and bottom bounce paths as floats 7, 8 and 9 descended to the bottom, and a direct and surface bounce path thereafter. Float 11 left the bottom prior to floats 7, 8 and 9 reaching the bottom as shown in Table VIII-2. The direct path between float 11 and the bottomed floats is visible throughout the experiment, except for a few records when float 11 had difficulty hearing float 7 (re Figure IX.9i).

X. RMS Pressure and Velocity

In order to quickly scan the VLF data from all channels of all floats, the root mean squared pressure (for the hydrophone) and root mean squared velocity (for the geophone) were calculated and are plotted in Figures X.1 through X.12. The plots are presented in order of increasing depth of deployment of the floats. These RMS power series have been corrected for the AGC gain, but are otherwise uncalibrated; the vertical axis is in units of volts at the A/D converter (re Appendix 1 for a block diagram of the VLF data recording system). Each RMS level value results from taking the square root of the average of the squared amplitude levels over a five second (or 250 point) period. Since each record is 2250 points long (which equals 45 seconds since the data sampling rate is 50 Hz), then nine RMS power values are calculated for each record. The RMS value for the last five-second period of each record includes one second of zeros. The one second of zeros represents the time during which no data is sampled while data in a temporary buffer is being written to cassette tape.

Aspects of these plots common to all Swallow float deployments (e.g. the upward-curving part of each RMS plot over the first 25 records due to the decrease of the AGC gain) have been discussed elsewhere [1,2] and only the unique features of this data set will be discussed here.

a) VLF Hydrophone-Equipped Swallow Floats

One unusual aspect of this deployment was the data collected by the VLF hydrophones installed on floats 10, 3, 5, and 11. The shape of the RMS power level curves plotted for the hydrophone data generally agree with those curves plotted for the geophone data. However, during some times, e.g. around record 150 in float 10's data, record 125 in float 3's data, around record 125 in float 5's data, and between records 100 and 150 in float 11's data, the hydrophone RMS power levels are strikingly lower than the geophone levels. This is believed to be due to an overloading of the hydrophone electronic circuit from a large dc voltage output from the hydrophone itself. The reason for the large hydrophone output is mostly due to a pyroelectric effect; laboratory tests have shown that a large voltage is output by the hydrophone in response to a temperature change. The voltage drives the front-end amplifier into saturation, thus eliminating the circuit amplification. The circuit does not immediately recover after the large voltage output from the hydrophone has stopped; laboratory tests have determined that a pair of silicon diodes, installed in the system to protect the amplifier from large voltages, takes 10 to 15 minutes to discharge the circuit to the level where the amplifier is no longer saturated. The saturation of the amplifier for an extended period of time typically occurs at times near the beginning of the float deployment and the VLF data during those times are usually of little interest. However, the possible occurrence of this condition in the future has been eliminated by a change in the front-end hydrophone electronics (re Appendix 1).

Note that another cause of a large hydrophone output voltage appears to be operating. The fact that float 11's hydrophone, which descended rapidly through the water column to the ocean bottom, lost sensitivity for a longer period of time than the hydrophones on midwater floats 10, 3, and 5 (about 40 minutes versus 5 to 15 minutes) and that it suffered a brief loss in sensitivity just after the float's weight reached the ocean bottom at record 250 (re Figure X.9b) are still unexplained.

For records written after the VLF-hydrophone-equipped floats stabilized at depth, the RMS power levels of the hydrophone data are generally higher than the geophone levels. However, because the hydrophone system electronics are independent of the geophone system electronics, and since the power series presented here are uncalibrated, no physical interpretation of differences in absolute RMS levels can be made. In fact, the difference in average power levels is due to a greater sensitivity in the hydrophone system than in the geophone system; the pre-deployment engineering design of the two data acquisition systems specified a 4 dB difference in their relative receiving sensitivity so that the hydrophone levels would control the AGC gain.

Since the hydrophone data acquisition systems are identical in floats 10, 3, 5, and 11, intercomparisons of the relative RMS power levels can be made. During the period of time after record 25 and before the floats were deployed, the RMS power levels recorded by float 10's hydrophone (Figure X.1a) are inexplicably lower than those of the other three floats with VLF hydrophones, 1.5 RMS volts versus 2.0 RMS

volts. However, float 10's hydrophone appeared to have operated properly throughout the deployment; the calibrated spectral levels calculated from the hydrophone data agree quite well with those derived from the geophone velocity data (re Section XII). A similar situation occurred with float 2's y geophone component (Figure X.6a) which is believed to be due to the y-component geophone resting against its stop during this time.

b) Midwater Swallow Float Data

The dominating feature of the midwater Swallow float RMS power plots once the floats stabilized at depth are spikes separated by about 2.7 records, or almost exactly 2 minutes. The source of these spikes is as yet unknown, but they are obviously the reason for the anomalously low AGC levels in this experiment (re Section VII). The source(s) appear to be moving; at some times, the spikes are largest on the horizontal axes, e.g. between records 725 and 750 in float 10's data, and at other times, the vertical axis spikes are largest, e.g. between records 750 and 800 in float 10's data (Figure X.1d). Possible explanations are that the source was close, it was moving quickly, more than one source was present, and/or the propagation characteristics between the source(s) and receivers changed quickly with a small change in source(s) position, e.g. the source(s) was located over the Patton Escarpment. Evidence supporting a source(s) location over the Patton Escarpment can be gotten by determining the float compass heading at a time when the spikes occurred predominantly on a horizontal geophone component. Between records 725 and 750 in float 10's data, the spikes occurred mostly on the x axis (Figure X.1d) and the float's heading during this time was around 0° (Figure VII.1). Since the y axis of the geophone is aligned with 0°-180° line on the compass, then the source(s) must be either due west or due east. Float 2's RMS power data between records 775 and 800 (Figure X.6d) and its compass heading data (Figure VII.6) show a similar pattern. Firm conclusions on the source(s) location must await further data analysis. However, because of the consistent two-minute repetition rate of the RMS power spikes, it seems likely that the source(s) of the contamination was man-made.

Other jumps in RMS power levels consistent across the components of all midwater Swallow floats can be found in the data. One such prominent jump occurs around record 560 (16:31, 30 August). Its cause may be partially due to range pulses issued by the floats; the scientific personnel on the Sproul were making in situ float clock drift measurements during this time (re Section III). (An increase in power levels around record 720 on the floats' z axes is probably associated with a float range survey being conducted at this time). However, since float 3's RMS levels, in Figure X.2c, show a similar jump and its 8 kHz hydrophone did not generate acoustic energy (re Section VIII), then another source, as yet unknown, must have contributed to the increase in power levels. Another jump in power levels occurs after record 1939 (09:45, 31 August) in floats' 0, 1, and 2 data (these were the only midwater floats still recording data). This jump is probably due to the passage of the New Horizon near the array (re Section IIc), although Sproul-radiated sound which was topographically coupled into the sound channel may have contributed.

Spikes with a one-record repetition rate are also visible in many of the floats' plots, e.g. float 11's geophone data in Figure X.9d. These spikes are caused by cassette-tape-recorder-induced contamination at the beginning of each record. Occasional dropouts (e.g. record 204 for float 6, Figure X.8b), are due to bad data records (re Figure V.1).

c) Bottom-Mounted Swallow Float Data

Figures X.10 through X.12 show the RMS velocity plots for the bottom-mounted floats, floats 7, 8, and 9. For much of the time after the floats reached the ocean bottom, their data are contaminated by tether effects. (During their relatively rapid descent to the bottom, the bottom floats' data are dominated by float rocking). However, at certain times, and on certain geophone components, useful information can be obtained. Most notable is the set of float 9's vertical geophone component data from record 800 to record 1000 (19:31, 30 August to 22:01, 30 August) shown in Figure X.12e. The timing of the arrivals from the contaminating source(s), discussed in first part of this section, is readily apparent; typically, three spikes of

large power, each separated by about two minutes, are each preceeded, by about 50 seconds, by a spike of smaller power. This sequence of six spikes repeats every 10.5 records (or 7 minutes, 50 seconds). Plots of float 9's uncalibrated time series for a 12-record sequence of data starting at record 900 which show the structure of the arrivals giving rise to these spikes, are presented in the next section. Note that at certain times, the sequence of spikes is composed of only two large spikes and two small spikes, rather than three, and that the timing between spikes and between sequences of spikes varies slightly.

The unusual appearance of float 9's RMS velocity data in the first 280 records is believed due to the loss of electrical power to the float's geophone circuit electronics (re Section VII, part c), either the geophone amplifier card or the low-pass filter card. The RMS power level in Figure X.12a does not equal zero immediately after record 11, the time the float apparently began to have trouble (re Figure VII.12). Instead, it hovers about a constant level of about a quarter RMS volt, until after record 25, as the AGC steps down to zero gain. The fact that the RMS levels do not increase as the AGC decreases (as seen in the first 25 records of the other floats' data) and that float 9's initial RMS level of 0.25 volts is about half the normal initial value indicates that the float probably had a bad connection immediately after synchronization. The power level finally drops to zero on the x axis at about the same time the AGC level reaches the maximum of 25.5 dB. The reverse situation occurred when the geophone regained power after record 235 (12:27, 30 August); the RMS power level hovers between 0 and 0.5 RMS volt as the AGC level decreases, until the AGC level reaches about 12 dB at which time the RMS levels begin to quickly rise to their maximum levels. The time at which the float's geophone regained power, 12:27, was just after float 8 had been deployed. Float 9 may have been moved into position for deployment at 12:27, thereby jostling the float into proper operation.

XI. Geophone and Hydrophone Time Series

Selected time series recorded by the geophones and the hydrophones, corrected for the AGC level but otherwise uncalibrated, are presented in this section. Each figure shows the time series recorded by a given float's component over a 12-record (9 minute) period; the record numbers are given on the left hand side of the plot. The data are sampled at 50 Hz (re Appendix 1), so that 2200 points from each channel are collected in the 44 seconds of each record (the 45th second of the record is made up of 50 zeros). Only every other sampled point is plotted. The scale of the plots' vertical axis is given at the top of each figure and is either ± 1.0 volts or ± 3.0 volts.

The time periods selected for plotting are;

Swallow Float VLF Time Series

Record Sequence	Local Time (Date)	Floats	Comments	Figure Numbers
30 - 41	09:53 - 10:02 (30 Aug)	2	The floats were still on the Sproul's deck.	XI.1
590 - 601	16:54 - 17:03 (30 Aug)	11	Float 11's AGC level was at its peak and changing rapidly.	XI.2
598 - 609	17:00 - 17:09 (30 Aug)	11	" "	XI.3
610 - 621	17:08 - 17:17 (30 Aug)	11	" "	XI.4
840 - 851	20:01 - 20:10 (30 Aug)	all midwater floats	Sproul was about 12 km to the southwest from the array.	XI.5 - XI.13
900 - 911	20:46 - 20:55 (30 Aug)	11 and 9	Contaminating noise is cleary visible on float 9's z axis.	XI.14 - XI.15
1175 - 1186	00:12 - 00:21 (31 Aug)	all midwater floats	AGC levels for the midwater floats were high.	XI.16 - XI.24
1230 - 1241	00:54 - 01:03 (31 Aug)	11 and bottom floats	Bottom float 9's AGC level was very high.	XI.25 - XI.28
1270 - 1281	01:24 - 01:33 (31 Aug)	all midwater floats	The floodlight bulb imploded in record 1272.	XI.29 - XI.37
1278 - 1289	01:30 - 01:39 (31 Aug)	all midwater floats	Seal bombs 1 and 2 exploded in records 1285 and 1287.	XI.38 - XI.46
1320 - 1331	02:01 - 02:10 (31 Aug)	all midwater floats	Start of leg 1 of Sproul maneuvers.	XI.47 - XI.55
1820 - 1831	08:16 - 08:25 (31 Aug)	0, 1, 2, 4, and 6	Seal bomb 3 exploded in record 1823.	XI.56 - XI.60
1860 - 1871	08:46 - 08:55 (31 Aug)	0, 1, 2, 4, and 6	Seal bomb 4 exploded in record 1862.	XI.61 - XI.65

1880 - 1891	09:01 - 09:10 (31 Aug)	0, 1, 2, 4, and 6	Seal bomb 6 exploded in record 1884.	XI.66 - XI.70
1908 - 1919	09:22 - 09:31 (31 Aug)	0, 1, 2, 4, and 6	Seal bomb 7 exploded in record 1914.	XI.71 - XI.75
1928 - 1939	09:37 - 09:46 (31 Aug)	0, 1, and 2	Seal bomb 8 exploded in record 1933.	XI.76 - XI.78

The figures for this section are presented in chronological order, and in order of increasing depth of the floats.

a) Comparison of Hydrophone and Geophone Time Series

Floats 10, 3, 5, and 11 were equipped with VLF hydrophones in addition to the VLF geophones installed on all the floats. Plots of the hydrophone time series recorded by one of these floats appear following its geophone time series plots. Note that the vertical axis scale in the geophone time series plots is ± 1.0 volt (except for float 9's geophone time series in records 900 through 911, Figures XI.15a through XI.15c, where it is ± 3.0 volts); in the hydrophone plots, it is ± 3.0 volts. The fact that the amplitudes recorded by the hydrophones were generally higher than those on the geophones is due to the greater sensitivity in the hydrophone channel versus the geophone channels. (Recall that the time series presented in this section are uncalibrated except for a correction of the AGC level).

The main difference between the hydrophone and geophone time series, besides the apparent difference in amplitude, is that the tape-recorder-induced contamination at the beginning of most of the geophone records does not appear to be present in the hydrophone records. For example, the beginning of each record in the geophone time series for float 11 in Figures XI.2 through XI.4 shows a characteristic and repeatable pattern; on the x axis, a 3 to 4 Hz signal riding on an initial upward swing from an initial large negative amplitude, an over-saturation of the y axis amplifier followed by recovery, and an upward swing from an initial large negative amplitude on the z axis. The beginning of each hydrophone time series record shows no evidence of this contamination. In addition, the 0.38 Hz rocking of float 11 seen on the horizontal geophone component time series, which is by far the most dominant feature in *calibrated* geophone time series [16], is not present in the hydrophone data. Tape-recorder-induced contamination is therefore non-acoustic in nature since the float motions are not accompanied by water-borne pressure fluctuations and this results in differences between the geophone and the hydrophone data. Further discussion of tape recorder contamination is given in part d of this section.

The appearance of the 8 kHz localization ping arrival on the geophone time series is different than on the hydrophone time series. In Figure XI.2c and XI.2d, float 11's localization ping occurs 20 seconds after the beginning of record 596 (recall that floats 10 and 11 pinged 20 seconds after the beginning of the records in which floats 5 and 6 pinged, respectively; re Section VIII). On the vertical geophone component, the ping is a sharp, impulsive arrival of about a quarter second duration (the localization ping itself is 10 msec in duration) with an approximately exponentially decaying amplitude; in the hydrophone time series, the ping arrival appears as a spike followed by a quarter second of data of nearly zero amplitude. The difference in appearance is due to the difference in response of the geophone and the hydrophone circuits; the ping arrival is sufficiently loud to drive the hydrophone front-end amplifier circuit into saturation and the nearly zero amplitude period represents the recovery of the circuit, whereas the geophone circuit is only clipped for a short period. Saturation of the hydrophone and geophone circuits occurs when the input signal level, converted to voltage, is greater than ± 5 volts; signal clipping occurs when the voltage is greater than ± 2.5 volts.

A second arrival appears almost 17 seconds after the localization ping in record 596. This arrival is a result of the in situ float clock drift measurements being made at this time (record 596 was written at 16:58, 30 August); float 11 issued a range pulse, which is about five times longer in duration than the localization ping, in response to an acoustic command from the Sproul. Note that the range pulse issued by float 11 is

clearly recorded by the horizontal geophone components whereas the localization ping does not appear to be present; re Figures XI.2a and XI.2b. Since the localization hydrophone is located directly below the float's glass sphere (re Figure 1), the localization and range pulses are expected to be recorded only on the vertical geophone component; the fact that the range pulse is heard by the horizontal components must be related to its longer duration, although the coupling mechanism is not yet understood. The difference in the recording of the localization ping and the range pulse has implications for the implementation of real-time transmission of the Swallow float data.

b) Unknown Source Contamination

As mentioned in the discussion of the floats' AGC levels (Section VII.c), the noise levels recorded during this deployment were much louder than in previous experiments at this study site. Arrivals from the unknown sound source(s), which are responsible for the low AGC levels, can be seen in almost all of the uncalibrated time series plots of this section; the exceptions being those plots recorded by the bottom-mounted floats when tether contamination was dominant.

Some observations of the properties of the unknown sound source(s) which caused the higher noise levels were made in parts b and c of the previous section. As pointed out there, the clearest display of the arrivals from the unknown source(s) is in portions of the data recorded by bottom float 9's vertical geophone component. Figure XI.15c shows a 12-record period, from record 900 to 911, of float 9's z axis time series. This sequence of records was written while the Sproul was returning to the float array from the southwest (re Section III). In this figure, the arrivals can be seen to be of two characteristic types. The first characteristic arrival is composed of 20 to 25 pulses (possibly a result of amplitude modulation), each pulse separated by about 0.7 seconds, followed by energy which is probably due to multipaths. The first few pulses do not cause clipping, but the remaining pulses do. The second characteristic arrival, which always follows the first type by about 46 to 47 minutes, is slightly shorter in duration (15 seconds versus 19 seconds), reaches amplitudes sufficient to cause clipping quicker (0.5 seconds from initial time of arrival versus 2 seconds), and appears to be monochromatic (about 17.9 Hz). It too is followed immediately by energy believed to be due to multipath arrivals.

The set of two arrivals, one of each characteristic type, is repeated twice, with a repetition rate varying somewhat between 120 and 125 seconds. The next group of six arrivals, three of each type, begins about 7 minutes, 55 seconds after the beginning of the previous group.

The time series recorded by float 11's z axis during records 900 - 911 are shown in Figure XI.14c. The distinct arrivals seen in float 9's data can also be seen in this figure. However, their amplitudes are smaller; the arrival composed of 20 to 25 pulses is not at all clipped and the monochromatic arrival is clipped for a smaller portion of the time than in float 9's data. (Note that the figures are plotted on the same scale). In addition, the arrival times in float 11's data appear to be delayed by about 0.4 seconds (equivalent to 600 meters) with respect to those measured in float 9's data. (This calculation of the delay does not take into account a difference in the two floats' clock drifts). Interestingly, the monochromatic arrival in float 11's data is composed of two packets of energy; the second packet follows the first by 10.5 seconds. The second packet may represent a multipath which is discernable in float 11's data due to decreased amplitudes and/or a different source/receiver geometry.

The overall pattern of arrivals appears to be maintained throughout most of the experiment. Variations do occur, e.g. a group is sometimes composed of only four, rather than six, arrivals, but the general regularity of the pattern suggests a man-made source(s). The source(s) may be moving (amplitudes of the arrivals on bottom-mounted float 9's z axis during records 1230 to 1241 in Figure XI.28c are significantly smaller than in records 900 to 911), although possible changes in source amplitude, the possibility of multiple sources, as well as the motion of the floats themselves complicate the situation. The Local Notice to Mariners, issued by the U.S. Coast Guard, indicate that several U.S. Navy activities were planned for the week of 28 August to 3 September. Which of these activities, if any, was responsible for the contaminating arrivals remains to be determined. Examination of digitized sonobuoy data, valid over a much larger frequency range than the Swallow float data, may help resolve this question. In addition, once the relative float clock drifts measured in Section VI are used to align the time bases, it may be possible to use the

Swallow float time series from the bottom-mounted floats to triangulate on the unknown source(s). Once the unknown source(s) has been identified, it may prove to be useful in applying various signal processing techniques to the data.

c) Floodlight Bulb and Seal Bomb Arrivals

The floodlight light bulb was thrown overboard from the Sproul at 01:25, 31 August and its implosion was heard on board the ship 32 seconds later. This time corresponds to the time when Swallow float record 1272 was being written. An examination of the Swallow float time series recorded at this time, Figures XI.29 through XI.37, shows that the implosion cannot be distinguished from the contamination caused by the unknown source(s). It is, however, audible on the sonobuoy analog magnetic data tapes. The potential use of floodlight bulb implosions as impulsive sound sources in Swallow float experiments must therefore be determined in a future deployment.

The following table lists the times, from the scientific log, of the eight seal bomb deployments in this experiment and the equivalent Swallow float record number;

Seal Bomb Number	Time (31 Aug)	Swallow Float Record Number
1	01:35	1285
2	01:36	1287
3	08:18	1823
4	08:48	1862
5(?)	09:03	1882
6	09:04	1884
7	09:27	1914
8	09:41	1933

(?) This seal bomb possibly did not detonate.

The first two detonations were clearly audible to the floats' geophones, Figures XI.38 through XI.46; they were, in fact, sufficiently loud to overload the front-end amplifier circuits on some of the geophone components, e.g. float 10's z axis (Figure XI.38c). However, the VLF hydrophones on floats 10, 3, 5, and 11 do not record the arrivals well, if at all. The reason for this difference is not yet clear.

The arrivals of the remaining seal bomb explosions, which detonated as the Sproul passed over the Patton escarpment (re Section IId), may be present in the Swallow floats' time series (that is, only for those floats not equipped with VLF hydrophones; VLF-hydrophone-equipped floats 10, 3, 5, and 11 had already filled their cassette data tapes by this time). However, it is impossible at present to unambiguously identify the seal bomb arrivals because of the contaminating noise source(s). A spike-like arrival 20 seconds after the beginning of record 1863 in float 2's vertical component data (Figure XI.63c), which also appears in float 0's y axis data (Figure XI.61b) and float 1's x axis data (Figure XI.62a), may be due to the explosion of seal bomb 4, but no firm conclusions can yet be made. It may be possible to identify these detonation arrivals once the time series are passed through a notch filter to eliminate the energy from the contaminating source. However, more information must be obtained about the contaminating source(s) before a study of the topographic coupling of sound into the sound channel can be undertaken.

d) Tape Recorder Contamination

As in previous deployments [1,2,3], an attempt was made in this experiment to reduce the contamination at the beginning of each 45-second record caused by the "noisy" type of Swallow float cassette tape recorder. ("Noisy" tape recorders are constructed so that their motor turns in the same direction as the cassette tape; "quiet" recorders are geared so that the motor and the tape turn in opposite directions). The tape recorder appears to impart an impulse to the float, causing the float to rock and thereby exciting other types of resonances, possibly including a radio beacon antenna oscillation at 4 to 5 Hz. To test whether

restriction of the antenna motion would reduce the contamination at 4 to 5 Hz, two nylon guy wires were attached to each of the radio beacon antennae on all but one of the floats. During deployment, many of the guy wires became entangled in the crane hook and were broken. The number of antenna guy wires which remained on each of the floats after deployment was;

Guy Wires on Swallow Float Antennae

Float I.D. Number	No. of Guy Wires after Deployment	Noisy (N) or Quiet (Q) Tape Recorder
10	1	Q
3	2	N
5	0	N
0	1	Q
1	0	Q
2	2	Q
4	2	N
6	2	Q
11	1	N
7	2	N
8	2	N
9	2	N

Examination of the geophone time series (tape recorder contamination does not appear in the hydrophone time series since it is non-acoustic) indicates that the only float with no antenna wires and equipped with a noisy tape recorder, float 5, suffered the greatest amount of 4 Hz contamination at the beginning of each record. The contamination occurs predominantly on the horizontal axes, although a small amount can be seen on the vertical axis. The duration of the contamination is about 3 seconds. This is shorter than in previous deployments [4] possibly because, strangely, no low frequency rocking can be seen in float 5's uncalibrated time series.

Float rocking is obviously present in float 11's horizontal component time series. The rocking may have forced antenna oscillations, explaining the presence of 4 Hz contamination on float 11's x axis even though one guy wire was attached to the antenna. Rocking is also strong in float 3's data, especially on the x geophone axis. However, no 4 Hz contamination is apparent, probably because the two guy wires attached to the antenna restricted its motion.

The time series recorded by the remaining midwater-column float with a noisy tape recorder, float 4, shows strong, low frequency float rocking. However, the 4 Hz contamination doesn't seem to be present; the initial one to two seconds of each record are dominated by recovery of the geophone circuits to overloading.

The data collected by those floats with quiet tape recorders contain much less tape-recorder-induced contamination. Of these floats, float 1 appears to have suffered the largest amount of 4 Hz contamination, although it is not predominant. This float was the only other float (in addition to float 5) which had no antenna support wires.

The conclusion from this antenna support test is that, barring the installation of quiet tape recorders in all the midwater floats (which would also significantly reduce the other types of tape recorder contamination, notably float rocking) the motion of the radio beacon antennae of all midwater floats should somehow be restricted. The 4 Hz contamination is apparent for only the first few seconds of each record, and to the degree that it is coherent from record to record, it can be removed by signal processing [17]. However, any relative motion of the antenna with the surrounding water, however generated, probably results in some in-band contamination in the geophone time series which cannot be removed. For example, a large spike of unknown origin was recorded on float 6's horizontal axes at the beginning of record 845 (20:05, 30 August) in Figures XI.12a,b. This arrival appears to have induced float rocking (re [16] for a calculation of the amount of float rocking due to an acoustic arrival of a given intensity) which could then result in antenna oscillation. Also, float 6's 8 kHz ping appeared to have caused antenna oscillation on the x axis in record 1186 (Figure XI.23a).

e) Tether Contamination

Contamination by the tether can be seen in most of the bottom-mounted Swallow float time series. Float 9's x axis (and to a lesser extent, the y axis) in record 900-911 (Figure XI.15a) show a 0.5 to 0.6 Hz oscillation due to float rocking driven by the tether and the prevailing ocean current. The tether-driven oscillations in float 7's and 8's data (Figures XI.26 and XI.27), on the other hand, occur at about 1.25 Hz and 1.5 Hz, respectively. These frequencies, as well as these variations in the frequency, of bottom-mounted float rocking have been seen in other deployments in which the bottom tethers were of different length [1,2]. The dynamics of bottom-mounted float rocking therefore appear to be independent of tether length (re [16] for a discussion of bottom-mounted float rocking). In addition, the amount of bottom-mounted float data in this experiment which is reasonably free of tether contamination is about the same as in previous experiments [1,2,3]. Therefore, the increase in the tether length to 18 meters in this experiment appears to have had little effect on the quality of the bottom-mounted floats' geophone data.

f) Sproul Generated Signals

Starting at 02:05, 31 August, the Sproul began a series of maneuvers (Section IIa and III) in order to use the ship-generated sound in future beamforming efforts. This sound is clearly recorded by float 10, especially on the z geophone axis, in records 1320 through 1325 (in Figures XI.47). It is difficult to identify the Sproul signal in the deeper Swallow floats' time series during this time (Figures XI.48 through XI.55). Power spectral estimates calculated from these data are presented in the next section.

g) Other Unknown Signals in the Time Series

Spikes of unknown origin appear intermittently in some of the Swallow floats' time series. Float 10's x geophone axis (Figure XI.16a) recorded a spike about 33 seconds into record 1176, one a few seconds after the beginning of record 1177, and another one about 16 seconds into record 1177. Float 3 appears to have heard this latter arrival on its y axis (Figure XI.17b), but it also recorded an arrival on all three geophone components about 16 seconds into record 1179. Additional spikes were heard by float 3, predominantly on its y geophone component, in records 1272 and 1278 (Figure XI.30b), 1283 and 1289 (Figure XI.39b), and 1320, 1323, 1327, and 1328 (Figure XI.48b). Most of these spikes recorded by float 3 were not heard by the other floats, nor by float 3's hydrophone. On the other hand, float 11's y geophone axis also recorded spikes, mostly between records 1283 and 1289 (Figure XI.46b), which were also heard by float 11's hydrophone (Figure XI.46d). Further investigation into the source of the spikes in float 3's geophone time series is warranted in order to determine whether they were caused by a geophone circuit glitch.

An unusual and predominant arrival, starting 20 to 25 seconds into record 1282 (01:33, 31 August), occurs in all the midwater floats' time series (Figures XI.38 through XI.46). It is most strongly recorded on the horizontal geophone components and it has an appearance unlike the arrivals from the unknown source(s). Another arrival in record 1179 (100:15, 31 August) has the same characteristics as the one in 1282.

h) Geophone Time Series Recorded on the Sproul's Deck

Figures XI.1a through 1c show the geophone time series recorded by float 2 while it was still on board the Sproul. These time series were plotted in order to determine why float 2's y axis RMS power levels were anomalously low prior to deployment (re Figure X.6a). The x axis time series show packets of clipped energy, each two to four seconds in duration, separated by a second or two of signal with relatively low amplitude. This pattern is probably a result of the rocking of the ship under the influence of ocean surface waves. The signal is low in amplitude when the geophone coil pendulum is resting against its stop, this

occurs twice in each surface wave period, and the signal is clipped when the coil pendulum is freely oscillating. The ship rocking period is therefore around 10 seconds, a typical period for ocean surface waves. The z geophone axis time series show a similar pattern, although this component's pendulum apparently spent less time resting against its stop. However, the y axis time series is uniformly low in amplitude. Since its appearance is similar to the low-amplitude portion of the x axis time series, its pendulum was probably either stuck or resting against its stop during the whole pre-deployment period.

The geophone time series in these figures appear to be harmonic in nature. (This also holds true for the other floats' time series at this time). A power spectral estimate indicates that almost all of the energy occurs at 20 Hz. This is probably the characteristic frequency of vibration of the ship's deck; the ship's generator operates at 1200 rpm (or 20 Hz) and 20 Hz is the largest subharmonic of 60 Hz in the Swallow float frequency band. The possibility of a 20 Hz signal intrinsic to the floats geophone circuit, although unlikely, has not yet been completely eliminated.

XII. Velocity and Acoustic Pressure Power Spectra

The *calibrated* power spectral estimates from data collected by each geophone and hydrophone component during selected periods of time are presented in Figures XII.1 through XII.80. The spectral estimates were made by dividing a 40.96-second piece of data, gotten from the 44 seconds of data in each record after skipping the first three seconds in order to reduce tape recorder contamination, into seven 512-point segments (each segment is 10.24 seconds long) with a 50 % overlap between segments. The segments were Fourier transformed after being windowed with a Kaiser-Bessel window of $\alpha = 2.5$. The seven spectra were then incoherently averaged in order to reduce the variance of the power spectral estimates; the resulting 90 % confidence limits are + 3.3 dB to -2.3 dB. The power spectra were also properly normalized (re Appendix 1) to give the power in units of dB re 1 $(m/sec)^2/Hz$ for the geophone components and dB re 1 $(\mu Pa)^2/Hz$ for the hydrophone component. (However, refer to part b of Appendix 1 for a discussion of the corrections to these calibrated spectral estimates).

The time periods selected for calculating the spectral estimates are;

Times of Swallow Float Spectral Estimates

Record Number	Local Time (Date)	Floats	Comments	Figure Numbers
41	10:02 (30 Aug)	10 and 2	Floats were setting on the Sproul's deck.	XII.1 - XII.2
590 - 621	16:54 - 17:17 (30 Aug)	11	Float 11's AGC level was at its peak and changing rapidly.	XII.3 - XII.34
840	20:01 (30 Aug)	all midwater floats	Sproul was about 12 km to the southwest from the array.	XII.36 - XII.44
900	20:46 (30 Aug)	9	Contaminating arrival of the first type is present on 9's z axis.	XII.45
901	20:47 (30 Aug)	9	Contaminating arrival of the second type is present on 9's z axis.	XII.46
908	20:52 (30 Aug)	9	Contaminating noise is apparently not present.	XII.47
1182	00:18 (31 Aug)	all midwater floats	AGC levels for the midwater floats were high.	XII.48 - XII.56
1240	01:01 (31 Aug)	11 and bottom float 9	Bottom float 9's AGC level was very high.	XII.60 - XII.61
1272	01:25 (31 Aug)	all midwater floats	The floodlight bulb imploded.	XII.62 - XII.70
1320	02:01 (31 Aug)	all midwater floats	Start of leg 1 of Sproul maneuvers.	XII.71 - XII.79

The figures in this section are placed in chronological order, and in order of increasing depth of the floats. Note that plots of spectral differences, including Figures XII.35, XII.57 through XII.59, and XII.80 as well

as others, are embedded with the spectral estimate plots. Also note that Figures XII.81 and XII.82, which are also not listed in the table above, are plots of spectral estimates from data taken during the September, 1987 experiment [3].

a) Comparison of Hydrophone and Geophone Pressure Spectra

The installation of the VLF hydrophones on some of the Swallow floats allows for the comparison of the pressure spectra derived from the velocity data collected by the geophones with the pressure spectra estimated from the hydrophone data. The geophone and hydrophone spectral estimates are completely independent of one another and are based upon data collected at the same time and the same place (that is, almost the same place; the VLF hydrophone and the geophone on a float are separated by about a half meter). The procedure used in deriving the pressure spectral estimates from the geophone velocity data is based upon an acoustic plane wave assumption [14]. Ramifications of this assumption are discussed in [15].

In those figures for floats equipped with a VLF hydrophone, floats 10, 3, 5, and 11, the *derived* pressure spectral estimate from the geophone data are plotted with the hydrophone pressure spectral estimate in the uppermost plot. Immediately following most of these figures is a figure showing the spectral difference between the hydrophone pressure spectrum and the geophone pressure spectrum. Spectral differences greater than zero indicate that the derived geophone spectral levels are greater than the hydrophone levels; negative spectral differences indicate that the hydrophone levels are greater. In this part of the section, the order in which the geophone and hydrophone spectral estimates are compared are from the shallowest float to the deepest float, i.e. 10, 3, 5, 11.

The pressure spectral difference from float 10's data written before the float was deployed (Figure XII.1b) shows a much greater spectral level (an average of about 10 dB above 1 Hz) was heard on the geophone than on the hydrophone. This was probably due mostly to the large amount of clipping of the geophone time series, although non-acoustic vibrations of the Sproul's deck may also contribute to the differences.

The spectral differences between the two pressure spectra for float 10 after the float was deployed, Figures XII.36b, XII.48b, XII.62b, and XII.71b, show that the geophone pressure spectral levels are almost always greater than the hydrophone levels. This is not due to excess clipping on the geophone channels; in general, the hydrophone channel contains a greater number of clipped samples because of its greater receiving sensitivity. The geophone levels are offset by about 3.5 dB from the hydrophone spectra above 2.5 Hz. Near 1.5 Hz, the geophone levels differ from the hydrophone levels by about 8 dB. The large 30 dB spike at 0.22 Hz occurs at the frequency at which the float rocks (re [16] for a comparison between a theoretical calculation and a measurement of the frequency of float rocking); float rocking is recorded on the geophones, but not the hydrophones.

Float 3's differences in pressure spectral estimates are plotted in Figures XII.37b, XII.49b, XII.63b, and XII.72b. The differences again are almost always positive (indicating that the geophone pressure spectral levels are greater than the hydrophone levels); they are about zero near the upper limit of the frequency band, but show a steadily increasing difference, about a quarter dB per Hz, with decreasing frequency, to a lower limit of 2.5 Hz. Below 2 Hz, float rotational resonances, the motion of the ballast at 1.3 Hz [16] and the float rocking at 0.36 Hz, dominate the geophone spectral levels. The rocking of float 3, recorded predominantly on the x component of the geophone (re float 3's time series in the previous section), is especially strong, often exceeding 40 dB above the noise heard by the hydrophone. The large differences seen in record 1320 (Figure XII.72b) are due to the spikes of unknown origin in this float's geophone time series (re Section XI.g and Figures XI.48).

The pressure spectral difference plots for float 5, Figures XII.38b, XII.50b, XII.64b, and XII.73b, are quite similar to the plots of float 10's differences and the comments pertaining to those figures hold here. One aspect of note of float 5's spectral differences is that the difference peak due to float rocking varies by over 10 dB in amplitude in these four plots (and it has been observed to vary by over 20 dB in comparison with some plots not presented here). The cause of the variation in the difference peak amplitude appears to be mostly a result of variations in float 5's hydrophone spectra and not due to variations in the amplitude of the rocking peak in the geophone spectra. It may be due to variations in the amount of clipping in the

hydrophone time series.

The pressure spectral levels reported by float 11's geophone and hydrophone agree quite closely across the whole frequency band above 0.75 Hz during records 1182 and 1240 (Figures XII.56b and XII.70b) and for many of the records in the 590-to-621-record sequence (Figures XII.3 through XII.34). Below 0.75 Hz, the float rocking resonance again dominates the geophone spectrum. Curiously, a secondary peak at 0.1 Hz occurs in addition to the rocking peak at 0.38 Hz. The spectral difference peak at 0.1 Hz is a result of a "plateau" in the calibrated pressure spectrum measured by the VLF hydrophone concurrent with a continued increase in spectral levels with decreasing frequency measured by the geophone. The plateau in the hydrophone spectrum is possibly due to the decrease in ambient ocean noise spectral levels below the microseismic peak at 0.14 Hz; the geophone may be unable to detect the decrease below the microseismic peak because of the float rocking resonance.

In records 840, 1272, and 1320, float 11's hydrophone spectral levels are *higher* (negative difference values) than the geophone levels at some frequencies. A broad "trough" centered around 5 Hz and a sharp "valley" at 3.0 Hz are typical features of Figures XII.44b, 70b, and 79b. Examination of float 11's time series in Section XI shows that these features of the spectral difference plots are directly relatable to the amount of clipping of the hydrophone time series (recall that the fixed gains in the geophone and hydrophone circuits were set so that the hydrophone component would dictate the AGC level). The power spectral estimate is distorted (power is smeared across the spectrum and false spectral peaks can arise) when significant clipping occurs. The sharp spectral difference peaks in Figure XII.79b at 17.2 Hz and 21.5 Hz are as yet unexplained.

Non-zero differences between the hydrophone and geophone pressure spectra can also arise because of the 8 kHz localization ping. Float 11's spectral plots for record 596 (in Figure XII.9) indicate that the difference between the two pressure spectra are due to the z geophone component spectrum. Recall (from Section XI) that it was in this record that both a localization ping and a range ping were issued by float 11. The difference in the two pressure spectral curves is therefore due to the difference in the response to large signals of the two sensors' electronic circuits.

In summary, the pressure spectral levels derived from geophone particle velocity data in general agree with those calculated directly from hydrophone data. Differences between levels can usually be explained by clipping on either the hydrophone channel or one of the geophone channels, by the difference in the way the sensors' electronic circuits respond to large signals (e.g. the 8 kHz localization ping), or by the known, non-acoustic, float rotational resonances which contaminate the geophone data. Positive spectral differences across the whole frequency band *may* be a result of a violation of the plane wave assumption used in deriving the geophone pressure spectra; the derived geophone pressure spectral estimate is actually an *upper bound* on the true pressure power spectrum [15]. Note that the spectral difference correction curve, shown in Figure A1.8 and discussed in Appendix 1, part b, accounts for some of the difference seen in the plots below a few Hz; above 5 Hz, the correction is only about 0.8 dB.

b) Contaminating Noise

The contamination from the unknown source(s), discussed in Sections X.b, X.c, and XI.b, has a power spectrum which varies from one record to the next. This variability can be seen by examining the 32-record sequence of spectra calculated from data recorded by float 11 in records 590 through 621. The "lump" of energy between 15 and 20 Hz, which is the main spectral feature associated with the contaminating noise, can have an appearance which varies from a sharp, peaky structure (re Figure XII.32) to a broad, bumpy plateau (re Figure XII.26). The bumpiness in the spectra can extend to frequencies above 20 Hz (re Figure XII.27). The energy is typically centered about 18 Hz and can be as much as 35 dB above the background levels in these records (and as much as 40 dB in other records).

Most of the record-to-record spectral variability can probably be explained by the varying percentages that each of the two characteristic types of arrivals from the contaminating source (Section XI.b) contribute to each record, including the degree of clipping that the arrivals cause. The power spectrum of a record containing mostly the first characteristic type of arrival, which is a sequence of 20 to 25 pulses separated by about 0.7 seconds, is shown in Figure XII.45. This record was written when the

contaminating source was very clearly recorded on bottom-mounted float 9's vertical geophone axis. The main features of the spectra are peaks on the horizontal axes at 7.3, 8.1, and 8.9 Hz, and multiple lumps of energy above 15 Hz, starting at about 17.2 Hz. These lumps are separated by about 1.4 Hz. Local maxima also occur at roughly 1.4 Hz intervals below 15 Hz in the z axis spectrum. The multiple lumps in the spectrum are due to the pulse-like structure of the time series with the 1.4 Hz interval corresponding to the 0.7-second pulse separation.

The following figure, Figure XII.46, shows the power spectrum of a record which is dominated by the second characteristic type of arrival from the unknown source(s). In this figure, the 7.3 Hz peak is a striking feature of all three geophone component spectra, especially the y axis. The lump of energy between 15 and 20 Hz is now a much sharper, peakier structure, centered at 18.1 Hz. The 8.1 Hz peak is also present on the x axis spectrum. Additional secondary peaks occur at 14.8 Hz and 19.9 Hz (both these peaks also appear in the spectra in Figure XII.45). The unusual shape of the z axis spectral curve around 3 Hz is probably a result of the significant clipping of the time series in this record.

Presented in Figure XII.47 is the component spectra from float 9's data in record 908 when no unknown source(s) arrivals were predominant. The horizontal axes spectra are almost identical to those in record 901, except for a 10 dB decrease in the 7.3 Hz power level on the y axis. However, the vertical axis spectrum is quite different form that in record 901; the hump around 3 Hz has disappeared and the lump at 18 Hz has decreased in level by almost 20 dB. The peak at 8.1 Hz is now more apparent on the z axis, but this is because the background level has decreased by about 10 dB. The 8.1 Hz peak is, therefore, seemingly unaffected by the decrease in the unknown source arrival levels.

Both the 7.3 Hz and 8.1 Hz peaks also appear in float 11's spectra for records 590 through 621. The 7.3 Hz peak occurs mainly on the horizontal geophone axes' spectra as in float 9's spectra for record 900, but the 8.1 Hz peak now appears predominantly on the vertical axis. An additional peak in the horizontal spectra at 14.1 Hz also appears and a lump of energy centered at 11.8 Hz is present on the vertical geophone axis in many of the spectra. Since these peaks are predominant on different geophone axes, this suggests that more than one source is contributing to the power levels during this time. It is uncertain at present whether these peaks are caused by the same source(s) as that of the lump of energy at 18 Hz. The 7.3 Hz peak appears in the midwater float spectra from record 840 (Figures XII.36 through XII.44); there, it appears mainly on the vertical geophone axis of floats deployed shallower than 1500 meters. It does not stand out (or is not present) in spectra from records 1182, 1240, 1272, or 1320. The peak at 8.1 Hz occurs regularly in all the geophone components' spectra from records 840, 1182, and 1240. The 14.1 Hz peak appears infrequently in other spectra, e.g. float 11's spectra for record 1182 (Figure XII.56a) and floats 10, 3, 5, 0, and 1 in record 1320.

The effect of the unknown contaminating source(s) arrivals on the *background* power spectral levels can be determined by comparing this experiment's spectra with those from previous experiments. Figures XII.57 through XII.59 are plots of the difference in spectra of data collected in the May, 1987 experiment [2] and data collected in this experiment. Both experiments were conducted at the same site and the environmental conditions were similar. The comparison was made for those midwater floats which operated properly in both deployments. Note that float 4 in the May, 1987 experiment was renumbered as float 10 in this experiment. The times chosen for comparison, record 1520 (04:56, 6 May) and record 1182 (00:18, 31 August) were times when the AGC levels of the floats were relatively high. The background pressure spectral levels above 5 Hz for record 1182 are about 70 to 75 dB re 1 $\mu Pa^2/Hz$, except for float 11's spectra in which the background levels are about 65 dB (re Figures XII.48 through XII.56). The pressure spectral differences in the uppermost panel of the figures are the differences in the derived geophone pressure spectra since no floats were equipped with VLF hydrophones in the 1987 deployments. Although the floats were deployed at different depths, 1590 meters for float 4 in May versus 425 meters for float 10 in this experiment, 1700 meters versus about 550 meters for float 3, and 1800 meters versus 975 meters for float 2, the spectral levels are quite similar below 15 Hz. (Note that the float 2 comparison in Figure XII.59 is distorted due to the 8 kHz ping arrival in record 1182. The exception is the 28 dB difference peak at 11.7 Hz on the vertical component comparison. A peak, or lump, at 11.7 Hz is a feature of the spectra for record 1182, as well as almost all the other spectra presented in this section. The notable exception is in record 840, where a peak at 12.3 Hz occurs on the horizontal geophone components. Above 15 Hz, the lump of energy due to the contaminating source(s) dominates. This is especially true on the z axis where

the difference reaches a maximum of 40 dB at 18.1 Hz. (Note that the strong rocking seen on the x axis of float 3 in Section XI was not present in the May, 1987 experiment; re the 20 dB peak at 0.3 Hz in the x axis difference plot. The installation of the VLF hydrophone must have changed the float rocking characteristics).

In summary, the contaminating arrivals from the unknown source(s) appears to significantly affect the background spectral levels only above 15 Hz, except when it causes clipping. Its effect is variable due to the different types of arrivals from the source(s). Below 15 Hz, peaks occur in the spectra, e.g. at 7.3, 8.1, and 11.7 Hz which may or may not be associated with the contamination.

c) Sproul-Generated Noise

The data written during record 1320 were taken at the beginning of the Sproul maneuvers for beamforming purposes, as the ship departed the array area (Section IIa). Ship-generated noise are clearly visible in float 10's (the shallowest float) time series, as discussed in Section XIf. Figures XII.71 through XII.79 present the calibrated component spectra for all midwater floats at this time. In addition, Figure XII.80 shows the difference in spectra for data recorded during this time and data recorded while the Sproul was about 12 km from the array. The most remarkable feature of these spectra is the peak at 20.3 Hz. It stands out on the z axis spectra, although this is mostly a result of the higher background noise levels on the horizontal axes. Evidence that this peak is generated by the Sproul can be gotten by looking at the spectra from data recorded while the floats were on the Sproul's deck. Figures XII.1 and XII.2 show the spectra during record 41 (10:02, 30 August). These two floats' data were chosen for analysis since float 10's VLF hydrophone RMS power (Figure X.1a) and float 2's y axis geophone RMS power (Figure X.6a) appeared anomalously low in the period after synchronization and before deployment. Again, the predominant feature of the spectra is the peak at 20.3 Hz. In addition, spectral measurements using the Clevite hydrophone and a Hewlett-Packard spectrum analyzer indicated a spectral peak at 20 Hz at ship speeds of 0.5 knots and less (Section IIb). The 20 Hz peak may not have been visible in these measurements above 0.5 knots because of contamination by flow noise. This peak is believed to be due to the ship's generator which rotates at 1200 rpm.

A final piece of evidence supporting the Sproul generation of the 20 Hz line can be obtained by examining two spectra recorded by float 2 in the September, 1987 experiment, a deployment in which the Sproul was also used [3]. Figures XII.81 and XII.82 show float 2's spectra estimated from data in two blocks of data, records 1100 - 1119 and records 1190 - 1209. In calculating these spectra, 2048-point FFTs (40.96 seconds) were calculated from each record's data, after skipping the first three seconds, resulting in greater frequency resolution than in the 512-point FFTs. In order to stabilize the spectral estimates, twenty such FFTs from twenty sequential records were then incoherently averaged. During record 1100 (07:40, 18 September), the Sproul was about 16 km from the float and steaming at about 7 knots towards the array; during record 1190 (08:48, 18 September), it was about 2 km away. A 20 Hz peak is prominent on the vertical axis spectrum for records 1190 - 1209 (the float was deployed at 1000 meters) and is not present in the spectra during records 1100 - 1119.

A small peak also appears near 14 Hz in record 1320's spectra. This *may* be associated with the Sproul; it also appears in float 11's spectra for records 590 through 621 and record 1182, but does not seem to occur in any of the other spectra.

Acknowledgements

We would like to thank Marvin Darling and Chris Nickles, other members of MPL's Swallow float team, for their numerous and various contributions to the project. We would also like to thank Jim McEachern and Mary Beth Dormuth of the Naval Air Development Center for providing the sonobuoy instrumentation and expertise and Joe Rice of the Naval Oceans Systems Center for providing the PAEL buoys. The crew of the R/V R. G. Sproul was very helpful and patient.

This work was supported by the Office of Naval Research under contract #N00014-87C-0127.

References

[1] G. L. D'Spain, R. L. Culver, W. S. Hodgkiss, and G. L. Edmonds, "Freely drifting Swallow float array: April, 1987 trip report" MPL Tech. Mem. 397, Marine Physical Laboratory, Scripps Institution of Oceanography, San Diego, CA (1987).

[2] G. L. D'Spain, R. L. Culver, W. S. Hodgkiss, and G. L. Edmonds, "Freely drifting Swallow float array: May, 1987 trip report" MPL Tech. Mem. 402, Marine Physical Laboratory, Scripps Institution of Oceanography, San Diego, CA (1988).

[3] G. L. D'Spain, W. S. Hodgkiss, and G. L. Edmonds, "Freely drifting Swallow float array: September, 1987 trip report" Marine Physical Laboratory, Scripps Institution of Oceanography, San Diego, CA (in preparation).

[4] R. L. Culver, W. S. Hodgkiss, G. L. Edmonds, and V. C. Anderson, "Freely drifting Swallow float array: September, 1986 trip report" MPL Tech. Mem. 391, Marine Physical Laboratory, Scripps Institution of Oceanography, San Diego, CA (1987).

[5] J. Rice, "STRAP data collection quick-look report" NOSC memorandum Ser 541/24-85, Naval Ocean Systems Center, San Diego, CA (1985).

[6] J. Churgin and S. J. Halminski, Temperature, Salinity, Oxygen, and Phosphate in Waters off the United States, Eastern North Pacific, National Oceanographic Data Center, 3, (1974).

[7] K. V. Mackenzie, "Nine-term equation for sound speed in the oceans" J. Acoust. Soc. Am., 70 (3), (1981).

[8] "Naval Air Development Center event A test plan" Naval Air Development Center, Warminster, PA 18974-5000, (1988).

[9] R. L. Culver, G. L. D'Spain, W. S. Hodgkiss, and G. L. Edmonds, "Estimating 8 kHz pulse travel times and travel time errors from Swallow float localization system measurements" Marine Physical Laboratory, Scripps Institution of Oceanography, San Diego, CA (in preparation).

[10] G. L. D'Spain and W. S. Hodgkiss, "Comparison of Swallow float, ocean bottom seismometer, and sonobuoy data in the VLF band" Marine Physical Laboratory, Scripps Institution of Oceanography, San Diego, CA (1988).

[11] G. L. D'Spain, "Resonant response of the Swallow float glass sphere" Marine Physical Laboratory, Scripps Institution of Oceanography, San Diego, CA (unpublished notes).

[12] R. L. Culver and G. L. Edmonds, "February, 1987 one-day Swallow float sea trip" Marine Physical Laboratory, Scripps Institution of Oceanography, San Diego, CA (unpublished memorandum).

[13] R. Urick, Principles of Underwater Sound, 3rd ed., McGraw-Hill, (1983).

[14] R. L. Culver, "Infrasonic ambient ocean noise spectra from freely drifting sensors" SIO Ref. 85-22, Marine Physical Laboratory, Scripps Institution of Oceanography, San Diego, CA (1985).

[15] G. L. D'Spain, "The calculation of acoustic pressure spectra from particle velocity spectra revisited" Marine Physical Laboratory, Scripps Institution of Oceanography, San Diego, CA (unpublished notes).

[16] G. L. D'Spain, "Swallow float rocking due to vertical asymmetry" Marine Physical Laboratory, Scripps Institution of Oceanography, San Diego, CA (in preparation).

[17] R. L. Culver, W. S. Hodgkiss, G. L. Edmonds, and V. C. Anderson, "Removing resonant oscillation signals from Swallow float data" MPL Tech. Mem. 395, Marine Physical Laboratory, Scripps Institution of Oceanography, San Diego, CA (1987).

[18] M. Pieuchot, Seismic Instrumentation, vol. 2, from Handbook of Geophysical Exploration, Section I - Seismic Exploration, ed. K. Helbig and S. Treitel, Geophysical Press (1982).

[19] R. Urick, Ambient Noise in the Sea, Peninsula Publ. (1984).

[20] A. B. Williams, Electronic Filter Design Handbook, McGraw-Hill (1981).

[21] A. Antoniou, Digital Filters: Analysis and Design, McGraw-Hill (1979).

[22] E. S. Maloney, Dutton's Navigation and Piloting, Naval Institute Press, 13th ed., (1978).

Appendix 1 - Swallow Float VLF Data Acquisition System

a) System Response

A block diagram of the Swallow float very low frequency (VLF) system appears in Figure A1.1. Only four of the floats, floats 10, 3, 5, and 11, were equipped with Ocean and Atmospheric Science (OAS) model E-4SD hydrophones in addition to the three-component Geo Space geophones installed in all the floats. The geophone channels will be described first, followed by a description of the hydrophone channel.

The water particle motion (and float rocking) is first coupled into motion at the geophone. The particle velocity at the geophone is then converted into voltages representing the three orthogonal components of particle velocity. The geophones are electromagnetic transducers in which a voltage is produced across a moving, conducting coil by its motion through the magnetic field lines produced by a permanent magnet [18]. The resulting voltage is proportional to the velocity of the coil with respect to the magnet. Constraining the coil to move in only one direction are elastic springs connecting the coil to the instrument casing. (Laboratory tests have determined that the geophones can withstand a maximum tilt from vertical of about 15°). The geophone package in each Swallow float is composed of three such transducers oriented to measure in three orthogonal directions.

The geophone amplitude and phase response was calculated using the theoretical equation of motion for this system [18]. (The amplitude response curve is nearly identical to the manufacturer's calibration curve provided with the geophones). Near-critical damping of the coil is achieved using a 60 kΩ shunt resistor. Note that the f^2 roll-off of the geophone amplitude response below the natural frequency of 8 Hz effectively pre-whitens the ocean ambient noise so that no additional pre-whitening needs to be implemented.

The three signals next undergo a fixed gain of 95 dB before being input to the automatic gain control (AGC). Included in the geophone channel circuitry are nine RC circuits. Five of these RC circuits act as high pass filters, with poles located at 0.000034, 0.034, 0.07, 0.26, and 0.47 Hz, in order to eliminate DC bias and decrease ultra-low frequency self noise. The other four RC circuits act as low pass filters, with poles at 34, 34, 72, and 337 Hz, in order to eliminate AC coupling noise (i.e. "cross-talk"). These RC circuits are lumped together with the geophone channel "fixed gain" in Figure A1.1.

The water-borne pressure fluctuations (acoustic and non-acoustic) are converted into voltage fluctuations by the sensing material in the hydrophone. The sensing material is electrostrictive; that is, it develops a voltage in response to an implied stress [13]. (From laboratory tests, it has been determined that the sensing material is also pyroelectric, i.e. it generates a voltage in response to a change in temperature). The electrostrictive material in the OAS hydrophones is pre-polarized lead zirconate-titanate, a polycrystalline ceramic. The hydrophone has a sensitivity of -182 dB re 1 V/μPa and a frequency response which is flat (within ±1 dB) from 0 to 5 kHz. Because the ocean ambient noise spectrum increases as f^{-4} below about 5 Hz [19], the pressure-induced voltage output by the hydrophone is then passed through a pre-whitening filter. This high-pass filter is comprised of two RC circuits in cascade, both with corner frequencies of about 8 Hz, the same as the natural frequency of the geophone components.

The "fixed gain" triangle for the VLF hydrophone channel in Figure A1.1 represents somewhat different circuitry than in the geophone channels. The fixed gain is set to 80 dB, rather than 95 dB, since the hydrophones are more sensitive than the geophones; -182 dB re 1 V/μPa for the hydrophones versus about -201 dB re 1 V/μPa above 8 Hz for the geophones. Also, since the hydrophone pre-whitening filter already includes two high pass RC circuits, only two additional high-pass circuits, with poles located at 0.034 and 0.47 Hz, needed to be added. An additional equivalent high-pass RC circuit is formed by the capacitance of the hydrophone itself and the resistance of two diodes; for the August, 1988 sea trip the resonant pole for this circuit was located at about 2.6 Hz. As discussed in the following paragraph, the hydrophone circuit has since been changed so that this equivalent RC pole is located at 0.2 Hz. These three high-pass RC circuits are included in the "fixed gain" triangle along with four low-pass circuits, with poles at 34, 34, 72, and 339 Hz.

Laboratory measurements made after the August, 1988 sea trip indicated that two silicon diodes, connected in parallel in the front end of the hydrophone system in order to protect the electronic components from large voltages, had finite equivalent resistances. The forward-biased diode had an equivalent resistance of about 22 MΩ and the reversed-biased diode had a resistance of 53 MΩ. These diodes, in series with the equivalent capacitance of 0.004 μf of the hydrophone itself, form an additional RC circuit with a resonant pole at about 2.6 Hz. The laboratory tests also determined that the resistance of the silicon diodes was temperature sensitive; in the forward-biased state, it changed from 12.5 MΩ at 22° C to 25 MΩ at 0° C. The hydrophone's equivalent capacitance was also found to be slightly temperature dependent; however, the change in capacitance partially offsets the change in diode resistance. The total effect was a change in resonant pole frequency of 10 %, from 2.66 Hz to 2.41 Hz, for a temperature change of 4.7° C over the equilibrium depths of float 10 (425 meters) and float 11 (3360 meters) in the August, 1988 experiment. Even though this change in resonant pole location resulted in slight differences in the total hydrophone system response, the diodes have since been removed and replaced by a temperature-stable Zener diode. This change eliminates the possibility of an extended loss in circuit amplification due to time it takes for the silicon diodes to discharge the circuit (as discussed in Section X). Also, a temperature-stable, metal film, 200 MΩ resistor was placed in series with the hydrophone in order to move the equivalent resonant pole location to 0.2 Hz.

The hydrophone component voltage and all three geophone component voltages are then sent to a automatic gain control (AGC) amplifier. The AGC is a variable gain amplifier with a range of 0 to 25 dB gain which allows the full dynamic range of the eight-bit A/D converter to be used. The AGC gain always changes by a 0.5 dB step between records; if more than 1 % of all data samples from the last 40 seconds of each record are clipped, then the AGC decreases by 0.5 dB. Otherwise, it increases. Plots of the AGC level for each float during every record are given in Section VII.

Before digitizing, the signals are passed through a five-pole, four-zero, elliptic, anti-aliasing filter. Elliptic filters theoretically have the sharpest transition region for a given number of poles and circuit complexity. The filter frequency response and the pole, zero locations in the *s* plane are shown in Figure A1.2 [20,21]. Incoming signals are amplified by a maximum of 4.6 dB in the passband, which has a 0.28 dB equal ripple. The cut-off frequency (the highest frequency at which the amplitude gain is equal to the minimum passband gain) is 20 Hz, and the attenuation is 19 5 dB at the Nyquist frequency of 25 Hz. The maximum equal ripple level in the stop band is 50.1 dB below the level in the pass band and is first reached at 31 Hz. Before installation in the floats, all filters were adjusted so that broadband noise input to the filters yielded the same amplitude response and same null location at the filters' output.

The geophone channel response, including all components in the system except the AGC gain (which varies over the time of the experiment) is plotted in Figure A1.3. The hydrophone channel response, including all components in the channel except the AGC gain, is plotted in Figure A1.4. In deriving the phase response in Figure A1.4, it was assumed that no phase shift was introduced by the hydrophone's electrostrictive material in the conversion of pressure to voltage.

The four (or three) signals are then digitized at a 50 Hz sampling rate and put into a temporary buffer. After 44 seconds of data (equal to one data record) have accumulated in the buffer, a one second period of writing the data to cassette tape takes place. During this time, no data is sampled. The 45 second cycle then repeats until the cassette tape is full. The cassette tape can store up to 17 Mbytes of unformatted data, which is sufficient space for up to 2100 three-component data records and 1600 four-component data records.

Both the RMS power plots discussed in Section X and the time series plots of Section XI have been corrected for the variable AGC level. No other adjustments have been made in these plots. The power spectral plots of Section XII, however, have been corrected for all electronic system gains including the geophone/hydrophone sensitivities and the anti-aliasing filter response and therefore report estimates of the approximate power level at the input to the sensors. However, the RC circuit responses have *not* been included in the calibration of either the geophone or the hydrophone spectra, for the reasons discussed in part b below.

Excellent agreement between the laboratory-measured and theoretically-predicted amplitude and phase responses of both the geophone and hydrophone channel circuitry, excluding the sensors themselves, has been obtained. Additional calibration measurements of the Swallow float VLF data acquisition system

are in progress.

b) Correction to the Swallow Float Calibrated Spectra

The nine RC circuits in the Swallow float geophone signal conditioning electronics had previously been assumed to have a negligible effect in the VLF band. However, the recent calibration measurements of the geophone system have shown that they actually have a significant effect at certain VLF frequencies. All previously reported Swallow float calibrated spectra, including those in references 1 through 4, 10, 12, and 14, have therefore under-estimated the power spectral levels. Figure A1.5 shows the amount to be added to the reported Swallow float geophone spectra in order to obtain the true calibrated spectral levels. The lower panel of Figure A1.7 shows these same data plotted on the same scale as the spectral plots in Section XII.

For the sake of comparison with previously reported spectra, the geophone spectra presented in this report were calibrated without taking into account the effect of the RC circuits. The hydrophone spectra were likewise uncorrected for the RC circuits' response, or for the diode-hydrophone equivalent RC response. Figure A1.6 shows the plot of the corrections to the hydrophone spectra to get the true calibrated spectra and the upper panel of Figure A1.7 shows these same data plotted on the same scale as the spectral plots in Section XII. Figure A1.8 plots the difference in the hydrophone and the geophone correction curves so that the spectral difference plots of Section XII can be properly interpreted.

c) Data Record Format

The installation of the VLF hydrophone required a change in the format of the data records. Shown in Figure A1.9 is the format of the geophone-only records. Each record is composed of 7646 bytes, 7120 bytes of which are VLF acoustic data (including resynchronization and checksum bytes). Figure A1.10 presents the new 9766-byte record format for the VLF-hydrophone equipped floats. Interleaved with the geophone data are the hydrophone data, resulting in 9240 bytes of VLF data in each record.

Appendix 2 - Loran-C Position Fixes

This short discussion is based upon the material on pp. 708-725 of [22].

Loran, or Long Range Navigation, is based upon the measurement of time differences between pulse radio emissions, with a carrier frequency of 100 kHz, issued from two or more transmitting stations. Loran-C is characterized by the use of multiple pulses, allowing a higher signal-to-noise ratio with the same power output at a transmitting station, and by the use of a phase matching procedure to refine the time-of-arrival estimates.

Position accuracy depends upon the variation in propagation conditions along the signal path and on the position of the ship with respect to the transmitting stations, as well as on the distance from the chain of stations. Therefore, an interval of accuracies, rather than a single value, is given. Our study site was about 400 km from the nearest station; this results in an accuracy interval of about 25-100 meters, or 0.01-0.06 minute.

Loran-C position fixes, however, can be expected to much more precise than accurate. The relative distances between a number of fixes made in the same general area are much more reliable than the absolute position of any one fix. This is because all the fixes are affected by the same propagation effects and station-receiver geometry.

Appendix 3 - Initial Results from a VLF-II Sonobuoy

The three figures in this appendix show the spectral characteristics of the sound field recorded by the VLF-II sonobuoy transmitting its data over radio frequency channel 14 (re Section I). The data were recorded during the early morning hours of 31 August. Note that the spectra are uncalibrated.

Figure A3.1 shows plots of the spectra for three different times. The times listed at the upper-left-hand corner of each plot contain an unknown offset so that only relative time can be determined; i.e., the three spectra were obtained from data taken in a 1½ minute interval. The range of the plots' horizontal axes is from 0 to 40 Hz, with a spacing of 4 Hz between the vertical dotted lines. The vertical axes' scale is from -10 to -90 dBV, and the horizontal dotted line separation is 10 dB. The interesting feature of these three plots is how the spectral characteristics of the loud unknown sound source(s) changed with time (see also Section XII.b). The uppermost plot shows a blob of noise power with a peak at about 17.8 Hz. Less than a half-minute later, the spectrum is dominated power spikes separated by 1.4 Hz, starting at almost 17 Hz and continuing up to 24 Hz. Almost a minute later, the spectrum, shown in the bottommost plot, has returned to approximately the form it had 1½ minutes earlier. However, the spectral structure of the noise power around 18 Hz is asymmetric with three peaks arising out of the broad background. In addition, power at 33.8 Hz appears. It does not appear to be harmonically related to the energy around 18 Hz in this spectrum.

Figure A3.2 shows the power spectra at two times separated by 1½ minutes. Again, only relative time can be obtained because of an unknown time offset. The vertical axes' scale is the same as in Figure A.1, but the horizontal axes' range is now from 0 to 100 Hz, with 10-Hz spacing between the tick marks. The uppermost spectrum shows a peak at 17.8 Hz, corresponding to the peak in the uppermost spectrum in Figure A3.1. In addition, a peak at 53.0 Hz is visible in this expanded frequency scale plot. The lower spectral plot in Figure A3.2 shows the power spikes with 1.4-Hz spacing starting at 16.9 Hz. Note that the 53-Hz peak is not present in this spectrum.

The final figure, Figure A3.3, shows two plots which are gray-scale plots of noise power versus frequency (on the horizontal axes) and time (on the vertical axes). The times listed on the vertical axes are Greenwich Mean Times; 7 hours are subtracted from these times to obtain local Pacific Daylight Times. The time span of the plots is about 5 minutes. The range of the frequency axis of the plot on the left is from 0 to 40 Hz with tick marks every 1 Hz; the range of the plot on the right is 0 to 80 Hz with tick marks every 2 Hz. The streak of power around 17 to 18 Hz due to the unknown sound source(s) is the dominant feature of both plots. The streak isn't of constant width in frequency with time, but rather broadens at a 45-to-50 second rate. The intermittent "fingering" of the spectra can be seen as intermittent vertical streaks at frequencies above 17 Hz. The blobs of power appearing near 18 Hz, 35 Hz and 54 Hz seem to have a frequency-sweep-like character, starting at a high frequency and decreasing to a lower frequency, over a 2-to-3 Hz band. These three frequencies, if not harmonically related, are very nearly so. The blobs of power around 54 Hz in the right-hand plot have a 20-to-25-second repetition rate. Streaks of power around 12 Hz and also around 4 Hz also appear. Some of this acoustic power may be associated with the Sproul since it was in the vicinity of the sonobuoy array conducting acoustic transmission tests during the time of these measurements (re Section III).

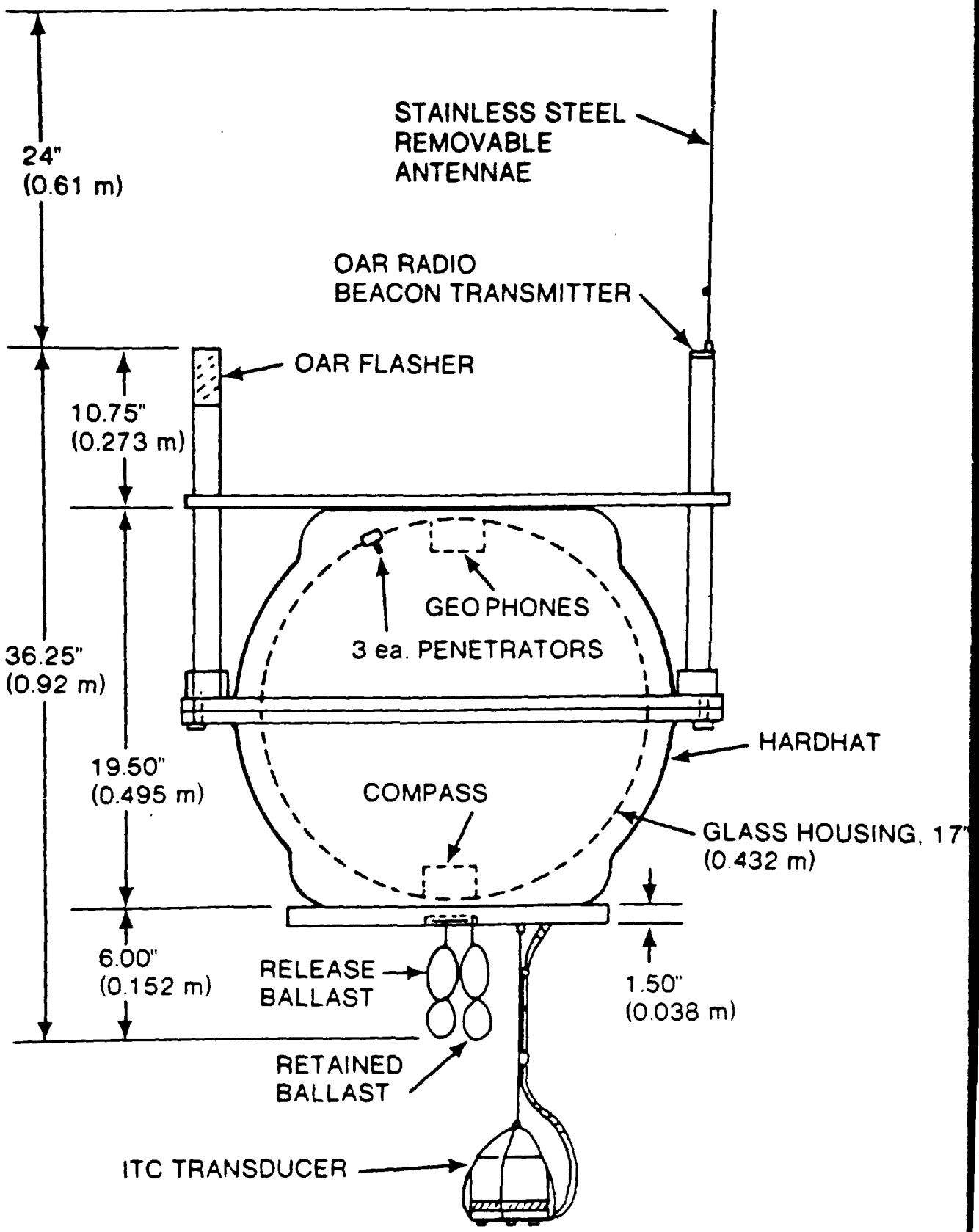

24"
(0.61 m)
STAINLESS STEEL
REMOVABLE
ANTENNAE
OAR RADIO
BEACON TRANSMITTER
OAR FLASHER
10.75"
(0.273 m)
GEO PHONES
3 ea. PENETRATORS
36.25"
(0.92 m)
HARDHAT
19.50"
(0.495 m)
COMPASS
GLASS HOUSING, 17"
(0.432 m)
6.00"
(0.152 m)
RELEASE
BALLAST
1.50"
(0.038 m)
RETAINED
BALLAST
ITC TRANSDUCER

Figure 1

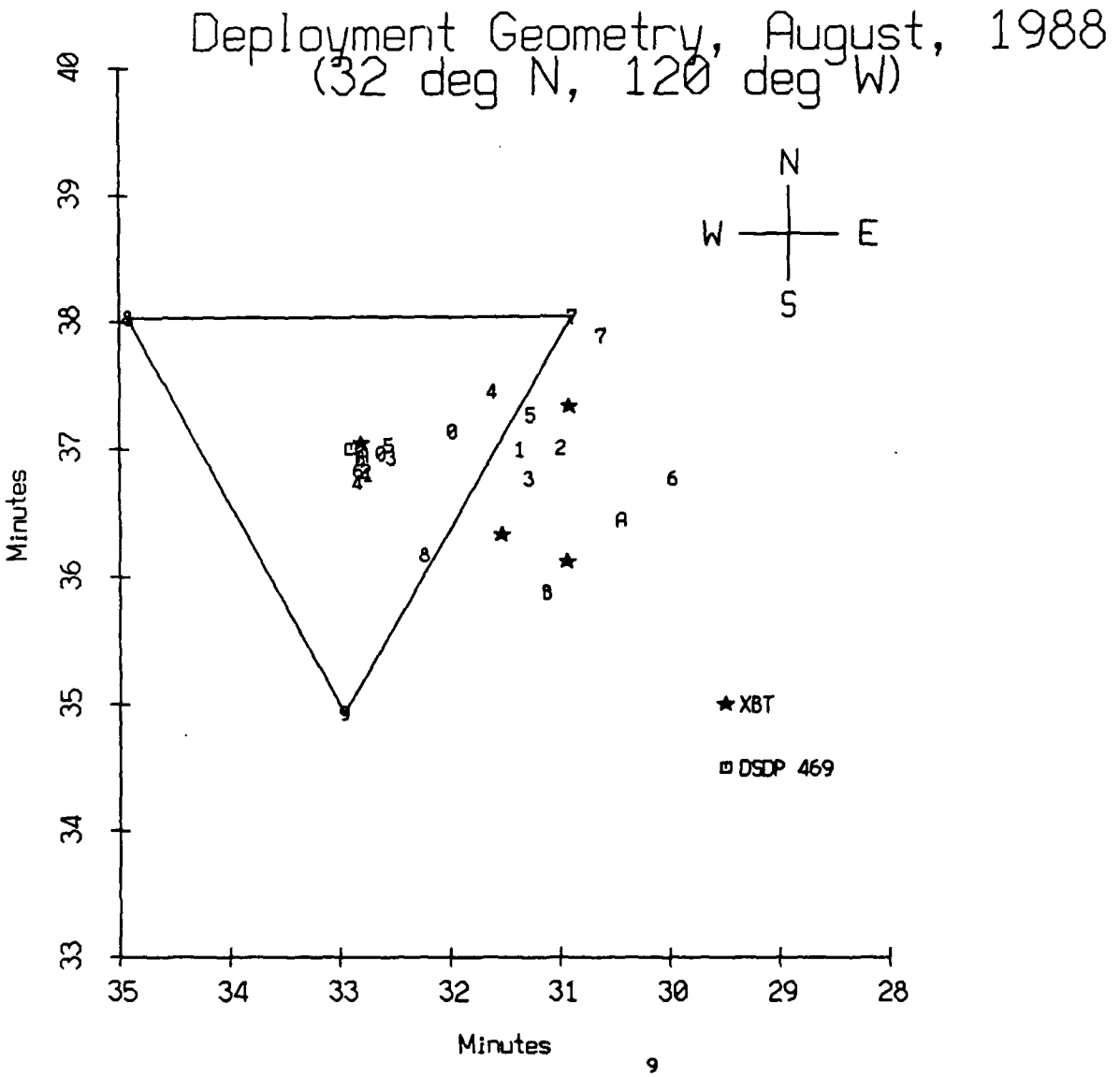

Deployment Geometry, August, 1988
(32 deg N, 120 deg W)
N
W
E
S
Minutes
40
39
38
37
36
35
34
33
35
34
33
32
31
30
29
28
Minutes
XBT
DSDP 469

Figure I.1

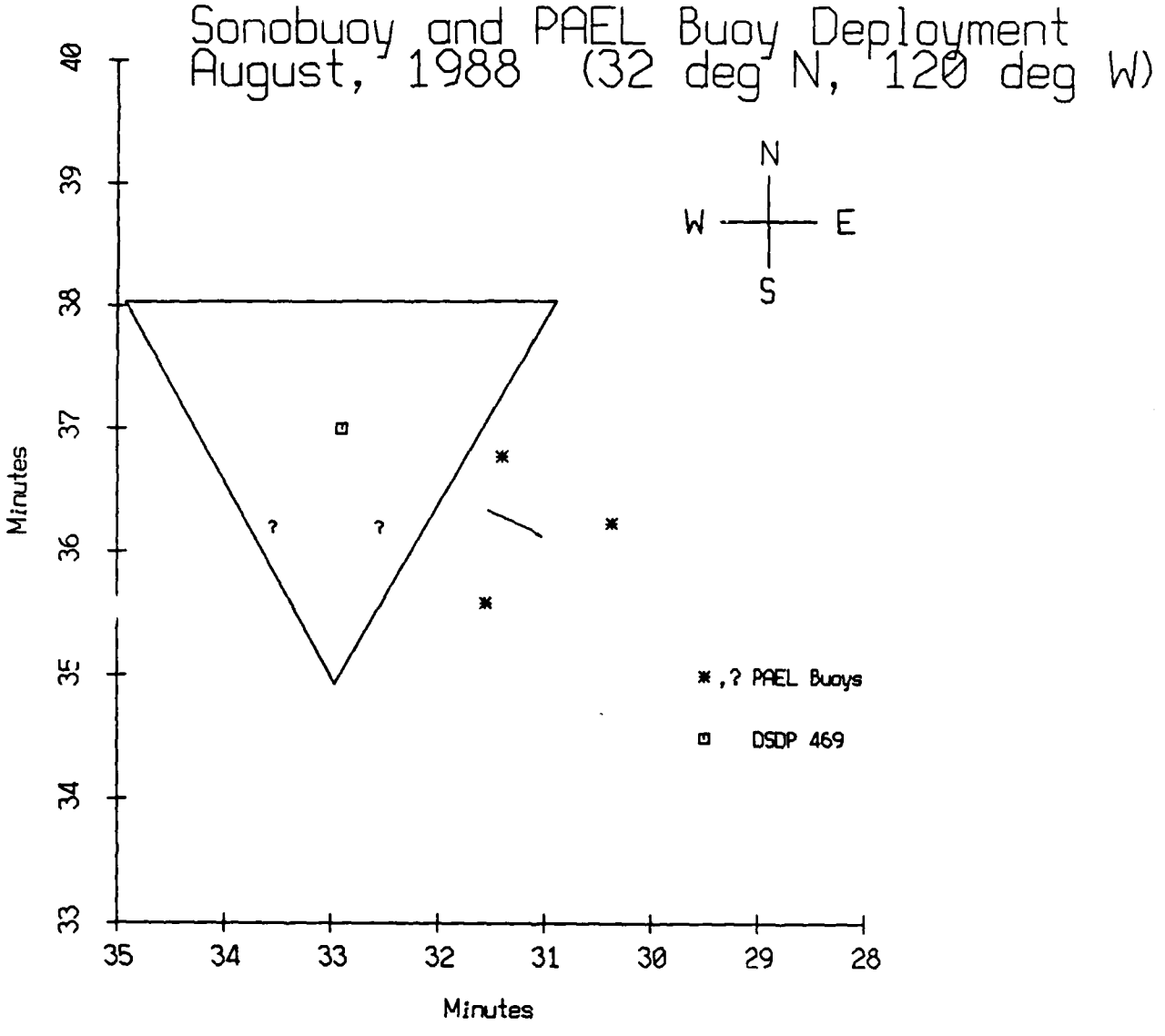

Sonobuoy and PAEL Buoy Deployment
August, 1988 (32 deg N, 120 deg W)
N
W
E
S
40
39
38
37
36
35
34
33
Minutes
35
34
33
32
31
30
29
28
Minutes
*,? PAEL Buoys
DSDP 469

Figure I.2

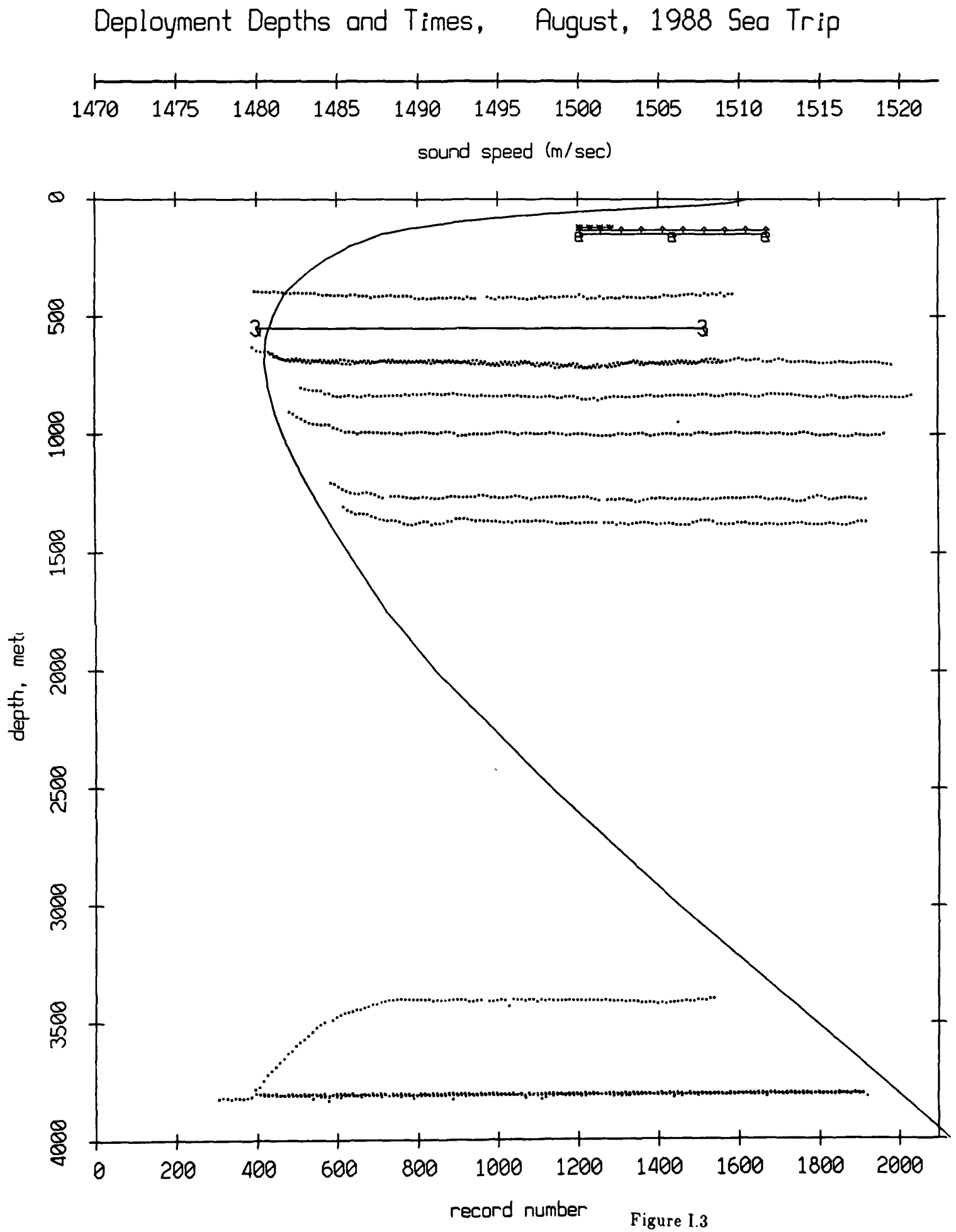

Deployment Depths and Times, August, 1988 Sea Trip
1470
1475
1480
1485
1490
1495
1500
1505
1510
1515
1520
sound speed (m/sec)
0
500
1000
1500
2000
2500
3000
3500
4000
depth, meti
0
200
400
600
800
1000
1200
1400
1600
1800
2000
record number

Figure I.3

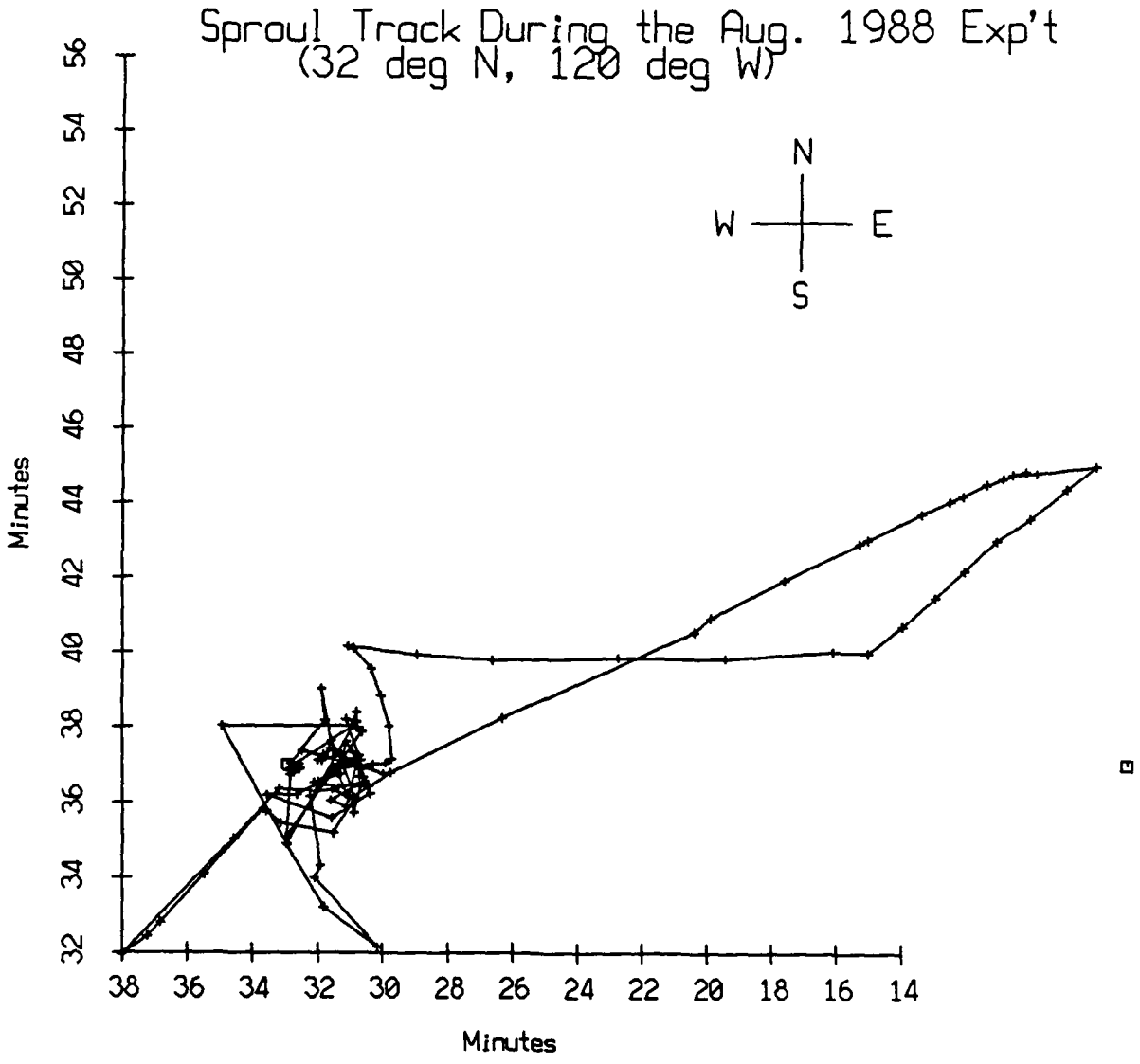

Sproul Track During the Aug. 1988 Exp't
(32 deg N, 120 deg W)
N
W
E
S
Minutes
56
54
52
50
48
46
44
42
40
38
36
34
32
38
36
34
32
30
28
26
24
22
20
18
16
14
Minutes

Figure II.1

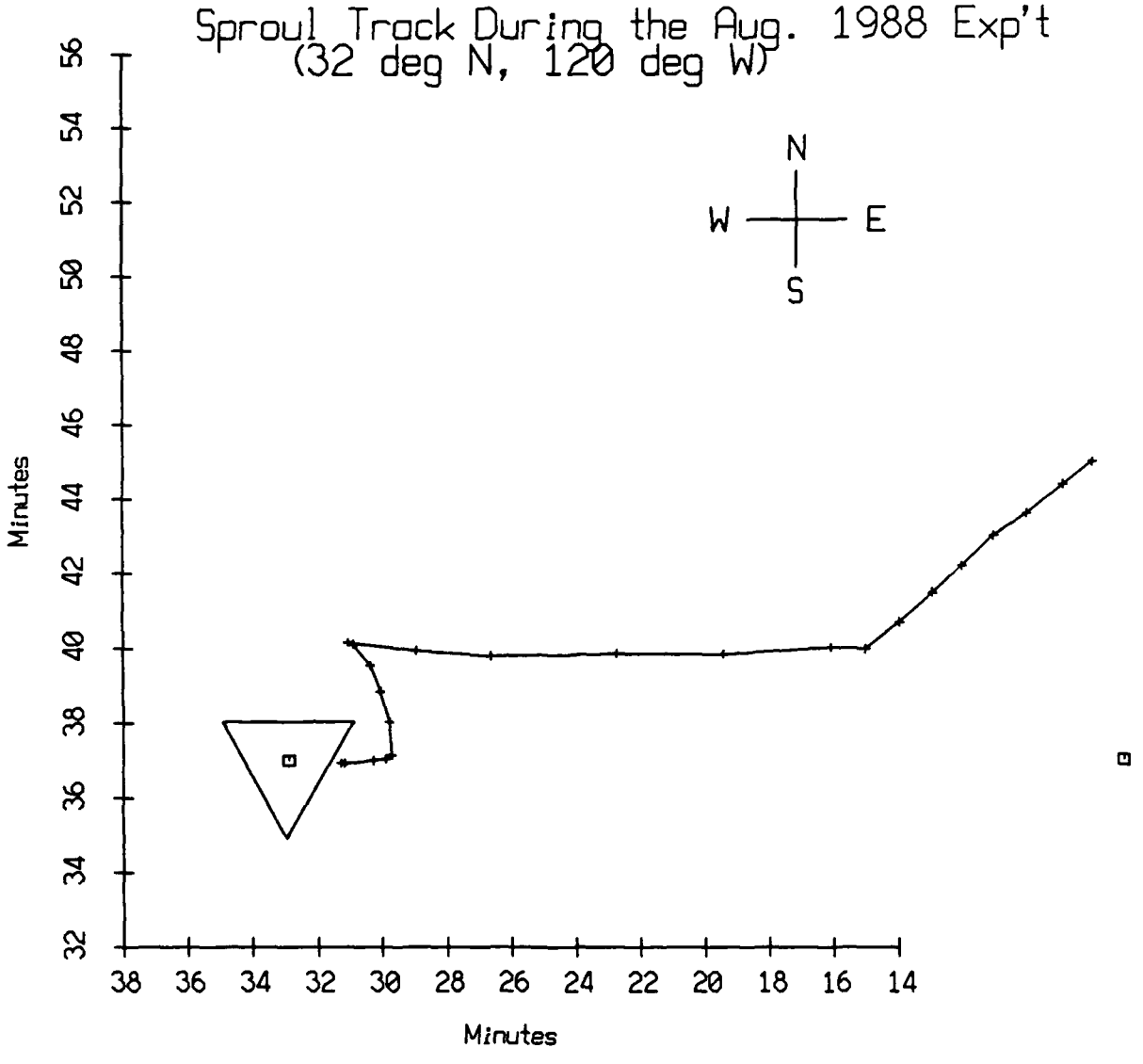

Sproul Track During the Aug. 1988 Exp't
(32 deg N, 120 deg W)
N
W
E
S
Minutes
56
54
52
50
48
46
44
42
40
38
36
34
32
38
36
34
32
30
28
26
24
22
20
18
16
14
Minutes

Figure II.2

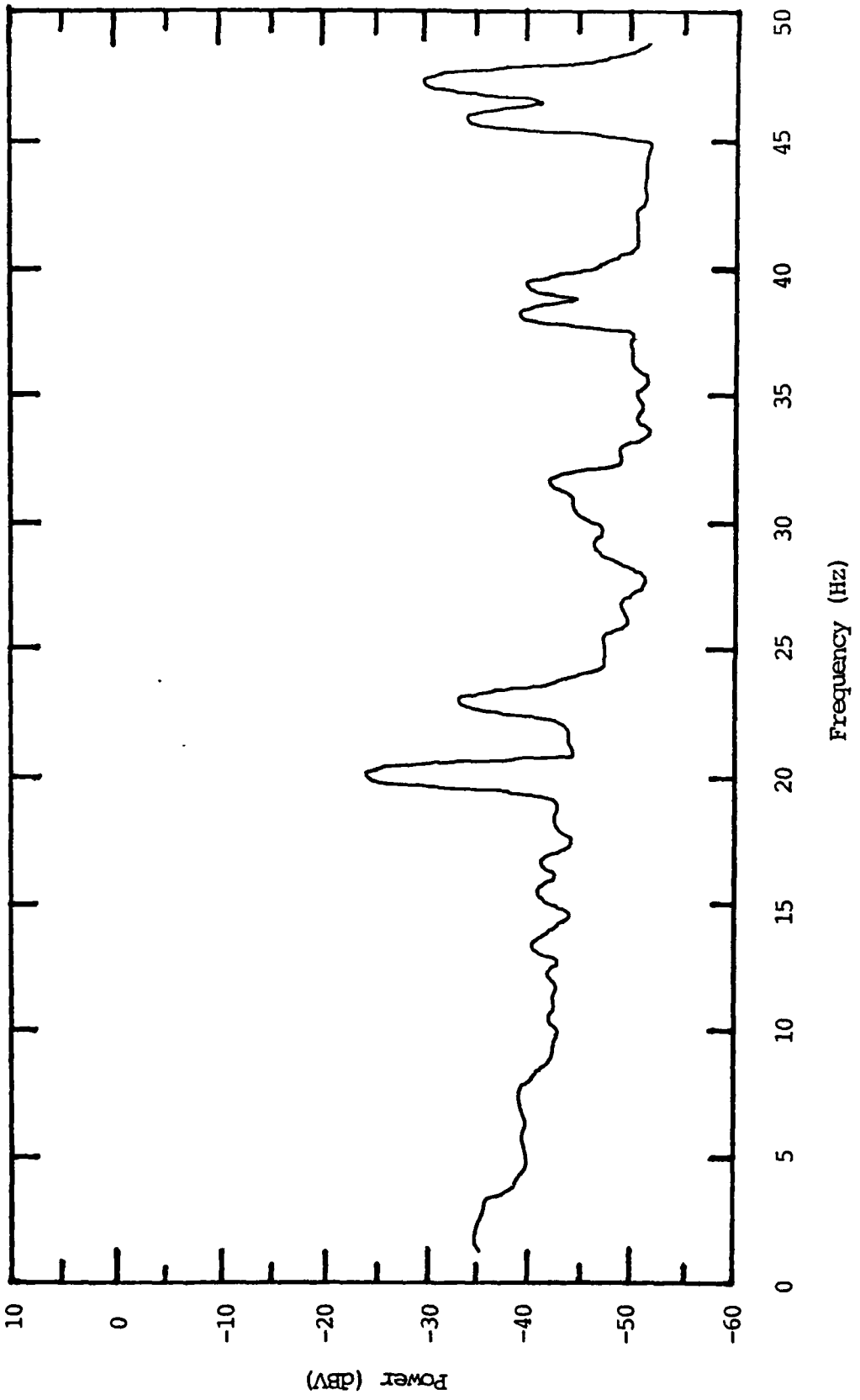

Power (dBV)
10
0
-10
-20
-30
-40
-50
-60
0
5
10
15
20
25
30
35
40
45
50
Frequency (Hz)

Figure II.3a

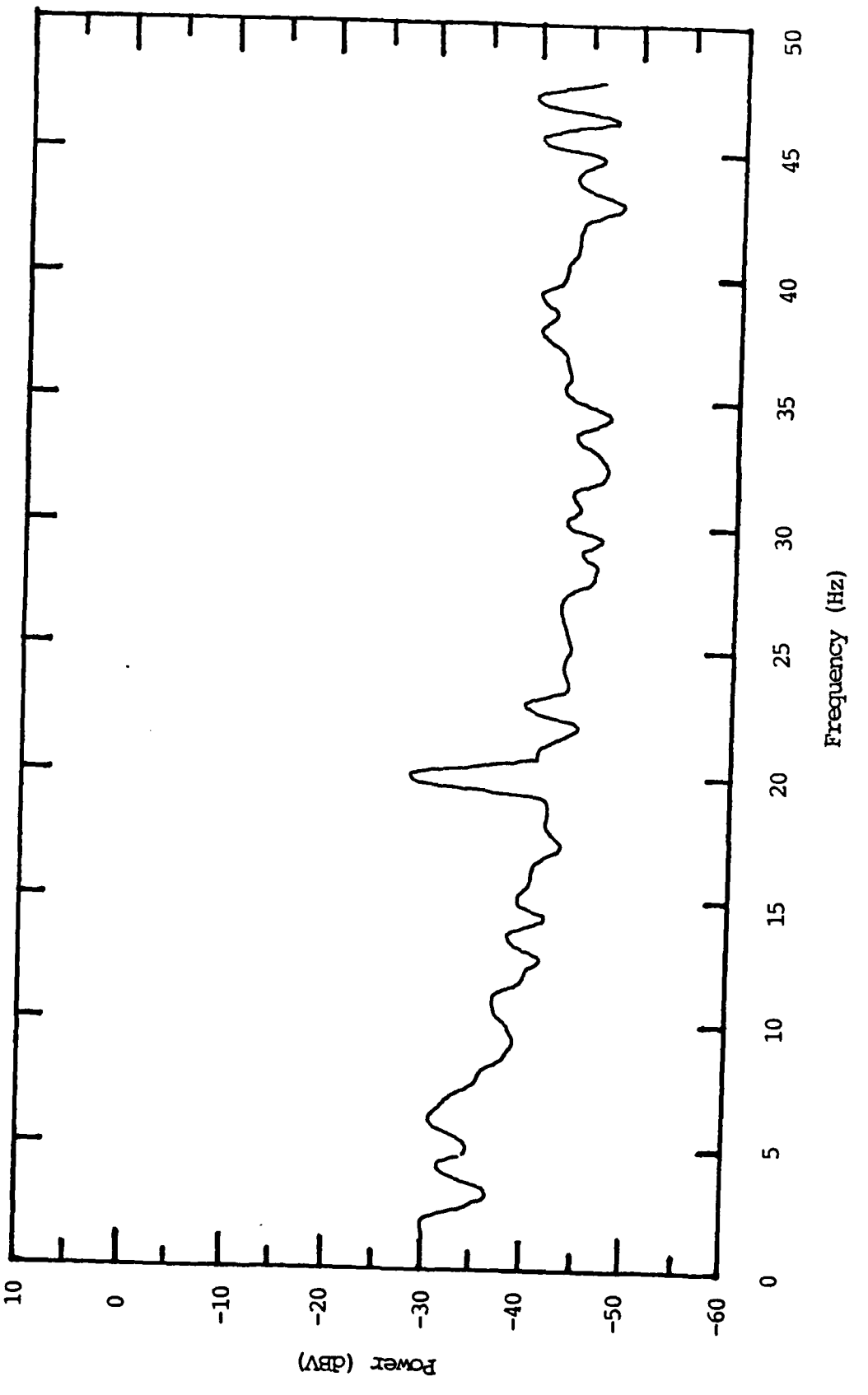

Power (dBV)
10
0
-10
-20
-30
-40
-50
-60
0
5
10
15
20
25
30
35
40
45
50
Frequency (Hz)

Figure II.3b

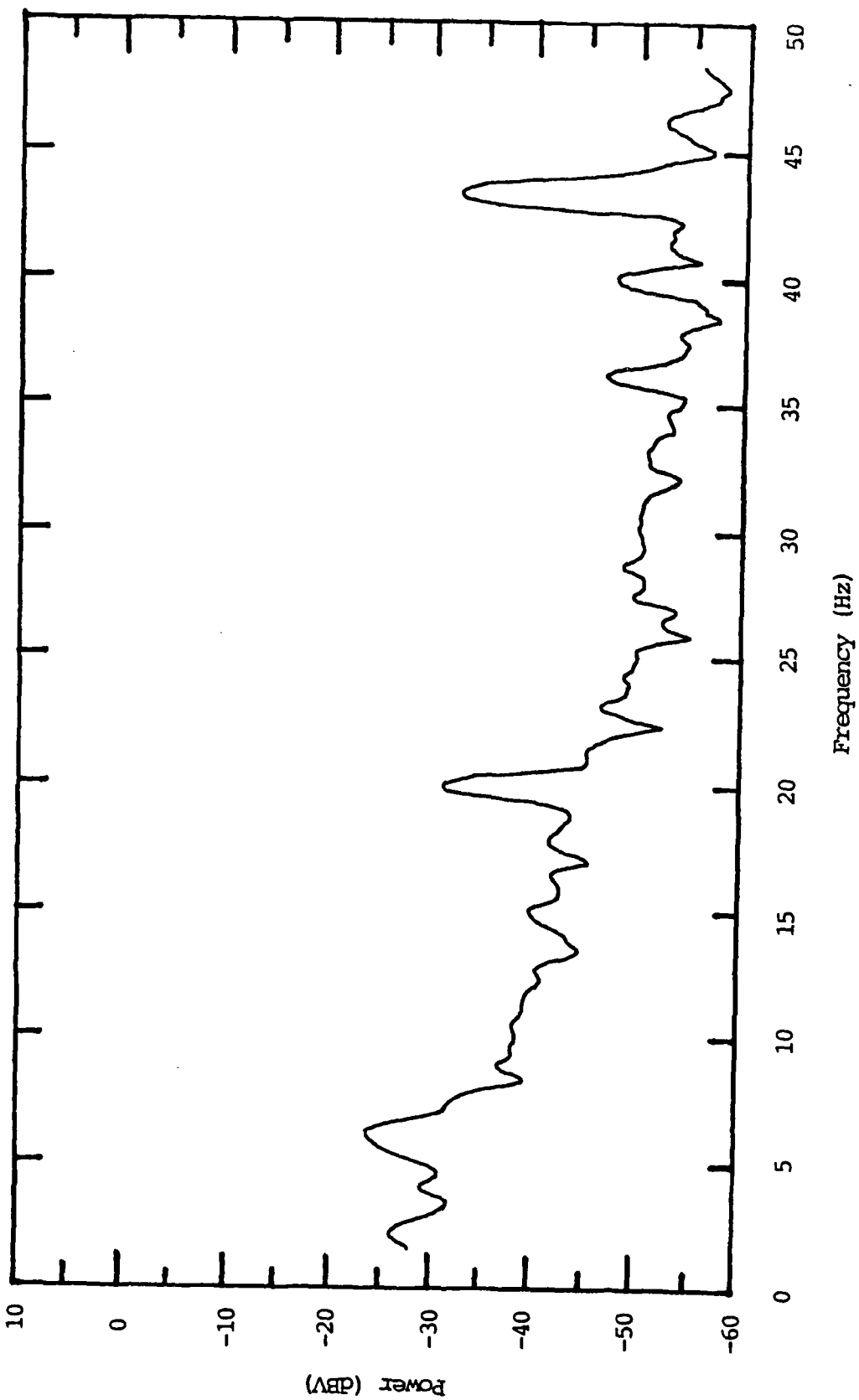

Power (dBV)
10
0
-10
-20
-30
-40
-50
-60
0
5
10
15
20
25
30
35
40
45
50
Frequency (Hz)

Figure II.3c

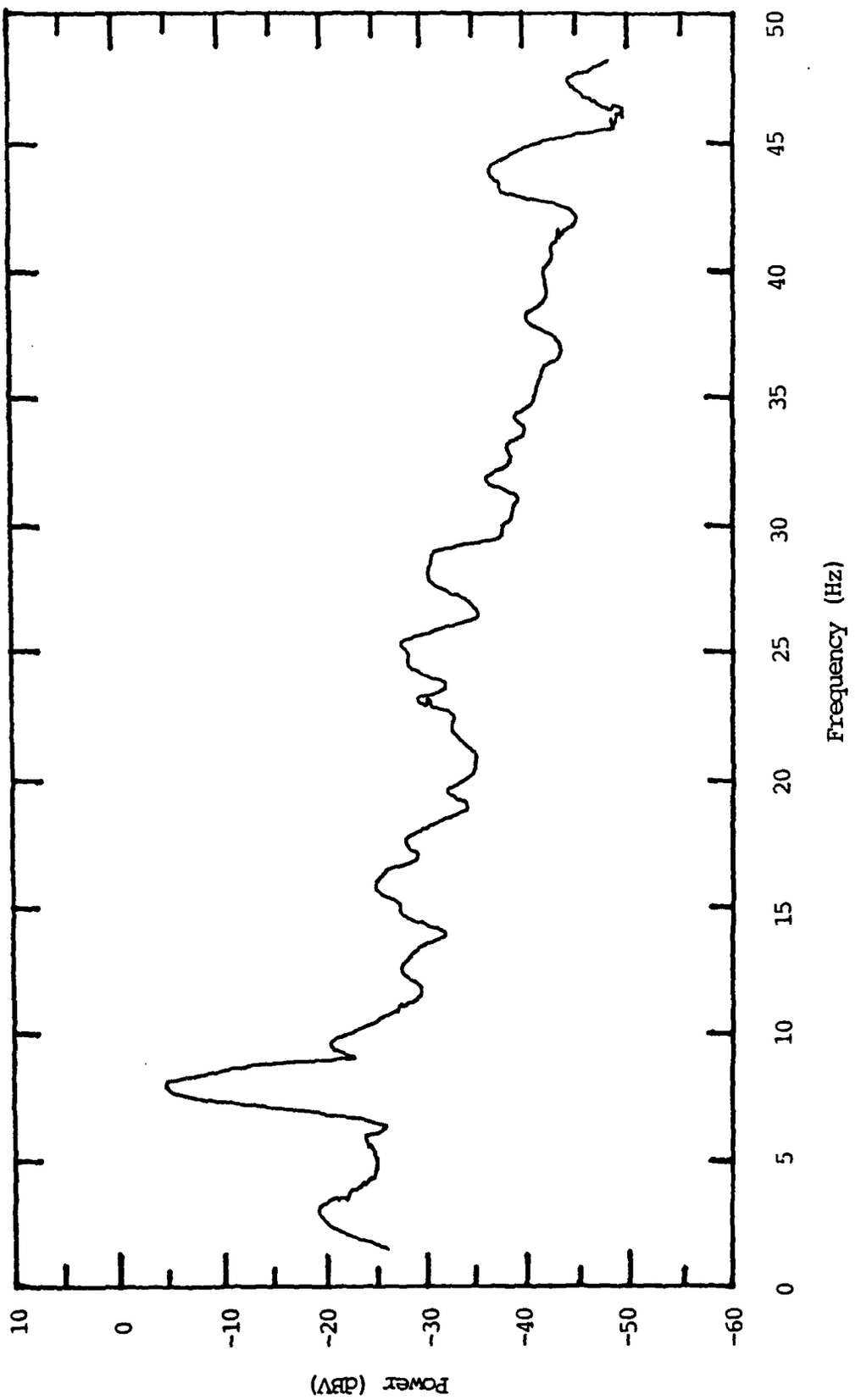

Power (dBV)
10
0
-10
-20
-30
-40
-50
-60
0
5
10
15
20
25
30
35
40
45
50
Frequency (Hz)

Figure II.3d

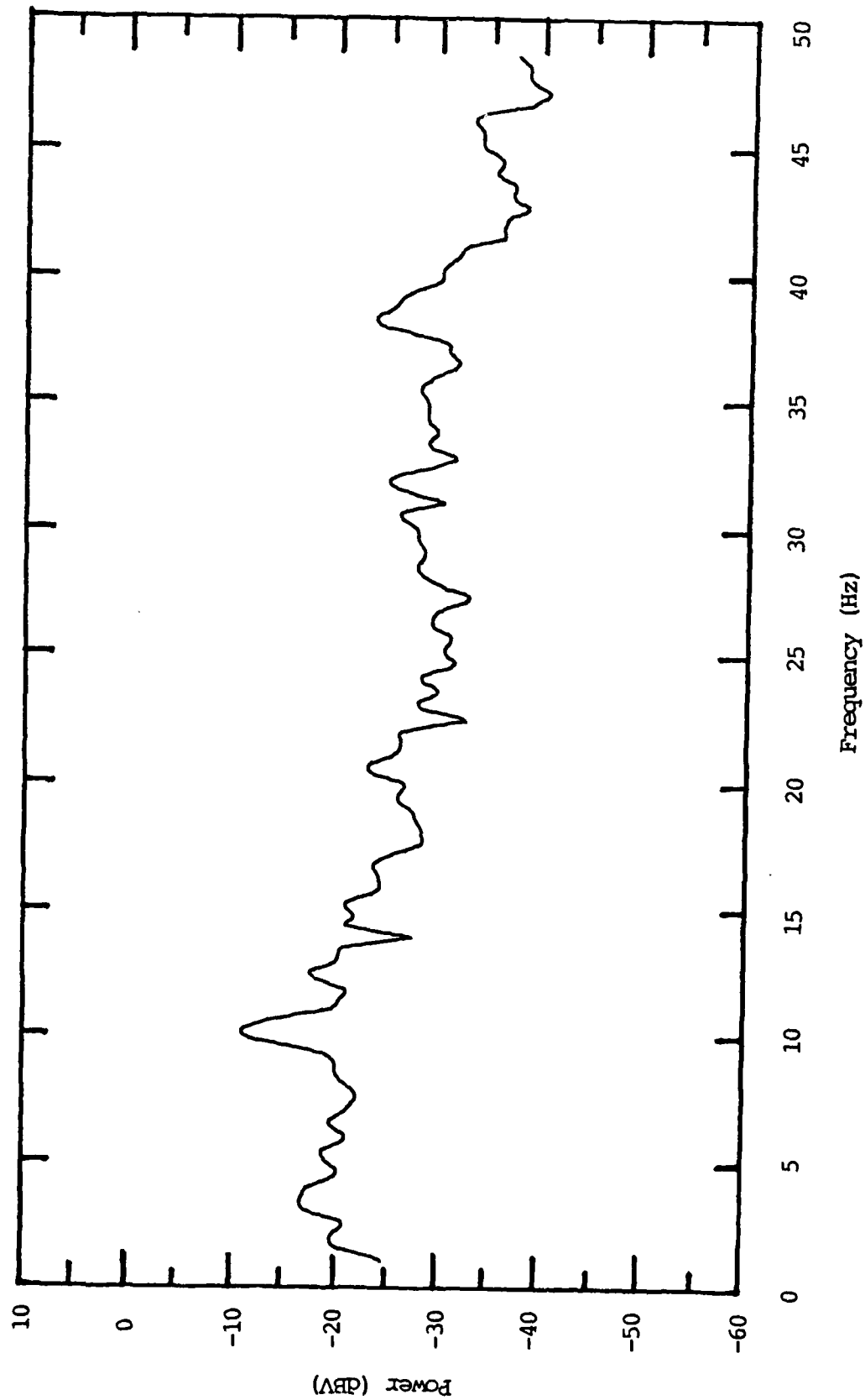

10
0
-10
-20
-30
-40
-50
-60
Power (dBV)
0
5
10
15
20
25
30
35
40
45
50
Frequency (Hz)

Figure II.3e

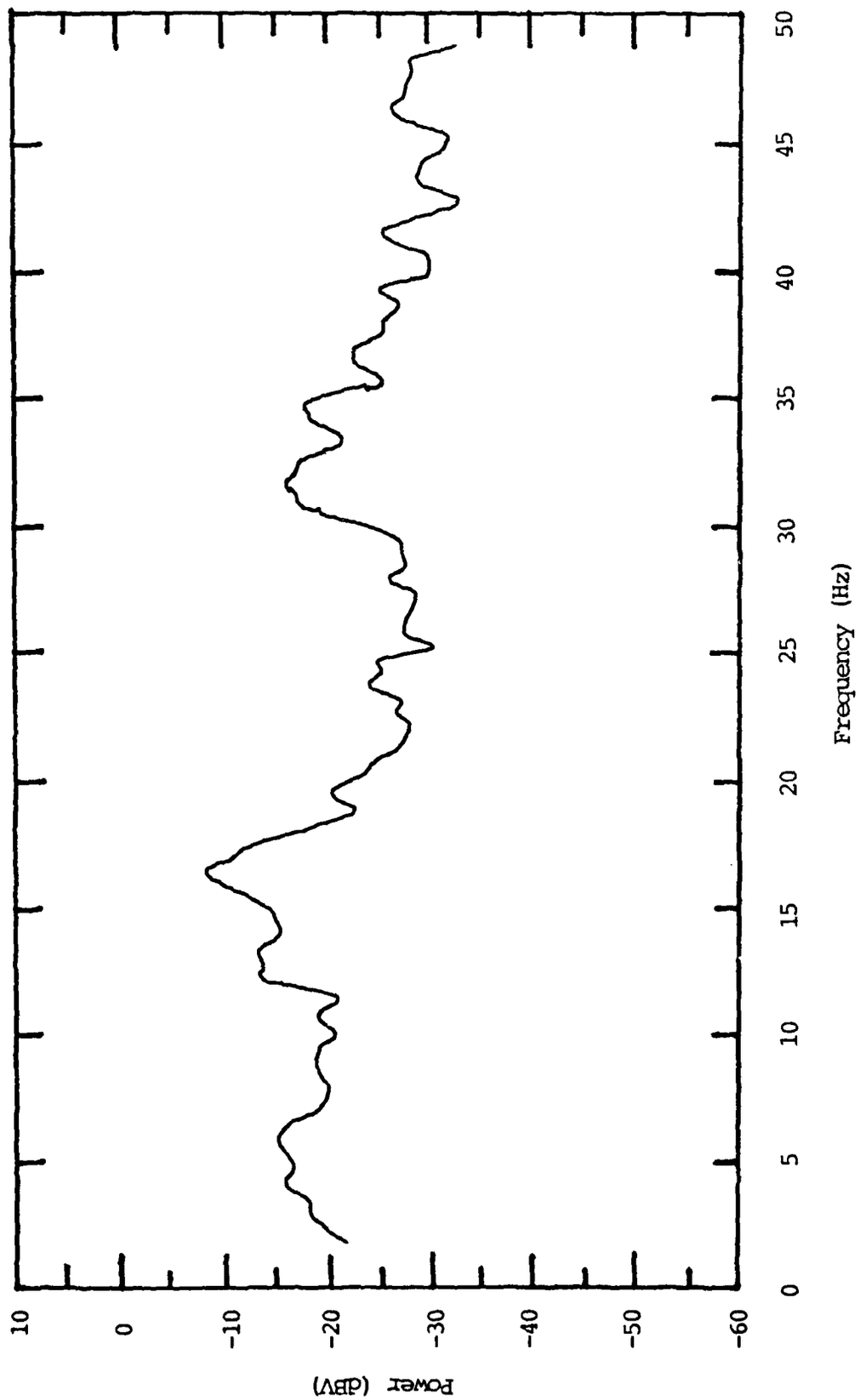

Power (dBV)
10
0
-10
-20
-30
-40
-50
-60
0
5
10
15
20
25
30
35
40
45
50
Frequency (Hz)

Figure II.3f

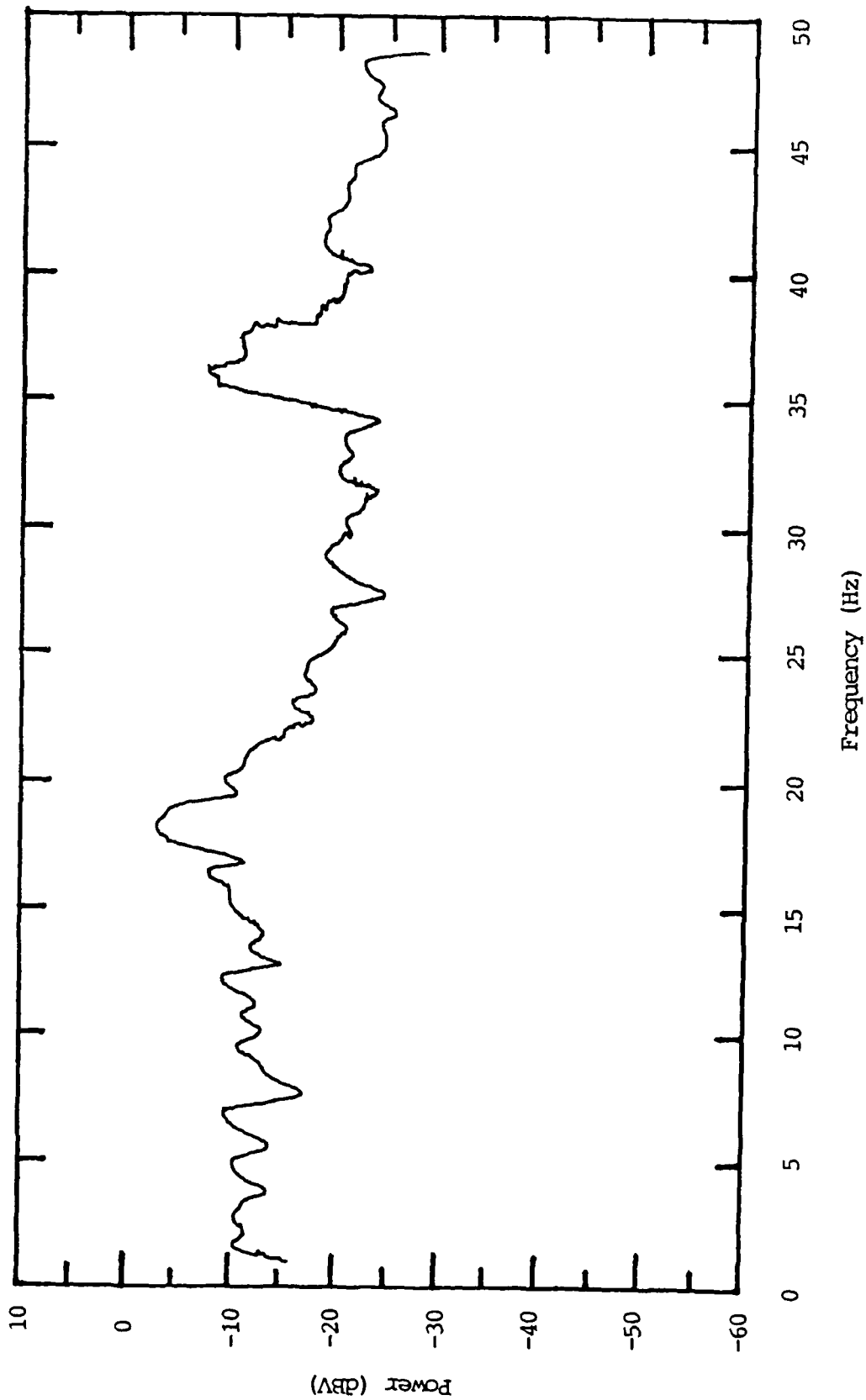

10
0
-10
-20
-30
-40
-50
-60
Power (dBV)
0
5
10
15
20
25
30
35
40
45
50
Frequency (Hz)

Figure II.3g

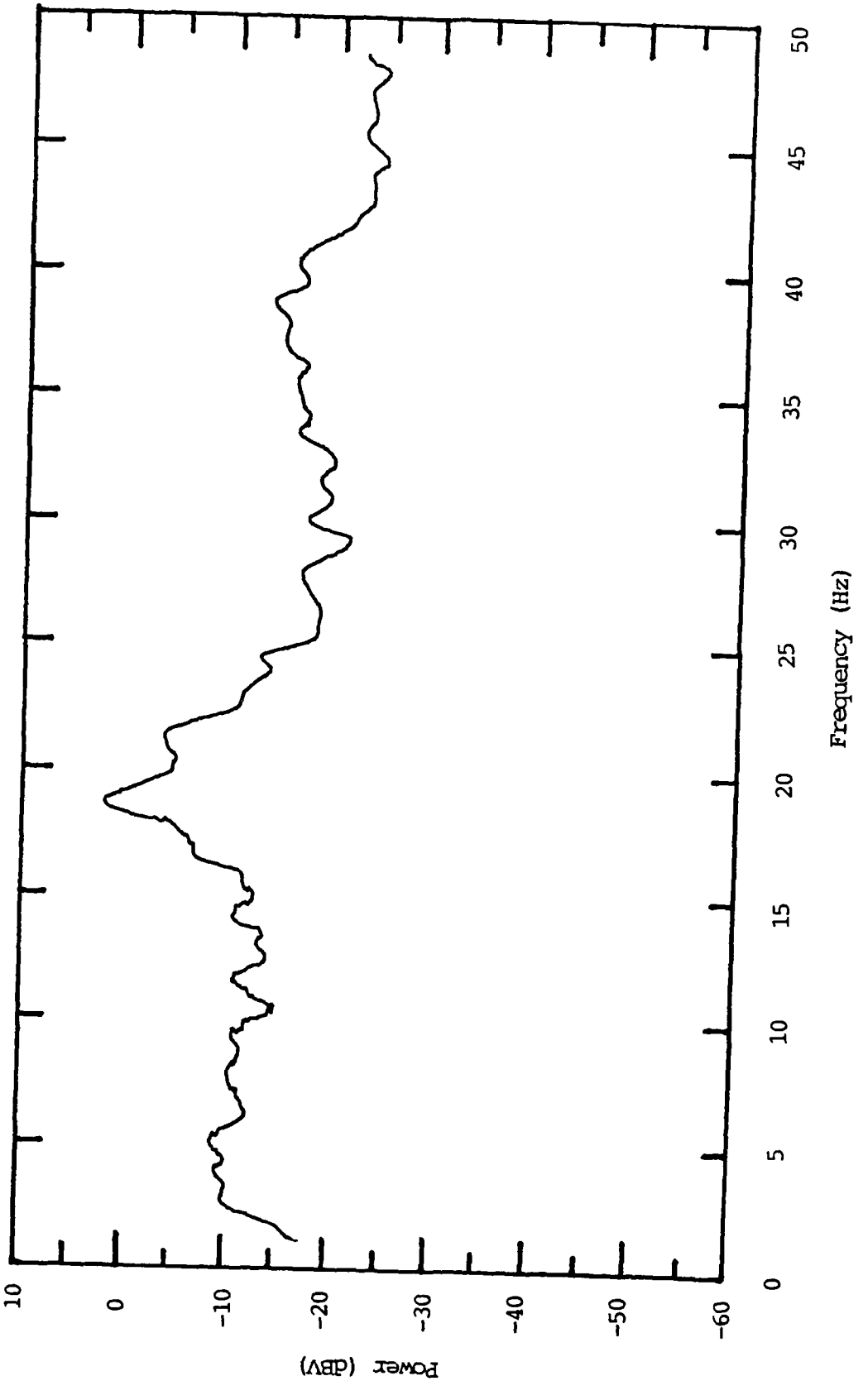

Power (dBV)
10
0
-10
-20
-30
-40
-50
-60
0
5
10
15
20
25
30
35
40
45
50
Frequency (Hz)

Figure II.3h

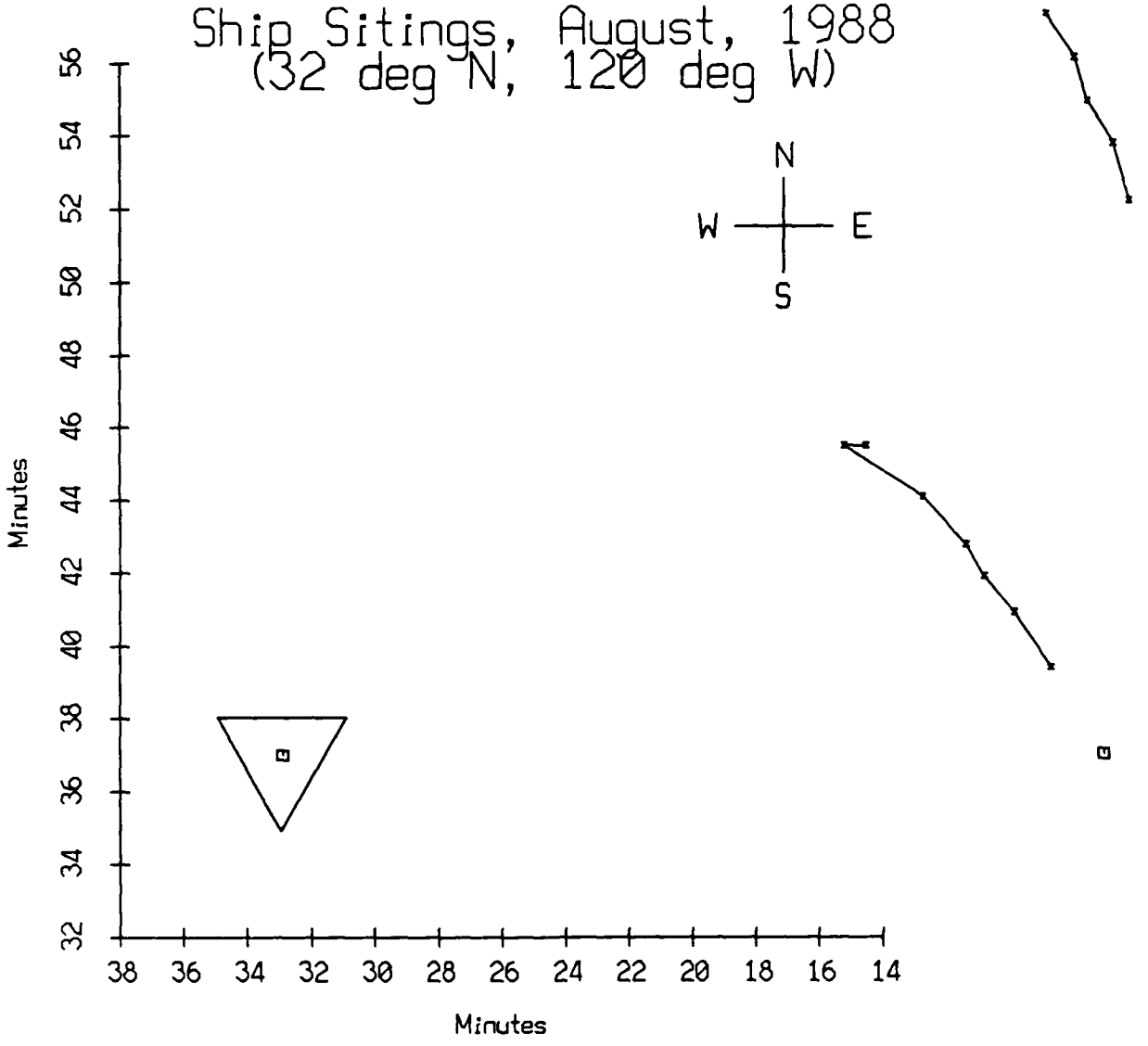

Ship Sitings, August, 1988
(32 deg N, 120 deg W)
N
W
E
S
Minutes
56
54
52
50
48
46
44
42
40
38
36
34
32
38 36 34 32 30 28 26 24 22 20 18 16 14
Minutes

Figure II.4

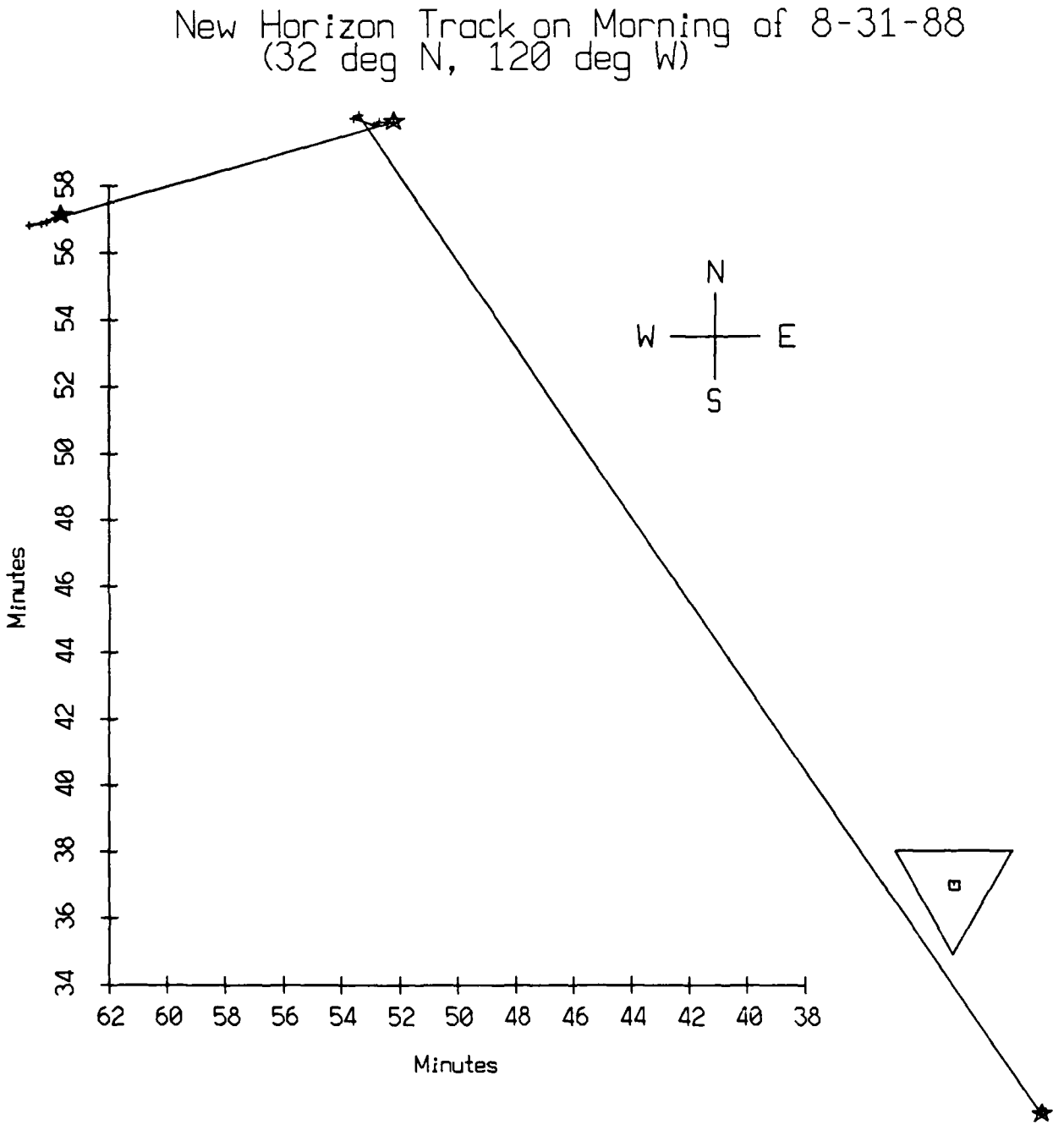

New Horizon Track on Morning of 8-31-88
(32 deg N, 120 deg W)
N
W
E
S
Minutes
58
56
54
52
50
48
46
44
42
40
38
36
34
62
60
58
56
54
52
50
48
46
44
42
40
38
Minutes

Figure II.5

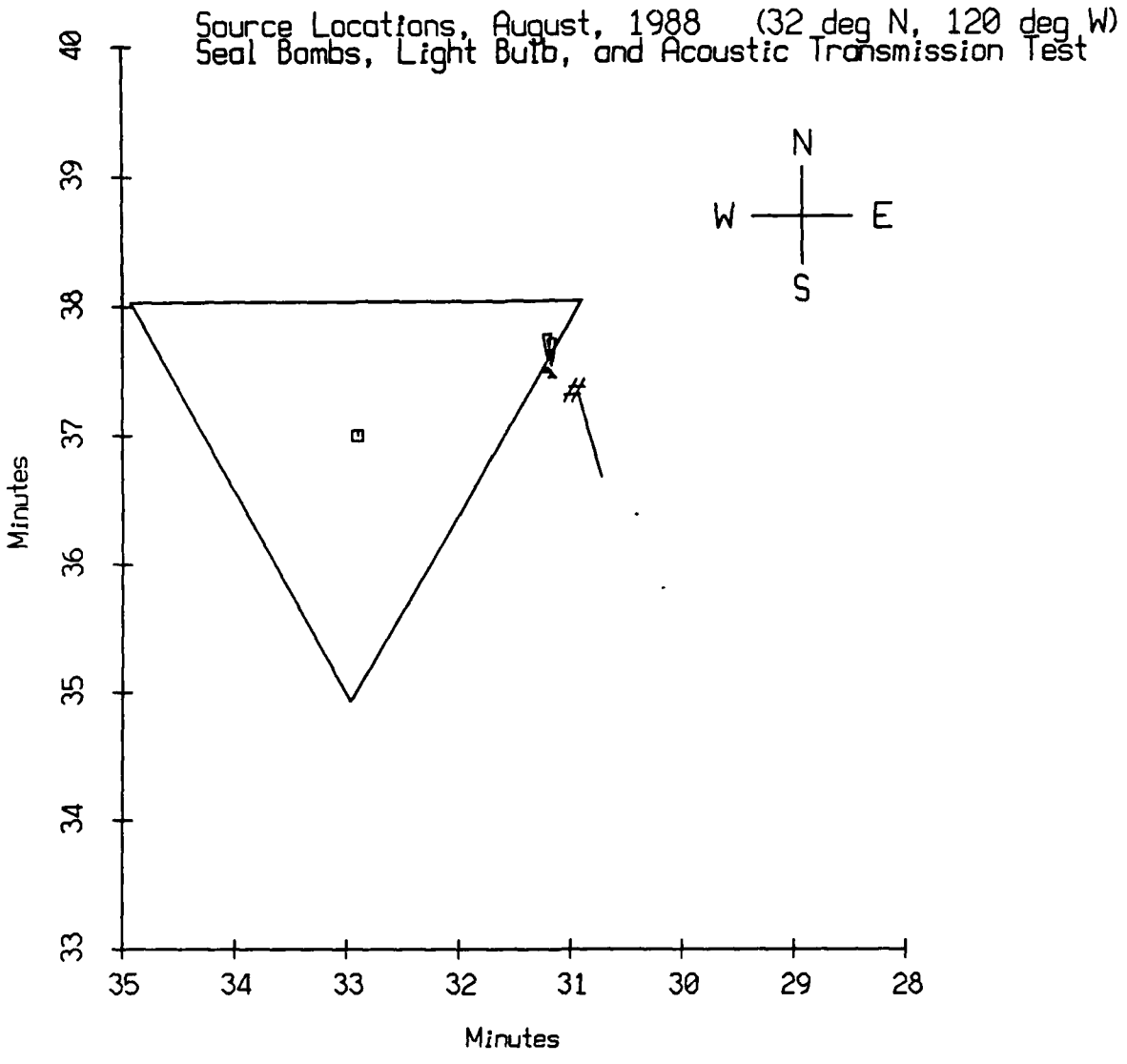

Source Locations, August, 1988 (32 deg N, 120 deg W)
Seal Bombs, Light Bulb, and Acoustic Transmission Test
N
W
E
S
Minutes
40
39
38
37
36
35
34
33
35
34
33
32
31
30
29
28
Minutes

Figure II.6

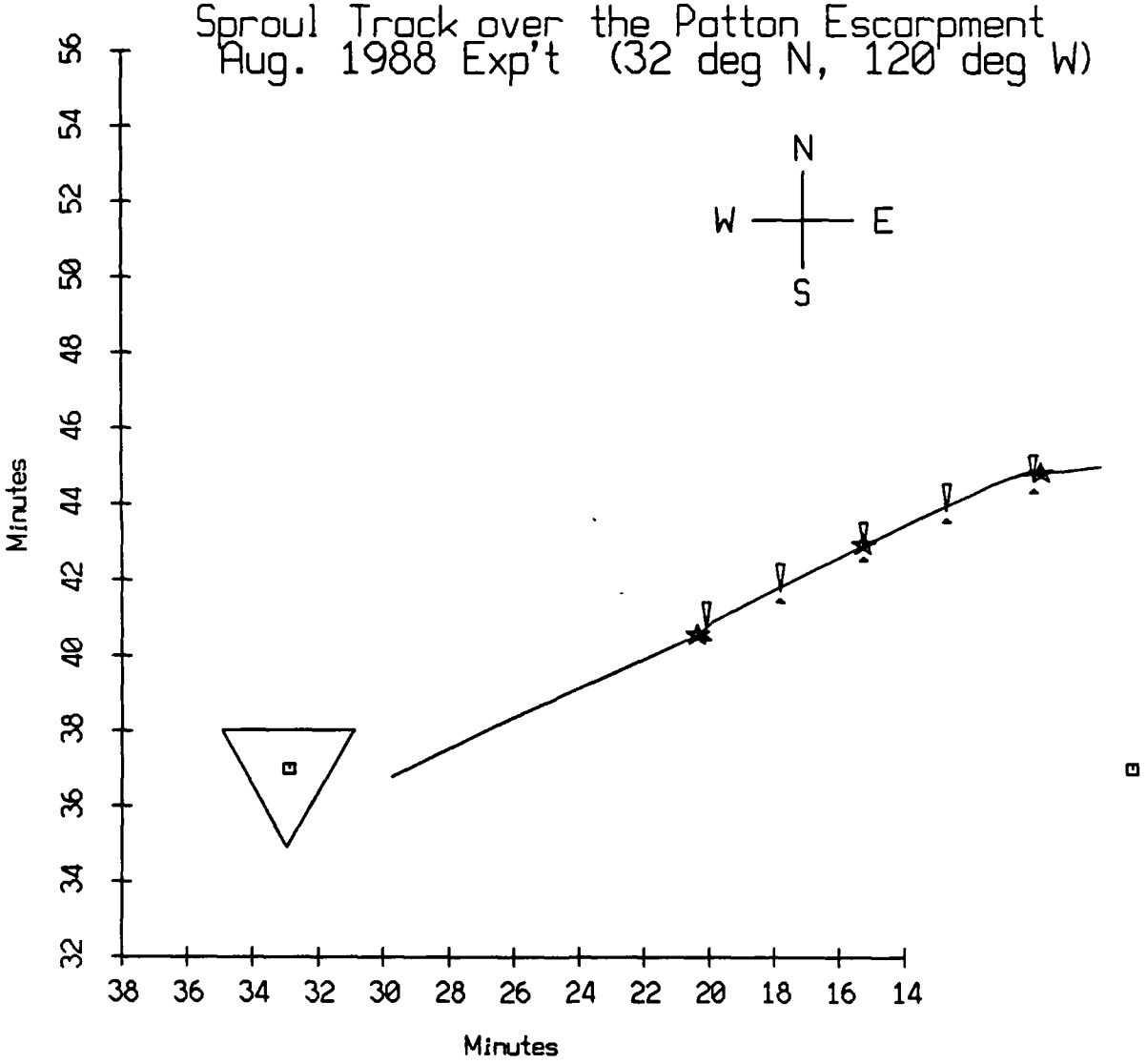

Sproul Track over the Patton Escarpment
Aug. 1988 Exp't (32 deg N, 120 deg W)
N
W
E
S
Minutes
56
54
52
50
48
46
44
42
40
38
36
34
32
38 36 34 32 30 28 26 24 22 20 18 16 14
Minutes

Figure II.7

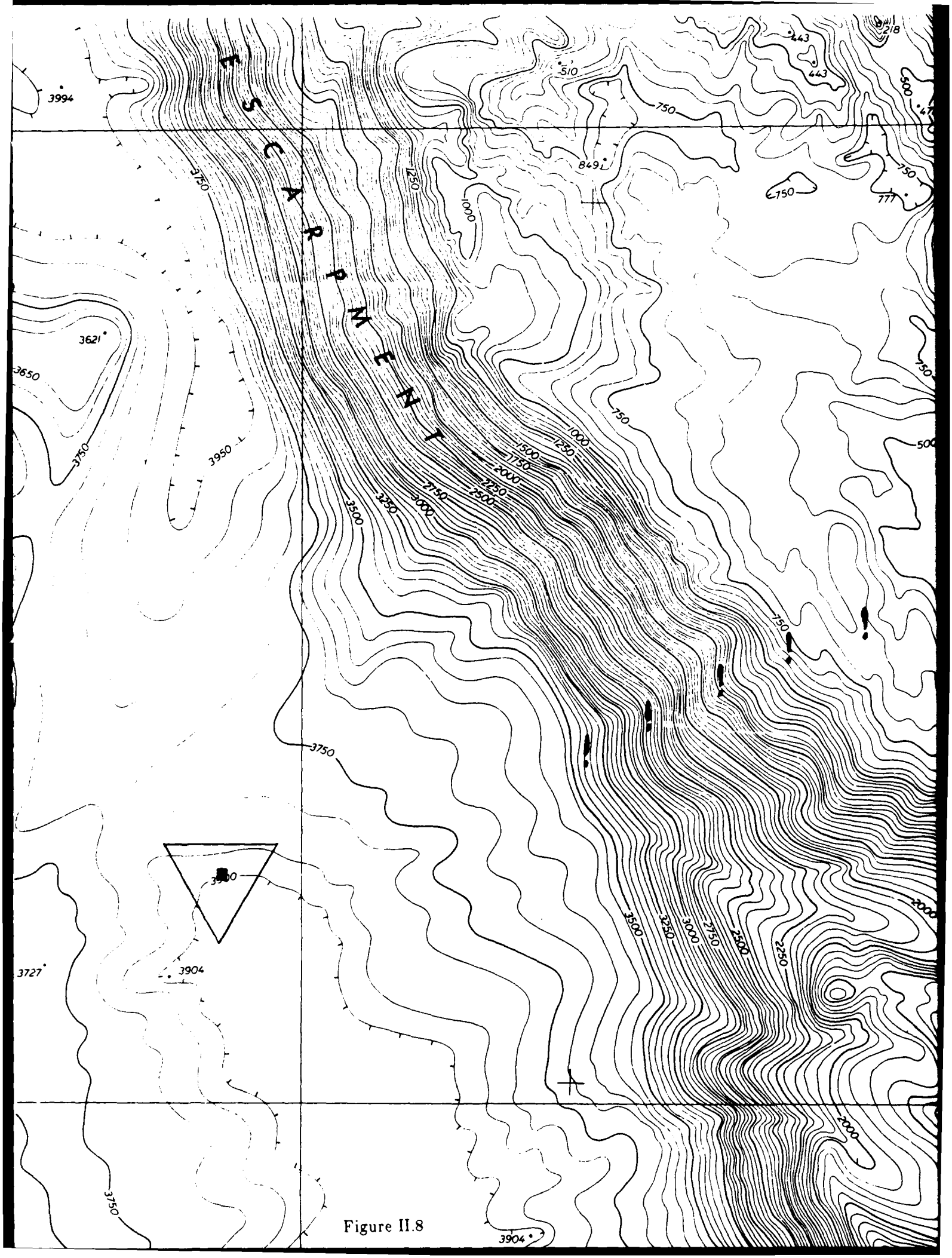

ESCARPMENT
3994
3621
3650
3750
3950
3727
3904
3904
510
443
443
218
849
777
750
1000
1250
1500
1750
2000
2250
2500
2750
3000
3250
3500

Figure II.8

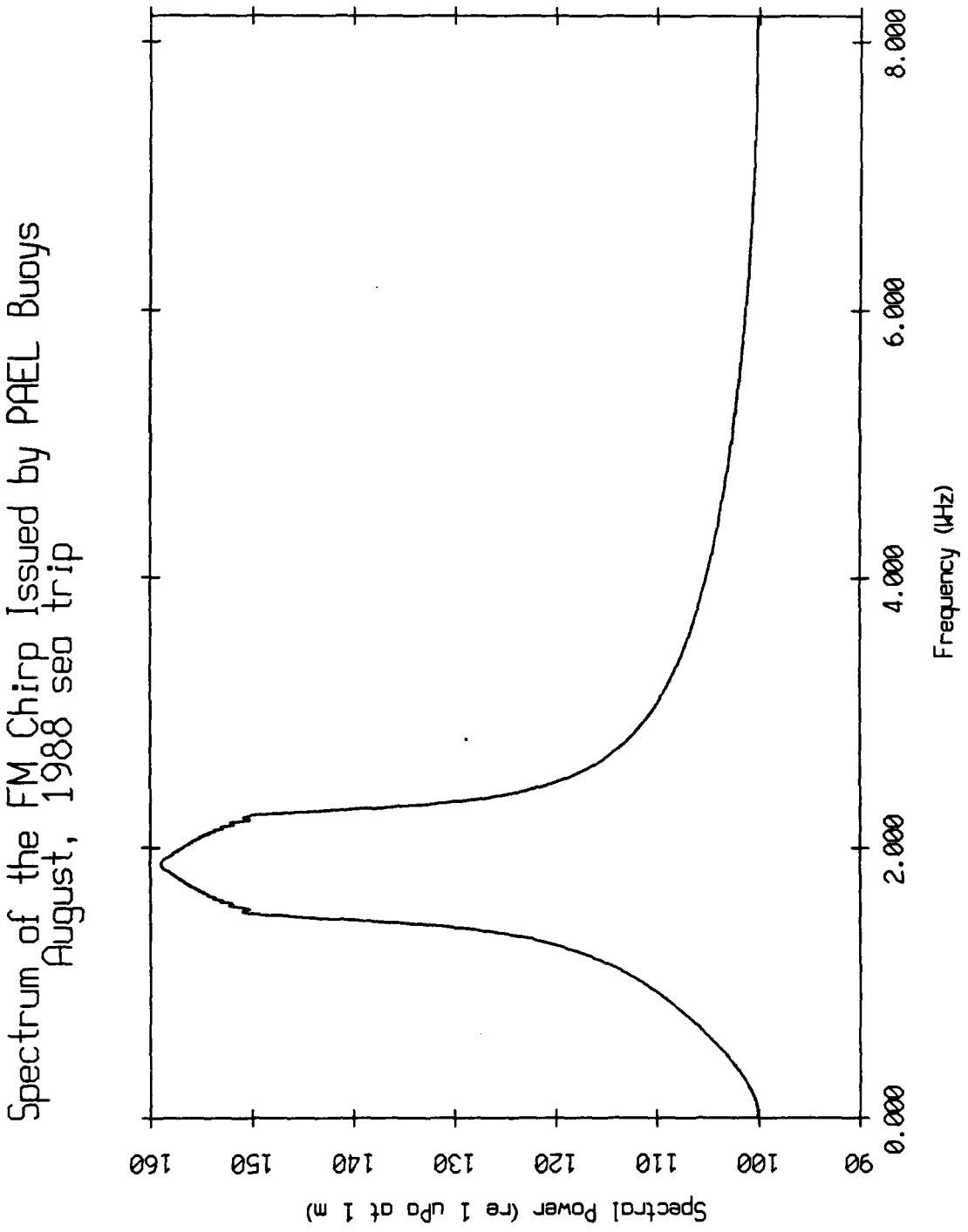

Spectrum of the FM Chirp Issued by PAEL Buoys
August, 1988 sea trip
Spectral Power (re 1 uPa at 1 m)
90
100
110
120
130
140
150
160
0.000
2.000
4.000
6.000
8.000
Frequency (kHz)

Figure II.9

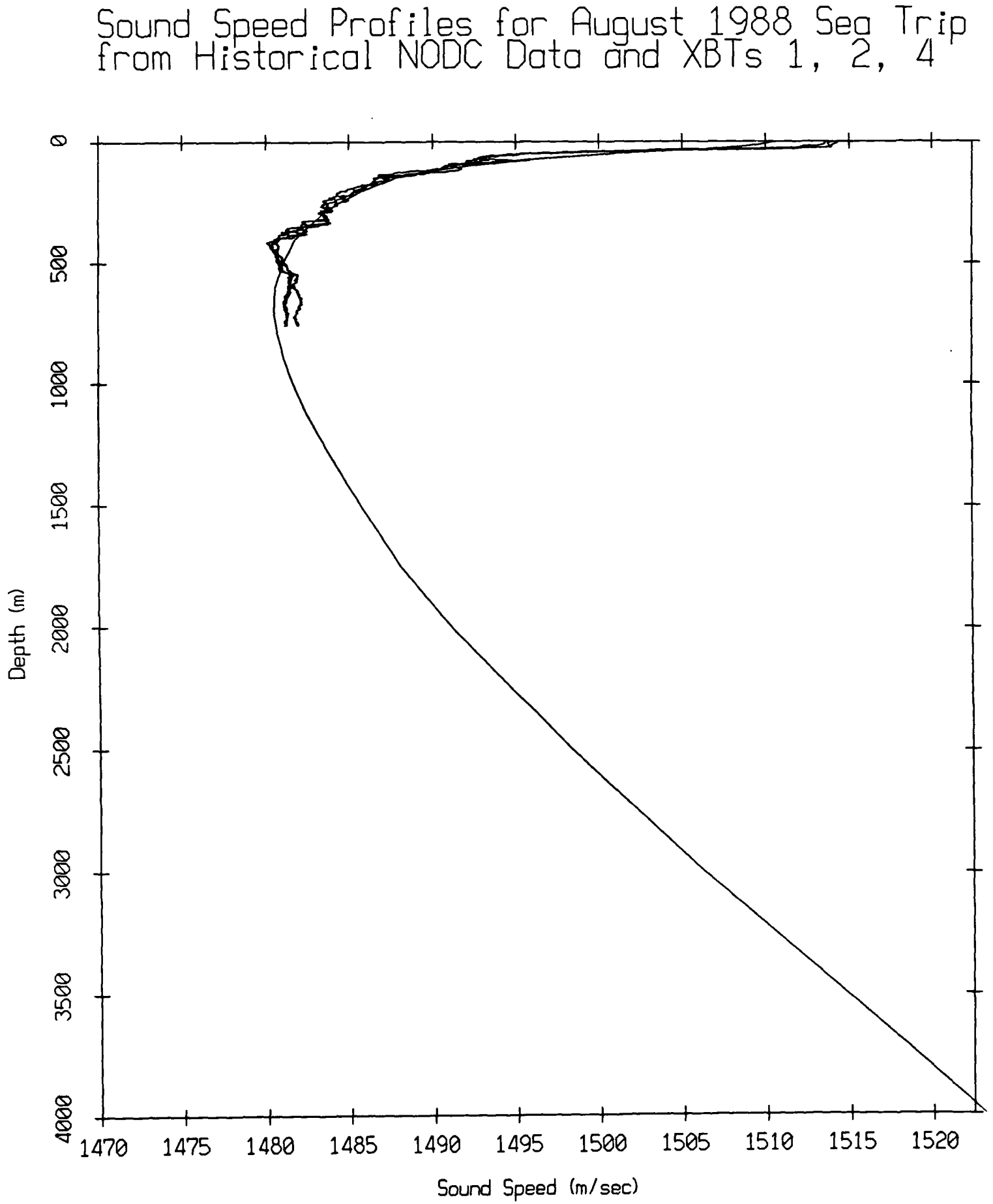

Sound Speed Profiles for August 1988 Sea Trip
from Historical NODC Data and XBTs 1, 2, 4
Depth (m)
0
500
1000
1500
2000
2500
3000
3500
4000
1470
1475
1480
1485
1490
1495
1500
1505
1510
1515
1520
Sound Speed (m/sec)

Figure IV.1

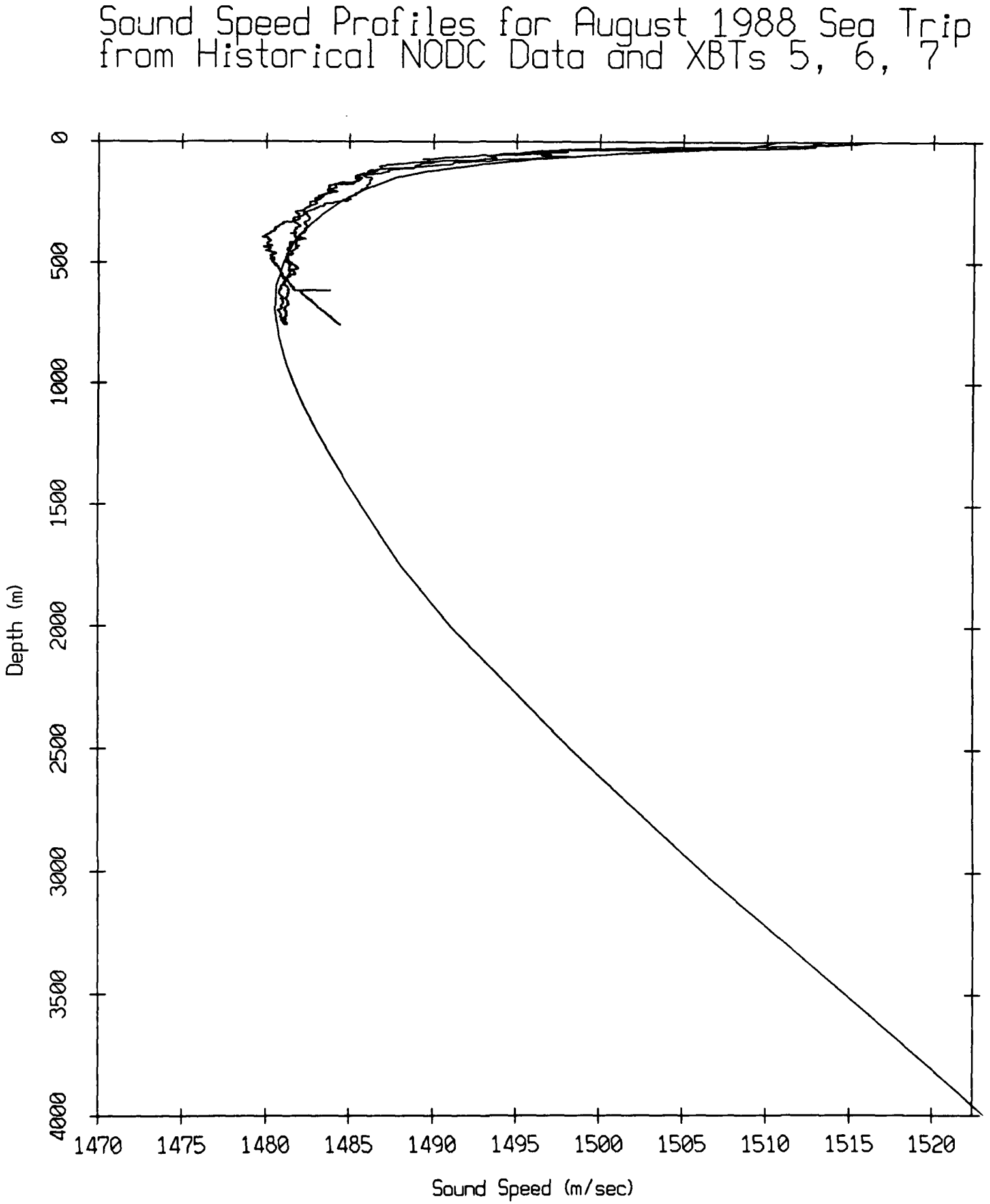

Sound Speed Profiles for August 1988 Sea Trip
from Historical NODC Data and XBTs 5, 6, 7
Depth (m)
0
500
1000
1500
2000
2500
3000
3500
4000
1470
1475
1480
1485
1490
1495
1500
1505
1510
1515
1520
Sound Speed (m/sec)

Figure IV.2

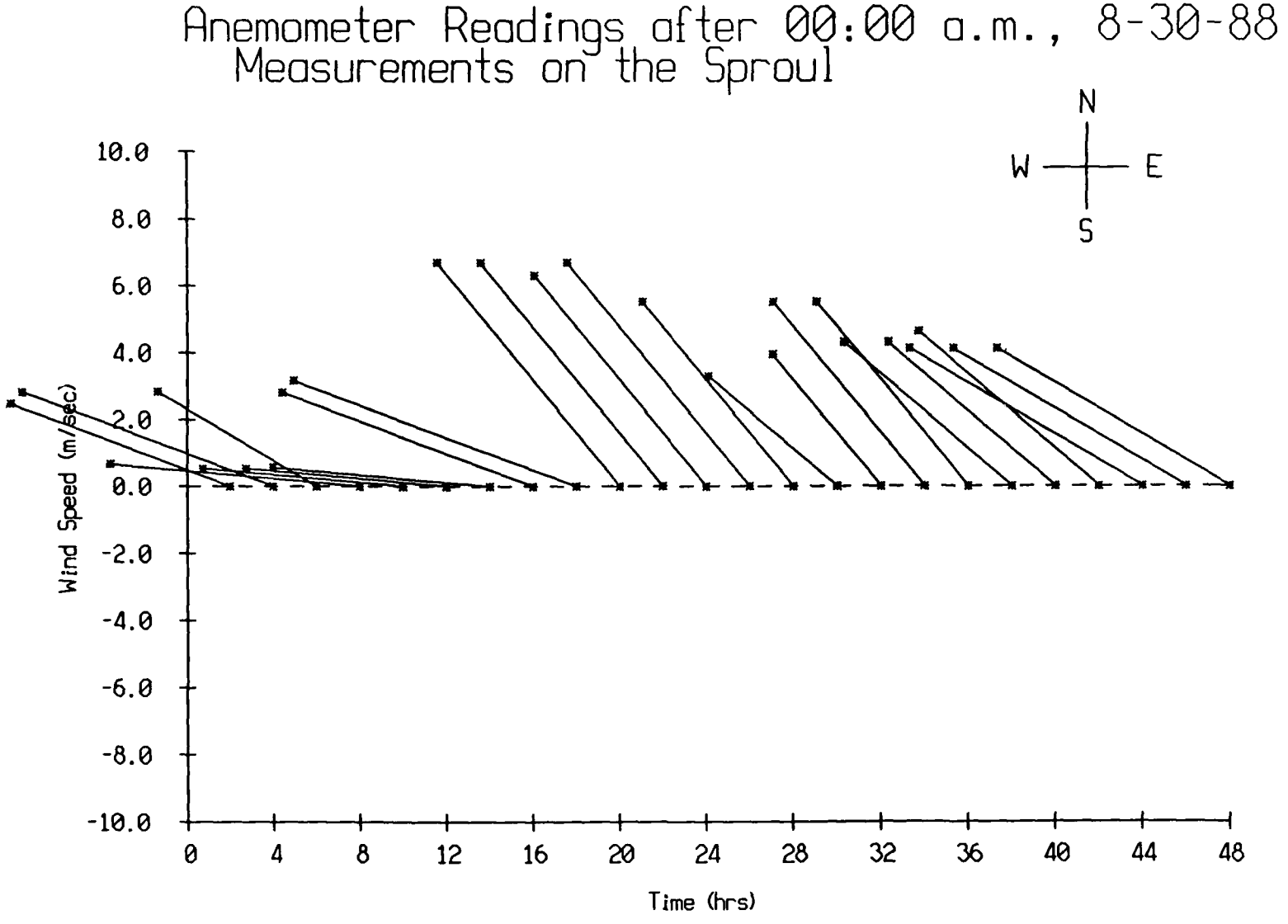

Anemometer Readings after 00:00 a.m., 8-30-88
Measurements on the Sproul
N
W
E
S
10.0
8.0
6.0
4.0
2.0
0.0
-2.0
-4.0
-6.0
-8.0
-10.0
Wind Speed (m/sec)
0
4
8
12
16
20
24
28
32
36
40
44
48
Time (hrs)

Figure IV.3

August 1988 Deployment Data Screening Results

record number	internal record number	# of bytes written	first missing resync	pass header checksum?	pass range checksum?	# of failed acoustic checksums?
			Float 0			
1987	1982	0	0	yes	yes	0
			Float 1			
463	461	7642	33	yes	yes	58
465	463	7642	6	yes	yes	84
1005	1004	7642	52	yes	yes	39
2030	2029	5690	0	yes	yes	1
2031	****	1240	1	no	no	10
2043	2040	0	0	yes	yes	0
			Float 2			
520	519	7642	15	yes	yes	76
674	673	1400	0	yes	yes	1
675	****	7658	1	no	no	88
975	973	2420	0	yes	yes	1
976	****	6272	1	no	no	72
981	978	3416	0	yes	yes	1
982	****	3504	1	no	no	38
983	****	228	1	no	no	38
985	980	7640	49	yes	yes	42
991	986	2178	0	yes	yes	1
992	987	416	0	yes	no	1
993	****	7676	1	no	no	88
1286	1280	7642	0	yes	no	0
1491	1485	7252	0	yes	yes	1
1498	1492	6648	0	yes	yes	1
1499	-7	284	1	no	no	1
1965	1958	7642	19	yes	yes	72
1975	1967	0	0	yes	yes	0
			Float 3			
806	802	9766	0	yes	yes	1
818	814	9766	0	yes	yes	1
895	891	9766	0	yes	yes	1
915	911	9766	0	yes	yes	1
935	931	9766	0	yes	yes	1

Figure V.1a

August 1988 Deployment Data Screening Results

record number	internal record number	# of bytes written	first missing resync	pass header checksum?	pass range checksum?	# of failed acoustic checksums?
943	939	9766	0	yes	yes	1
1007	1003	9766	0	yes	yes	1
1017	1013	9766	0	yes	yes	1
1106	1102	9766	0	yes	yes	1
1115	1111	9766	0	yes	yes	1
1220	1216	9766	39	yes	yes	52
1517	1512	0	0	yes	yes	1
			Float 4			
689	688	3878	0	yes	yes	1
690	****	4308	1	no	no	48
866	864	7642	41	yes	yes	50
1429	1427	2292	0	yes	yes	1
1430	****	4656	1	no	no	52
1925	1921	0	0	yes	yes	0
			Float 5			
566	565	9766	0	yes	yes	1
783	782	8160	0	yes	yes	2
784	****	1272	1	no	no	10
880	878	9766	0	yes	yes	1
969	967	9766	0	yes	yes	1
987	985	9766	0	yes	yes	1
1099	1097	9766	0	yes	yes	1
1132	1130	9766	0	yes	yes	1
1134	1132	9766	0	yes	yes	1
1166	1164	9766	0	yes	yes	1
1567	1564	0	0	yes	yes	1
1568	1947	7642	3	yes	yes	88
1569	9554	****	1	no	no	88
1570	****	****	1	no	no	88
1571	****	****	1	no	no	88
1572	****	****	1	no	no	88
1573	****	****	1	no	no	88
1574	****	****	1	no	no	88
1575	****	****	1	no	no	88
1576	****	****	1	no	no	88
1577	****	****	1	no	no	88
1578	****	****	1	no	no	88

Figure V.1b

August 1988 Deployment Data Screening Results

record number	internal record number	# of bytes written	first missing resync	pass header checksum?	pass range checksum?	# of failed acoustic checksums?
1579	****	-175	1	no	no	88
1580	****	****	1	no	no	88
1581	****	****	1	no	no	88
1582	****	****	1	no	no	88
1583	****	****	1	no	no	88
1584	****	****	1	no	no	88
1585	****	****	1	no	no	88
1586	425	426	1	no	no	88
1587	****	****	1	no	no	88
1588	****	****	1	no	no	88
1589	****	****	1	no	no	88
1590	****	****	1	no	no	88
1591	****	****	1	no	no	88
1592	****	****	1	no	no	88
1593	****	****	1	no	no	88
1594	****	****	1	no	no	88
1595	****	****	1	no	no	88
			Float 6			
92	91	3402	0	yes	yes	1
93	****	3548	1	no	no	38
204	0	7644	1	no	no	88
937	935	6484	0	yes	yes	1
938	****	470	1	no	no	1
1465	1462	7642	6	yes	yes	85
1927	1923	0	0	yes	yes	0
			Float 7			
27	26	7642	0	yes	yes	1
32	31	7642	0	yes	yes	1
183	182	860	0	yes	yes	1
184	382	6098	1	no	no	70
1912	1909	0	0	yes	yes	0
			Float 8			
484	****	7644	1	no	no	88
489	29	7644	1	no	no	88

Figure V.1c

August 1988 Deployment Data Screening Results

record number	internal record number	# of bytes written	first missing resync	pass header checksum?	pass range checksum?	# of failed acoustic checksums?
1811	****	7644	1	no	no	88
1893	1891	0	0	yes	yes	0
			Float 9			
1922	1920	0	0	yes	yes	0
			Float 10			
797	796	4168	0	yes	yes	2
798	****	4850	1	no	no	43
839	837	9766	0	yes	yes	1
864	862	9766	0	yes	yes	1
947	945	9766	0	yes	yes	1
981	979	9766	0	yes	yes	1
1084	1082	9766	0	yes	yes	1
1147	1145	9766	0	yes	yes	1
1184	1182	9766	0	yes	yes	1
1194	1192	9766	0	yes	yes	1
1595	1593	9634	0	yes	yes	1
1597	1594	0	0	yes	yes	1
			Float 11			
1	****	6020	1	no	no	53
917	913	9766	0	yes	yes	1
930	926	9766	0	yes	yes	1
936	932	9766	0	yes	yes	1
1010	1006	9766	0	yes	yes	1
1027	1023	9766	0	yes	yes	1
1029	1025	9766	0	yes	yes	1
1031	1027	9766	0	yes	yes	1
1056	1052	9766	0	yes	yes	1
1057	1053	9766	0	yes	yes	1
1098	1094	9766	0	yes	yes	1
1122	1118	9766	0	yes	yes	1
1549	1544	0	0	yes	yes	1

Figure V.1d

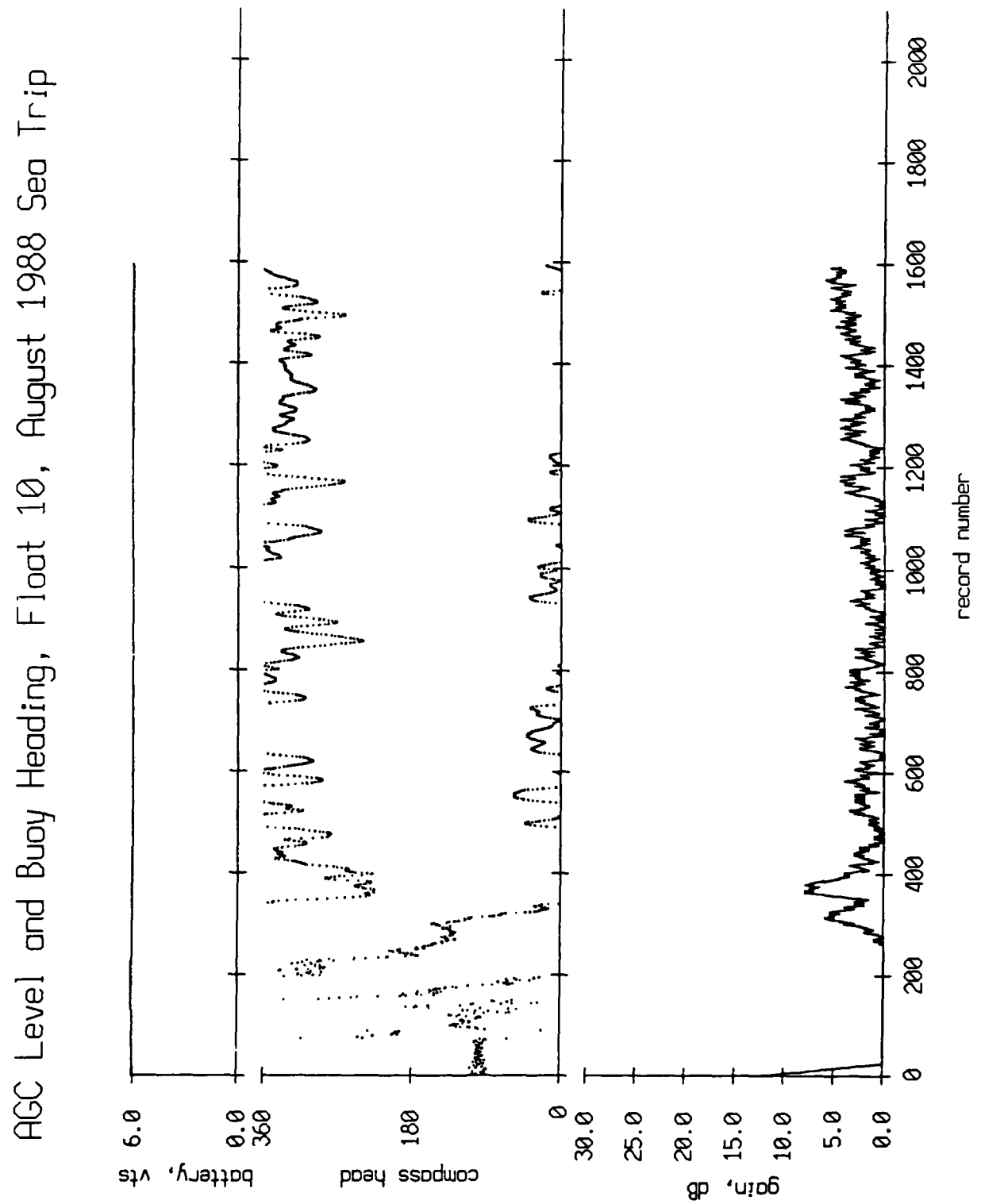

AGC Level and Buoy Heading, Float 10, August 1988 Sea Trip
battery, vts
6.0
0.0
compass head
360
180
0
gain, db
30.0
25.0
20.0
15.0
10.0
5.0
0.0
0
200
400
600
800
1000
1200
1400
1600
1800
2000
record number

Figure VII.1

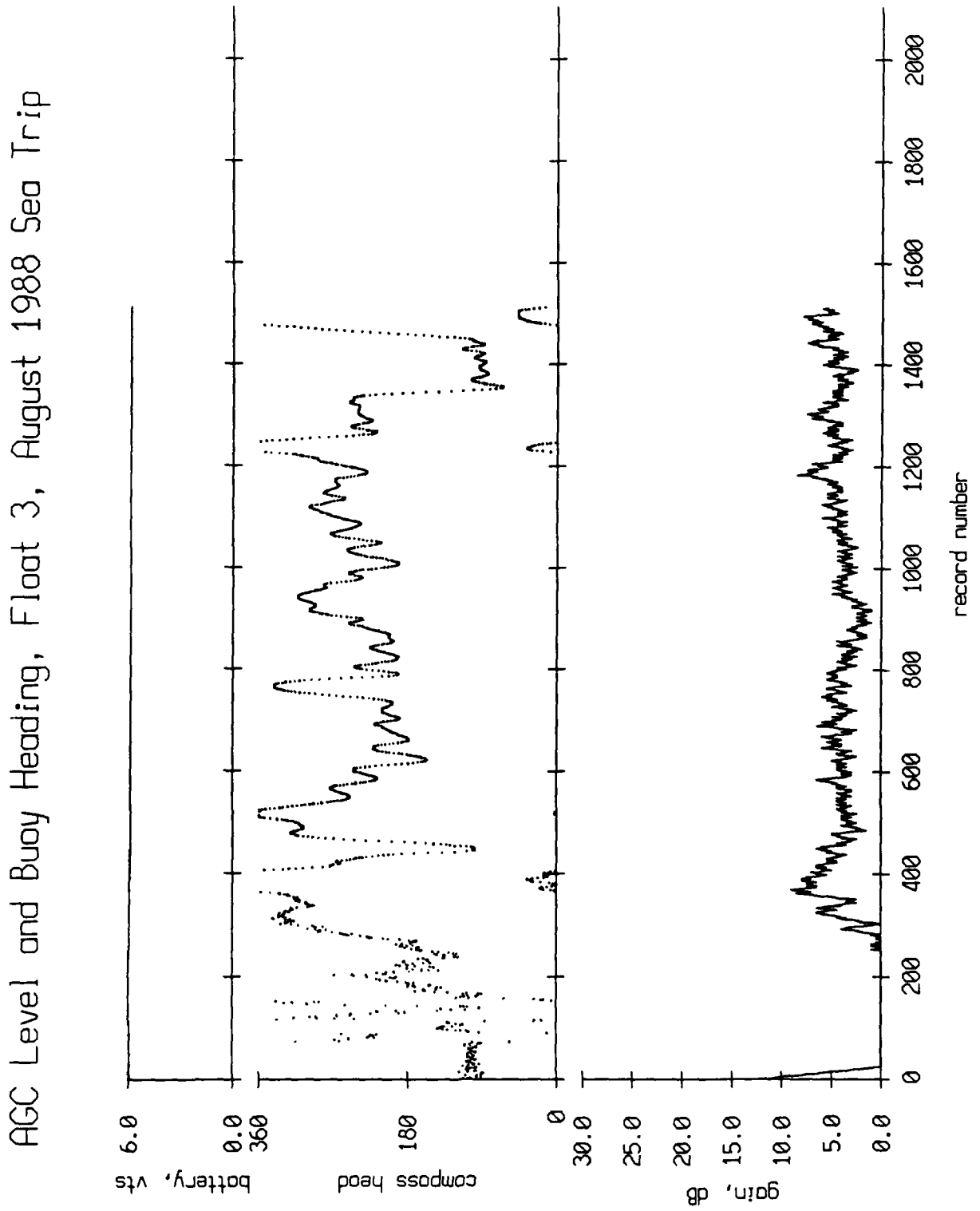

AGC Level and Buoy Heading, Float 3, August 1988 Sea Trip
battery, vts
6.0
0.0
compass head
360
180
0
gain, db
30.0
25.0
20.0
15.0
10.0
5.0
0.0
0
200
400
600
800
1000
1200
1400
1600
1800
2000
record number

Figure VII.2

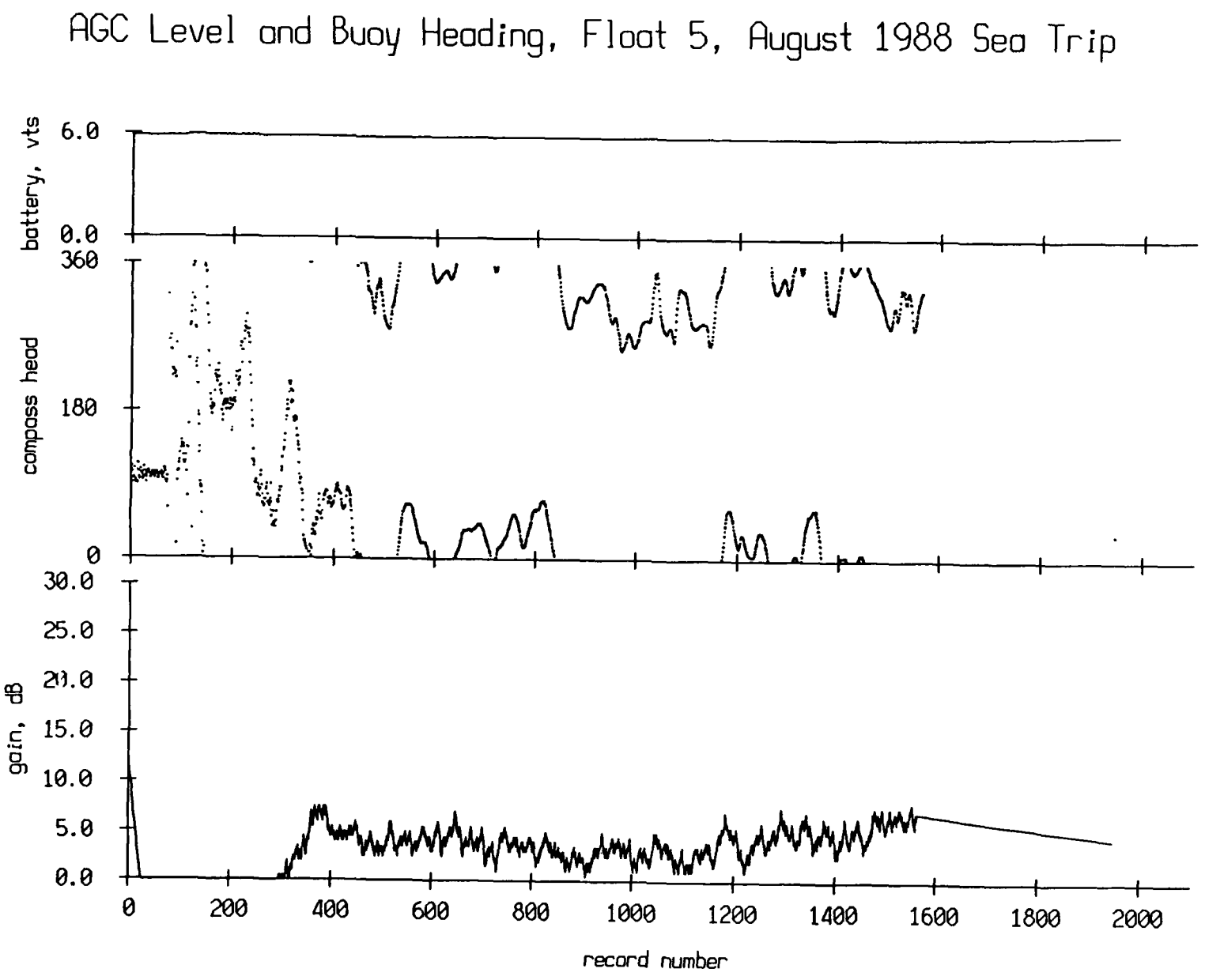

AGC Level and Buoy Heading, Float 5, August 1988 Sea Trip
battery, vts
6.0
0.0
compass head
360
180
0
gain, dB
30.0
25.0
20.0
15.0
10.0
5.0
0.0
0
200
400
600
800
1000
1200
1400
1600
1800
2000
record number

Figure VII.3

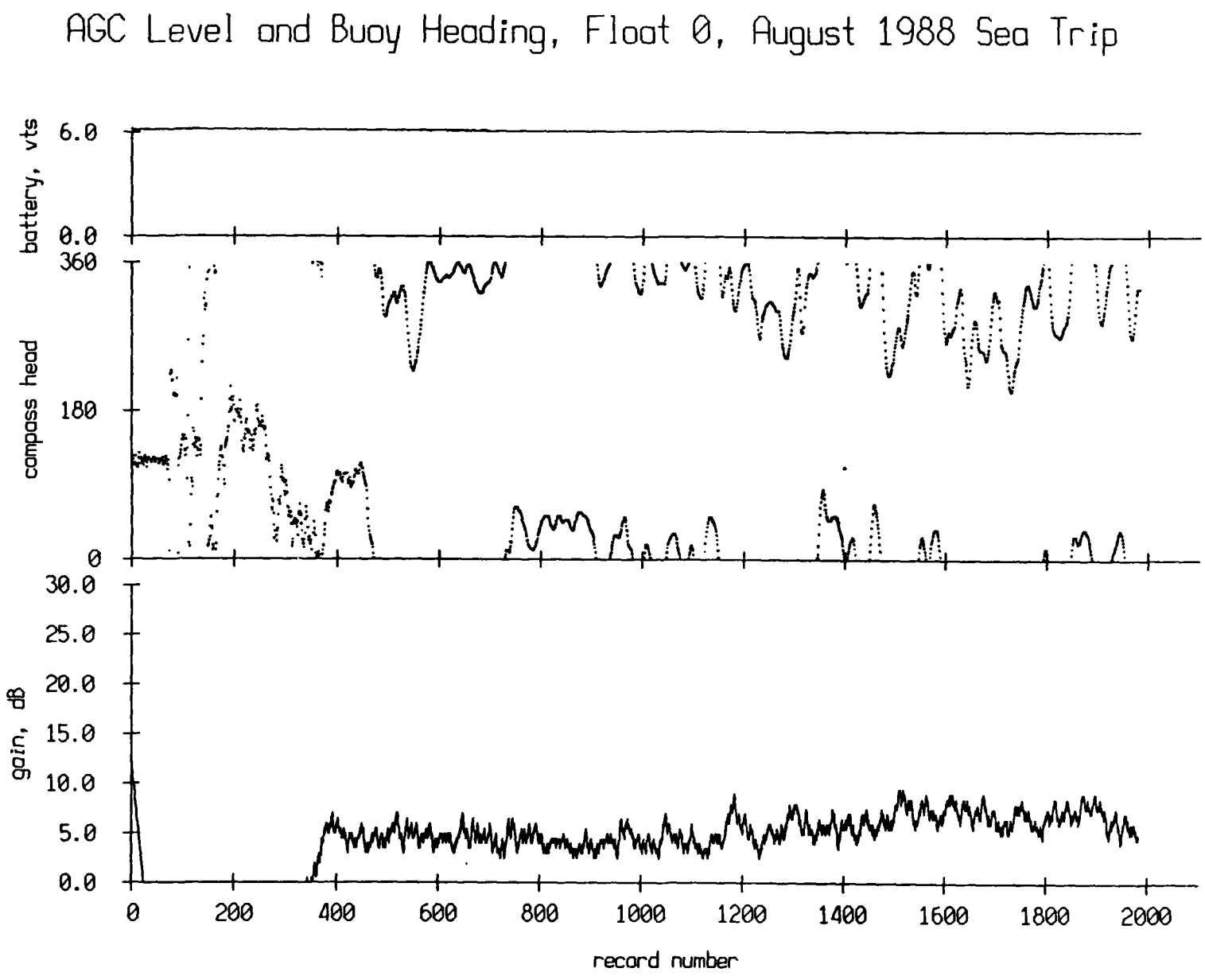

AGC Level and Buoy Heading, Float 0, August 1988 Sea Trip
battery, vts
6.0
0.0
compass head
360
180
0
gain, dB
30.0
25.0
20.0
15.0
10.0
5.0
0.0
0
200
400
600
800
1000
1200
1400
1600
1800
2000
record number

Figure VII.4

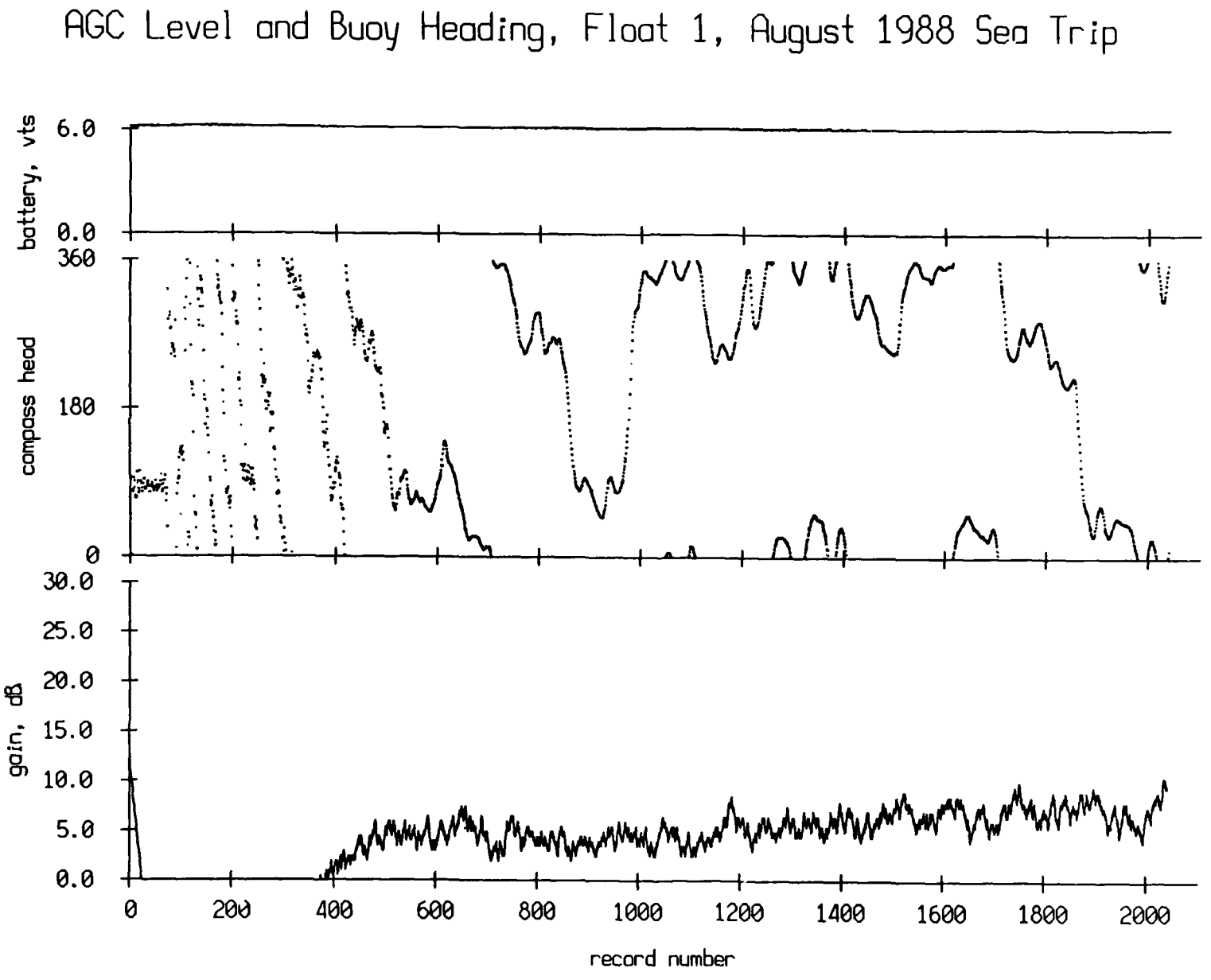

AGC Level and Buoy Heading, Float 1, August 1988 Sea Trip
battery, vts
6.0
0.0
compass head
360
180
0
gain, dB
30.0
25.0
20.0
15.0
10.0
5.0
0.0
0
200
400
600
800
1000
1200
1400
1600
1800
2000
record number

Figure VII.5

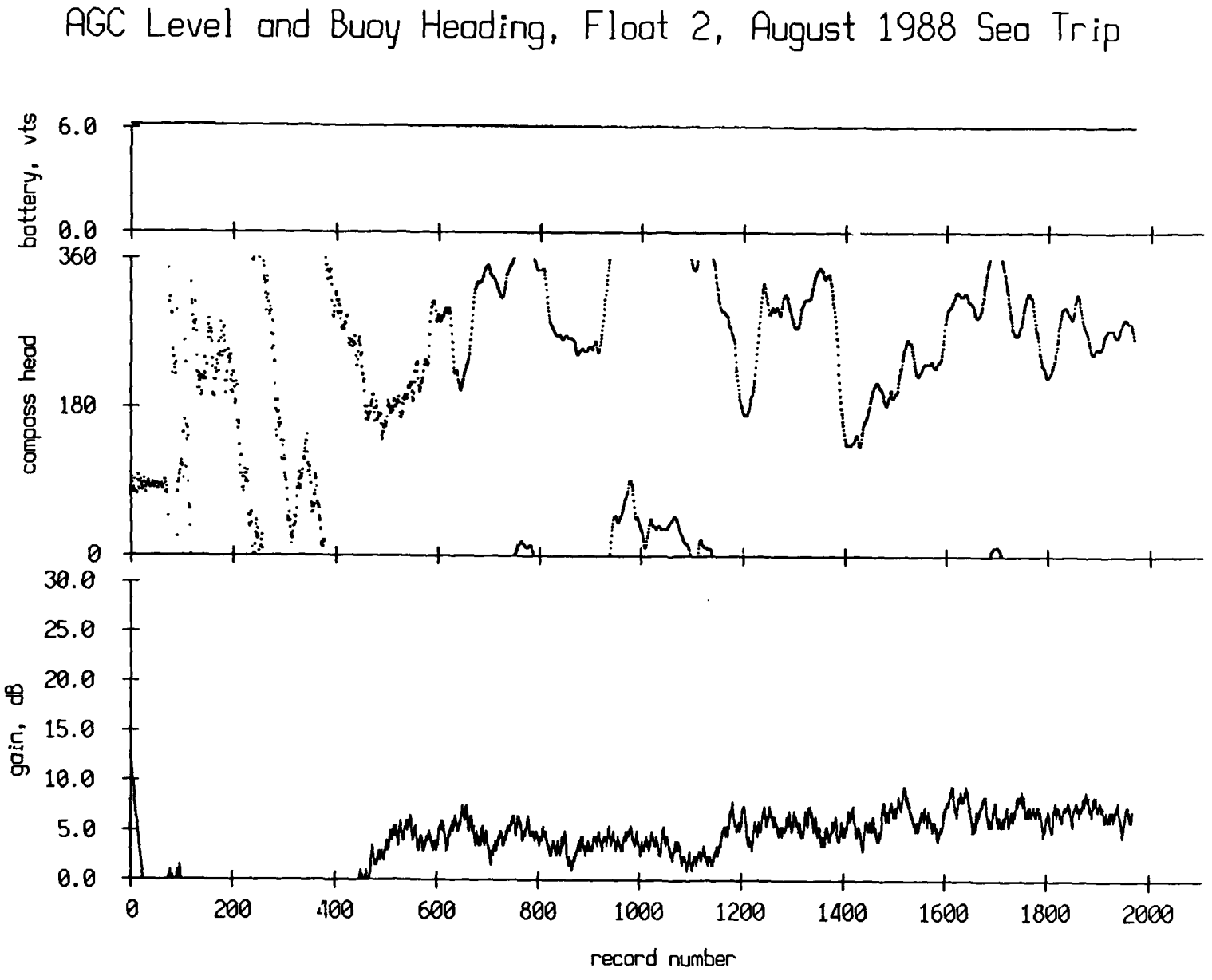

AGC Level and Buoy Heading, Float 2, August 1988 Sea Trip
battery, vts
6.0
0.0
compass head
360
180
0
gain, dB
30.0
25.0
20.0
15.0
10.0
5.0
0.0
0
200
400
600
800
1000
1200
1400
1600
1800
2000
record number

Figure VII.6

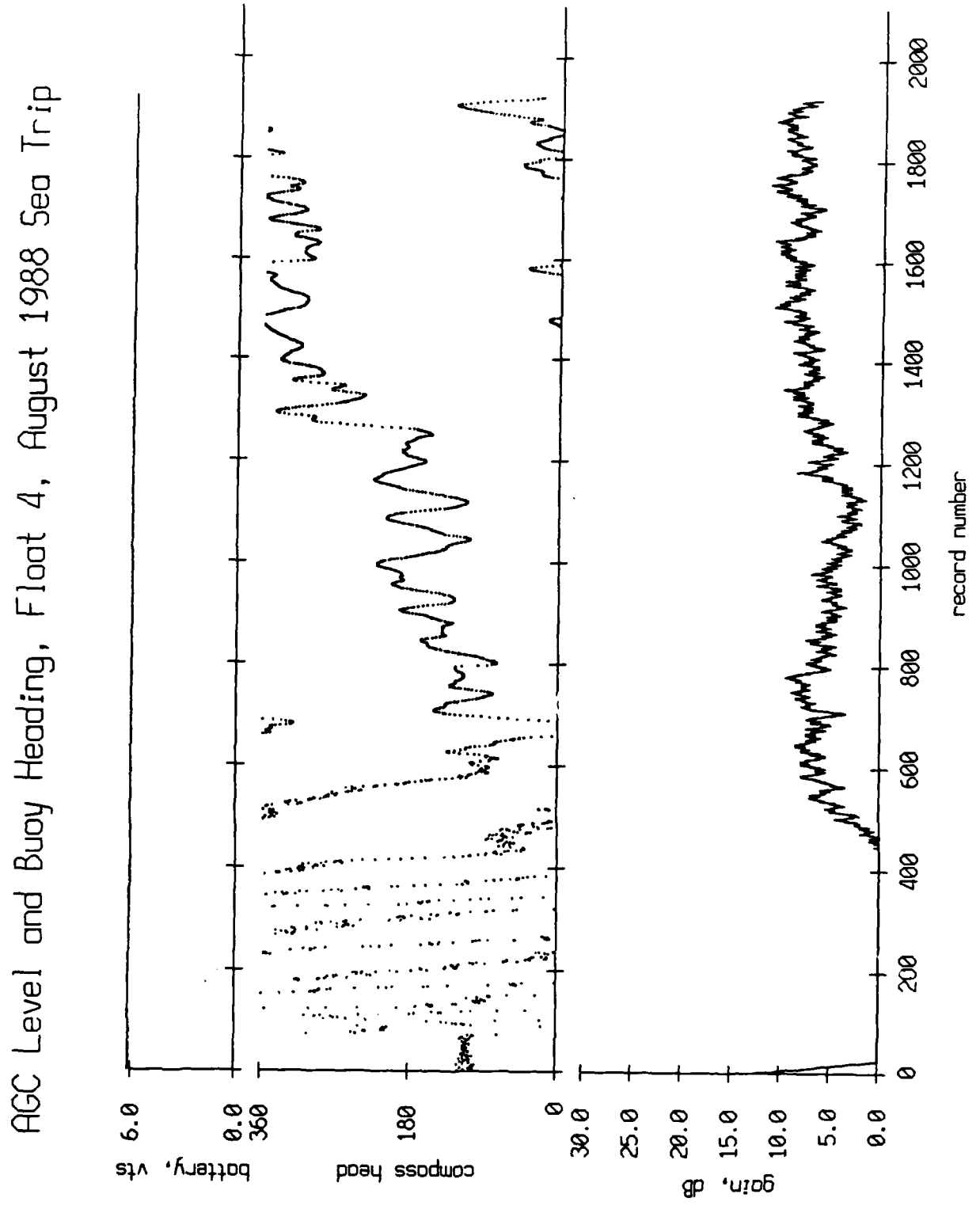

AGC Level and Buoy Heading, Float 4, August 1988 Sea Trip
battery, vts
6.0
0.0
compass head
360
180
0
gain, db
30.0
25.0
20.0
15.0
10.0
5.0
0.0
0
200
400
600
800
1000
1200
1400
1600
1800
2000
record number

Figure VII.7

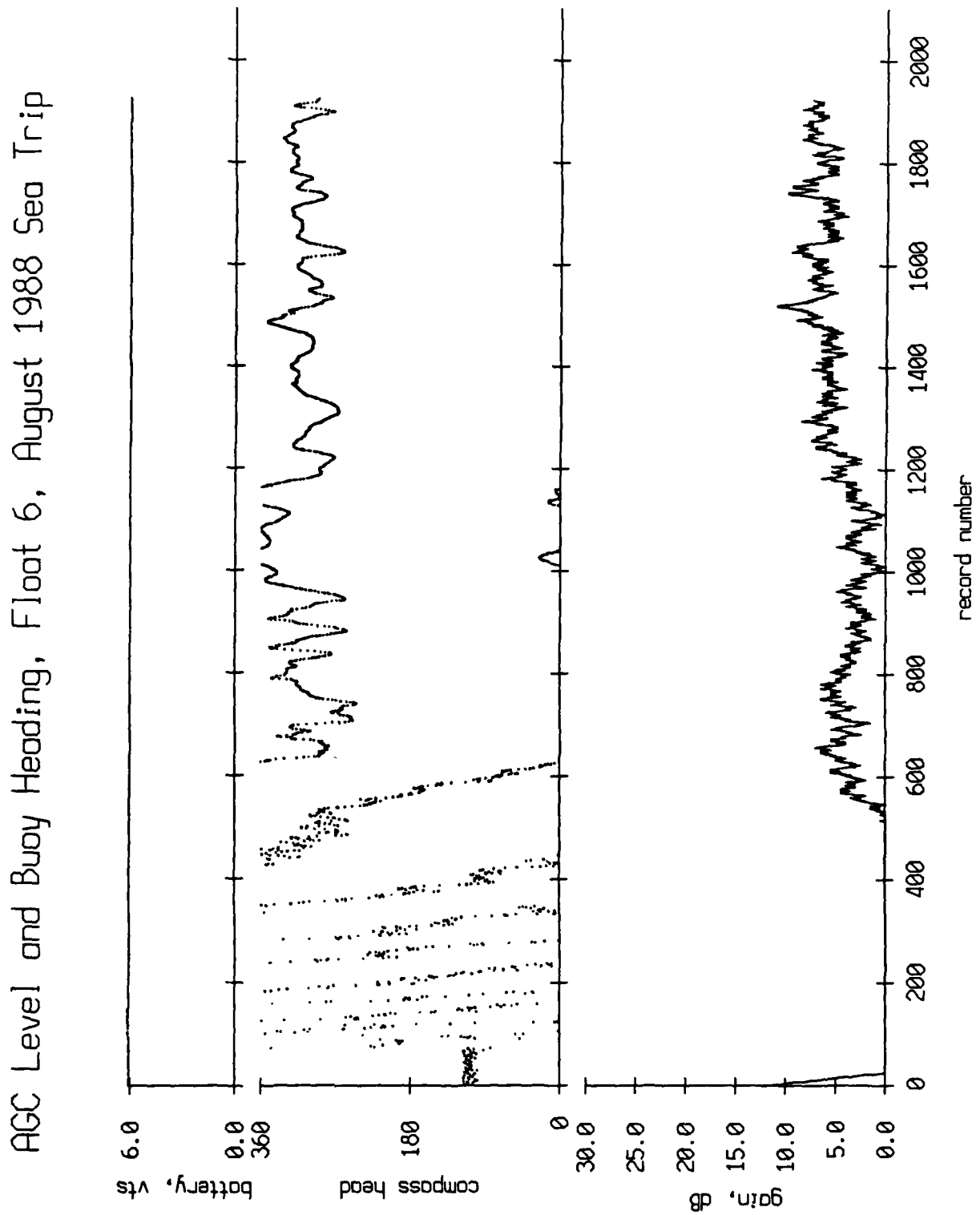

AGC Level and Buoy Heading, Float 6, August 1988 Sea Trip
battery, vts
6.0
0.0
compass head
360
180
0
gain, db
30.0
25.0
20.0
15.0
10.0
5.0
0.0
0
200
400
600
800
1000
1200
1400
1600
1800
2000
record number

Figure VII.8

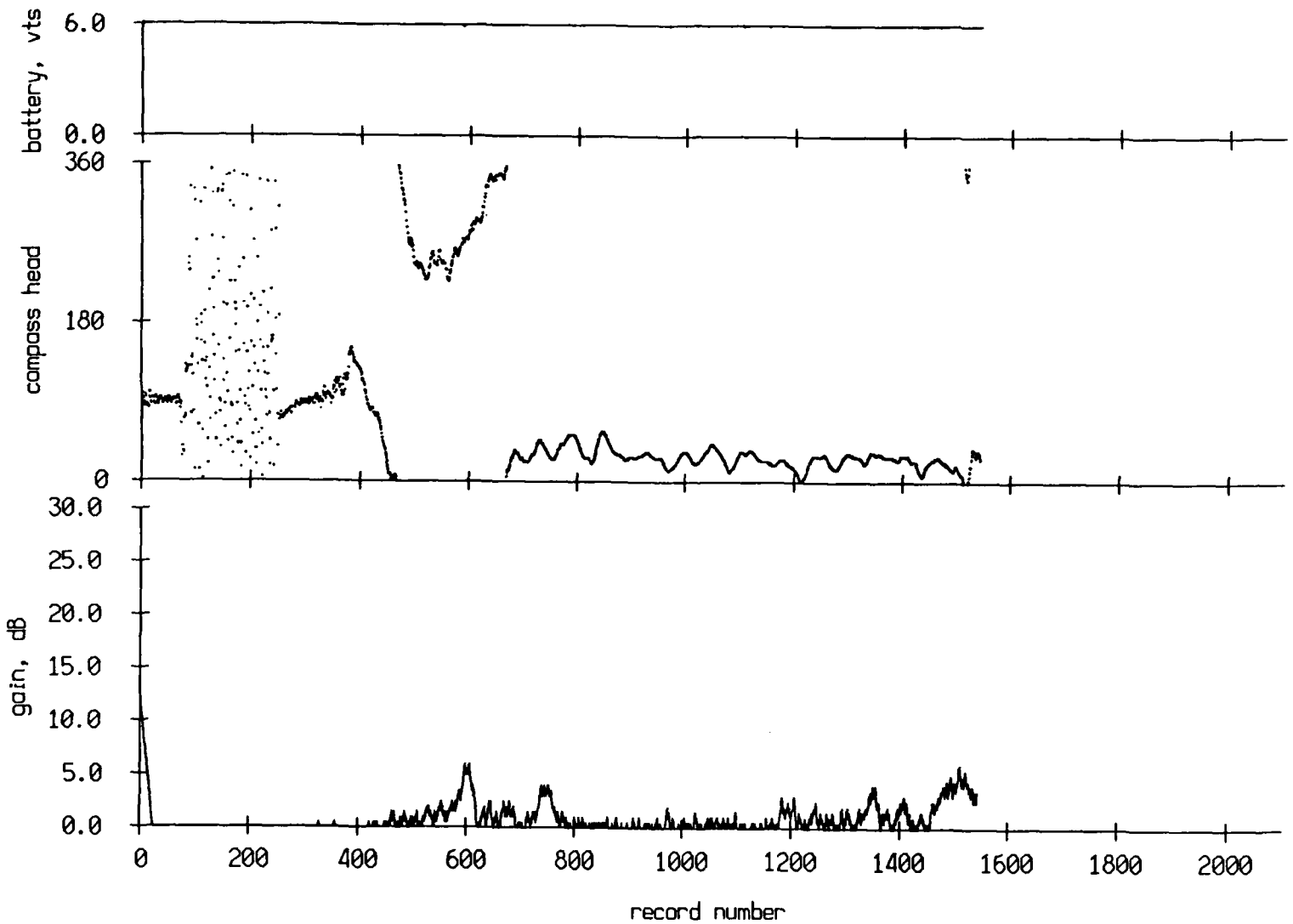

AGC Level and Buoy Heading, Float 11, August 1988 Sea Trip
battery, vts
6.0
0.0
compass head
360
180
0
gain, dB
30.0
25.0
20.0
15.0
10.0
5.0
0.0
0
200
400
600
800
1000
1200
1400
1600
1800
2000
record number

Figure VII.9

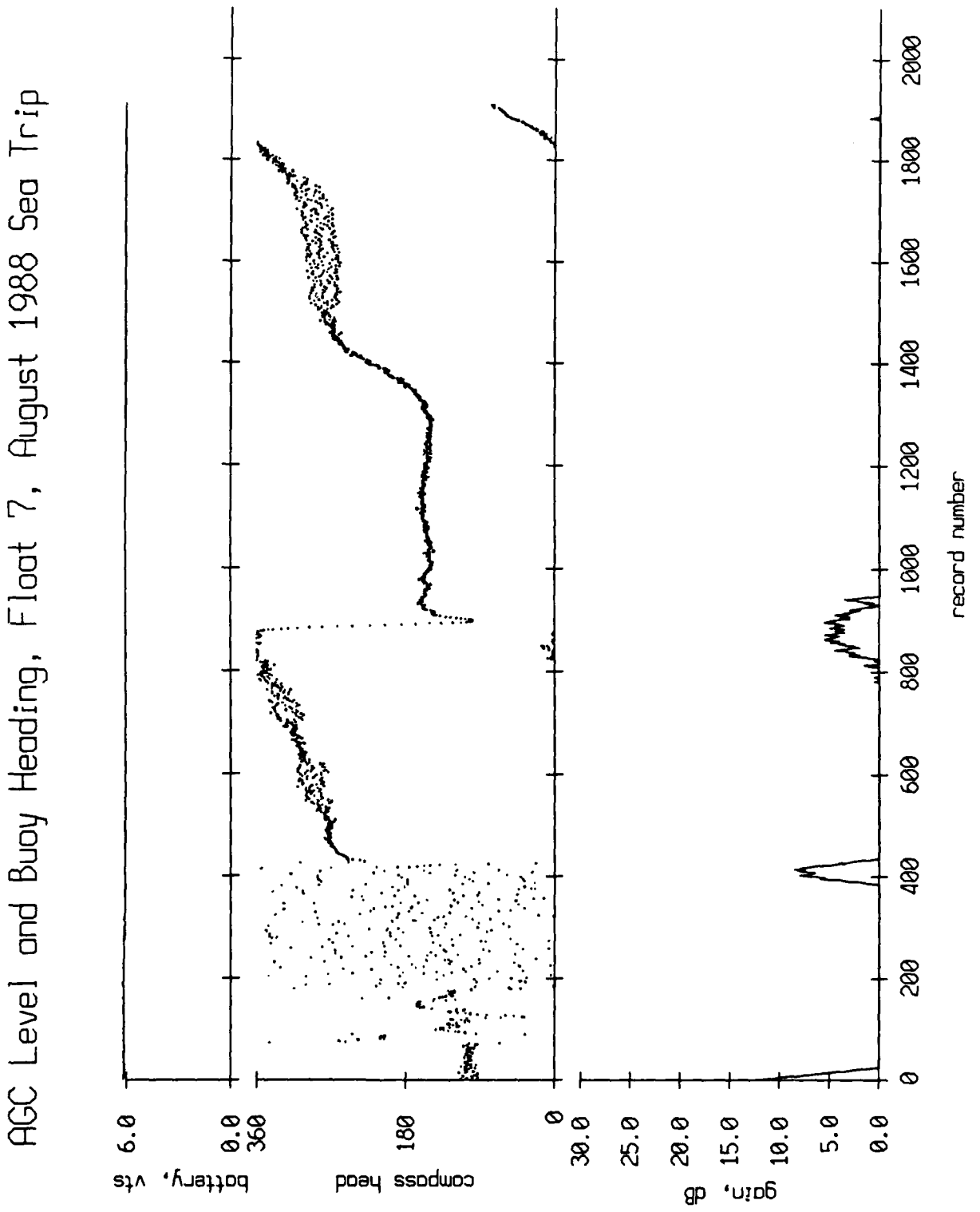


Figure VII.10

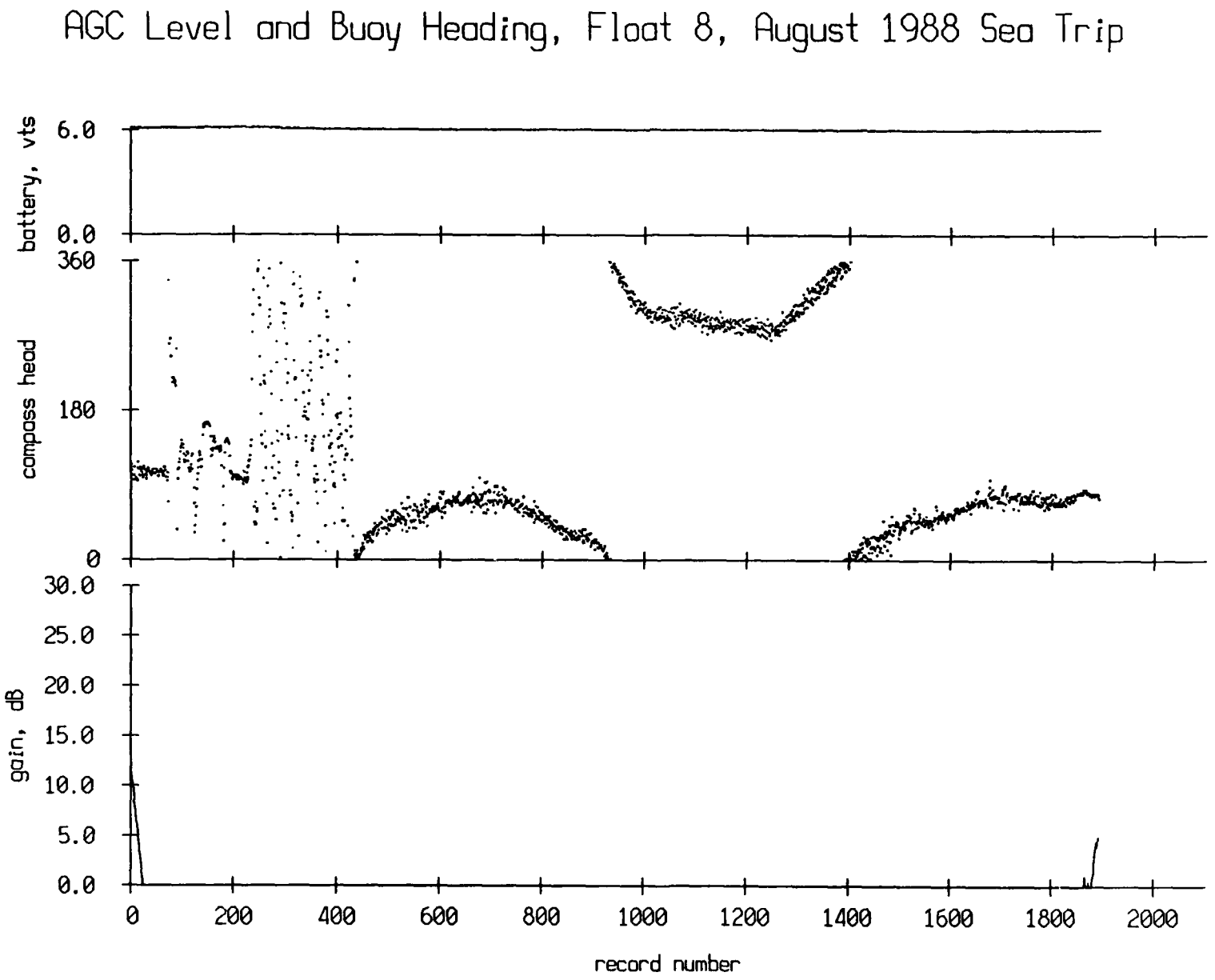


Figure VII.11

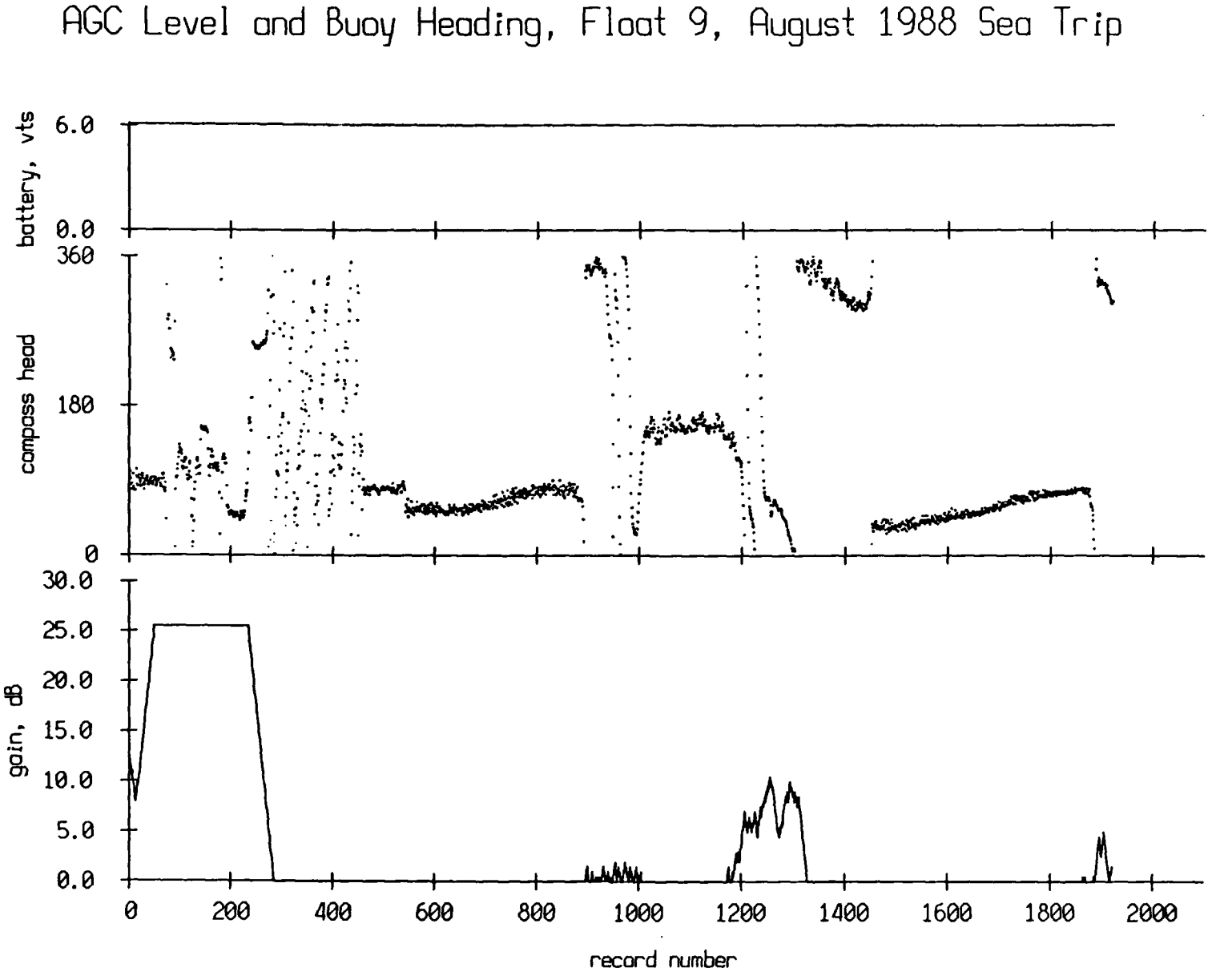


Figure VII.12

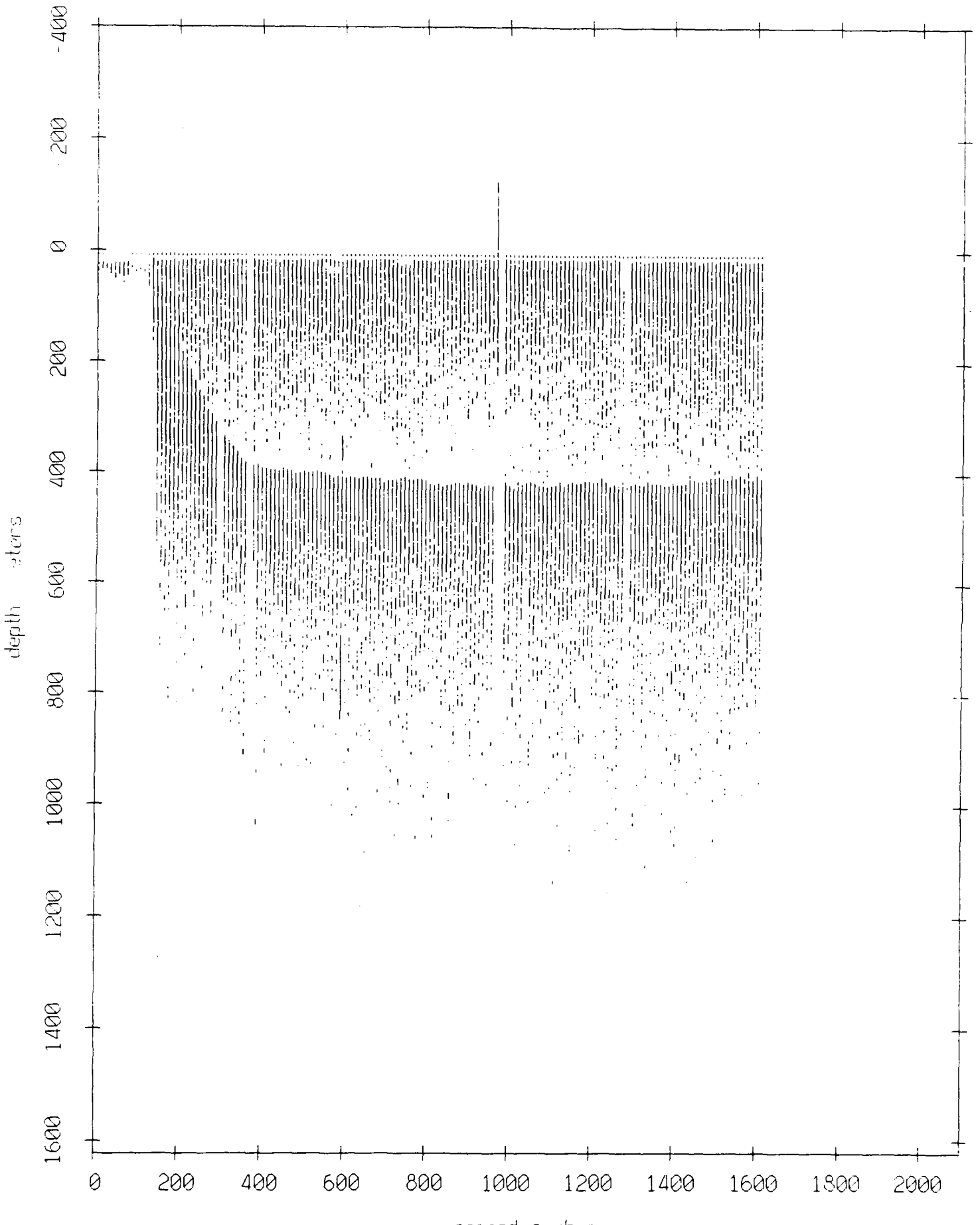


Figure VIII.1

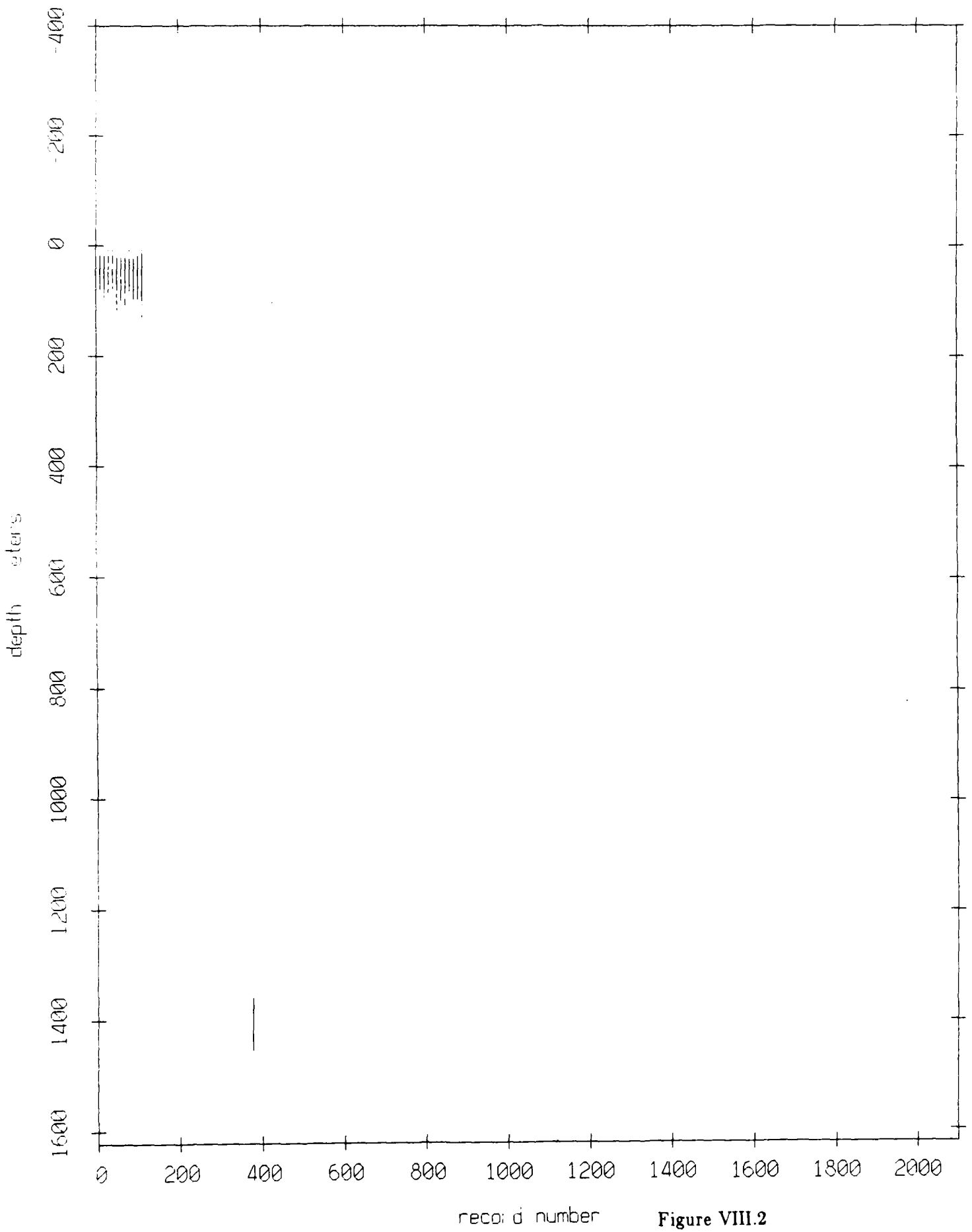


Figure VIII.2

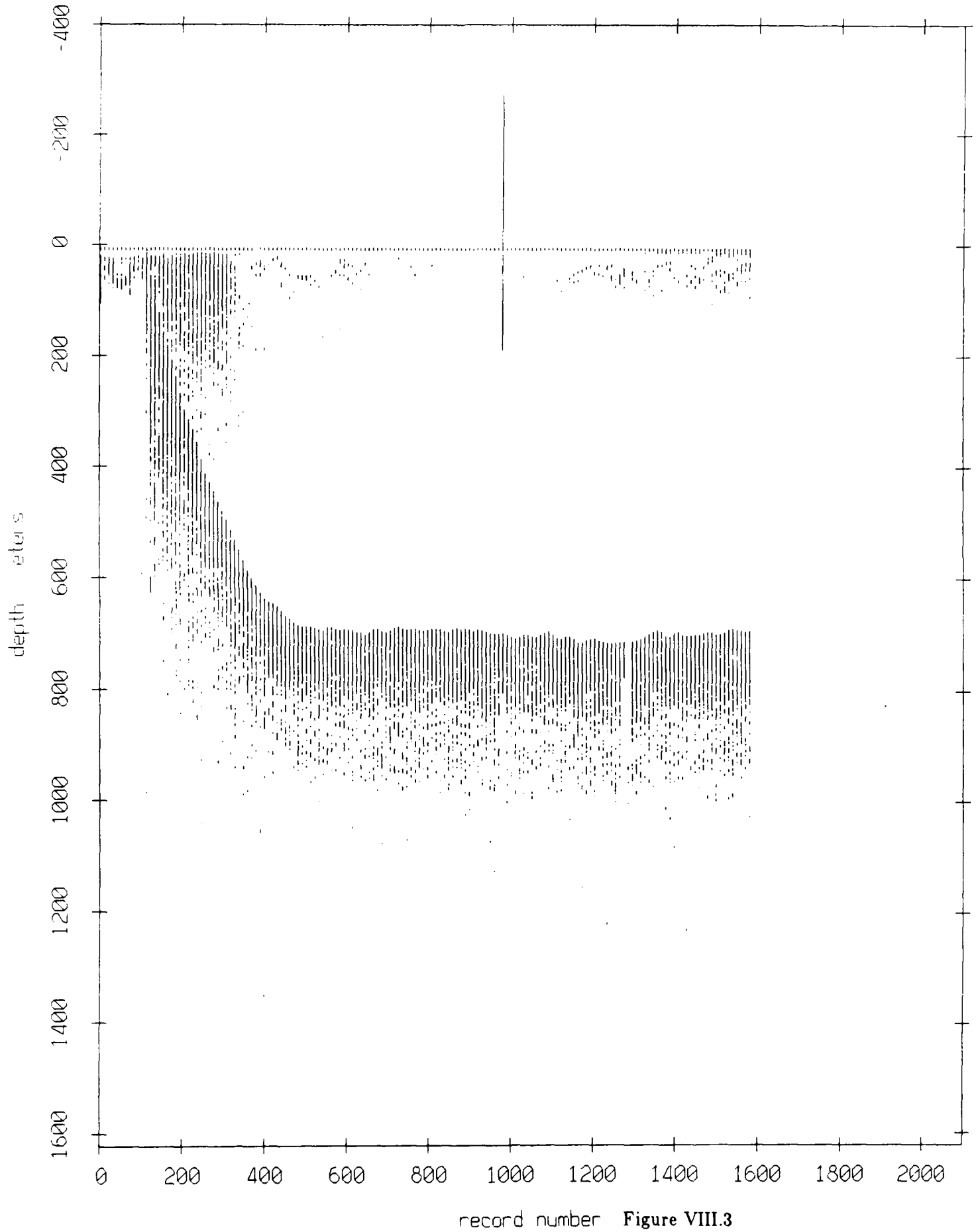


Figure VIII.3

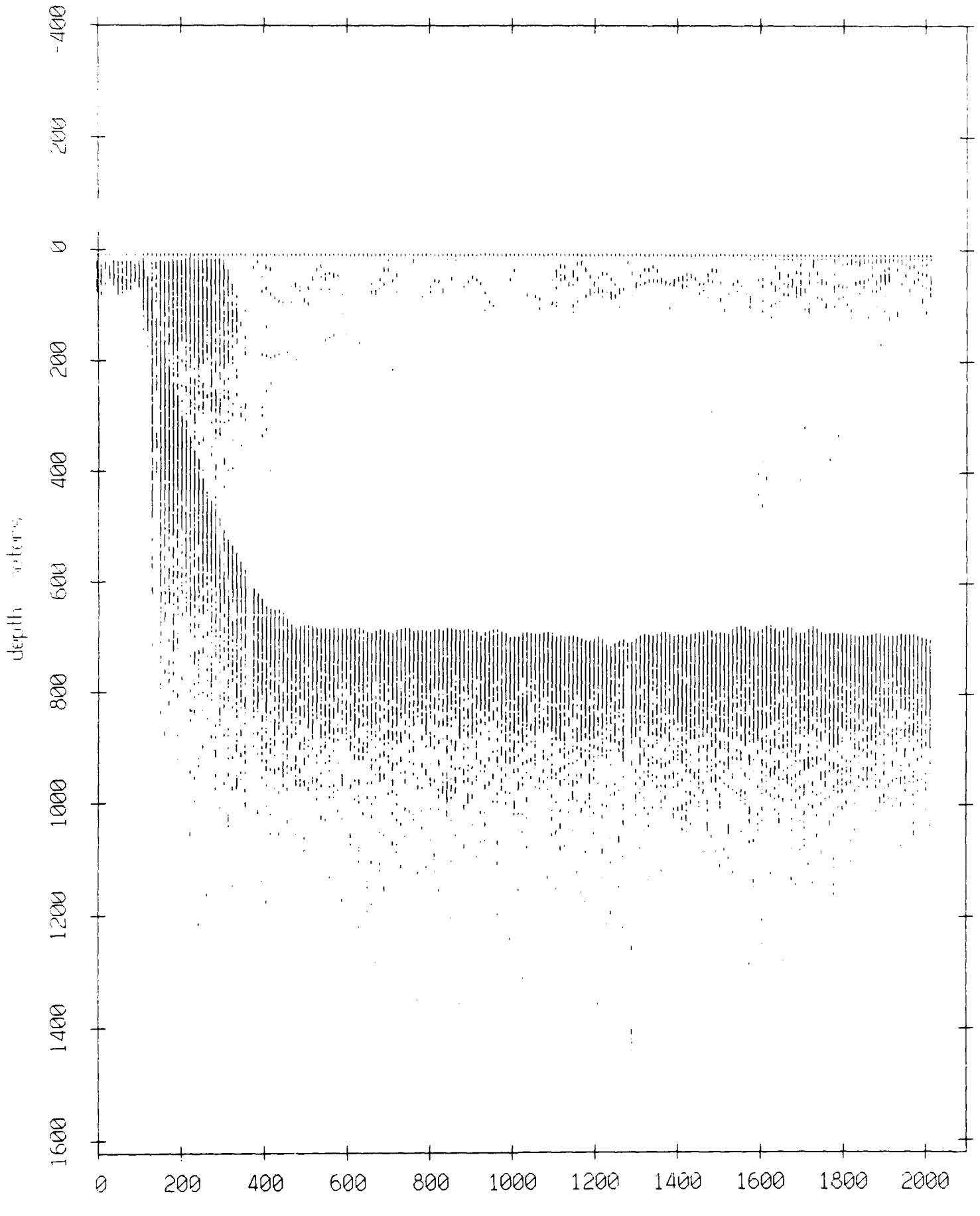


Figure VIII.4

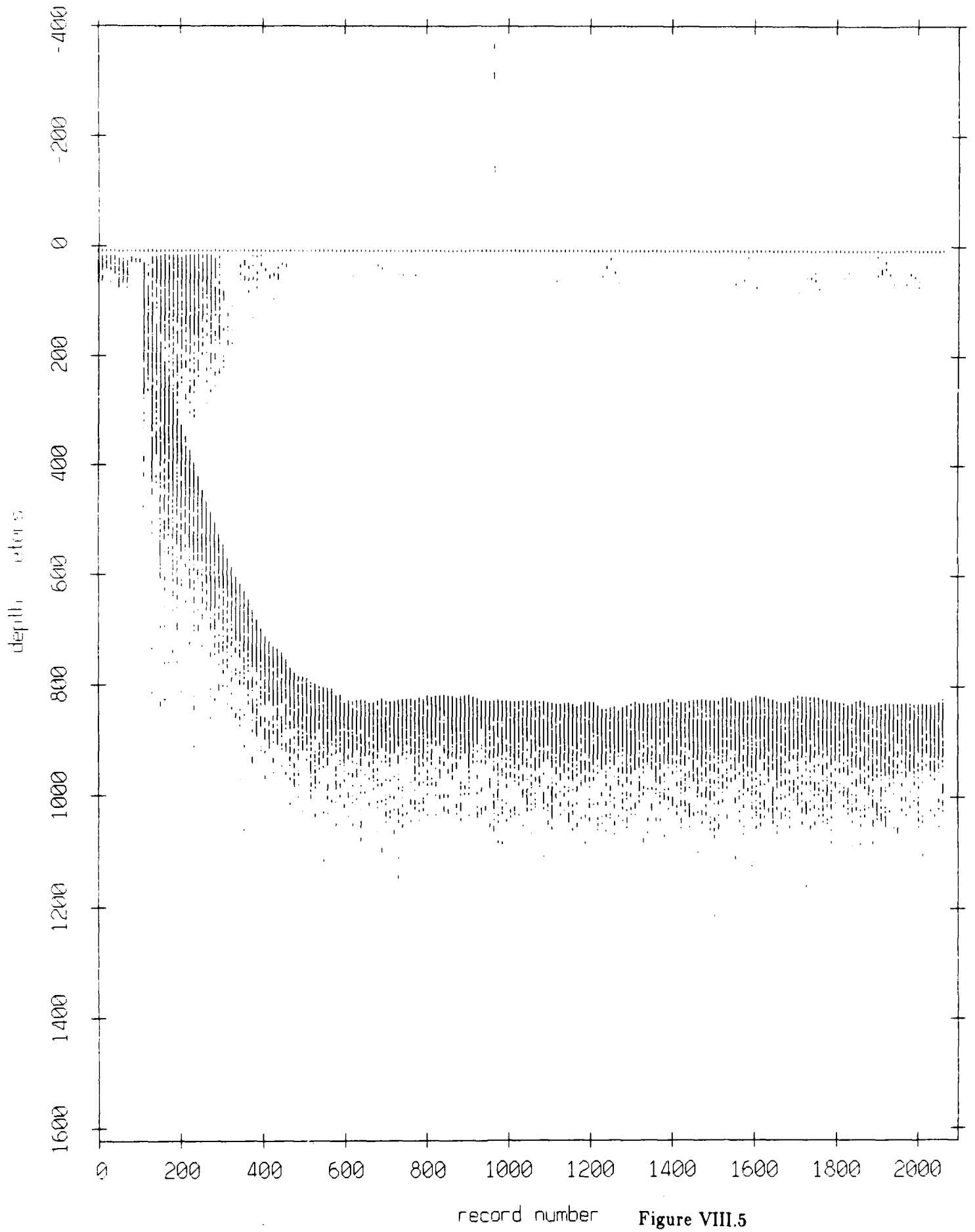


Figure VIII.5

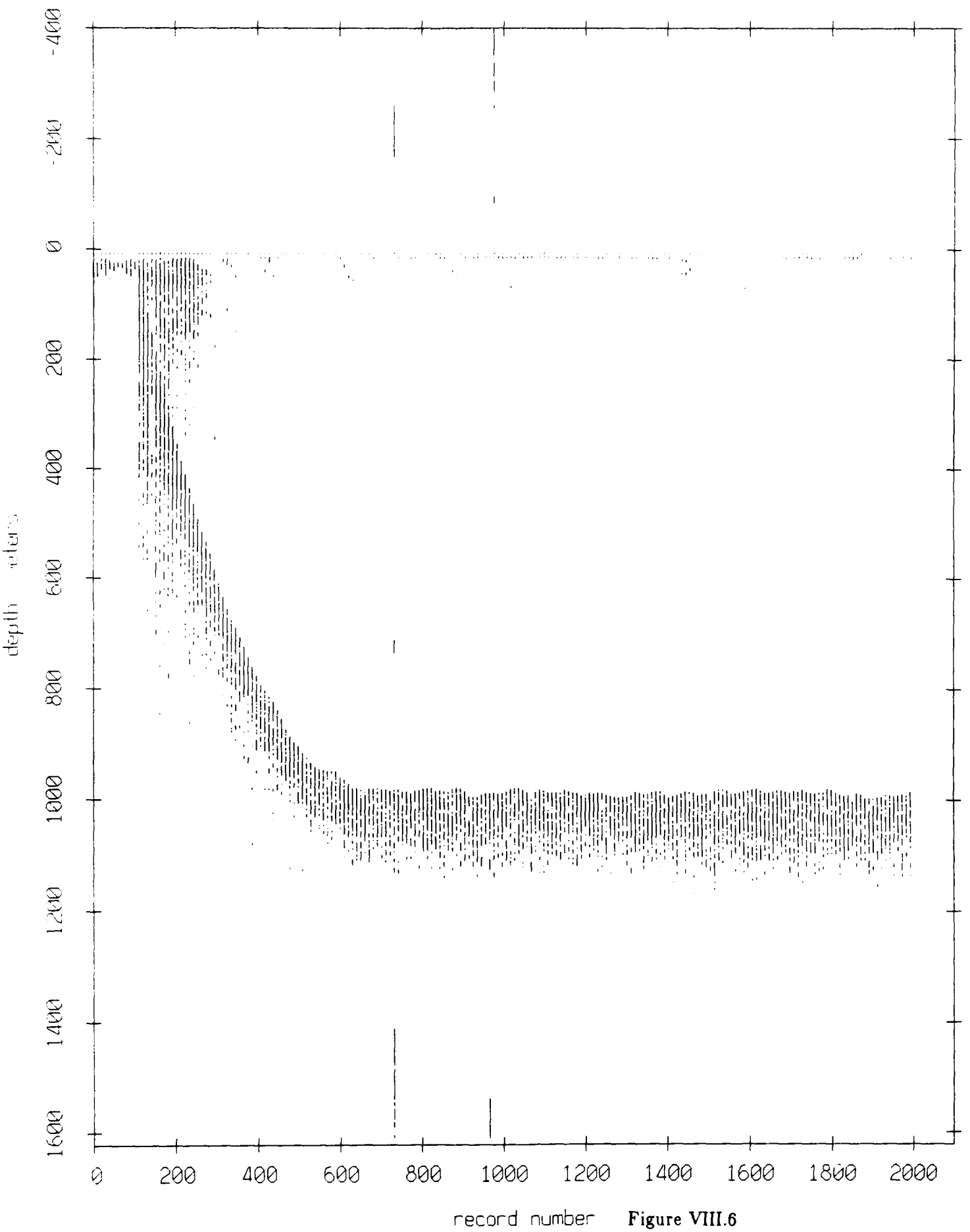


Figure VIII.6

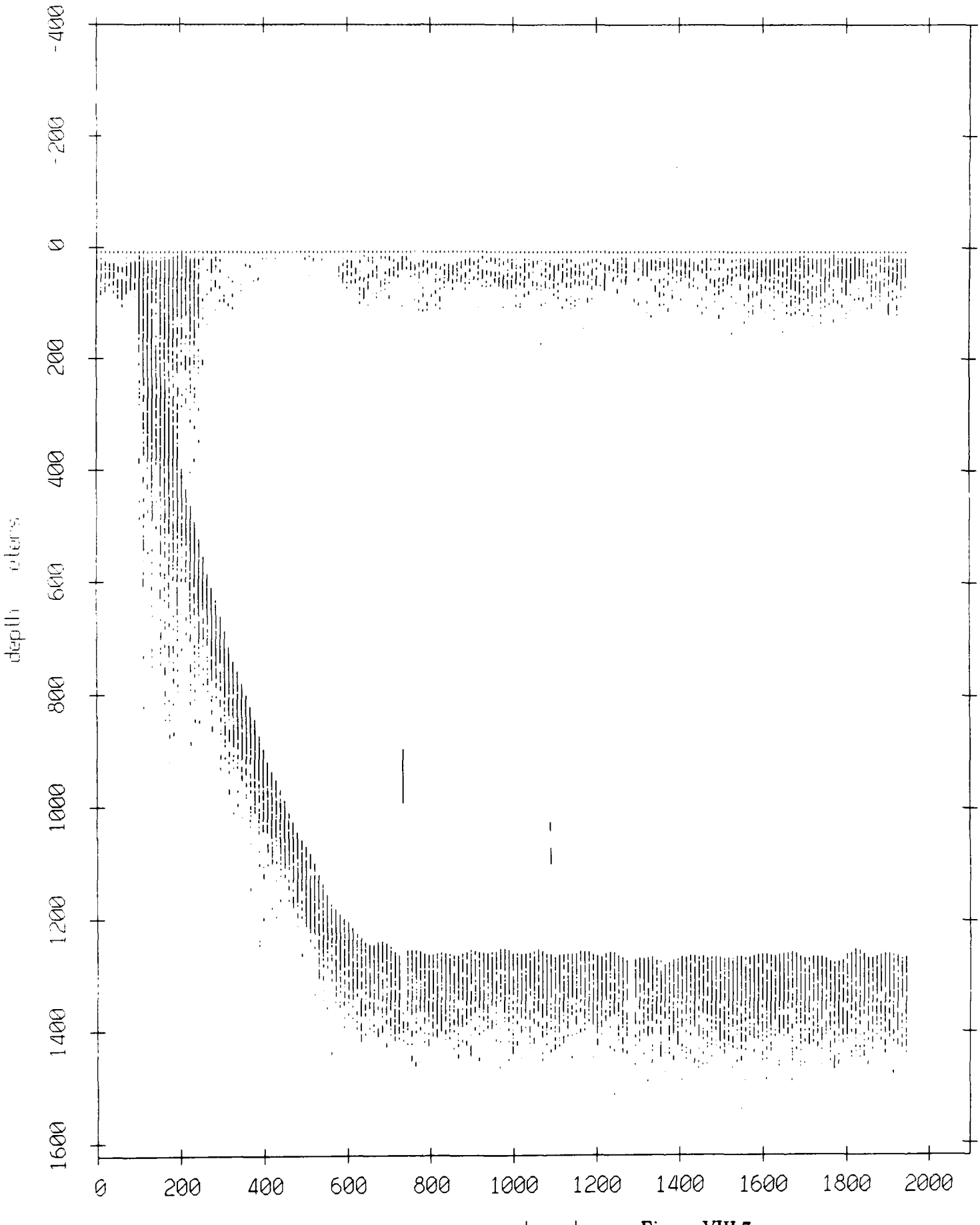


Figure VIII.7

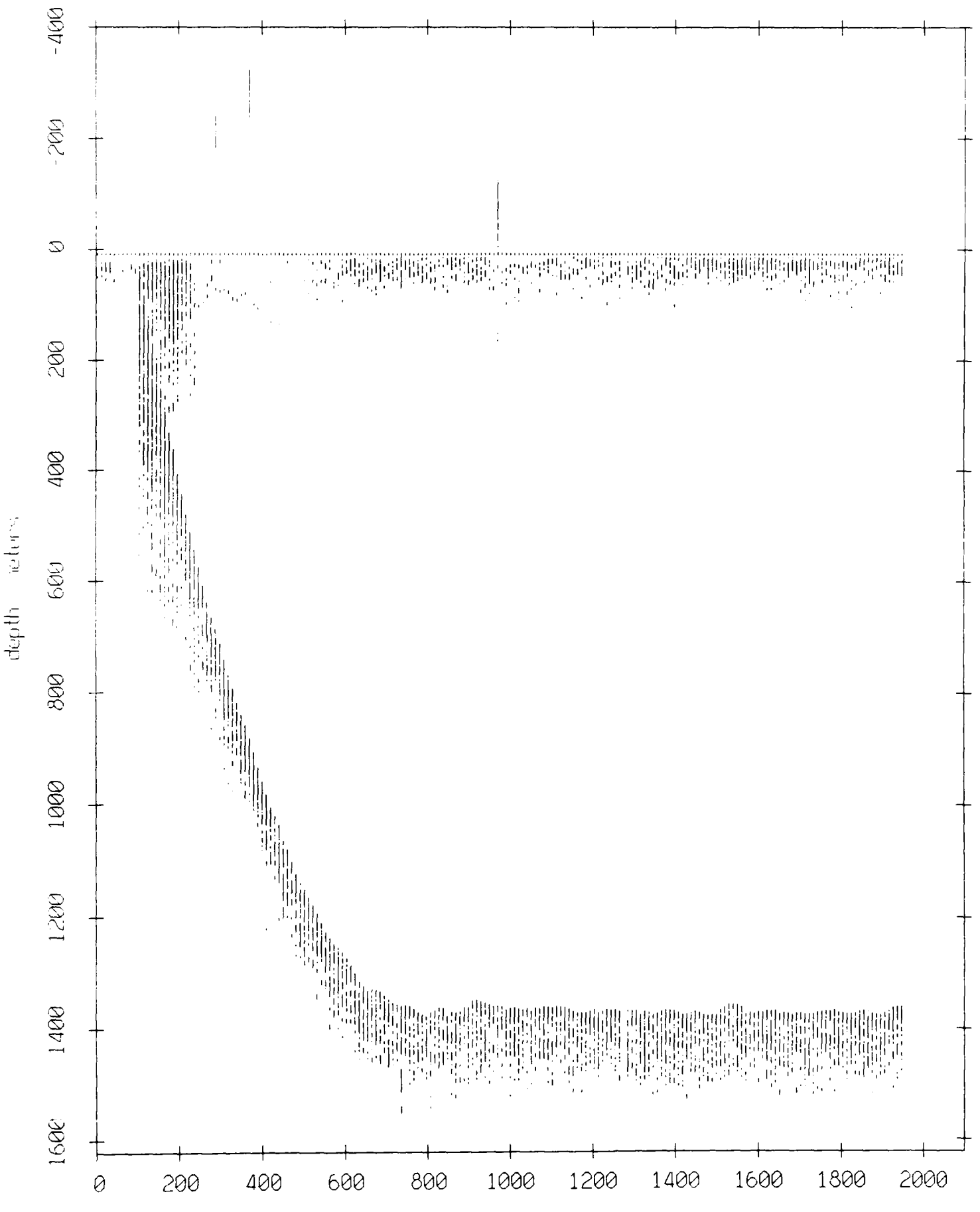


Figure VIII.8

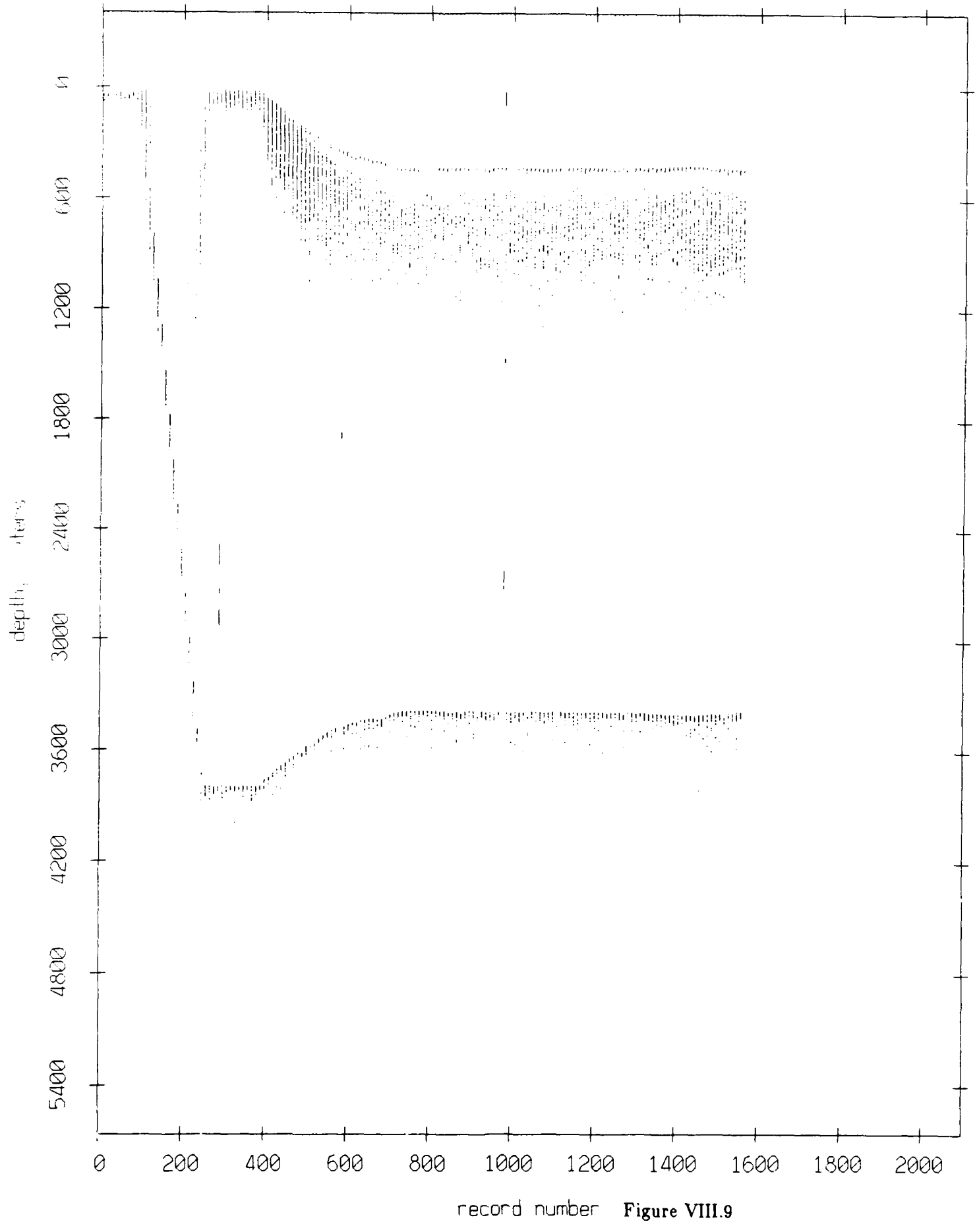


Figure VIII.9

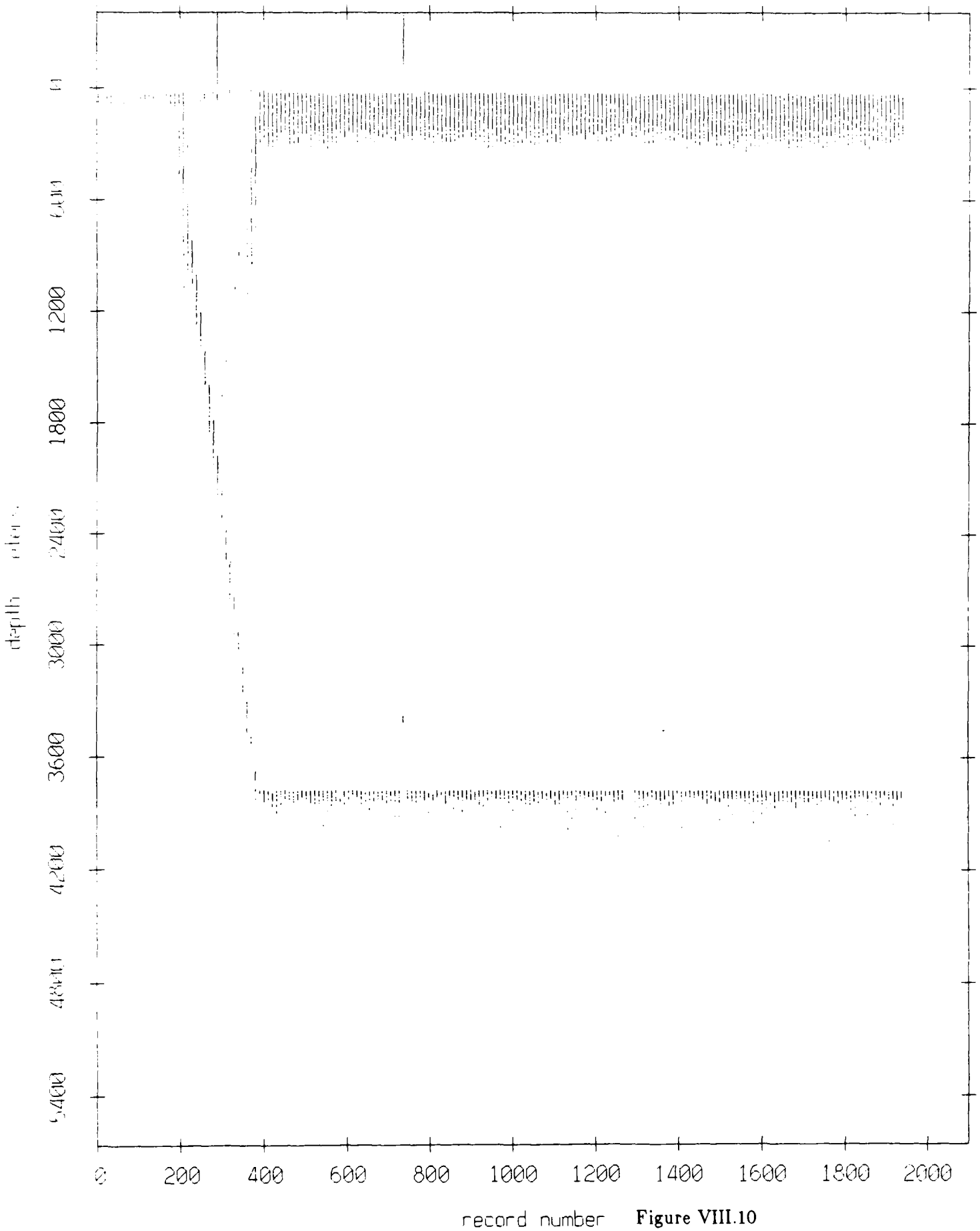


Figure VIII.10

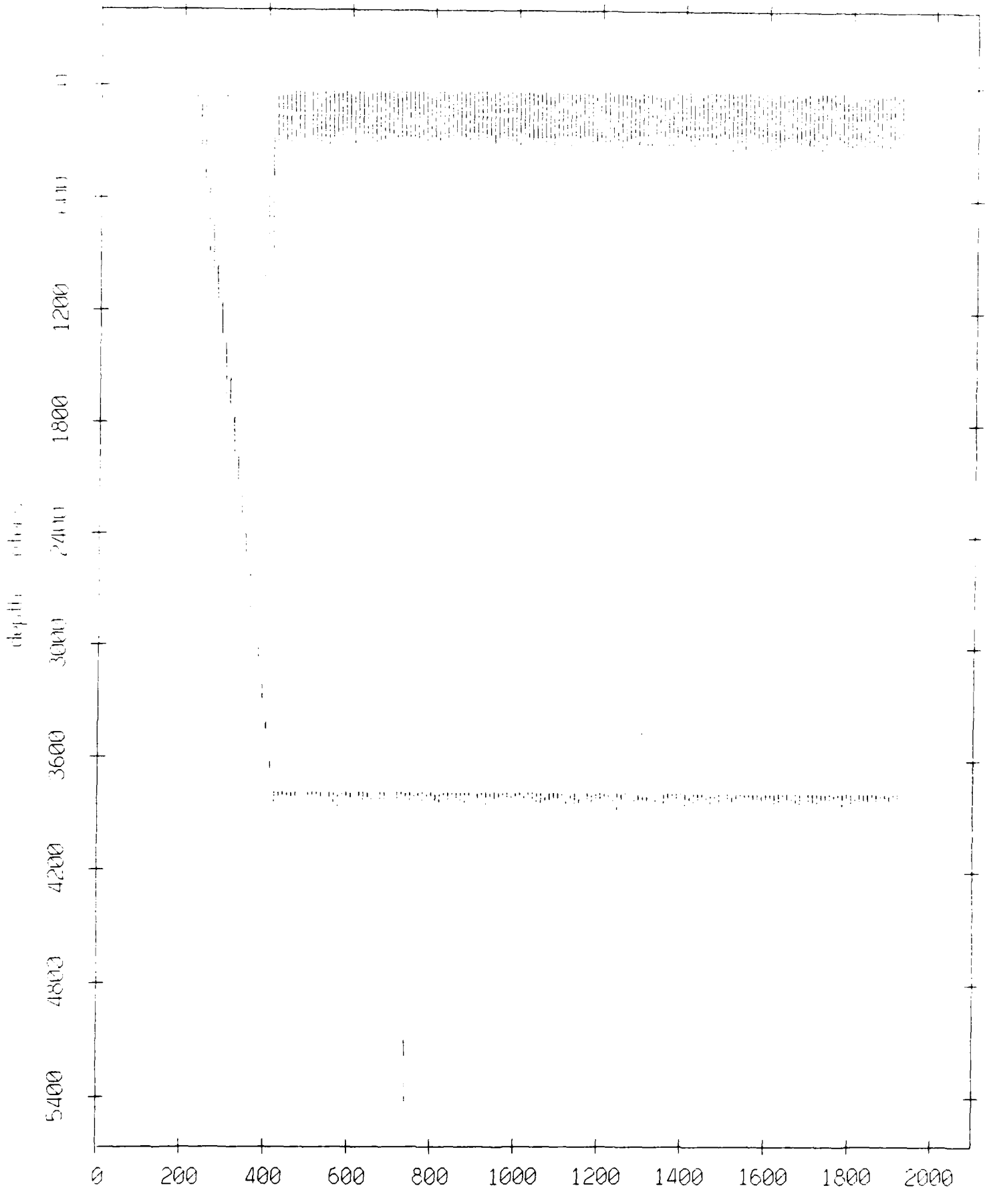


Figure VIII.11

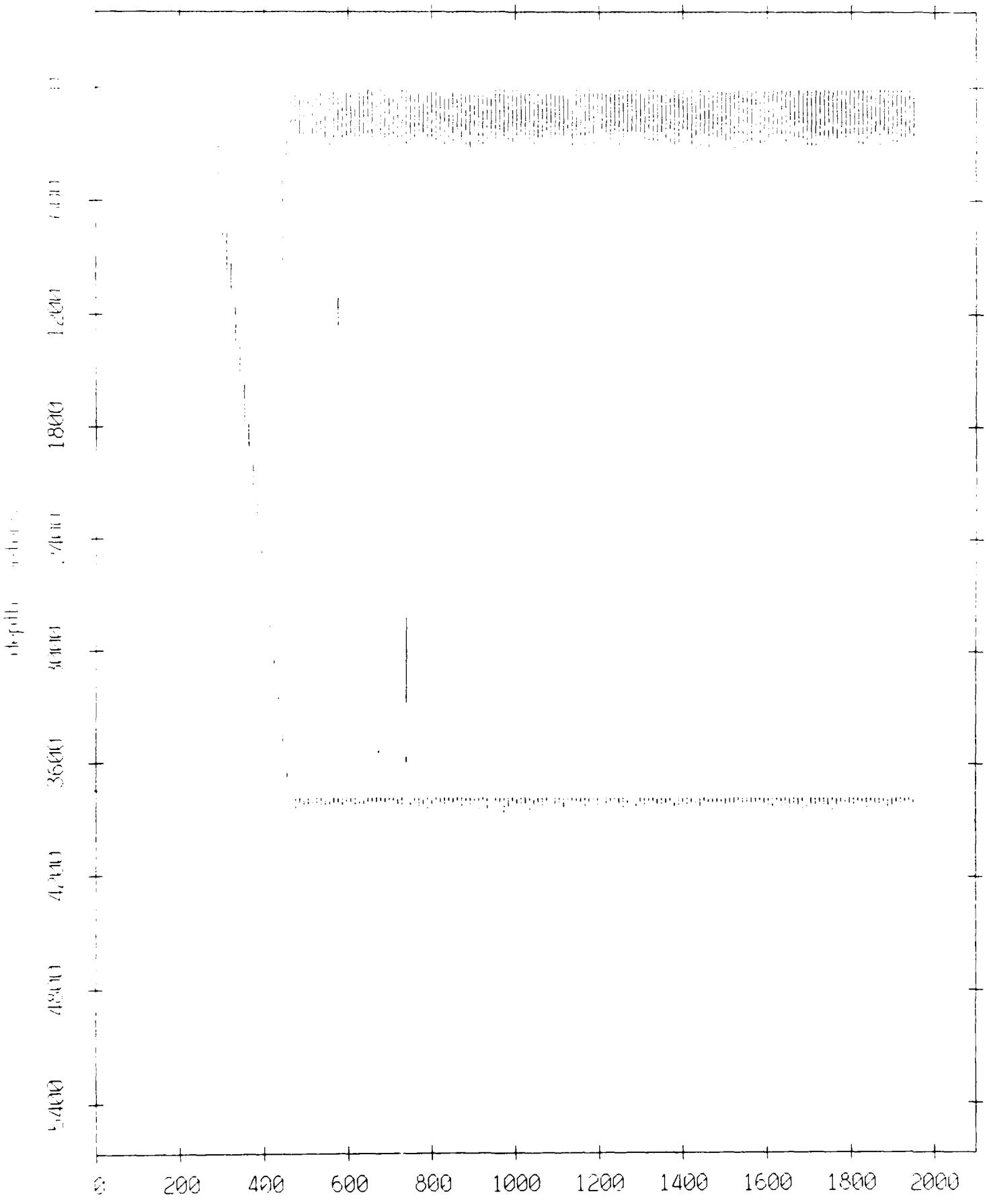


Figure VIII.12

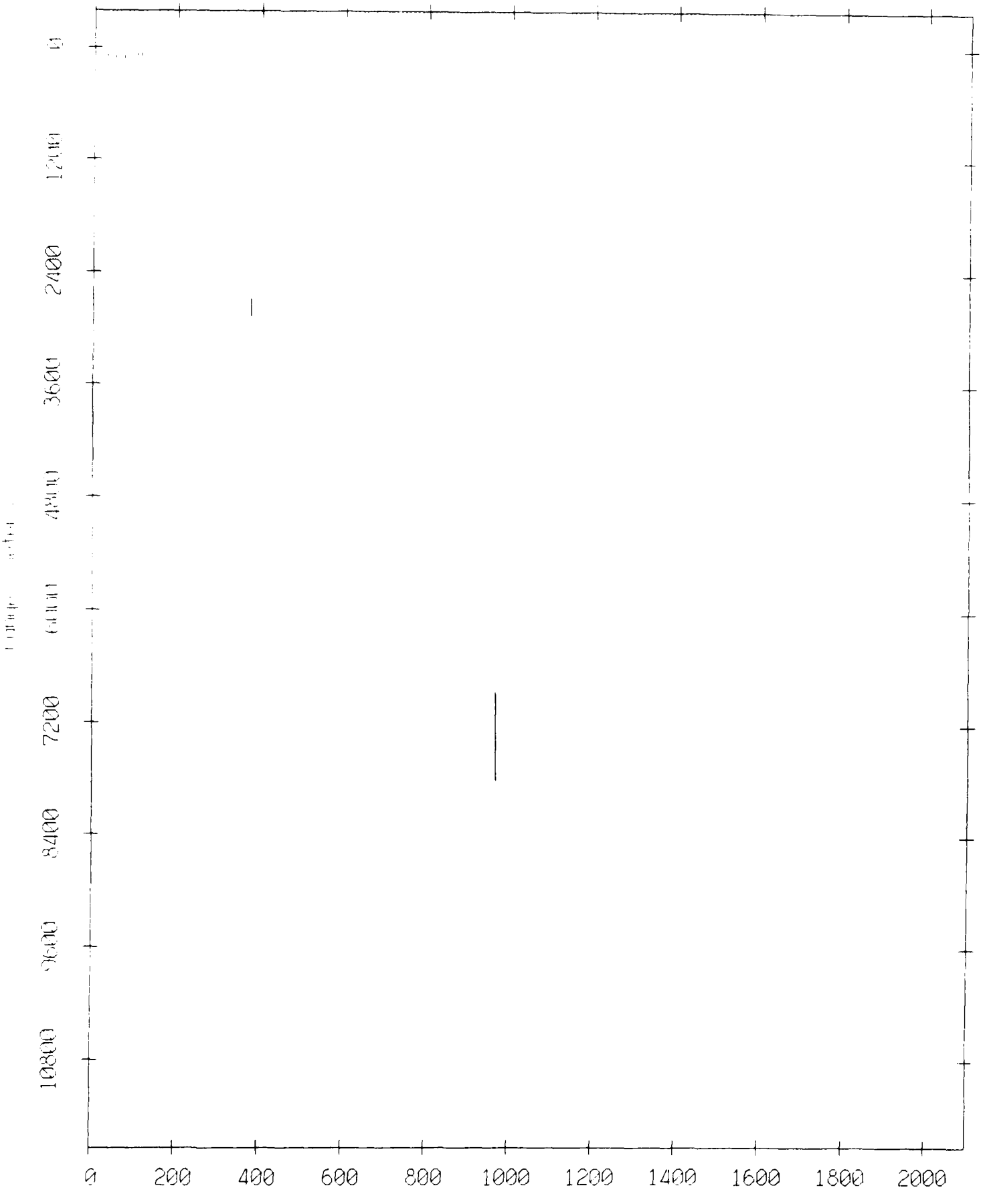

Float 10, August 1988 Experiment: range from float 3
0
2400
7200
10800
0
200
400
600
800
1000
1200
1400
1600
1800
2000
record number

Figure IX.1a

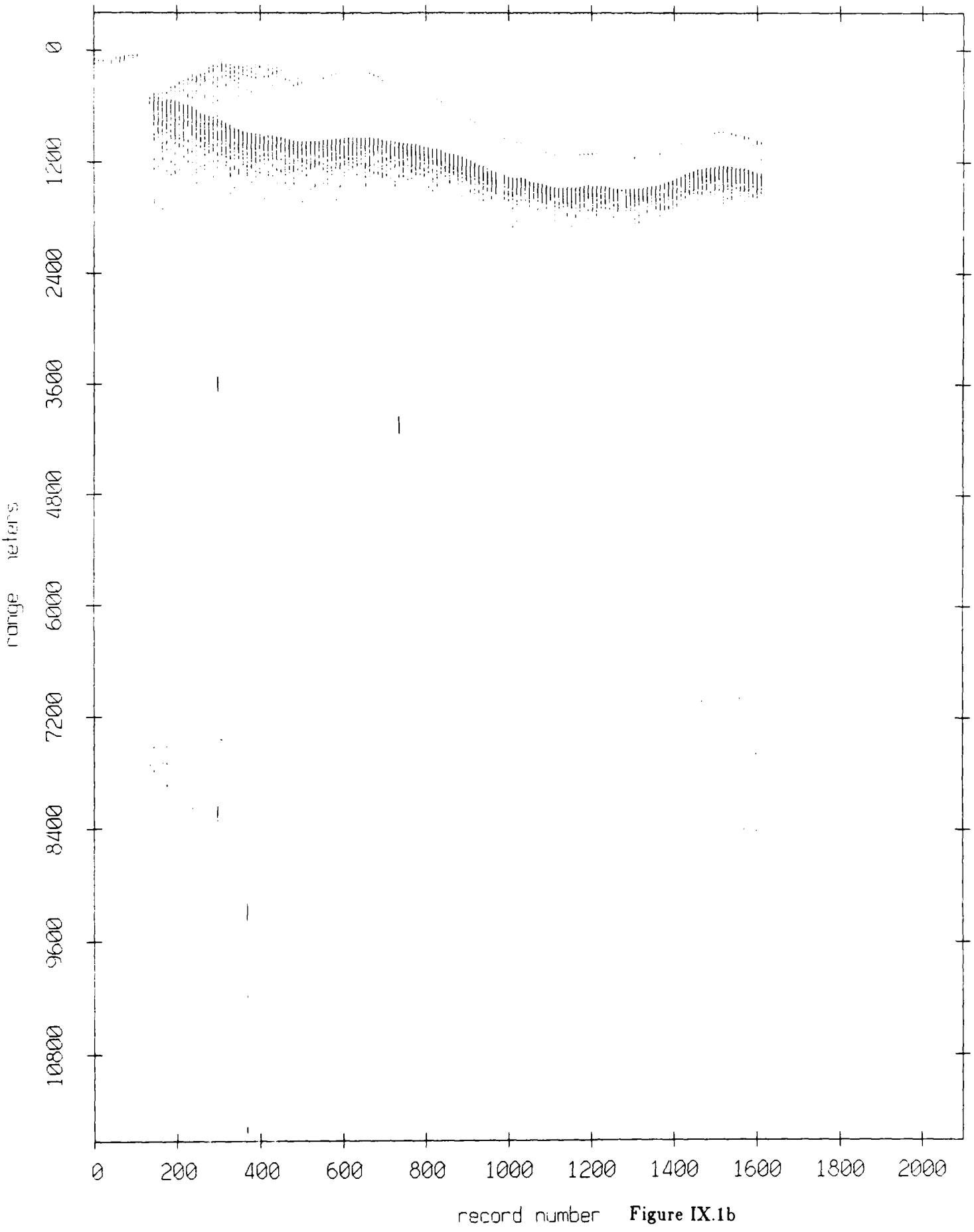

Float 10, August 1988 Experiment: range from float 5
range meters
0
1200
2400
3600
4800
6000
7200
8400
9600
10800
0
200
400
600
800
1000
1200
1400
1600
1800
2000
record number

Figure IX.1b

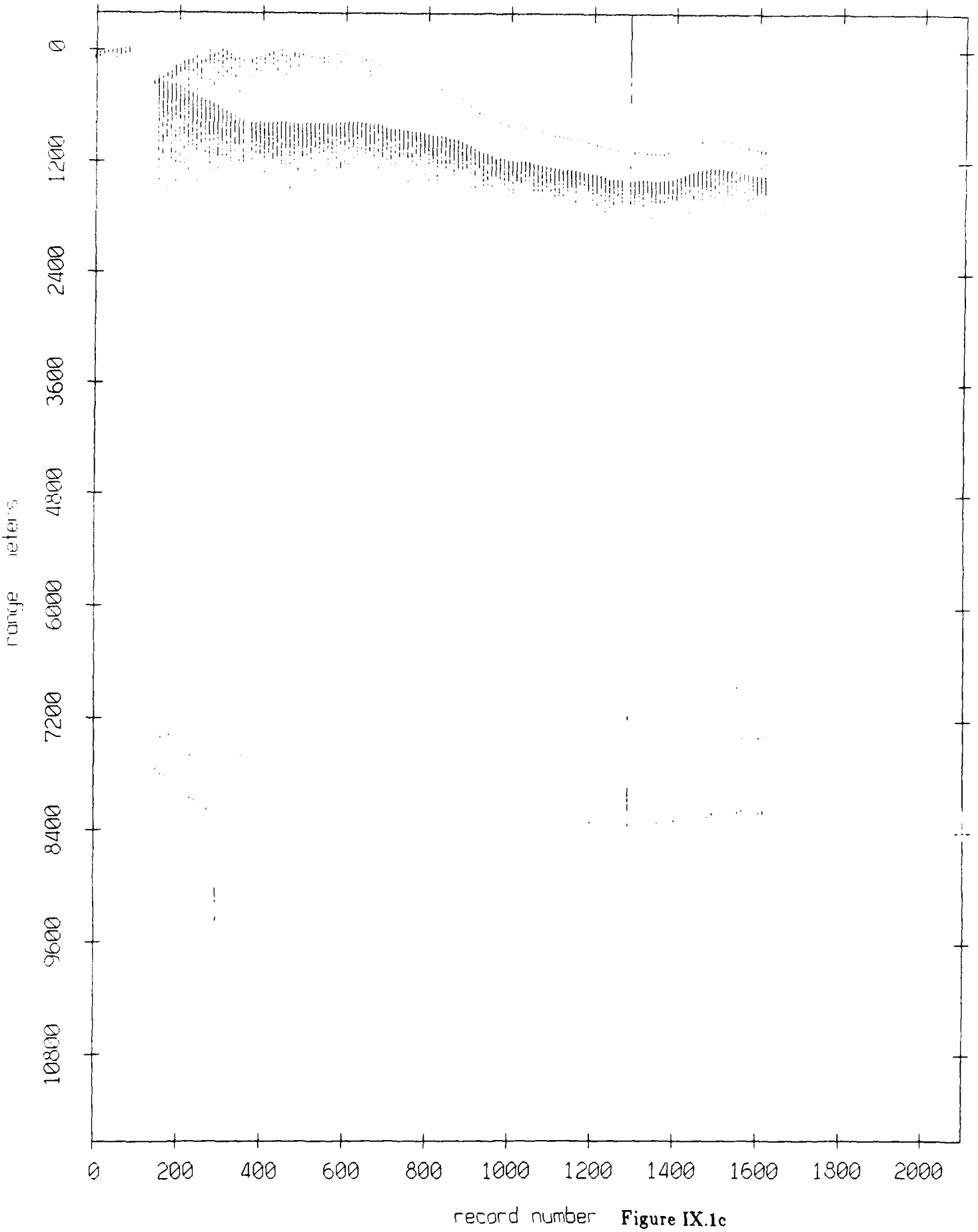

Float 10, August 1988 Experiment: range from float 0
range meters
0
1200
2400
3600
4800
6000
7200
8400
9600
10800
0
200
400
600
800
1000
1200
1400
1600
1800
2000
record number

Figure IX.1c

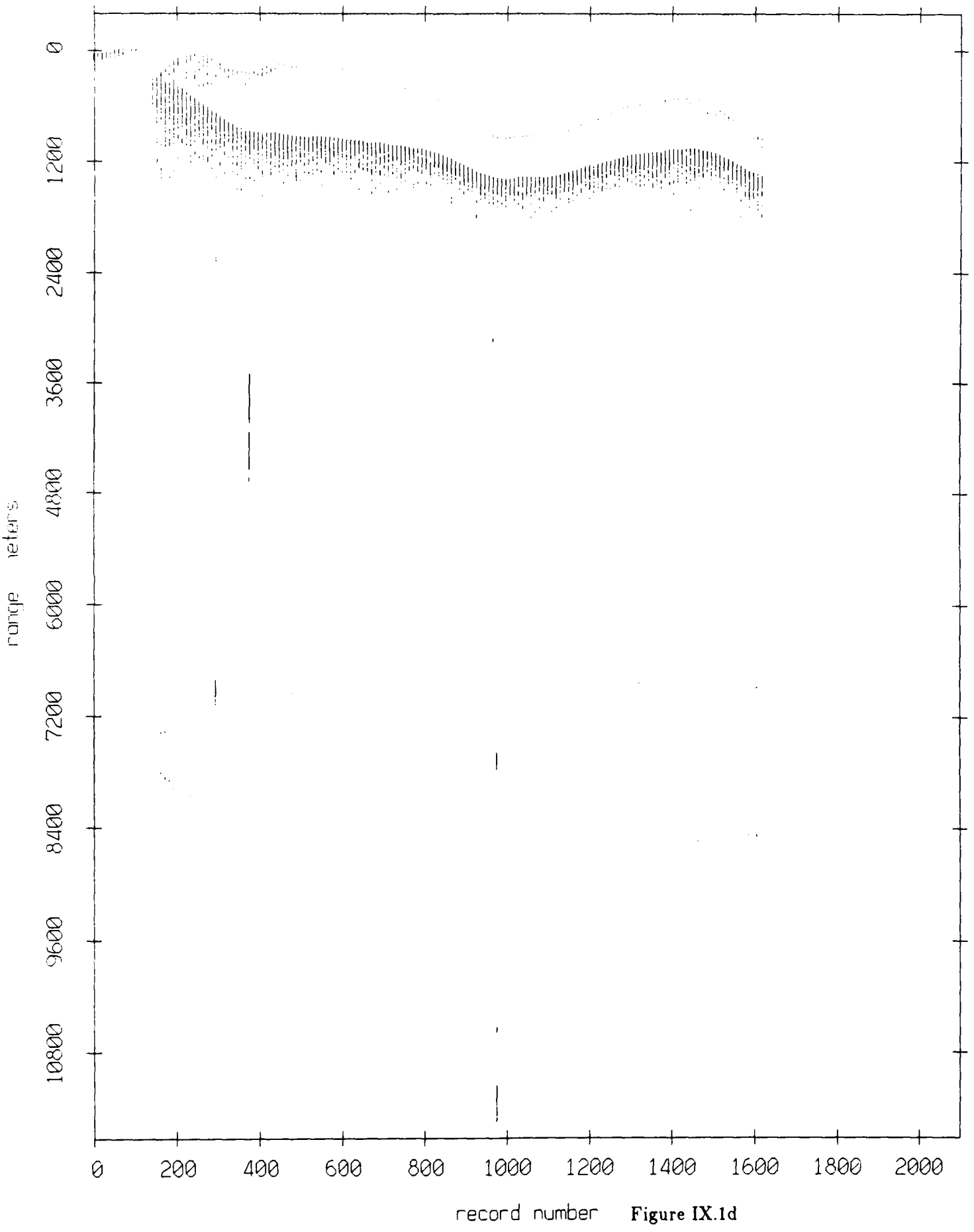

Float 10, August 1988 Experiment: range from float 1
range meters
0
1200
2400
3600
4800
6000
7200
8400
9600
10800
0
200
400
600
800
1000
1200
1400
1600
1800
2000
record number

Figure IX.1d

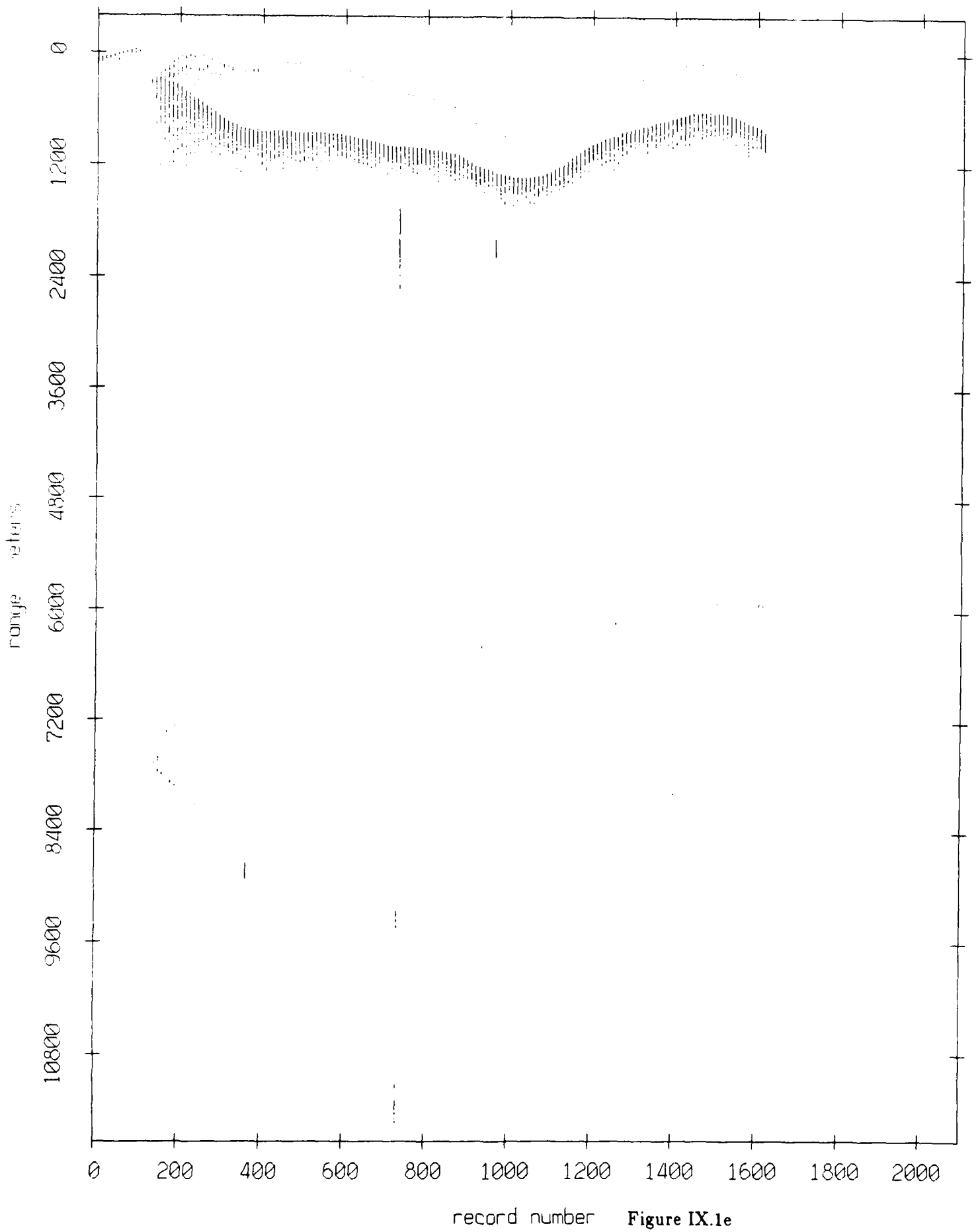

Float 10, August 1988 Experiment: range from float 2
range (km)
0
1200
2400
3600
4800
6000
7200
8400
9600
10800
0
200
400
600
800
1000
1200
1400
1600
1800
2000
record number

Figure IX.1e

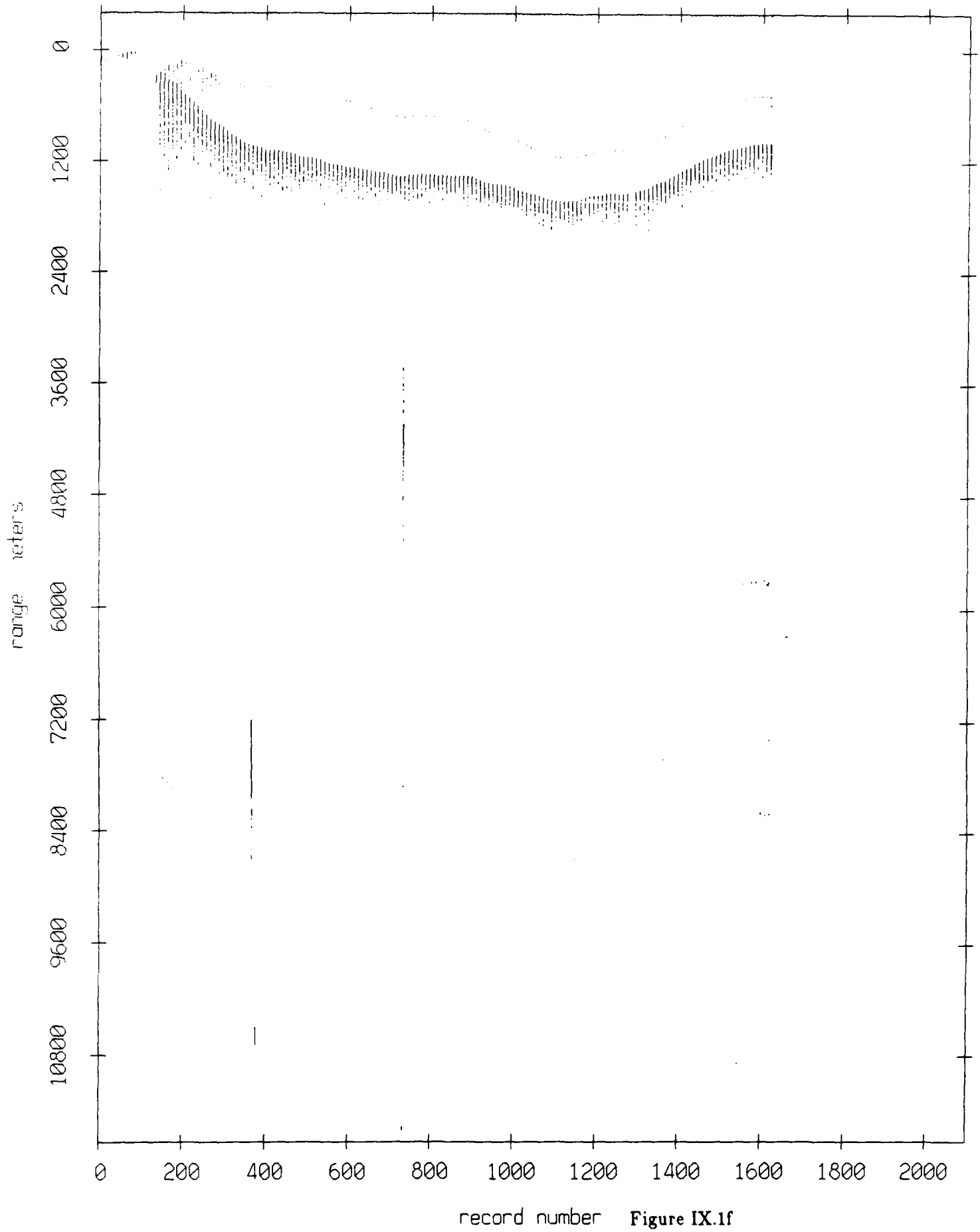

Float 10, August 1988 Experiment: range from float 4
range meters
0
1200
2400
3600
4800
6000
7200
8400
9600
10800
0
200
400
600
800
1000
1200
1400
1600
1800
2000
record number

Figure IX.1f

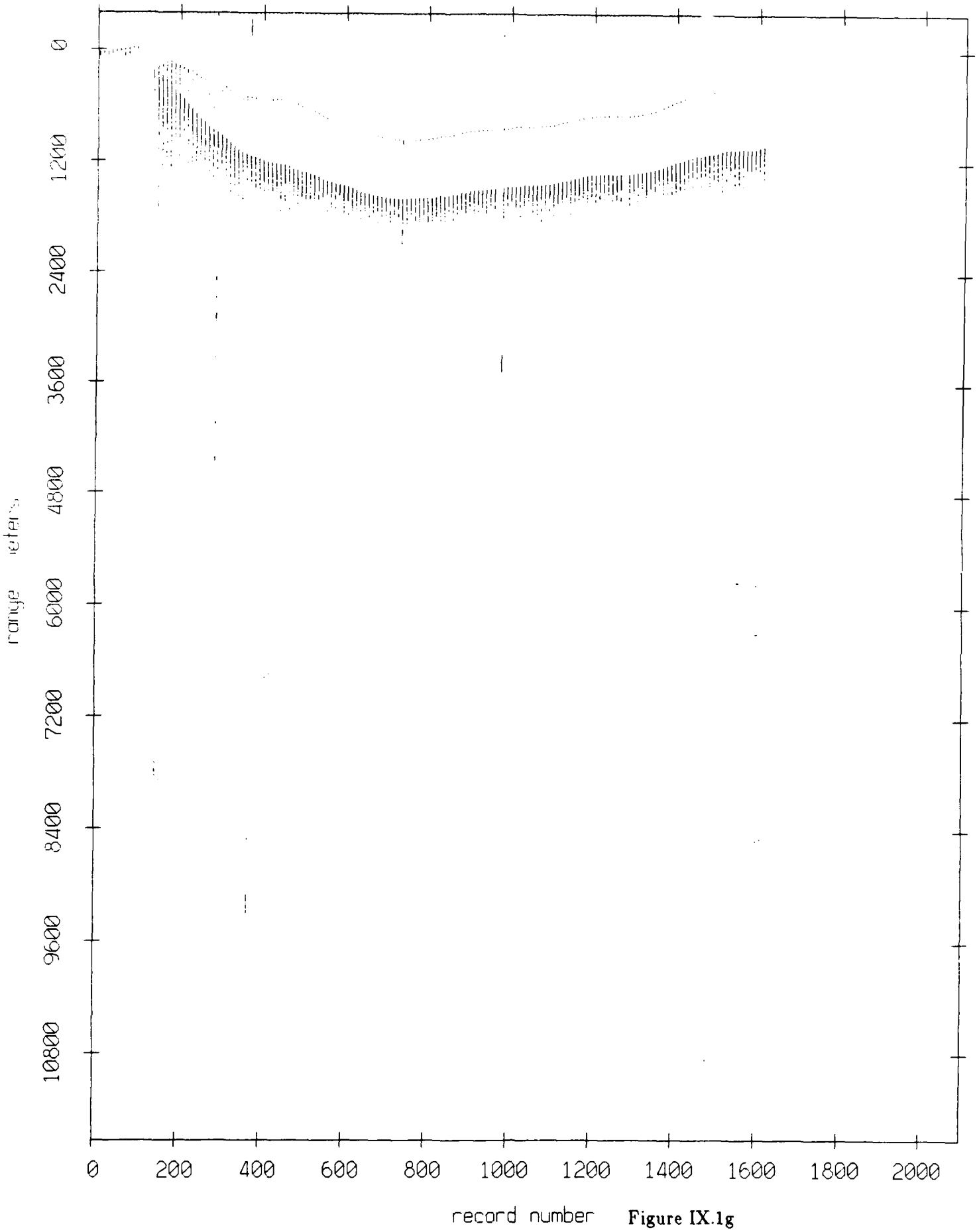

Float 10, August 1988 Experiment: range from float 6
range meters
0
1200
2400
3600
4800
6000
7200
8400
9600
10800
0
200
400
600
800
1000
1200
1400
1600
1800
2000
record number

Figure IX.1g

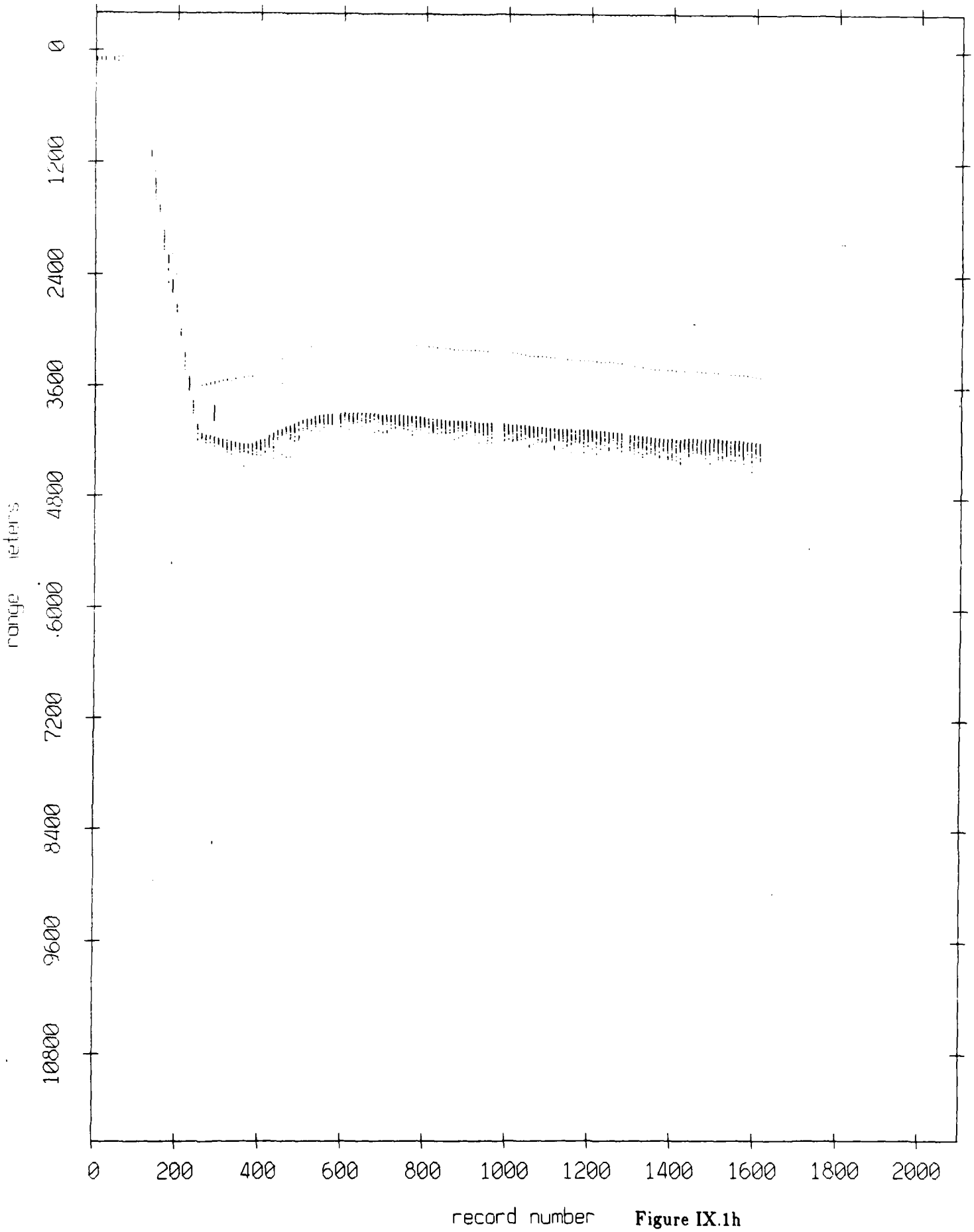

Float 10, August 1988 Experiment: range from float 11
range meters
0
1200
2400
3600
4800
6000
7200
8400
9600
10800
0
200
400
600
800
1000
1200
1400
1600
1800
2000
record number

Figure IX.1h

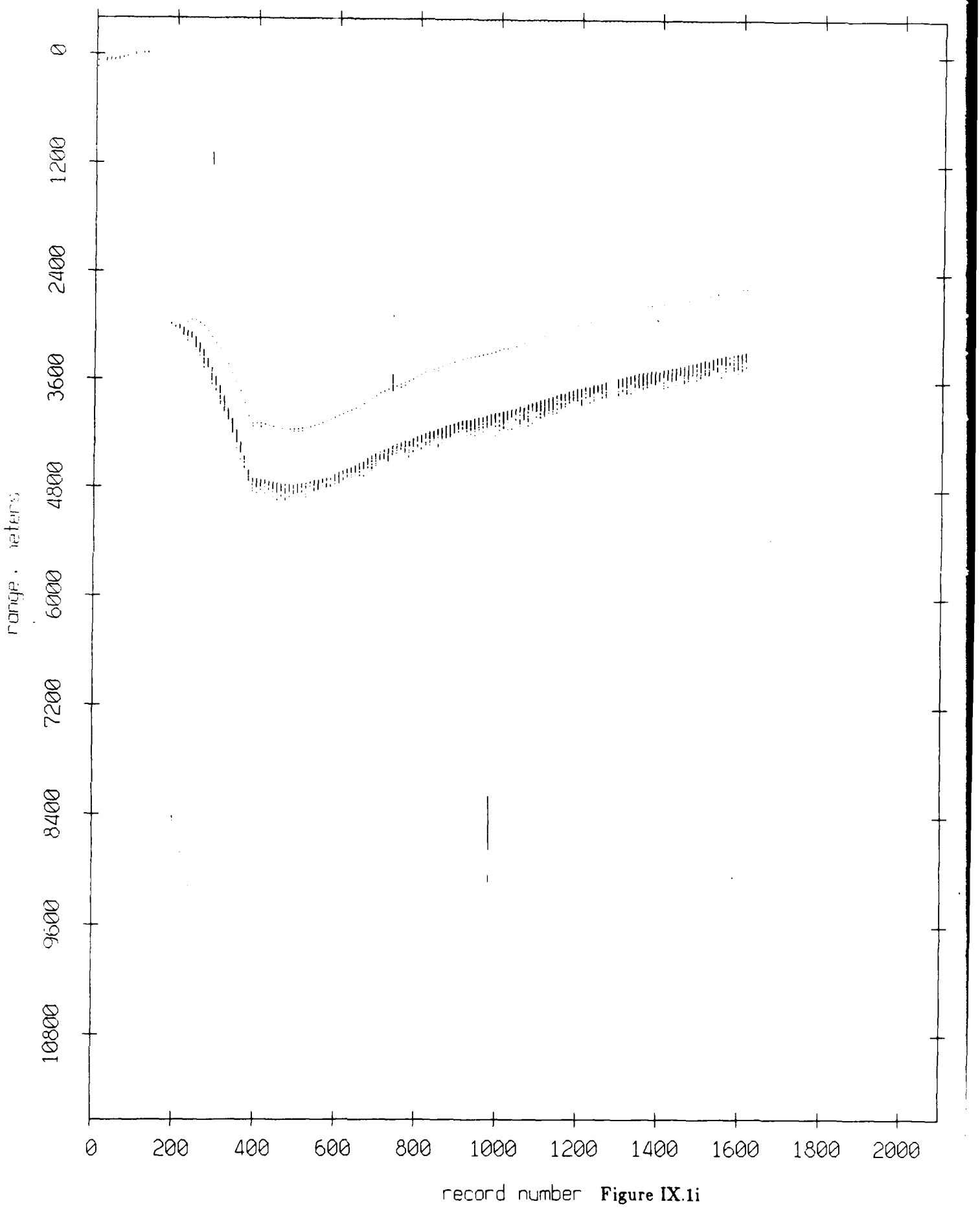

Float 10, August 1988 Experiment: range from float 7
range, meters
0
1200
2400
3600
4800
6000
7200
8400
9600
10800
0
200
400
600
800
1000
1200
1400
1600
1800
2000
record number

Figure IX.1i

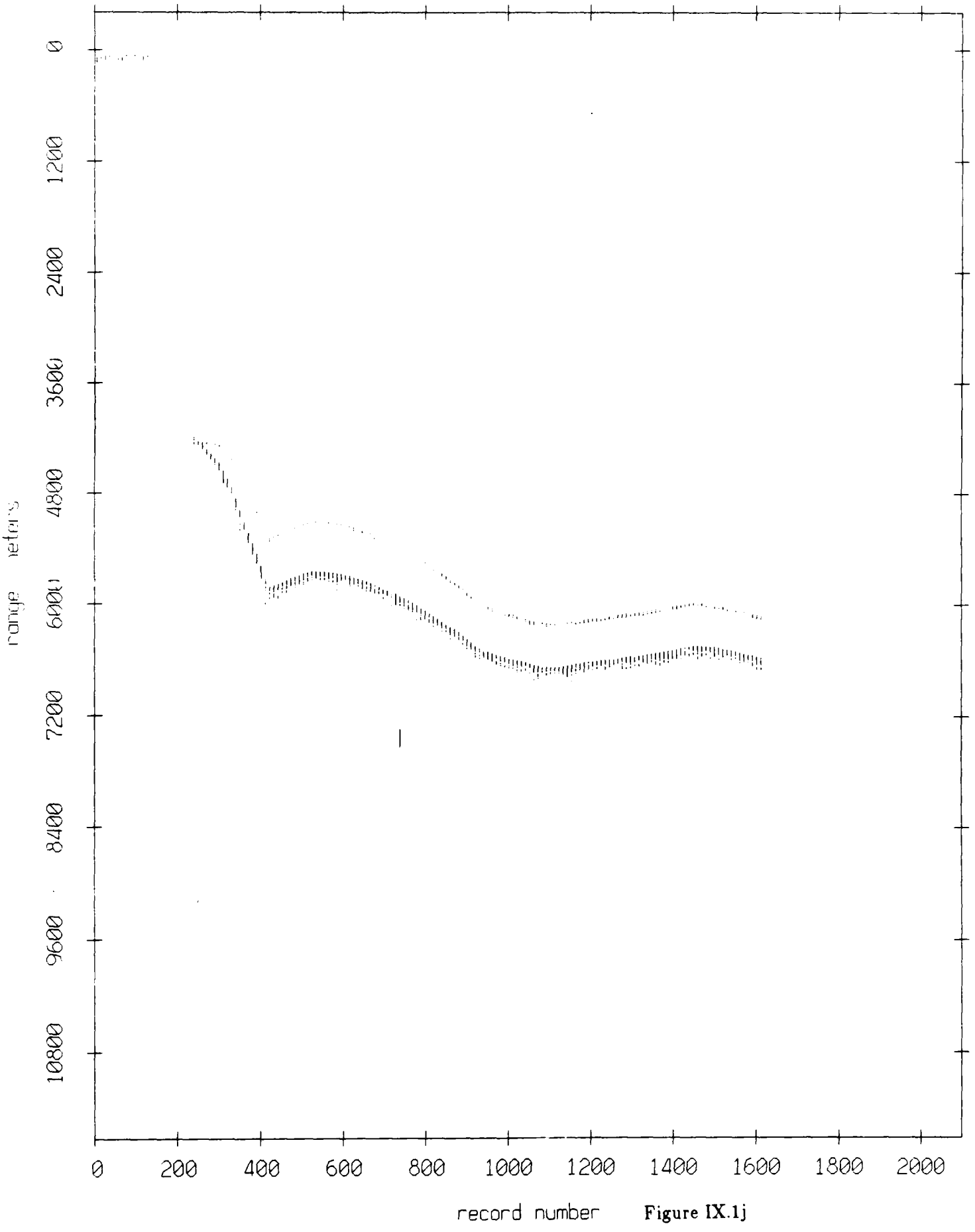

Float 10, August 1988 Experiment: range from float 8
range, meters
0
1200
2400
3600
4800
6000
7200
8400
9600
10800
0
200
400
600
800
1000
1200
1400
1600
1800
2000
record number

Figure IX.1j

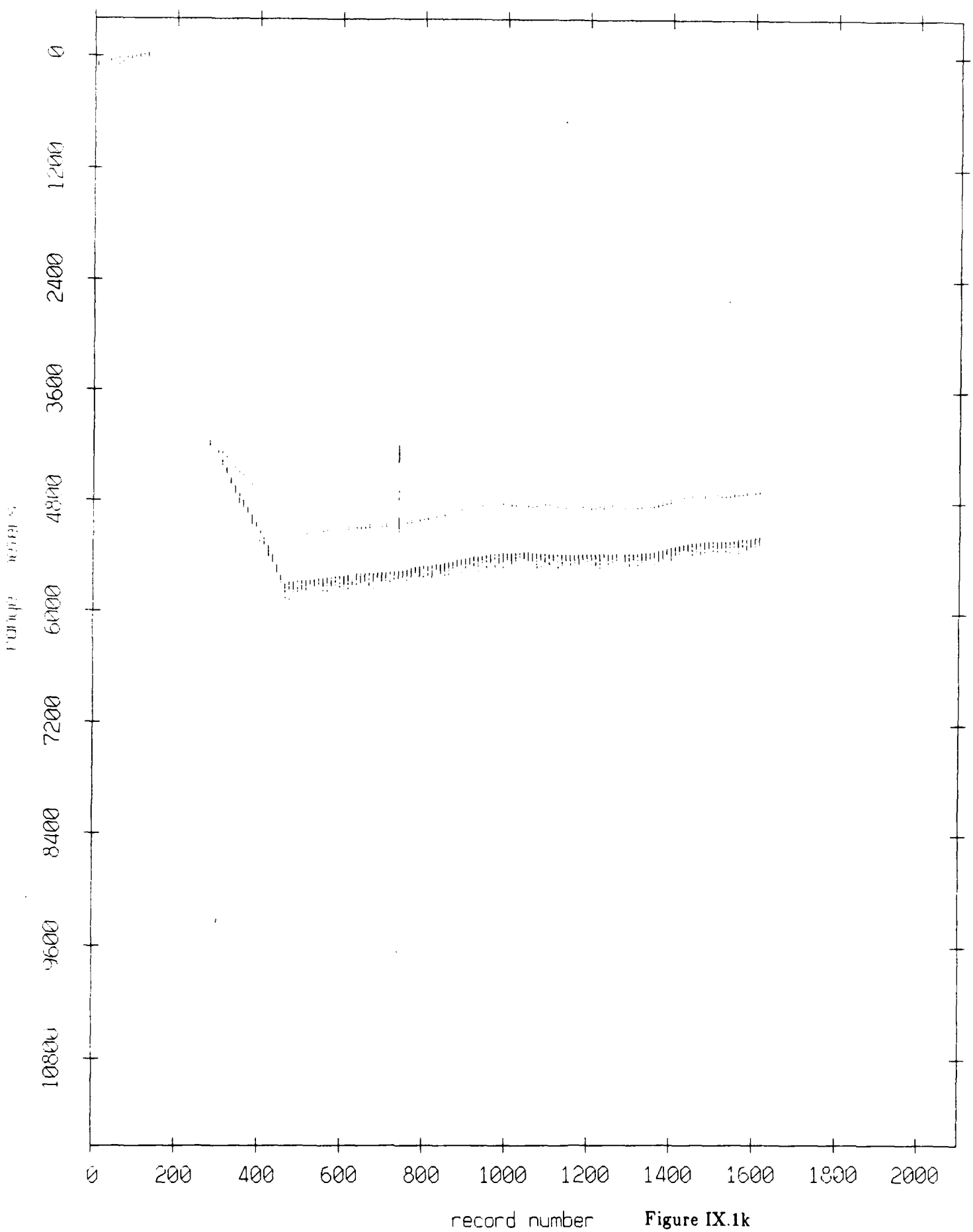

Float 10, August 1988 Experiment: range from float 9
0
1200
2400
3600
4800
6000
7200
8400
9600
10800
0
200
400
600
800
1000
1200
1400
1600
1800
2000
record number

Figure IX.1k

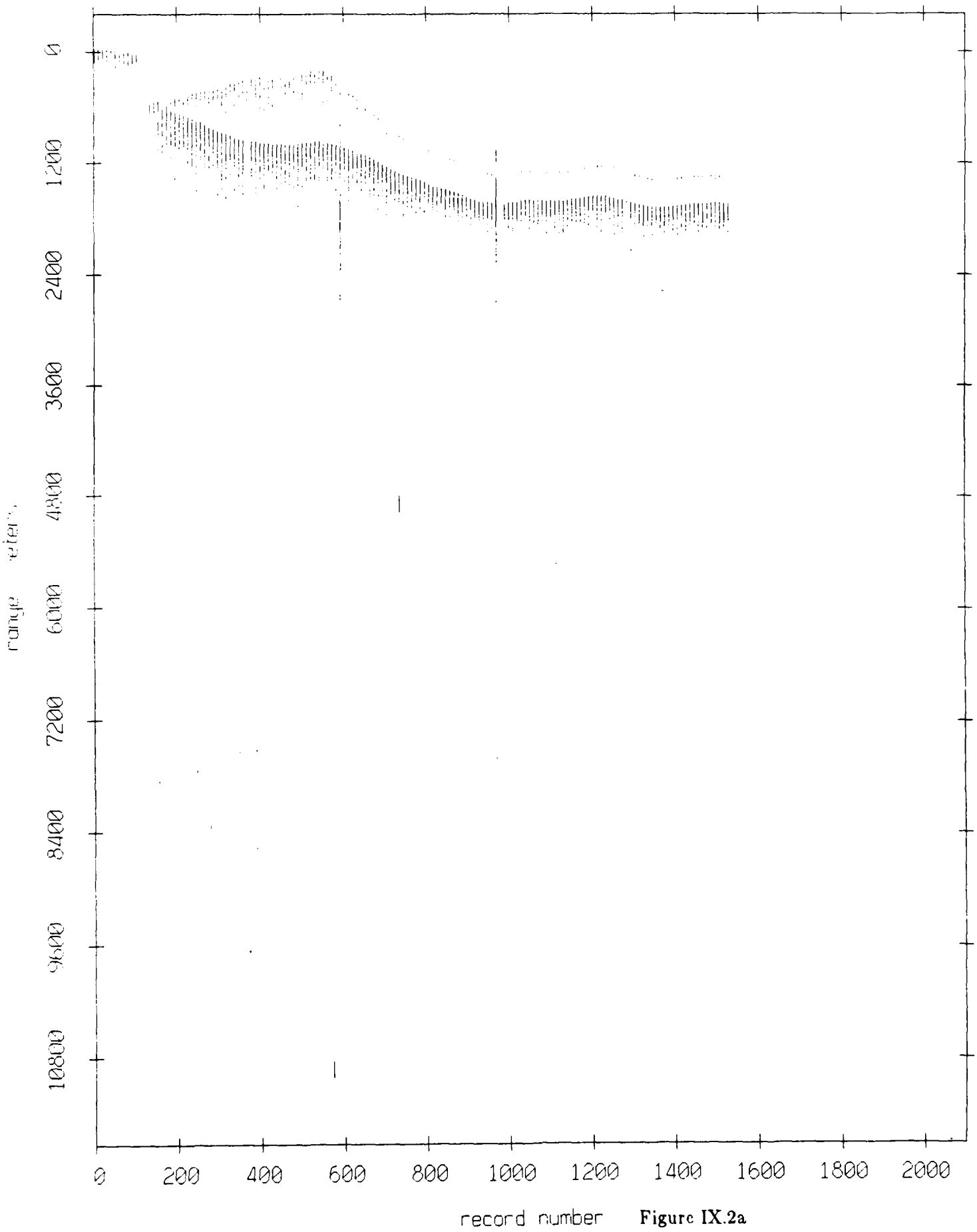

Float 3, August 1988 Experiment: range from float 10
range meters
0
1200
2400
3600
4800
6000
7200
8400
9600
10800
0
200
400
600
800
1000
1200
1400
1600
1800
2000
record number

Figure IX.2a

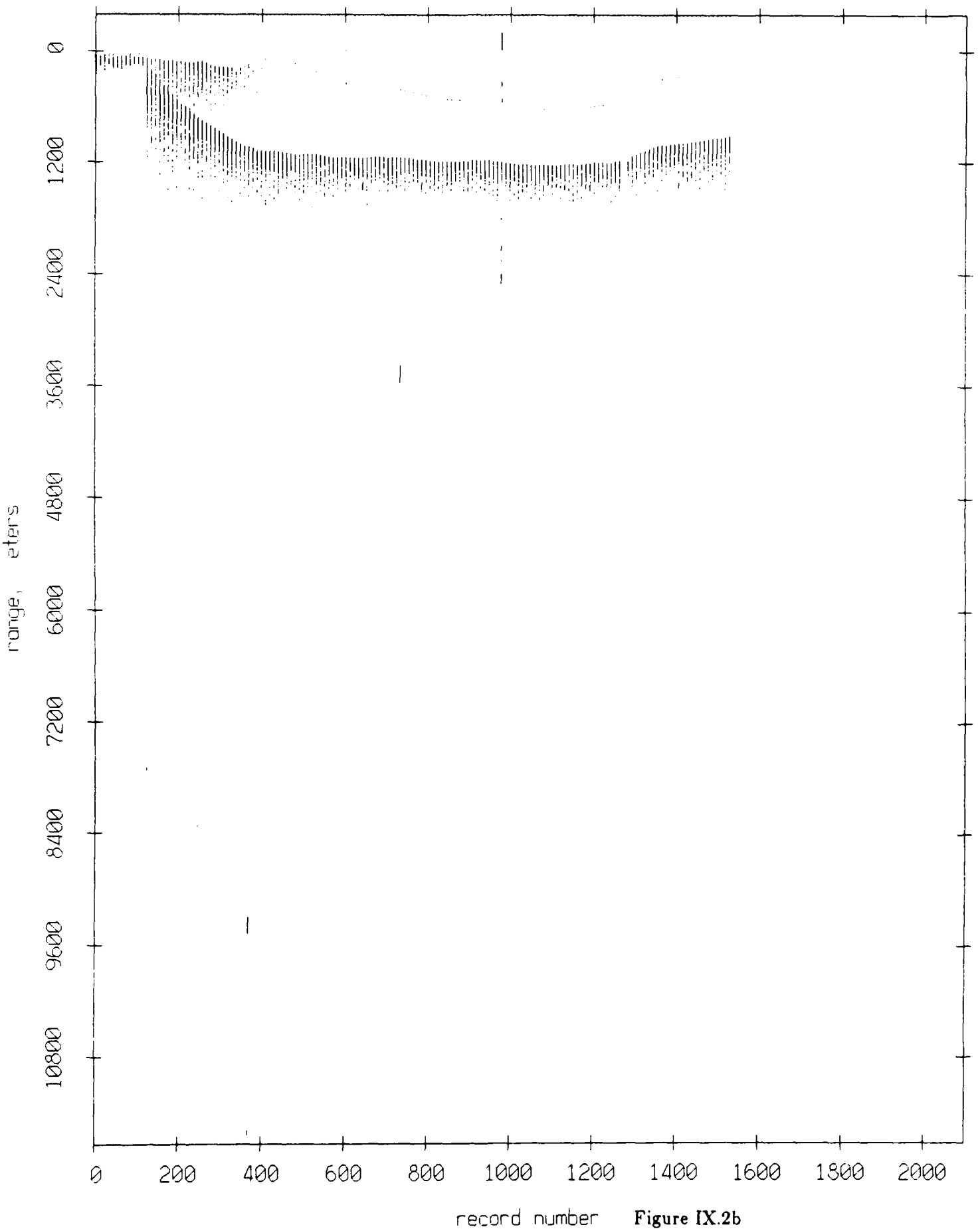

Float 3, August 1988 Experiment: range from float 5
range, eters
0
1200
2400
3600
4800
6000
7200
8400
9600
10800
0
200
400
600
800
1000
1200
1400
1600
1800
2000
record number

Figure IX.2b

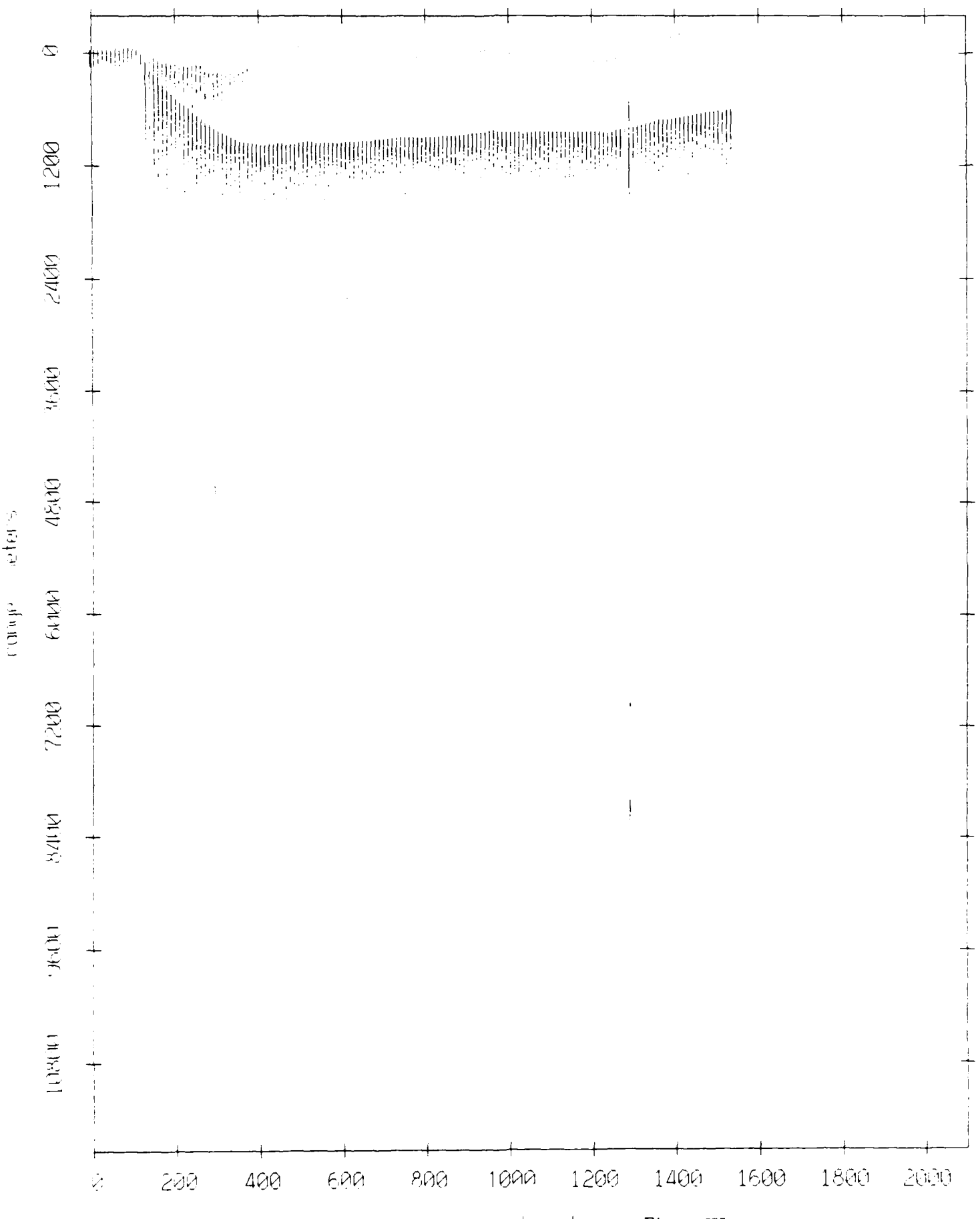

Float 3, August 1988 Experiment: range from float 0
0
1200
2400
4800
6000
7200
8400
9600
10800
0
200
400
600
800
1000
1200
1400
1600
1800
2000
record number

Figure IX.2c

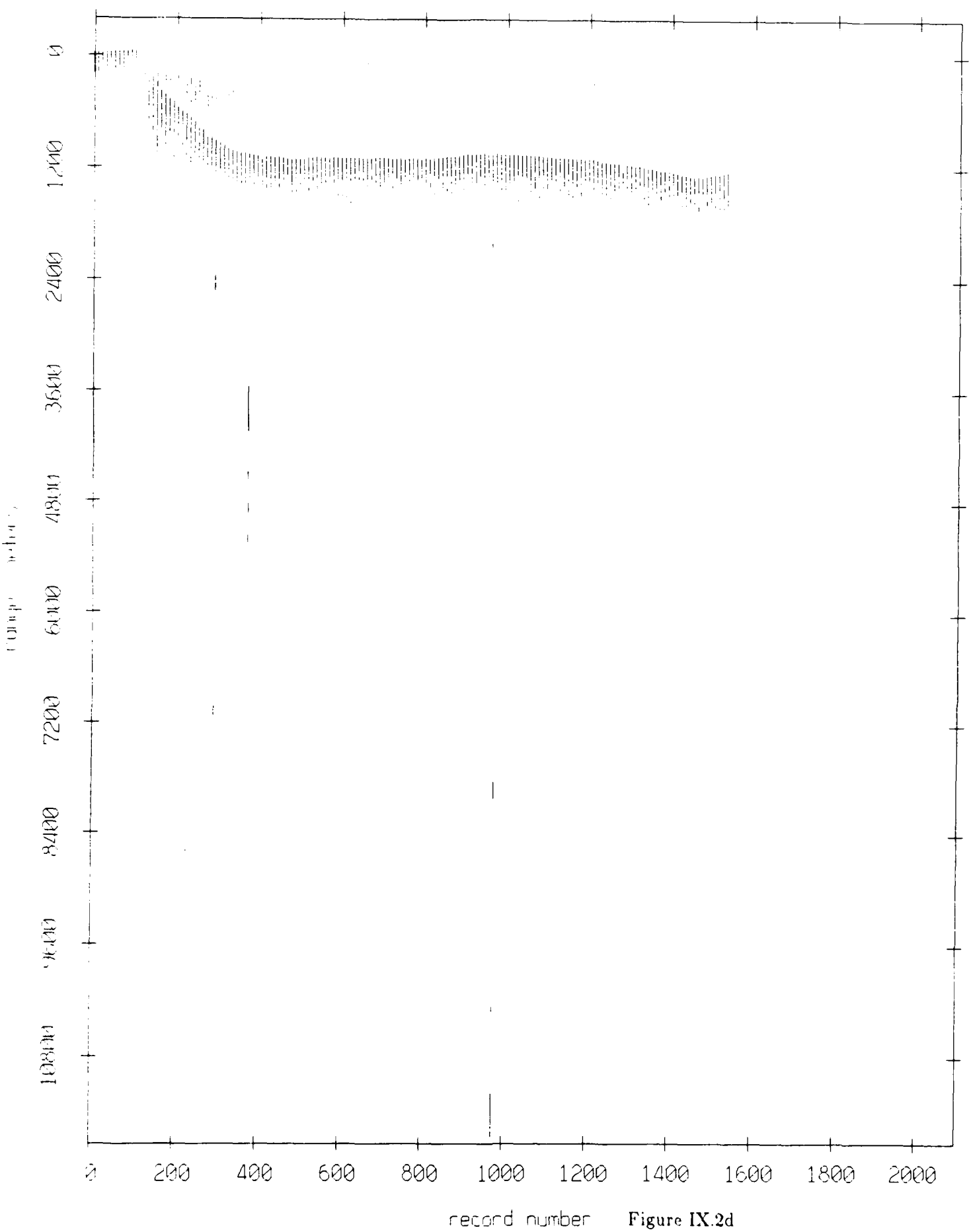

Float 3, August 1988 Experiment: range from float 1
0
1200
2400
3600
4800
6000
7200
8400
9600
10800
0
200
400
600
800
1000
1200
1400
1600
1800
2000
record number

Figure IX.2d

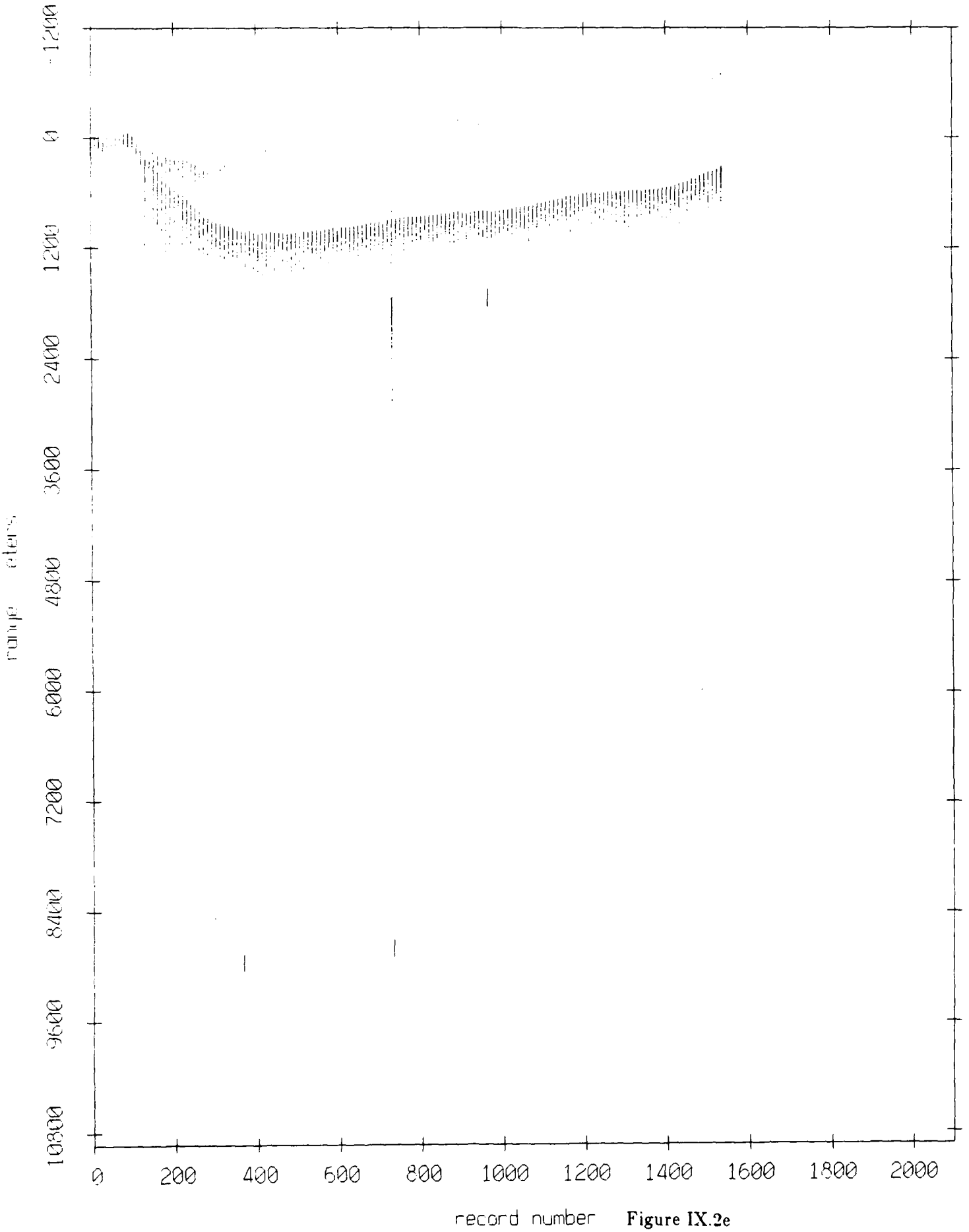

Float 3, August 1988 Experiment: range from float 2
range meters
-1200
0
1200
2400
3600
4800
6000
7200
8400
9600
10800
0
200
400
600
800
1000
1200
1400
1600
1800
2000
record number

Figure IX.2e

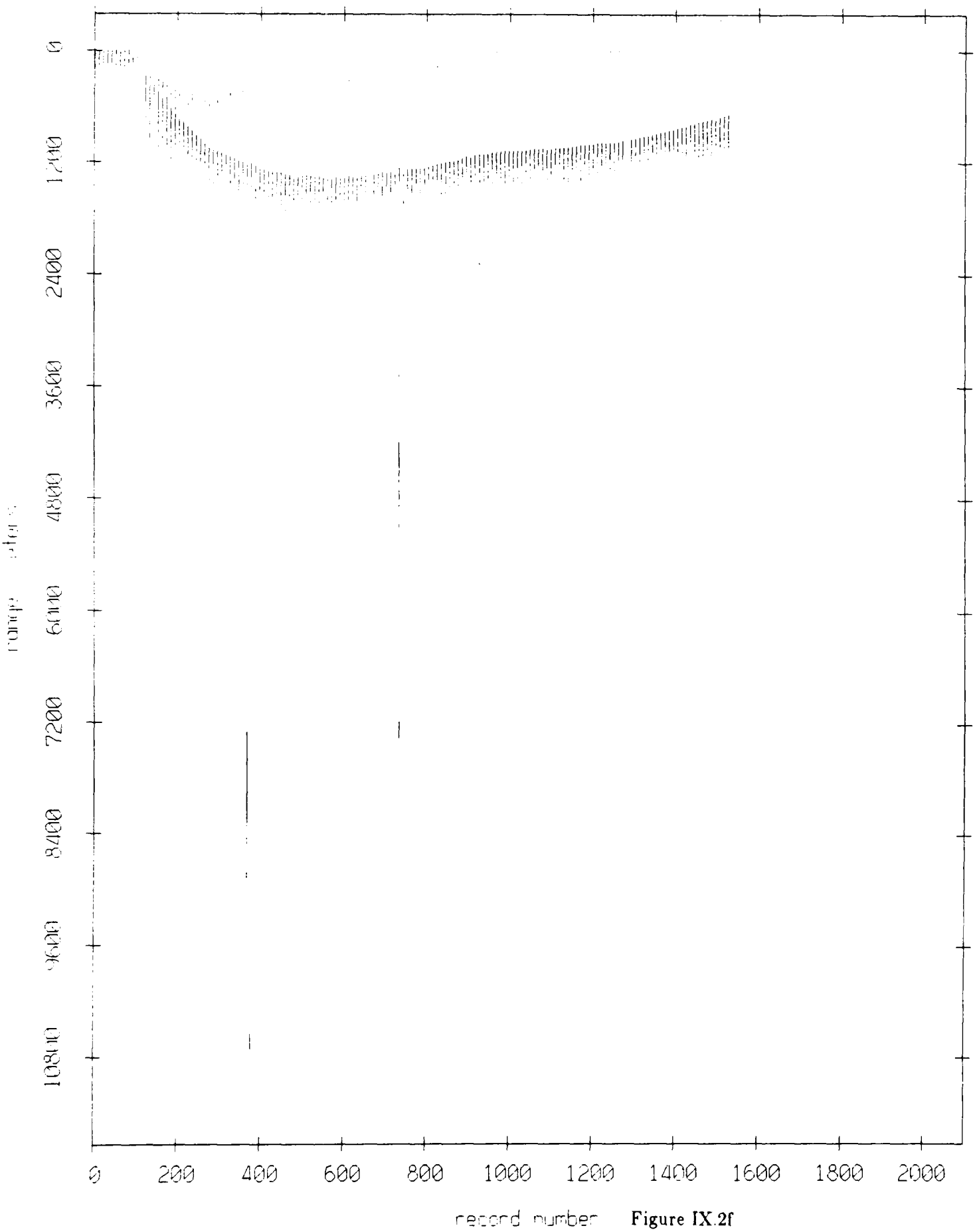

Float 3, August 1988 Experiment: range from float 4
0
1200
2400
3600
4800
6000
7200
8400
9600
10800
0
200
400
600
800
1000
1200
1400
1600
1800
2000
record number

Figure IX.2f

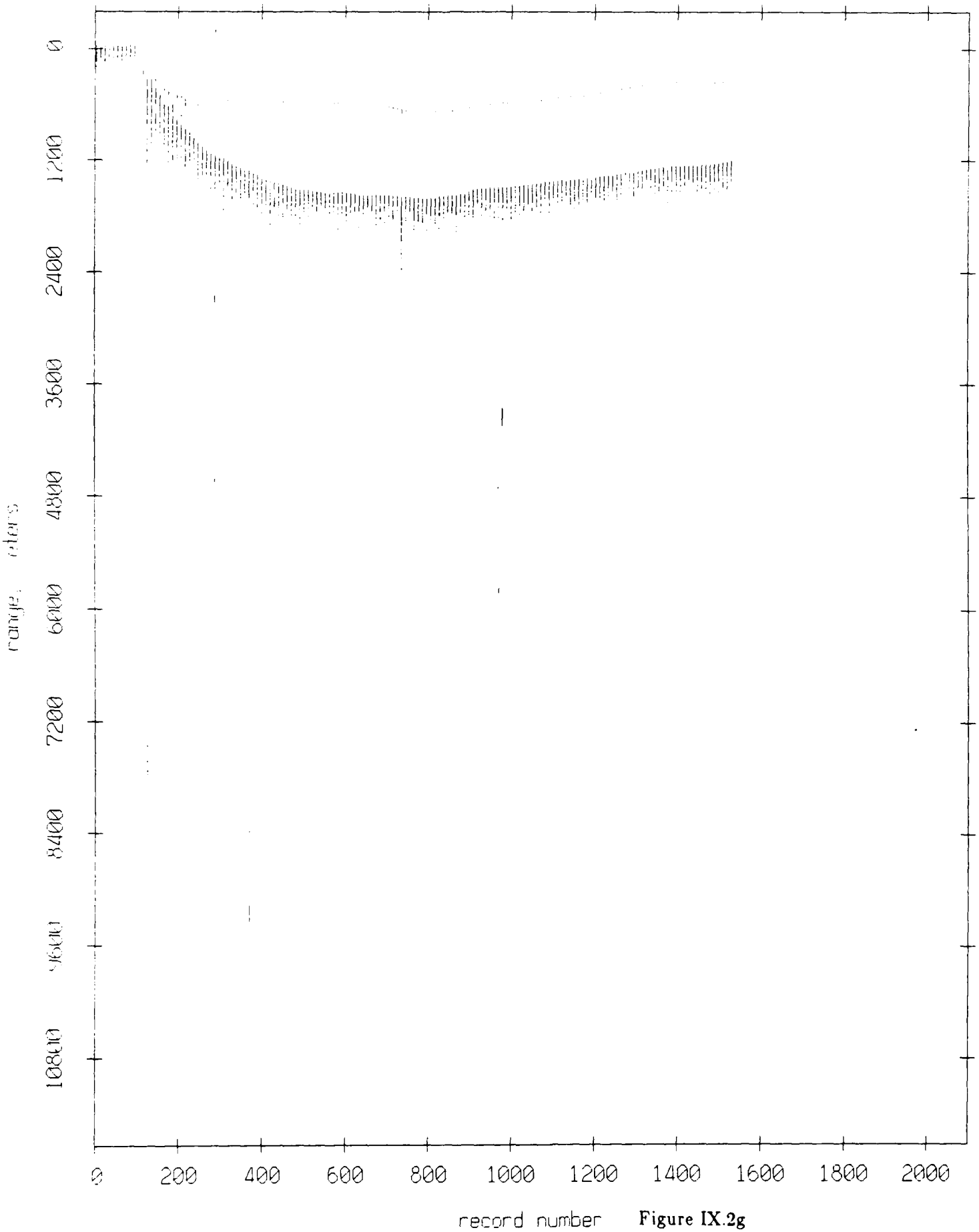

Float 3, August 1988 Experiment: range from float 6
range, meters
0
1200
2400
3600
4800
6000
7200
8400
9600
10800
0
200
400
600
800
1000
1200
1400
1600
1800
2000
record number

Figure IX.2g

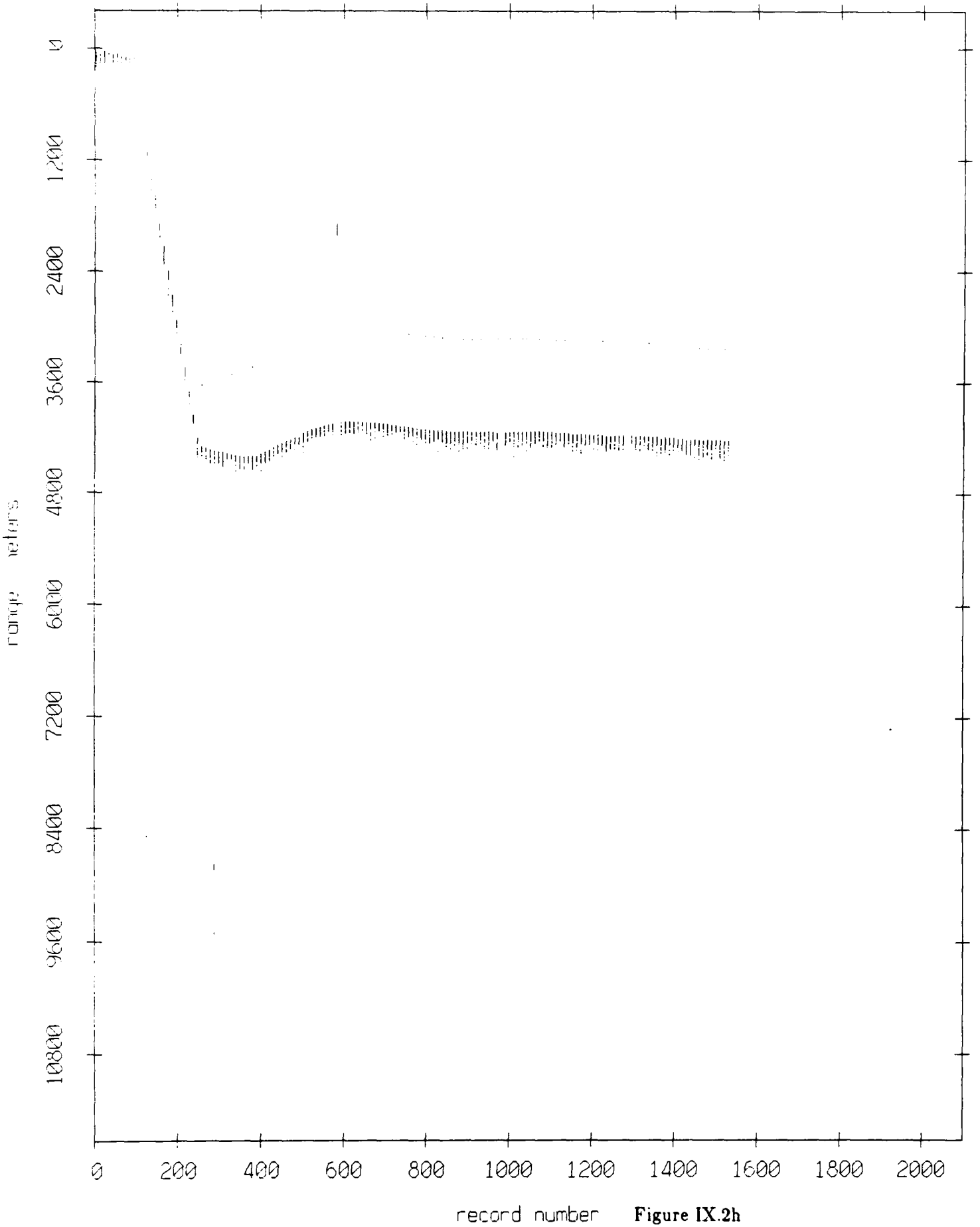

Float 3, August 1988 Experiment: range from float 11
range meters
0
1200
2400
3600
4800
6000
7200
8400
9600
10800
0
200
400
600
800
1000
1200
1400
1600
1800
2000
record number

Figure IX.2h

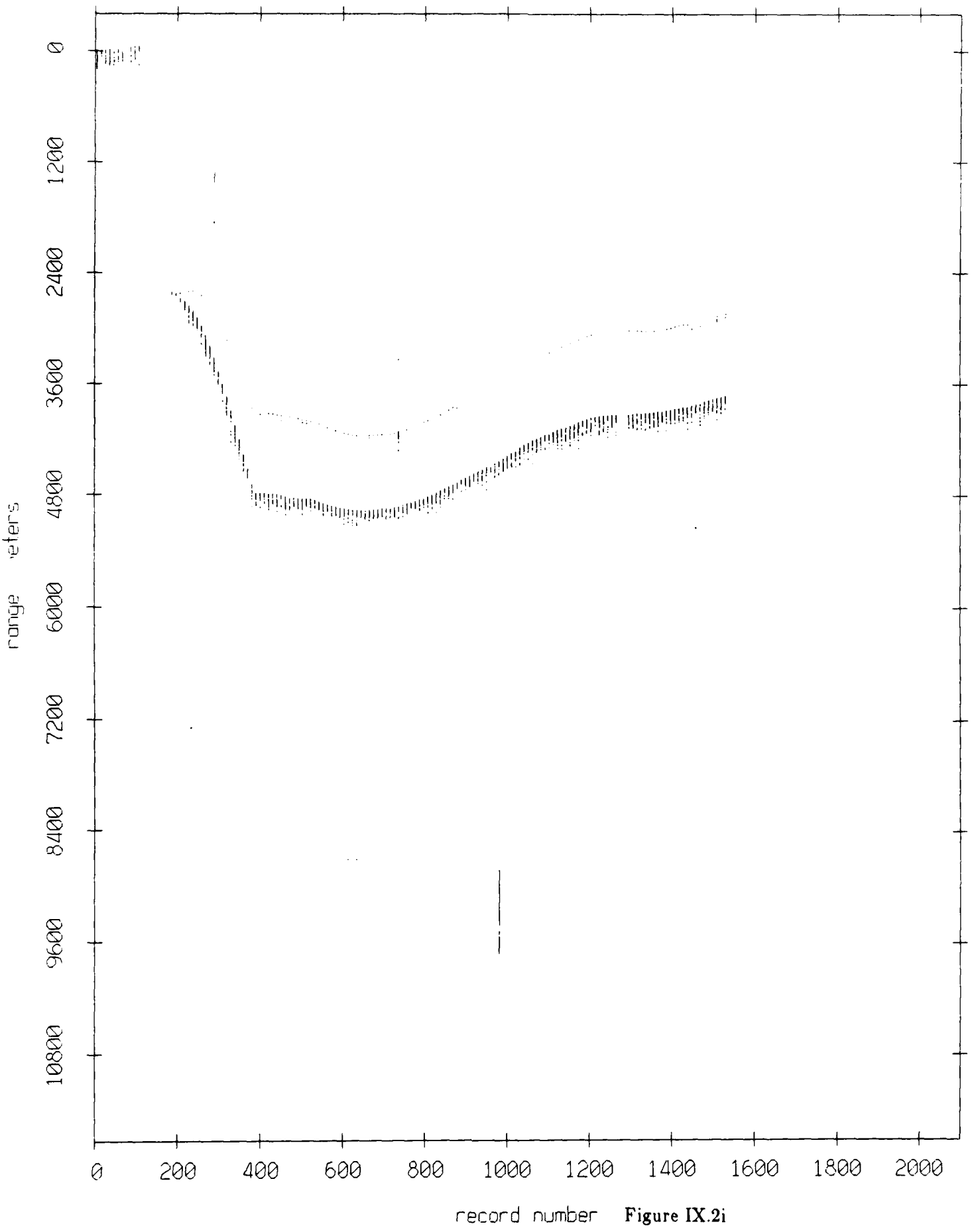

Float 3, August 1988 Experiment: range from float 7
range meters
0
1200
2400
3600
4800
6000
7200
8400
9600
10800
0
200
400
600
800
1000
1200
1400
1600
1800
2000
record number

Figure IX.2i

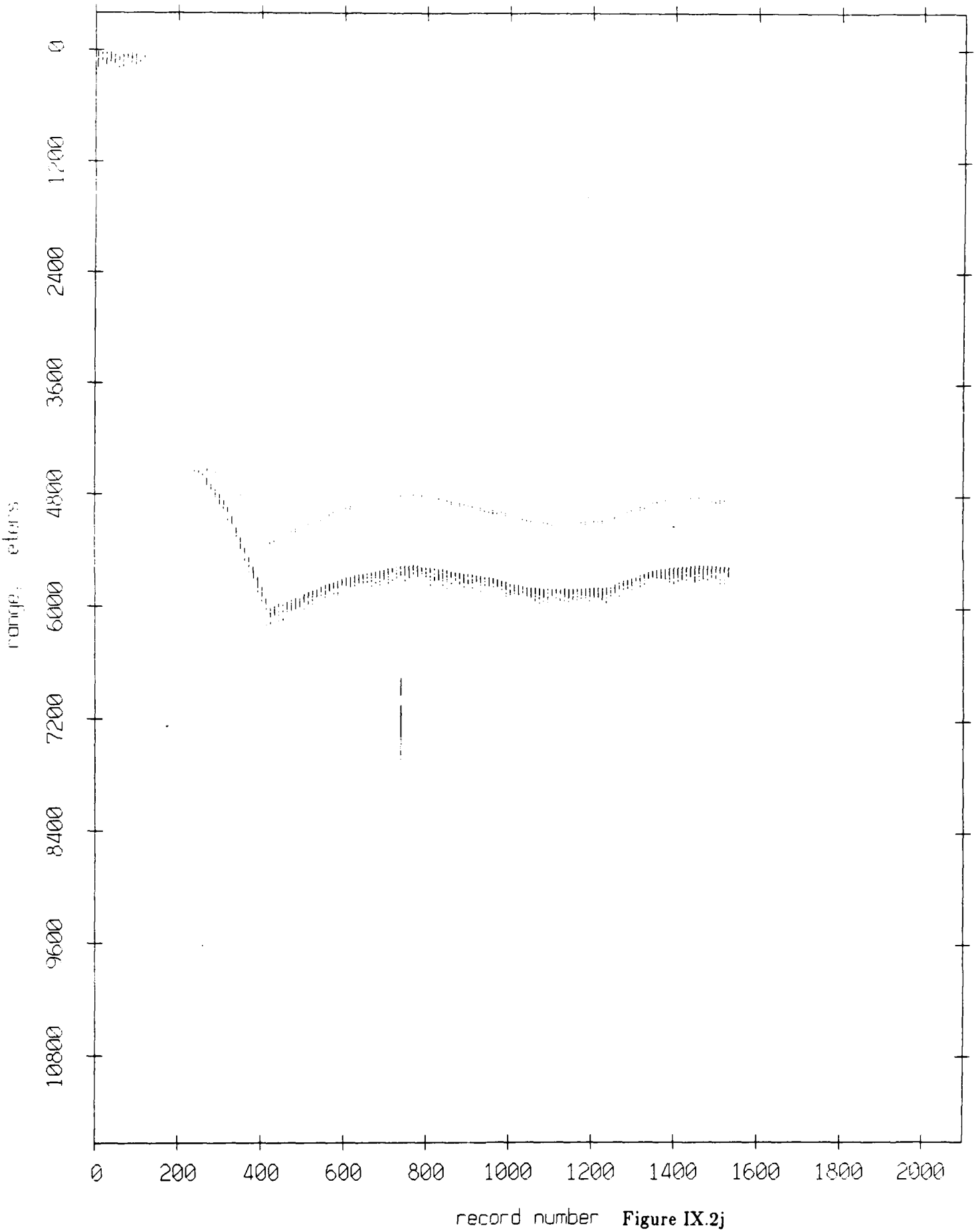

Float 3, August 1988 Experiment: range from float 8
range, etcrs
0
1200
2400
3600
4800
6000
7200
8400
9600
10800
0
200
400
600
800
1000
1200
1400
1600
1800
2000
record number

Figure IX.2j

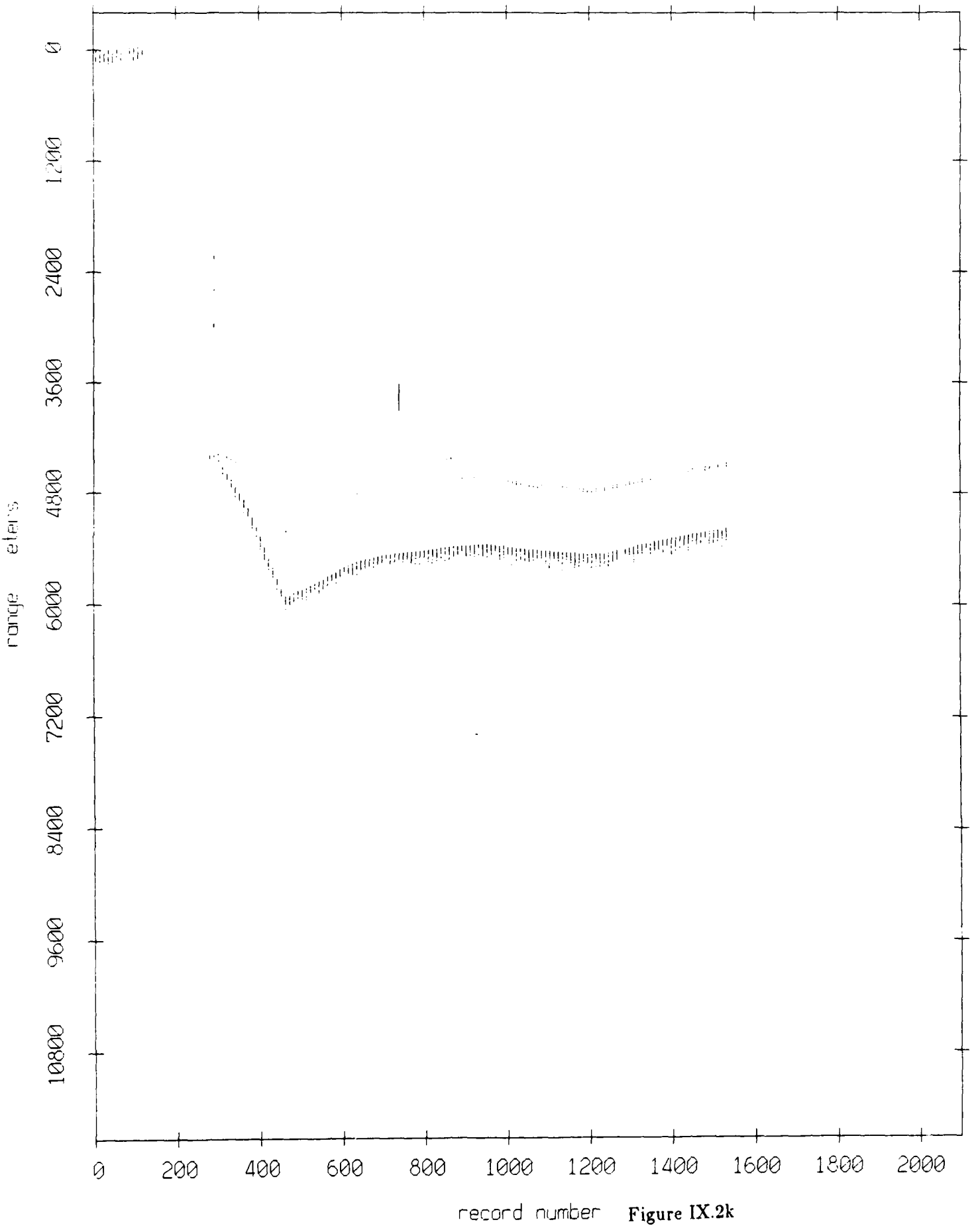

Float 3, August 1988 Experiment: range from float 9
range meters
0
1200
2400
3600
4800
6000
7200
8400
9600
10800
0
200
400
600
800
1000
1200
1400
1600
1800
2000
record number

Figure IX.2k

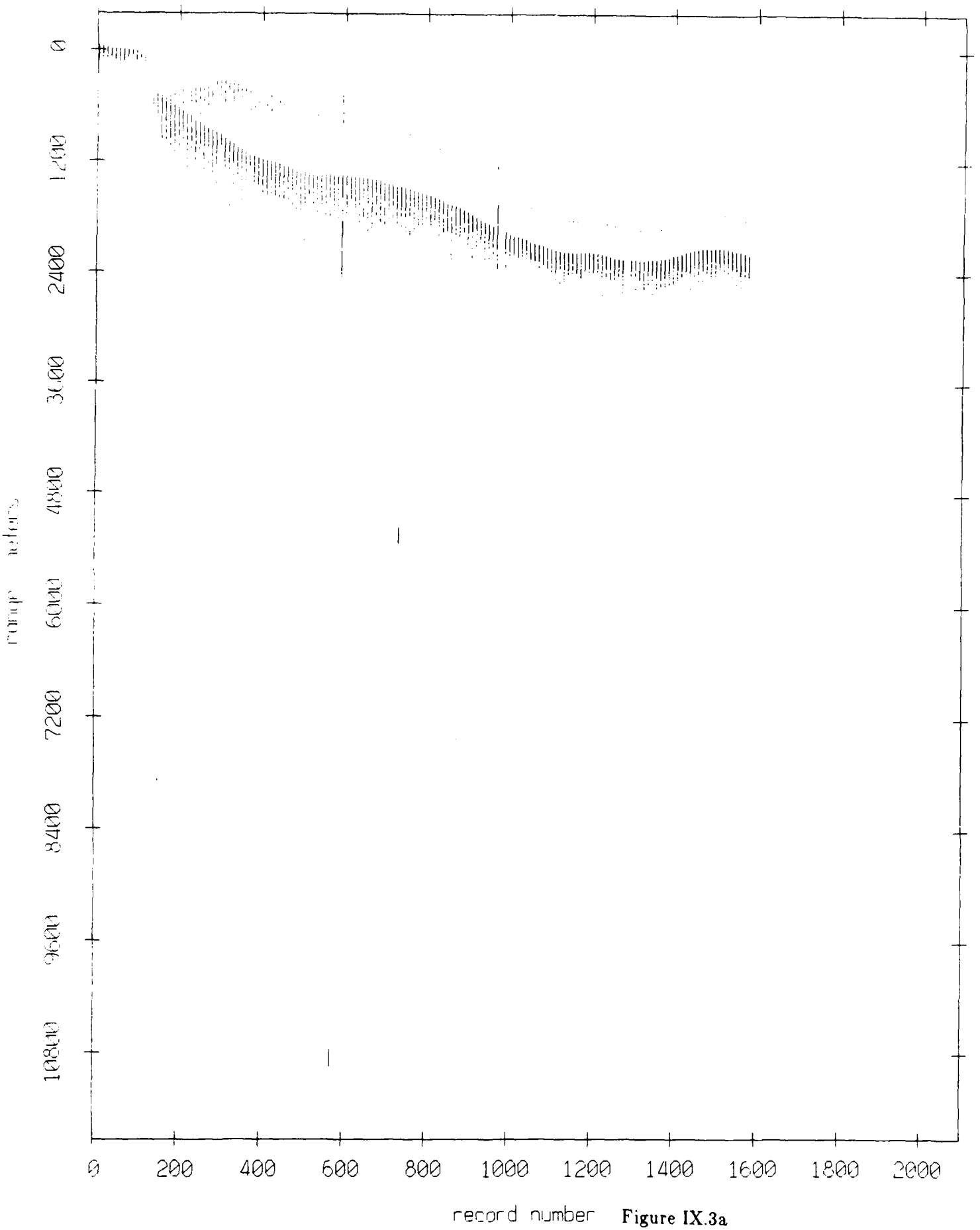

Float 5, August 1988 Experiment: range from float 10
0
1200
2400
3600
4800
6000
7200
8400
9600
10800
0
200
400
600
800
1000
1200
1400
1600
1800
2000
record number

Figure IX.3a

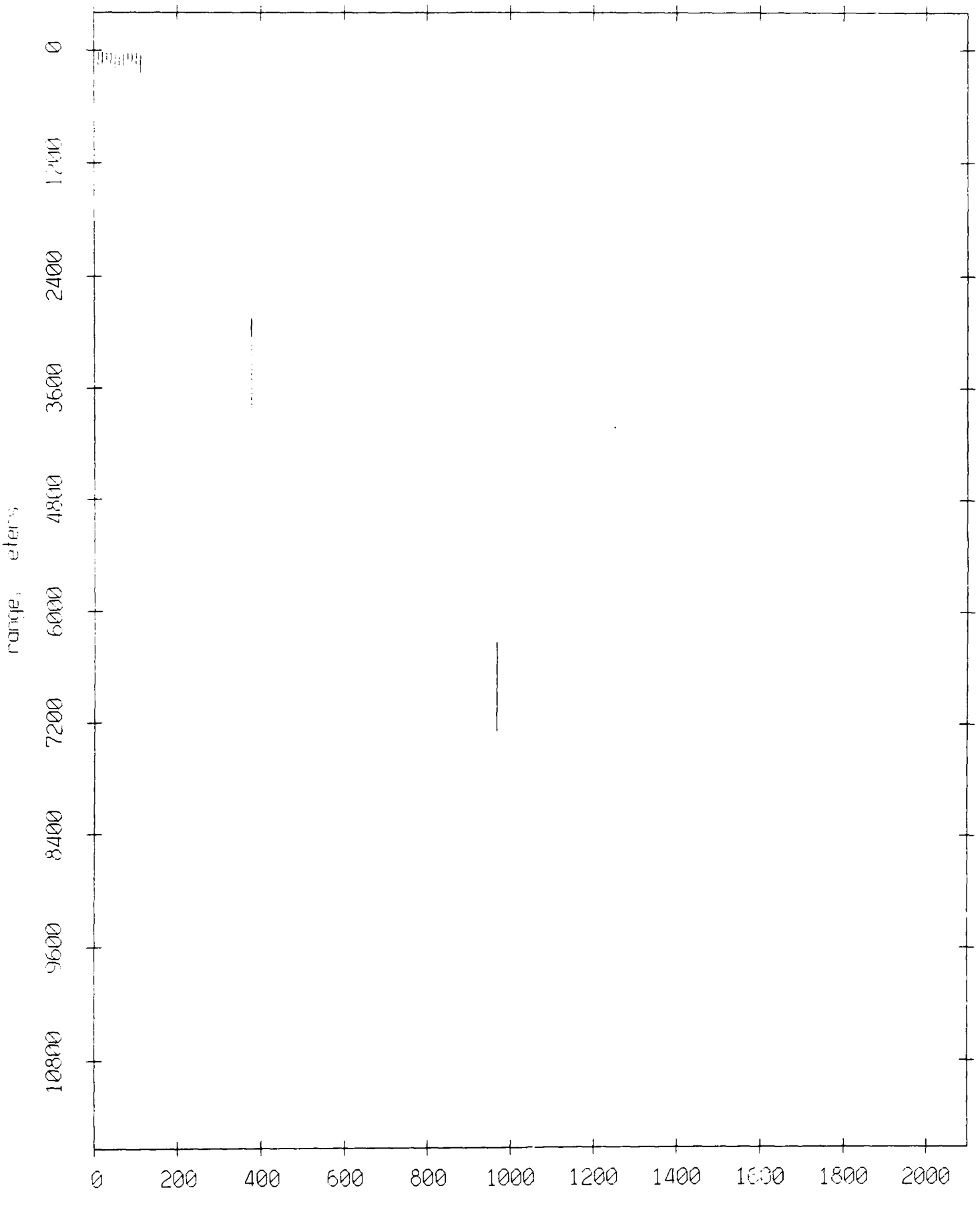

Float 5, August 1988 Experiment: range from float 3
range, meters
0
1200
2400
3600
4800
6000
7200
8400
9600
10800
0
200
400
600
800
1000
1200
1400
1600
1800
2000
record number

Figure IX.3b

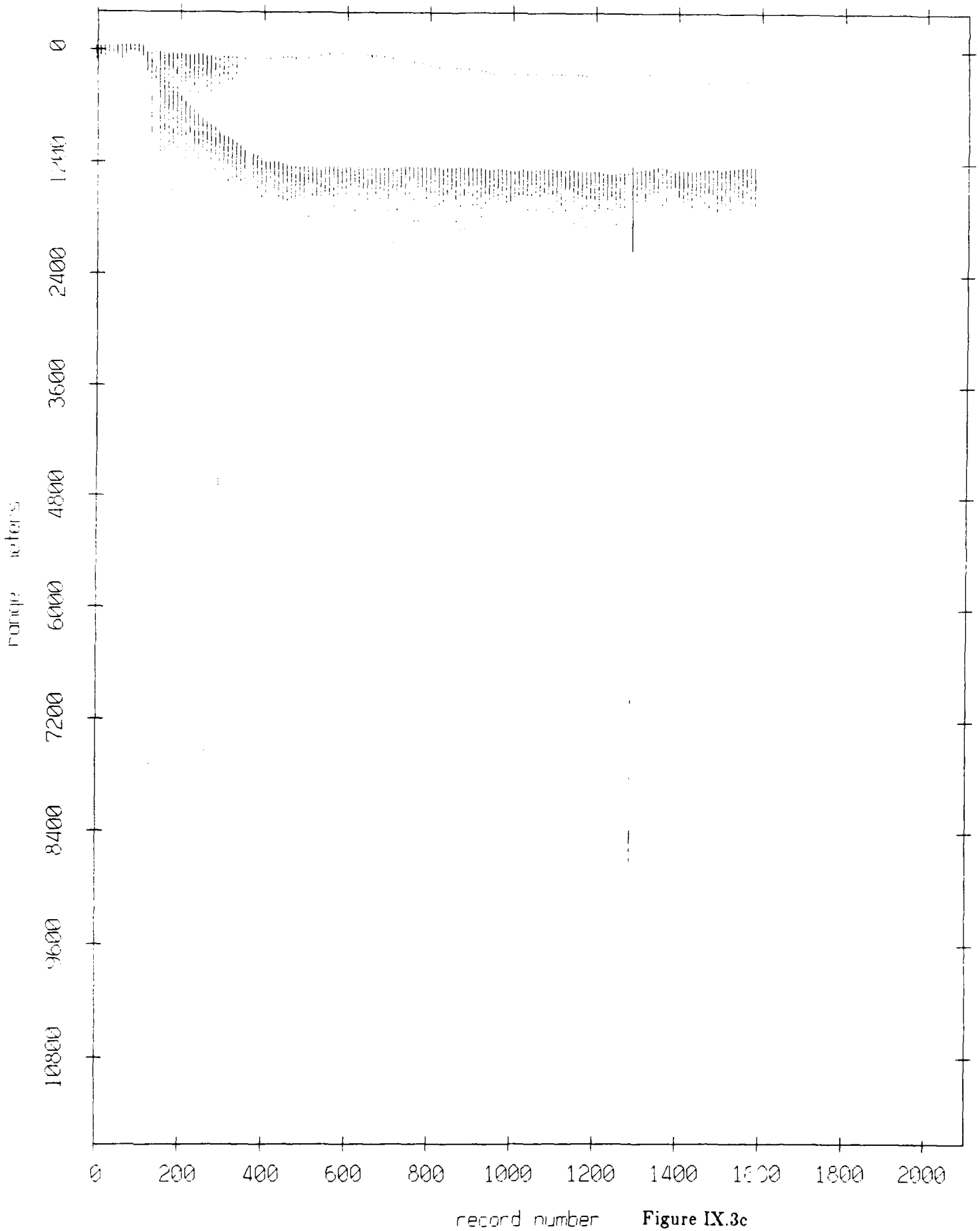

Float 5, August 1988 Experiment: range from float 0
range, meters
0
1200
2400
3600
4800
6000
7200
8400
9600
10800
0
200
400
600
800
1000
1200
1400
1600
1800
2000
record number

Figure IX.3c

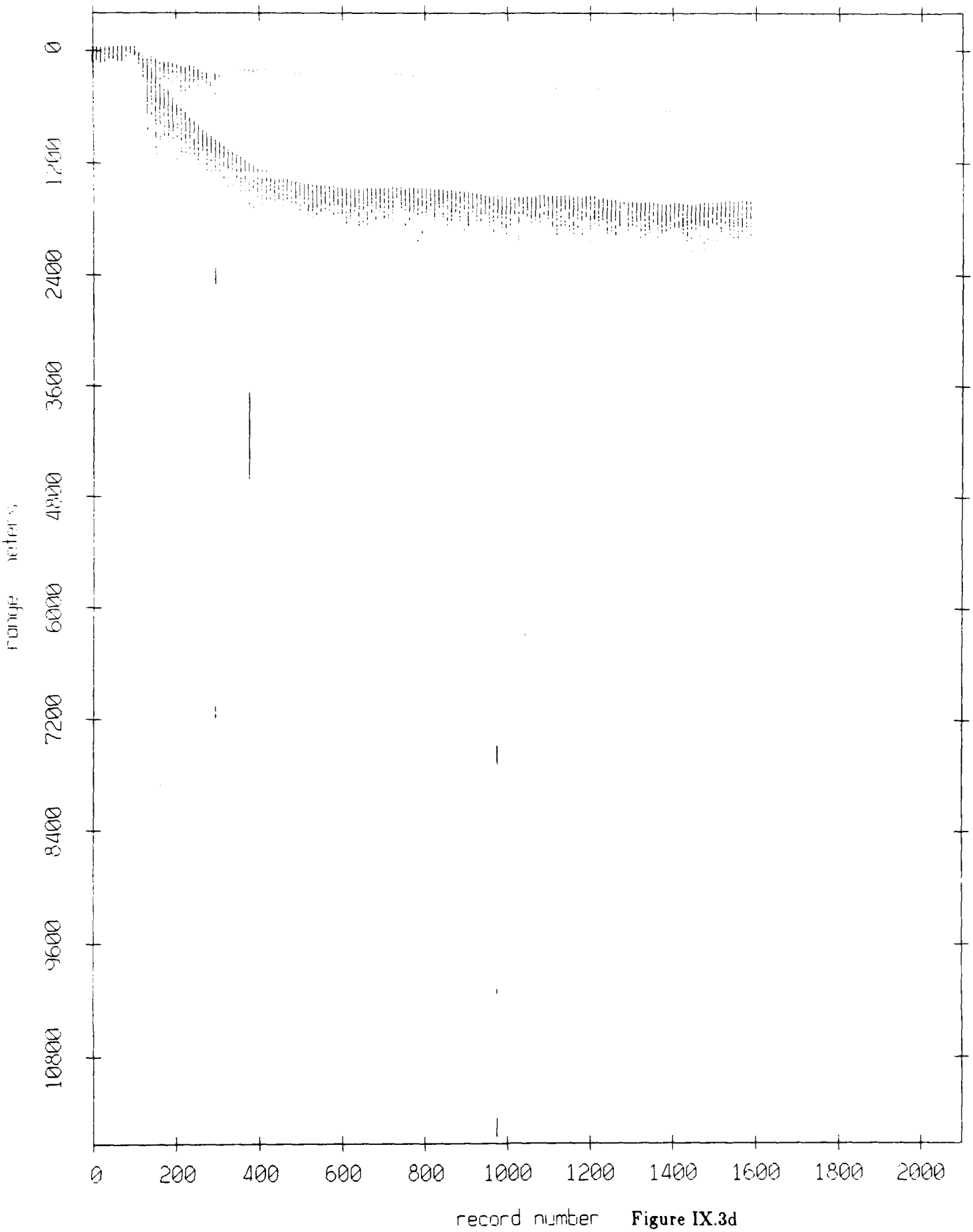

Float 5, August 1988 Experiment: range from float 1
range meters
0
1200
2400
3600
4800
6000
7200
8400
9600
10800
0
200
400
600
800
1000
1200
1400
1600
1800
2000
record number

Figure IX.3d

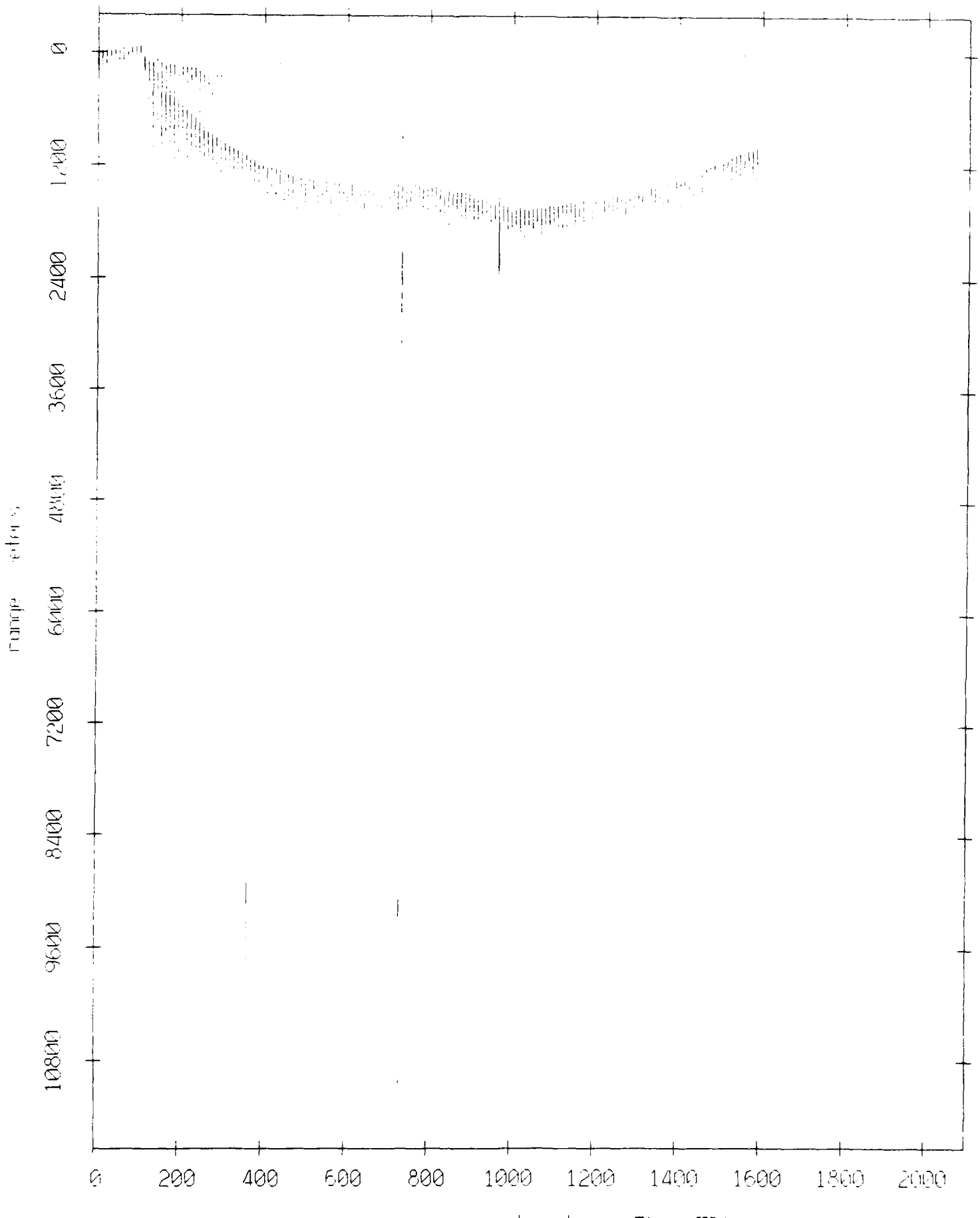

Float 5, August 1988 Experiment: range from float 2
range (km)
0
1200
2400
3600
4800
6000
7200
8400
9600
10800
0
200
400
600
800
1000
1200
1400
1600
1800
2000
record number

Figure IX.3e

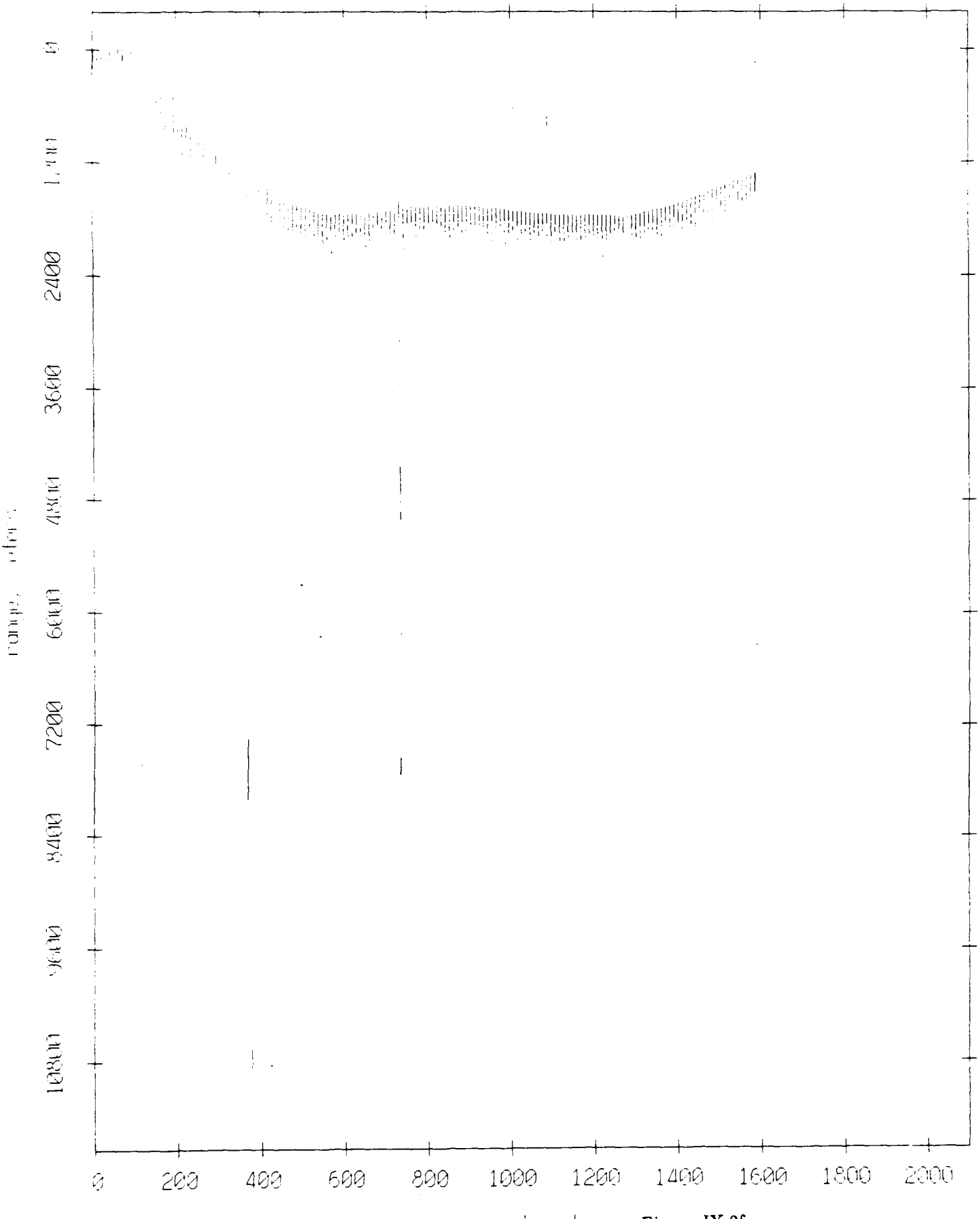

Float 5, August 1988 Experiment: range from float 4
2400
3600
7200
0
200
400
600
800
1000
1200
1400
1600
1800
2000
record number

Figure IX.3f

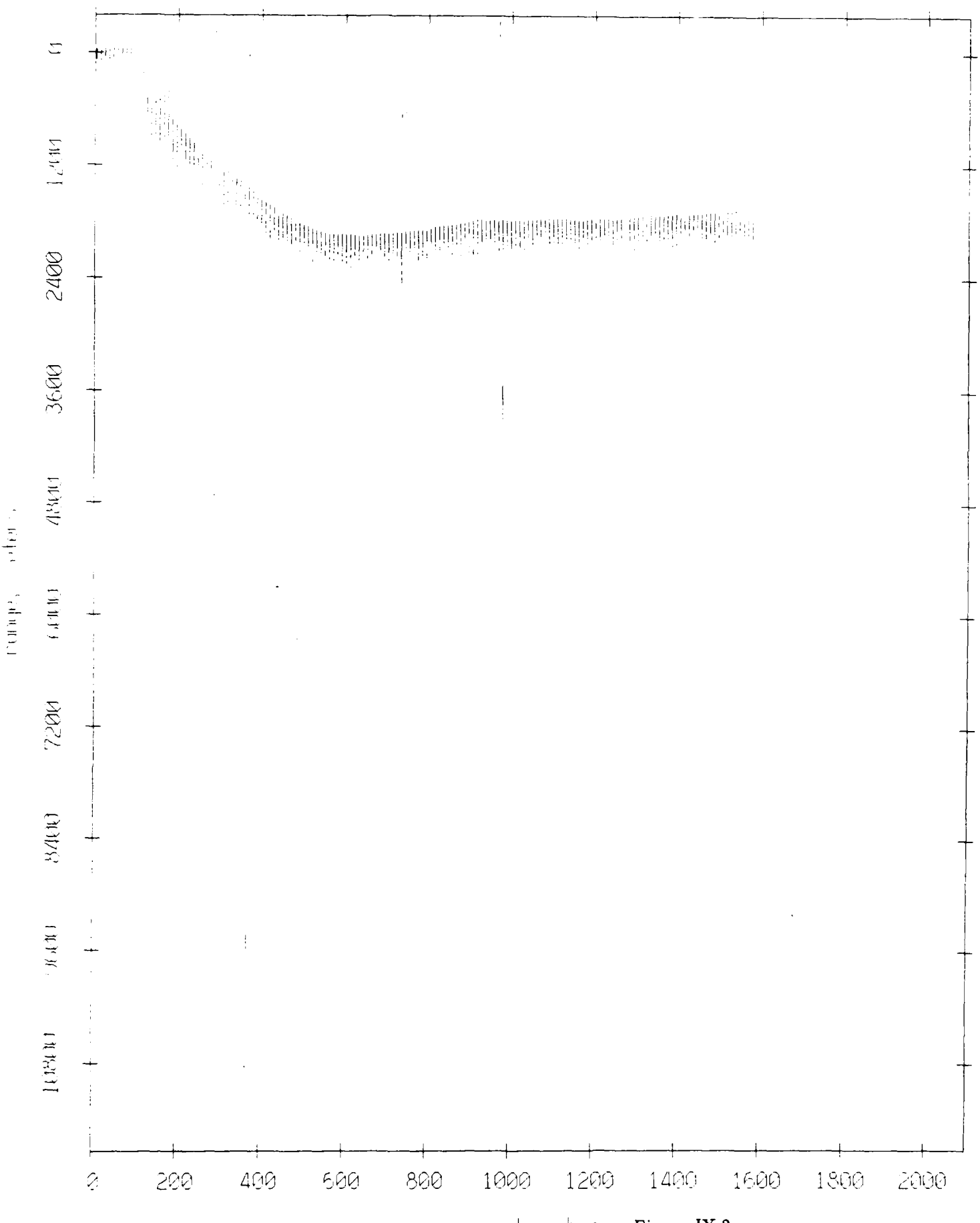

Float 5, August 1988 Experiment: range from float 6
2400
3600
7200
0
200
400
600
800
1000
1200
1400
1600
1800
2000
record number

Figure IX.3g

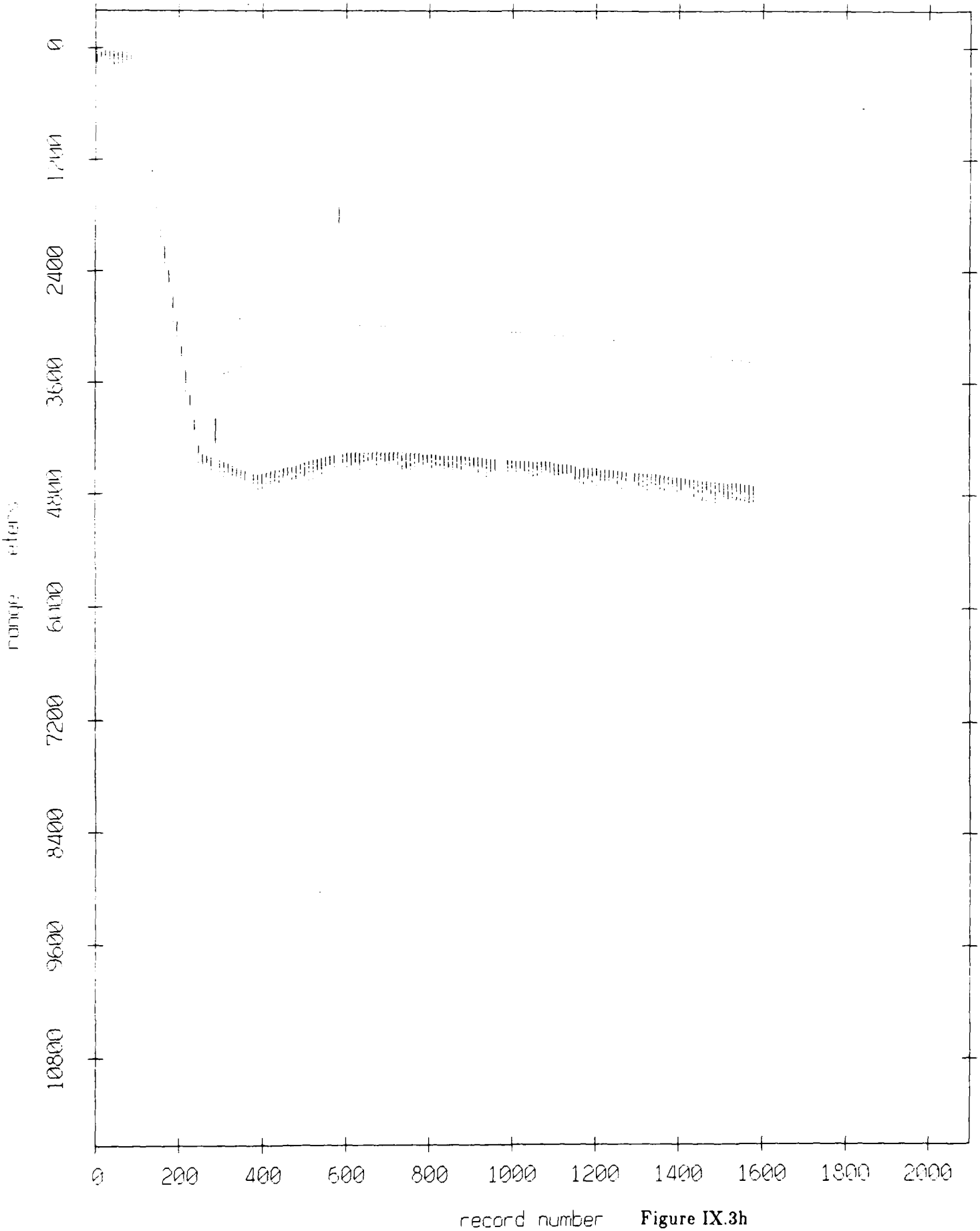

Float 5, August 1988 Experiment: range from float 11
0
1200
2400
3600
4800
6000
7200
8400
9600
10800
range (km)
0
200
400
600
800
1000
1200
1400
1600
1800
2000
record number

Figure IX.3h

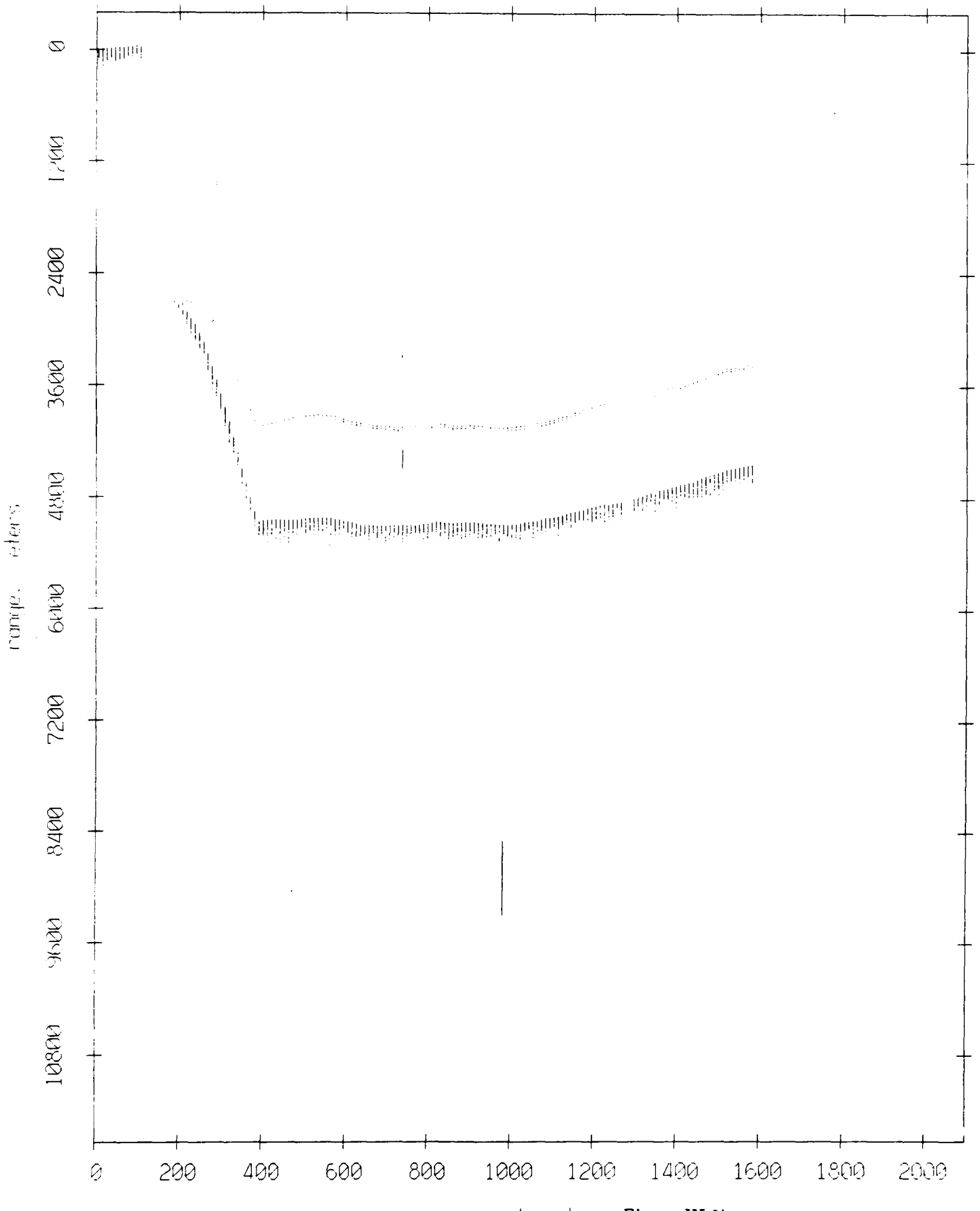

Float 5, August 1988 Experiment: range from float 7
0
1200
2400
3600
4800
6000
7200
8400
9600
10800
range, ctrs
0
200
400
600
800
1000
1200
1400
1600
1800
2000
record number

Figure IX.3i

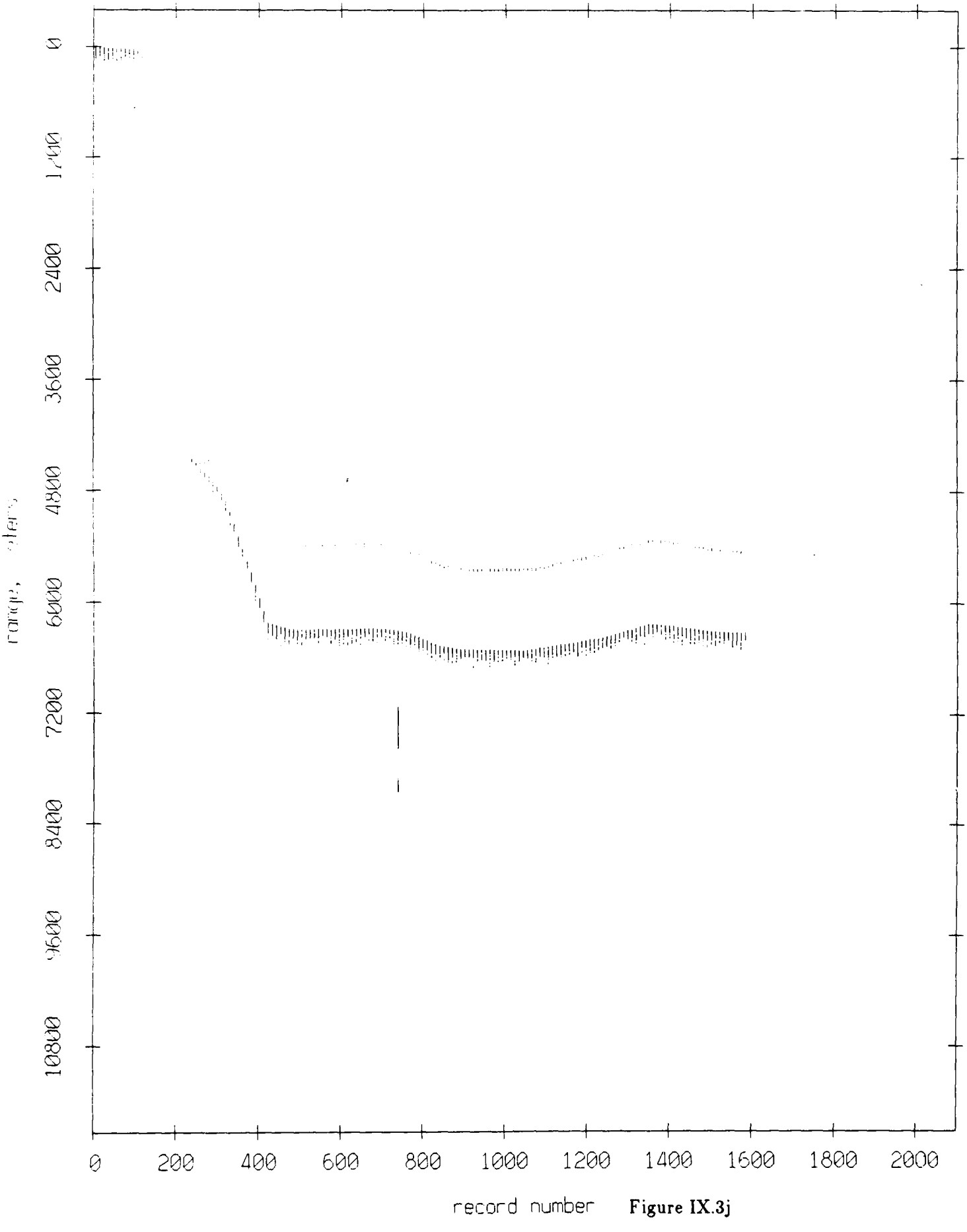

Float 5, August 1988 Experiment: range from float 8
0
1200
2400
3600
4800
6000
7200
8400
9600
10800
0
200
400
600
800
1000
1200
1400
1600
1800
2000
record number

Figure IX.3j

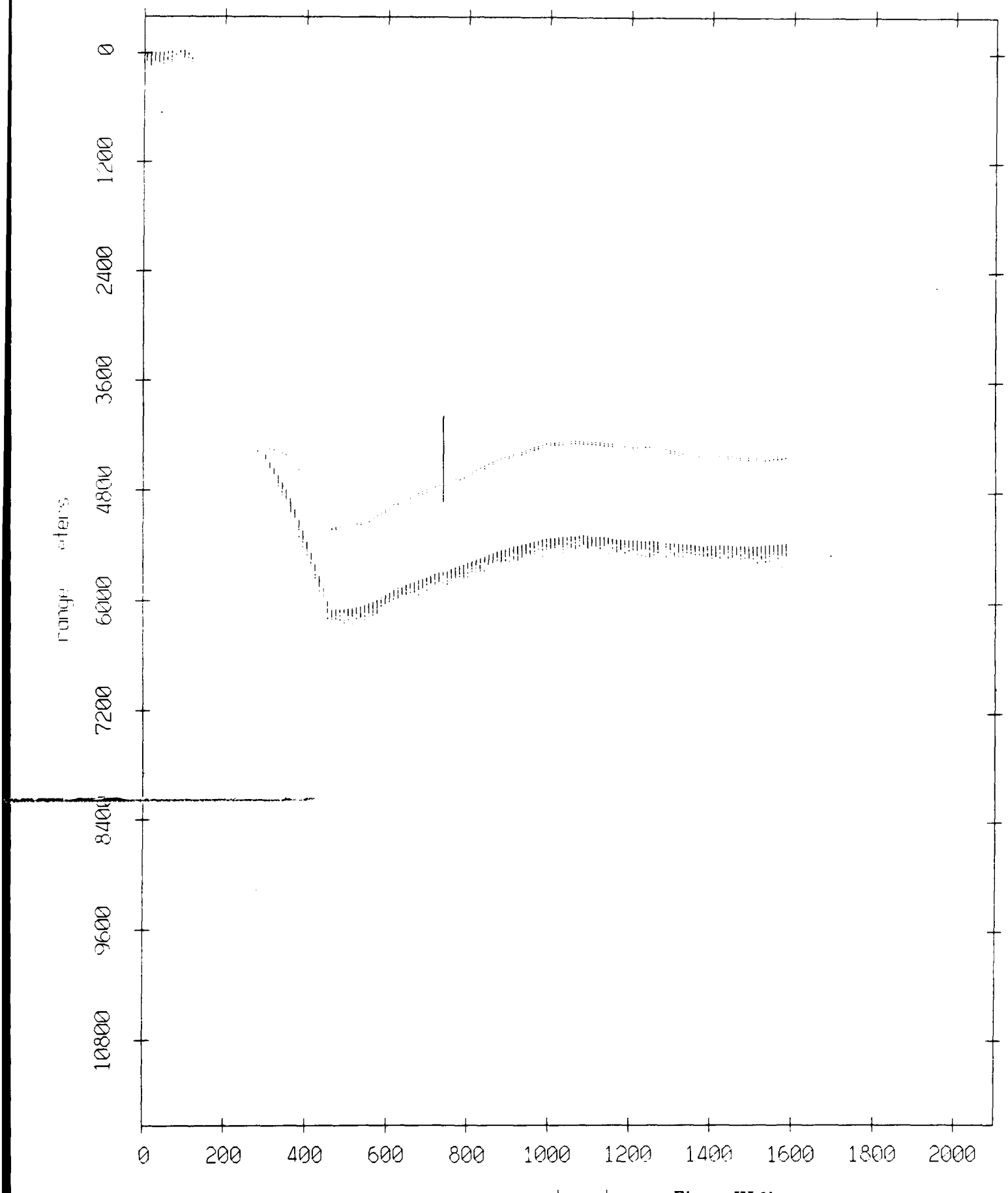

Float 5, August 1988 Experiment: range from float 9
0
1200
2400
3600
4800
6000
7200
8400
9600
10800
0
200
400
600
800
1000
1200
1400
1600
1800
2000
record number

Figure IX.3k

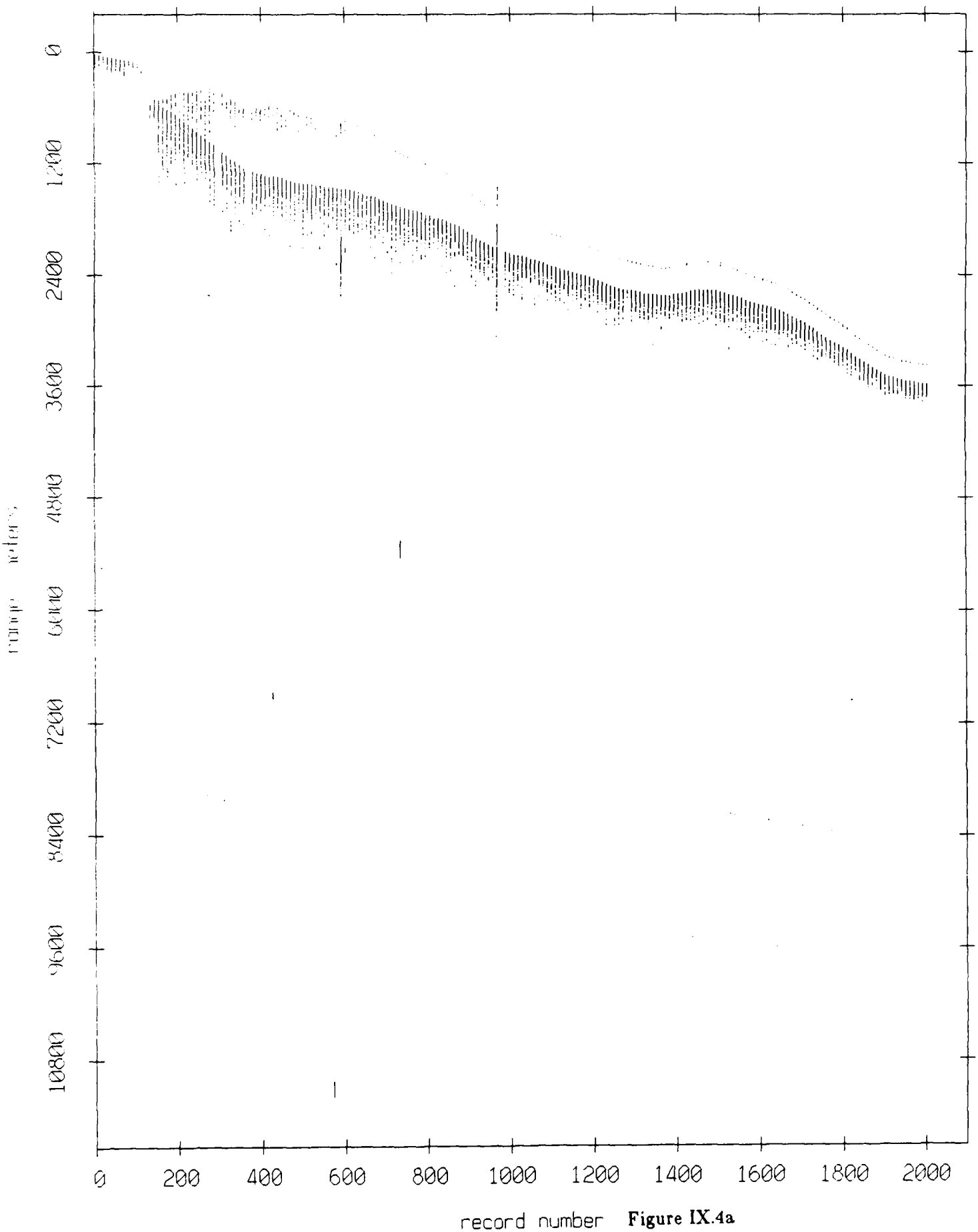

Float 0, August 1988 Experiment: range from float 10
0
1200
2400
3600
4800
6000
7200
8400
9600
10800
0
200
400
600
800
1000
1200
1400
1600
1800
2000
record number

Figure IX.4a

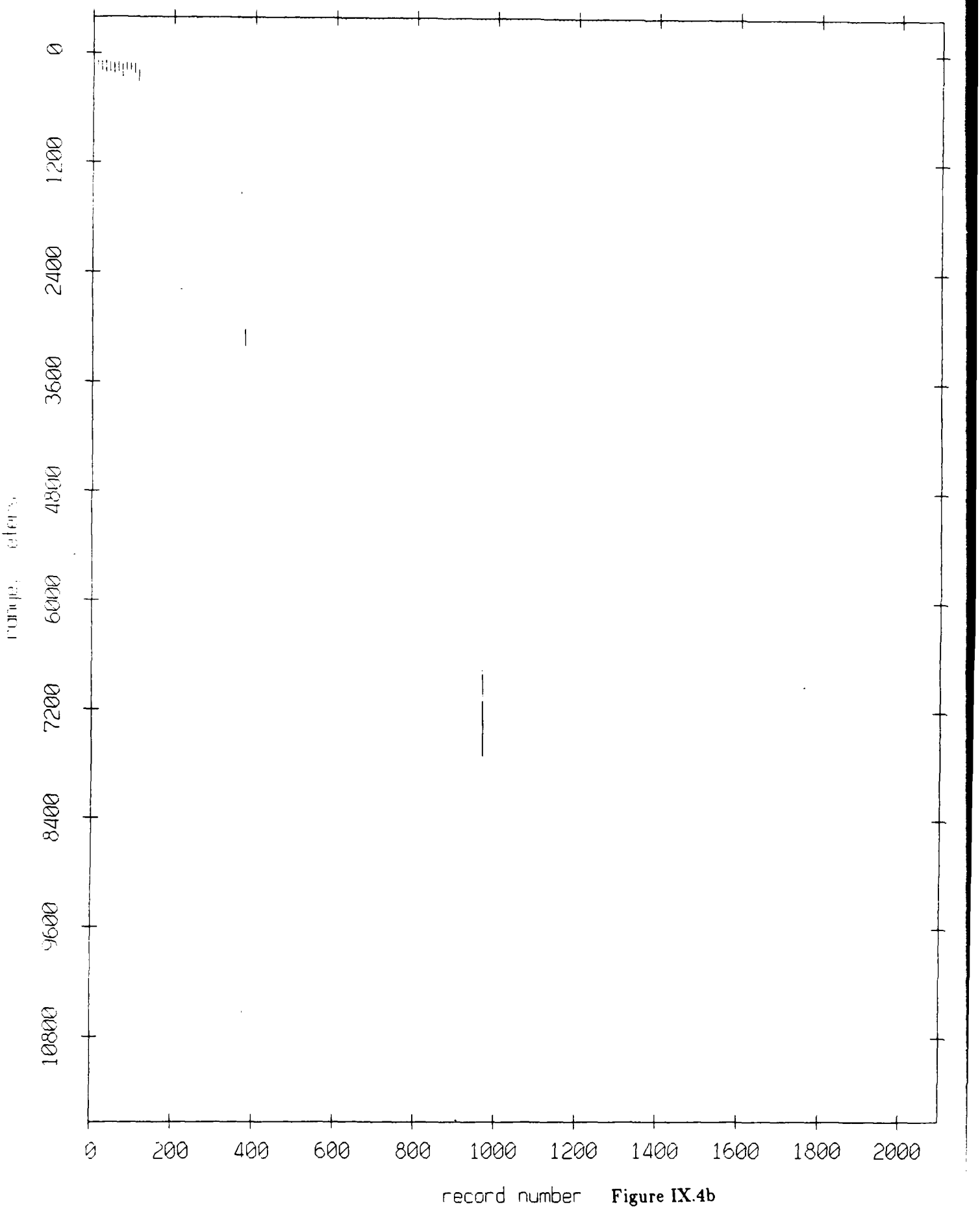

Float 0, August 1988 Experiment: range from float 3
0
1200
2400
3600
4800
6000
7200
8400
9600
10800
0
200
400
600
800
1000
1200
1400
1600
1800
2000
record number

Figure IX.4b

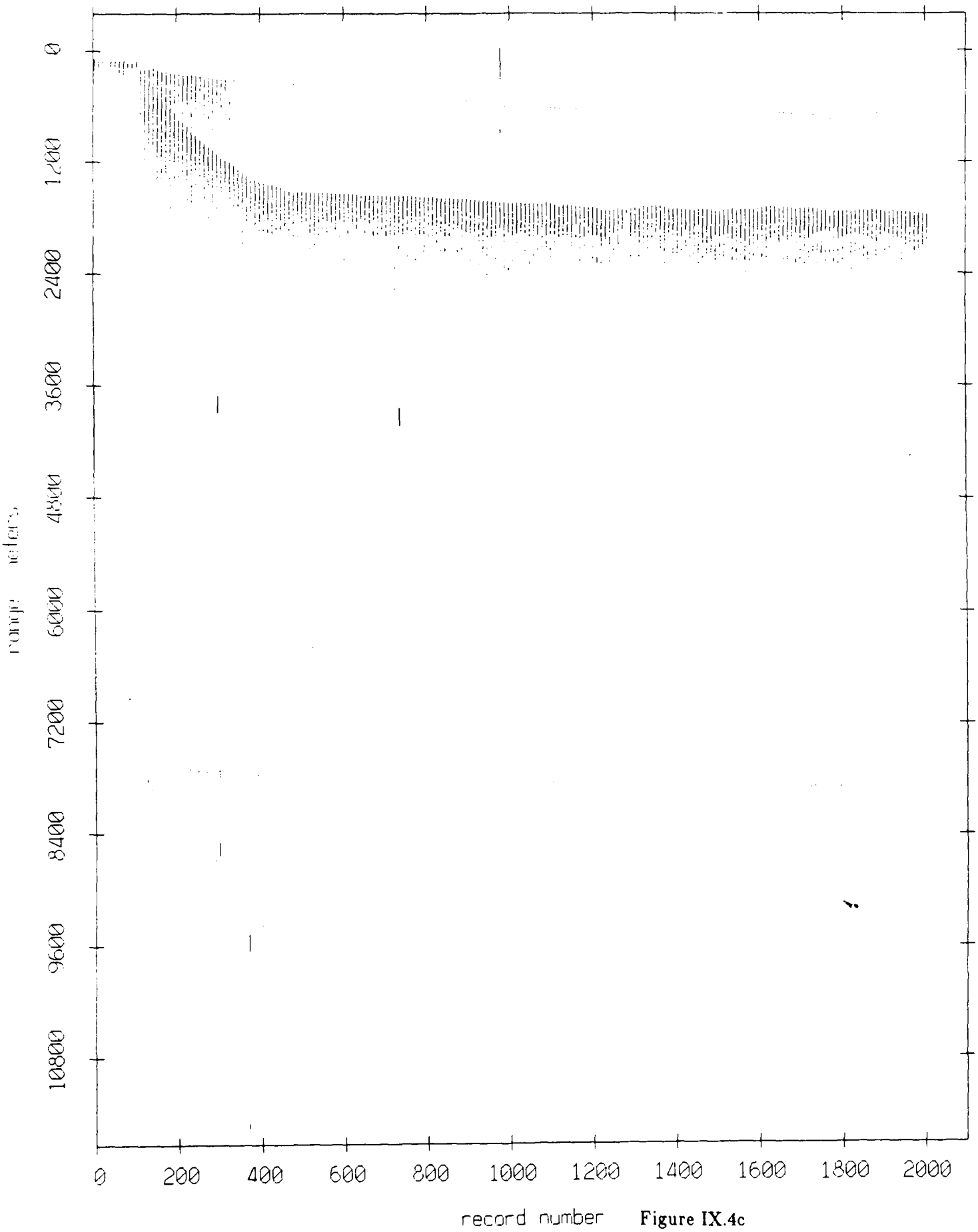

Float 0, August 1988 Experiment: range from float 5
0
1200
2400
3600
4800
6000
7200
8400
9600
10800
0
200
400
600
800
1000
1200
1400
1600
1800
2000
record number

Figure IX.4c

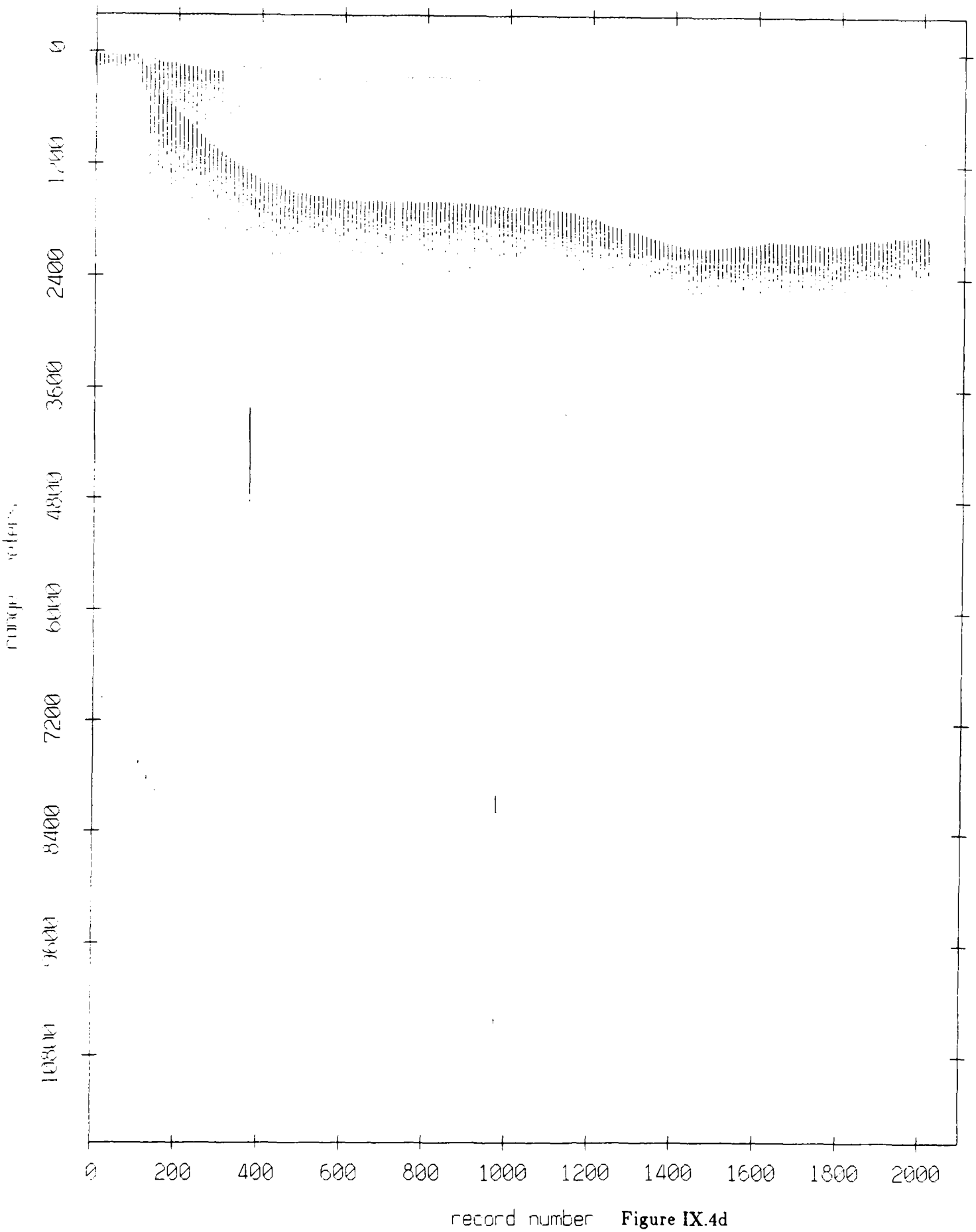

Float 0, August 1988 Experiment: range from float 1
0
1200
2400
3600
4800
6000
7200
8400
9600
10800
range, meters
0
200
400
600
800
1000
1200
1400
1600
1800
2000
record number

Figure IX.4d

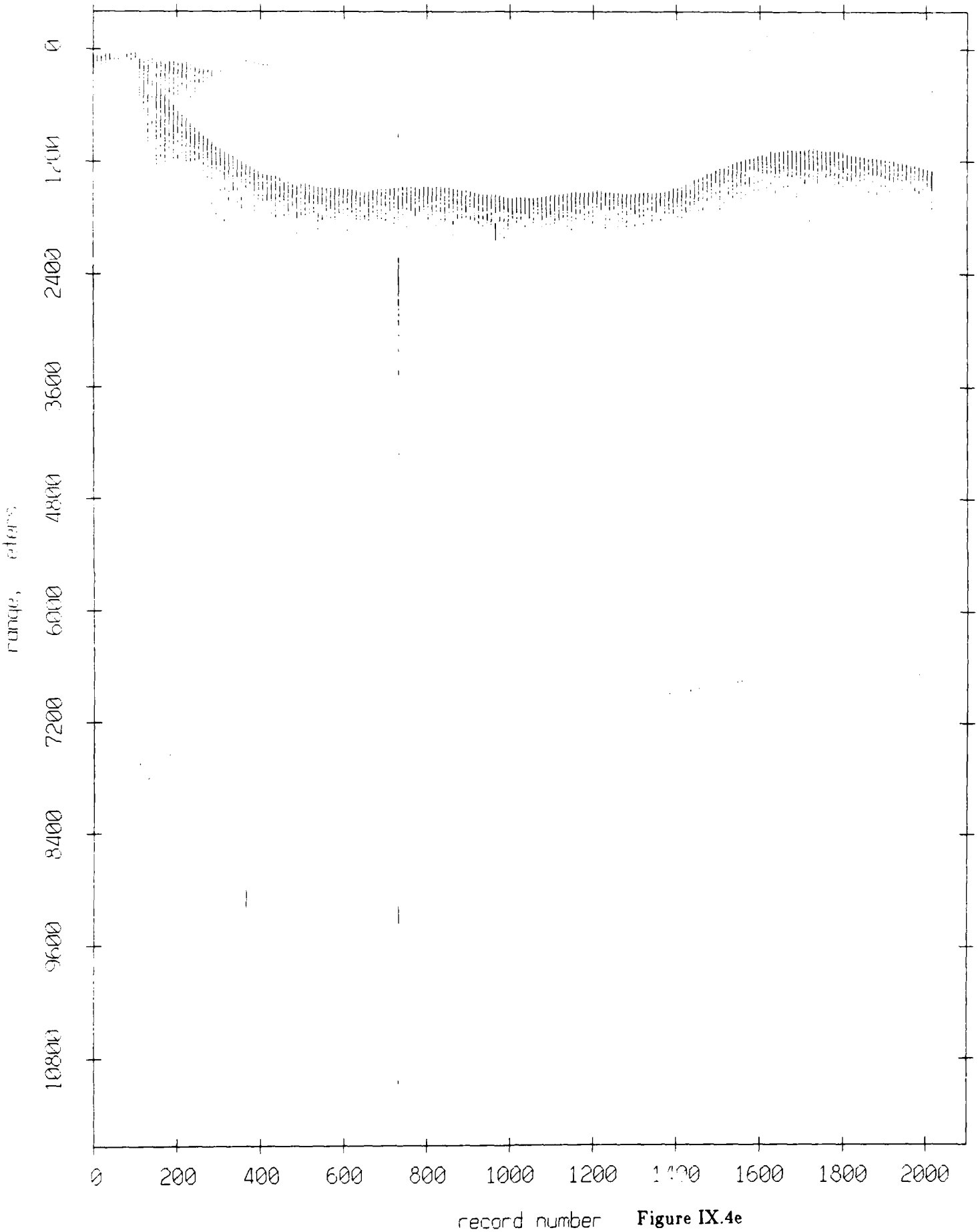

Float 0, August 1988 Experiment: range from float 2
range, ctors
0
1200
2400
3600
4800
6000
7200
8400
9600
10800
0
200
400
600
800
1000
1200
1400
1600
1800
2000
record number

Figure IX.4e

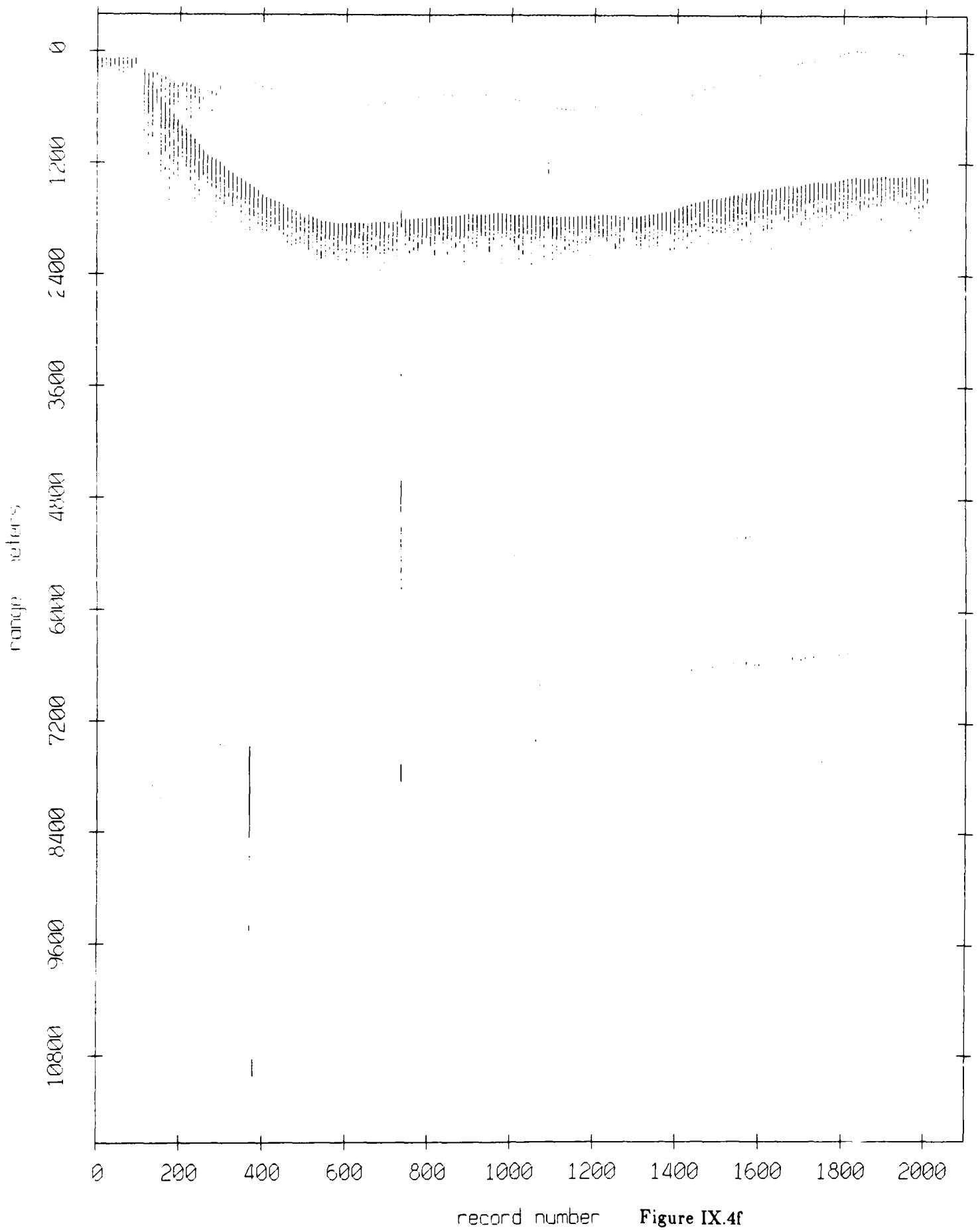

Float 0, August 1988 Experiment: range from float 4
range meters
0
1200
2400
3600
4800
6000
7200
8400
9600
10800
0
200
400
600
800
1000
1200
1400
1600
1800
2000
record number

Figure IX.4f

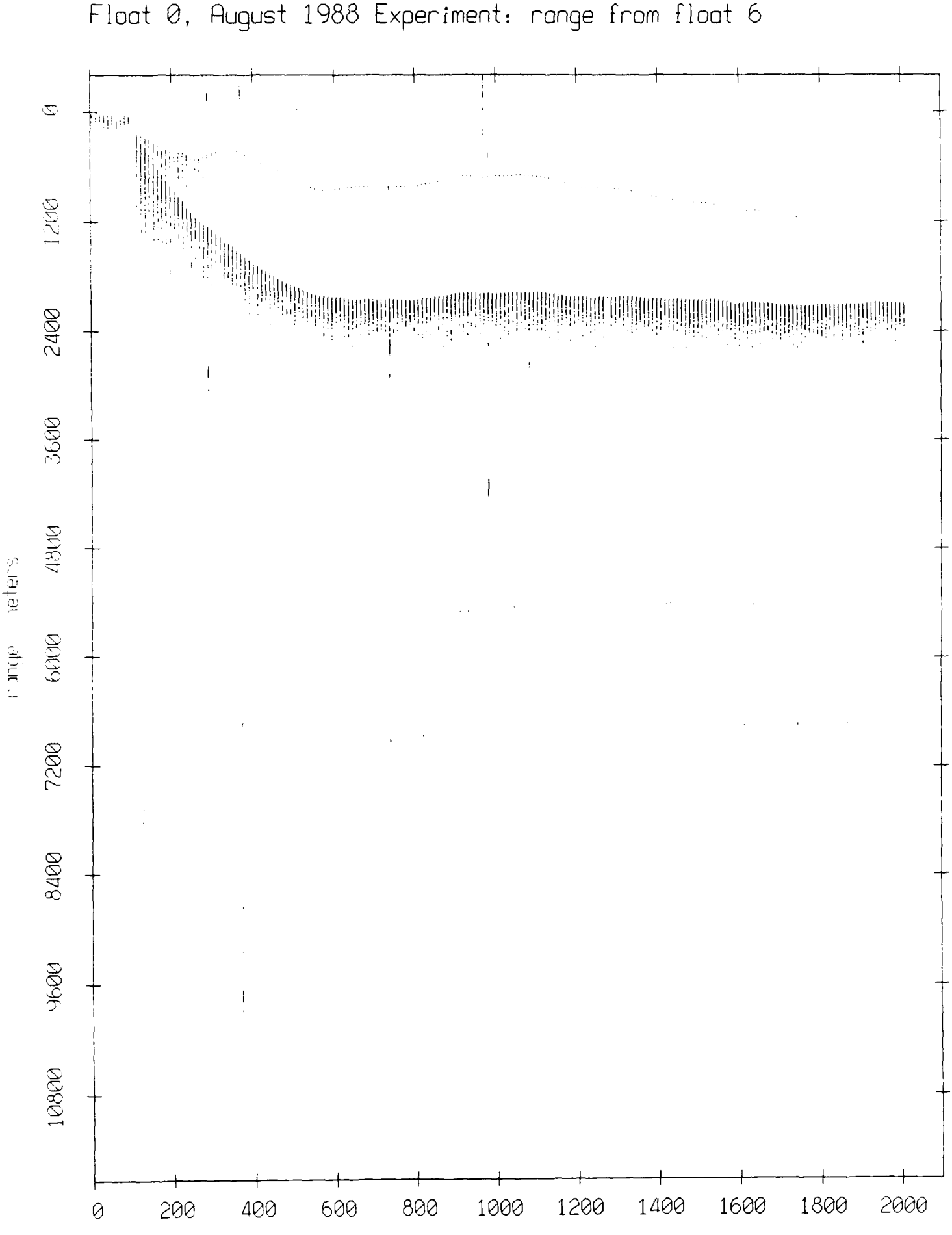

Float 0, August 1988 Experiment: range from float 6
0
1200
2400
3600
4800
6000
7200
8400
9600
10800
meters
0
200
400
600
800
1000
1200
1400
1600
1800
2000
record number

Figure IX.4g

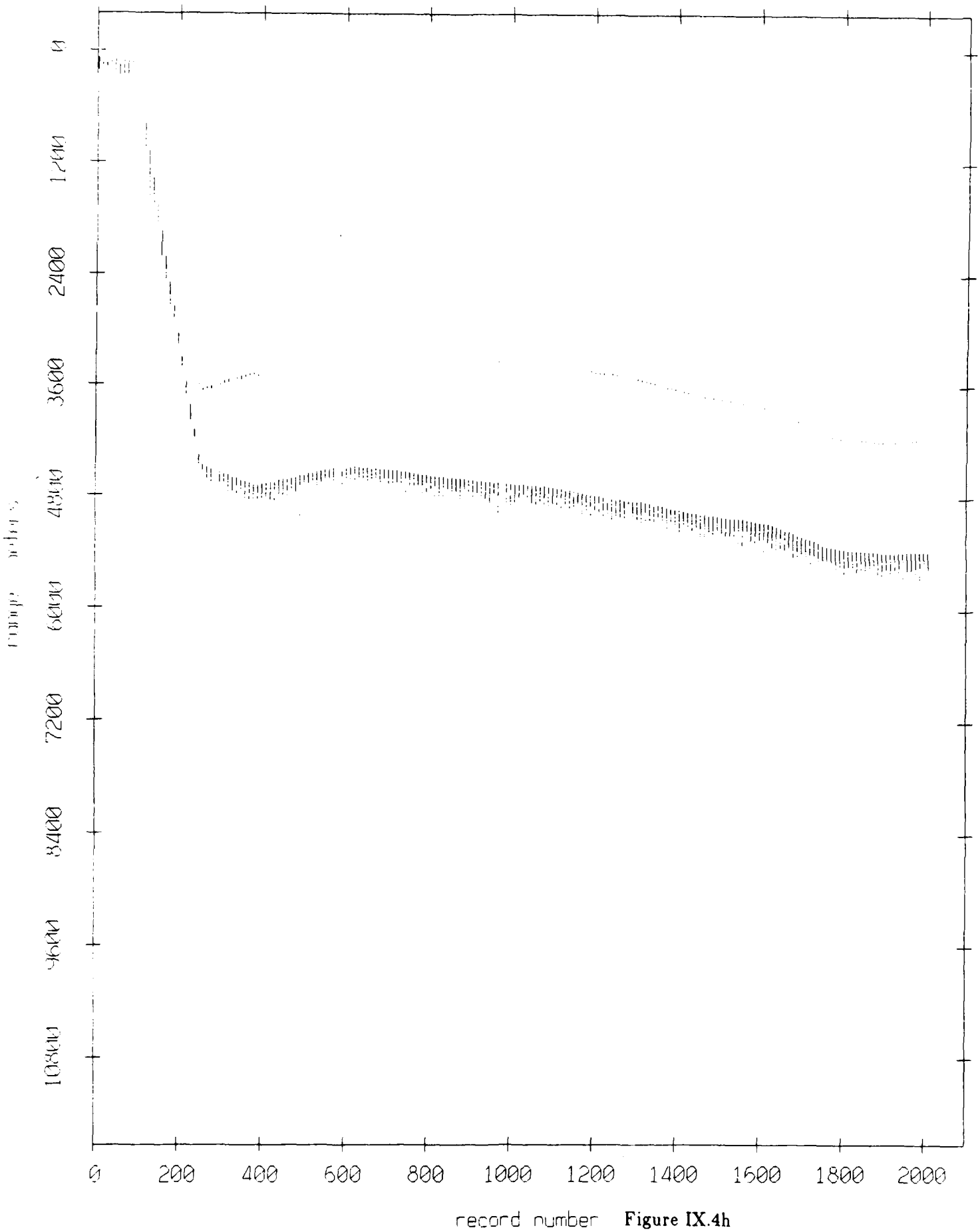

Float 0, August 1988 Experiment: range from float 11
0
1200
2400
3600
4800
6000
7200
8400
9600
10800
0
200
400
600
800
1000
1200
1400
1600
1800
2000
record number

Figure IX.4h

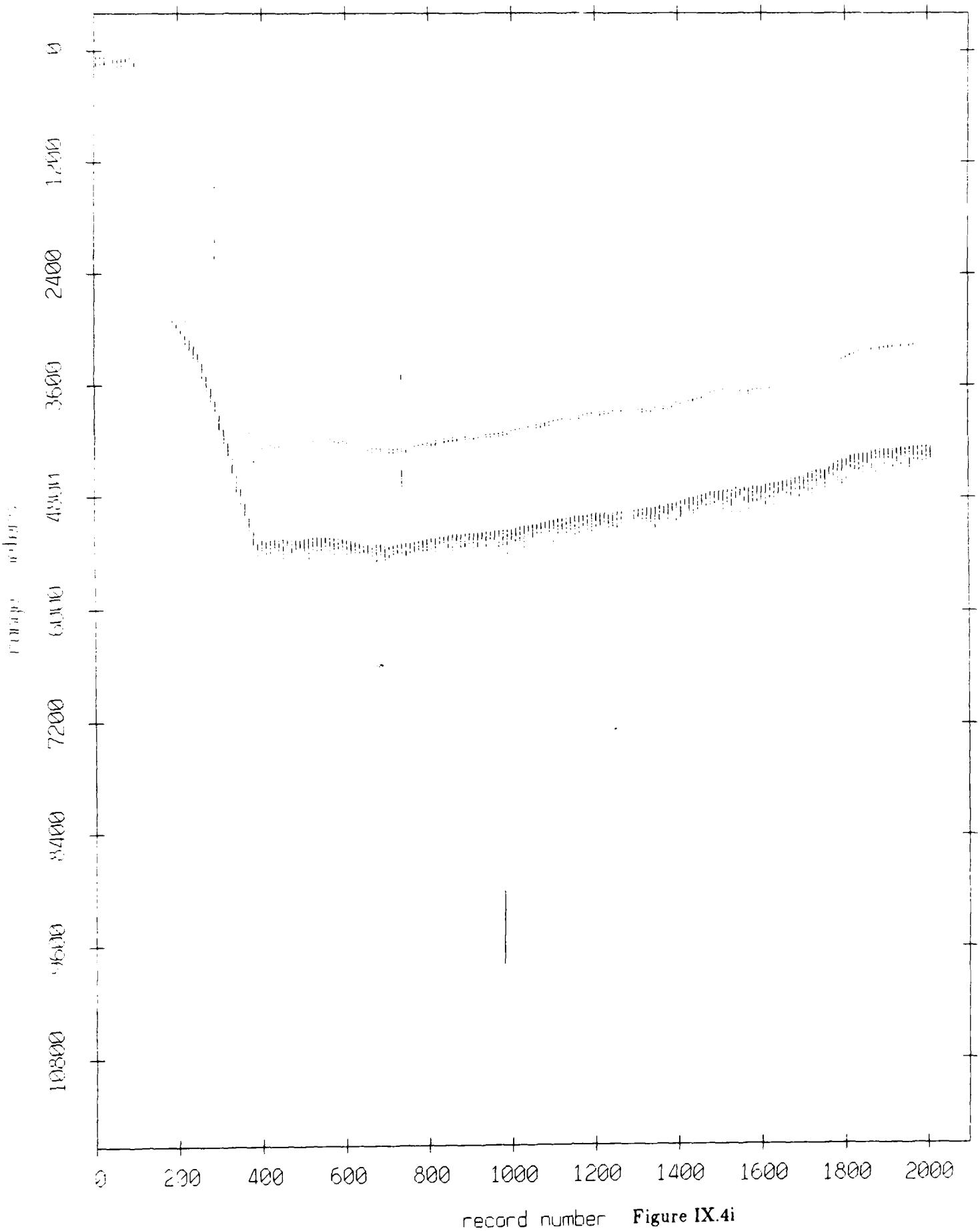

Float 0, August 1988 Experiment: range from float 7
0
1200
2400
3600
4800
6000
7200
8400
9600
10800
0
200
400
600
800
1000
1200
1400
1600
1800
2000
record number

Figure IX.4i

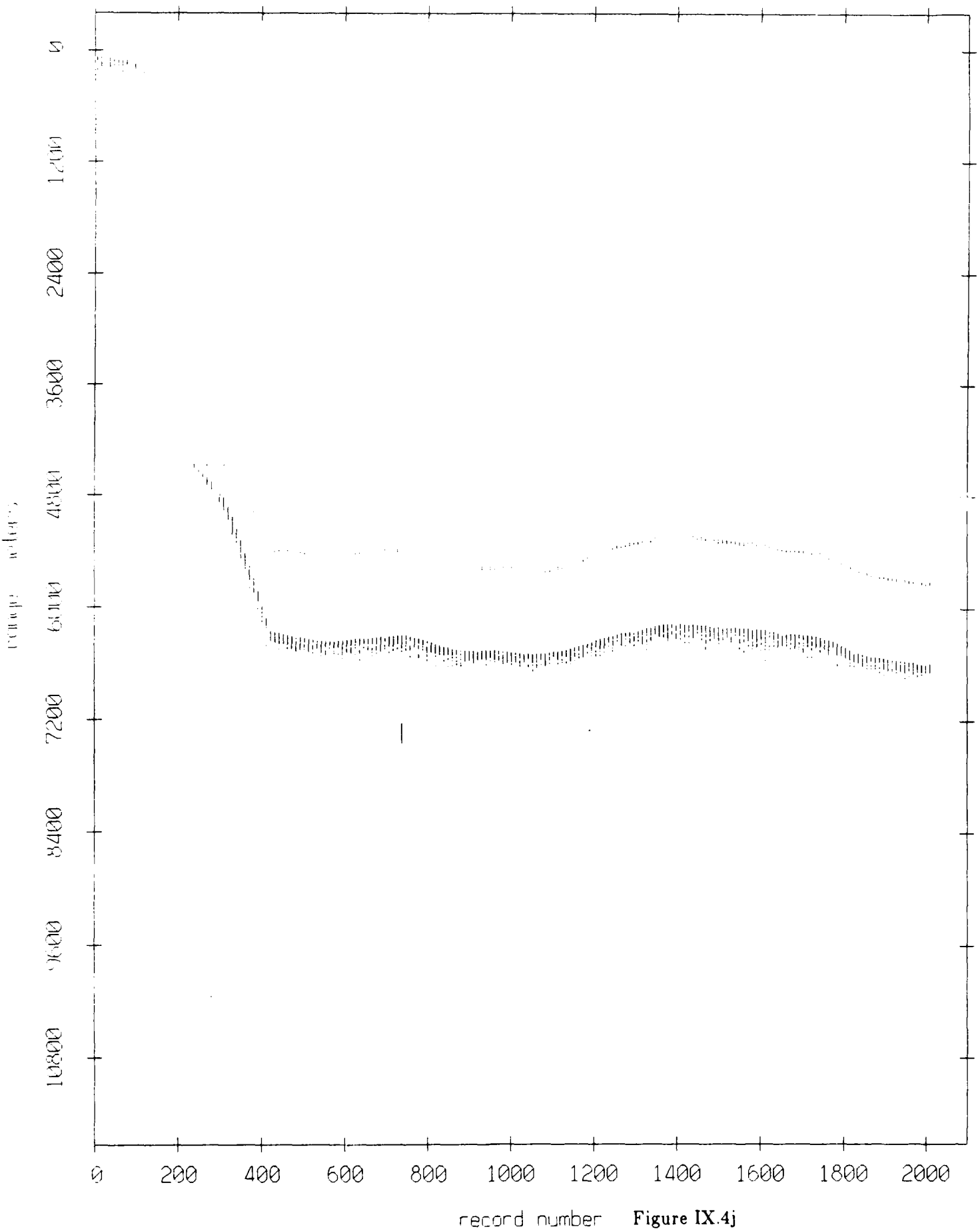

Float 0, August 1988 Experiment: range from float 8
2400
3600
7200
0
200
400
600
800
1000
1200
1400
1600
1800
2000
record number

Figure IX.4j

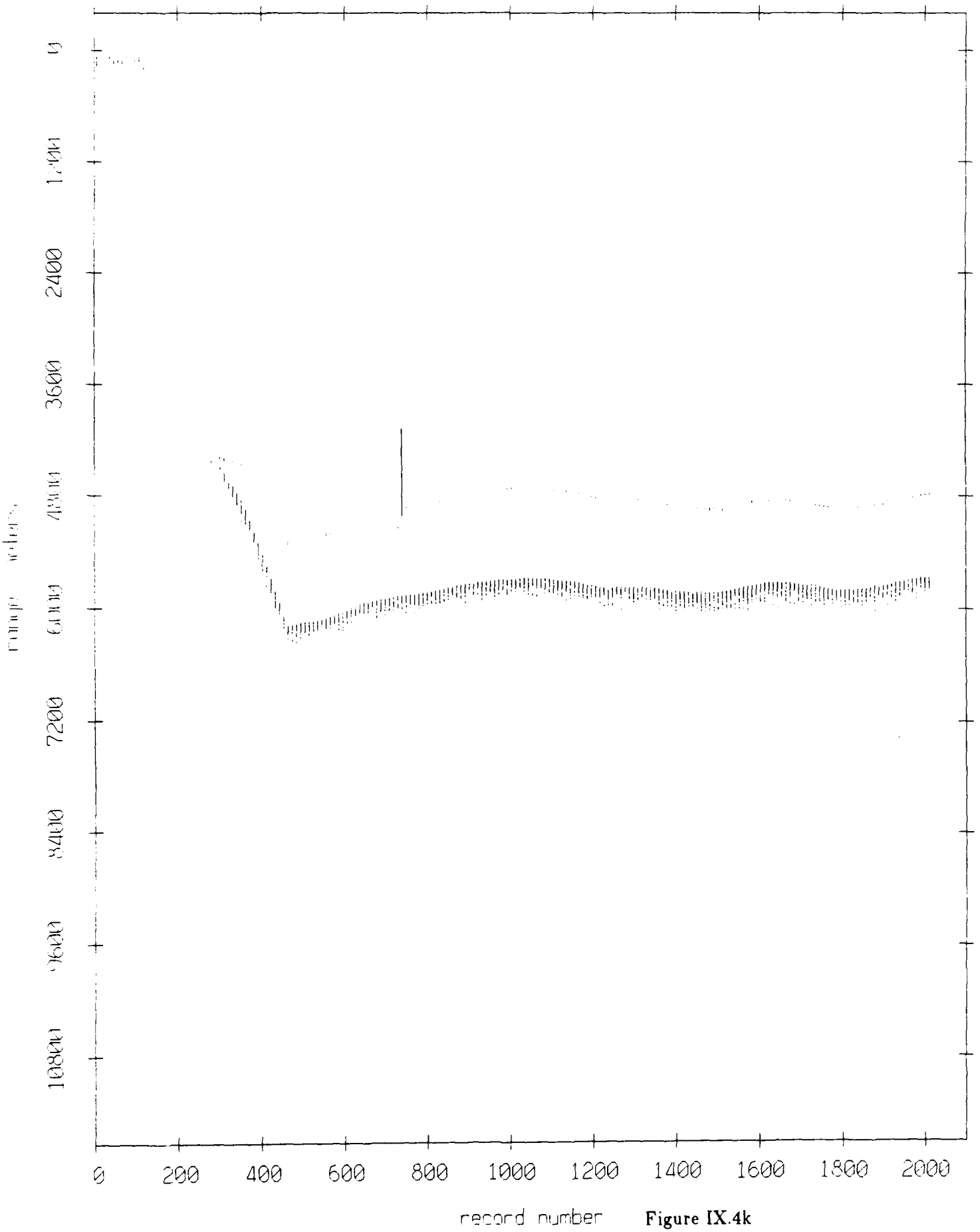

Float 0, August 1988 Experiment: range from float 9
3600
2400
7200
0
200
400
600
800
1000
1200
1400
1600
1800
2000
record number

Figure IX.4k

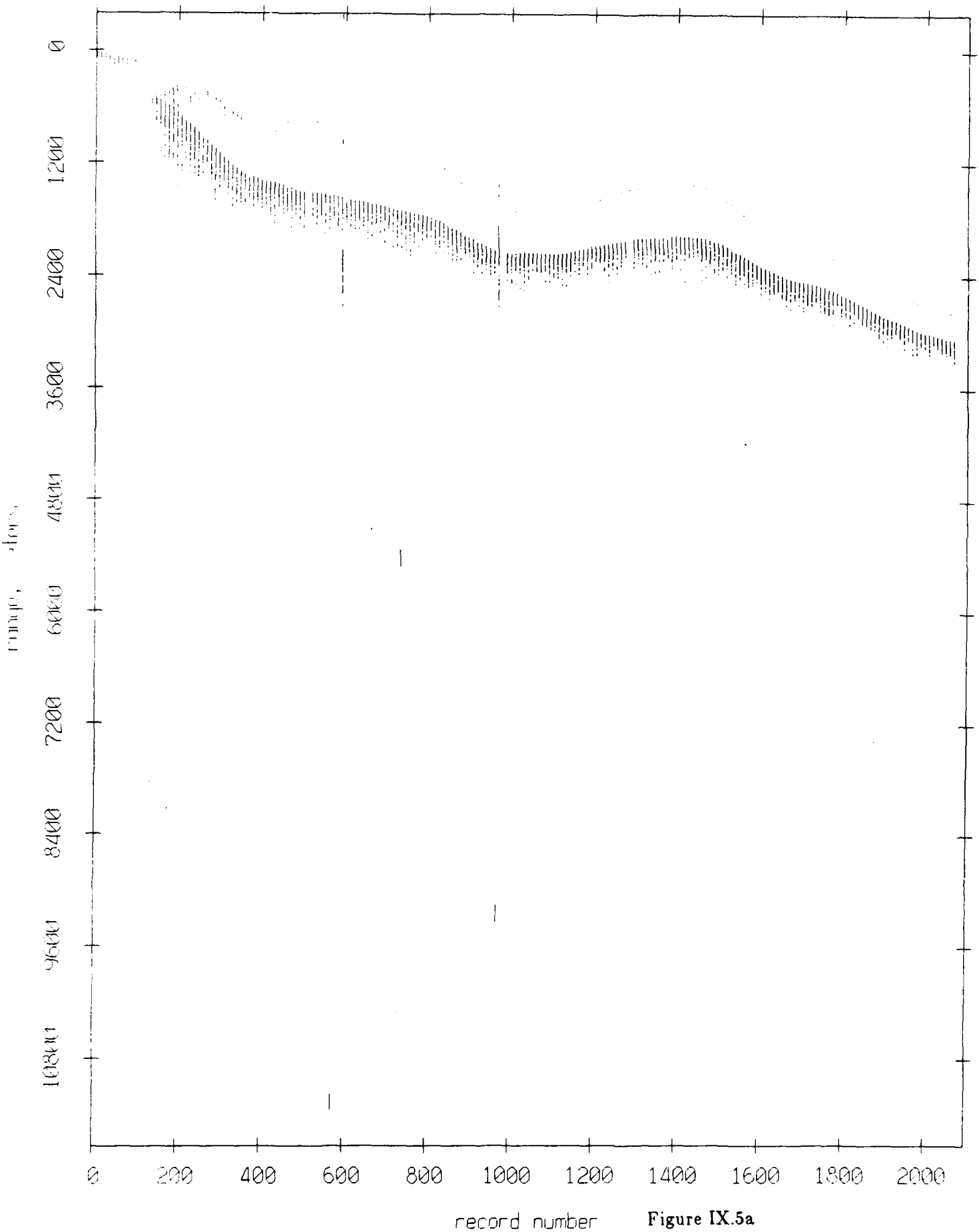

Float 1, August 1988 Experiment: range from float 10
0
1200
2400
3600
4800
6000
7200
8400
9600
10800
0
200
400
600
800
1000
1200
1400
1600
1800
2000
record number

Figure IX.5a

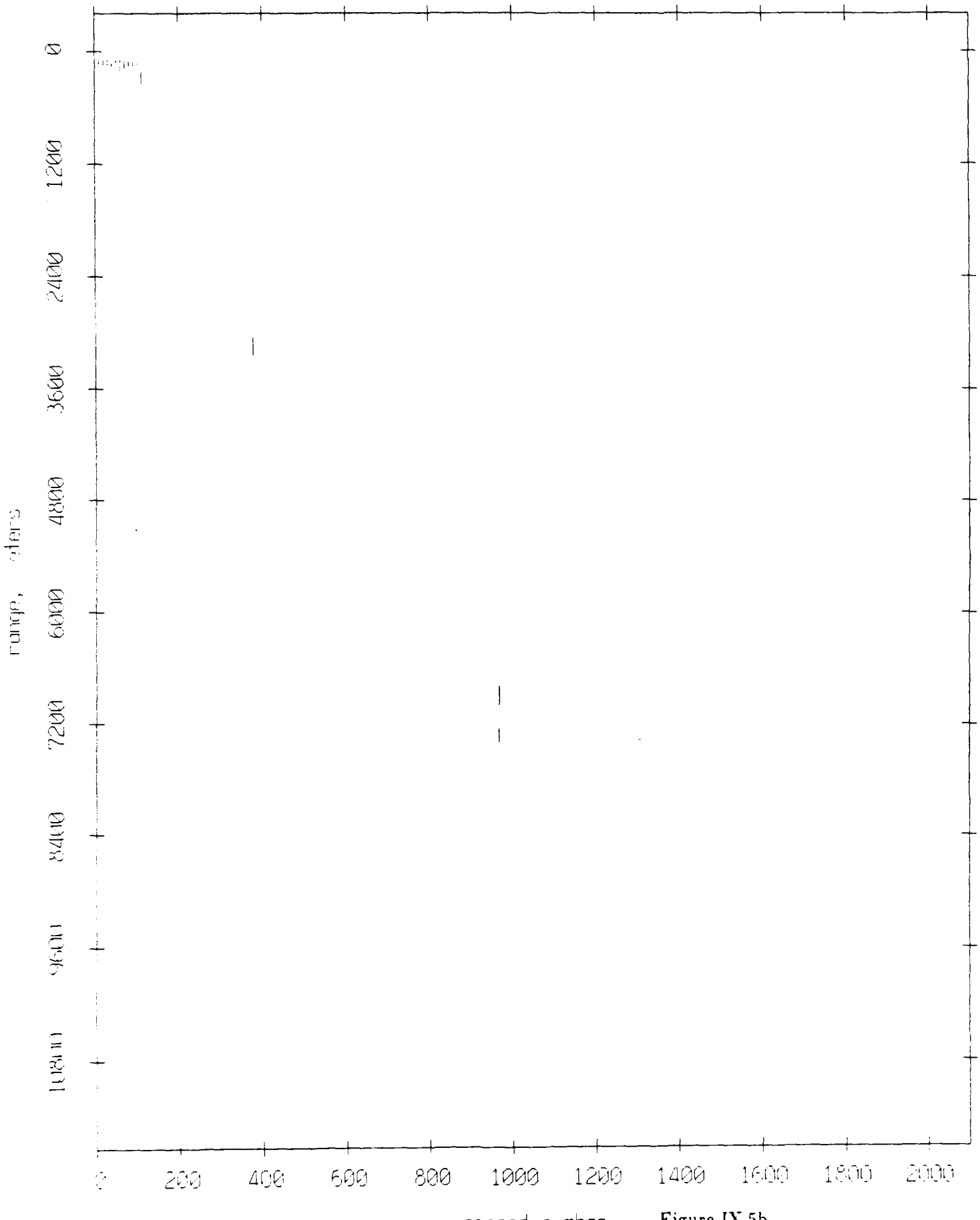

Float 1, August 1988 Experiment: range from float 3
range, meters
0
1200
2400
3600
4800
6000
7200
8400
9601
10801
0
200
400
600
800
1000
1200
1400
1600
1800
2000
record number

Figure IX.5b

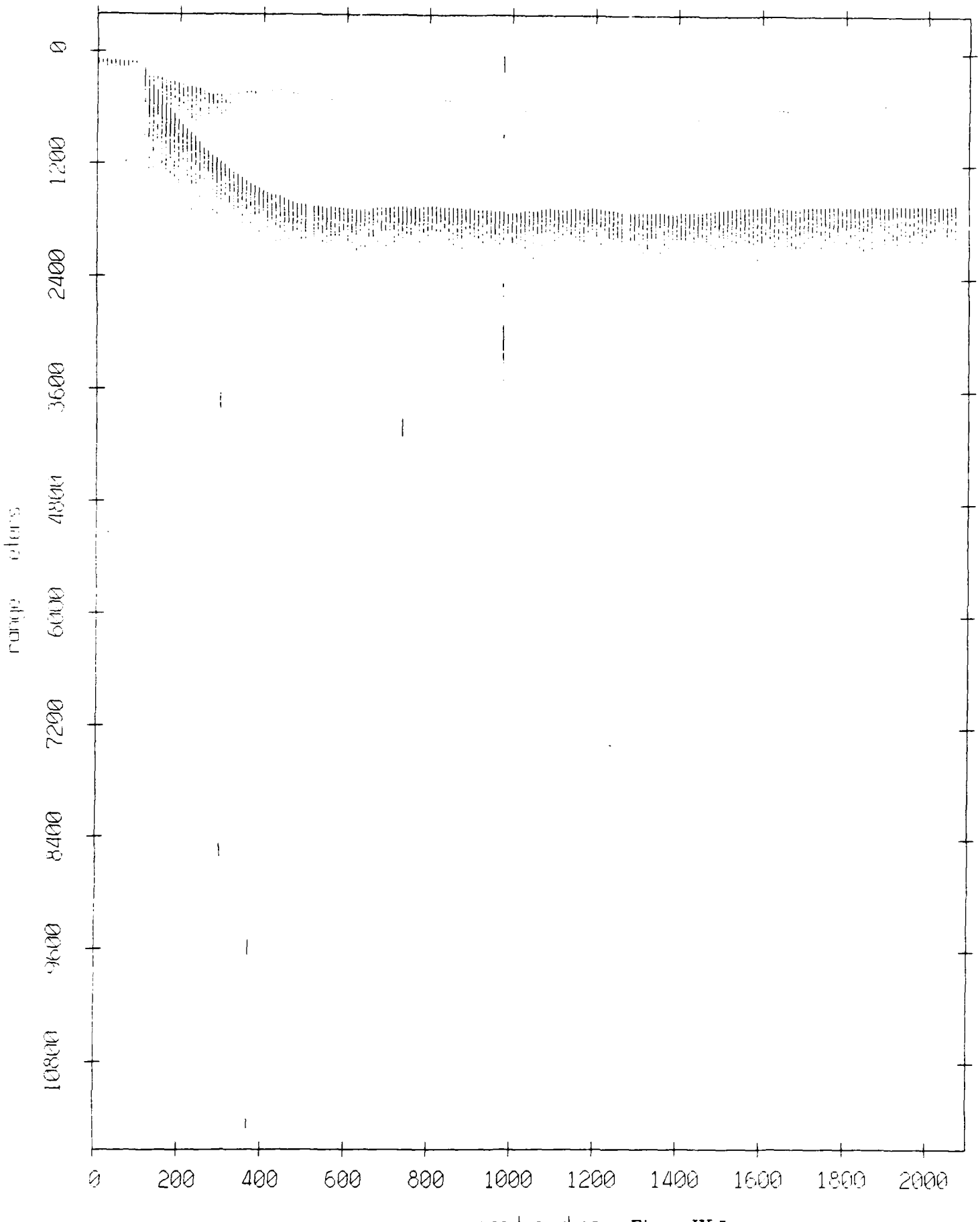

Float 1, August 1988 Experiment: range from float 5
range, others
0
1200
2400
3600
4800
6000
7200
8400
9600
10800
0
200
400
600
800
1000
1200
1400
1600
1800
2000
record number

Figure IX.5c

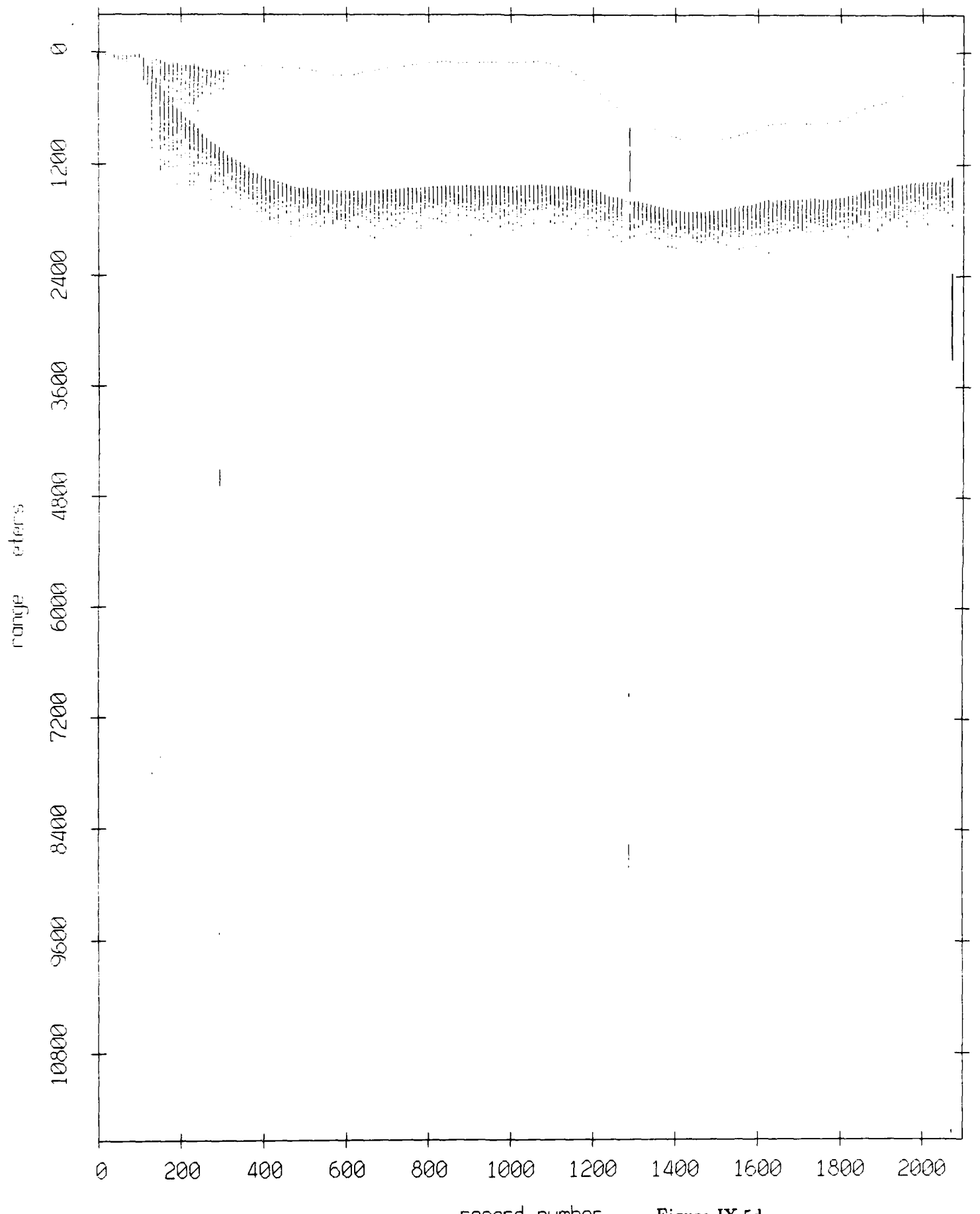

Float 1, August 1988 Experiment: range from float 0
range meters
0
1200
2400
3600
4800
6000
7200
8400
9600
10800
0
200
400
600
800
1000
1200
1400
1600
1800
2000
record number

Figure IX.5d

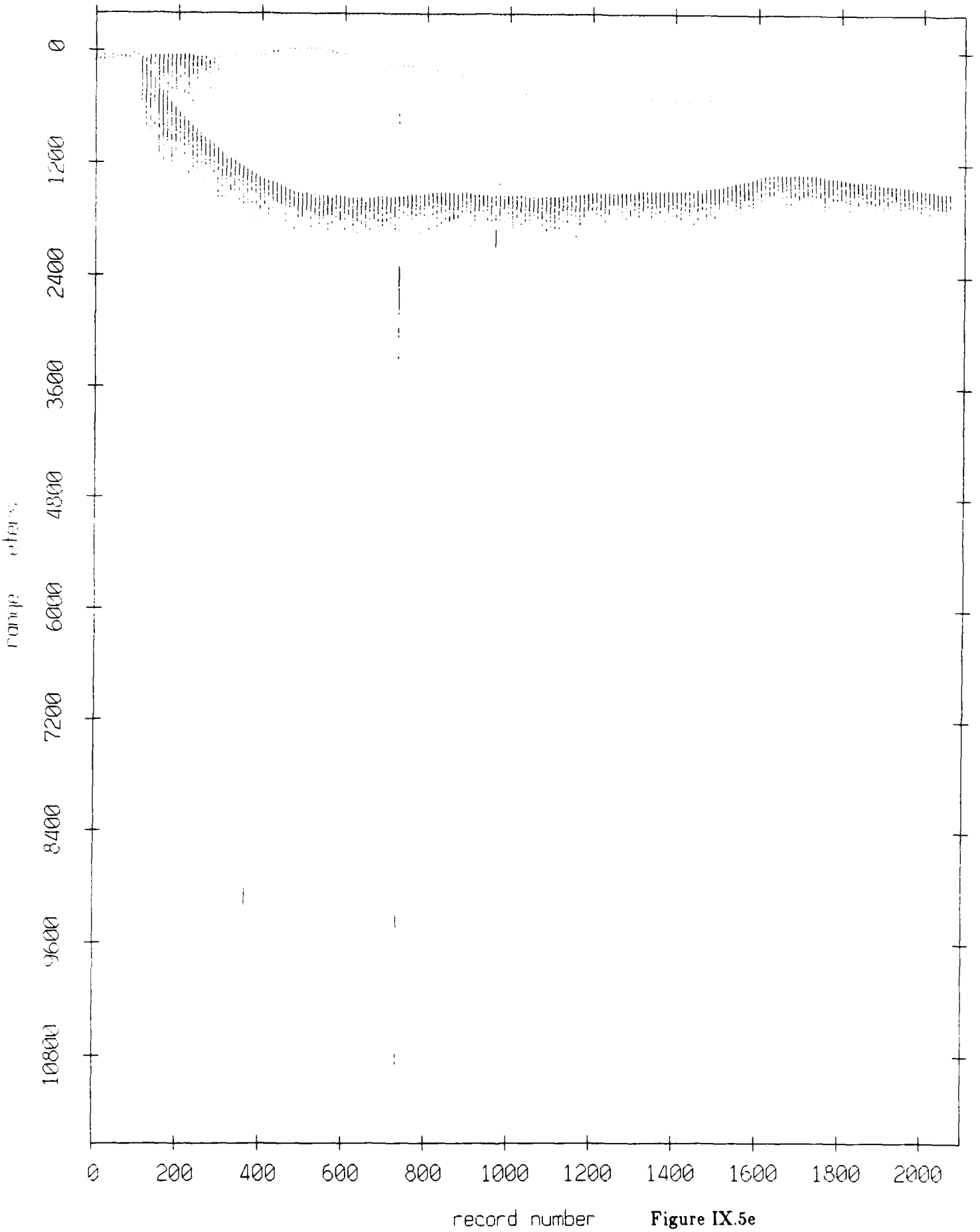

Float 1, August 1988 Experiment: range from float 2
0
1200
2400
3600
4800
6000
7200
8400
9600
10800
0
200
400
600
800
1000
1200
1400
1600
1800
2000
record number

Figure IX.5e

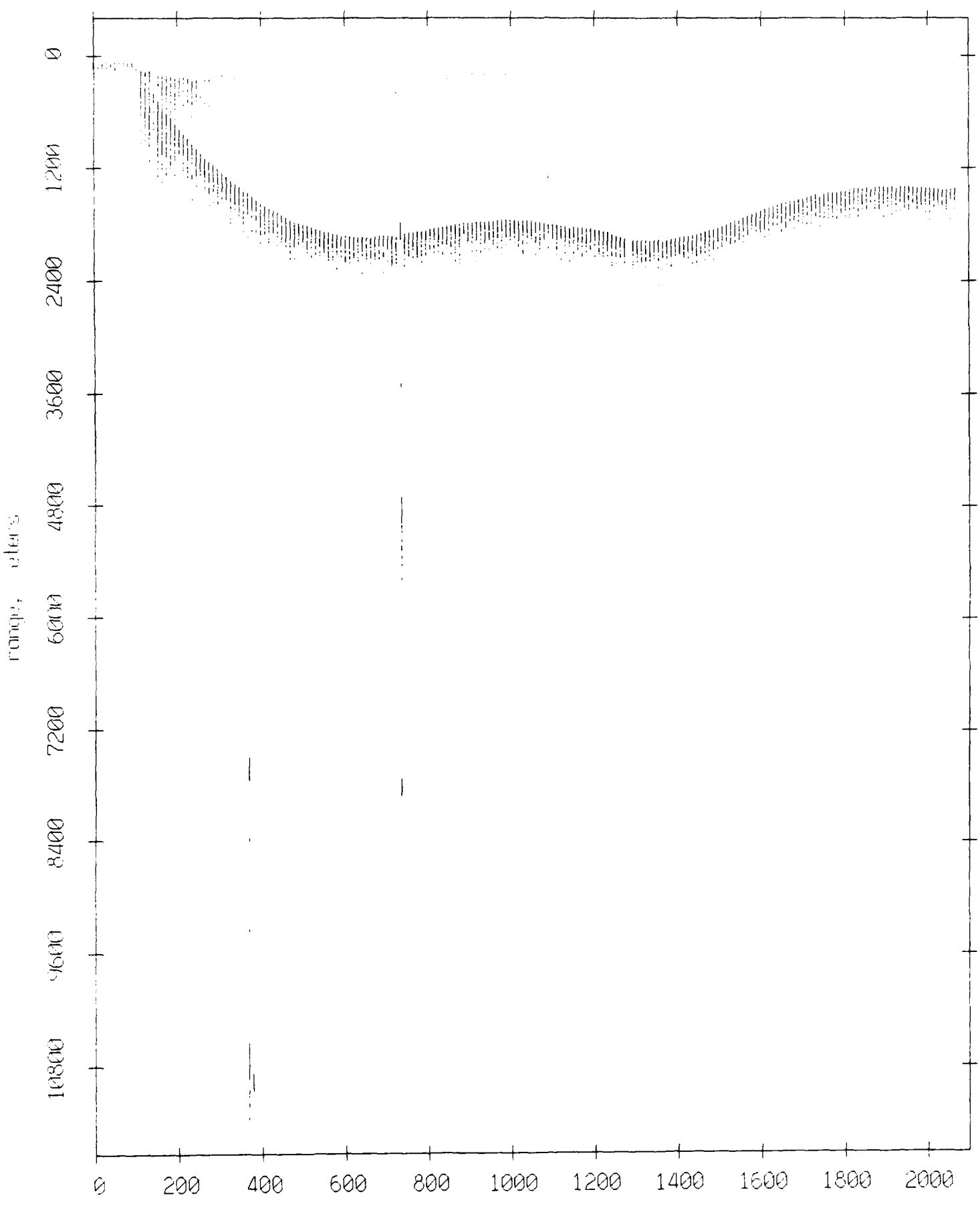

Float 1, August 1988 Experiment: range from float 4
range, ohms
0
1200
2400
3600
4800
6000
7200
8400
9600
10800
0
200
400
600
800
1000
1200
1400
1600
1800
2000
record number

Figure IX.5f

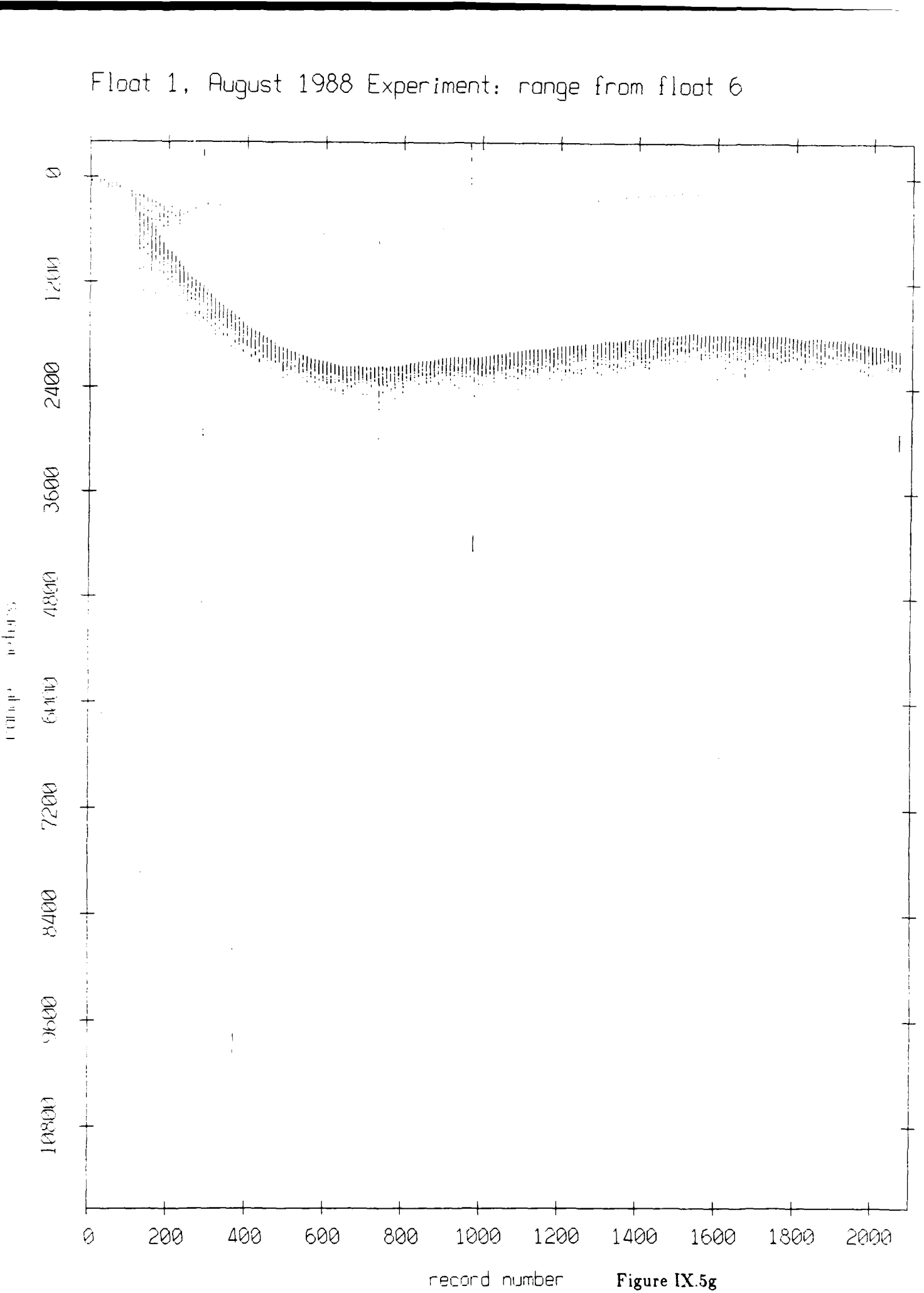

Float 1, August 1988 Experiment: range from float 6
0
1200
2400
3600
4800
6000
7200
8400
9600
10800
0
200
400
600
800
1000
1200
1400
1600
1800
2000
record number

Figure IX.5g

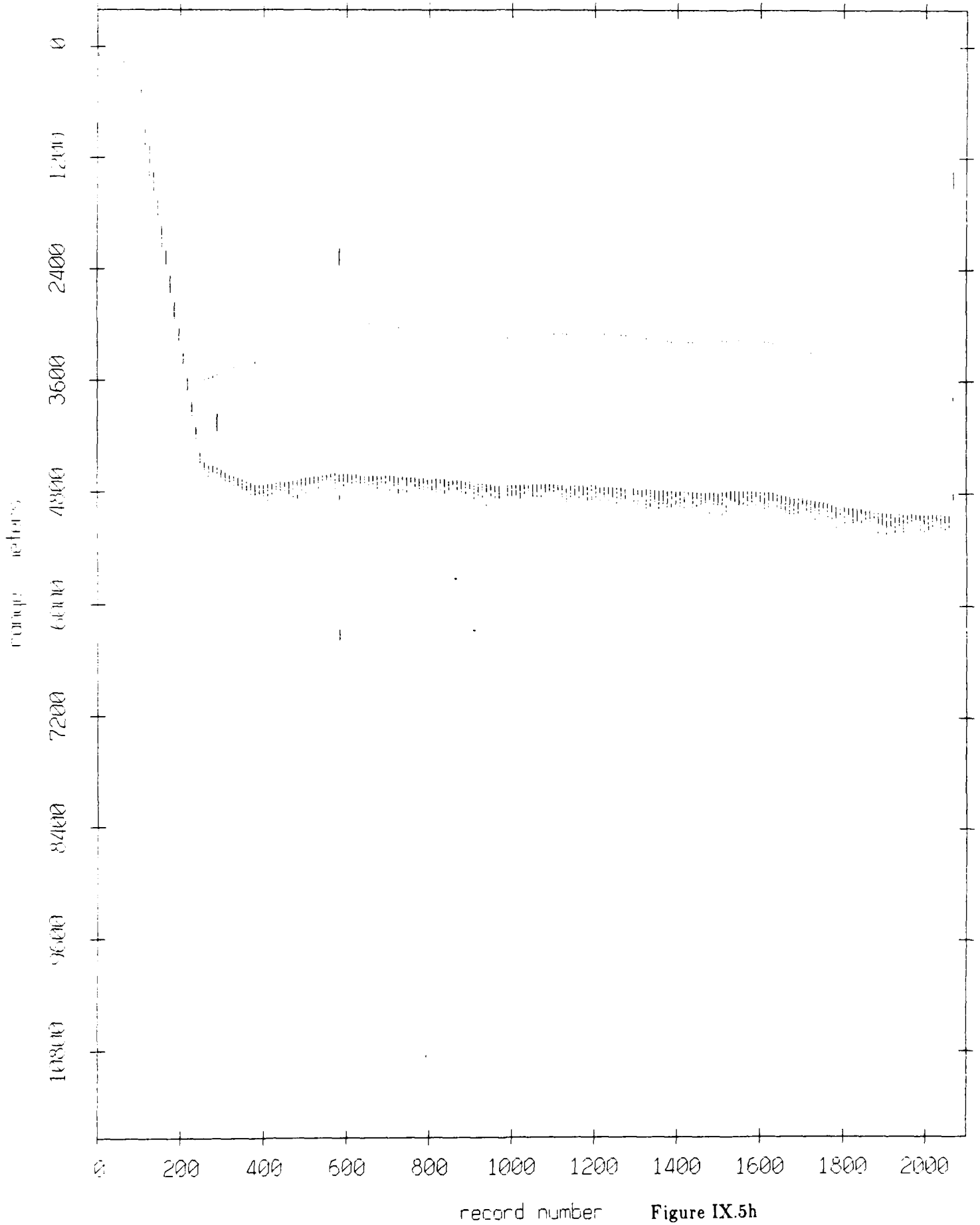

Float 1, August 1988 Experiment: range from float 11
0
1200
2400
3600
4800
6000
7200
8400
9600
10800
0
200
400
600
800
1000
1200
1400
1600
1800
2000
record number

Figure IX.5h

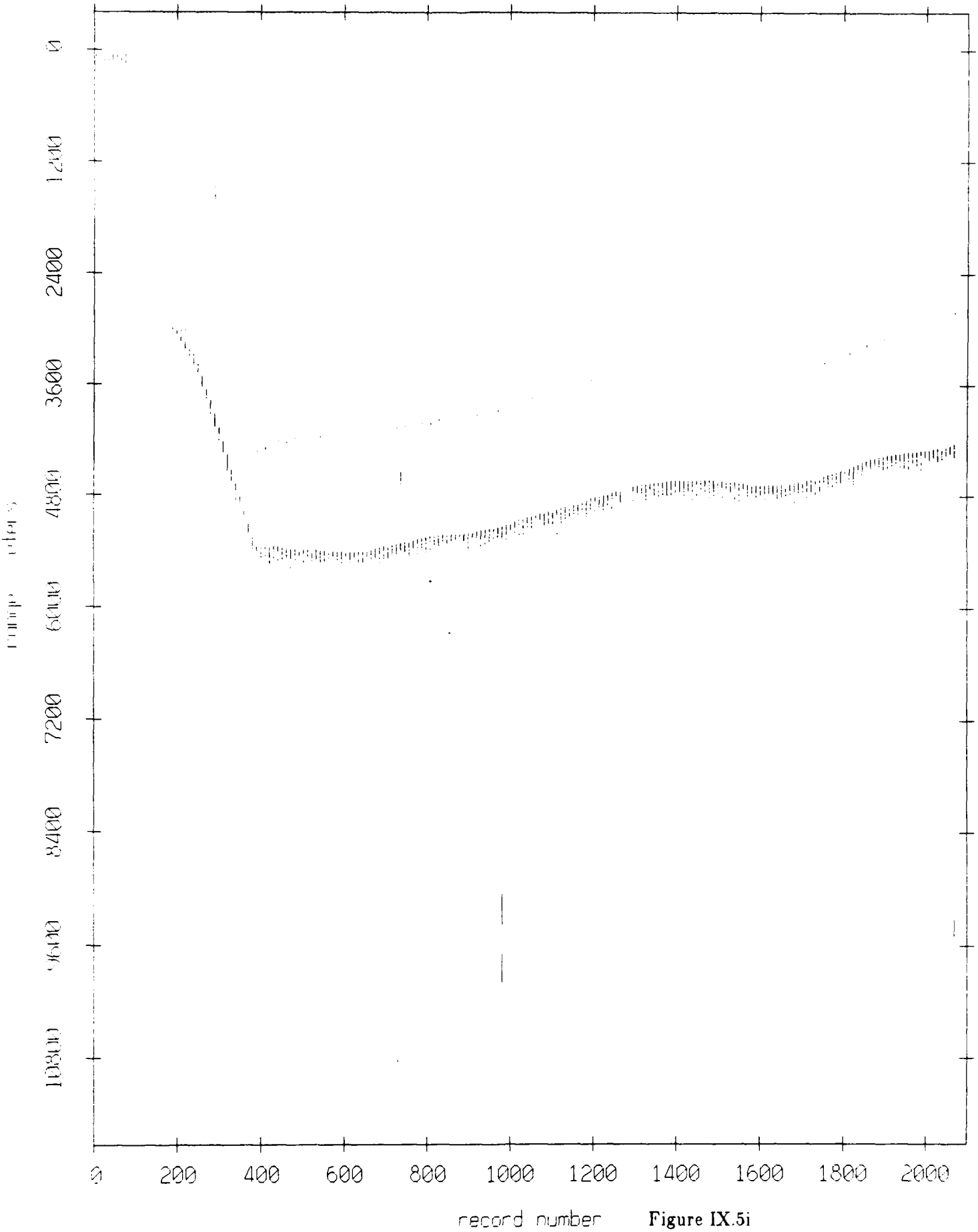

Float 1, August 1988 Experiment: range from float 7
0
1200
2400
3600
4800
6000
7200
8400
9600
10800
0
200
400
600
800
1000
1200
1400
1600
1800
2000
record number

Figure IX.5i

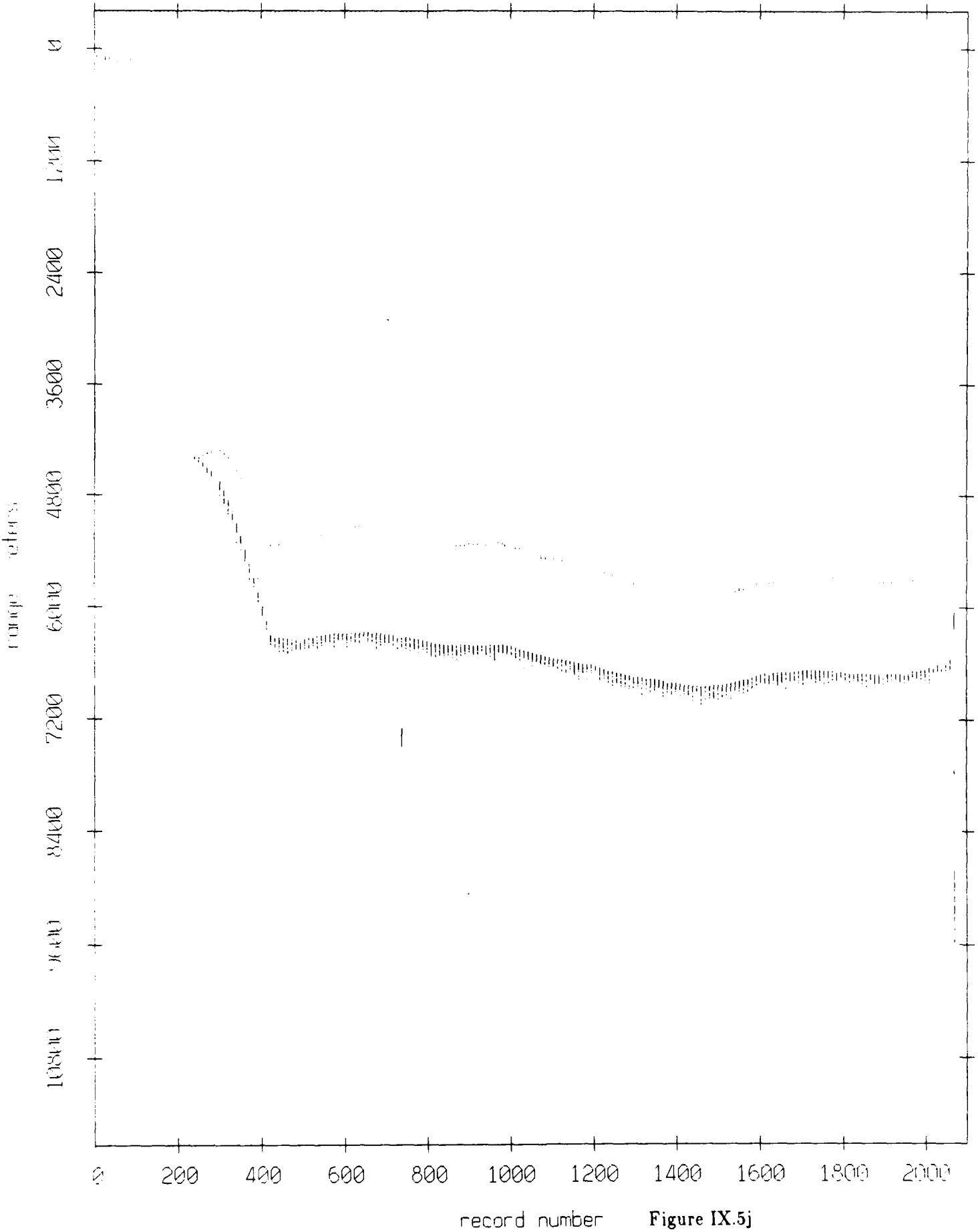

Float 1, August 1988 Experiment: range from float 8
0
1200
2400
3600
4800
6000
7200
8400
9600
10800
range, etc.
0
200
400
600
800
1000
1200
1400
1600
1800
2000
record number

Figure IX.5j

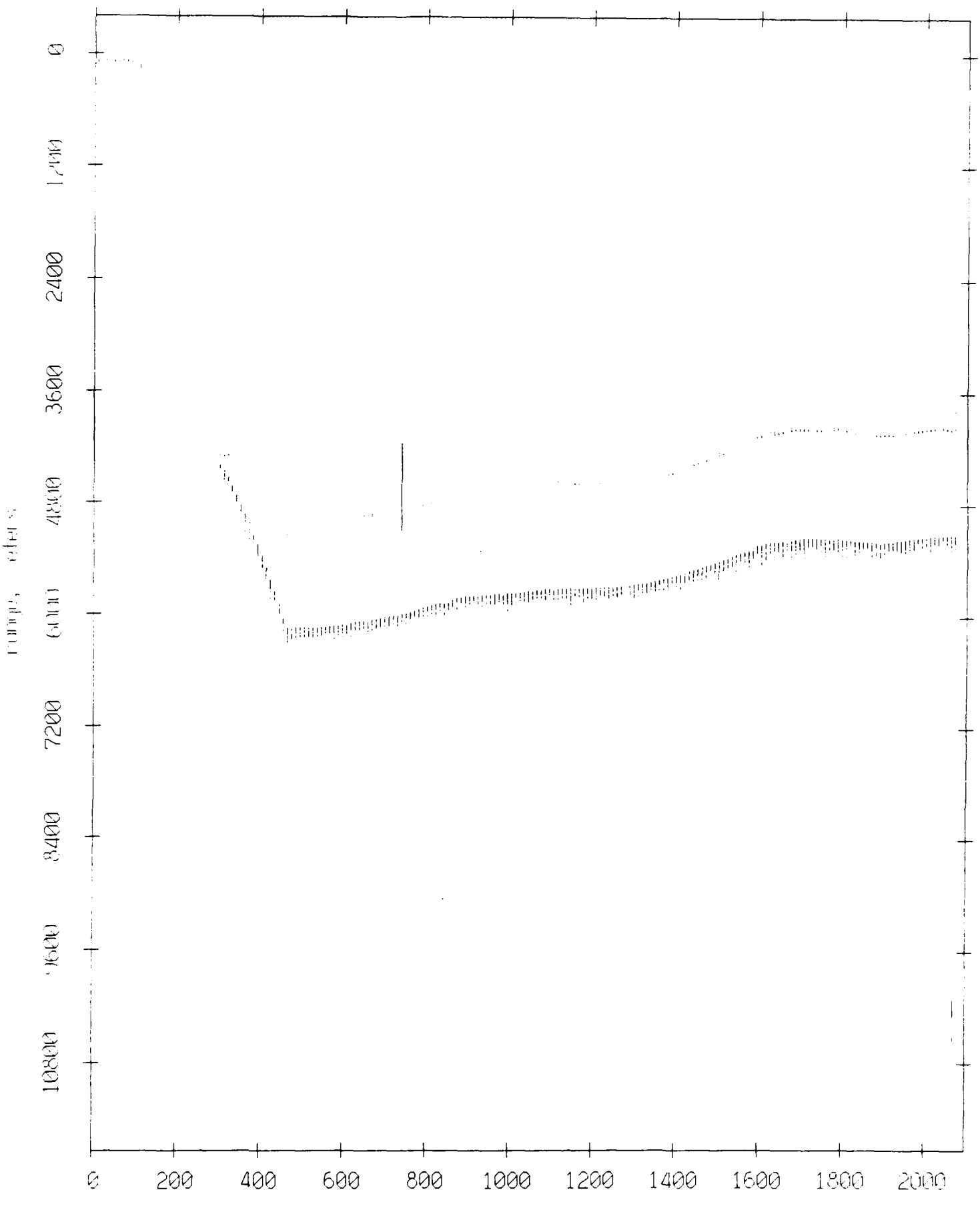

Float 1, August 1988 Experiment: range from float 9
0
1200
2400
3600
4800
6000
7200
8400
9600
10800
0
200
400
600
800
1000
1200
1400
1600
1800
2000
record number

Figure IX.5k

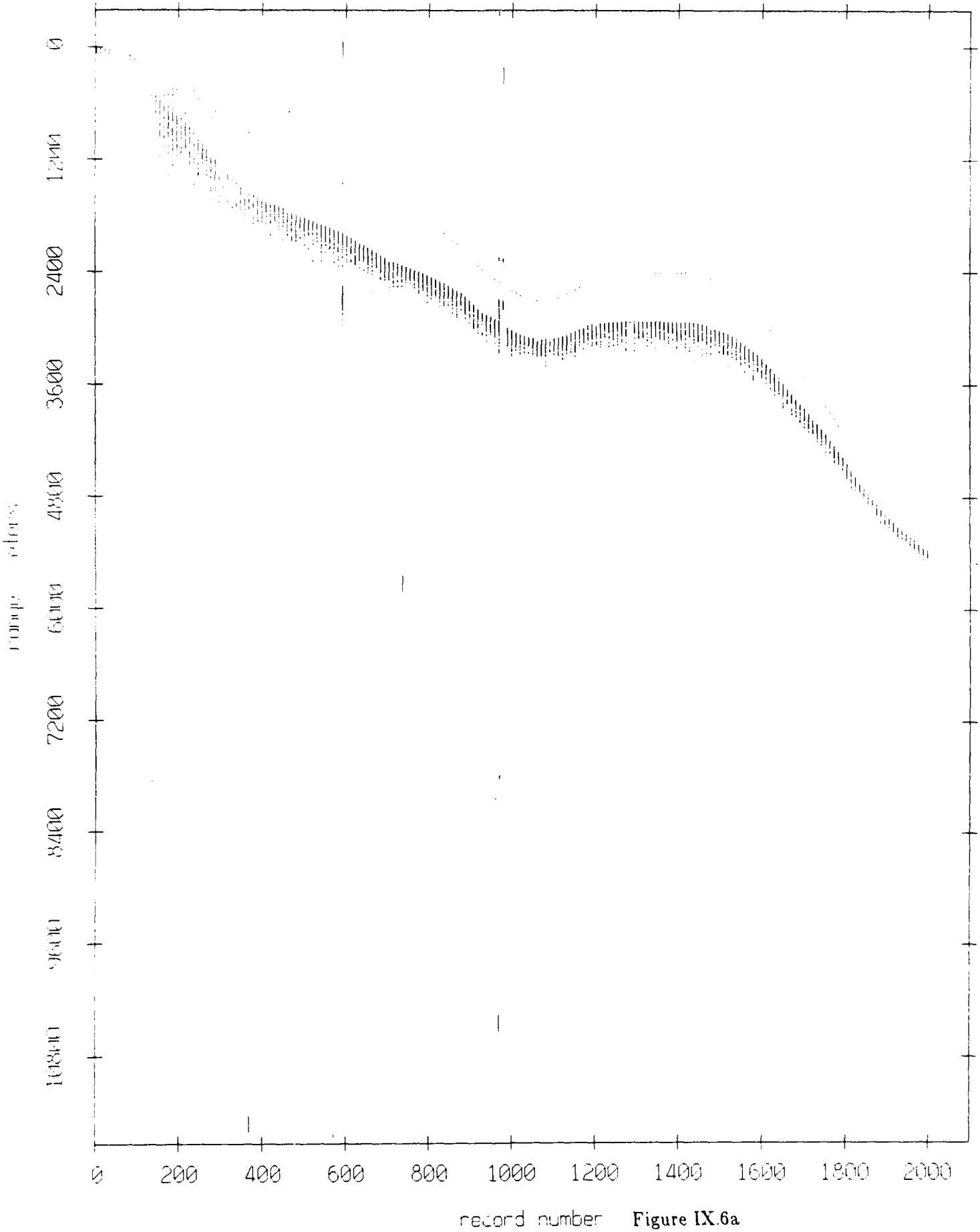

Float 2, August 1988 Experiment: range from float 10
0
1200
2400
3600
4800
6000
7200
8400
9600
10800
0
200
400
600
800
1000
1200
1400
1600
1800
2000
record number

Figure IX.6a

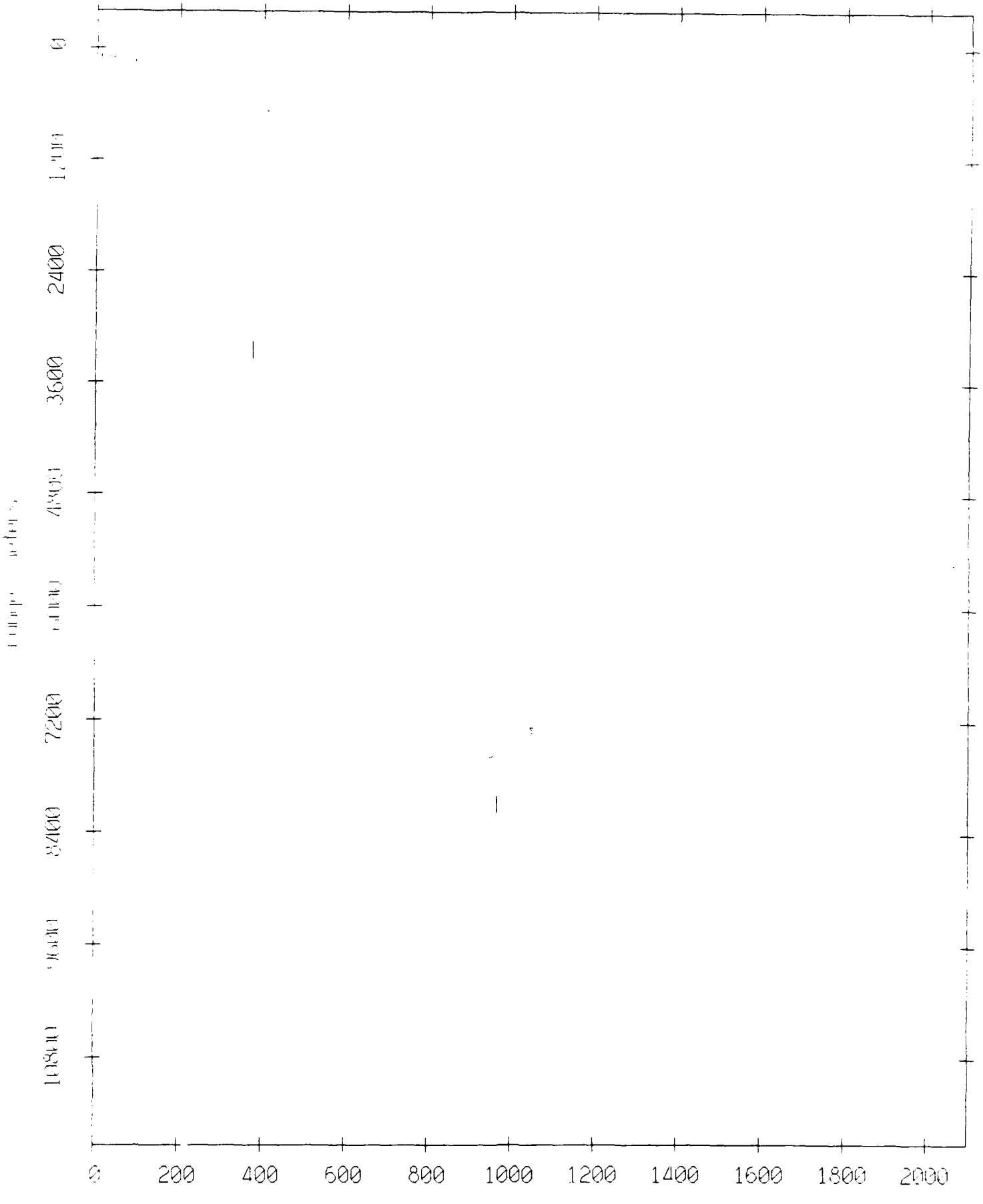

Float 2, August 1988 Experiment: range from float 3
2400
3600
72000
84000
0
200
400
600
800
1000
1200
1400
1600
1800
2000
record number

Figure IX.6b

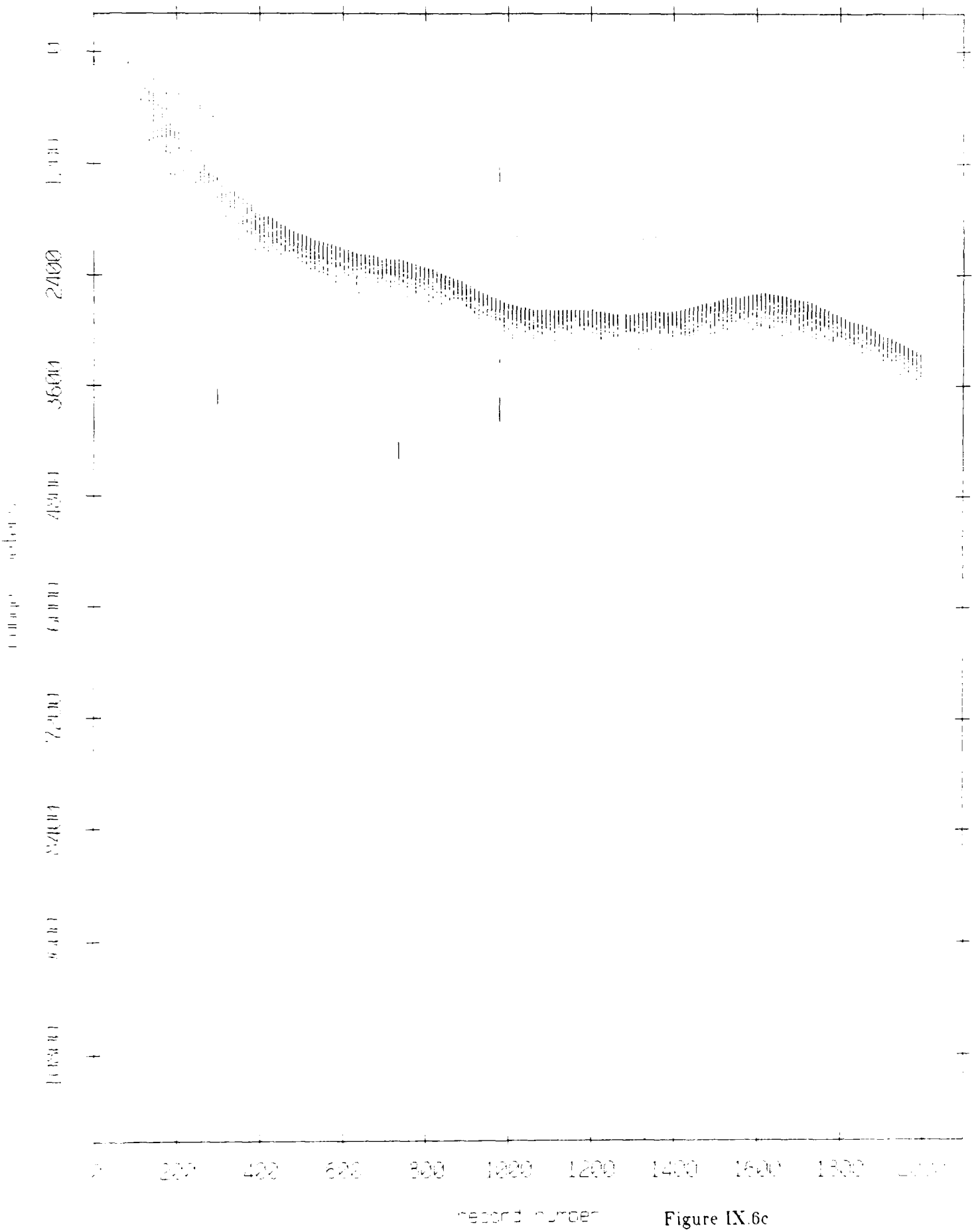

Float 2, August 1988 Experiment: range from float 5
2400
3600
record number

Figure IX.6c

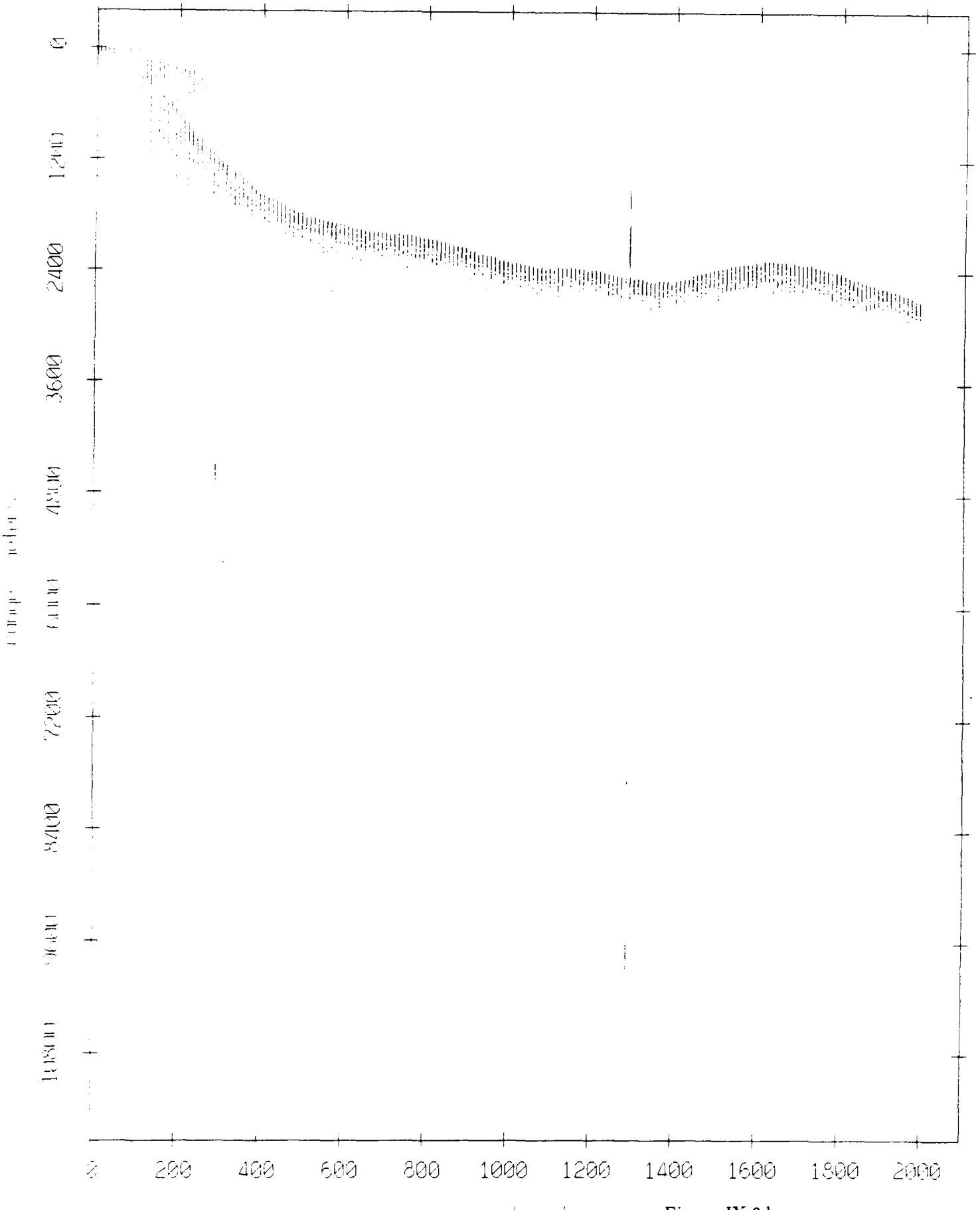

Float 2, August 1988 Experiment: range from float 0
0
1200
2400
3600
4800
6000
7200
8400
9600
10800
0
200
400
600
800
1000
1200
1400
1600
1800
2000
record number

Figure IX.6d

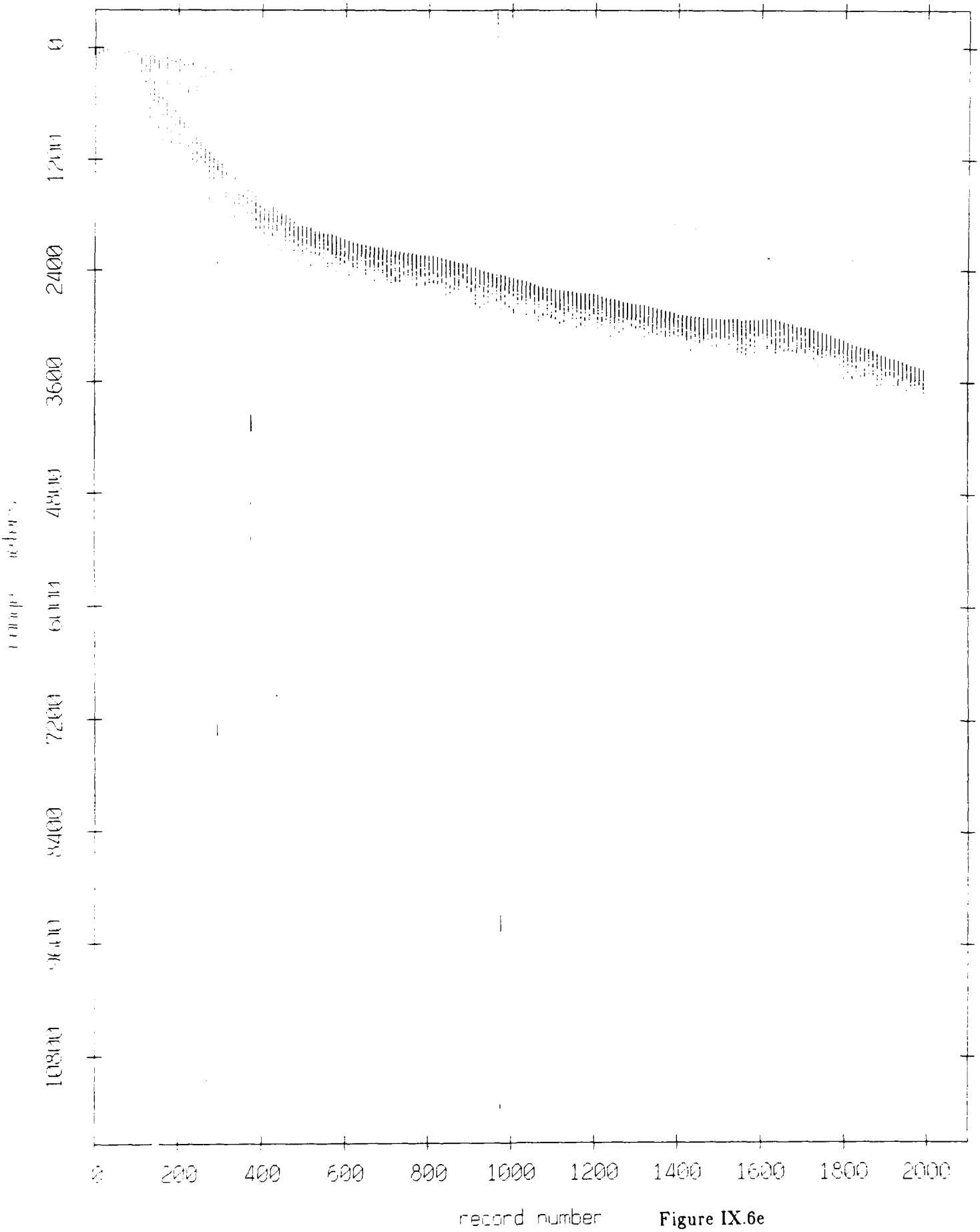

Float 2, August 1988 Experiment: range from float 1
0
1200
2400
3600
4800
6000
7200
8400
9600
10800
0
200
400
600
800
1000
1200
1400
1600
1800
2000
record number

Figure IX.6e

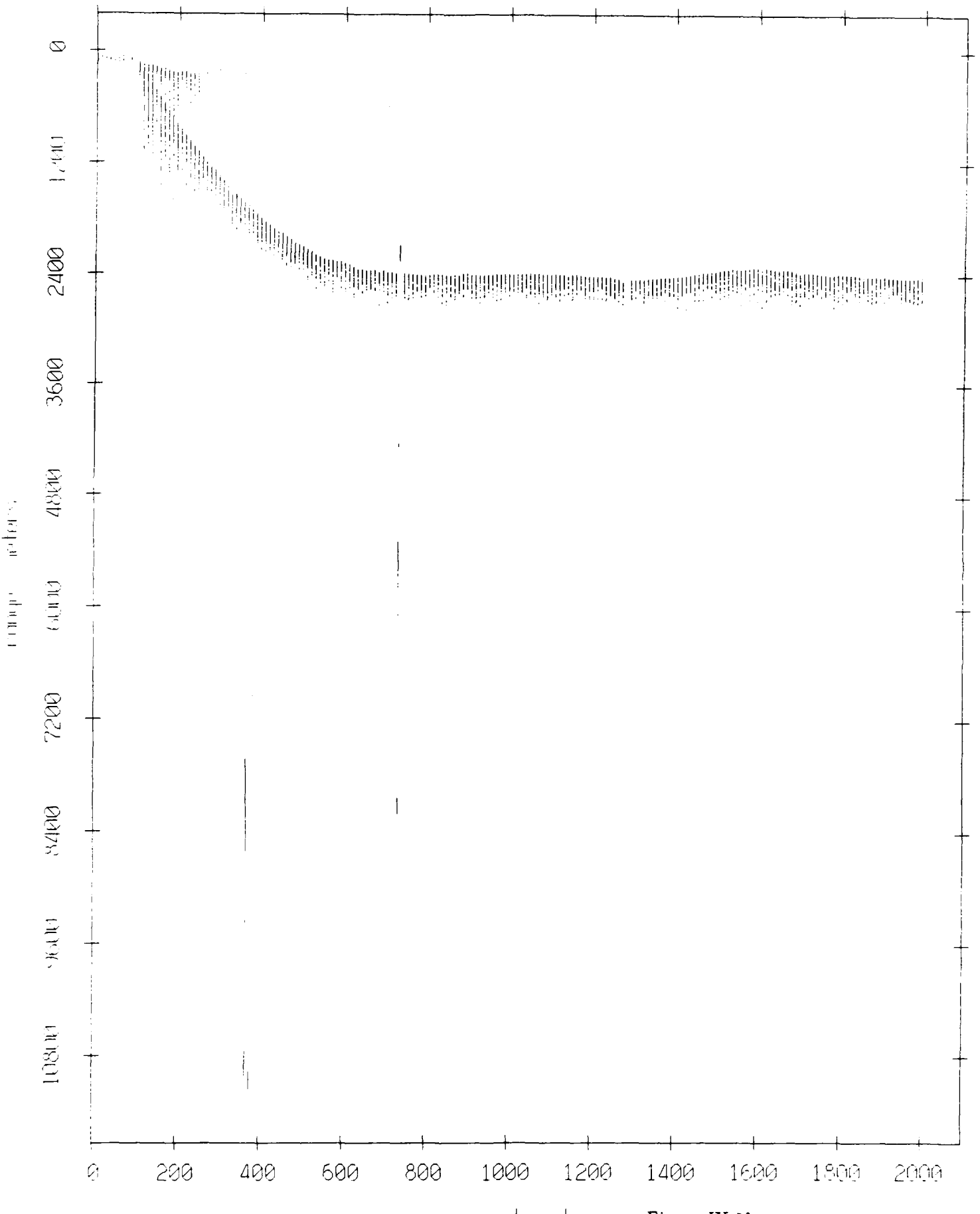

Float 2, August 1988 Experiment: range from float 4
0
2400
3600
7200
0
200
400
600
800
1000
1200
1400
1600
2000
record number

Figure IX.6f

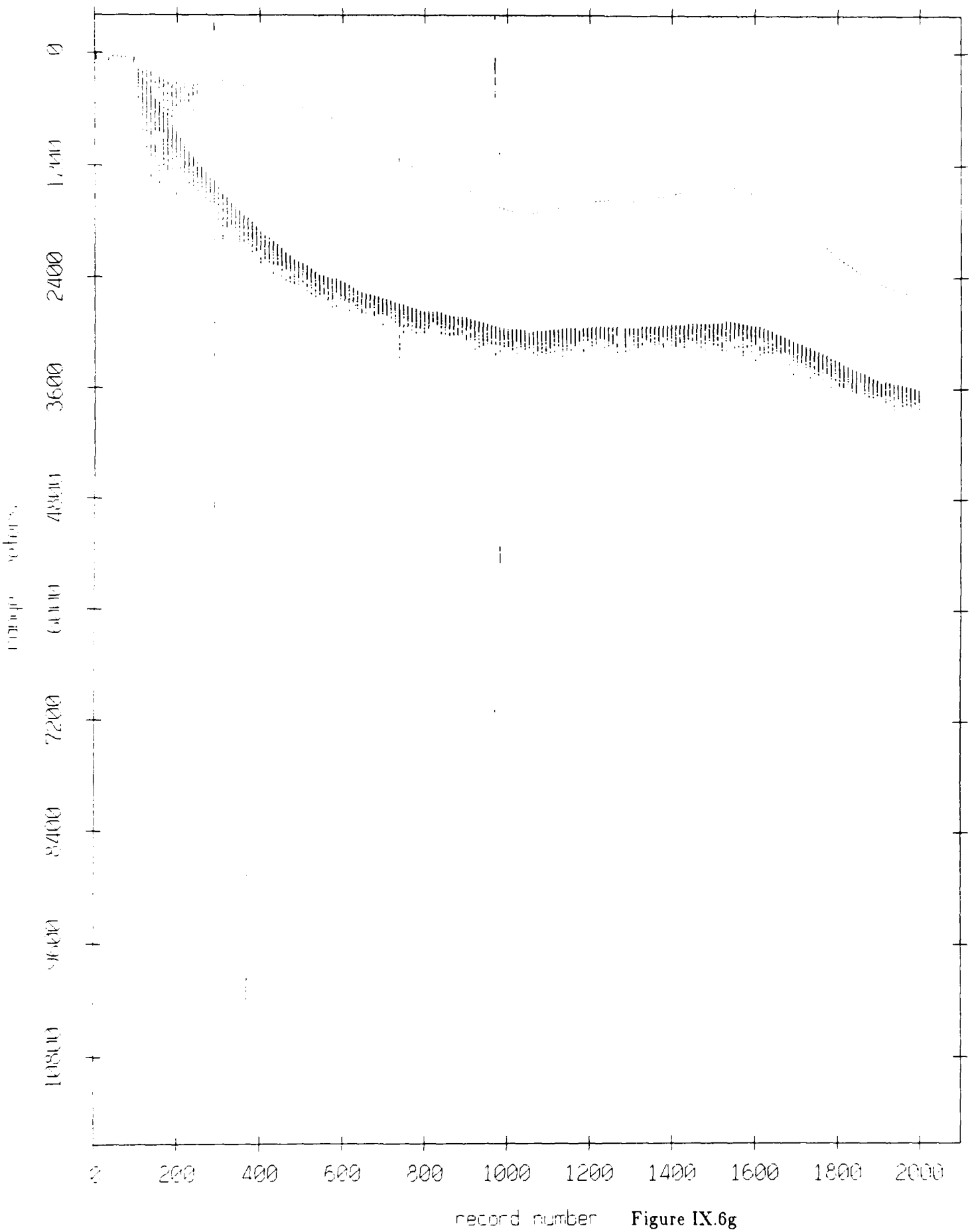

Float 2, August 1988 Experiment: range from float 6
0
1200
2400
3600
4800
6000
7200
8400
9600
10800
200
400
600
800
1000
1200
1400
1600
1800
2000
record number

Figure IX.6g

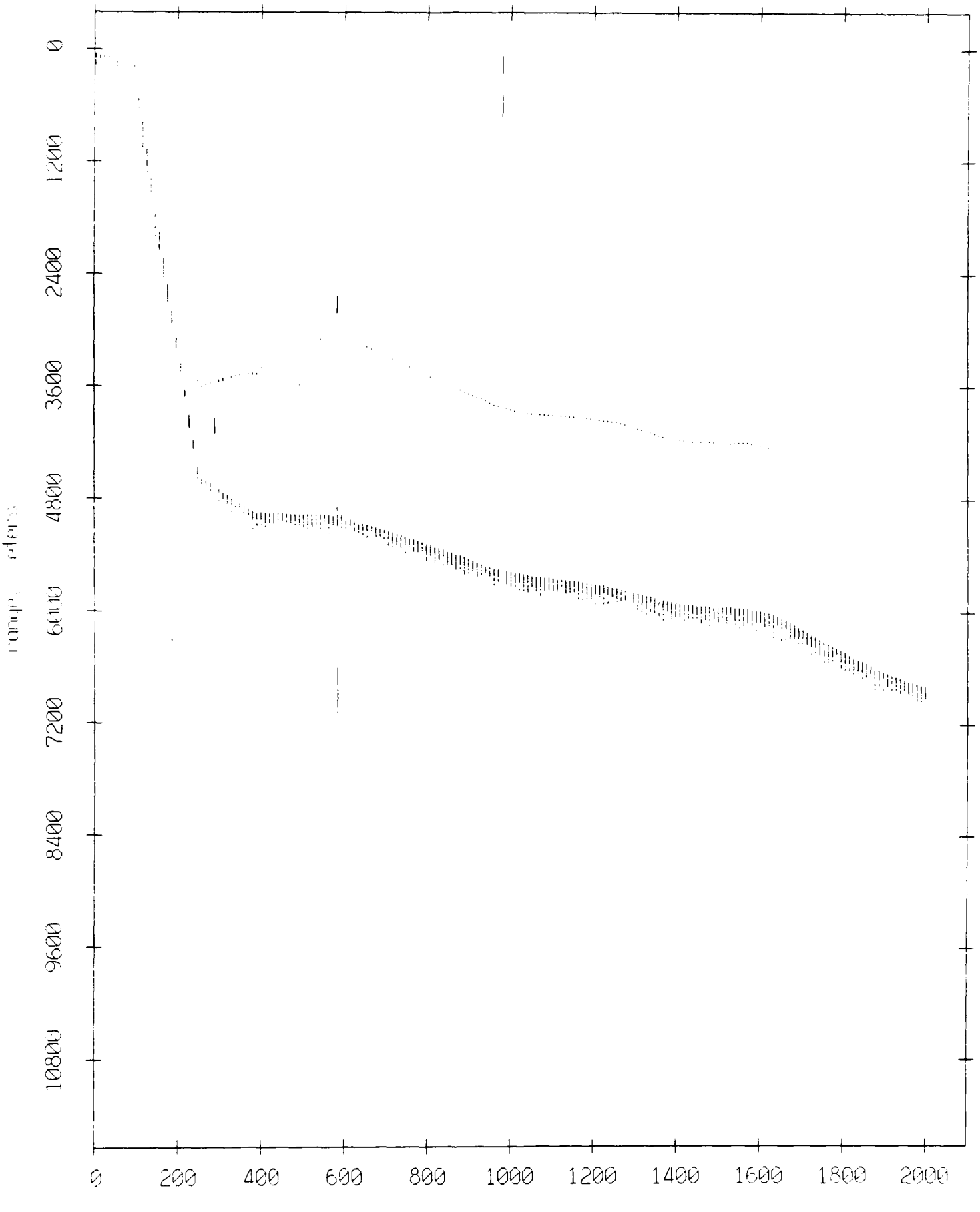

Float 2, August 1988 Experiment: range from float 11
0
1200
2400
3600
4800
6000
7200
8400
9600
10800
0
200
400
600
800
1000
1200
1400
1600
1800
2000
record number

Figure IX.6h

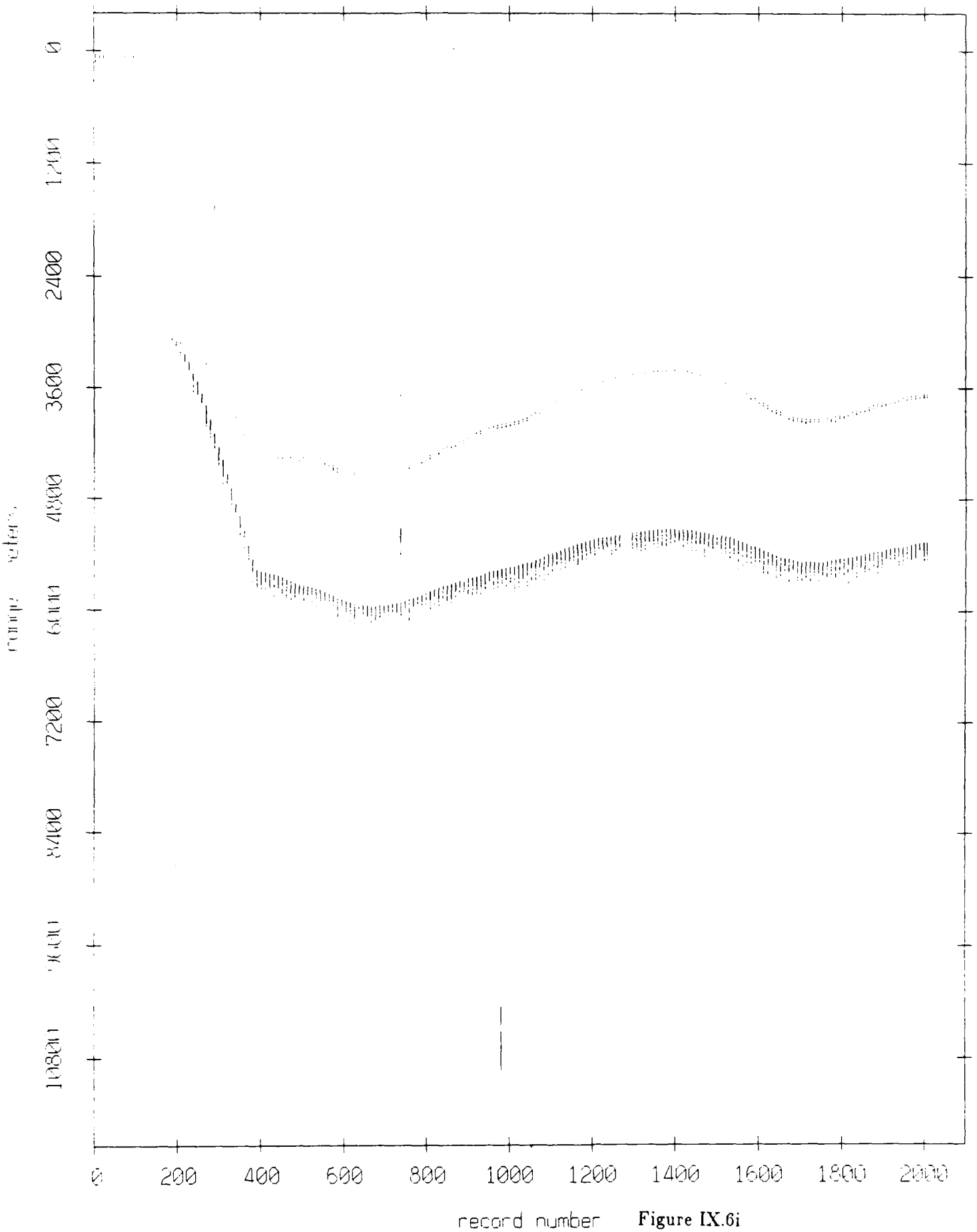

Float 2, August 1988 Experiment: range from float 7
0
1200
2400
3600
4800
6000
7200
8400
9600
10800
0
200
400
600
800
1000
1200
1400
1600
1800
2000
record number

Figure IX.6i

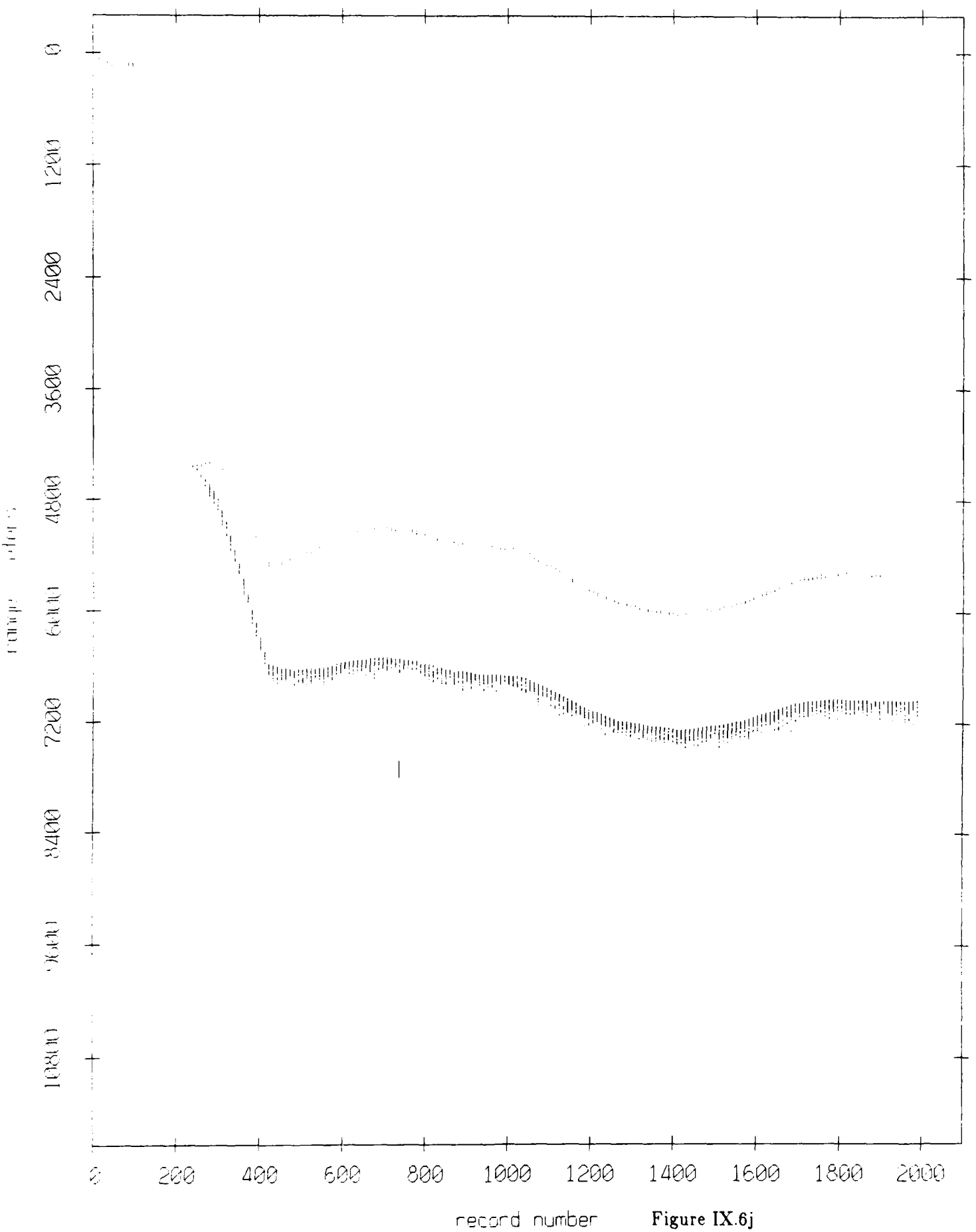

Float 2, August 1988 Experiment: range from float 8
0
1200
2400
3600
4800
6000
7200
8400
9600
10800
0
200
400
600
800
1000
1200
1400
1600
1800
2000
record number

Figure IX.6j

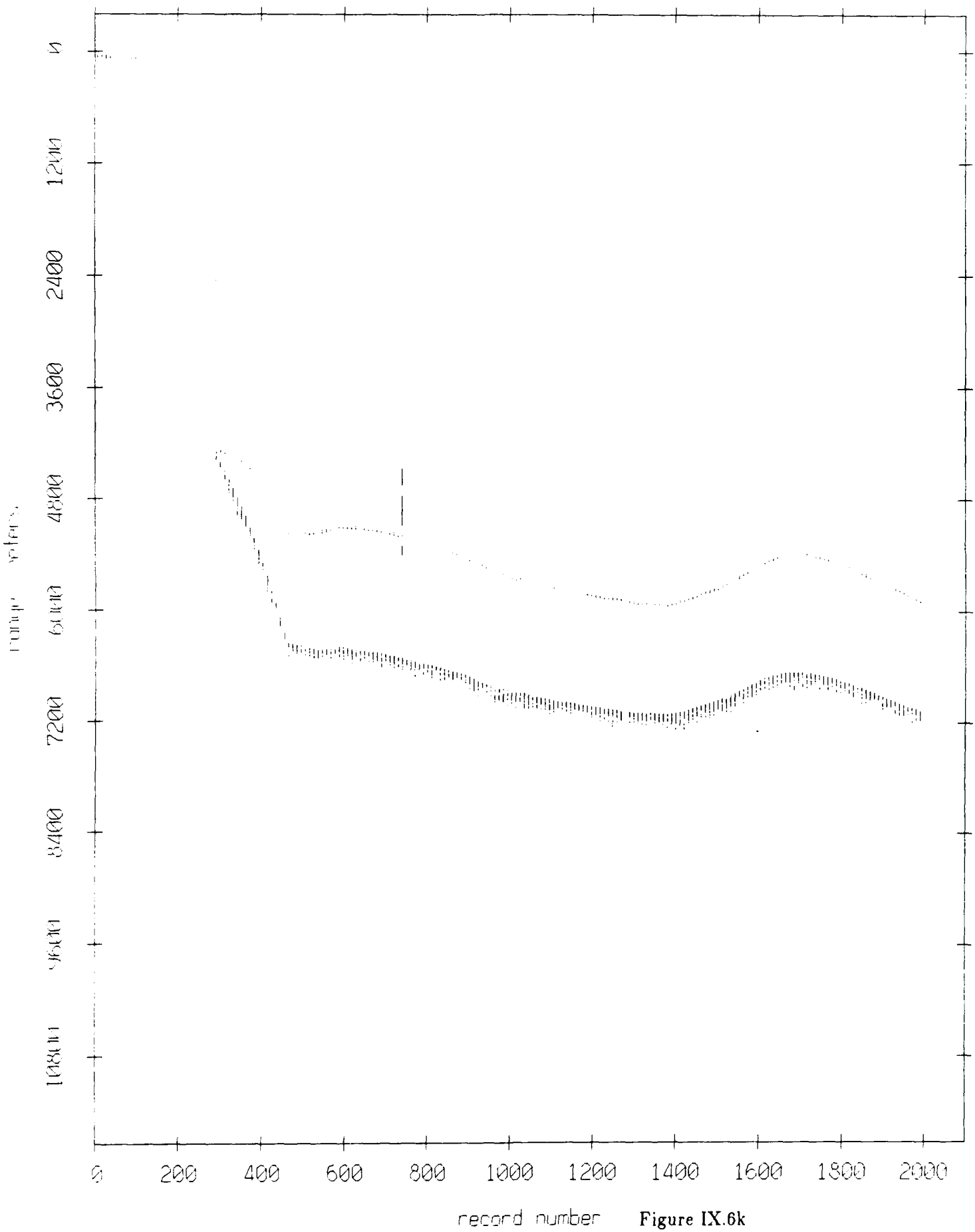

Float 2, August 1988 Experiment: range from float 9
0
200
400
600
800
1000
1200
1400
1600
1800
2000
record number

Figure IX.6k

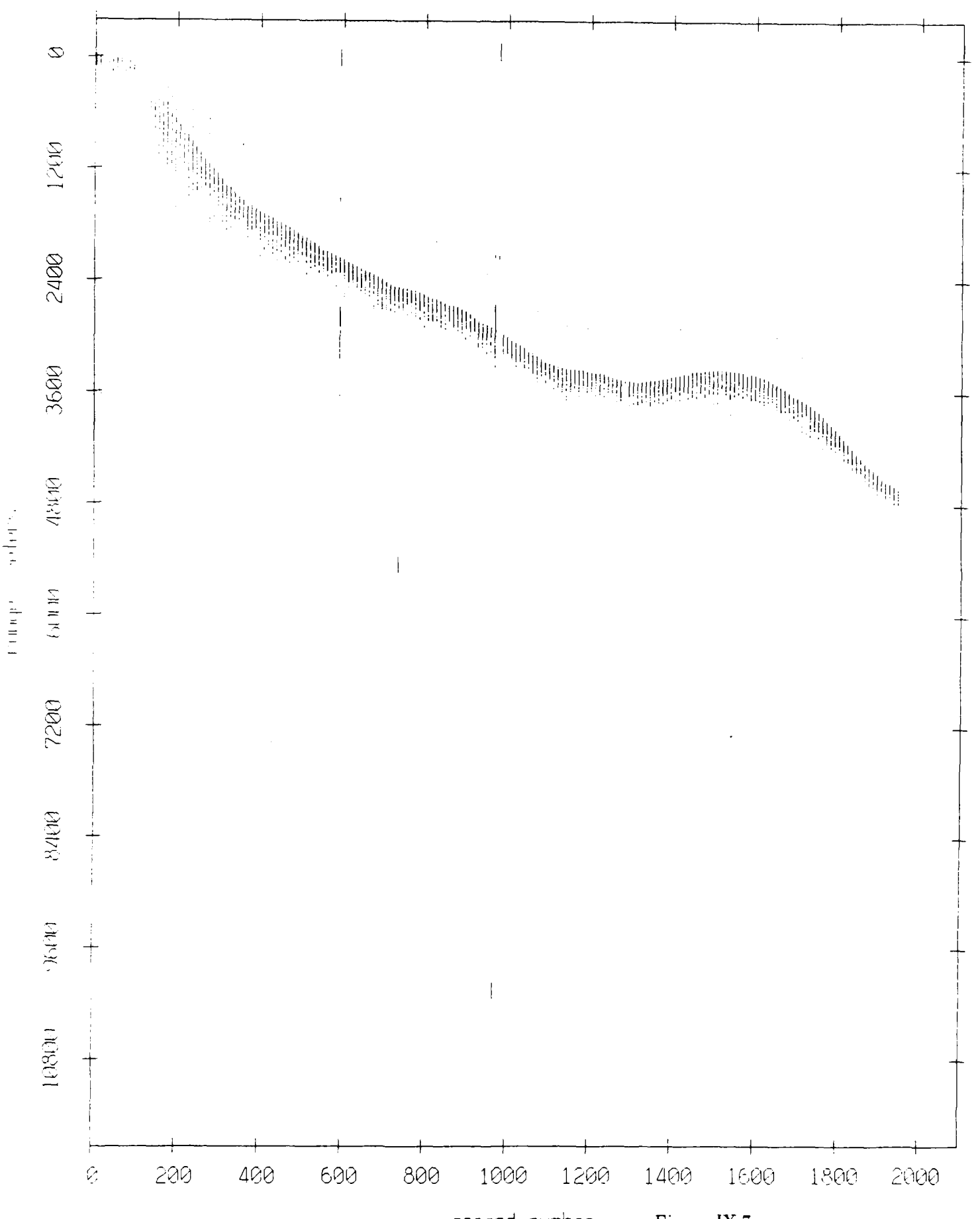

Float 4, August 1988 Experiment: range from float 10
0
1200
2400
3600
4800
6000
7200
8400
9600
10800
0
200
400
600
800
1000
1200
1400
1600
1800
2000
record number

Figure IX.7a

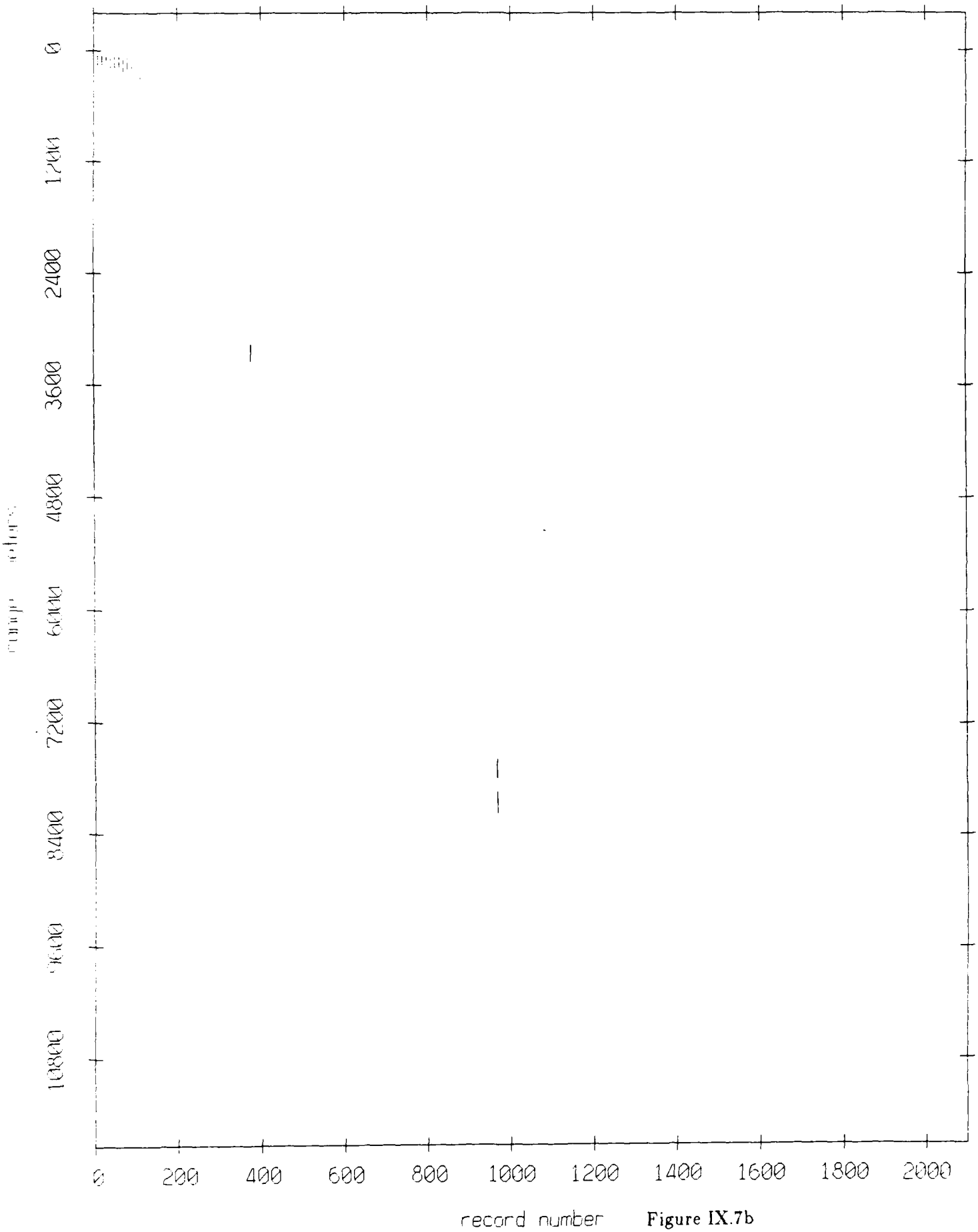

Float 4, August 1988 Experiment: range from float 3
0
1200
2400
3600
4800
7200
9600
12000
0
200
400
600
800
1000
1200
1400
1600
1800
2000
record number

Figure IX.7b

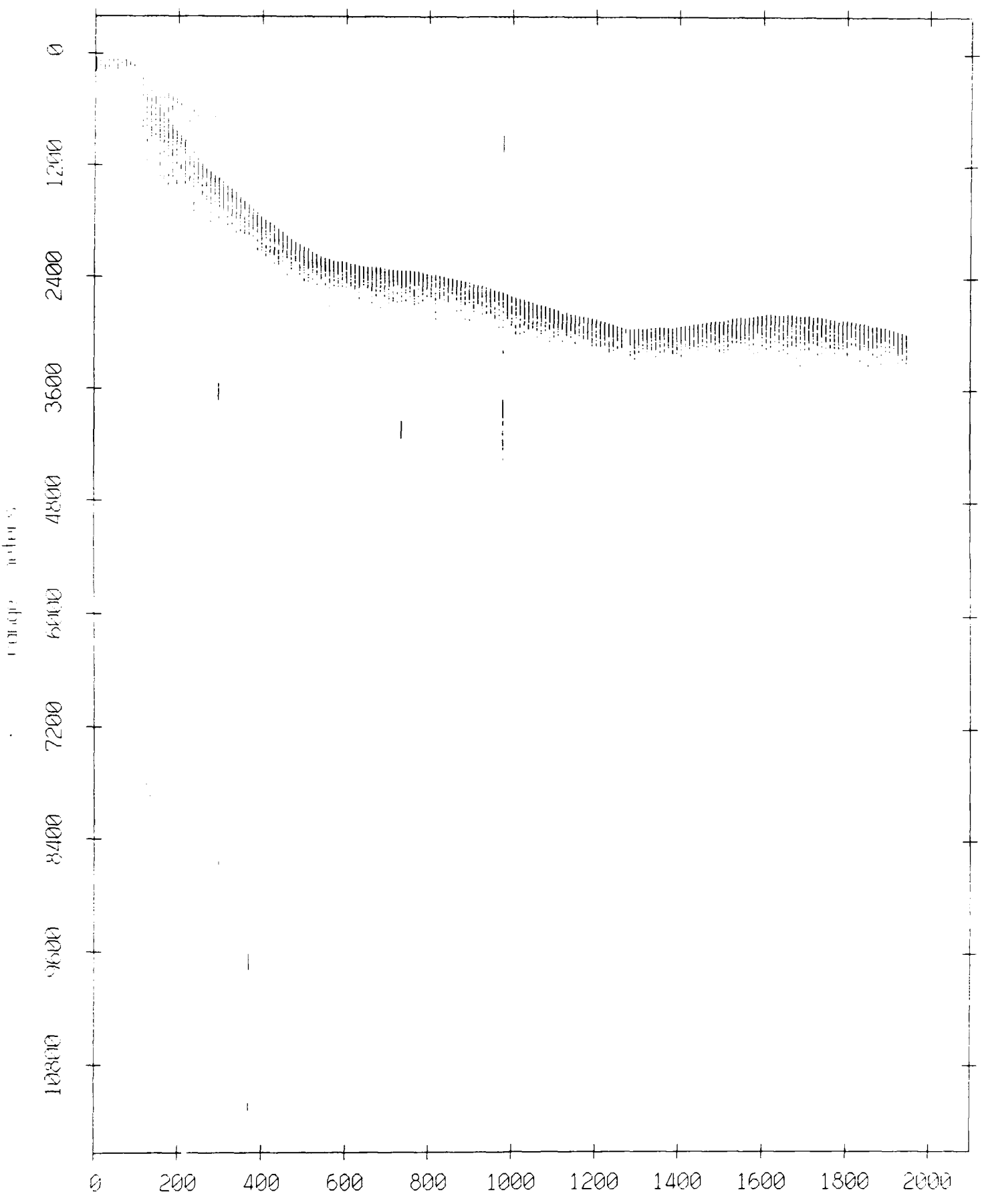

Float 4, August 1988 Experiment: range from float 5
0
1200
2400
3600
4800
6000
7200
8400
9600
10800
0
200
400
600
800
1000
1200
1400
1600
1800
2000
record number

Figure IX.7c

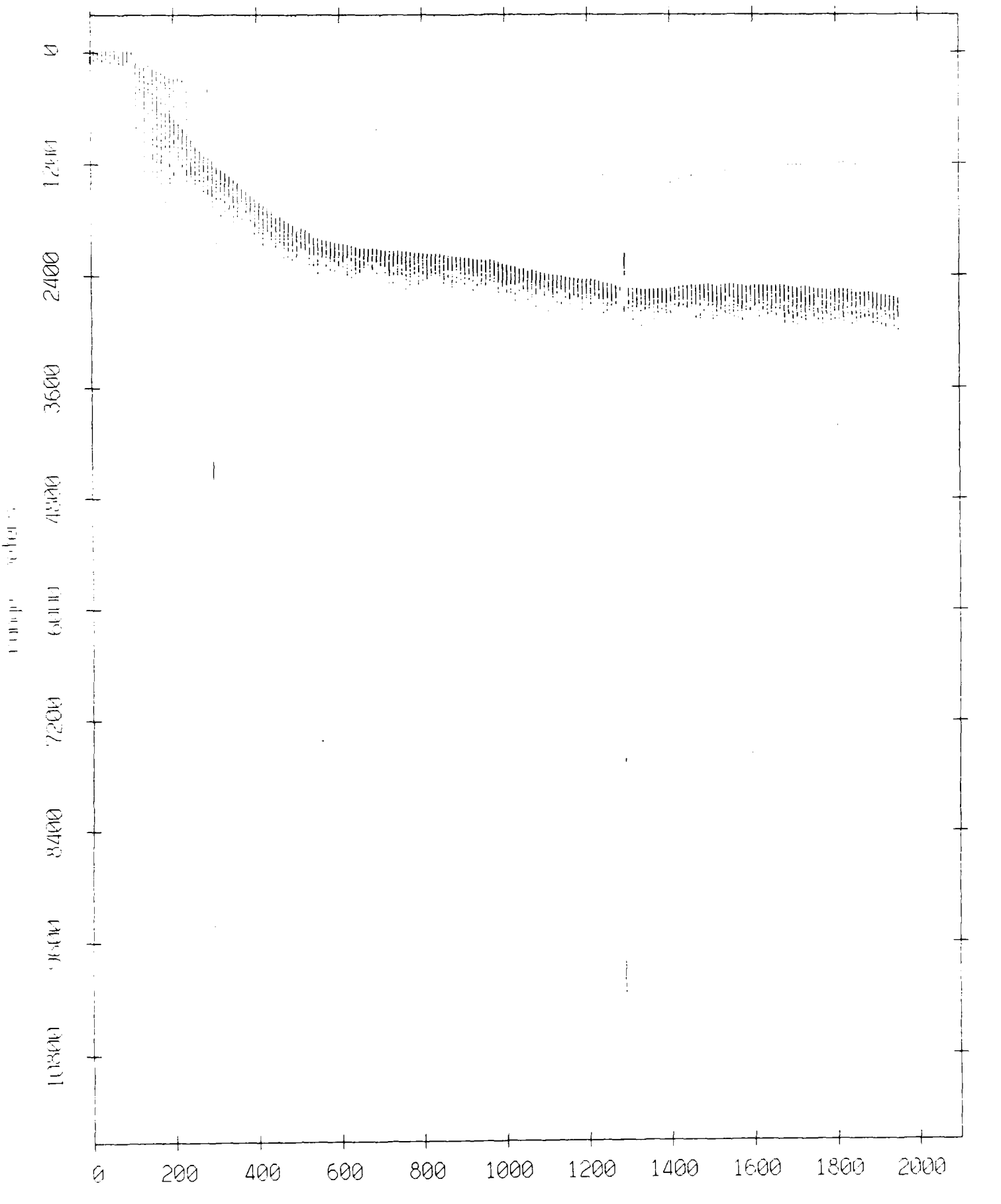

Float 4, August 1988 Experiment: range from float 0
0
2400
36000
0
200
400
600
800
1000
1200
1400
1600
1800
2000
record number

Figure IX.7d

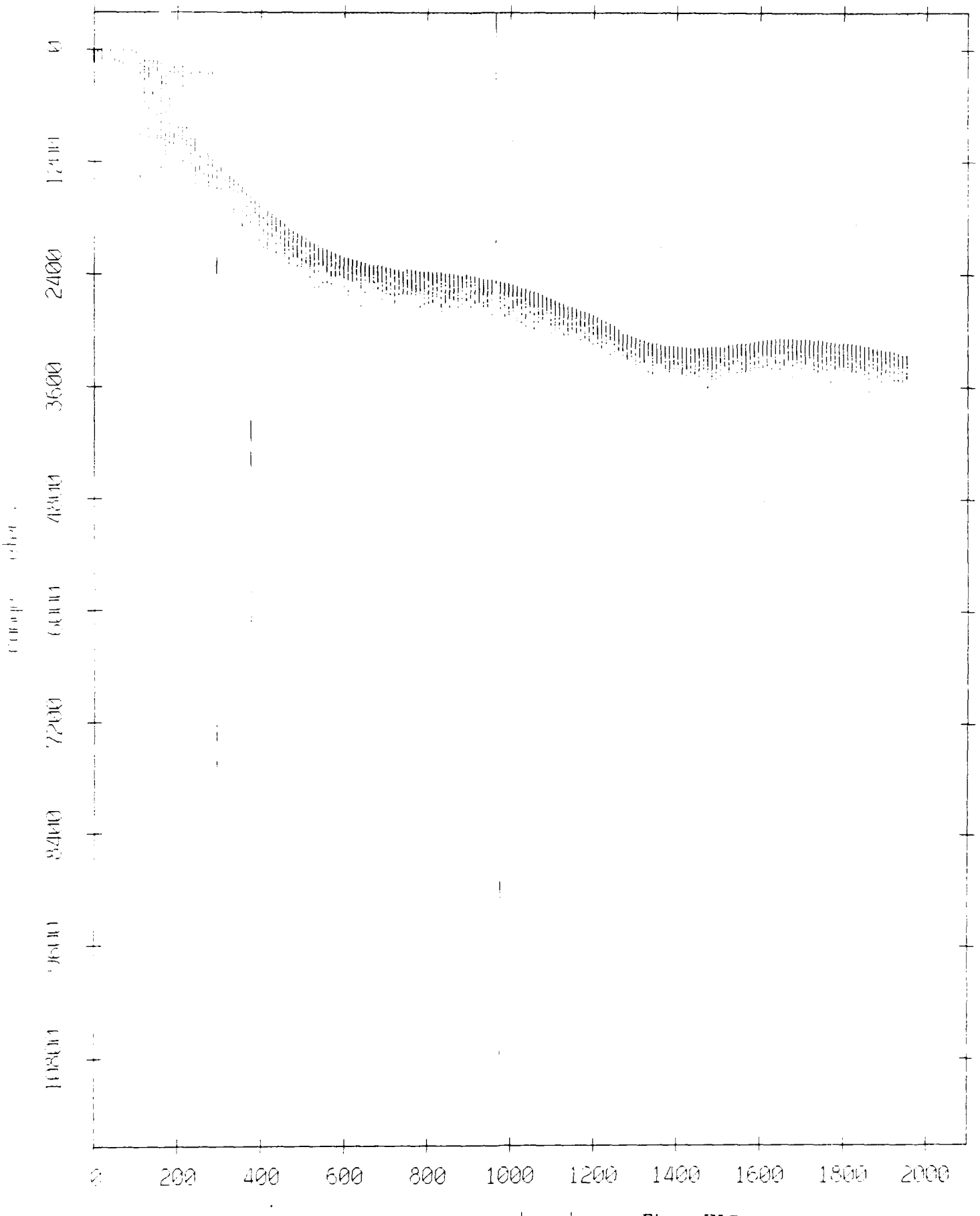

Float 4, August 1988 Experiment: range from float 1
24000
36000
200
400
600
800
1000
1200
1400
1600
1800
2000
record number

Figure IX.7e

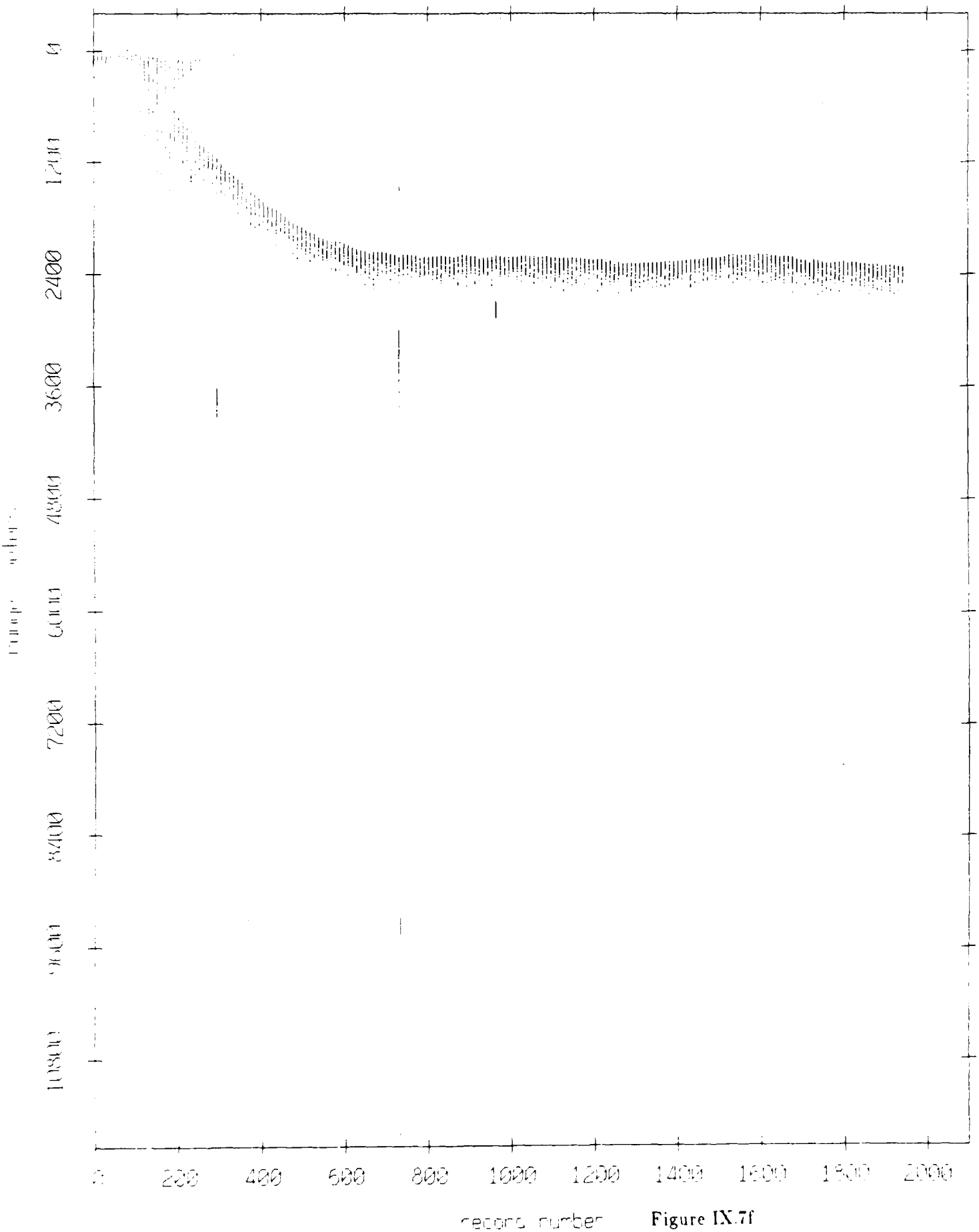

Float 4, August 1988 Experiment: range from float 2
2400
3600
7200
200
400
800
1000
1200
record number

Figure IX.7f

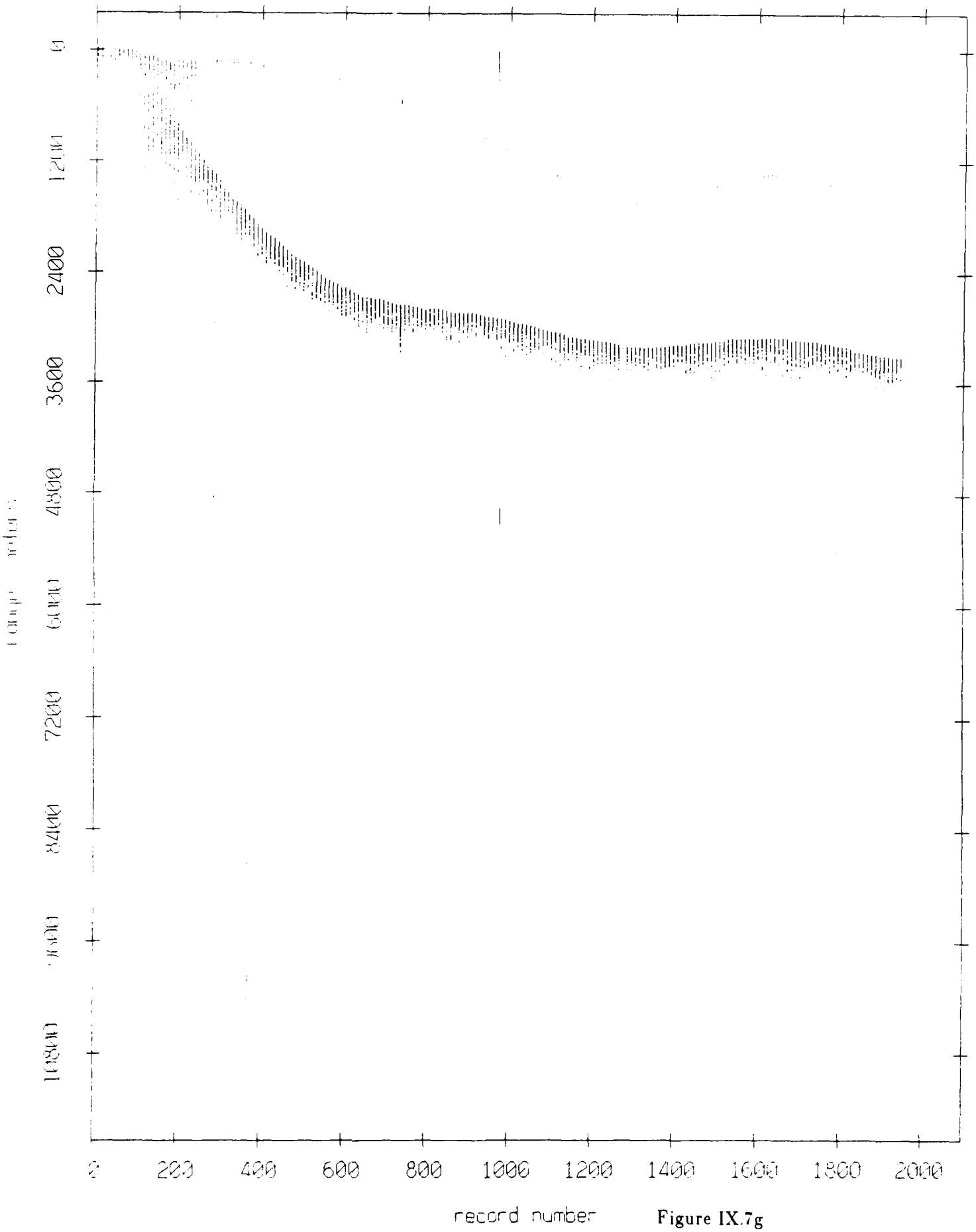

Float 4, August 1988 Experiment: range from float 6
0
1200
2400
3600
4800
6000
7200
8400
9600
10800
0
200
400
600
800
1000
1200
1400
1600
1800
2000
record number

Figure IX.7g

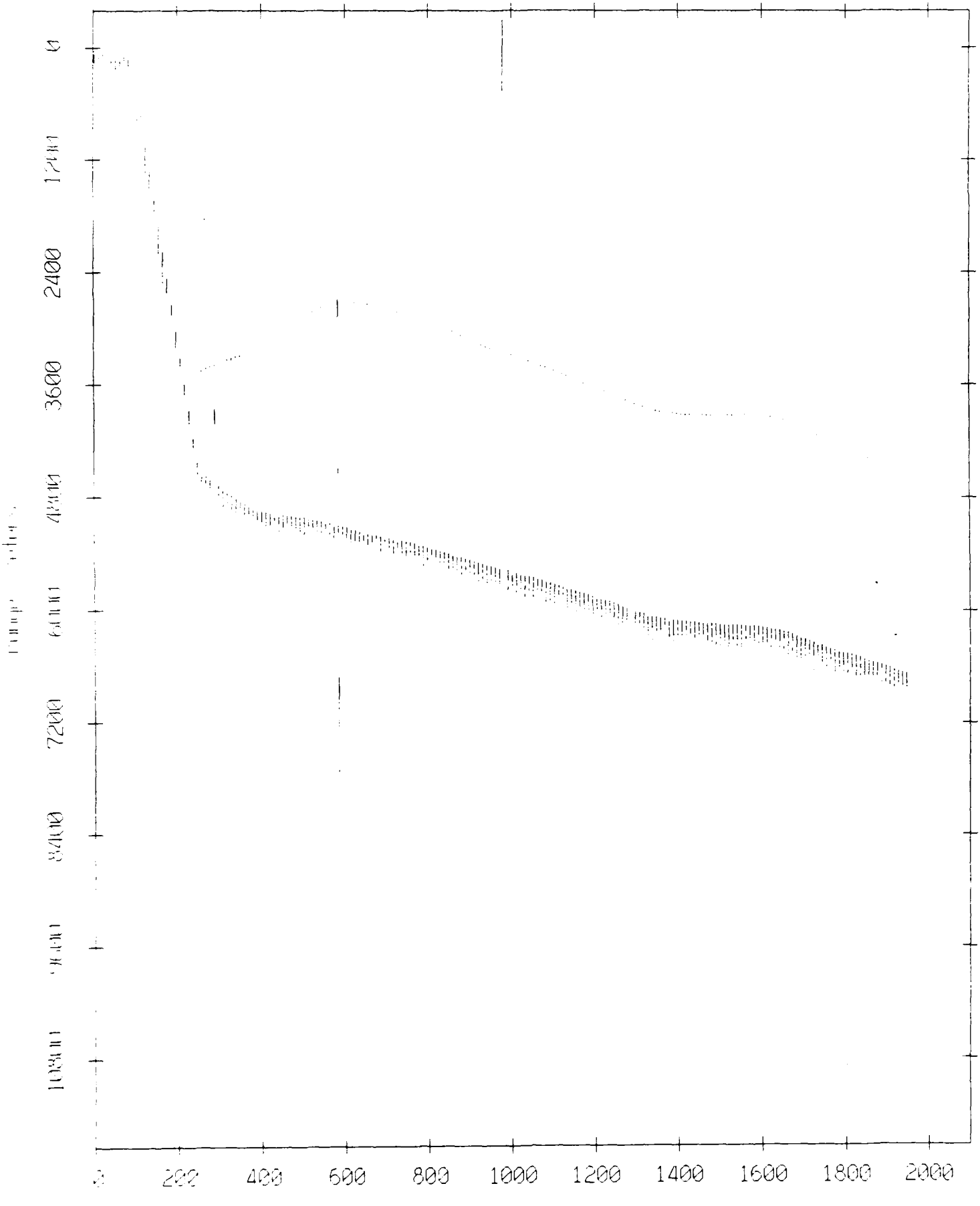

Float 4, August 1988 Experiment: range from float 11
2400
3600
7200
0
200
400
600
800
1000
1200
1400
1600
1800
2000
record number

Figure IX.7h

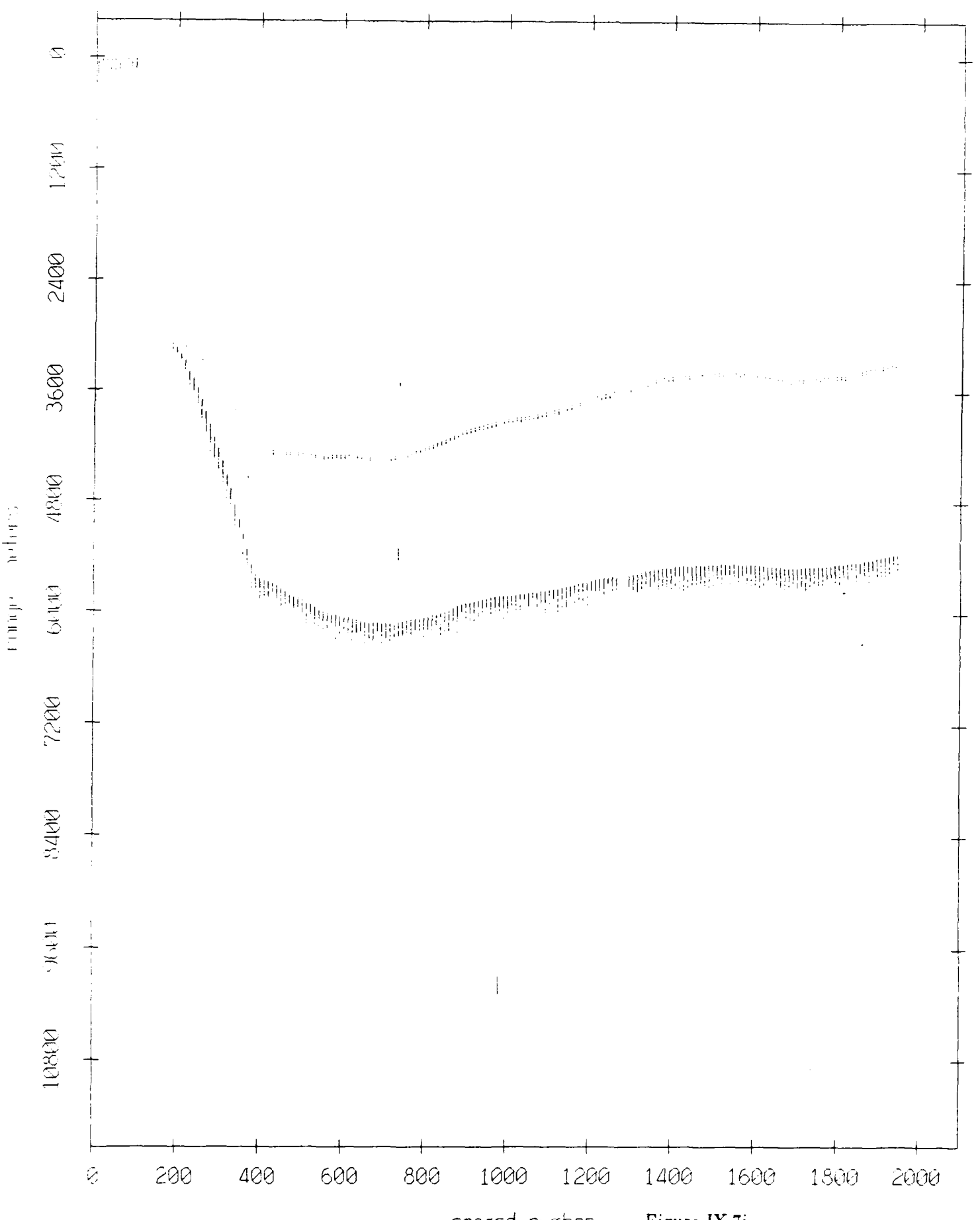

Float 4, August 1988 Experiment: range from float 7
0
1200
2400
3600
4800
6000
7200
8400
9600
10800
0
200
400
600
800
1000
1200
1400
1600
1800
2000
record number

Figure IX.7i

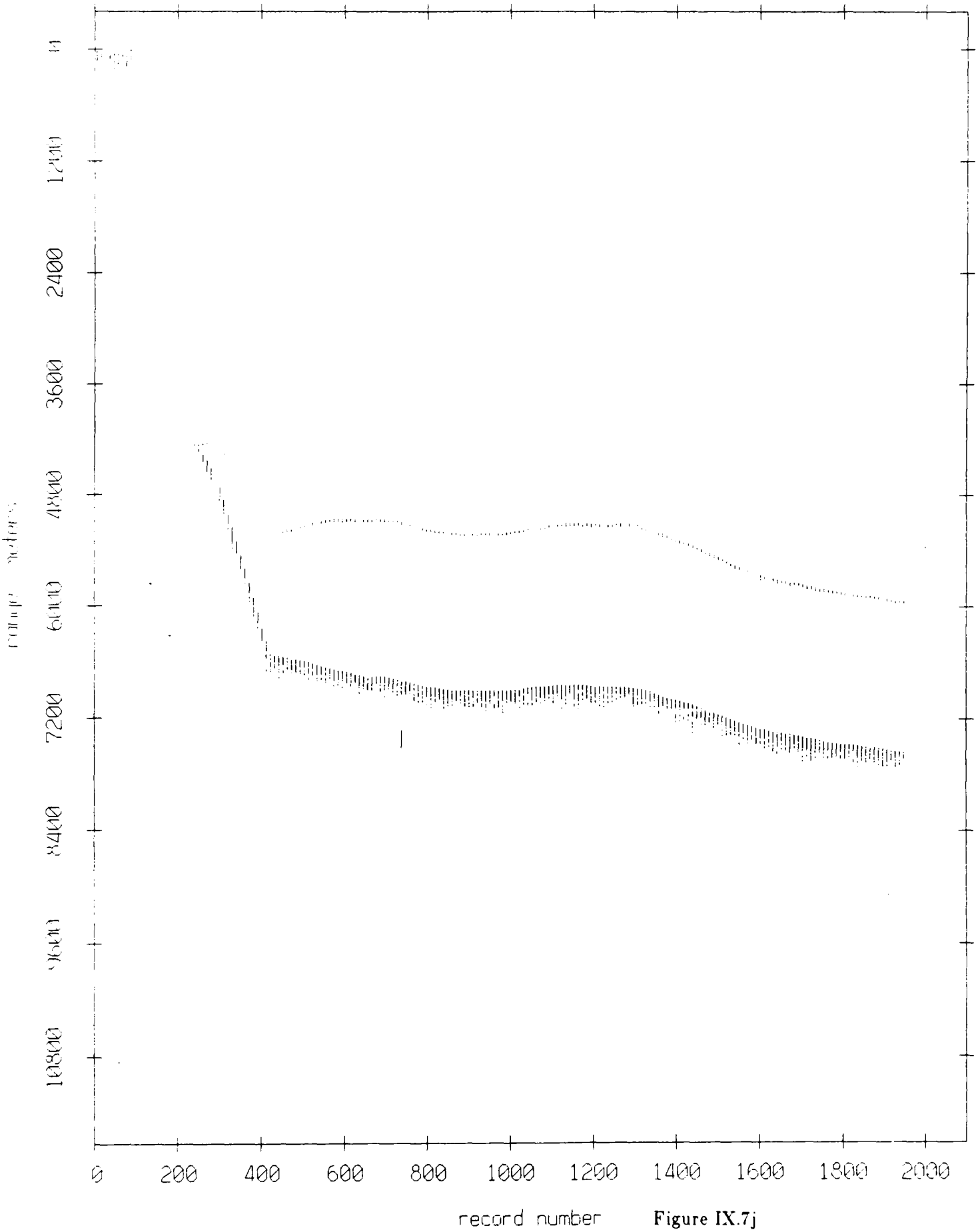

Float 4, August 1988 Experiment: range from float 8
2400
3600
4800
7200
8400
0
200
400
600
800
1000
1200
1400
1600
1800
2000
record number

Figure IX.7j

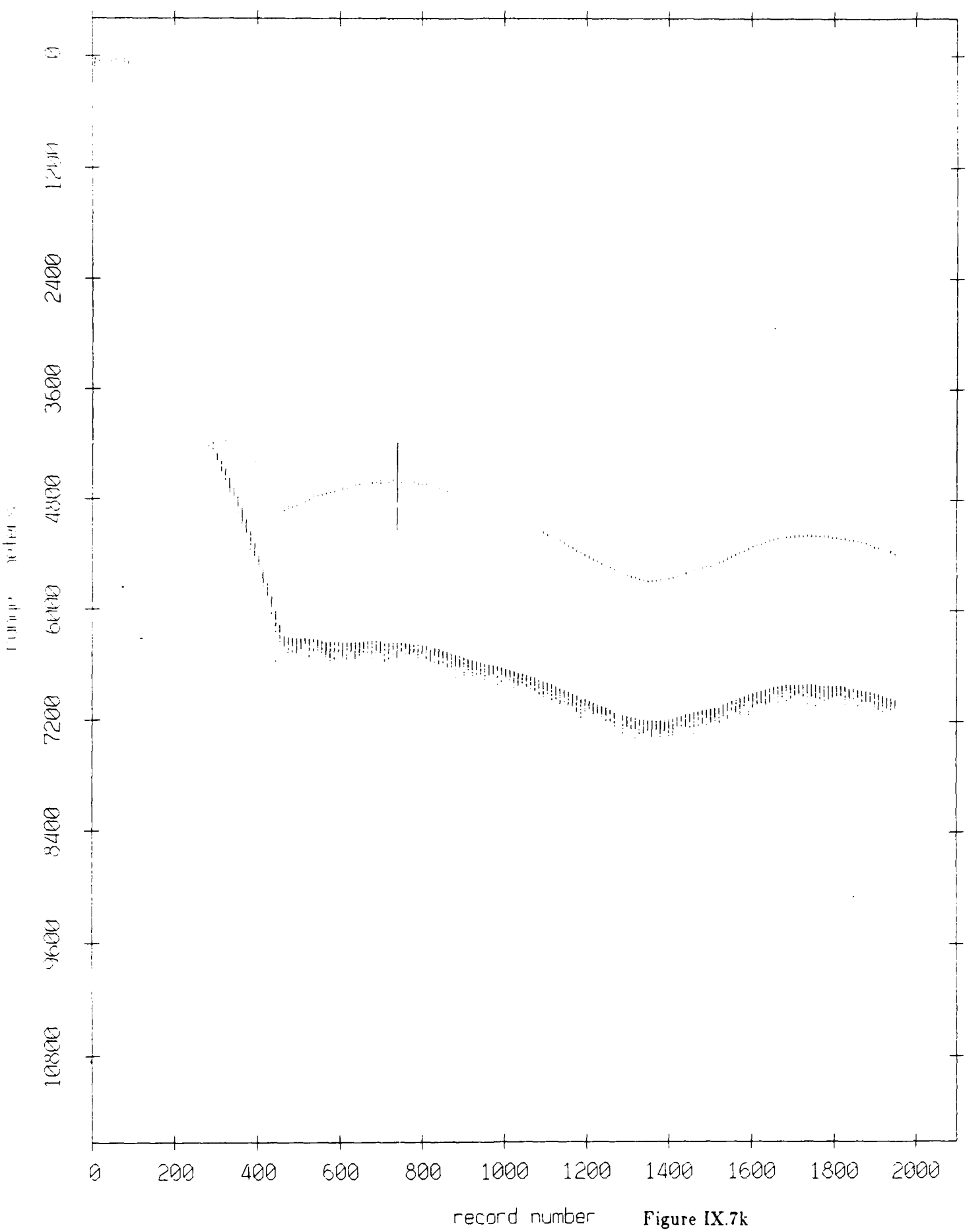

Float 4, August 1988 Experiment: range from float 9
0
2400
3600
4800
7200
8400
9600
10800
0
200
400
600
800
1000
1200
1400
1600
1800
2000
record number

Figure IX.7k

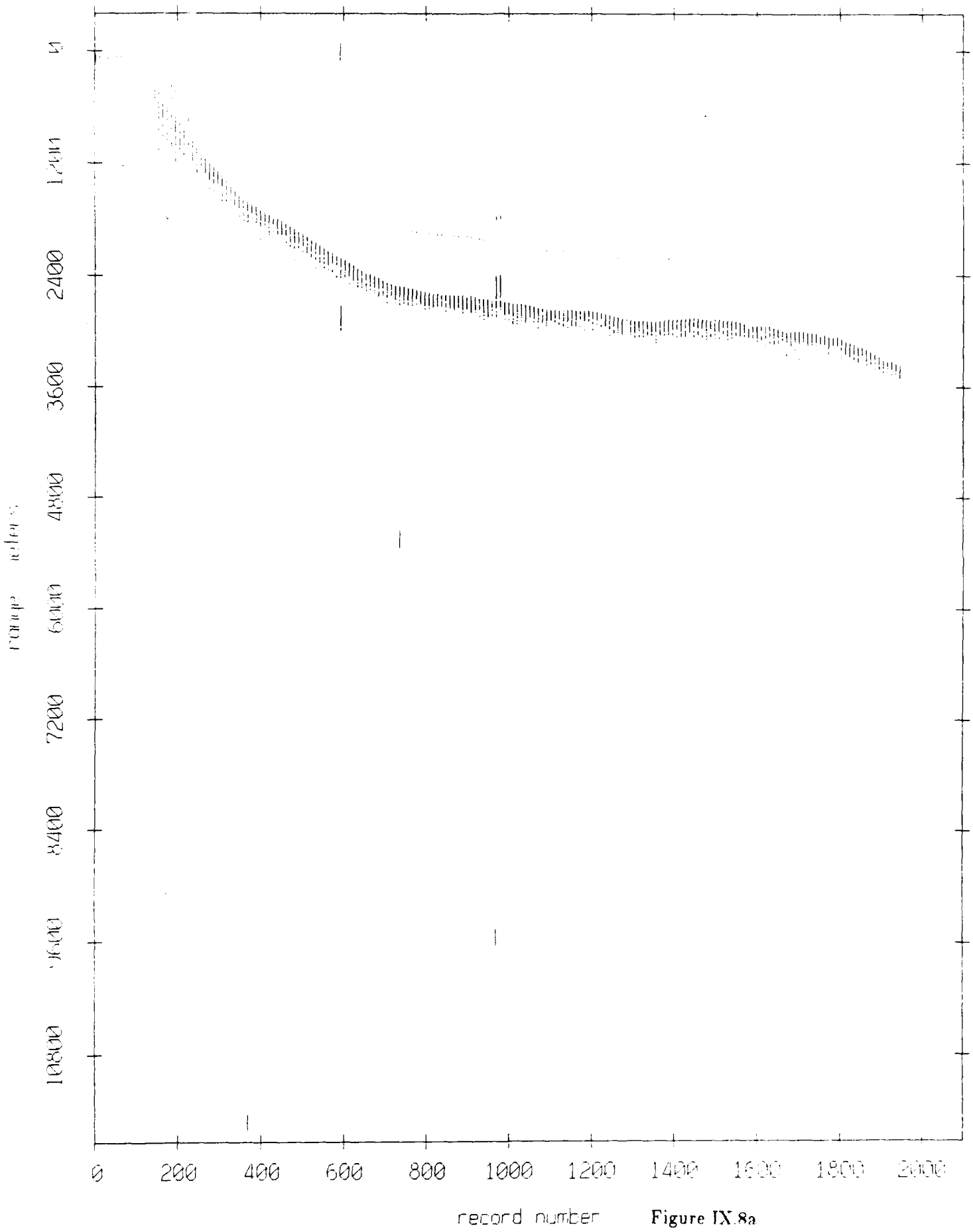

Float 6, August 1988 Experiment: range from float 10
0
2400
3600
4800
7200
9600
12000
84000
108000
0
200
400
600
800
1000
1200
1400
1600
1800
2000
record number

Figure IX.8a

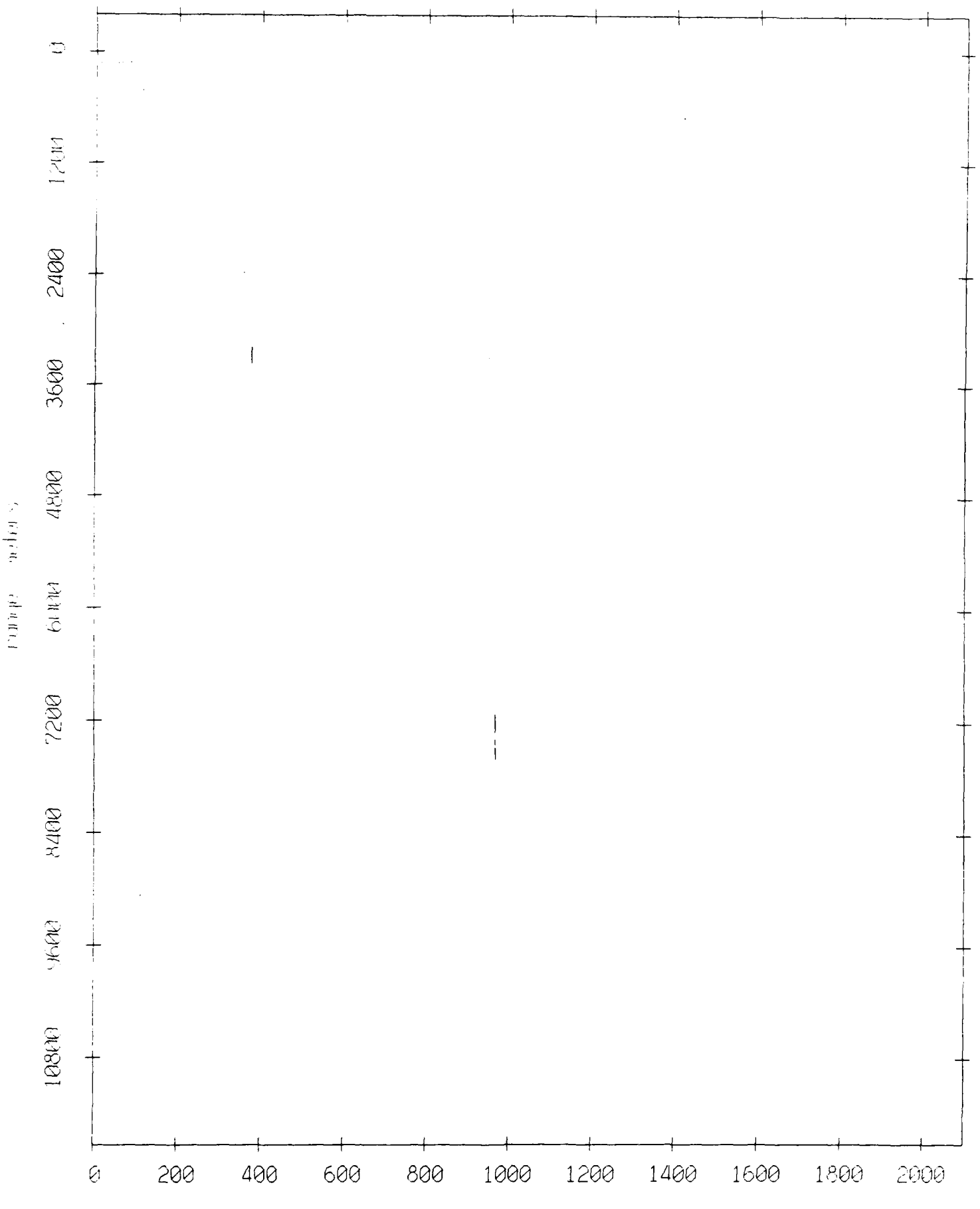

Float 6, August 1988 Experiment: range from float 3
0
2400
3600
4800
7200
8400
10800
0
200
400
600
800
1000
1200
1400
1600
1800
2000
record number

Figure IX.8b

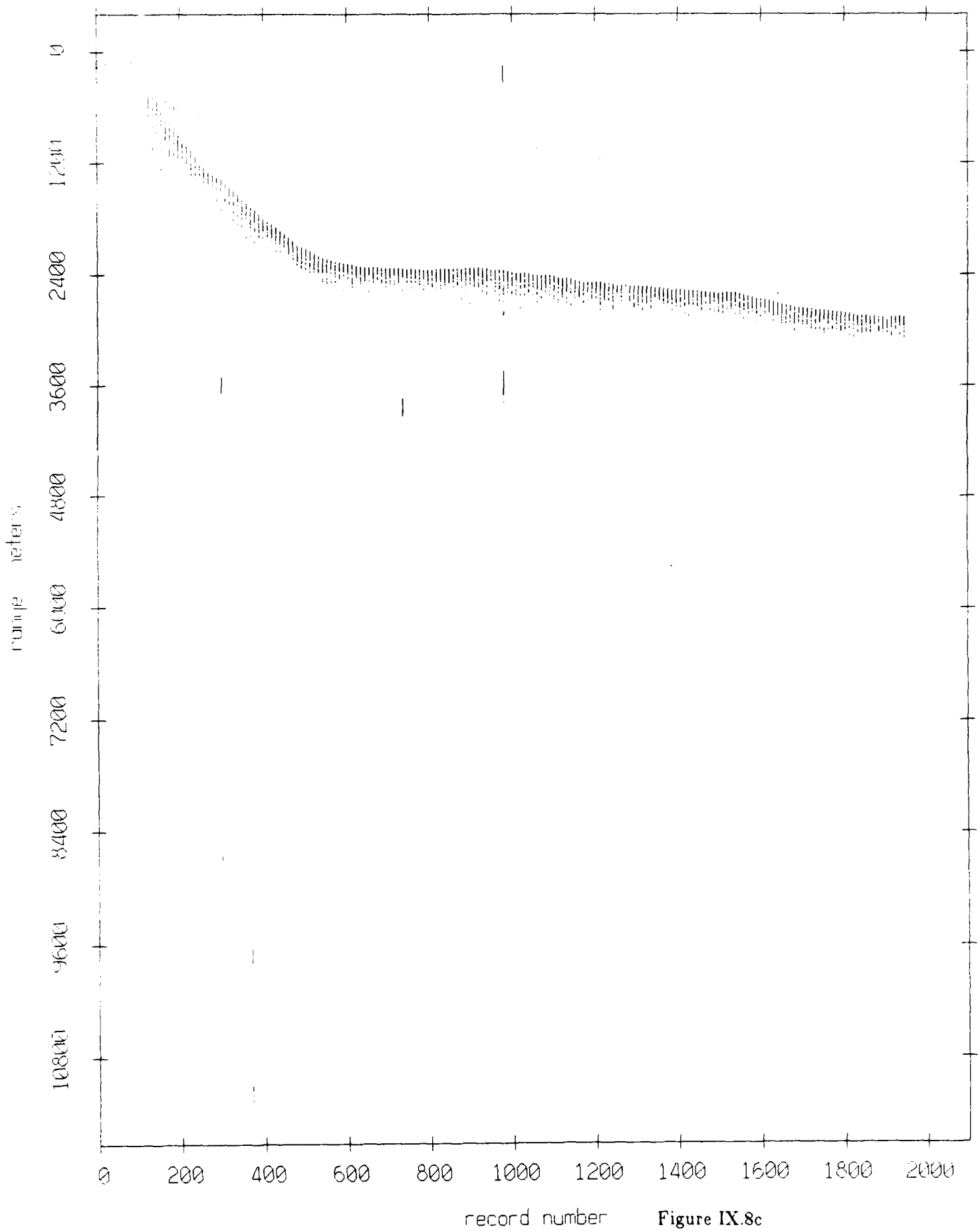

Float 6, August 1988 Experiment: range from float 5
range meters
0
1200
2400
3600
4800
6000
7200
8400
9600
10800
0
200
400
600
800
1000
1200
1400
1600
1800
2000
record number

Figure IX.8c

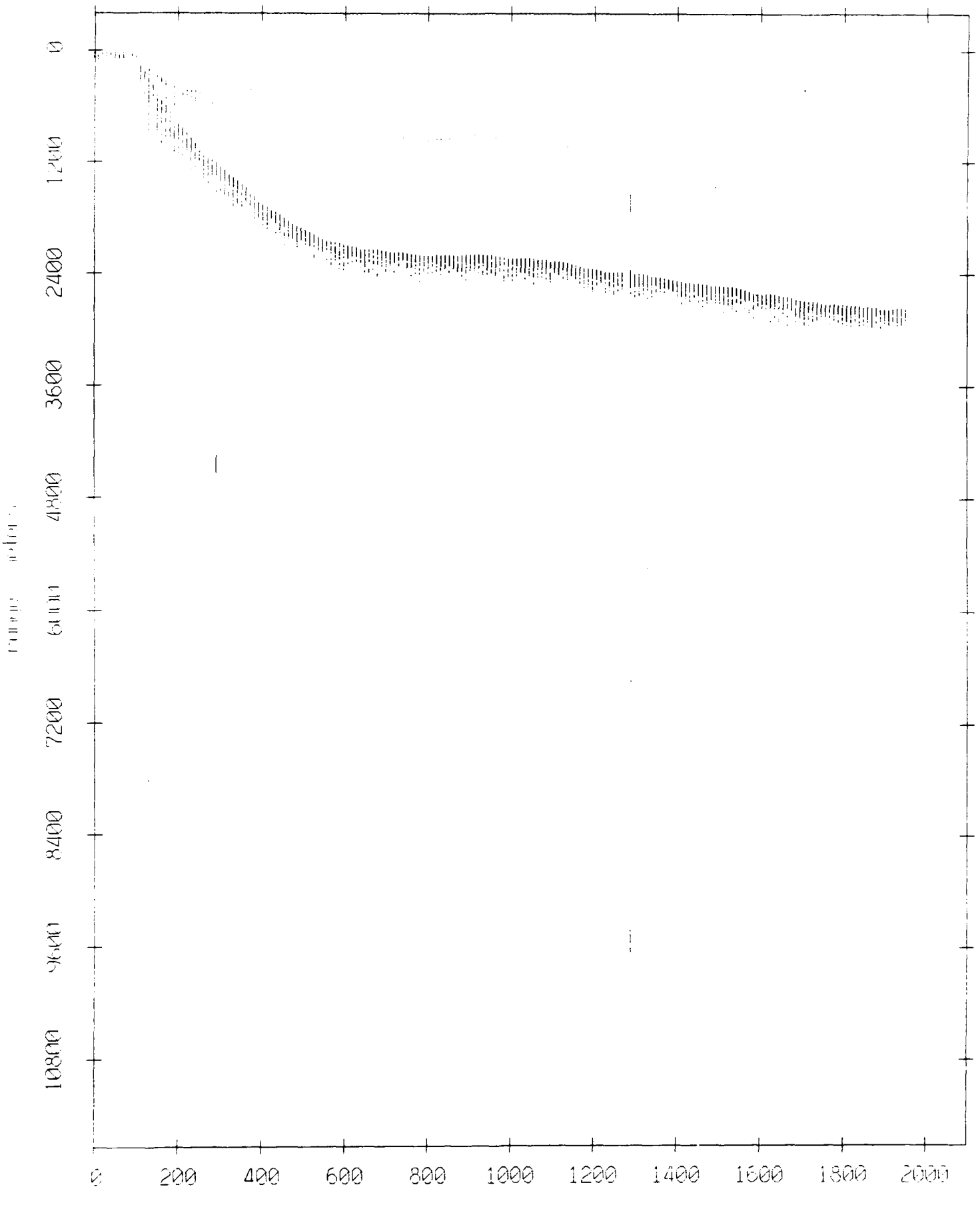

Float 6, August 1988 Experiment: range from float 0
0
1200
2400
3600
4800
6000
7200
8400
9600
10800
0
200
400
600
800
1000
1200
1400
1600
1800
2000
record number

Figure IX.8d

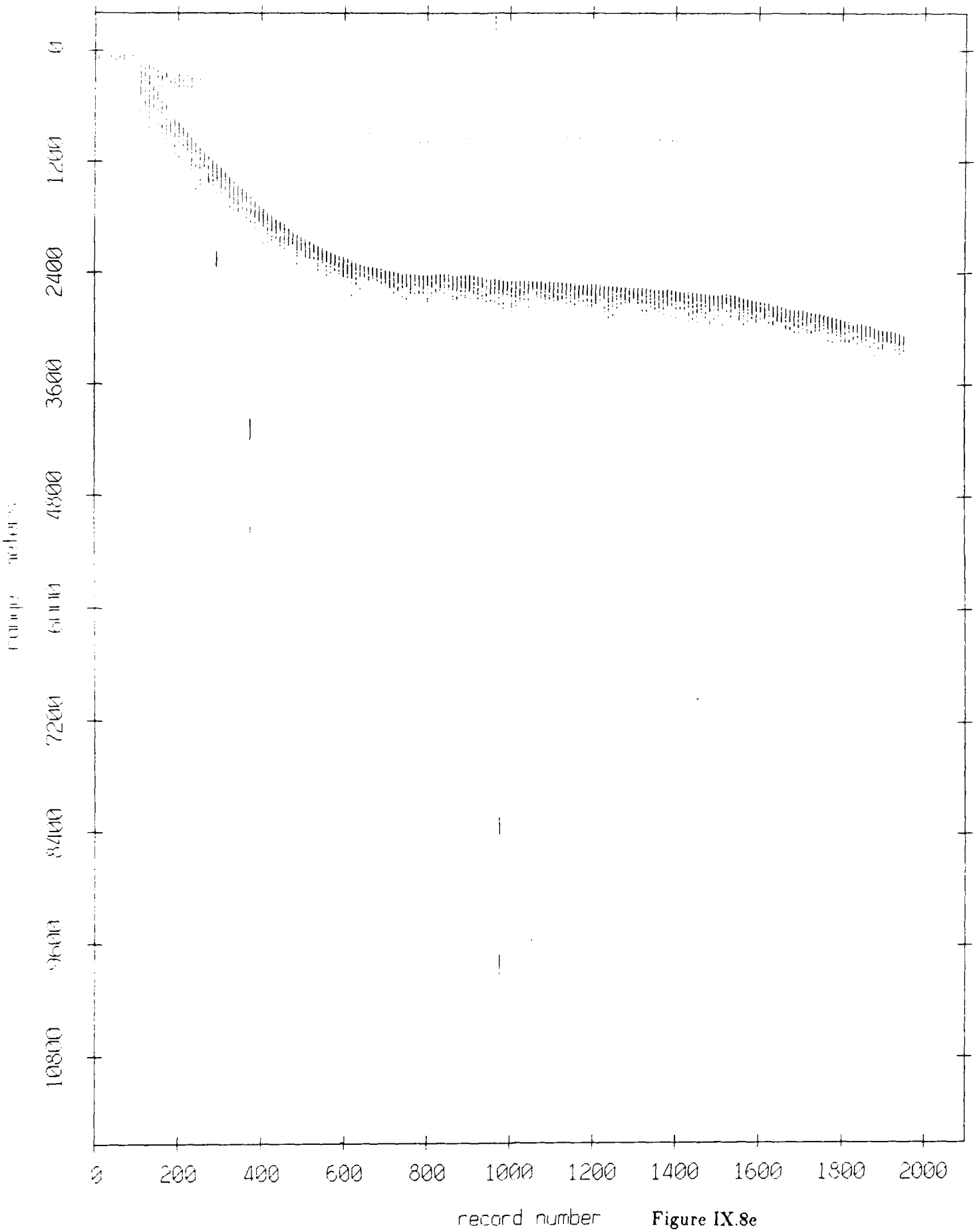

Float 6, August 1988 Experiment: range from float 1
12000
24000
36000
48000
60000
72000
84000
96000
108000
0
200
400
600
800
1000
1200
1400
1600
1800
2000
record number

Figure IX.8e

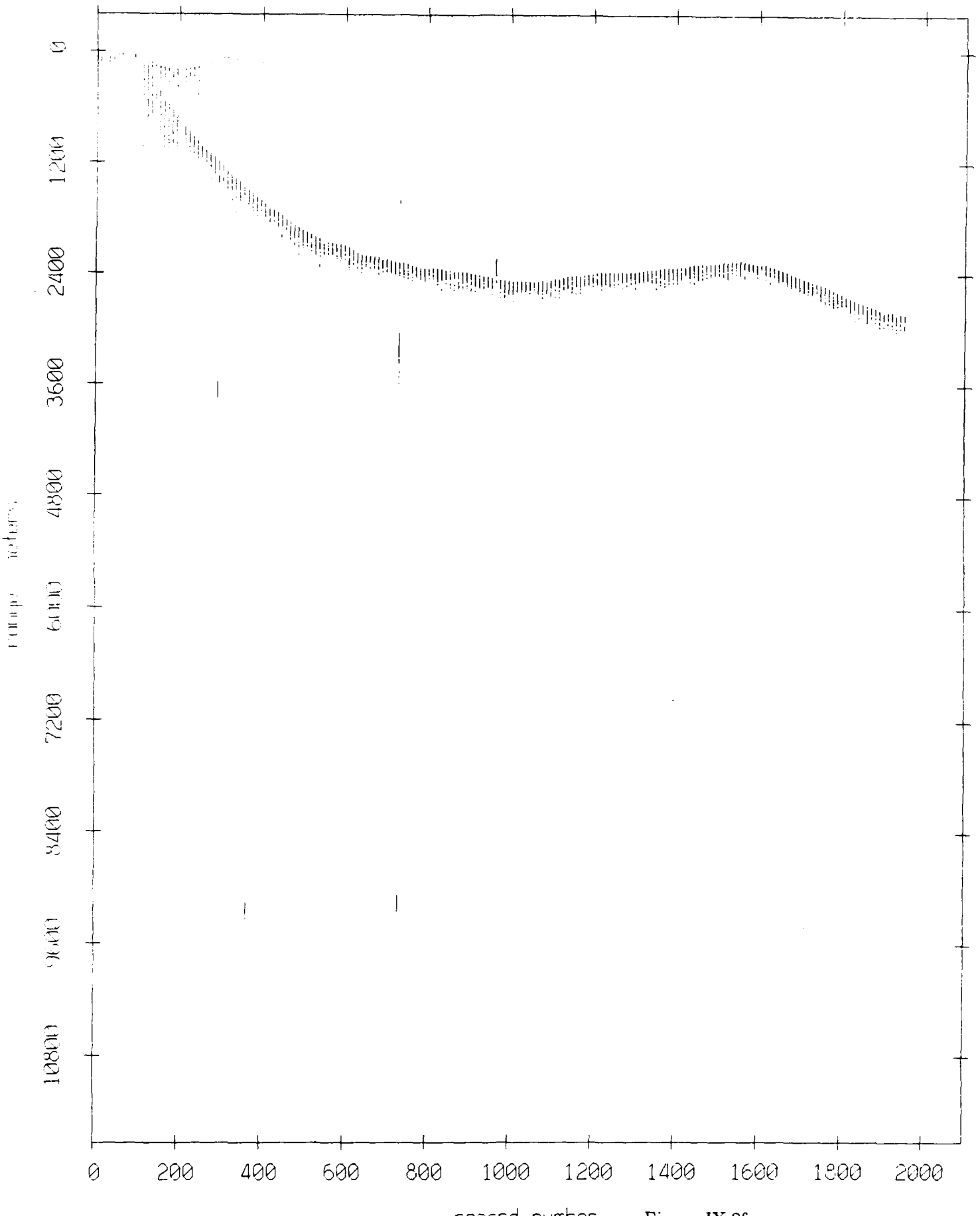

Float 6, August 1988 Experiment: range from float 2
0
1200
2400
3600
4800
6000
7200
8400
9600
10800
0
200
400
600
800
1000
1200
1400
1600
1800
2000
record number

Figure IX.8f

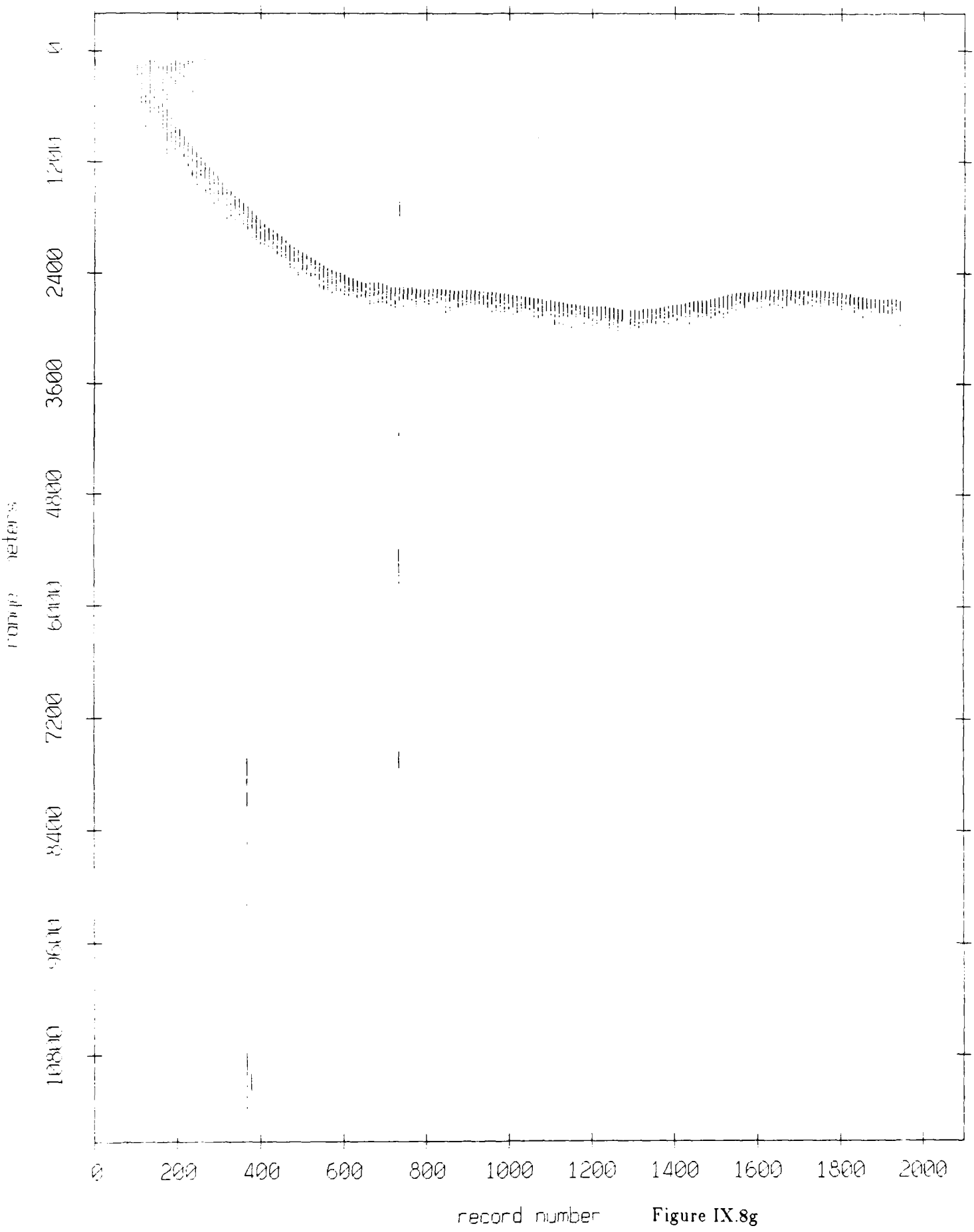

Float 6, August 1988 Experiment: range from float 4
0
1200
2400
3600
4800
6000
7200
8400
9600
10800
0
200
400
600
800
1000
1200
1400
1600
1800
2000
record number

Figure IX.8g

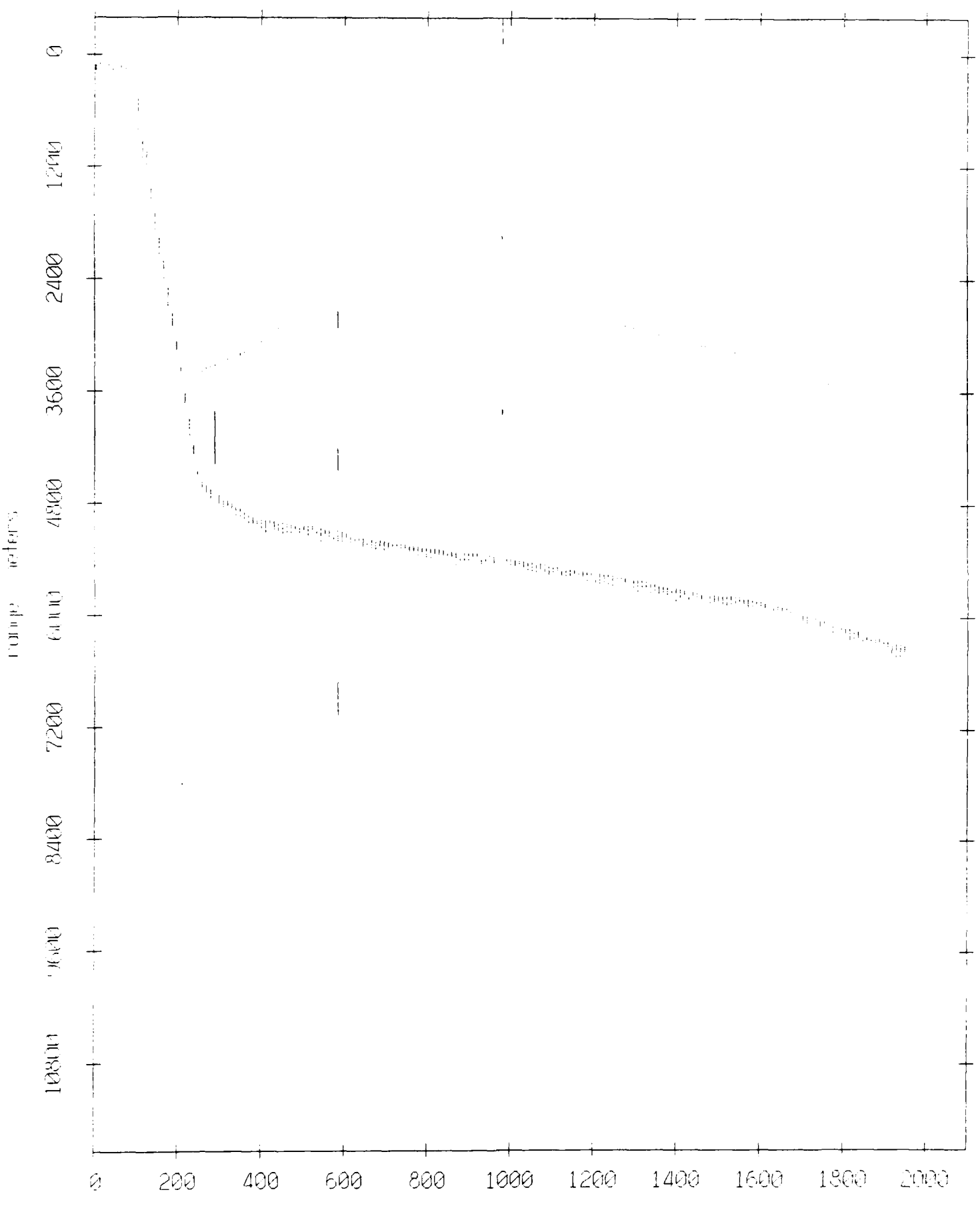

Float 6, August 1988 Experiment: range from float 11
0
1200
2400
3600
4800
7200
8400
0
200
400
600
800
1000
1200
1400
1600
1800
2000
record number

Figure IX.8h

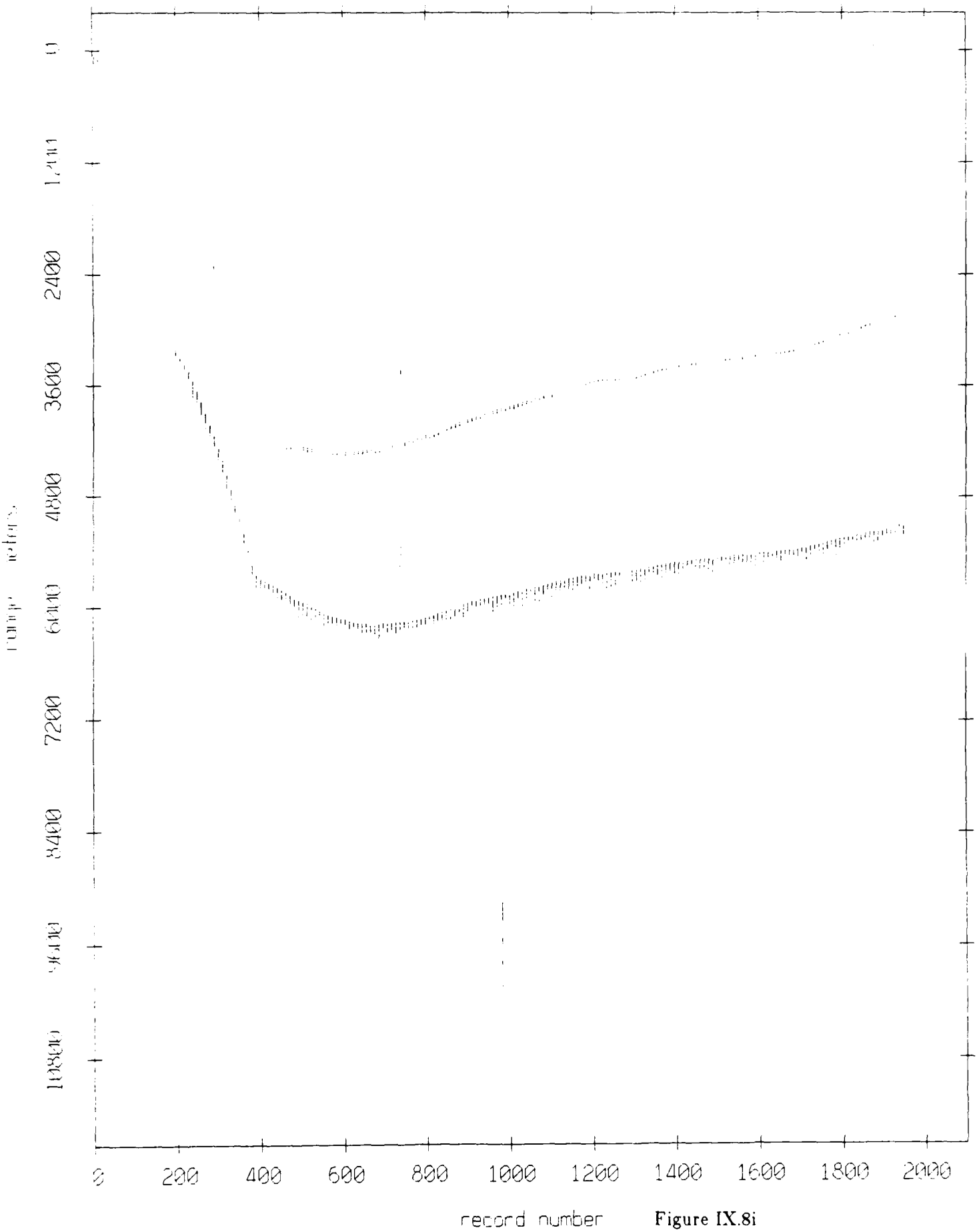

Float 6, August 1988 Experiment: range from float 7
2400
3600
4800
7200
8400
0
200
400
600
800
1000
1200
1400
1600
1800
2000
record number

Figure IX.8i

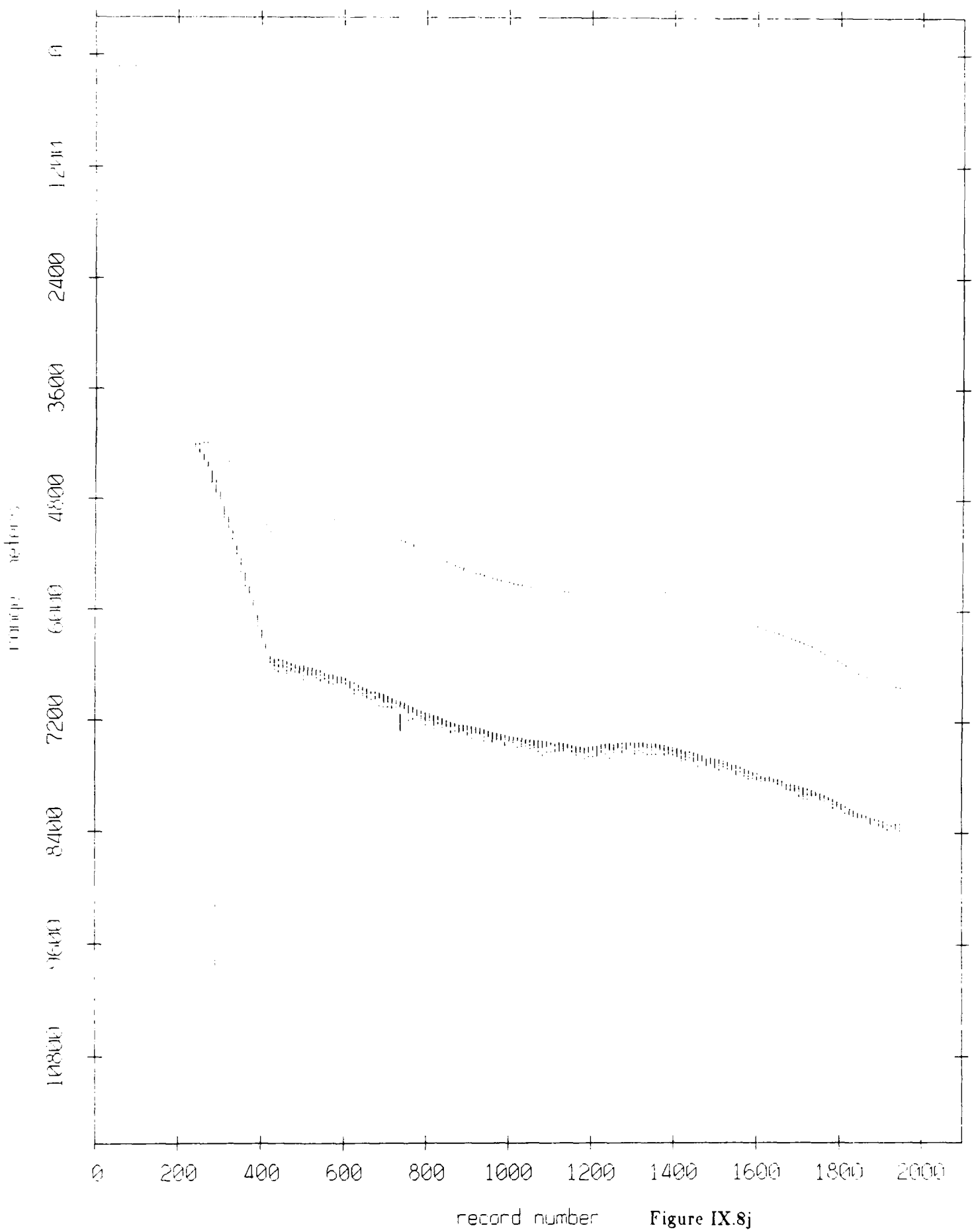

Float 6, August 1988 Experiment: range from float 8
0
200
400
600
800
1000
1200
1400
1600
1800
2000
record number

Figure IX.8j

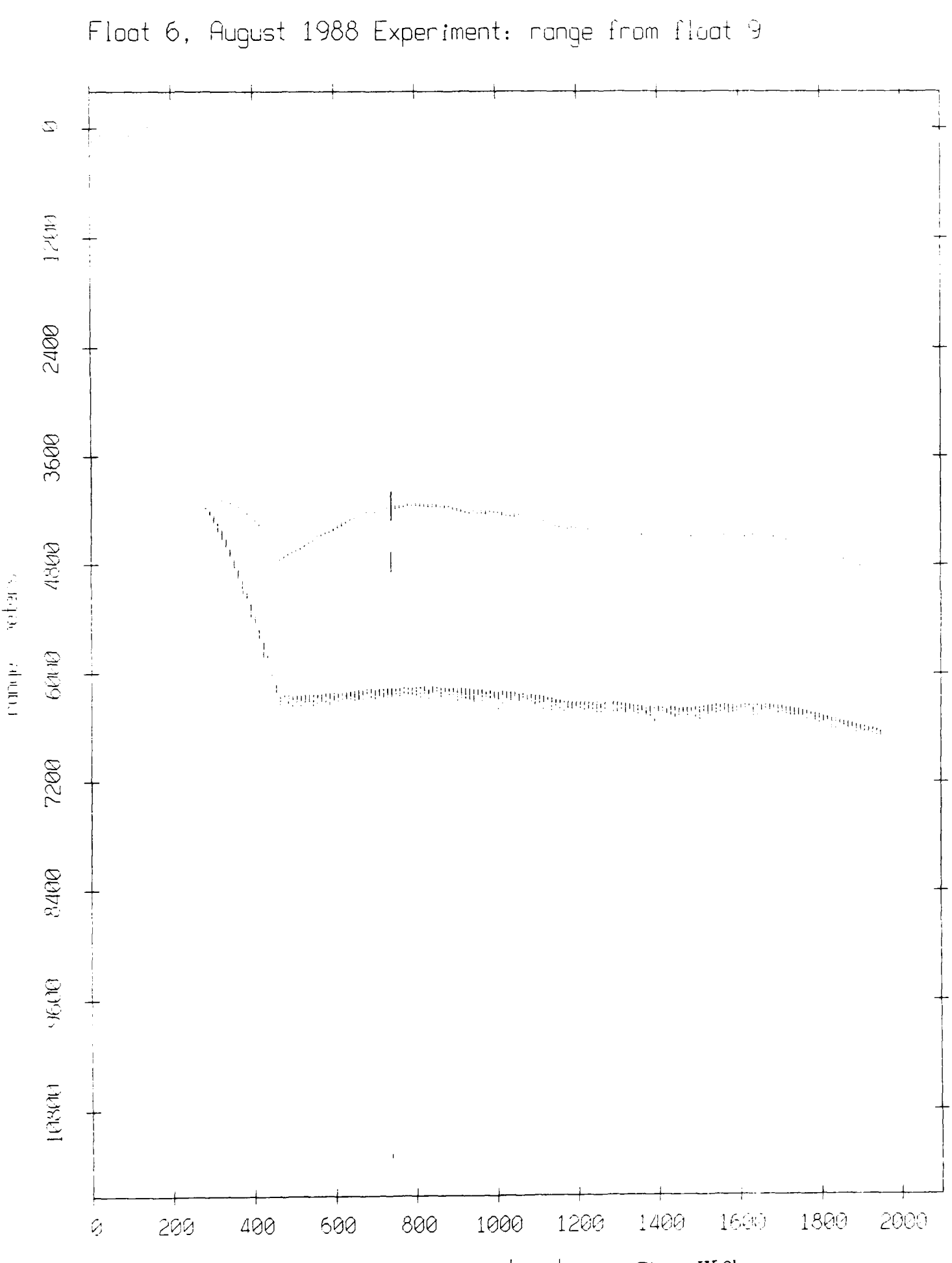

Float 6, August 1988 Experiment: range from float 9
2400
3600
7200
8400
0
200
400
600
800
1000
1200
1400
1800
2000
record number

Figure IX.8k

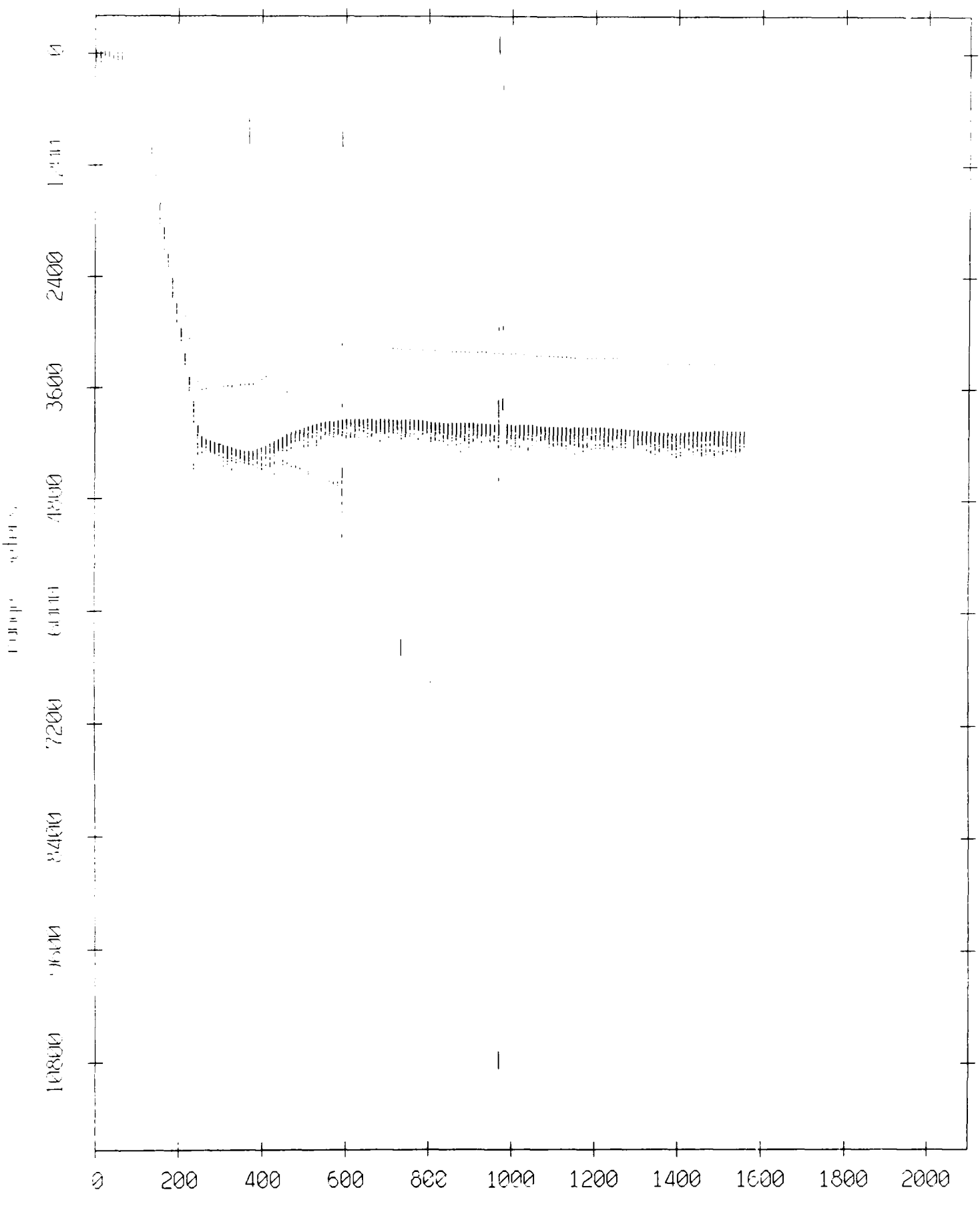

Float 11, August 1988 Experiment: range from float 10
2400
3600
0
200
400
600
800
1000
1200
1400
1600
1800
2000
record number

Figure IX.9a

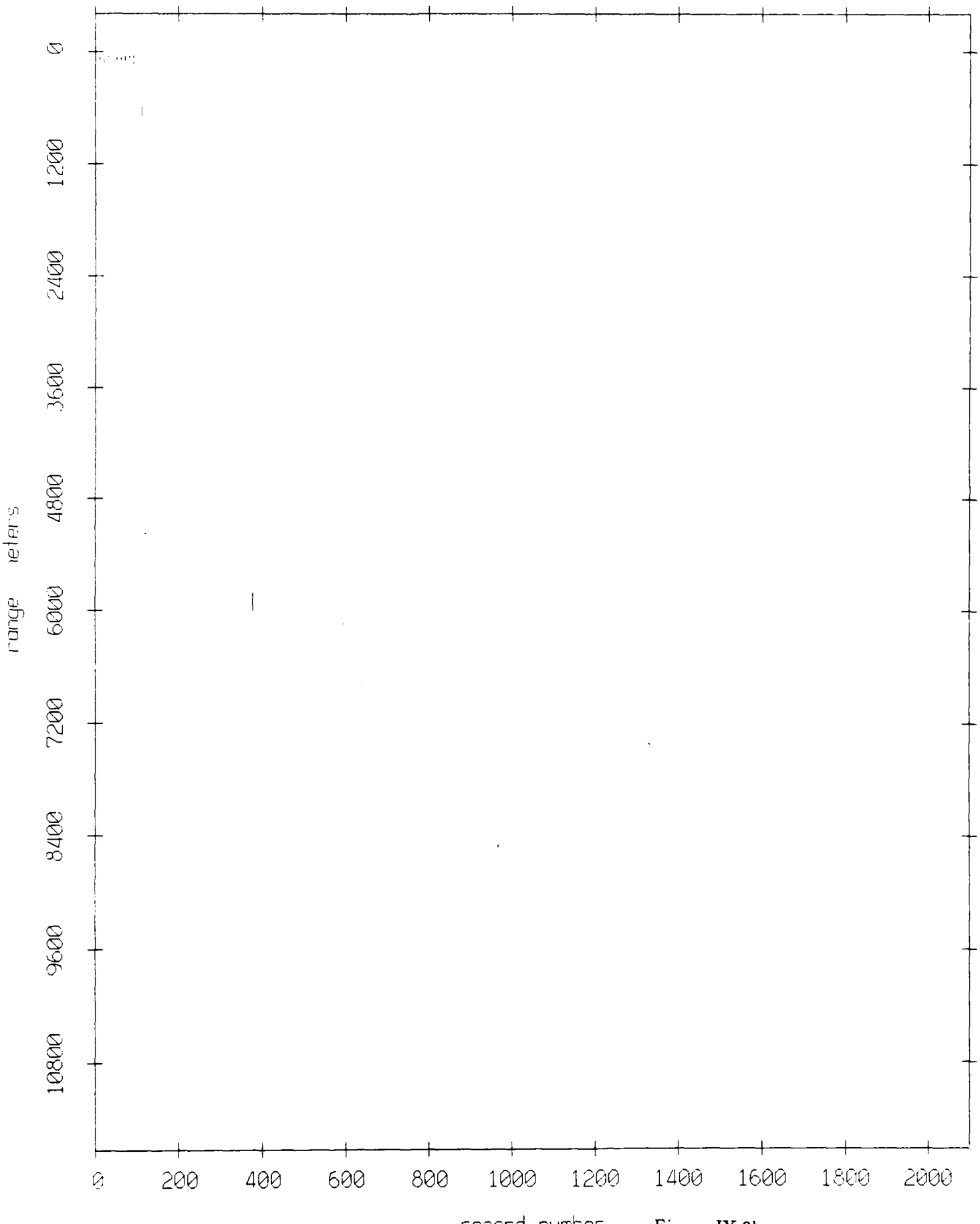

Float 11, August 1988 Experiment: range from float 3
range meters
0
1200
2400
3600
4800
6000
7200
8400
9600
10800
0
200
400
600
800
1000
1200
1400
1600
1800
2000
record number

Figure IX.9b

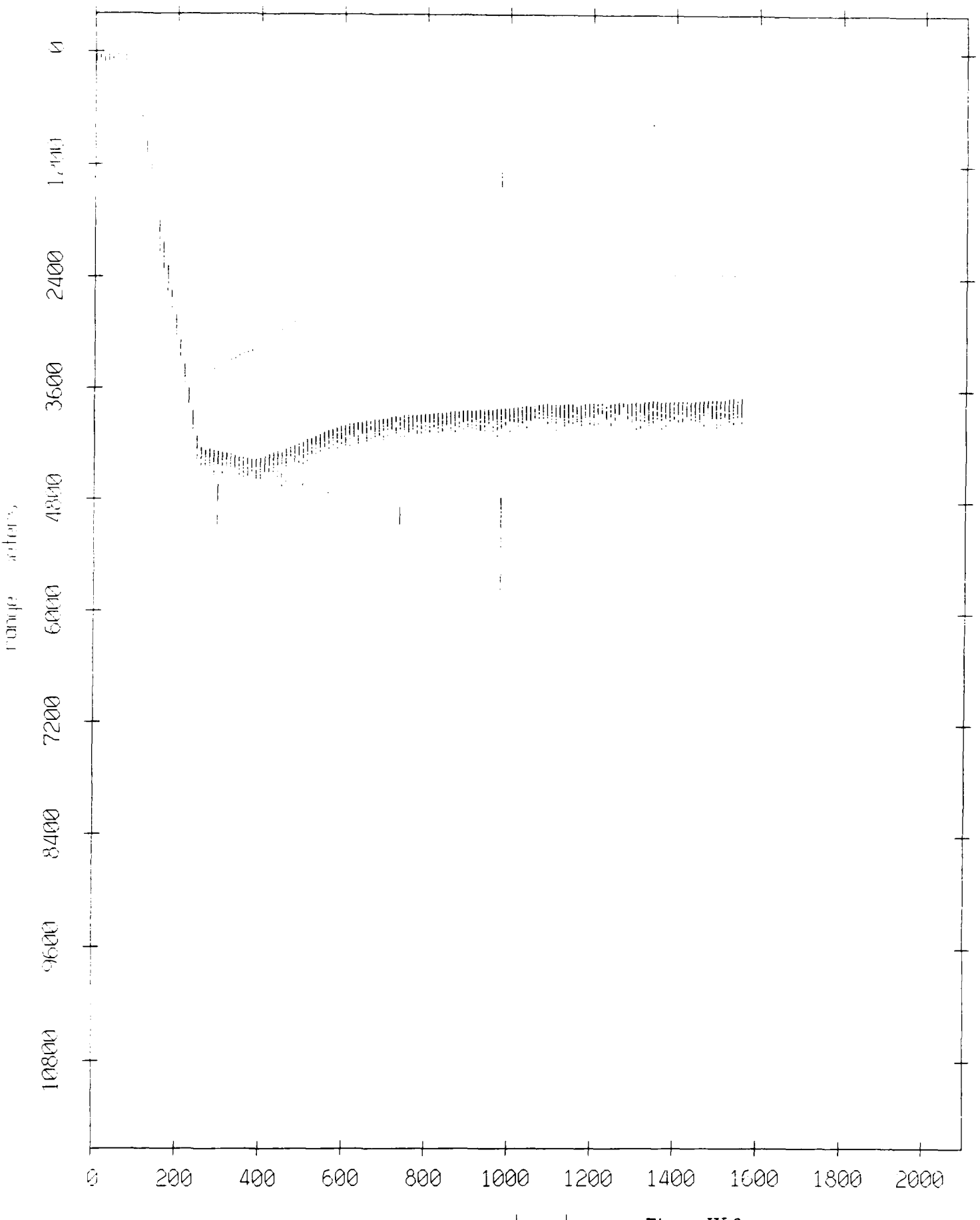

Float 11, August 1988 Experiment: range from float 5
0
1200
2400
3600
4800
6000
7200
8400
9600
10800
0
200
400
600
800
1000
1200
1400
1600
1800
2000
record number

Figure IX.9c

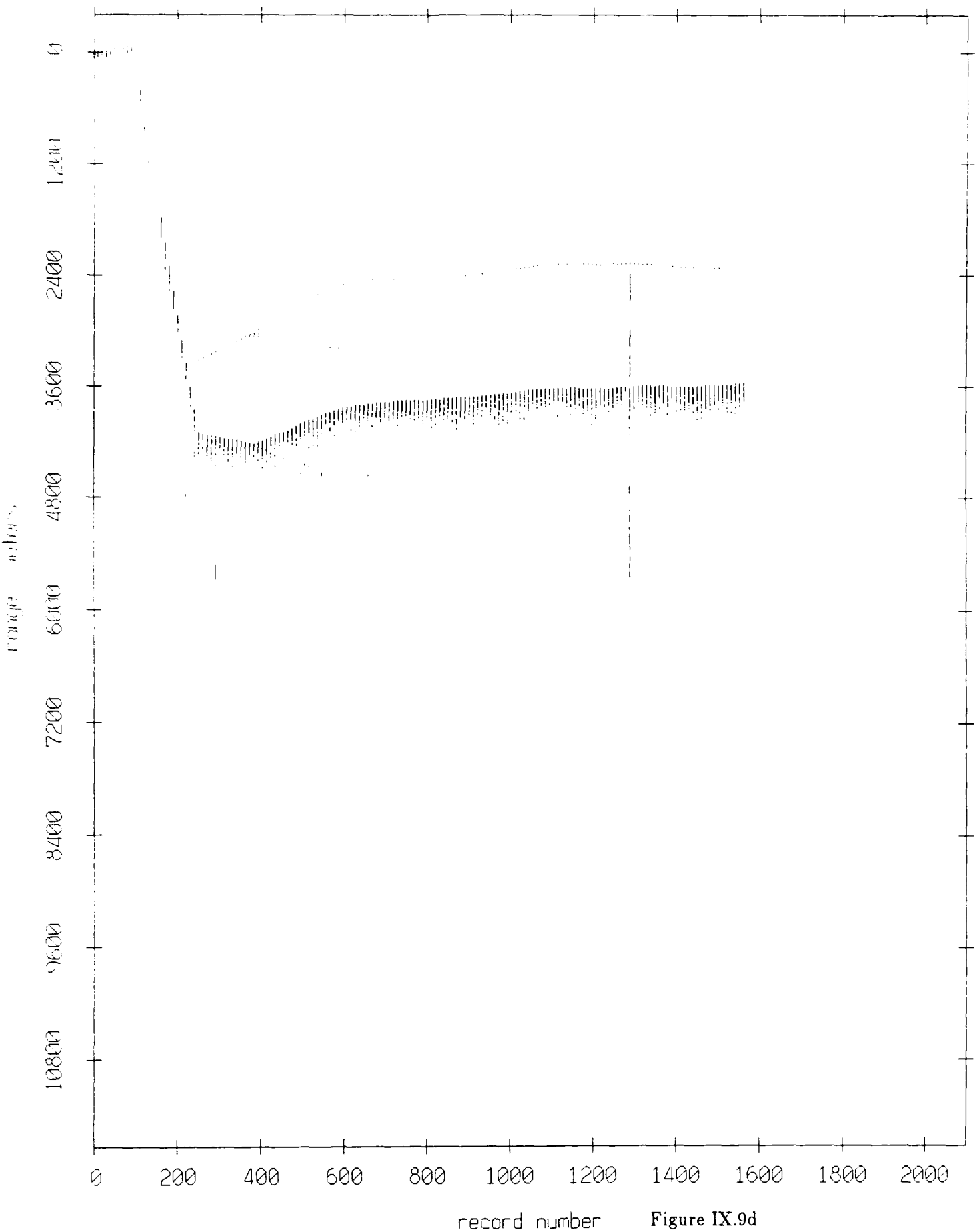

Float 11, August 1988 Experiment: range from float 0
range, m
0
1200
2400
3600
4800
6000
7200
8400
9600
10800
0
200
400
600
800
1000
1200
1400
1600
1800
2000
record number

Figure IX.9d

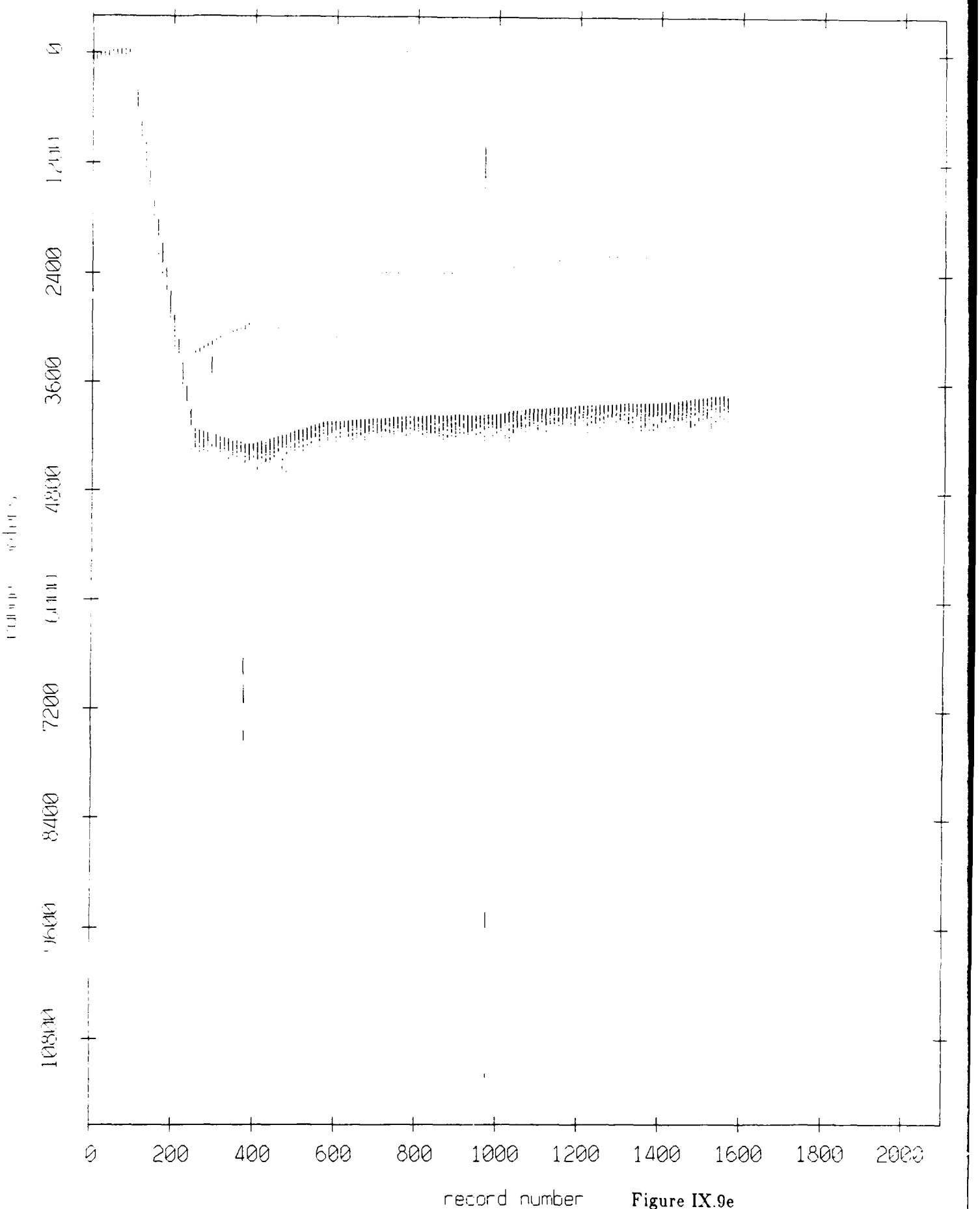

Float 11, August 1988 Experiment: range from float 1
0
2400
3600
7200
8400
0
200
400
600
800
1000
1200
1400
1600
1800
record number

Figure IX.9e

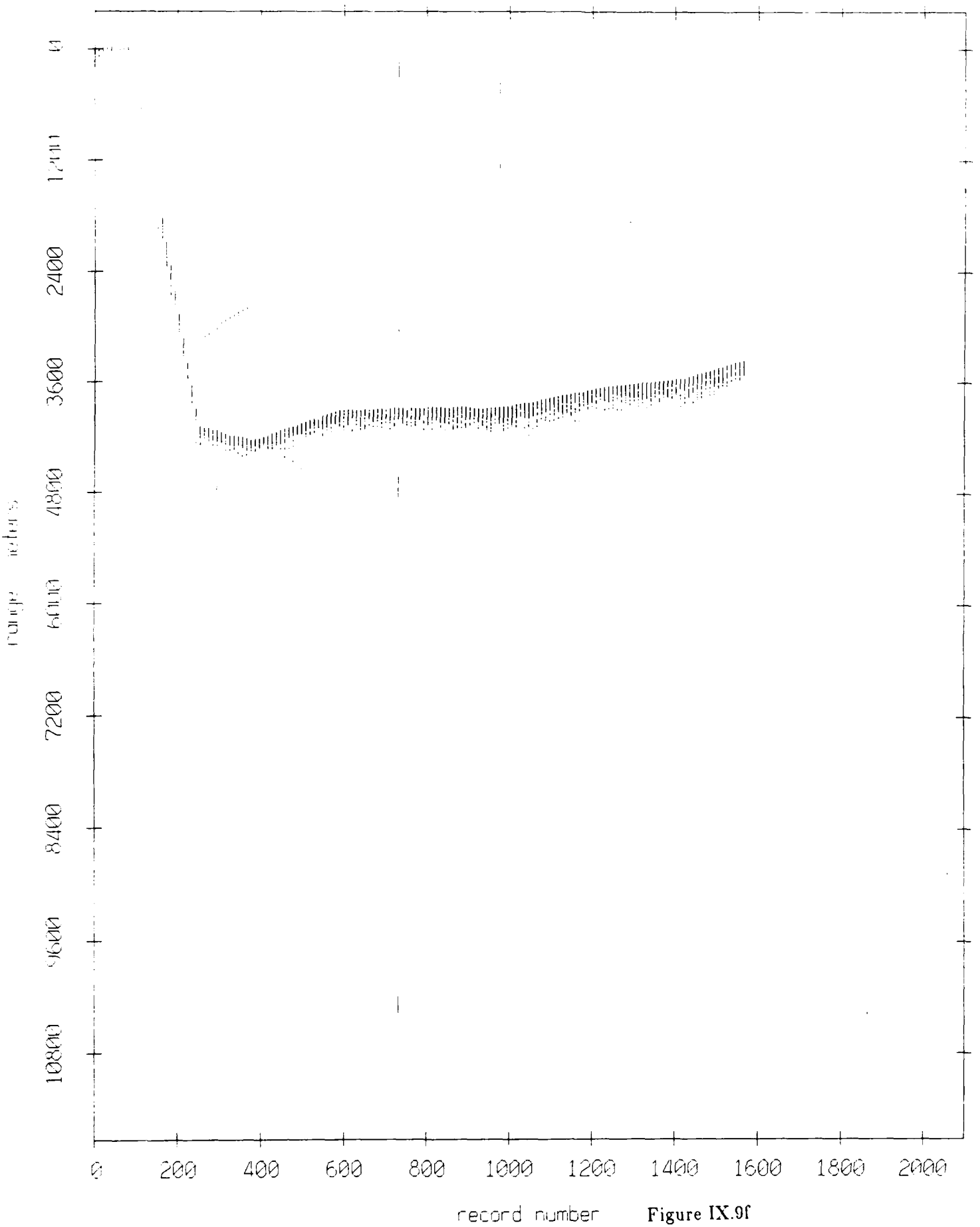

Float 11, August 1988 Experiment: range from float 2
2400
3600
4800
7200
8400
10800
0
200
400
600
800
1000
1200
1400
1600
1800
2000
record number

Figure IX.9f

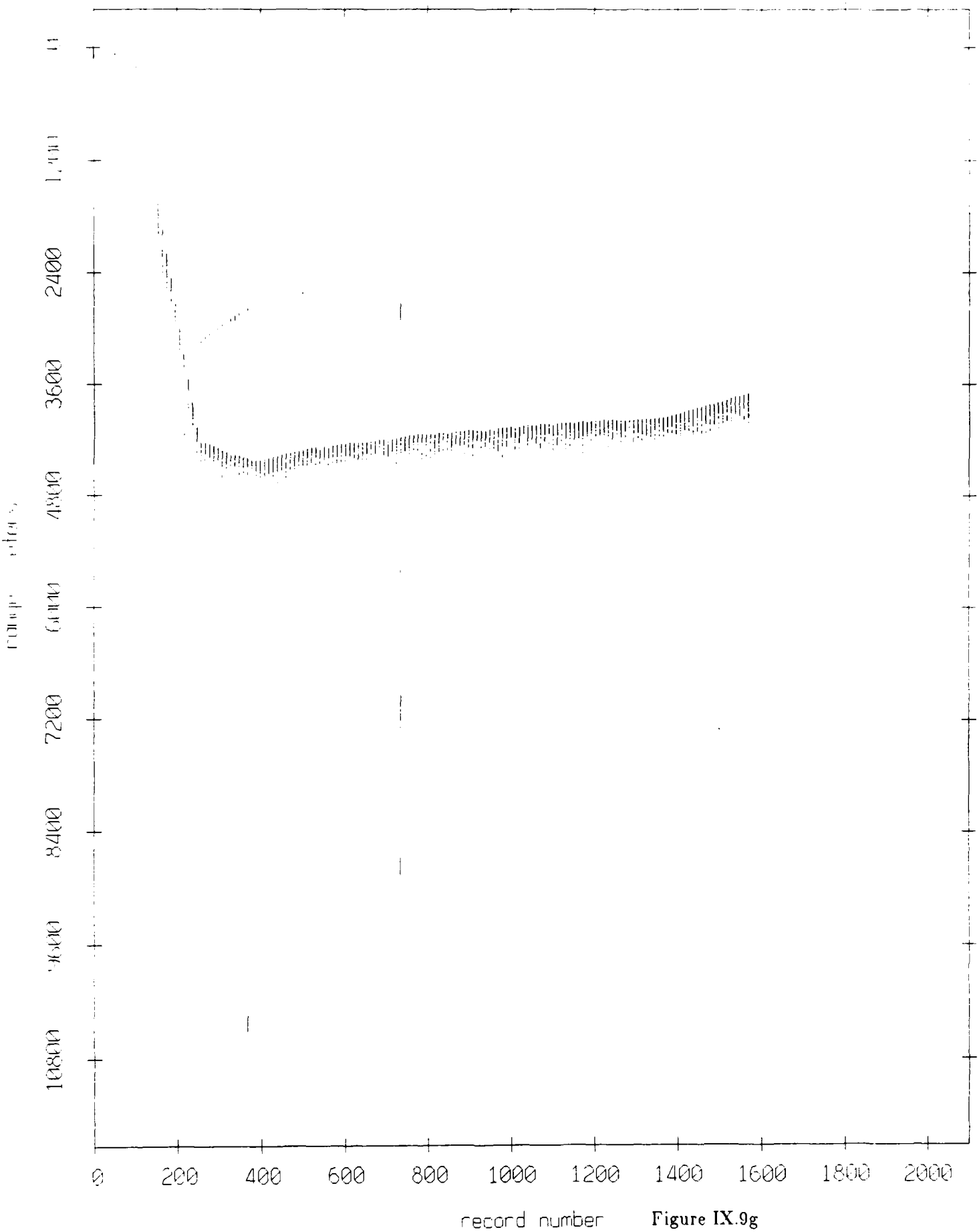

Float 11, August 1988 Experiment: range from float 4
10800
9600
8400
7200
6000
4800
3600
2400
1200
0
200
400
600
800
1000
1200
1400
1600
1800
2000
record number

Figure IX.9g

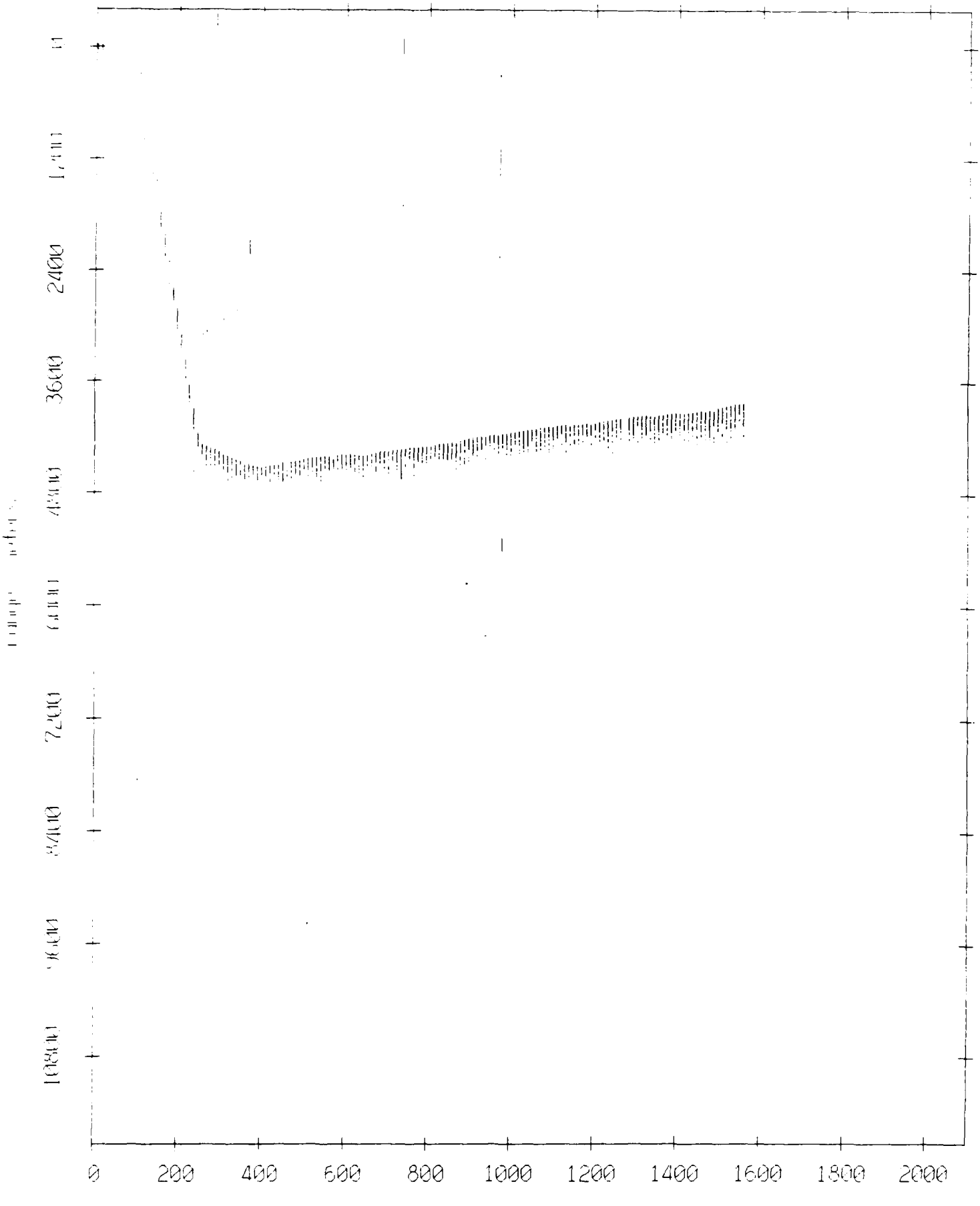

Float 11, August 1988 Experiment: range from float 6
24000
36000
0
200
400
600
800
1000
1200
1400
1600
1800
2000
record number

Figure IX.9h

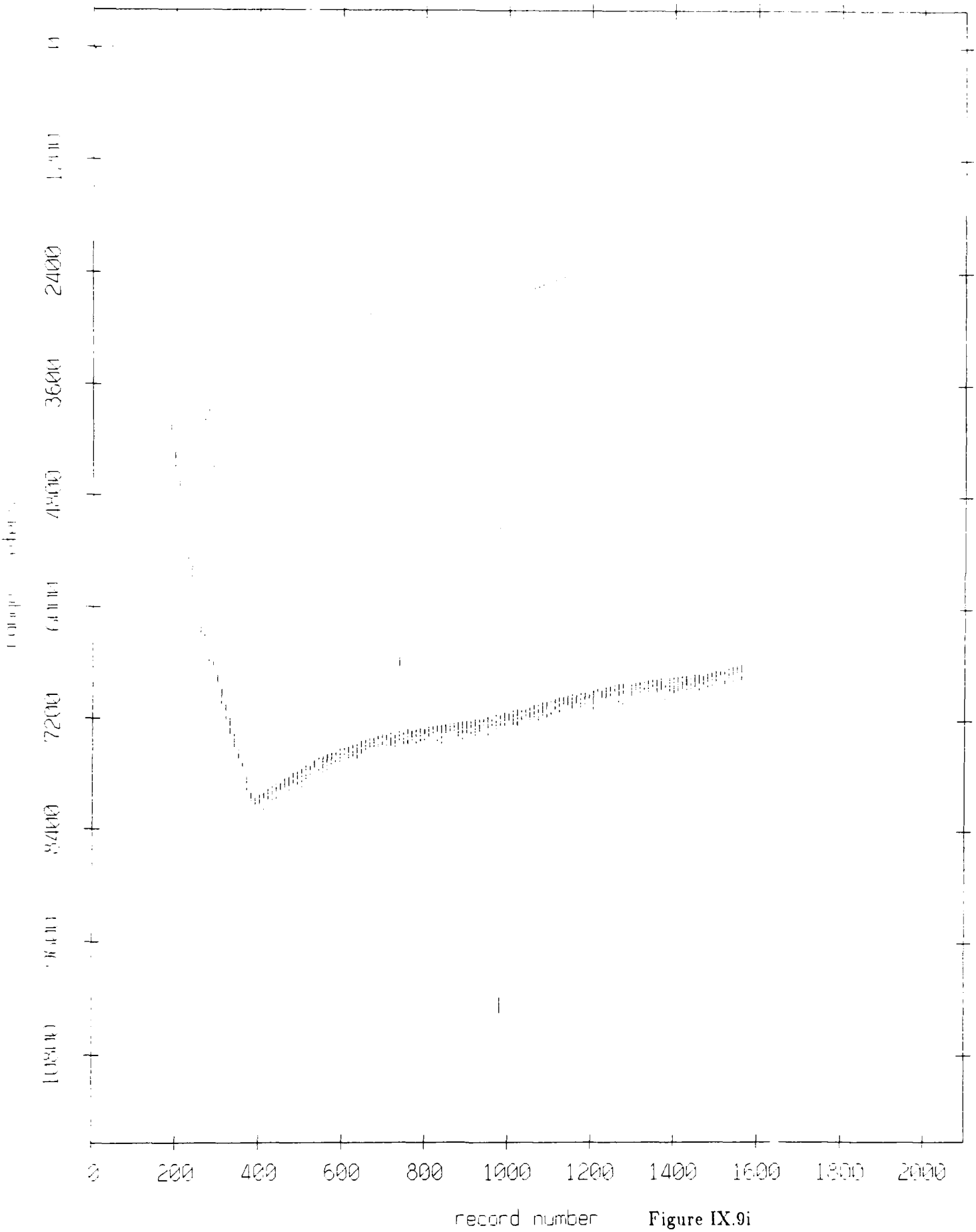

Float 11, August 1988 Experiment: range from float 7
2400
3600
4800
7200
9600
0
200
400
600
800
1000
1200
1400
1600
1800
2000
record number

Figure IX.9i

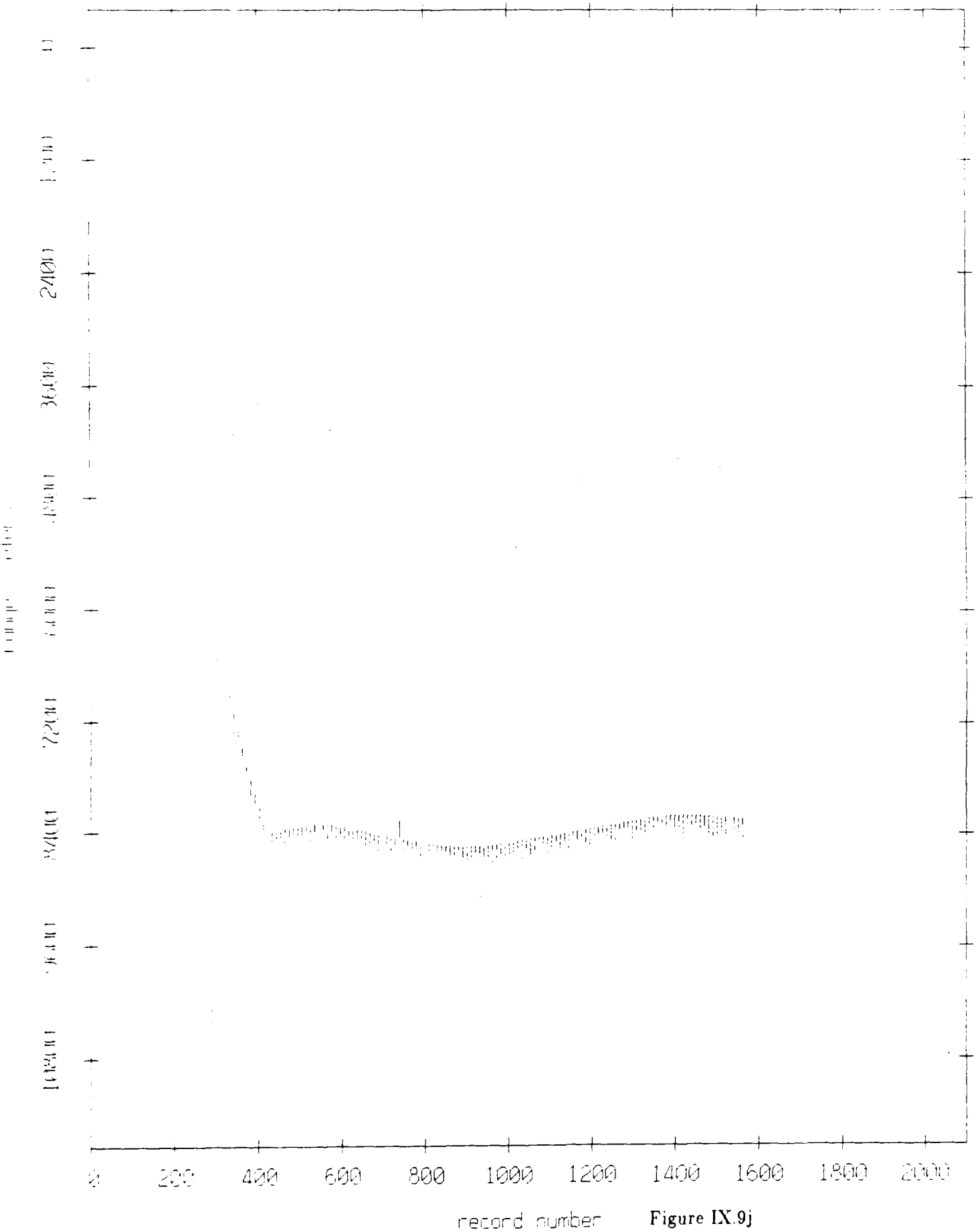

Float 11, August 1988 Experiment: range from float 8
2400
3600
7200
0
200
400
600
800
1000
1200
1400
1600
1800
2000
record number

Figure IX.9j

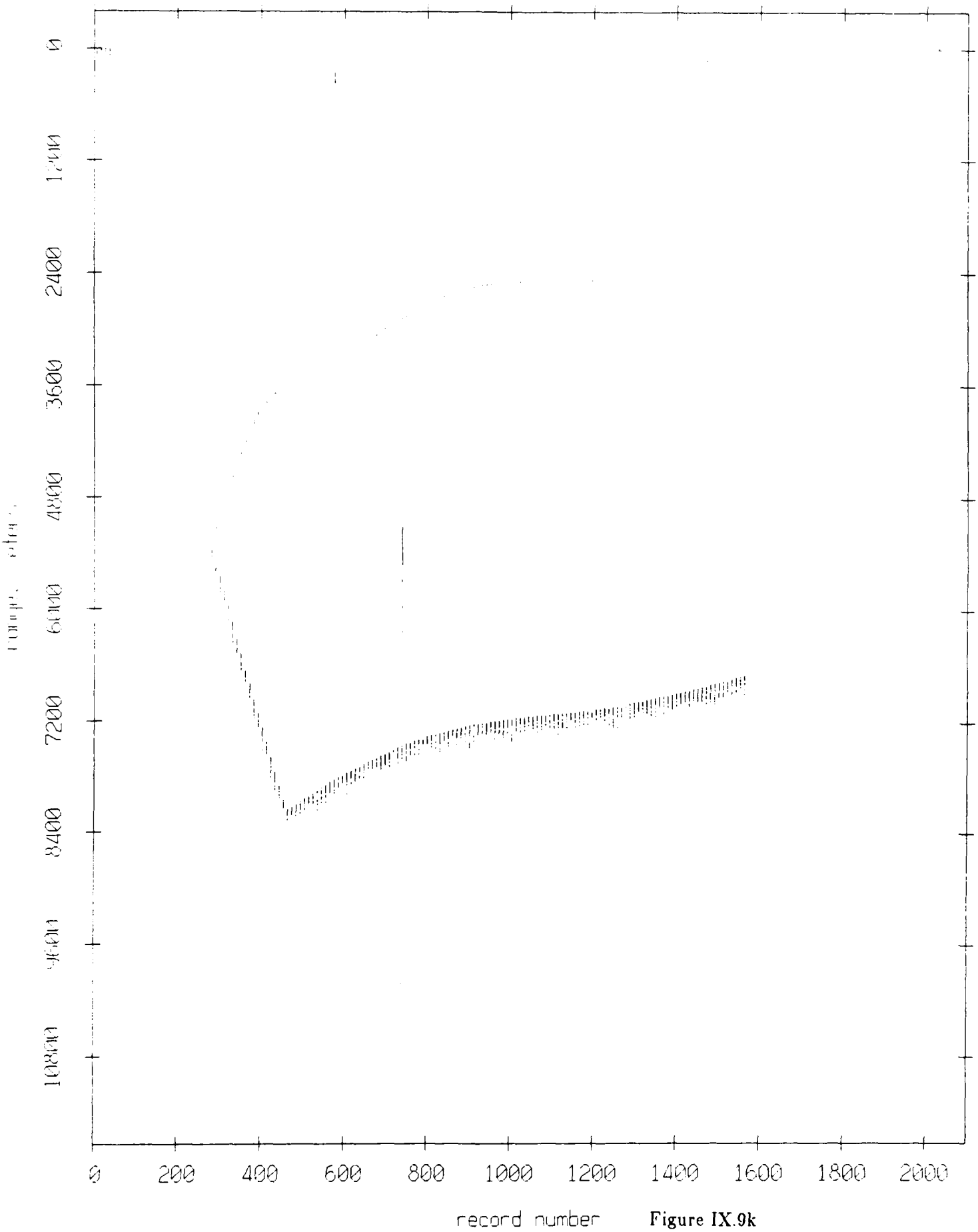

Float 11, August 1988 Experiment: range from float 9
0
1200
2400
3600
4800
6000
7200
8400
9600
10800
0
200
400
600
800
1000
1200
1400
1600
1800
2000
record number

Figure IX.9k

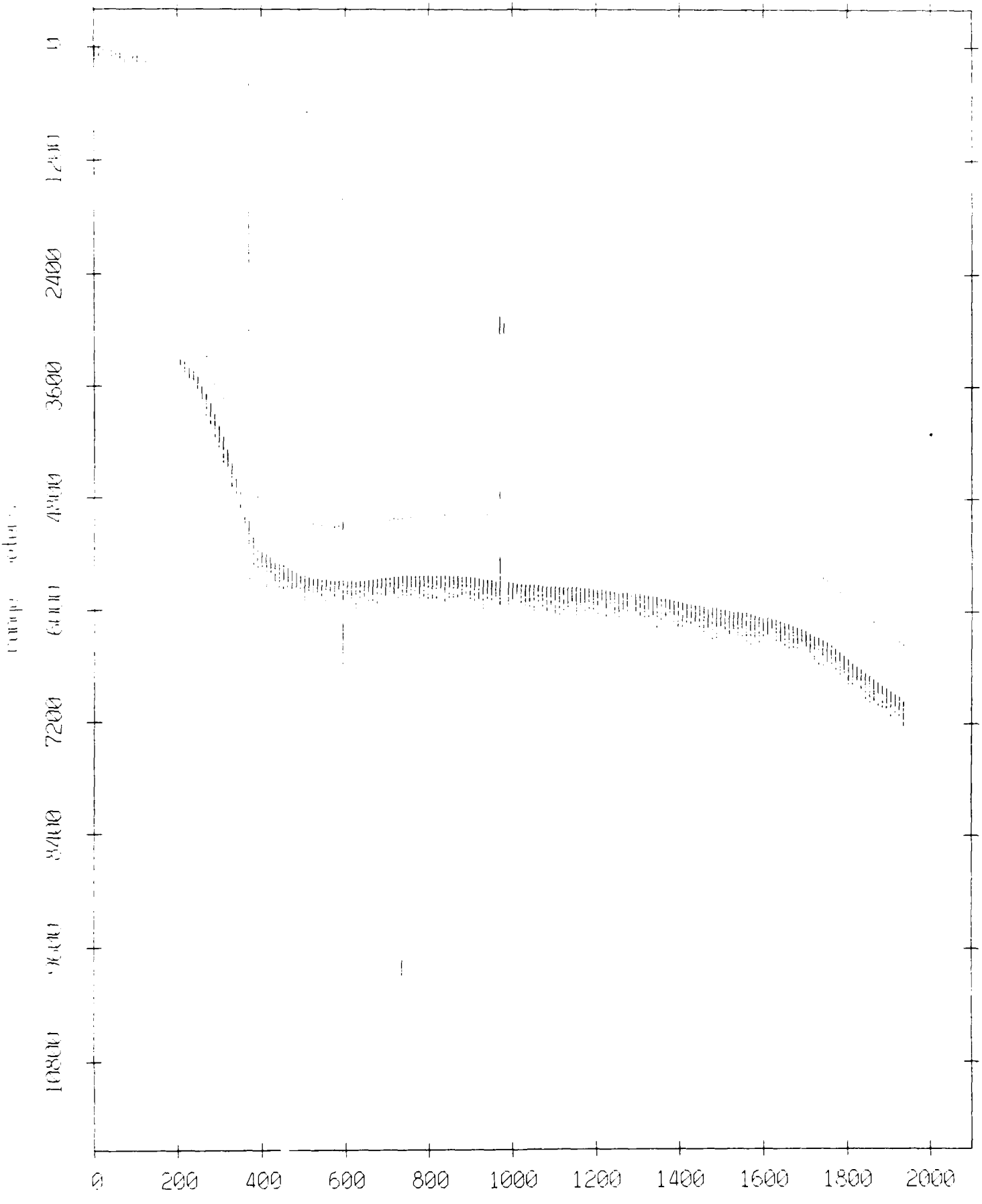


Figure IX.10a

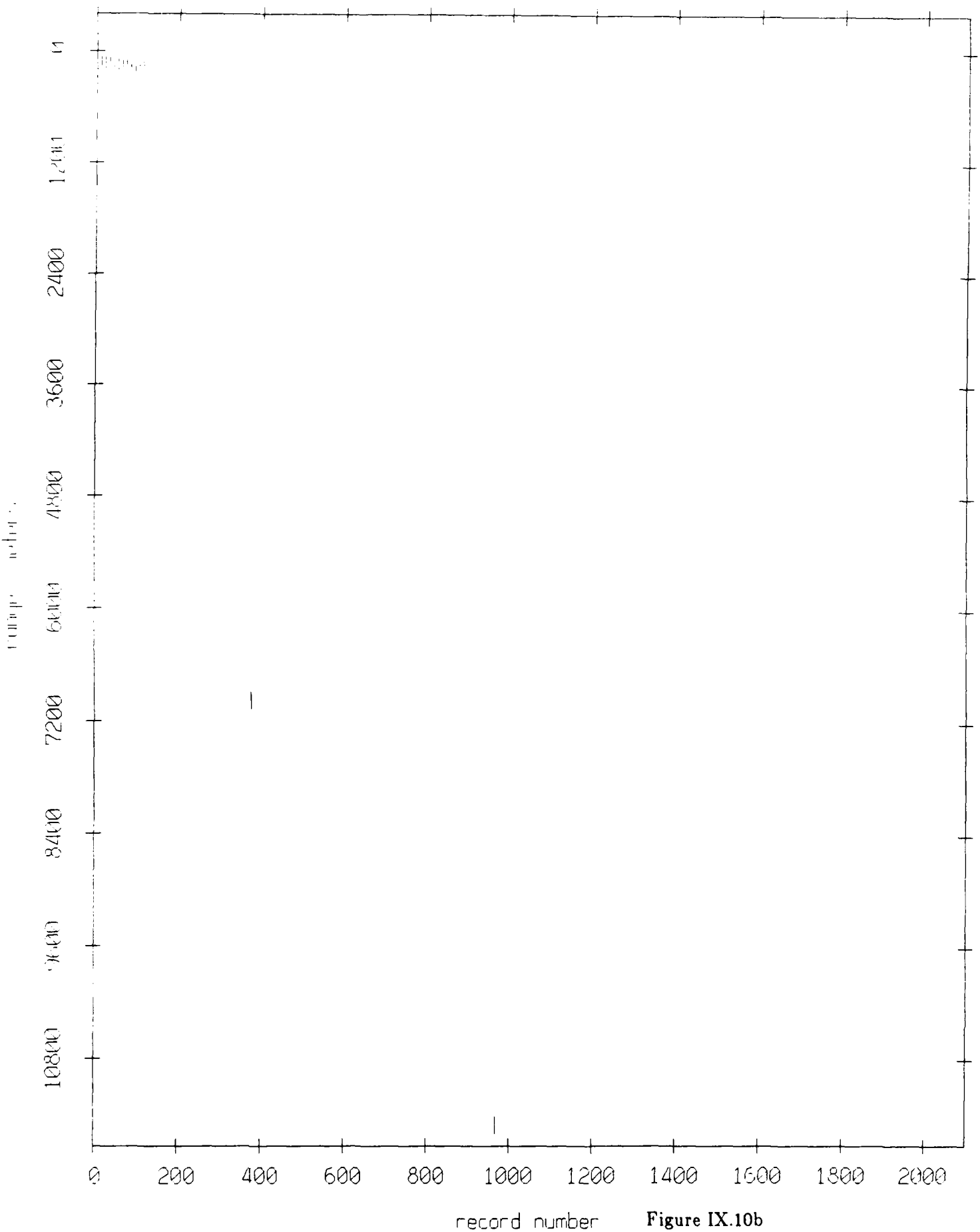


Figure IX.10b

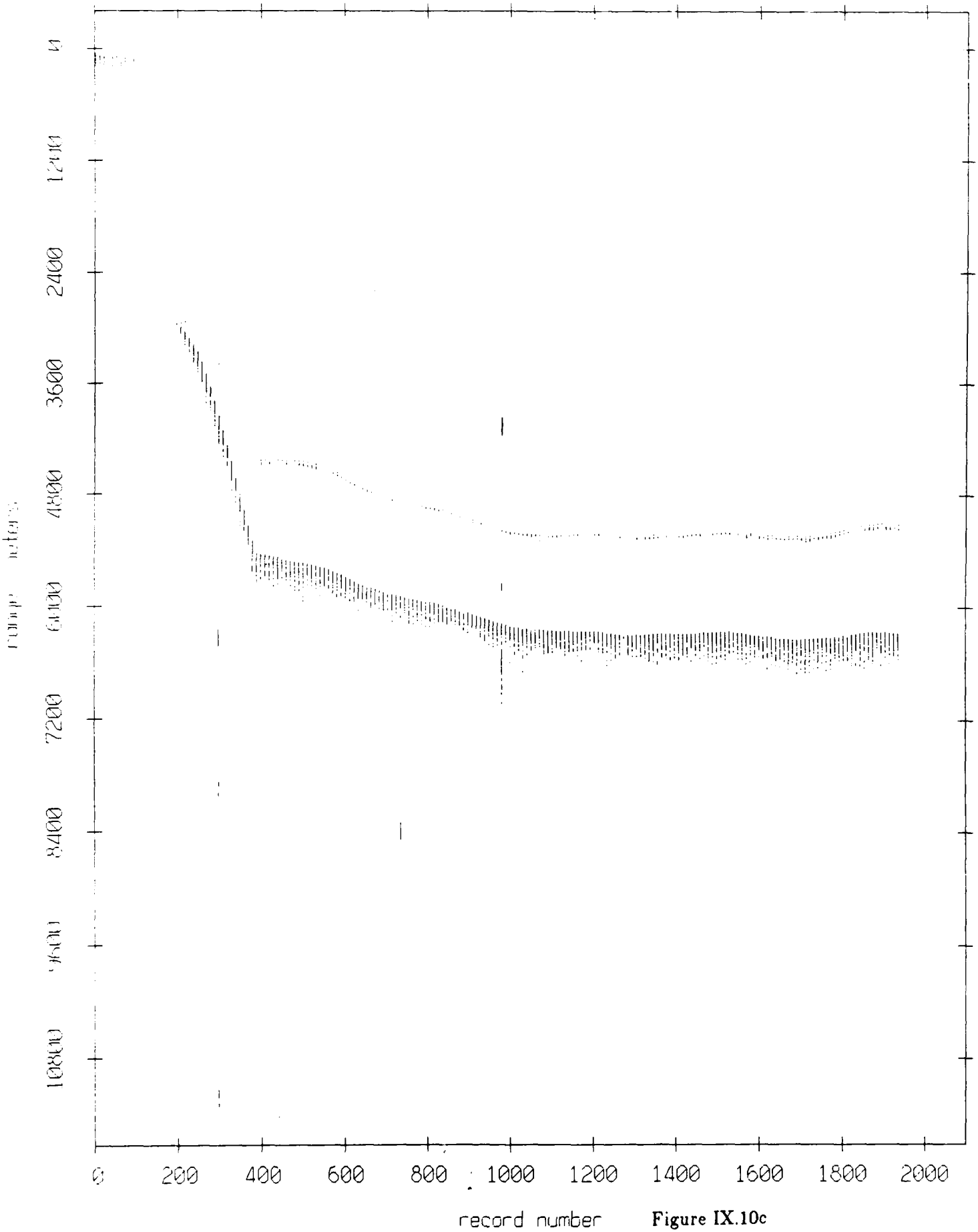


Figure IX.10c

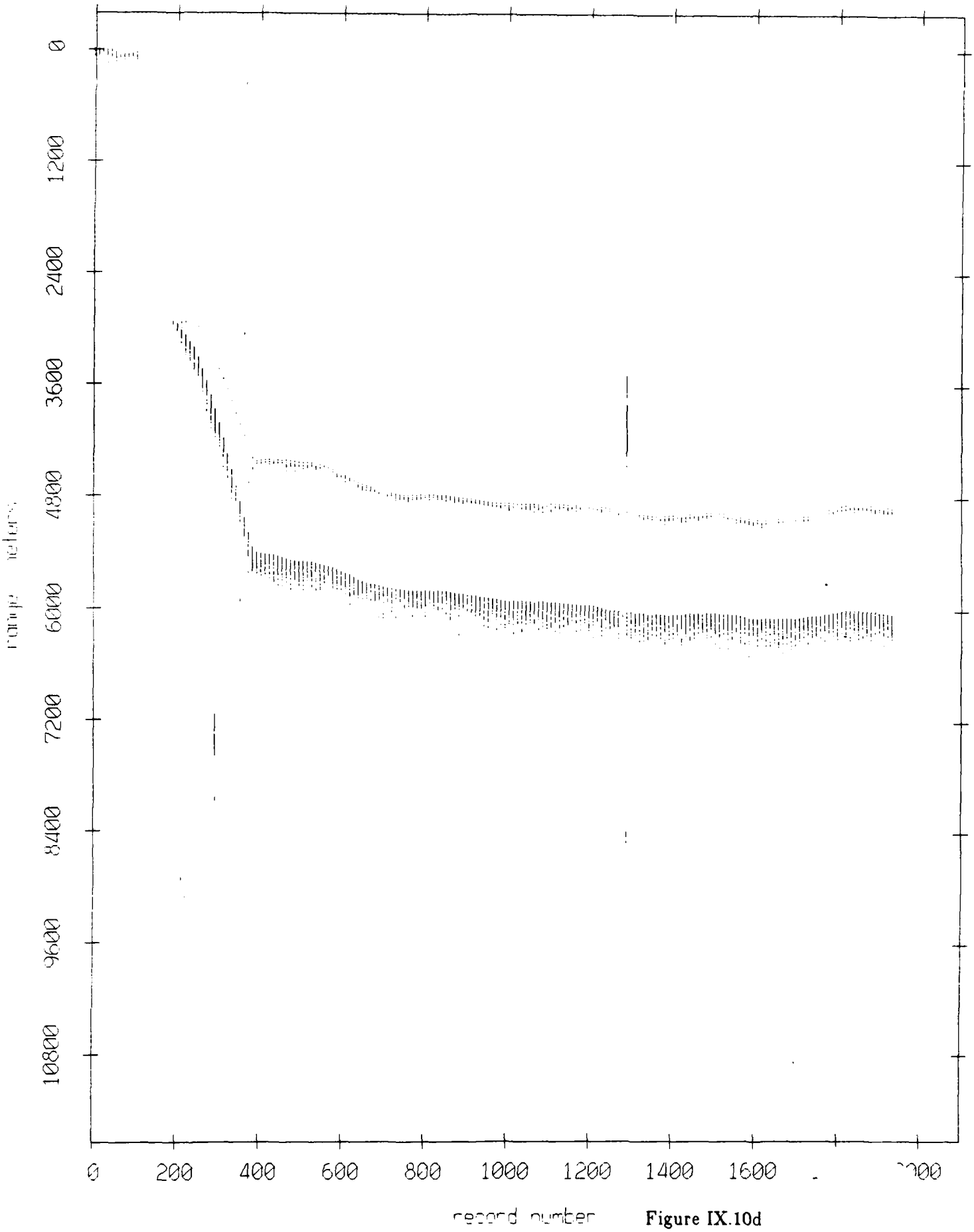


Figure IX.10d

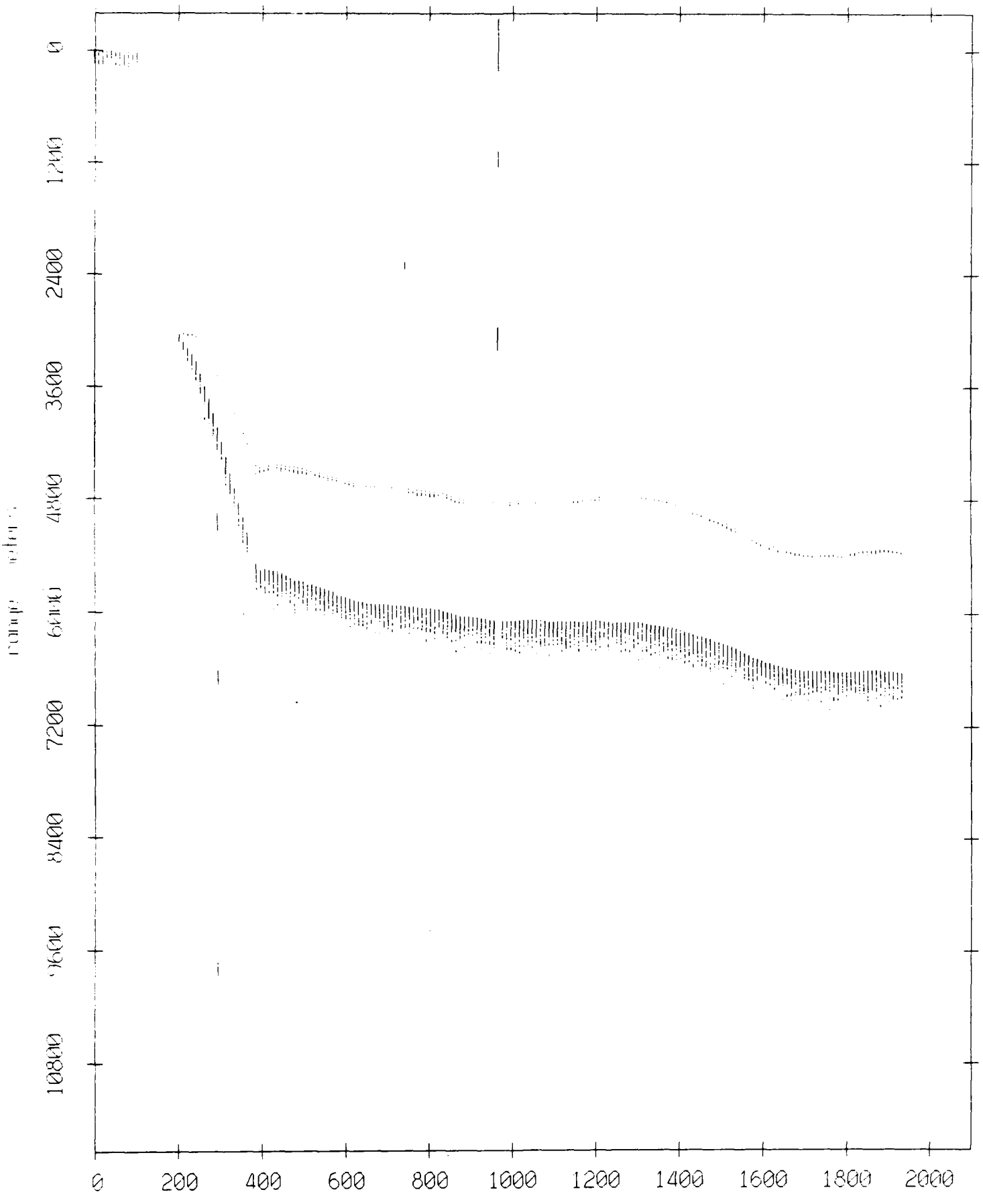


Figure IX.10e

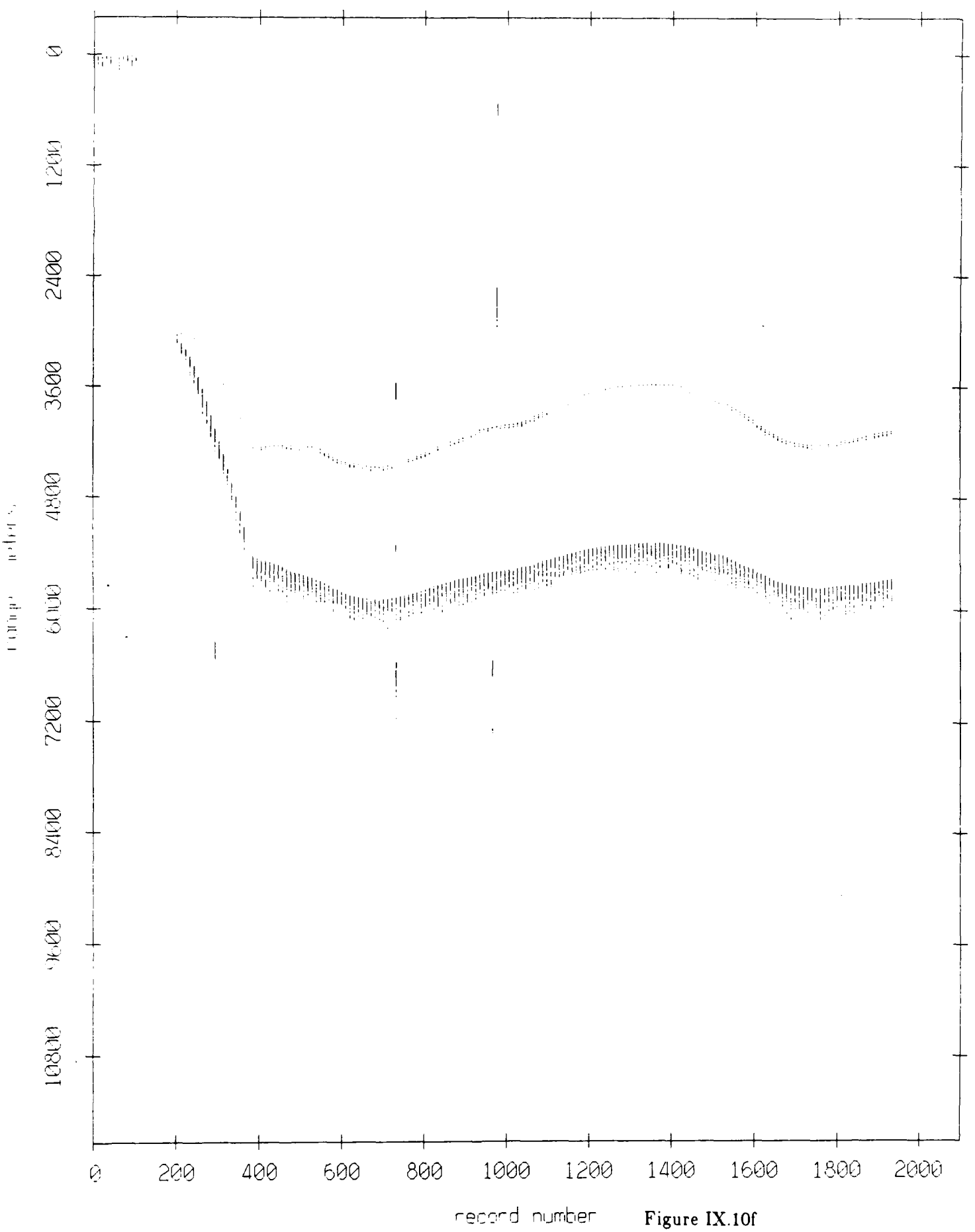


Figure IX.10f

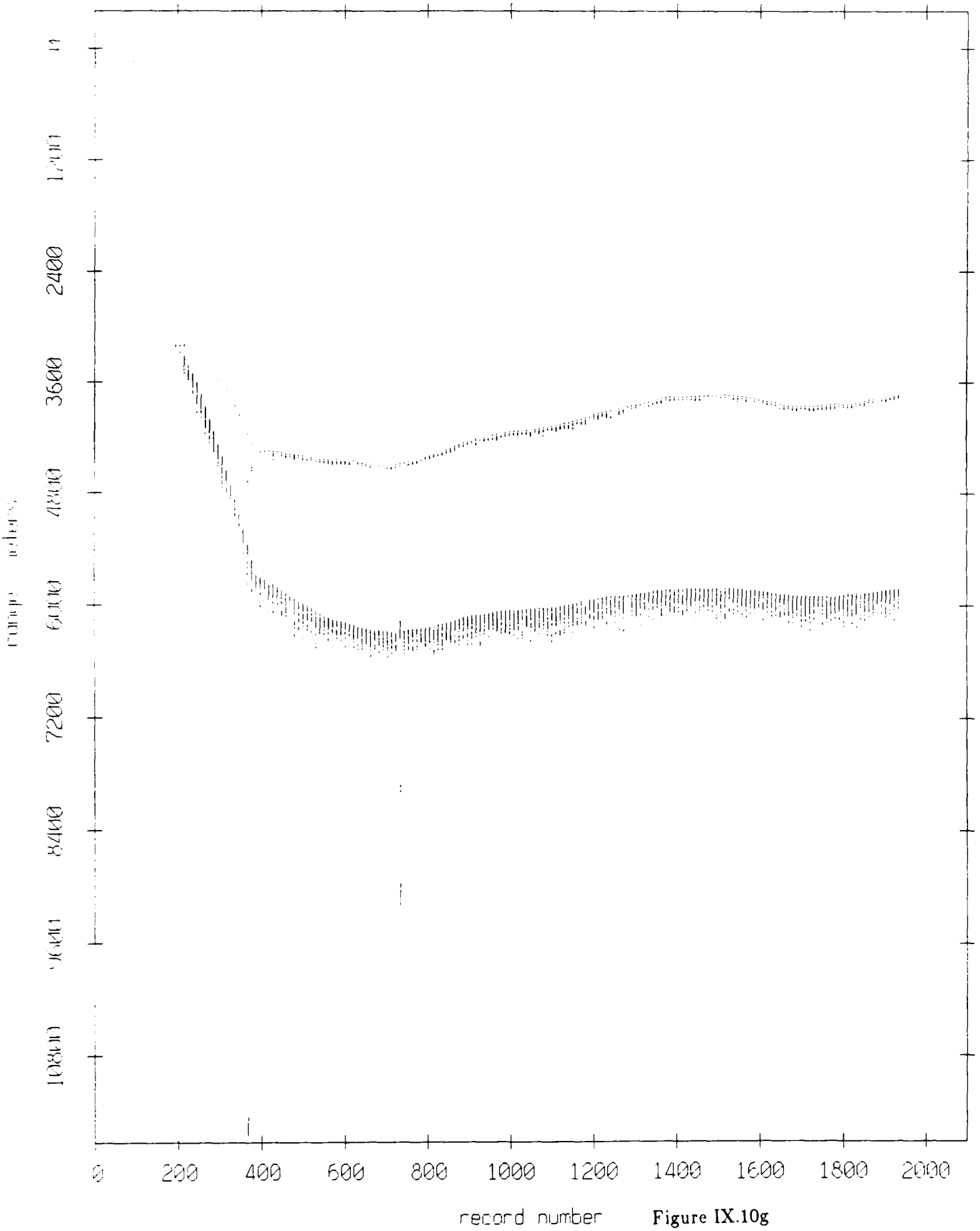


Figure IX.10g

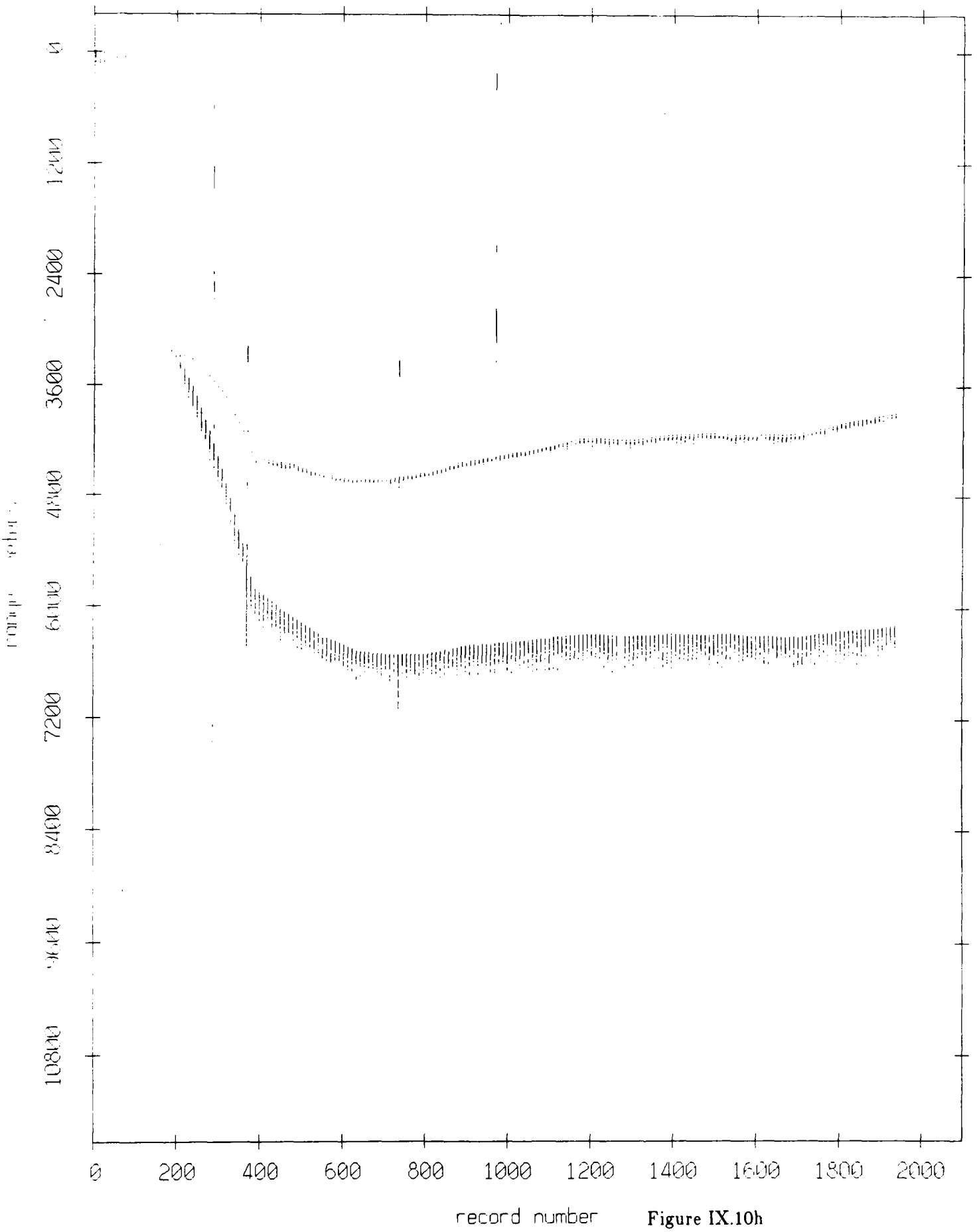


Figure IX.10h

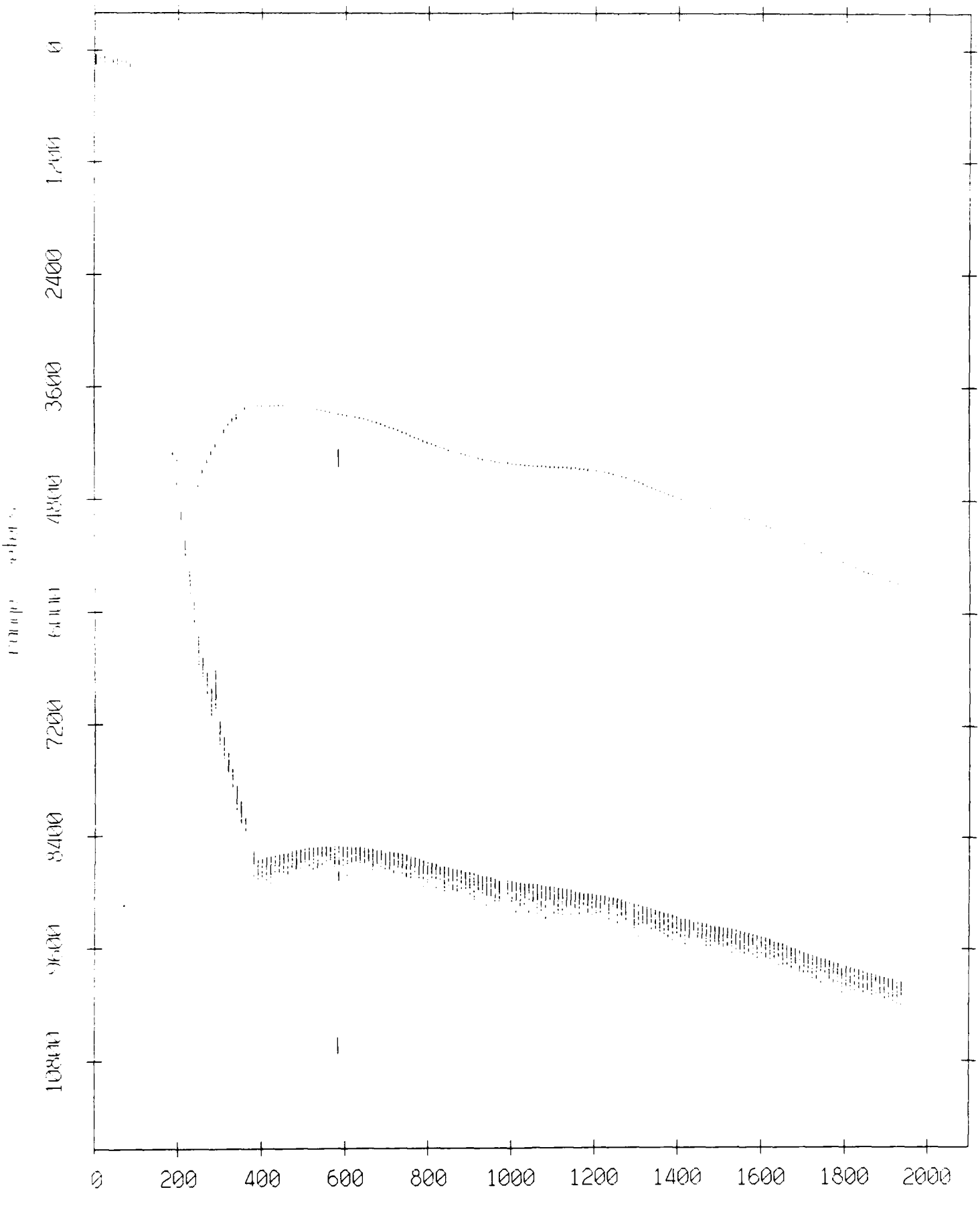


Figure IX.10i

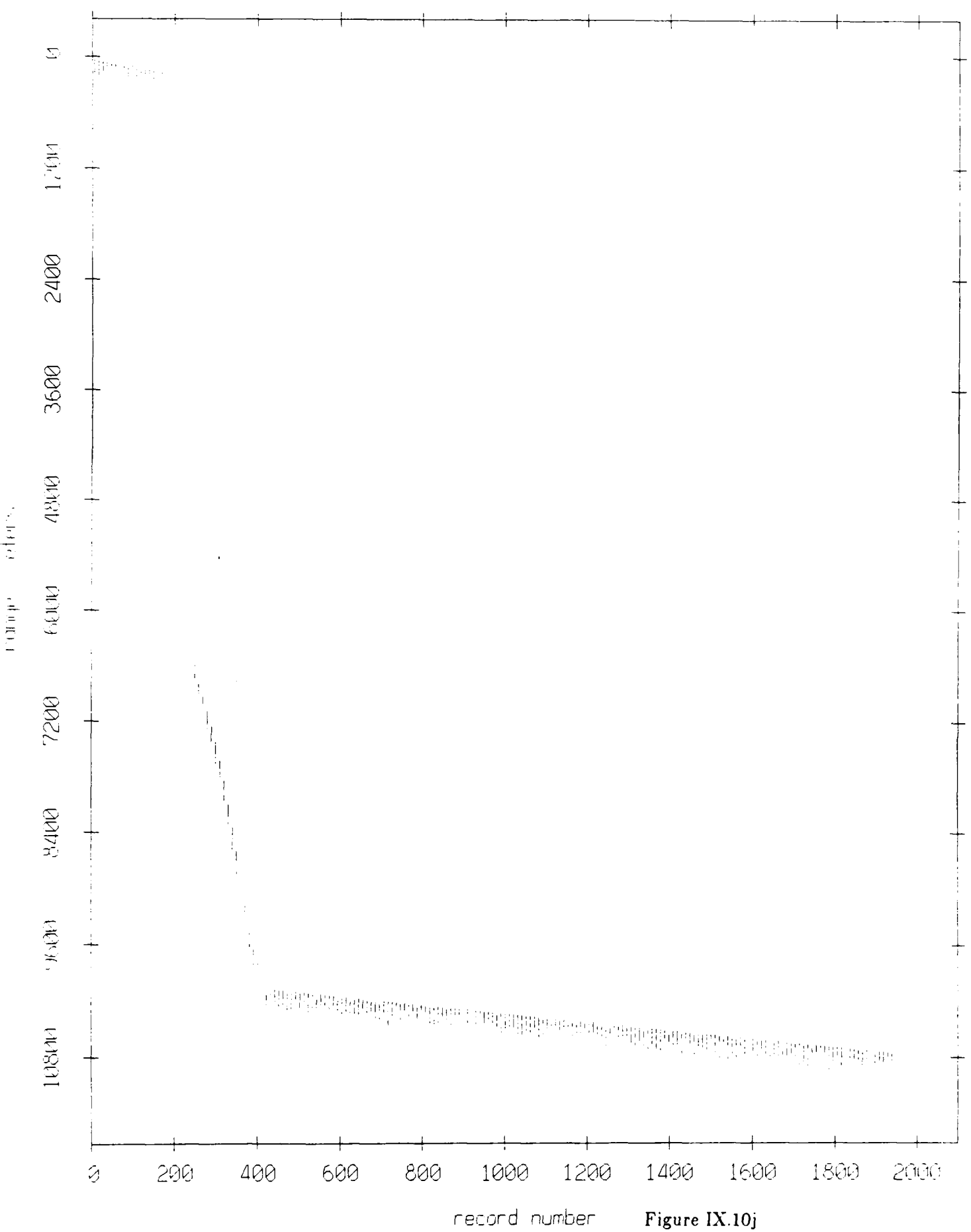


Figure IX.10j

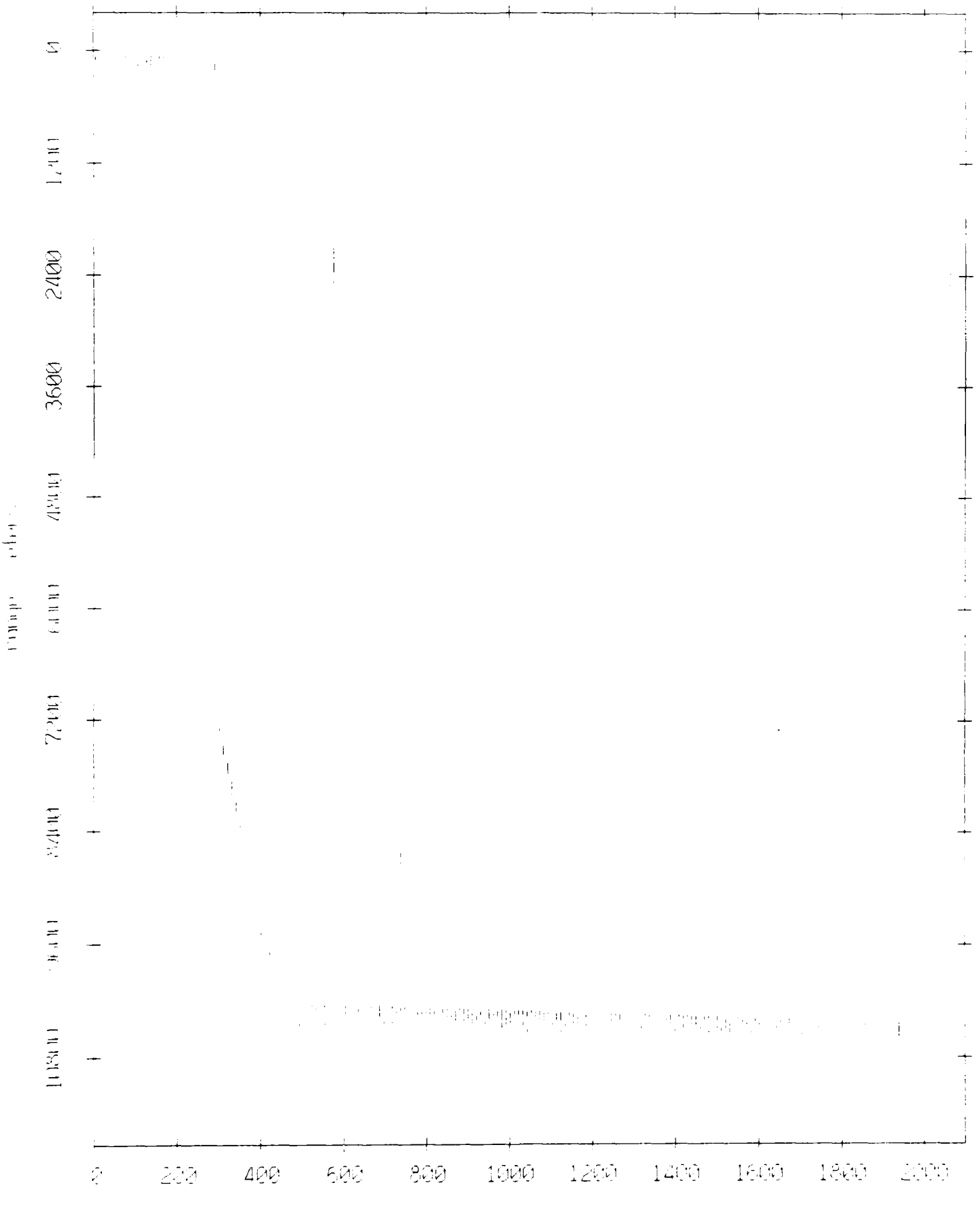


Figure IX.10k

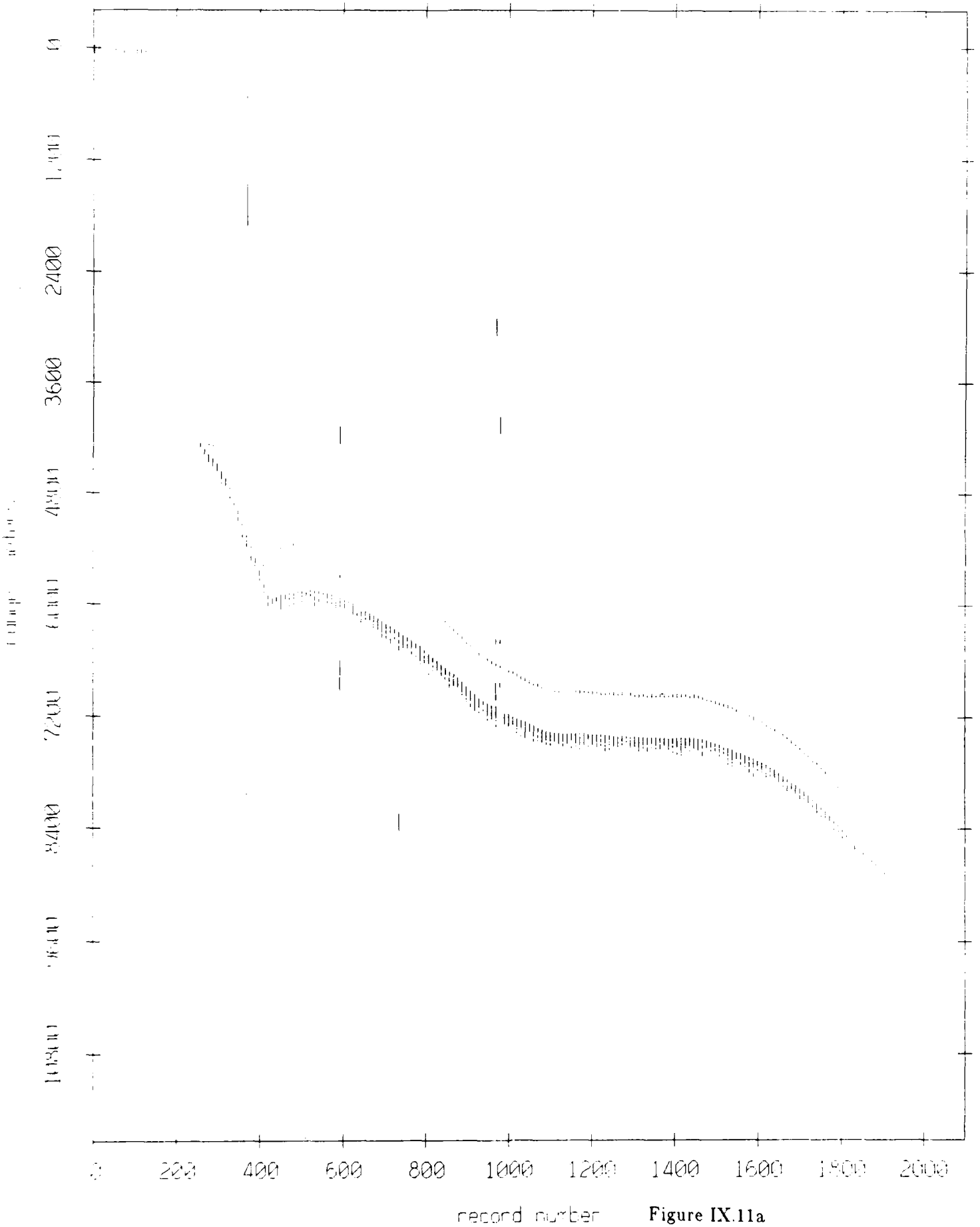


Figure IX.11a

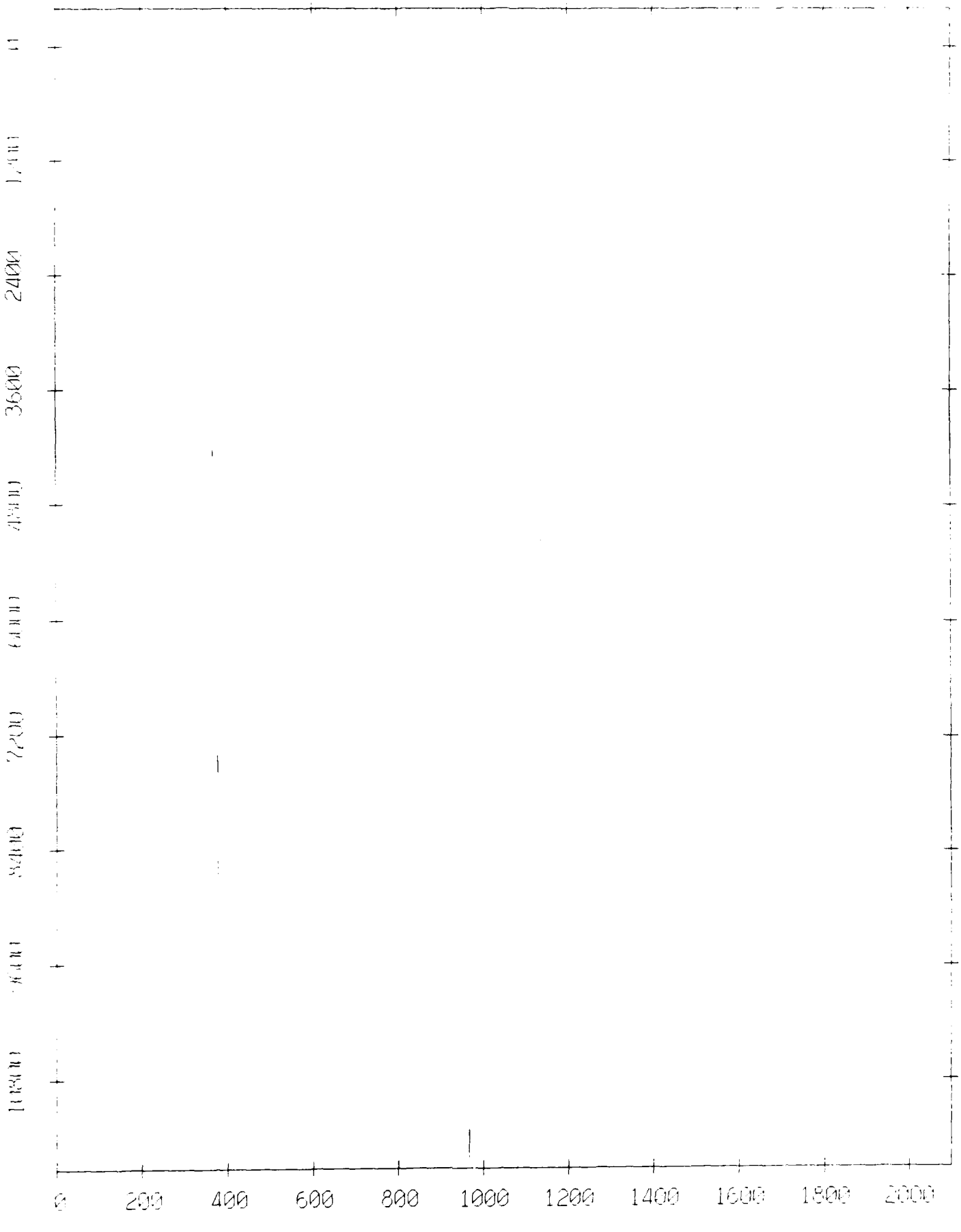


Figure IX.11b

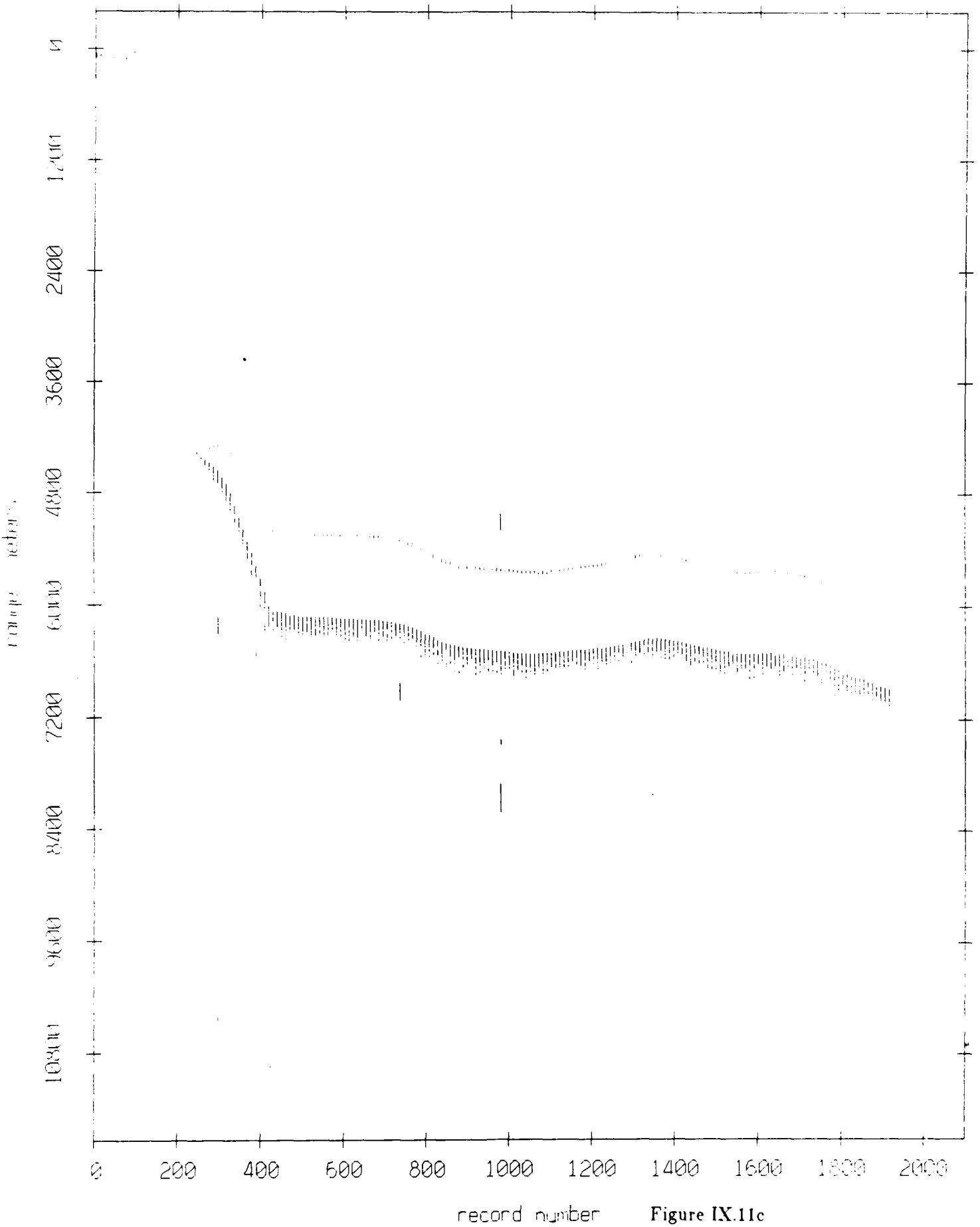


Figure IX.11c

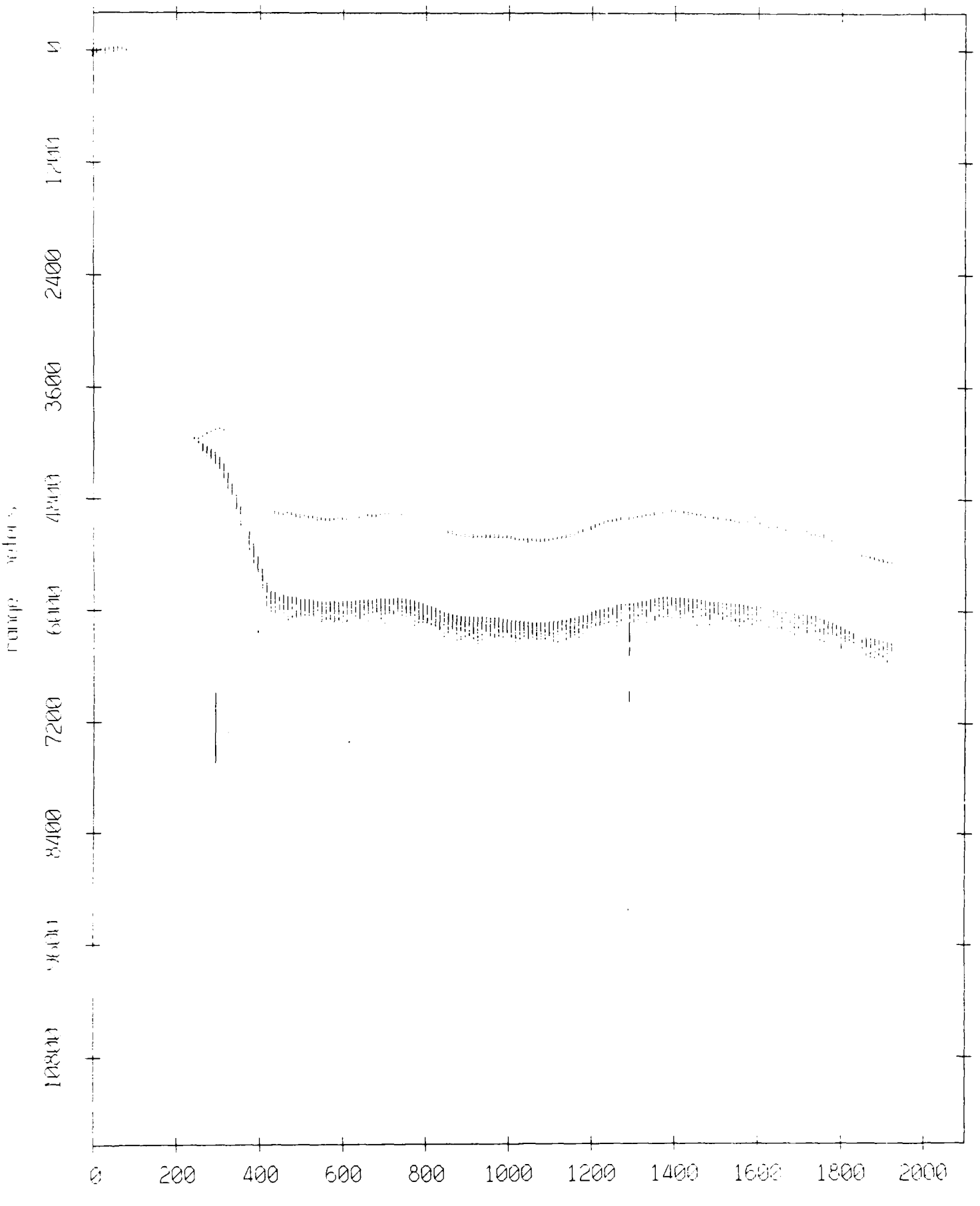


Figure IX.11d

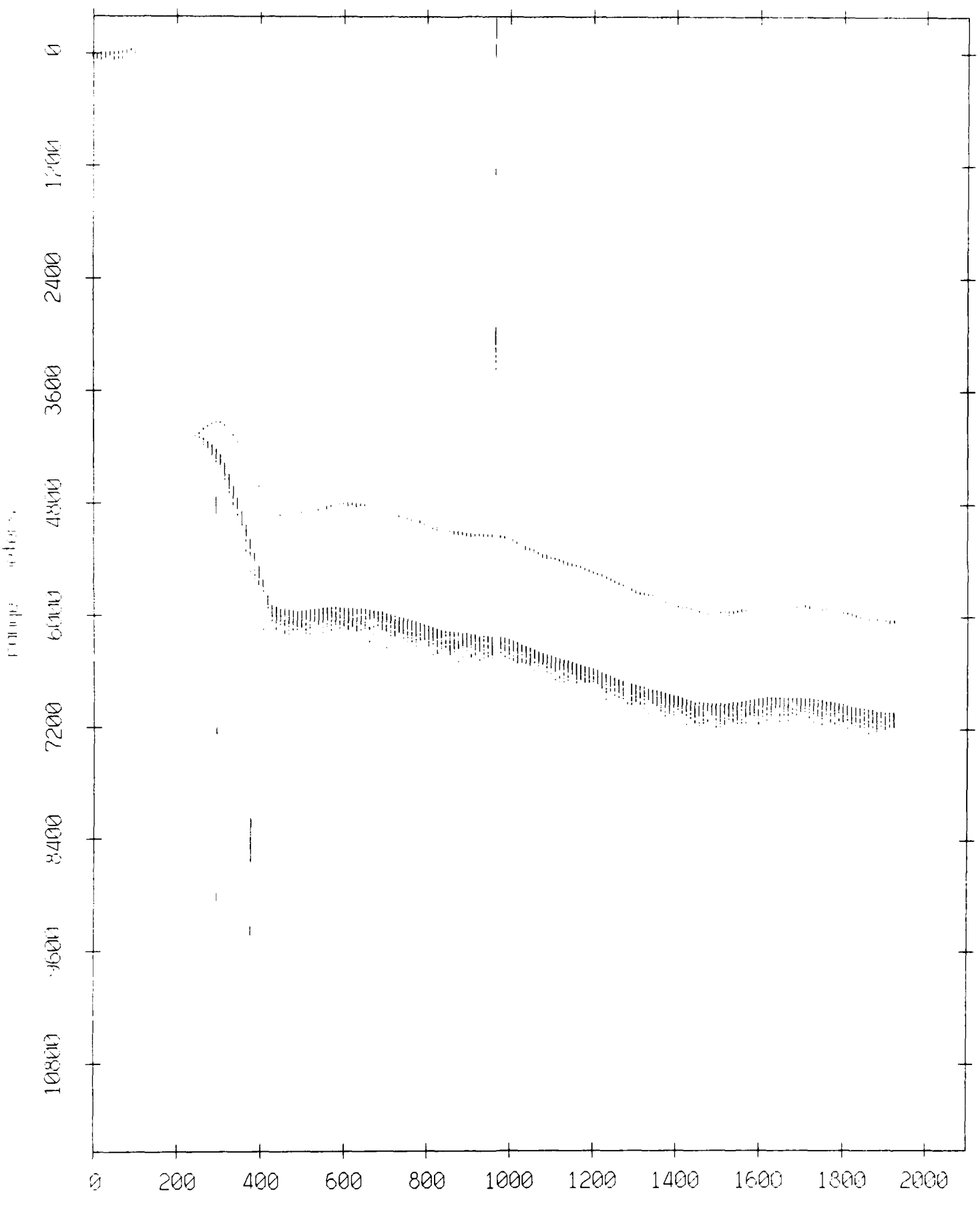


Figure IX.11e

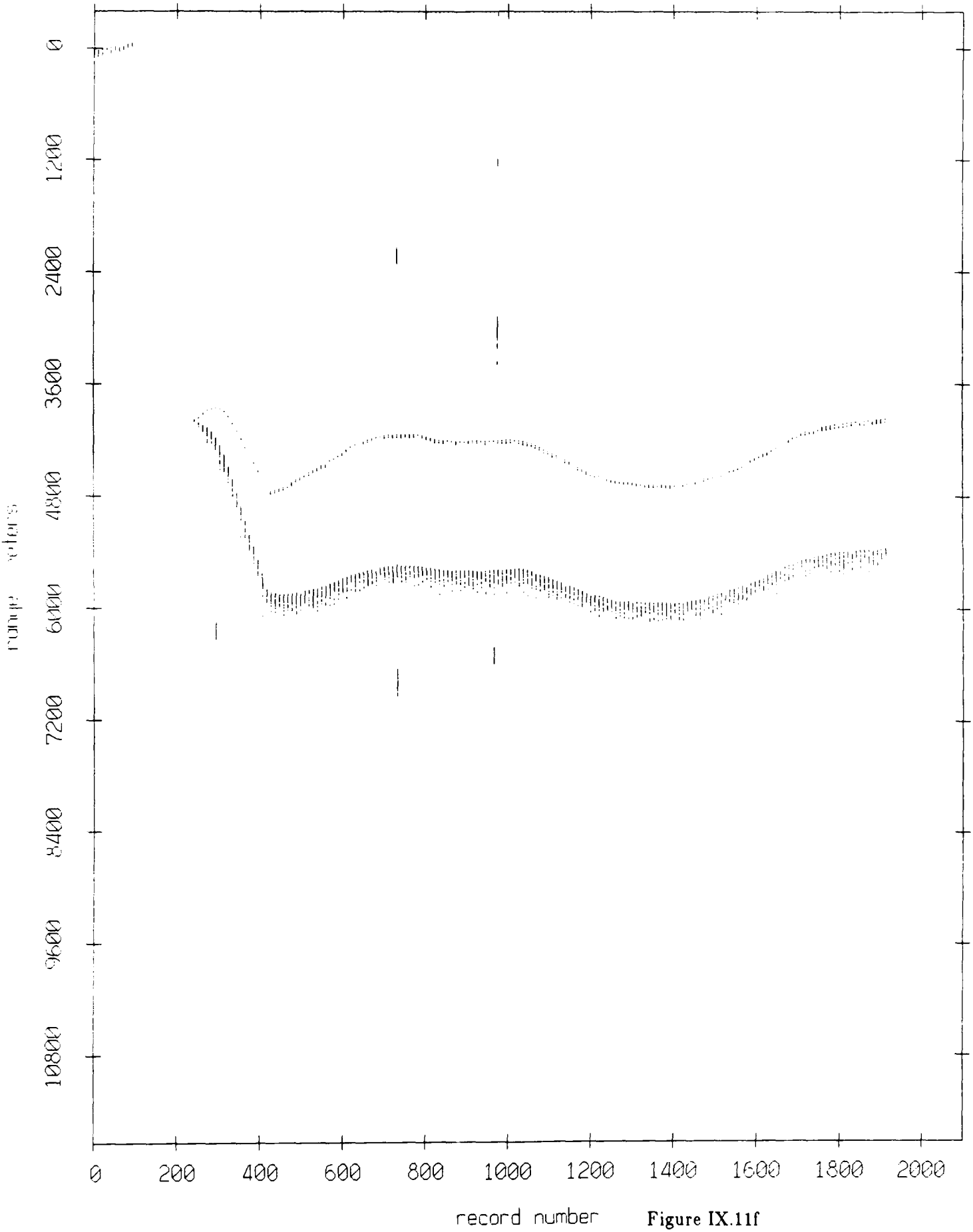


Figure IX.11f

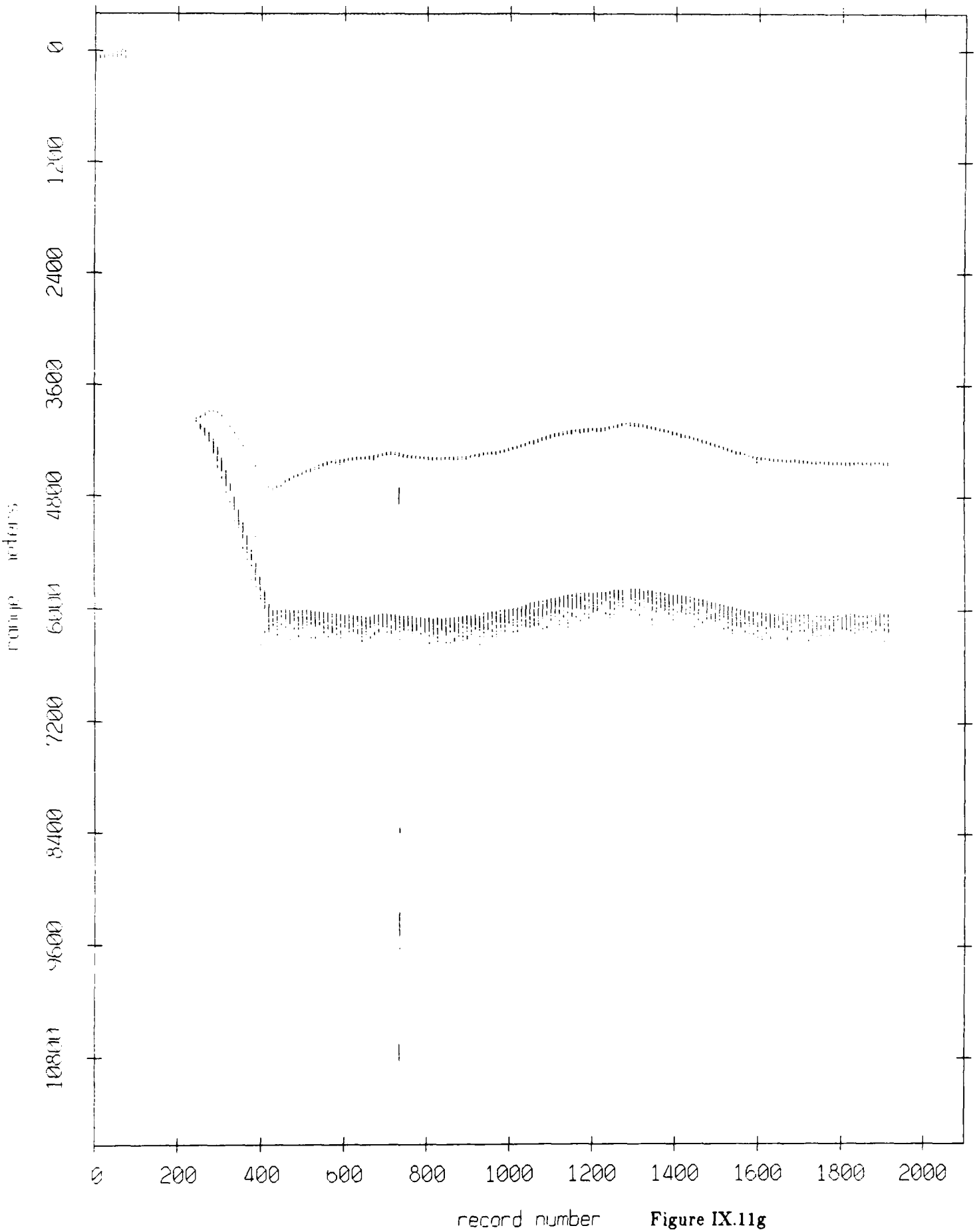


Figure IX.11g

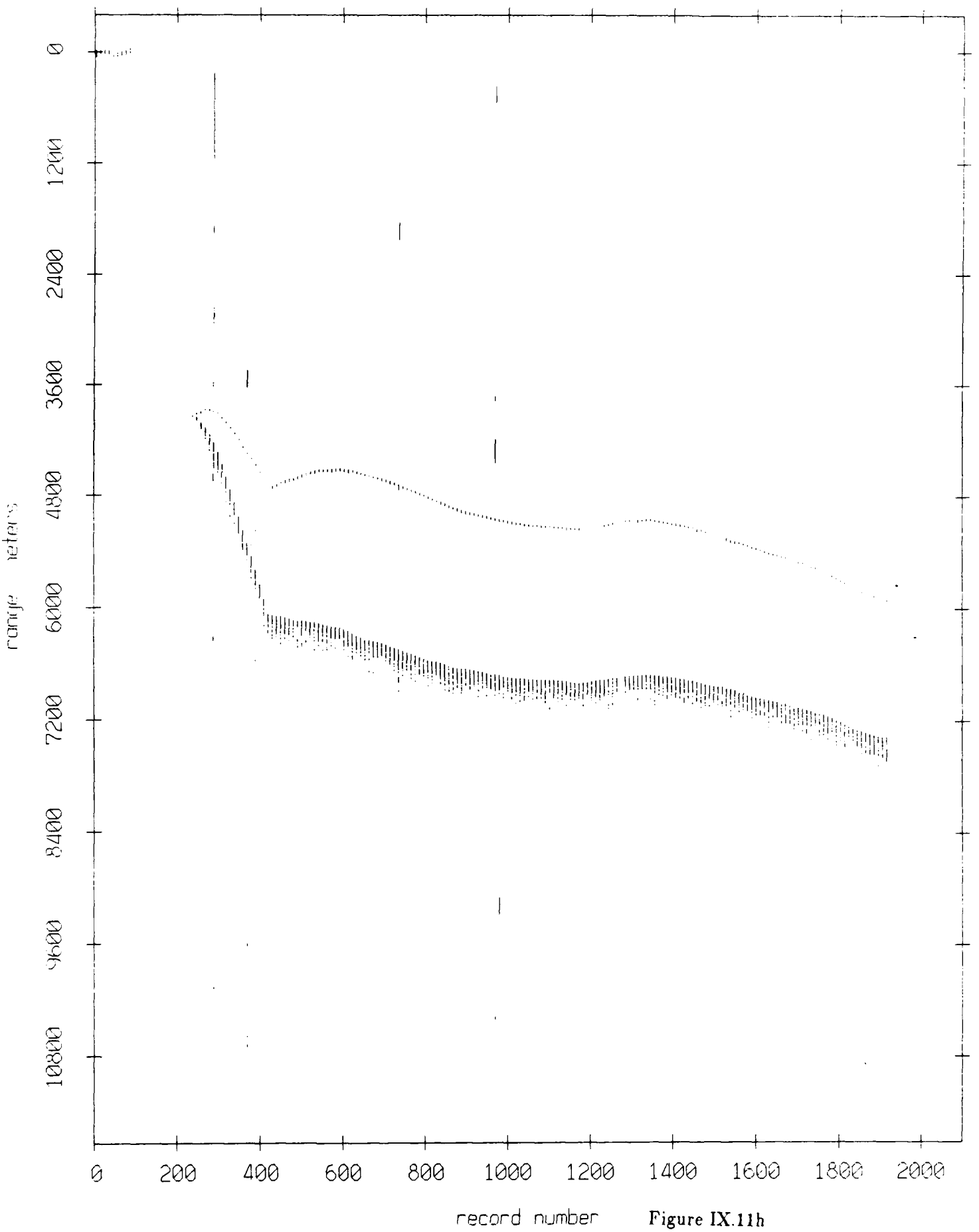


Figure IX.11h

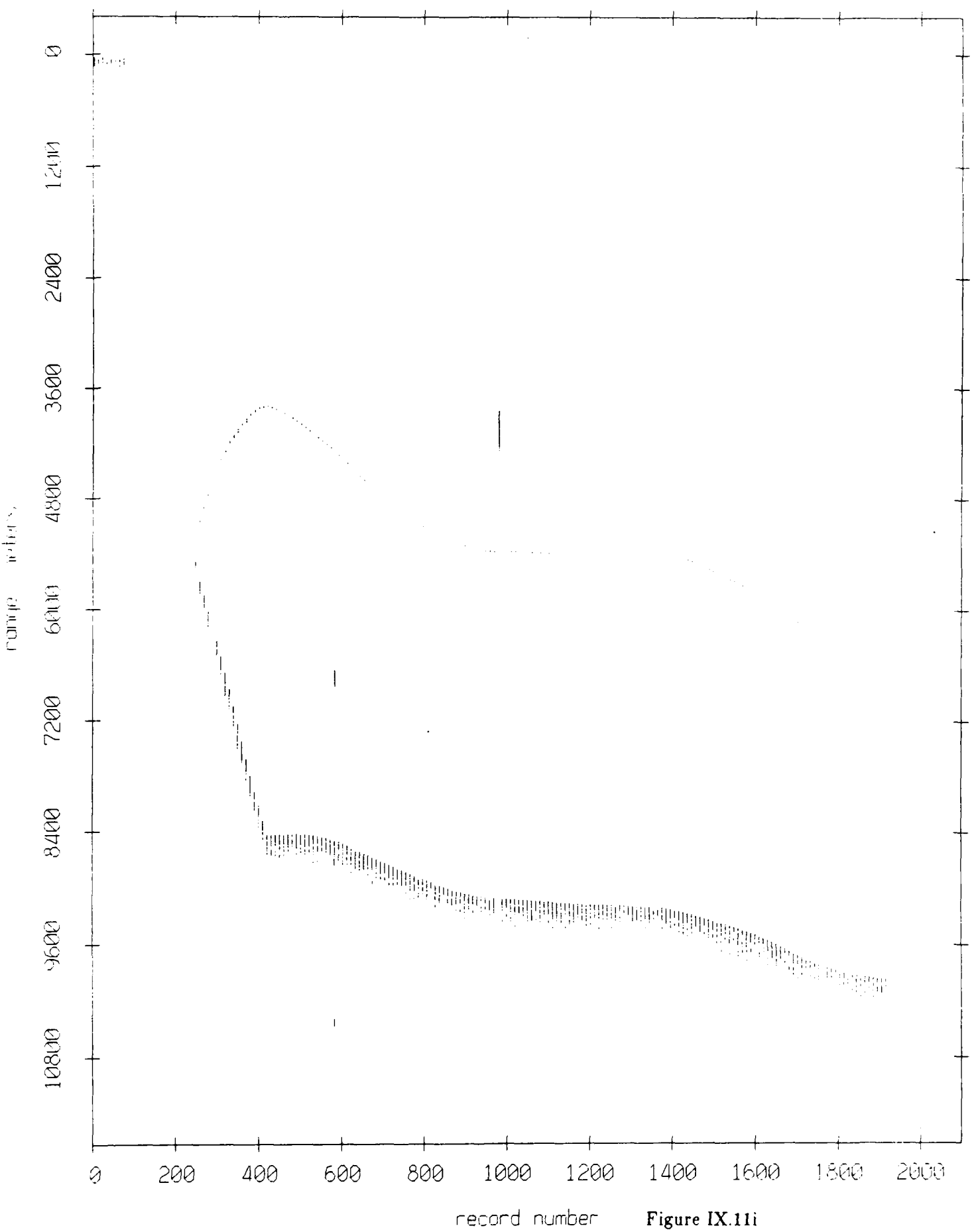


Figure IX.11i

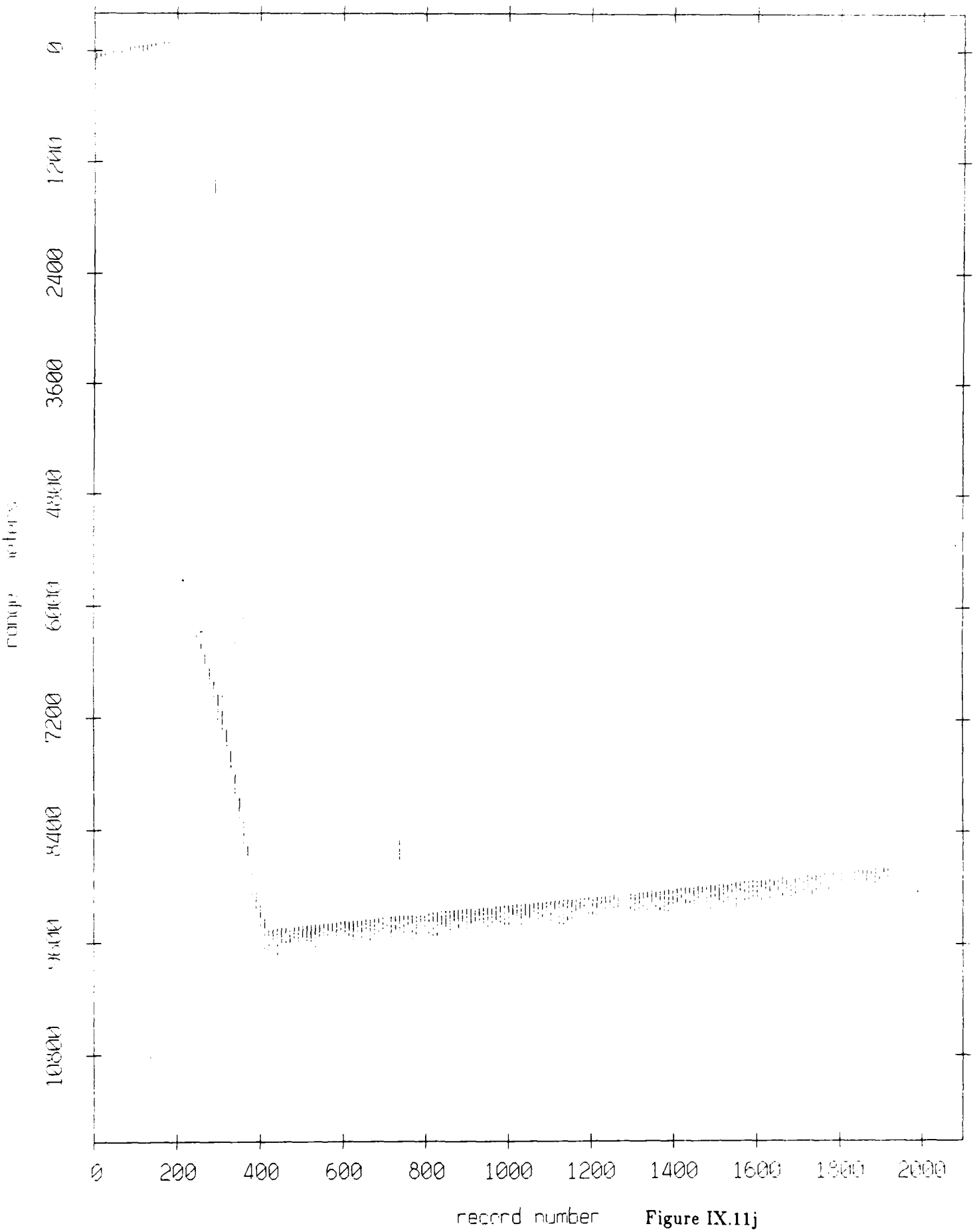


Figure IX.11j

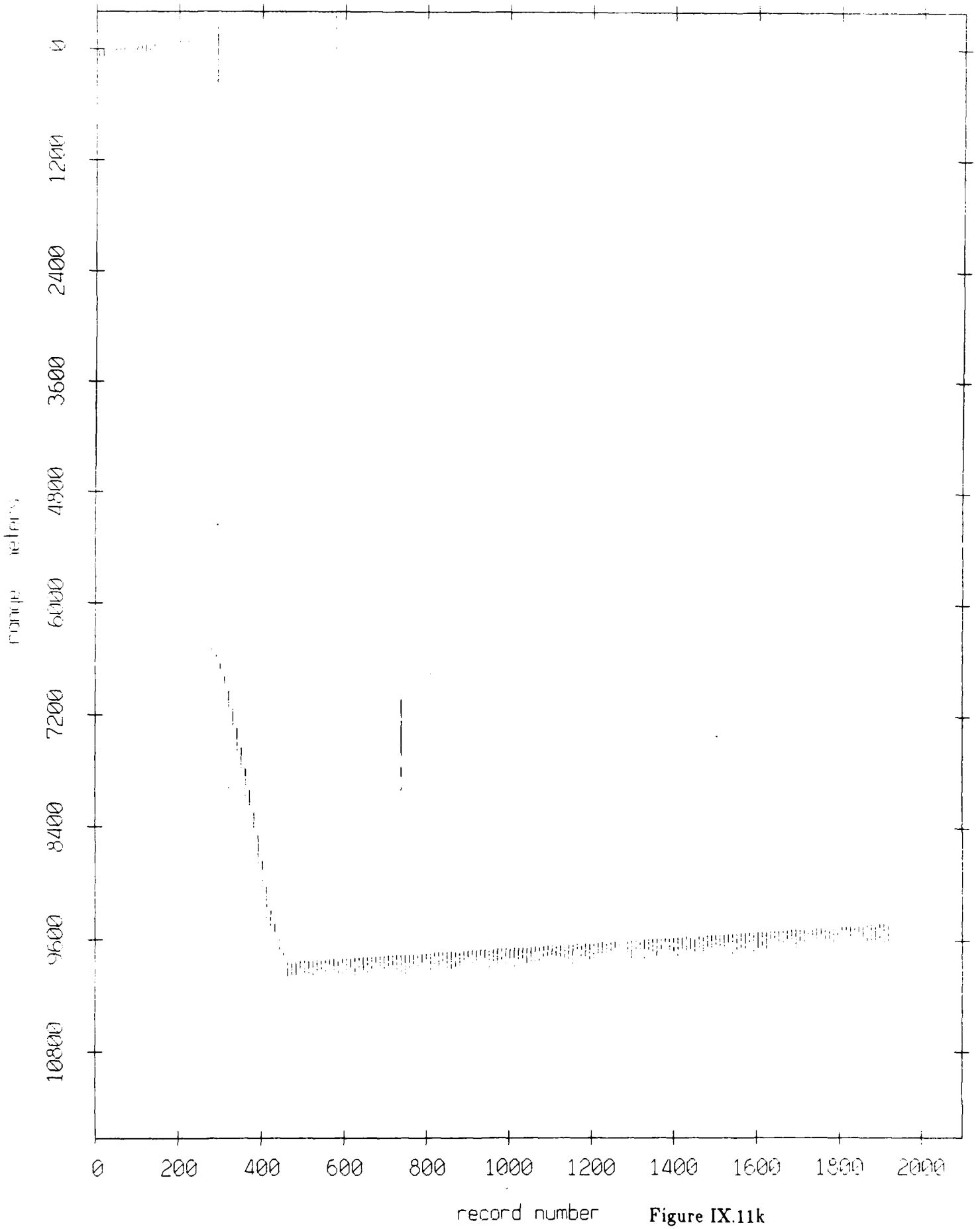


Figure IX.11k

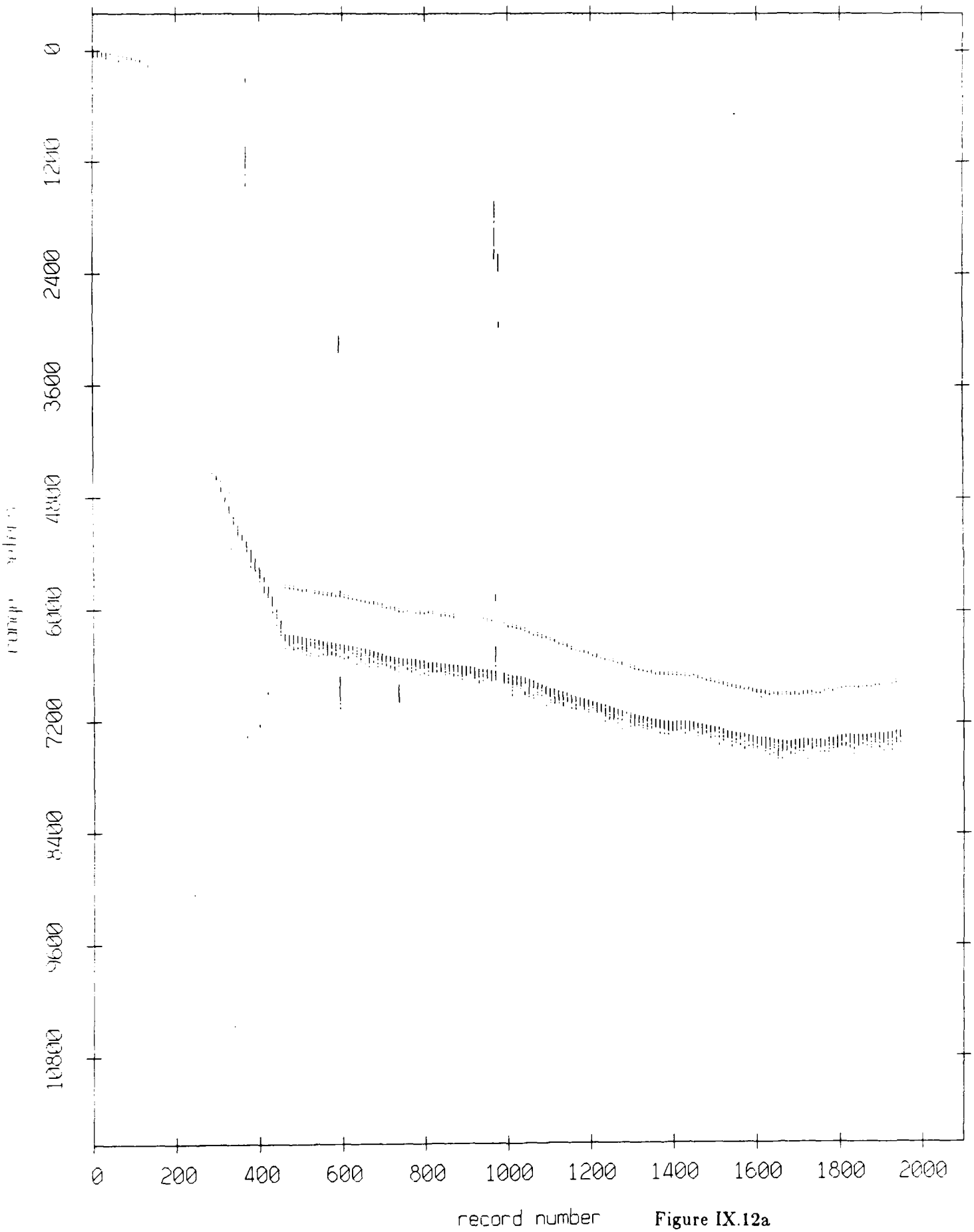


Figure IX.12a

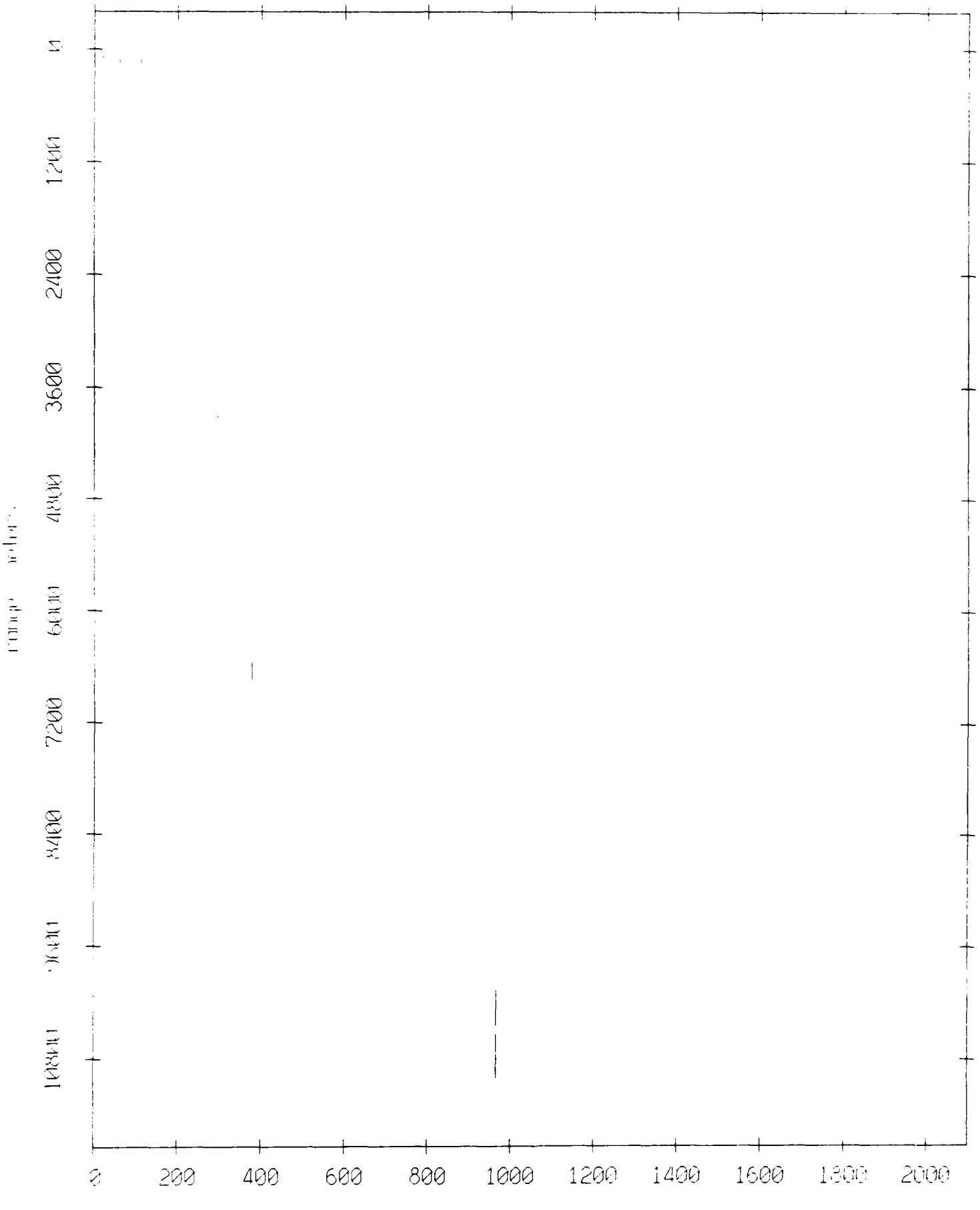


Figure IX.12b

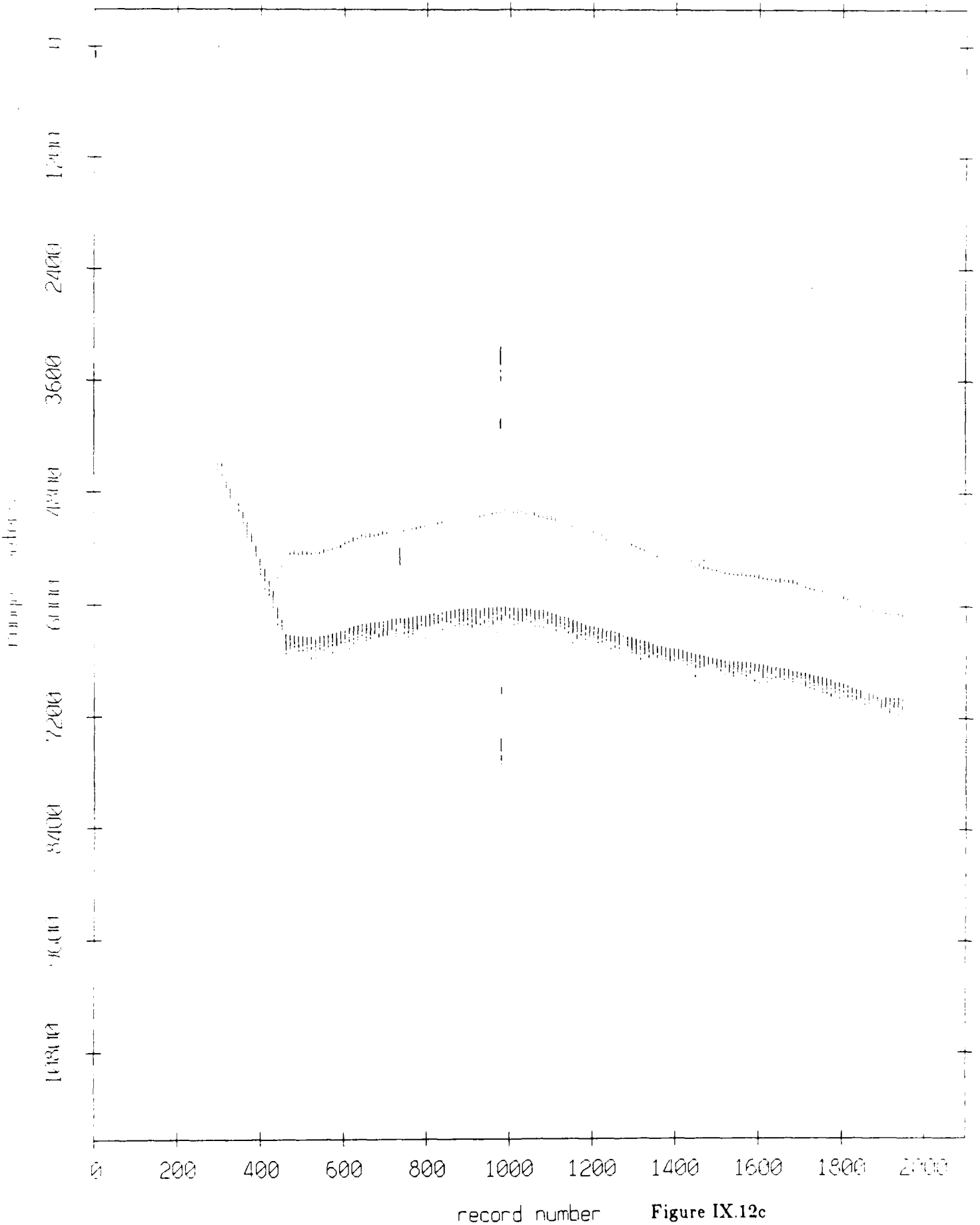


Figure IX.12c

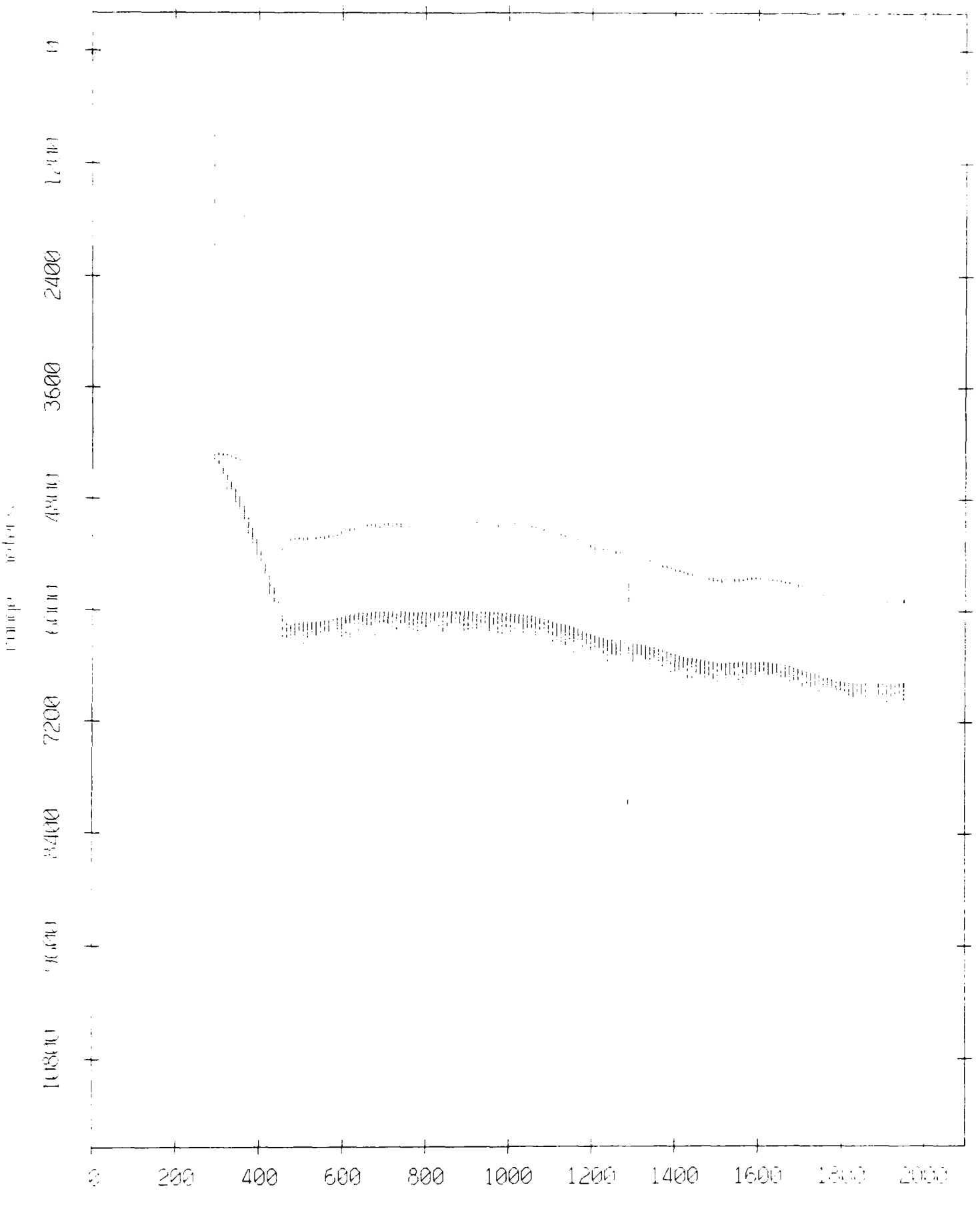


Figure IX.12d

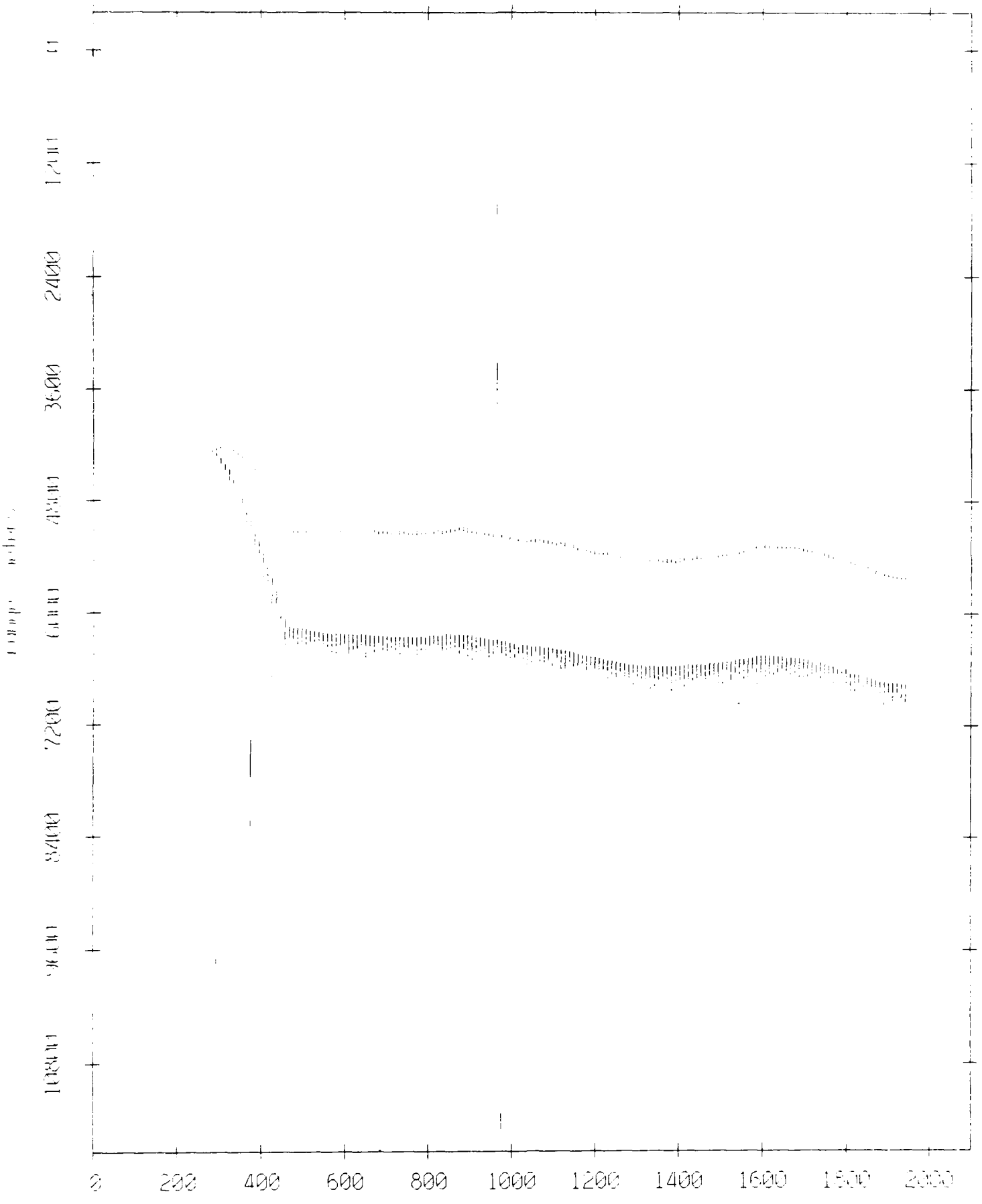


Figure IX.12e

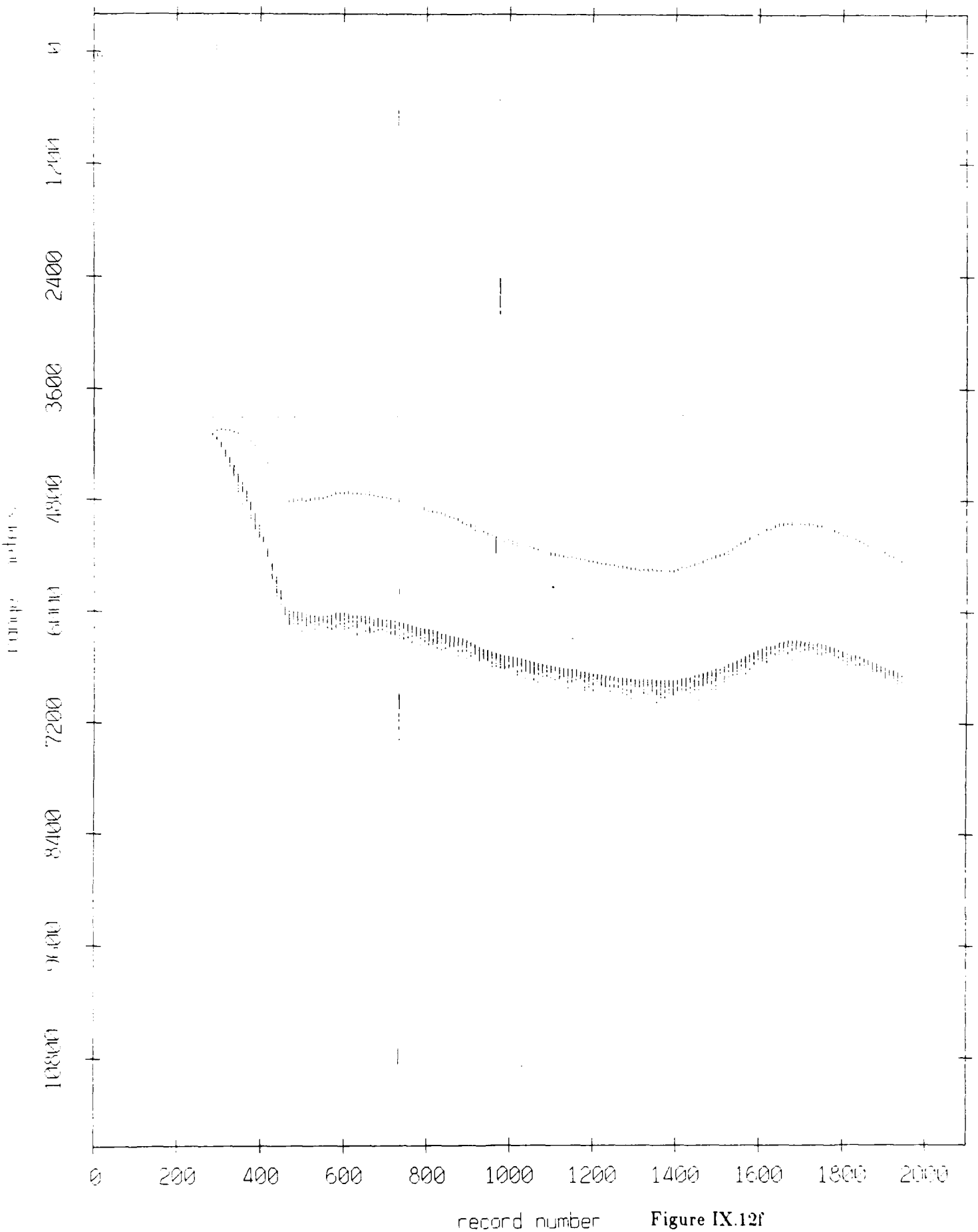


Figure IX.12f

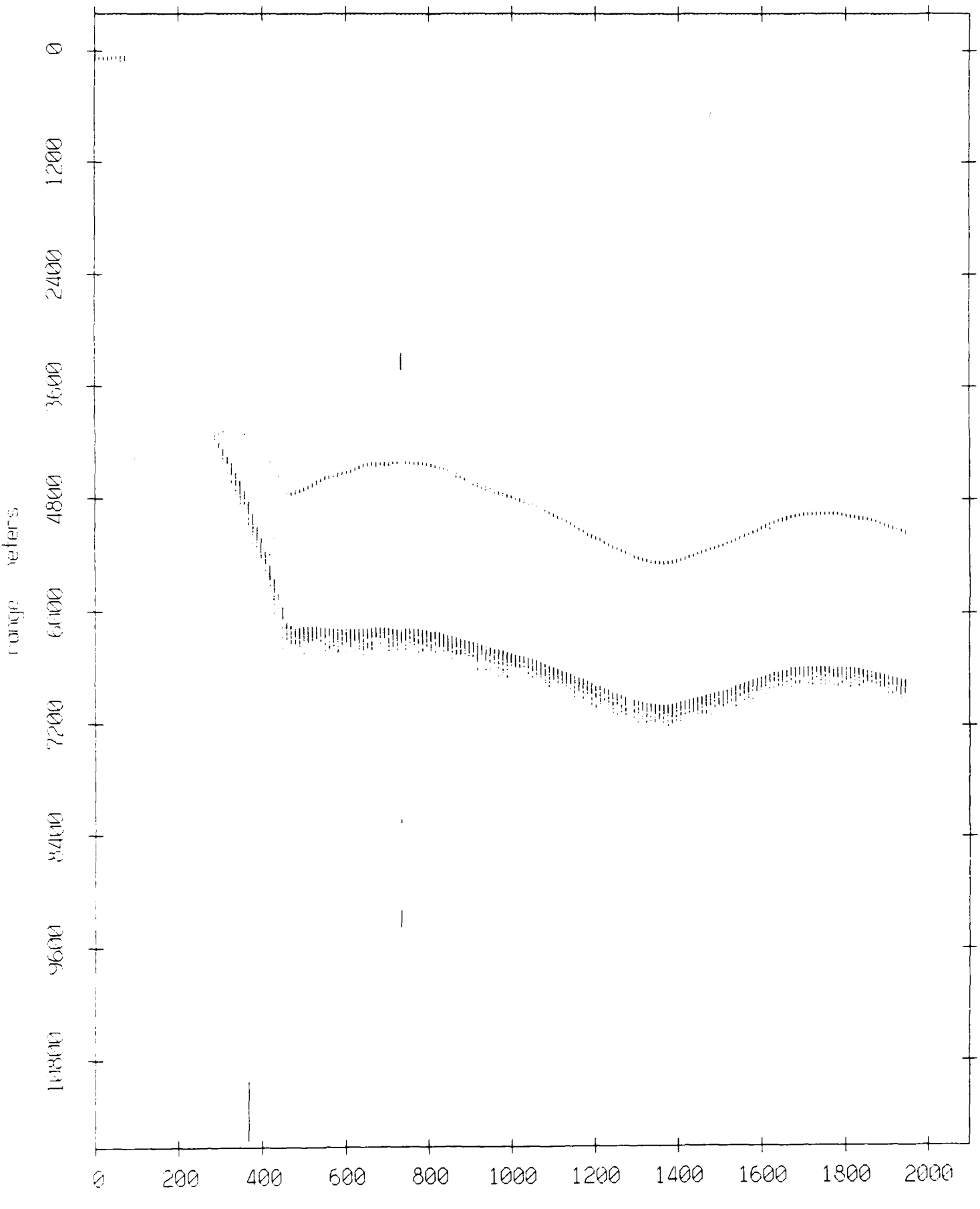


Figure IX.12g

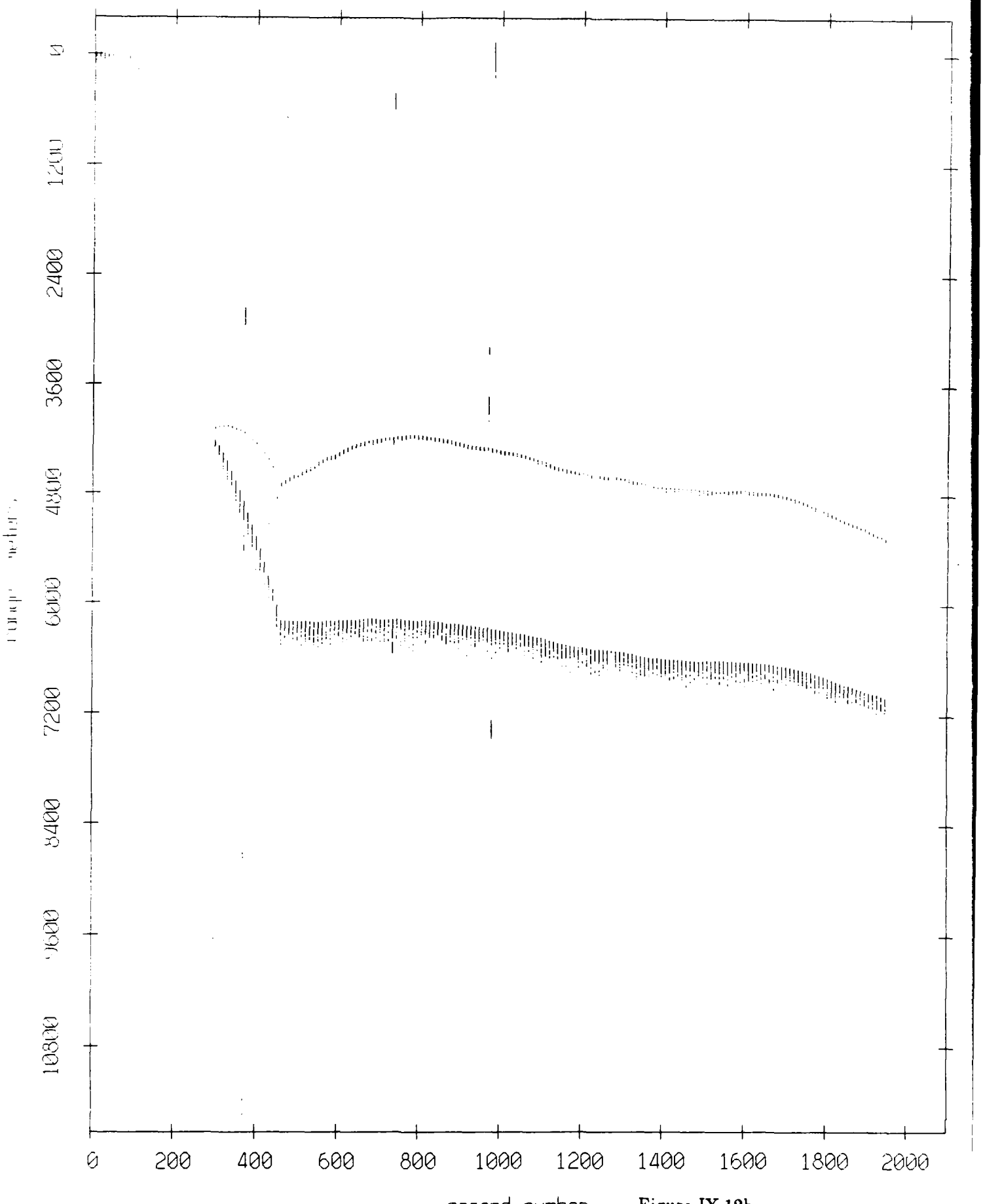


Figure IX.12h

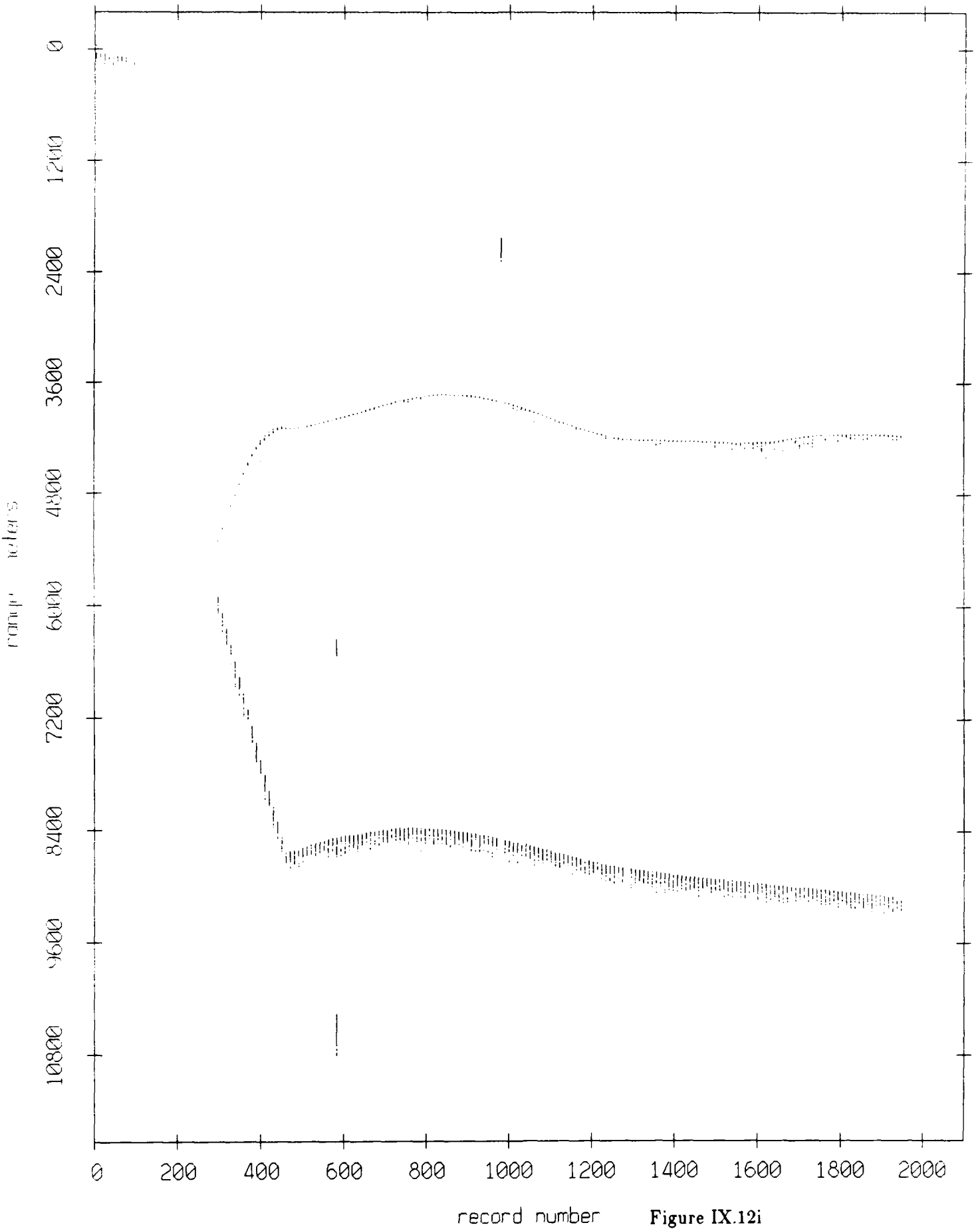


Figure IX.12i

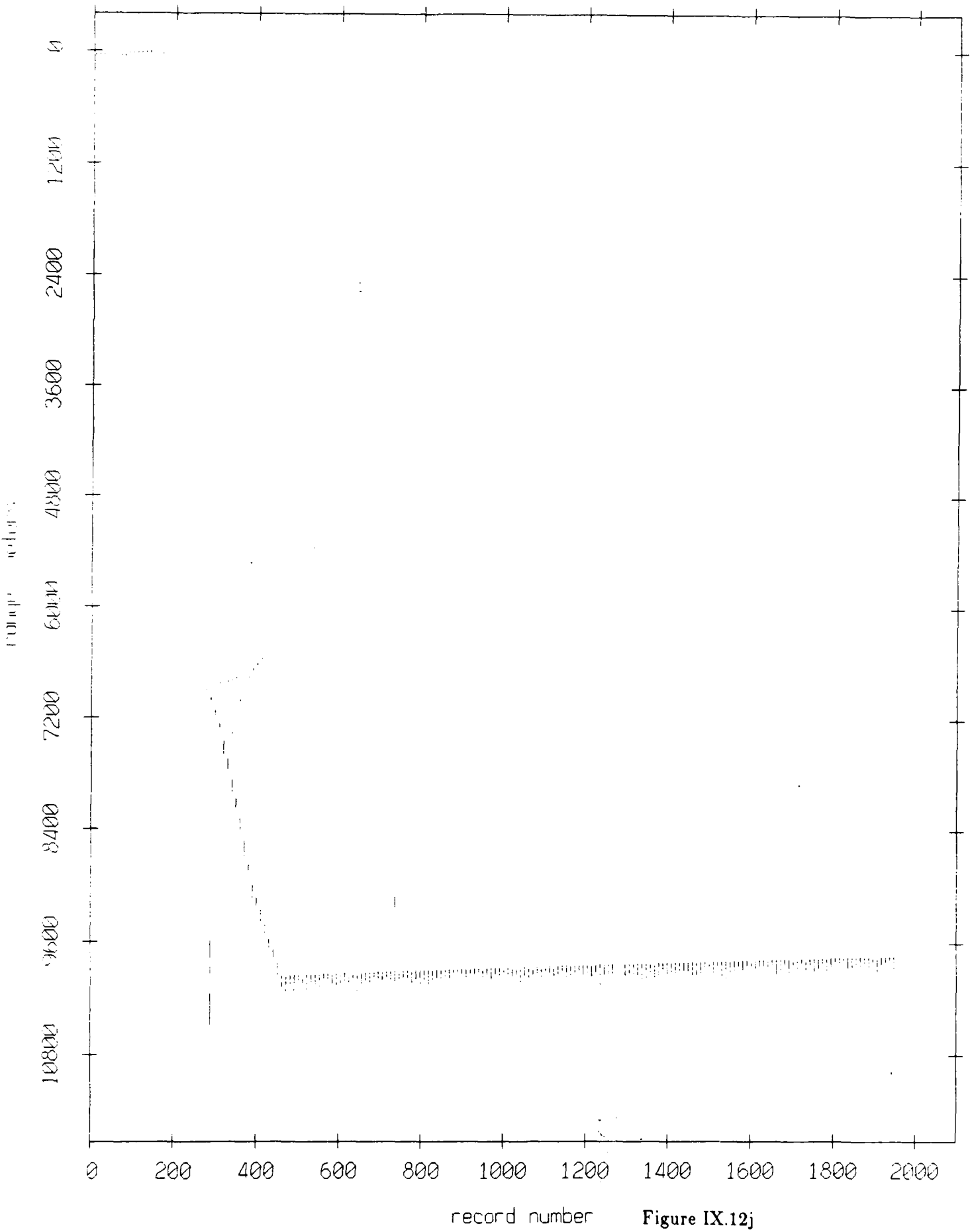


Figure IX.12j

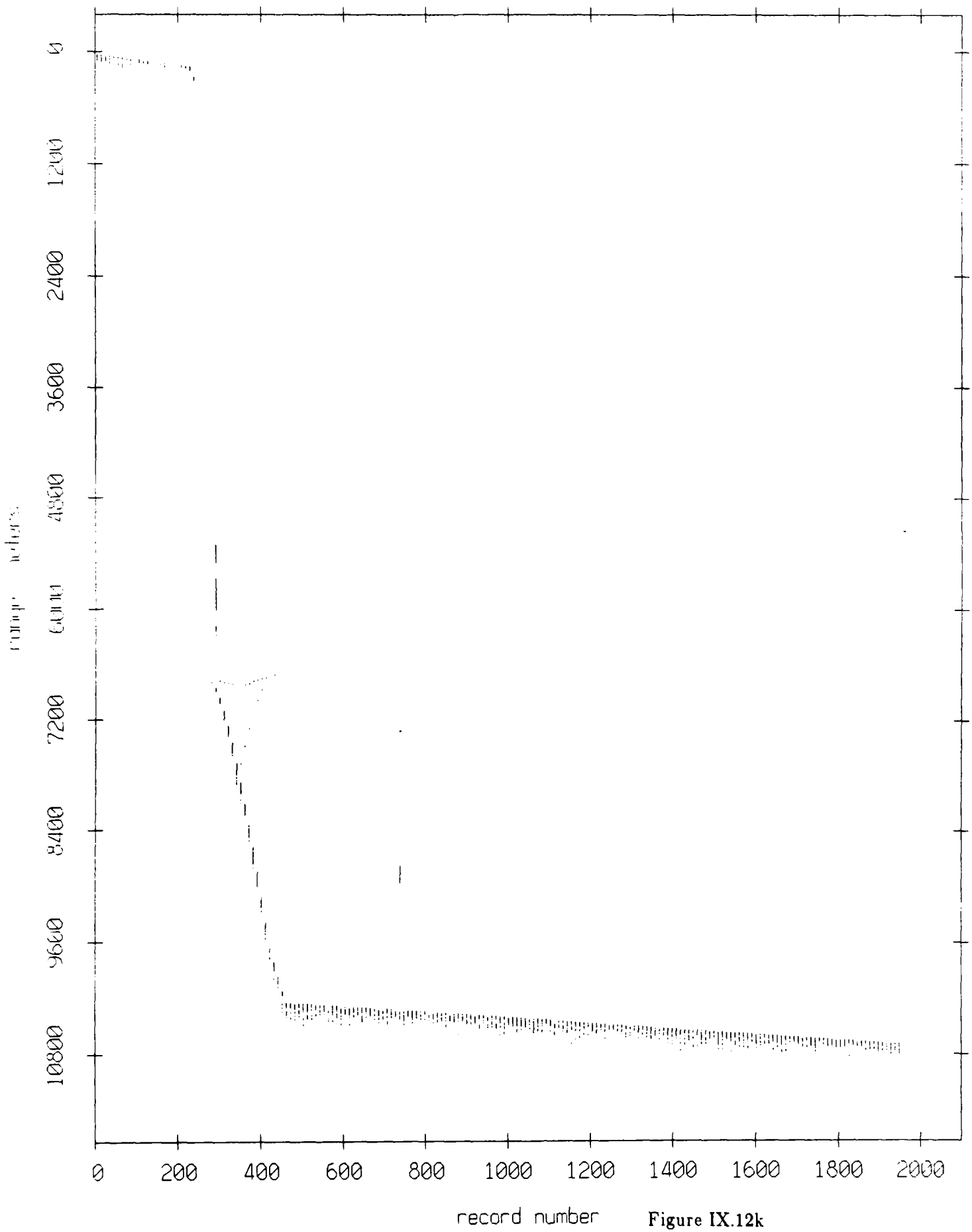


Figure IX.12k

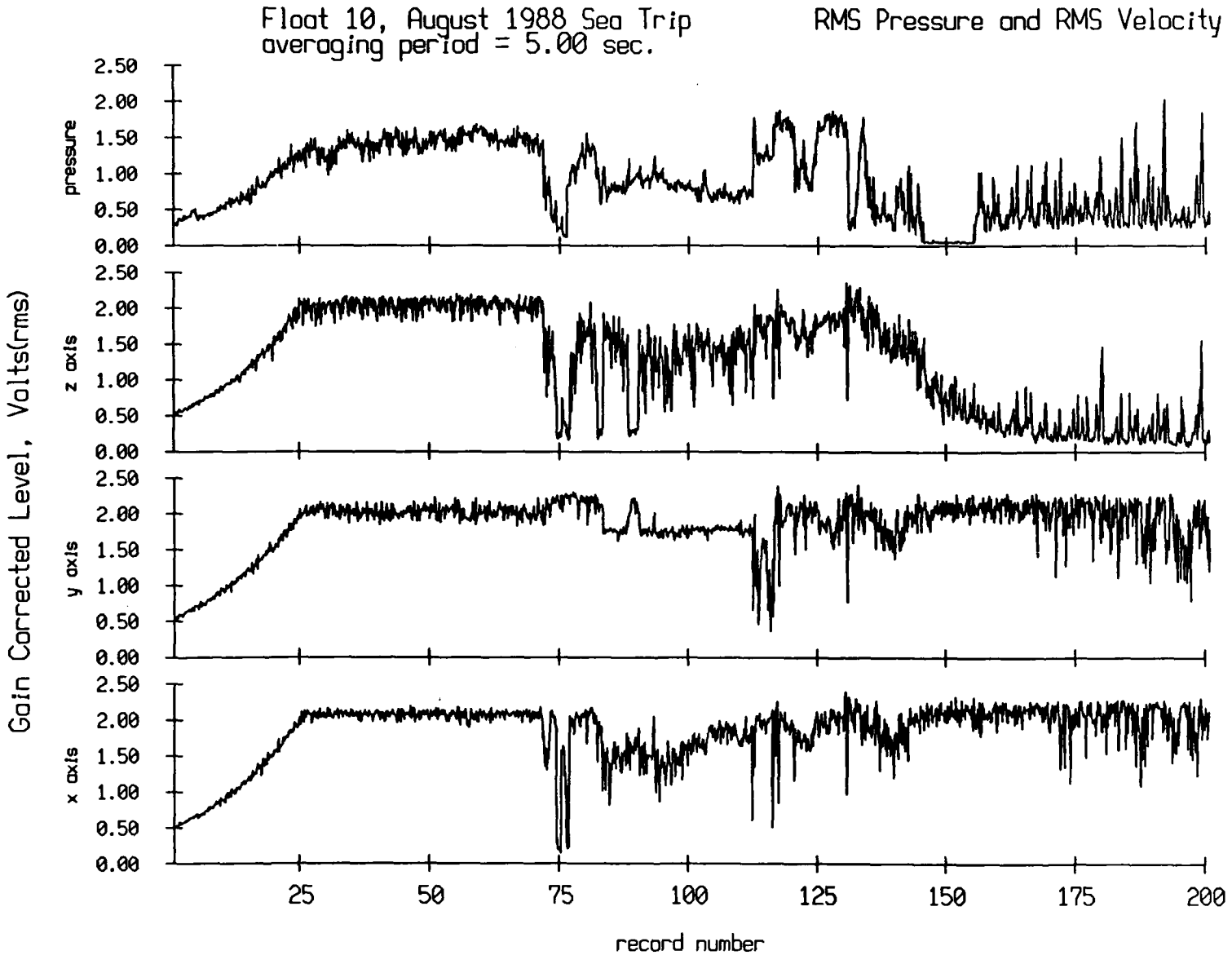

Float 10, August 1988 Sea Trip
averaging period = 5.00 sec.
RMS Pressure and RMS Velocity
Gain Corrected Level, Volts(rms)
pressure
z axis
y axis
x axis
2.50
2.00
1.50
1.00
0.50
0.00
25
50
75
100
125
150
175
200
record number

Figure X.1a

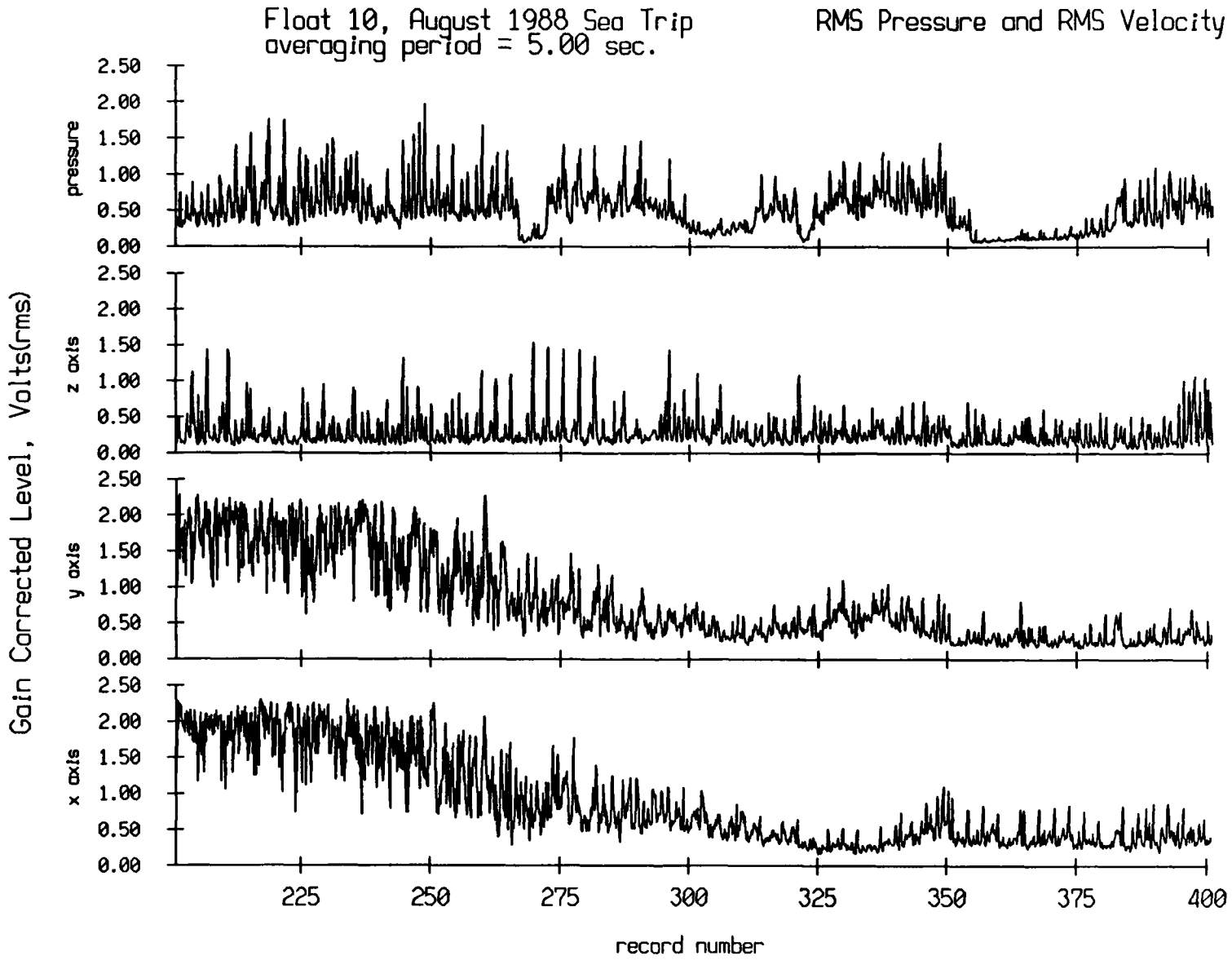

Float 10, August 1988 Sea Trip
averaging period = 5.00 sec.
RMS Pressure and RMS Velocity
Gain Corrected Level, Volts(rms)
pressure
z axis
y axis
x axis
2.50
2.00
1.50
1.00
0.50
0.00
225
250
275
300
325
350
375
400
record number

Figure X.1b

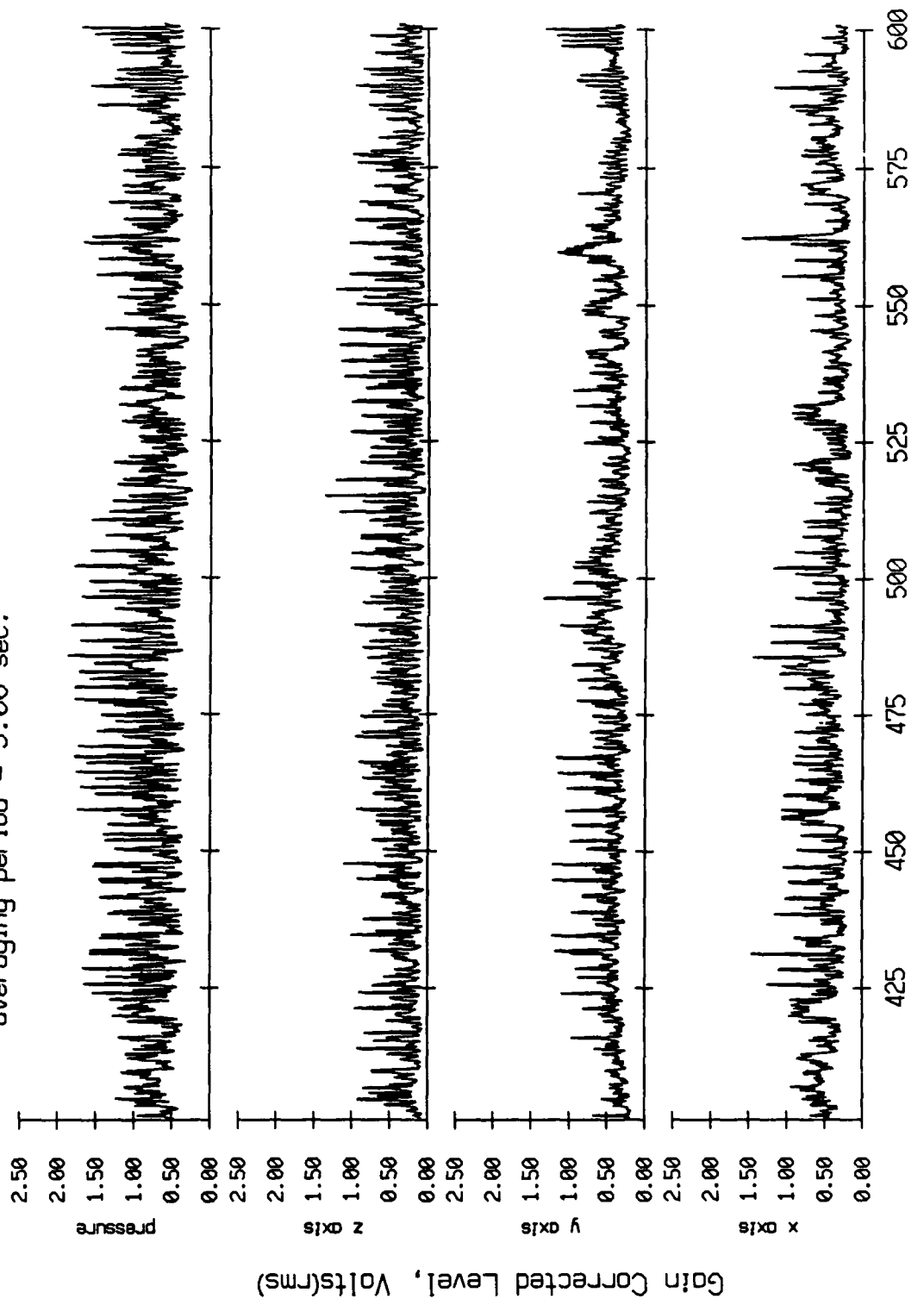

Float 10, August 1988 Sea Trip
averaging period = 5.00 sec.
RMS Pressure and RMS Velocity
Gain Corrected Level, Volts(rms)
pressure
z axis
y axis
x axis
2.50
2.00
1.50
1.00
0.50
0.00
425
450
475
500
525
550
575
600
record number

Figure X.1c

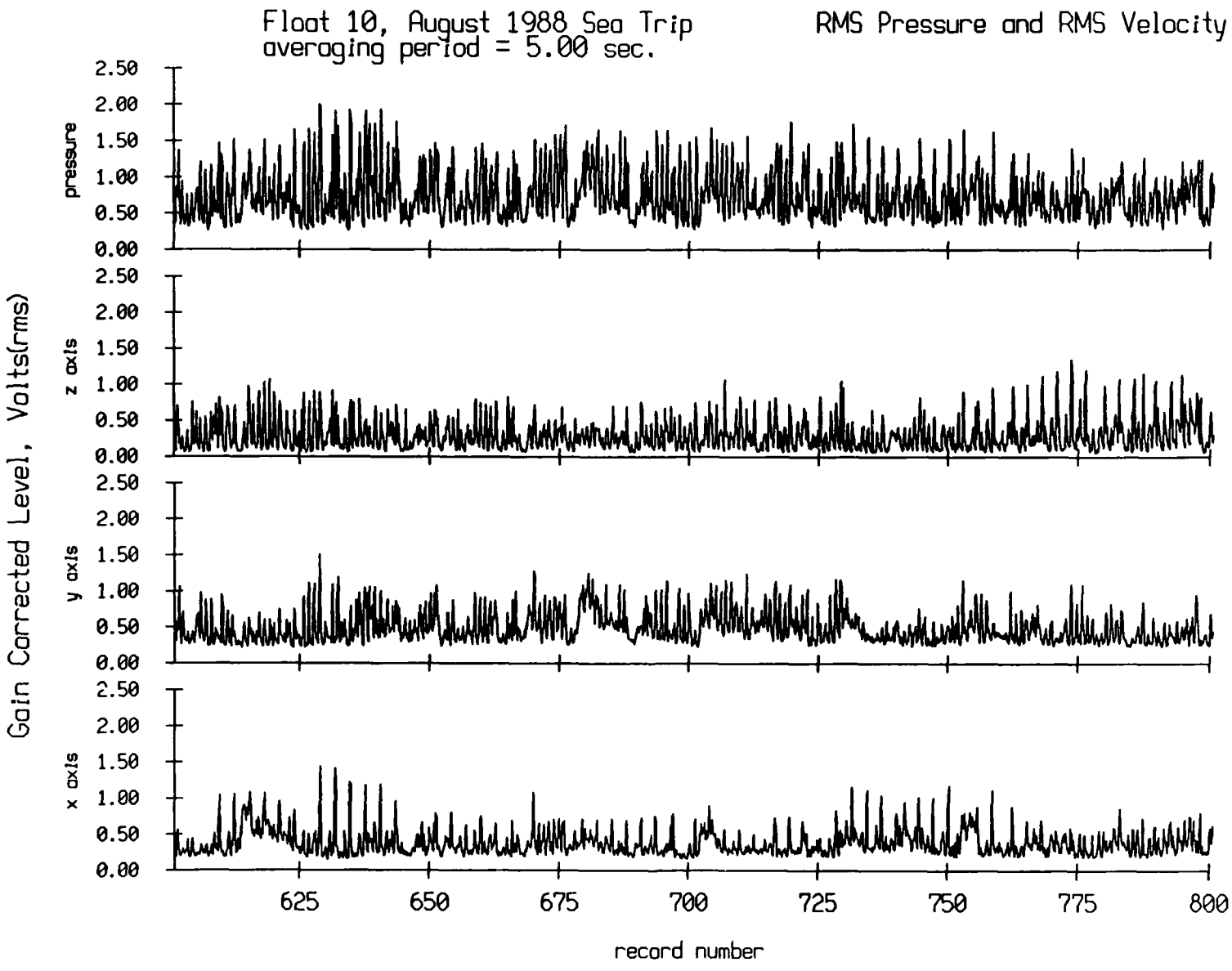

Float 10, August 1988 Sea Trip
averaging period = 5.00 sec.
RMS Pressure and RMS Velocity
Gain Corrected Level, Volts(rms)
pressure
z axis
y axis
x axis
2.50
2.00
1.50
1.00
0.50
0.00
625
650
675
700
725
750
775
800
record number

Figure X.1d

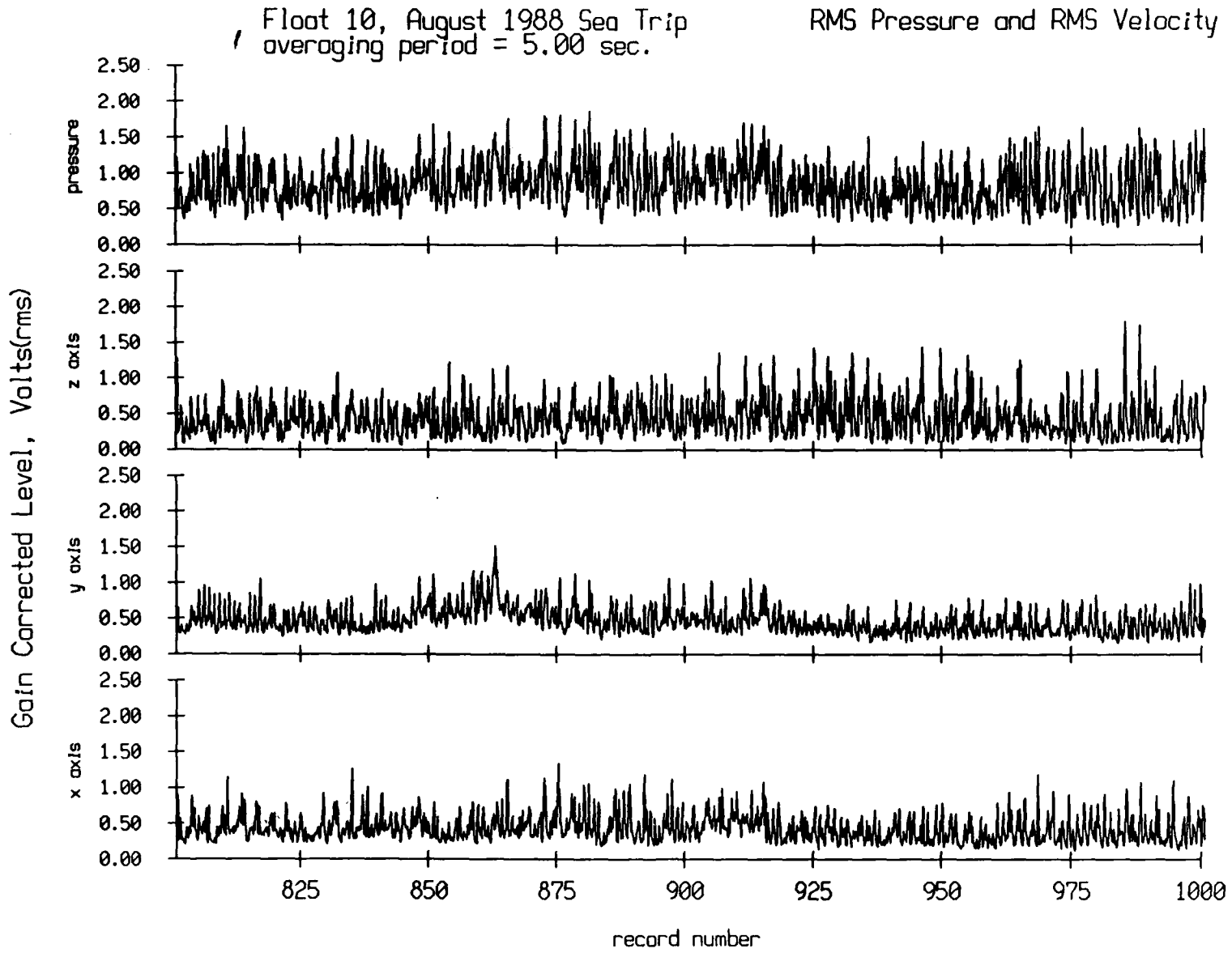

Float 10, August 1988 Sea Trip
averaging period = 5.00 sec.
RMS Pressure and RMS Velocity
Gain Corrected Level, Volts(rms)
pressure
z axis
y axis
x axis
2.50
2.00
1.50
1.00
0.50
0.00
825
850
875
900
925
950
975
1000
record number

Figure X.1e

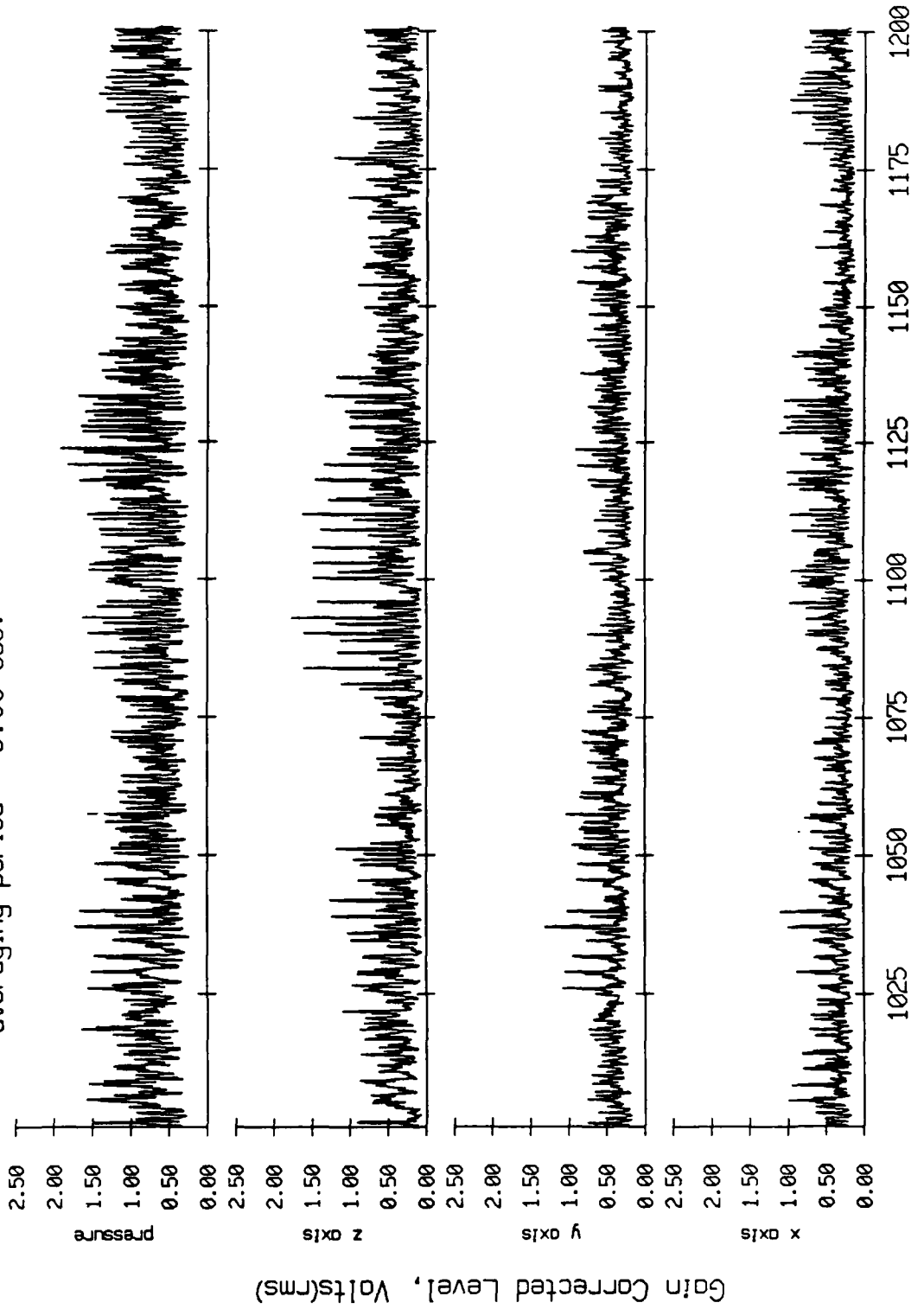

Float 10, August 1988 Sea Trip
averaging period = 5.00 sec.
RMS Pressure and RMS Velocity
Gain Corrected Level, Volts(rms)
pressure
z axis
y axis
x axis
2.50
2.00
1.50
1.00
0.50
0.00
1025
1050
1075
1100
1125
1150
1175
1200
record number

Figure X.1f

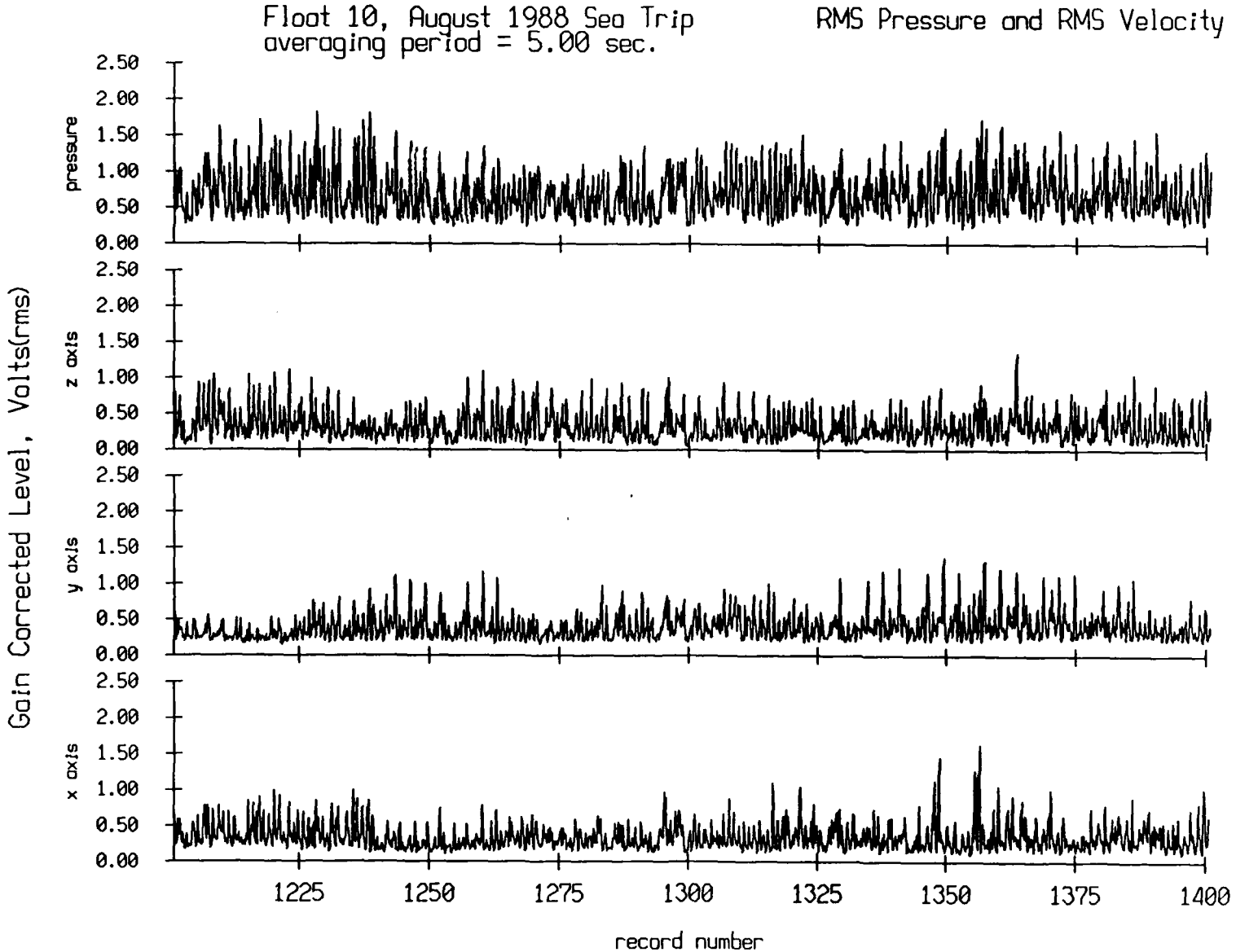

Float 10, August 1988 Sea Trip
averaging period = 5.00 sec.
RMS Pressure and RMS Velocity
Gain Corrected Level, Volts(rms)
pressure
z axis
y axis
x axis
2.50
2.00
1.50
1.00
0.50
0.00
1225
1250
1275
1300
1325
1350
1375
1400
record number

Figure X.1g

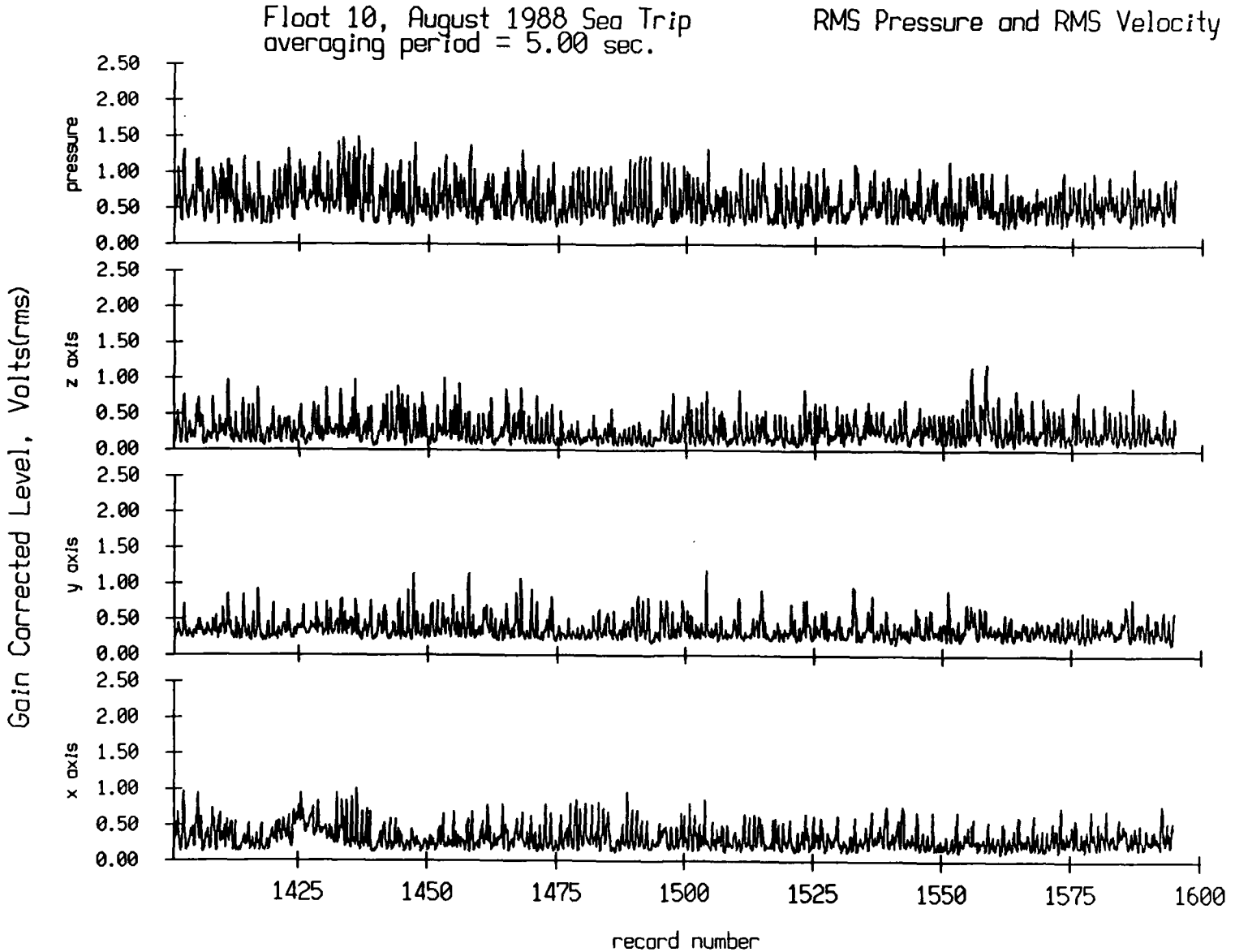

Float 10, August 1988 Sea Trip
overaging period = 5.00 sec.
RMS Pressure and RMS Velocity
Gain Corrected Level, Volts(rms)
pressure
z axis
y axis
x axis
2.50
2.00
1.50
1.00
0.50
0.00
1425
1450
1475
1500
1525
1550
1575
1600
record number

Figure X.1h

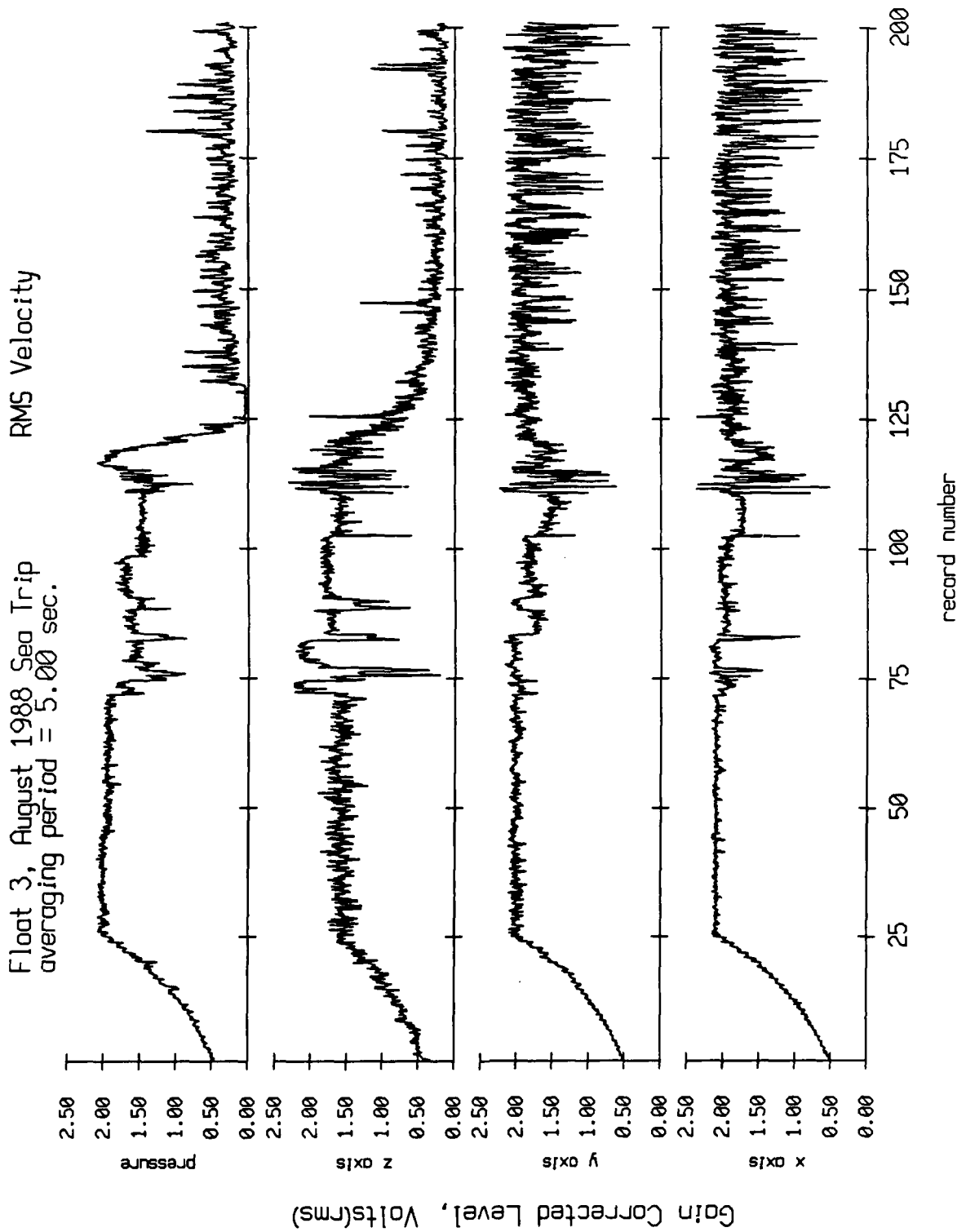

Float 3, August 1988 Sea Trip
averaging period = 5.00 sec.
RMS Velocity
Gain Corrected Level, Volts(rms)
pressure
z axis
y axis
x axis
2.50
2.00
1.50
1.00
0.50
0.00
25
50
75
100
125
150
175
200
record number

Figure X.2a

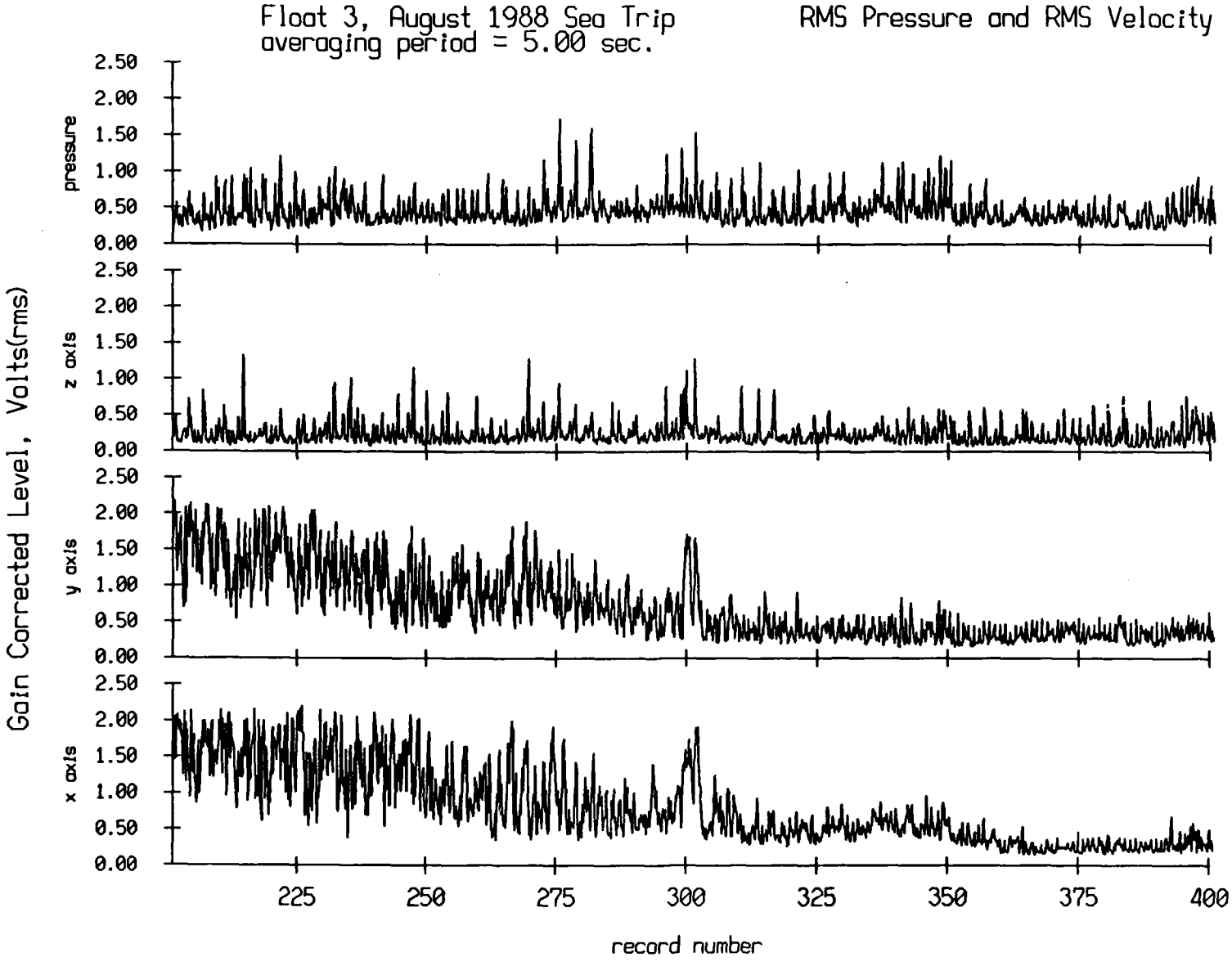

Float 3, August 1988 Sea Trip
averaging period = 5.00 sec.
RMS Pressure and RMS Velocity
Gain Corrected Level, Volts(rms)
pressure
z axis
y axis
x axis
2.50
2.00
1.50
1.00
0.50
0.00
225
250
275
300
325
350
375
400
record number

Figure X.2b

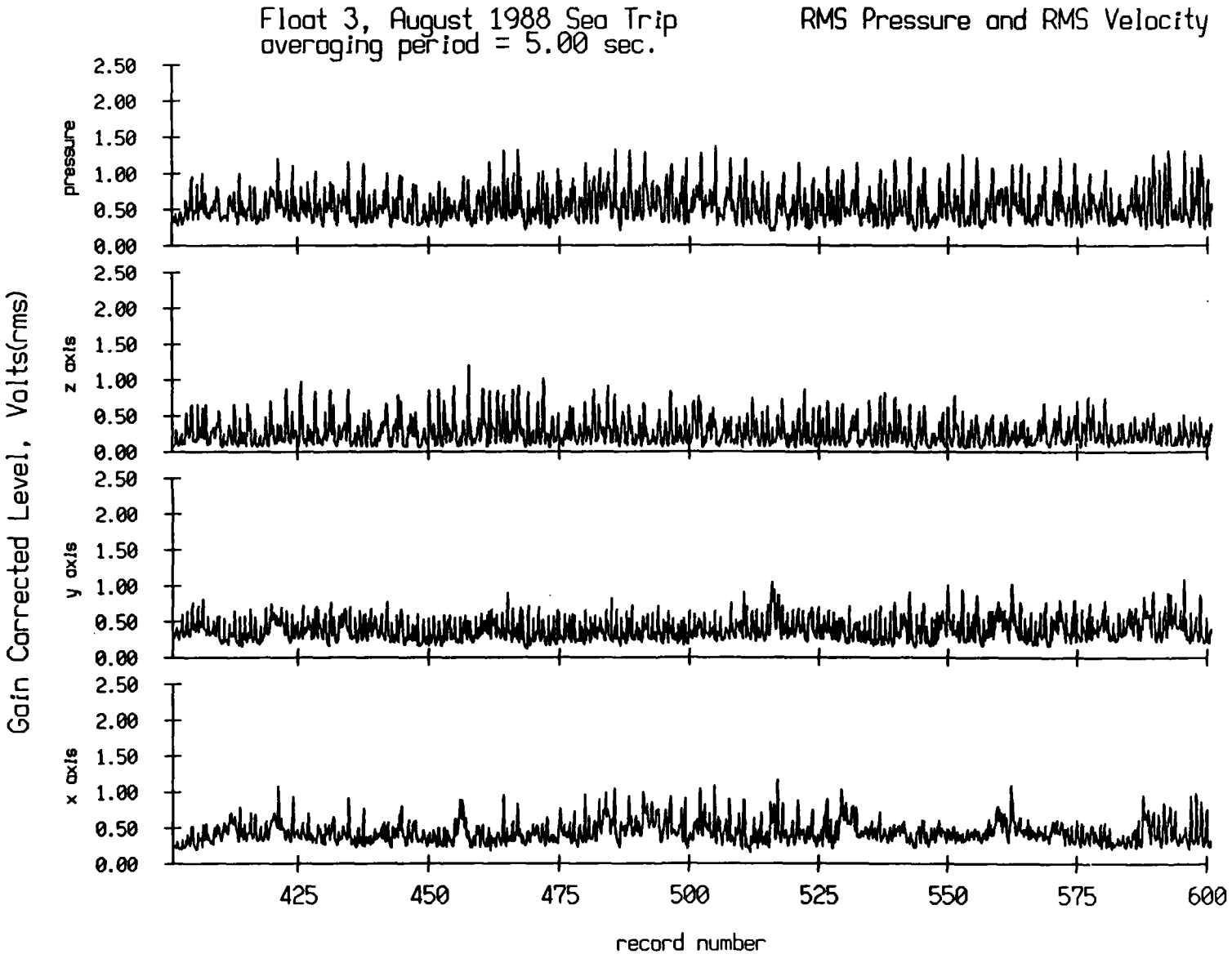

Float 3, August 1988 Sea Trip
averaging period = 5.00 sec.
RMS Pressure and RMS Velocity
Gain Corrected Level, Volts(rms)
pressure
z axis
y axis
x axis
2.50
2.00
1.50
1.00
0.50
0.00
425
450
475
500
525
550
575
600
record number

Figure X.2c

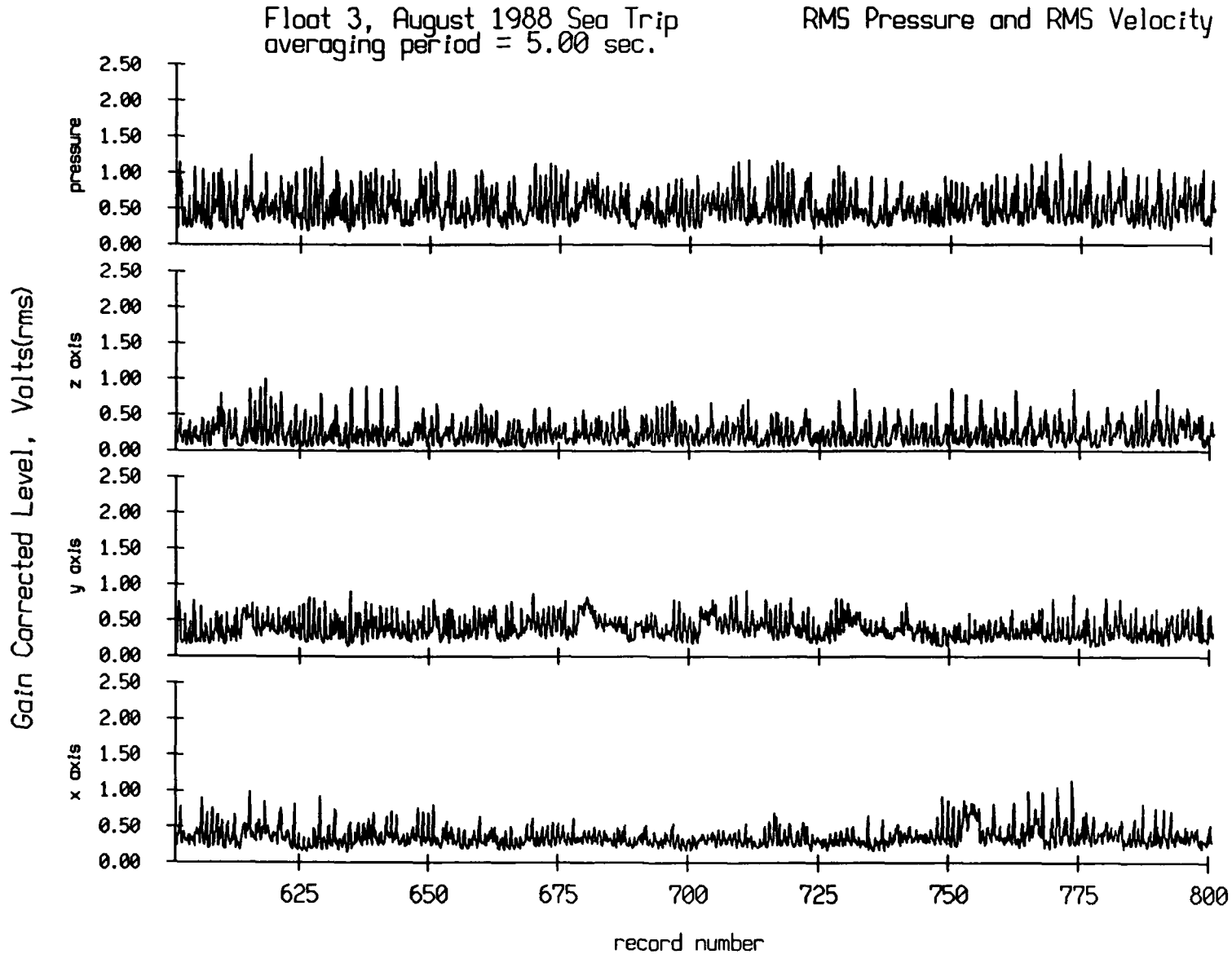

Float 3, August 1988 Sea Trip
averaging period = 5.00 sec.
RMS Pressure and RMS Velocity
Gain Corrected Level, Volts(rms)
pressure
z axis
y axis
x axis
2.50
2.00
1.50
1.00
0.50
0.00
625
650
675
700
725
750
775
800
record number

Figure X.2d

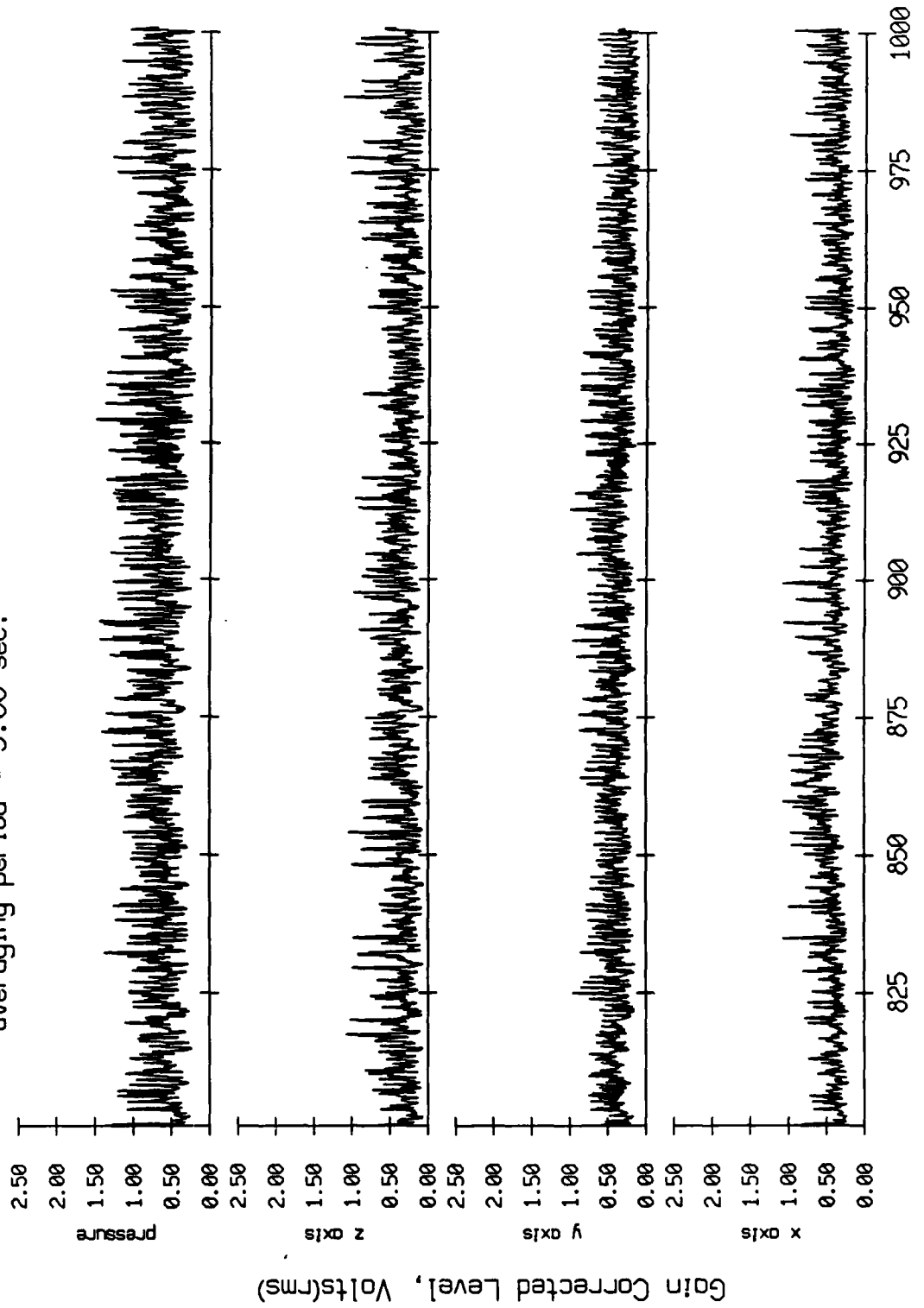

Float 3, August 1988 Sea Trip
averaging period = 5.00 sec.
RMS Pressure and RMS Velocity
Gain Corrected Level, Volts(rms)
pressure
z axis
y axis
x axis
2.50
2.00
1.50
1.00
0.50
0.00
825
850
875
900
925
950
975
1000
record number

Figure X.2e

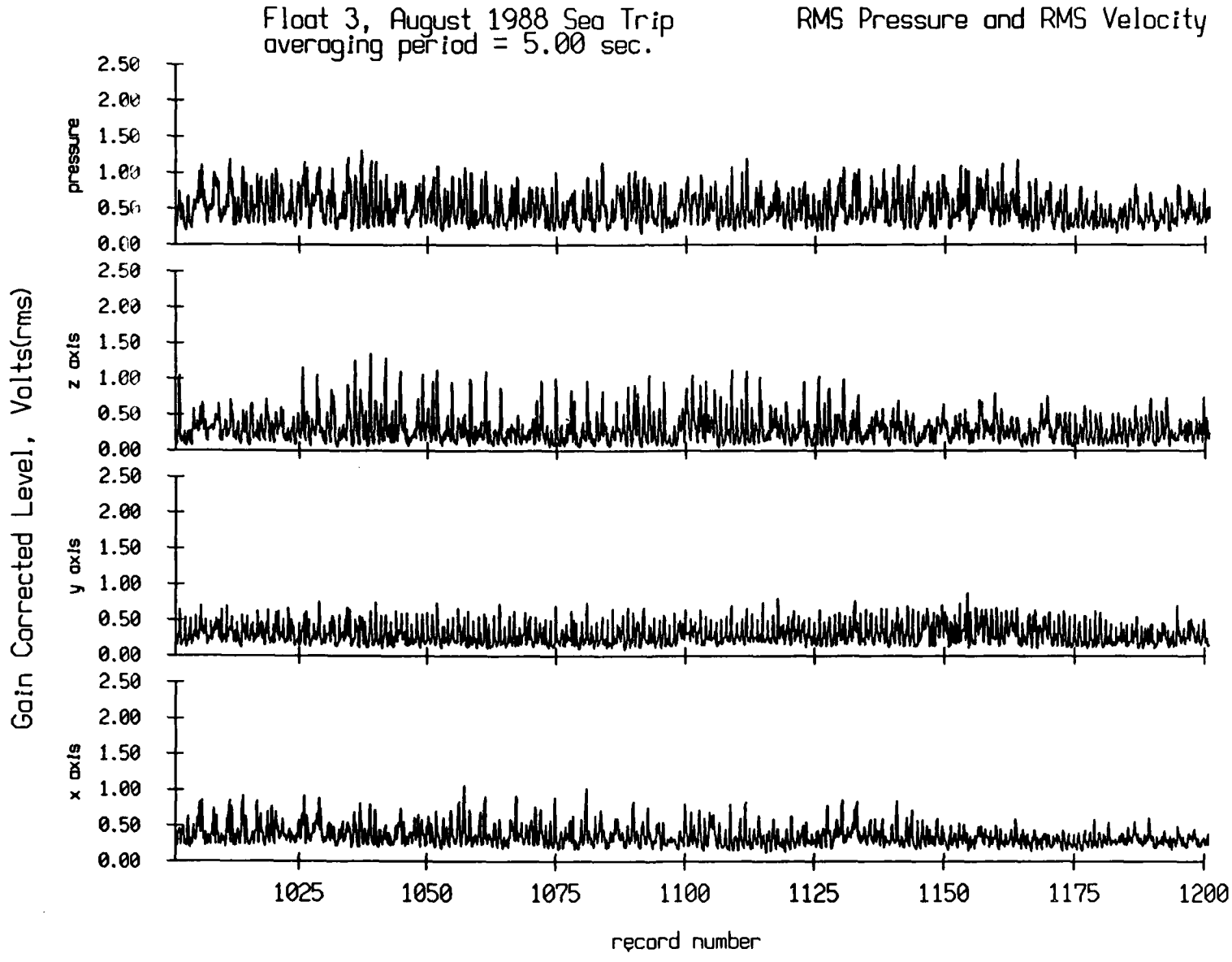

Float 3, August 1988 Sea Trip
averaging period = 5.00 sec.
RMS Pressure and RMS Velocity
Gain Corrected Level, Volts(rms)
pressure
z axis
y axis
x axis
2.50
2.00
1.50
1.00
0.50
0.00
1025
1050
1075
1100
1125
1150
1175
1200
record number

Figure X.2f

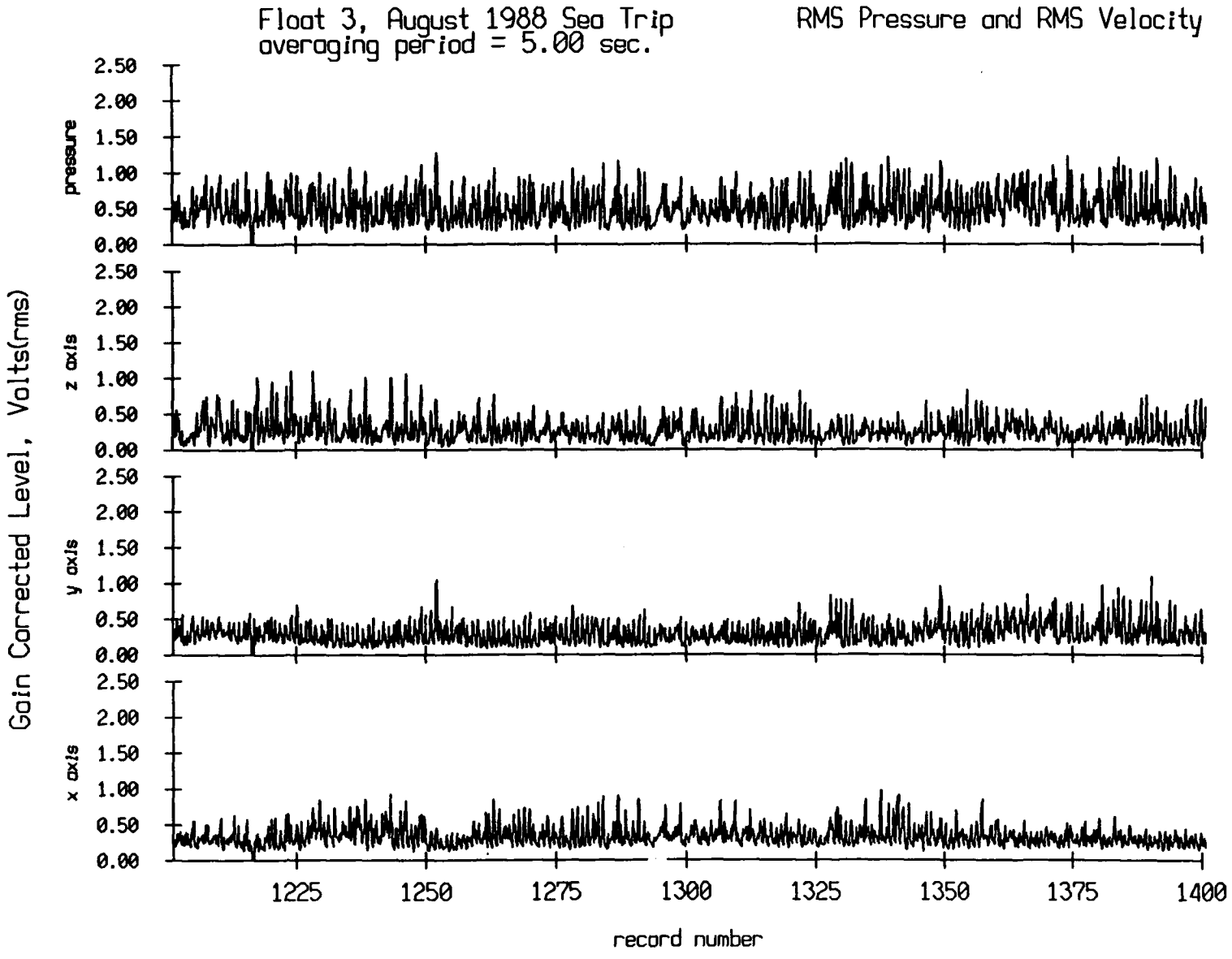

Float 3, August 1988 Sea Trip
overaging period = 5.00 sec.
RMS Pressure and RMS Velocity
Gain Corrected Level, Volts(rms)
pressure
z axis
y axis
x axis
2.50
2.00
1.50
1.00
0.50
0.00
1225
1250
1275
1300
1325
1350
1375
1400
record number

Figure X.28

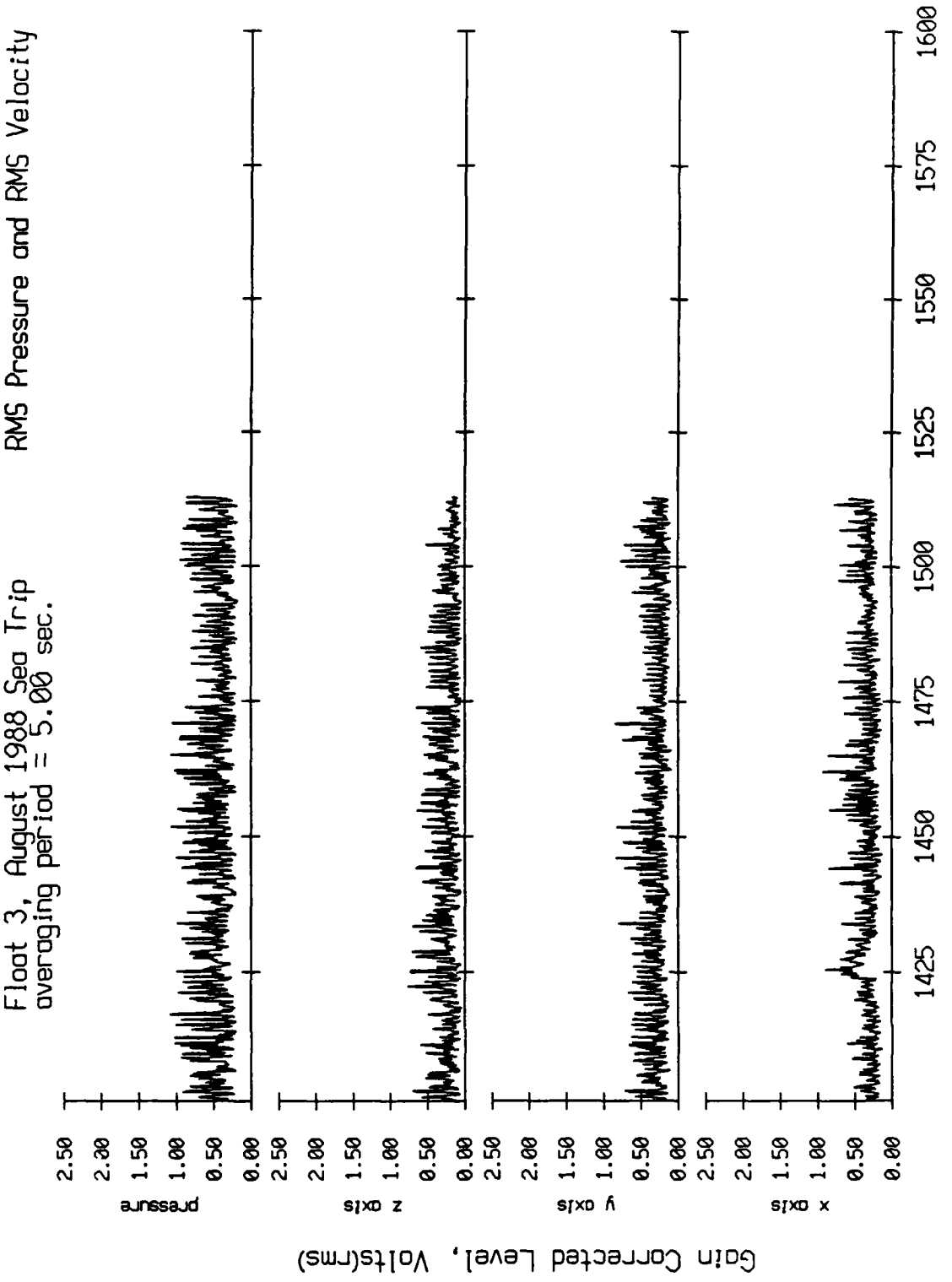

Float 3, August 1988 Sea Trip
averaging period = 5.00 sec.
RMS Pressure and RMS Velocity
Gain Corrected Level, Volts(rms)
pressure
z axis
y axis
x axis
2.50
2.00
1.50
1.00
0.50
0.00
1425
1450
1475
1500
1525
1550
1575
1600
record number

Figure X.2h

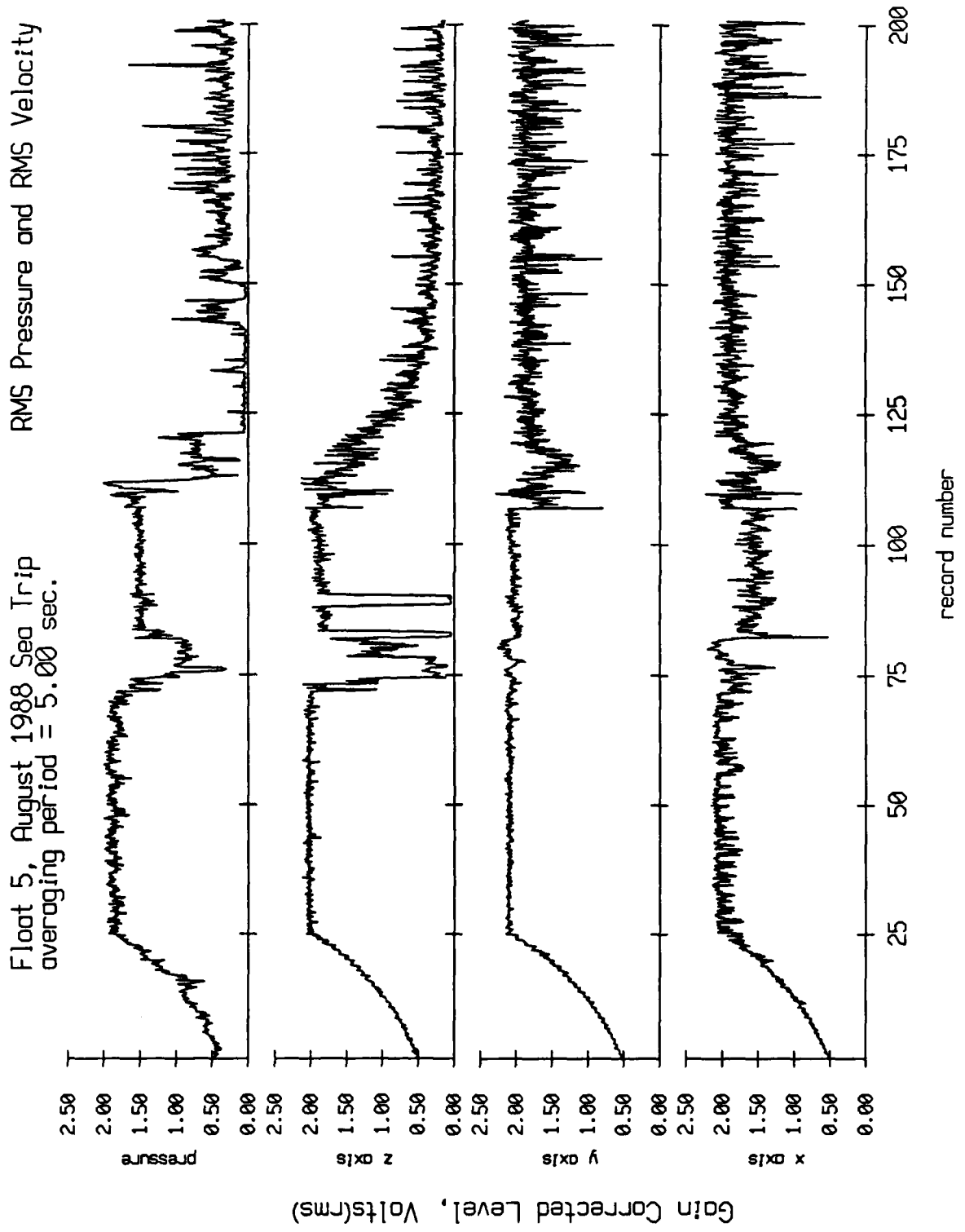

Float 5, August 1988 Sea Trip
averaging period = 5.00 sec.
RMS Pressure and RMS Velocity
Gain Corrected Level, Volts(rms)
pressure
z axis
y axis
x axis
2.50
2.00
1.50
1.00
0.50
0.00
25
50
75
100
125
150
175
200
record number

Figure X.3a

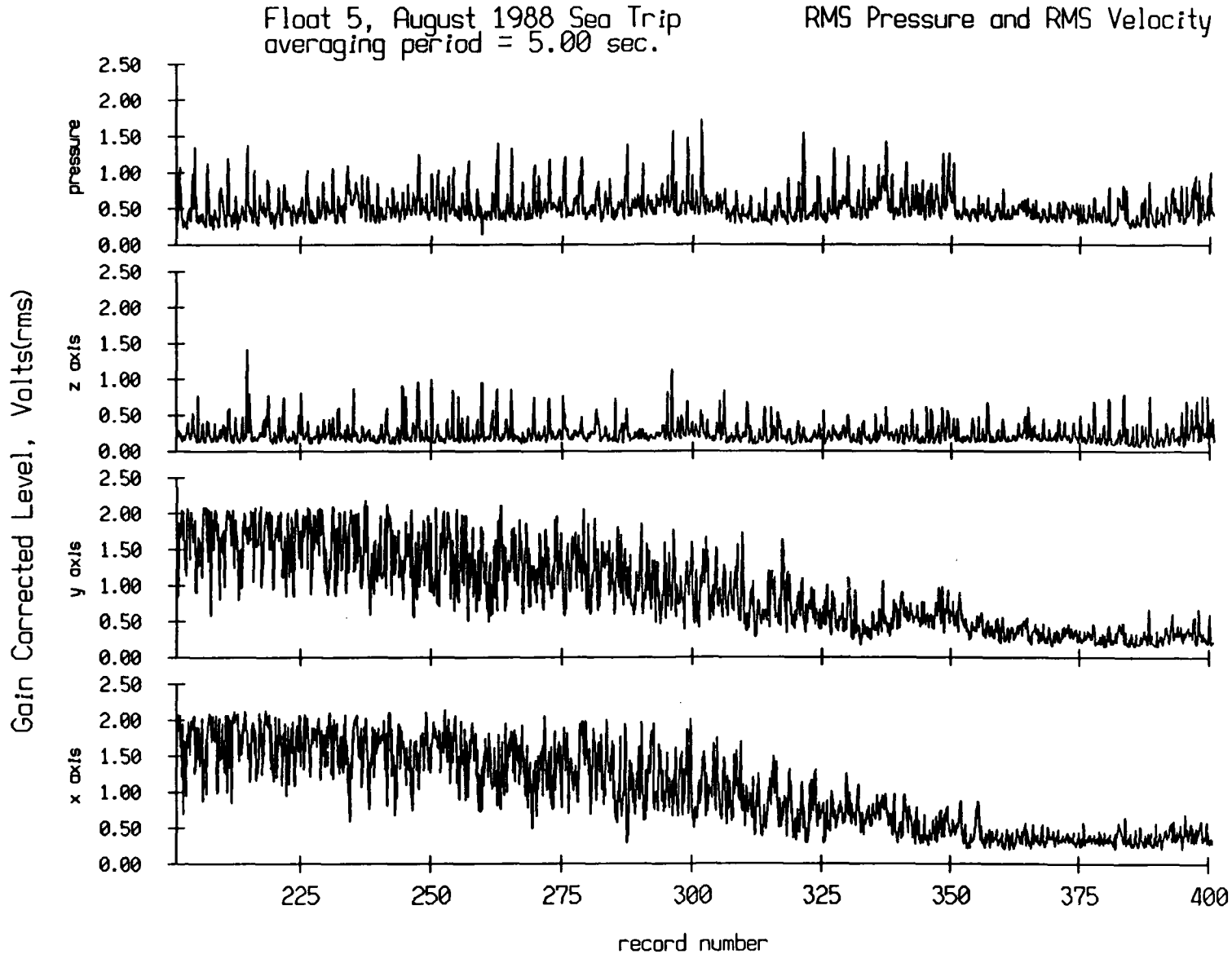

Float 5, August 1988 Sea Trip
averaging period = 5.00 sec.
RMS Pressure and RMS Velocity
Gain Corrected Level, Volts(rms)
pressure
z axis
y axis
x axis
2.50
2.00
1.50
1.00
0.50
0.00
225
250
275
300
325
350
375
400
record number

Figure X.3b

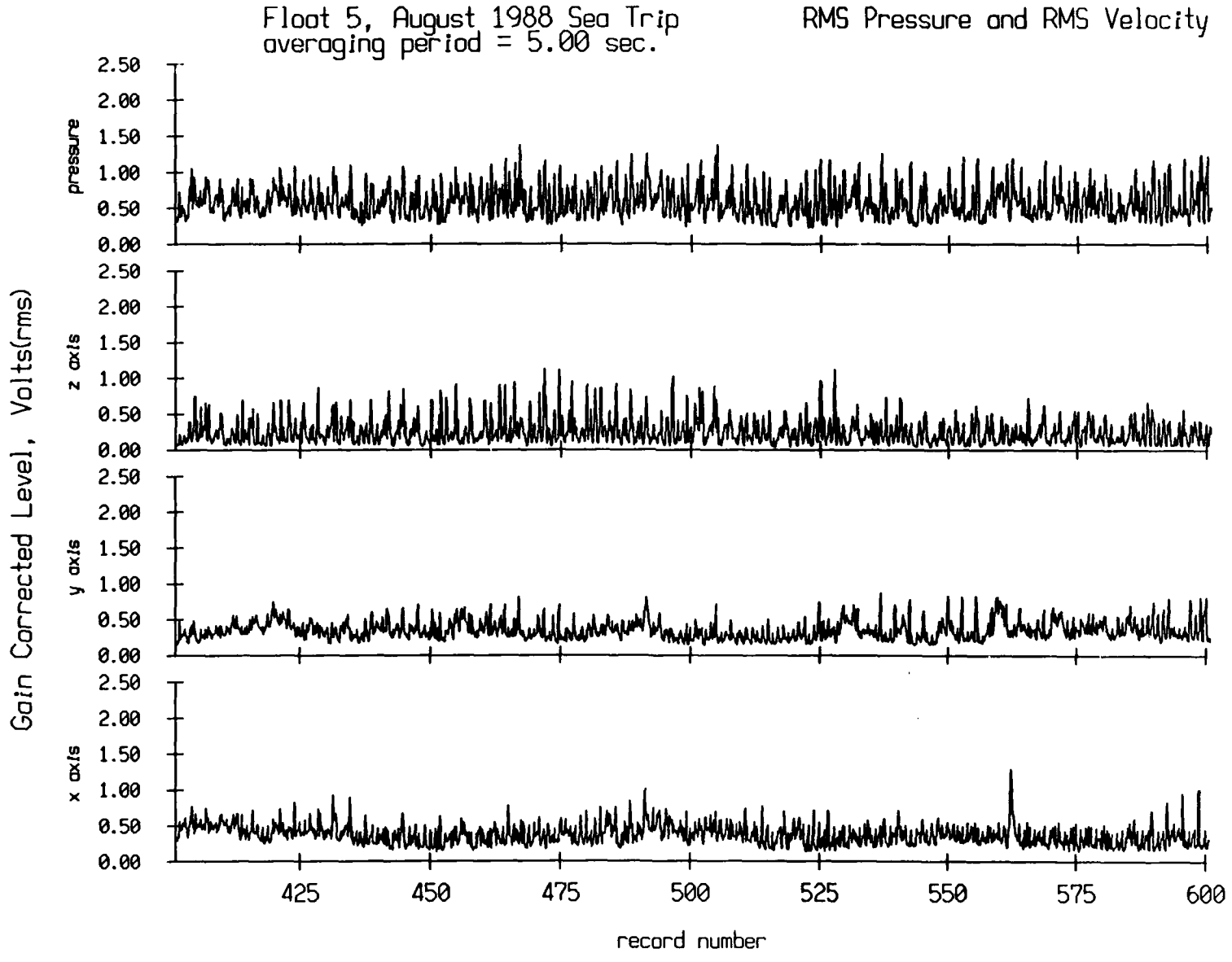

Float 5, August 1988 Sea Trip
averaging period = 5.00 sec.
RMS Pressure and RMS Velocity
Gain Corrected Level, Volts(rms)
pressure
z axis
y axis
x axis
2.50
2.00
1.50
1.00
0.50
0.00
425
450
475
500
525
550
575
600
record number

Figure X.3c

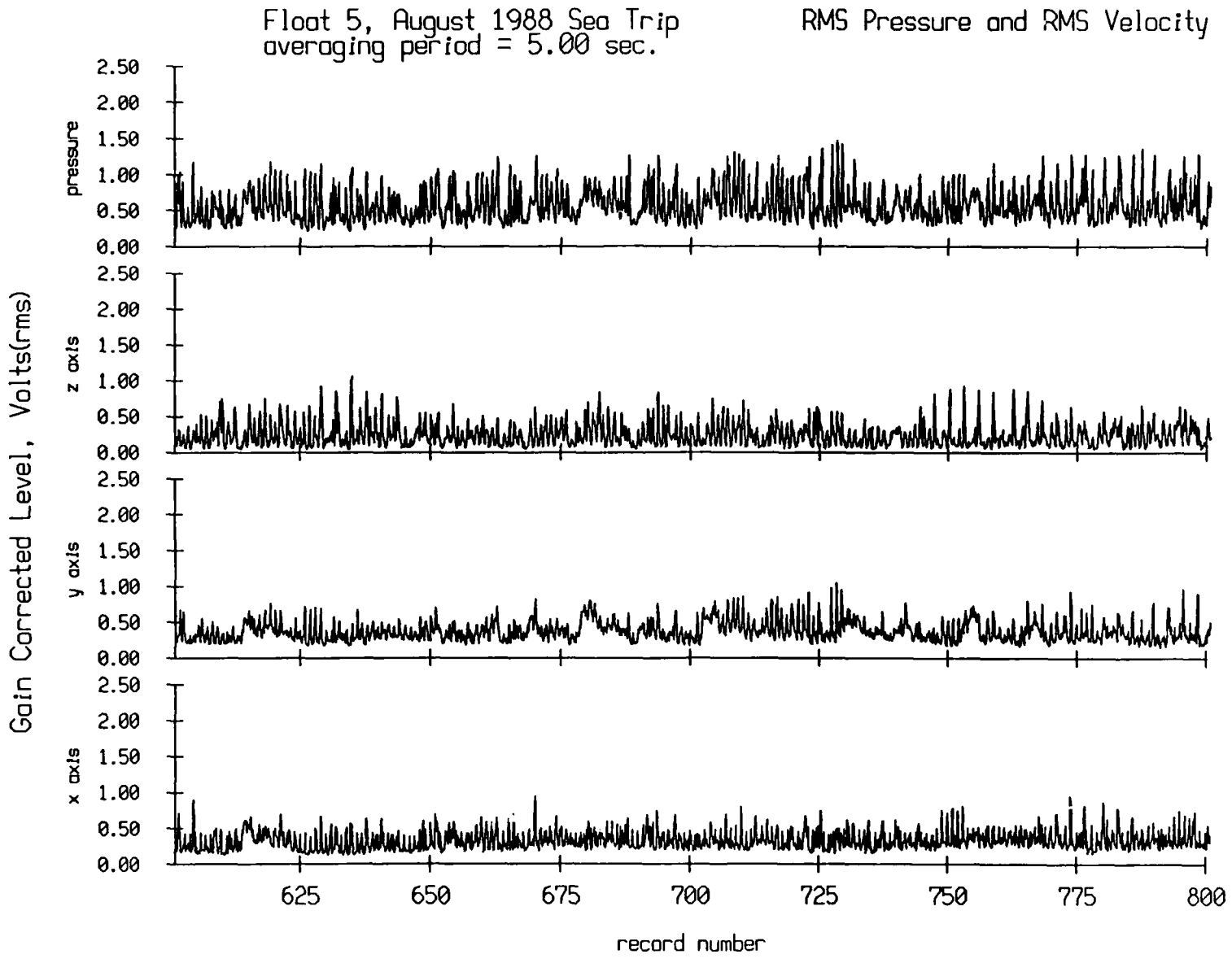

Float 5, August 1988 Sea Trip
averaging period = 5.00 sec.
RMS Pressure and RMS Velocity
Gain Corrected Level, Volts(rms)
pressure
z axis
y axis
x axis
2.50
2.00
1.50
1.00
0.50
0.00
625
650
675
700
725
750
775
800
record number

Figure X.3d

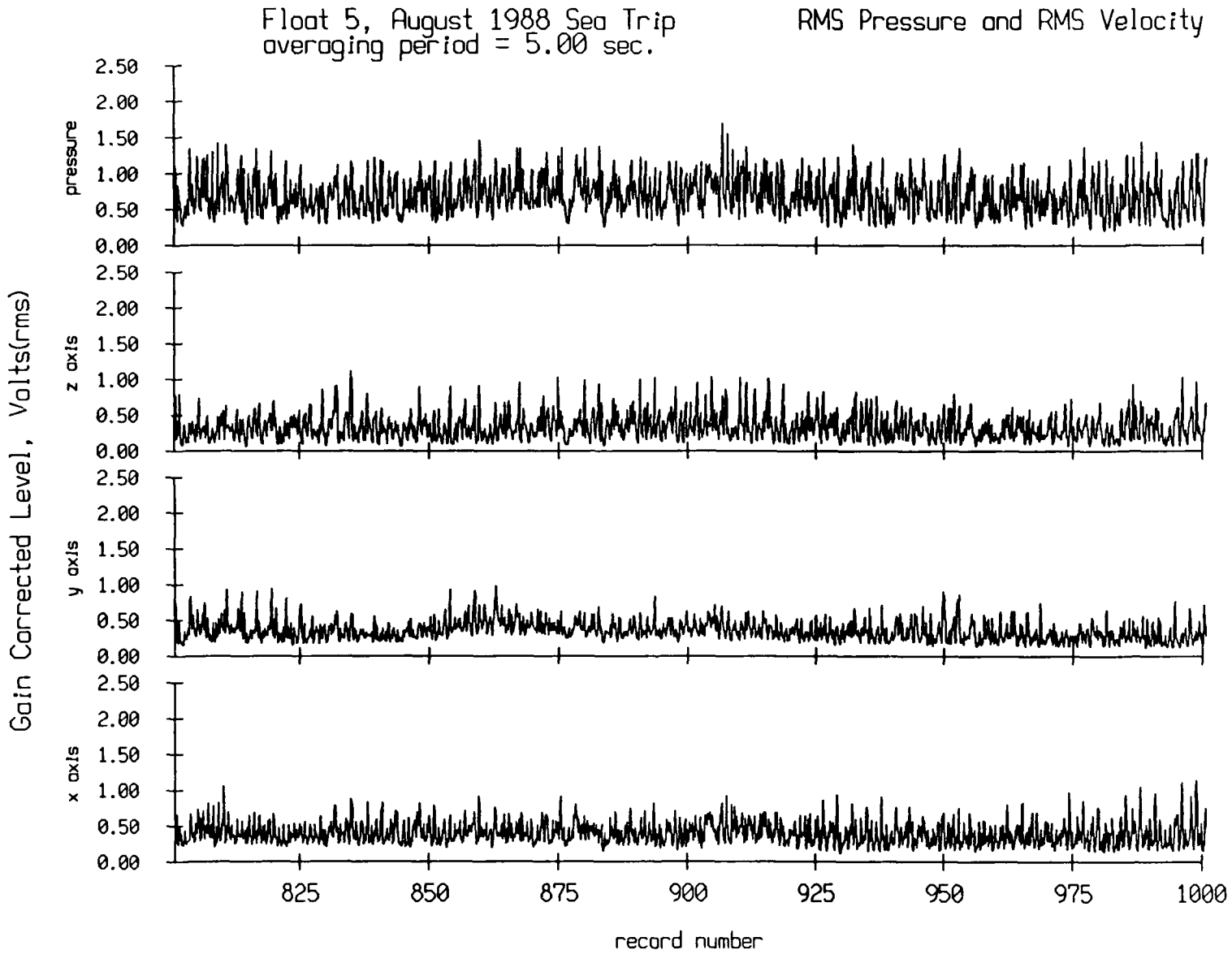

Float 5, August 1988 Sea Trip
averaging period = 5.00 sec.
RMS Pressure and RMS Velocity
Gain Corrected Level, Volts(rms)
pressure
z axis
y axis
x axis
2.50
2.00
1.50
1.00
0.50
0.00
825
850
875
900
925
950
975
1000
record number

Figure X.3e

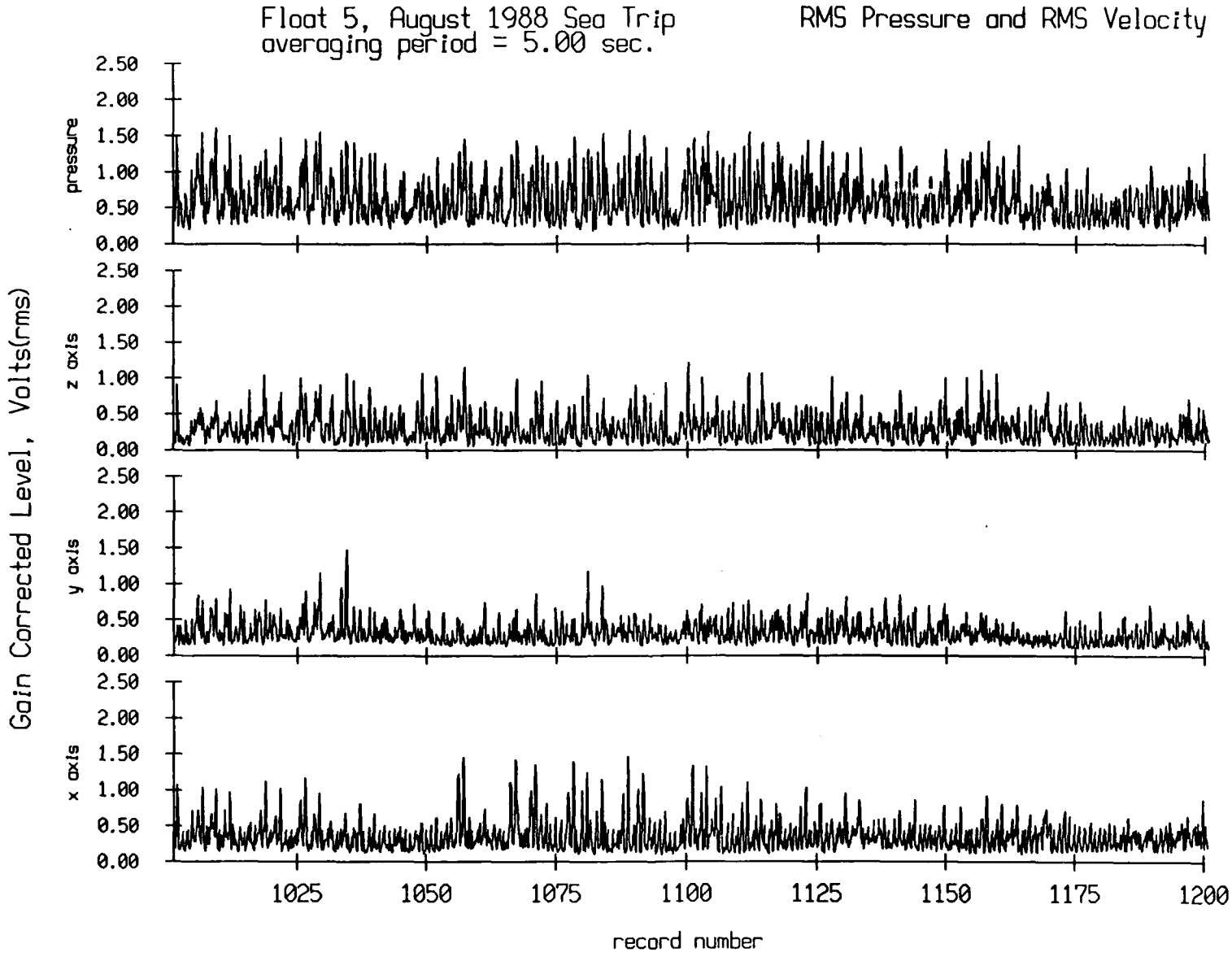

Float 5, August 1988 Sea Trip
averaging period = 5.00 sec.
RMS Pressure and RMS Velocity
Gain Corrected Level, Volts(rms)
pressure
z axis
y axis
x axis
2.50
2.00
1.50
1.00
0.50
0.00
1025
1050
1075
1100
1125
1150
1175
1200
record number

Figure X.3f

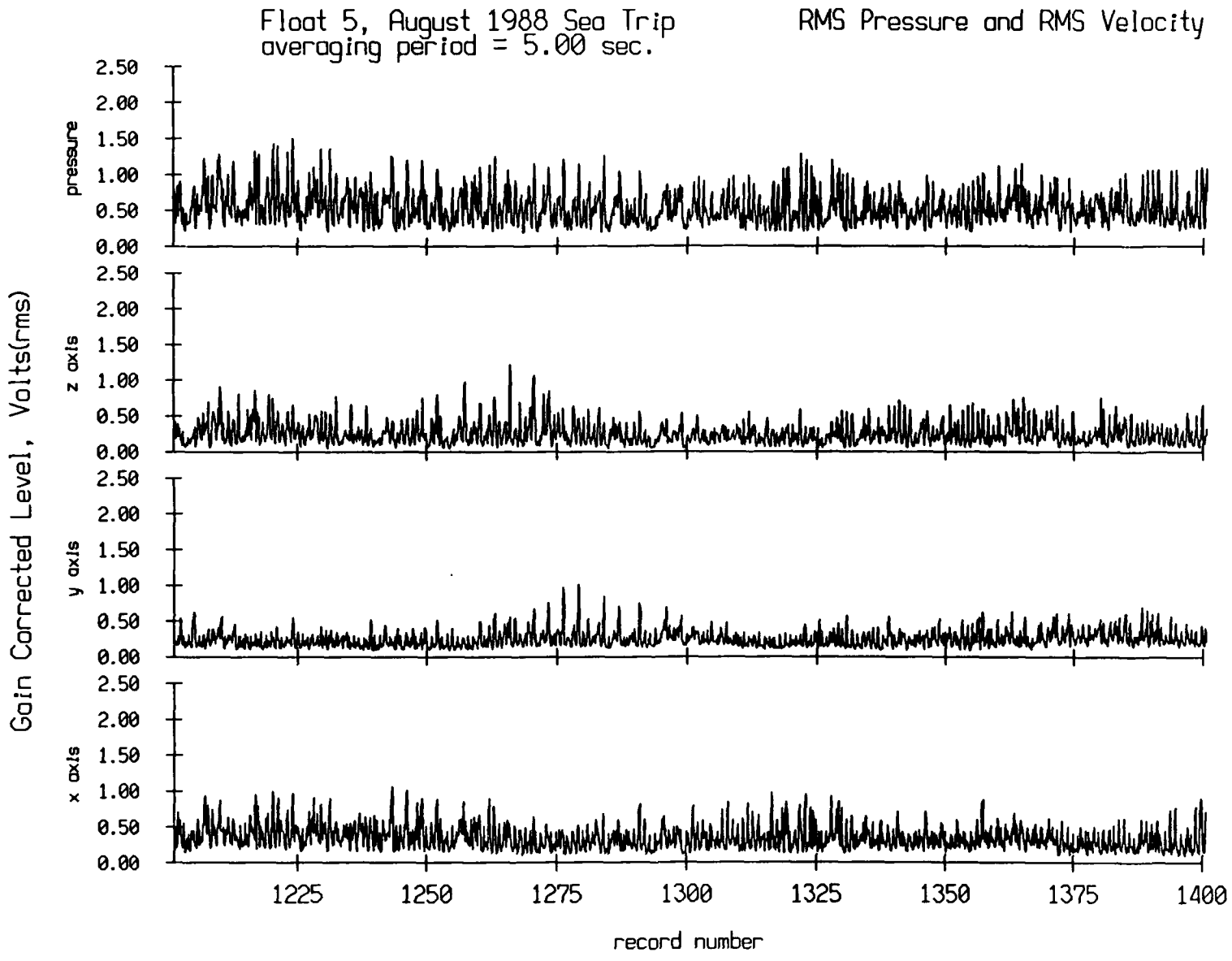

Float 5, August 1988 Sea Trip
averaging period = 5.00 sec.
RMS Pressure and RMS Velocity
Gain Corrected Level, Volts(rms)
pressure
z axis
y axis
x axis
2.50
2.00
1.50
1.00
0.50
0.00
1225
1250
1275
1300
1325
1350
1375
1400
record number

Figure X.3g

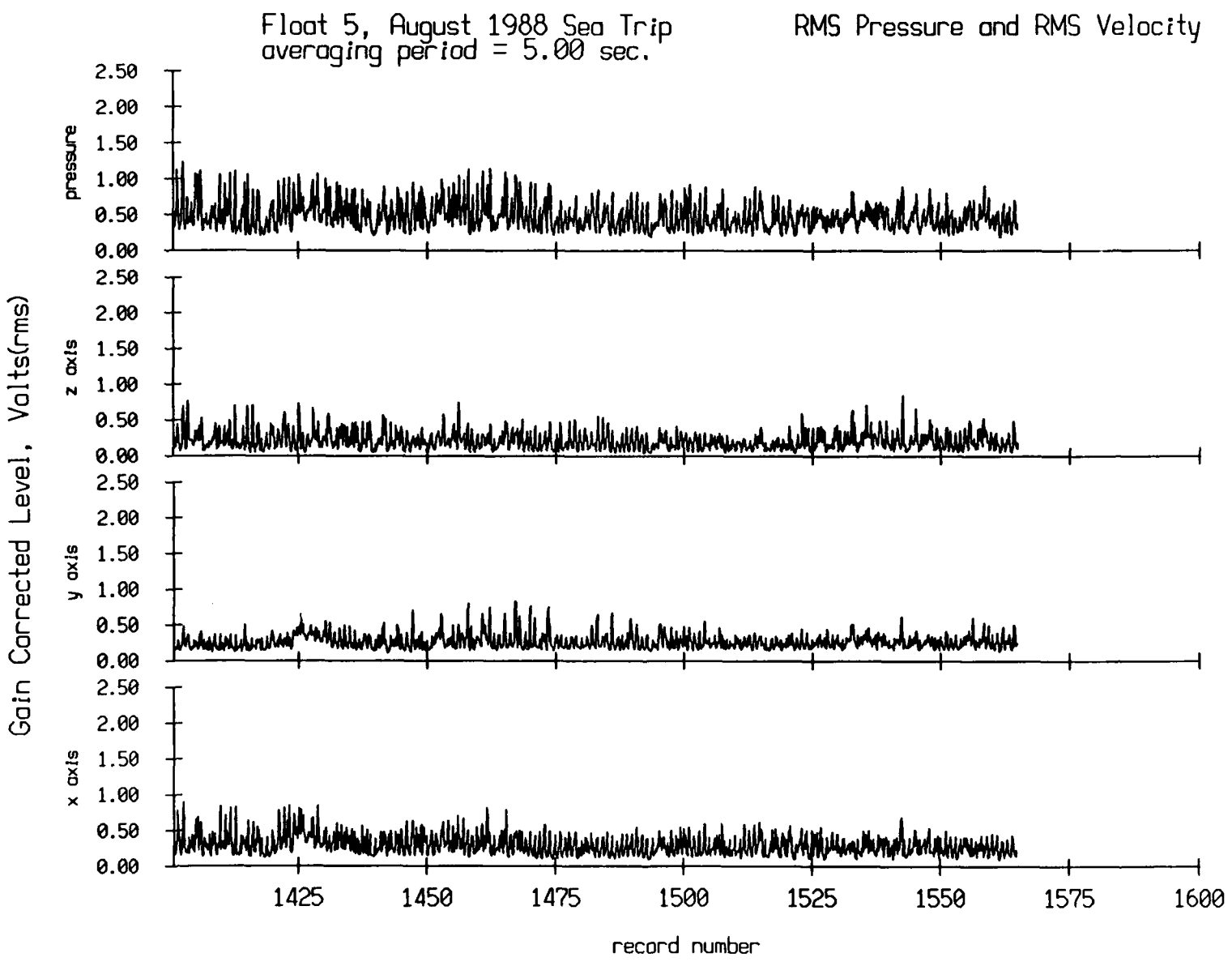

Float 5, August 1988 Sea Trip
averaging period = 5.00 sec.
RMS Pressure and RMS Velocity
Gain Corrected Level, Volts(rms)
pressure
z axis
y axis
x axis
2.50
2.00
1.50
1.00
0.50
0.00
1425
1450
1475
1500
1525
1550
1575
1600
record number

Figure X.3h

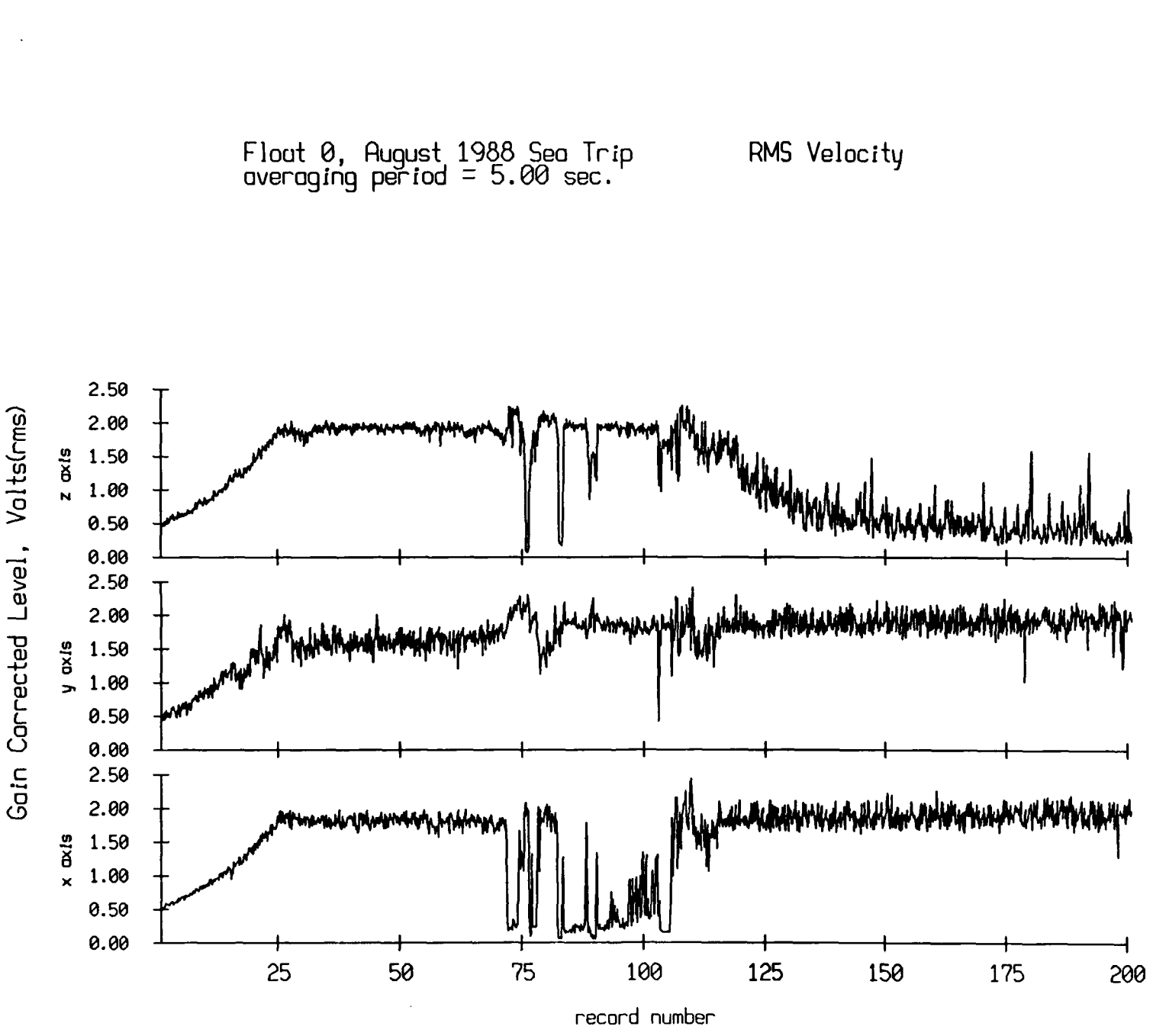

Float 0, August 1988 Sea Trip
averaging period = 5.00 sec.
RMS Velocity
Gain Corrected Level, Volts(rms)
z axis
y axis
x axis
2.50
2.00
1.50
1.00
0.50
0.00
25
50
75
100
125
150
175
200
record number

Figure X.4a

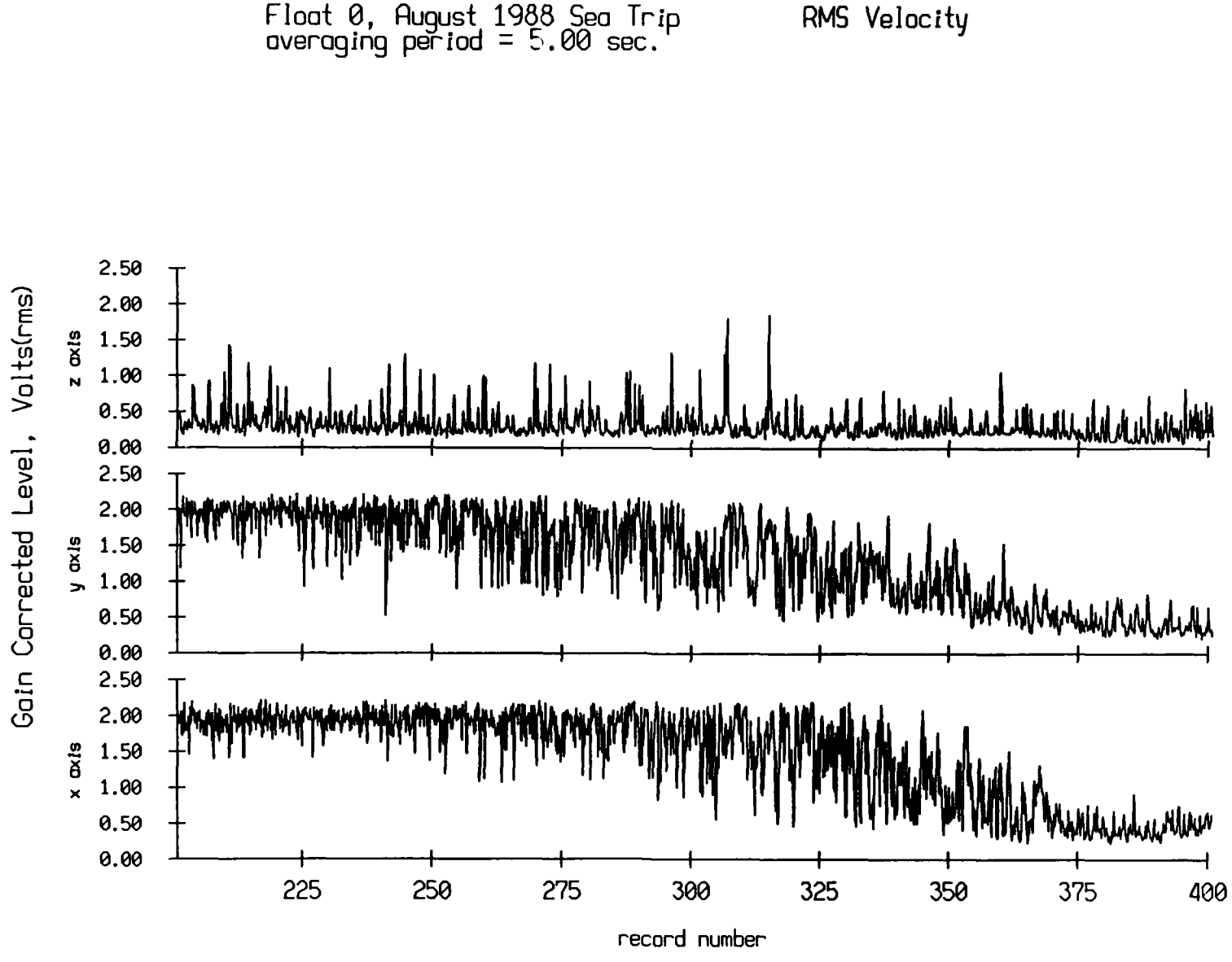

Float 0, August 1988 Sea Trip
averaging period = 5.00 sec.
RMS Velocity
Gain Corrected Level, Volts(rms)
z axis
y axis
x axis
2.50
2.00
1.50
1.00
0.50
0.00
225
250
275
300
325
350
375
400
record number

Figure X.4b

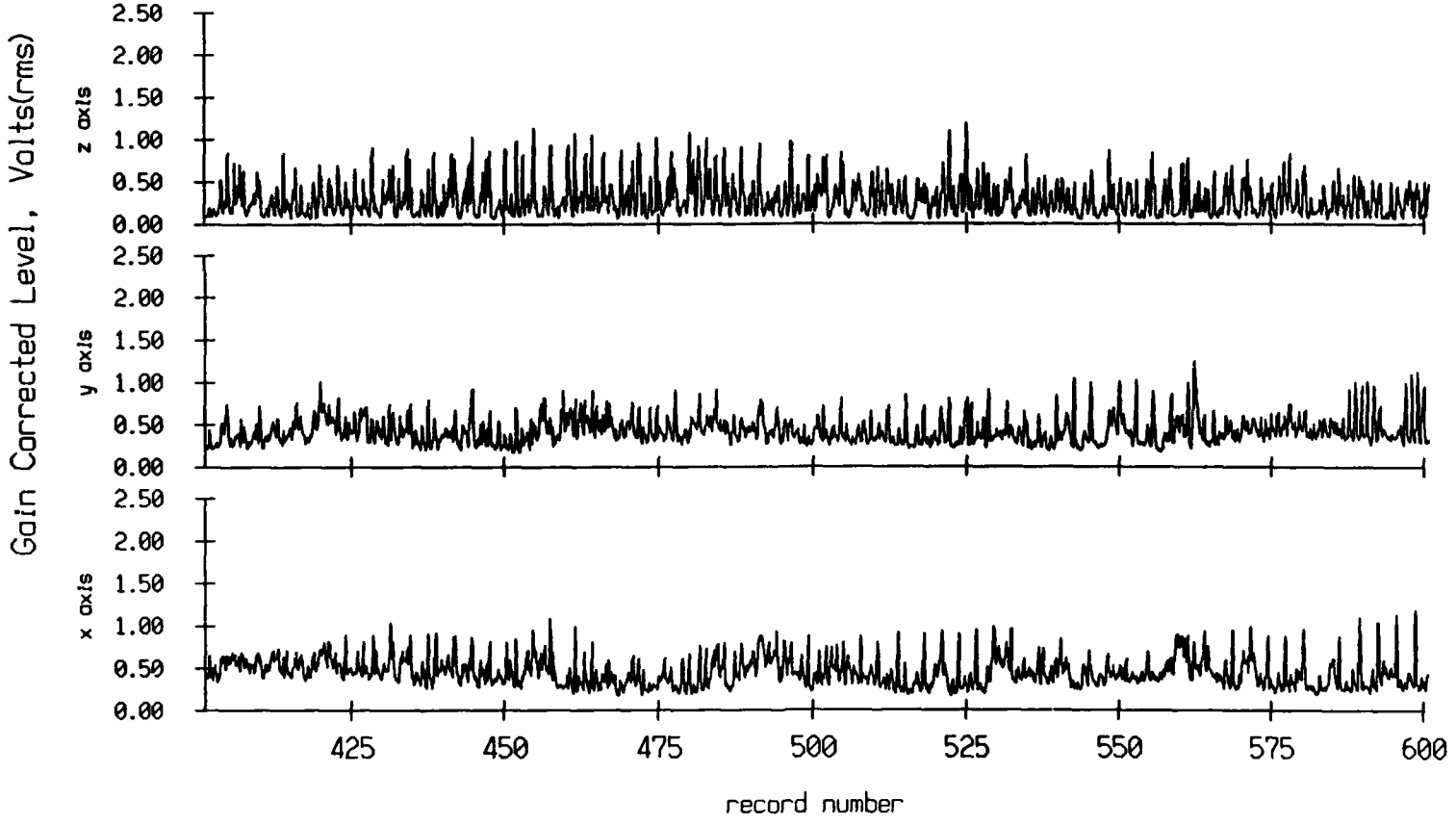

Float 0, August 1988 Sea Trip
averaging period = 5.00 sec.
RMS Velocity
Gain Corrected Level, Volts(rms)
z axis
y axis
x axis
2.50
2.00
1.50
1.00
0.50
0.00
425
450
475
500
525
550
575
600
record number

Figure X.4c

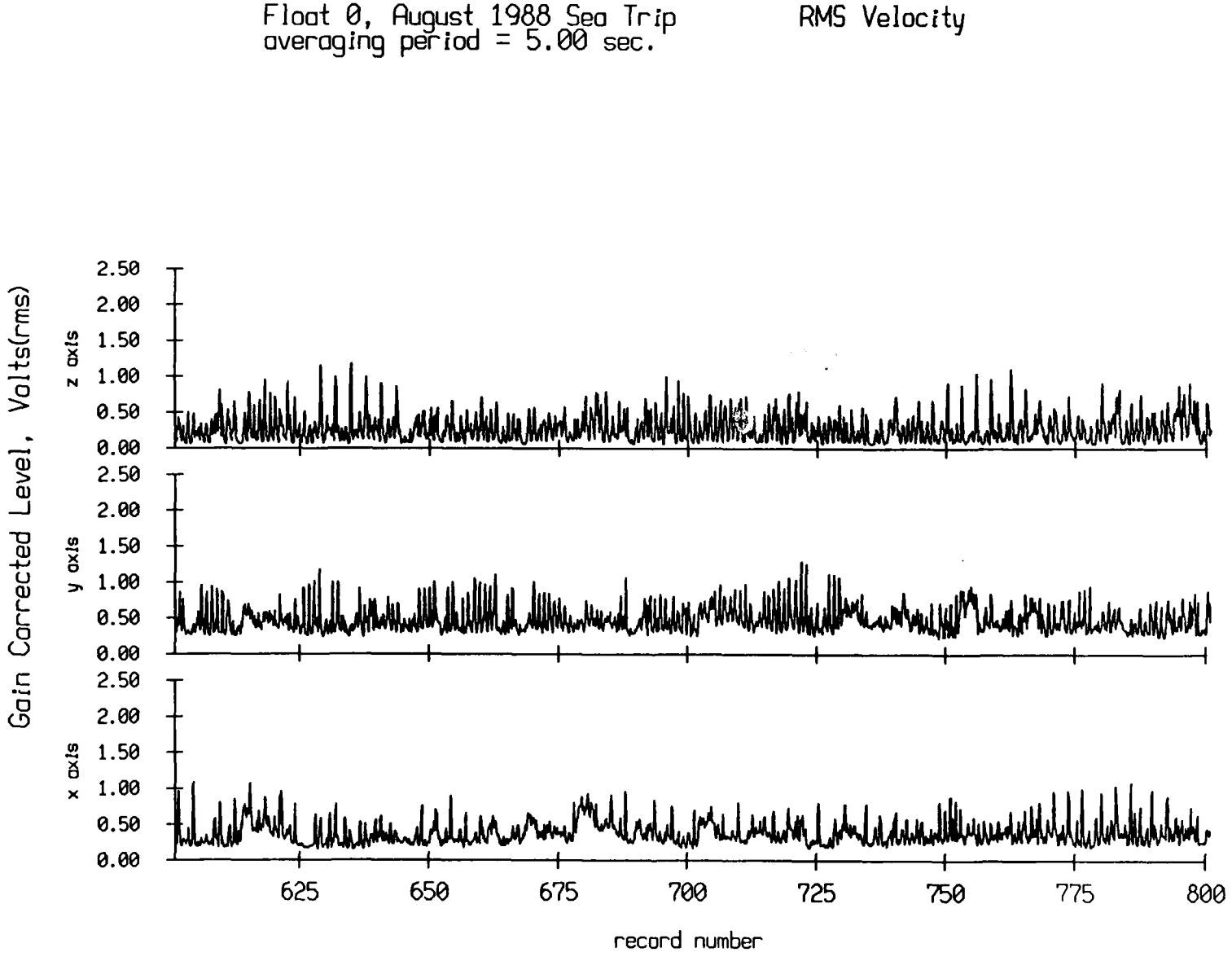

Float 0, August 1988 Sea Trip
averaging period = 5.00 sec.
RMS Velocity
Gain Corrected Level, Volts(rms)
z axis
y axis
x axis
2.50
2.00
1.50
1.00
0.50
0.00
625
650
675
700
725
750
775
800
record number

Figure X.4d

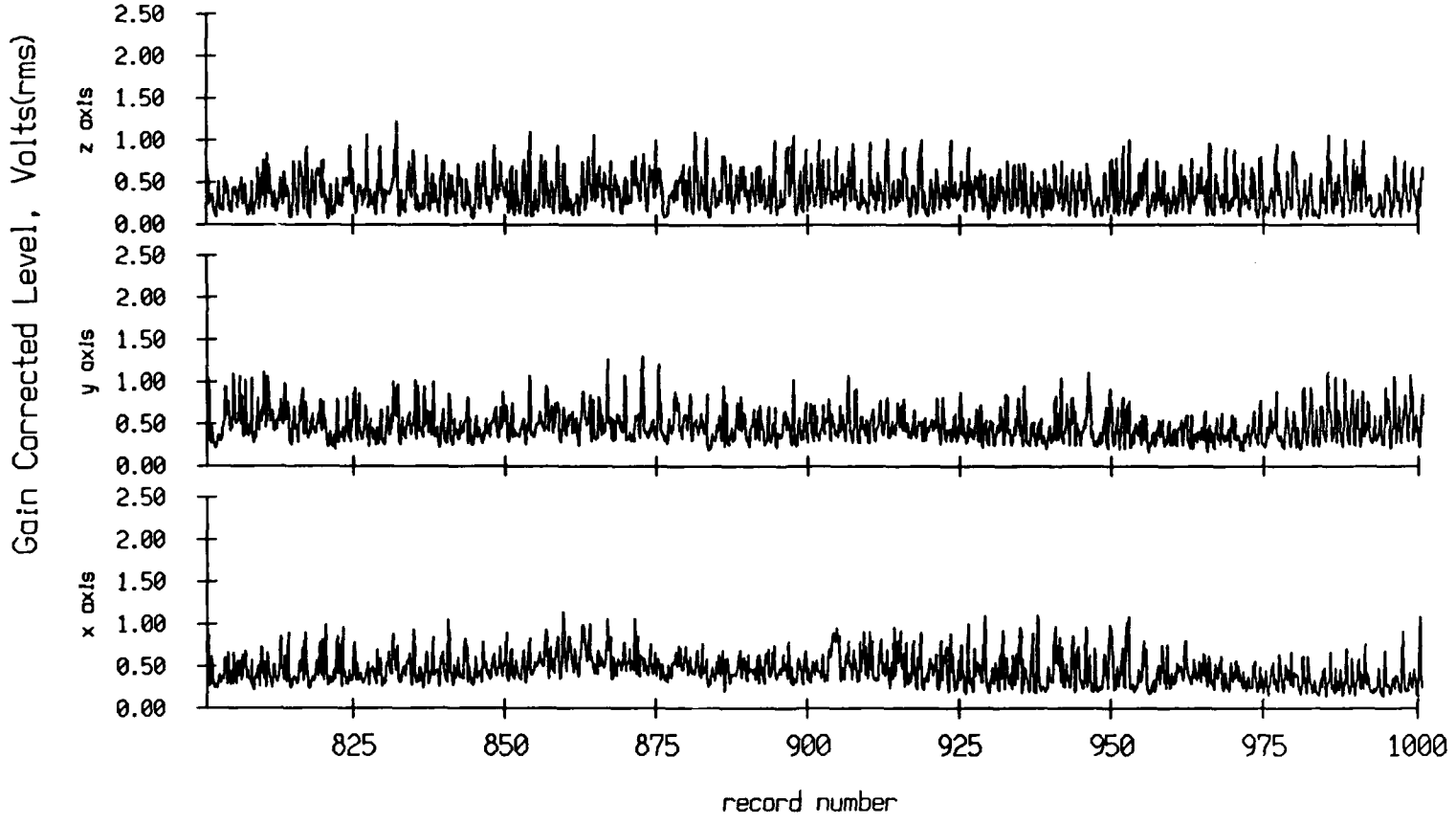

Float 0, August 1988 Sea Trip
averaging period = 5.00 sec.
RMS Velocity
Gain Corrected Level, Volts(rms)
z axis
y axis
x axis
2.50
2.00
1.50
1.00
0.50
0.00
825
850
875
900
925
950
975
1000
record number

Figure X.4e

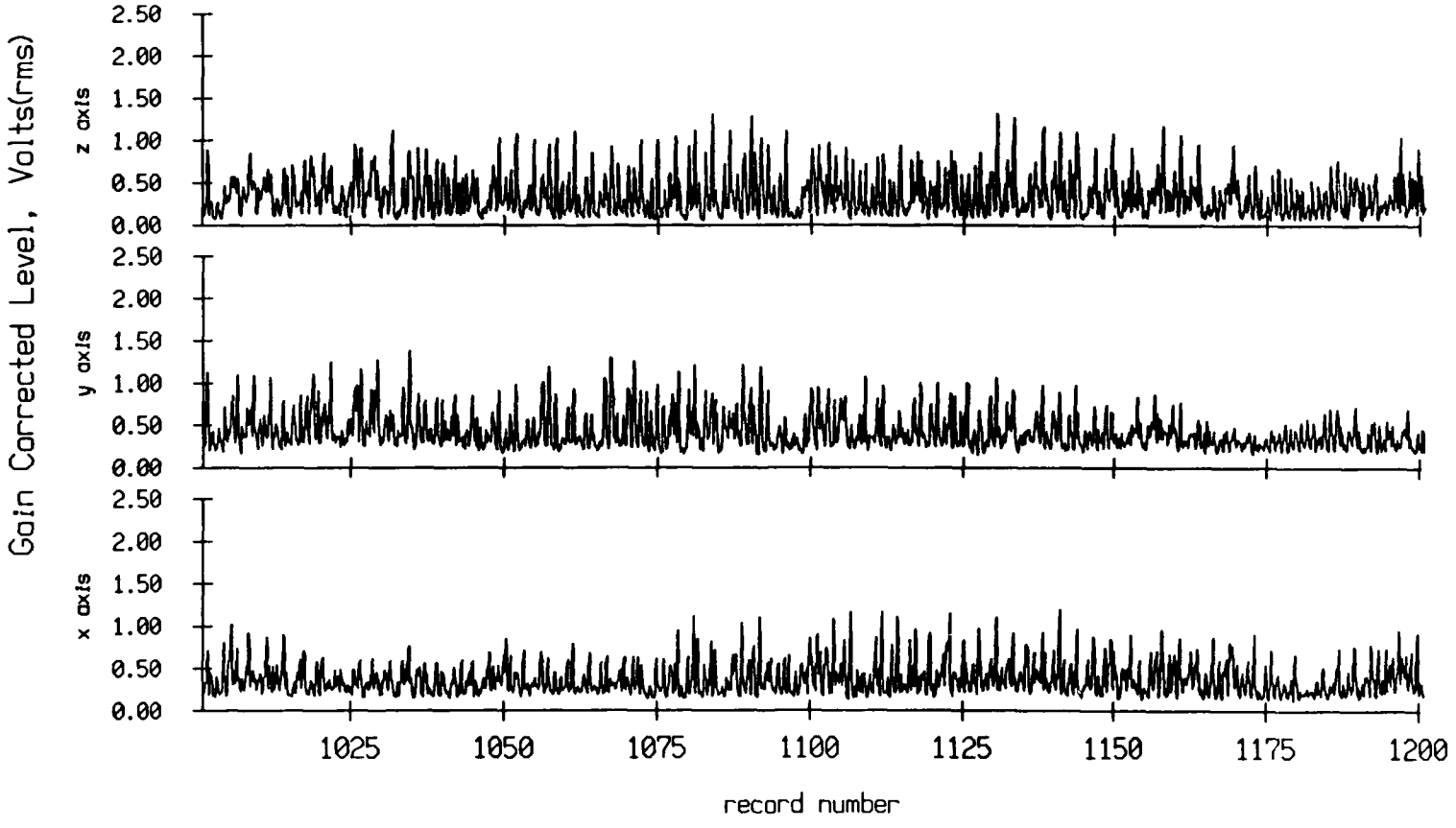

Float 0, August 1988 Sea Trip
overaging period = 5.00 sec.
RMS Velocity
Gain Corrected Level, Volts(rms)
z axis
y axis
x axis
2.50
2.00
1.50
1.00
0.50
0.00
1025
1050
1075
1100
1125
1150
1175
1200
record number

Figure X.4f

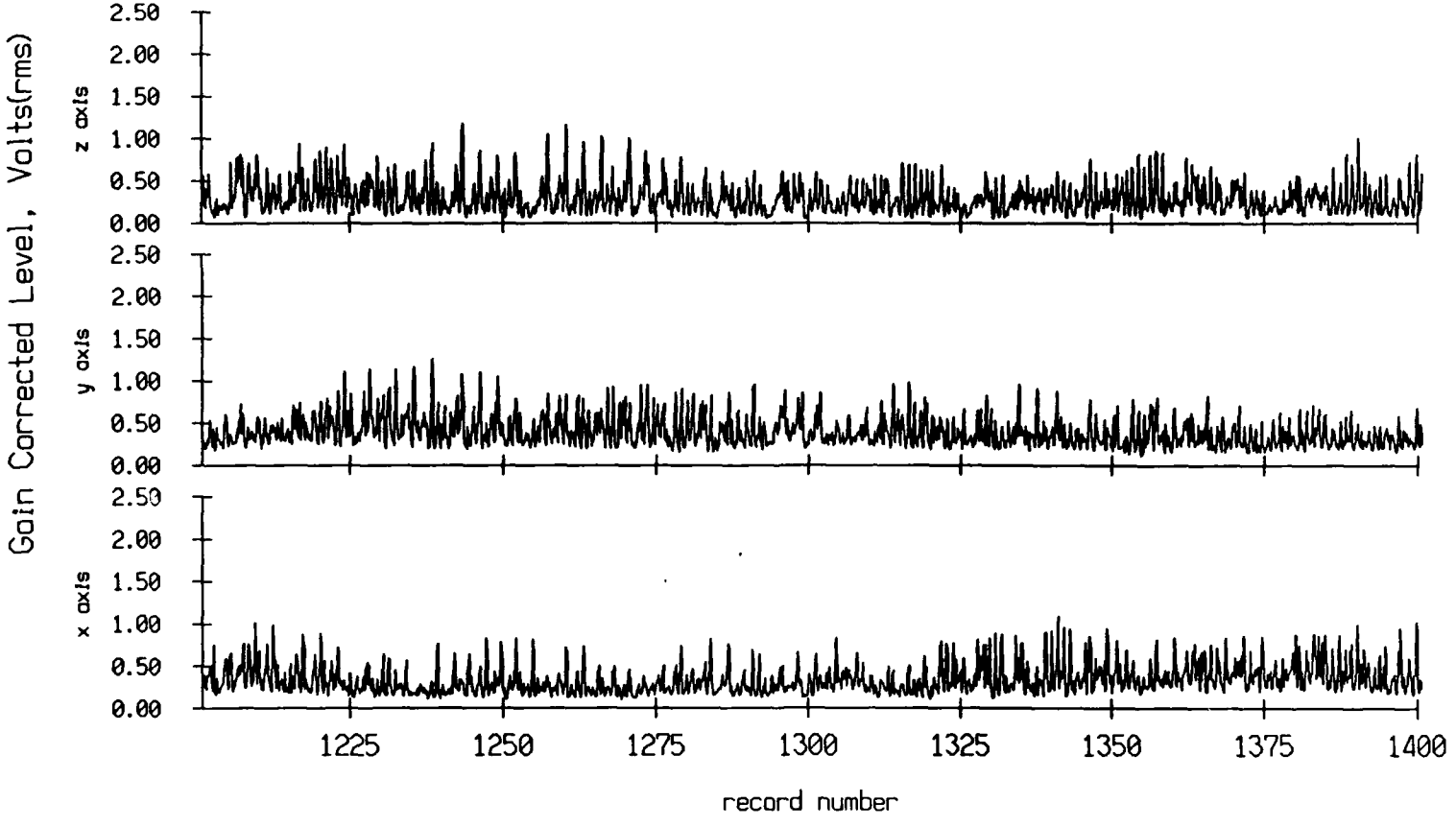

Float 0, August 1988 Sea Trip
averaging period = 5.00 sec.
RMS Velocity
Gain Corrected Level, Volts(rms)
z axis
y axis
x axis
2.50
2.00
1.50
1.00
0.50
0.00
1225
1250
1275
1300
1325
1350
1375
1400
record number

Figure X.4g

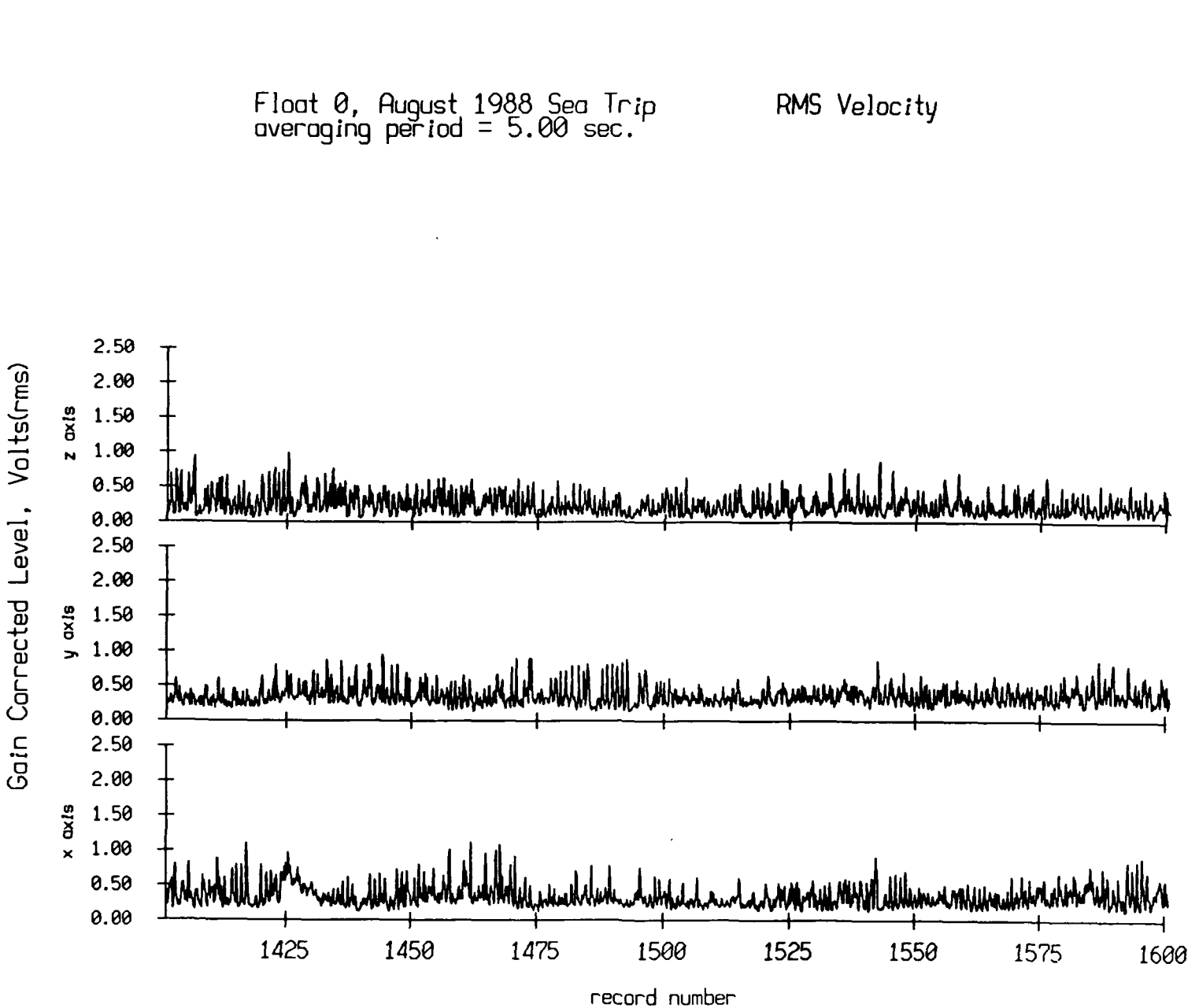

Float 0, August 1988 Sea Trip
averaging period = 5.00 sec.
RMS Velocity
Gain Corrected Level, Volts(rms)
z axis
y axis
x axis
2.50
2.00
1.50
1.00
0.50
0.00
1425
1450
1475
1500
1525
1550
1575
1600
record number

Figure X.4h

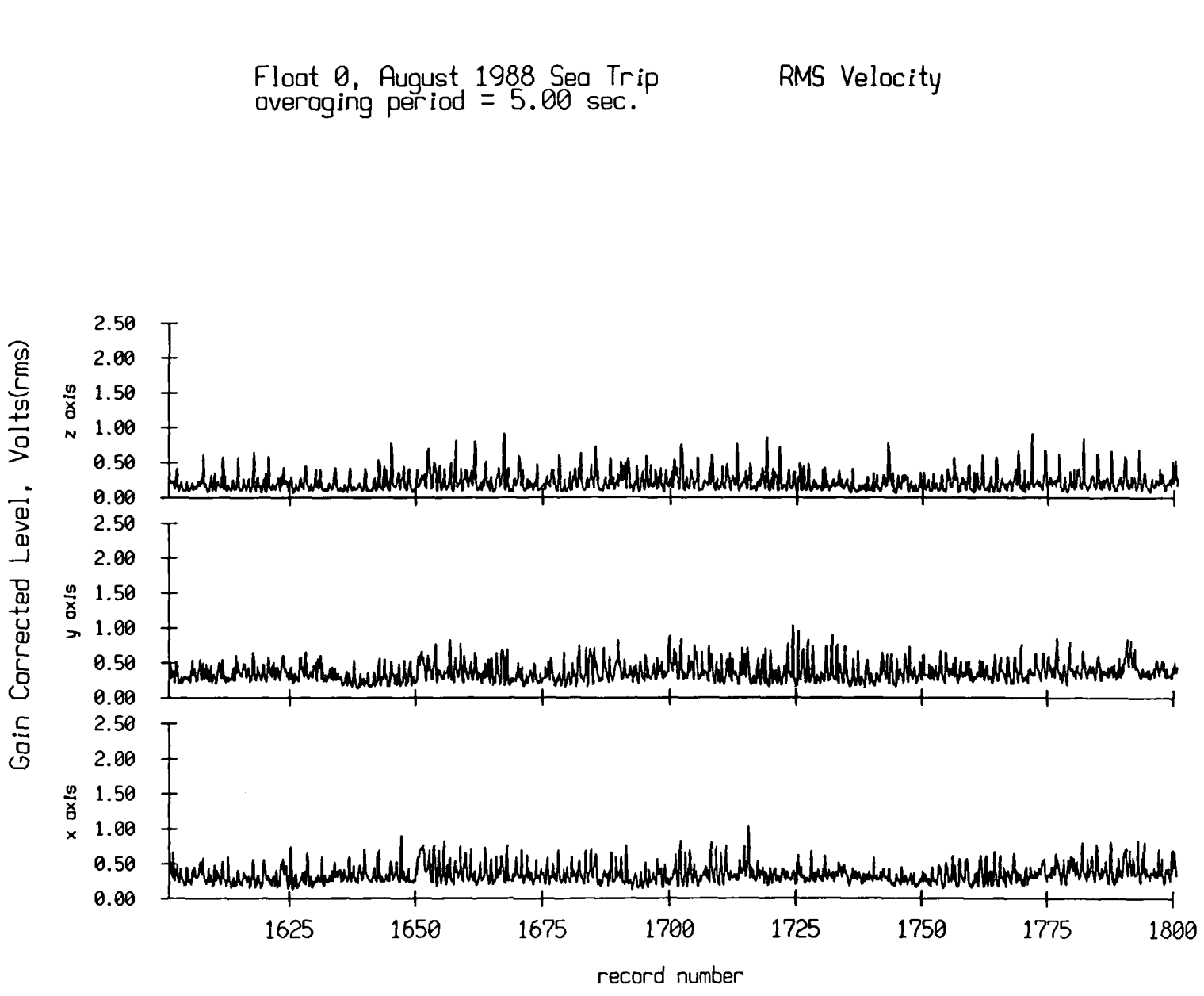

Float 0, August 1988 Sea Trip
averaging period = 5.00 sec.
RMS Velocity
Gain Corrected Level, Volts(rms)
z axis
y axis
x axis
2.50
2.00
1.50
1.00
0.50
0.00
1625
1650
1675
1700
1725
1750
1775
1800
record number

Figure X.4i

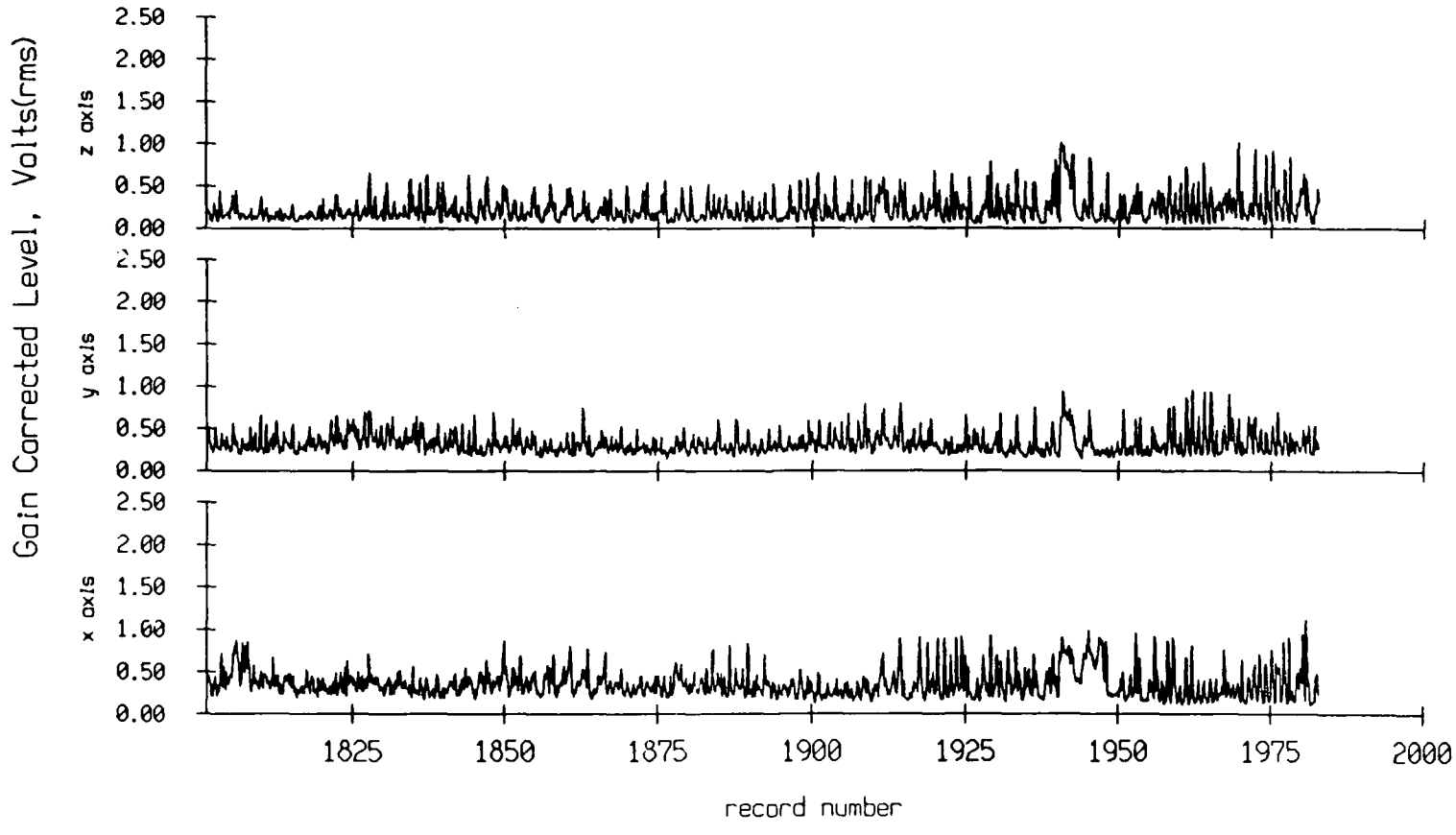

Float 0, August 1988 Sea Trip
averaging period = 5.00 sec.
RMS Velocity
Gain Corrected Level, Volts(rms)
z axis
y axis
x axis
2.50
2.00
1.50
1.00
0.50
0.00
1825
1850
1875
1900
1925
1950
1975
2000
record number

Figure X.4

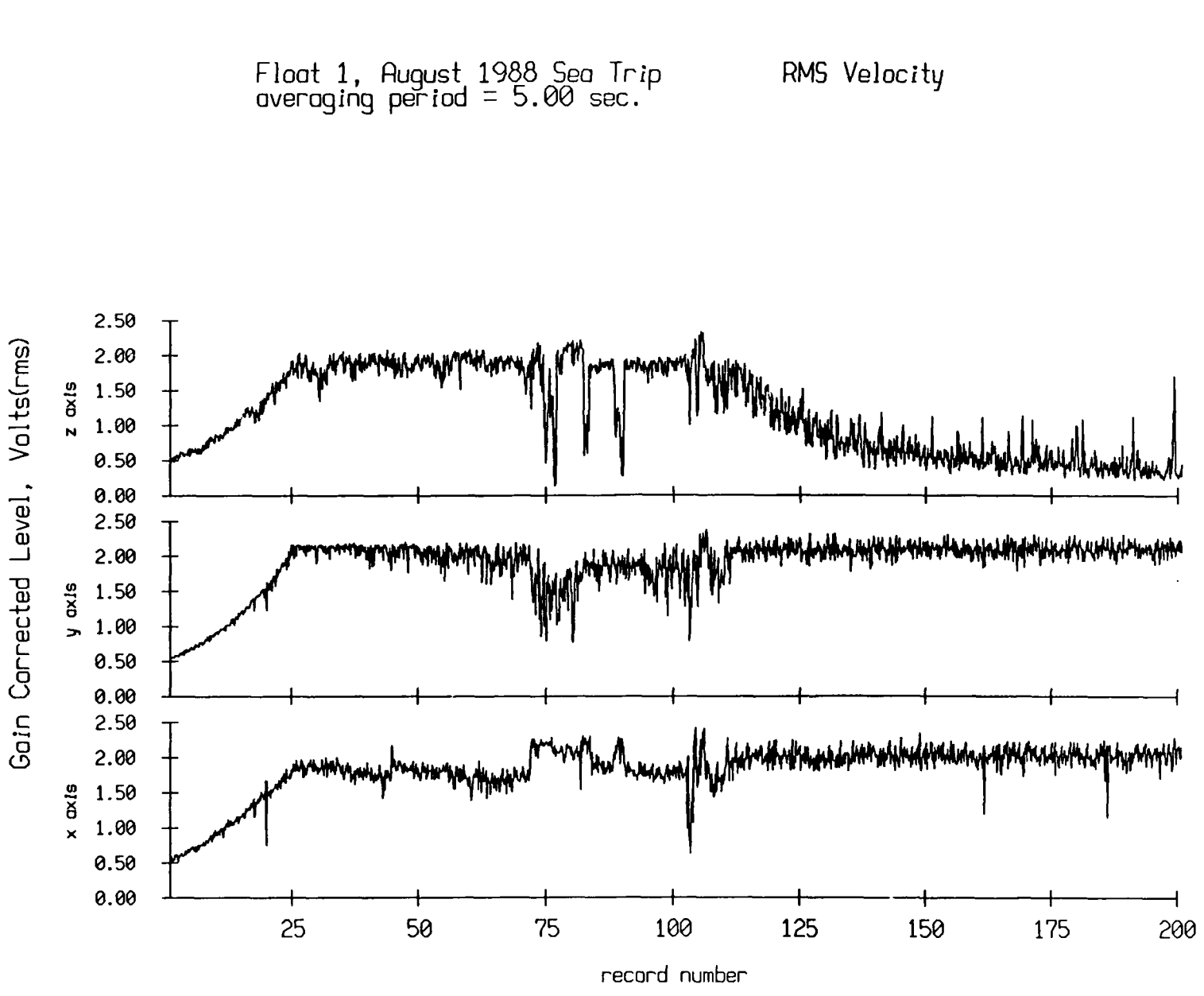

Float 1, August 1988 Sea Trip
averaging period = 5.00 sec.
RMS Velocity
Gain Corrected Level, Volts(rms)
z axis
y axis
x axis
2.50
2.00
1.50
1.00
0.50
0.00
25
50
75
100
125
150
175
200
record number

Figure X.5a

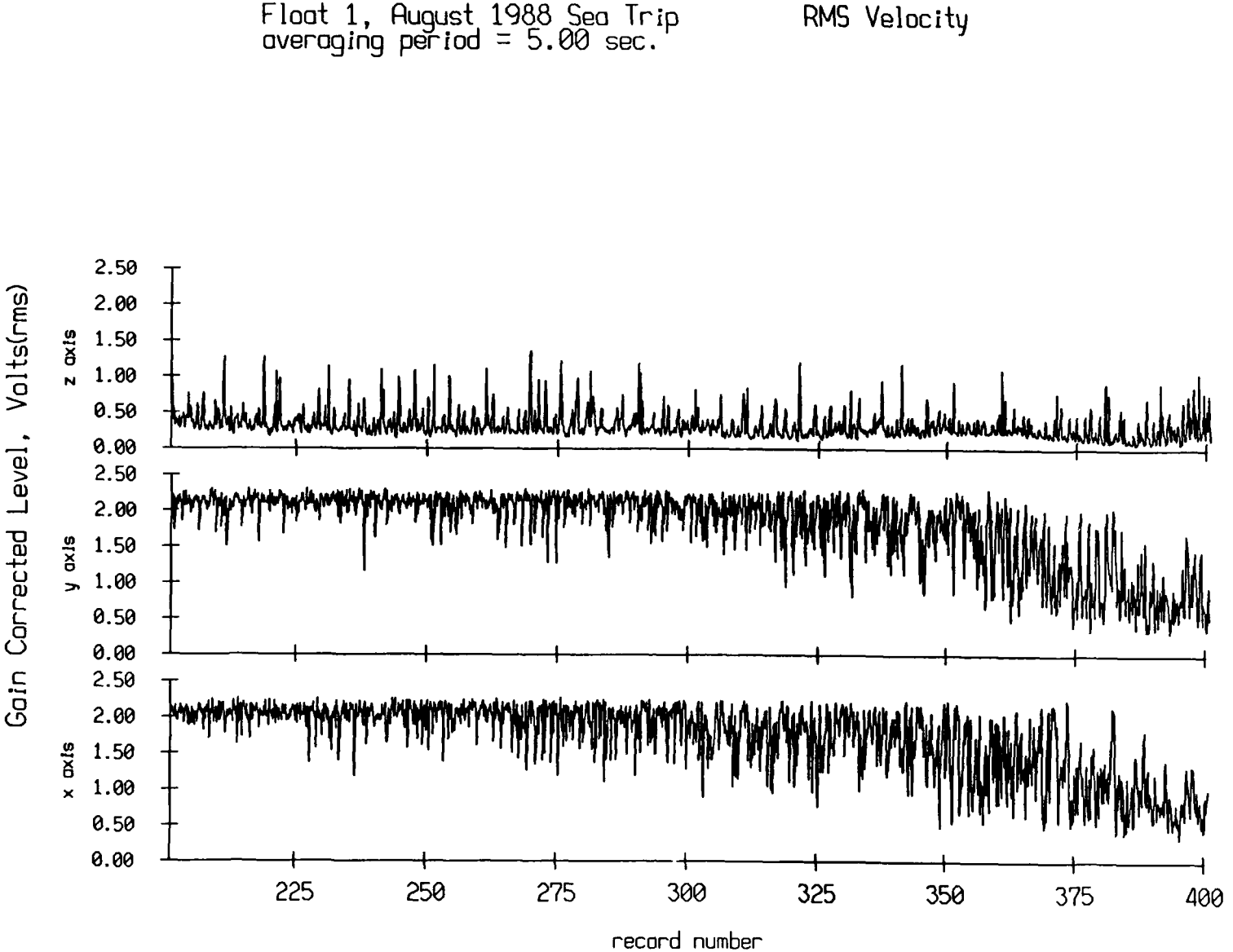

Float 1, August 1988 Sea Trip
averaging period = 5.00 sec.
RMS Velocity
Gain Corrected Level, Volts(rms)
z axis
y axis
x axis
2.50
2.00
1.50
1.00
0.50
0.00
225
250
275
300
325
350
375
400
record number

Figure X.5b

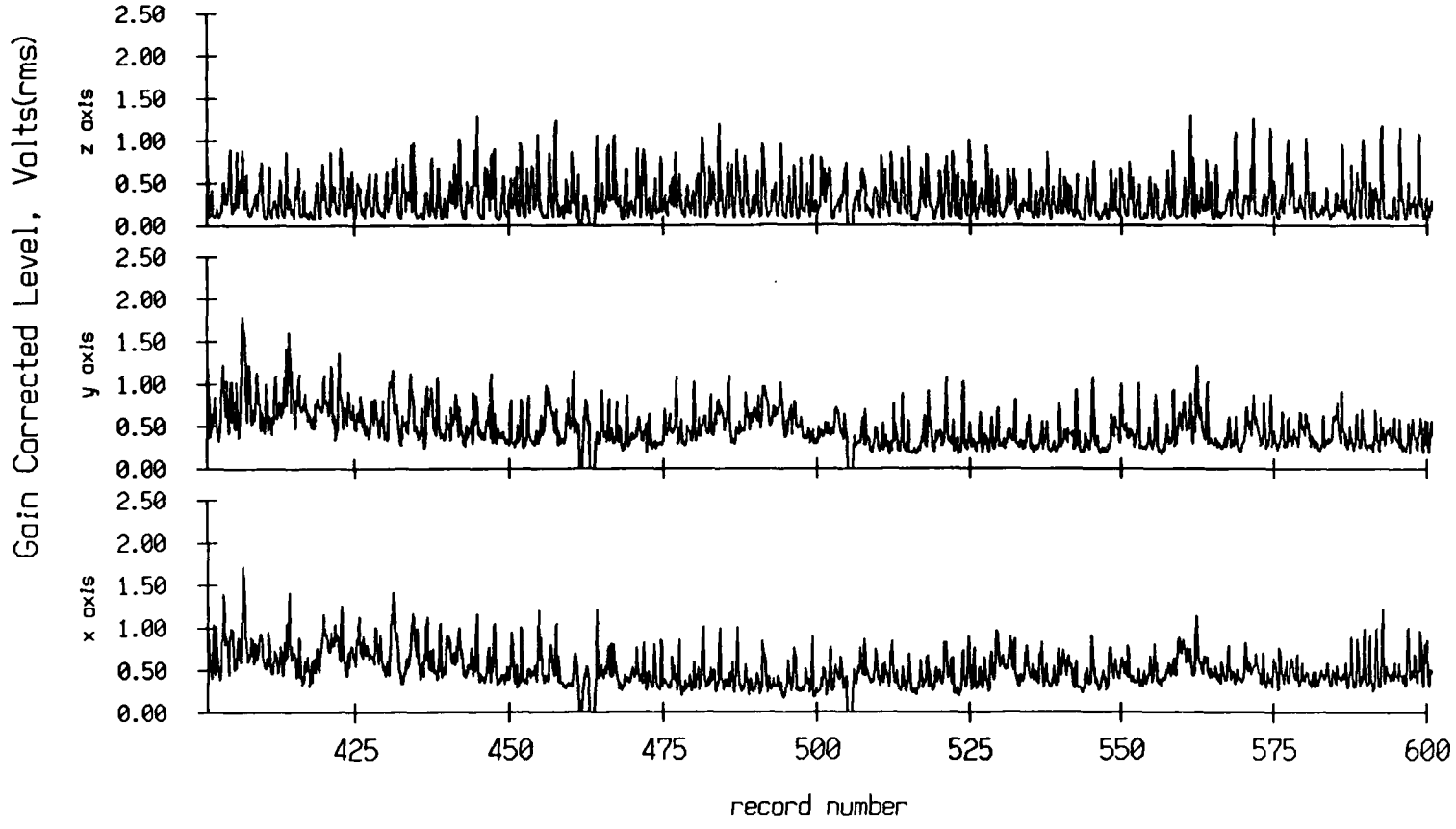

Float 1, August 1988 Sea Trip
averaging period = 5.00 sec.
RMS Velocity
Gain Corrected Level, Volts(rms)
z axis
y axis
x axis
2.50
2.00
1.50
1.00
0.50
0.00
425
450
475
500
525
550
575
600
record number

Figure X.5c

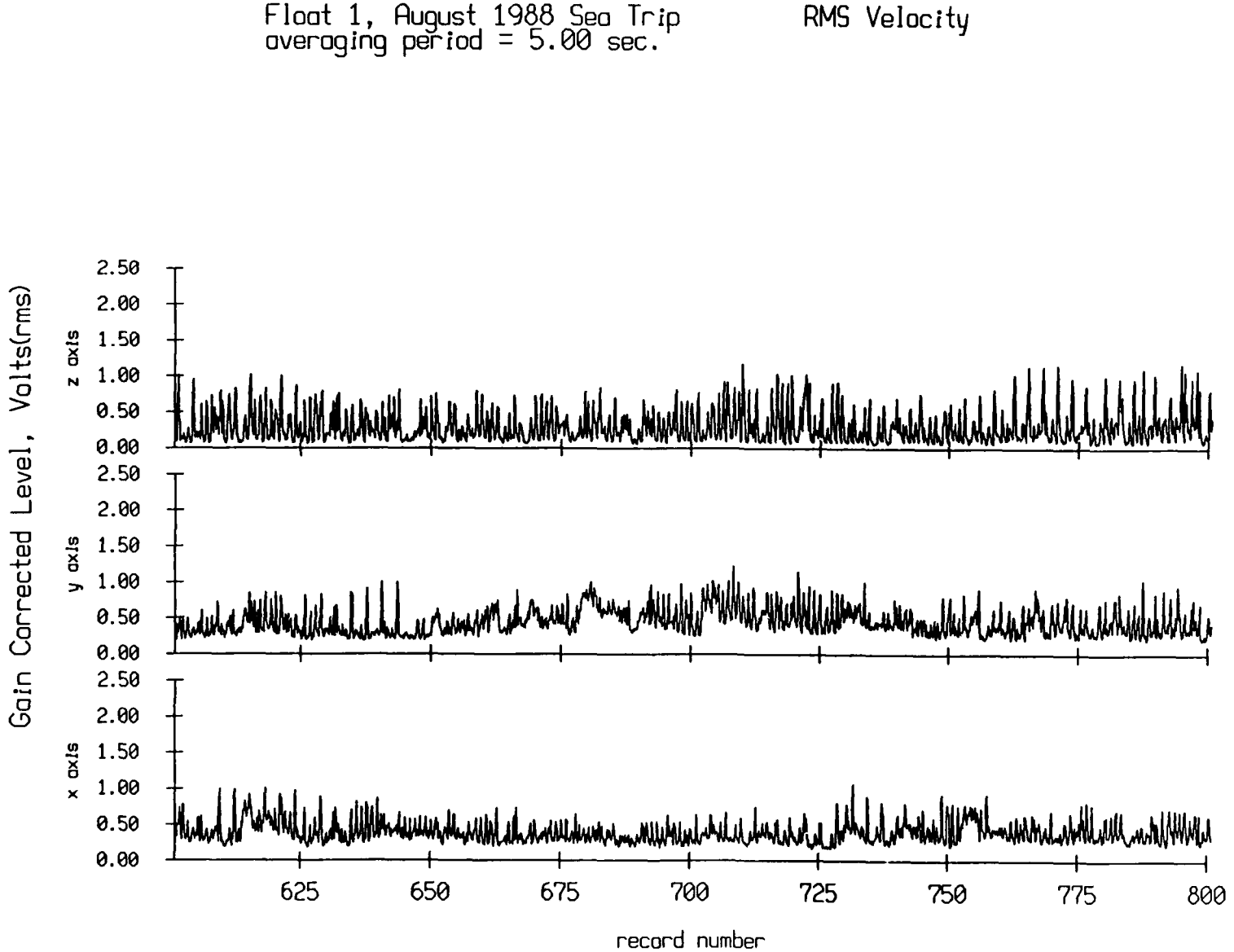

Float 1, August 1988 Sea Trip
averaging period = 5.00 sec.
RMS Velocity
Gain Corrected Level, Volts(rms)
z axis
y axis
x axis
2.50
2.00
1.50
1.00
0.50
0.00
625
650
675
700
725
750
775
800
record number

Figure X.5d

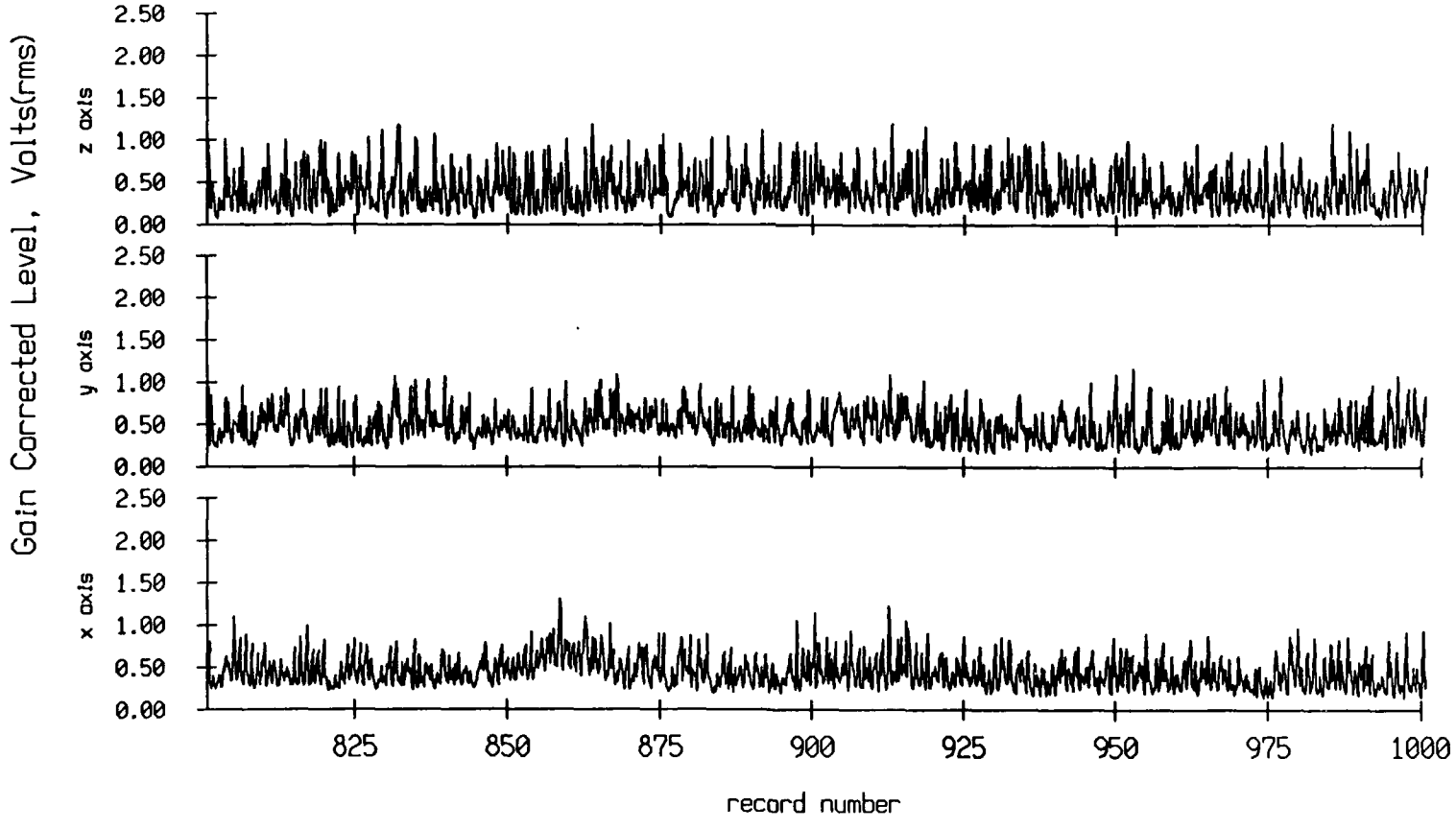

Float 1, August 1988 Sea Trip
averaging period = 5.00 sec.
RMS Velocity
Gain Corrected Level, Volts(rms)
z axis
y axis
x axis
2.50
2.00
1.50
1.00
0.50
0.00
825
850
875
900
925
950
975
1000
record number

Figure X.5e

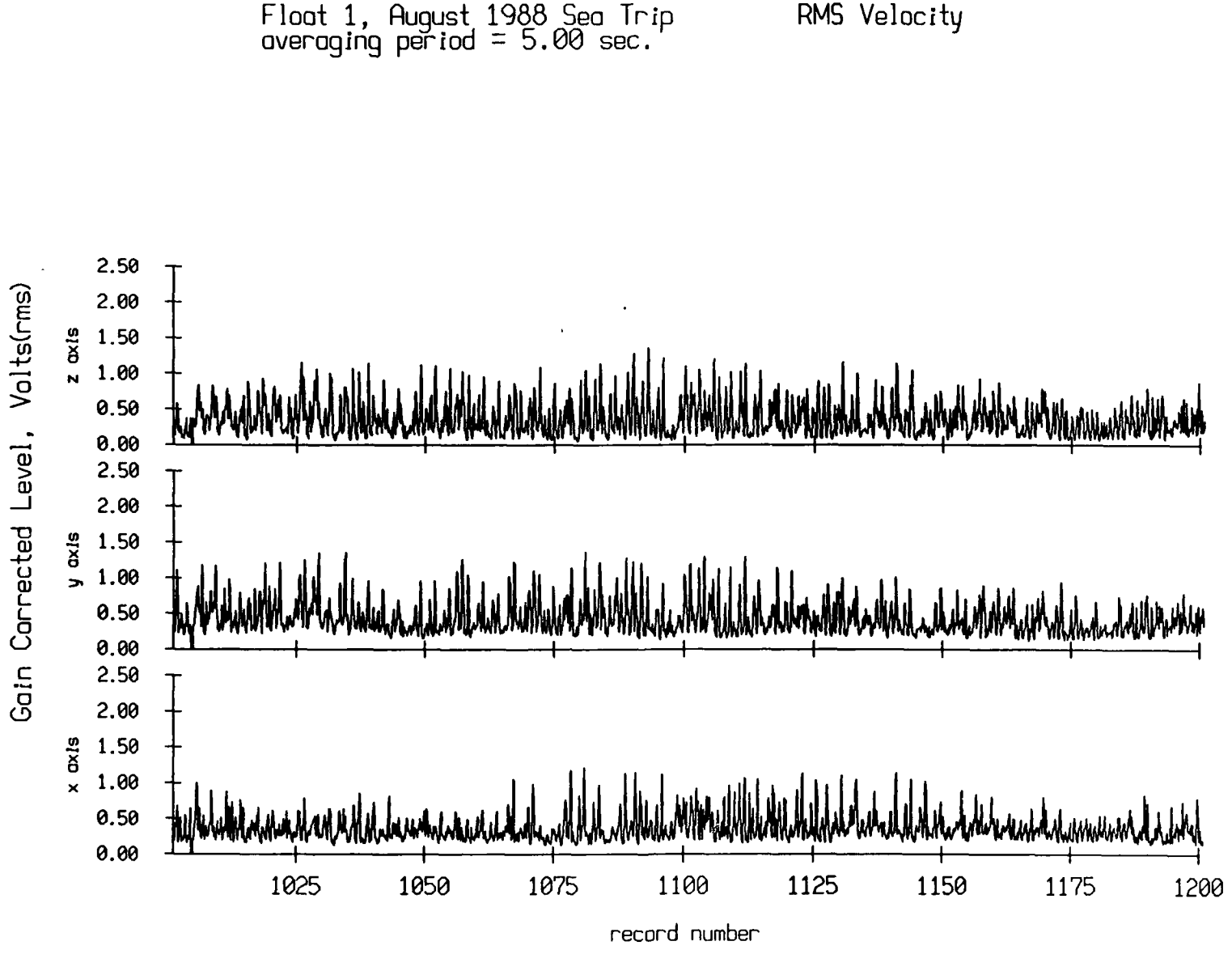

Float 1, August 1988 Sea Trip
averaging period = 5.00 sec.
RMS Velocity
Gain Corrected Level, Volts(rms)
z axis
y axis
x axis
2.50
2.00
1.50
1.00
0.50
0.00
1025
1050
1075
1100
1125
1150
1175
1200
record number

Figure X.5f

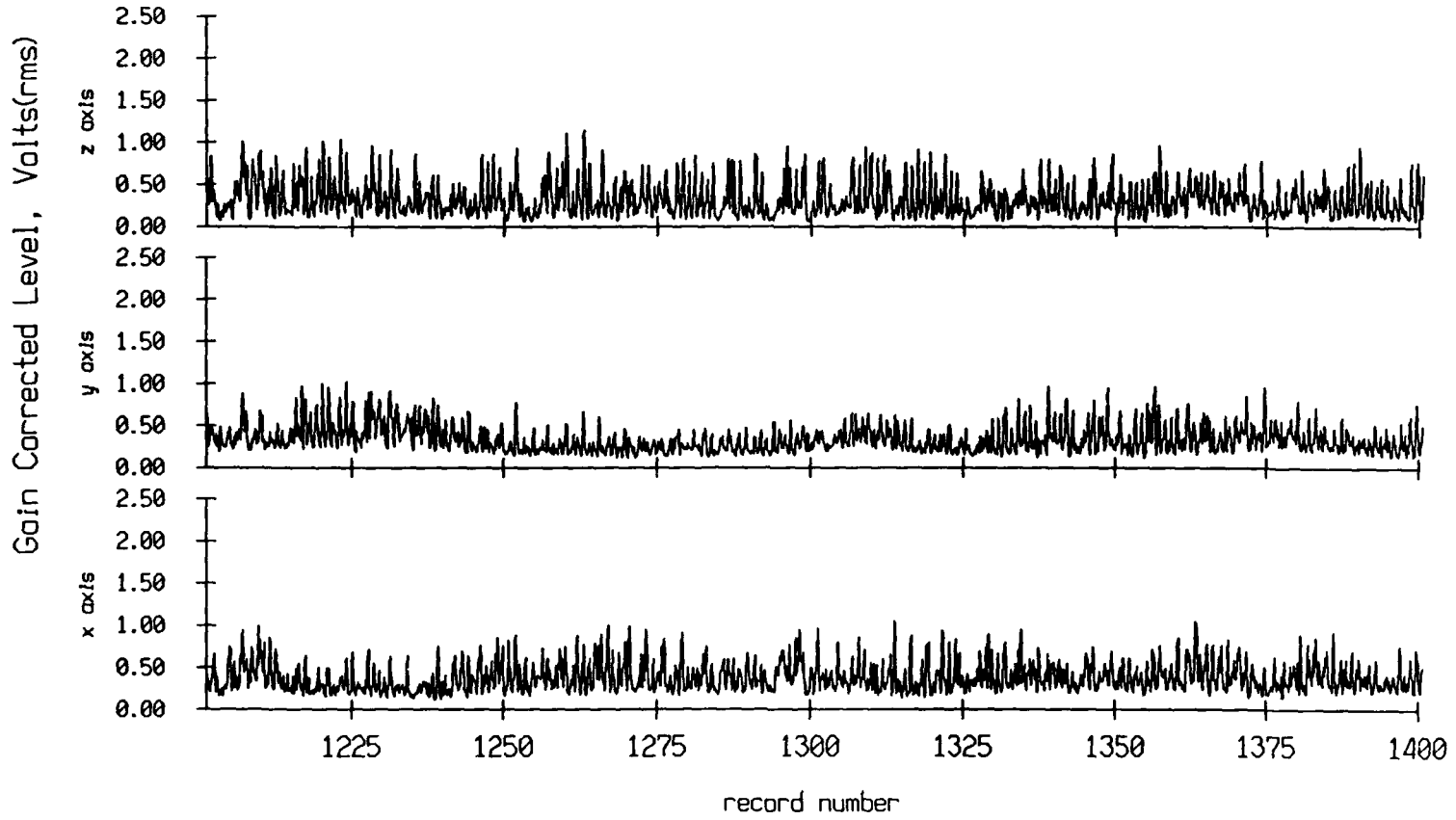

Float 1, August 1988 Sea Trip
averaging period = 5.00 sec.
RMS Velocity
Gain Corrected Level, Volts(rms)
z axis
y axis
x axis
2.50
2.00
1.50
1.00
0.50
0.00
1225
1250
1275
1300
1325
1350
1375
1400
record number

Figure X 5g

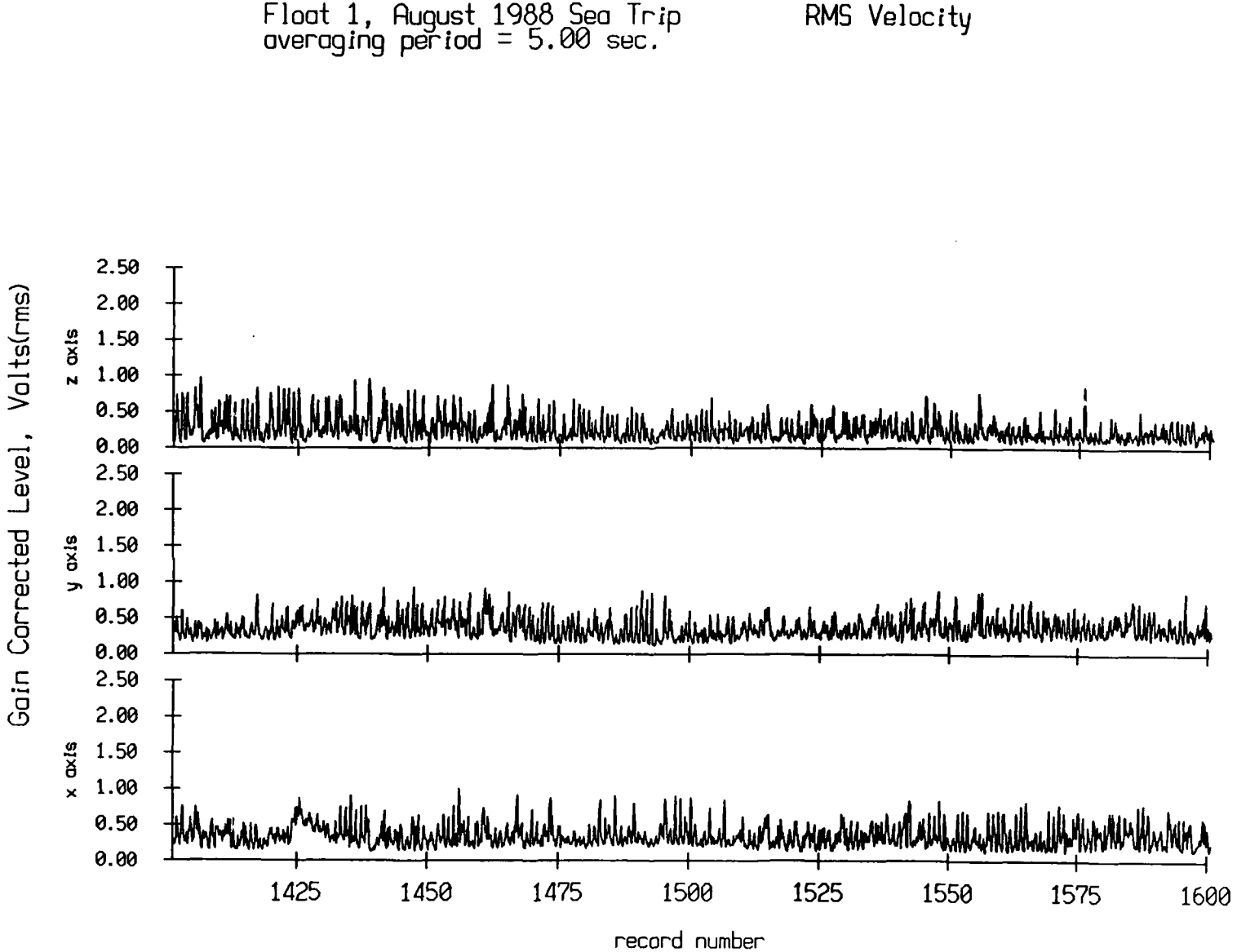

Float 1, August 1988 Sea Trip
averaging period = 5.00 sec.
RMS Velocity
Gain Corrected Level, Volts(rms)
z axis
y axis
x axis
2.50
2.00
1.50
1.00
0.50
0.00
1425
1450
1475
1500
1525
1550
1575
1600
record number

Figure X.5h

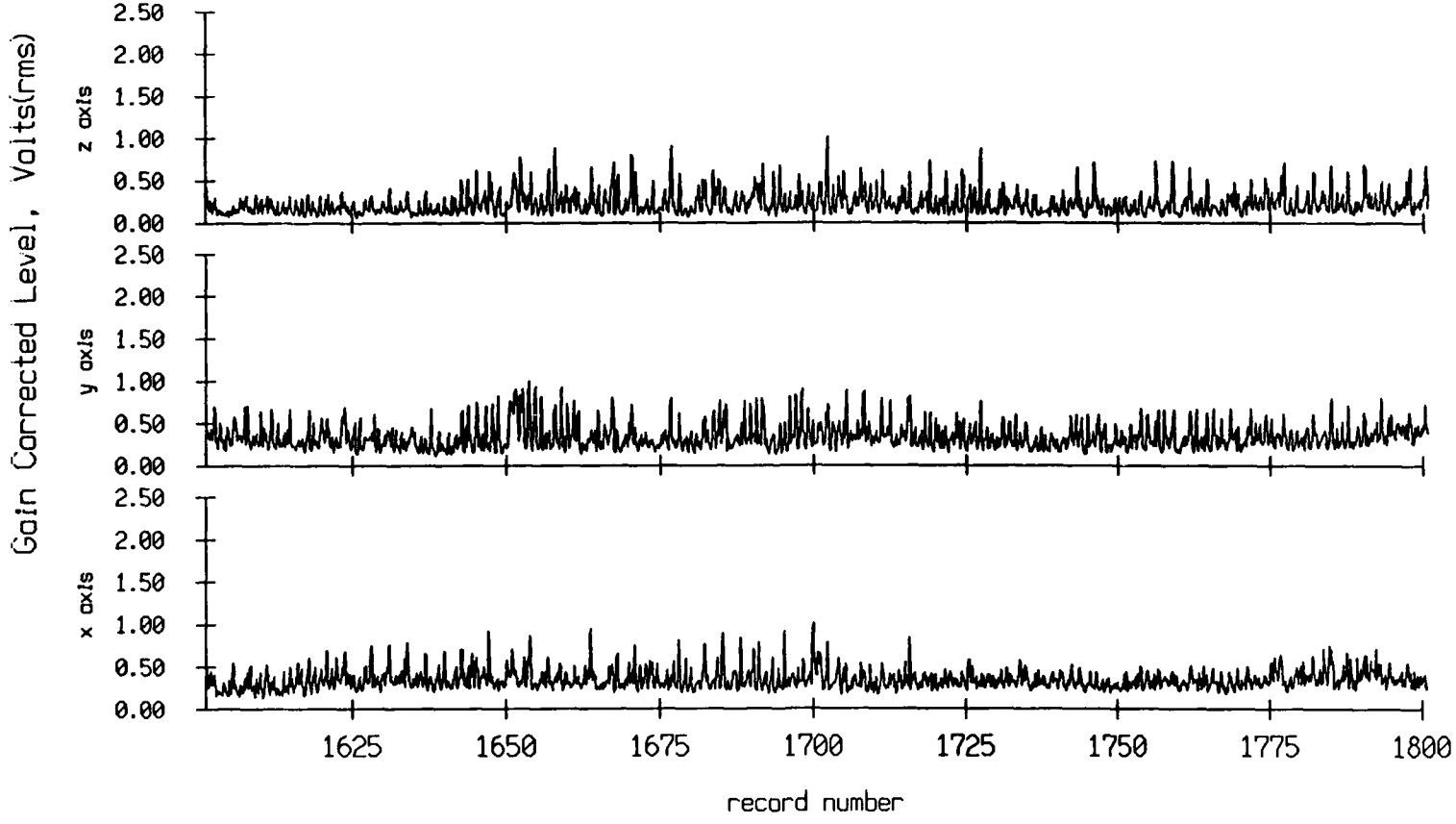

Float 1, August 1988 Sea Trip
averaging period = 5.00 sec.
RMS Velocity
Gain Corrected Level, Volts(rms)
z axis
y axis
x axis
2.50
2.00
1.50
1.00
0.50
0.00
1625
1650
1675
1700
1725
1750
1775
1800
record number

Figure X.5i

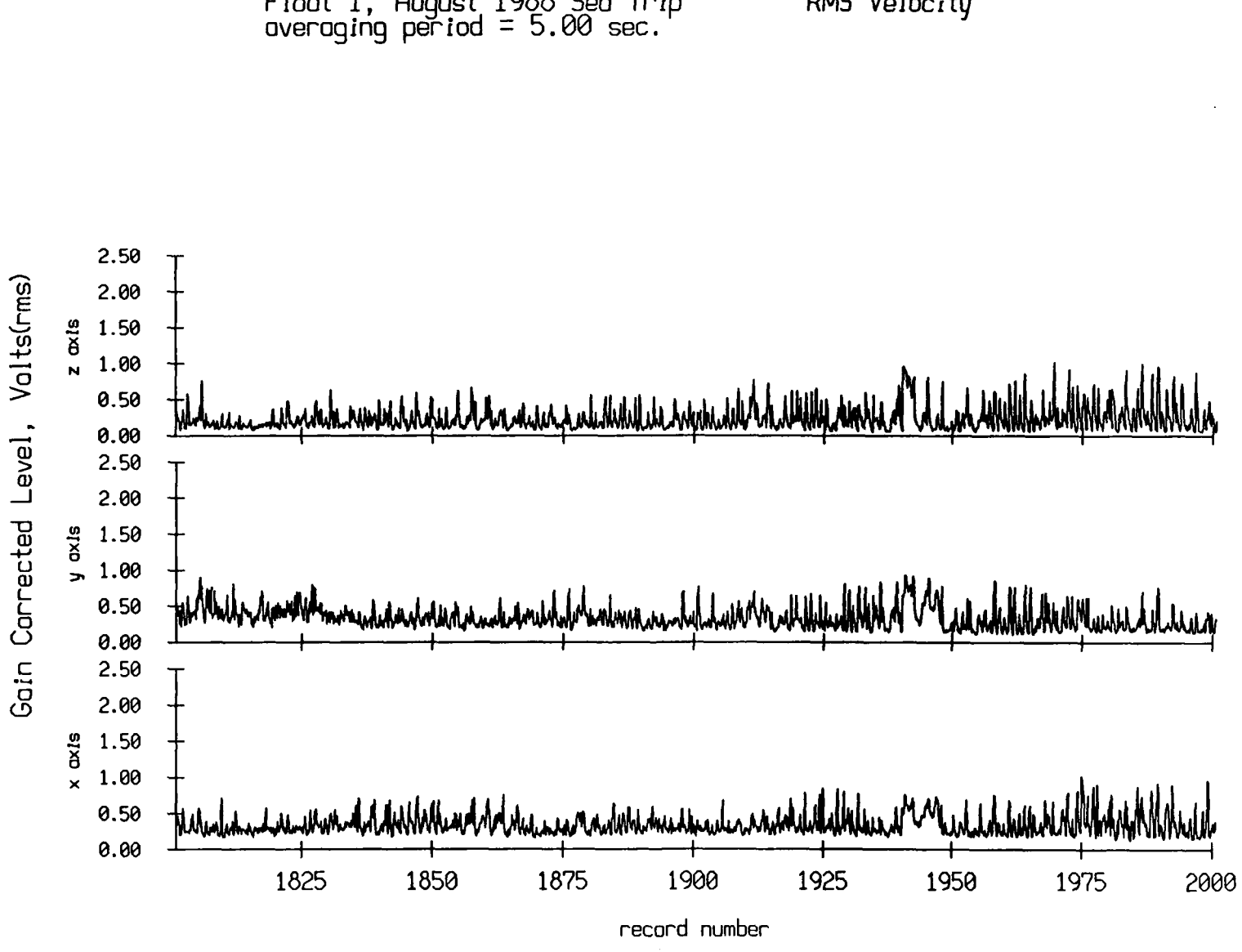

Float 1, August 1988 Sea Trip
averaging period = 5.00 sec.
RMS Velocity
Gain Corrected Level, Volts(rms)
z axis
y axis
x axis
2.50
2.00
1.50
1.00
0.50
0.00
1825
1850
1875
1900
1925
1950
1975
2000
record number

Figure X.5j

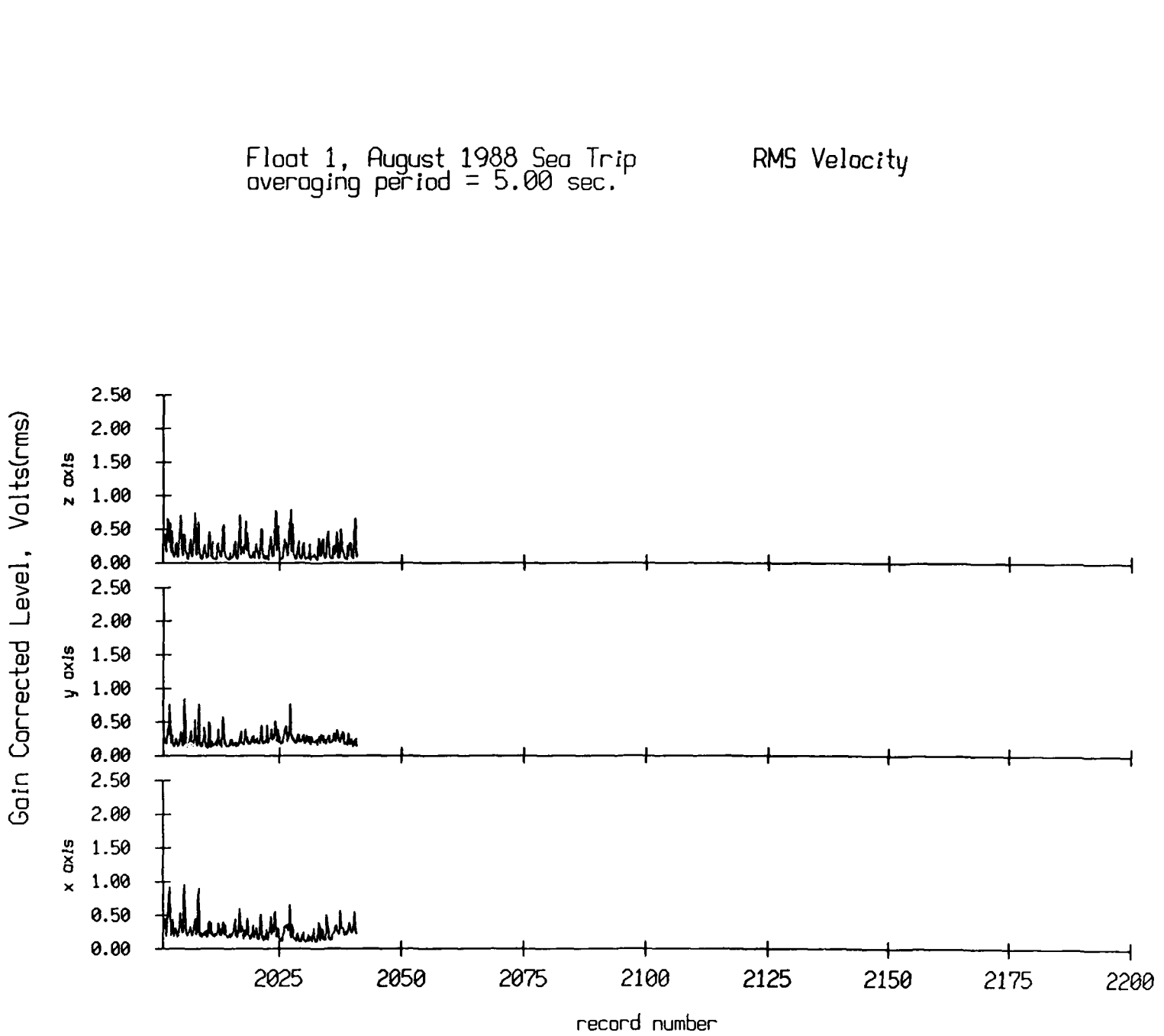

Float 1, August 1988 Sea Trip
averaging period = 5.00 sec.
RMS Velocity
Gain Corrected Level, Volts(rms)
z axis
y axis
x axis
2.50
2.00
1.50
1.00
0.50
0.00
2025
2050
2075
2100
2125
2150
2175
2200
record number

Figure X.5k

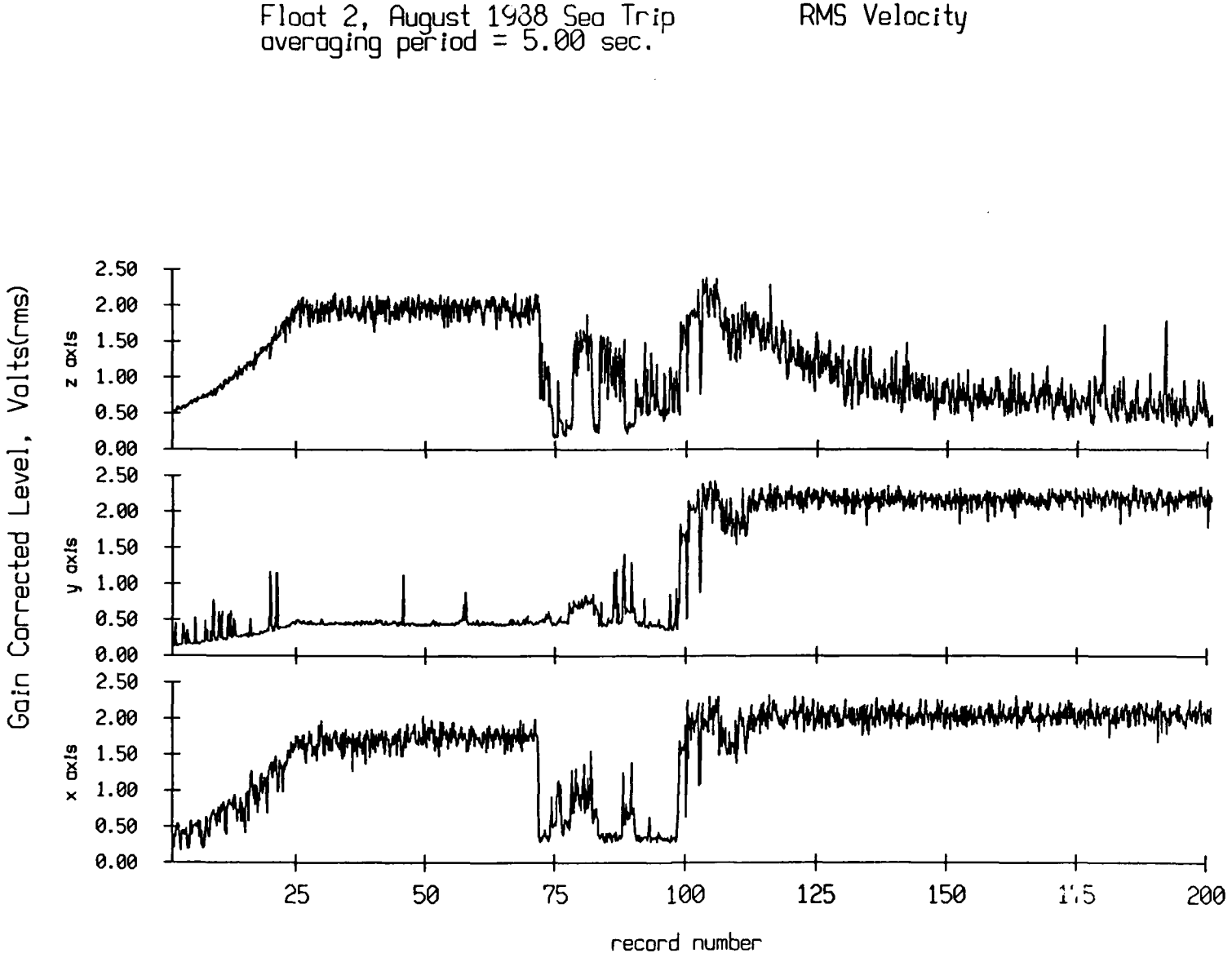

Float 2, August 1988 Sea Trip
averaging period = 5.00 sec.
RMS Velocity
Gain Corrected Level, Volts(rms)
z axis
y axis
x axis
2.50
2.00
1.50
1.00
0.50
0.00
25
50
75
100
125
150
175
200
record number

Figure X.6a

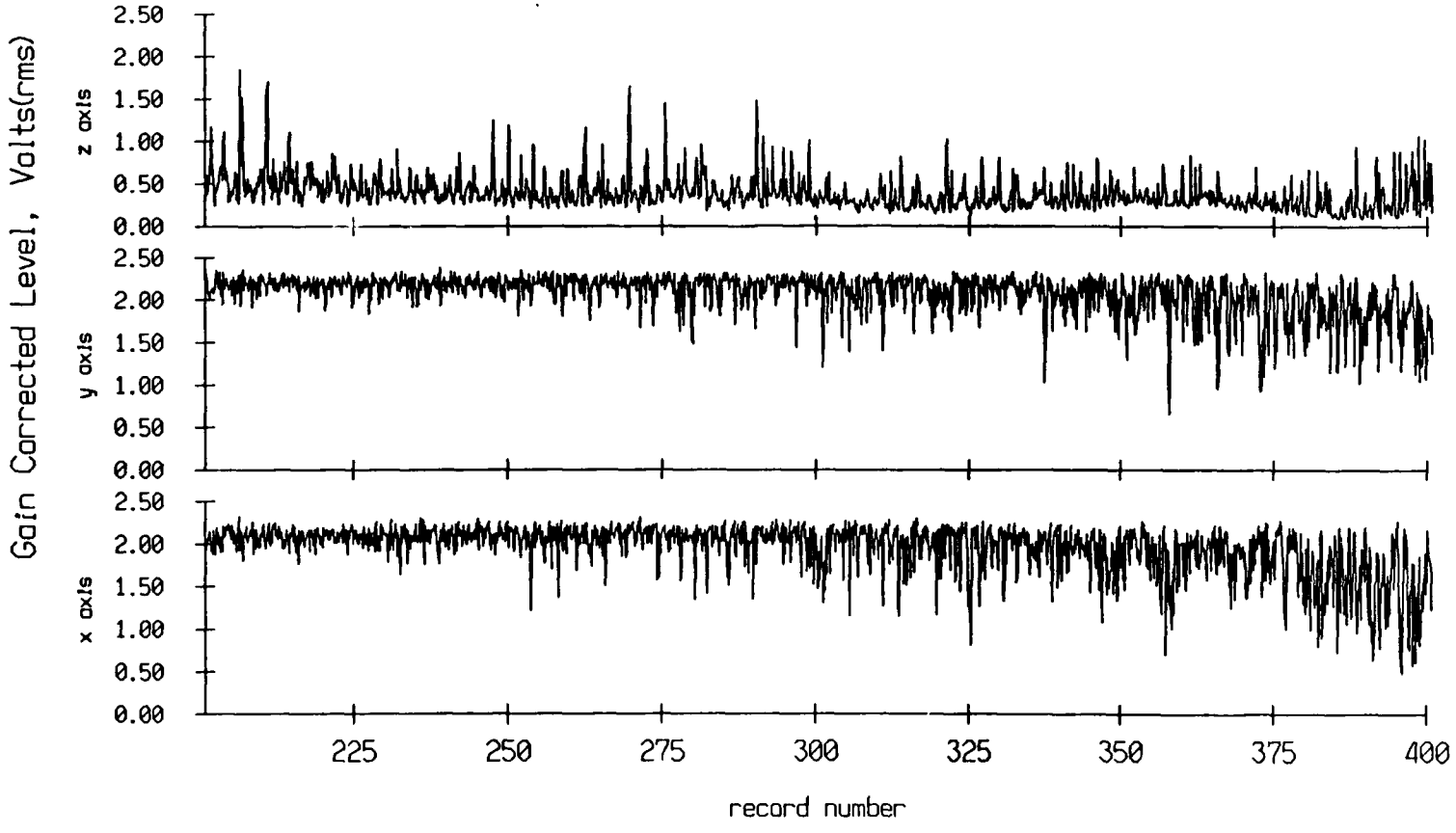

Float 2, August 1988 Sea Trip
averaging period = 5.00 sec.
RMS Velocity
Gain Corrected Level, Volts(rms)
z axis
y axis
x axis
2.50
2.00
1.50
1.00
0.50
0.00
225
250
275
300
325
350
375
400
record number

Figure X.6b

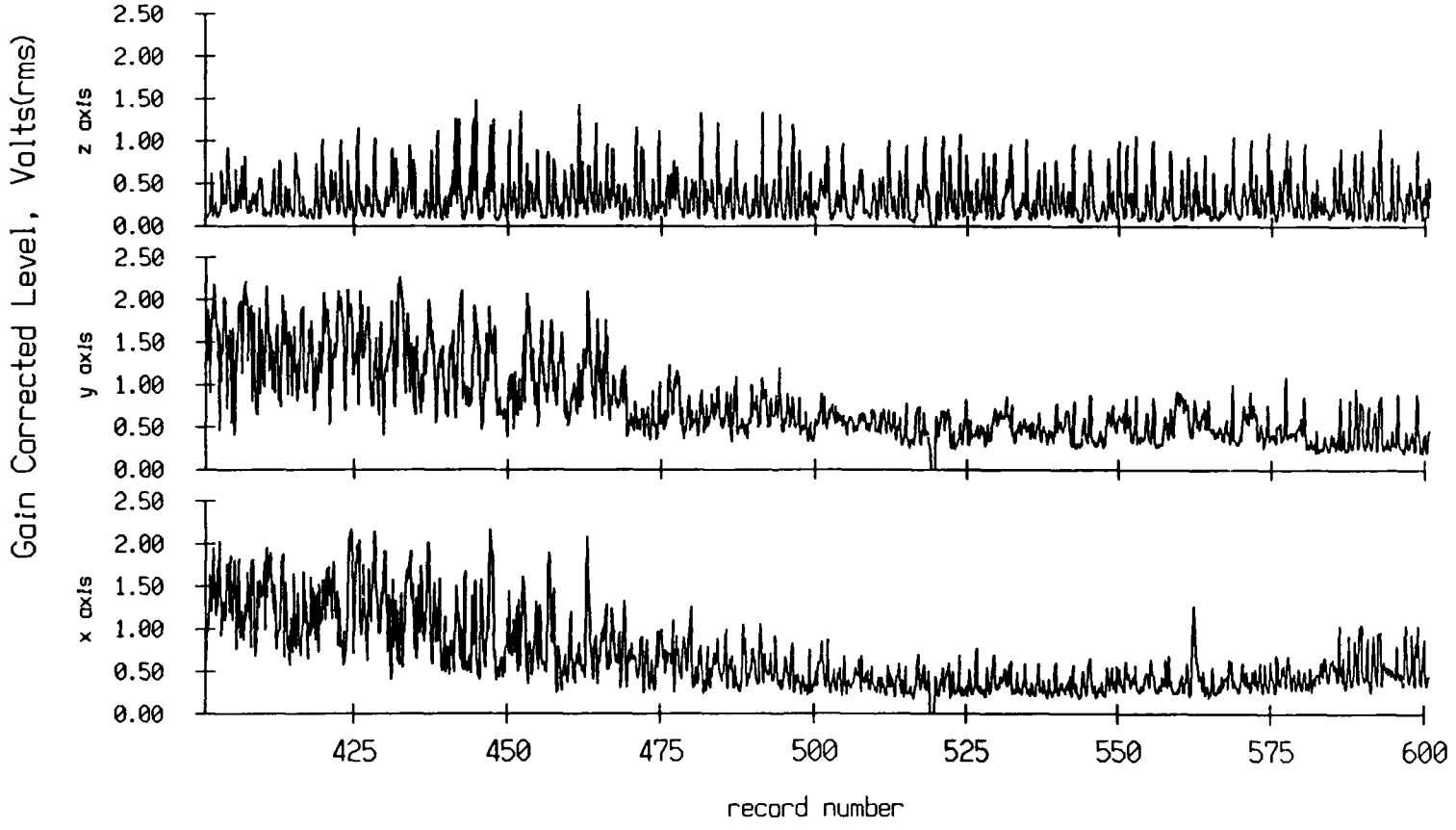

Float 2, August 1988 Sea Trip
averaging period = 5.00 sec.
RMS Velocity
Gain Corrected Level, Volts(rms)
z axis
y axis
x axis
2.50
2.00
1.50
1.00
0.50
0.00
425
450
475
500
525
550
575
600
record number

Figure X.6c

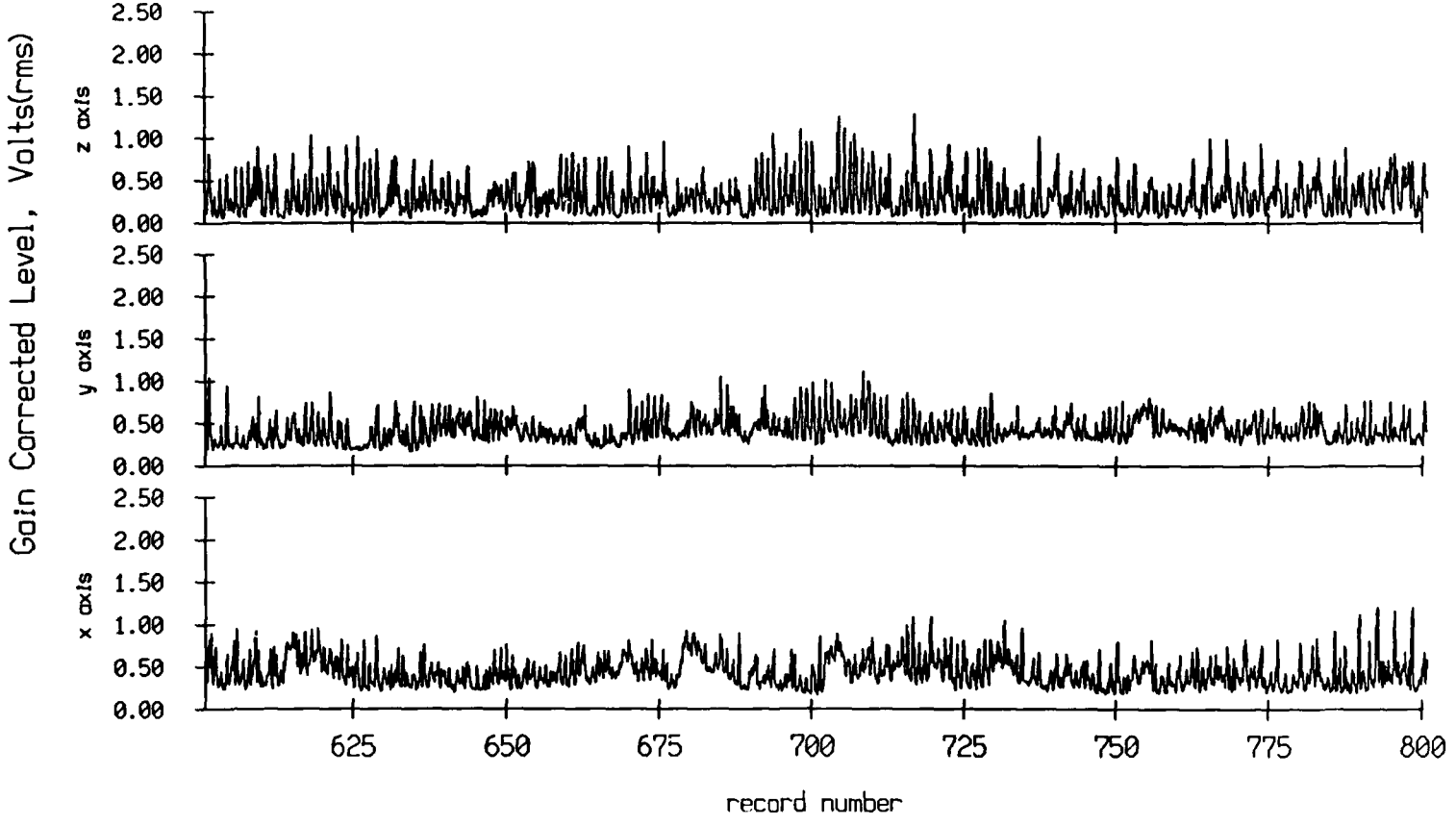

Float 2, August 1988 Sea Trip
averaging period = 5.00 sec.
RMS Velocity
Gain Corrected Level, Volts(rms)
z axis
y axis
x axis
2.50
2.00
1.50
1.00
0.50
0.00
625
650
675
700
725
750
775
800
record number

Figure X.6d

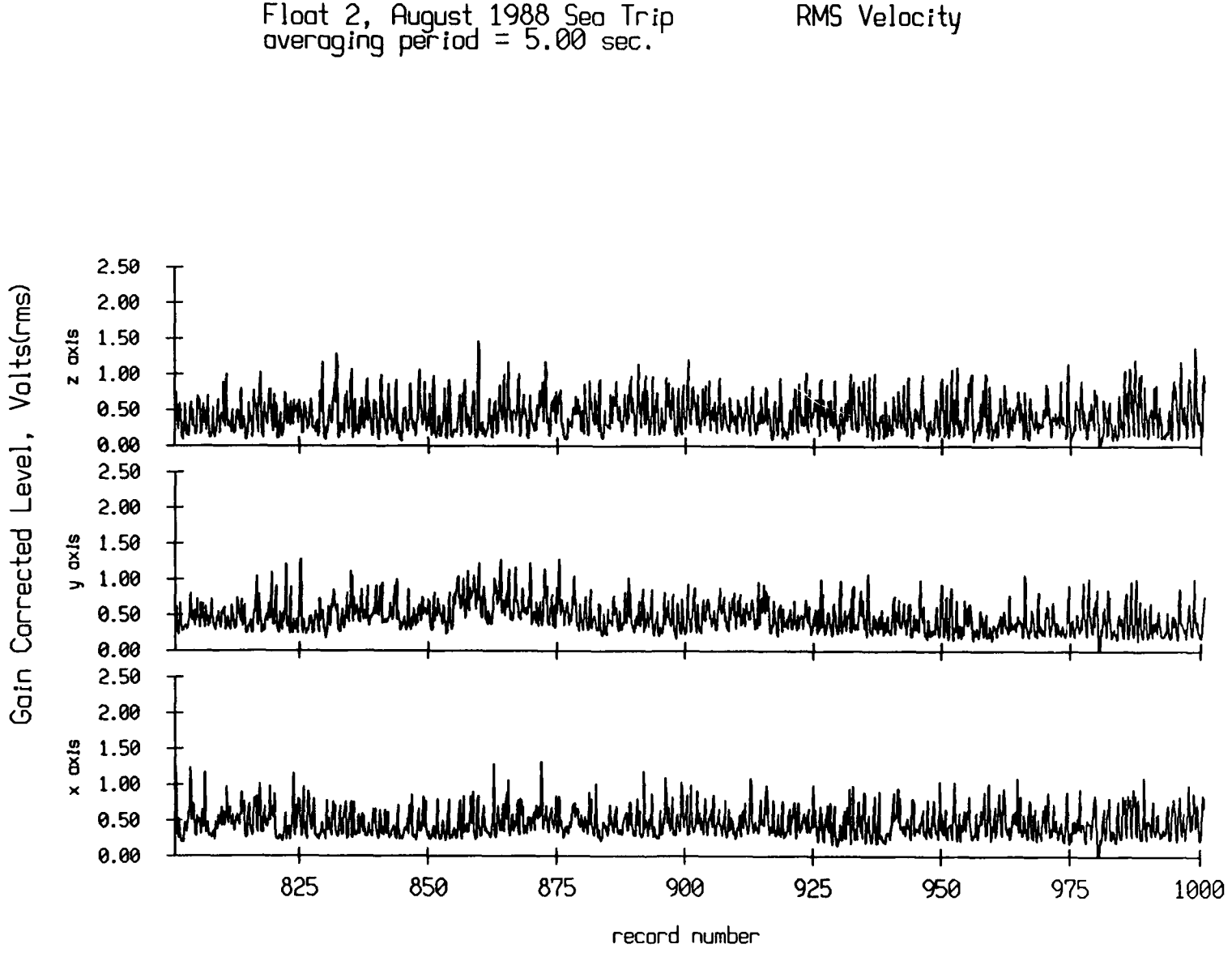

Float 2, August 1988 Sea Trip
averaging period = 5.00 sec.
RMS Velocity
Gain Corrected Level, Volts(rms)
z axis
y axis
x axis
2.50
2.00
1.50
1.00
0.50
0.00
825
850
875
900
925
950
975
1000
record number

Figure X.6e

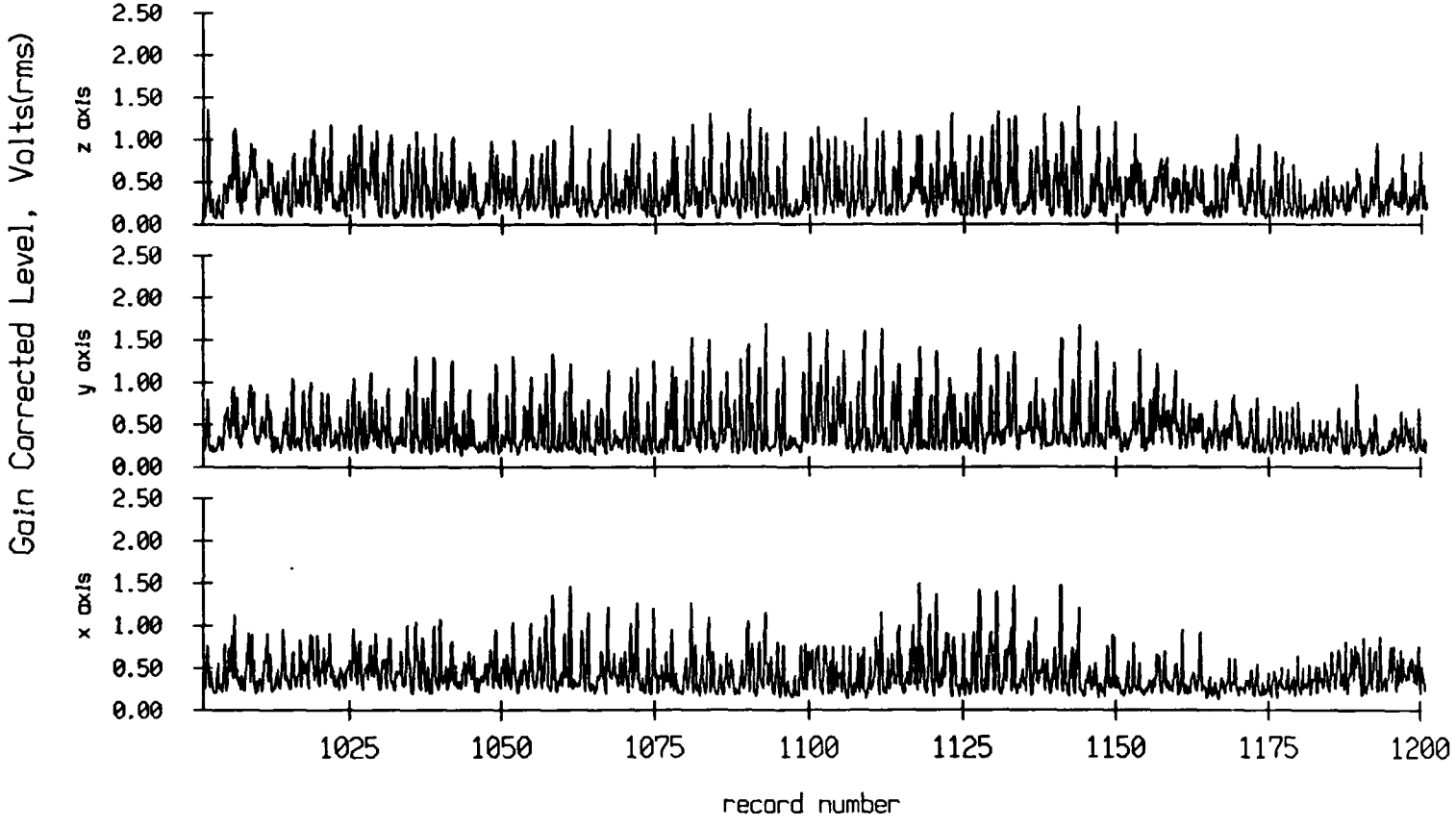
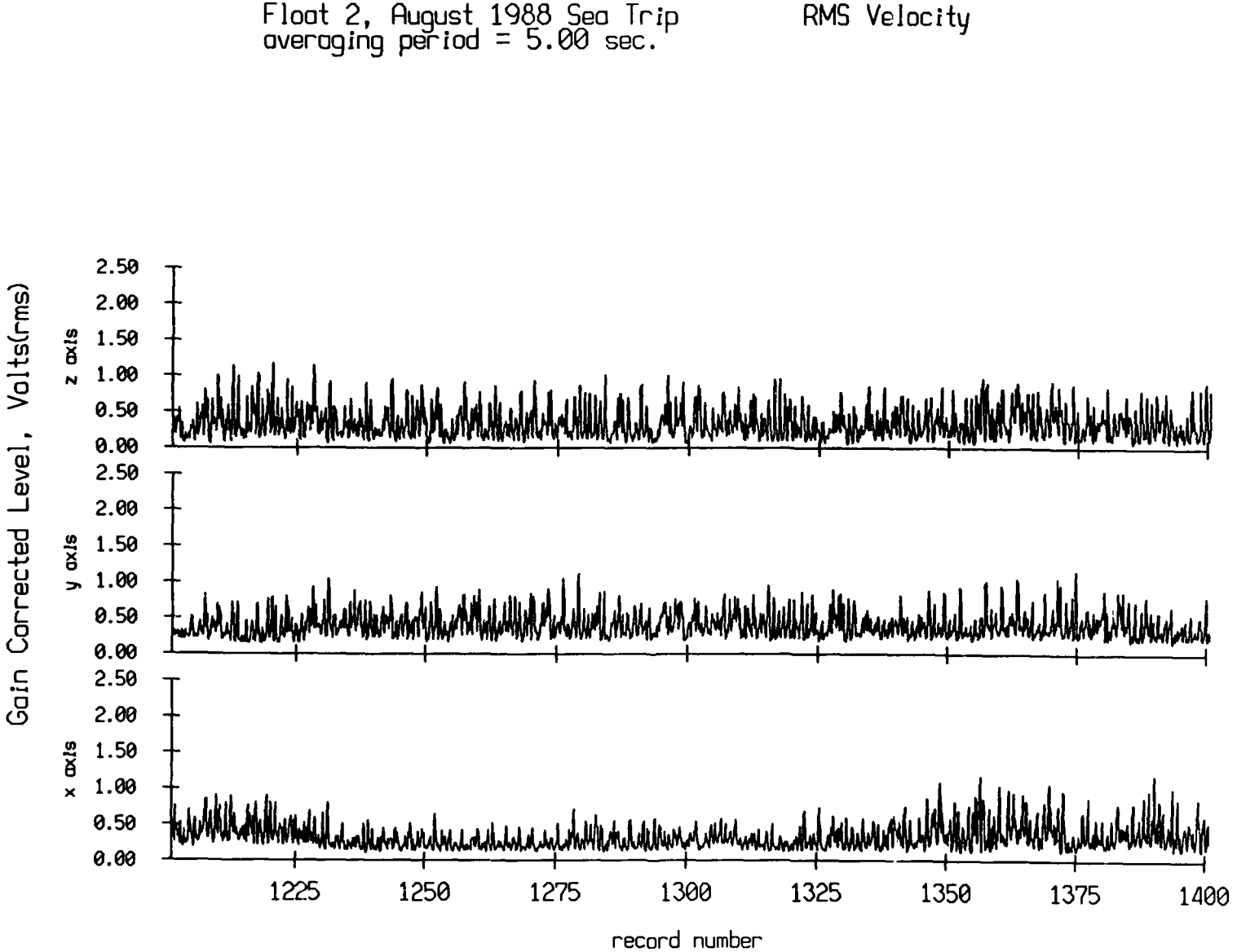

Float 2, August 1988 Sea Trip
averaging period = 5.00 sec.
RMS Velocity
Gain Corrected Level, Volts(rms)
z axis
y axis
x axis
2.50
2.00
1.50
1.00
0.50
0.00
1025
1050
1075
1100
1125
1150
1175
1200
record number

Figure X.6f

Figure X.8g


Float 2, August 1988 Sea Trip
averaging period = 5.00 sec.
RMS Velocity
Gain Corrected Level, Volts(rms)
z axis
y axis
x axis
2.50
2.00
1.50
1.00
0.50
0.00
1225
1250
1275
1300
1325
1350
1375
1400
record number

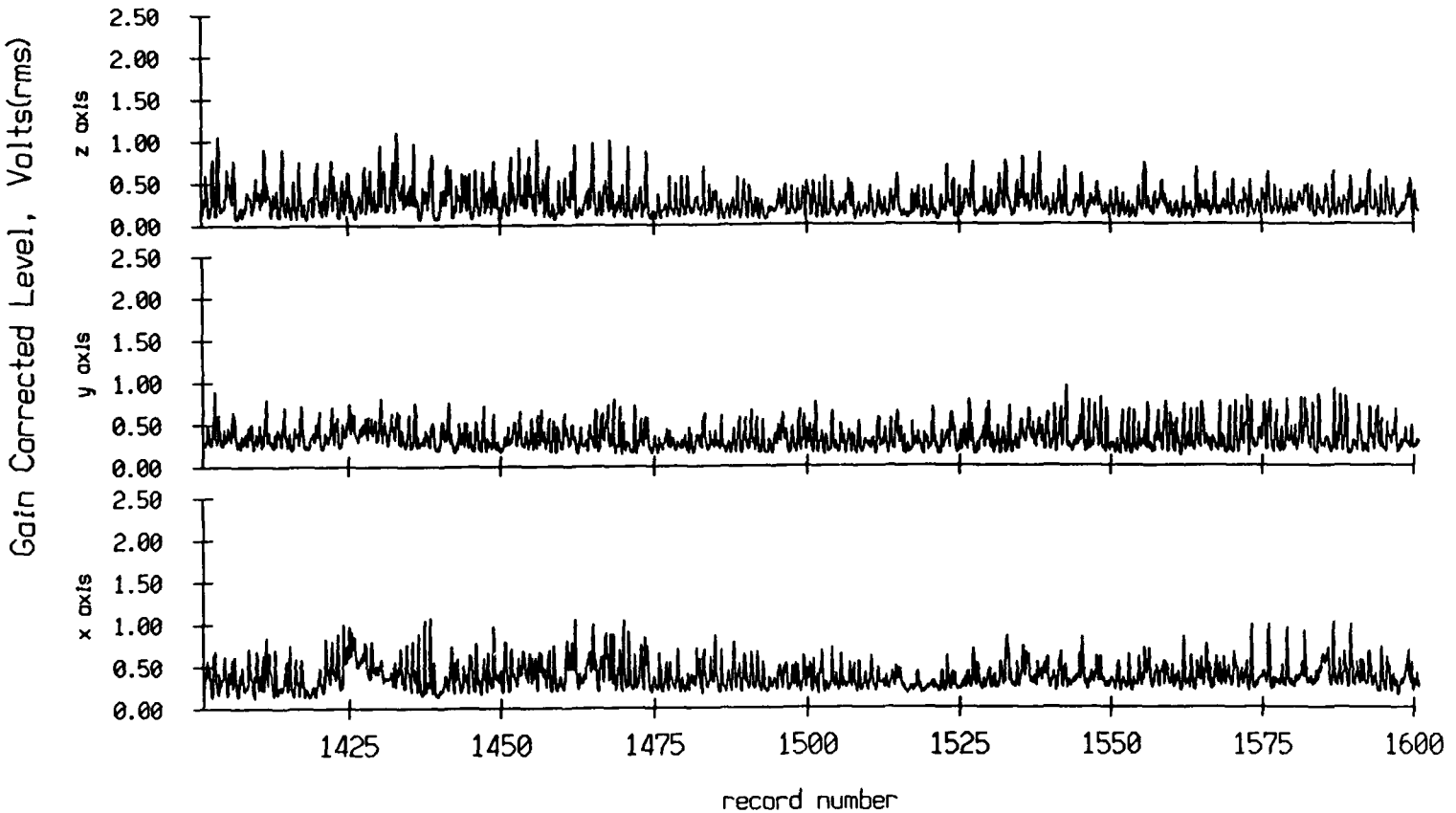

Float 2, August 1988 Sea Trip
averaging period = 5.00 sec.
RMS Velocity
Gain Corrected Level, Volts(rms)
z axis
y axis
x axis
2.50
2.00
1.50
1.00
0.50
0.00
1425
1450
1475
1500
1525
1550
1575
1600
record number

Figure X.6h

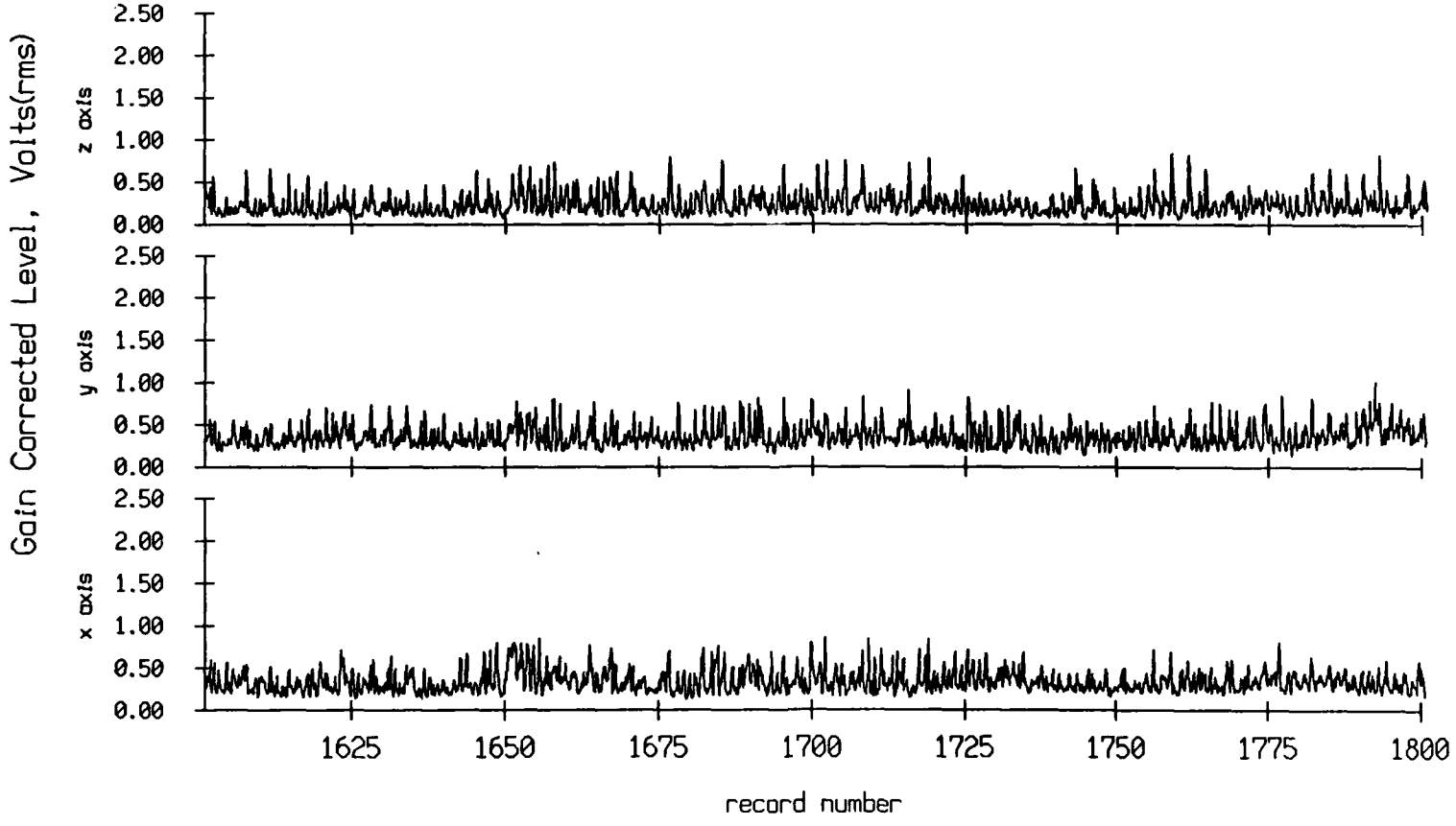

Float 2, August 1988 Sea Trip
averaging period = 5.00 sec.
RMS Velocity
Gain Corrected Level, Volts(rms)
z axis
y axis
x axis
2.50
2.00
1.50
1.00
0.50
0.00
1625
1650
1675
1700
1725
1750
1775
1800
record number

Figure X.6i

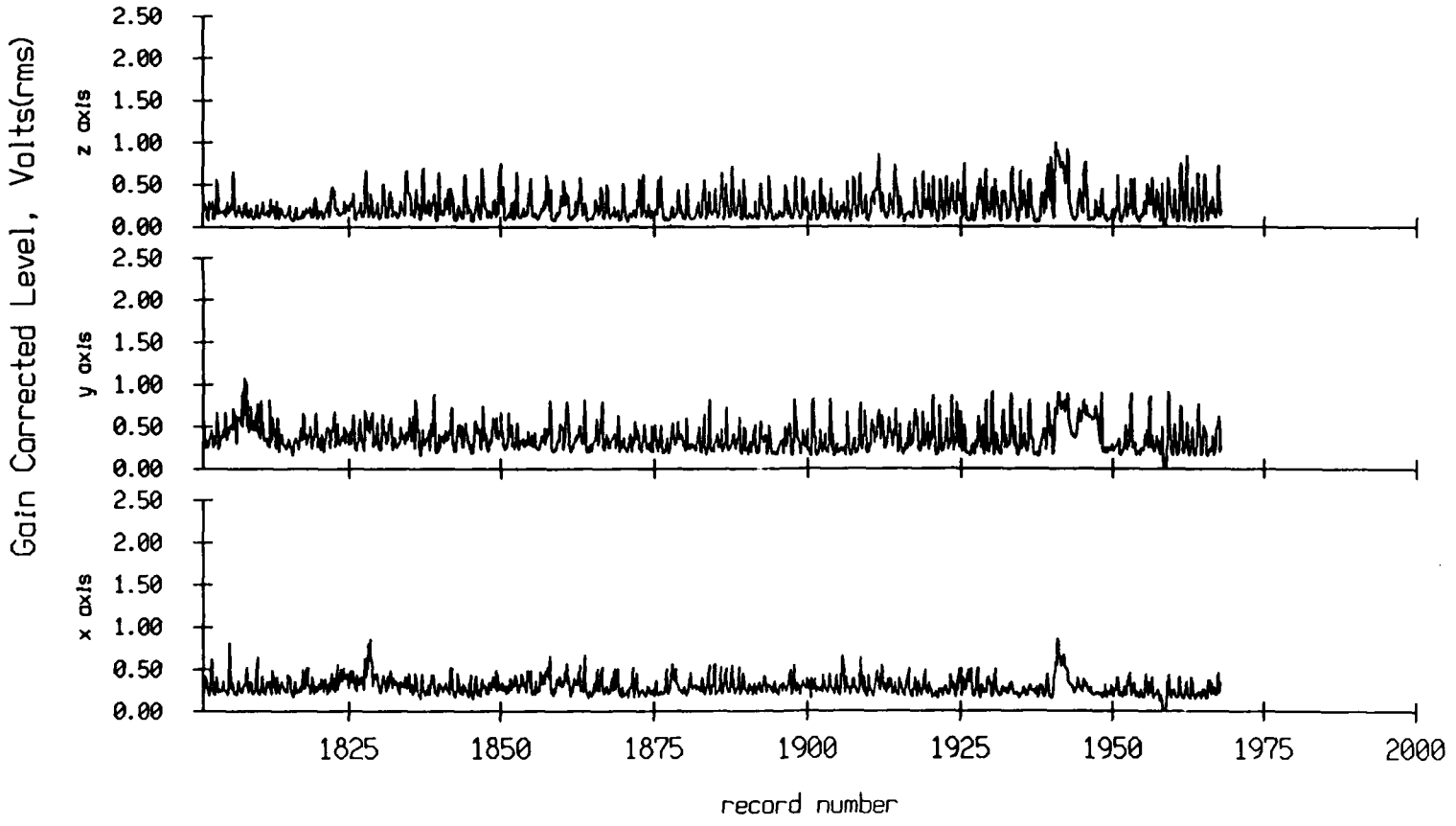

Float 2, August 1988 Sea Trip
averaging period = 5.00 sec.
RMS Velocity
Gain Corrected Level, Volts(rms)
z axis
y axis
x axis
2.50
2.00
1.50
1.00
0.50
0.00
1825
1850
1875
1900
1925
1950
1975
2000
record number

Figure X.6j

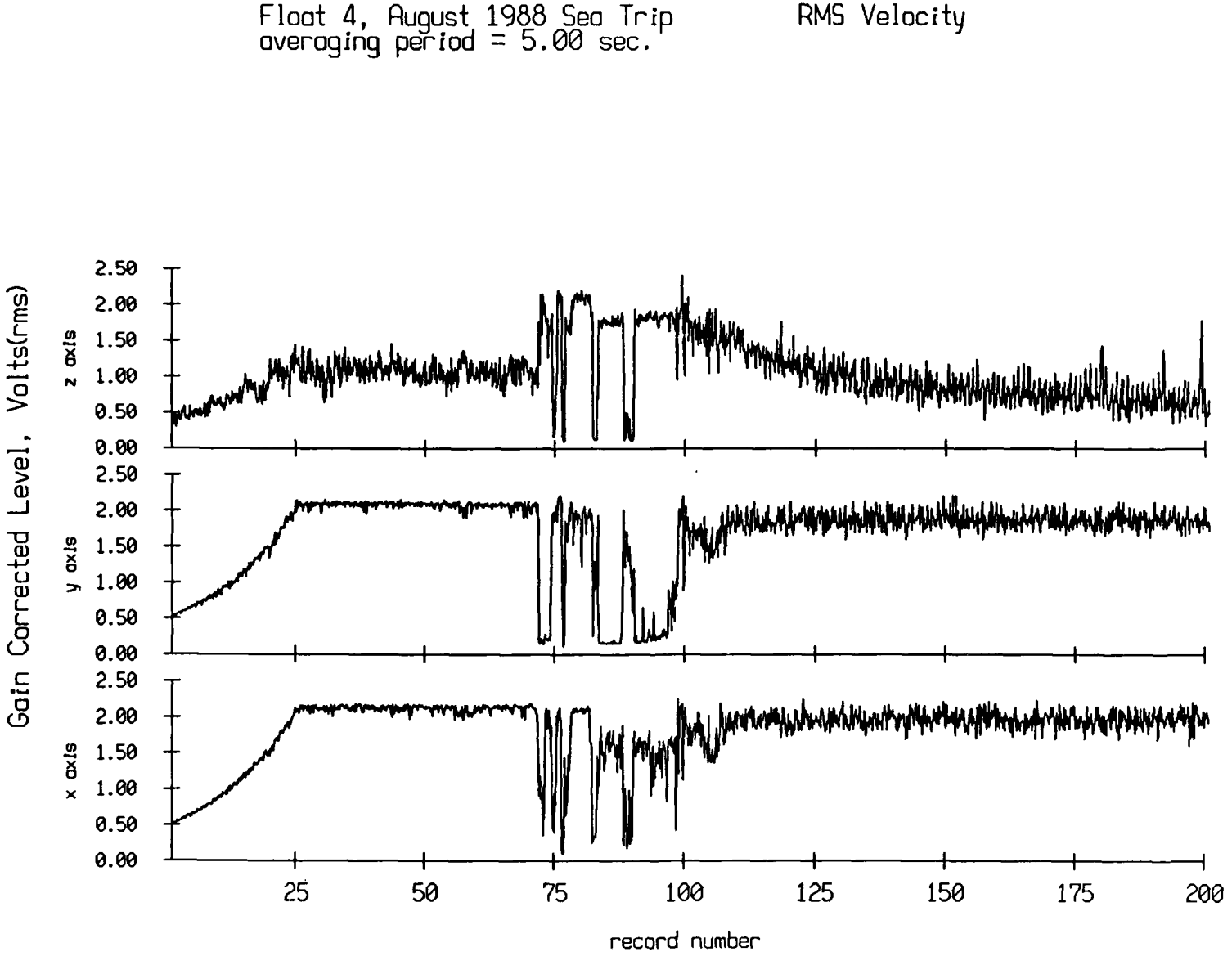

Float 4, August 1988 Sea Trip
averaging period = 5.00 sec.
RMS Velocity
Gain Corrected Level, Volts(rms)
z axis
y axis
x axis
2.50
2.00
1.50
1.00
0.50
0.00
25
50
75
100
125
150
175
200
record number

Figure X.7a

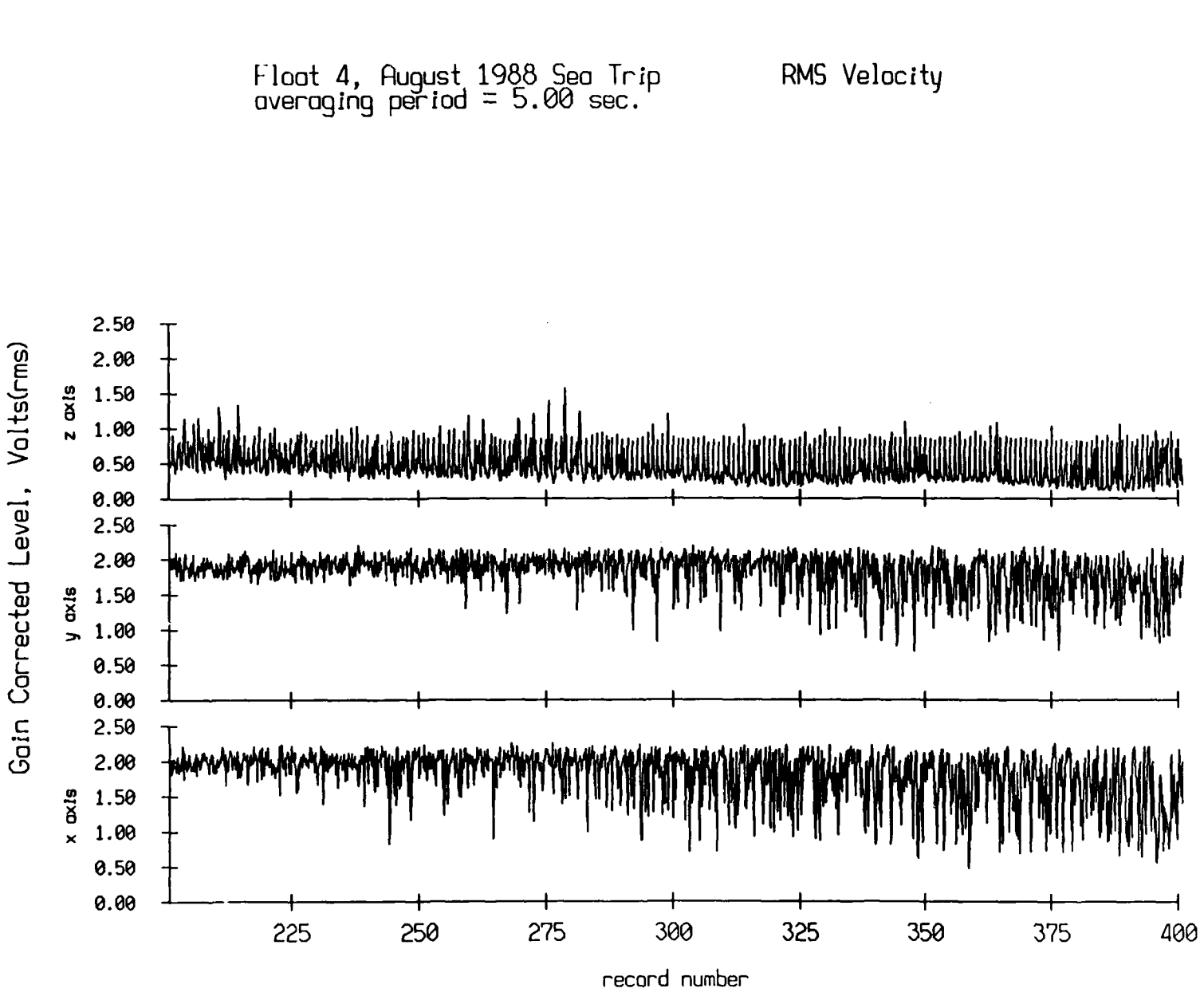

Float 4, August 1988 Sea Trip
averaging period = 5.00 sec.
RMS Velocity
Gain Corrected Level, Volts(rms)
z axis
y axis
x axis
2.50
2.00
1.50
1.00
0.50
0.00
225
250
275
300
325
350
375
400
record number

Figure X.7b

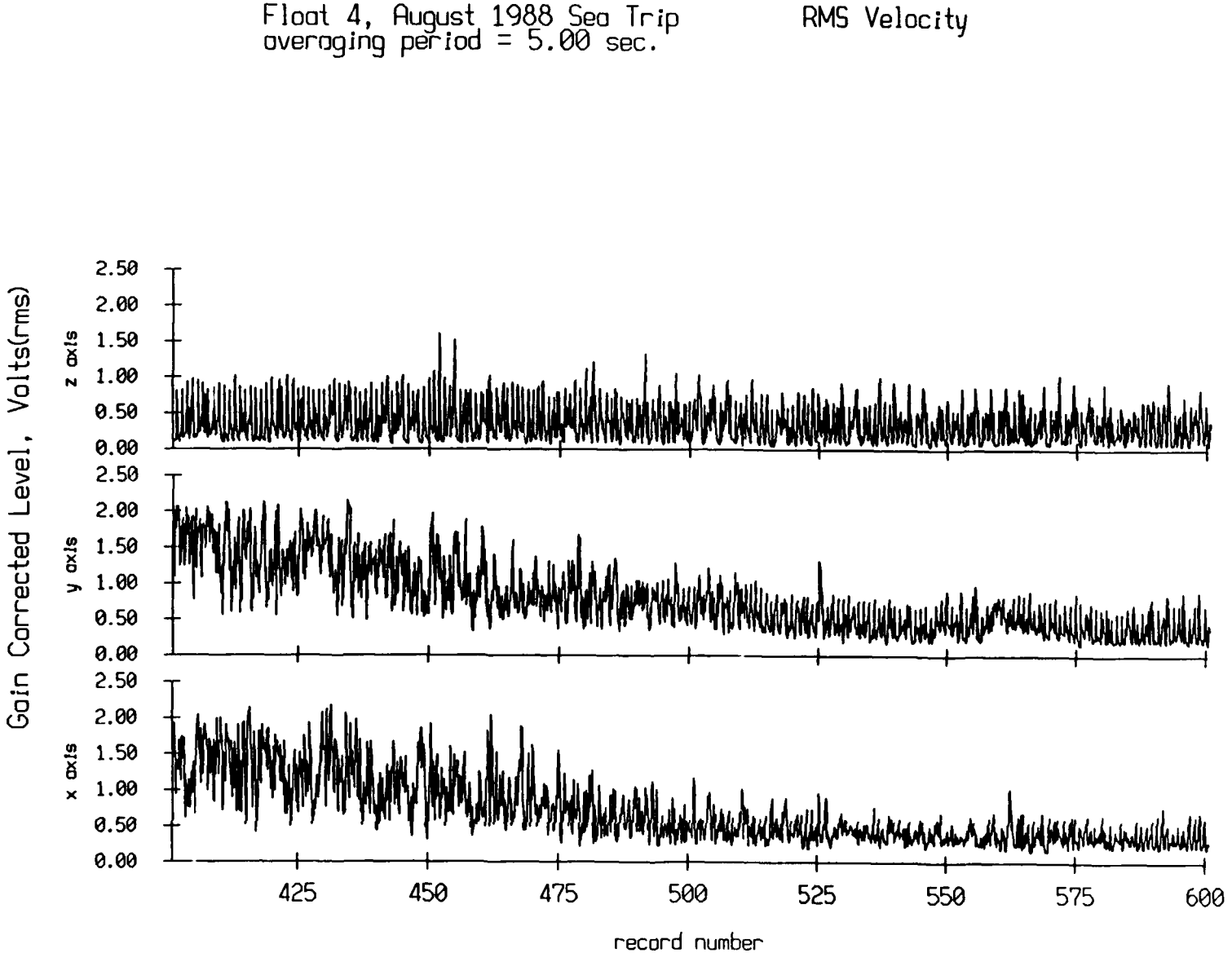

Float 4, August 1988 Sea Trip
averaging period = 5.00 sec.
RMS Velocity
Gain Corrected Level, Volts(rms)
z axis
y axis
x axis
2.50
2.00
1.50
1.00
0.50
0.00
425
450
475
500
525
550
575
600
record number

Figure X.7c

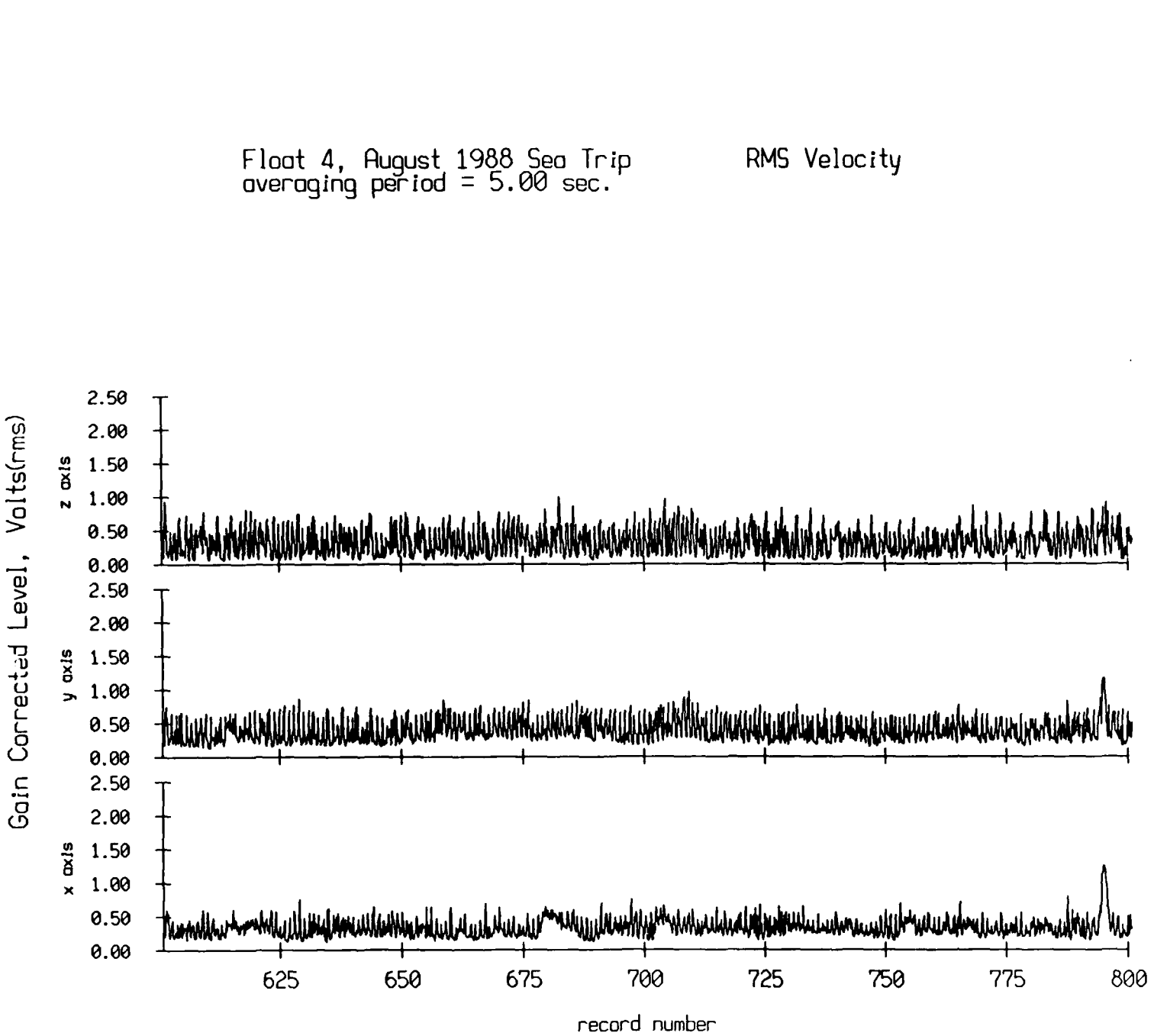

Float 4, August 1988 Sea Trip
averaging period = 5.00 sec.
RMS Velocity
Gain Corrected Level, Volts(rms)
z axis
y axis
x axis
2.50
2.00
1.50
1.00
0.50
0.00
625
650
675
700
725
750
775
800
record number

Figure X.7d

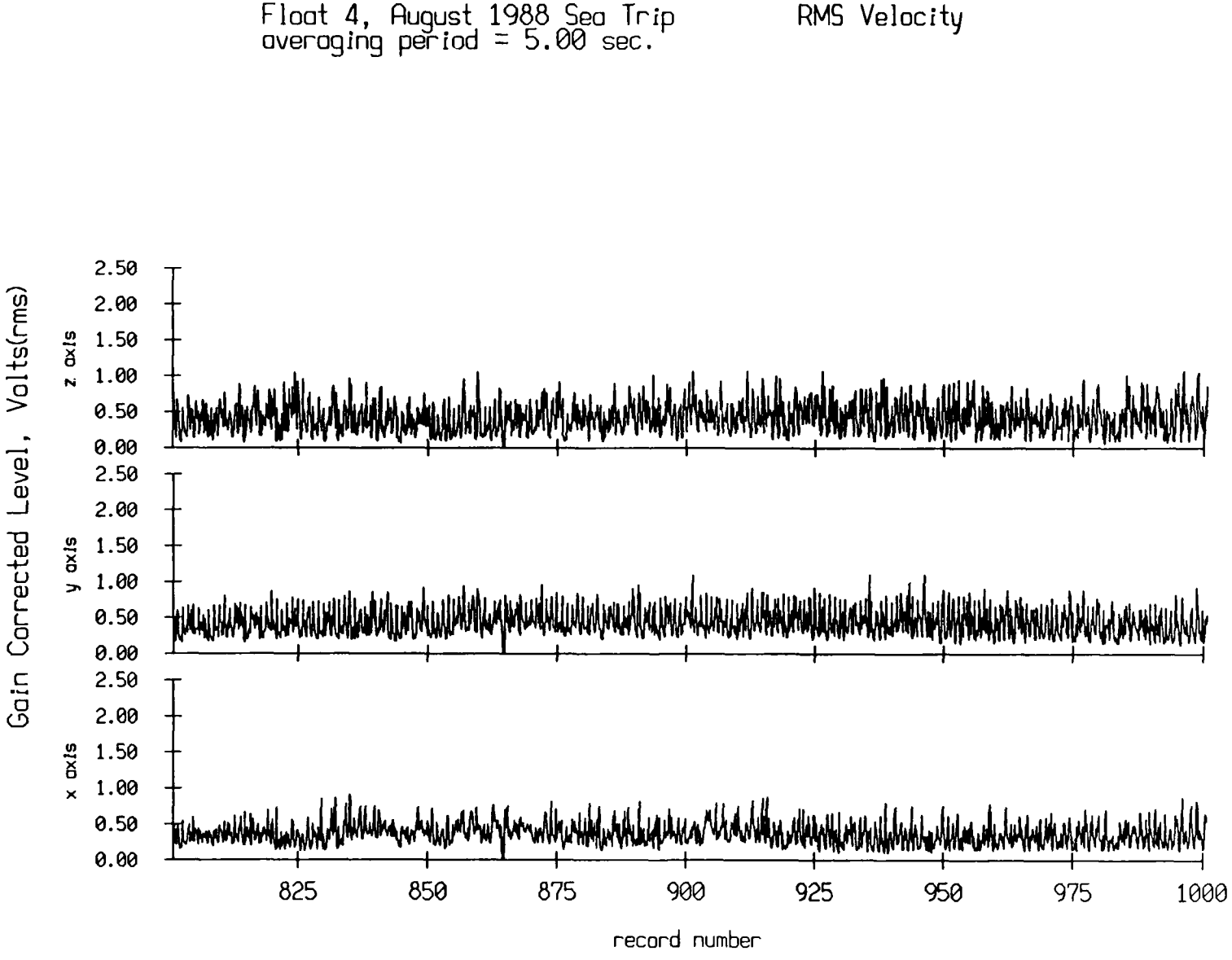

Float 4, August 1988 Sea Trip
averaging period = 5.00 sec.
RMS Velocity
Gain Corrected Level, Volts(rms)
z axis
y axis
x axis
2.50
2.00
1.50
1.00
0.50
0.00
825
850
875
900
925
950
975
1000
record number

Figure X.7e

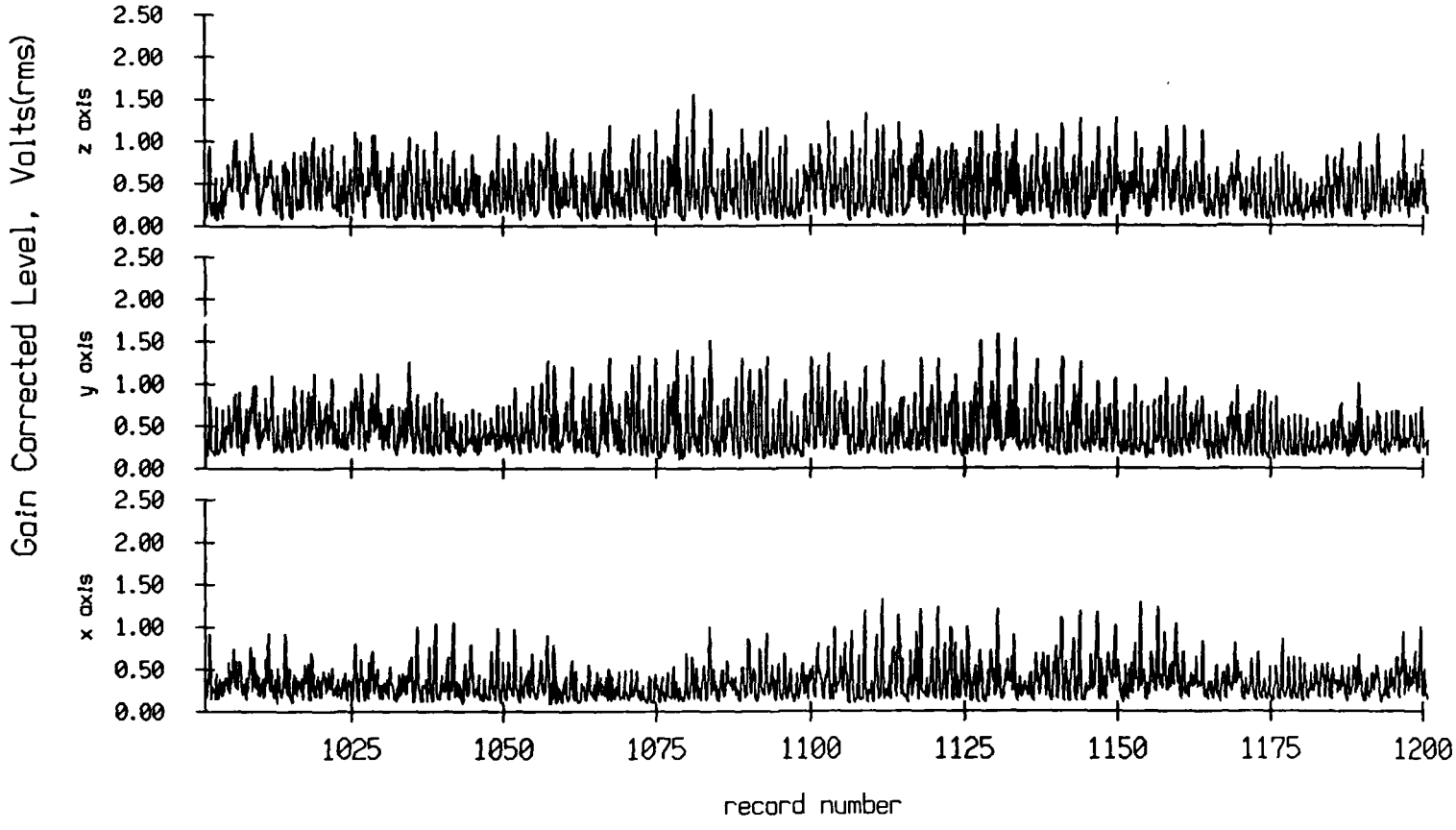

Float 4, August 1988 Sea Trip
averaging period = 5.00 sec.
RMS Velocity
Gain Corrected Level, Volts(rms)
z axis
y axis
x axis
2.50
2.00
1.50
1.00
0.50
0.00
1025
1050
1075
1100
1125
1150
1175
1200
record number

Figure X.7f

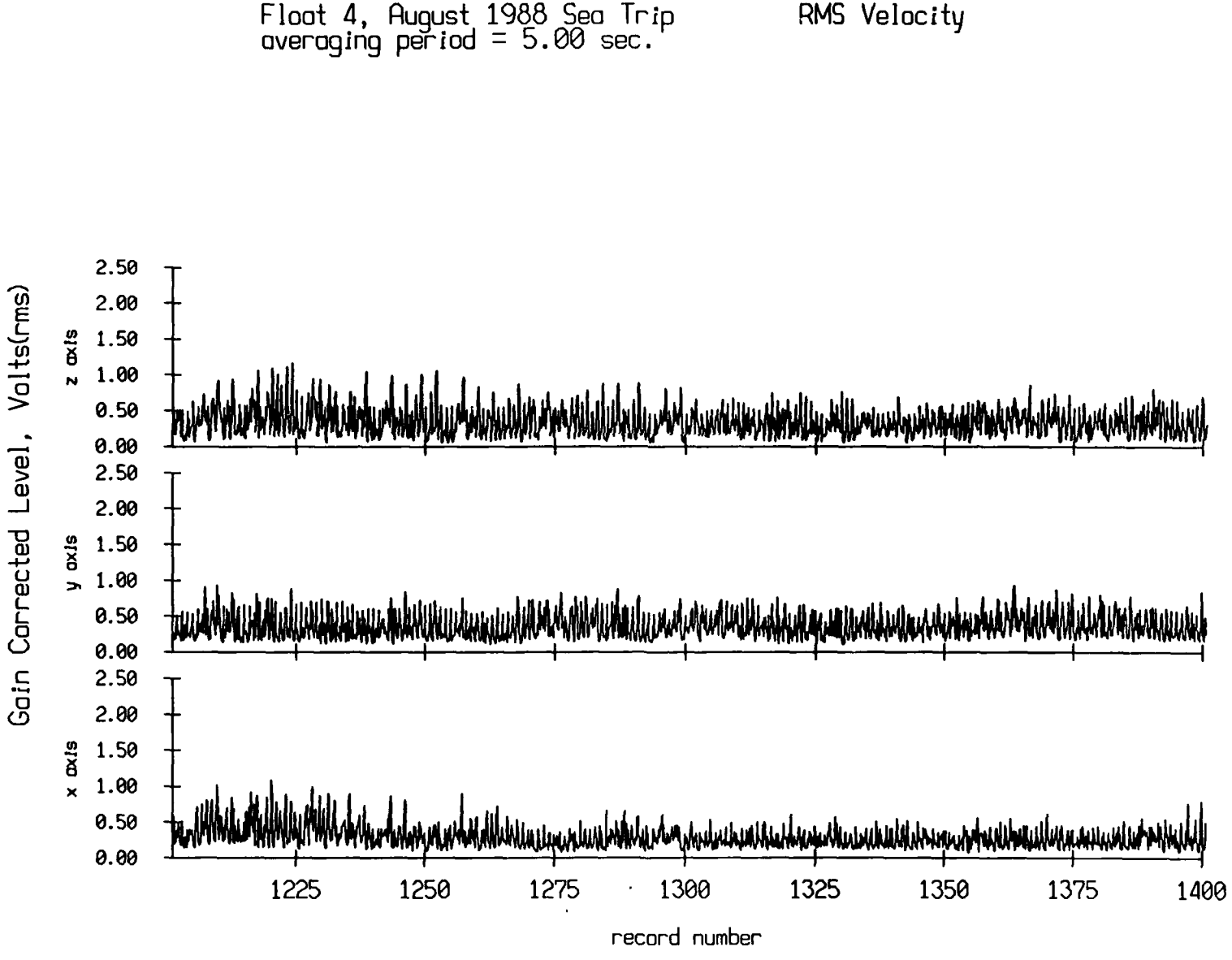

Float 4, August 1988 Sea Trip
averaging period = 5.00 sec.
RMS Velocity
Gain Corrected Level, Volts(rms)
z axis
y axis
x axis
2.50
2.00
1.50
1.00
0.50
0.00
1225
1250
1275
1300
1325
1350
1375
1400
record number

Figure X.7g

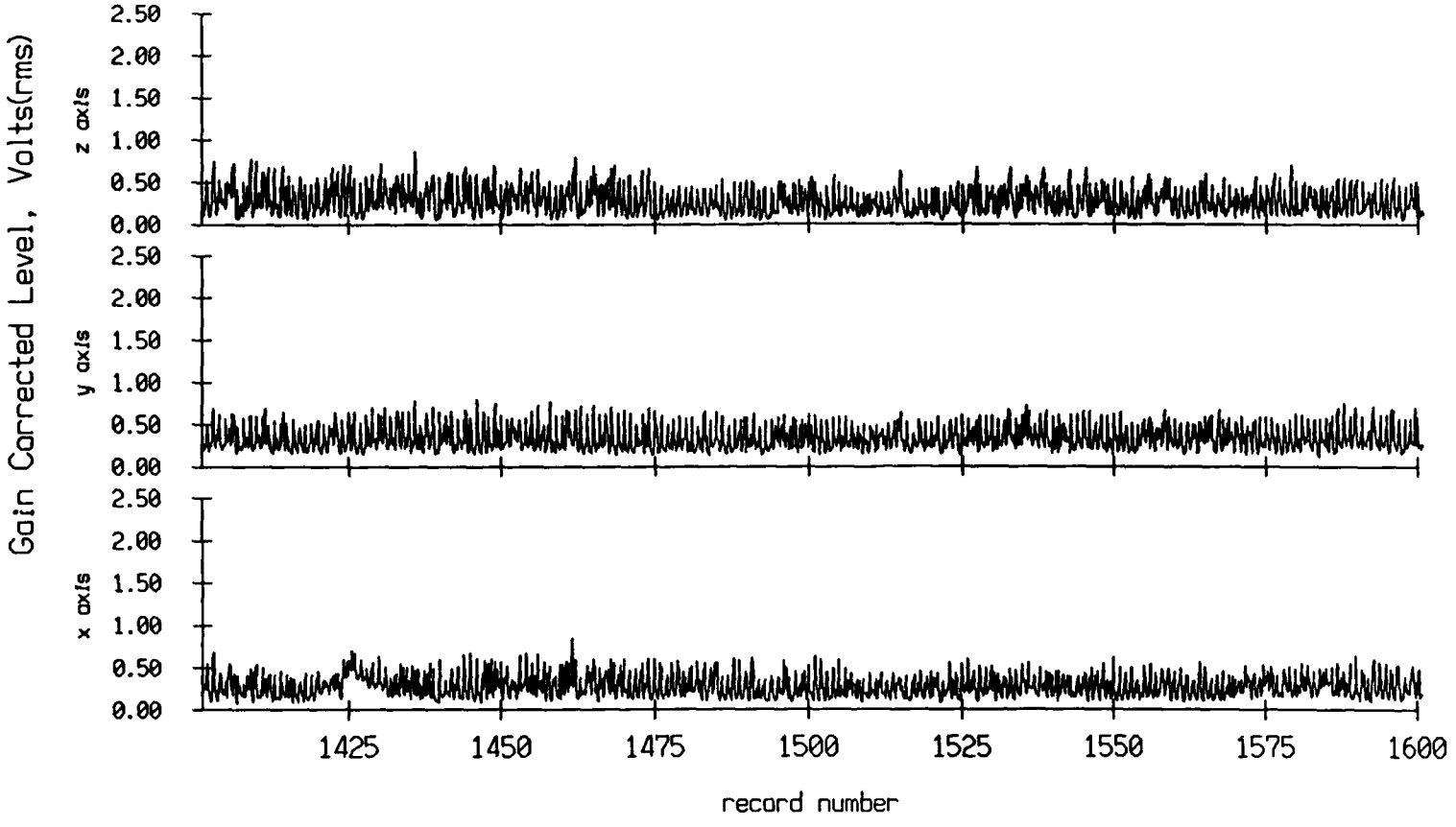

Float 4, August 1988 Sea Trip
averaging period = 5.00 sec.
RMS Velocity
Gain Corrected Level, Volts(rms)
z axis
y axis
x axis
2.50
2.00
1.50
1.00
0.50
0.00
1425
1450
1475
1500
1525
1550
1575
1600
record number

Figure X.7h

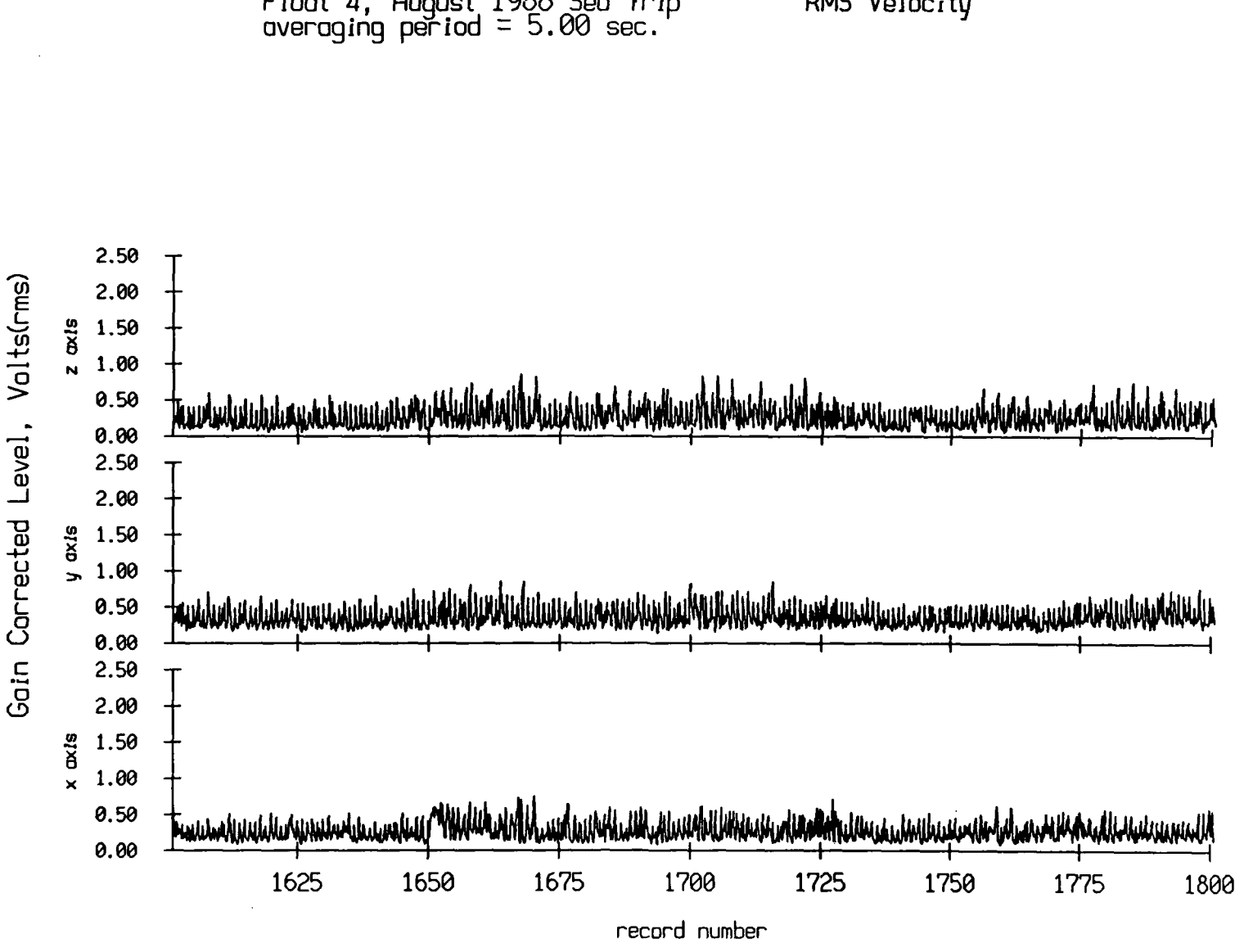

Float 4, August 1988 Sea Trip
averaging period = 5.00 sec.
RMS Velocity
Gain Corrected Level, Volts(rms)
z axis
y axis
x axis
2.50
2.00
1.50
1.00
0.50
0.00
1625
1650
1675
1700
1725
1750
1775
1800
record number

Figure X.7i

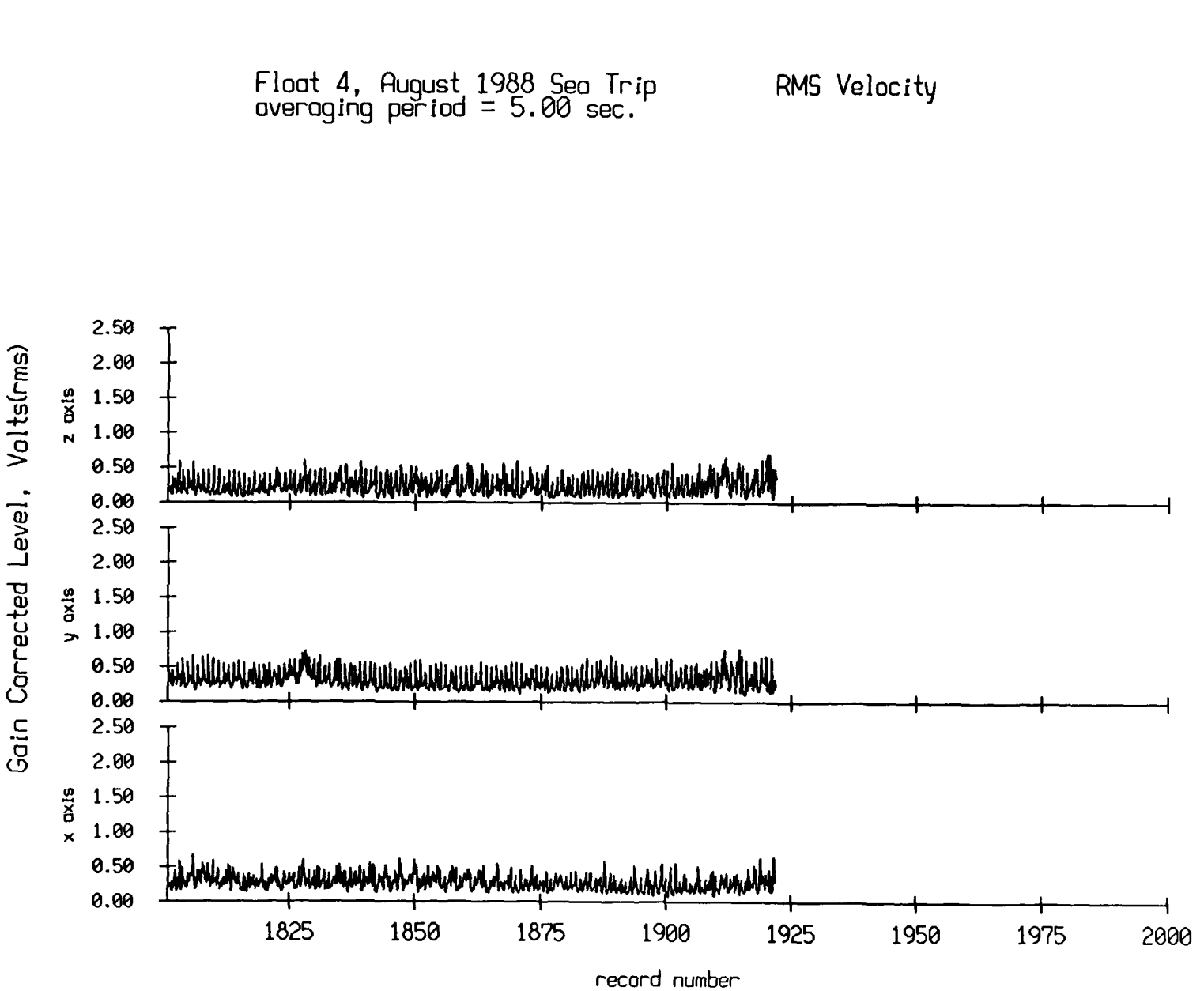

Float 4, August 1988 Sea Trip
averaging period = 5.00 sec.
RMS Velocity
Gain Corrected Level, Volts(rms)
z axis
y axis
x axis
2.50
2.00
1.50
1.00
0.50
0.00
1825
1850
1875
1900
1925
1950
1975
2000
record number

Figure X.7j

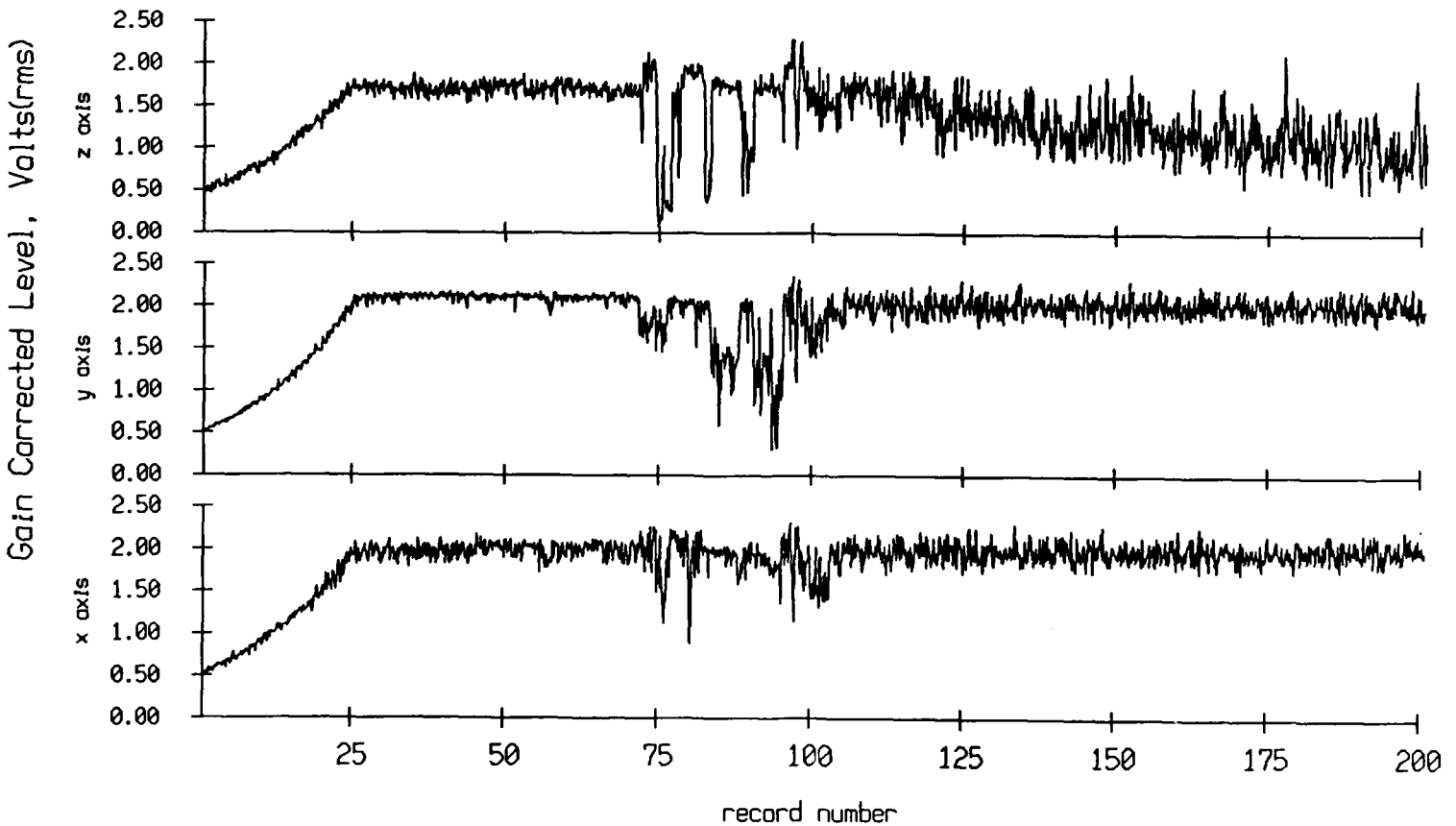

Float 6, August 1988 Sea Trip
averaging period = 5.00 sec.
RMS Velocity
Gain Corrected Level, Volts(rms)
z axis
y axis
x axis
2.50
2.00
1.50
1.00
0.50
0.00
25
50
75
100
125
150
175
200
record number

Figure X.8a

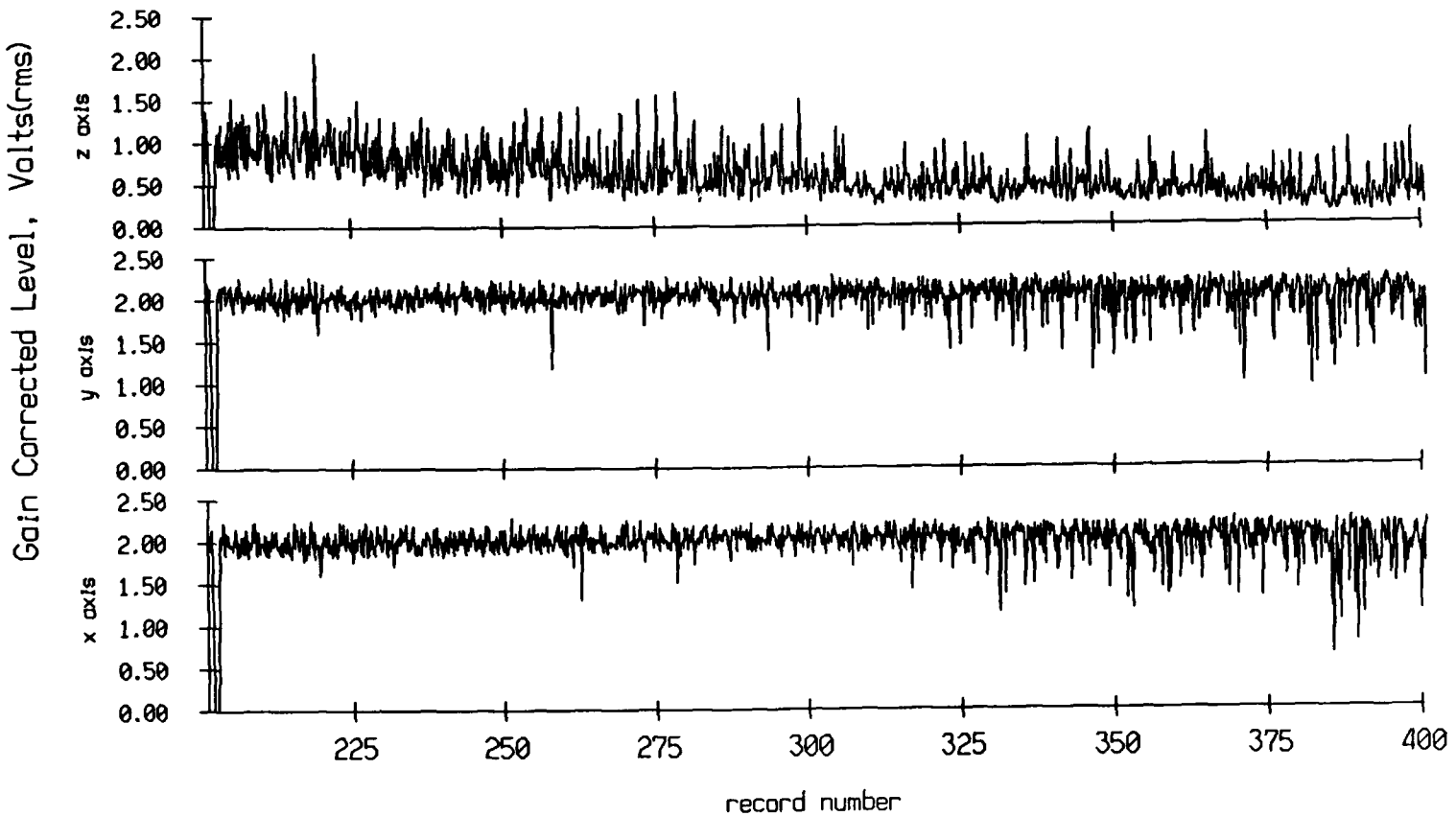

Float 6, August 1988 Sea Trip
averaging period = 5.00 sec.
RMS Velocity
Gain Corrected Level, Volts(rms)
z axis
y axis
x axis
2.50
2.00
1.50
1.00
0.50
0.00
225
250
275
300
325
350
375
400
record number

Figure X.8b

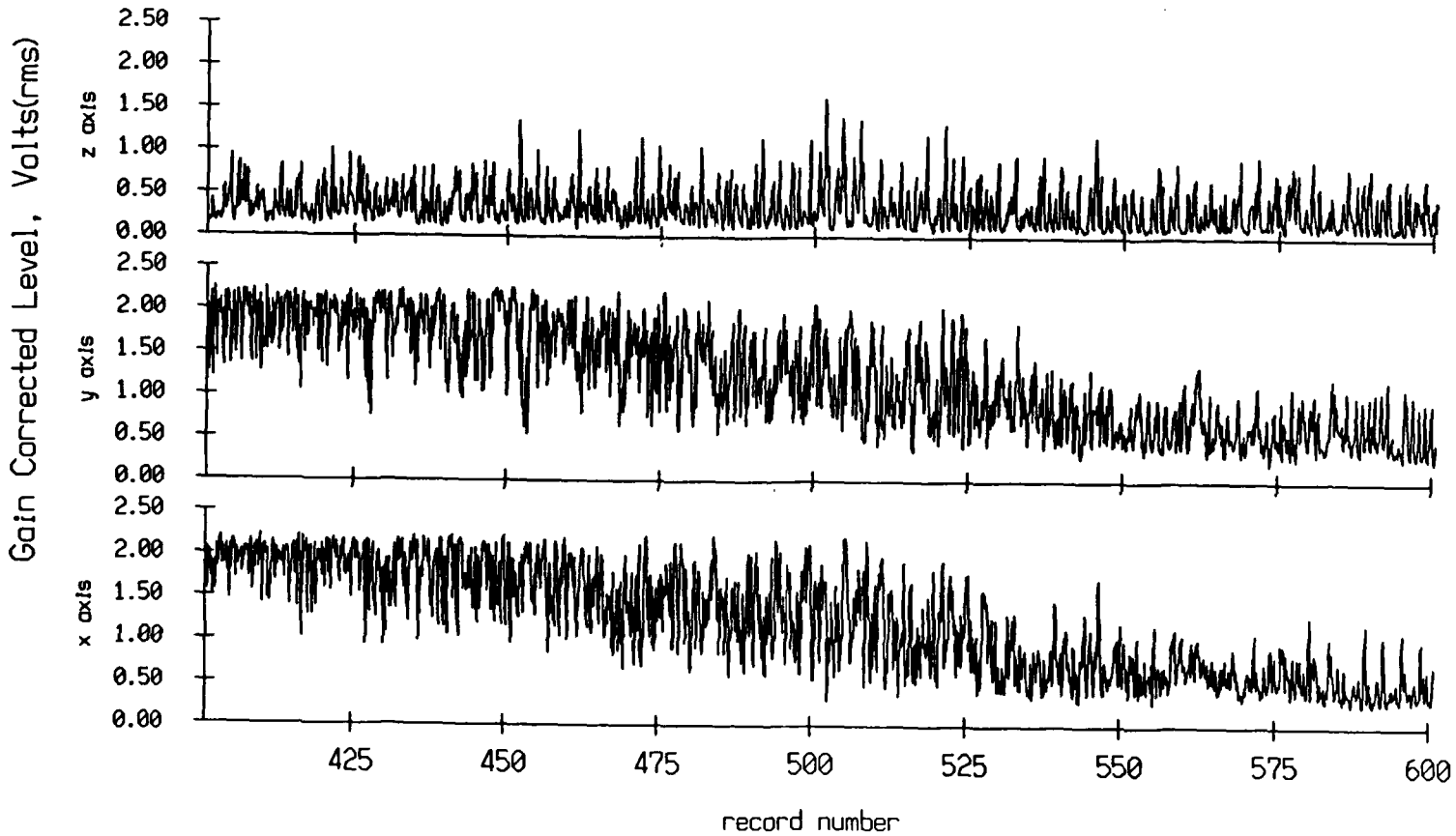

Float 6, August 1988 Sea Trip
averaging period = 5.00 sec.
RMS Velocity
Gain Corrected Level, Volts(rms)
z axis
y axis
x axis
2.50
2.00
1.50
1.00
0.50
0.00
425
450
475
500
525
550
575
600
record number

Figure X.8c

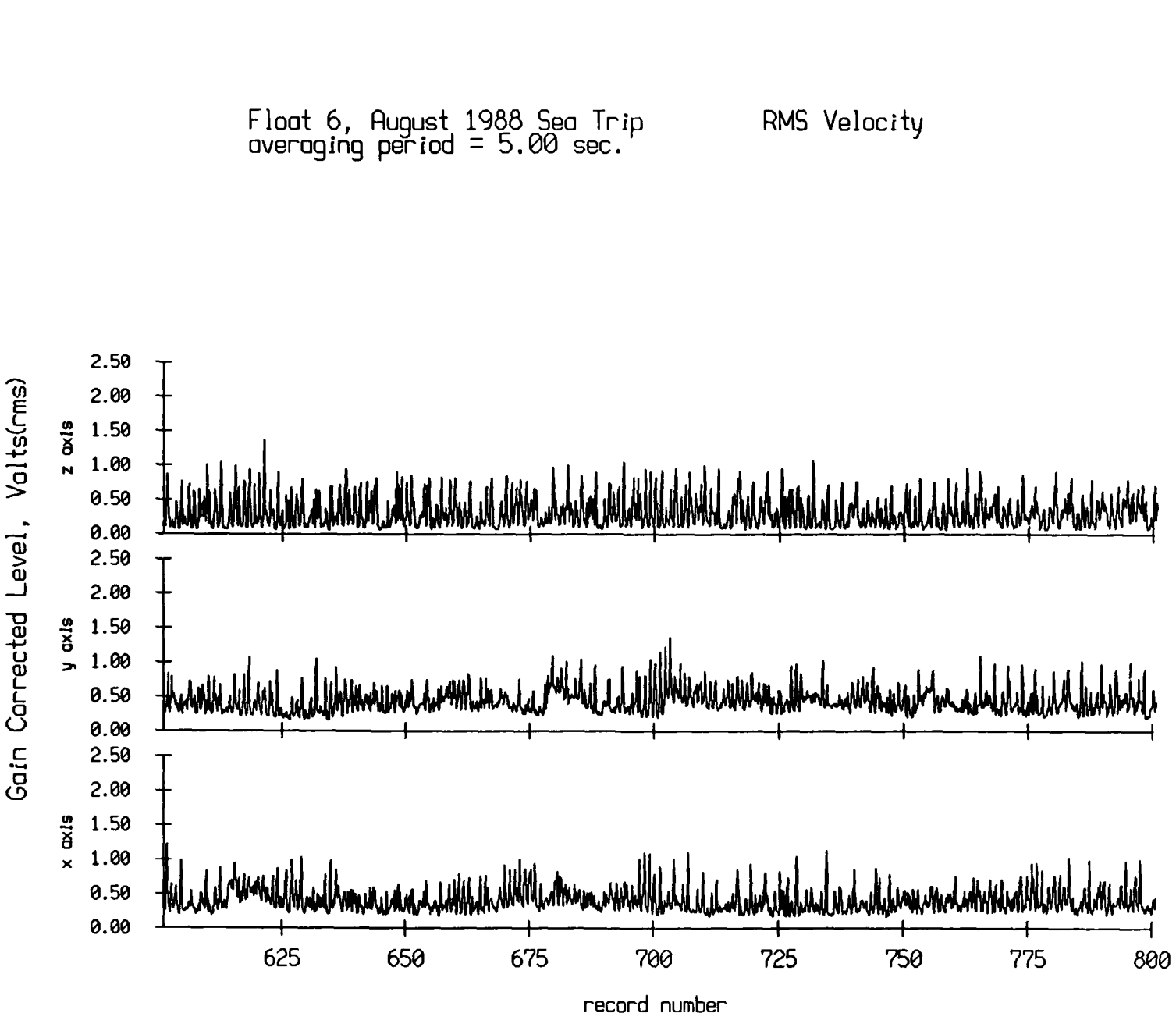

Float 6, August 1988 Sea Trip
averaging period = 5.00 sec.
RMS Velocity
Gain Corrected Level, Volts(rms)
z axis
y axis
x axis
2.50
2.00
1.50
1.00
0.50
0.00
625
650
675
700
725
750
775
800
record number

Figure X.8d

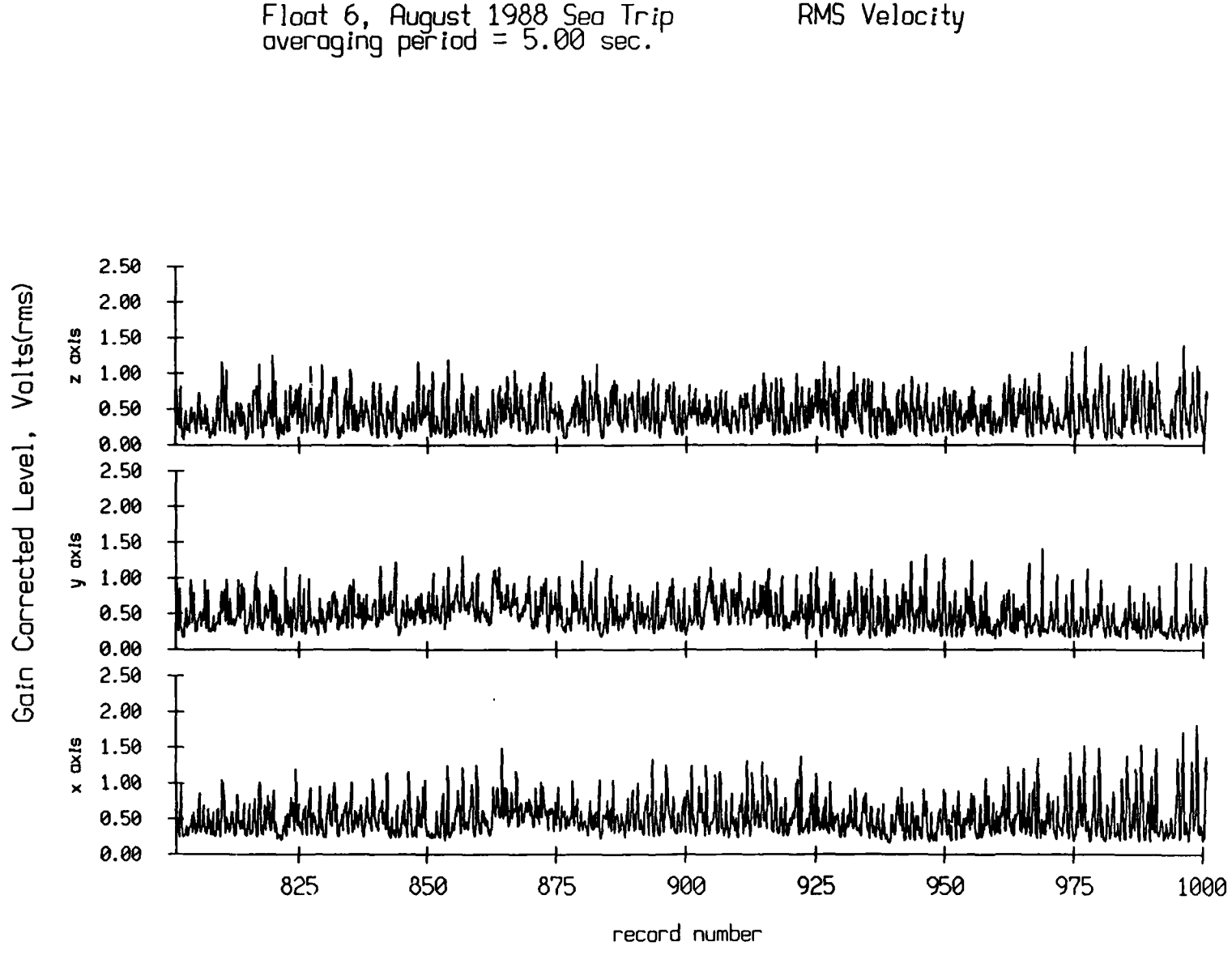

Float 6, August 1988 Sea Trip
averaging period = 5.00 sec.
RMS Velocity
Gain Corrected Level, Volts(rms)
z axis
y axis
x axis
2.50
2.00
1.50
1.00
0.50
0.00
825
850
875
900
925
950
975
1000
record number

Figure X.8e

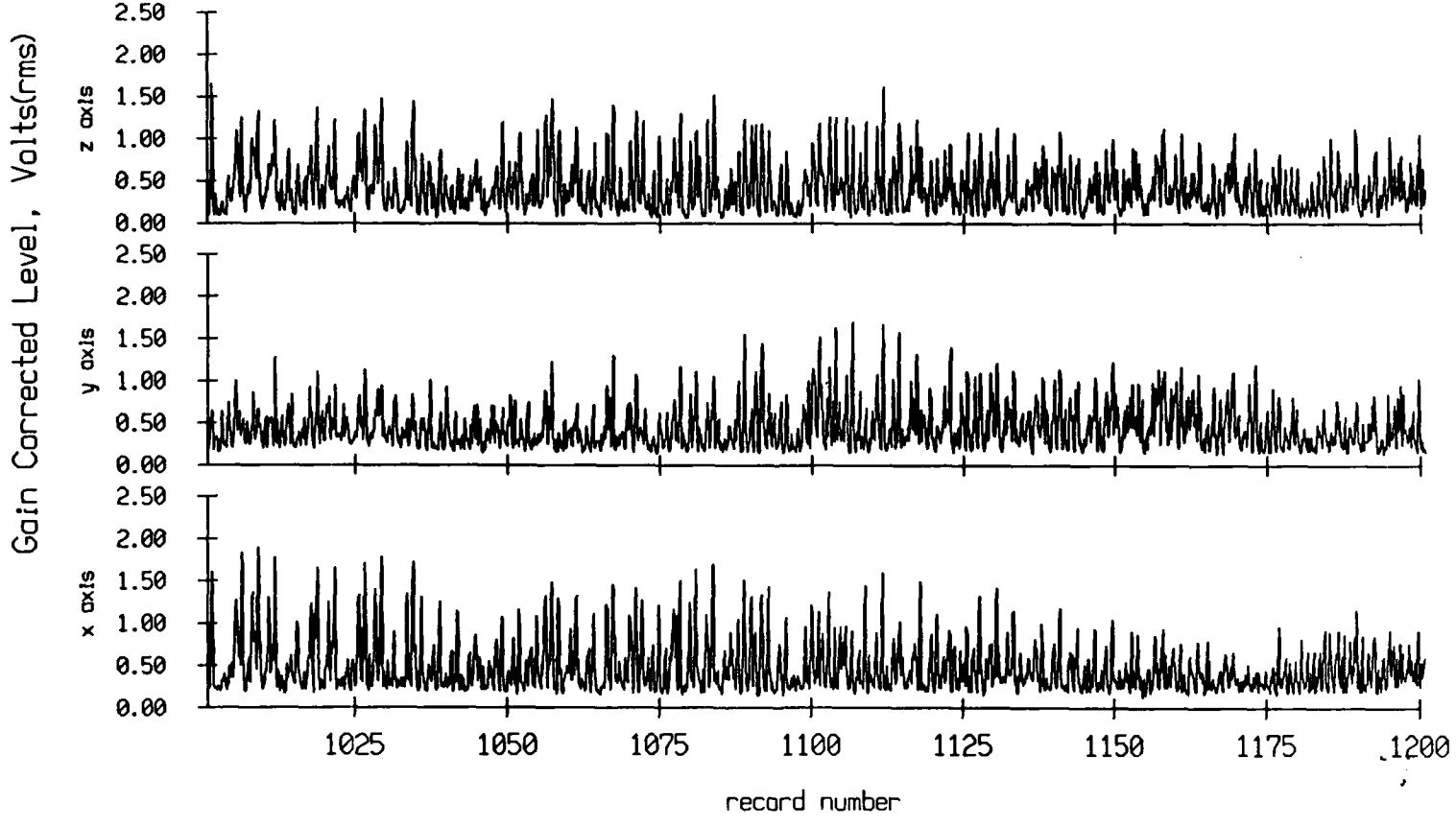

Float 6, August 1988 Sea Trip
averaging period = 5.00 sec.
RMS Velocity
Gain Corrected Level, Volts(rms)
z axis
y axis
x axis
2.50
2.00
1.50
1.00
0.50
0.00
1025
1050
1075
1100
1125
1150
1175
1200
record number

Figure X.8f

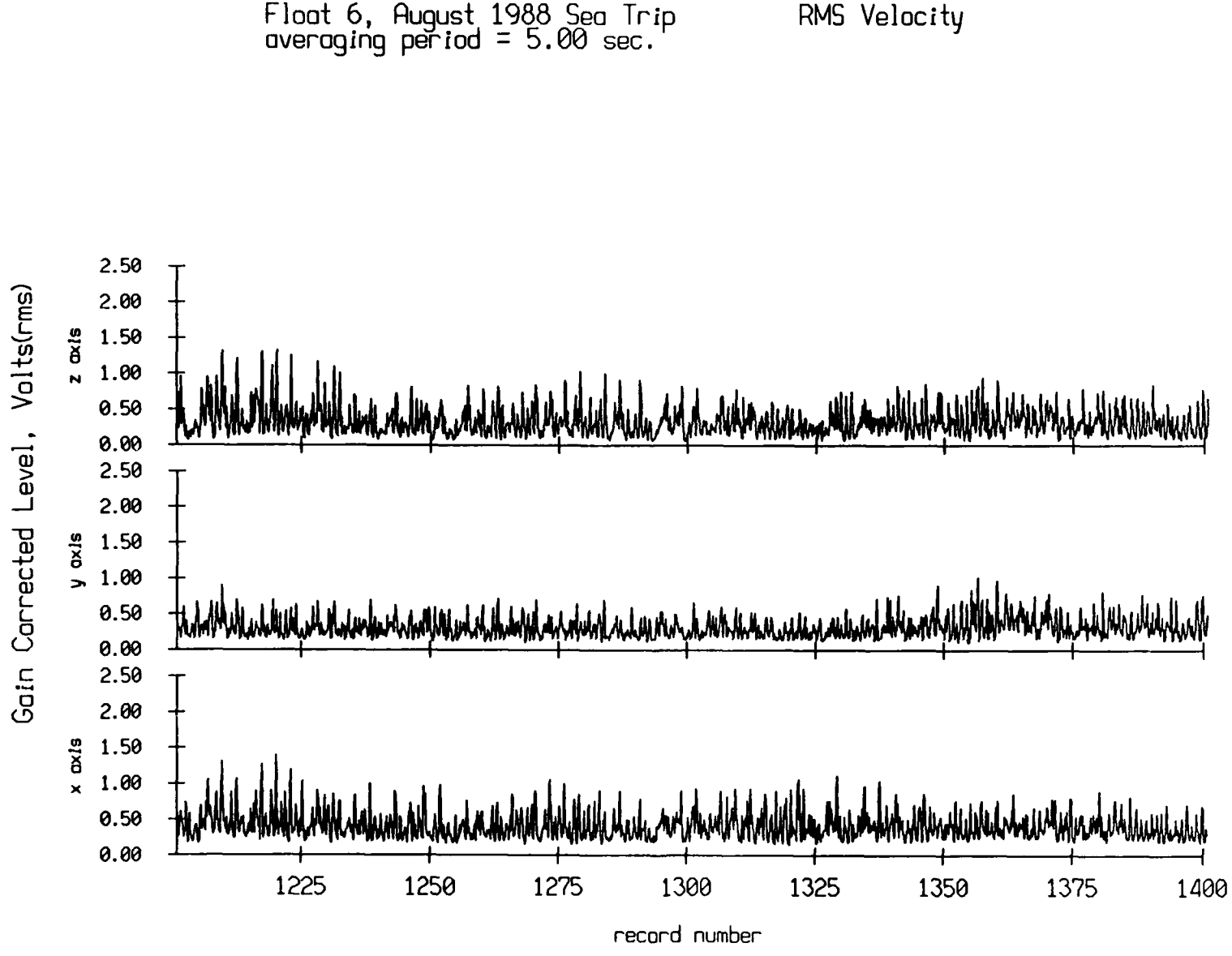

Float 6, August 1988 Sea Trip
averaging period = 5.00 sec.
RMS Velocity
Gain Corrected Level, Volts(rms)
z axis
y axis
x axis
2.50
2.00
1.50
1.00
0.50
0.00
1225
1250
1275
1300
1325
1350
1375
1400
record number

Figure X.8g

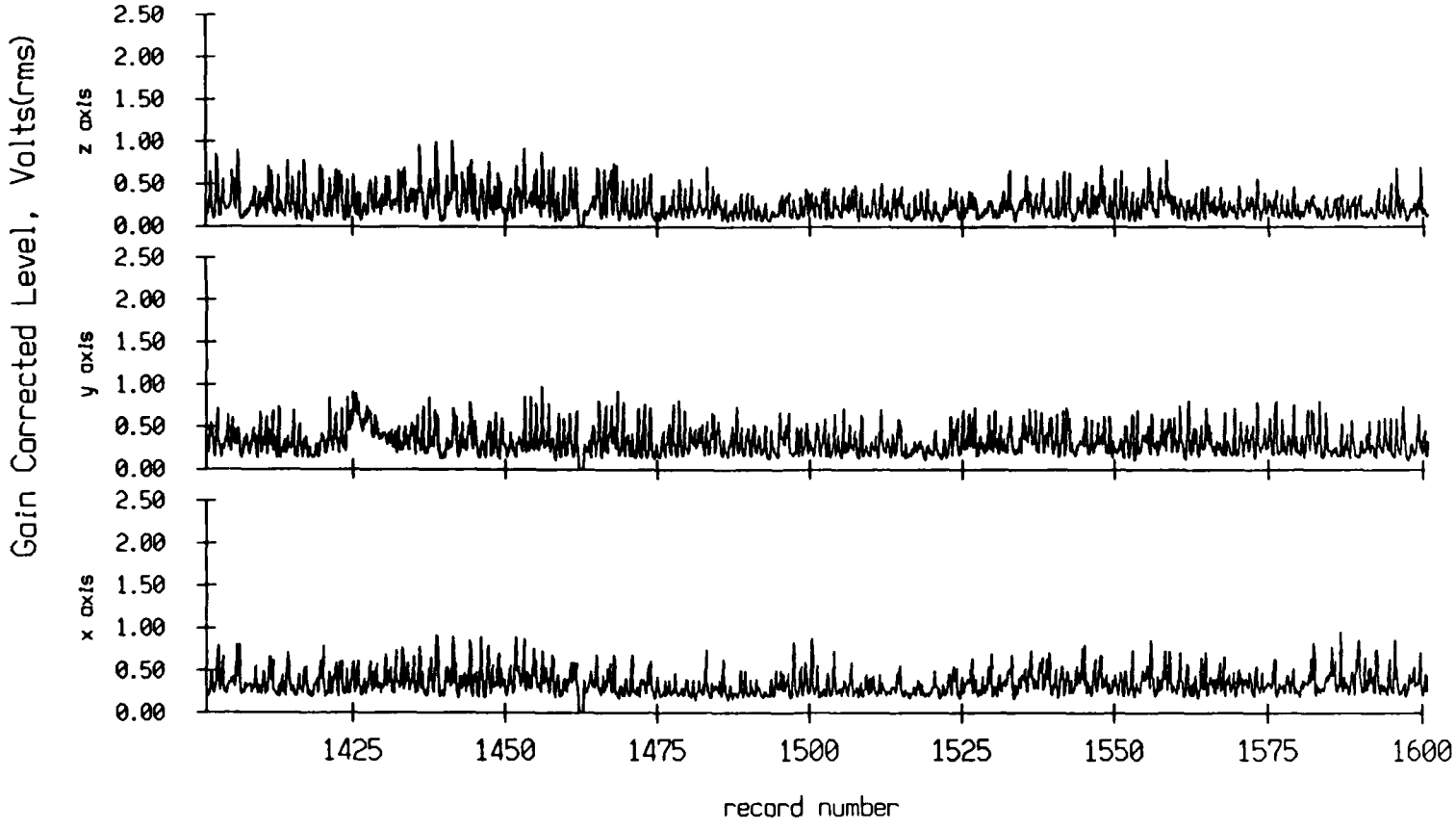

Float 6, August 1988 Sea Trip
averaging period = 5.00 sec.
RMS Velocity
Gain Corrected Level, Volts(rms)
z axis
y axis
x axis
2.50
2.00
1.50
1.00
0.50
0.00
1425
1450
1475
1500
1525
1550
1575
1600
record number

Figure X.8h

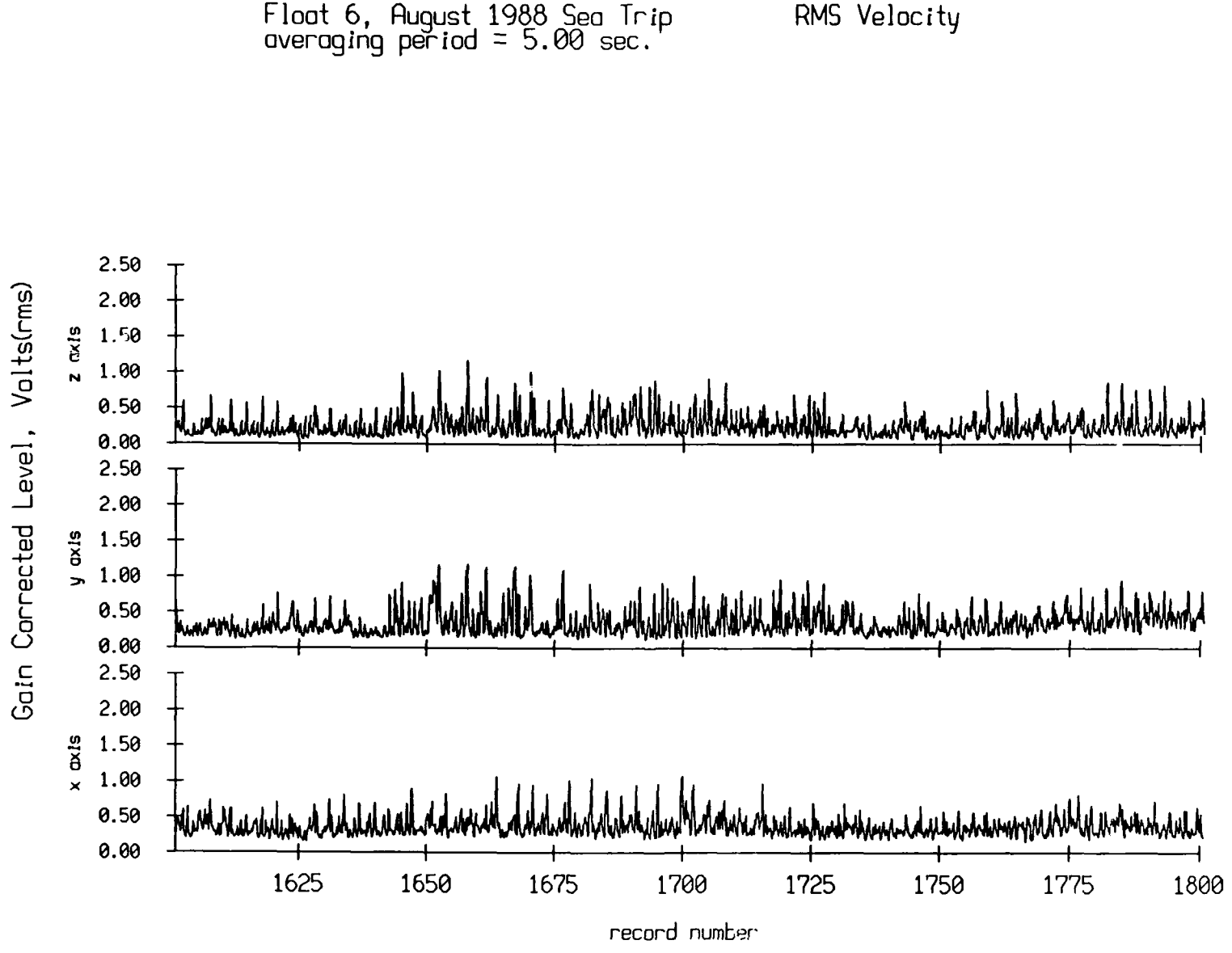

Float 6, August 1988 Sea Trip
averaging period = 5.00 sec.
RMS Velocity
Gain Corrected Level, Volts(rms)
z axis
y axis
x axis
2.50
2.00
1.50
1.00
0.50
0.00
1625
1650
1675
1700
1725
1750
1775
1800
record number

Figure X.8i

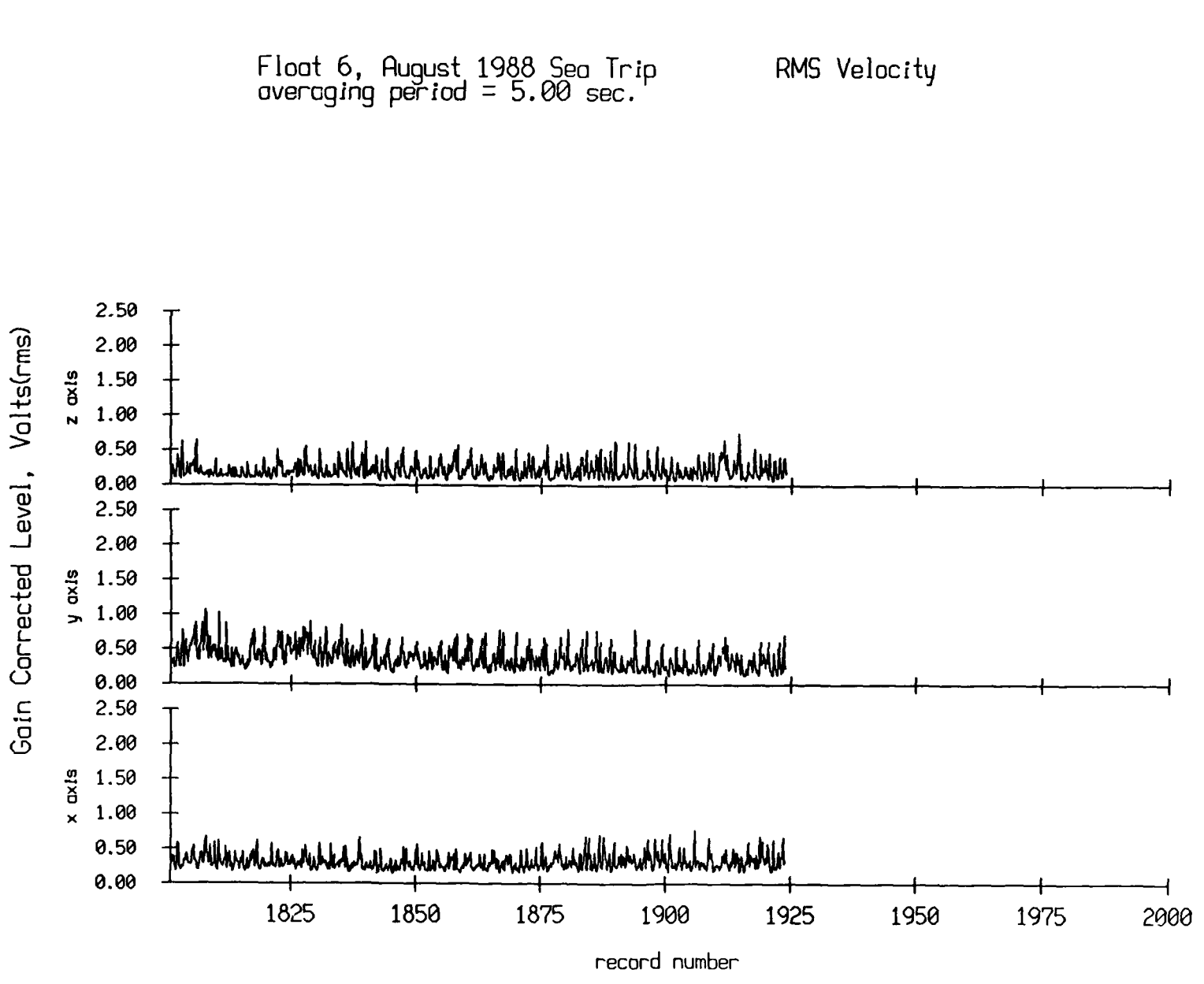

Float 6, August 1988 Sea Trip
averaging period = 5.00 sec.
RMS Velocity
Gain Corrected Level, Volts(rms)
z axis
y axis
x axis
2.50
2.00
1.50
1.00
0.50
0.00
1825
1850
1875
1900
1925
1950
1975
2000
record number

Figure X.8j

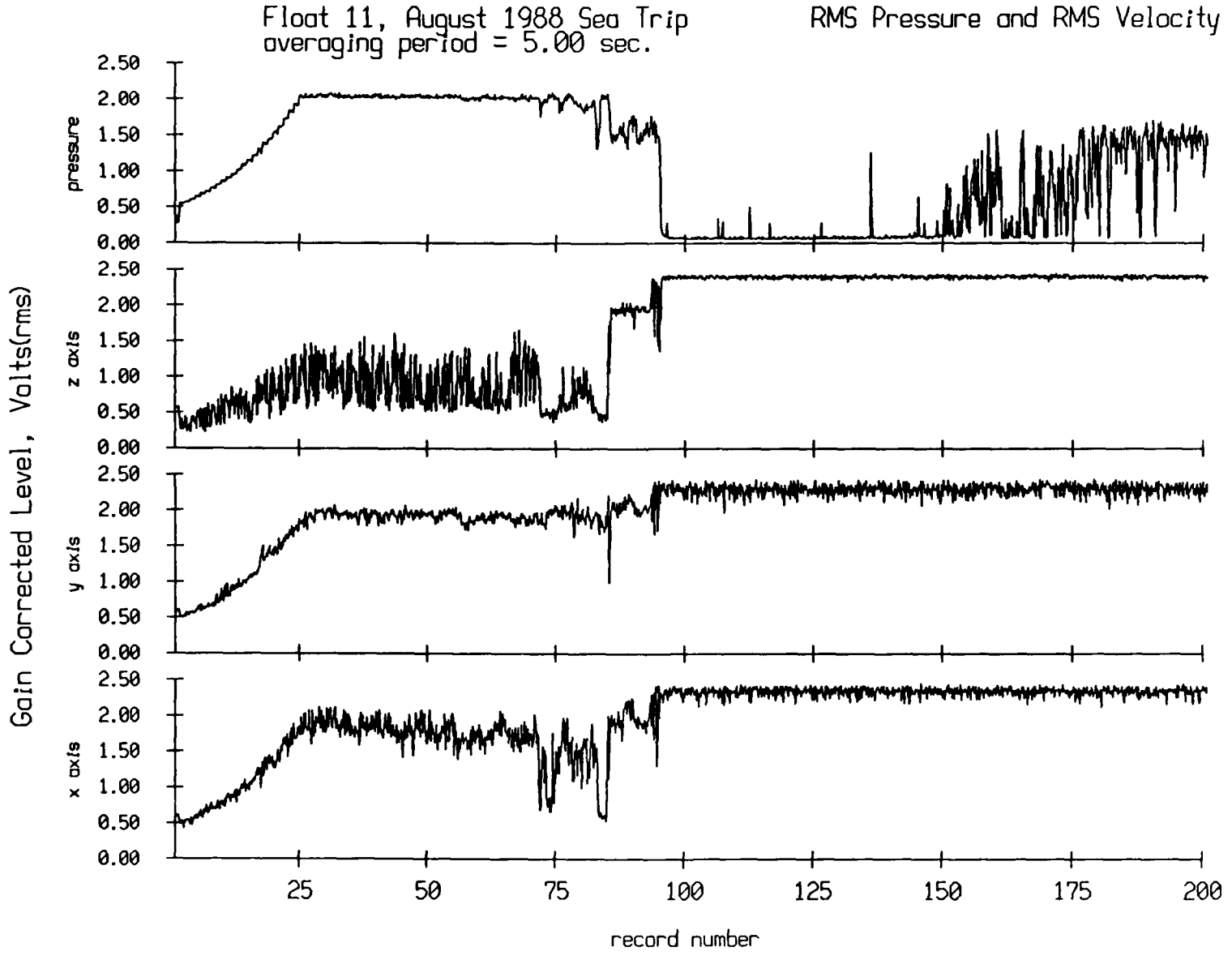

Float 11, August 1988 Sea Trip
averaging period = 5.00 sec.
RMS Pressure and RMS Velocity
Gain Corrected Level, Volts(rms)
pressure
z axis
y axis
x axis
2.50
2.00
1.50
1.00
0.50
0.00
25
50
75
100
125
150
175
200
record number

Figure X.9a

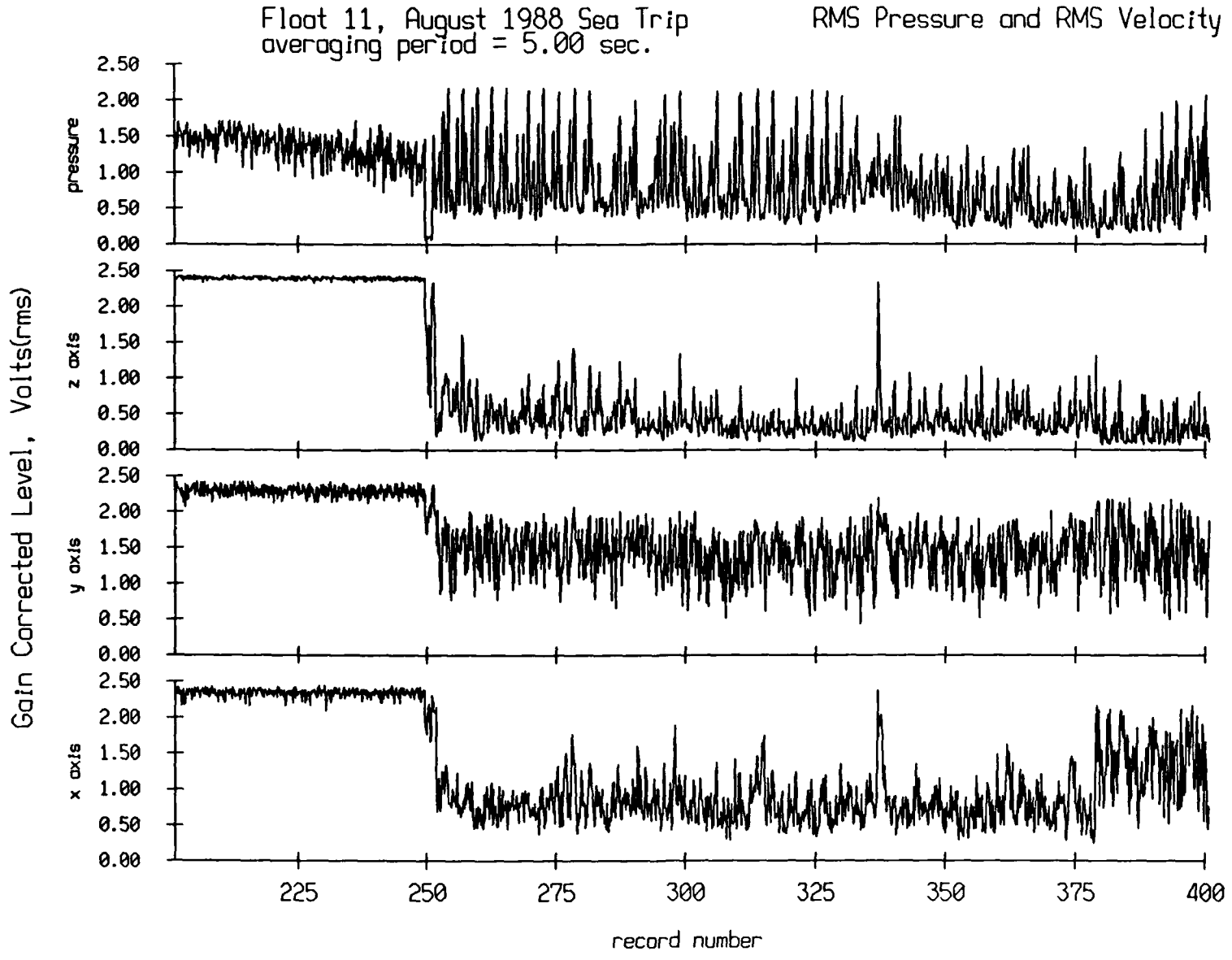

Float 11, August 1988 Sea Trip
averaging period = 5.00 sec.
RMS Pressure and RMS Velocity
Gain Corrected Level, Volts(rms)
pressure
z axis
y axis
x axis
2.50
2.00
1.50
1.00
0.50
0.00
225
250
275
300
325
350
375
400
record number

Figure X.9b

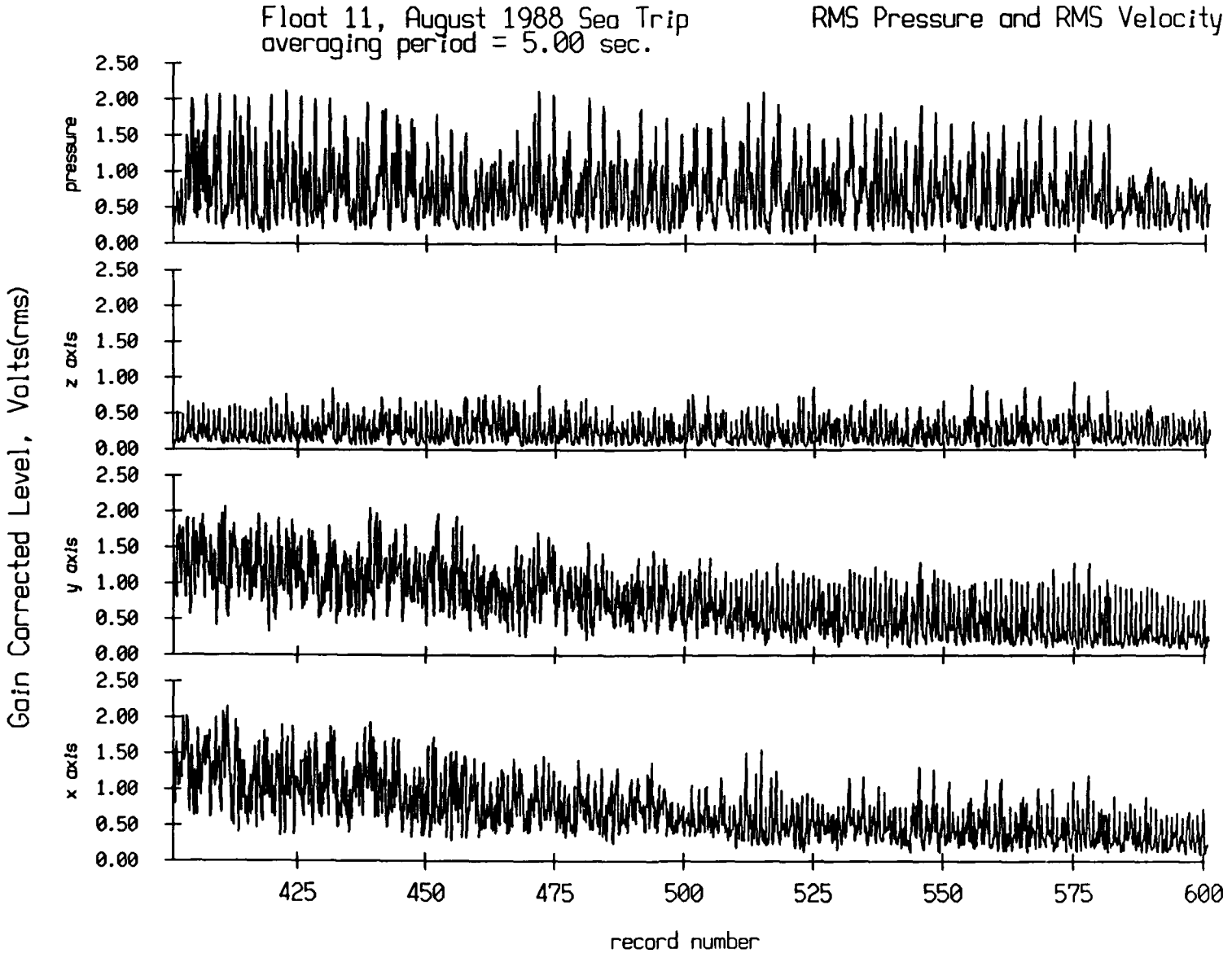

Float 11, August 1988 Sea Trip
averaging period = 5.00 sec.
RMS Pressure and RMS Velocity
Gain Corrected Level, Volts(rms)
pressure
z axis
y axis
x axis
2.50
2.00
1.50
1.00
0.50
0.00
425
450
475
500
525
550
575
600
record number

Figure X.9c

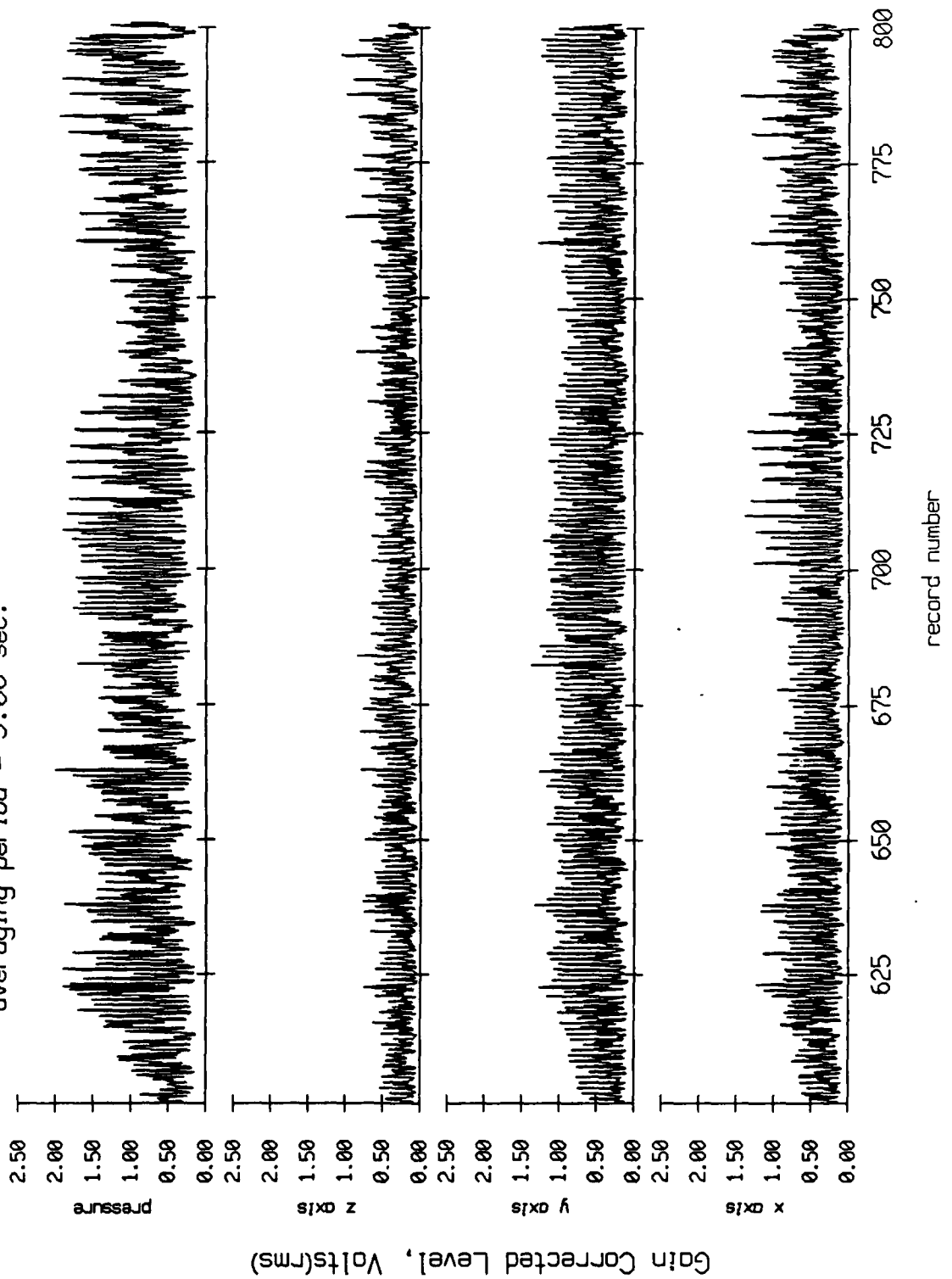

Float 11, August 1988 Sea Trip
averaging period = 5.00 sec.
RMS Pressure and RMS Velocity
Gain Corrected Level, Volts(rms)
pressure
z axis
y axis
x axis
2.50
2.00
1.50
1.00
0.50
0.00
625
650
675
700
725
750
775
800
record number

Figure X.9d

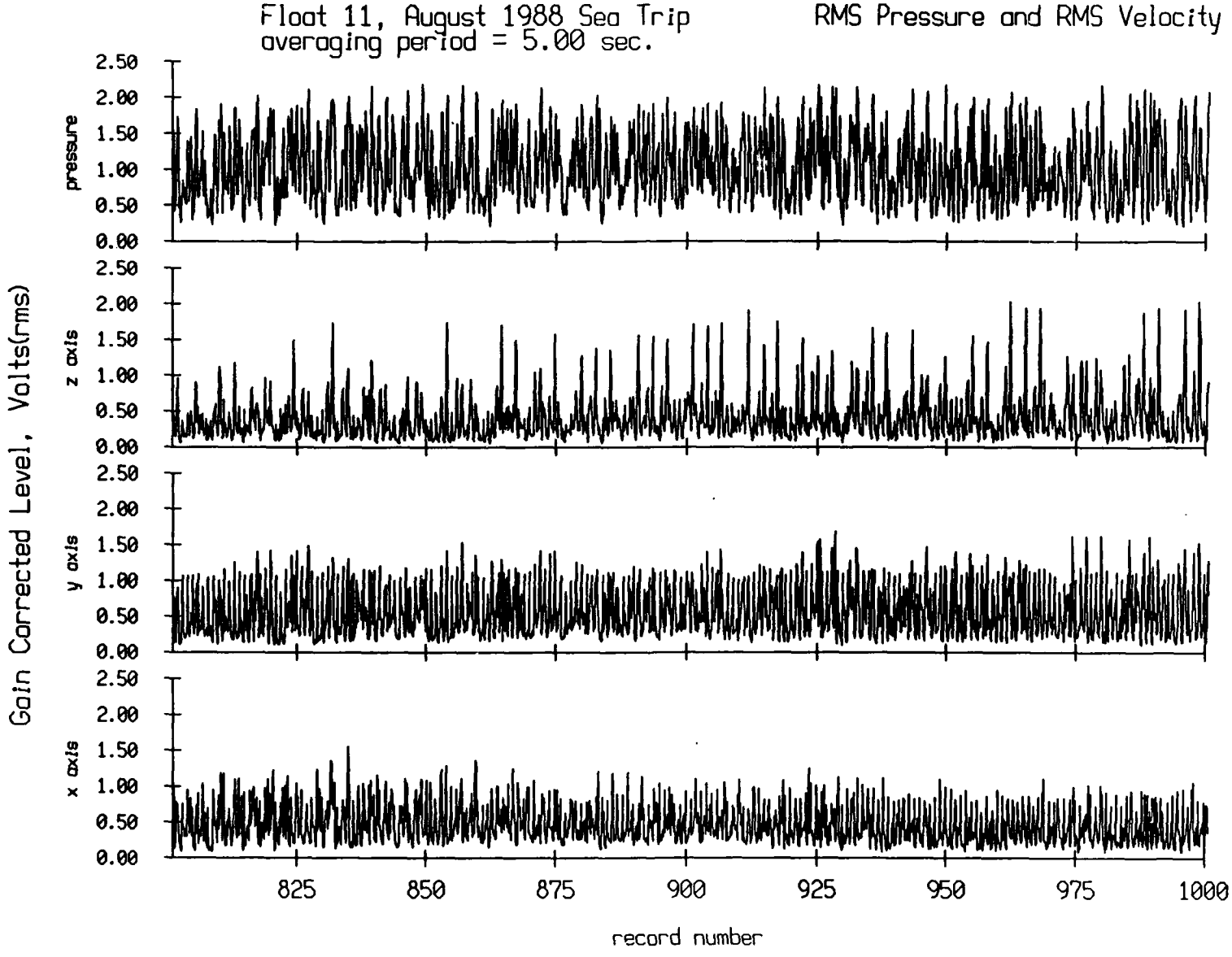

Float 11, August 1988 Sea Trip
averaging period = 5.00 sec.
RMS Pressure and RMS Velocity
Gain Corrected Level, Volts(rms)
pressure
z axis
y axis
x axis
2.50
2.00
1.50
1.00
0.50
0.00
825
850
875
900
925
950
975
1000
record number

Figure X.9e

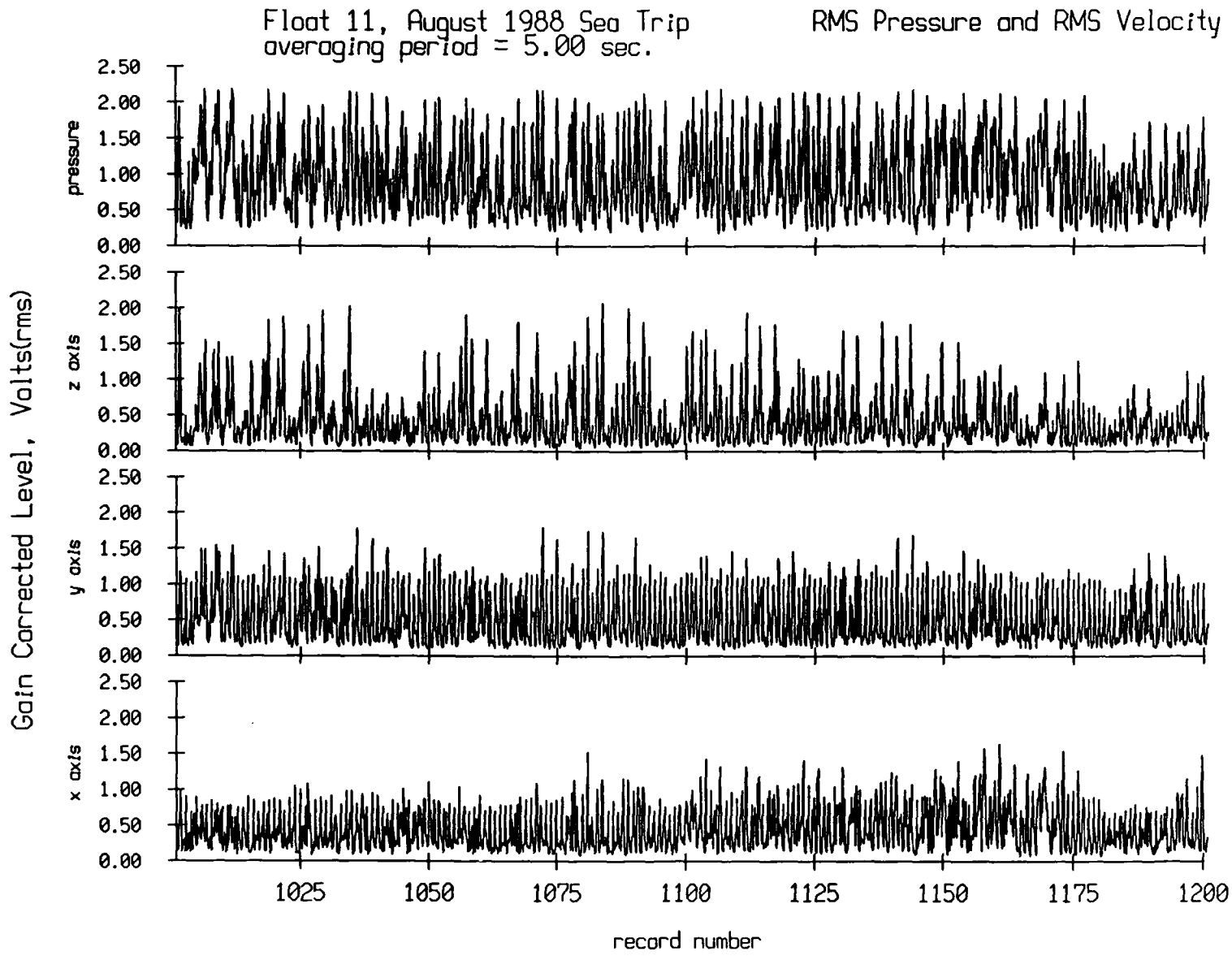

Float 11, August 1988 Sea Trip
averaging period = 5.00 sec.
RMS Pressure and RMS Velocity
Gain Corrected Level, Volts(rms)
pressure
z axis
y axis
x axis
2.50
2.00
1.50
1.00
0.50
0.00
1025
1050
1075
1100
1125
1150
1175
1200
record number

Figure X.9f

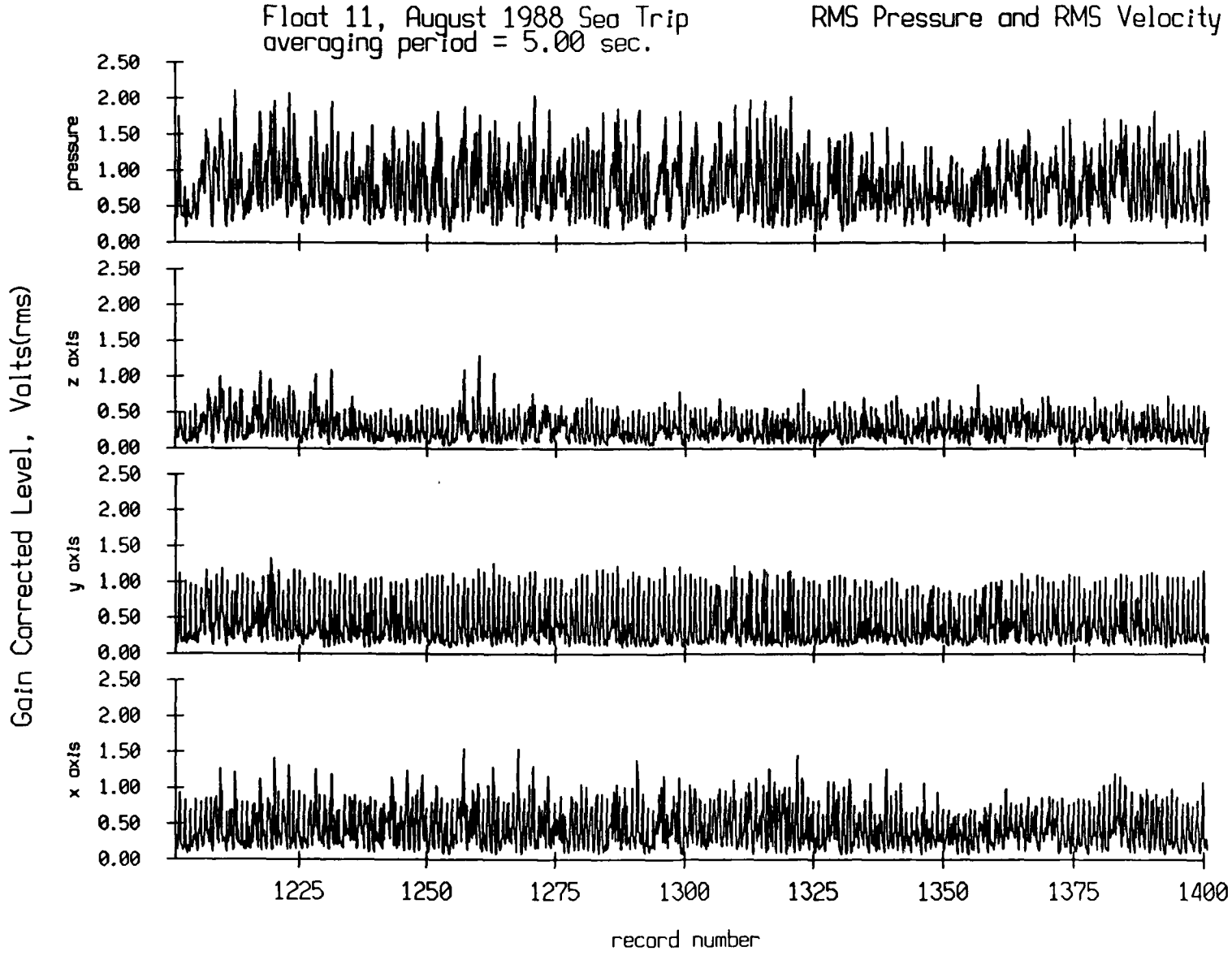

Float 11, August 1988 Sea Trip
averaging period = 5.00 sec.
RMS Pressure and RMS Velocity
Gain Corrected Level, Volts(rms)
pressure
z axis
y axis
x axis
2.50
2.00
1.50
1.00
0.50
0.00
1225
1250
1275
1300
1325
1350
1375
1400
record number

Figure X.9g

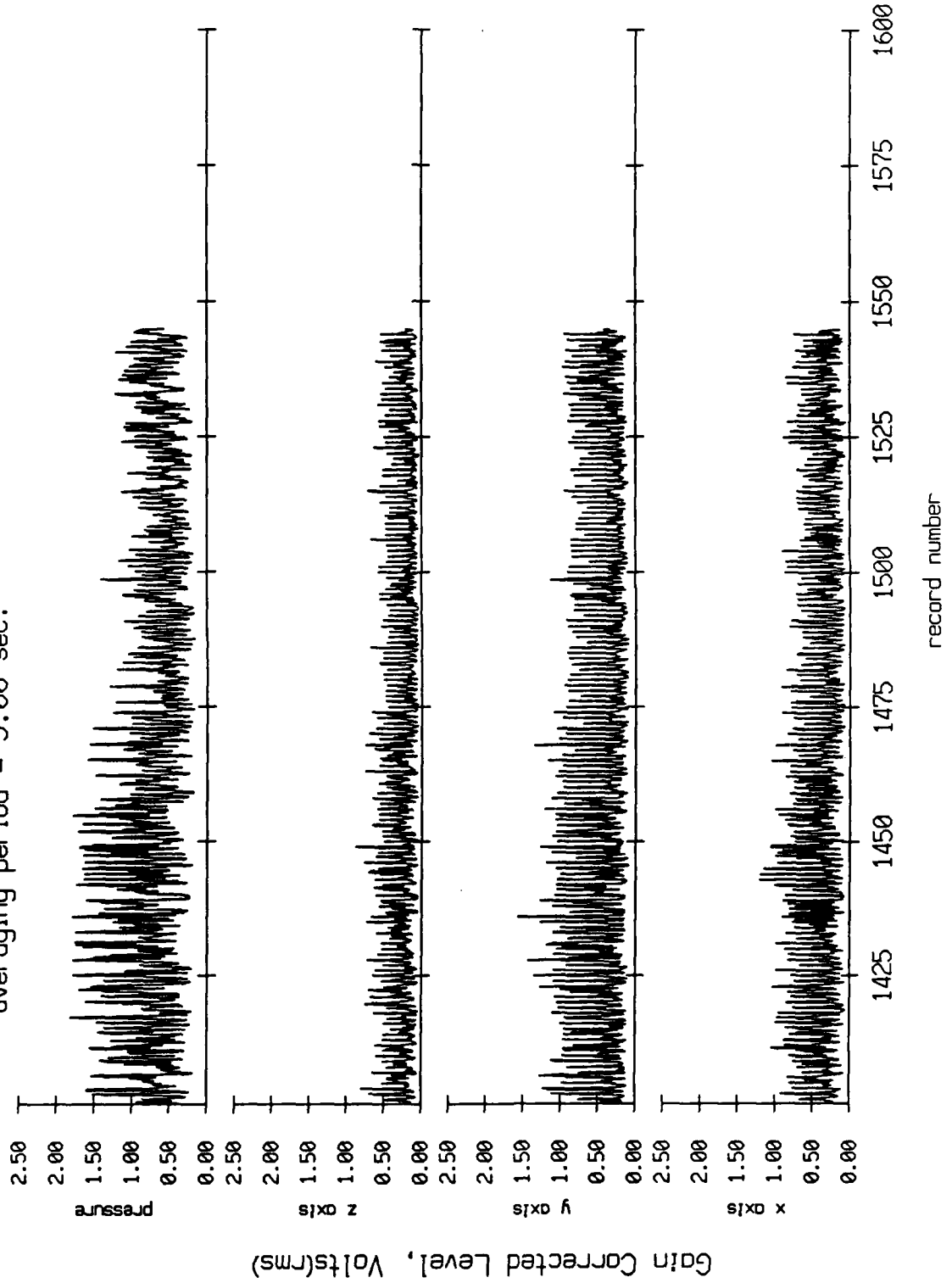

Float 11, August 1988 Sea Trip
averaging period = 5.00 sec.
RMS Pressure and RMS Velocity
Gain Corrected Level, Volts(rms)
pressure
z axis
y axis
x axis
2.50
2.00
1.50
1.00
0.50
0.00
1425
1450
1475
1500
1525
1550
1575
1600
record number

Figure X.9h

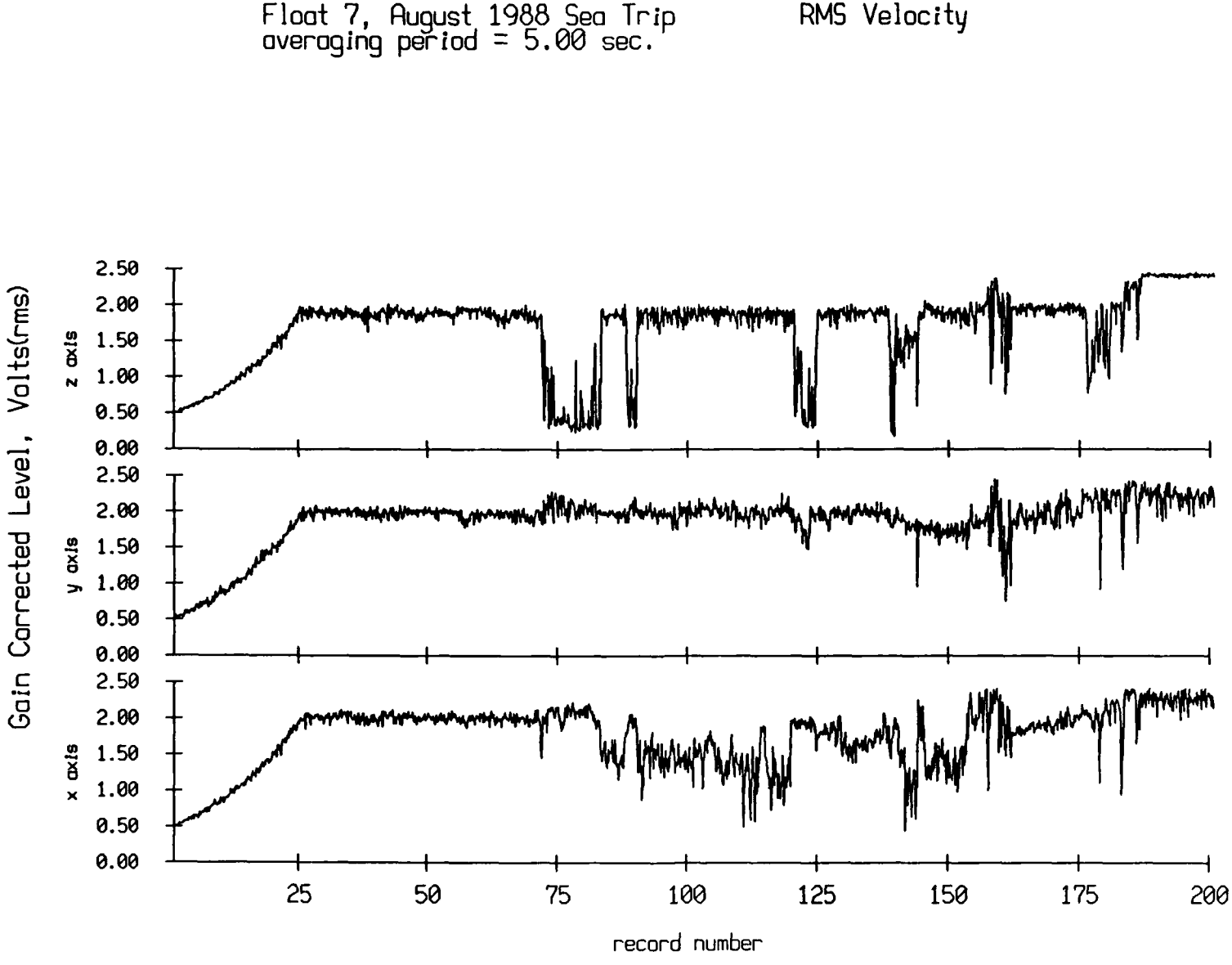

Float 7, August 1988 Sea Trip
averaging period = 5.00 sec.
RMS Velocity
Gain Corrected Level, Volts(rms)
z axis
y axis
x axis
2.50
2.00
1.50
1.00
0.50
0.00
25
50
75
100
125
150
175
200
record number

Figure X.10a

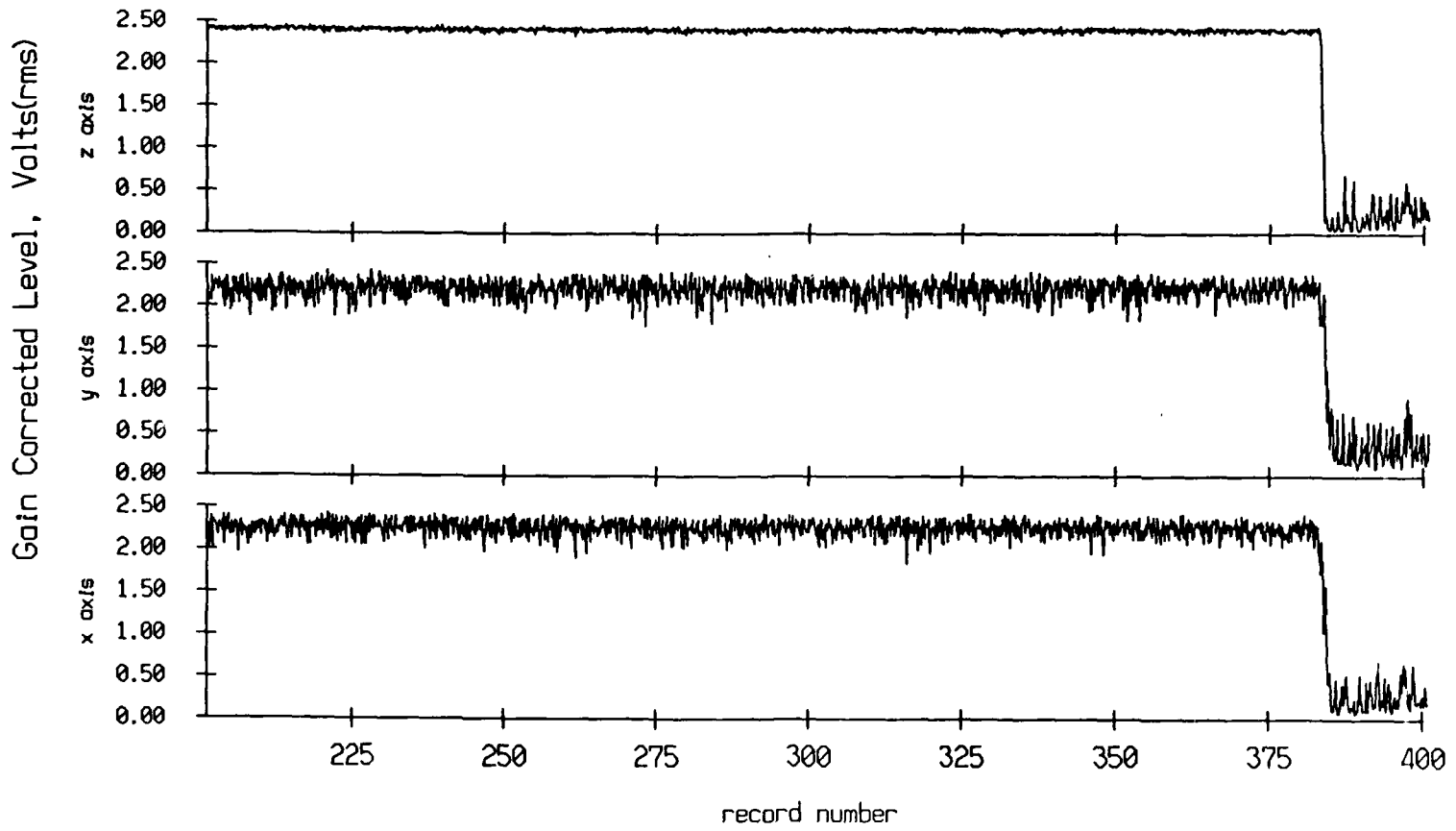

Float 7, August 1988 Sea Trip
averaging period = 5.00 sec.
RMS Velocity
Gain Corrected Level, Volts(rms)
z axis
y axis
x axis
2.50
2.00
1.50
1.00
0.50
0.00
225
250
275
300
325
350
375
400
record number

Figure X.10b

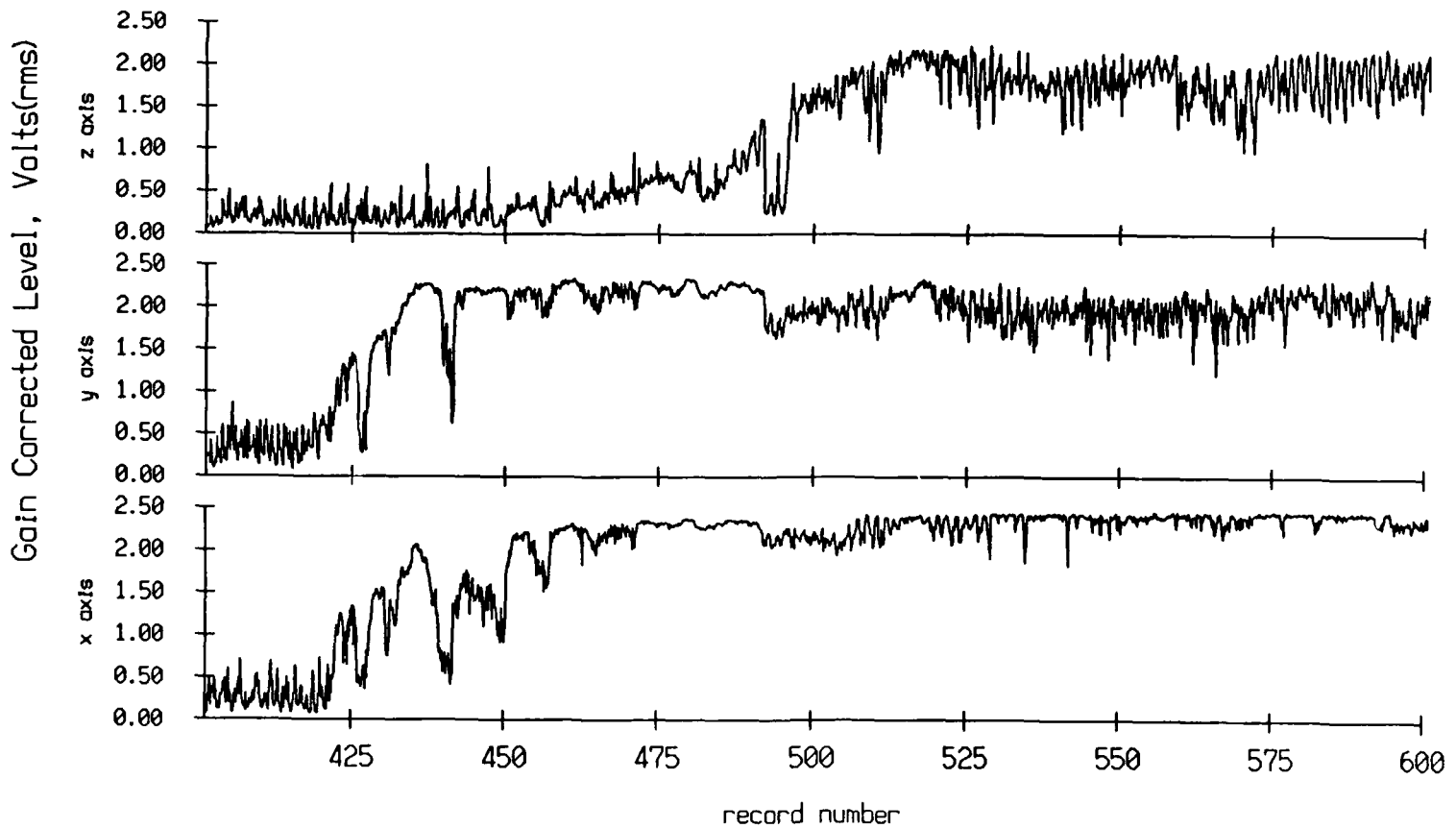

Floot 7, August 1988 Sea Trip
overaging period = 5.00 sec.
RMS Velocity
Gain Corrected Level, Volts(rms)
z axis
y axis
x axis
2.50
2.00
1.50
1.00
0.50
0.00
425
450
475
500
525
550
575
600
record number

Figure X.10c

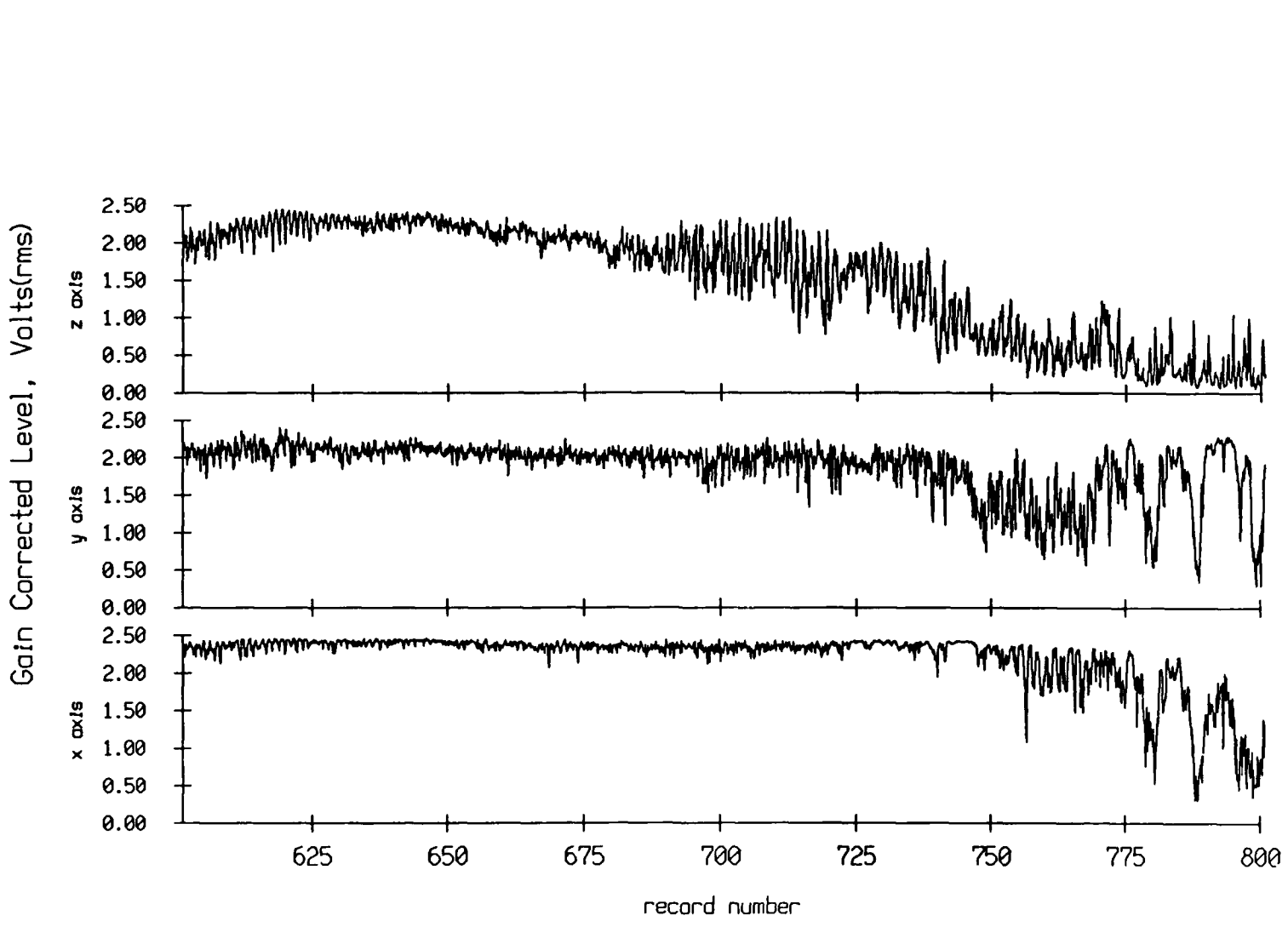

Float 7, August 1988 Sea Trip
averaging period = 5.00 sec.
RMS Velocity
Gain Corrected Level, Volts(rms)
z axis
y axis
x axis
2.50
2.00
1.50
1.00
0.50
0.00
625
650
675
700
725
750
775
800
record number

Figure X.10d

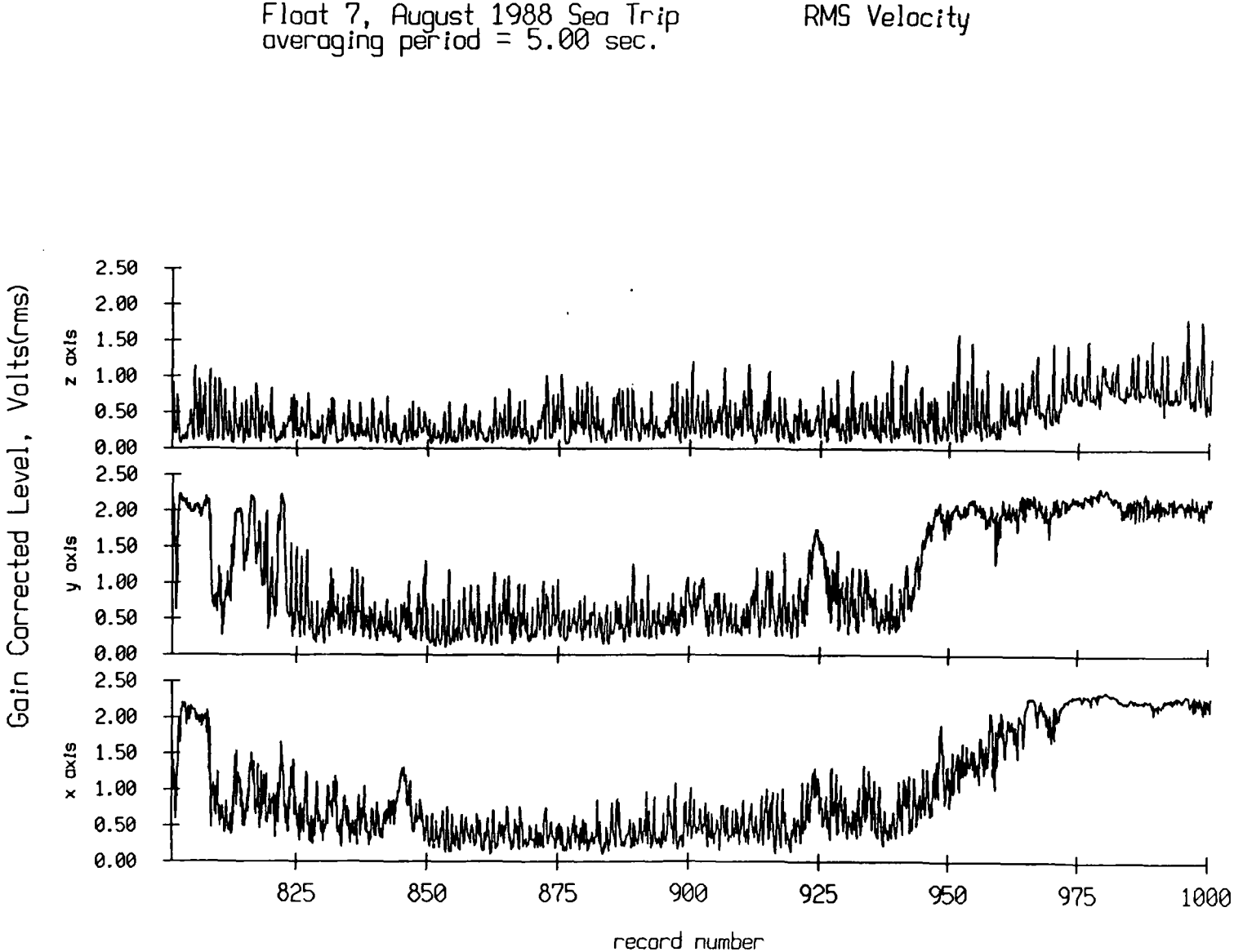

Float 7, August 1988 Sea Trip
averaging period = 5.00 sec.
RMS Velocity
Gain Corrected Level, Volts(rms)
z axis
y axis
x axis
2.50
2.00
1.50
1.00
0.50
0.00
825
850
875
900
925
950
975
1000
record number

Figure X.10e

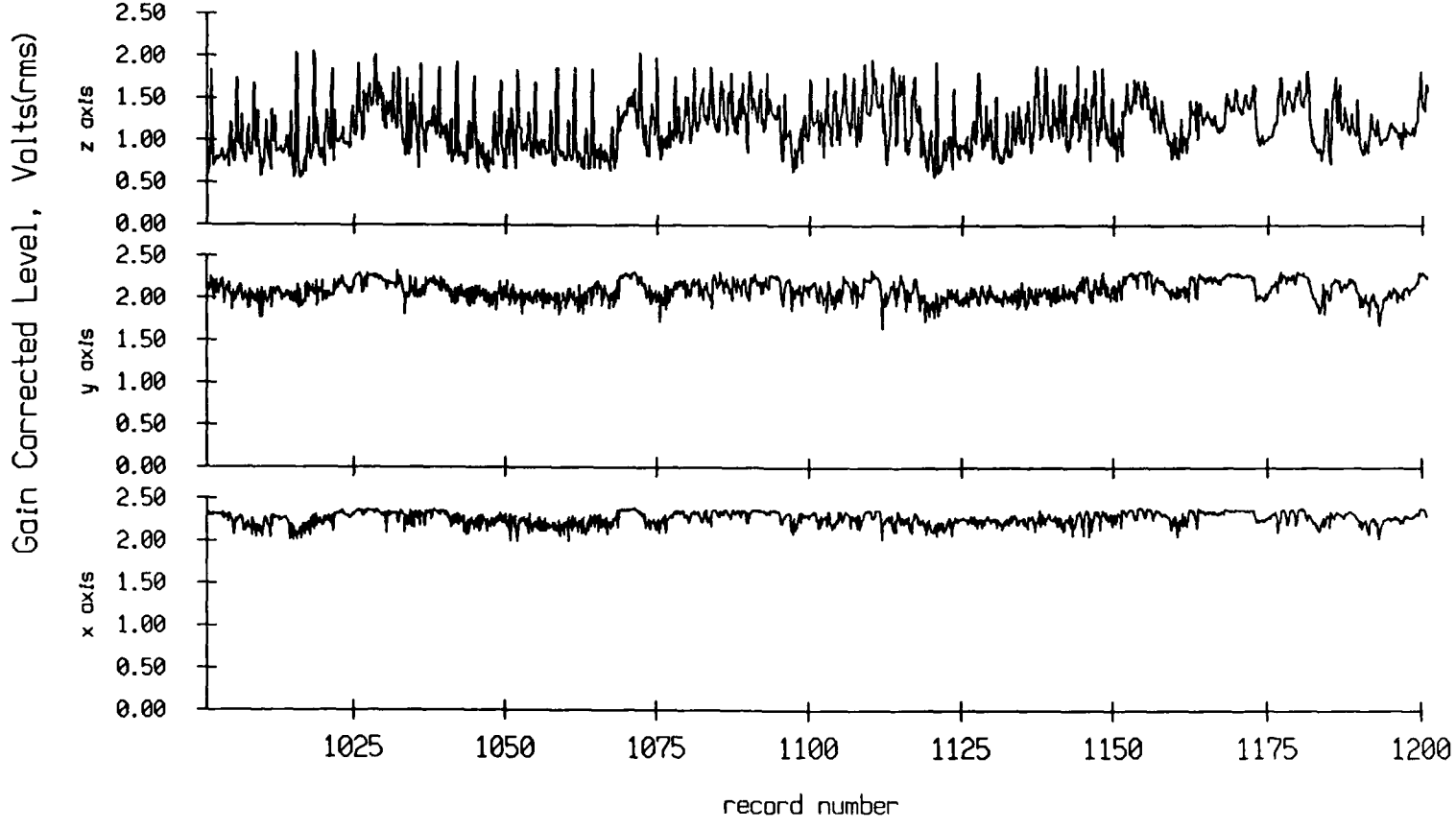

Float 7, August 1988 Sea Trip
averaging period = 5.00 sec.
RMS Velocity
Gain Corrected Level, Volts(rms)
z axis
y axis
x axis
2.50
2.00
1.50
1.00
0.50
0.00
1025
1050
1075
1100
1125
1150
1175
1200
record number

Figure X.10f

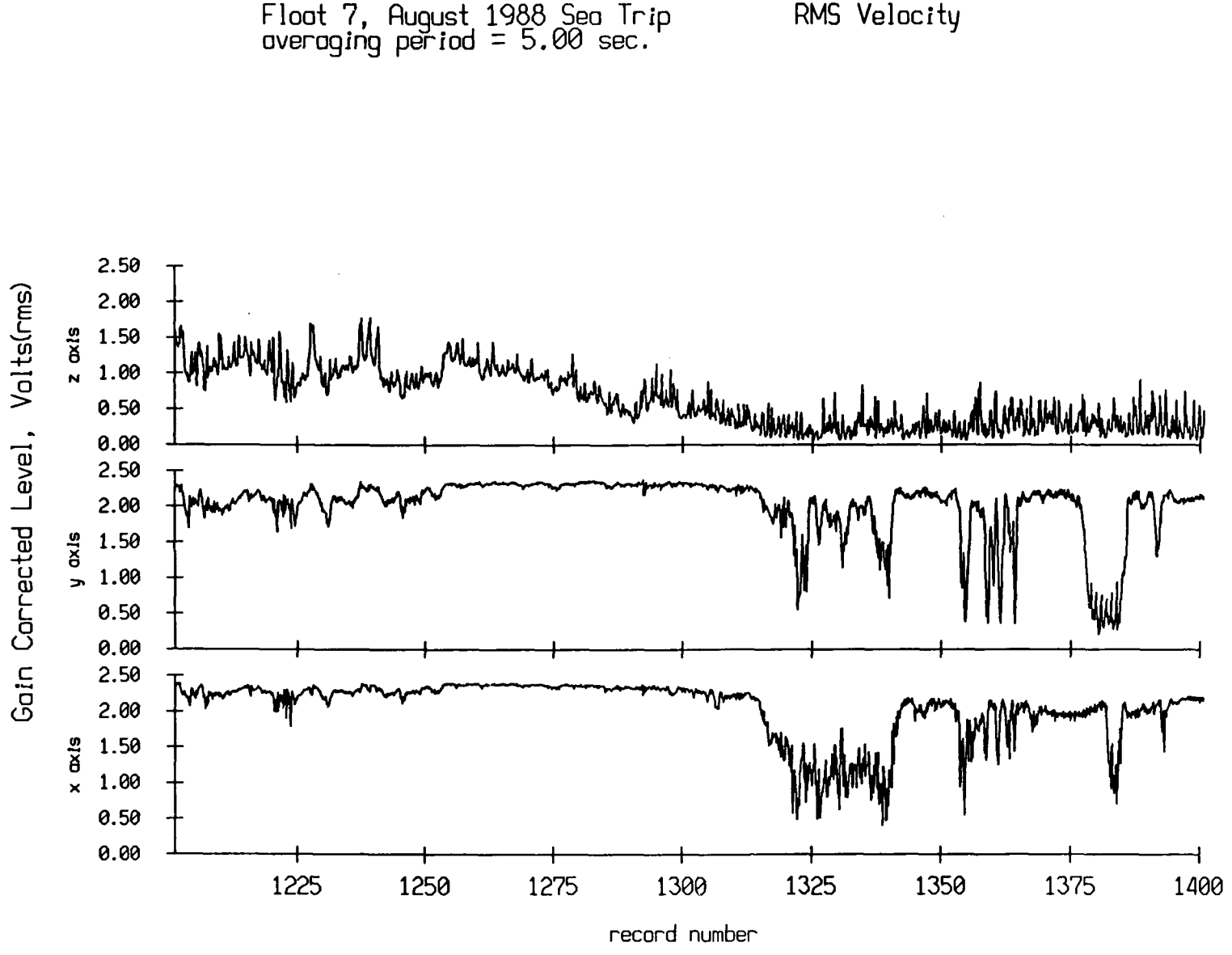

Float 7, August 1988 Sea Trip
averaging period = 5.00 sec.
RMS Velocity
Gain Corrected Level, Volts(rms)
z axis
y axis
x axis
2.50
2.00
1.50
1.00
0.50
0.00
1225
1250
1275
1300
1325
1350
1375
1400
record number

Figure X.10g

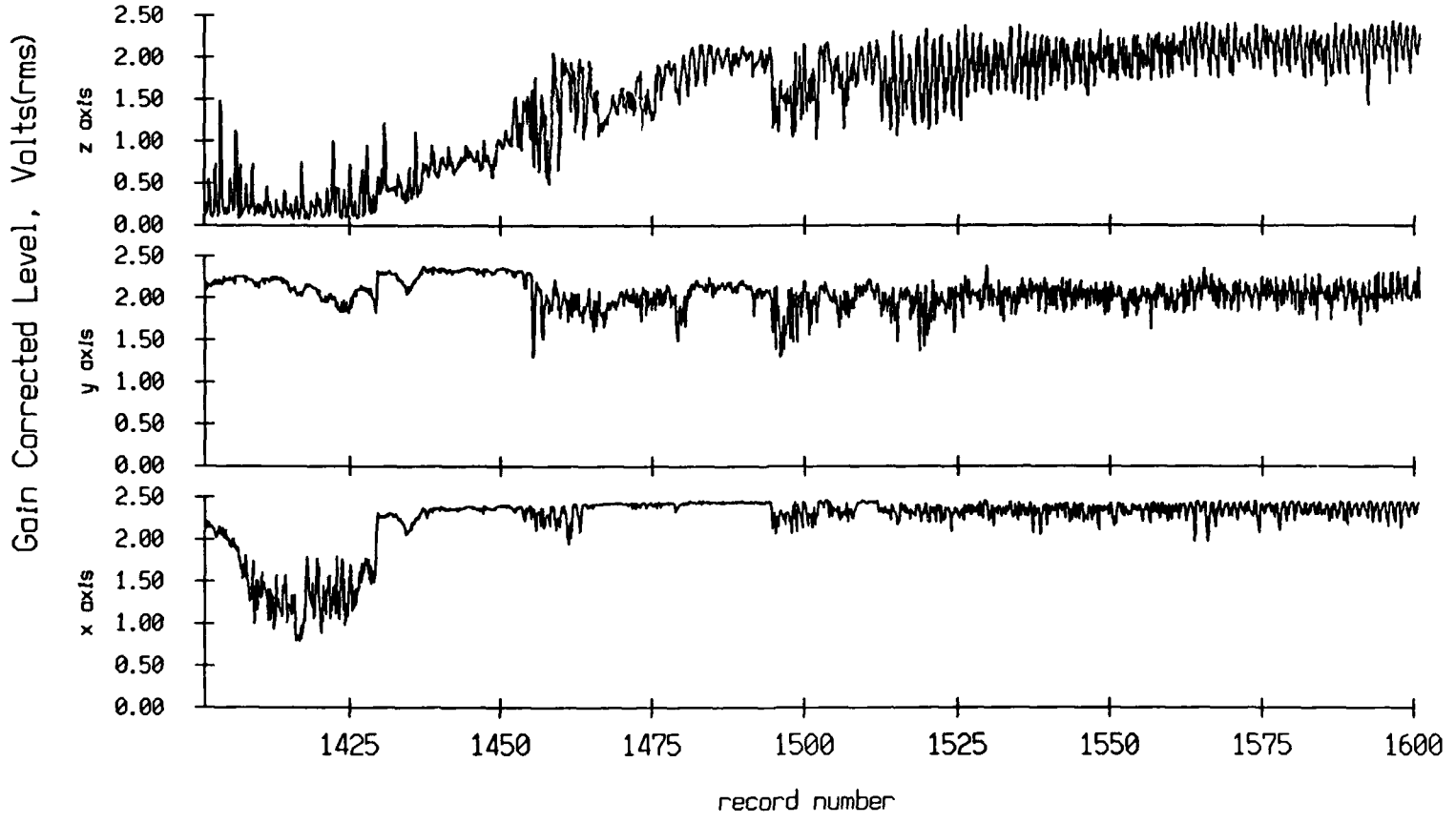

Float 7, August 1988 Sea Trip
averaging period = 5.00 sec.
RMS Velocity
Gain Corrected Level, Volts(rms)
z axis
y axis
x axis
2.50
2.00
1.50
1.00
0.50
0.00
1425
1450
1475
1500
1525
1550
1575
1600
record number

Figure X.10h

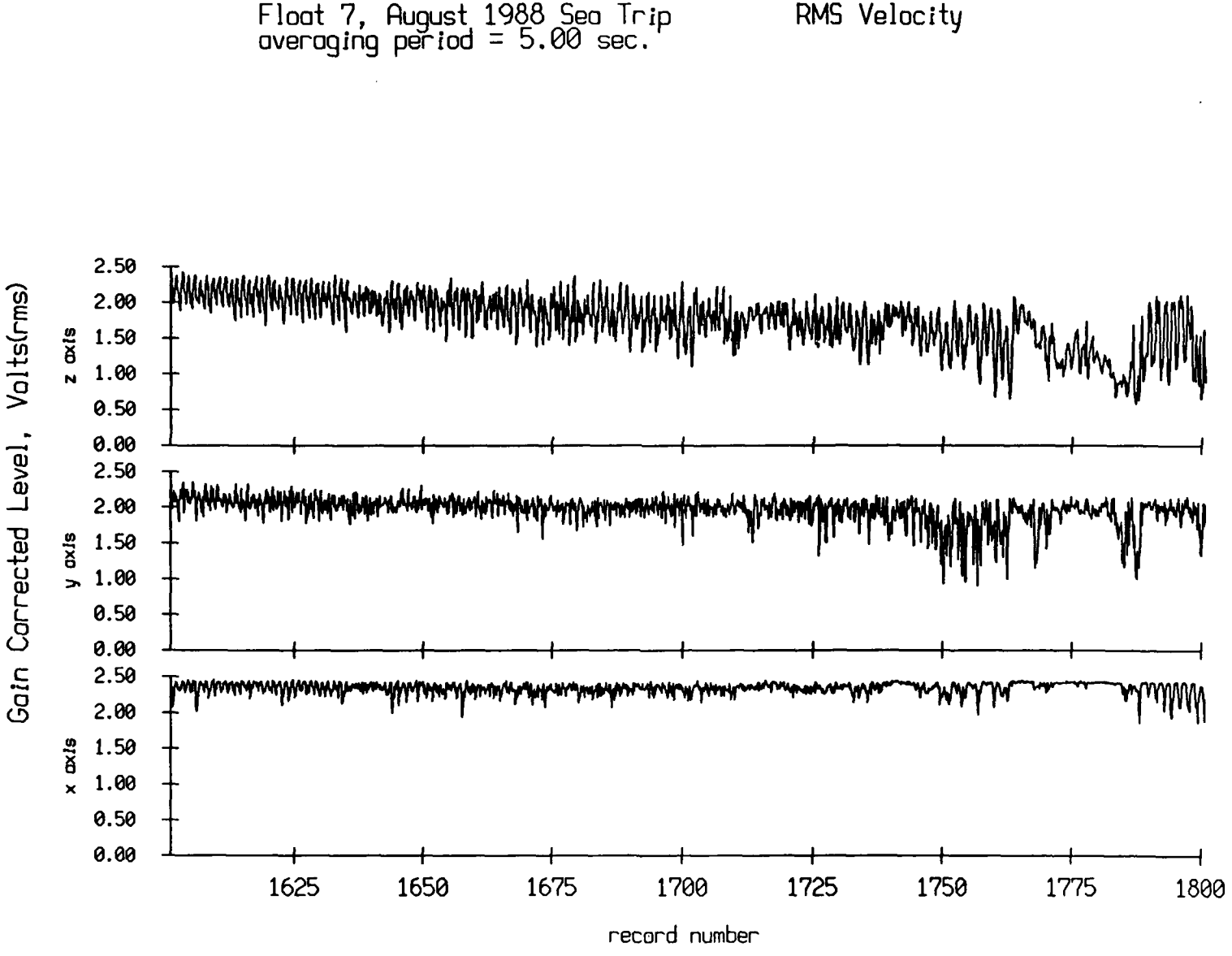

Float 7, August 1988 Sea Trip
averaging period = 5.00 sec.
RMS Velocity
Gain Corrected Level, Volts(rms)
z axis
y axis
x axis
2.50
2.00
1.50
1.00
0.50
0.00
1625
1650
1675
1700
1725
1750
1775
1800
record number

Figure X.10i

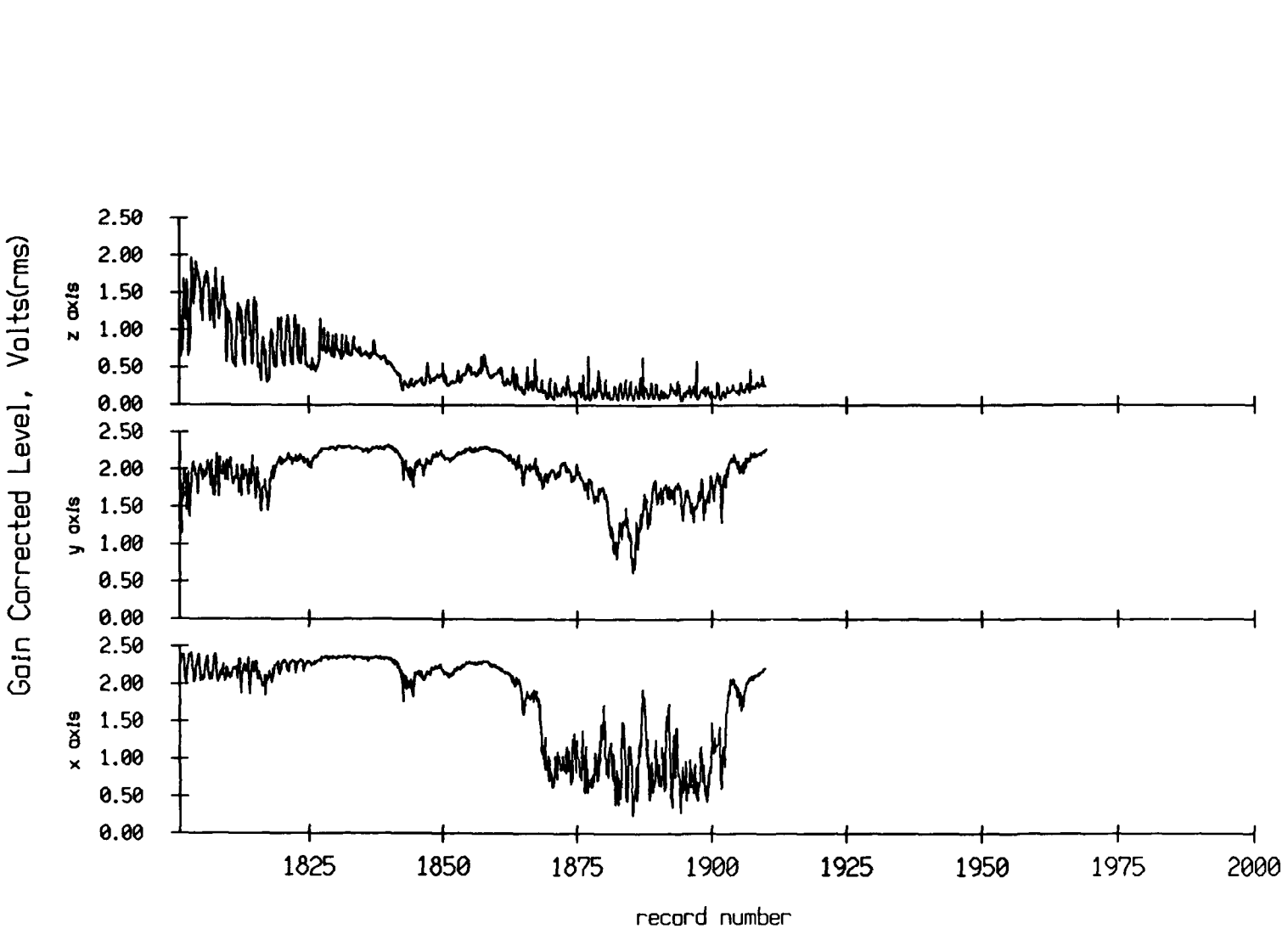

Float 7, August 1988 Sea Trip
averaging period = 5.00 sec.
RMS Velocity
Gain Corrected Level, Volts(rms)
z axis
y axis
x axis
2.50
2.00
1.50
1.00
0.50
0.00
1825
1850
1875
1900
1925
1950
1975
2000
record number

Figure X.10j

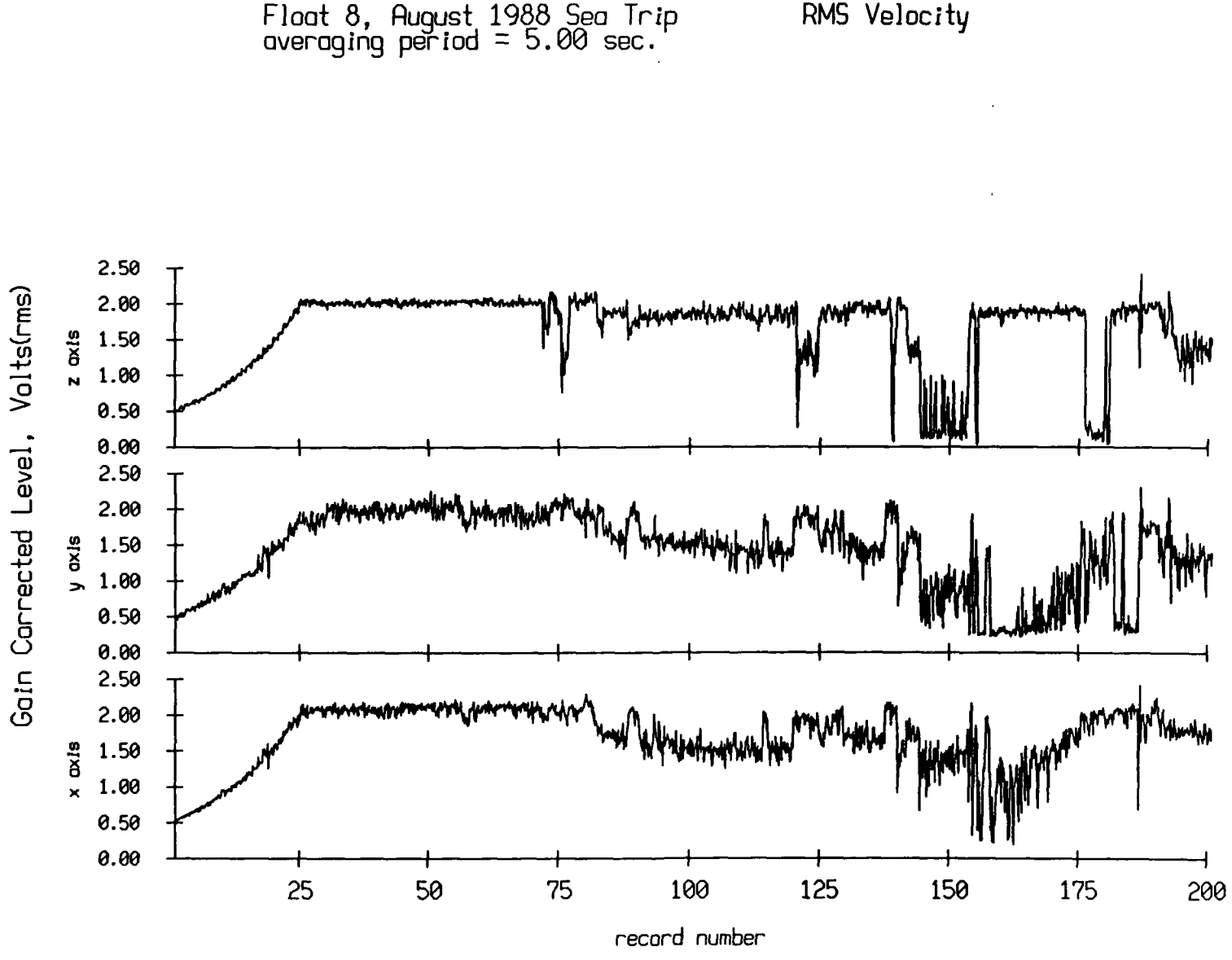

Float 8, August 1988 Sea Trip
averaging period = 5.00 sec.
RMS Velocity
Gain Corrected Level, Volts(rms)
z axis
y axis
x axis
2.50
2.00
1.50
1.00
0.50
0.00
25
50
75
100
125
150
175
200
record number

Figure X.11a

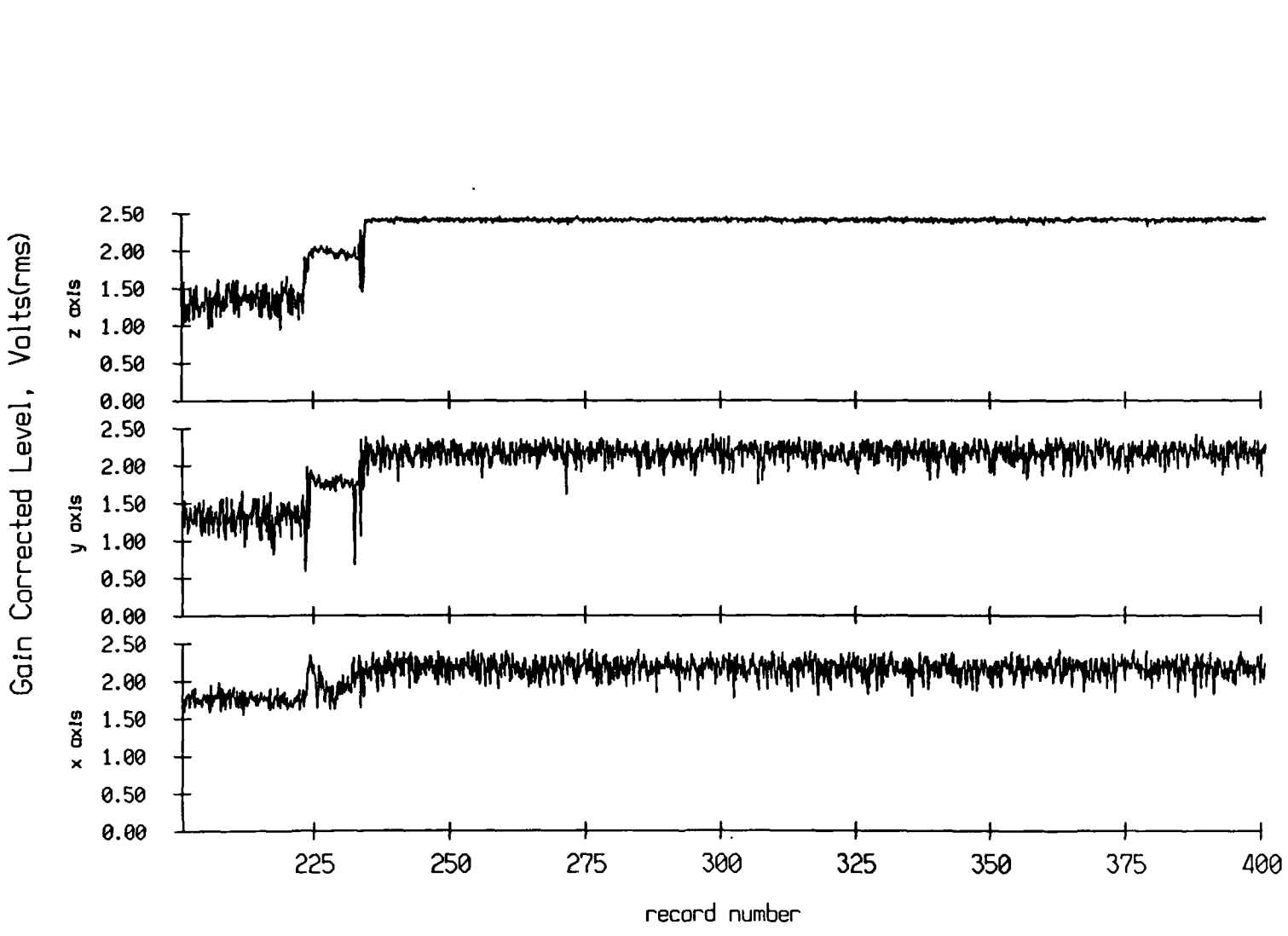

Float 8, August 1988 Sea Trip
averaging period = 5.00 sec.
RMS Velocity
Gain Corrected Level, Volts(rms)
z axis
y axis
x axis
2.50
2.00
1.50
1.00
0.50
0.00
225
250
275
300
325
350
375
400
record number

Figure X.11b

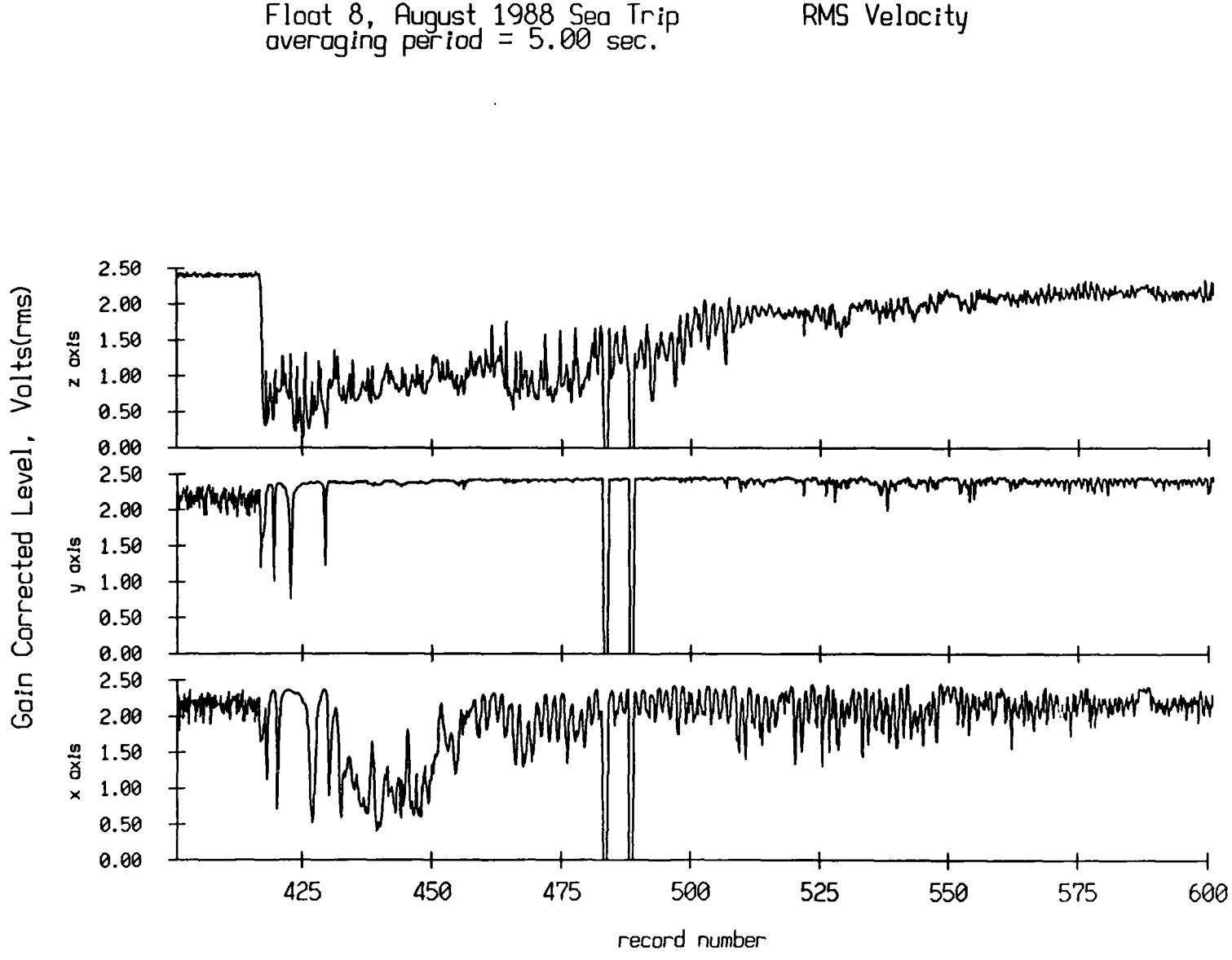

Float 8, August 1988 Sea Trip
averaging period = 5.00 sec.
RMS Velocity
Gain Corrected Level, Volts(rms)
z axis
y axis
x axis
2.50
2.00
1.50
1.00
0.50
0.00
425
450
475
500
525
550
575
600
record number

Figure X.11c

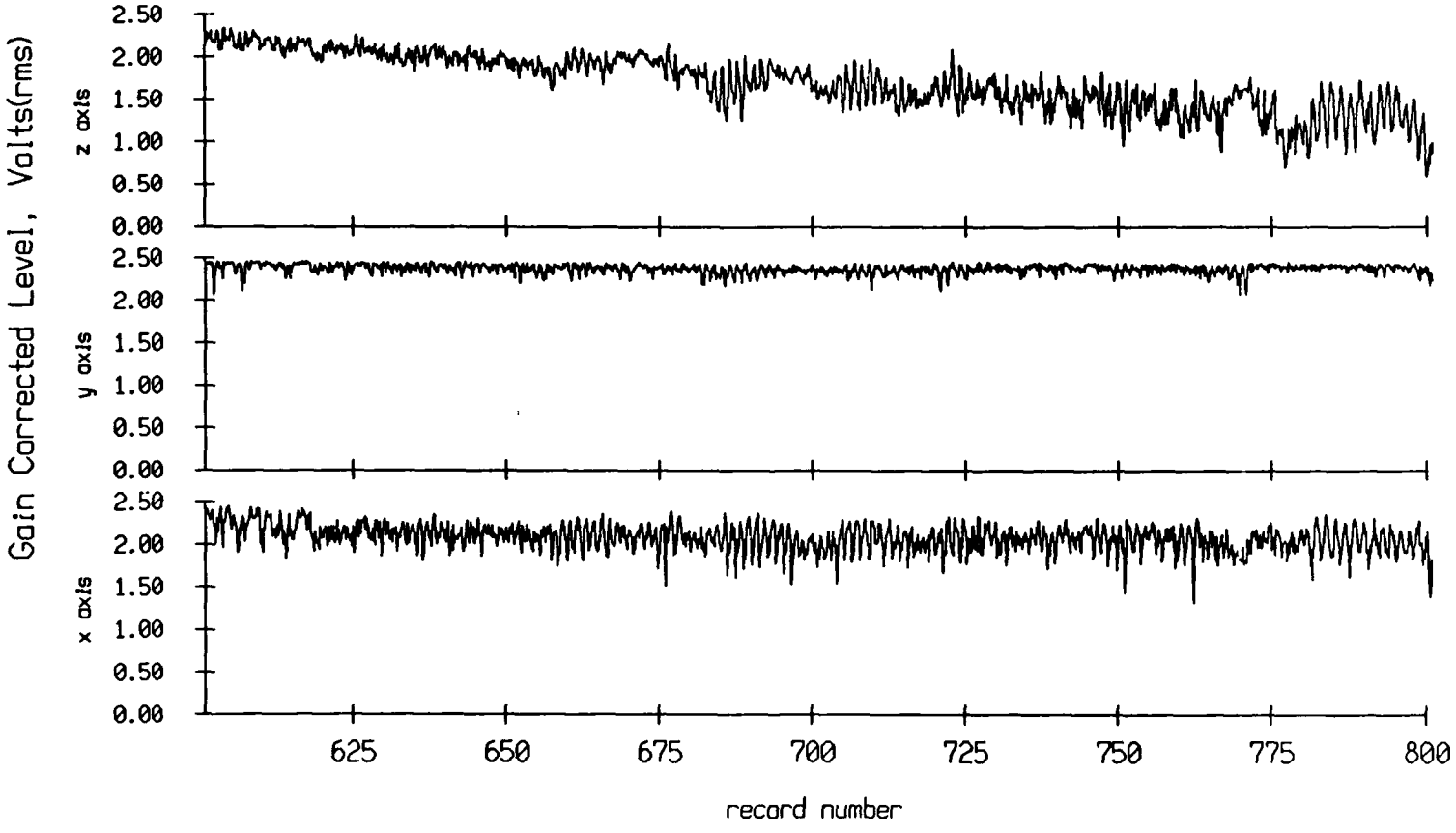

Float 8, August 1988 Sea Trip
averaging period = 5.00 sec.
RMS Velocity
Gain Corrected Level, Volts(rms)
z axis
y axis
x axis
2.50
2.00
1.50
1.00
0.50
0.00
625
650
675
700
725
750
775
800
record number

Figure XIId

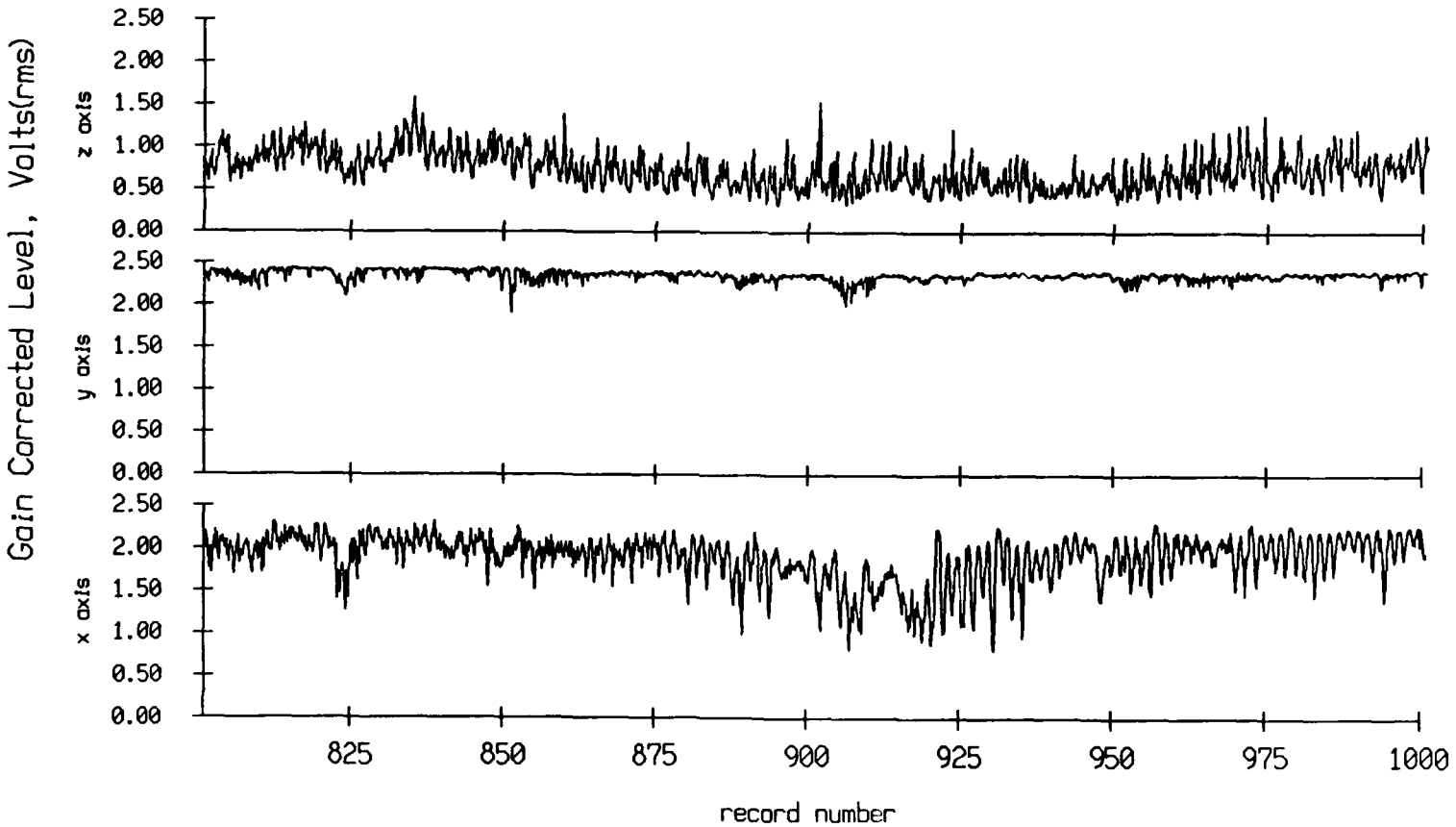

Float 8, August 1988 Sea Trip
averaging period = 5.00 sec.
RMS Velocity
Gain Corrected Level, Volts(rms)
z axis
y axis
x axis
2.50
2.00
1.50
1.00
0.50
0.00
825
850
875
900
925
950
975
1000
record number

Figure X.11e

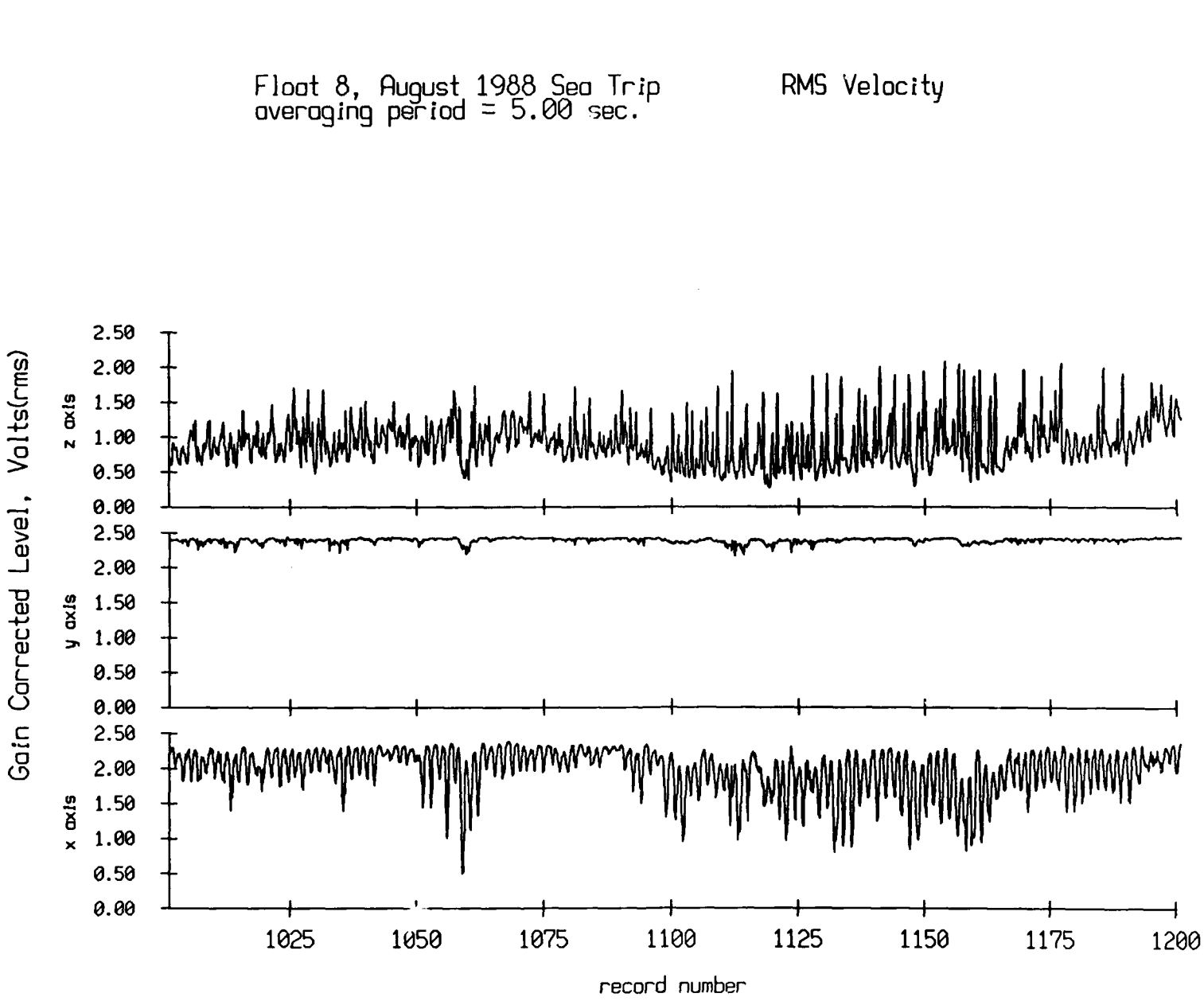

Float 8, August 1988 Sea Trip
averaging period = 5.00 sec.
RMS Velocity
Gain Corrected Level, Volts(rms)
z axis
y axis
x axis
2.50
2.00
1.50
1.00
0.50
0.00
1025
1050
1075
1100
1125
1150
1175
1200
record number

Figure X.11f

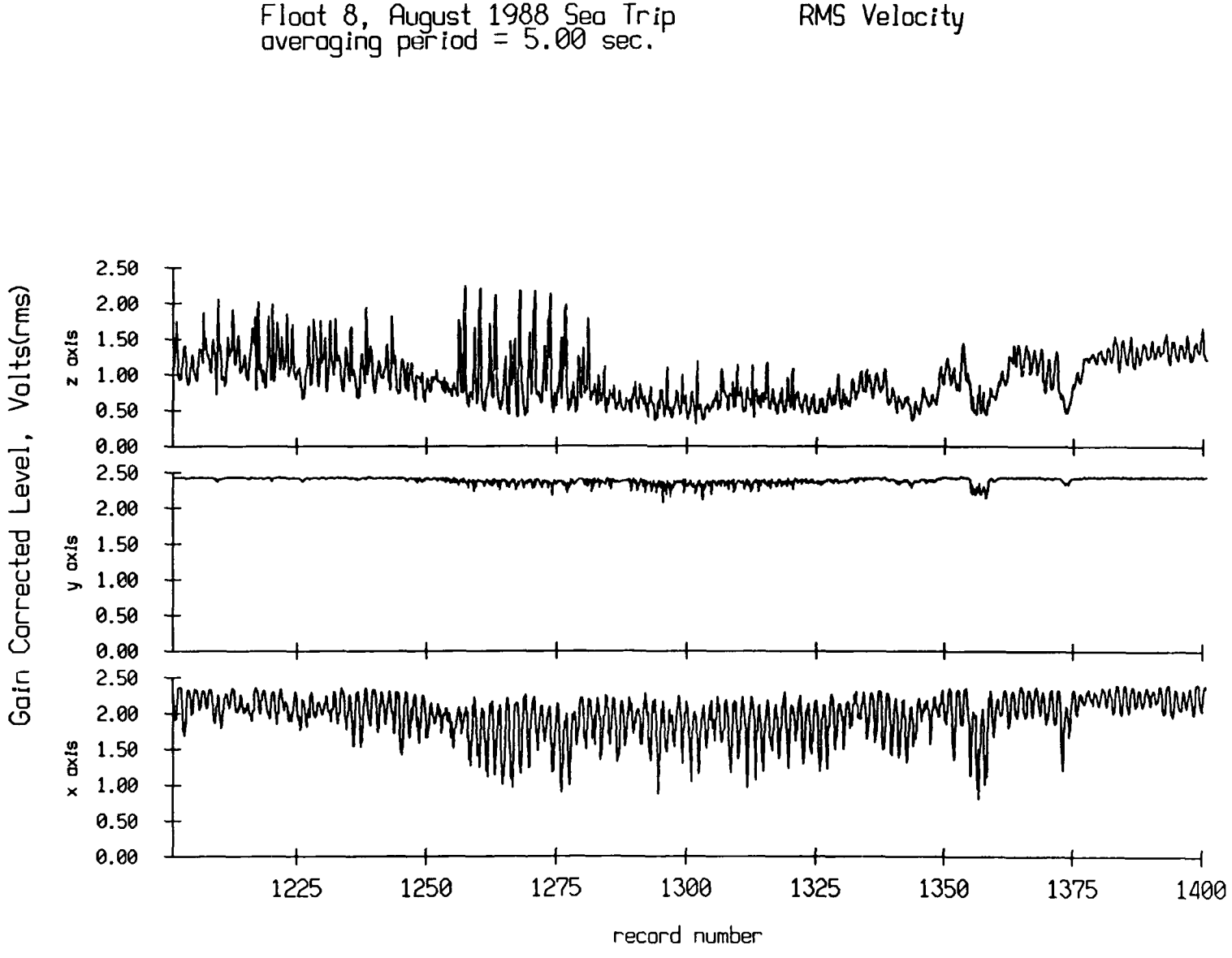

Float 8, August 1988 Sea Trip
averaging period = 5.00 sec.
RMS Velocity
Gain Corrected Level, Volts(rms)
z axis
y axis
x axis
2.50
2.00
1.50
1.00
0.50
0.00
1225
1250
1275
1300
1325
1350
1375
1400
record number

Figure X.11g

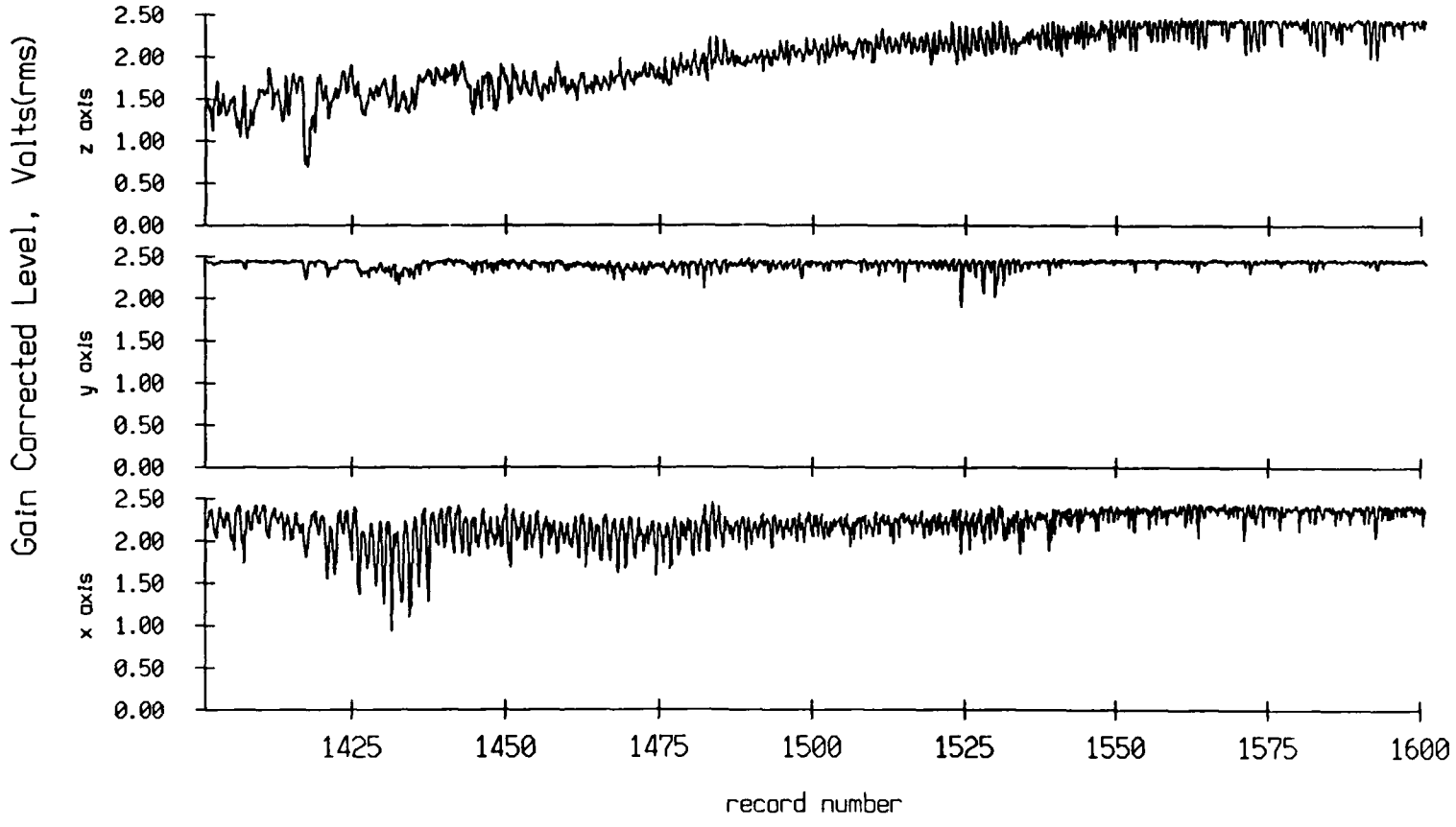

Float 8, August 1988 Sea Trip
averaging period = 5.00 sec.
RMS Velocity
Gain Corrected Level, Volts(rms)
z axis
y axis
x axis
2.50
2.00
1.50
1.00
0.50
0.00
1425
1450
1475
1500
1525
1550
1575
1600
record number

Figure X.11h

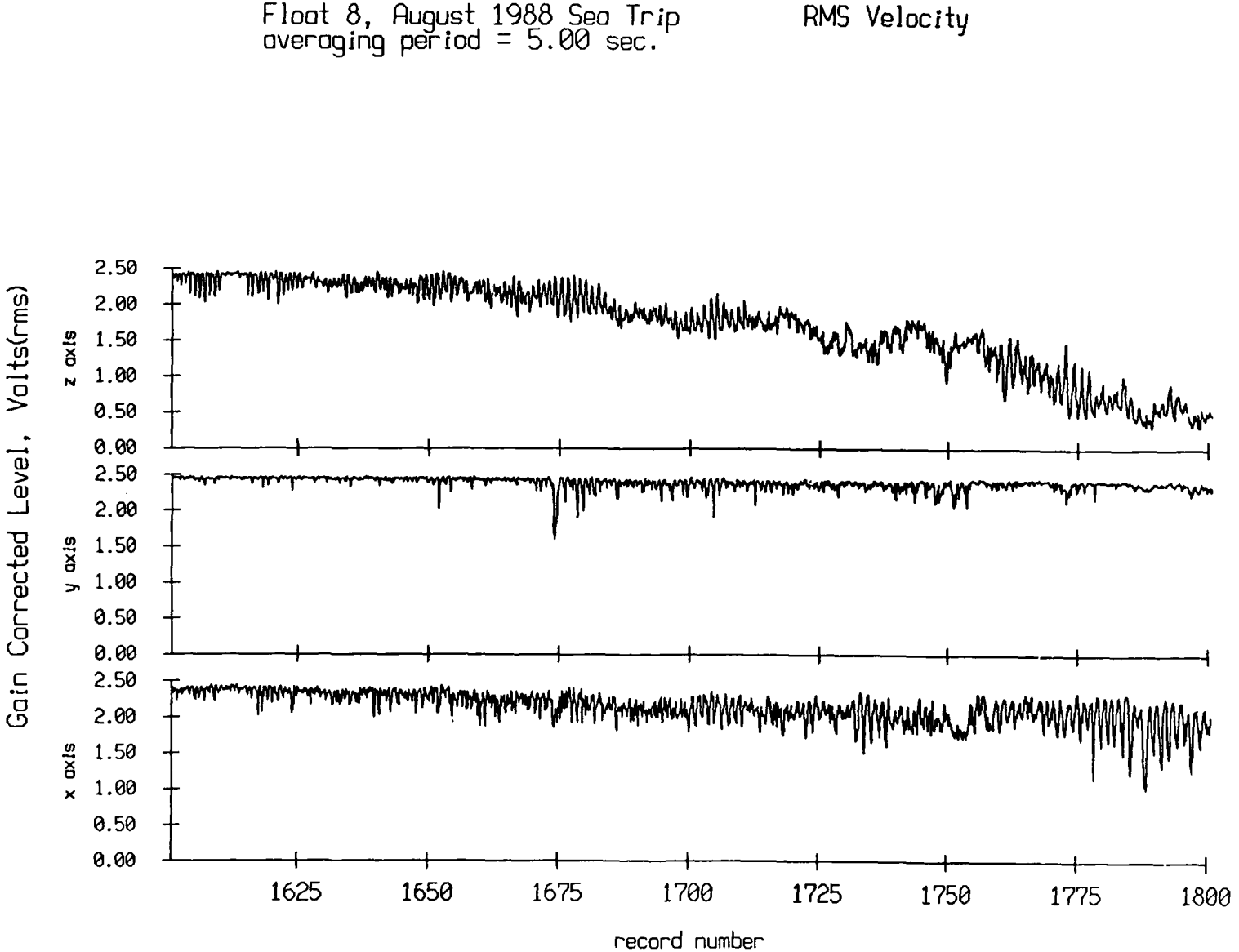

Float 8, August 1988 Sea Trip
averaging period = 5.00 sec.
RMS Velocity
Gain Corrected Level, Volts(rms)
z axis
y axis
x axis
2.50
2.00
1.50
1.00
0.50
0.00
1625
1650
1675
1700
1725
1750
1775
1800
record number

Figure X.11i

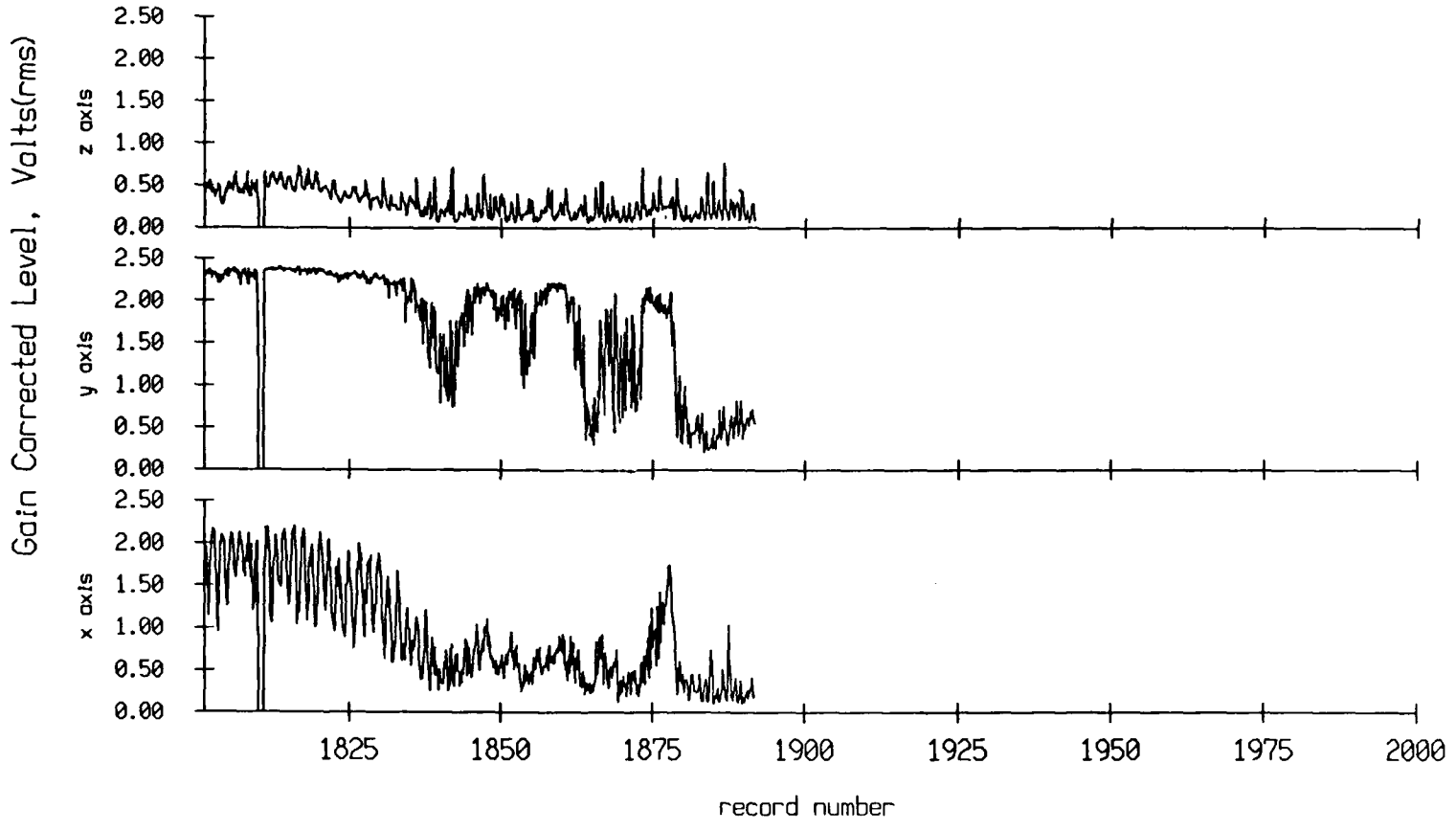

Float 8, August 1988 Sea Trip
averaging period = 5.00 sec.
RMS Velocity
Gain Corrected Level, Volts(rms)
z axis
y axis
x axis
2.50
2.00
1.50
1.00
0.50
0.00
1825
1850
1875
1900
1925
1950
1975
2000
record number

Figure X.11j

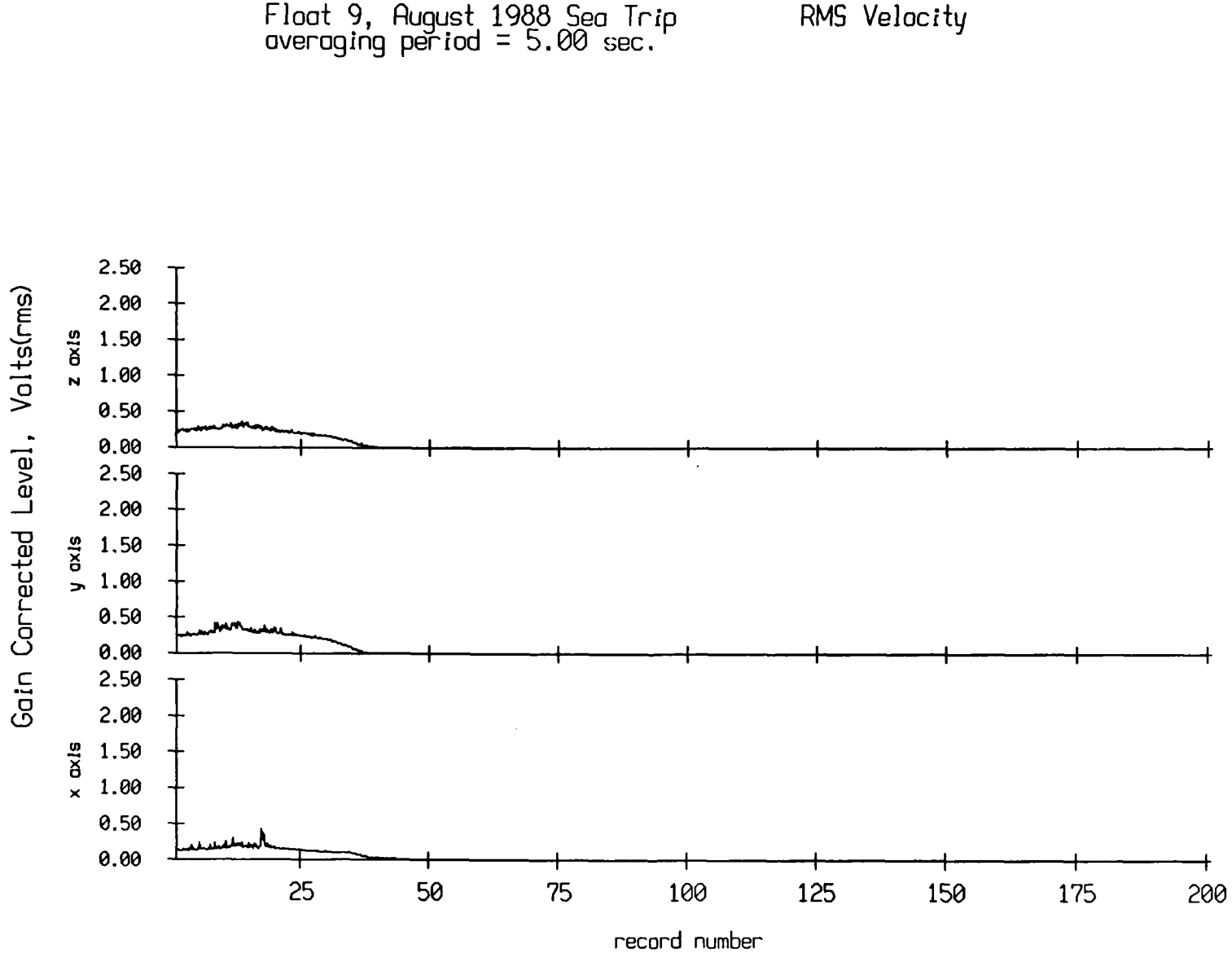

Float 9, August 1988 Sea Trip
averaging period = 5.00 sec.
RMS Velocity
Gain Corrected Level, Volts(rms)
z axis
y axis
x axis
2.50
2.00
1.50
1.00
0.50
0.00
25
50
75
100
125
150
175
200
record number

Figure X.12a

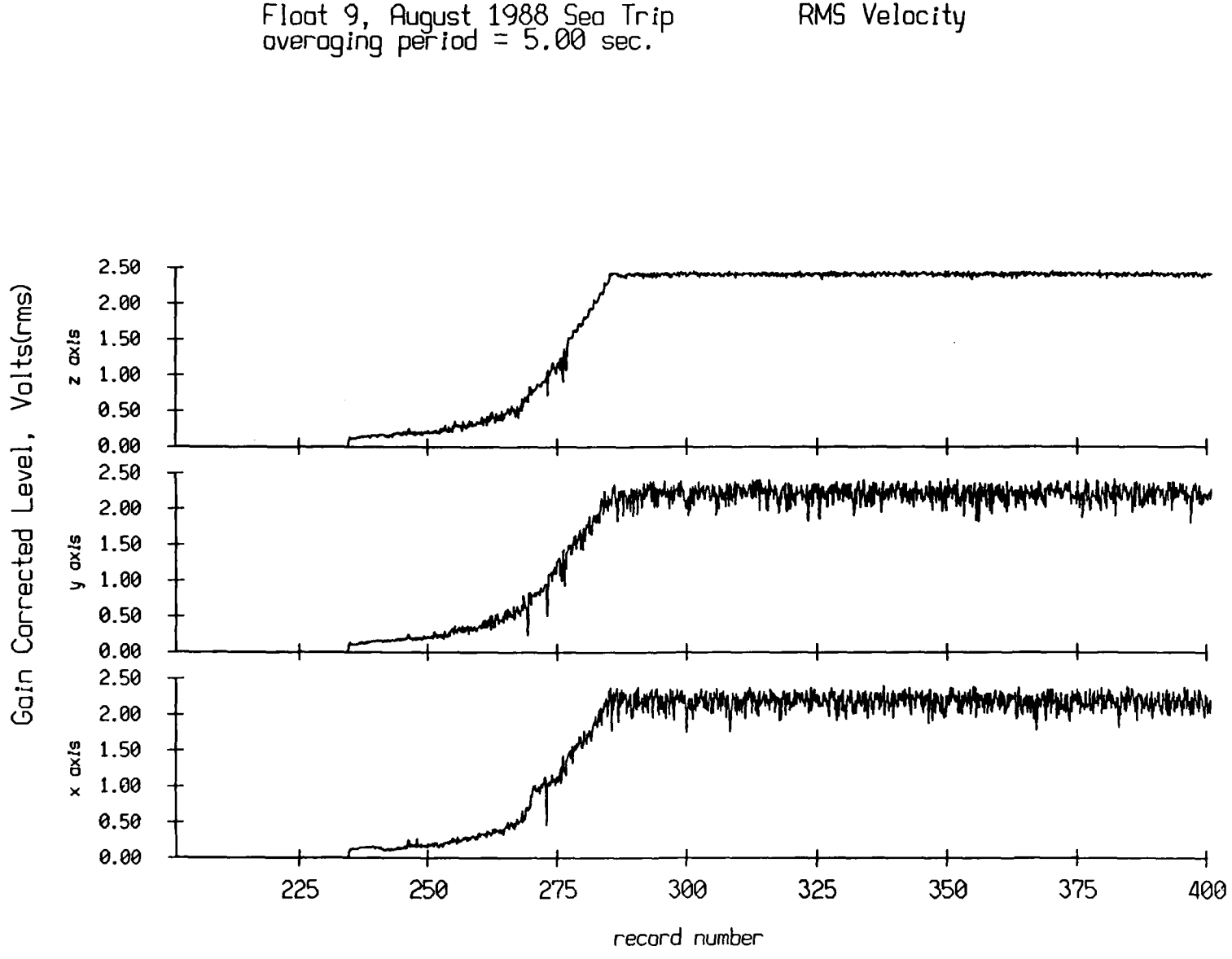

Float 9, August 1988 Sea Trip
averaging period = 5.00 sec.
RMS Velocity
Gain Corrected Level, Volts(rms)
z axis
y axis
x axis
2.50
2.00
1.50
1.00
0.50
0.00
225
250
275
300
325
350
375
400
record number

Figure X.12b

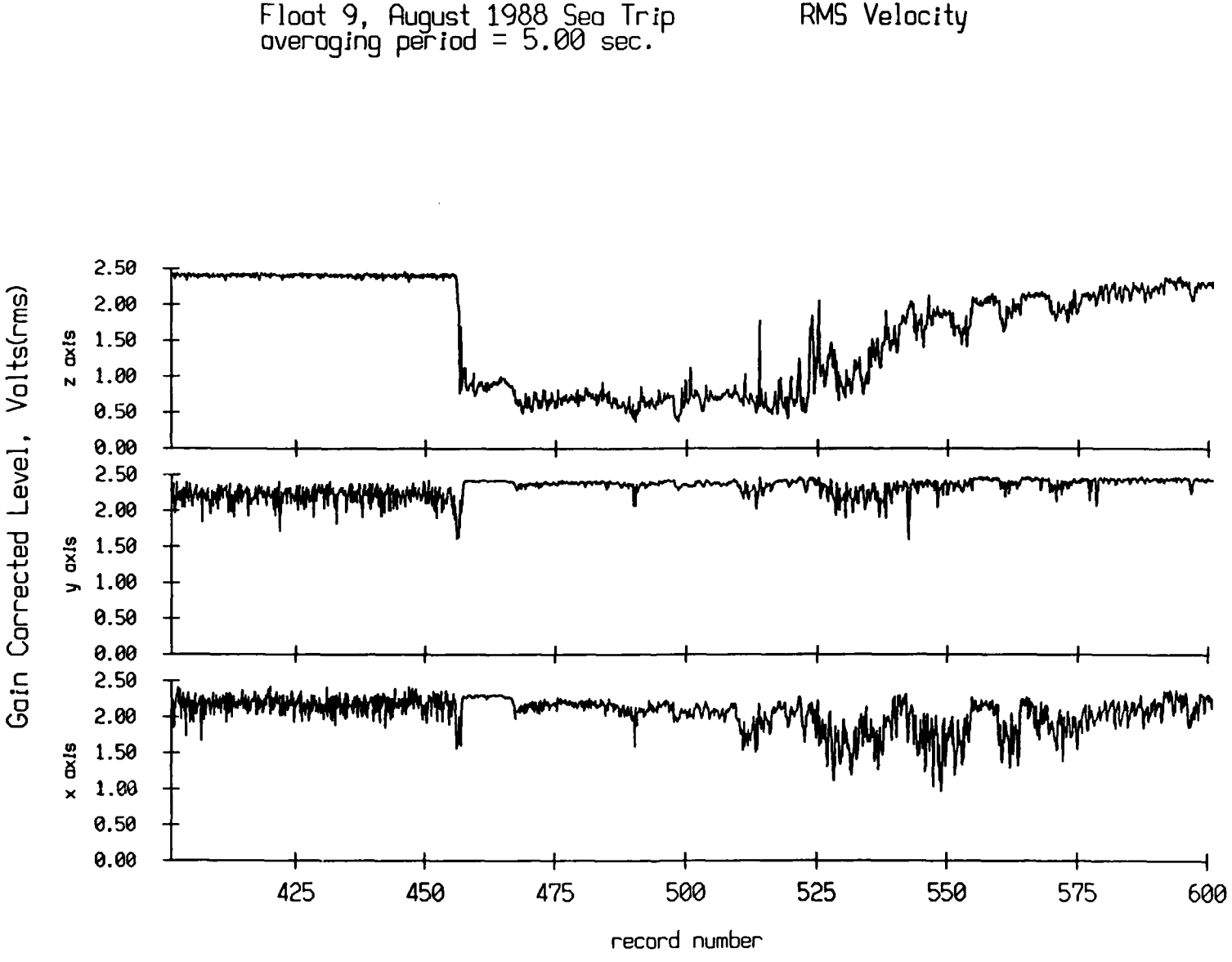

Float 9, August 1988 Sea Trip
overoging period = 5.00 sec.
RMS Velocity
Gain Corrected Level, Volts(rms)
z axis
y axis
x axis
2.50
2.00
1.50
1.00
0.50
0.00
425
450
475
500
525
550
575
600
record number

Figure X.12c

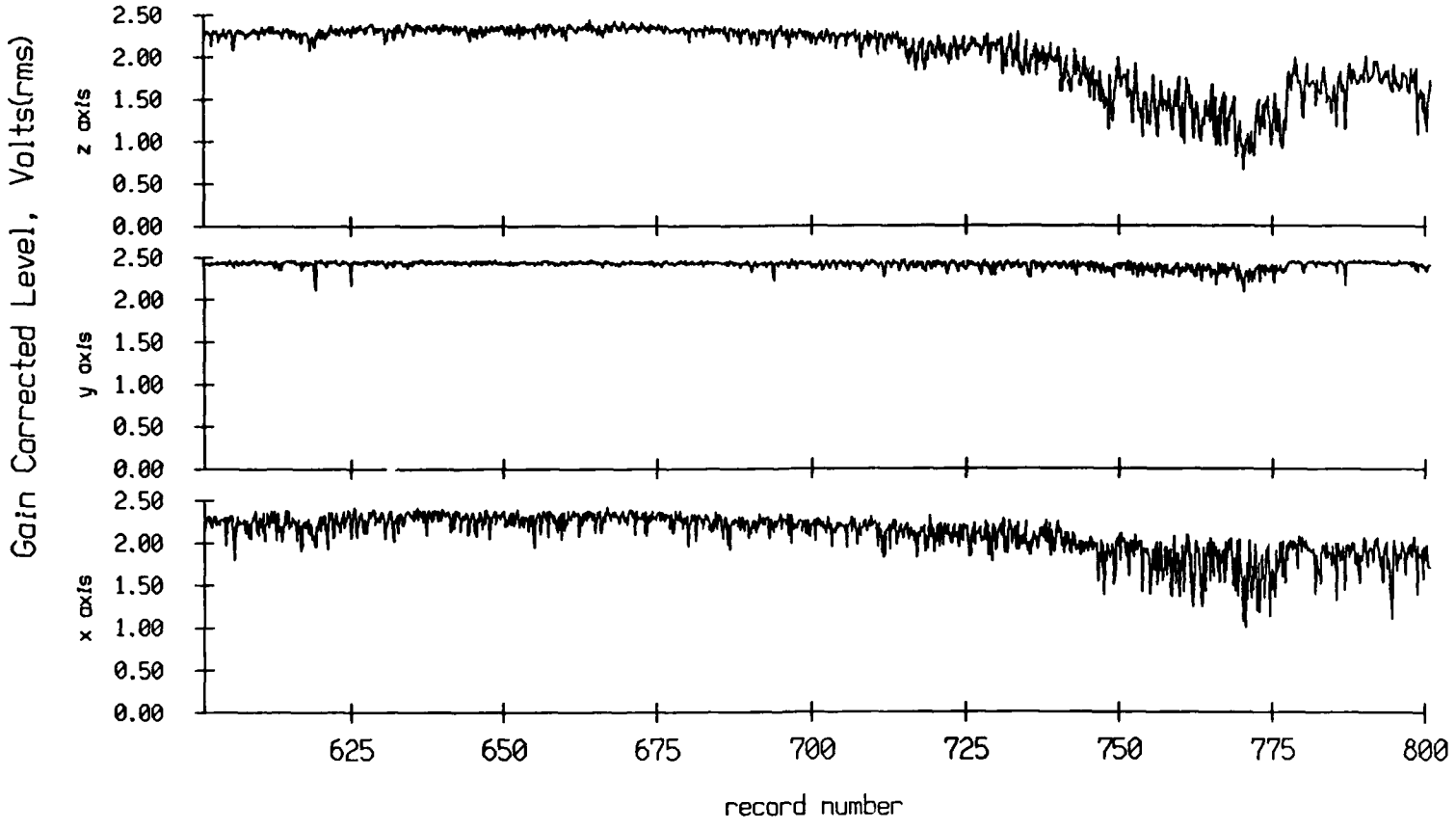

Float 9, August 1988 Sea Trip
averaging period = 5.00 sec.
RMS Velocity
Gain Corrected Level, Volts(rms)
z axis
y axis
x axis
2.50
2.00
1.50
1.00
0.50
0.00
625
650
675
700
725
750
775
800
record number

Figure X.12d

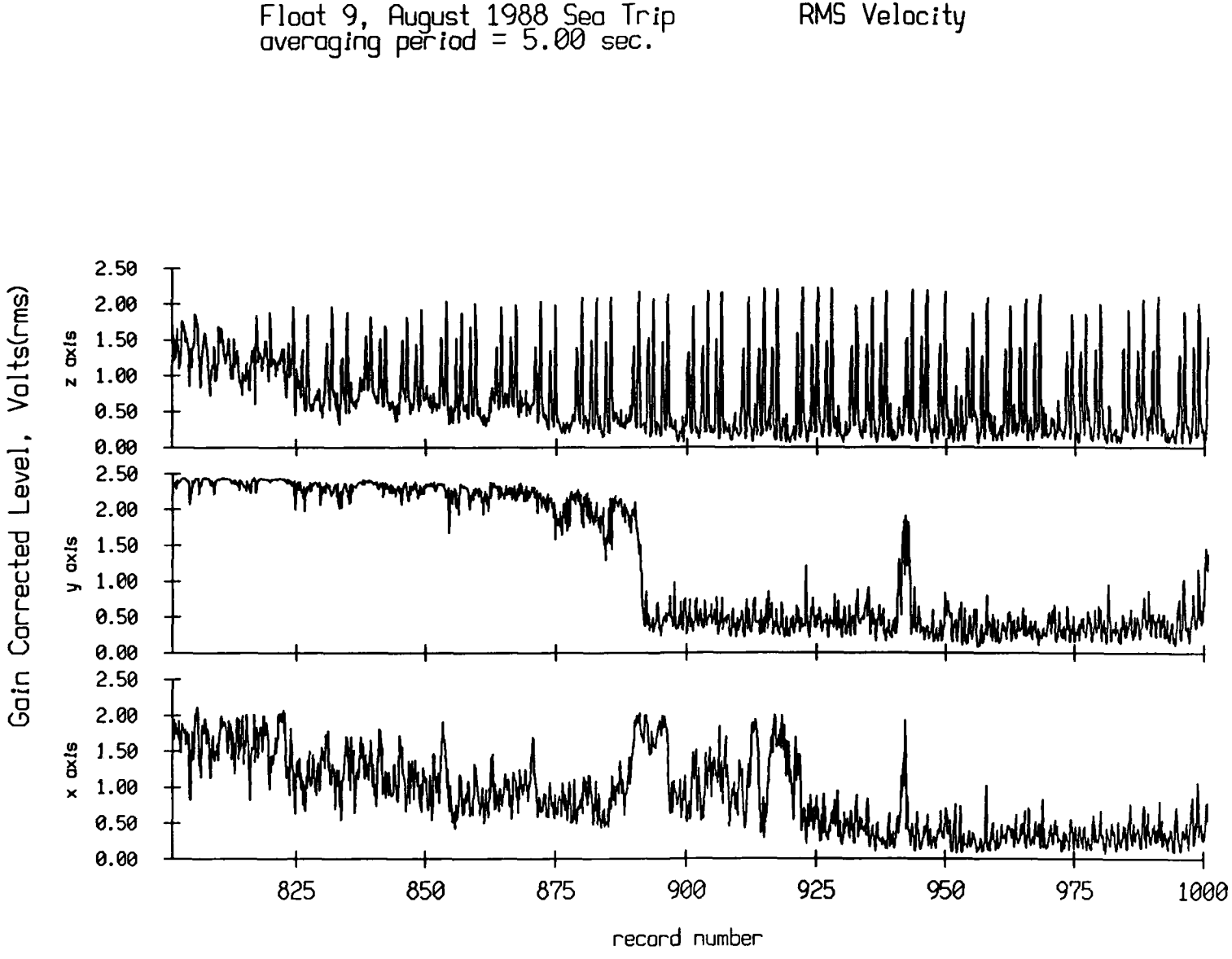

Float 9, August 1988 Sea Trip
averaging period = 5.00 sec.
RMS Velocity
Gain Corrected Level, Volts(rms)
z axis
y axis
x axis
2.50
2.00
1.50
1.00
0.50
0.00
825
850
875
900
925
950
975
1000
record number

Figure X.12e

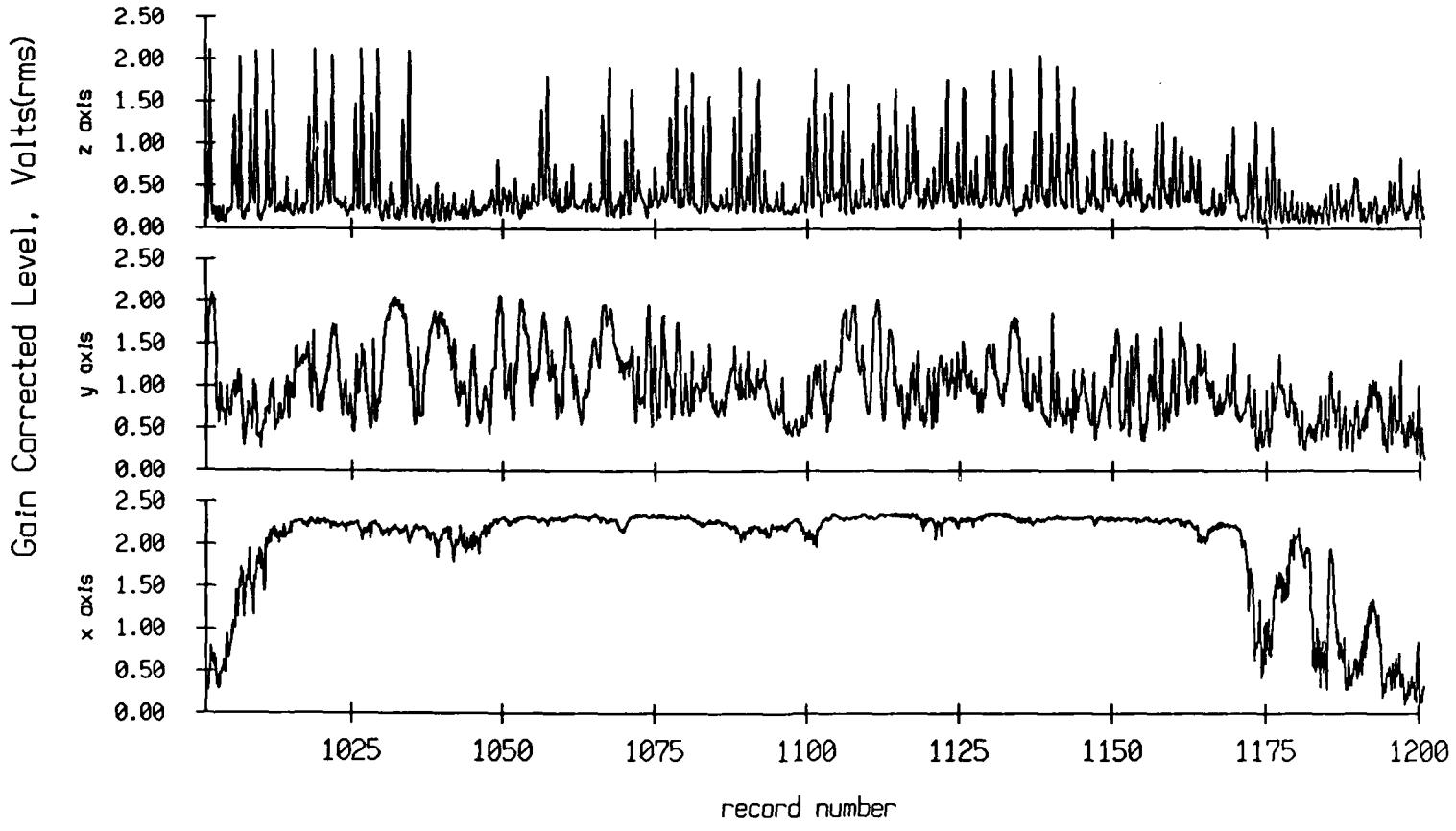

Float 9, August 1988 Sea Trip
averaging period = 5.00 sec.
RMS Velocity
Gain Corrected Level, Volts(rms)
z axis
y axis
x axis
2.50
2.00
1.50
1.00
0.50
0.00
1025
1050
1075
1100
1125
1150
1175
1200
record number

Figure X.1.jf

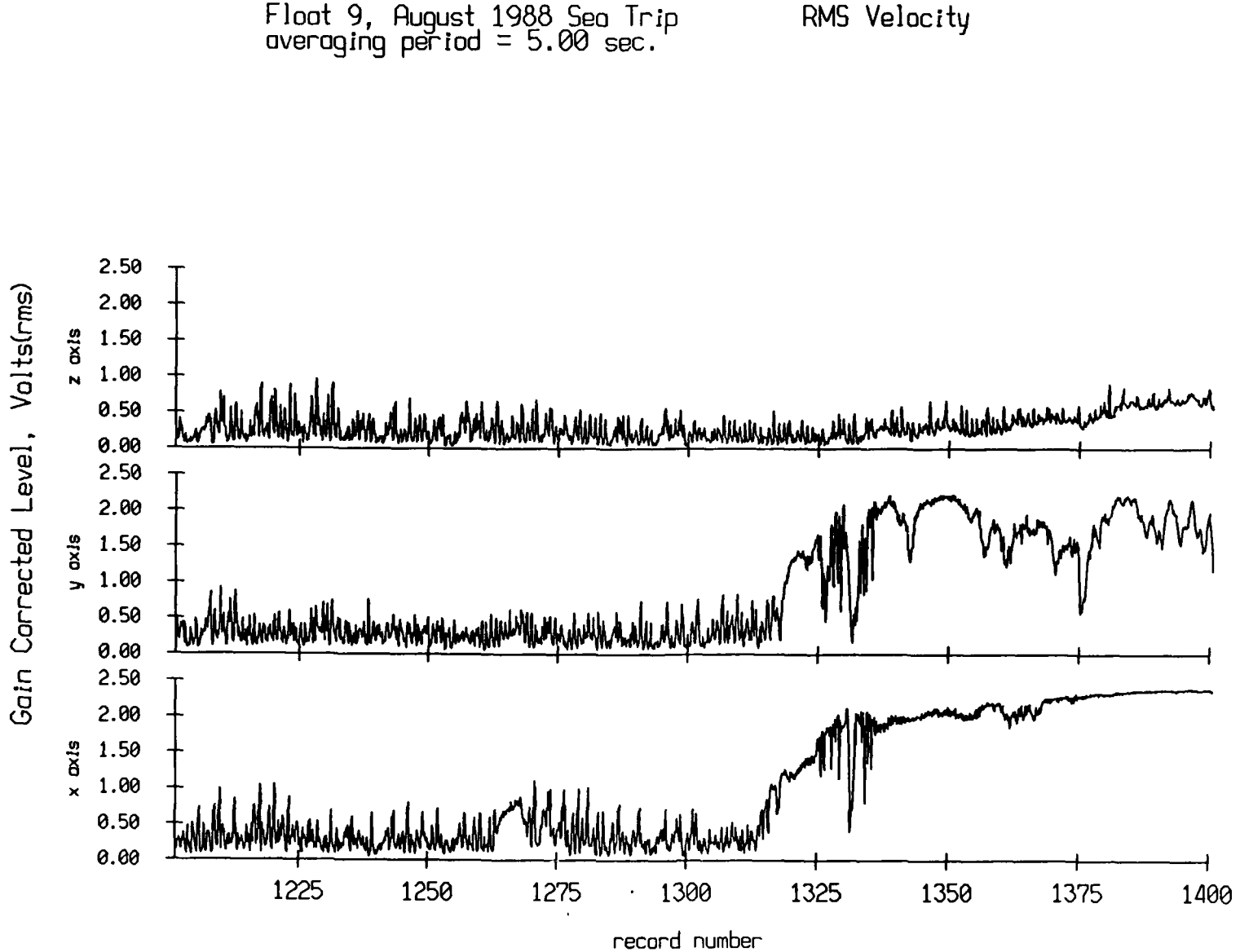

Float 9, August 1988 Sea Trip
averaging period = 5.00 sec.
RMS Velocity
Gain Corrected Level, Volts(rms)
z axis
y axis
x axis
2.50
2.00
1.50
1.00
0.50
0.00
1225
1250
1275
1300
1325
1350
1375
1400
record number

Figure X.12g

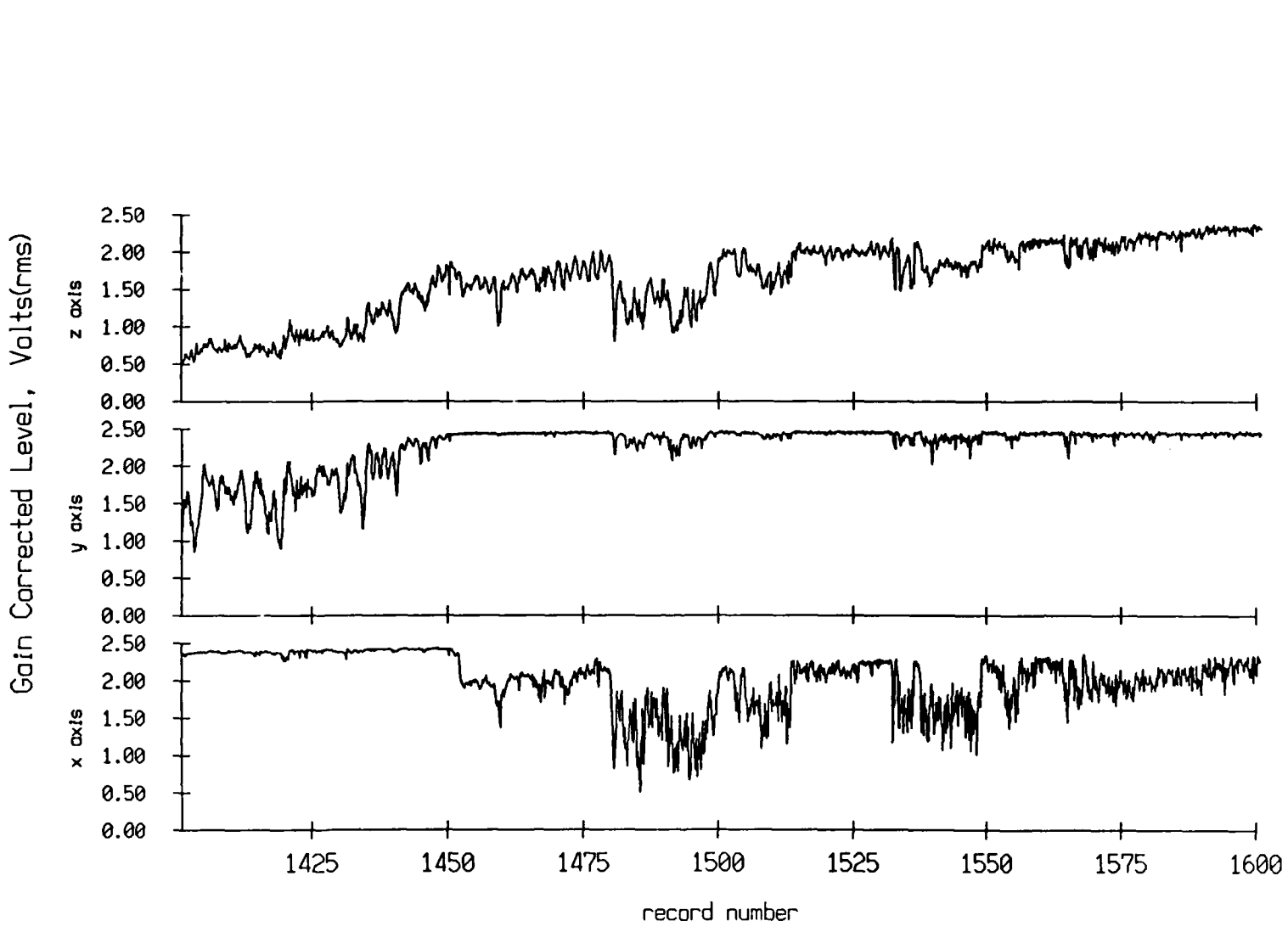

Float 9, August 1988 Sea Trip
averaging period = 5.00 sec.
RMS Velocity
Gain Corrected Level, Volts(rms)
z axis
y axis
x axis
2.50
2.00
1.50
1.00
0.50
0.00
1425
1450
1475
1500
1525
1550
1575
1600
record number

Figure X.12h

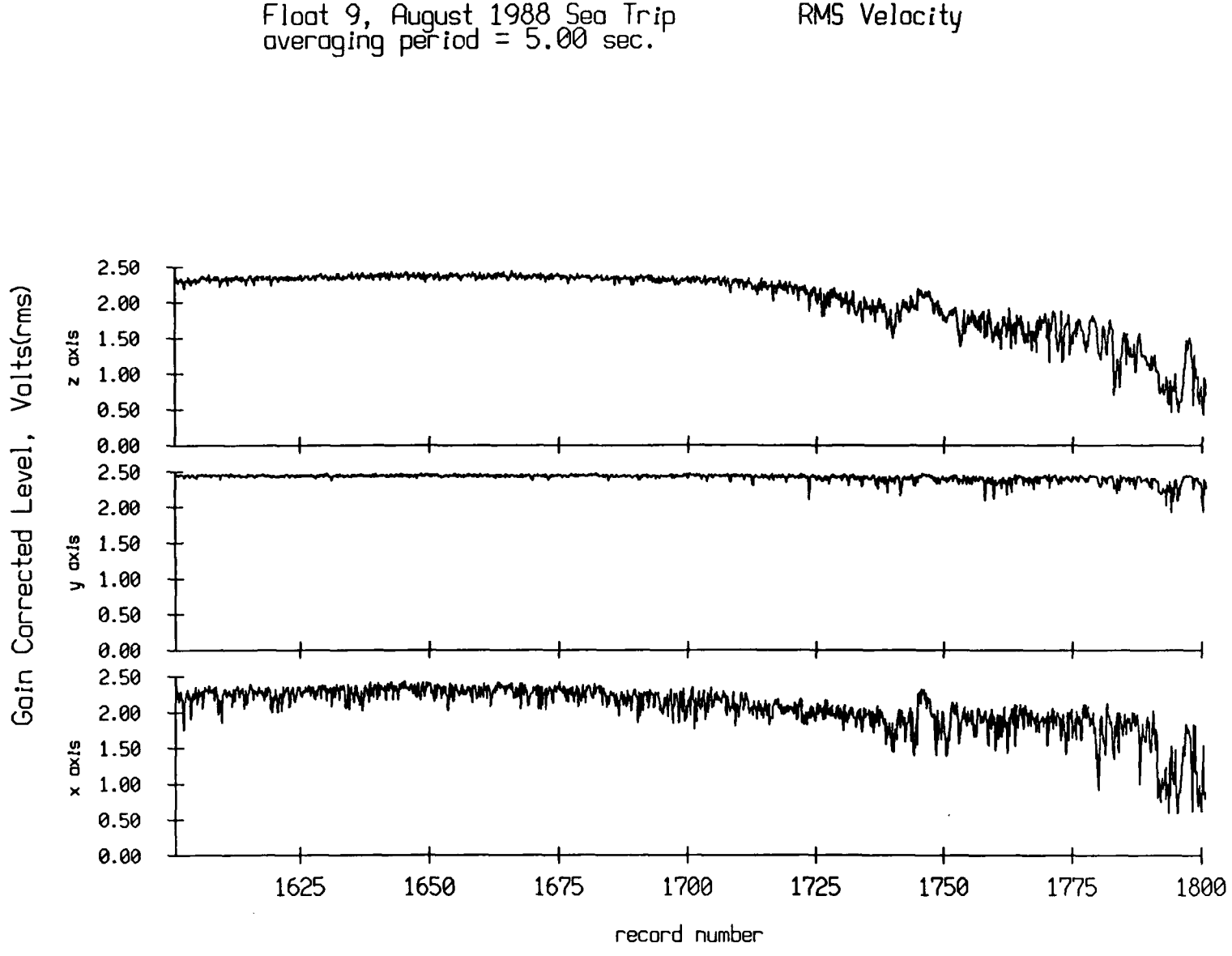

Float 9, August 1988 Sea Trip
averaging period = 5.00 sec.
RMS Velocity
Gain Corrected Level, Volts(rms)
z axis
y axis
x axis
2.50
2.00
1.50
1.00
0.50
0.00
1625
1650
1675
1700
1725
1750
1775
1800
record number

Figure X.12i

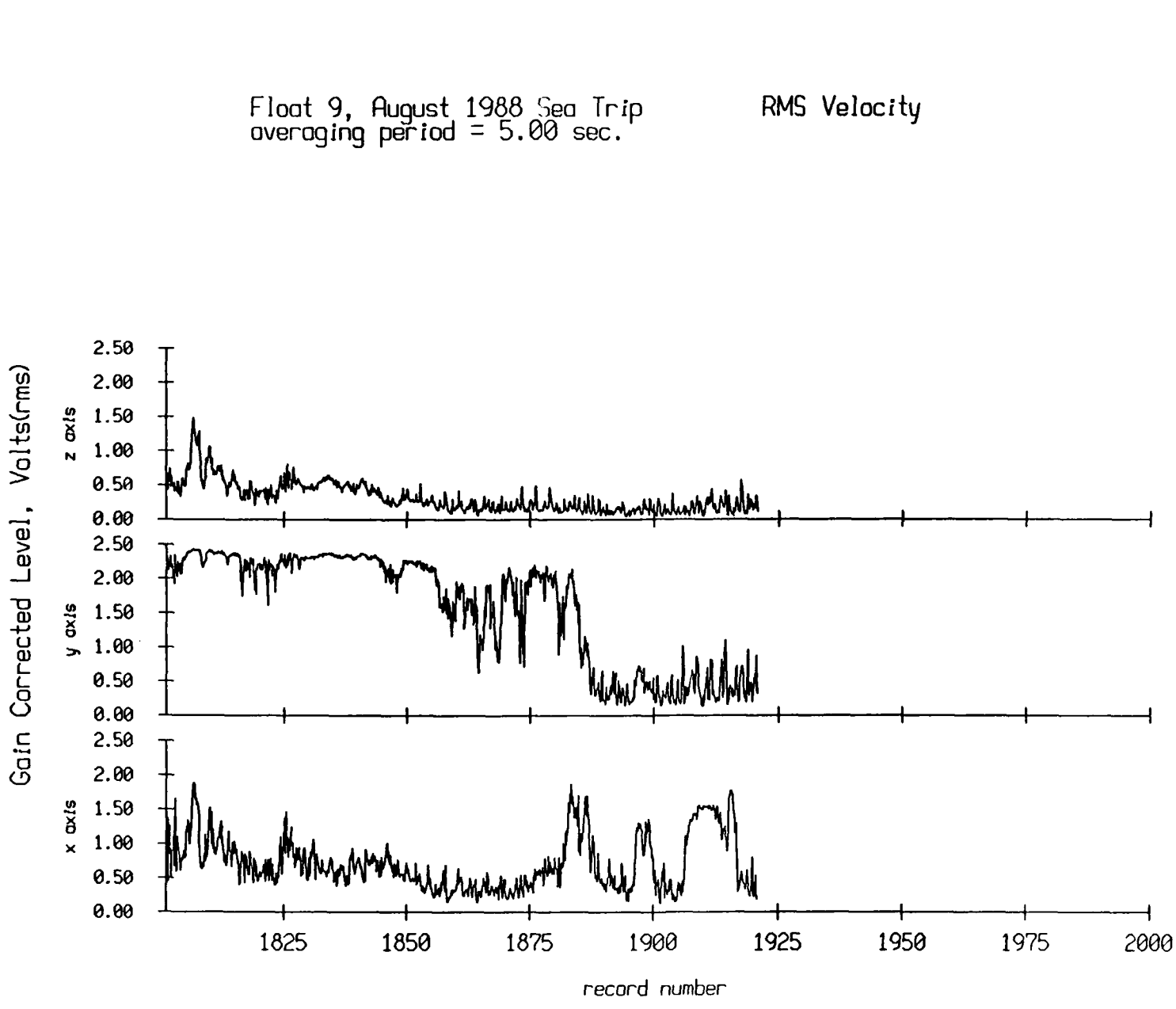

Float 9, August 1988 Sea Trip
averaging period = 5.00 sec.
RMS Velocity
Gain Corrected Level, Volts(rms)
z axis
y axis
x axis
2.50
2.00
1.50
1.00
0.50
0.00
1825
1850
1875
1900
1925
1950
1975
2000
record number

Figure X.12j

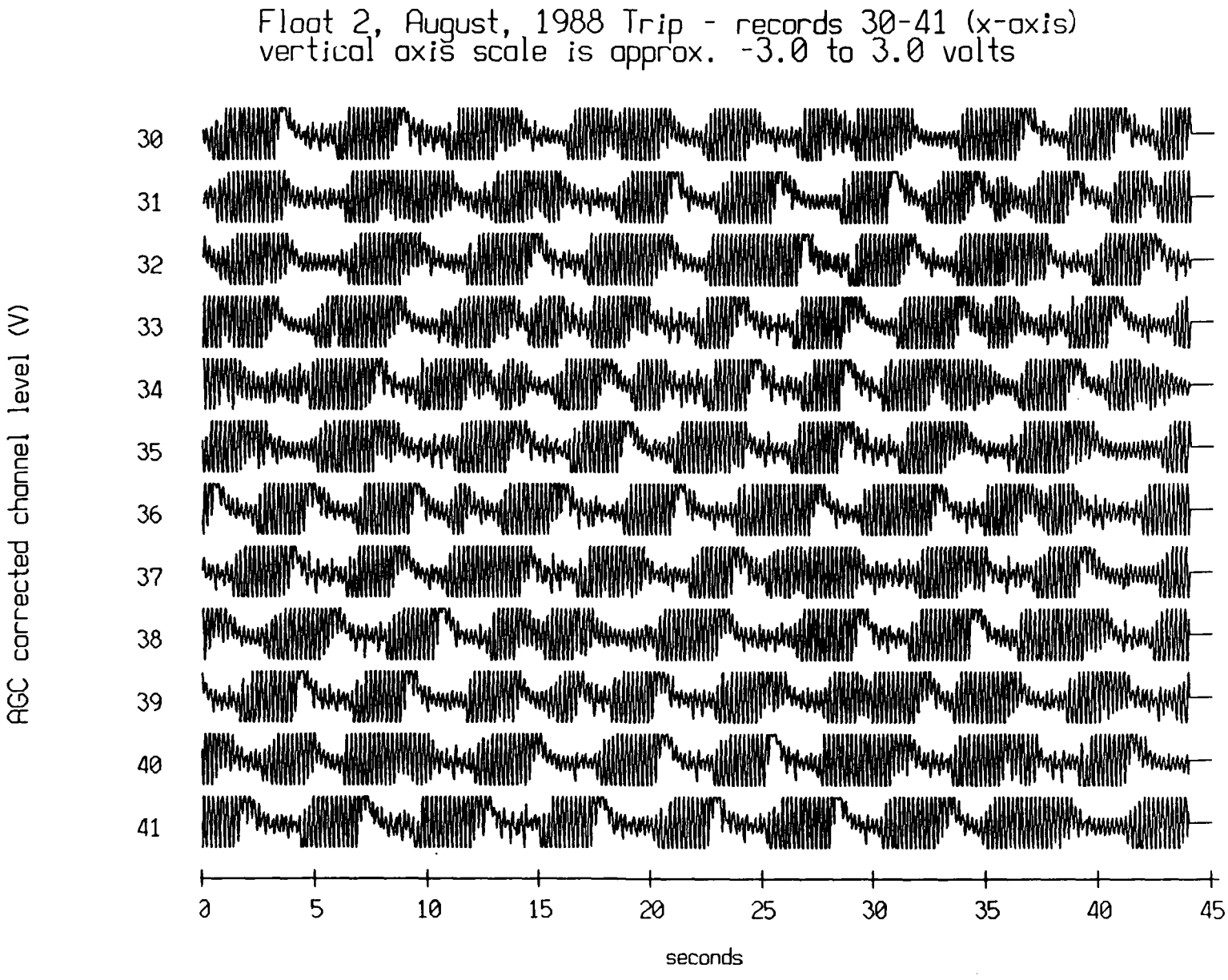

Float 2, August, 1988 Trip - records 30-41 (x-axis)
vertical axis scale is approx. -3.0 to 3.0 volts
AGC corrected channel level (V)
30
31
32
33
34
35
36
37
38
39
40
41
0
5
10
15
20
25
30
35
40
45
seconds

Figure XI.1a

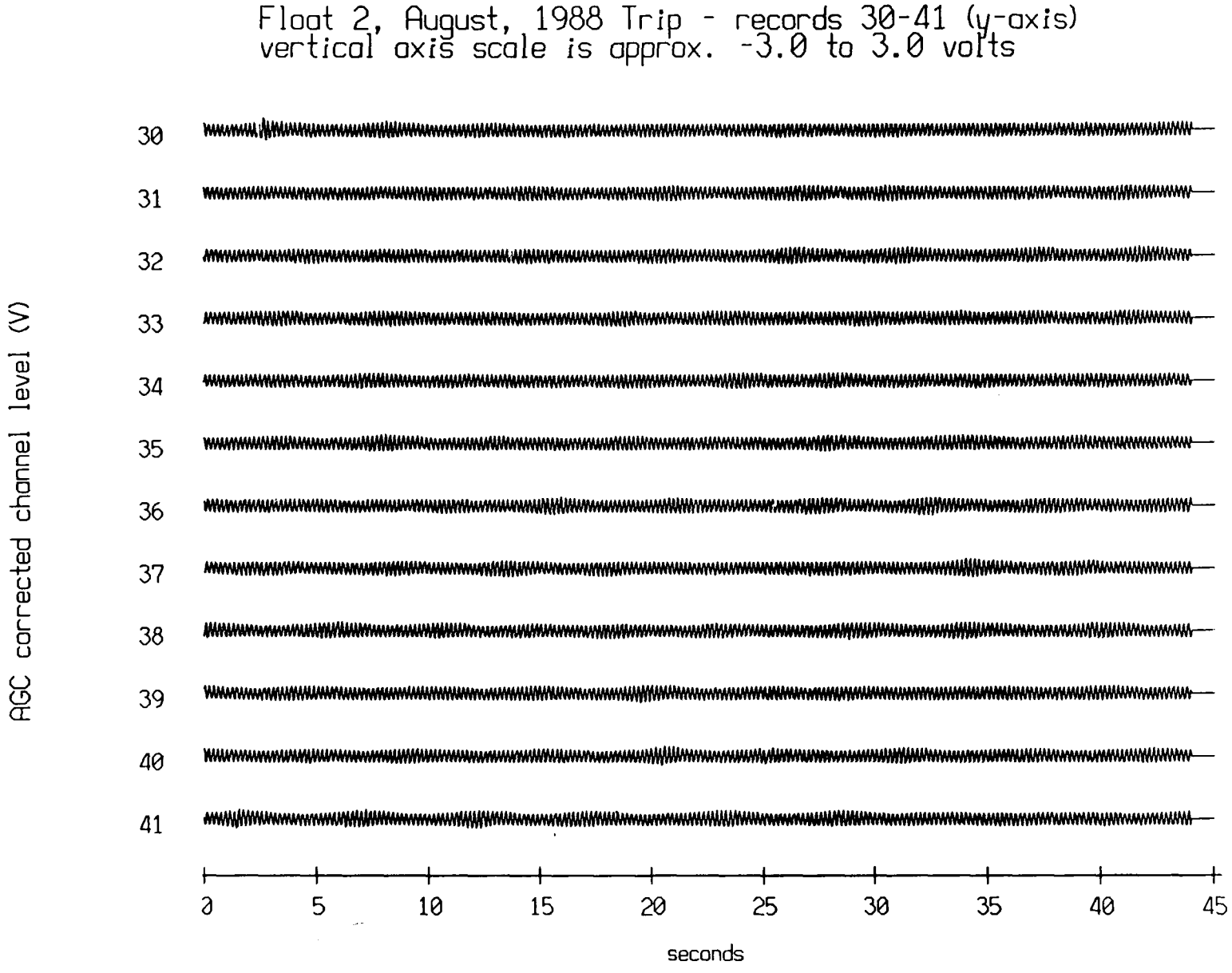

Float 2, August, 1988 Trip - records 30-41 (y-axis)
vertical axis scale is approx. -3.0 to 3.0 volts
AGC corrected channel level (V)
30
31
32
33
34
35
36
37
38
39
40
41
0
5
10
15
20
25
30
35
40
45
seconds

Figure XI.1b

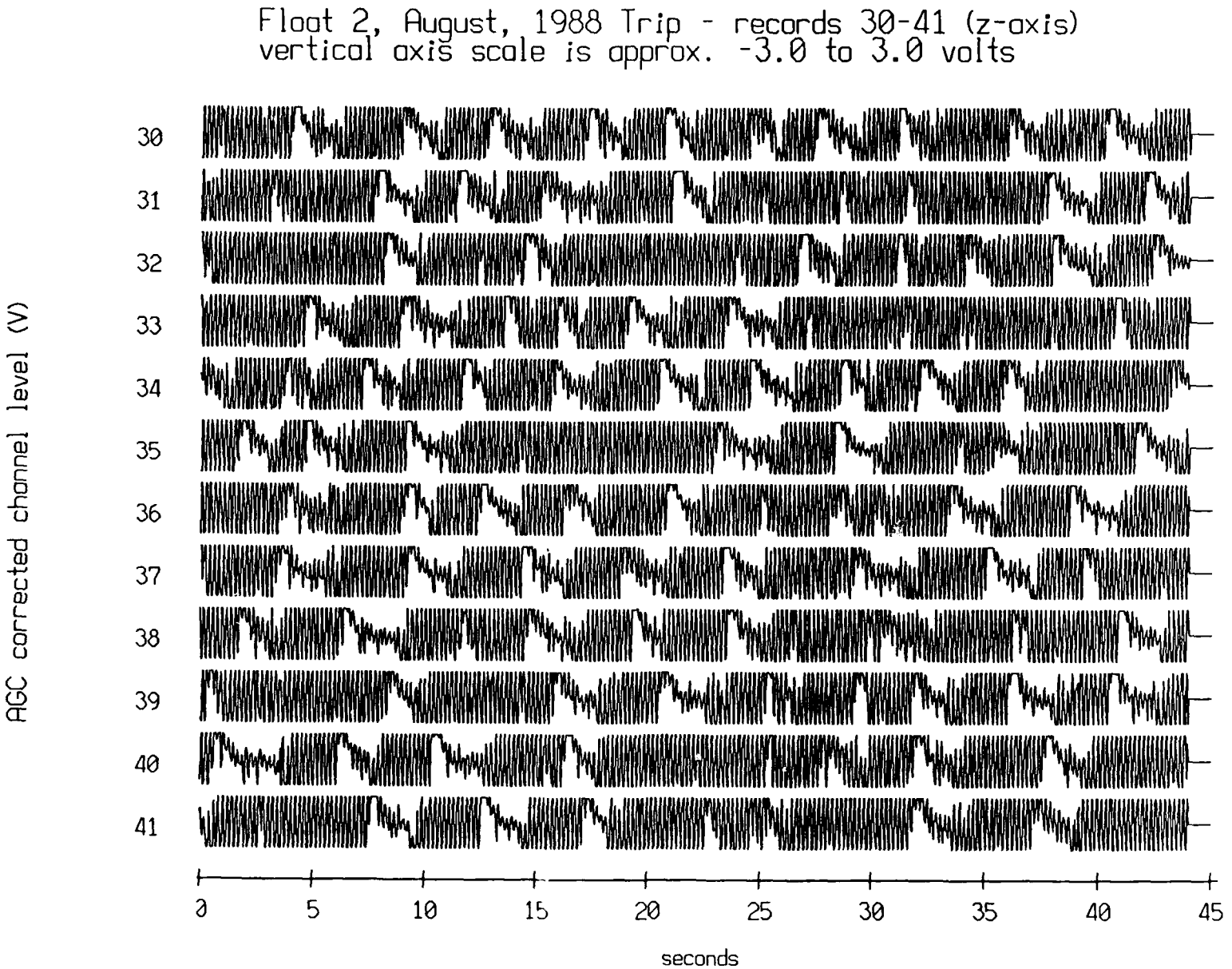

Float 2, August, 1988 Trip - records 30-41 (z-axis)
vertical axis scale is approx. -3.0 to 3.0 volts
AGC corrected channel level (V)
30
31
32
33
34
35
36
37
38
39
40
41
0
5
10
15
20
25
30
35
40
45
seconds

Figure XI.1c

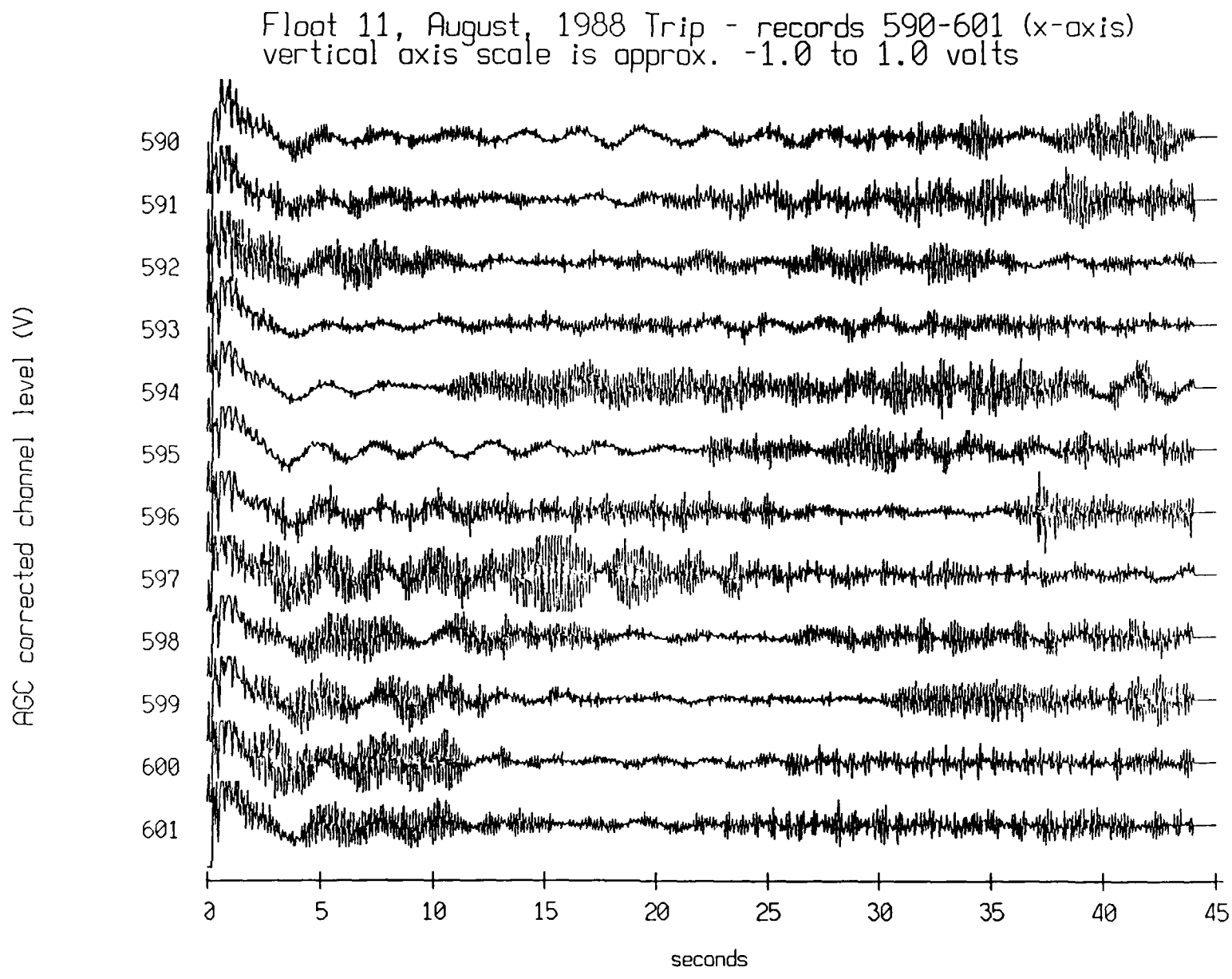

Float 11, August, 1988 Trip - records 590-601 (x-axis)
vertical axis scale is approx. -1.0 to 1.0 volts
AGC corrected channel level (V)
590
591
592
593
594
595
596
597
598
599
600
601
0
5
10
15
20
25
30
35
40
45
seconds

Figure XI.2a

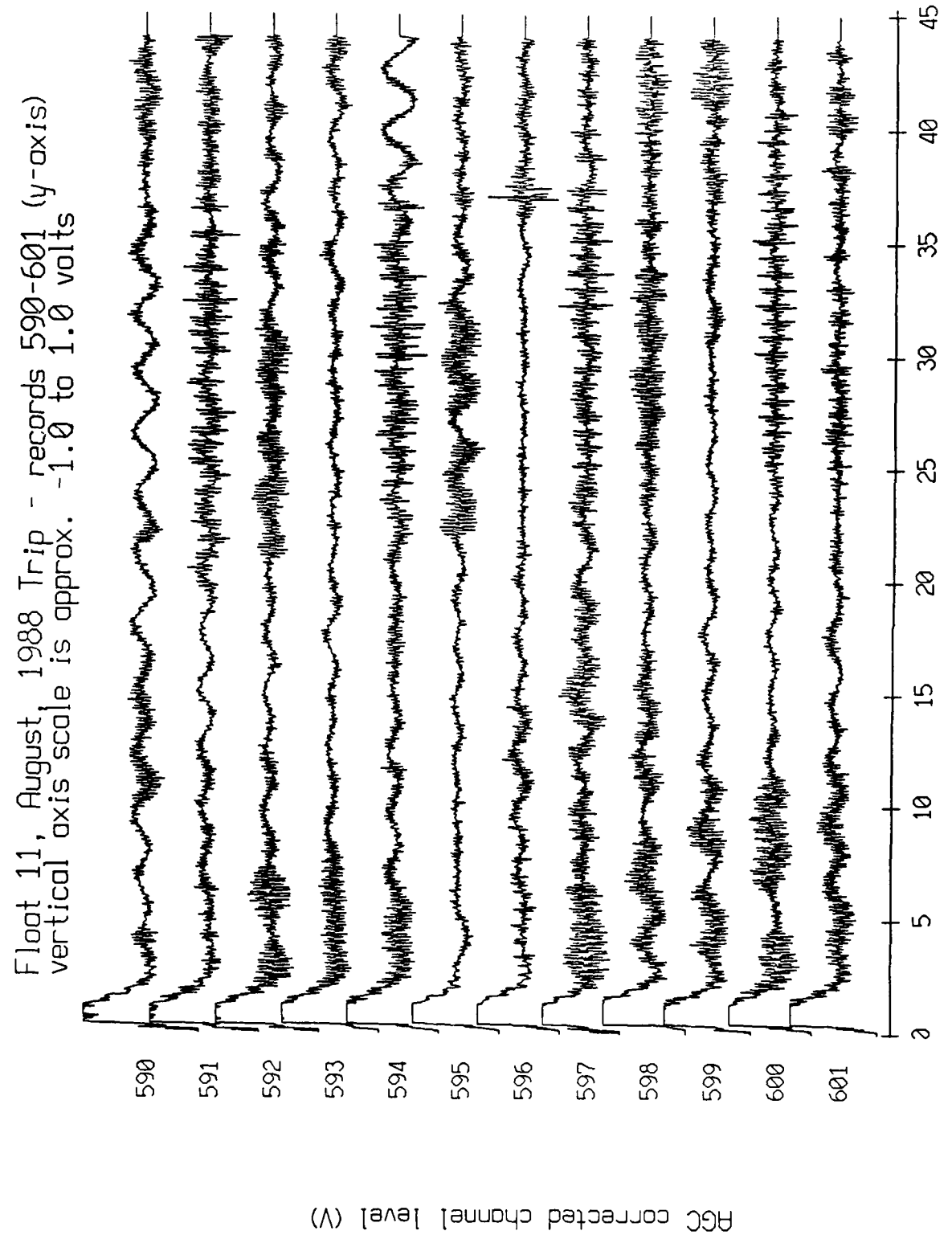

Float 11, August 1988 Trip - records 590-601 (y-axis)
vertical axis scale is approx. -1.0 to 1.0 volts
590
591
592
593
594
595
596
597
598
599
600
601
0
5
10
15
20
25
30
35
40
45
seconds
AGC corrected channel level (V)

Figure XI.2b

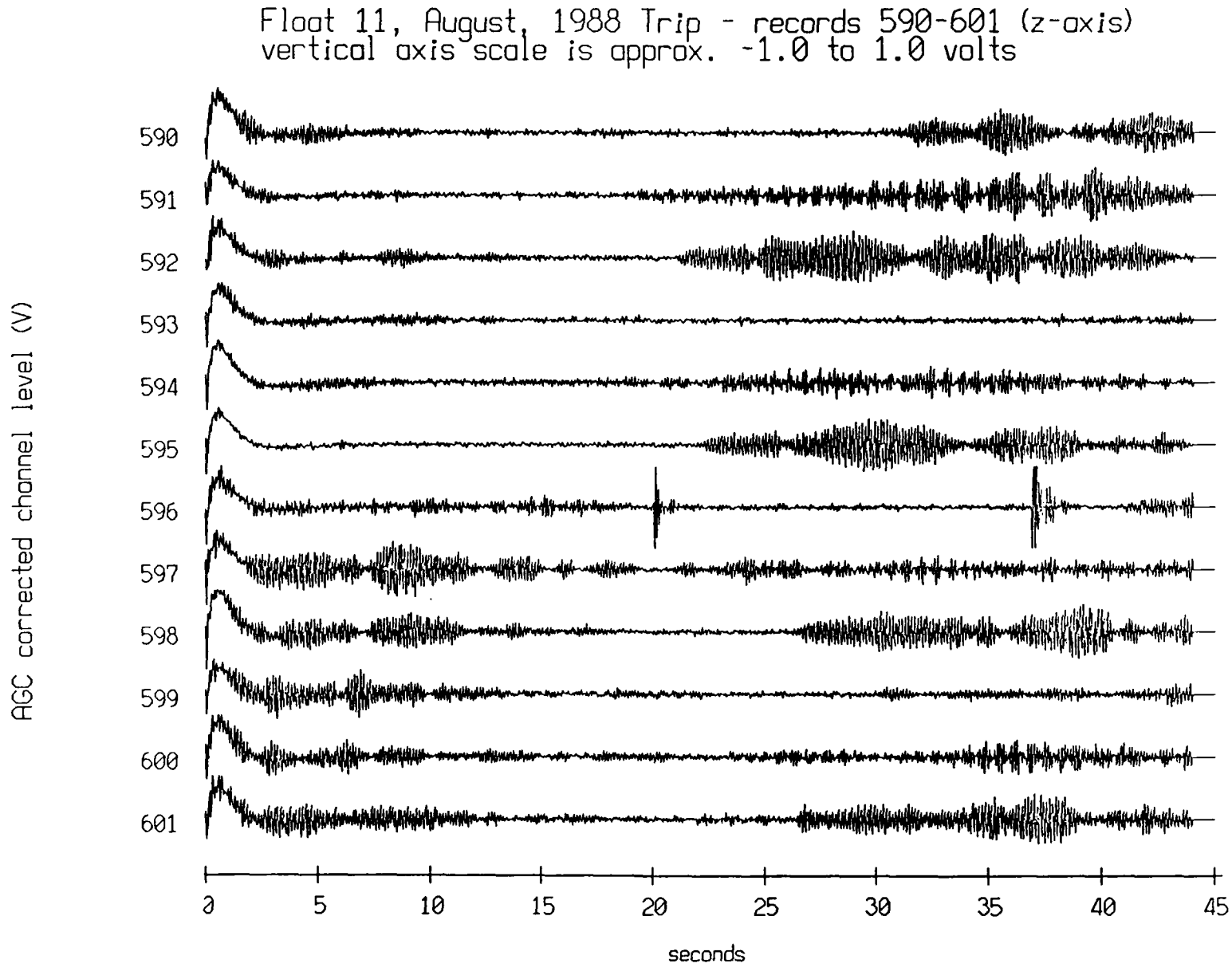

Float 11, August, 1988 Trip - records 590-601 (z-axis)
vertical axis scale is approx. -1.0 to 1.0 volts
AGC corrected channel level (V)
590
591
592
593
594
595
596
597
598
599
600
601
0
5
10
15
20
25
30
35
40
45
seconds

Figure XI.2c

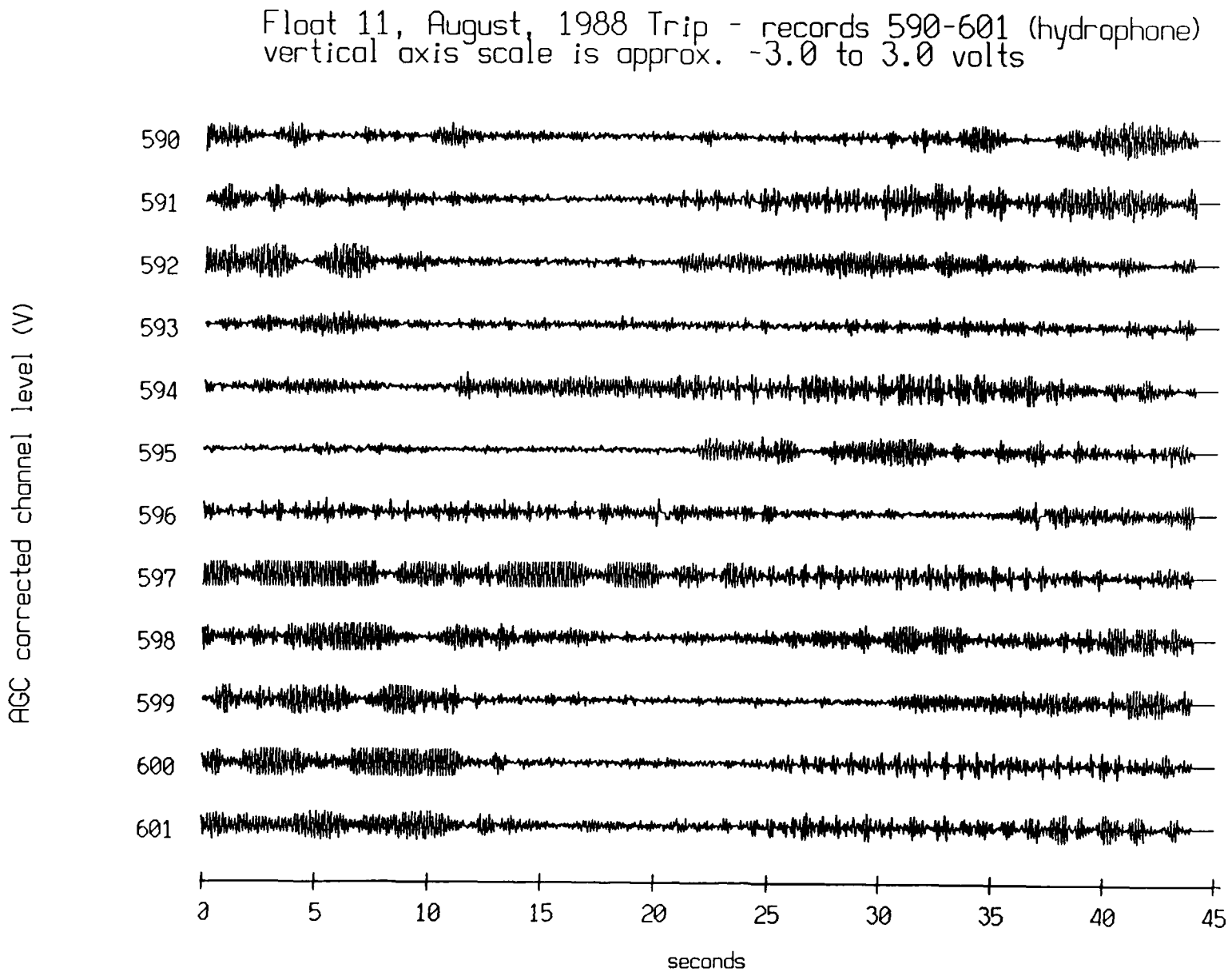

Float 11, August, 1988 Trip - records 590-601 (hydrophone)
vertical axis scale is approx. -3.0 to 3.0 volts
AGC corrected channel level (V)
590
591
592
593
594
595
596
597
598
599
600
601
0
5
10
15
20
25
30
35
40
45
seconds

Figure XI.2d

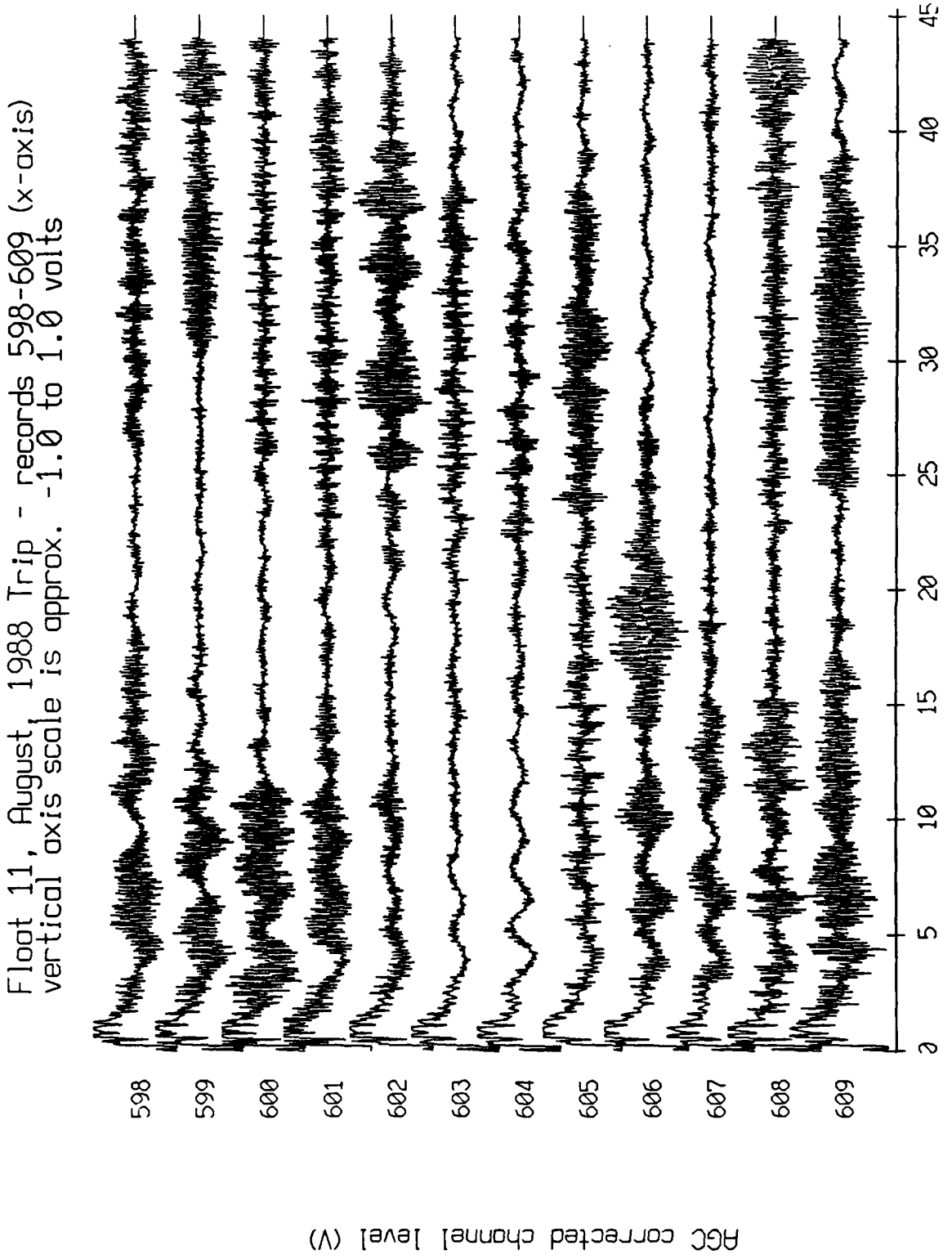

Float 11, August, 1988 Trip - records 598-609 (x-axis)
vertical axis scale is approx. -1.0 to 1.0 volts
AGC corrected channel level (V)
598
599
600
601
602
603
604
605
606
607
608
609
0
5
10
15
20
25
30
35
40
45
seconds

Figure XI.3a

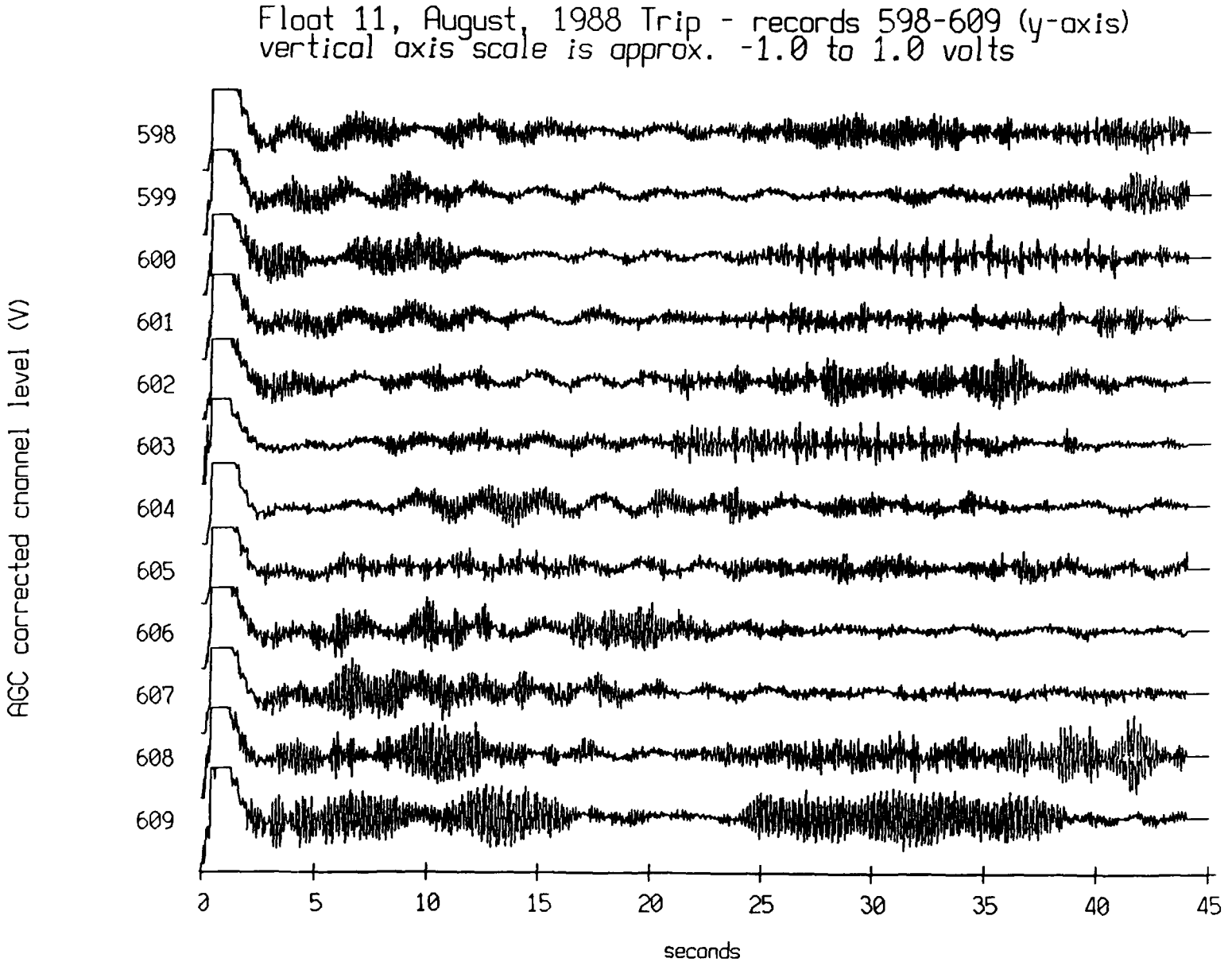

Float 11, August, 1988 Trip - records 598-609 (y-axis)
vertical axis scale is approx. -1.0 to 1.0 volts
AGC corrected channel level (V)
598
599
600
601
602
603
604
605
606
607
608
609
0
5
10
15
20
25
30
35
40
45
seconds

Figure XI.3b

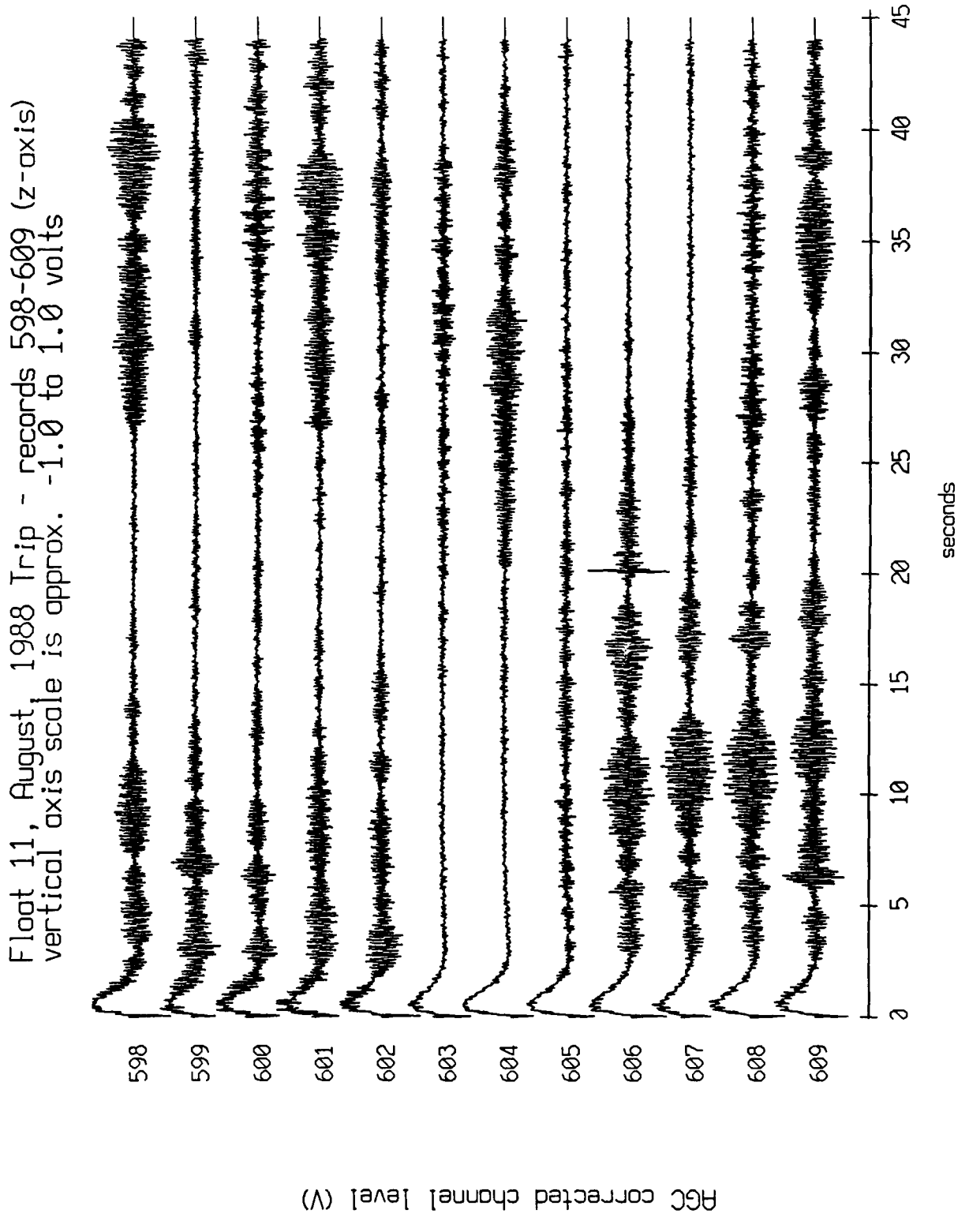

Float 11, August 1988 Trip - records 598-609 (z-axis)
vertical axis scale is approx. -1.0 to 1.0 volts
AGC corrected channel level (V)
598
599
600
601
602
603
604
605
606
607
608
609
0
5
10
15
20
25
30
35
40
45
seconds

Figure XI.3c

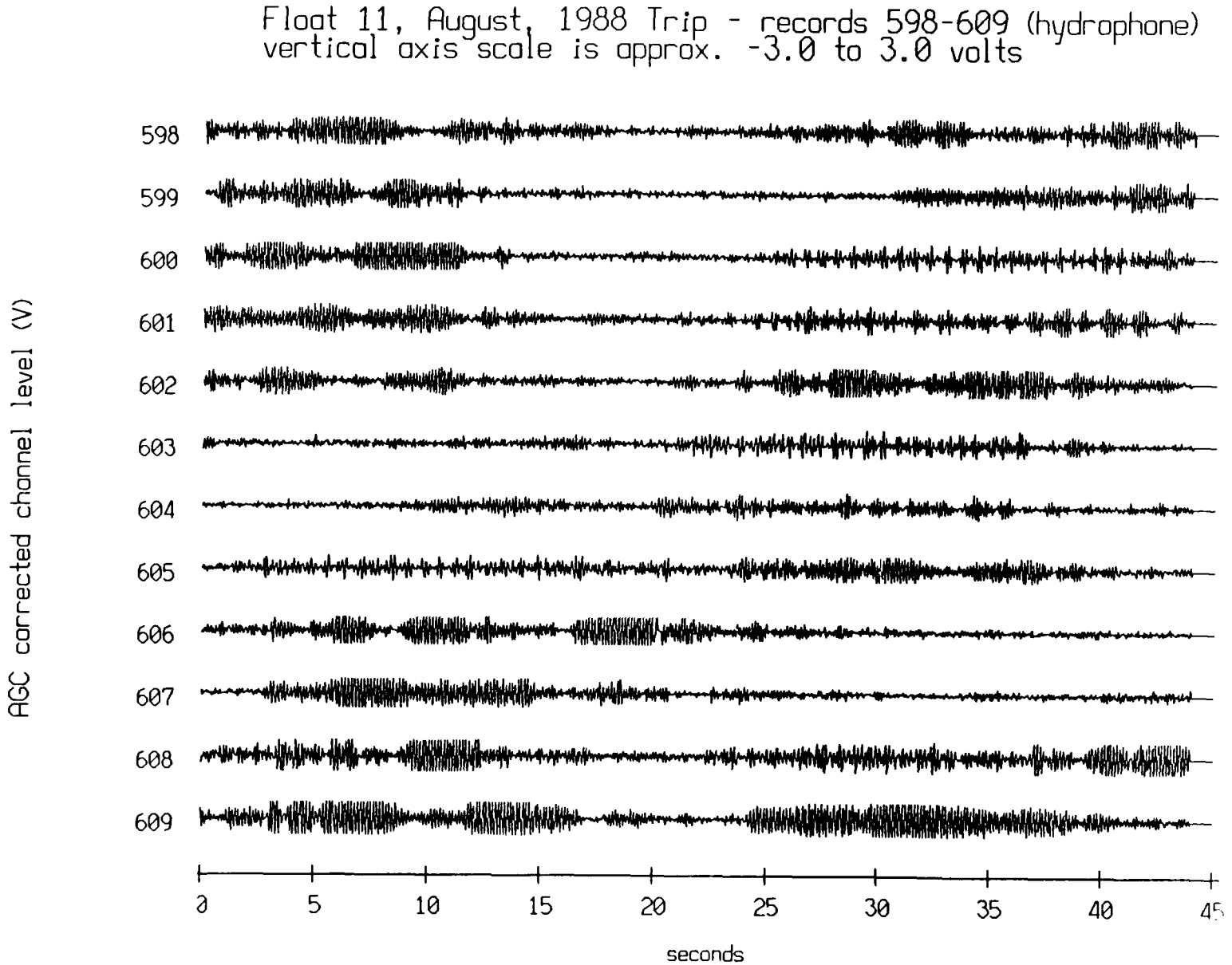

Float 11, August, 1988 Trip - records 598-609 (hydrophone)
vertical axis scale is approx. -3.0 to 3.0 volts
AGC corrected channel level (V)
598
599
600
601
602
603
604
605
606
607
608
609
0
5
10
15
20
25
30
35
40
45
seconds

Figure XI.3d

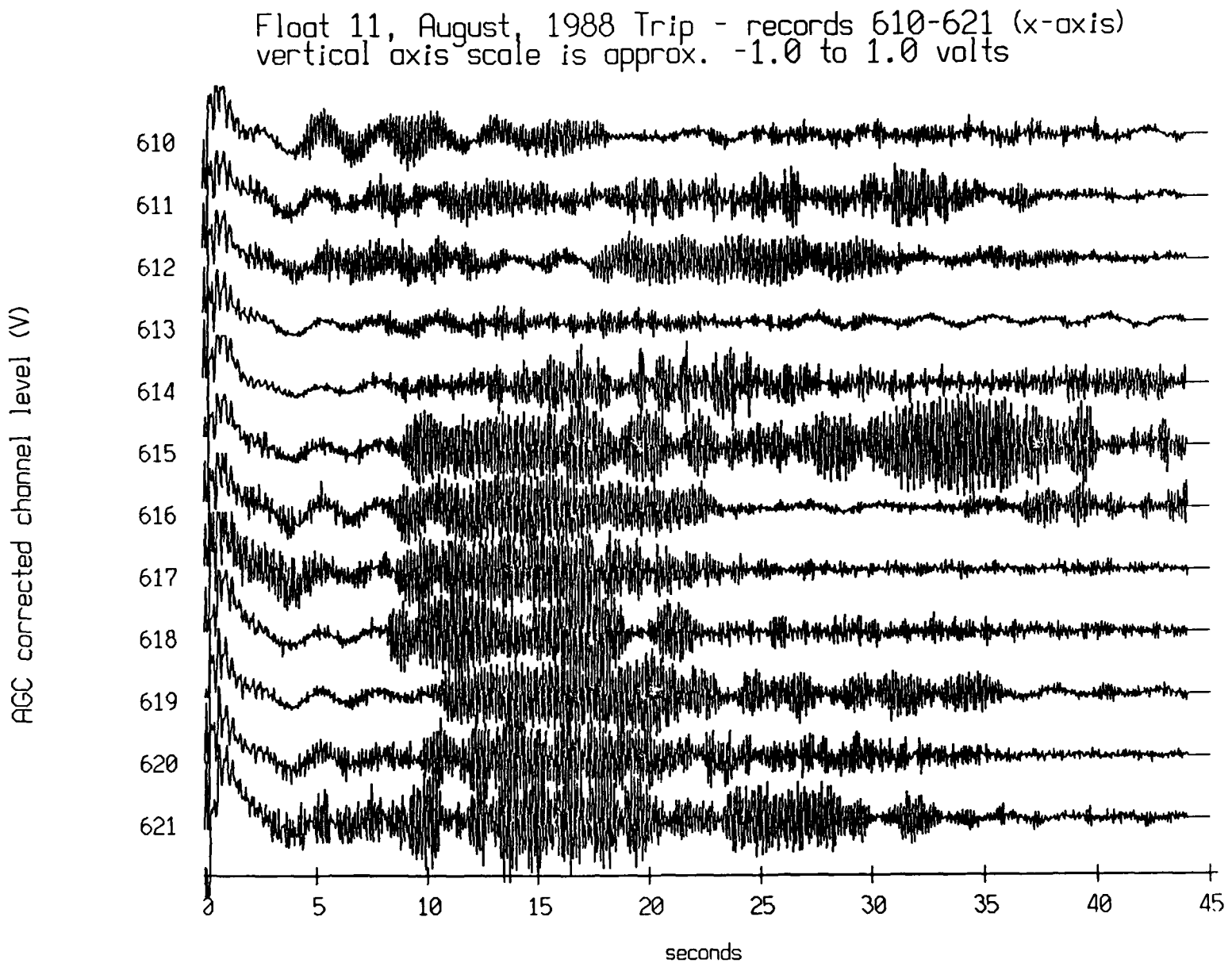

Float 11, August, 1988 Trip - records 610-621 (x-axis)
vertical axis scale is approx. -1.0 to 1.0 volts
AGC corrected channel level (V)
610
611
612
613
614
615
616
617
618
619
620
621
0
5
10
15
20
25
30
35
40
45
seconds

Figure XI.4a

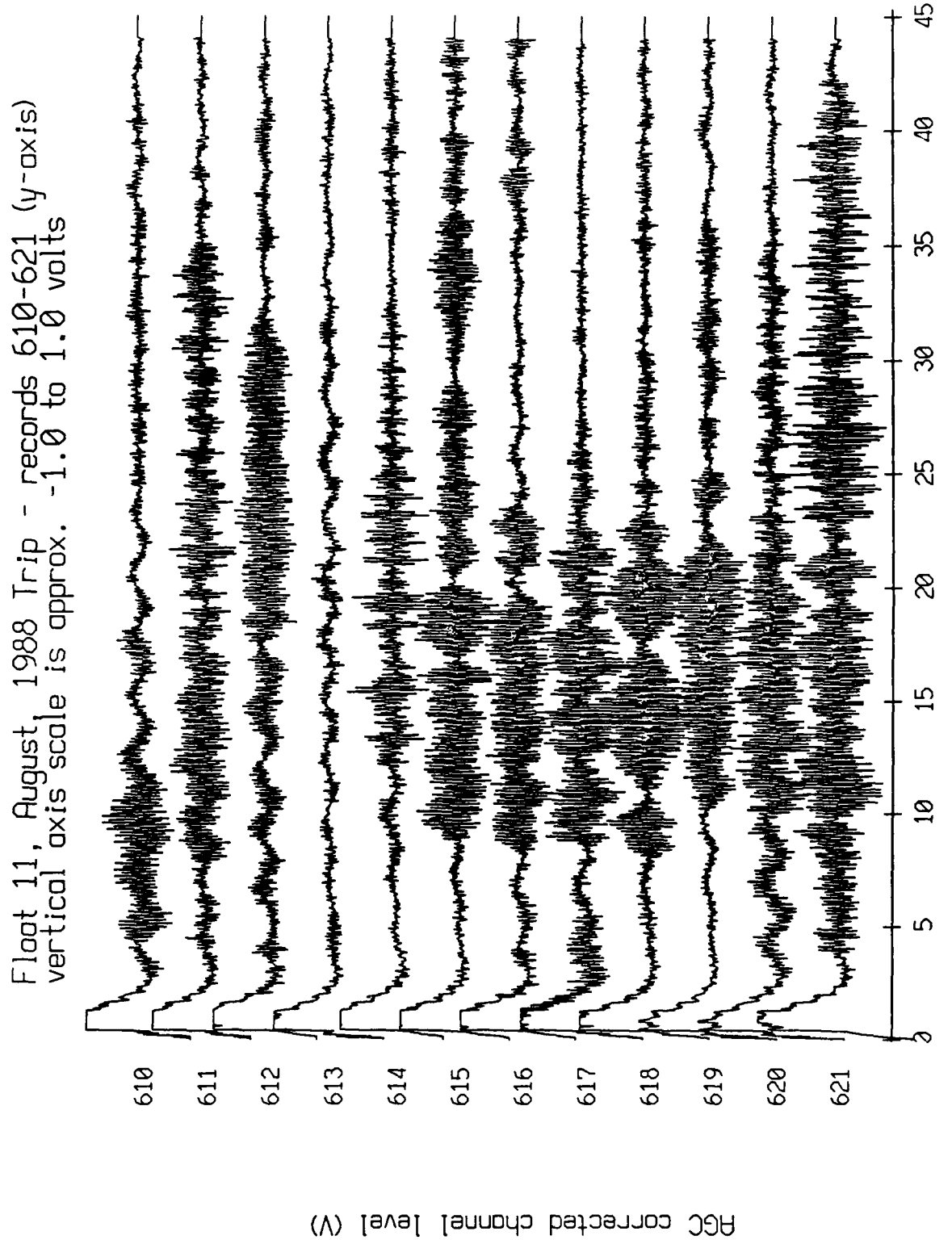

Float 11, August 1988 Trip - records 610-621 (y-axis)
vertical axis scale is approx. -1.0 to 1.0 volts
610
611
612
613
614
615
616
617
618
619
620
621
0
5
10
15
20
25
30
35
40
45
seconds
AGC corrected channel level (V)

Figure XI.4b

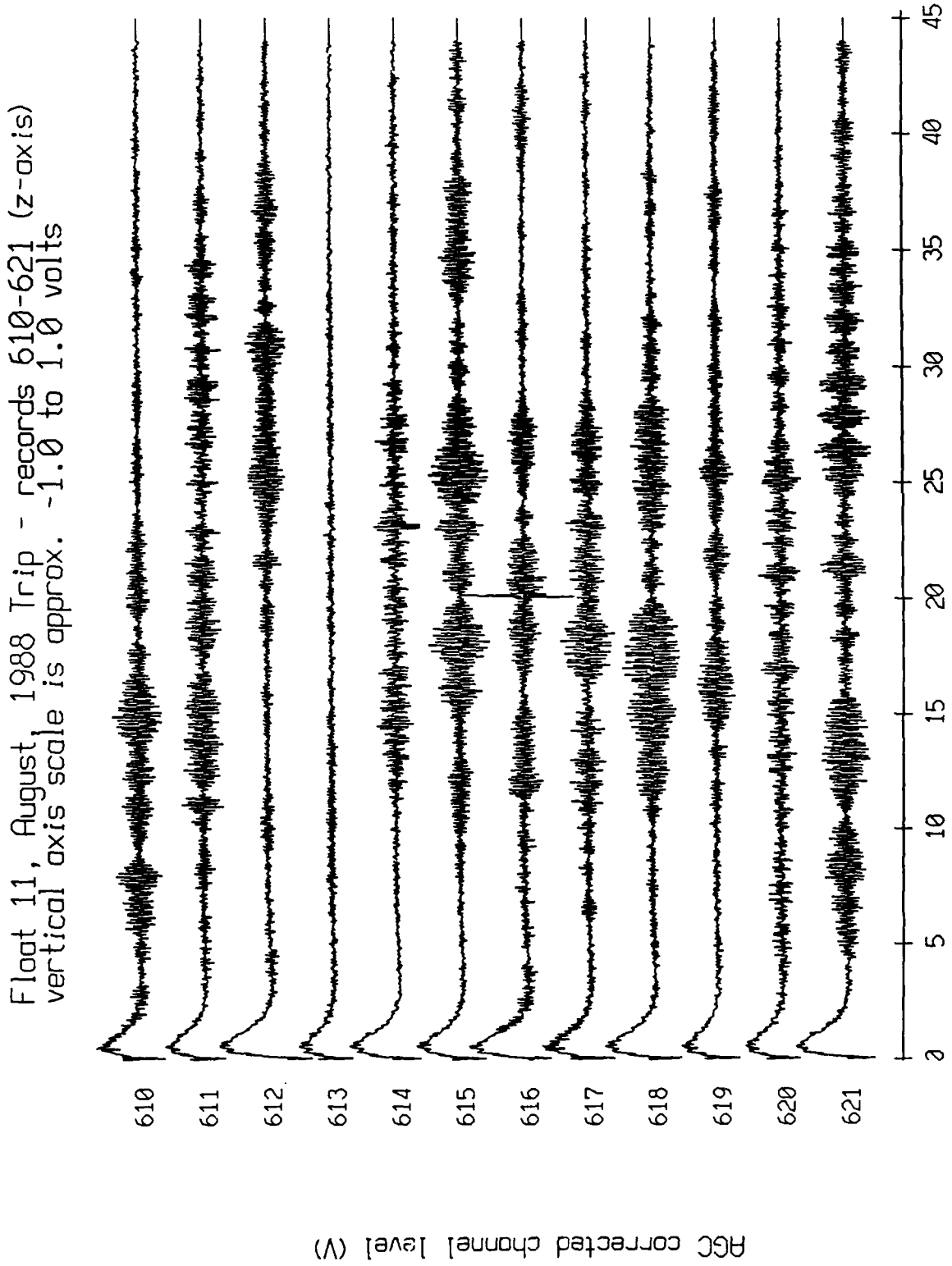

Float 11, August 1988 Trip - records 610-621 (z-axis)
vertical axis scale is approx. -1.0 to 1.0 volts
610
611
612
613
614
615
616
617
618
619
620
621
0
5
10
15
20
25
30
35
40
45
seconds
AGC corrected channel level (V)

Figure XI.4c

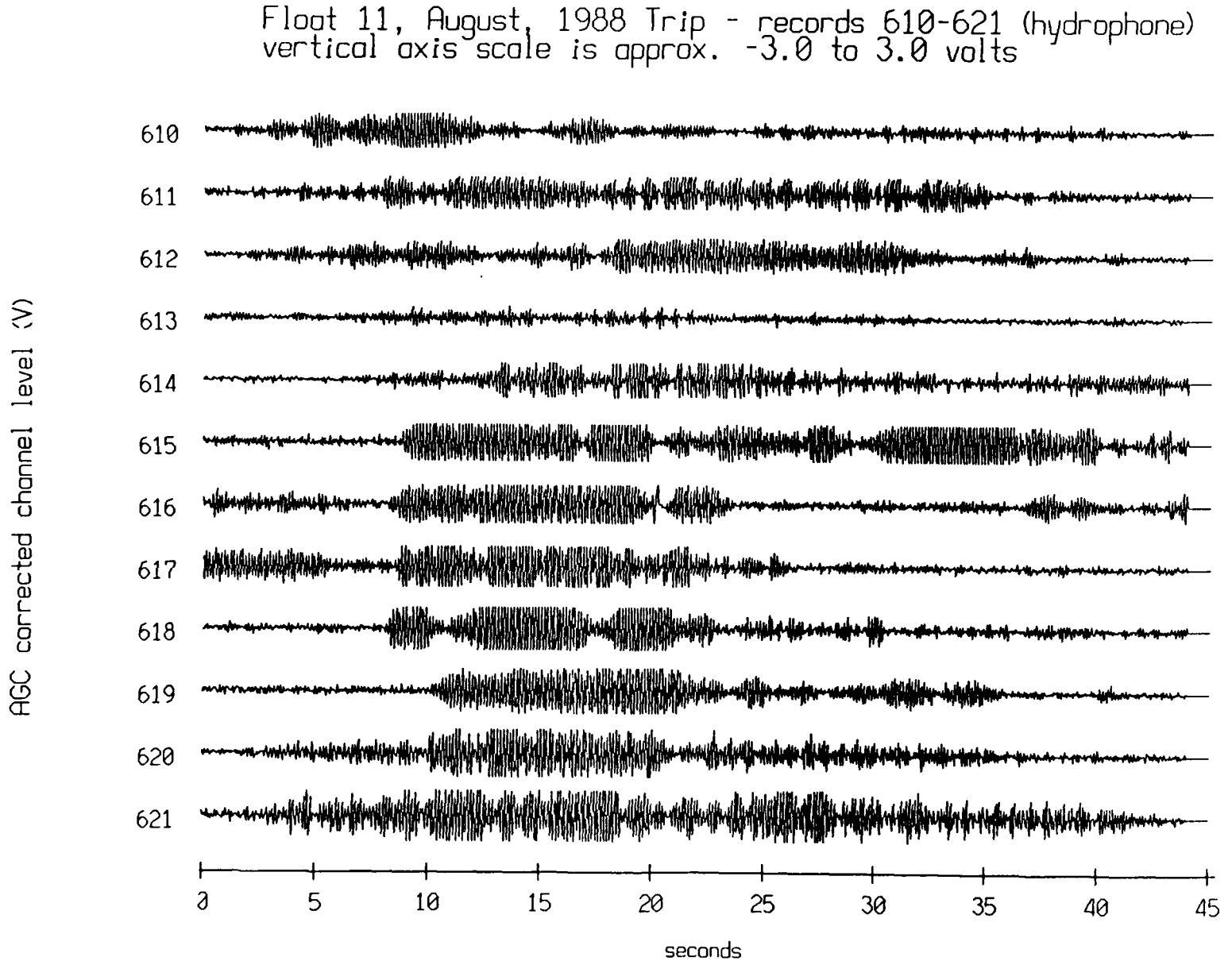

Float 11, August, 1988 Trip - records 610-621 (hydrophone)
vertical axis scale is approx. -3.0 to 3.0 volts
610
611
612
613
614
615
616
617
618
619
620
621
AGC corrected channel level (V)
0
5
10
15
20
25
30
35
40
45
seconds

Figure XI.4d

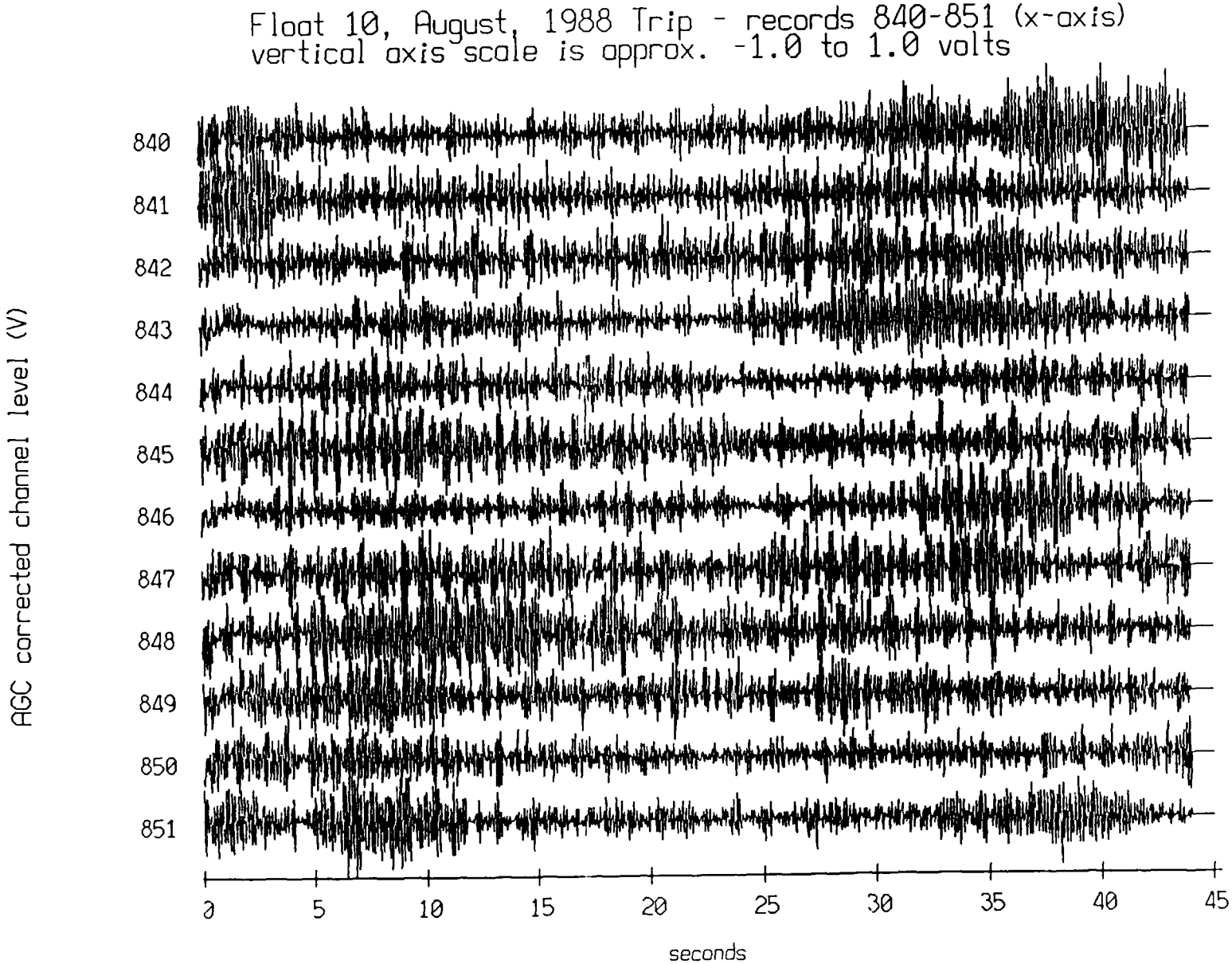

Float 10, August, 1988 Trip - records 840-851 (x-axis)
vertical axis scale is approx. -1.0 to 1.0 volts
AGC corrected channel level (V)
840
841
842
843
844
845
846
847
848
849
850
851
0
5
10
15
20
25
30
35
40
45
seconds

Figure XI.5a

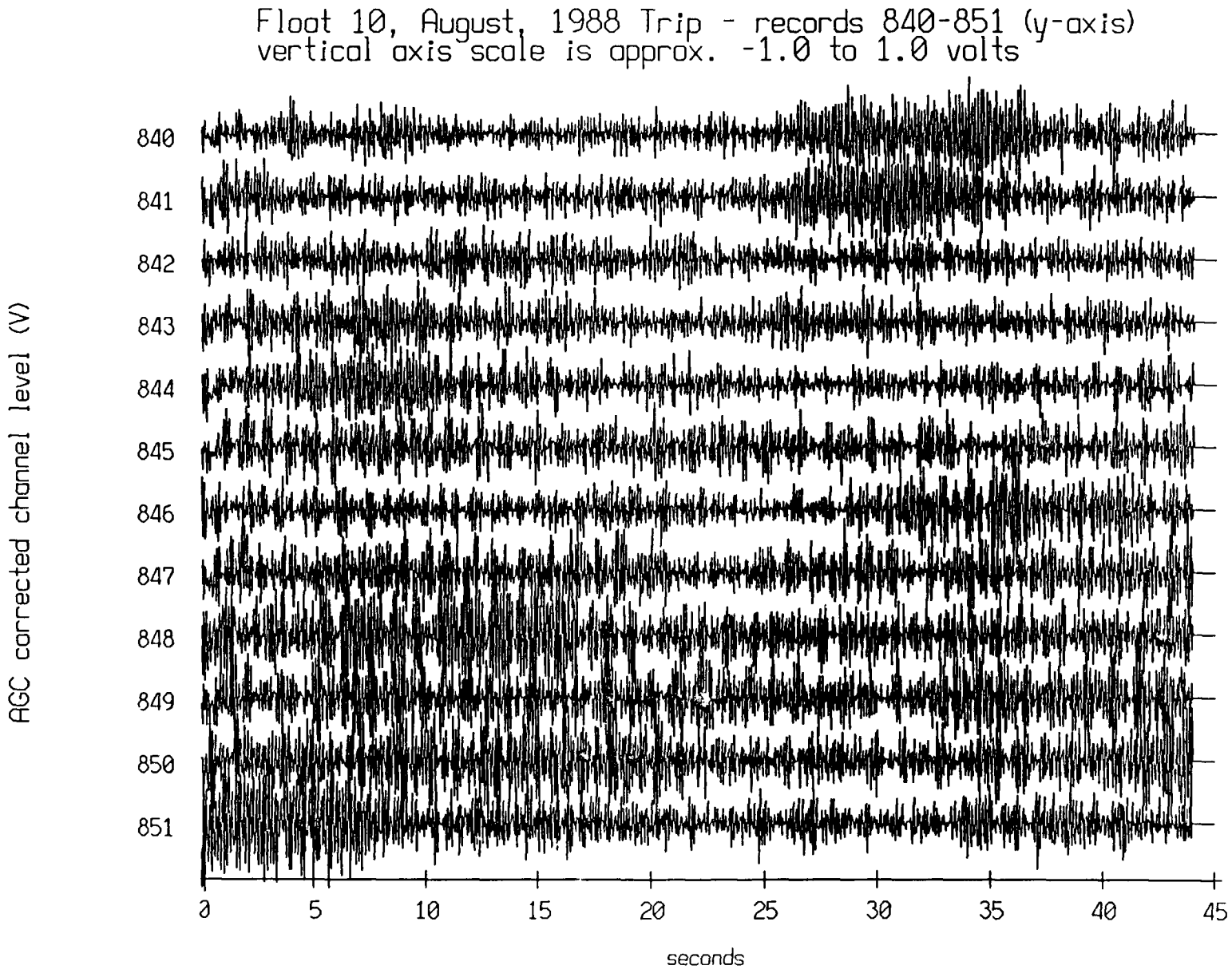

Float 10, August, 1988 Trip - records 840-851 (y-axis)
vertical axis scale is approx. -1.0 to 1.0 volts
AGC corrected channel level (V)
840
841
842
843
844
845
846
847
848
849
850
851
0
5
10
15
20
25
30
35
40
45
seconds

Figure XI.5b

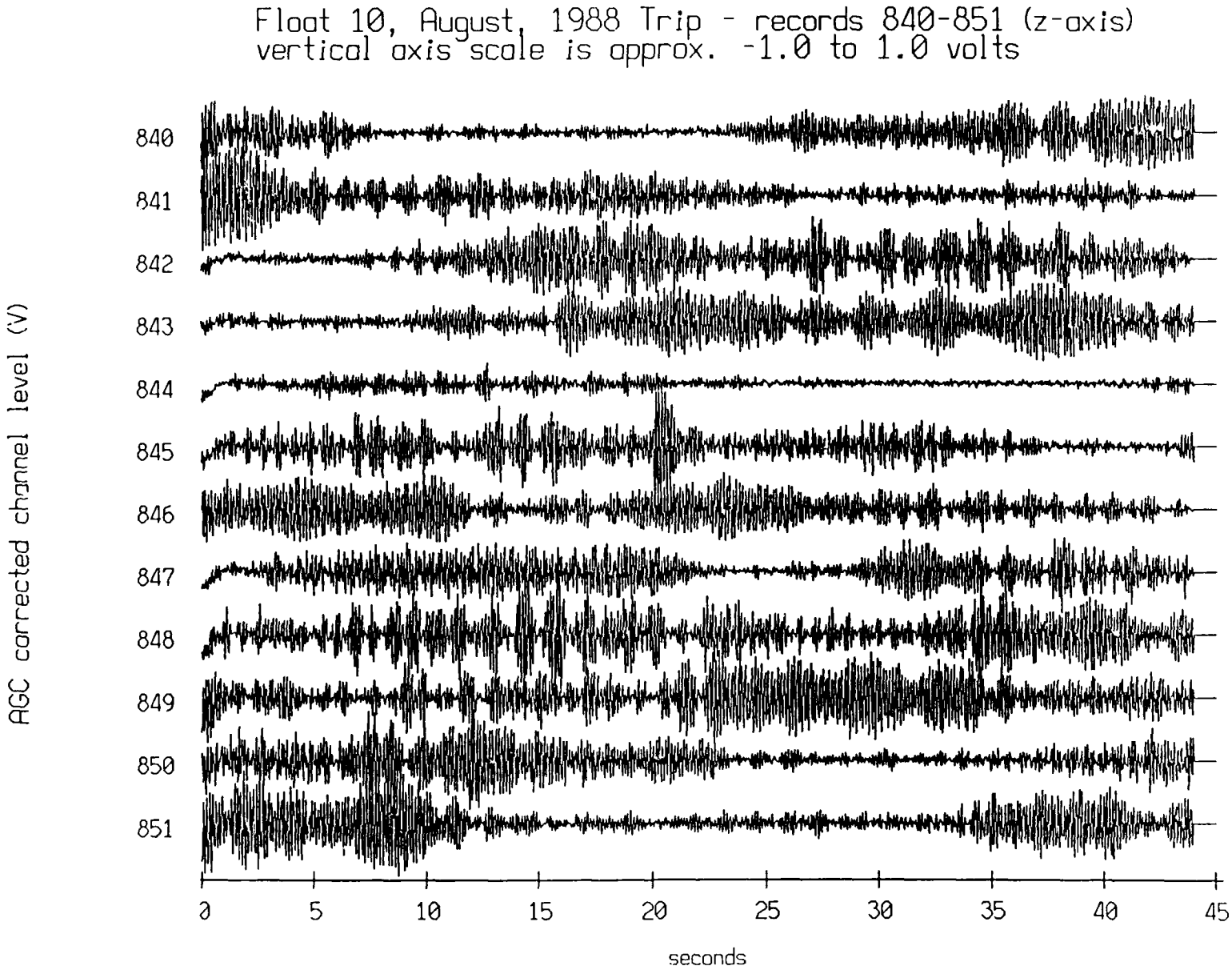


Figure XIV-5c

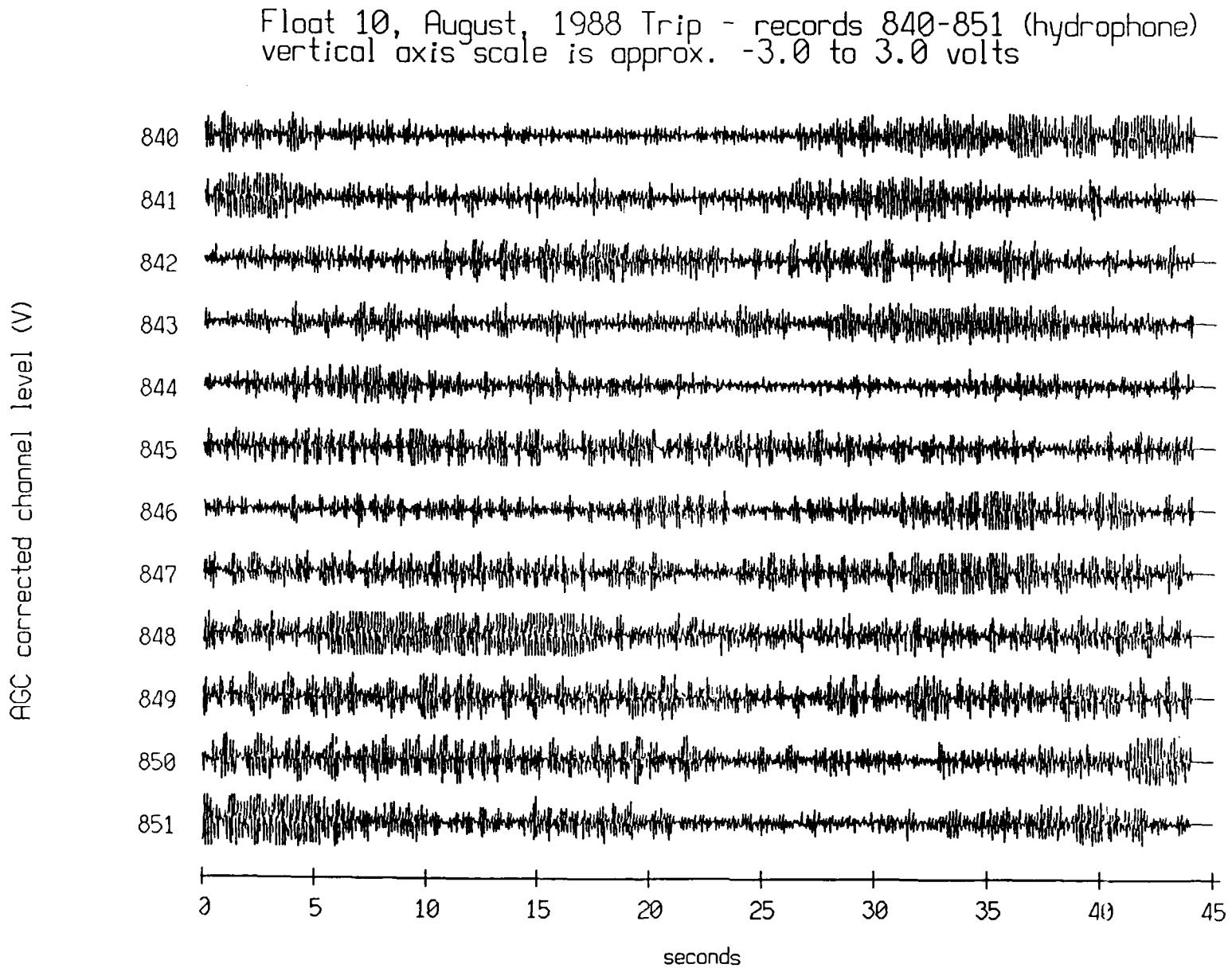

Float 10, August, 1988 Trip - records 840-851 (hydrophone)
vertical axis scale is approx. -3.0 to 3.0 volts
AGC corrected channel level (V)
840
841
842
843
844
845
846
847
848
849
850
851
0
5
10
15
20
25
30
35
40
45
seconds

Figure XI.5d

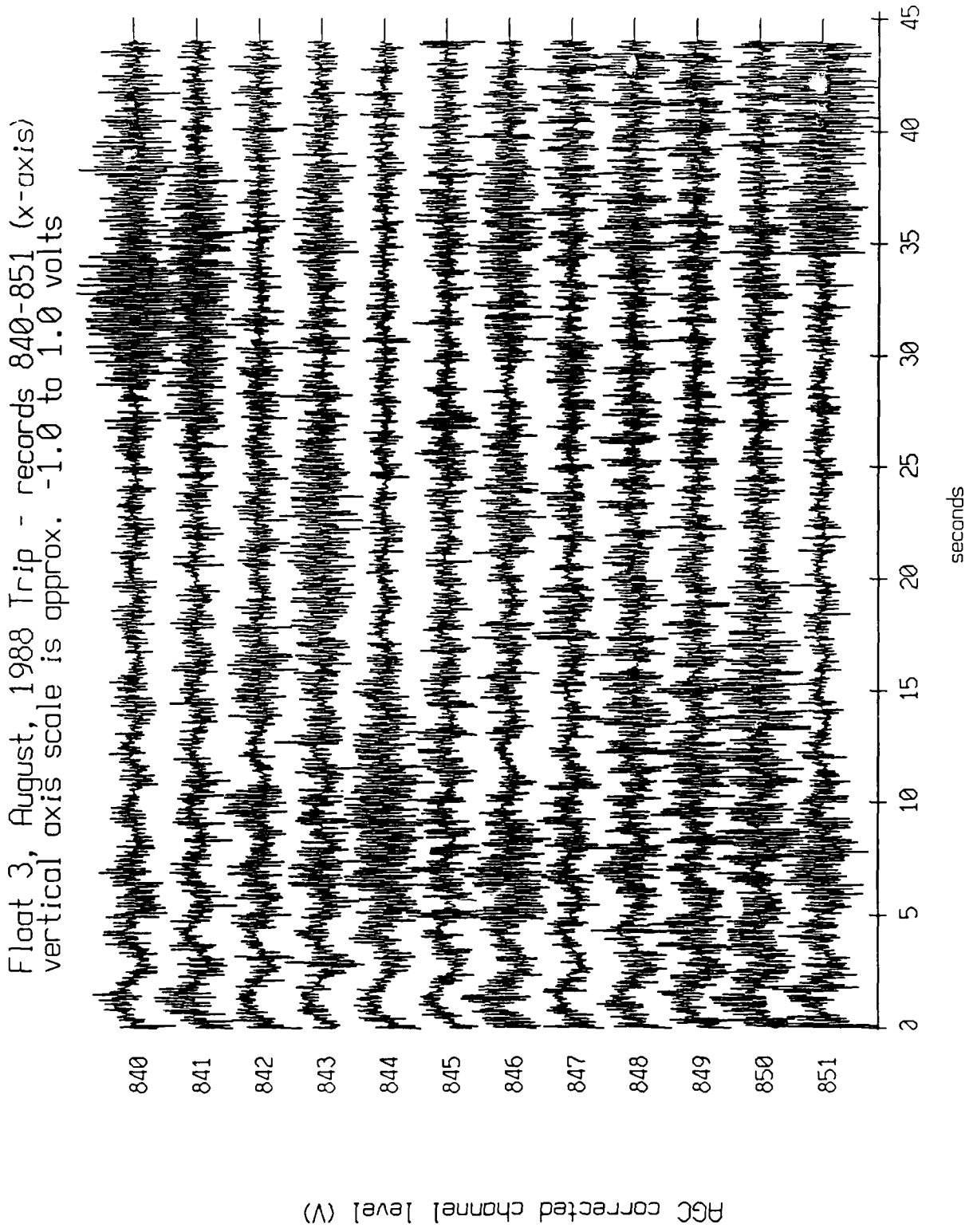

Float 3, August, 1988 Trip - records 840-851 (x-axis)
vertical axis scale is approx. -1.0 to 1.0 volts
AGC corrected channel level (V)
840
841
842
843
844
845
846
847
848
849
850
851
0
5
10
15
20
25
30
35
40
45
seconds

Figure XI.6a

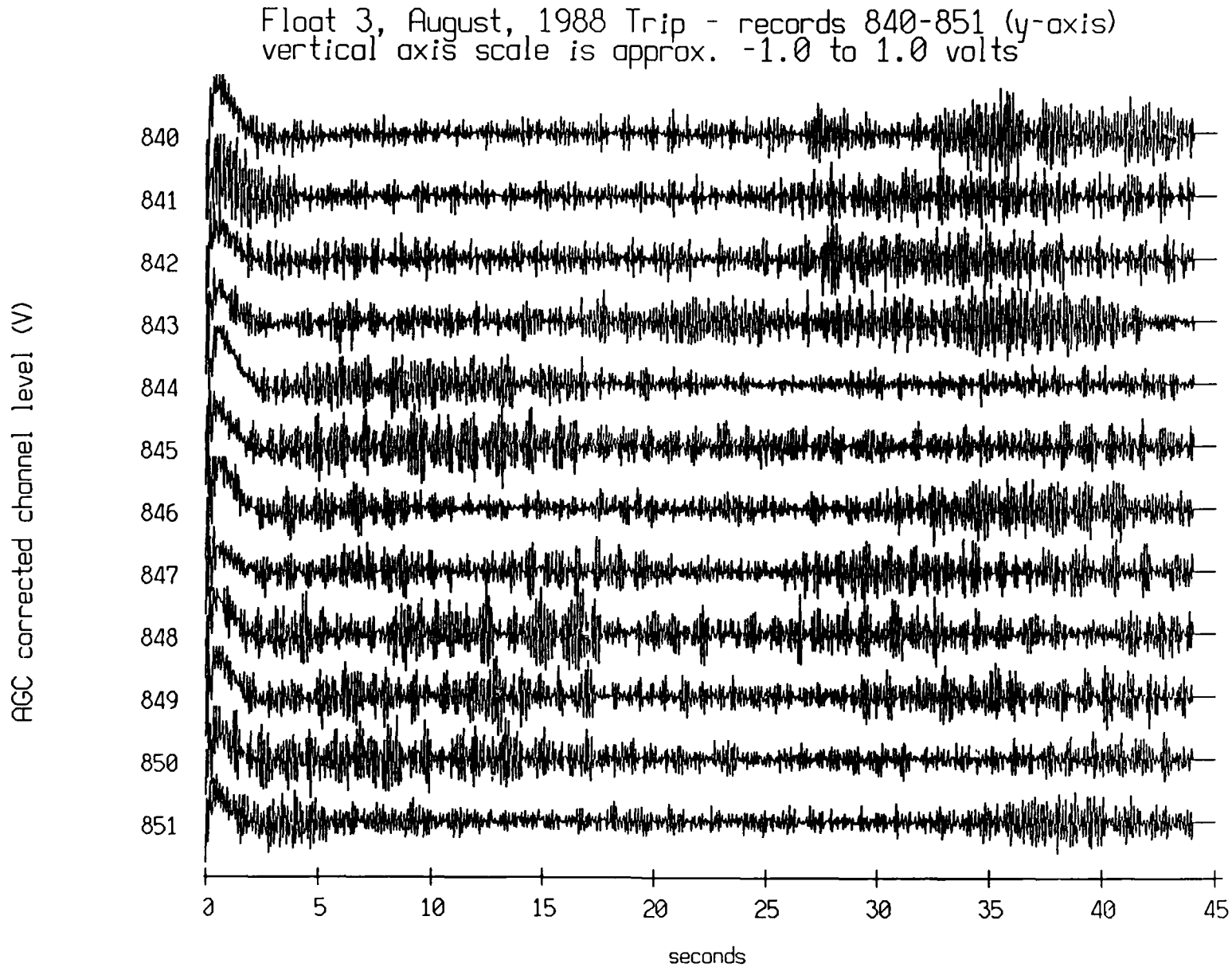

Float 3, August, 1988 Trip - records 840-851 (y-axis)
vertical axis scale is approx. -1.0 to 1.0 volts
AGC corrected channel level (V)
840
841
842
843
844
845
846
847
848
849
850
851
0
5
10
15
20
25
30
35
40
45
seconds

Figure XI.6b

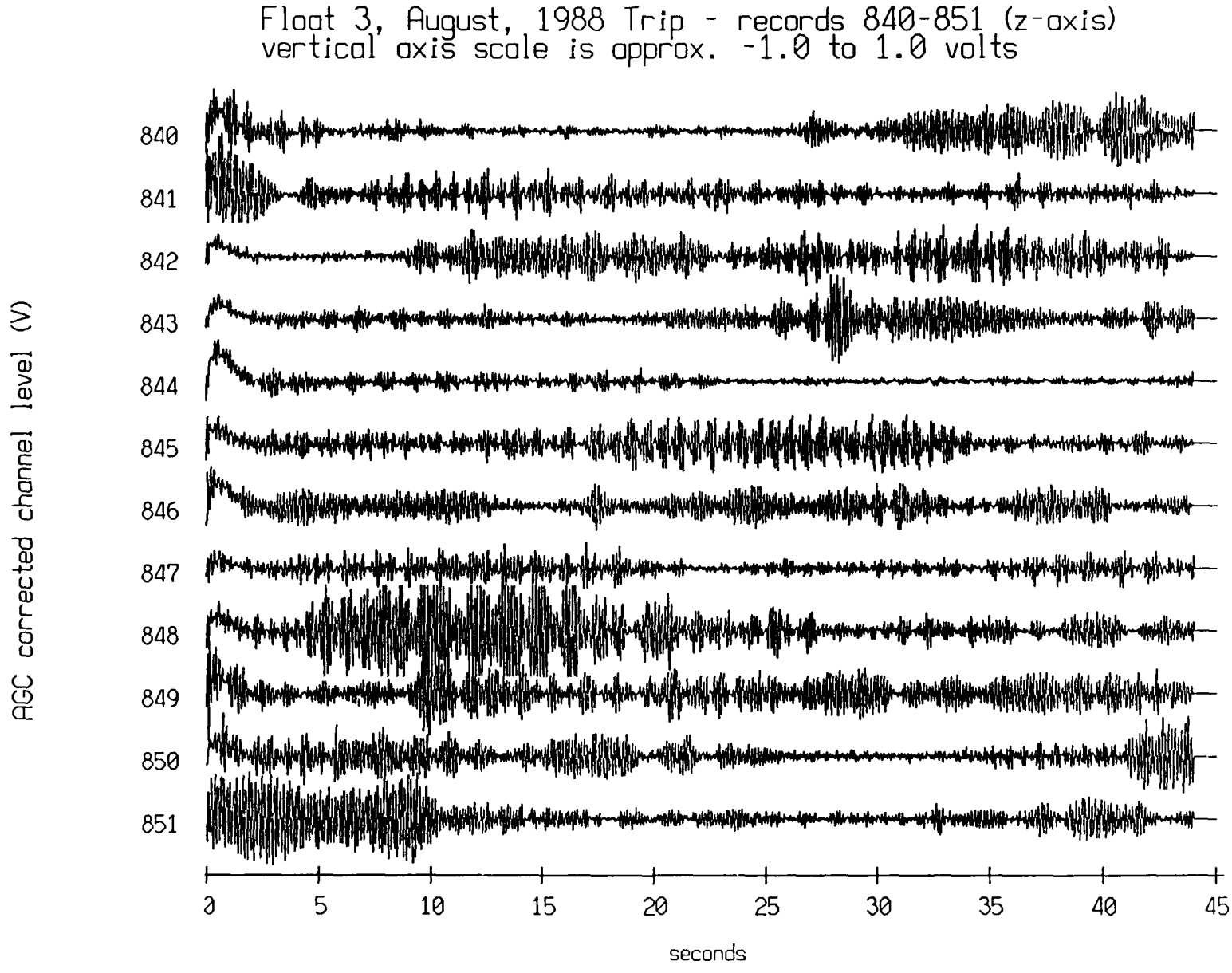

Float 3, August, 1988 Trip - records 840-851 (z-axis)
vertical axis scale is approx. -1.0 to 1.0 volts
AGC corrected channel level (V)
840
841
842
843
844
845
846
847
848
849
850
851
0
5
10
15
20
25
30
35
40
45
seconds

Figure XI.6c

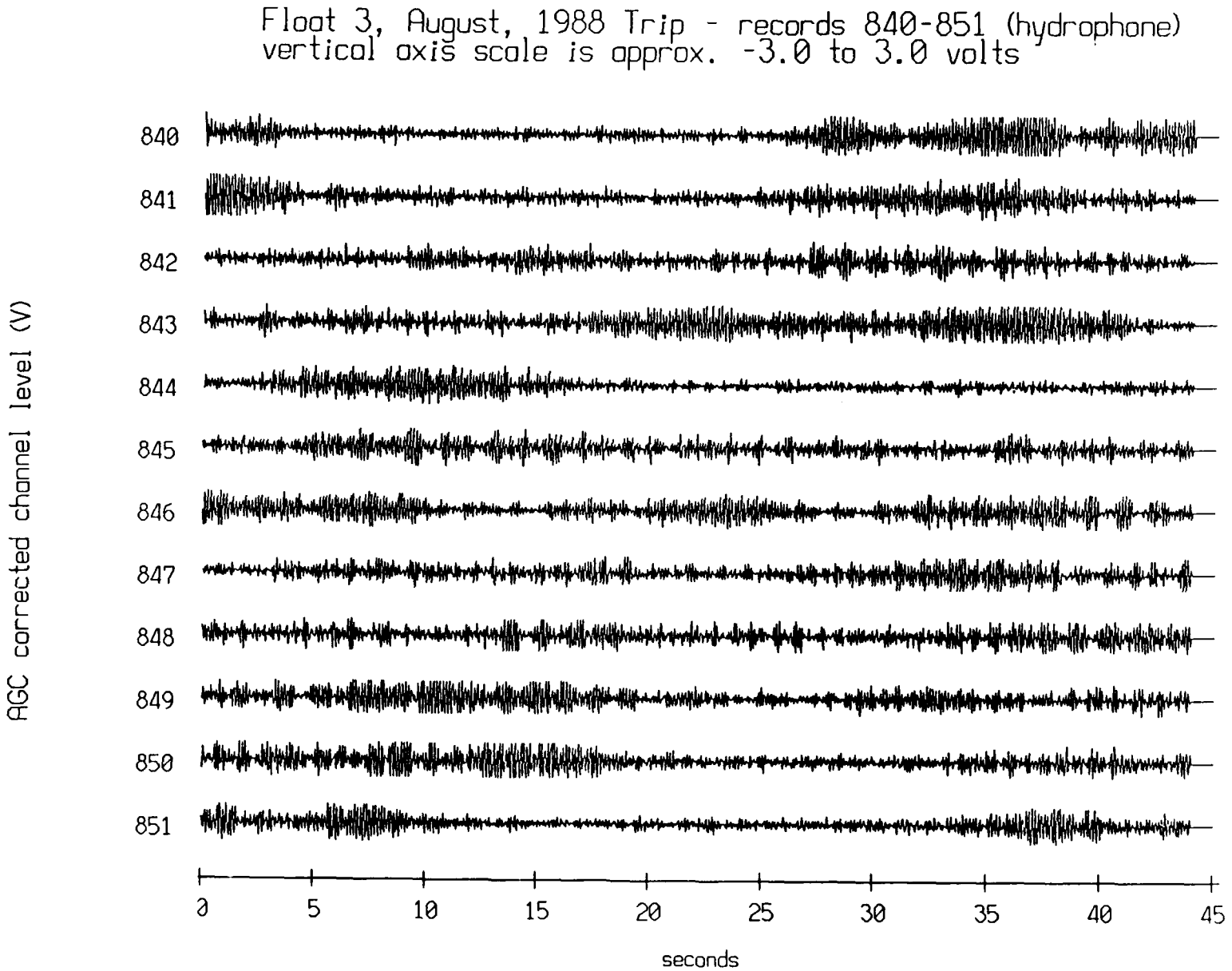

Float 3, August, 1988 Trip - records 840-851 (hydrophone)
vertical axis scale is approx. -3.0 to 3.0 volts
AGC corrected channel level (V)
840
841
842
843
844
845
846
847
848
849
850
851
0
5
10
15
20
25
30
35
40
45
seconds

Figure XI.6d

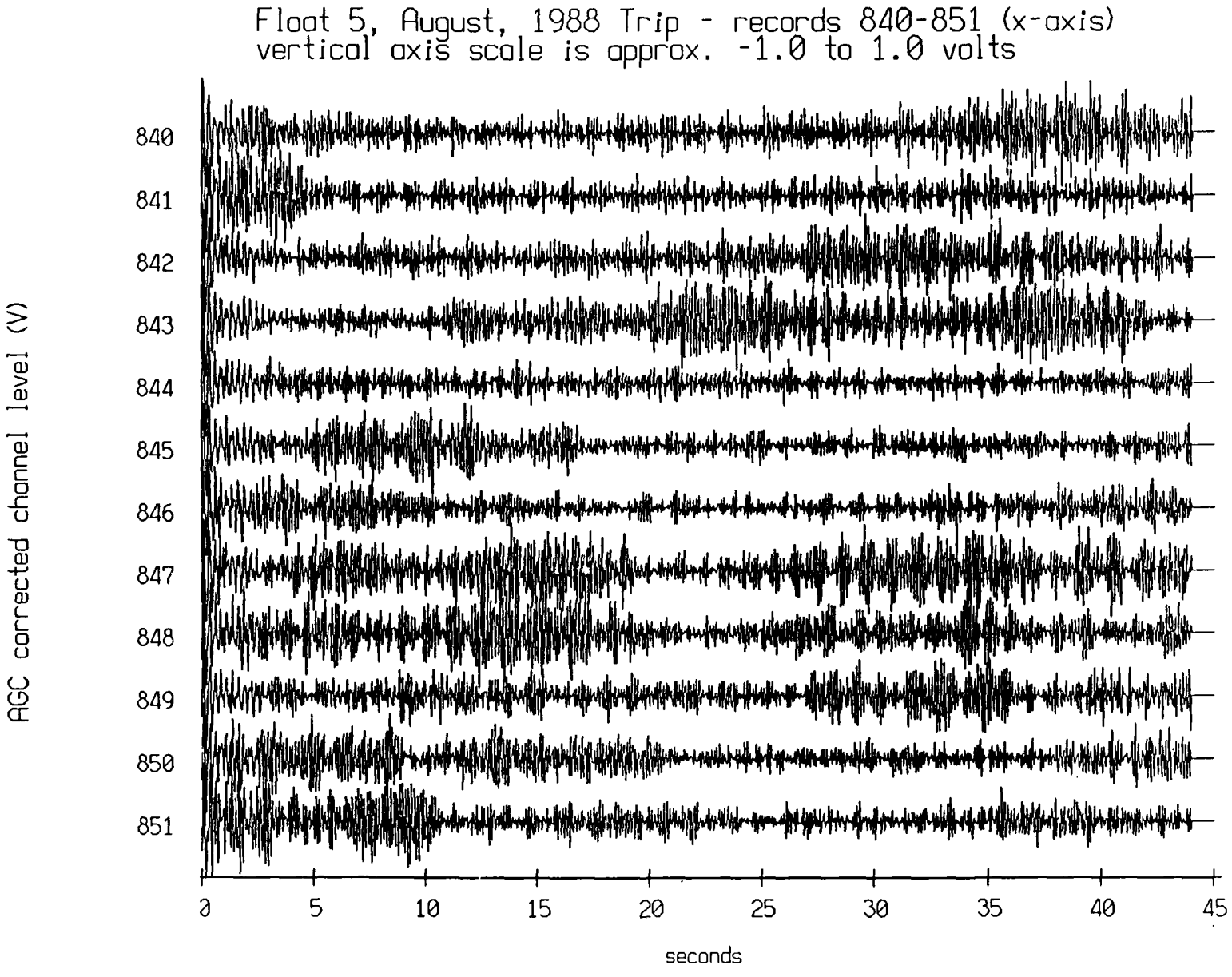

Float 5, August, 1988 Trip - records 840-851 (x-axis)
vertical axis scale is approx. -1.0 to 1.0 volts
AGC corrected channel level (V)
840
841
842
843
844
845
846
847
848
849
850
851
0
5
10
15
20
25
30
35
40
45
seconds

Figure XI.7a

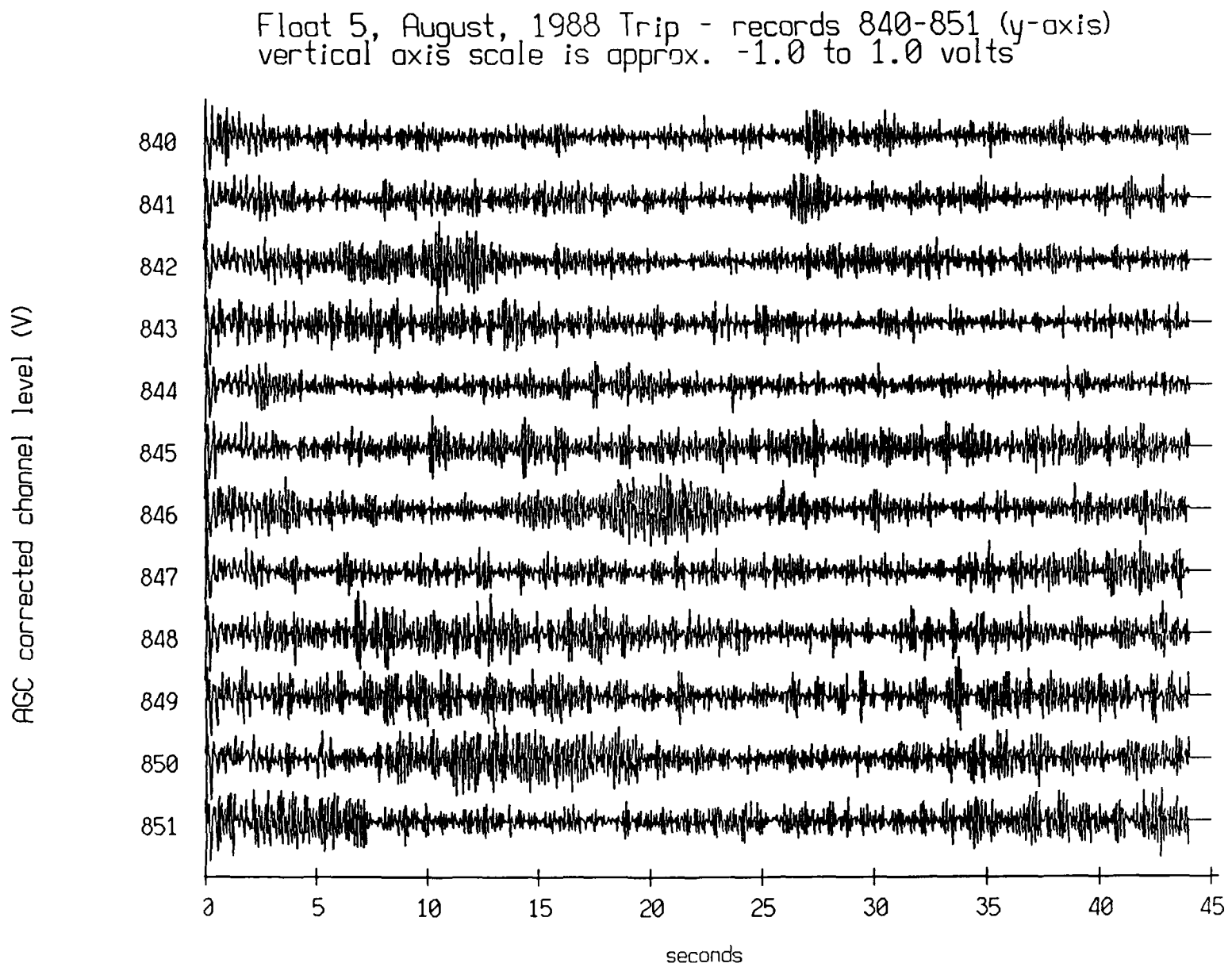

Float 5, August, 1988 Trip - records 840-851 (y-axis)
vertical axis scale is approx. -1.0 to 1.0 volts
AGC corrected channel level (V)
840
841
842
843
844
845
846
847
848
849
850
851
0
5
10
15
20
25
30
35
40
45
seconds

Figure XI.7b

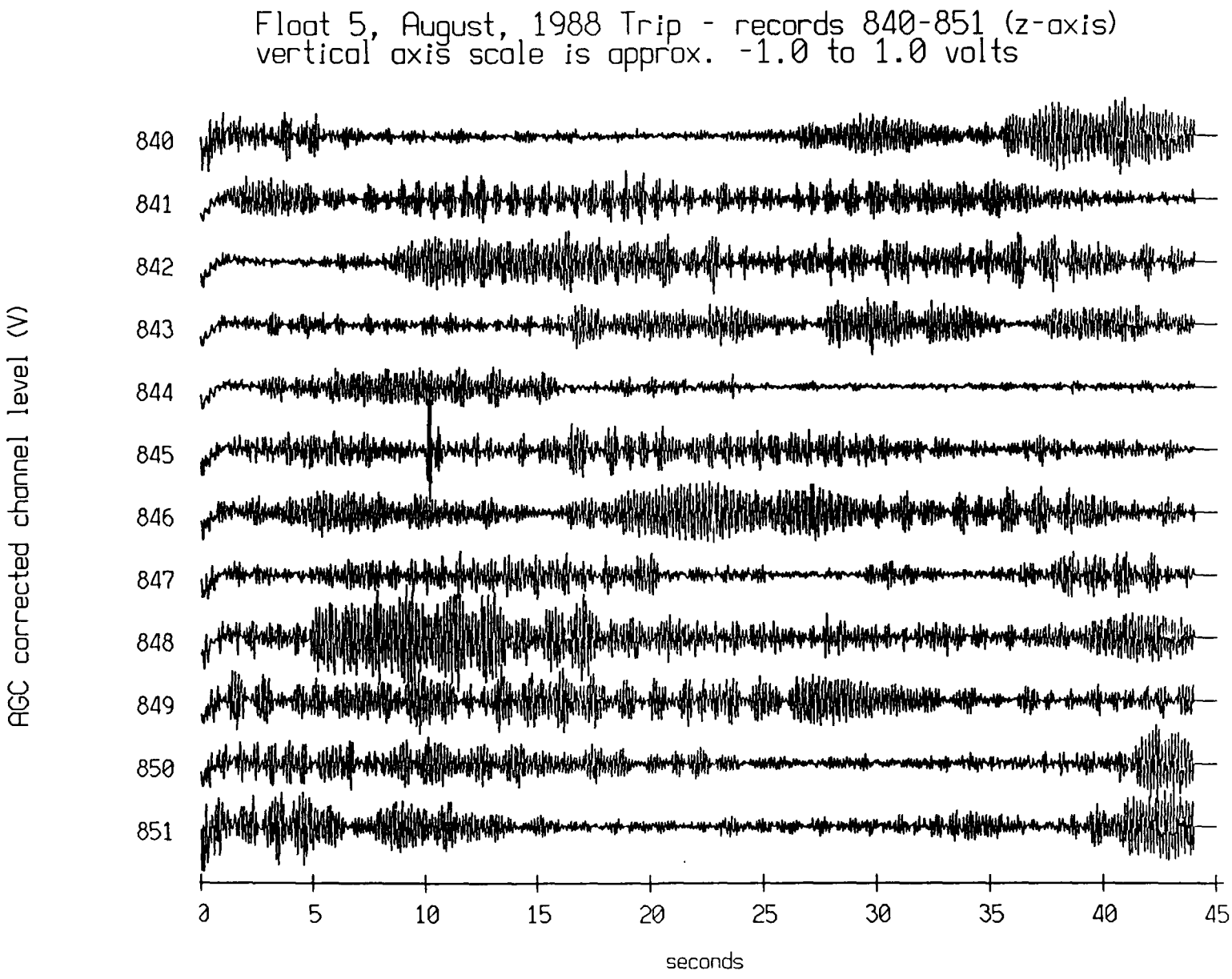

Float 5, August, 1988 Trip - records 840-851 (z-axis)
vertical axis scale is approx. -1.0 to 1.0 volts
AGC corrected channel level (V)
840
841
842
843
844
845
846
847
848
849
850
851
0
5
10
15
20
25
30
35
40
45
seconds

Figure XI.7c

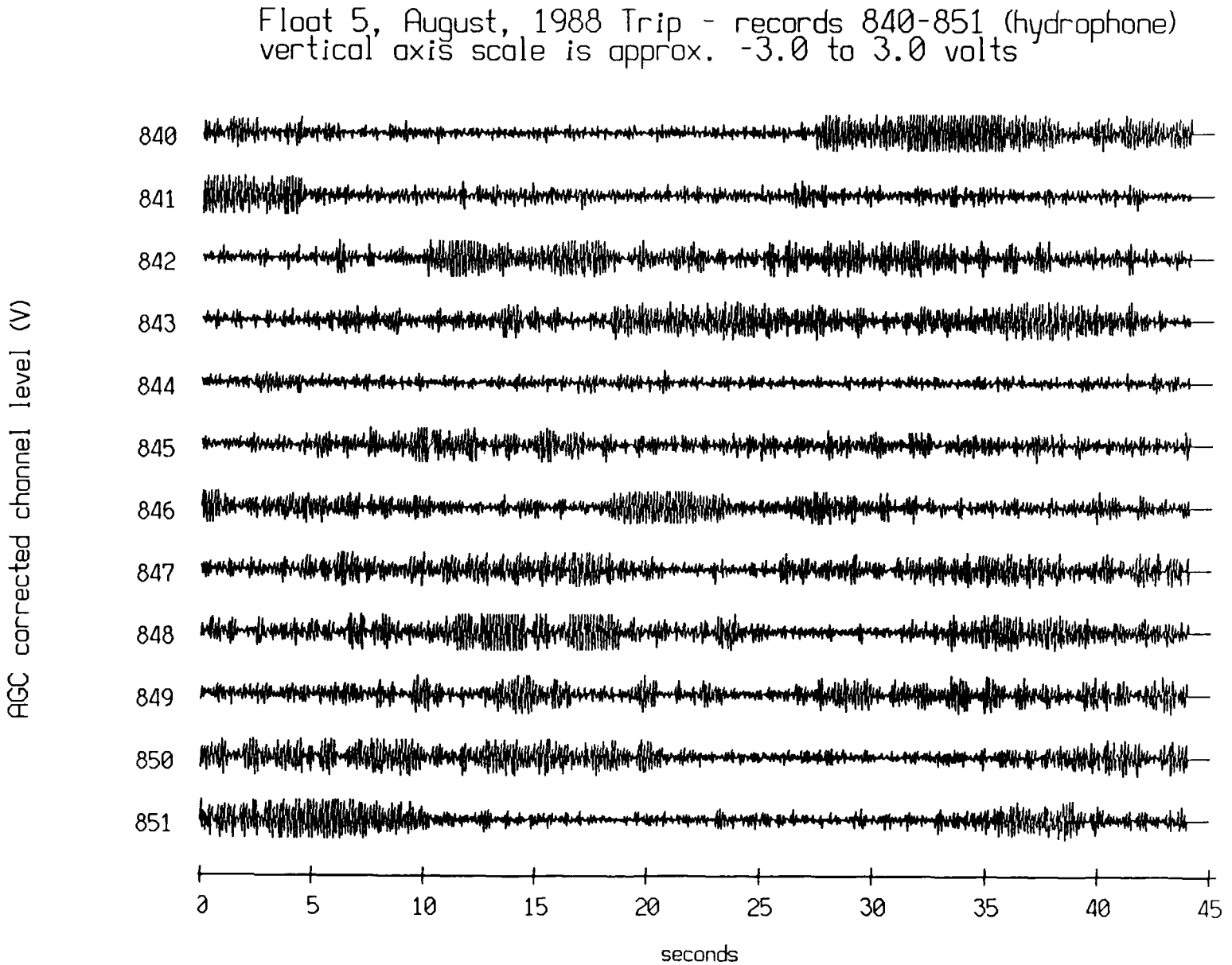

Float 5, August, 1988 Trip - records 840-851 (hydrophone)
vertical axis scale is approx. -3.0 to 3.0 volts
AGC corrected channel level (V)
840
841
842
843
844
845
846
847
848
849
850
851
0
5
10
15
20
25
30
35
40
45
seconds

Figure XI.7d

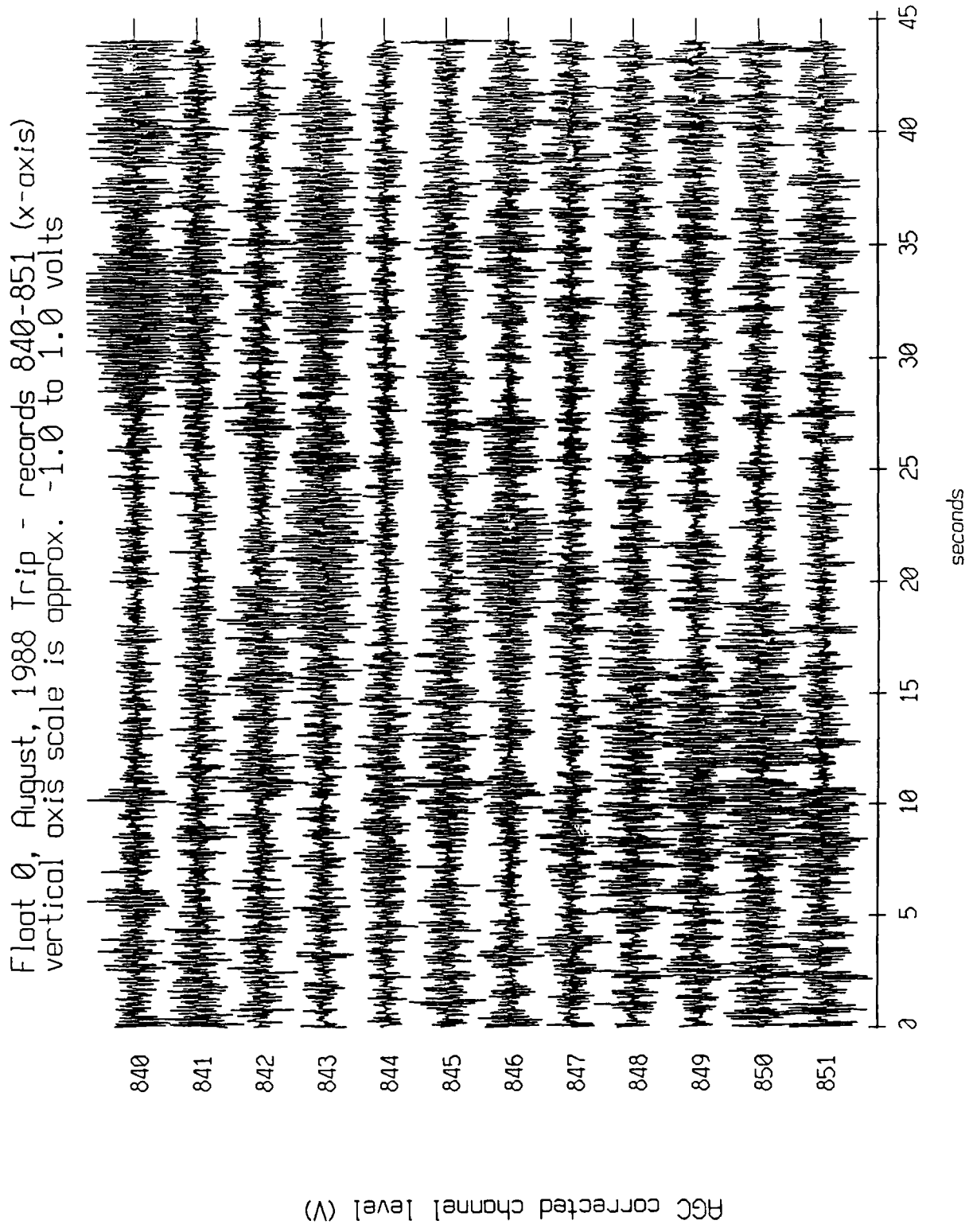

Float 0, August, 1988 Trip - records 840-851 (x-axis)
vertical axis scale is approx. -1.0 to 1.0 volts
AGC corrected channel level (V)
840
841
842
843
844
845
846
847
848
849
850
851
0
5
10
15
20
25
30
35
40
45
seconds

Figure XI.8a

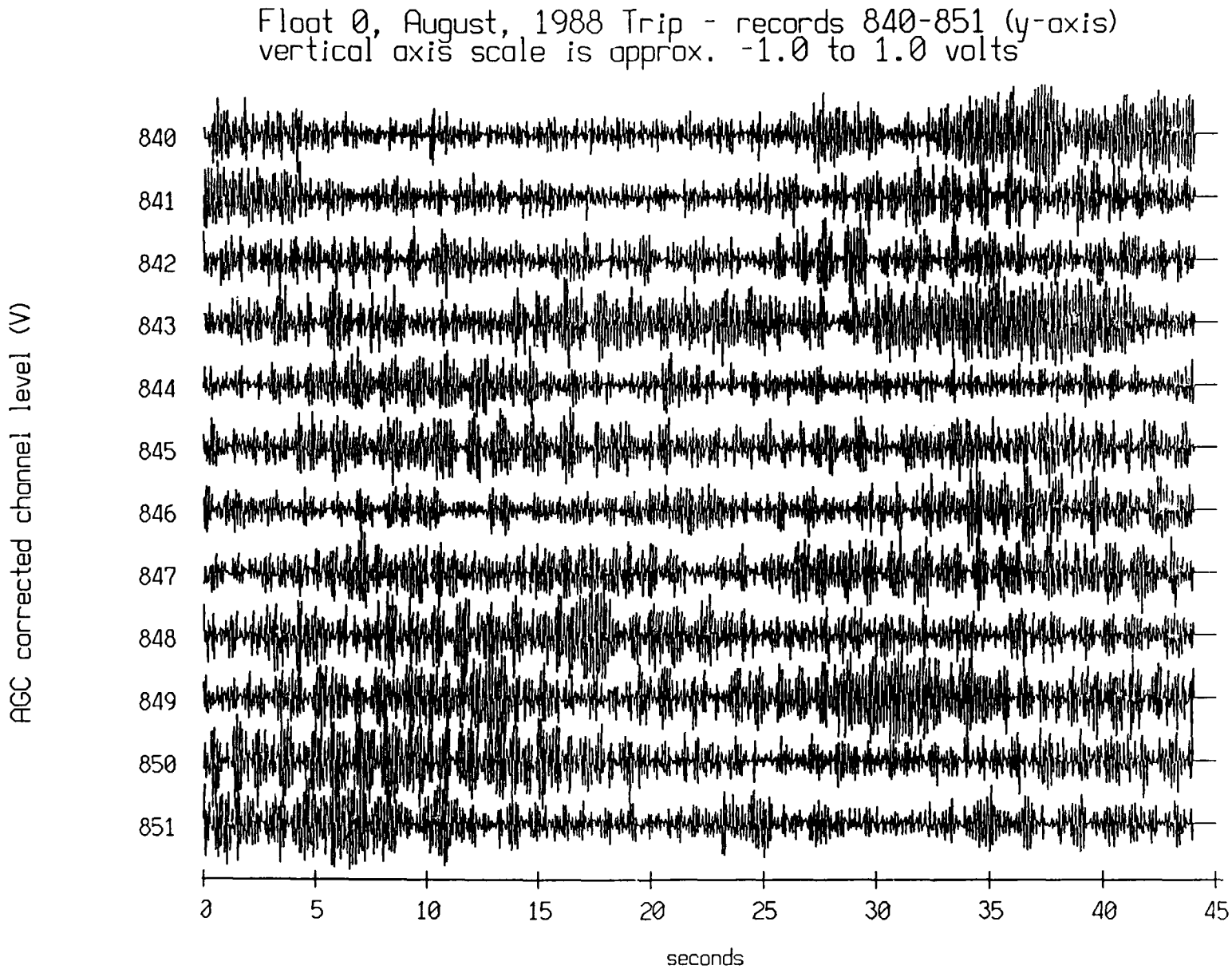

Float 0, August, 1988 Trip - records 840-851 (y-axis)
vertical axis scale is approx. -1.0 to 1.0 volts
AGC corrected channel level (V)
840
841
842
843
844
845
846
847
848
849
850
851
0
5
10
15
20
25
30
35
40
45
seconds

Figure XI.5b

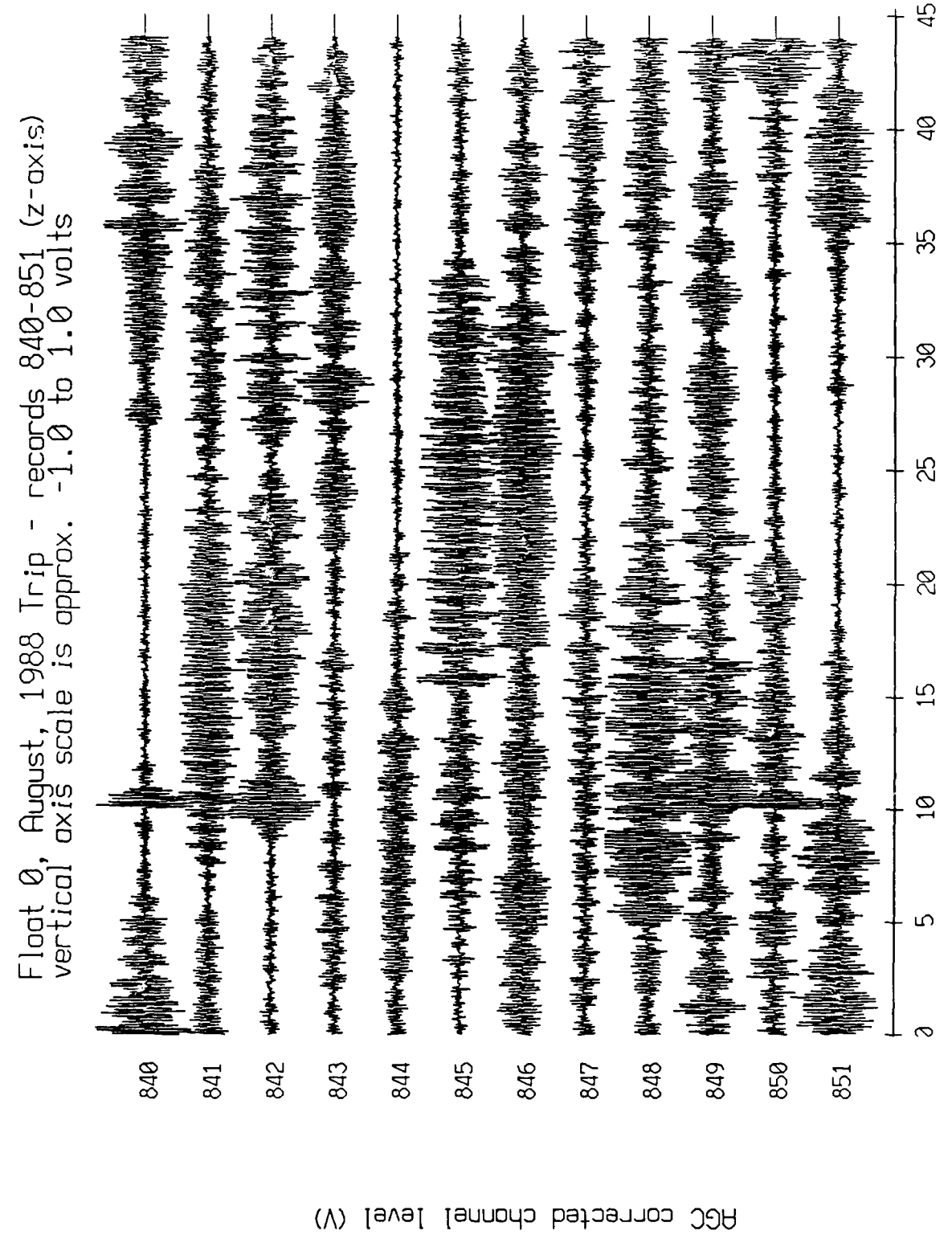

Float 0, August, 1988 Trip - records 840-851 (z-axis)
vertical axis scale is approx. -1.0 to 1.0 volts
840
841
842
843
844
845
846
847
848
849
850
851
0
5
10
15
20
25
30
35
40
45
seconds
RGC corrected channel level (V)

Figure XI.8c

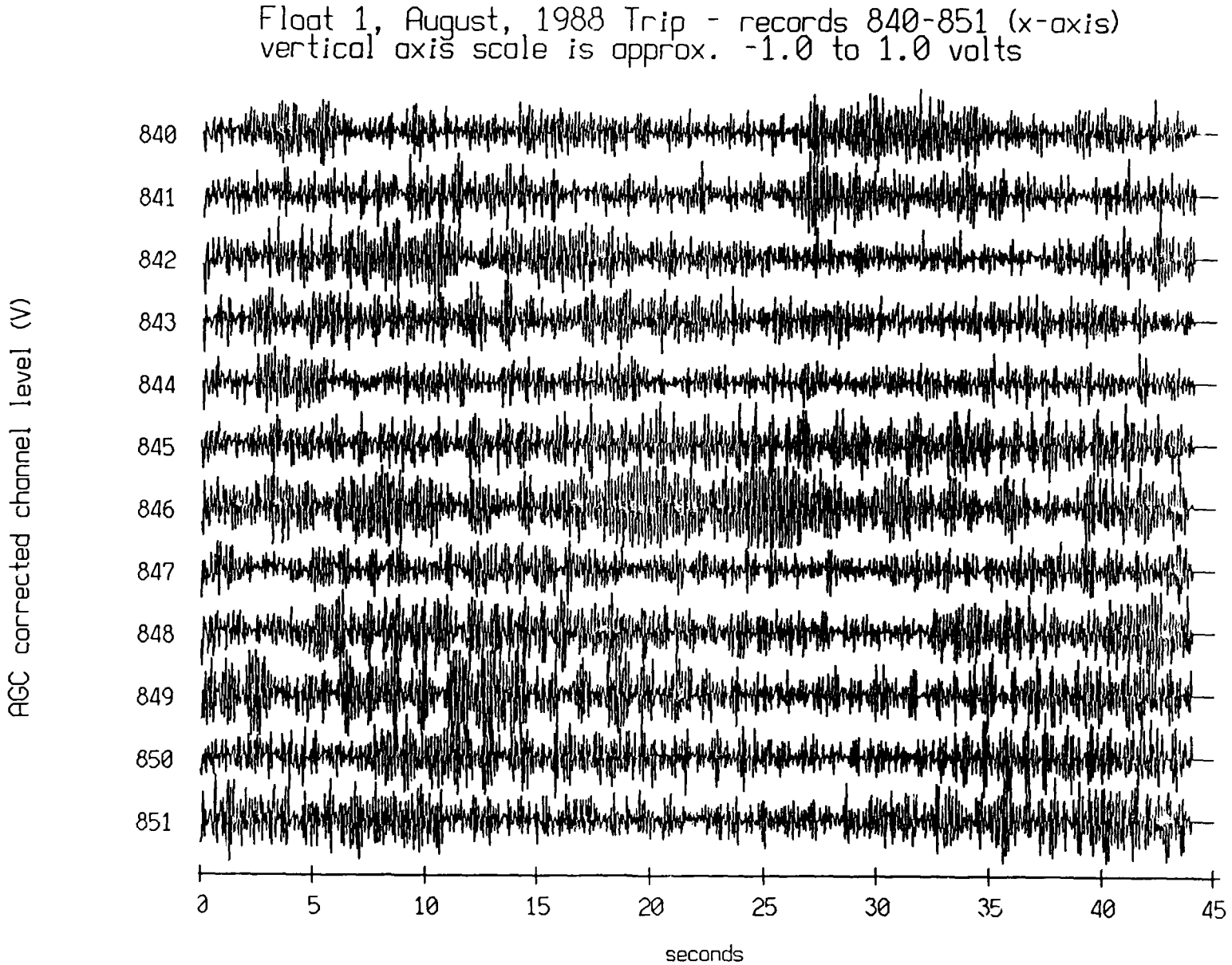

Float 1, August, 1988 Trip - records 840-851 (x-axis)
vertical axis scale is approx. -1.0 to 1.0 volts
AGC corrected channel level (V)
840
841
842
843
844
845
846
847
848
849
850
851
0
5
10
15
20
25
30
35
40
45
seconds

Figure XI.9a

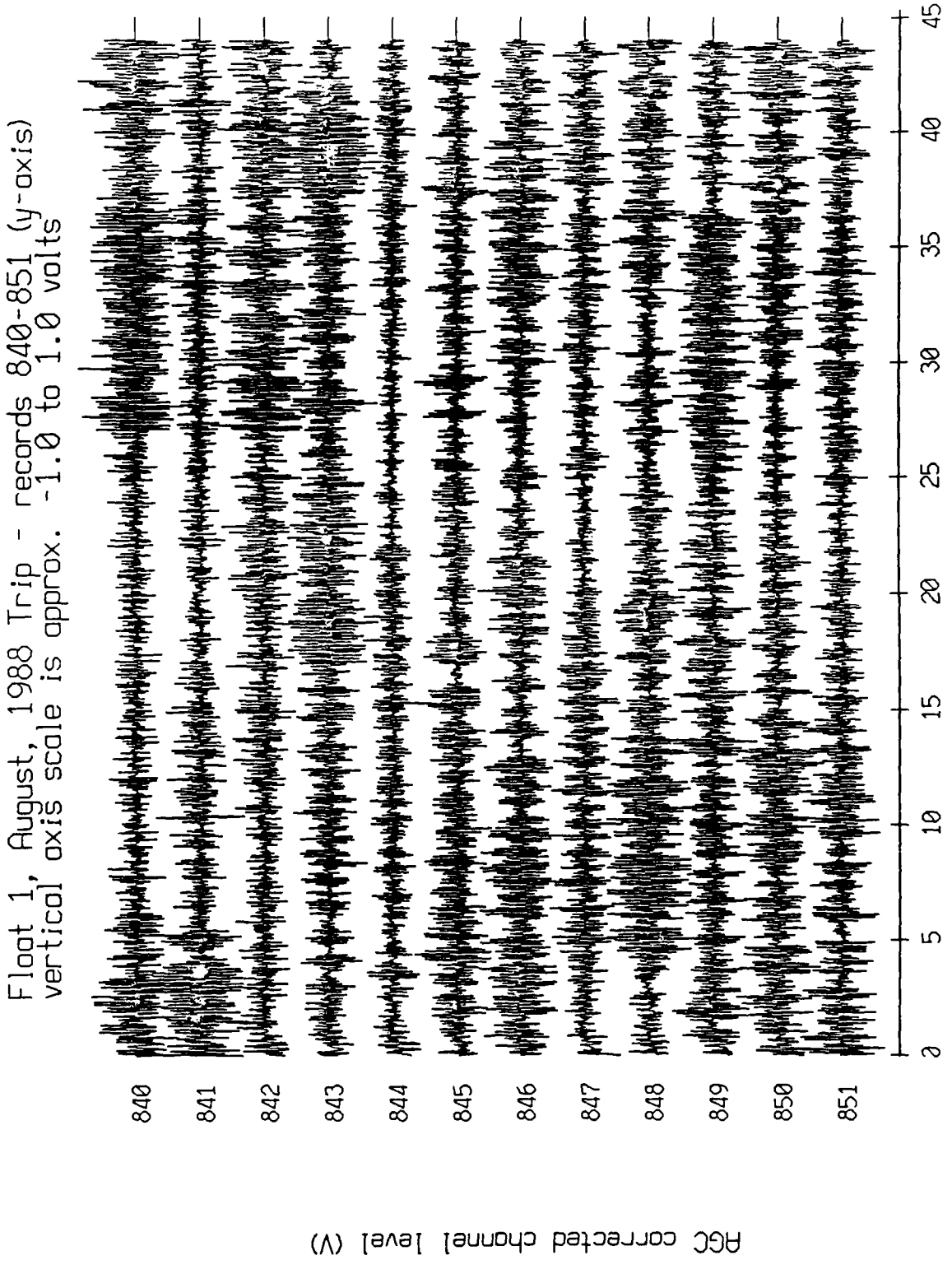

Float 1, August, 1988 Trip - records 840-851 (y-axis)
vertical axis scale is approx. -1.0 to 1.0 volts
840
841
842
843
844
845
846
847
848
849
850
851
0
5
10
15
20
25
30
35
40
45
seconds
AGC corrected channel level (V)

Figure XI.9b

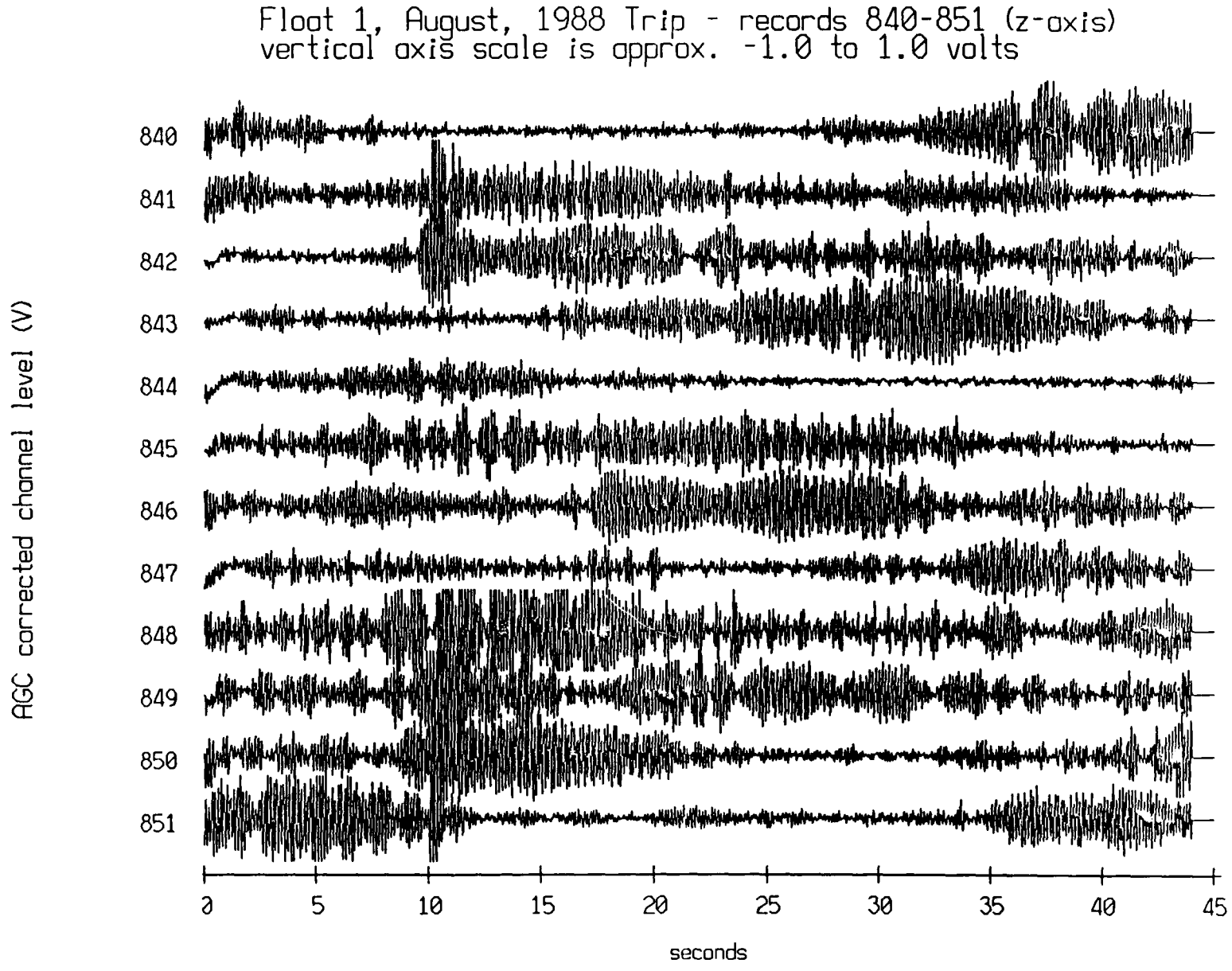

Float 1, August, 1988 Trip - records 840-851 (z-axis)
vertical axis scale is approx. -1.0 to 1.0 volts
AGC corrected channel level (V)
840
841
842
843
844
845
846
847
848
849
850
851
0
5
10
15
20
25
30
35
40
45
seconds

Figure XI.9c

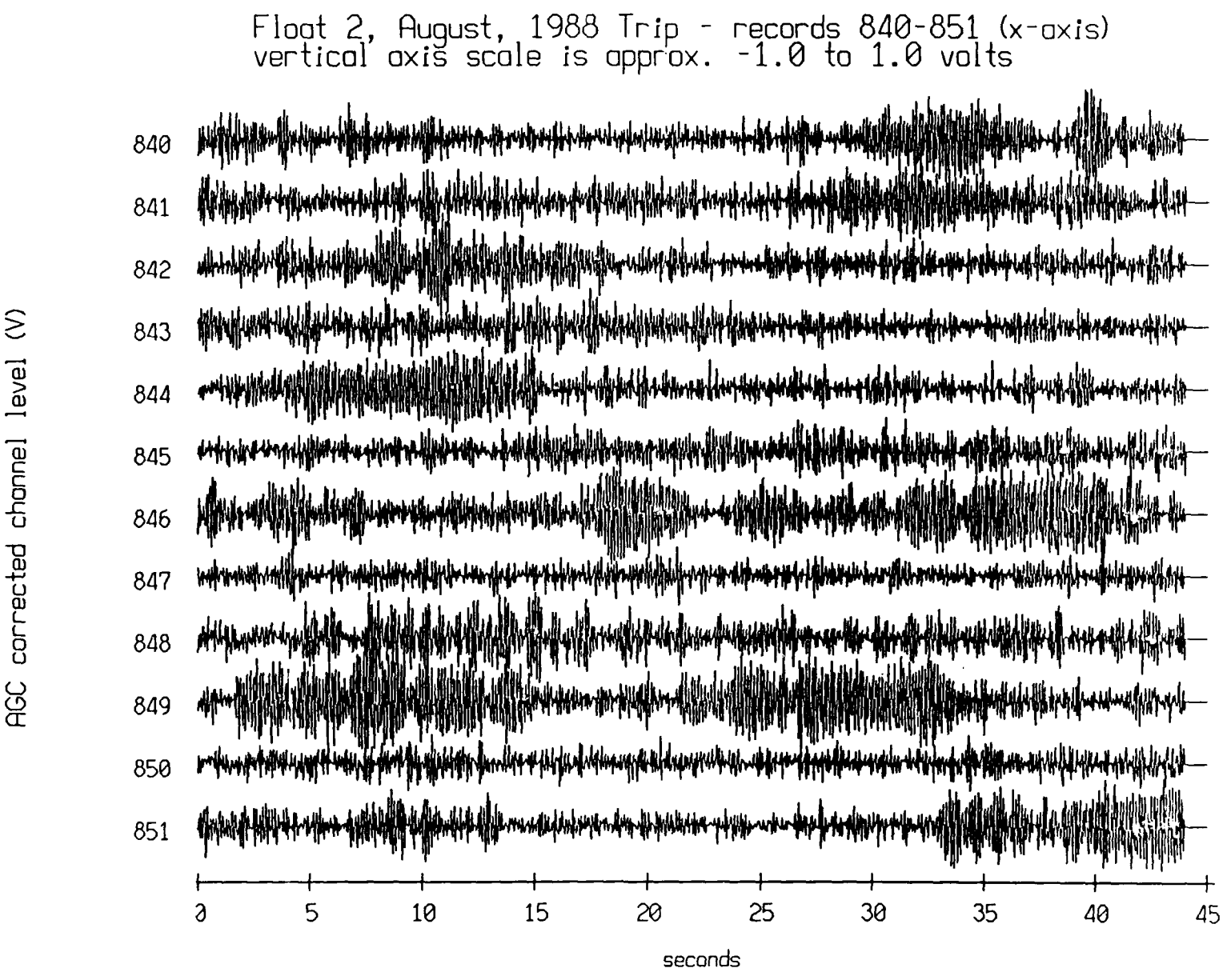


Figure XI.10a

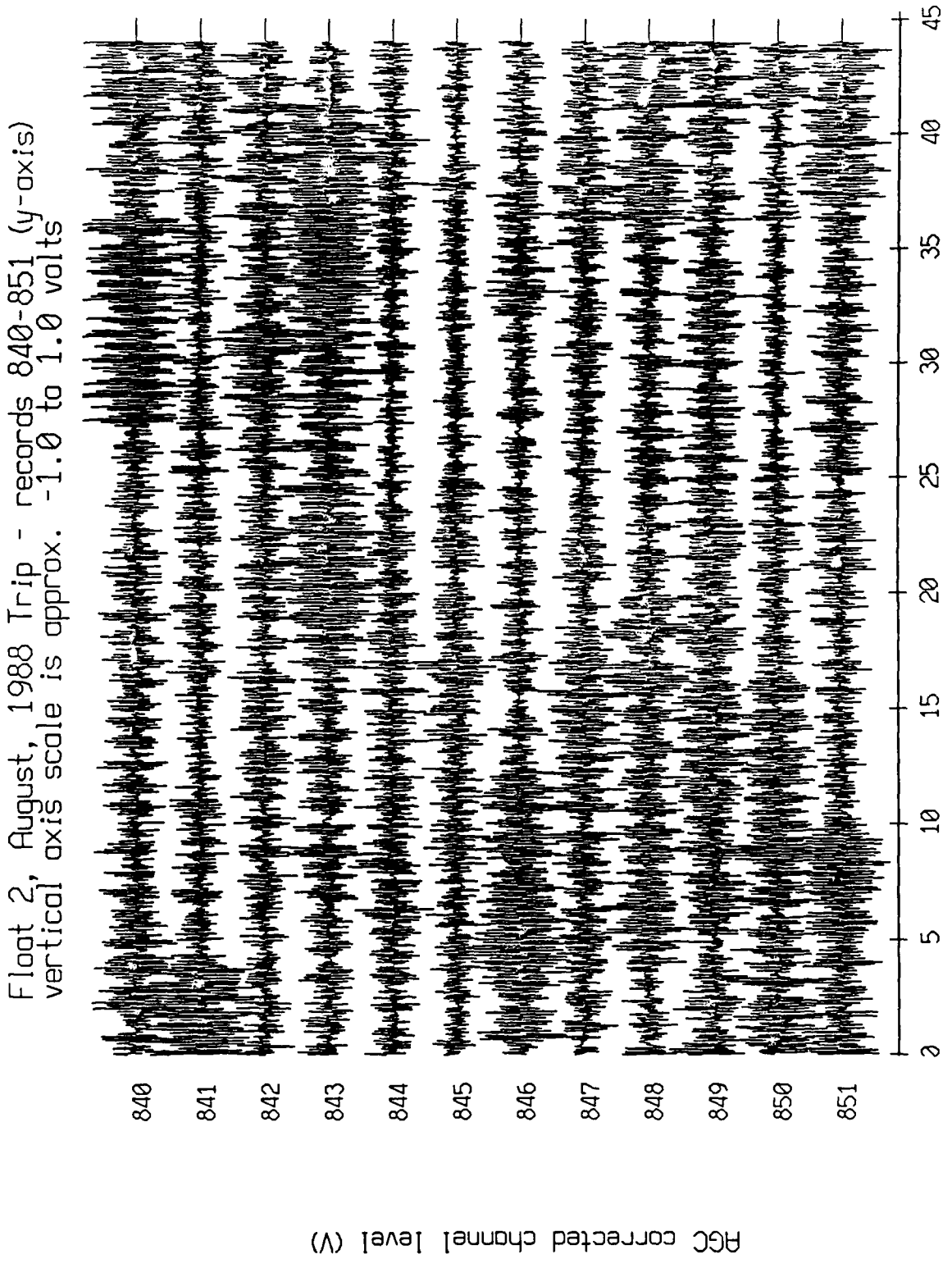


Figure XI.10b

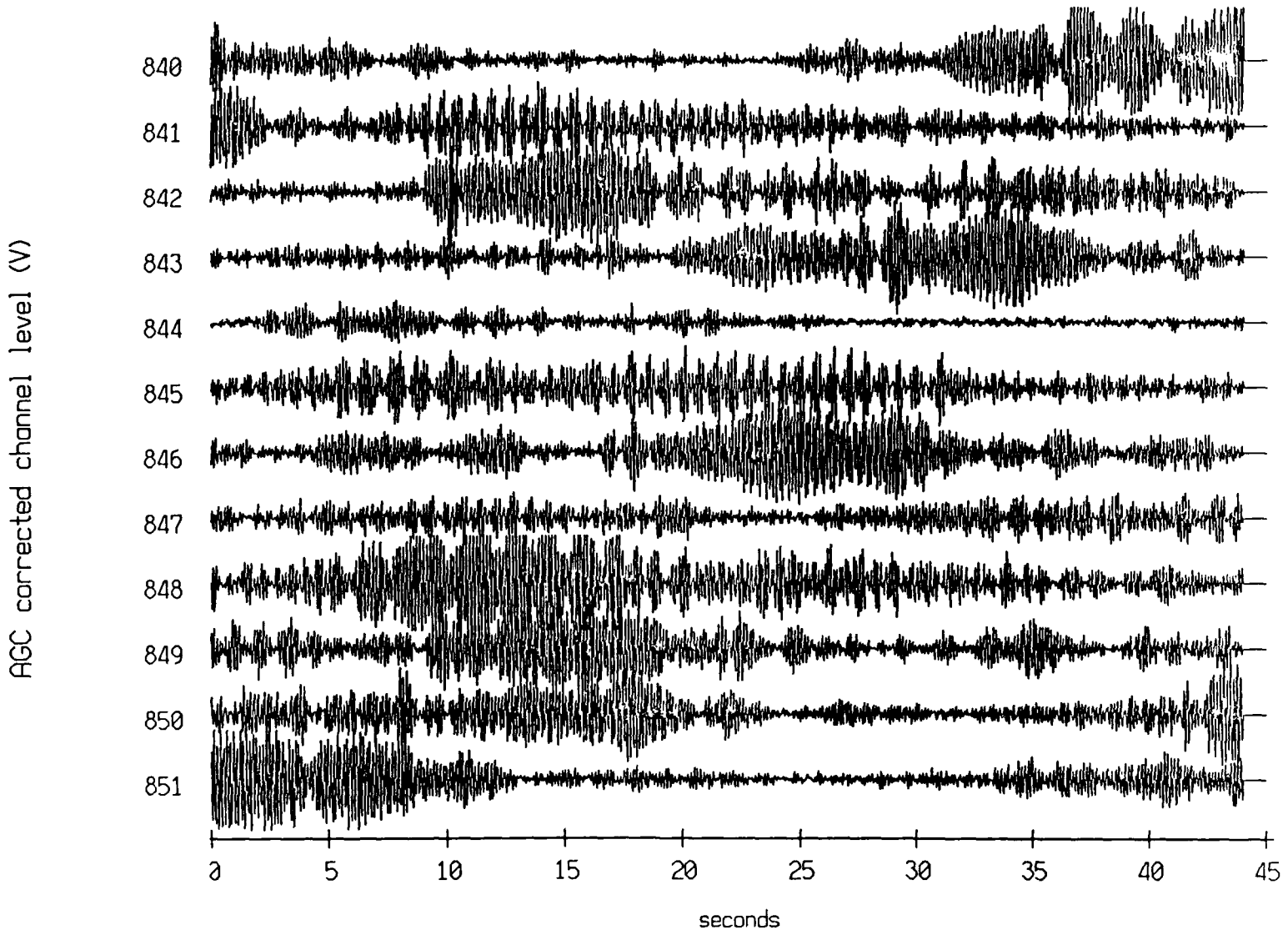


Figure XI.10c

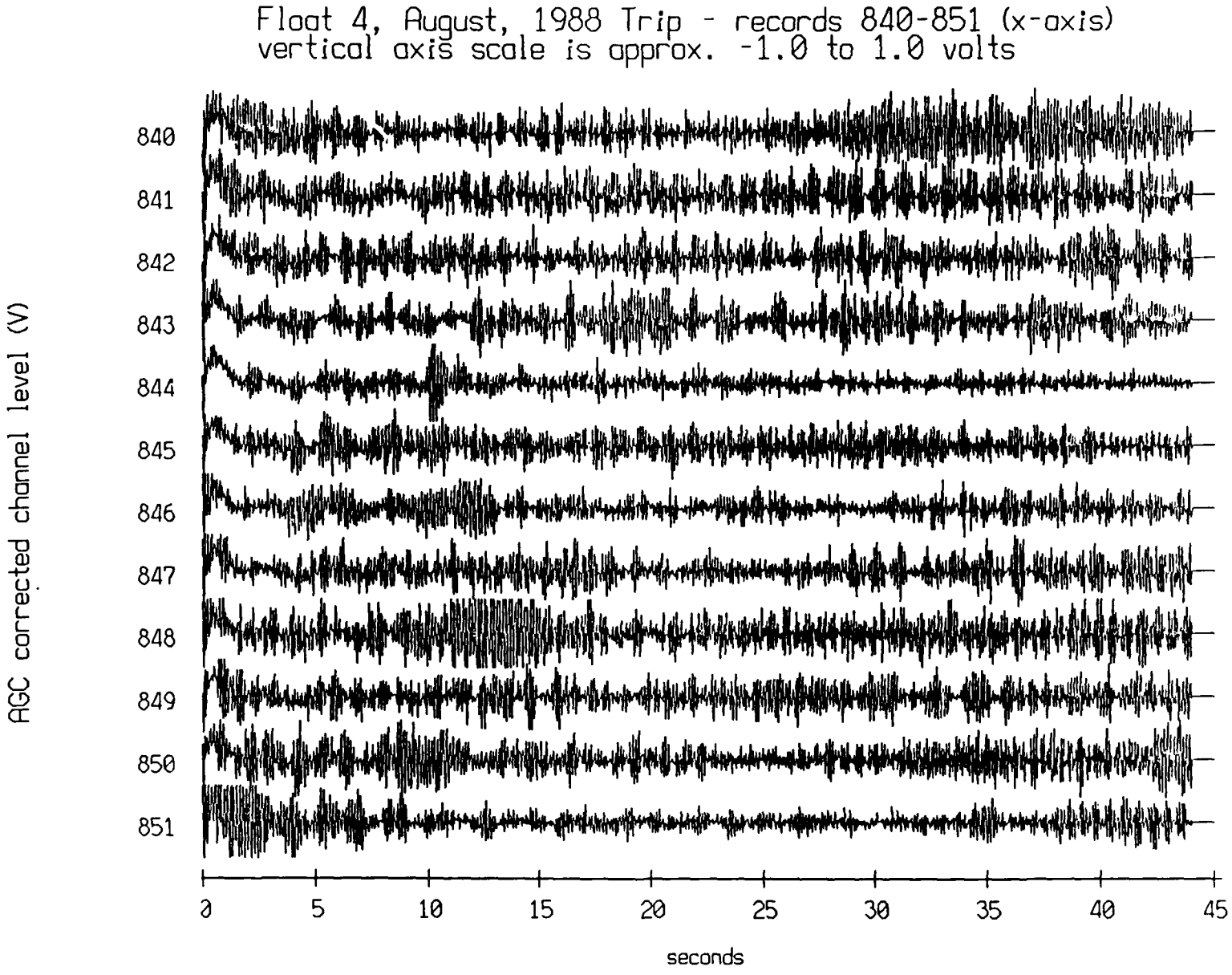


Figure XI.11a

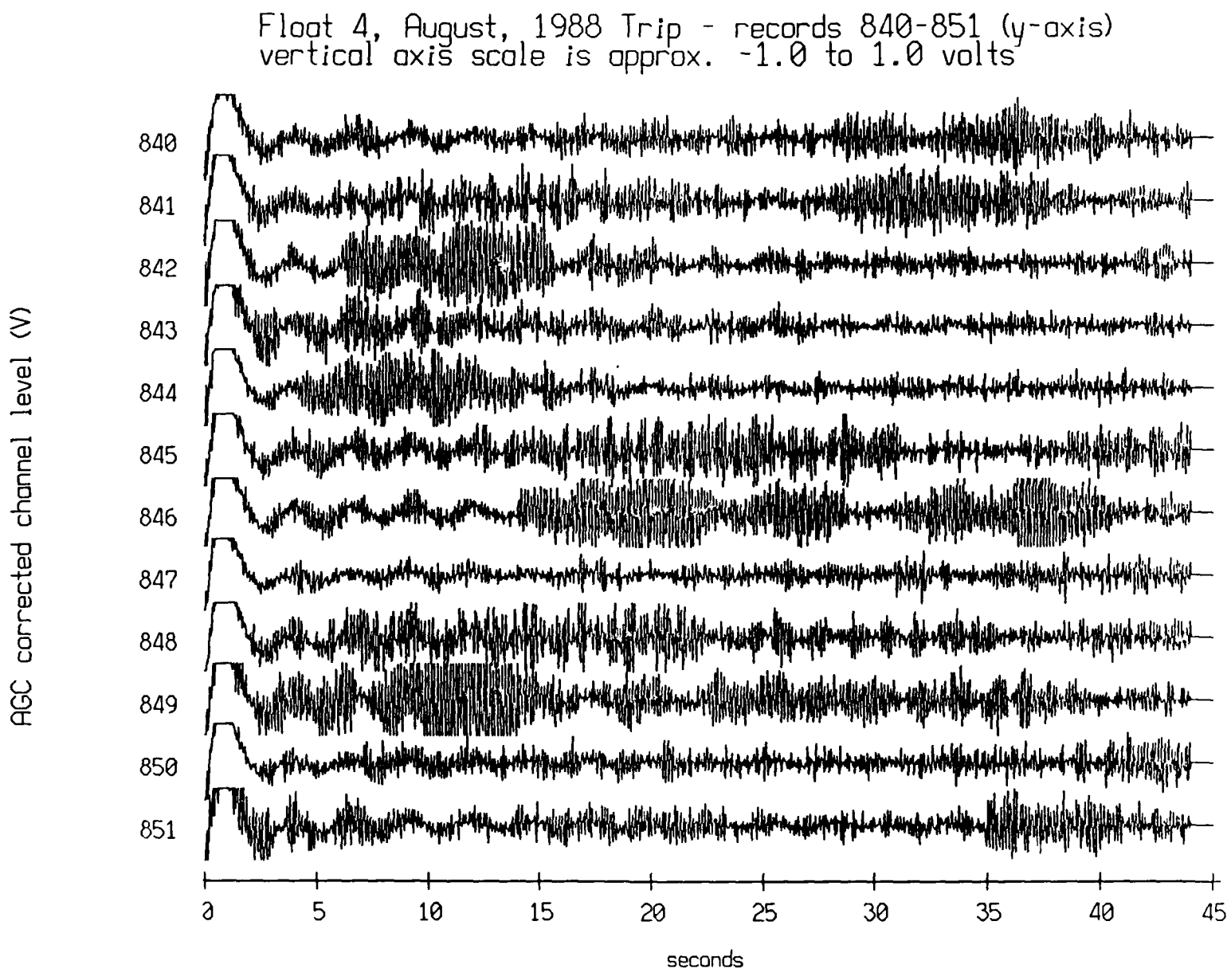


Figure XI.11b

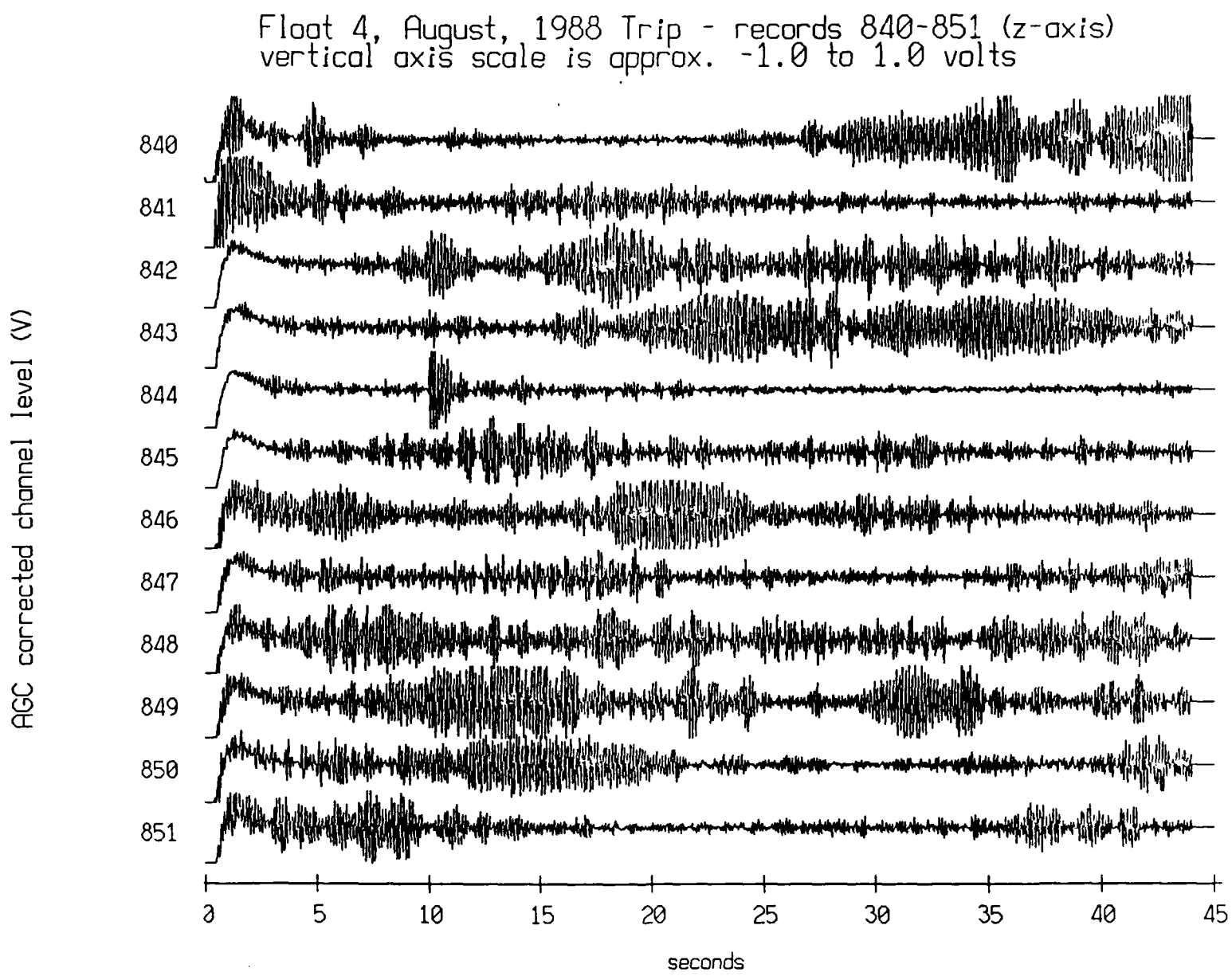


Figure XI.11c

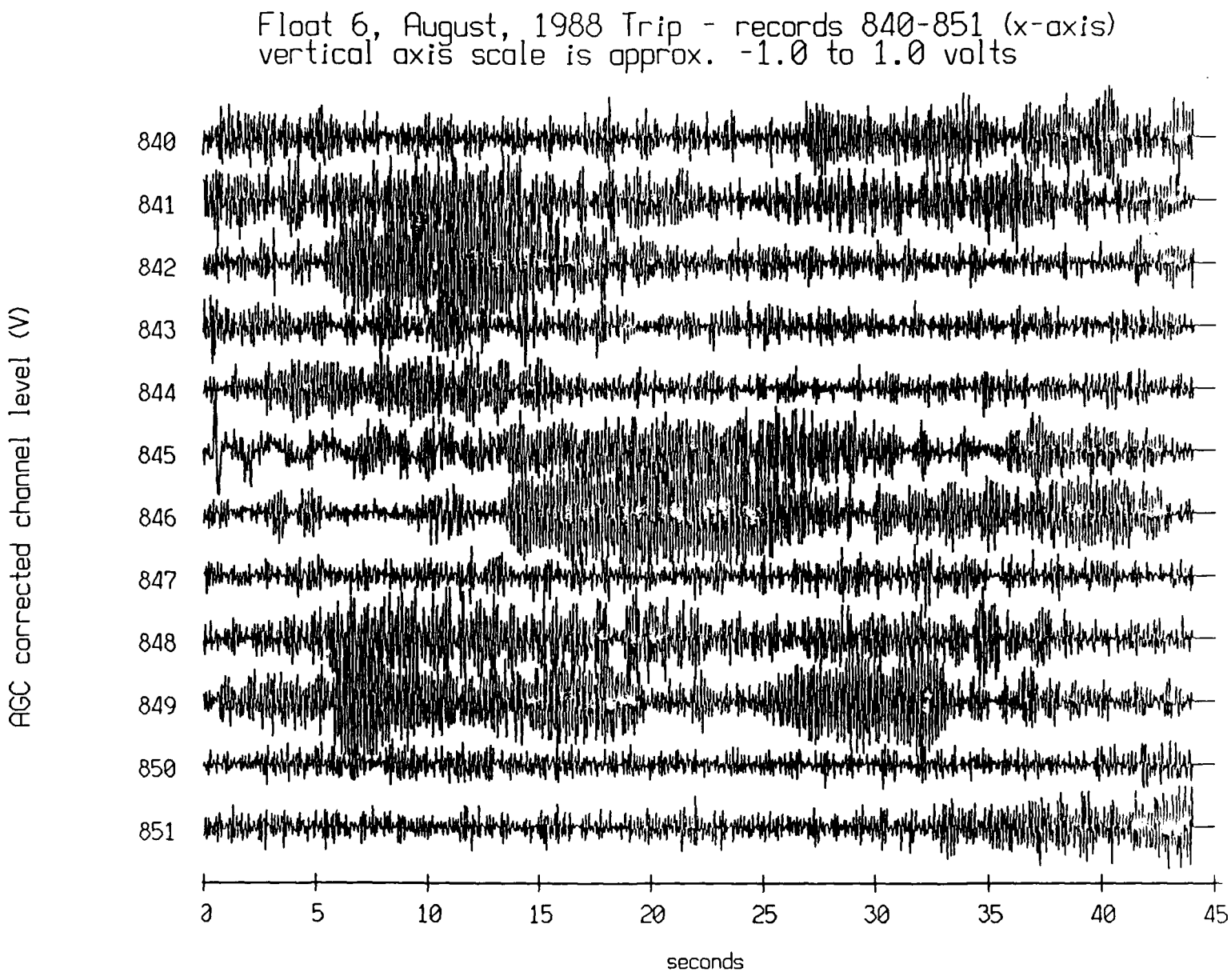


Figure XI.12a

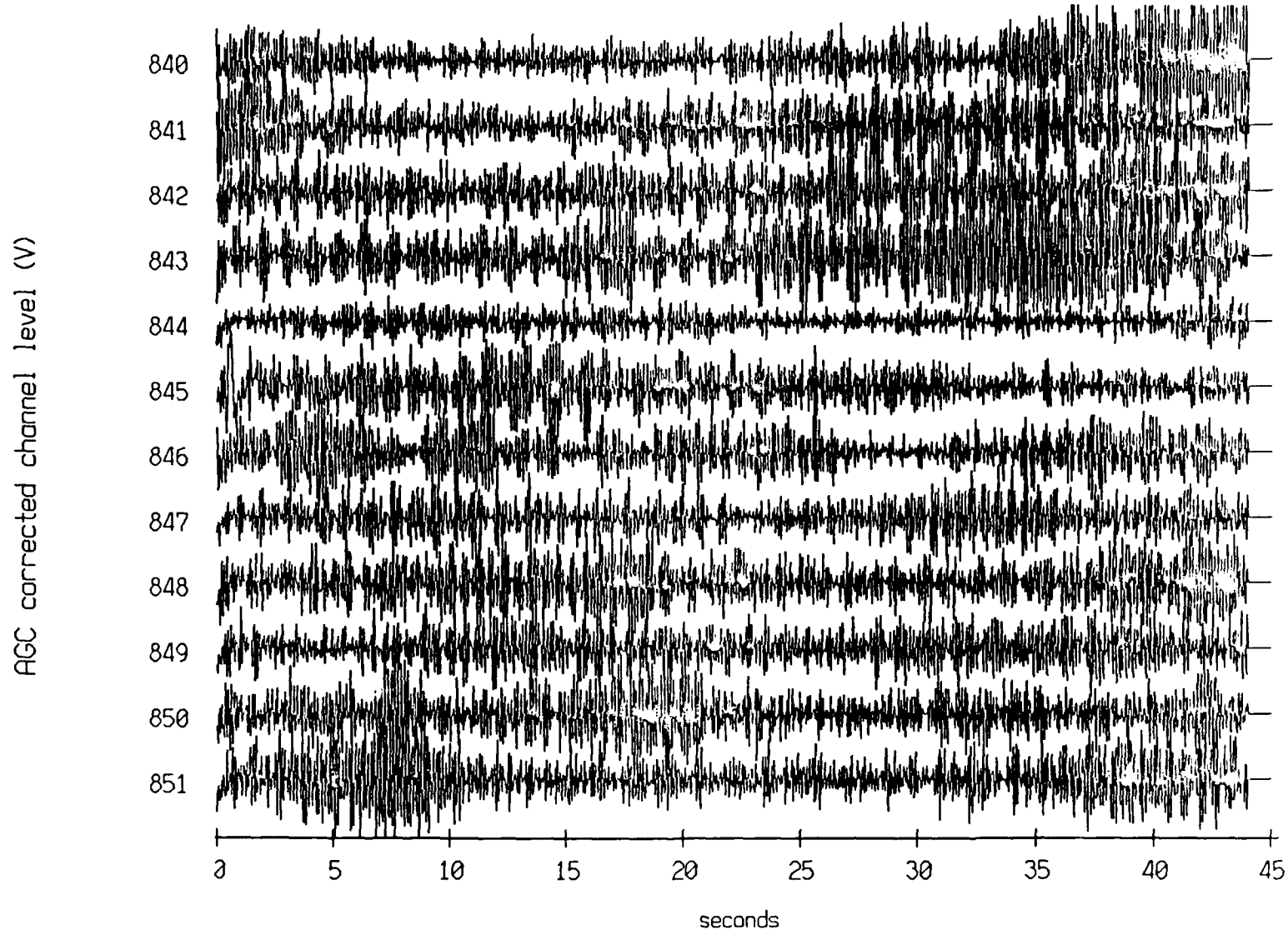


Figure XI.12b

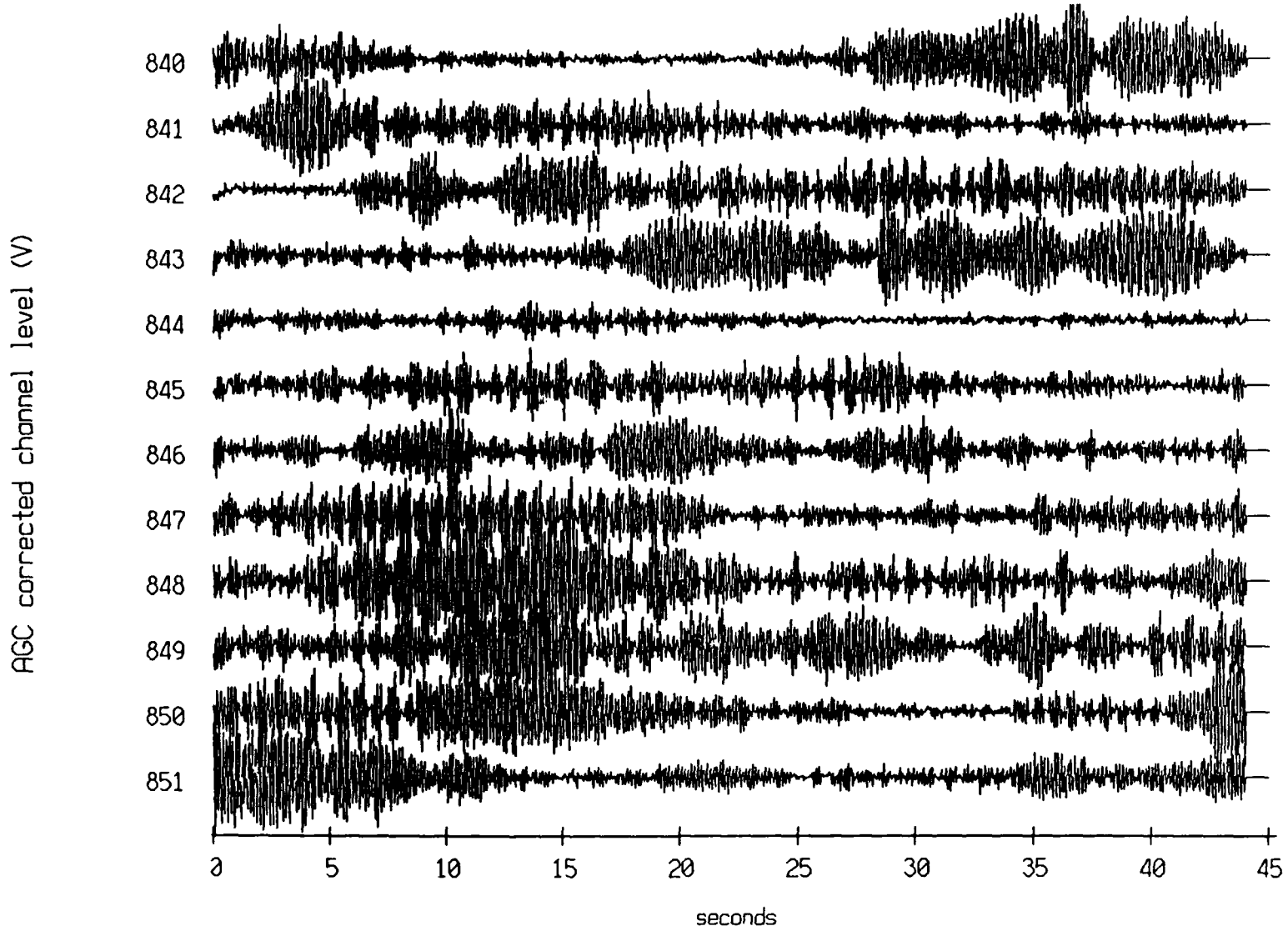


Figure XI.12c

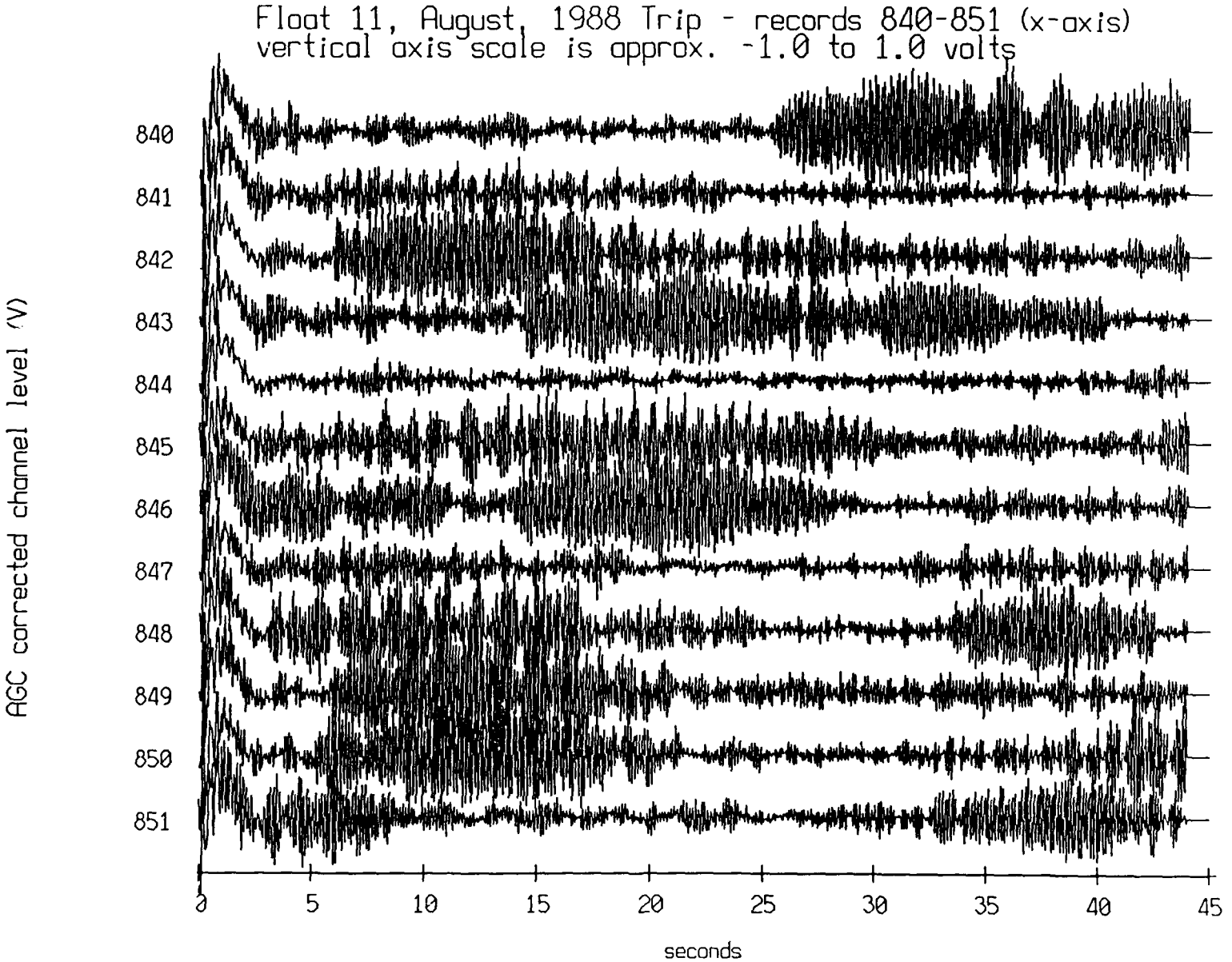


Figure XI.13a

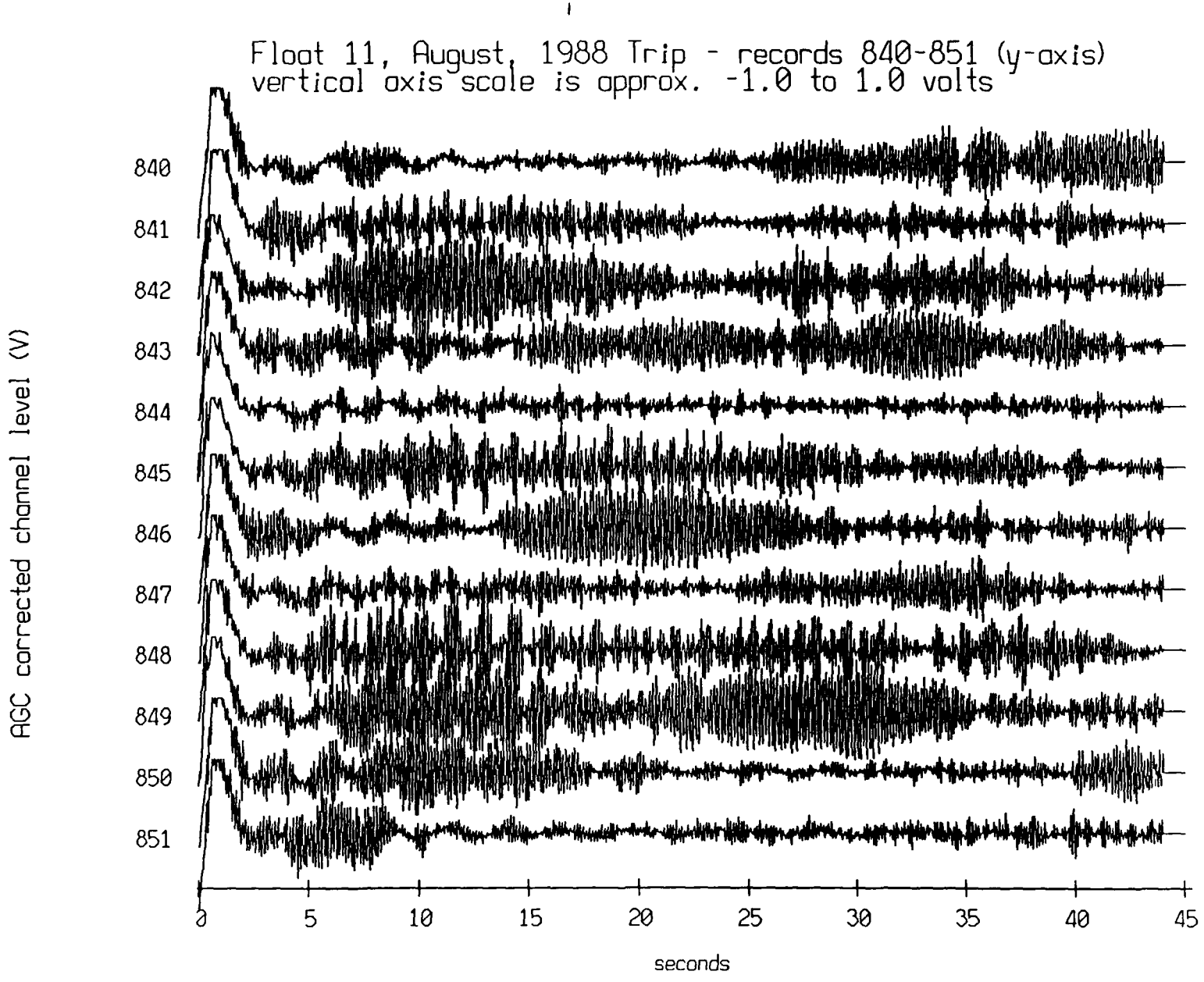


Figure XI.13b

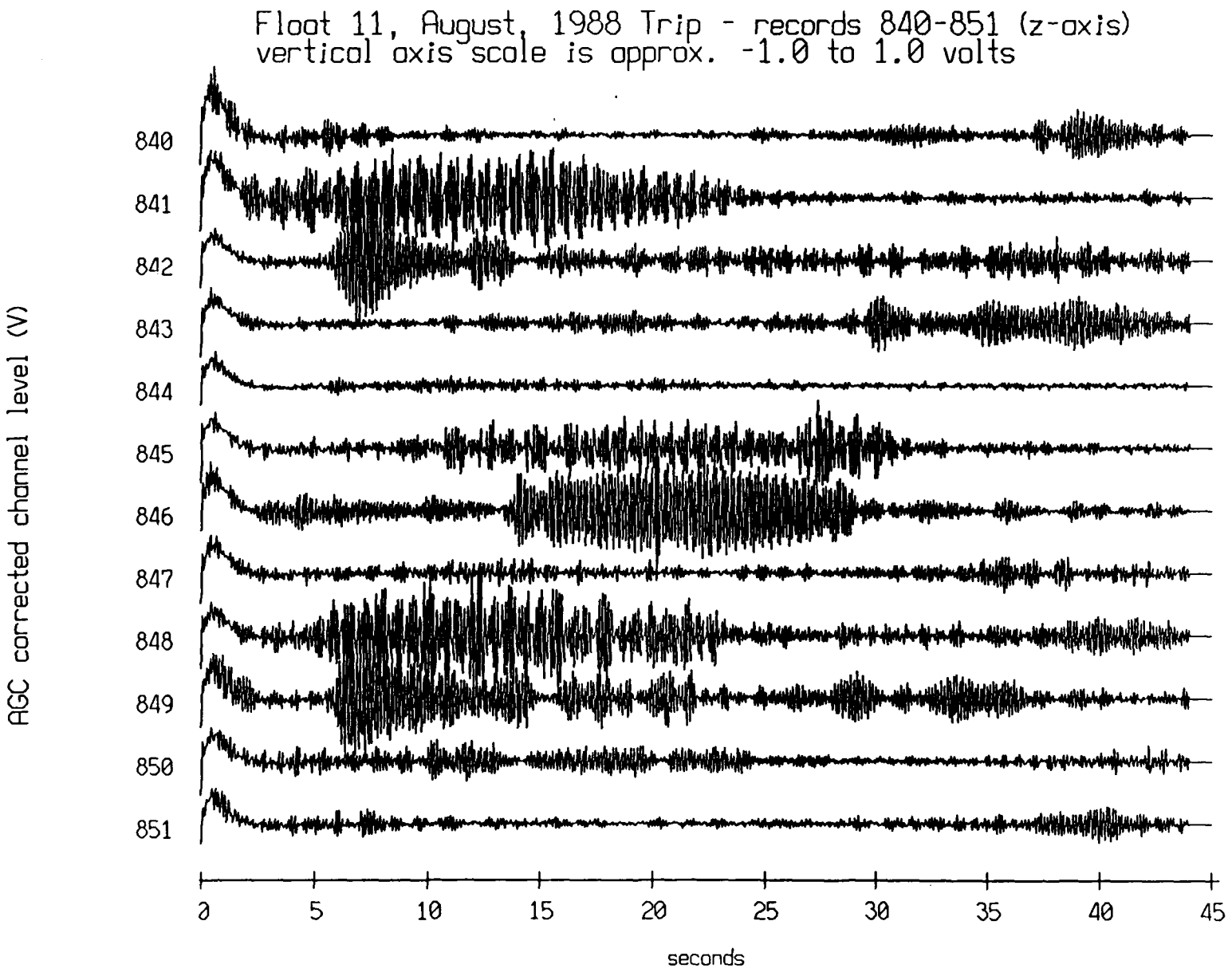


Figure XI.13c

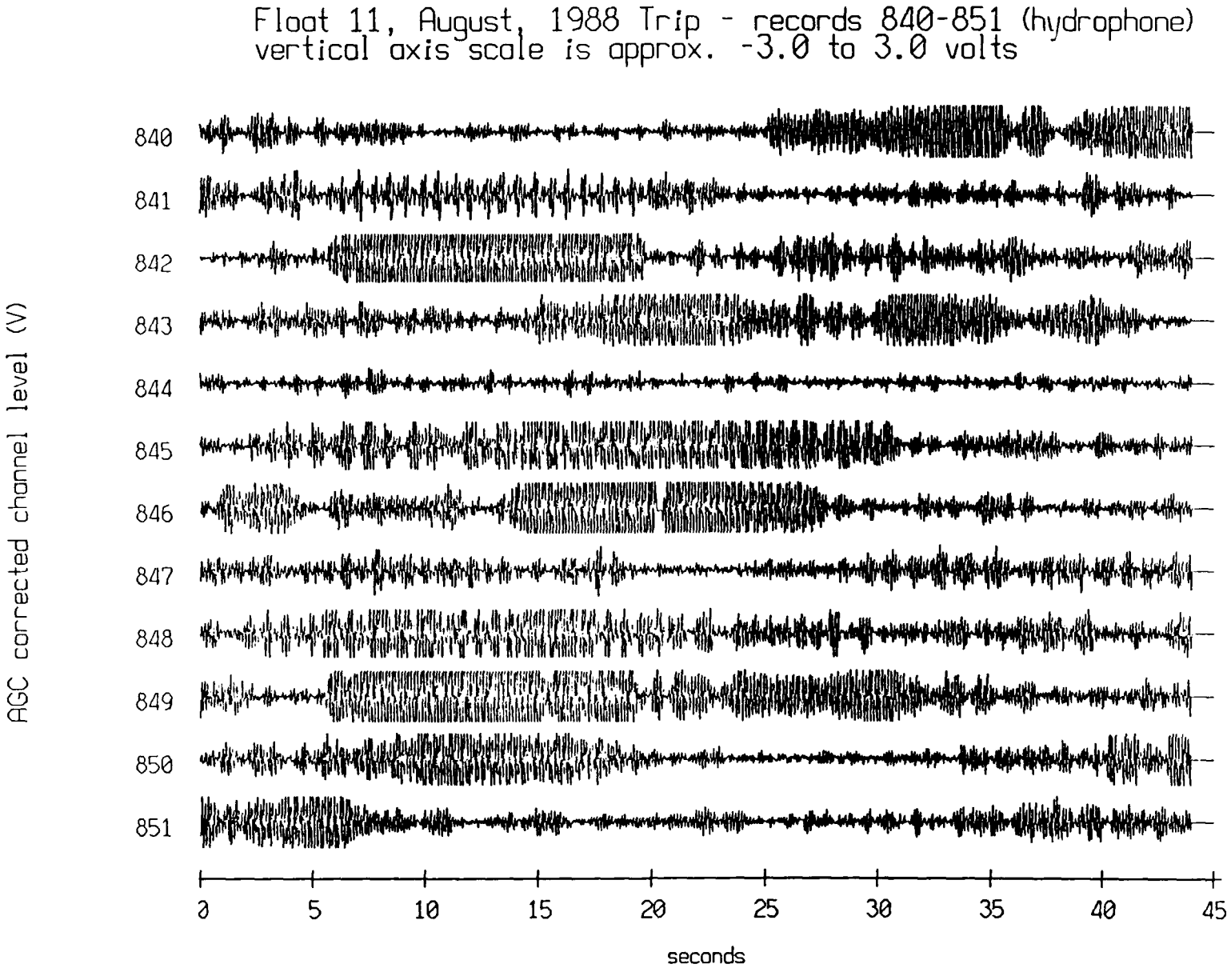


Figure XI.13d

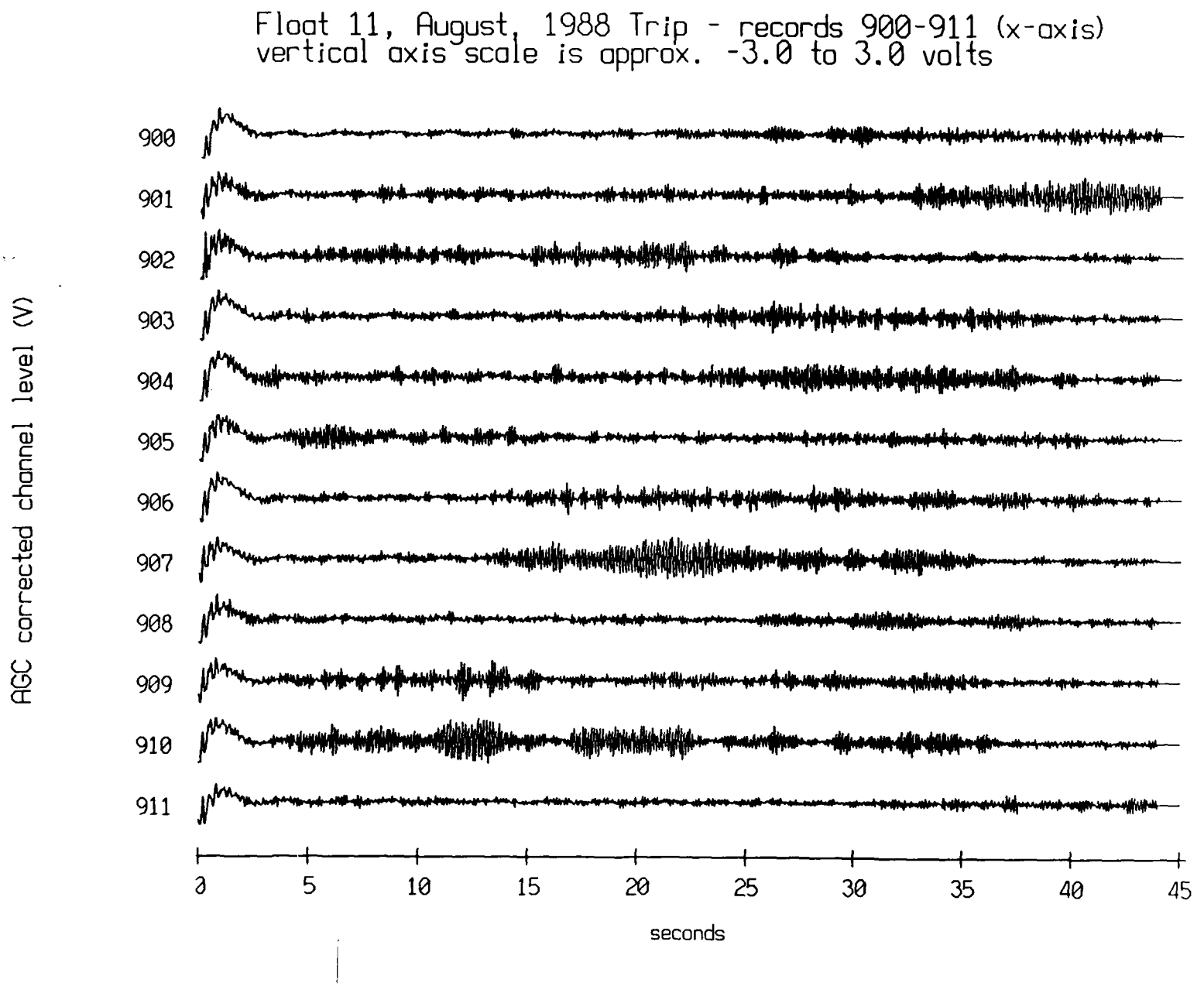


Figure XI.14a

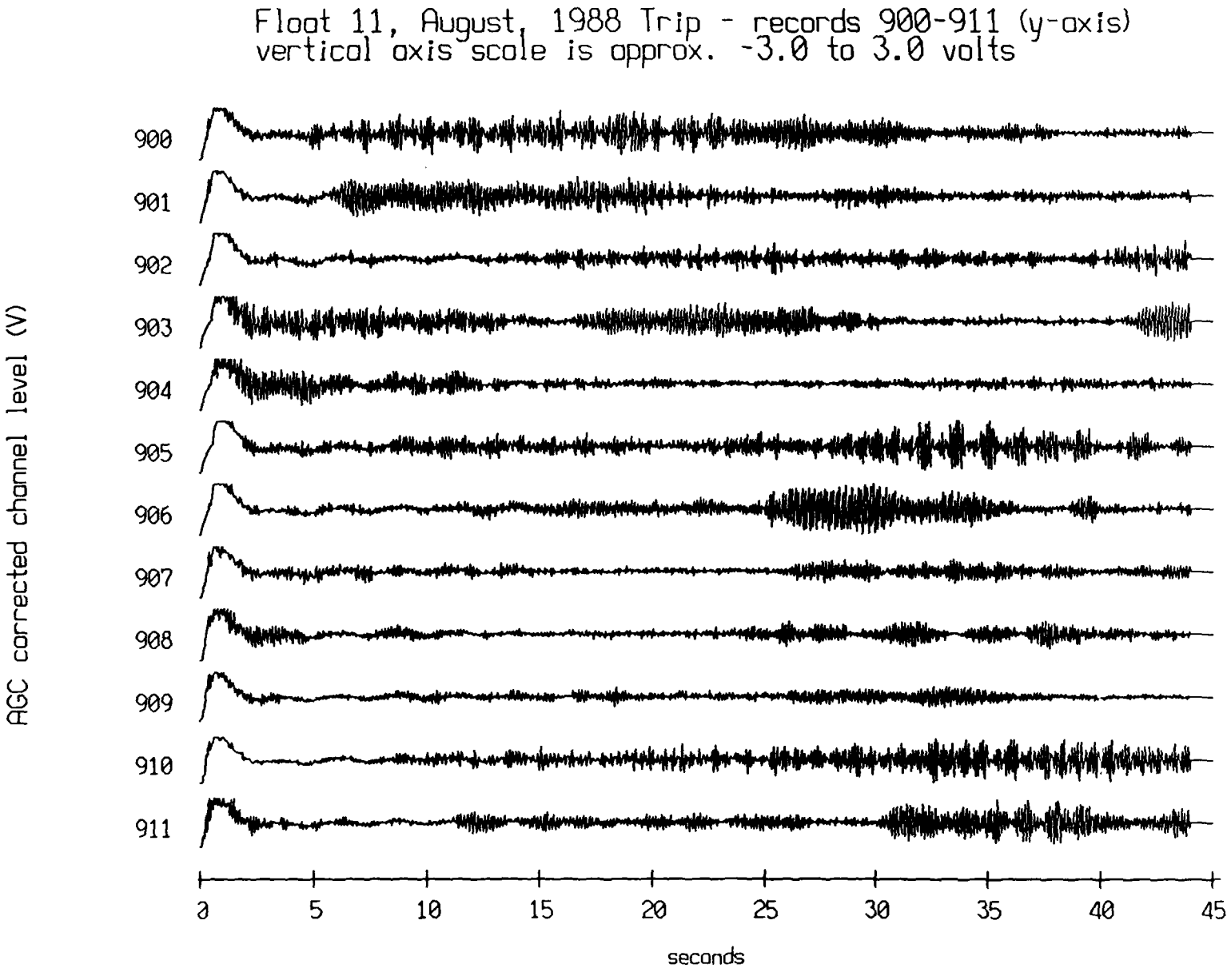


Figure XI.14b

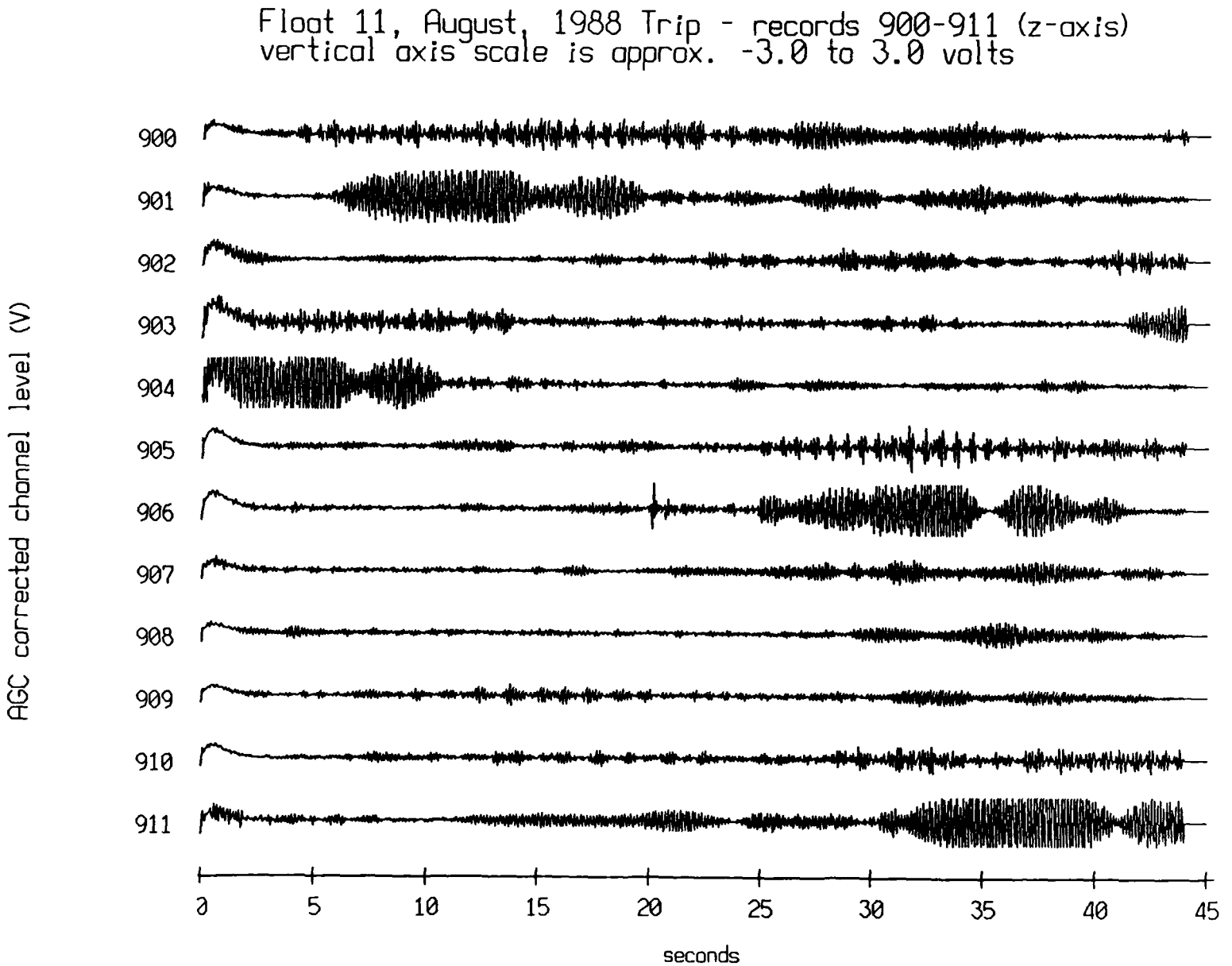


Figure XI.14c

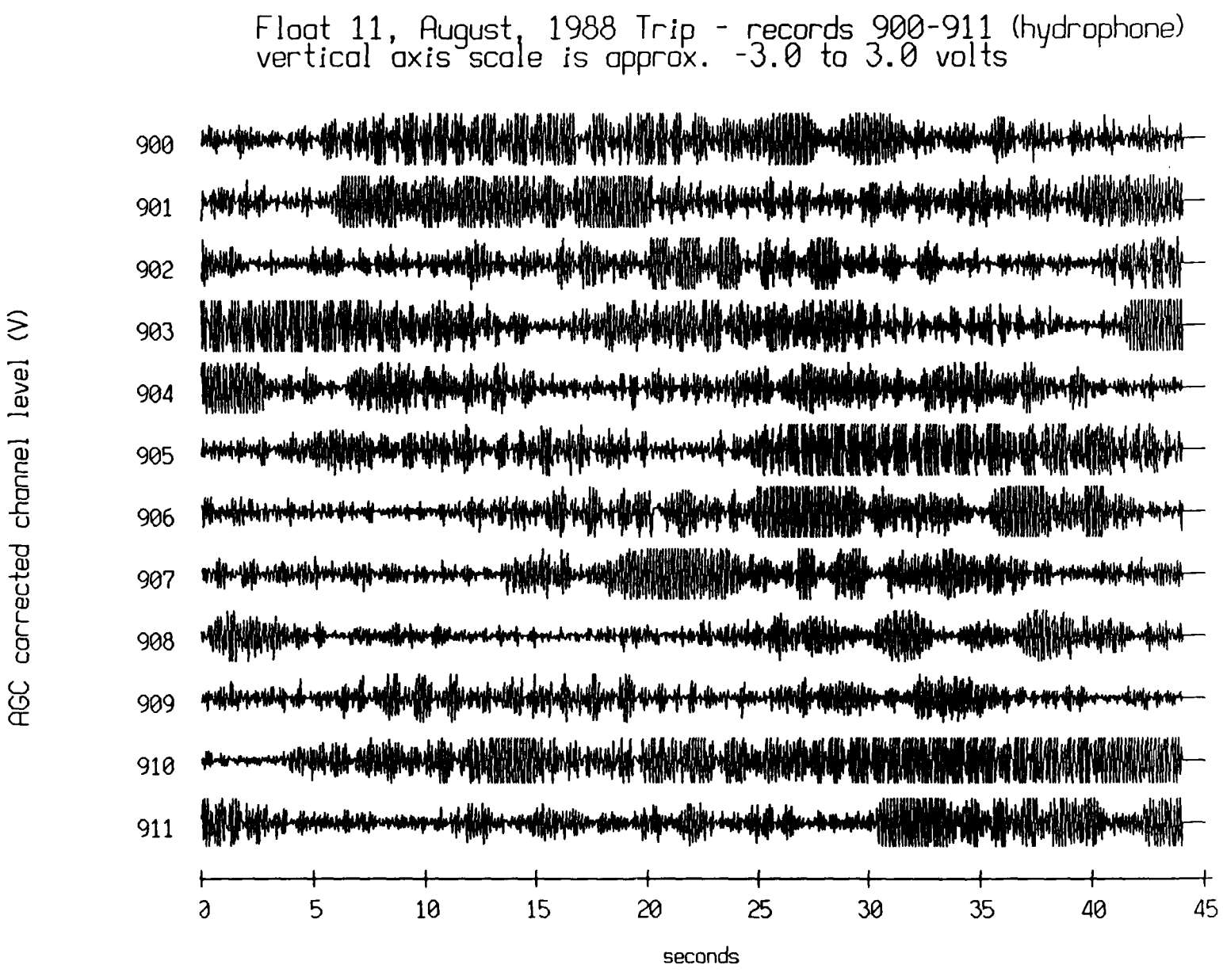


Figure XI.11d

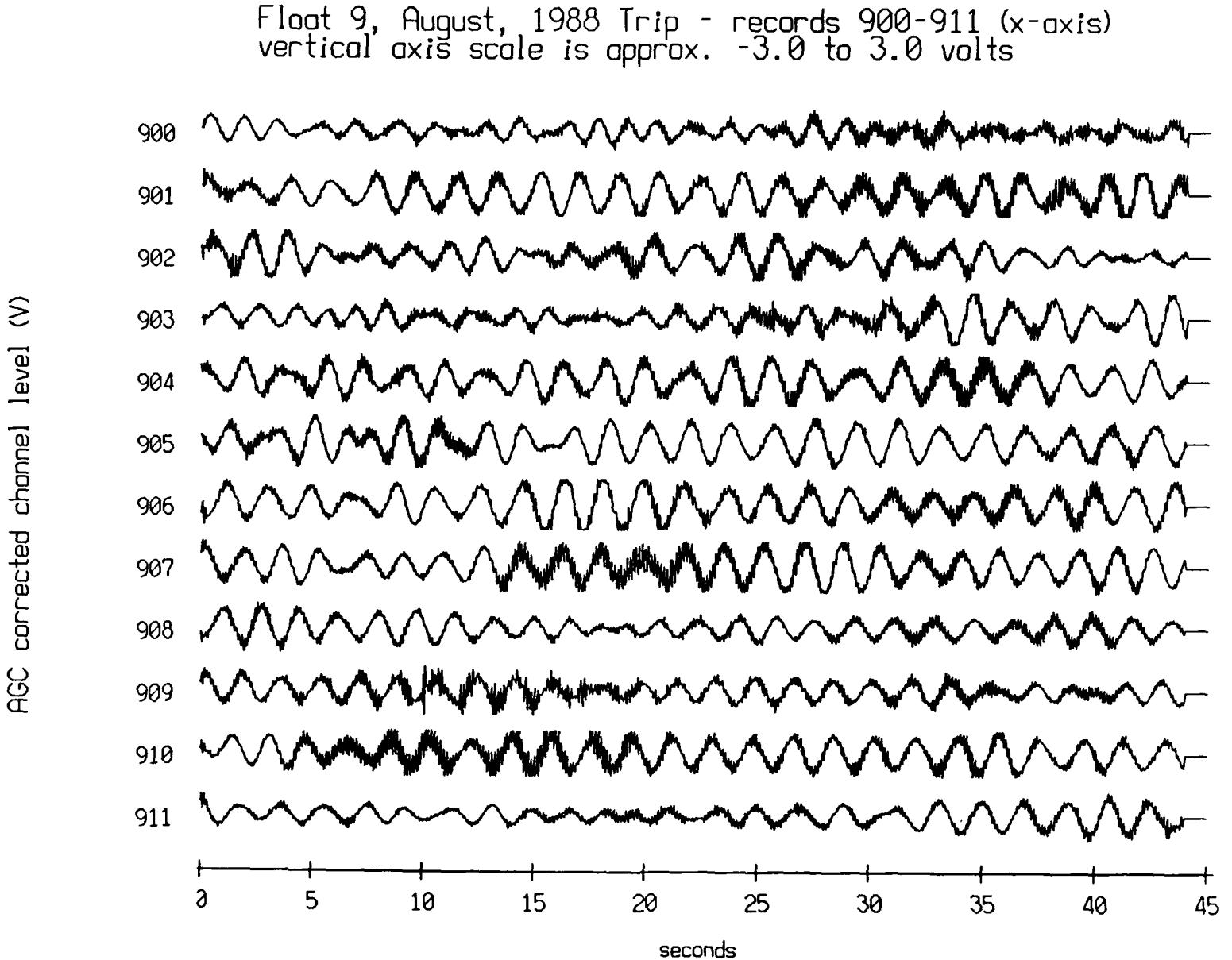


Figure XI.15a

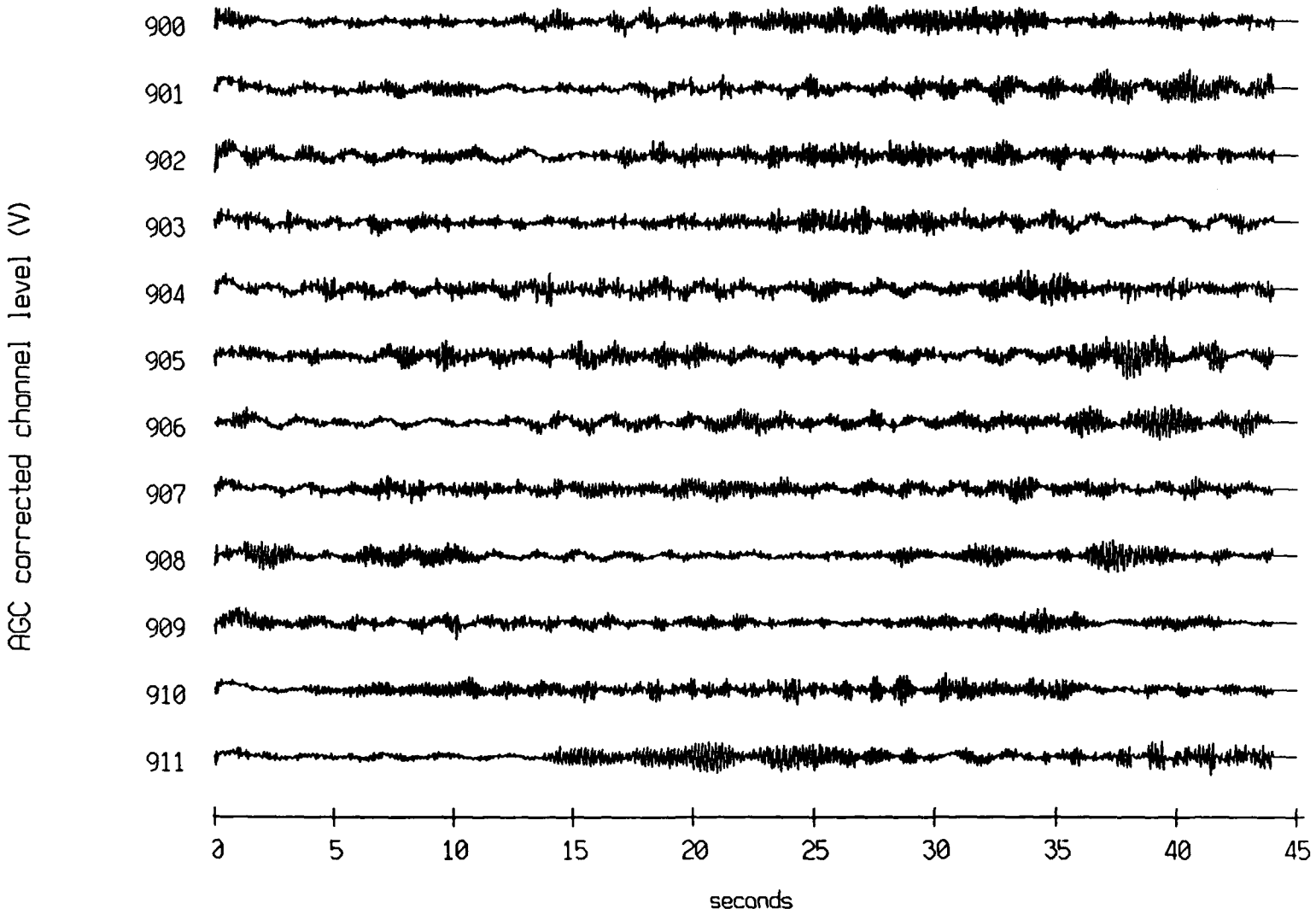


Figure XI.15b

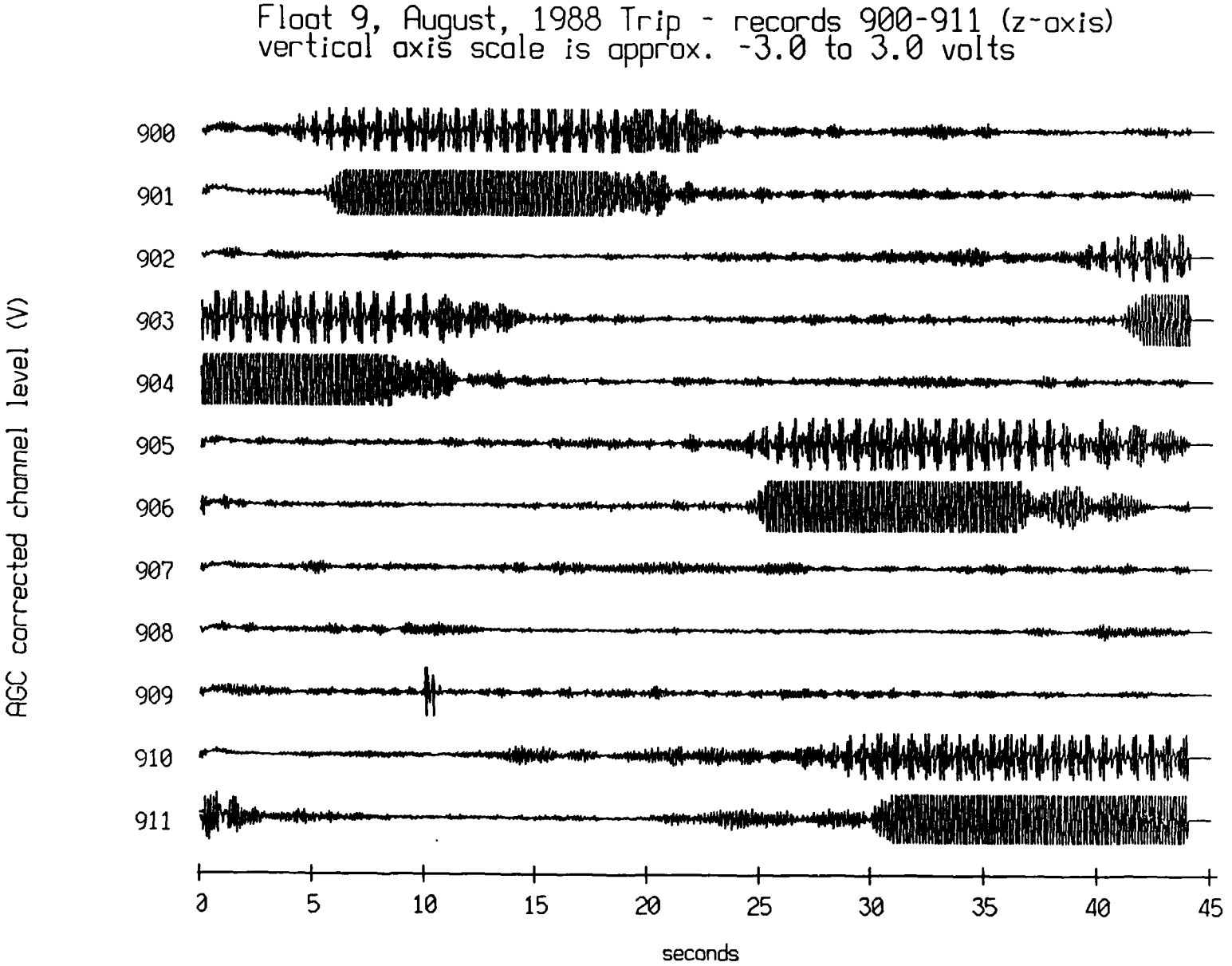


Figure XI.15c

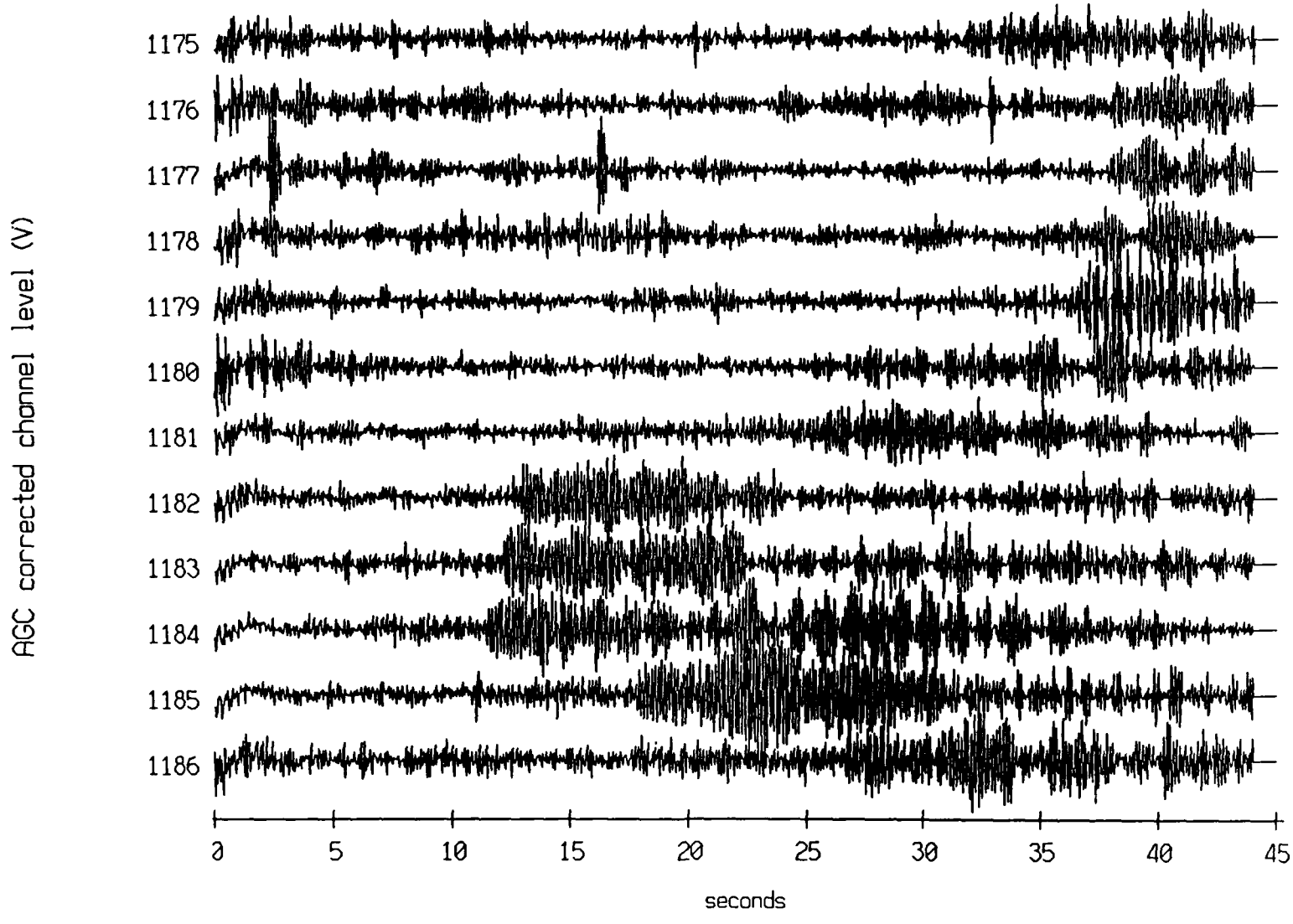


Figure XI.16a

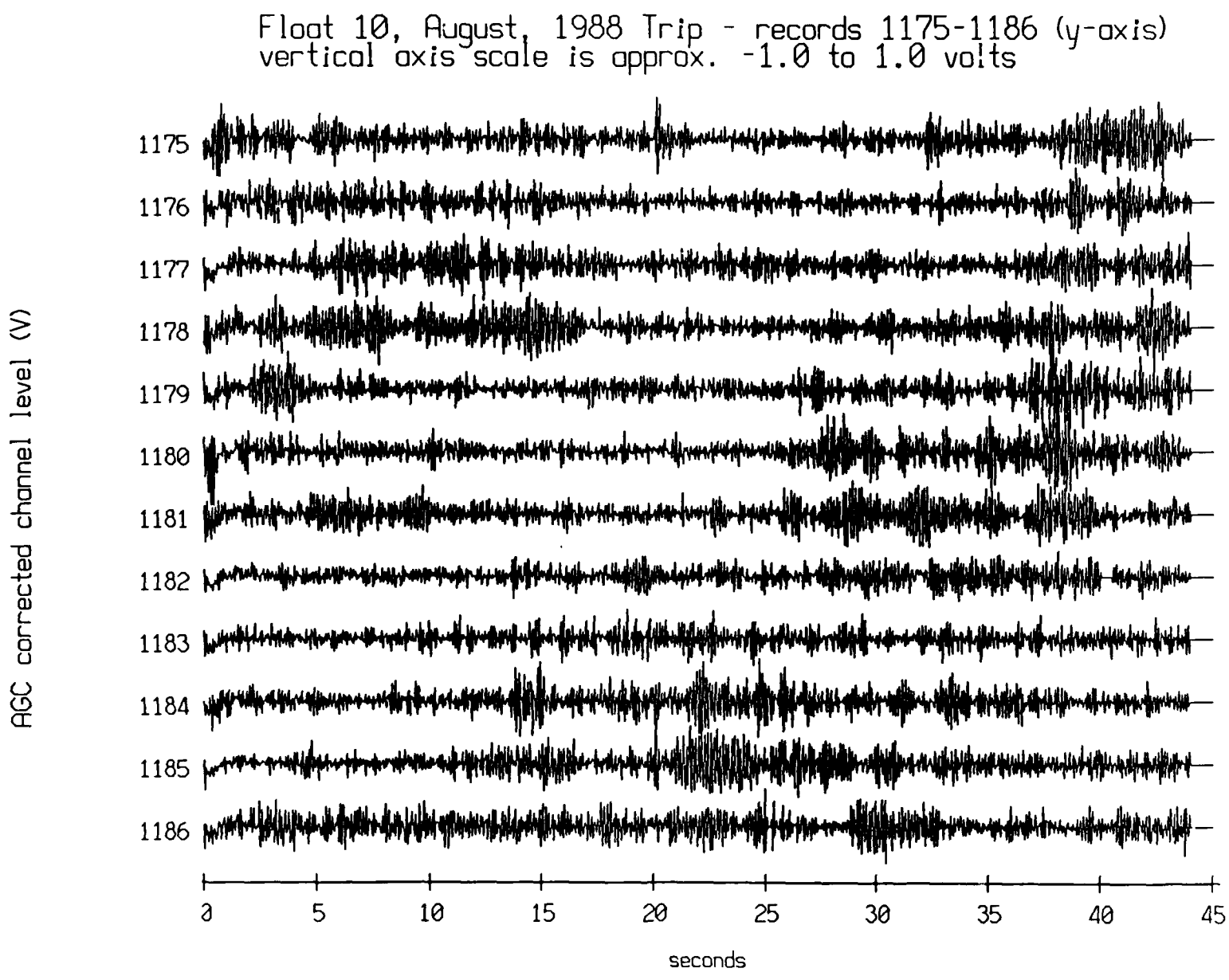


Figure XI.16b

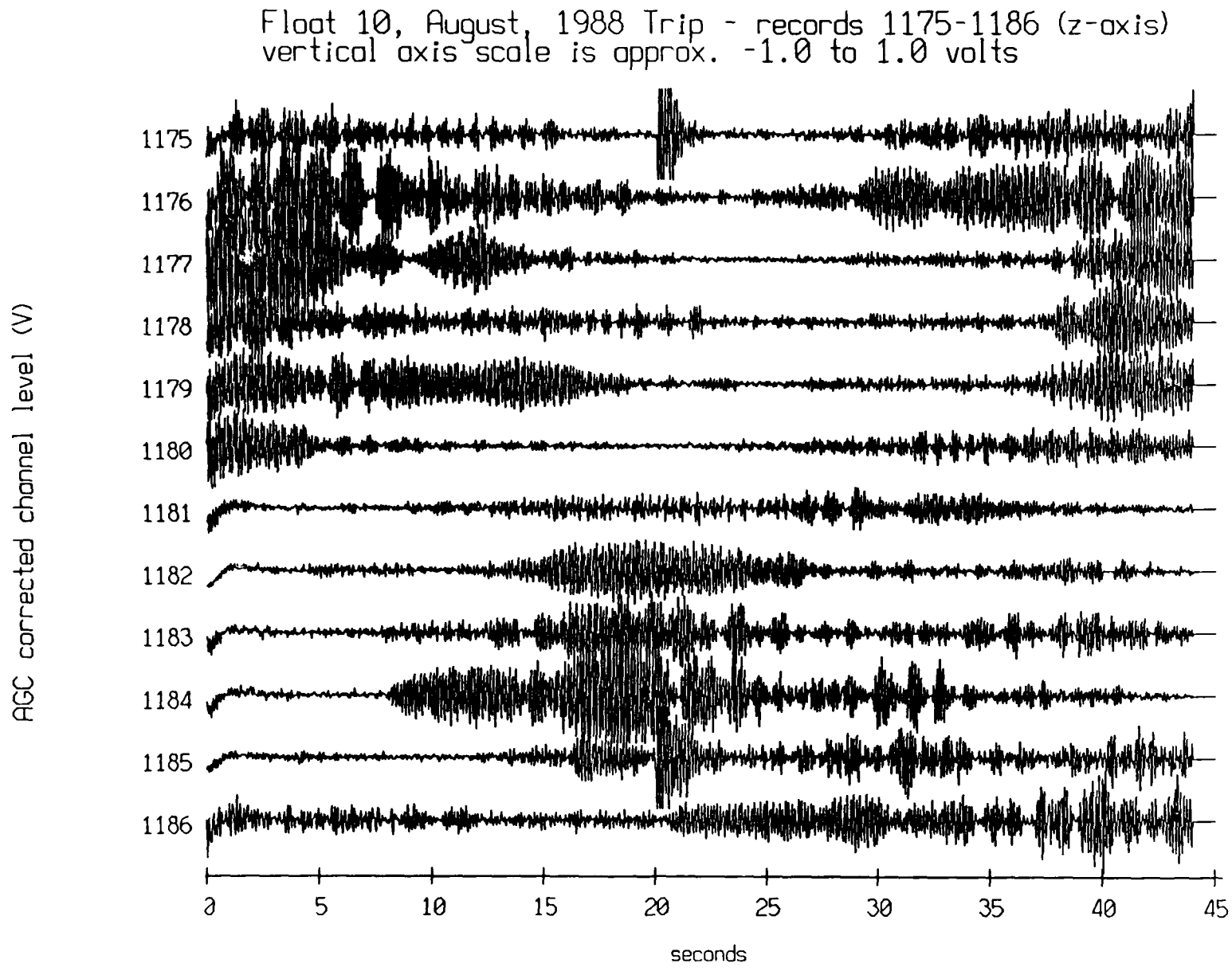


Figure XI.16c

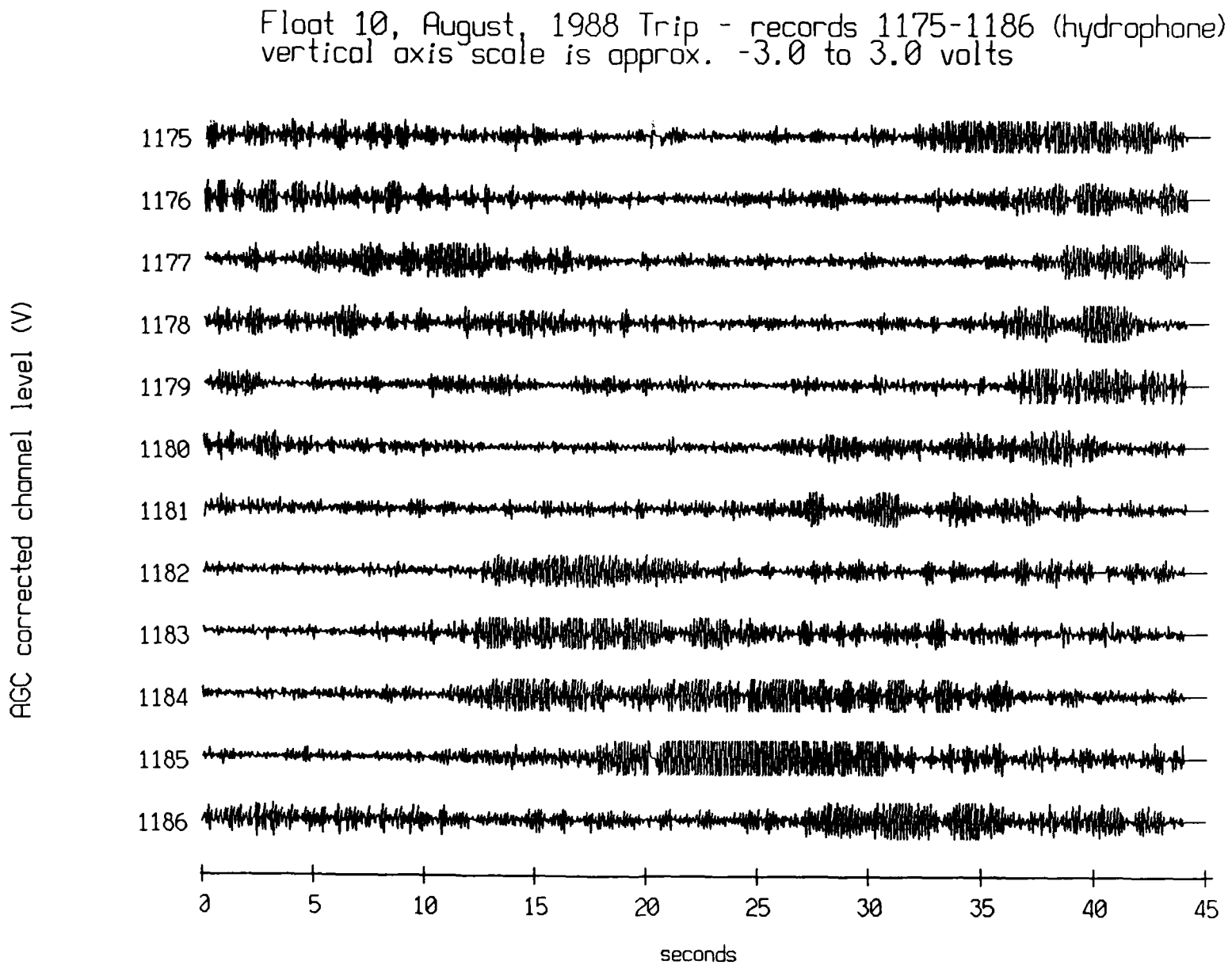


Figure XI.16d

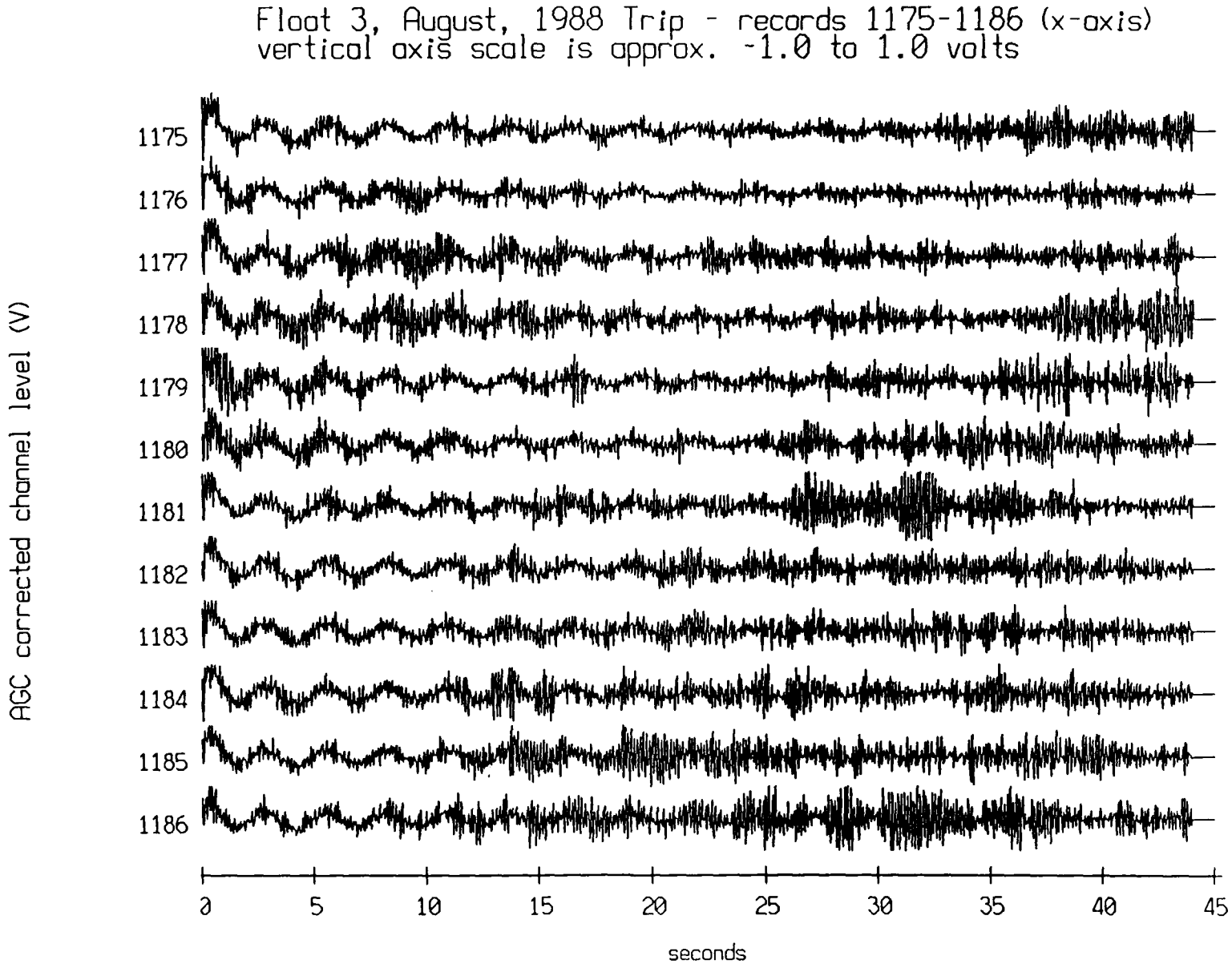


Figure XI.17a

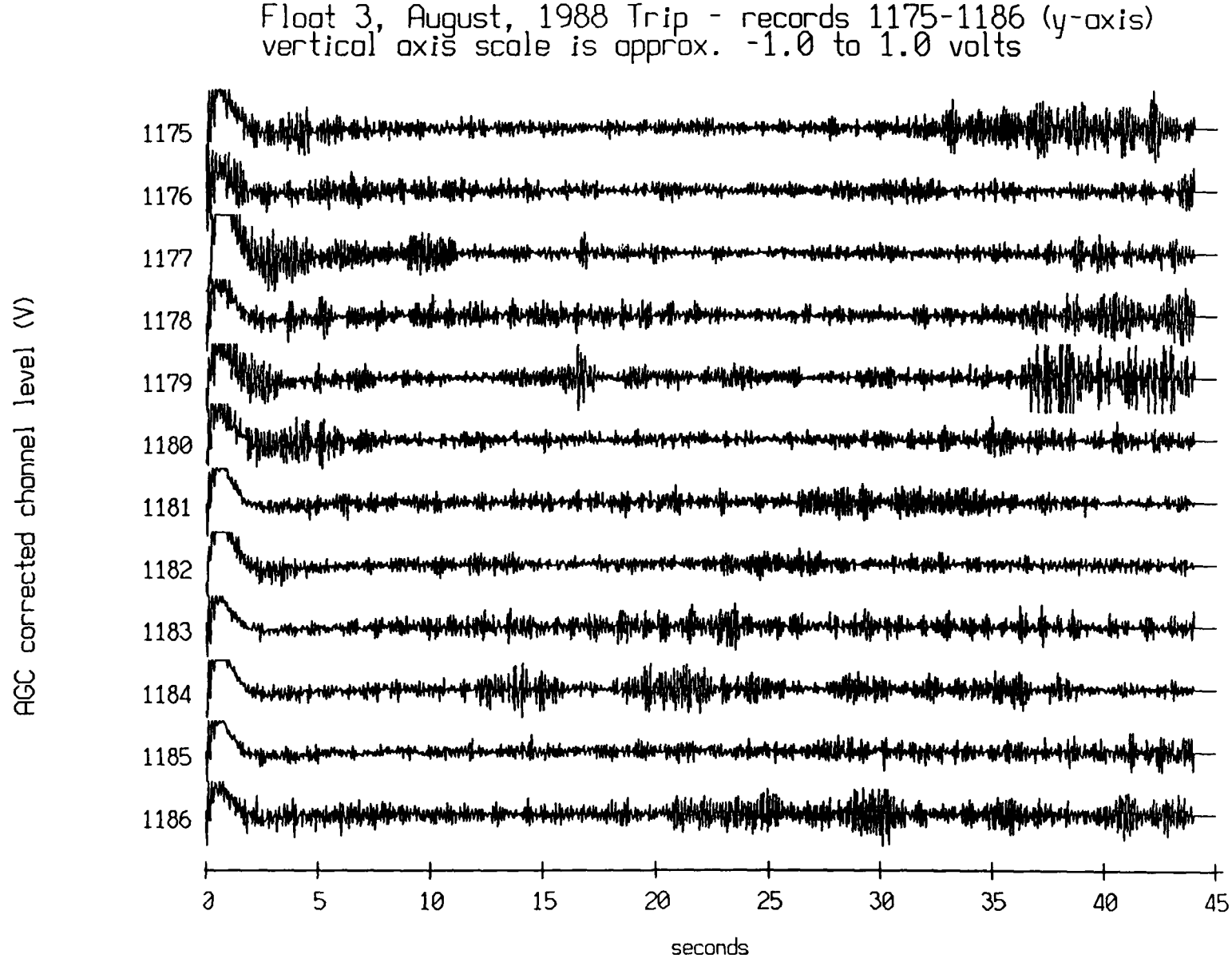


Figure XI.17b

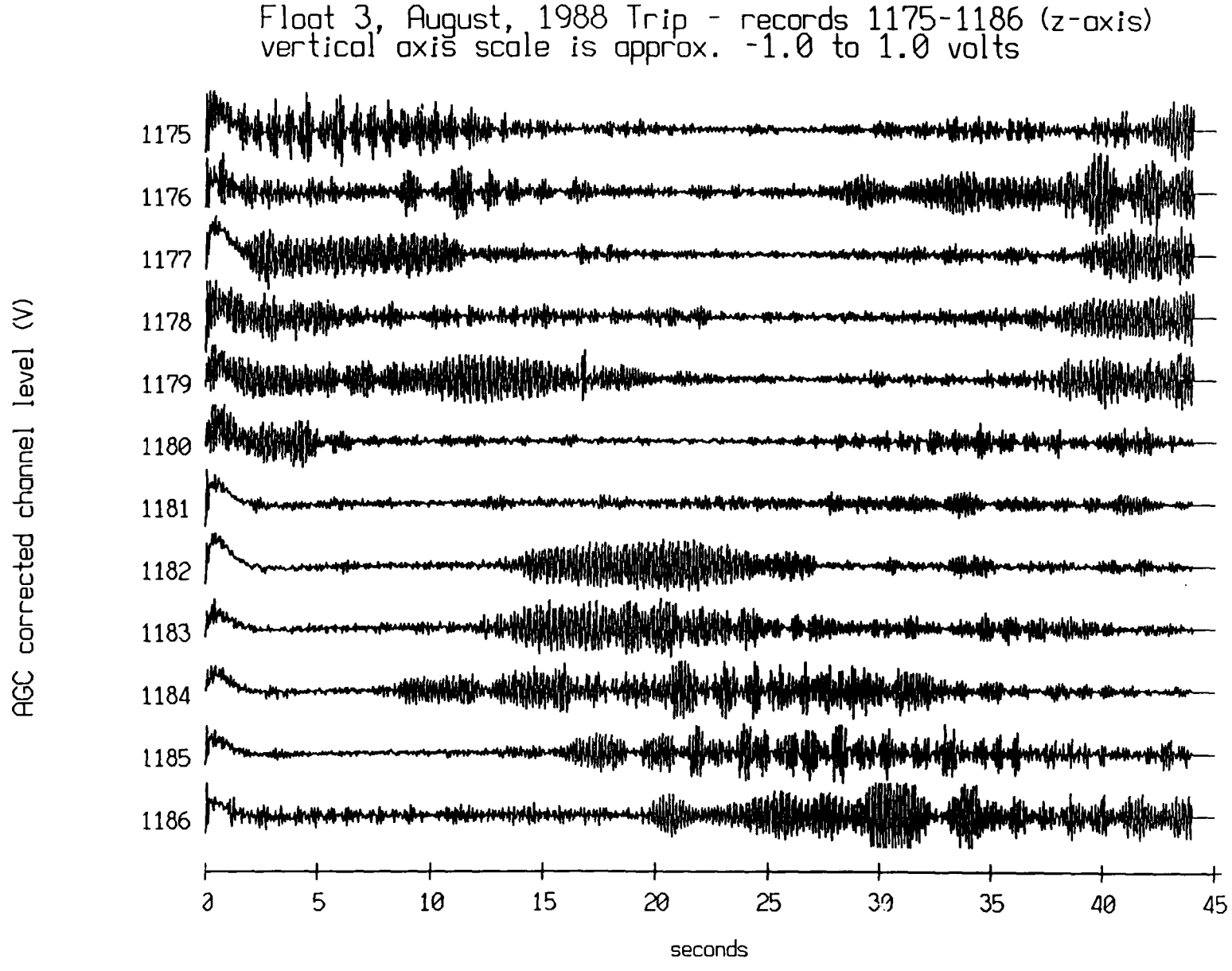

Float 3, August, 1988 Trip - records 1175-1186 (z-axis)
vertical axis scale is approx. -1.0 to 1.0 volts
AGC corrected channel level (V)
1175
1176
1177
1178
1179
1180
1181
1182
1183
1184
1185
1186
0
5
10
15
20
25
30
35
40
45
seconds

Figure XI.7c

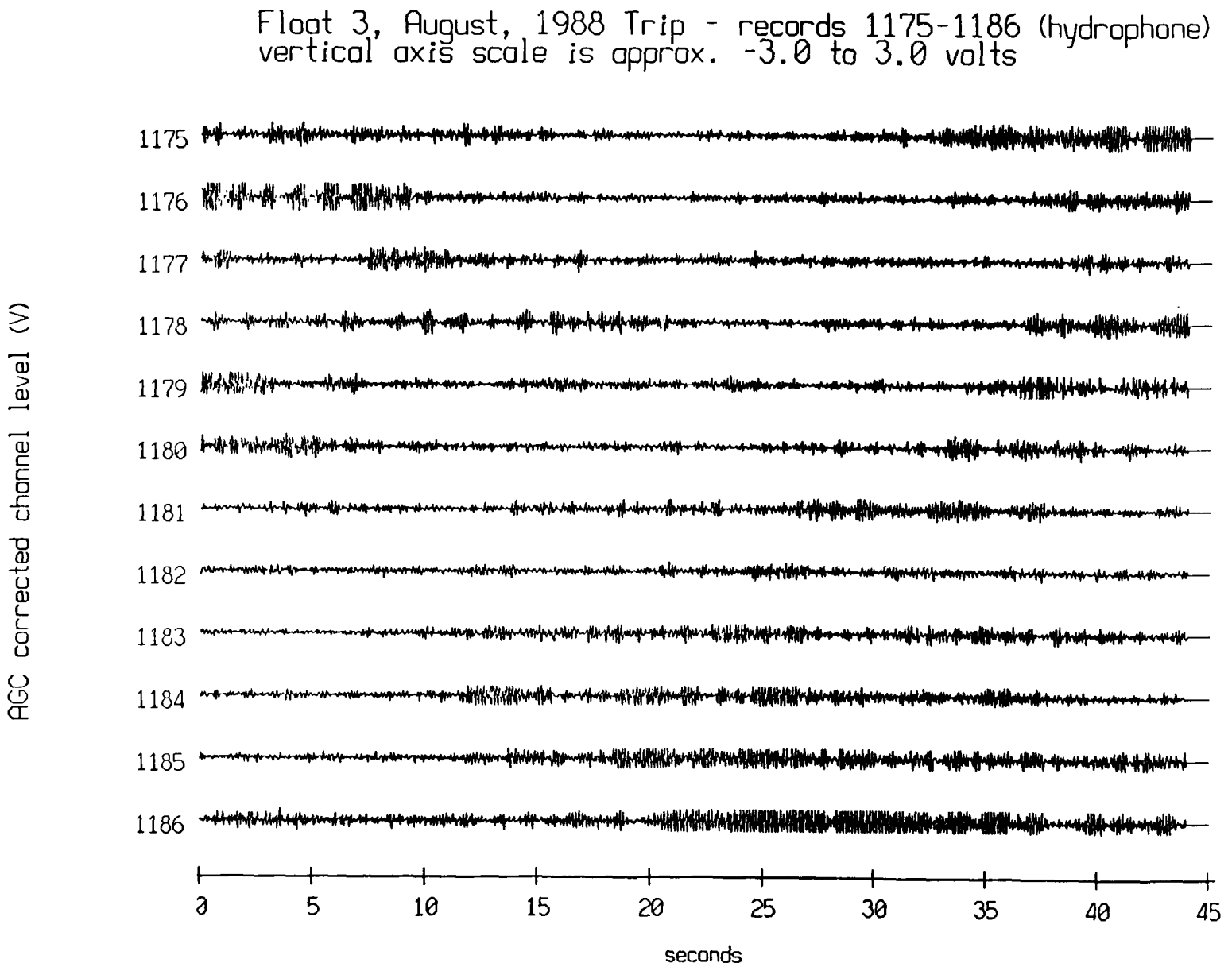


Figure XI.17d

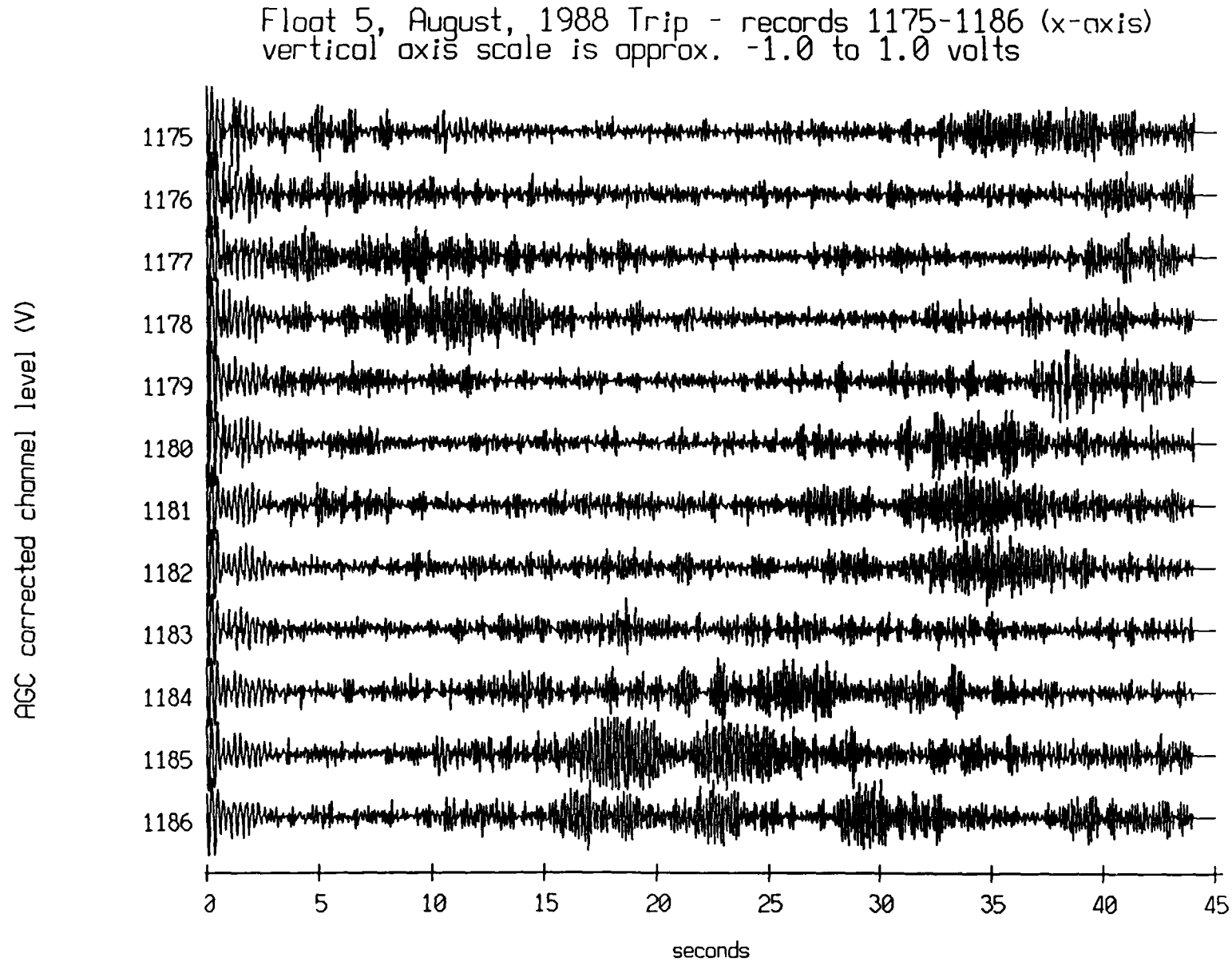


Figure XI.18a

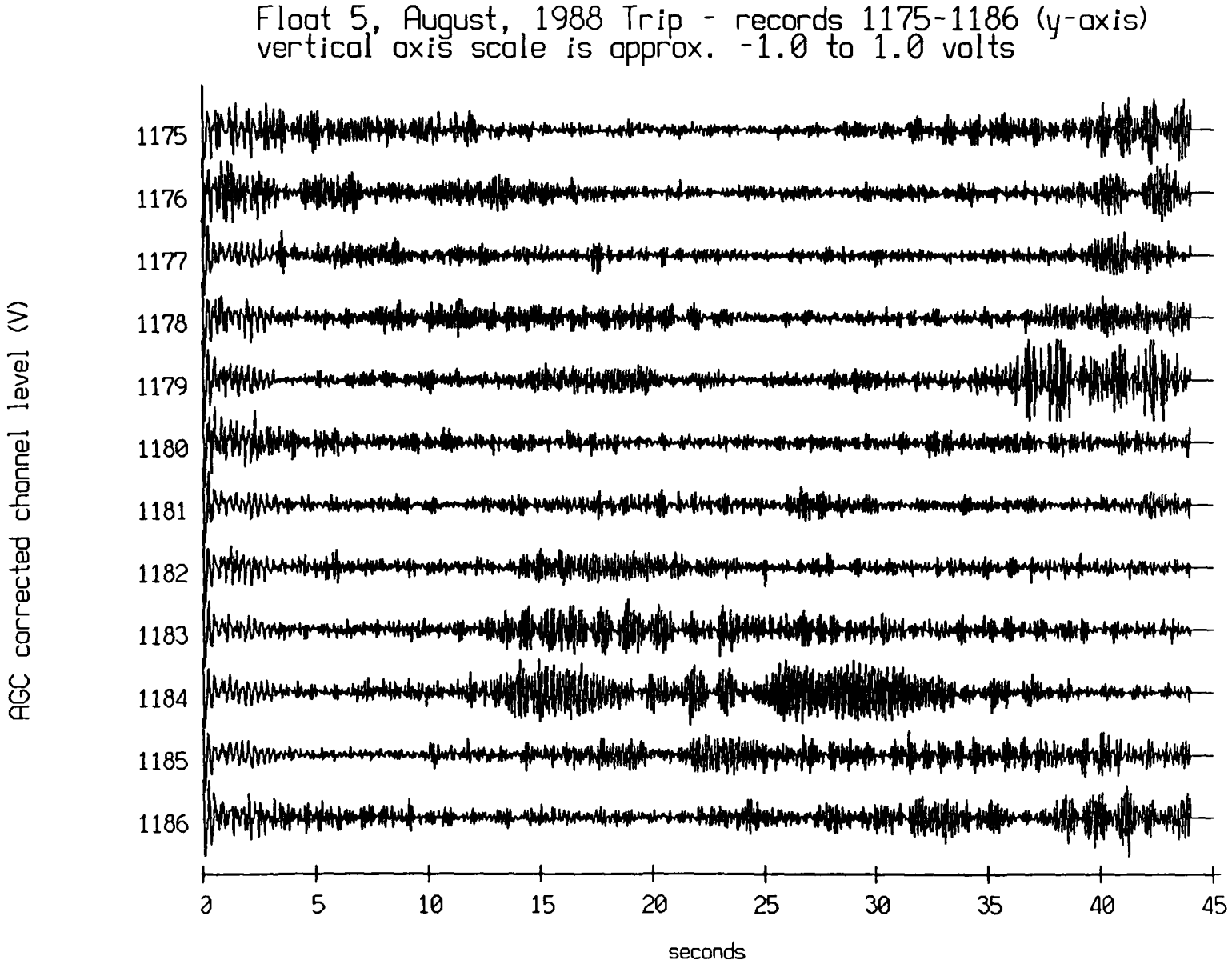


Figure XI.18b

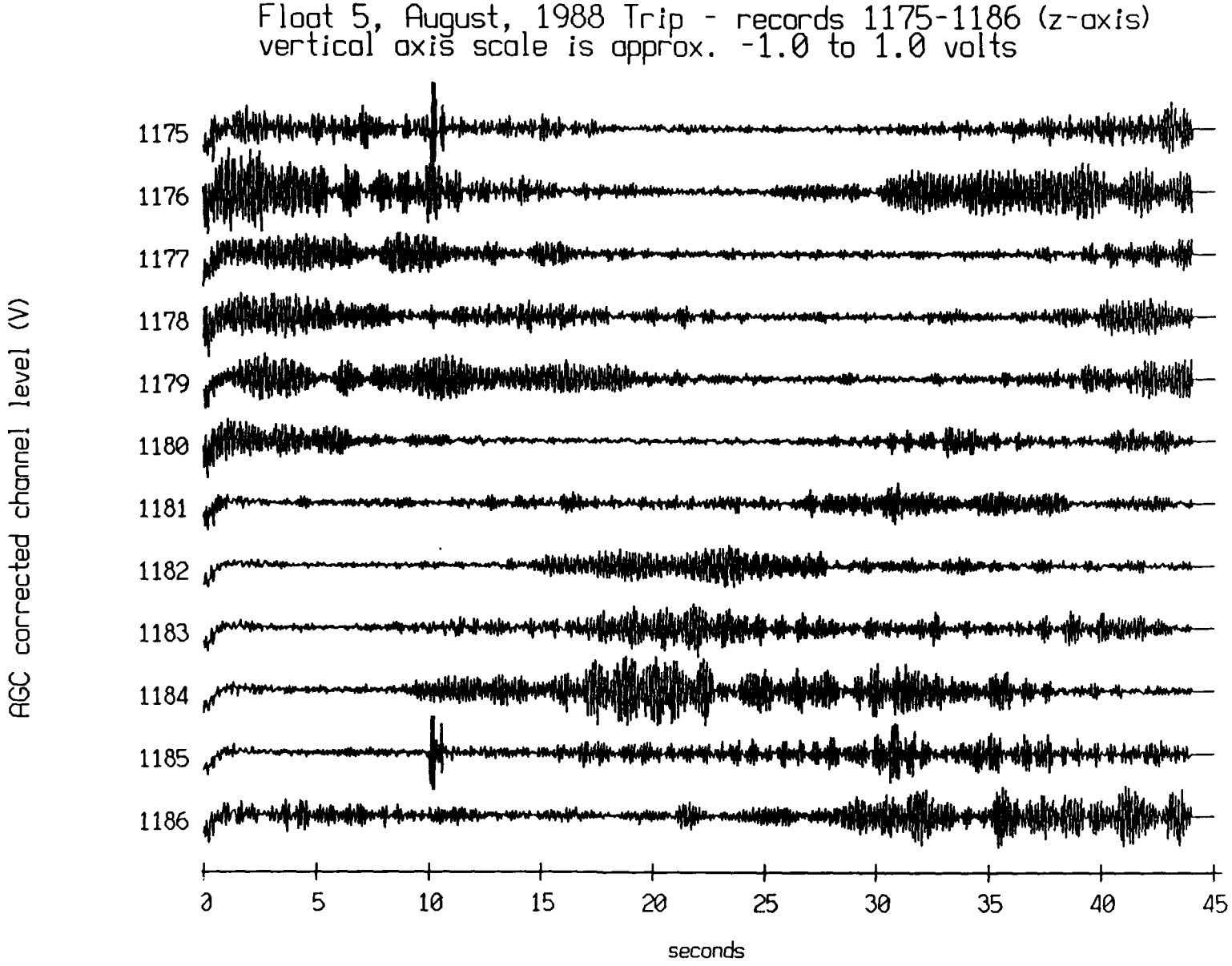


Figure XI.18c

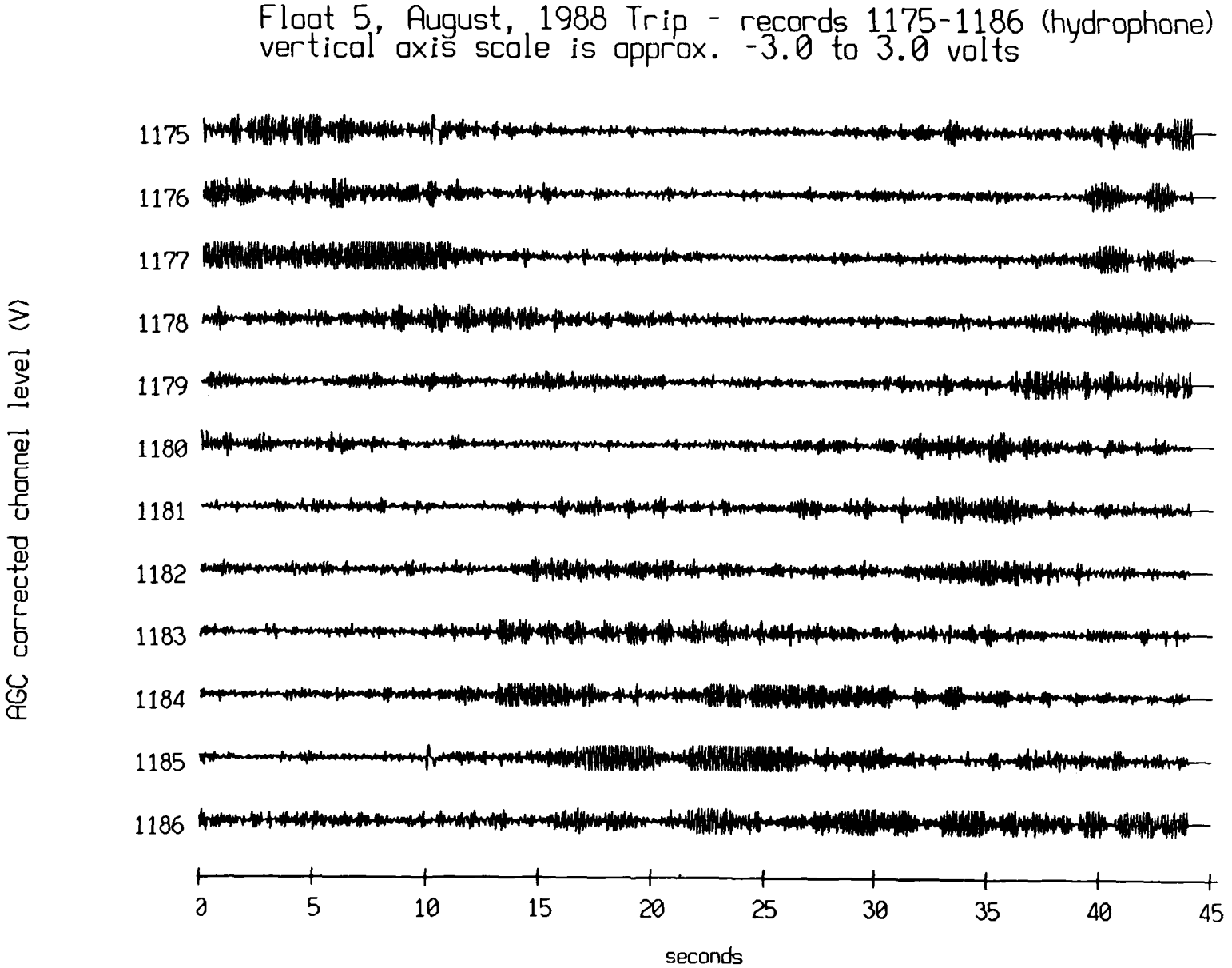


Figure XI.18d

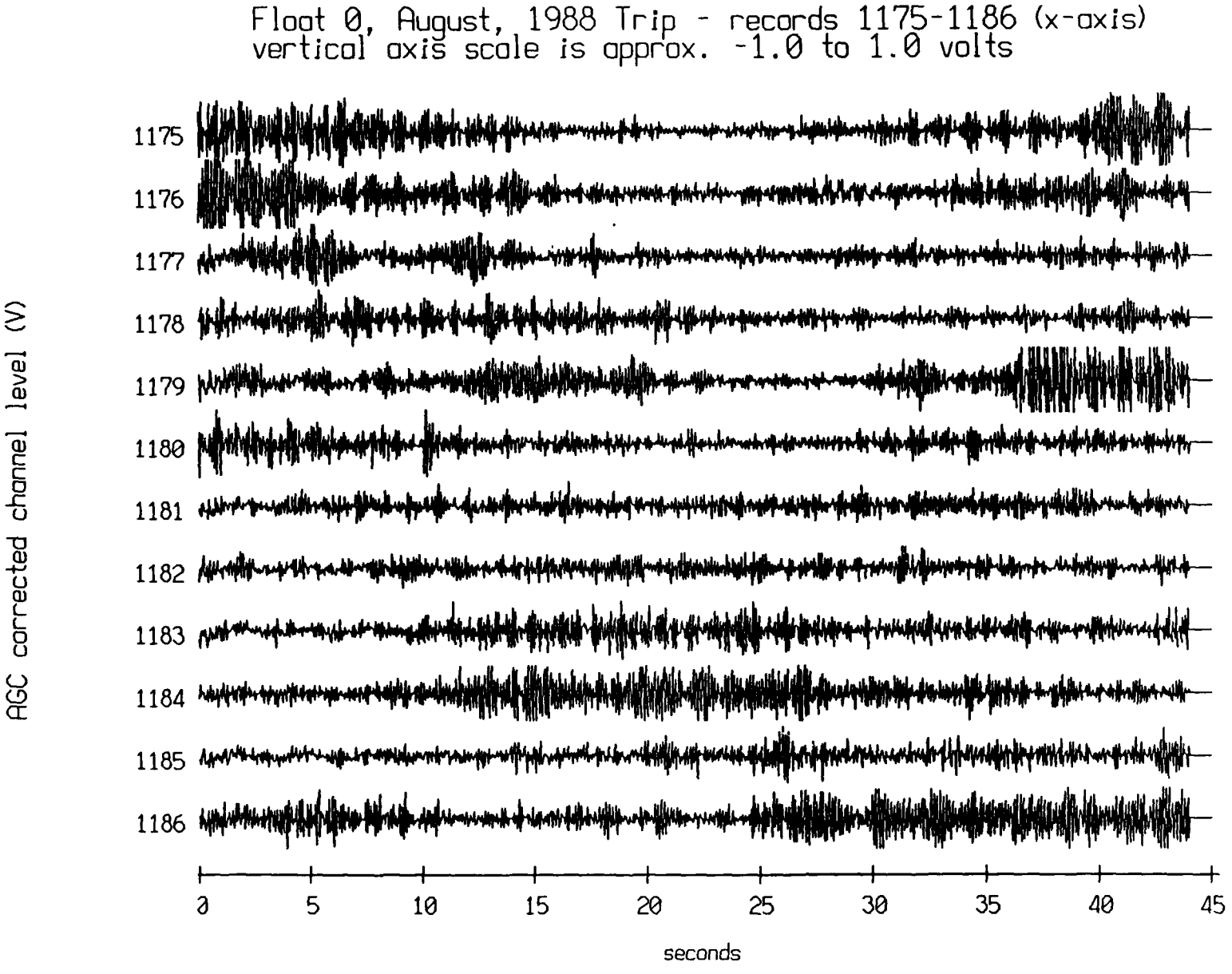


Figure XI.19a

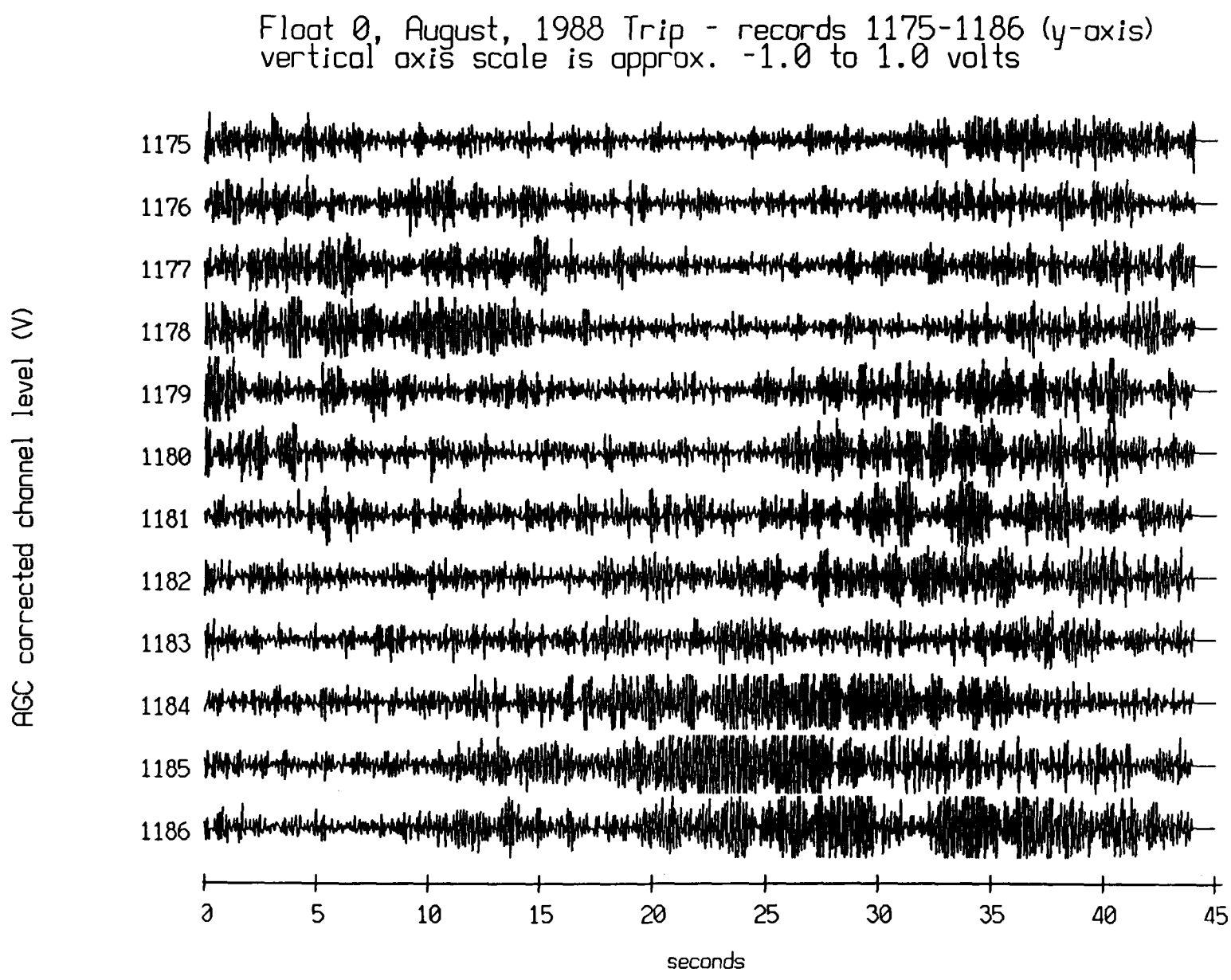


Figure XI.19b

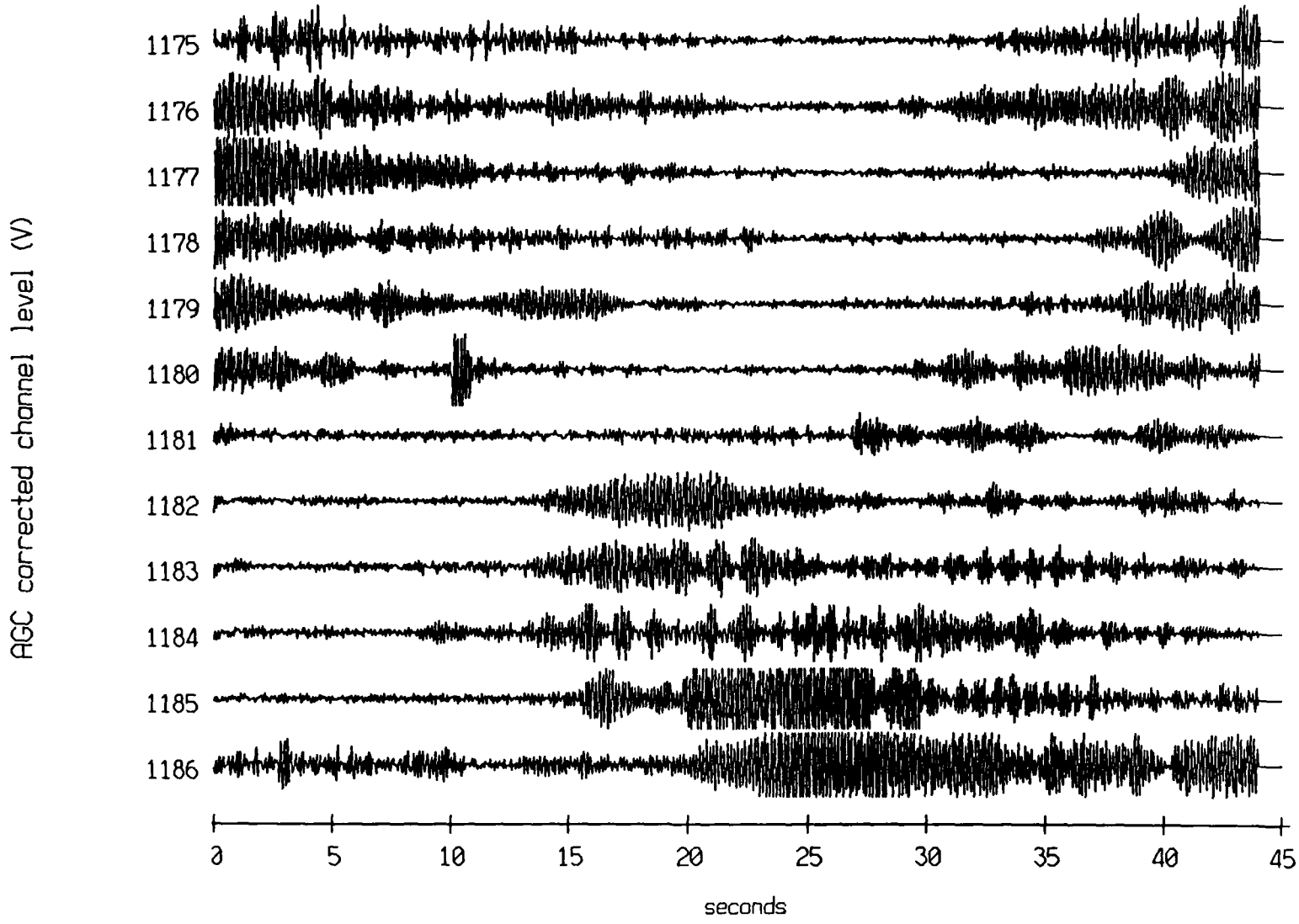


Figure XI.19c

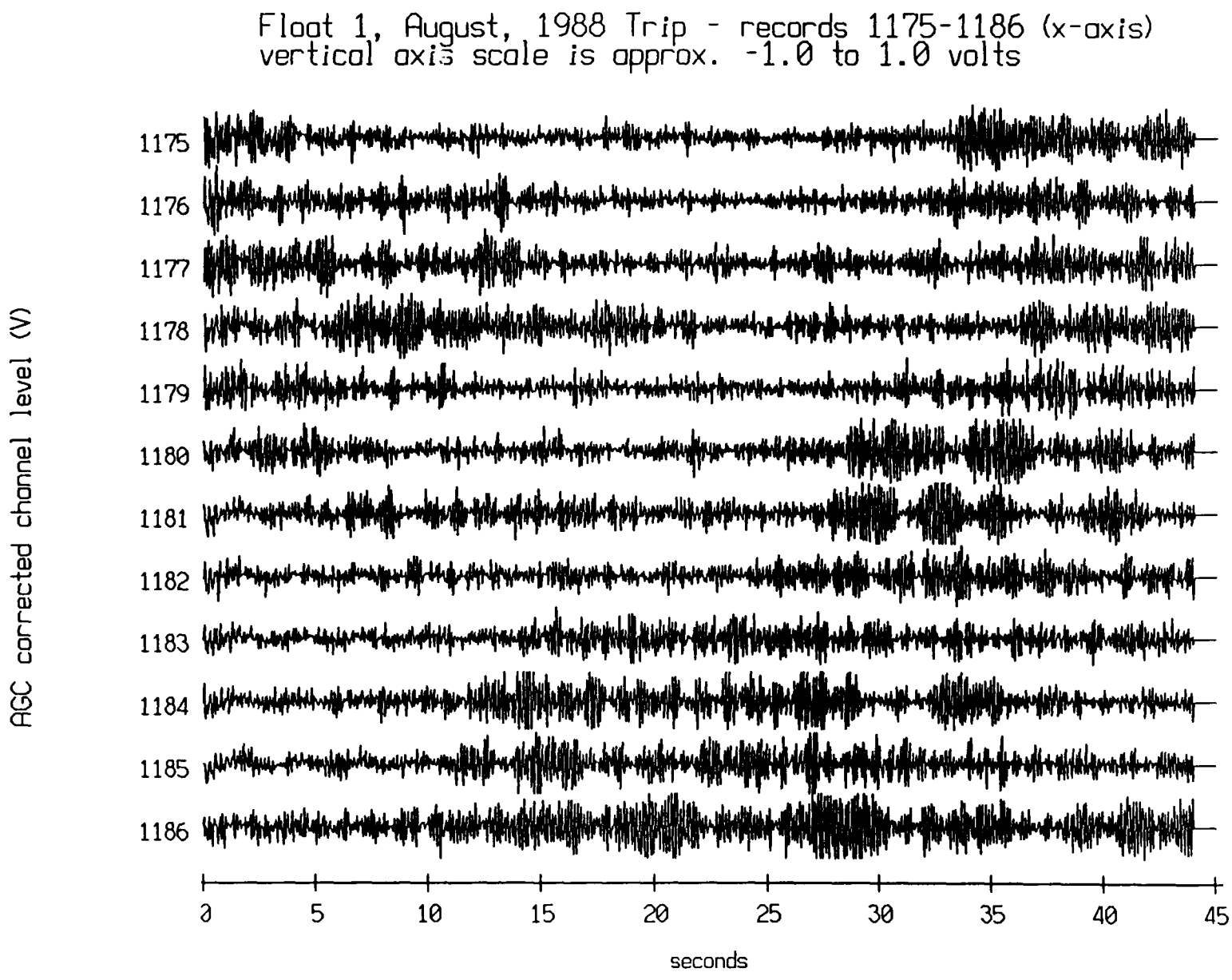


Figure XI.20a

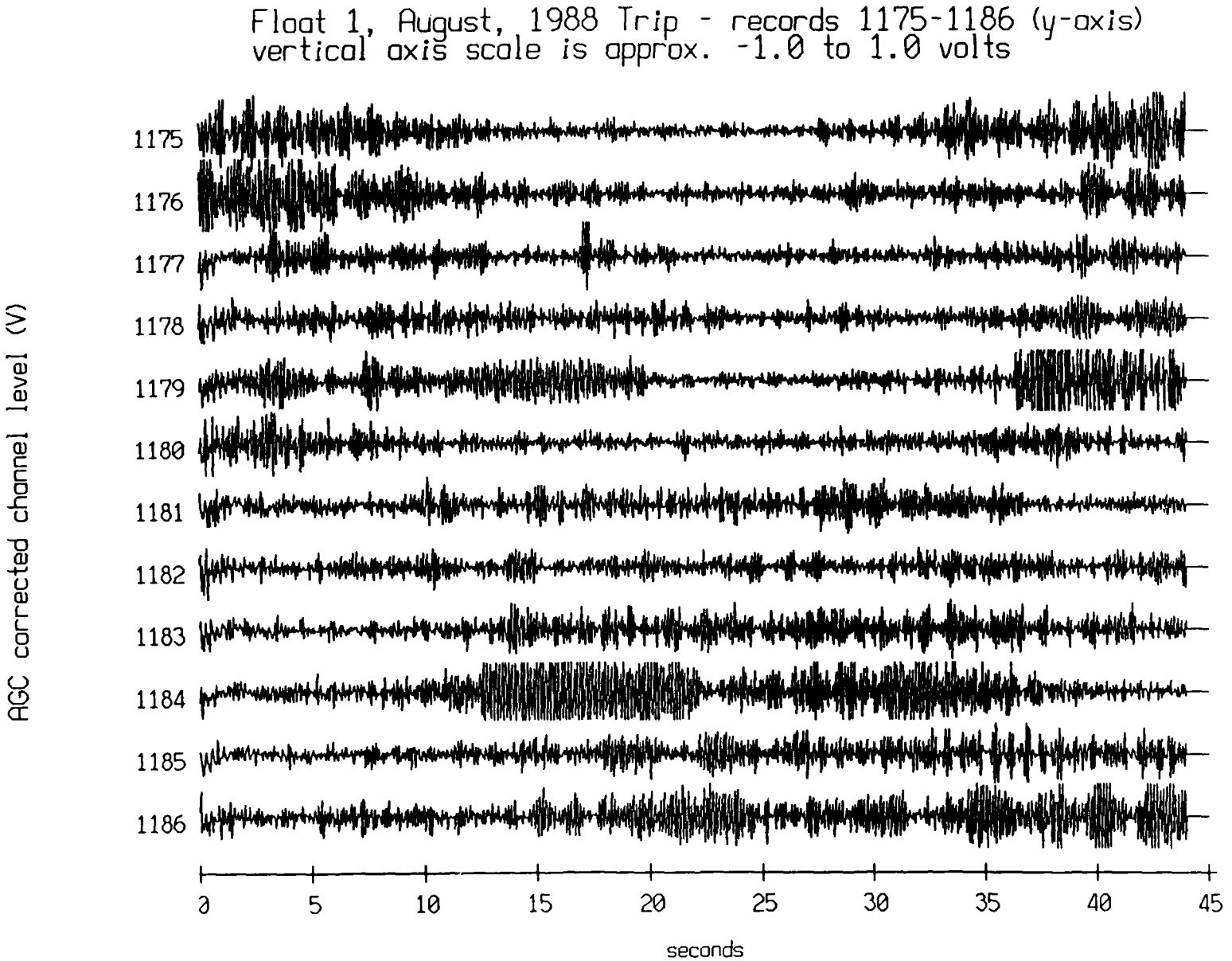


Figure XI.20b

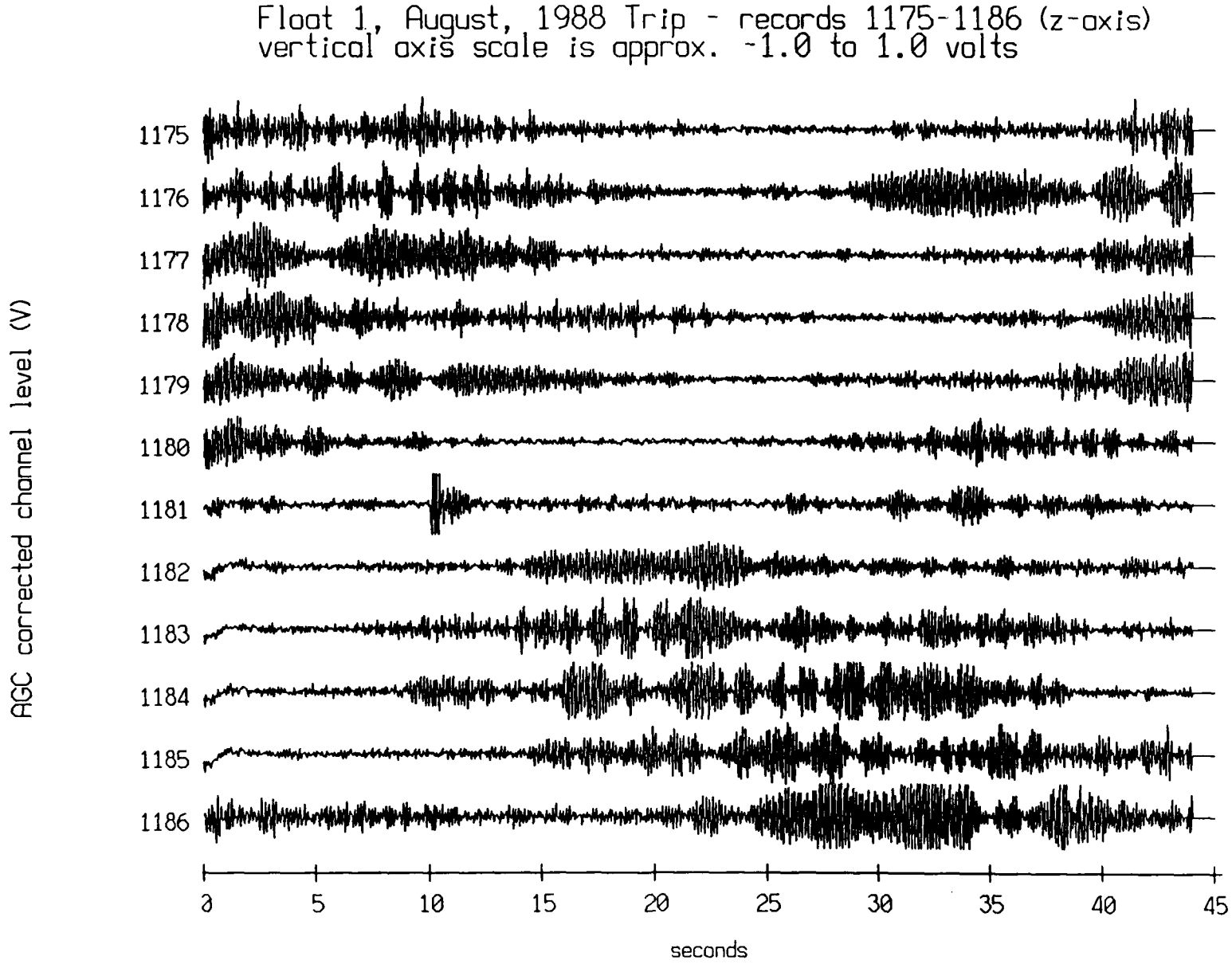


Figure XI.20c

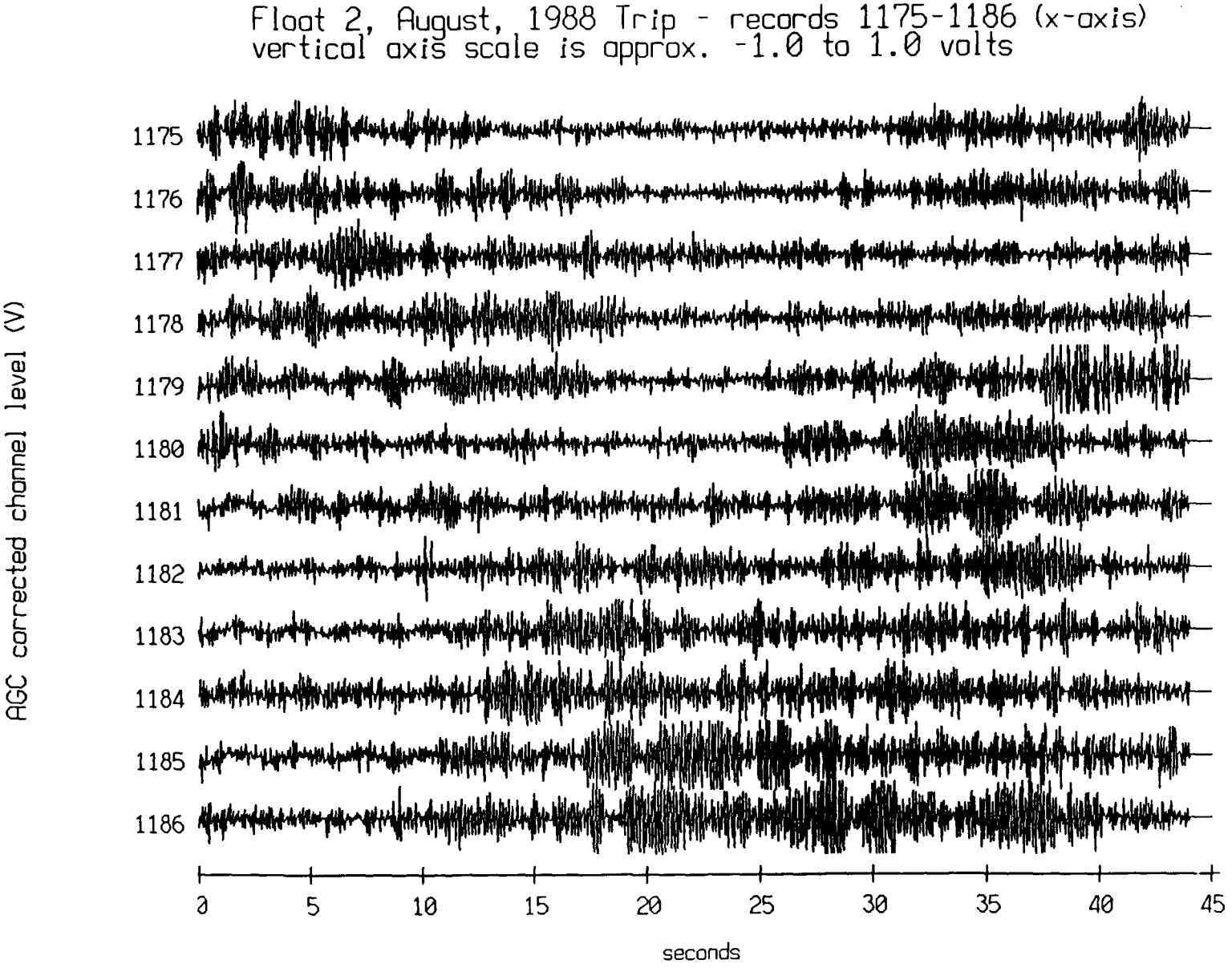


Figure XI.21a

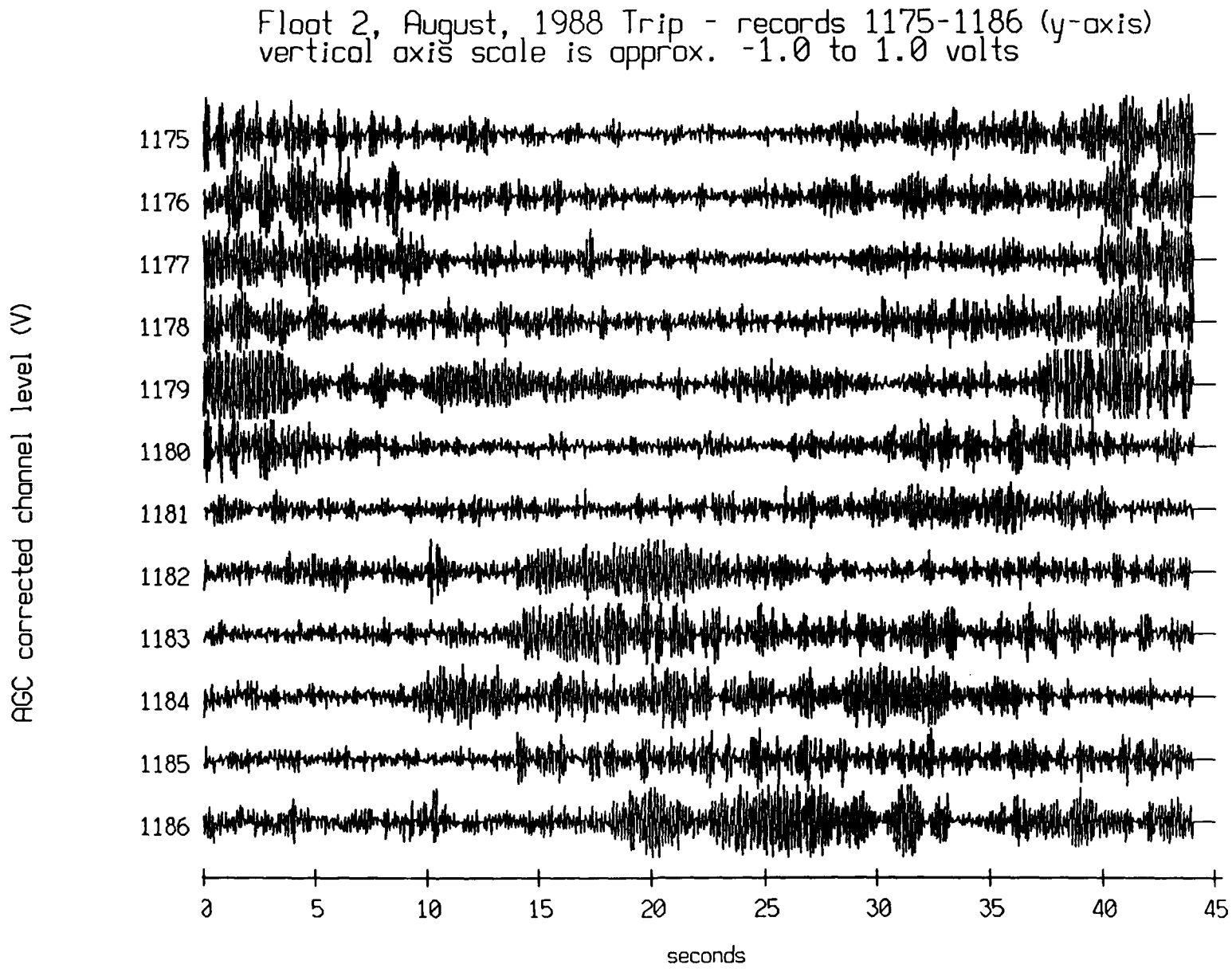


Figure XI.21b

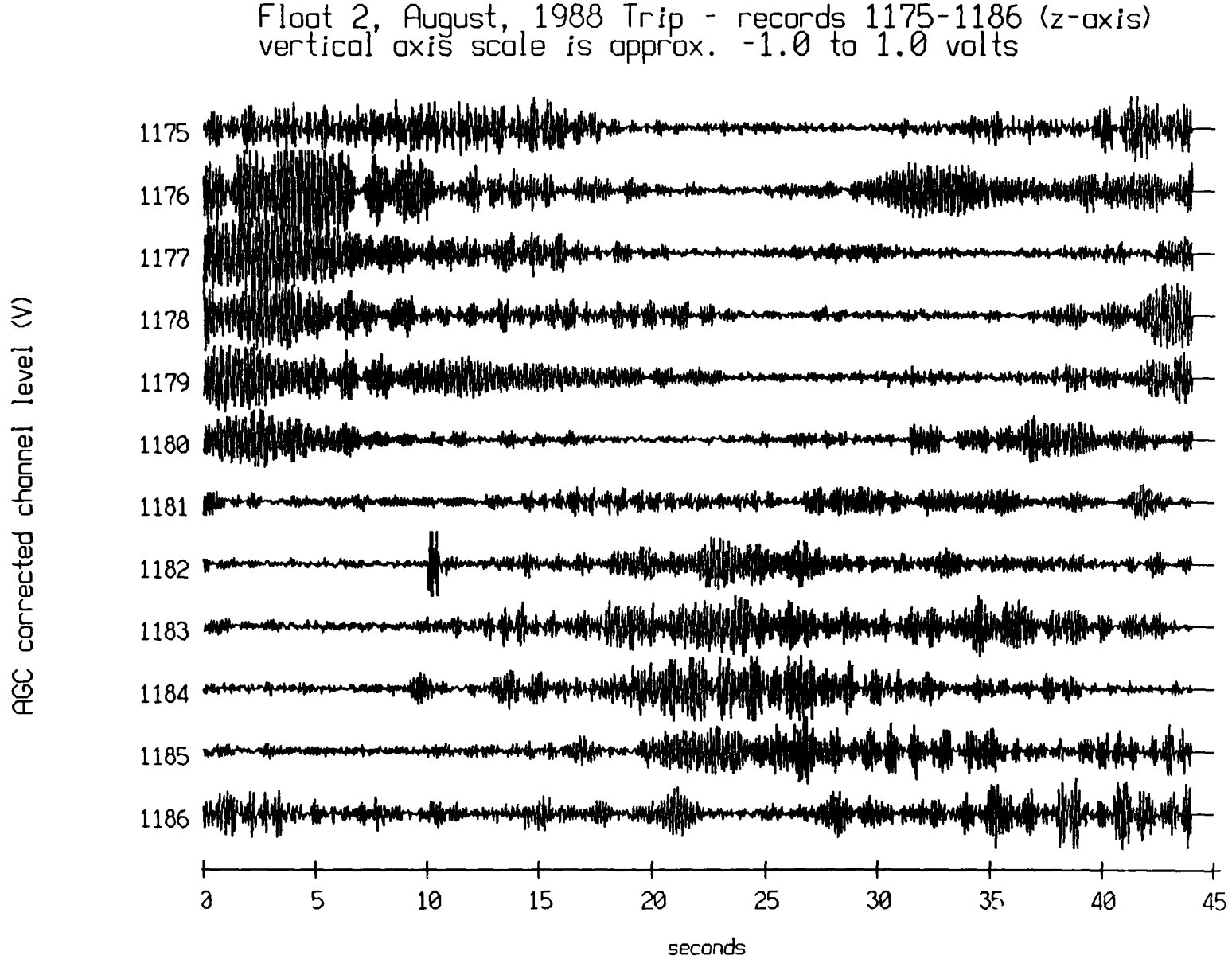


Figure XI.21c

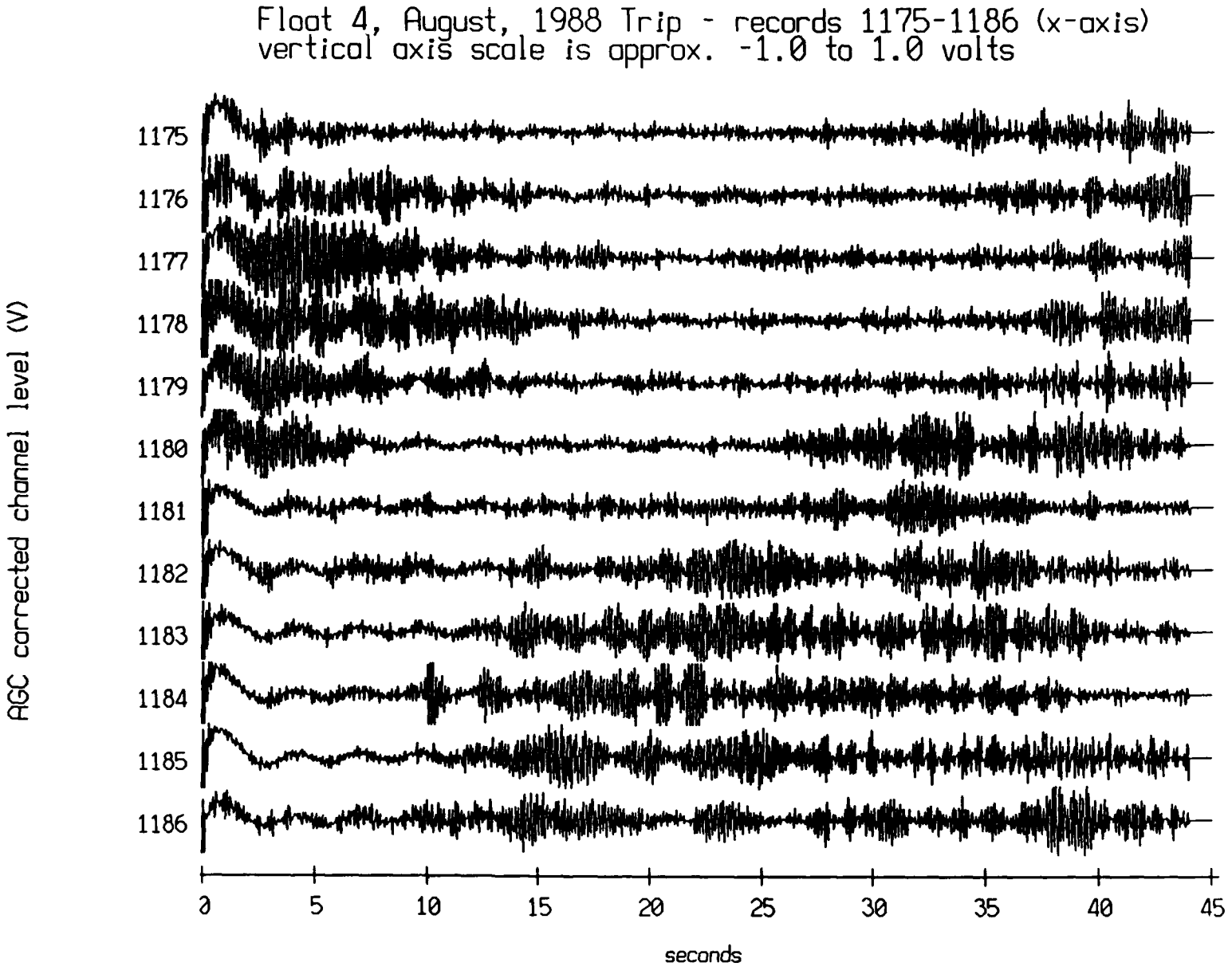


Figure XI.22a

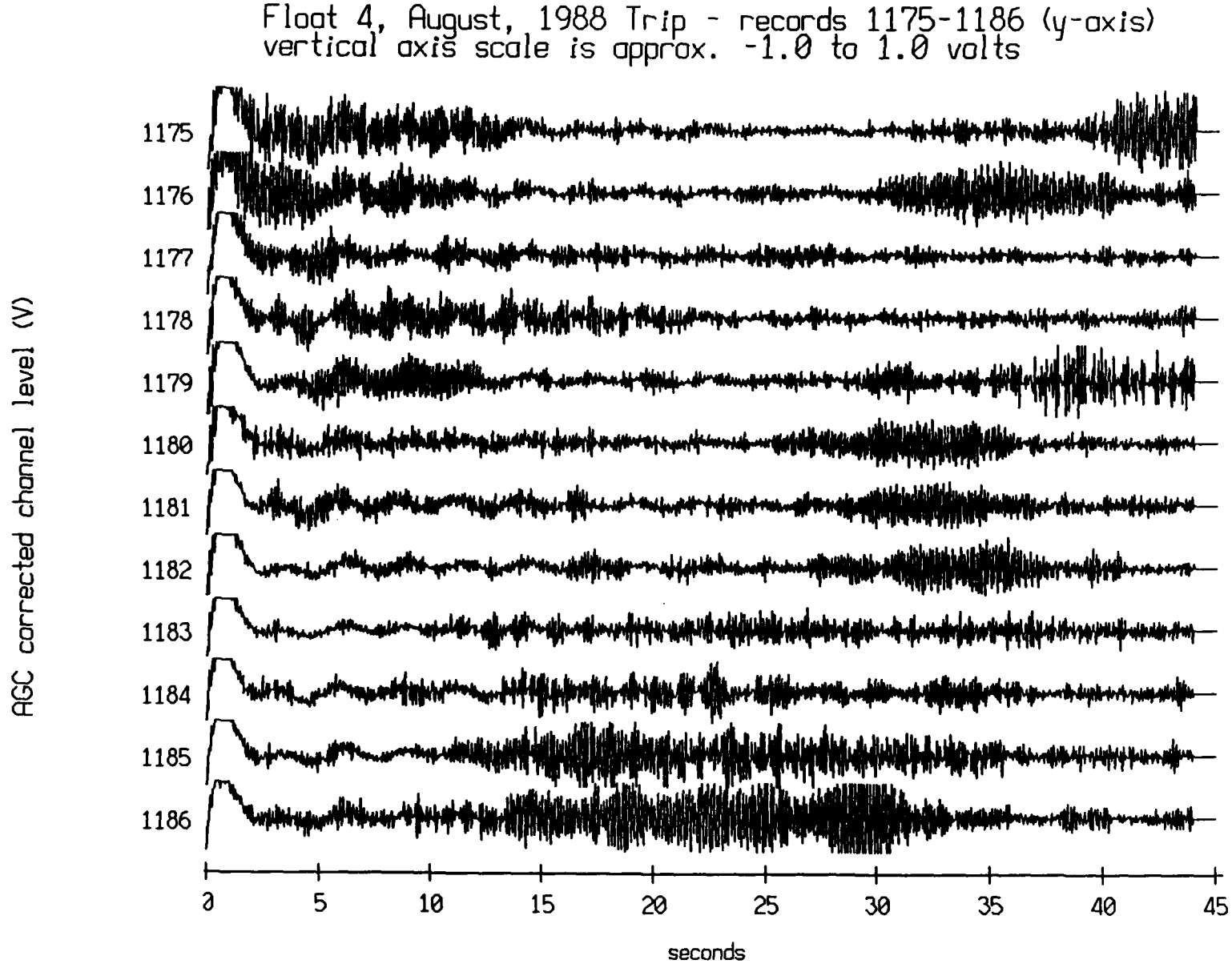


Figure XI.22b

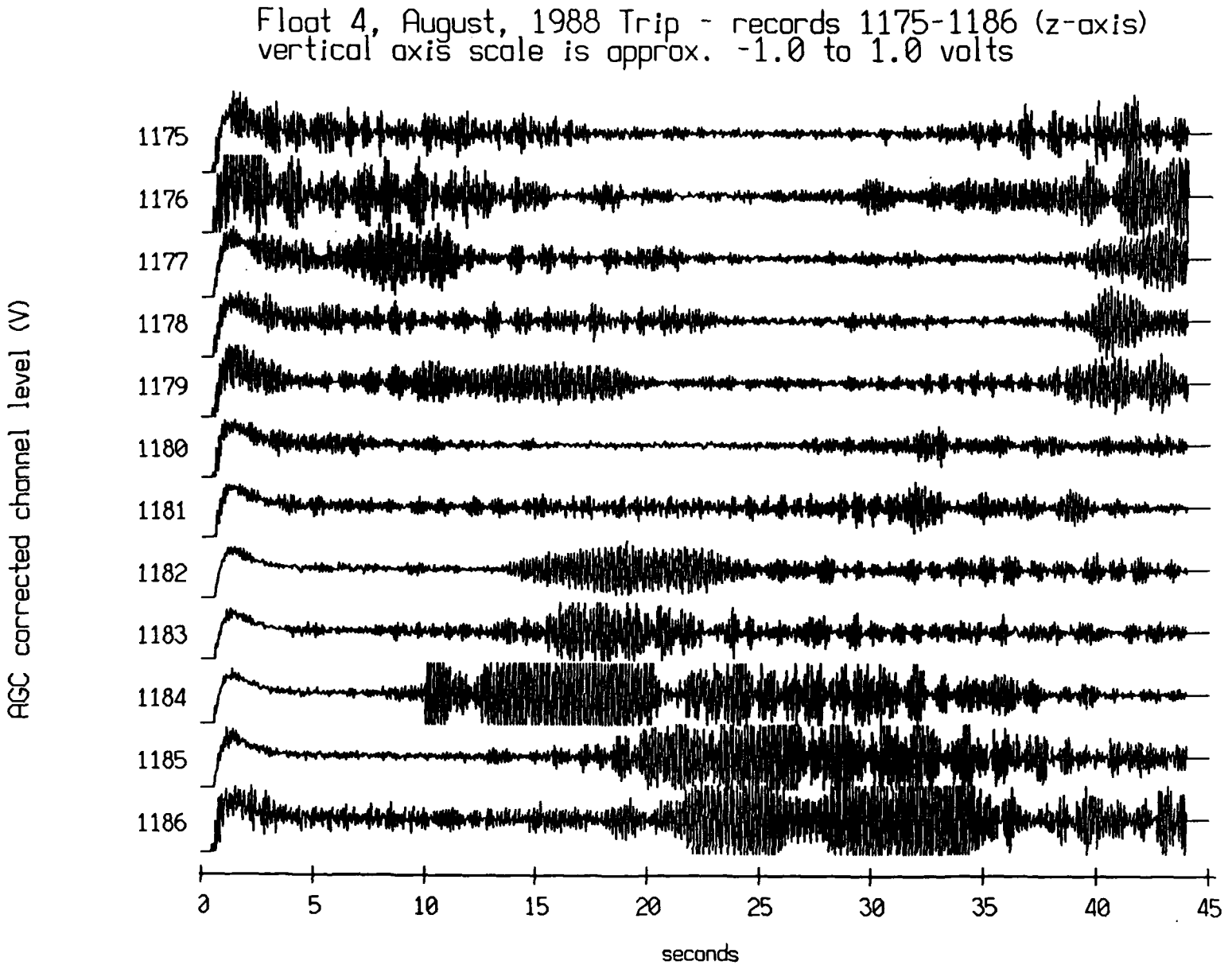


Figure XI.22c

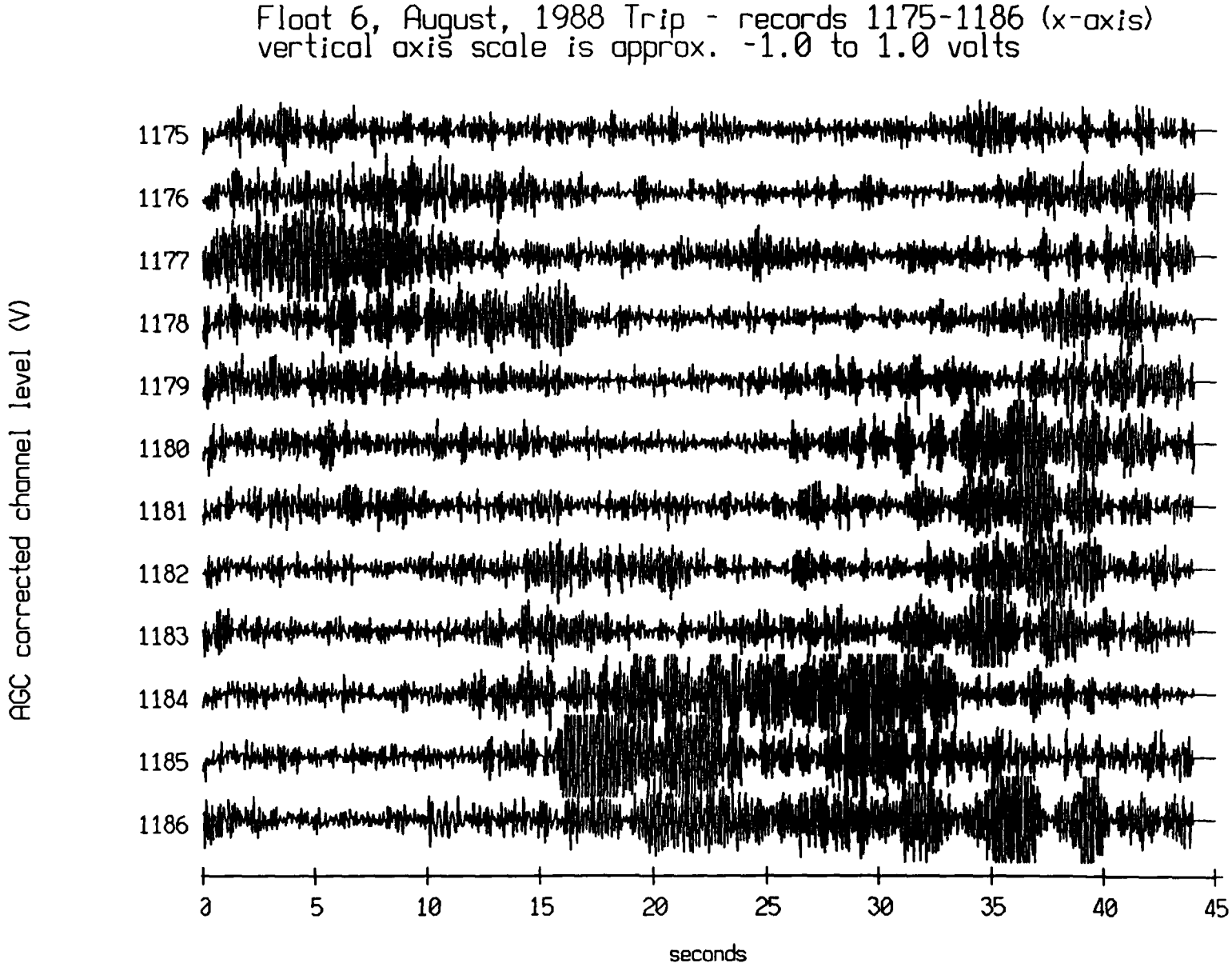


Figure XI.23a

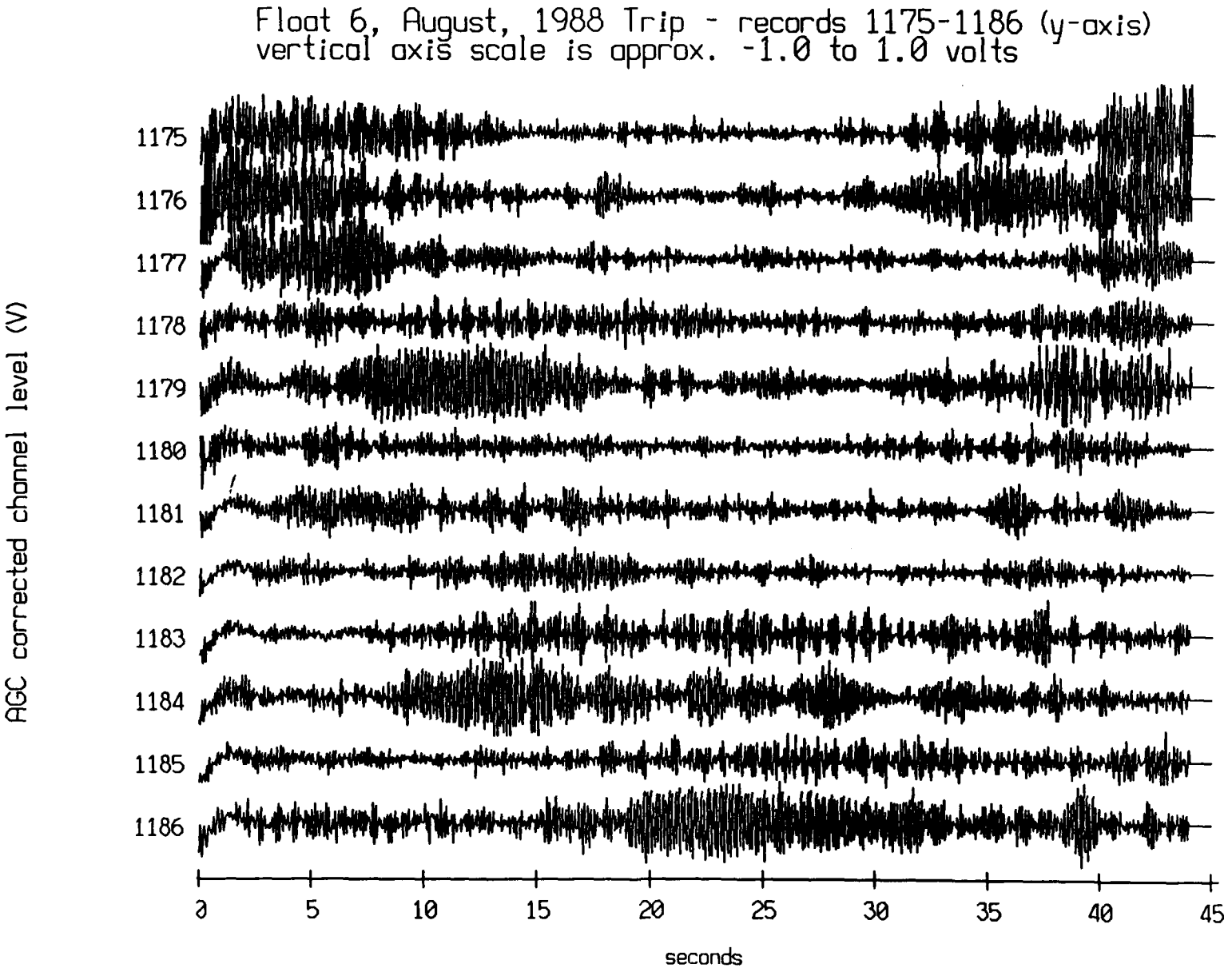


Figure XI.23b

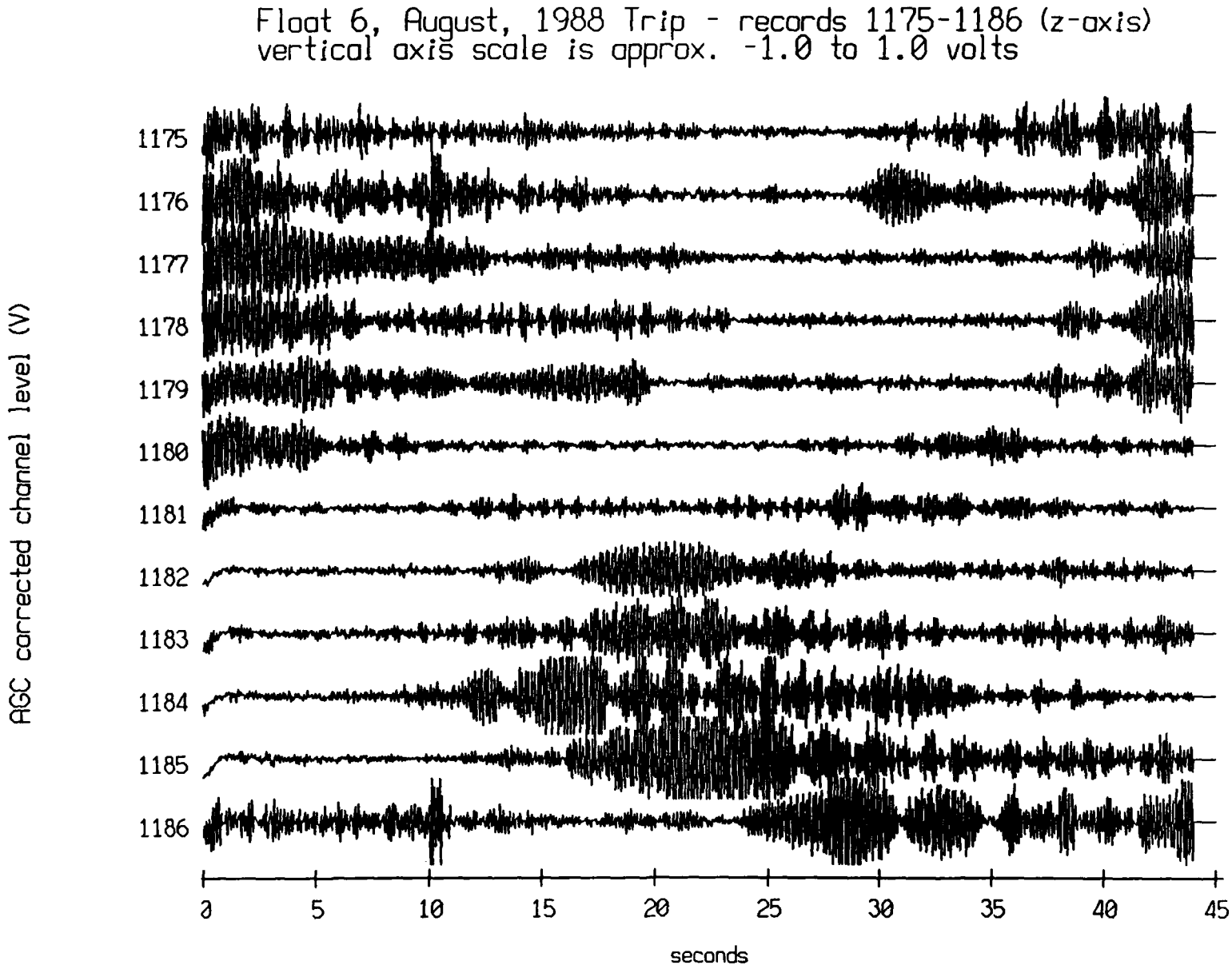


Figure XI.23c

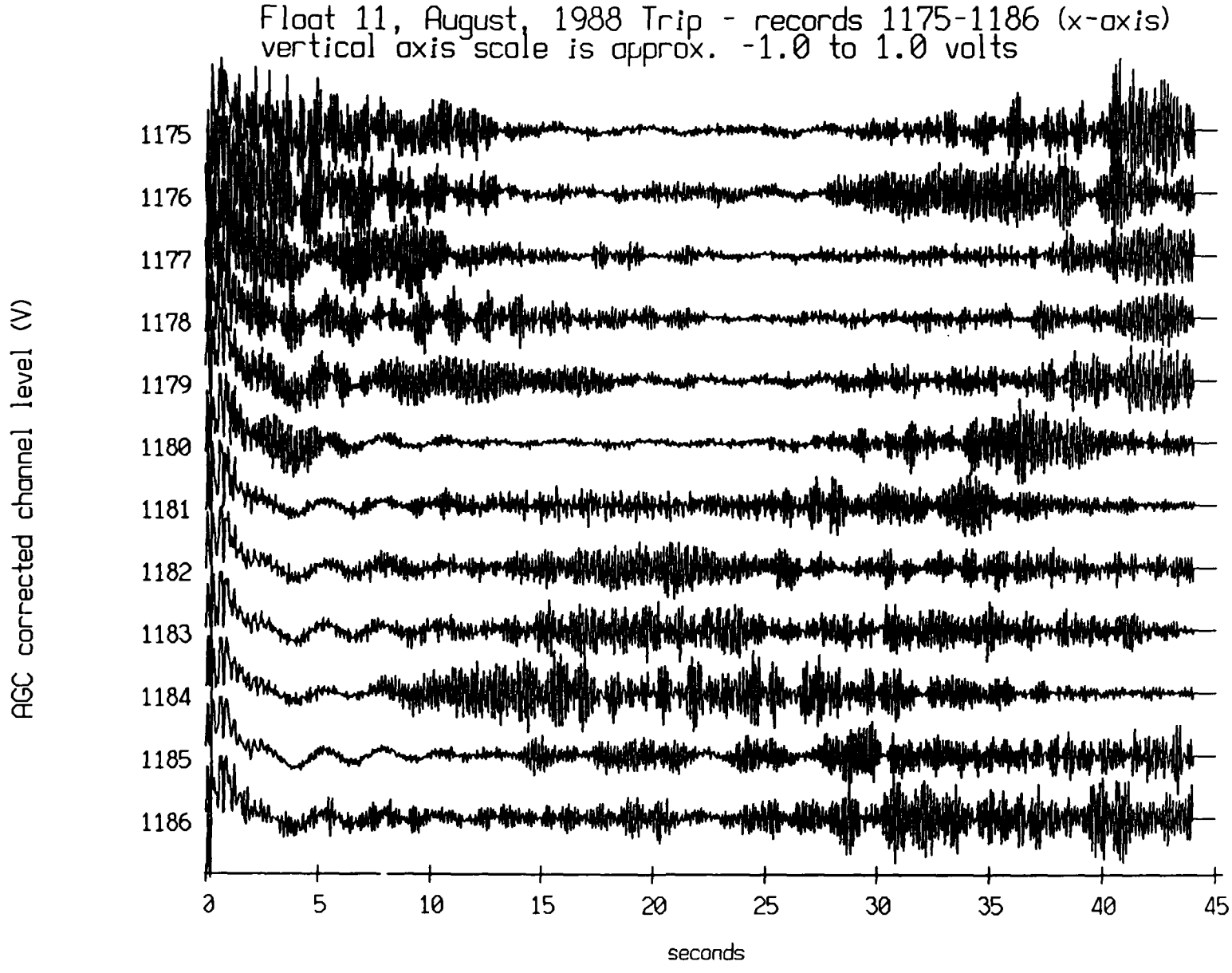


Figure XI.24a

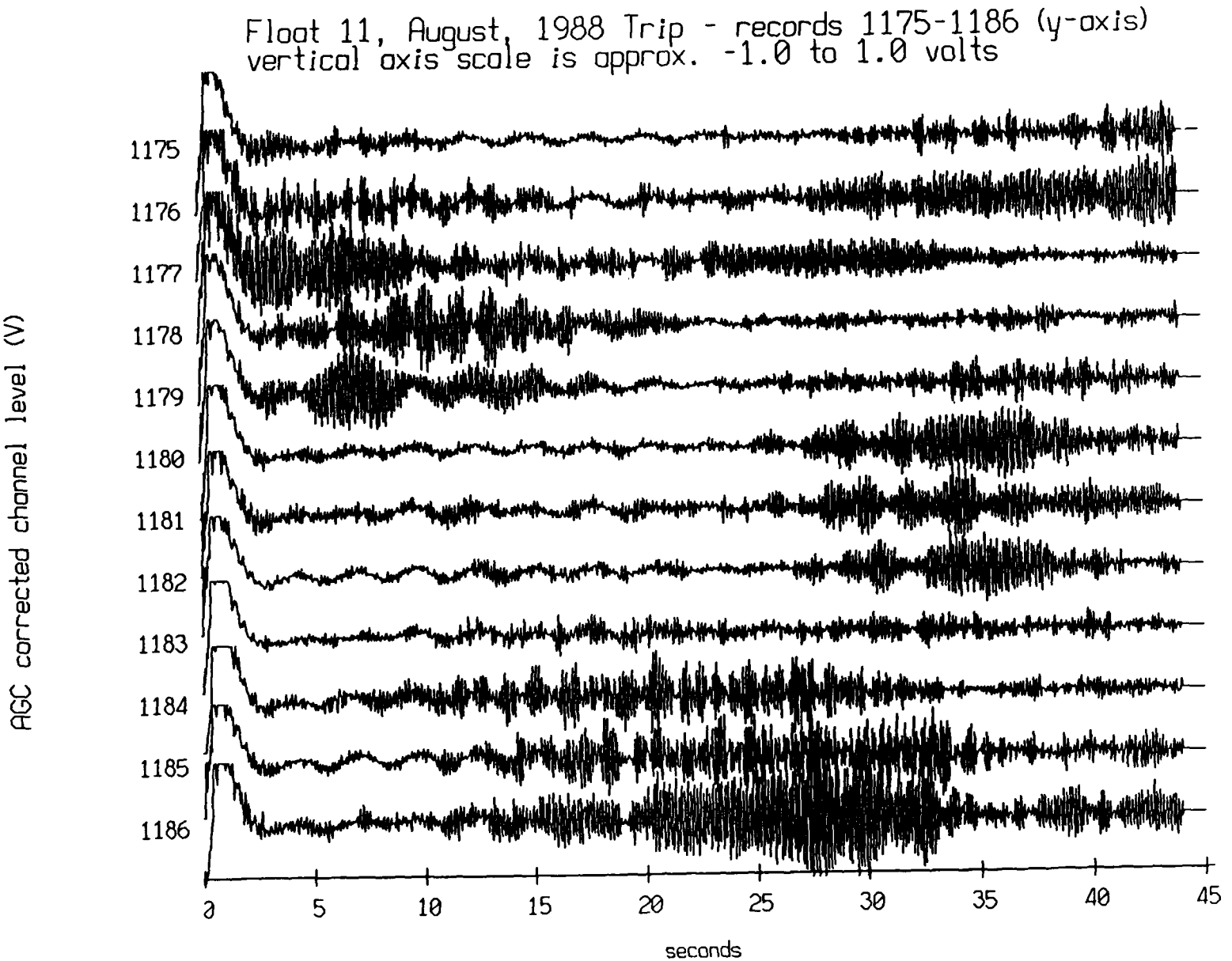


Figure XI.24b

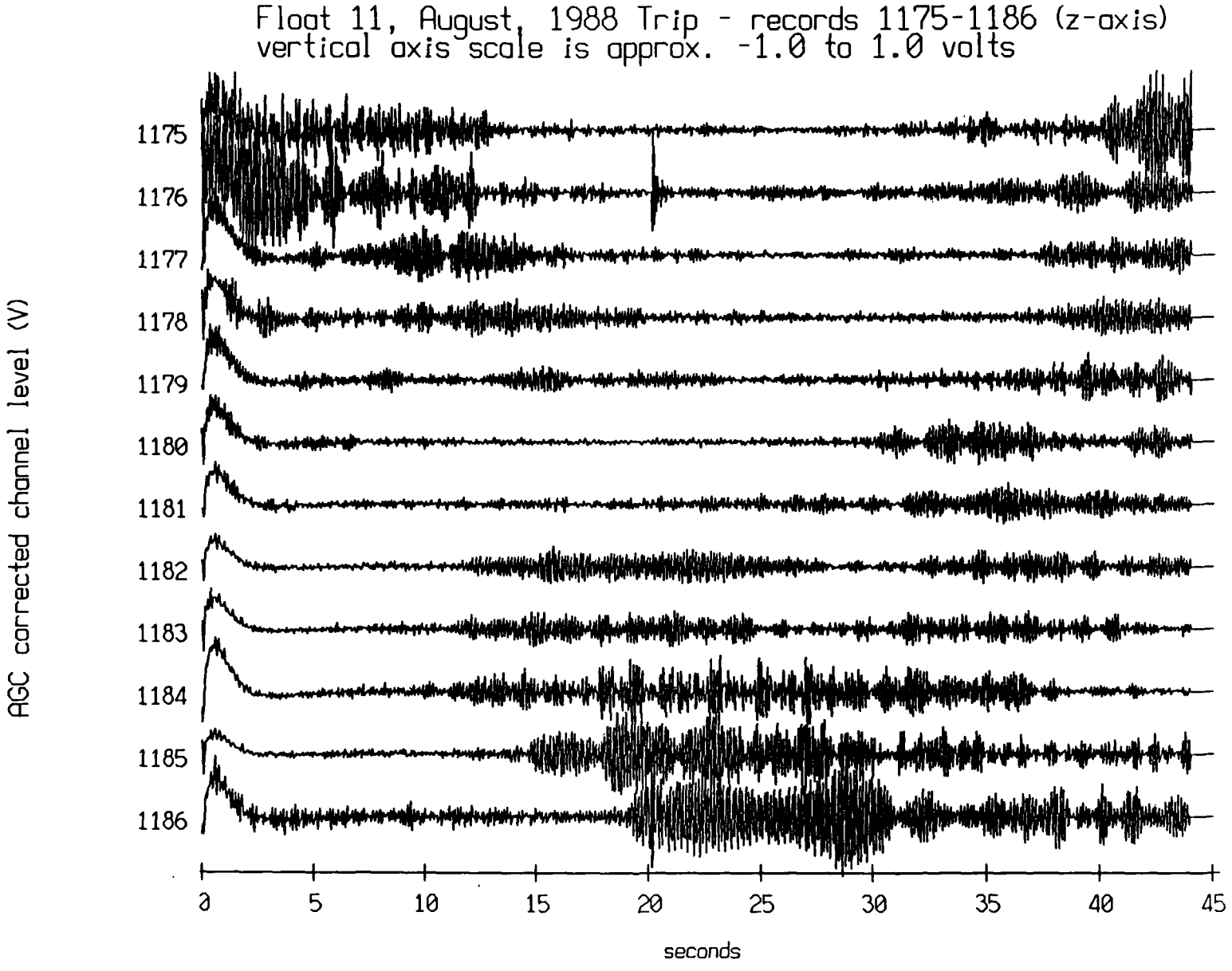


Figure XI.24c

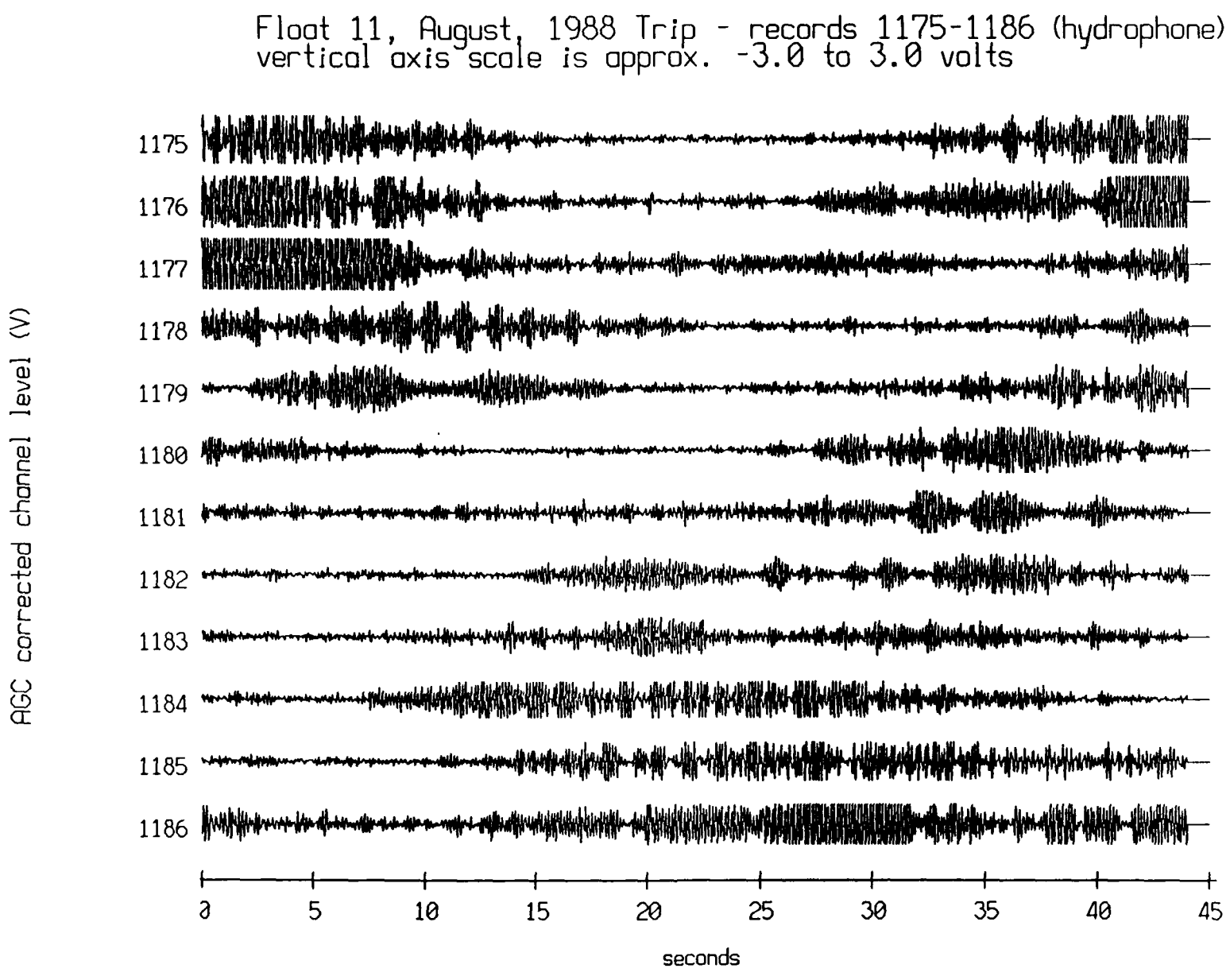


Figure XI.2.4d

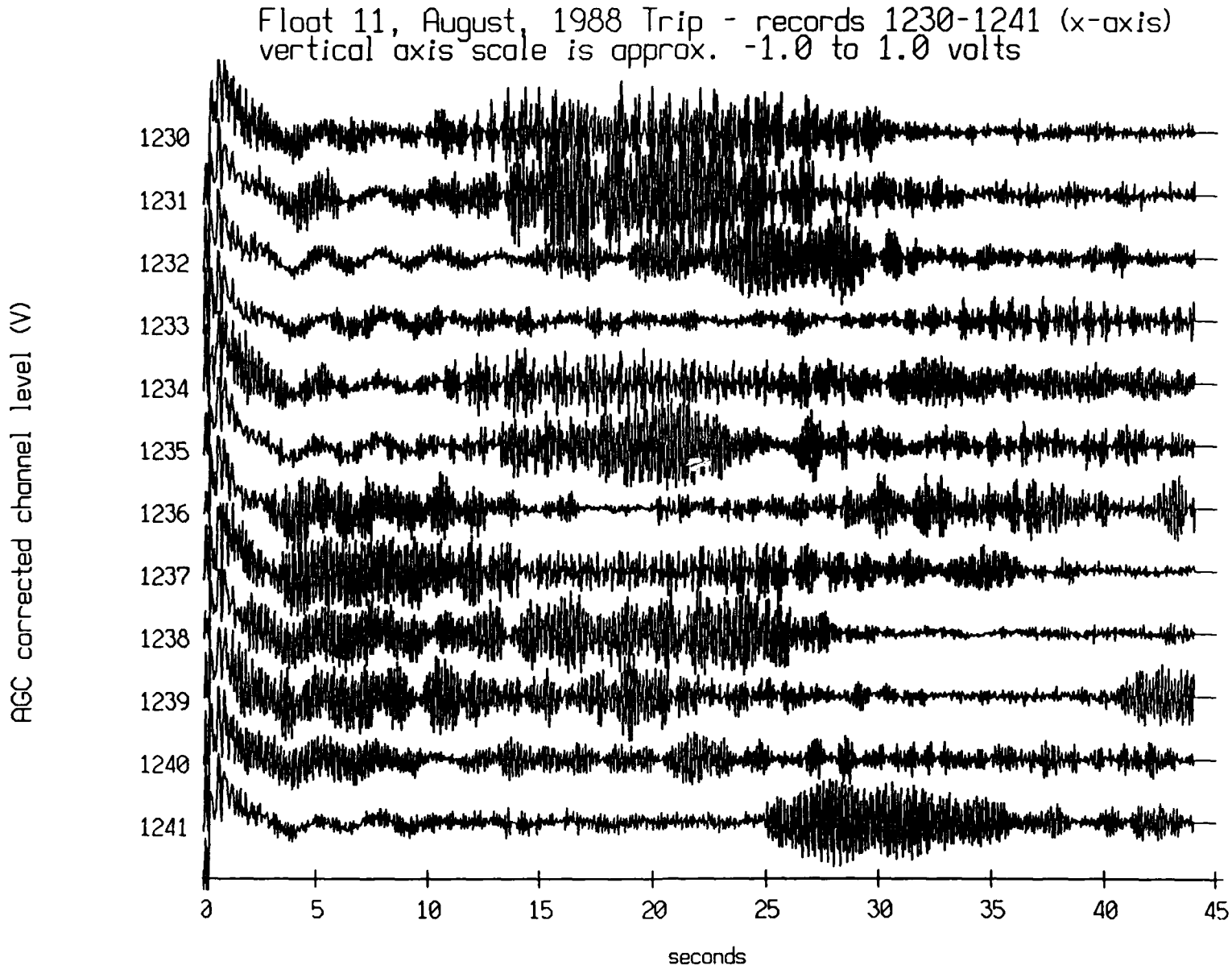


Figure XI.25a

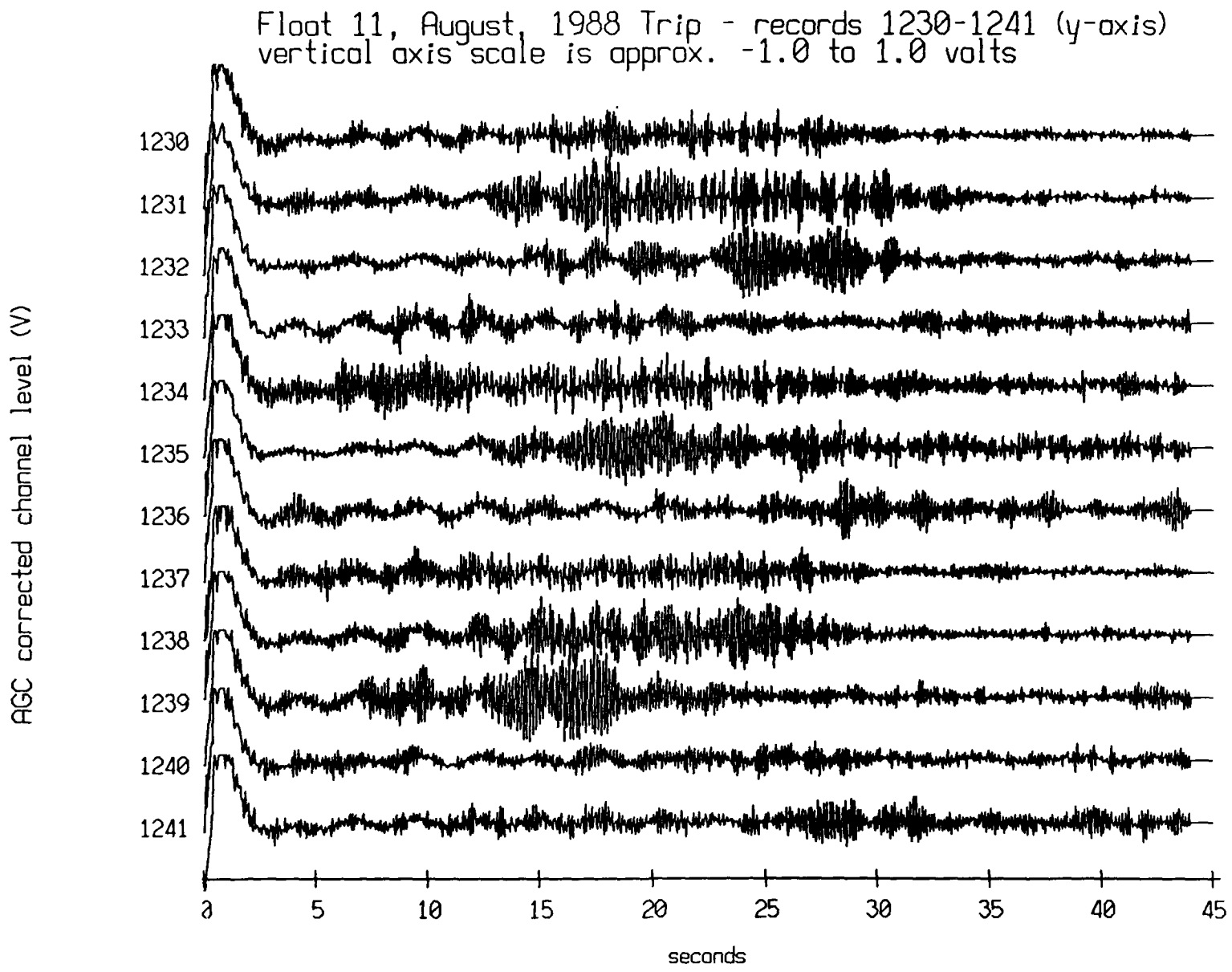


Figure XI.25b

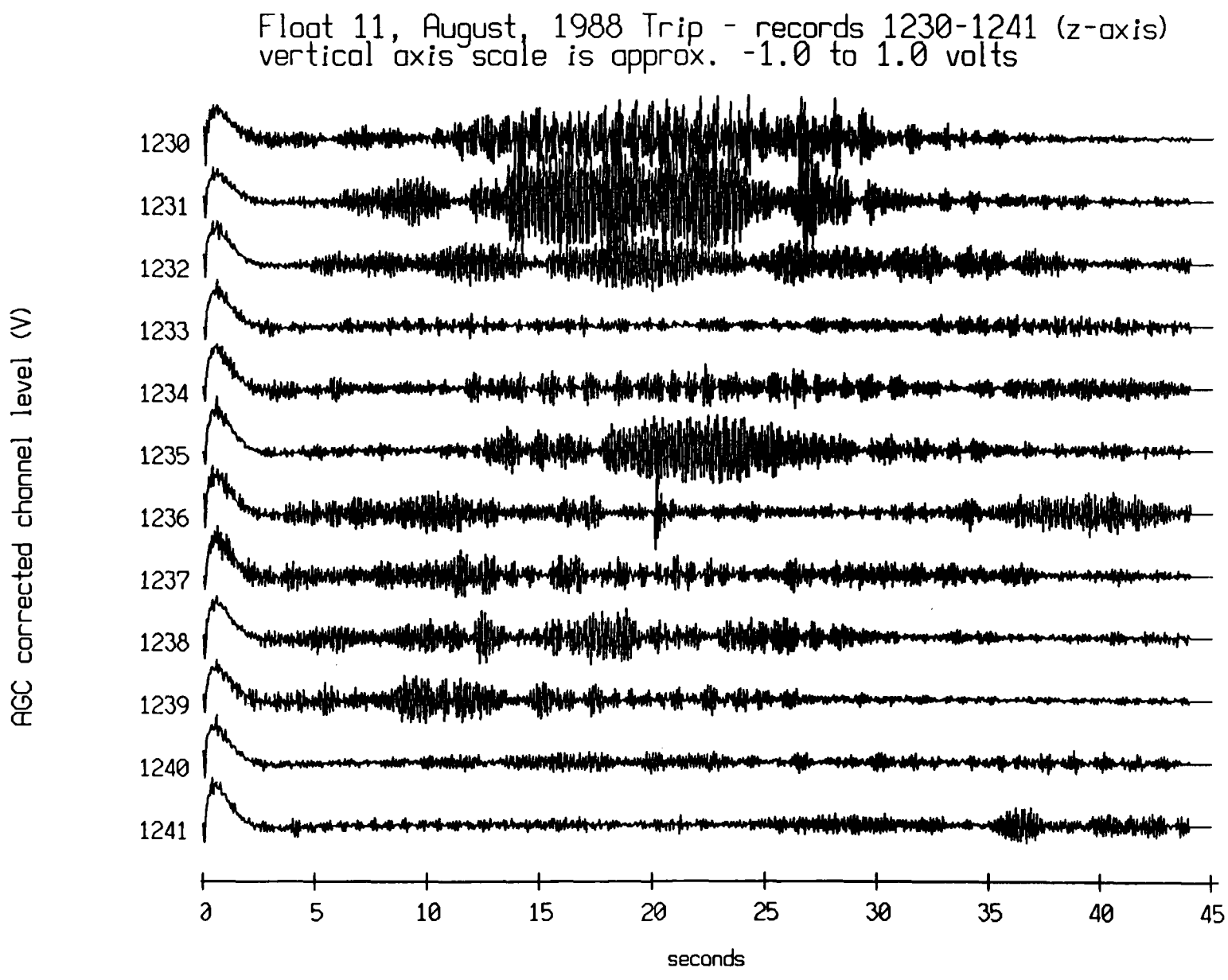


Figure XI.25c

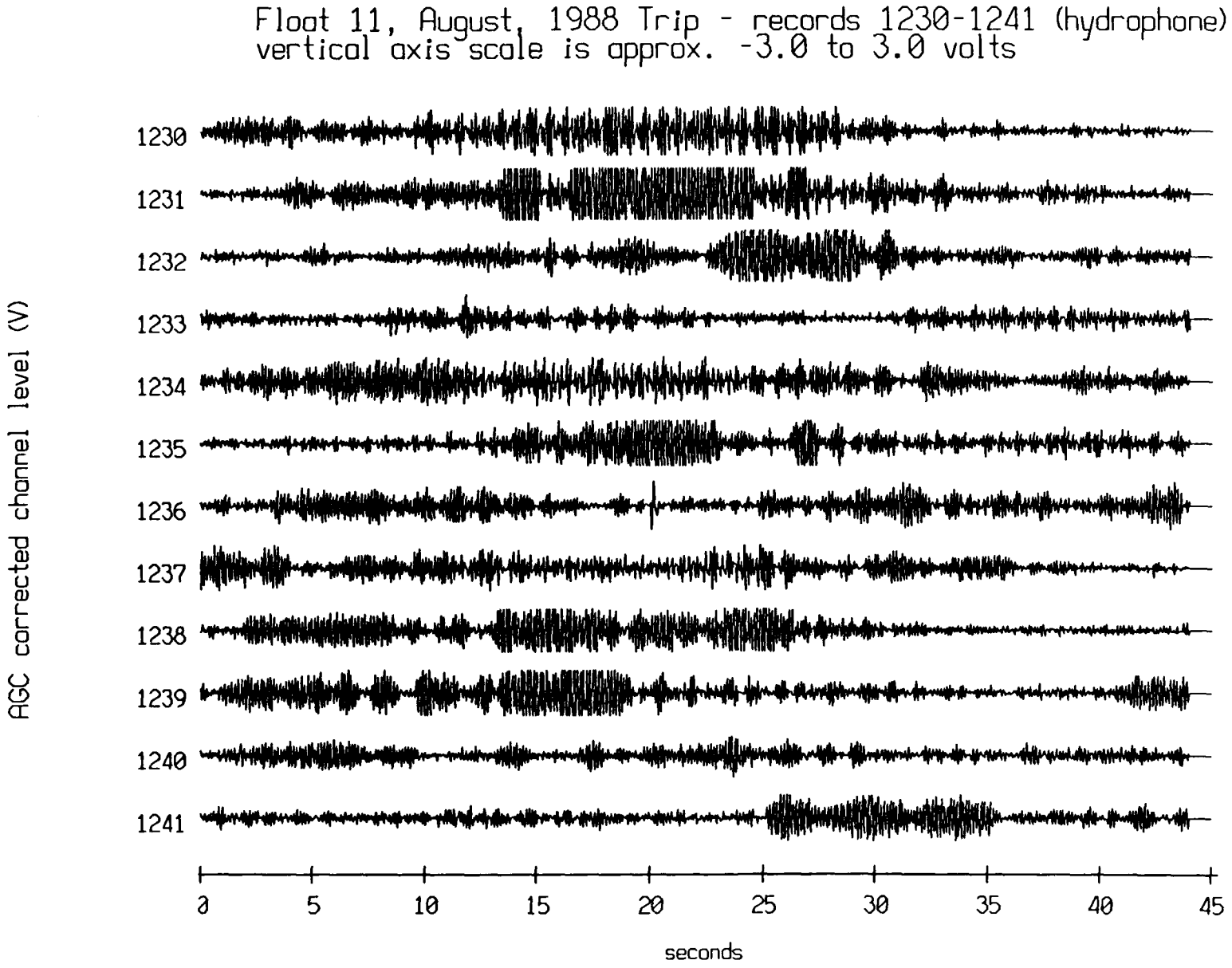


Figure XI.25d

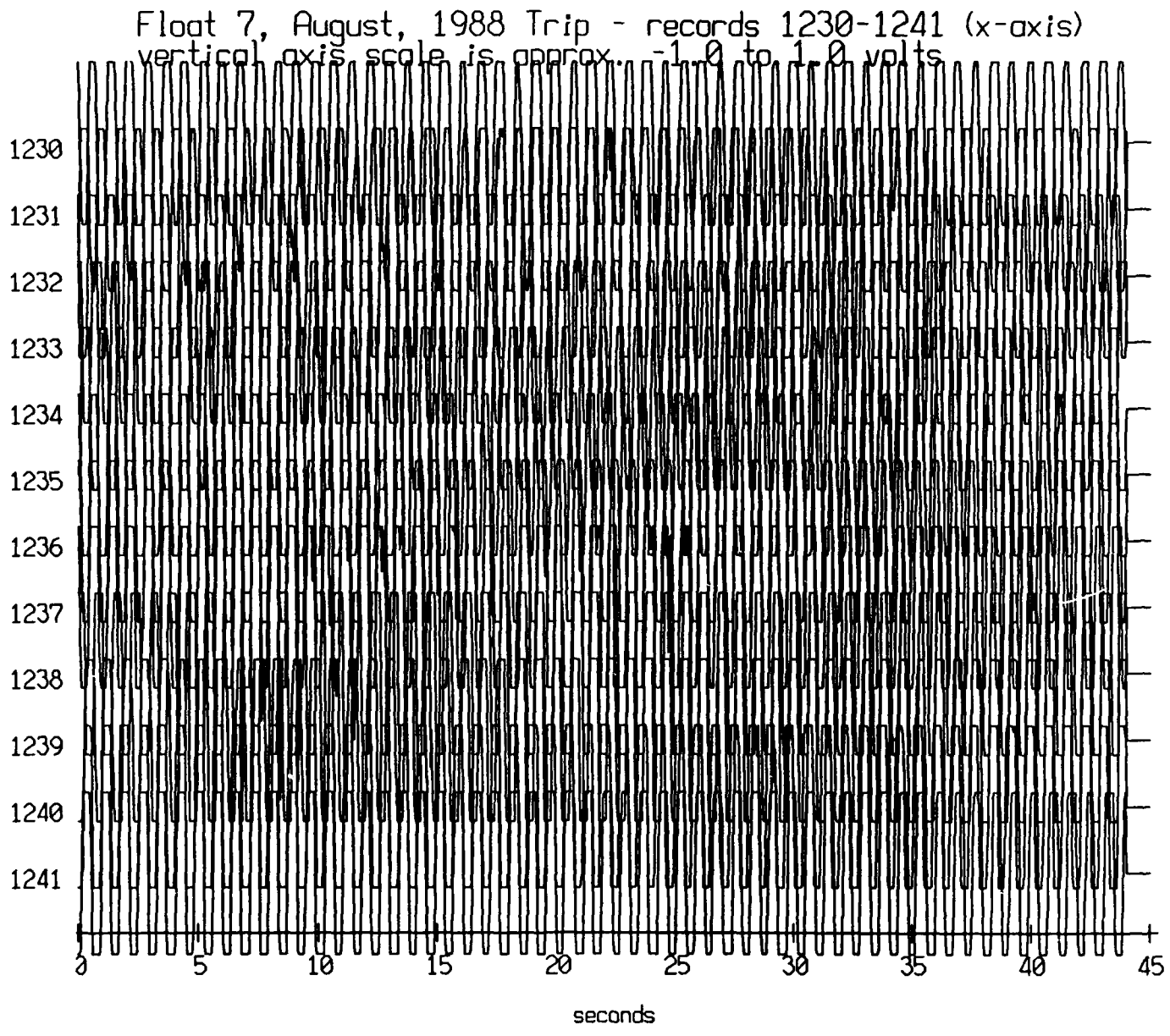


Figure XI.26a

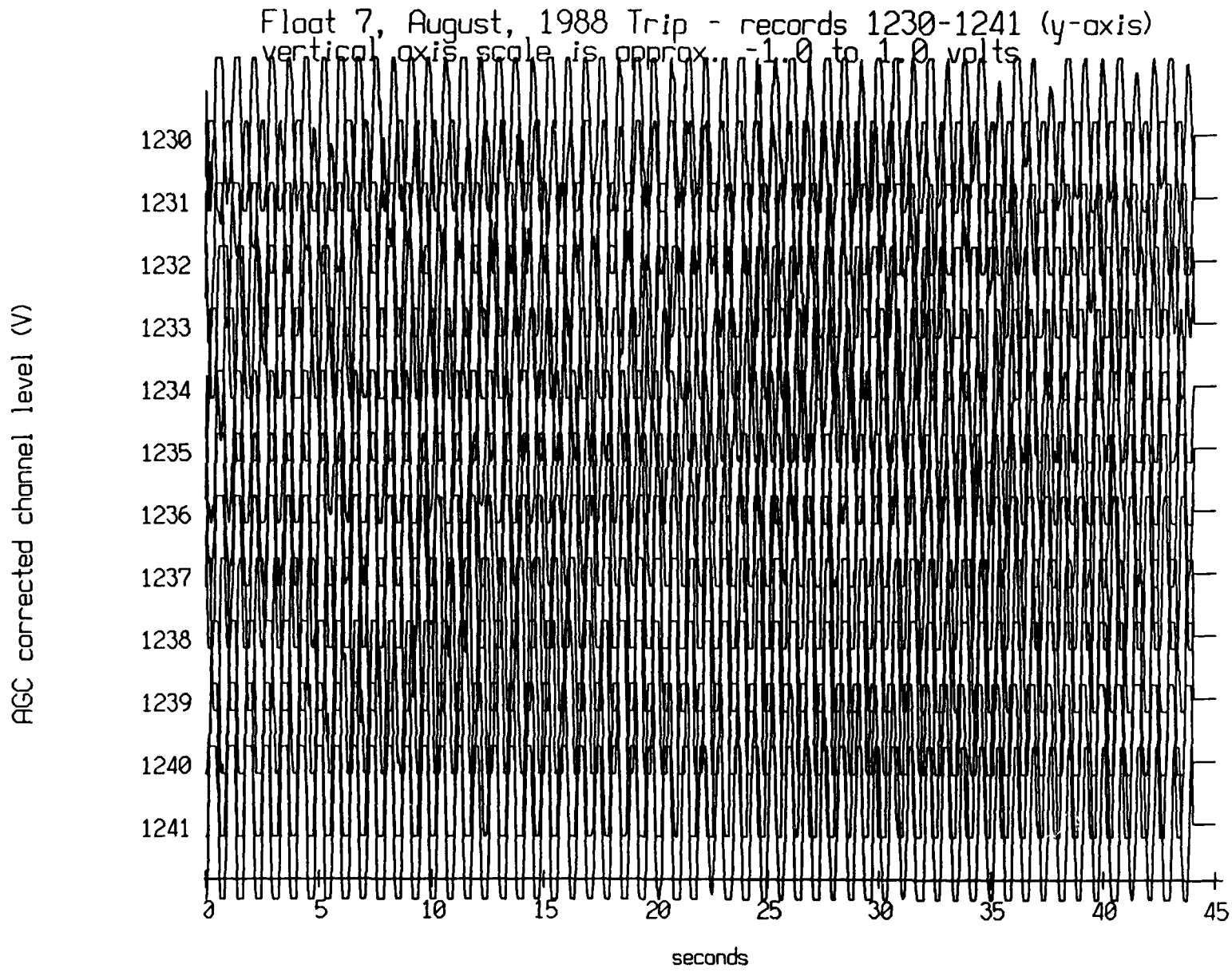


Figure XI.26b

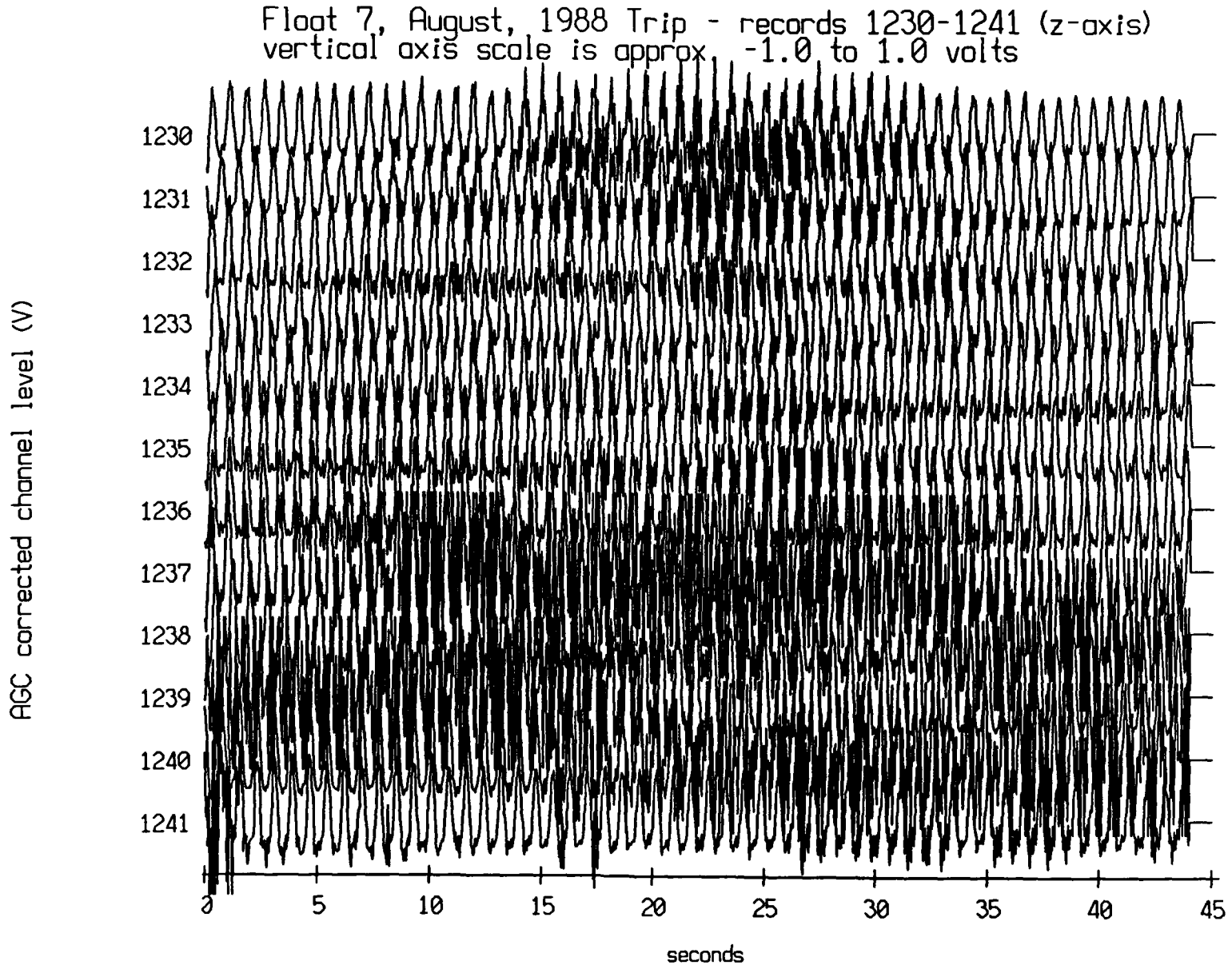


Figure XI.26c

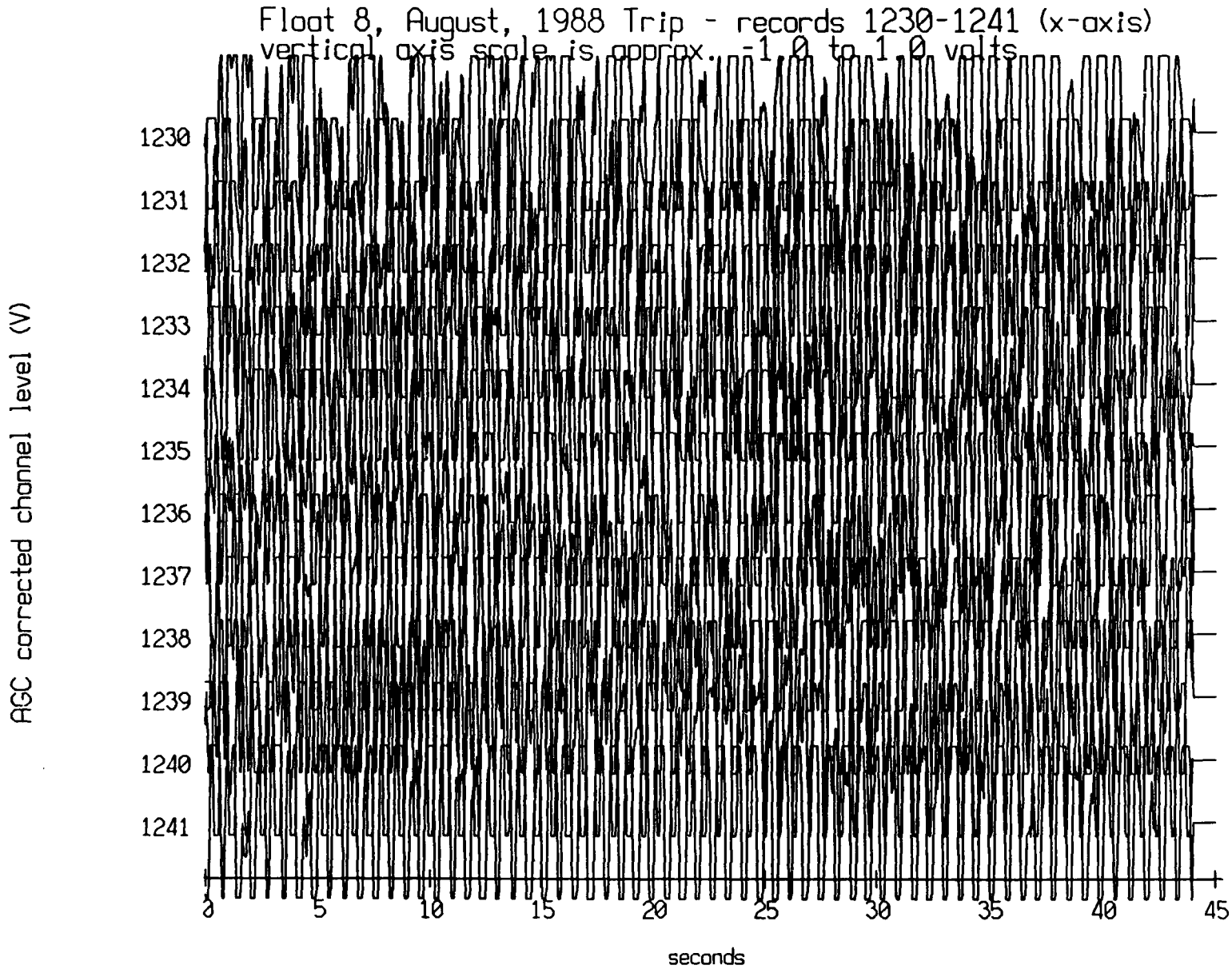


Figure XI.27a

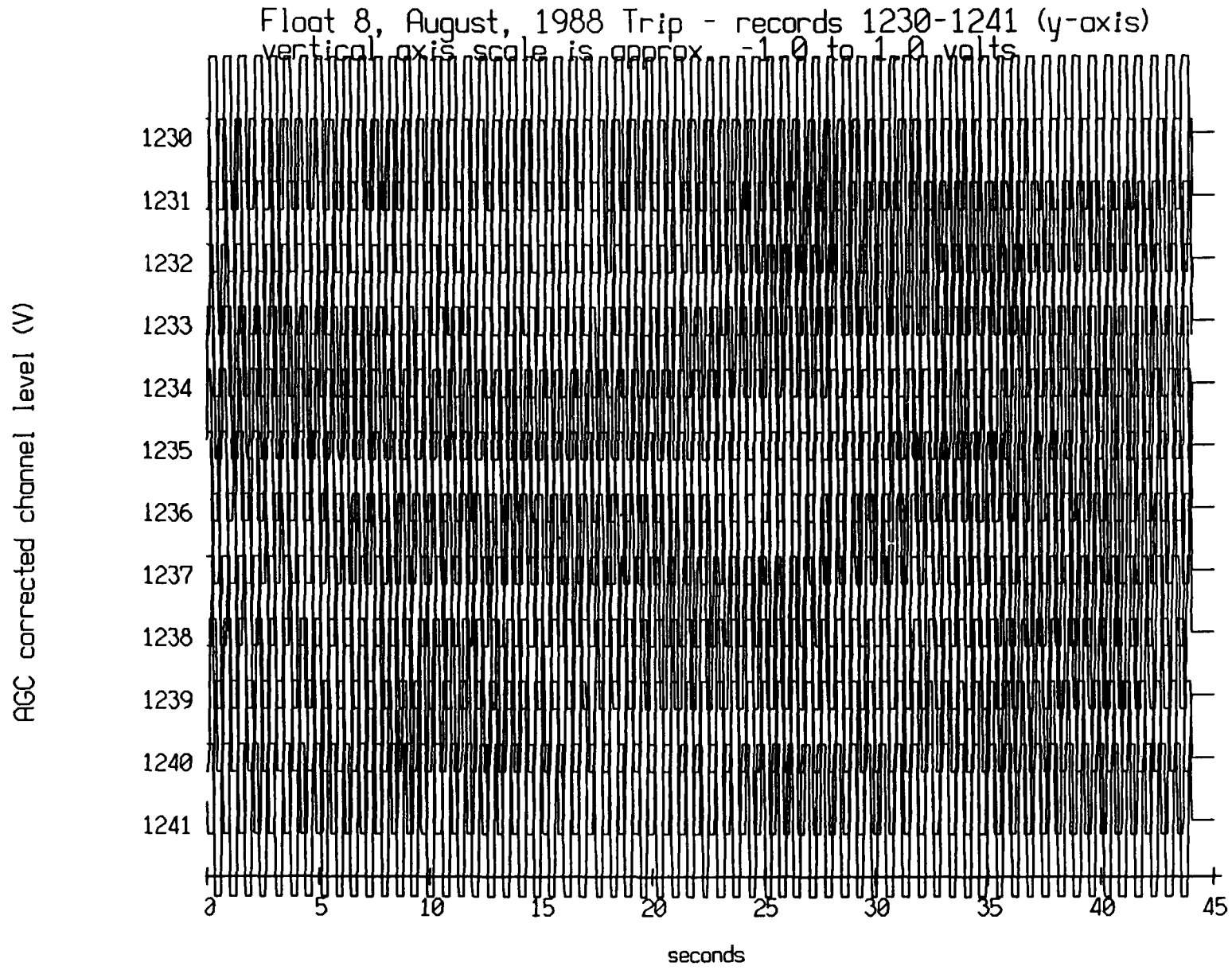


Figure XI.27b

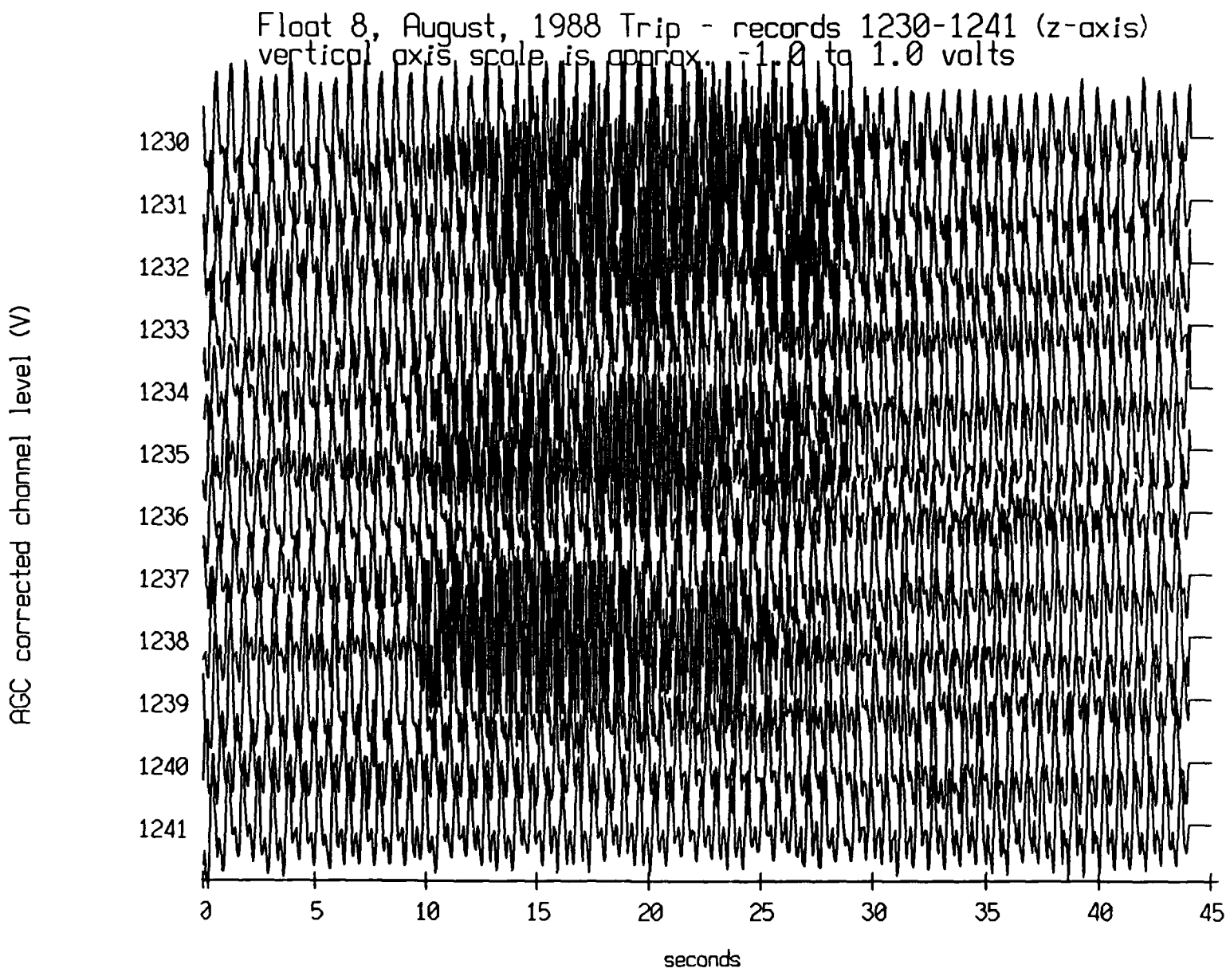


Figure XI.27c

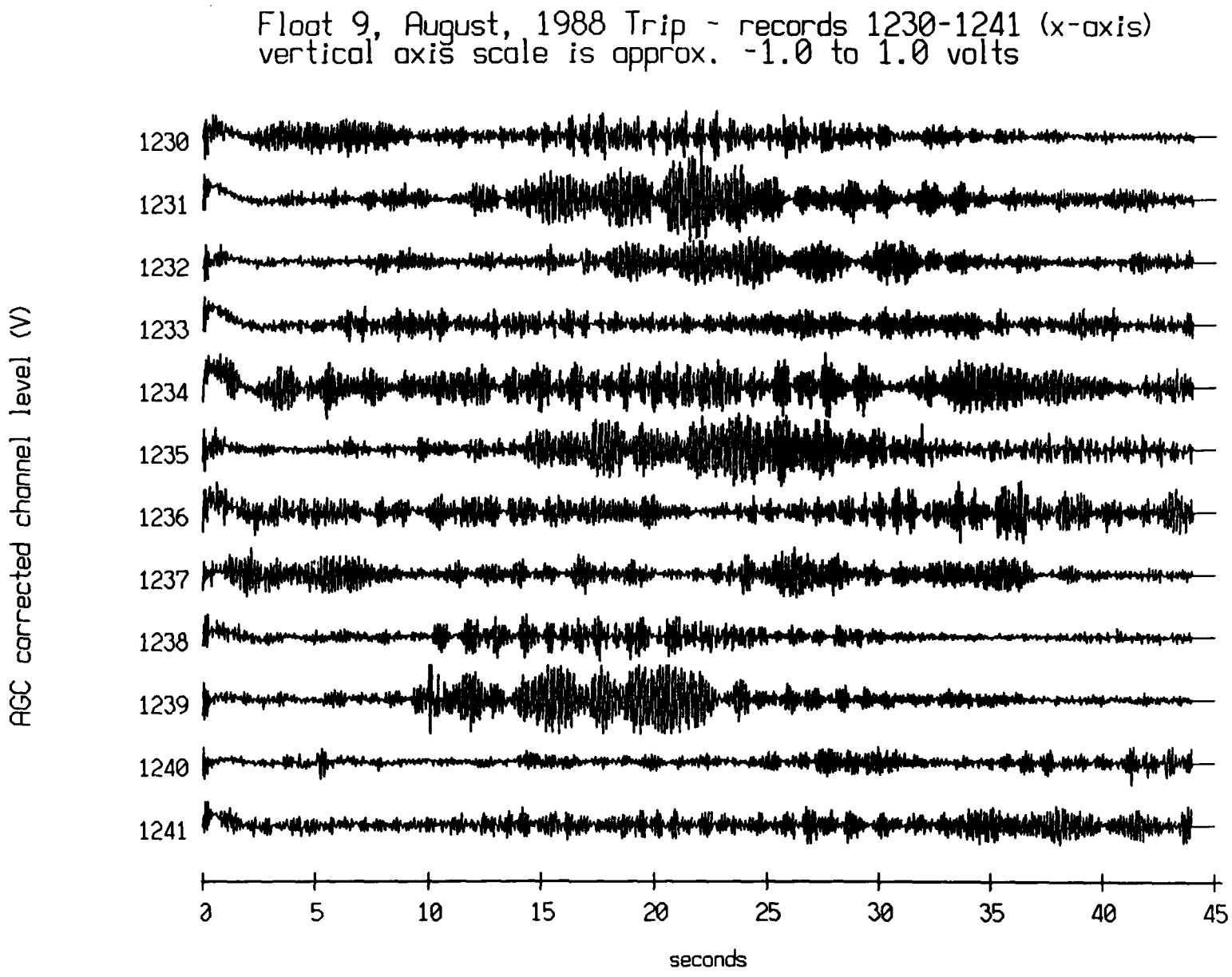


Figure XI.28a

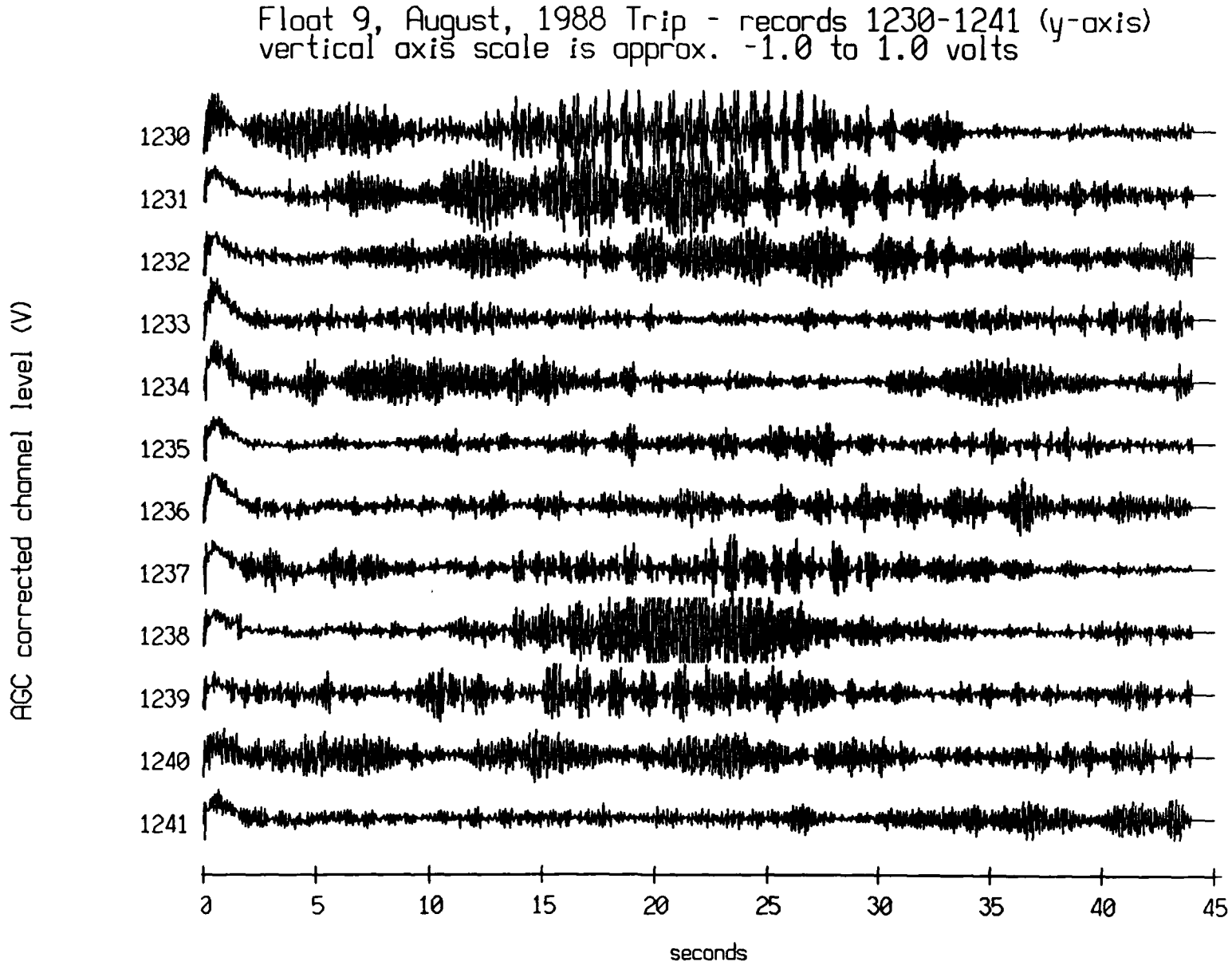


Figure XI.28b

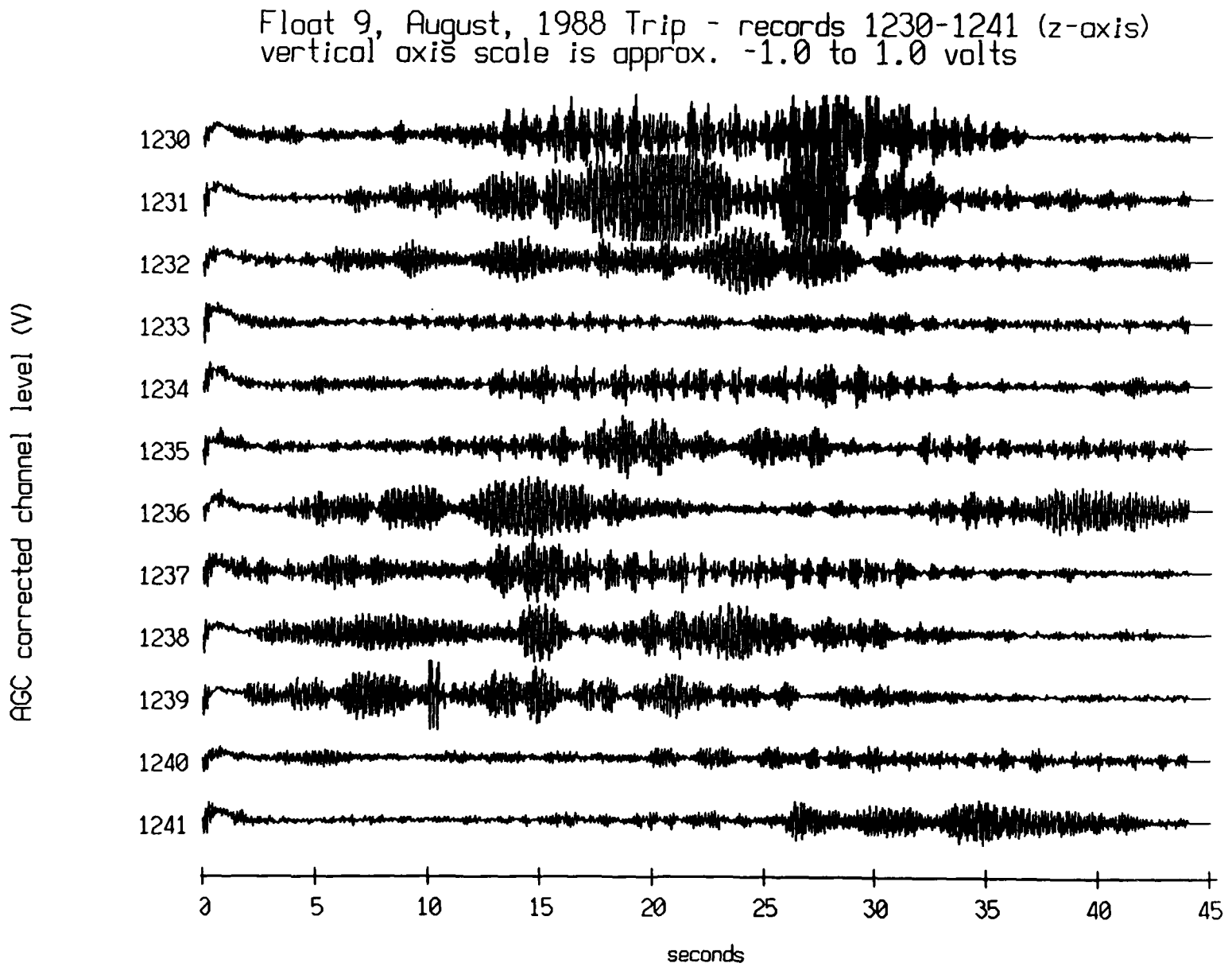


Figure XI.28c

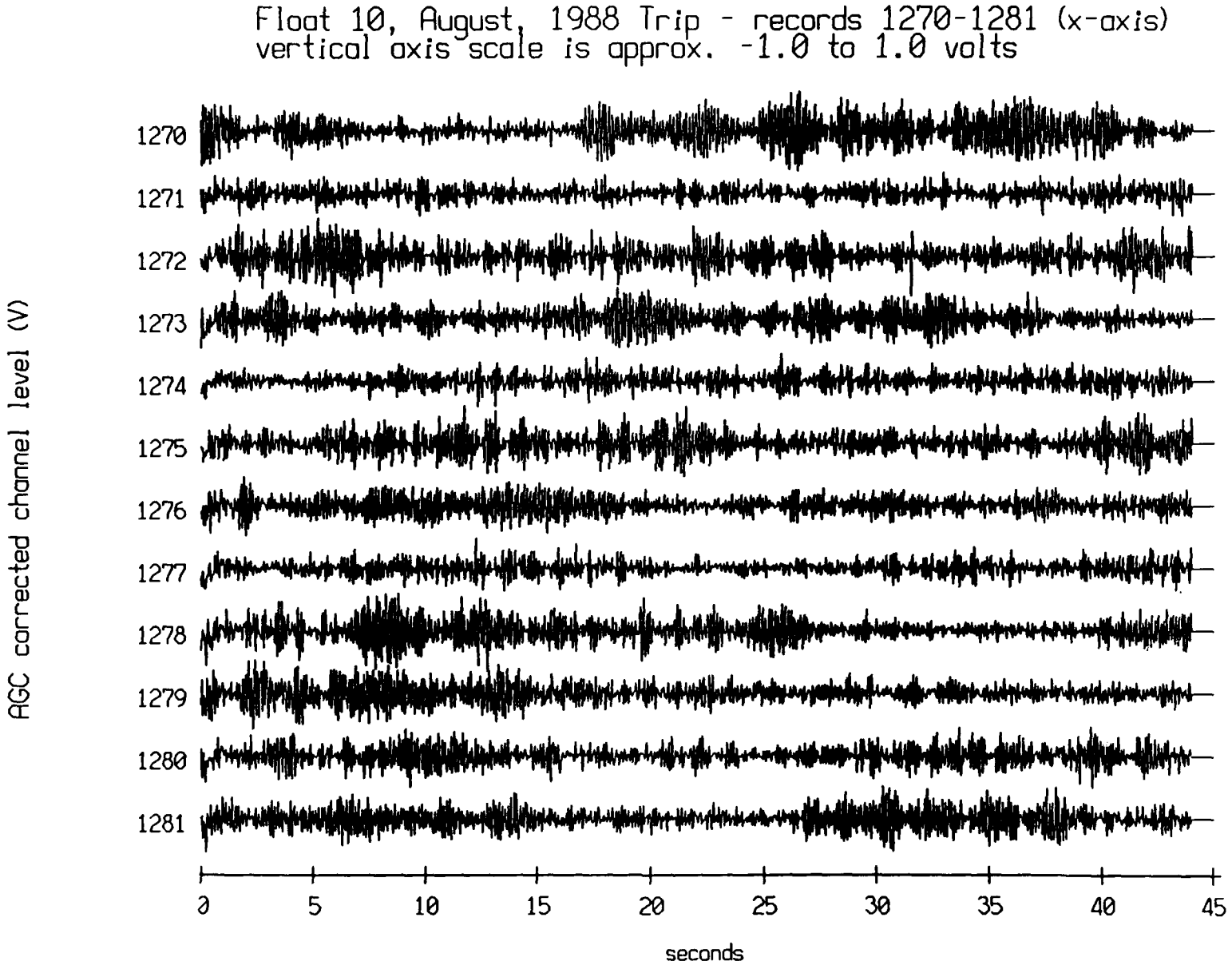


Figure XI.29a

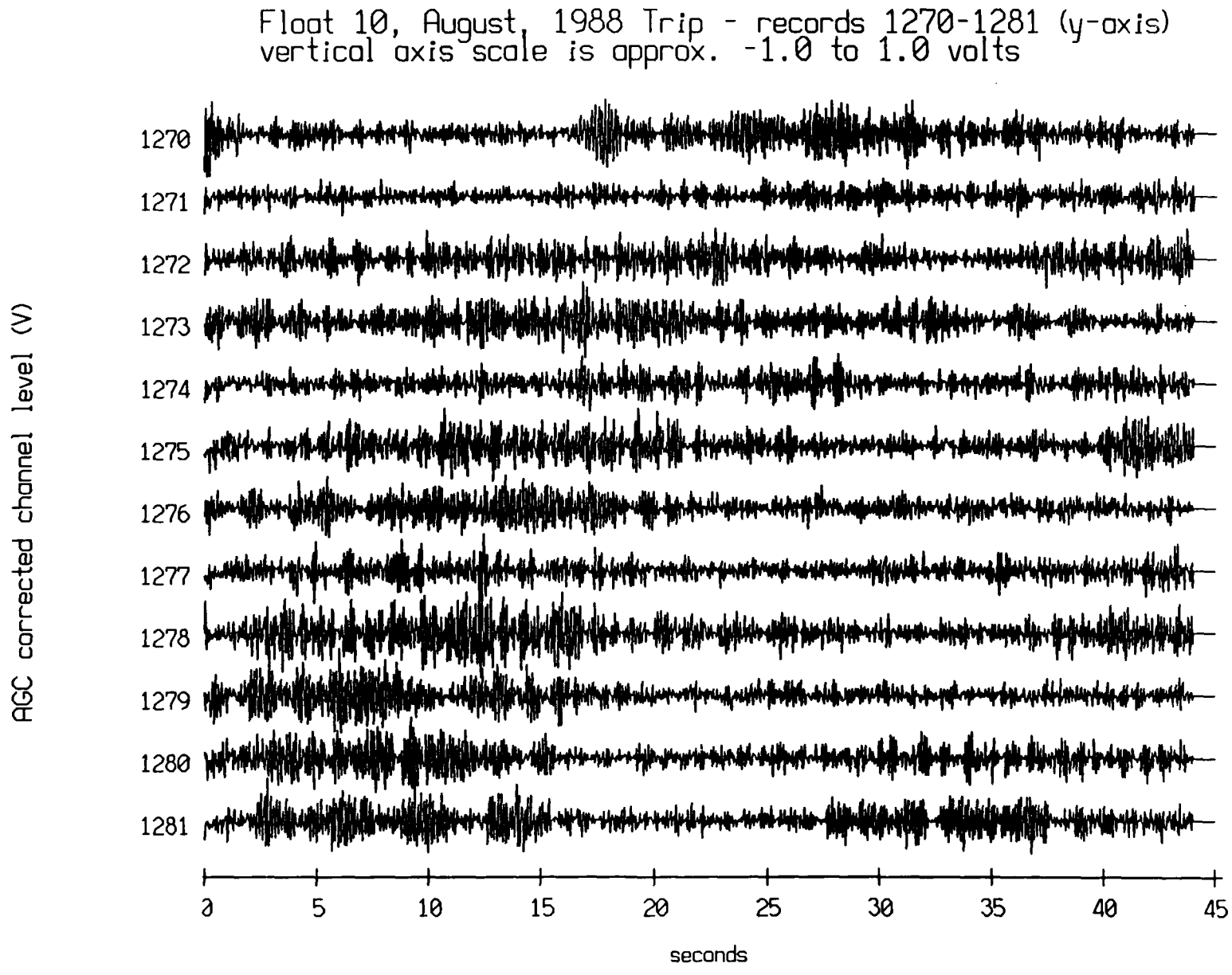


Figure XI.29b

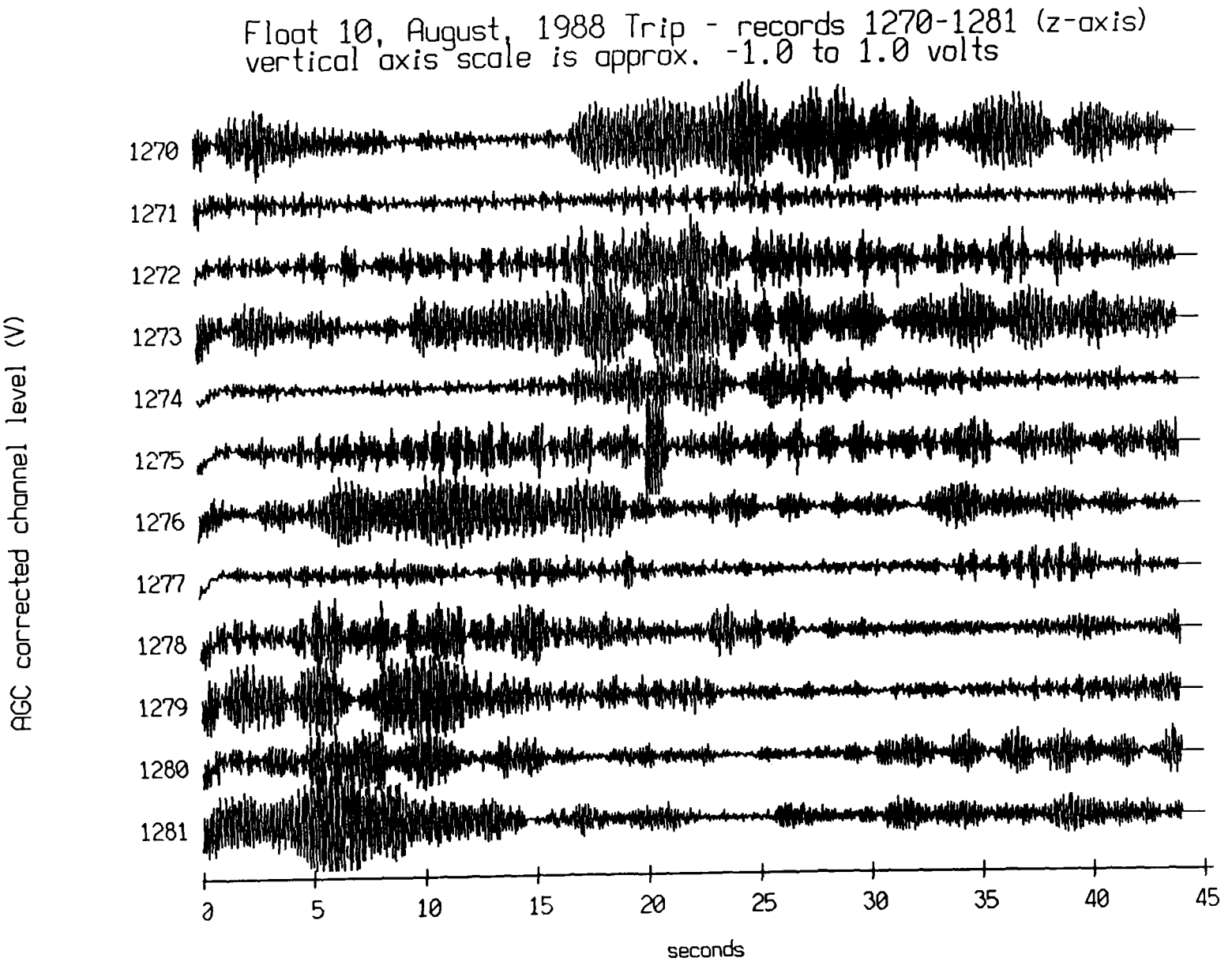


Figure XI.29c

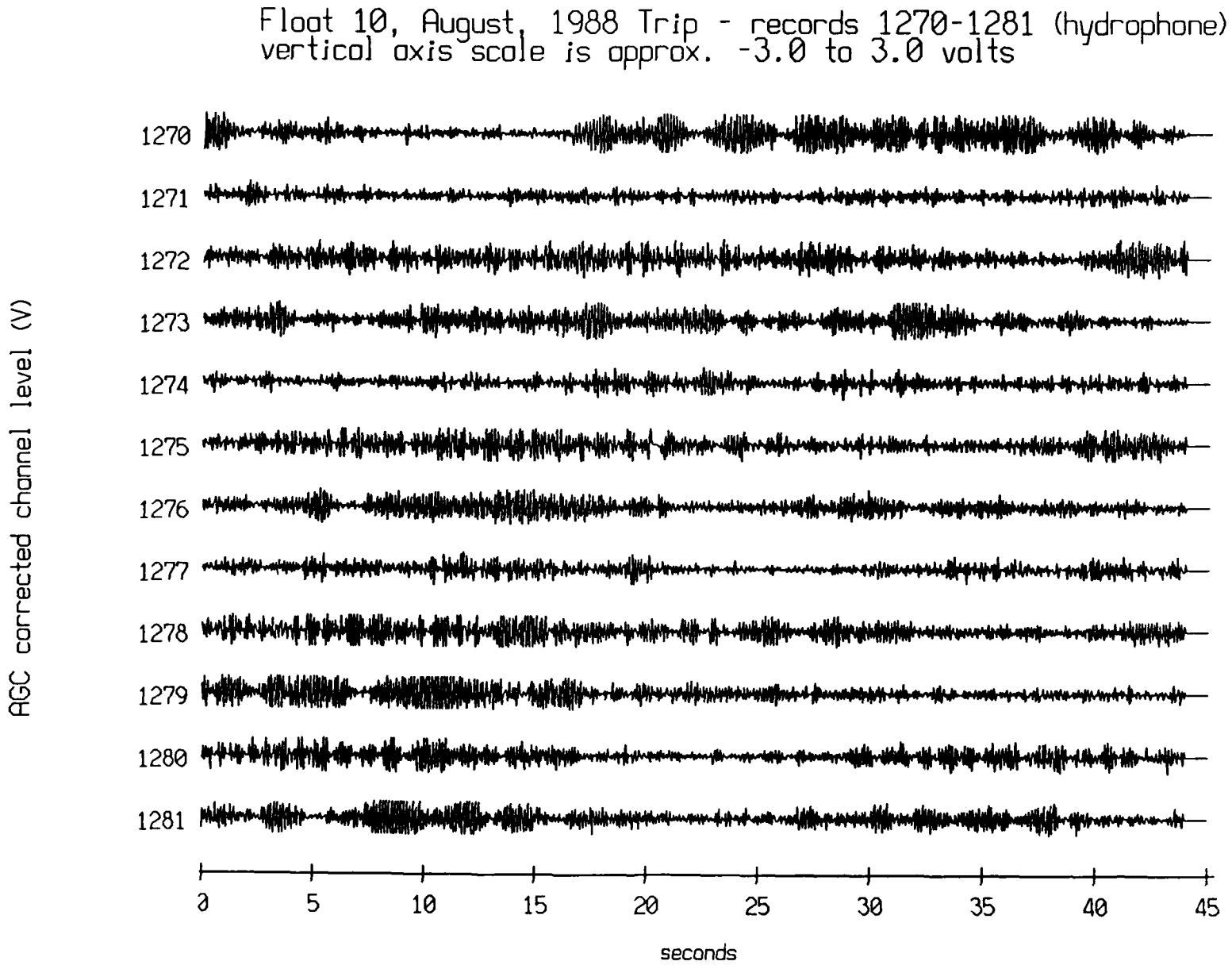


Figure XI.29d

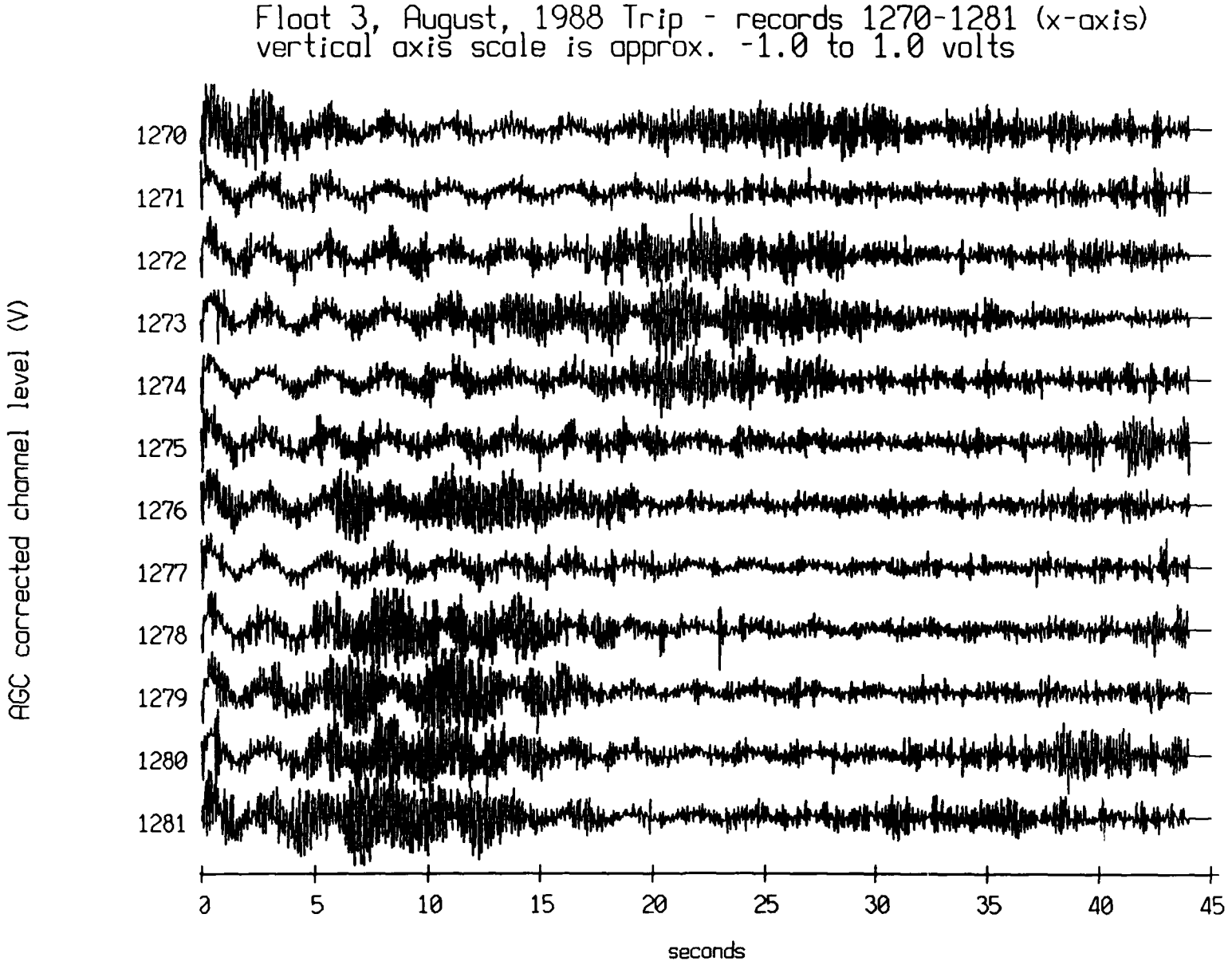


Figure XI.30a

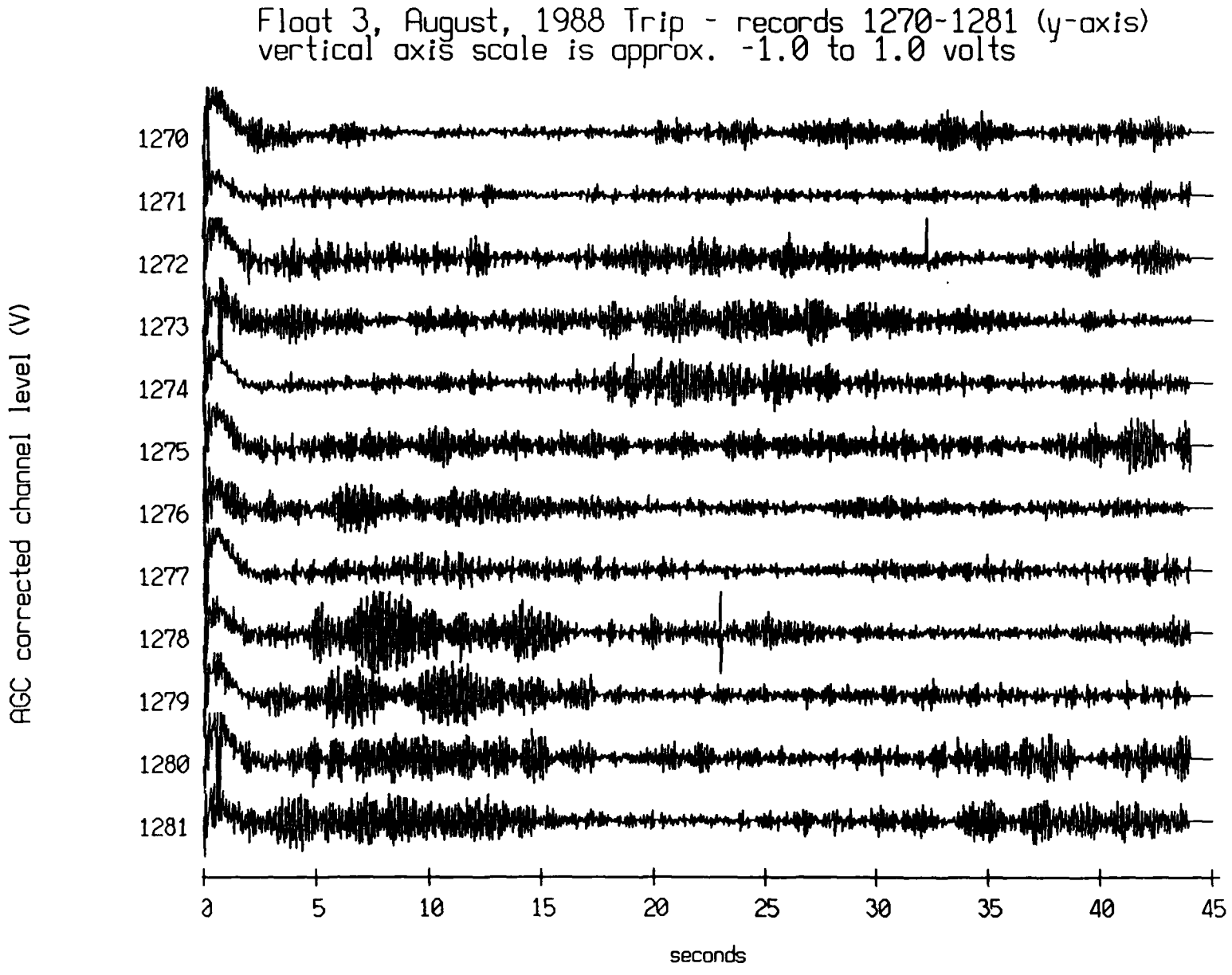


Figure XI.30b

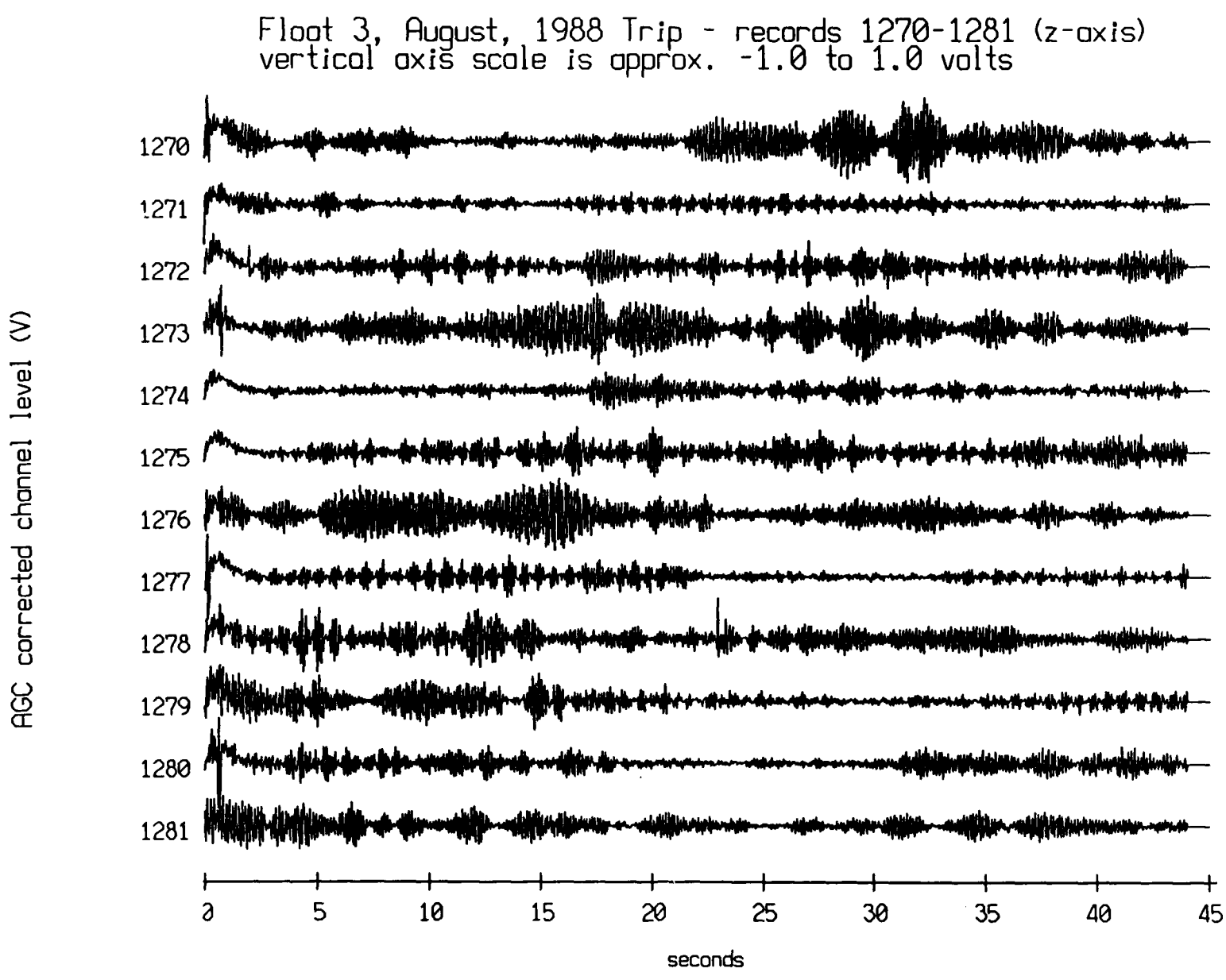


Figure X1.30c

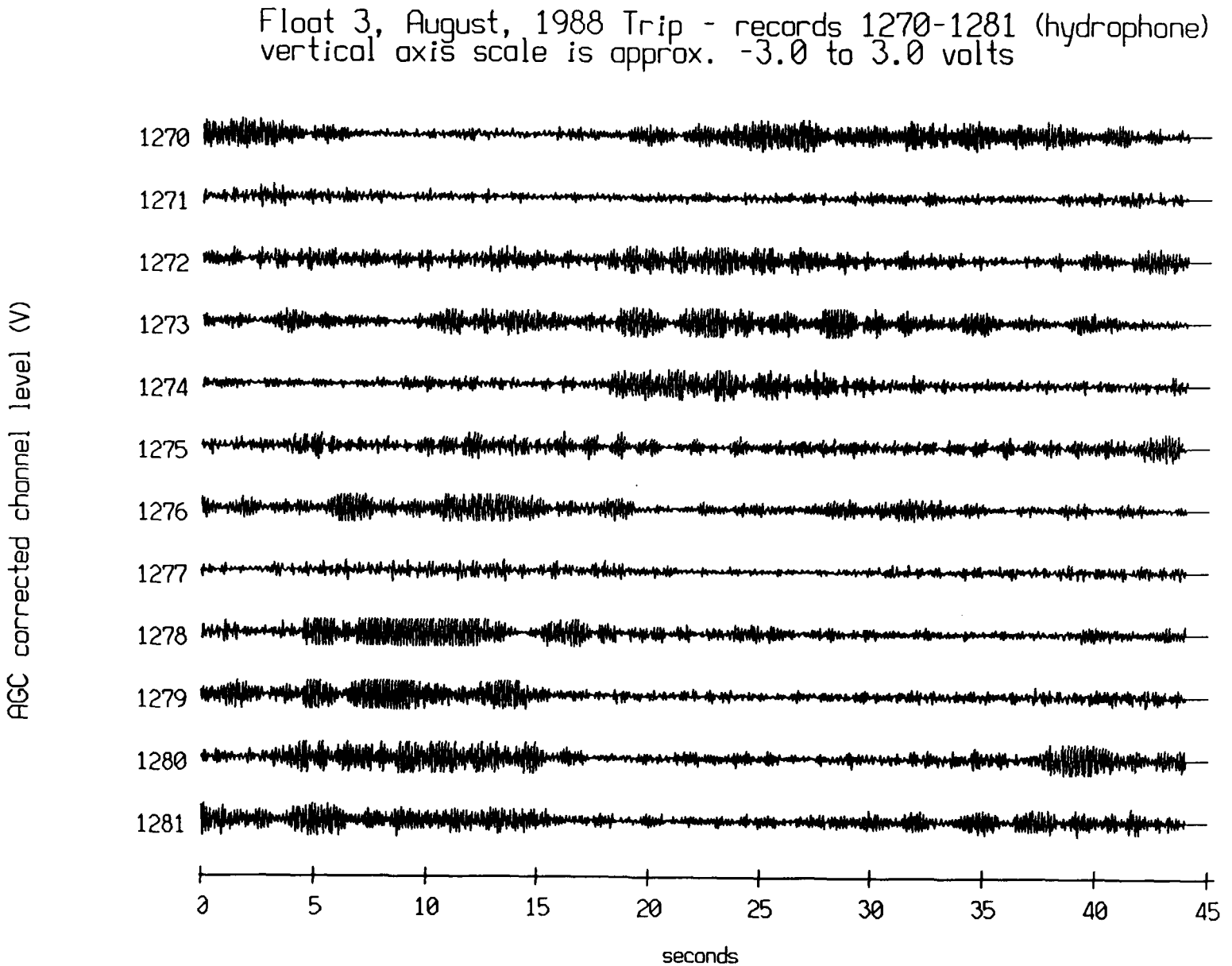


Figure XI.30d

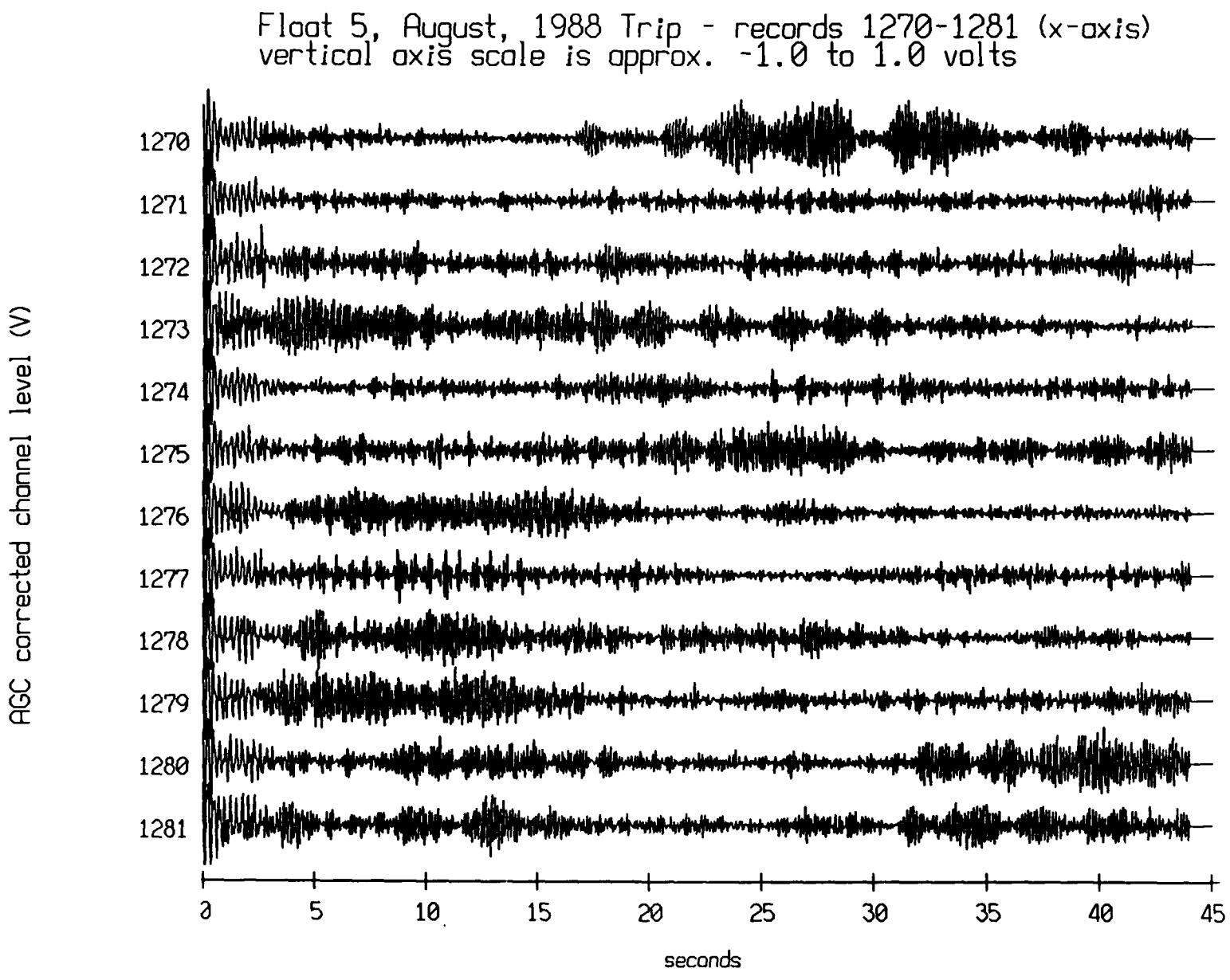


Figure XI.31a

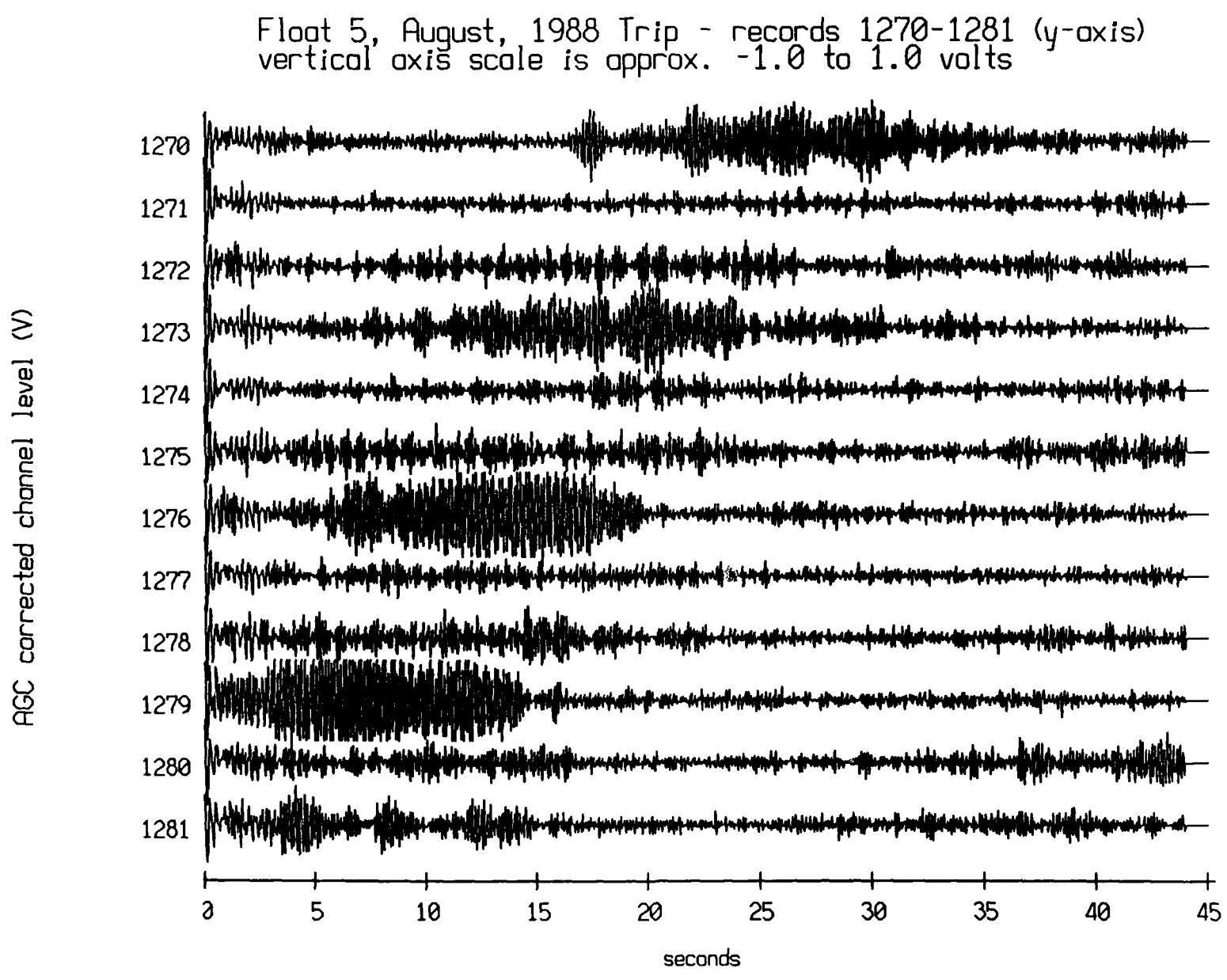


Figure XI.31b

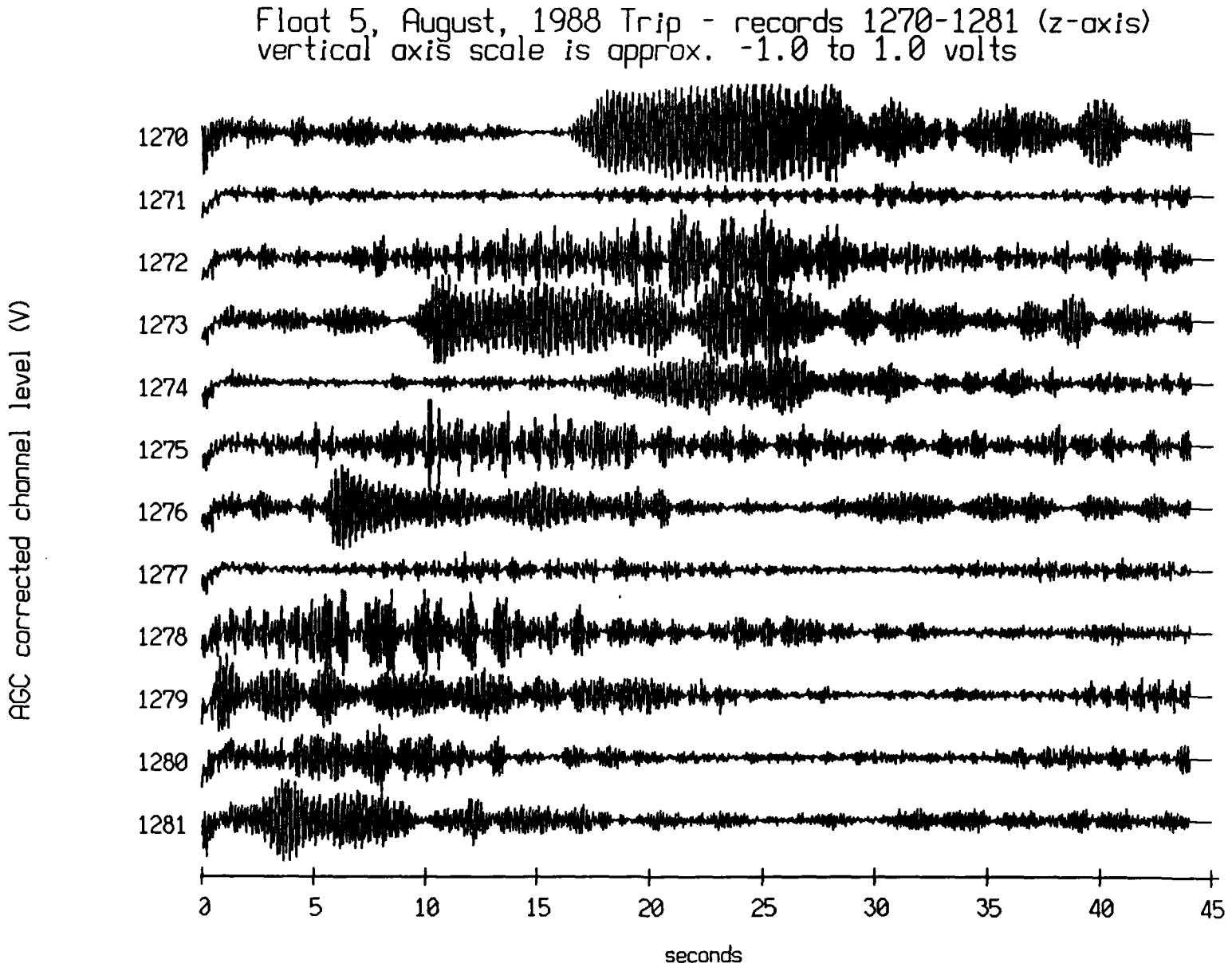


Figure XI.31c

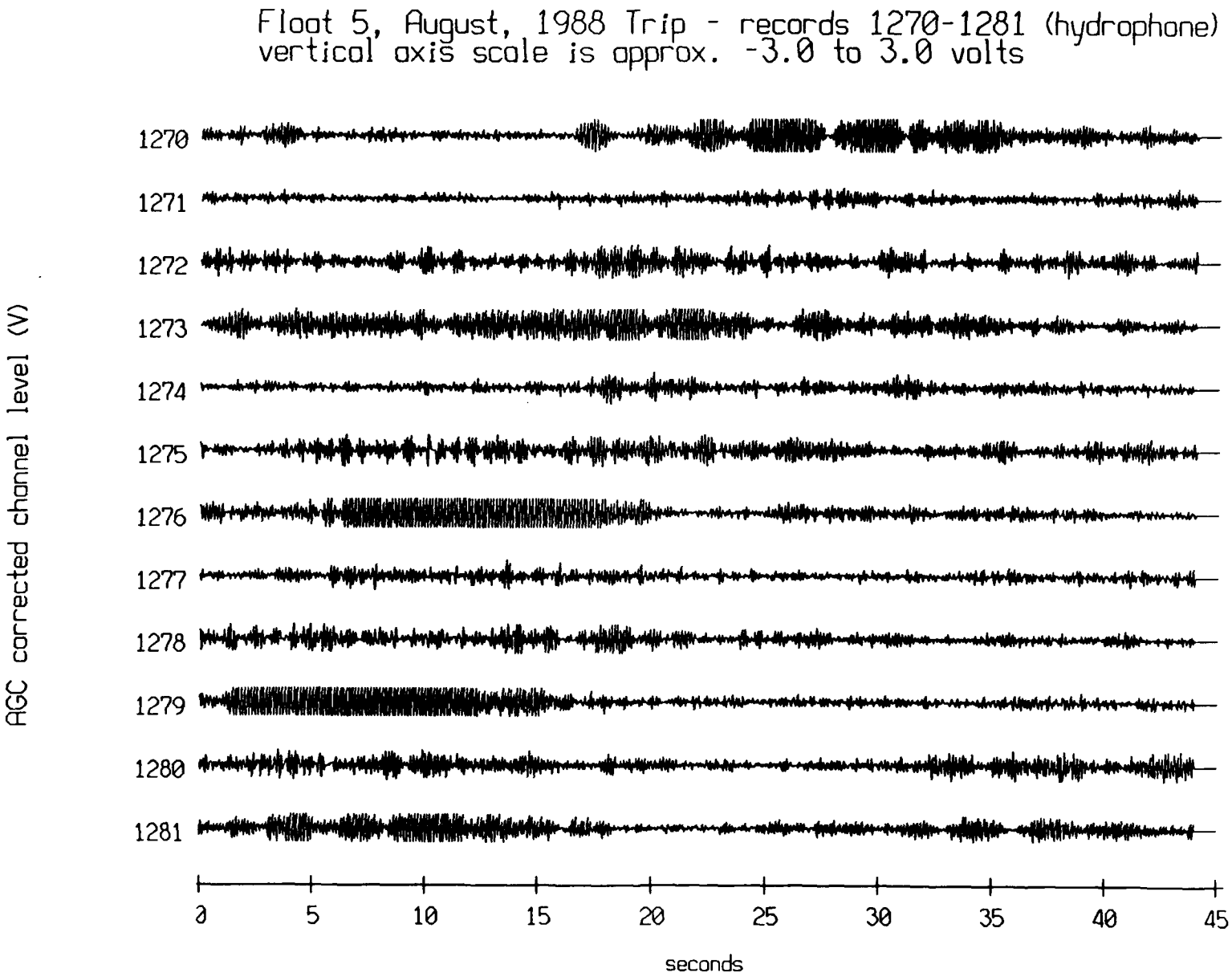


Figure XI.31d

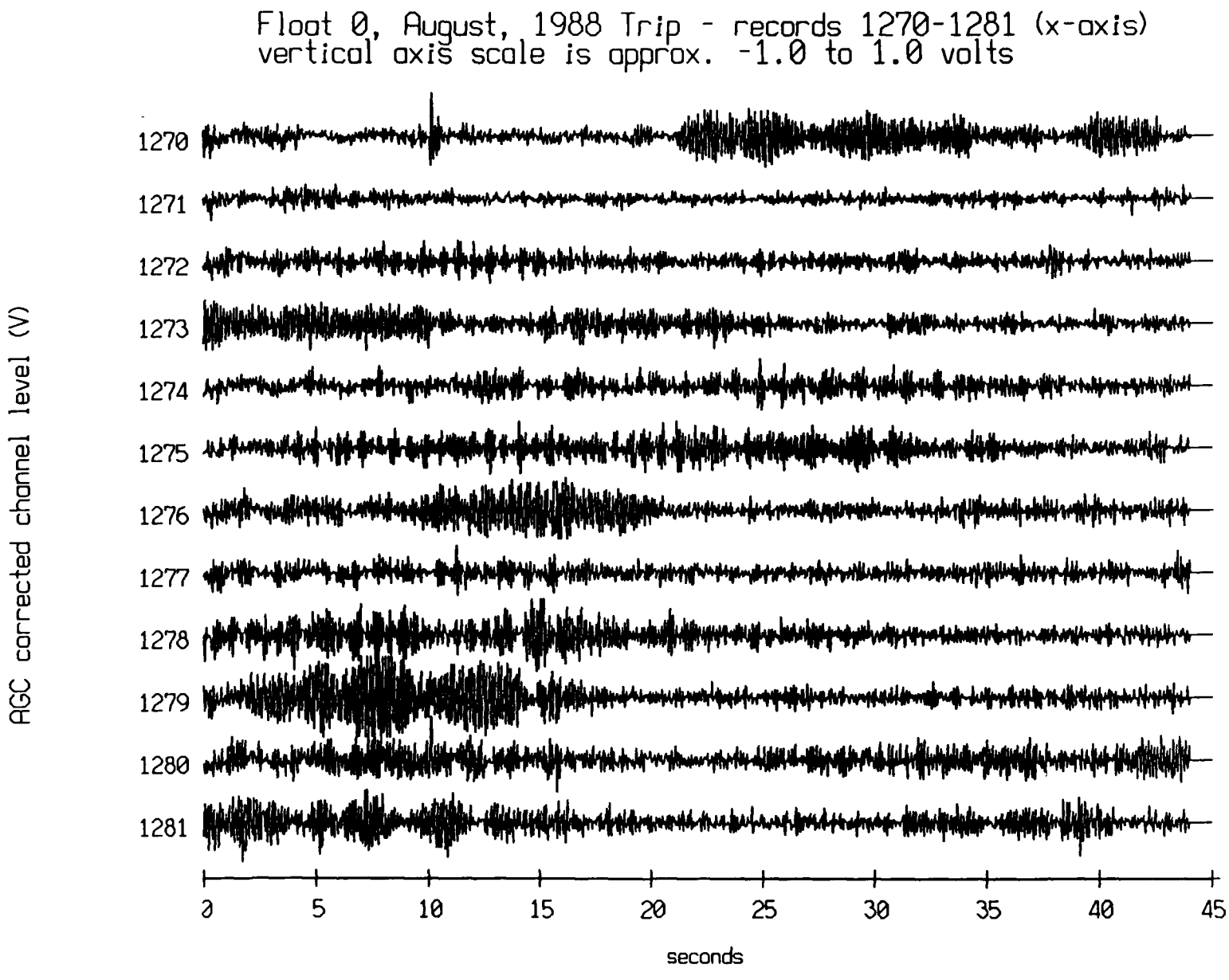


Figure XI.32a

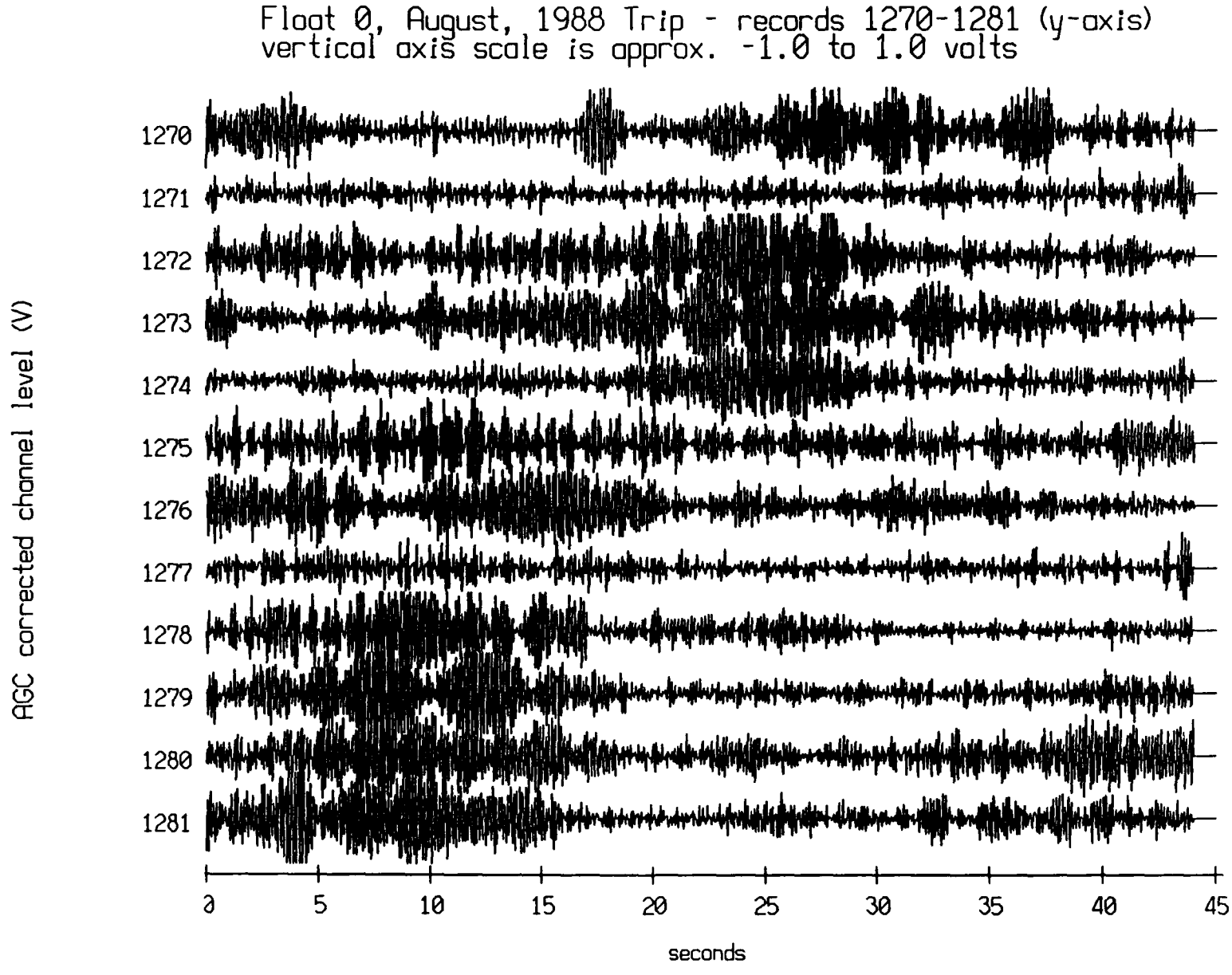


Figure XI.32b

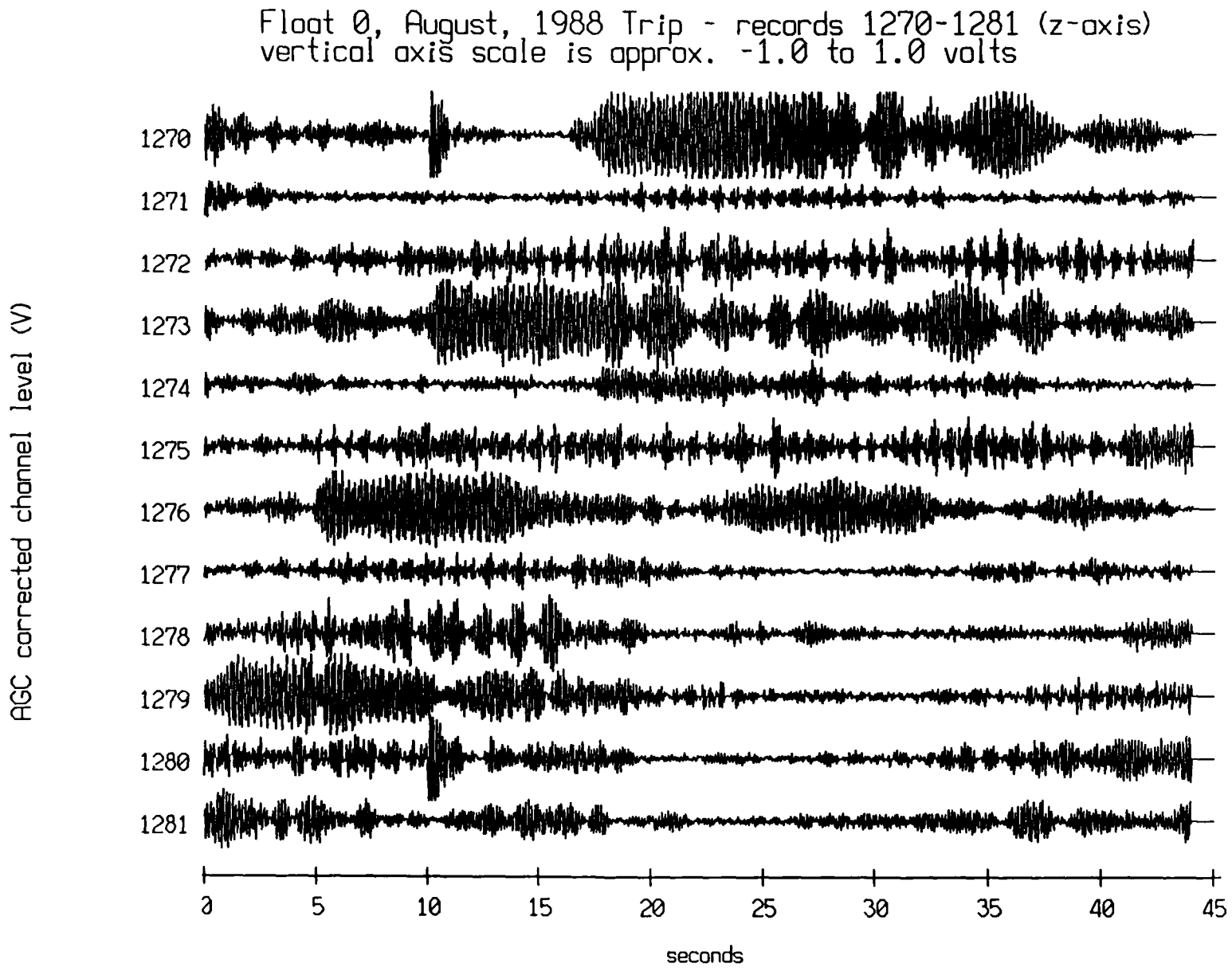


Figure XI.32c

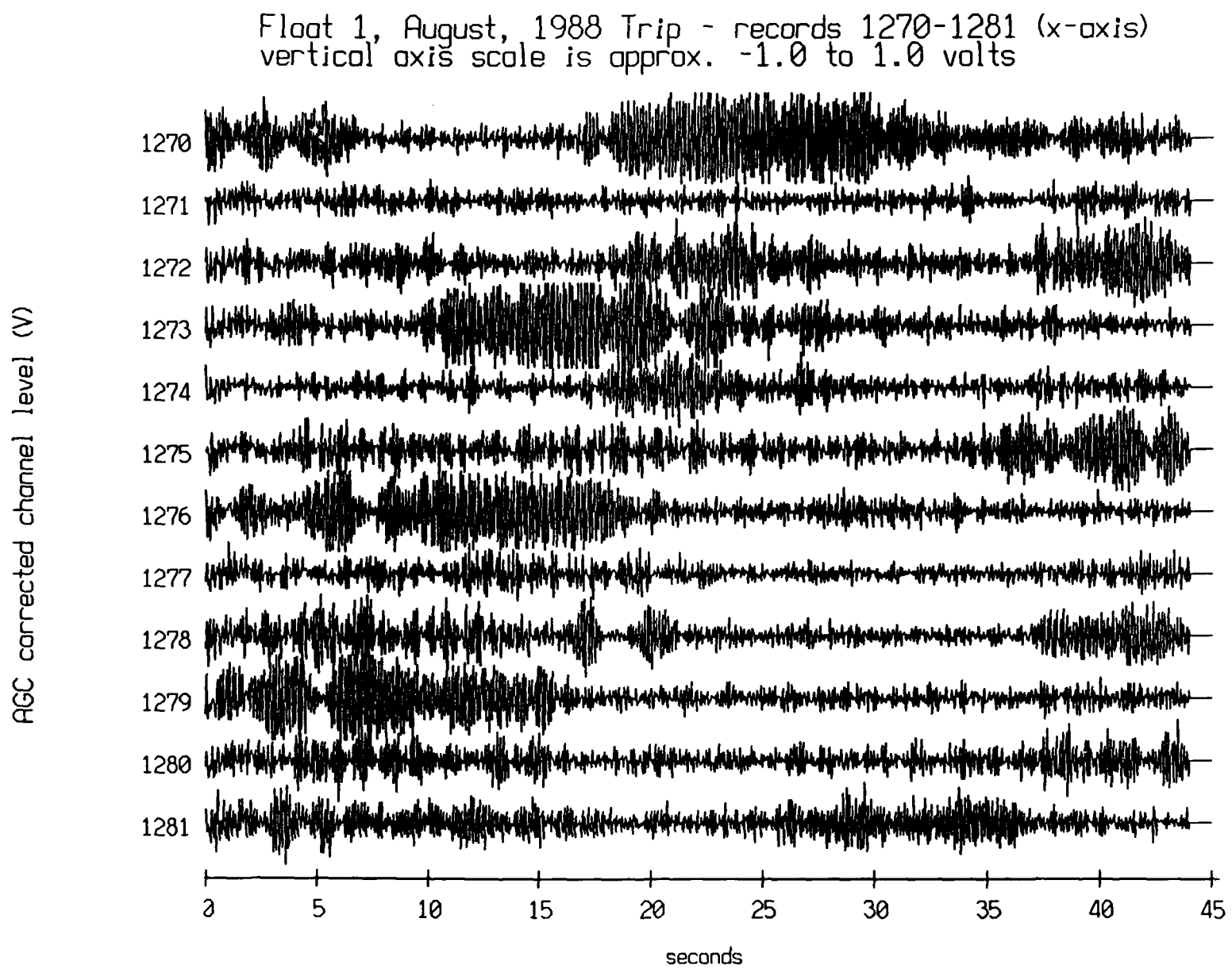


Figure XI.33a

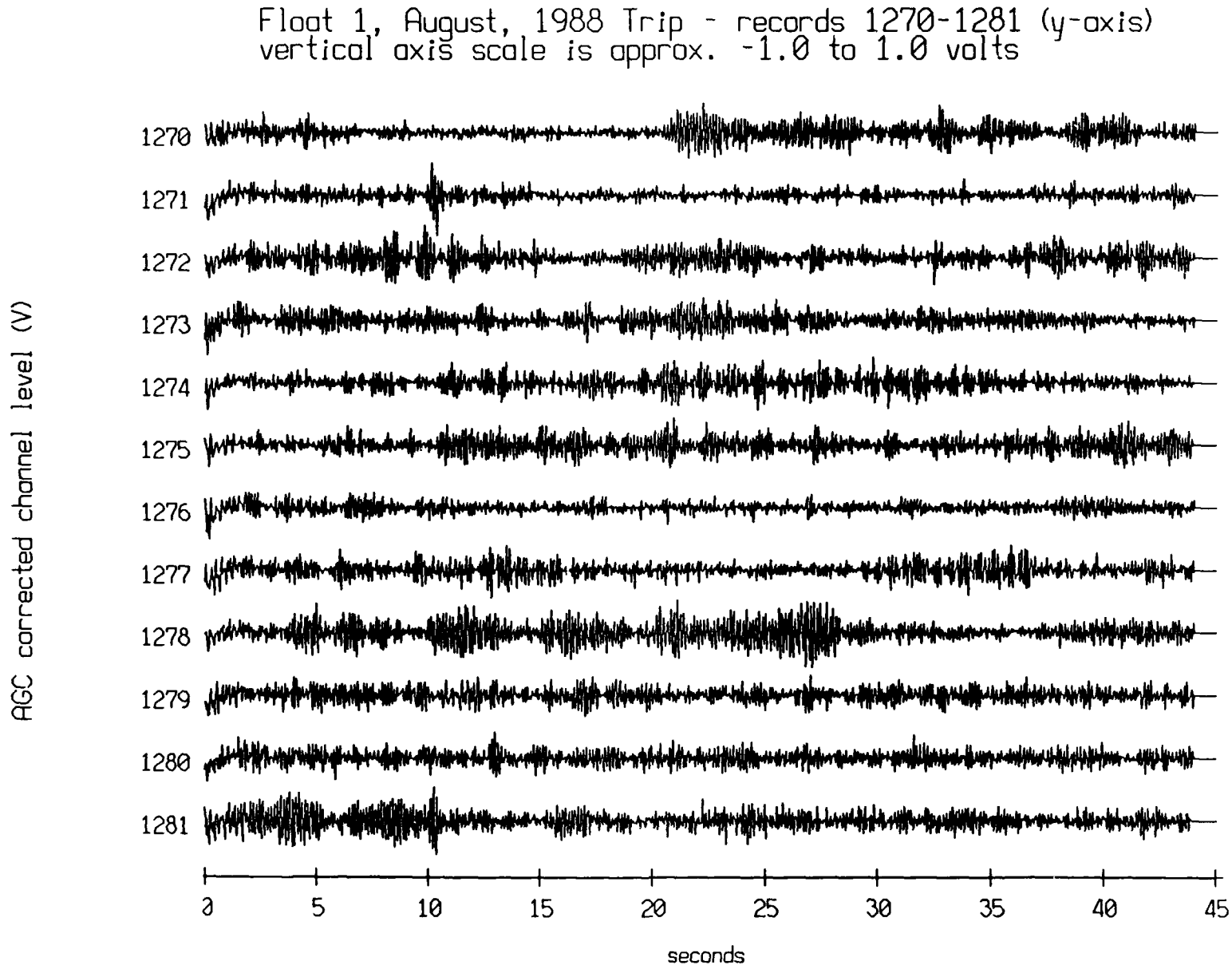


Figure XI.33b

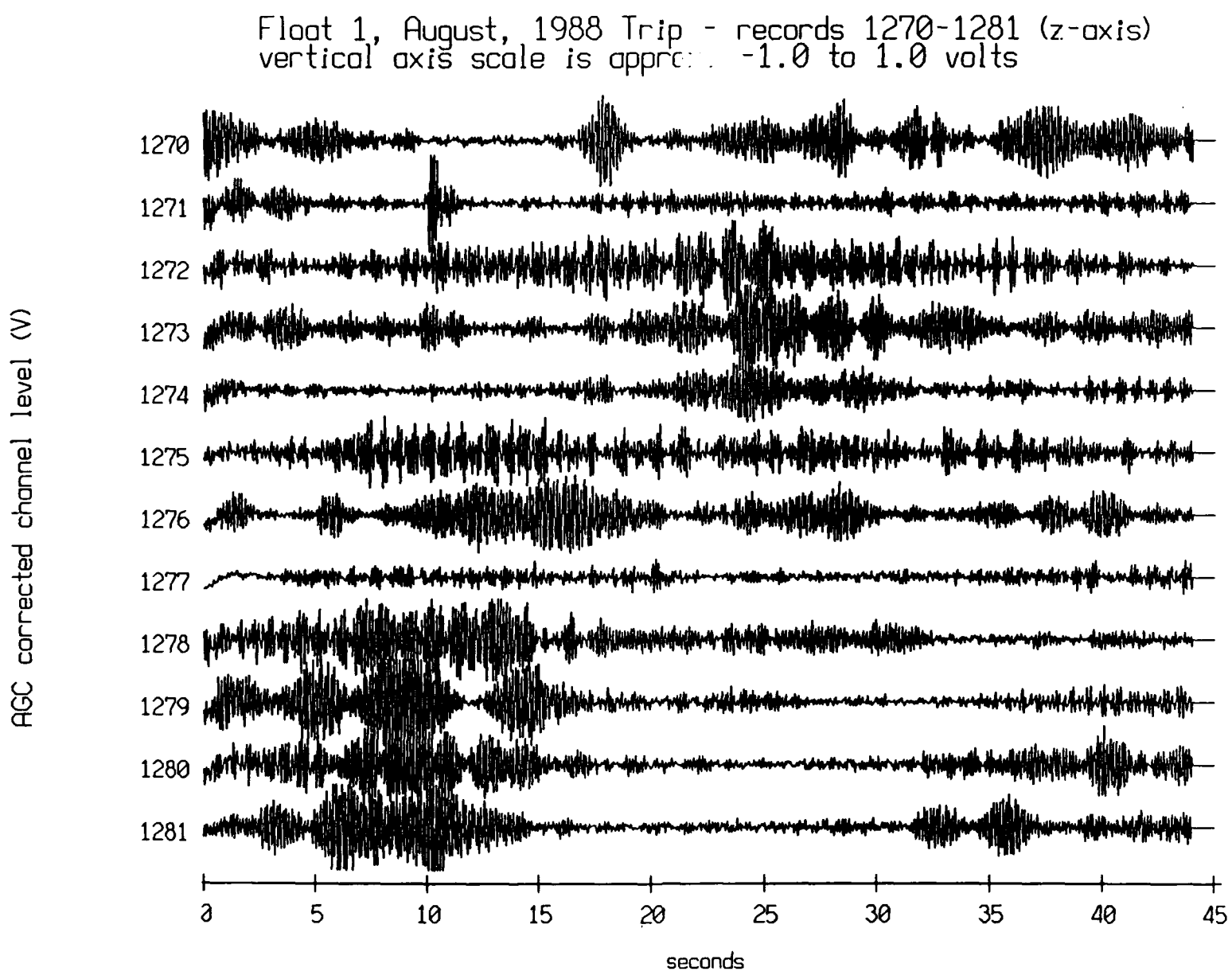


Figure XI.33c

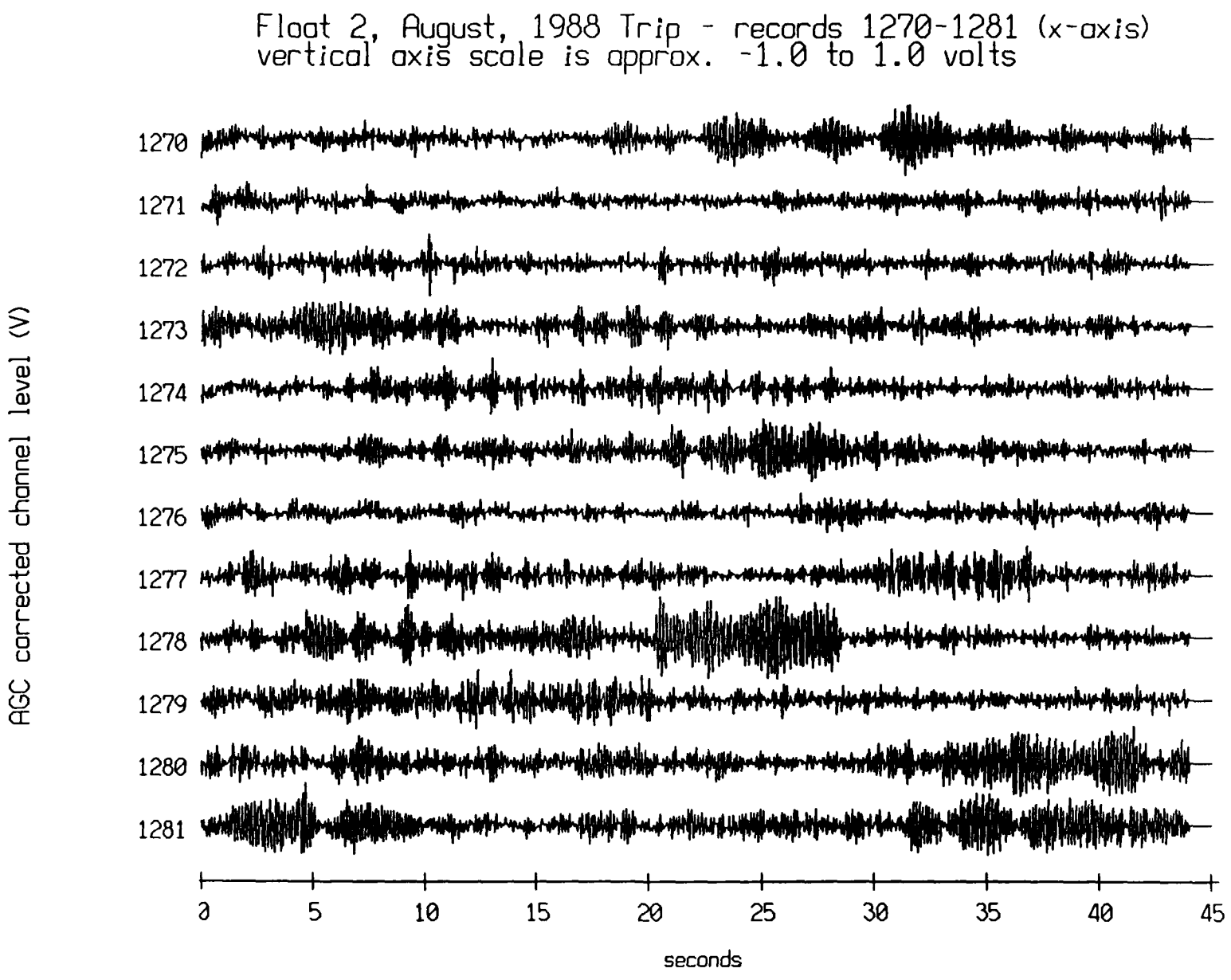


Figure XI.31a

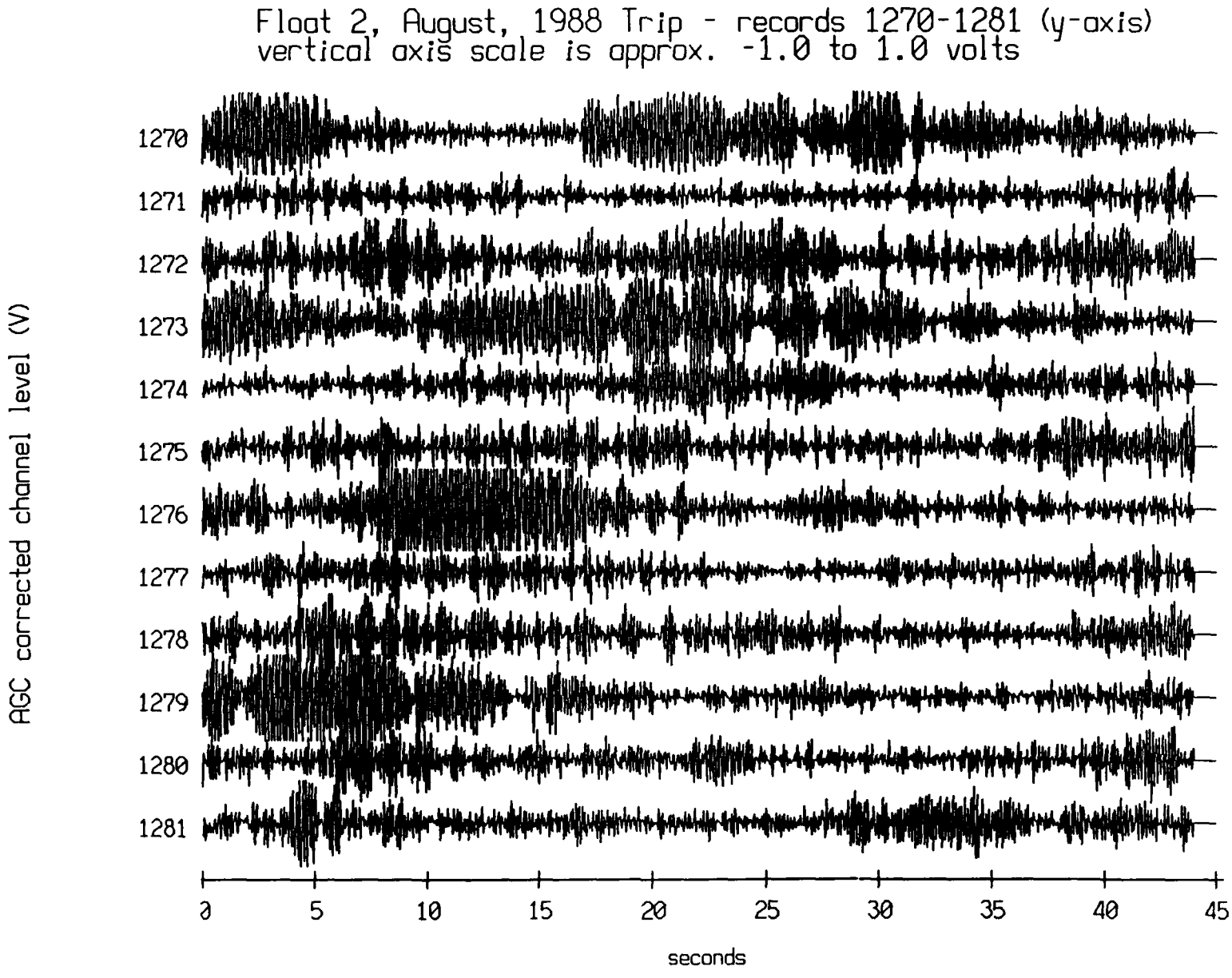


Figure XI.34b

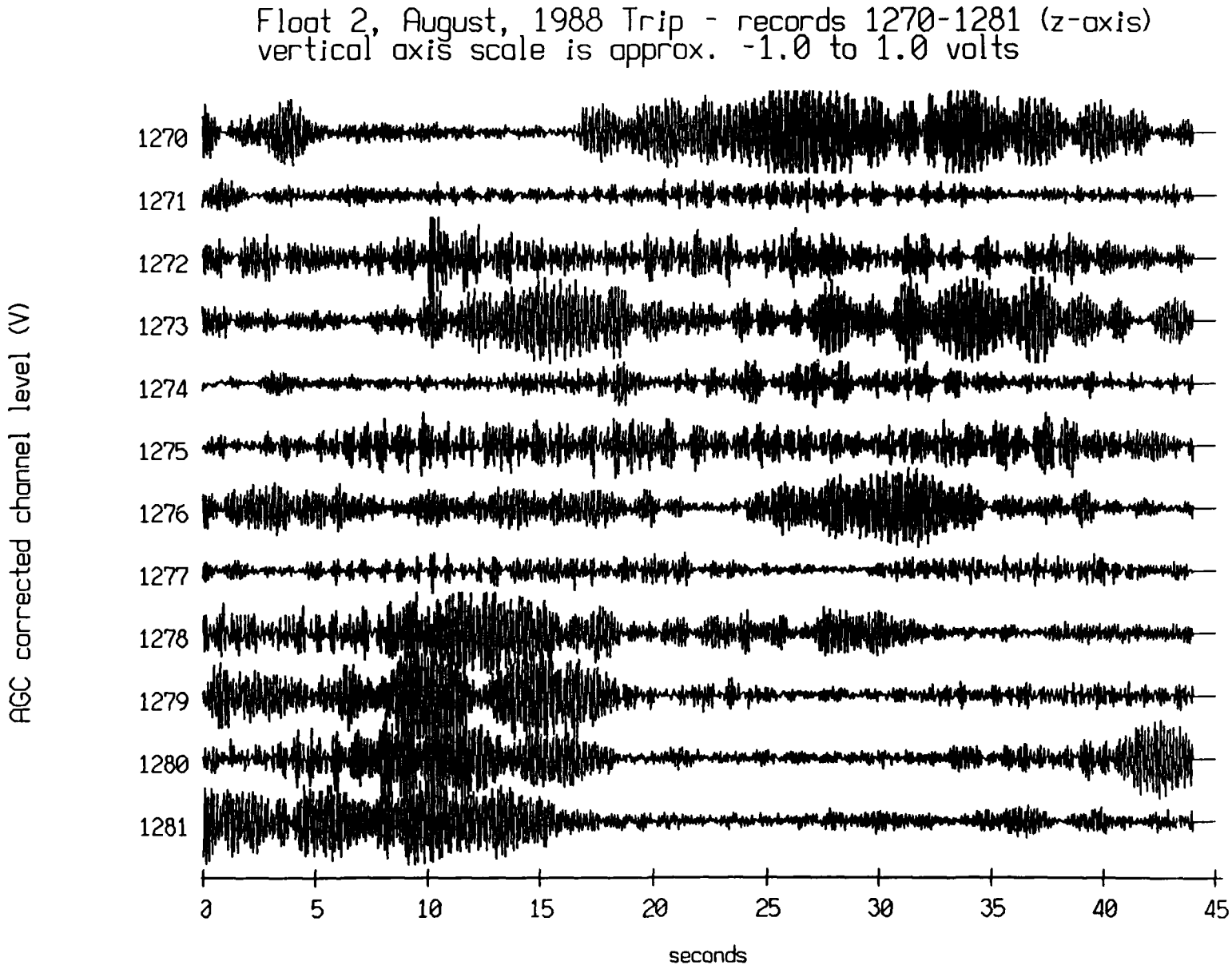


Figure XI.34c

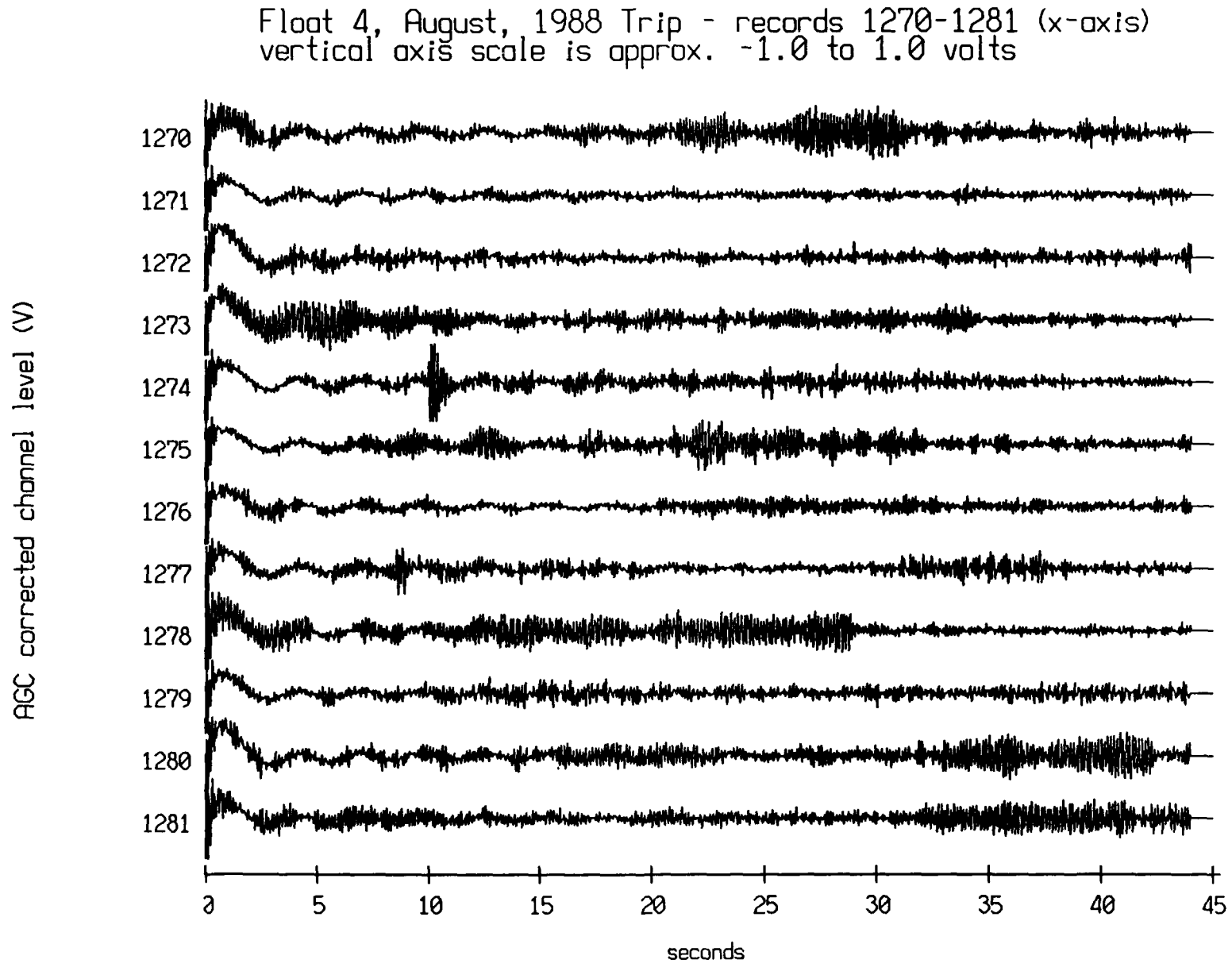


Figure XI.35a

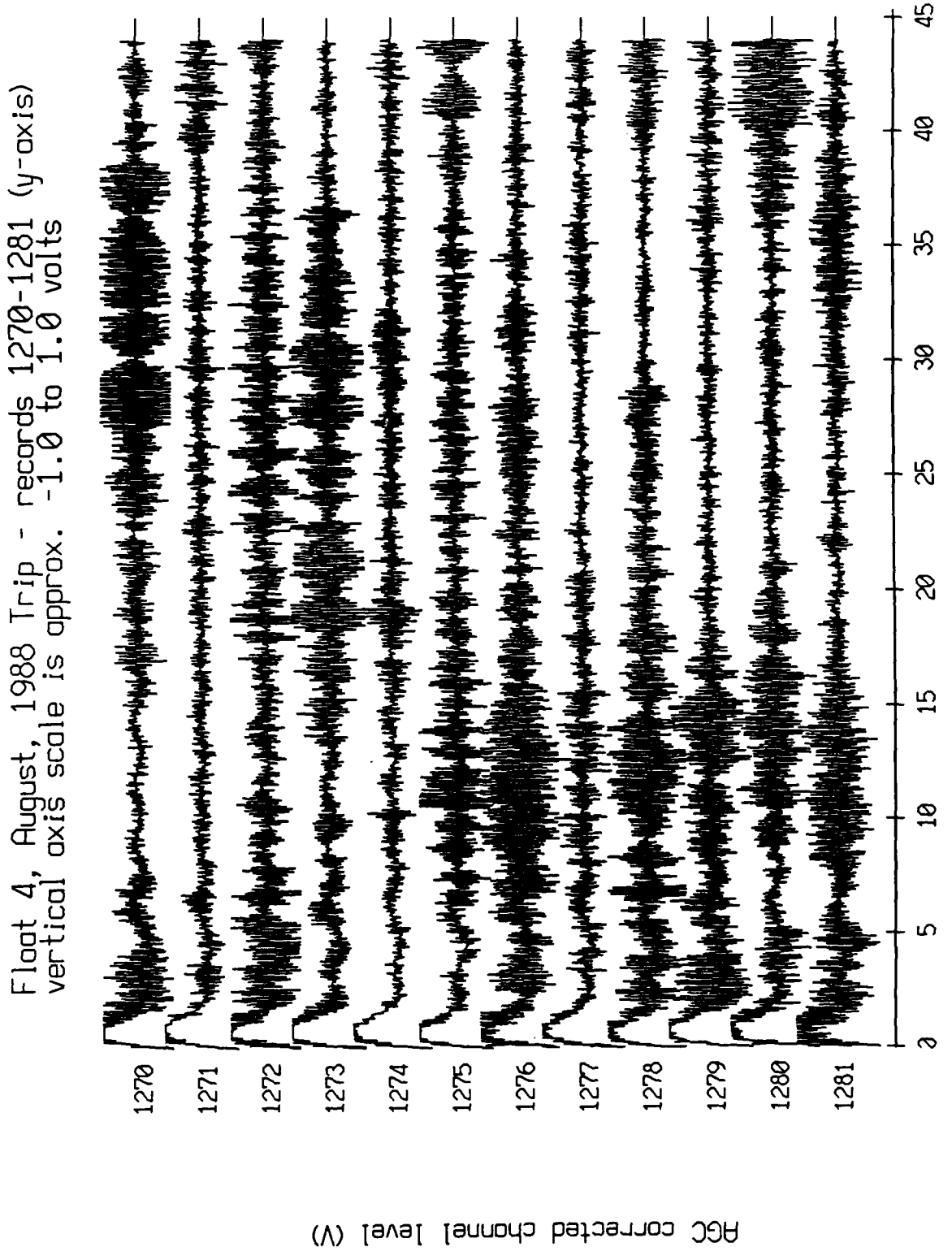


Figure XI.35b

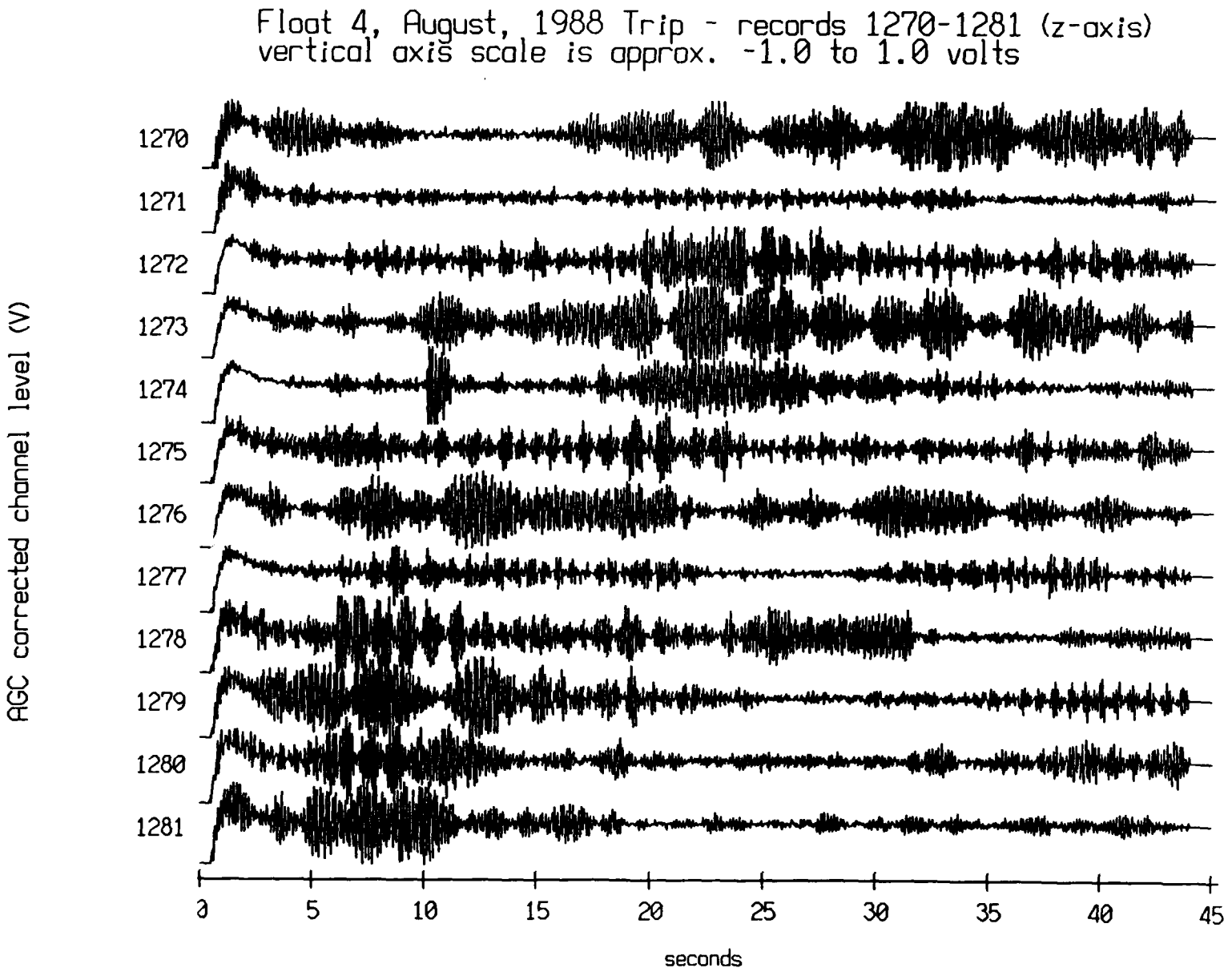


Figure XI.35c

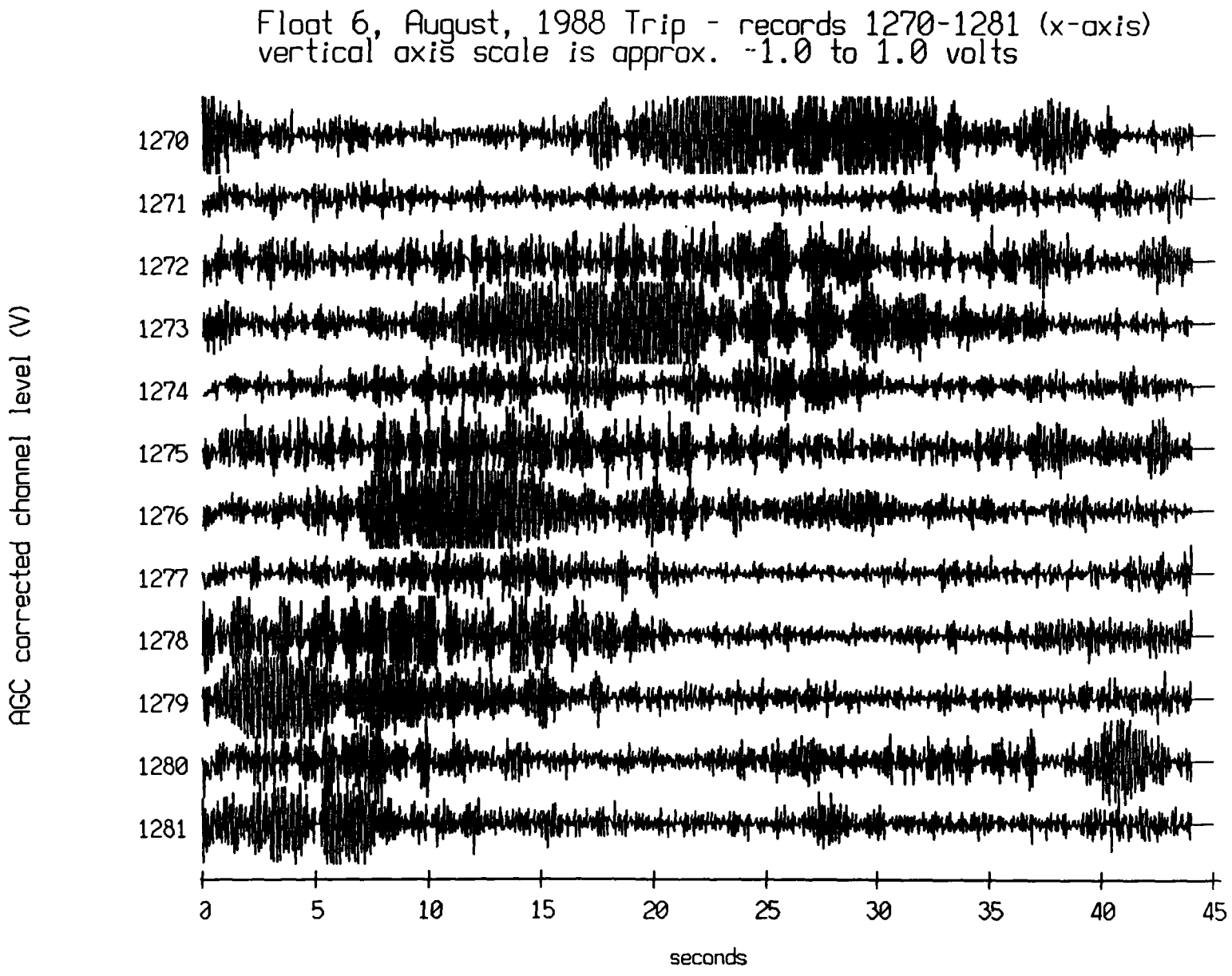


Figure XI.36a

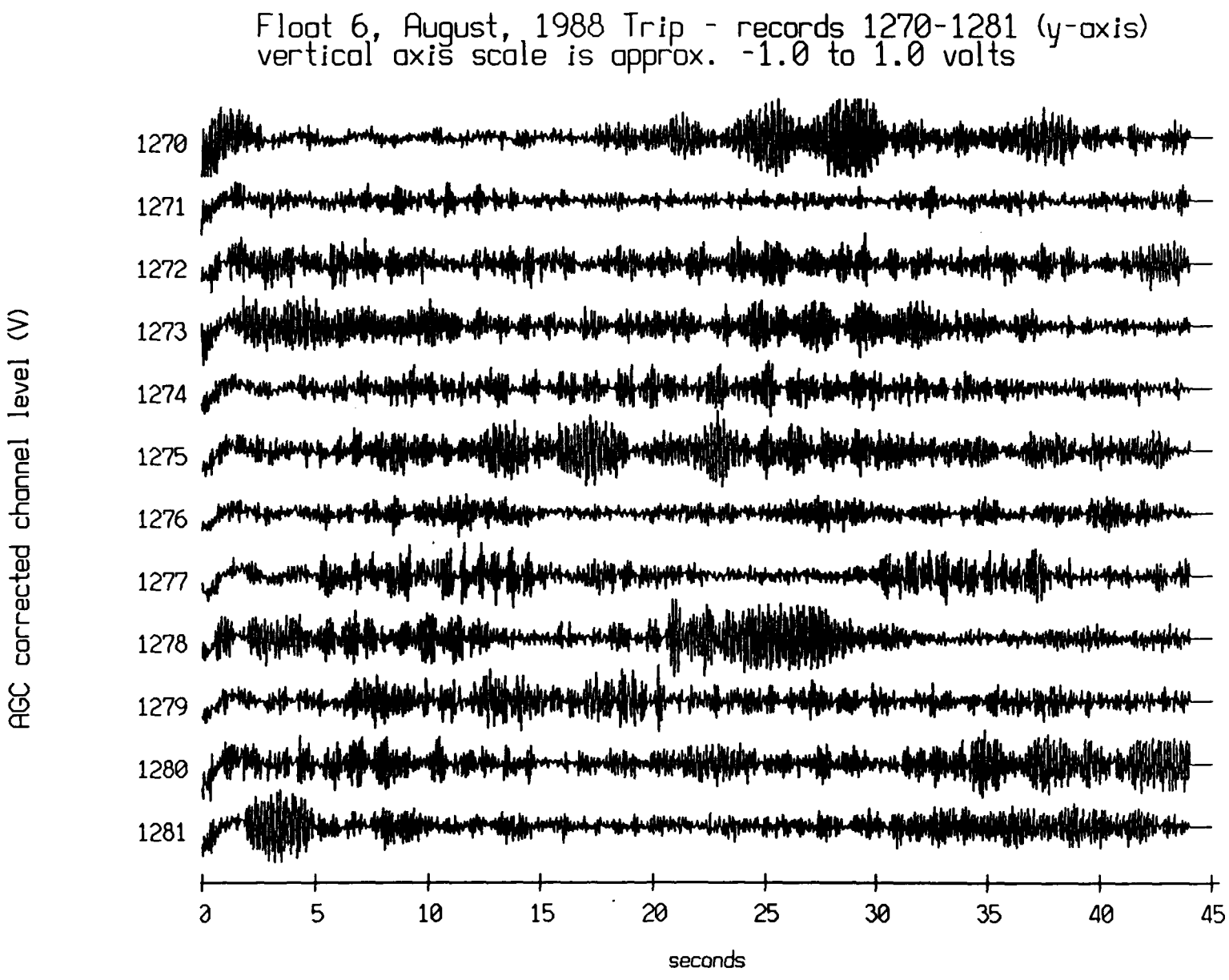


Figure XI.36b

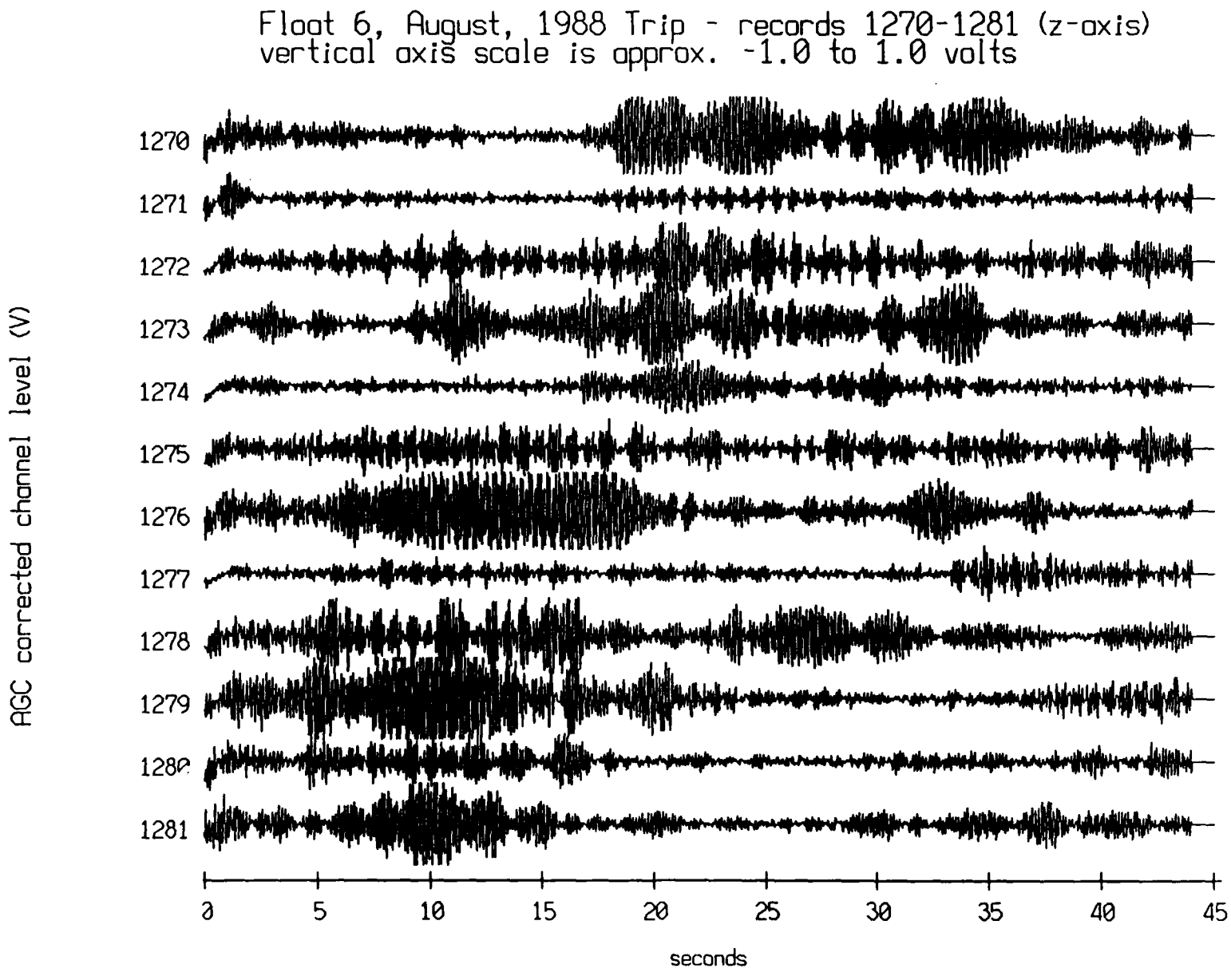


Figure XI.36c

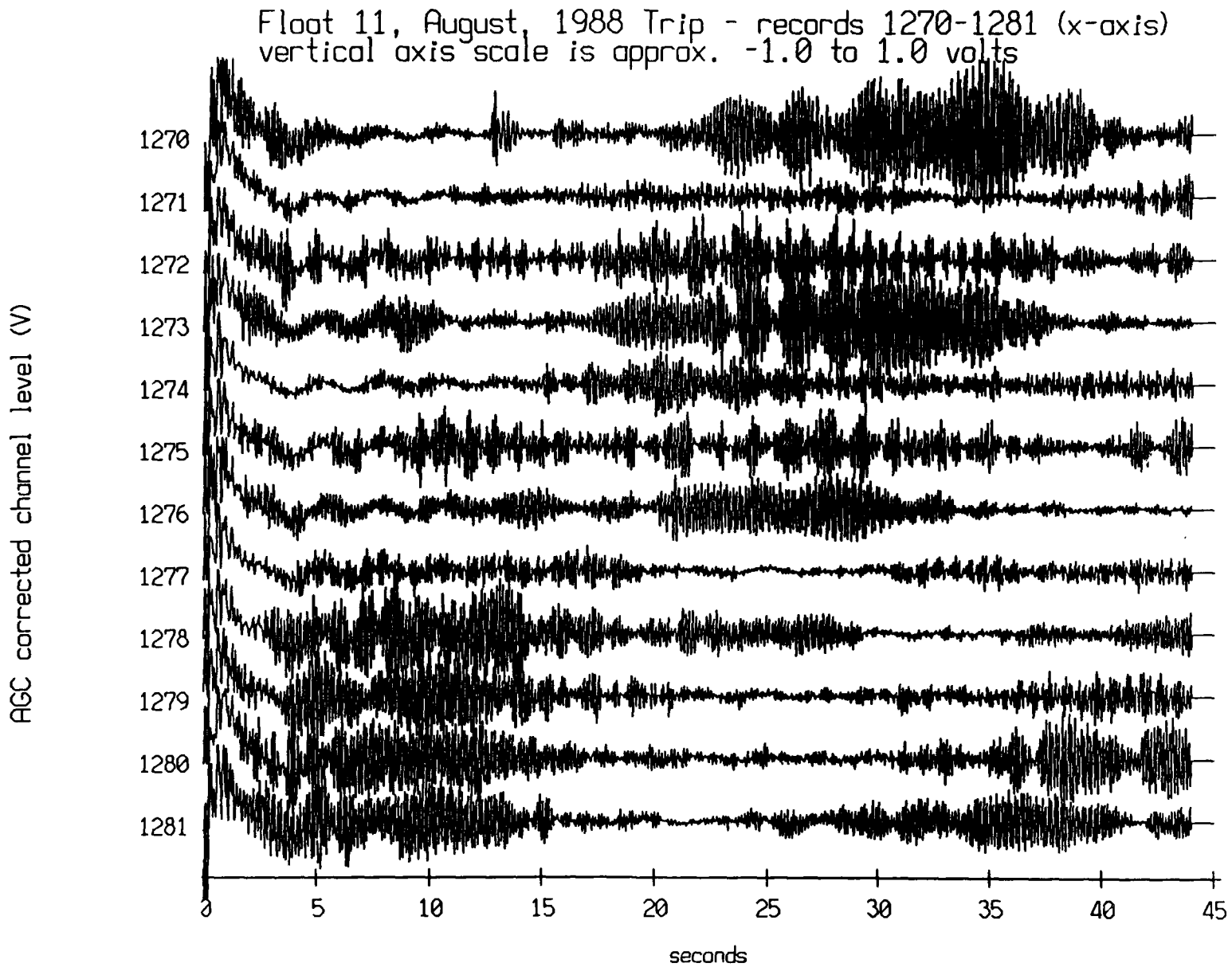


Figure XI.37a

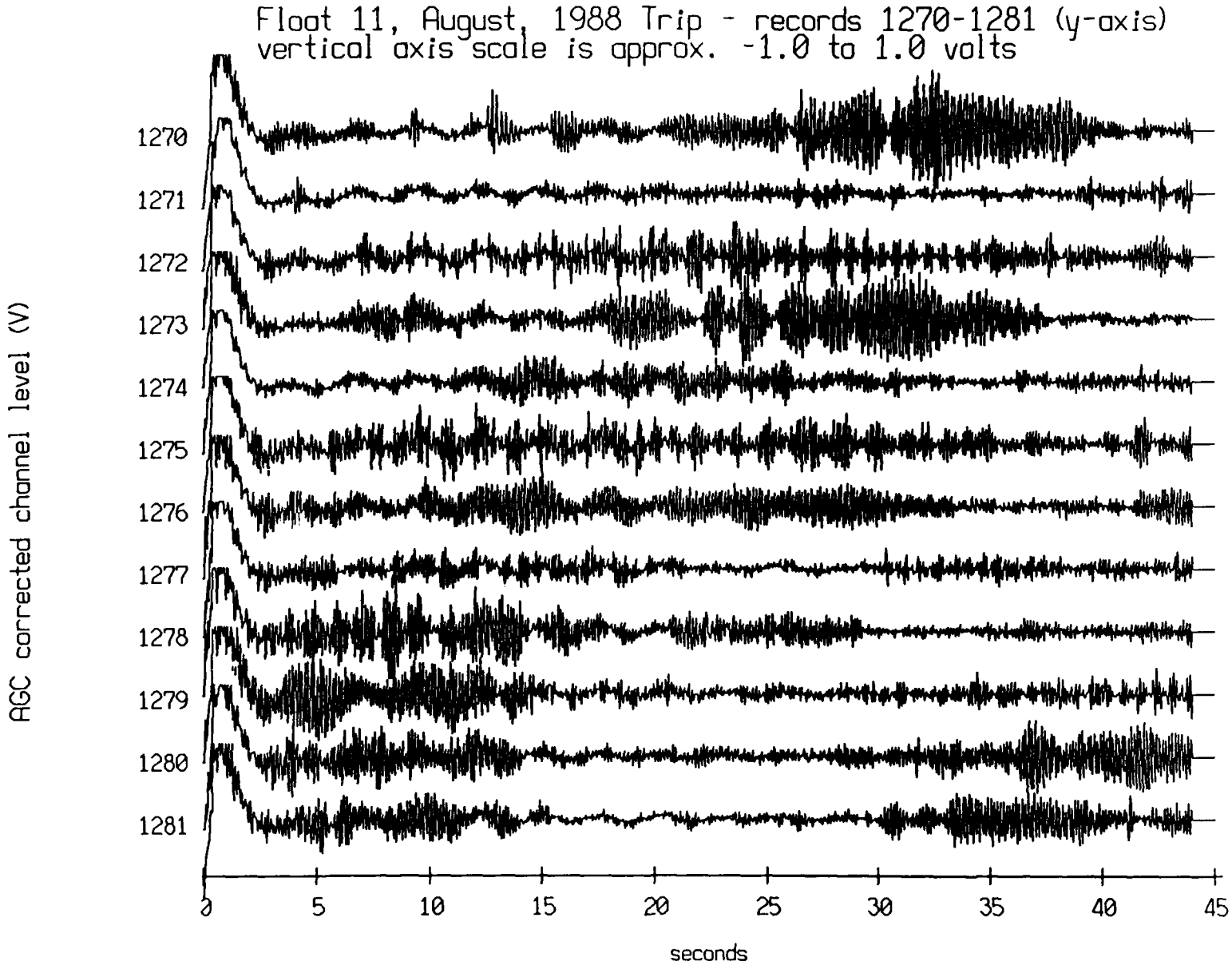


Figure XI.37b

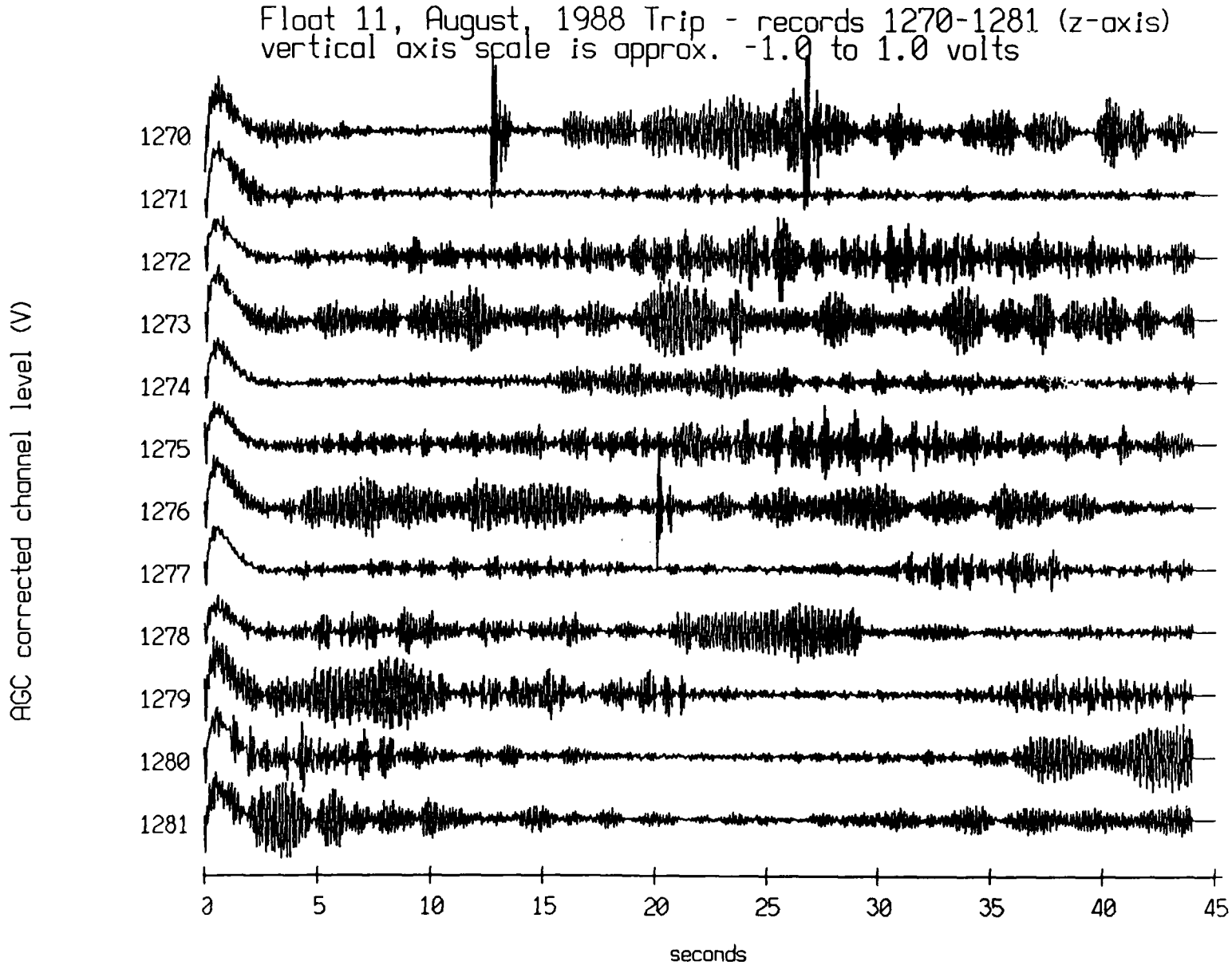


Figure XI.37c

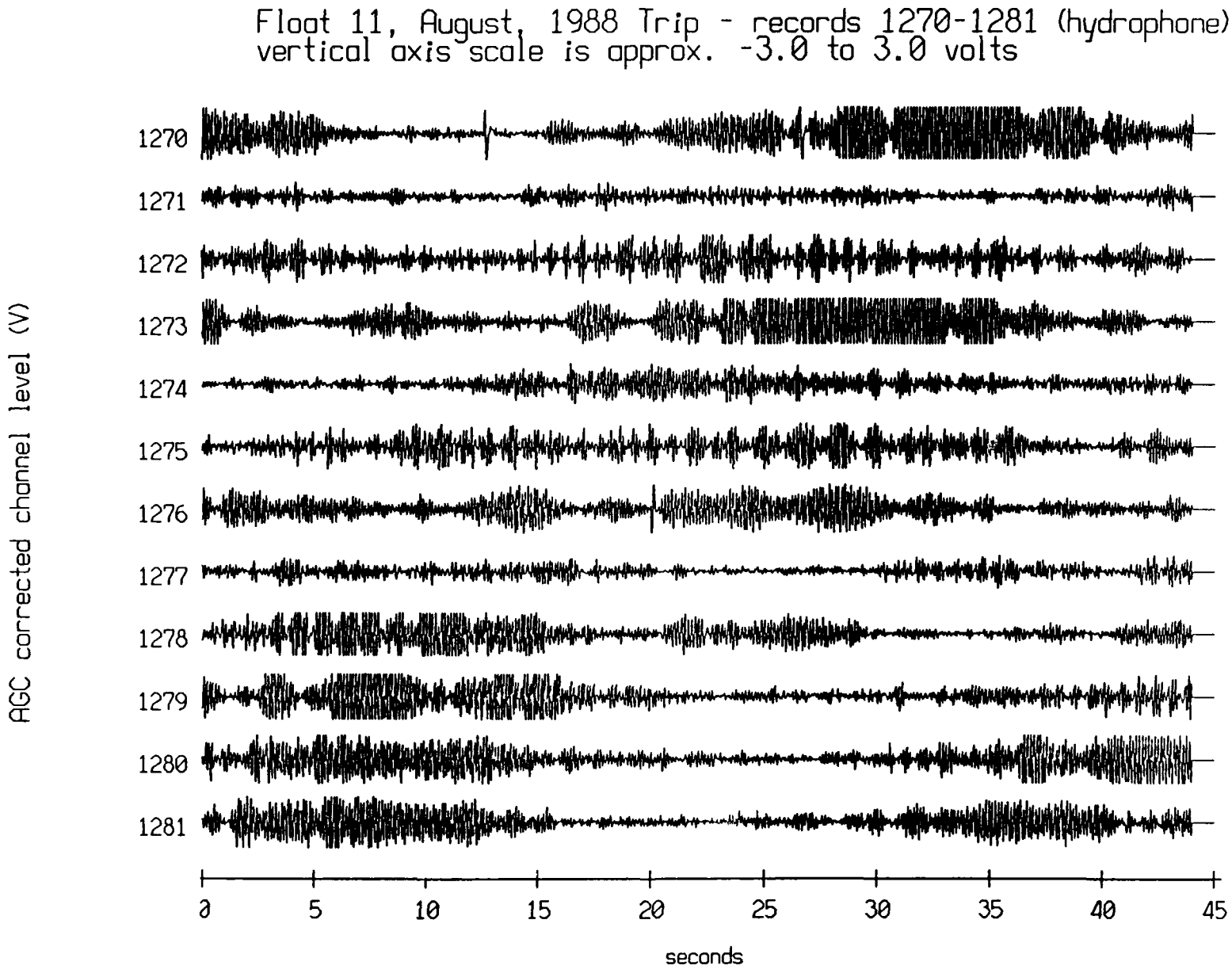


Figure XI.37d

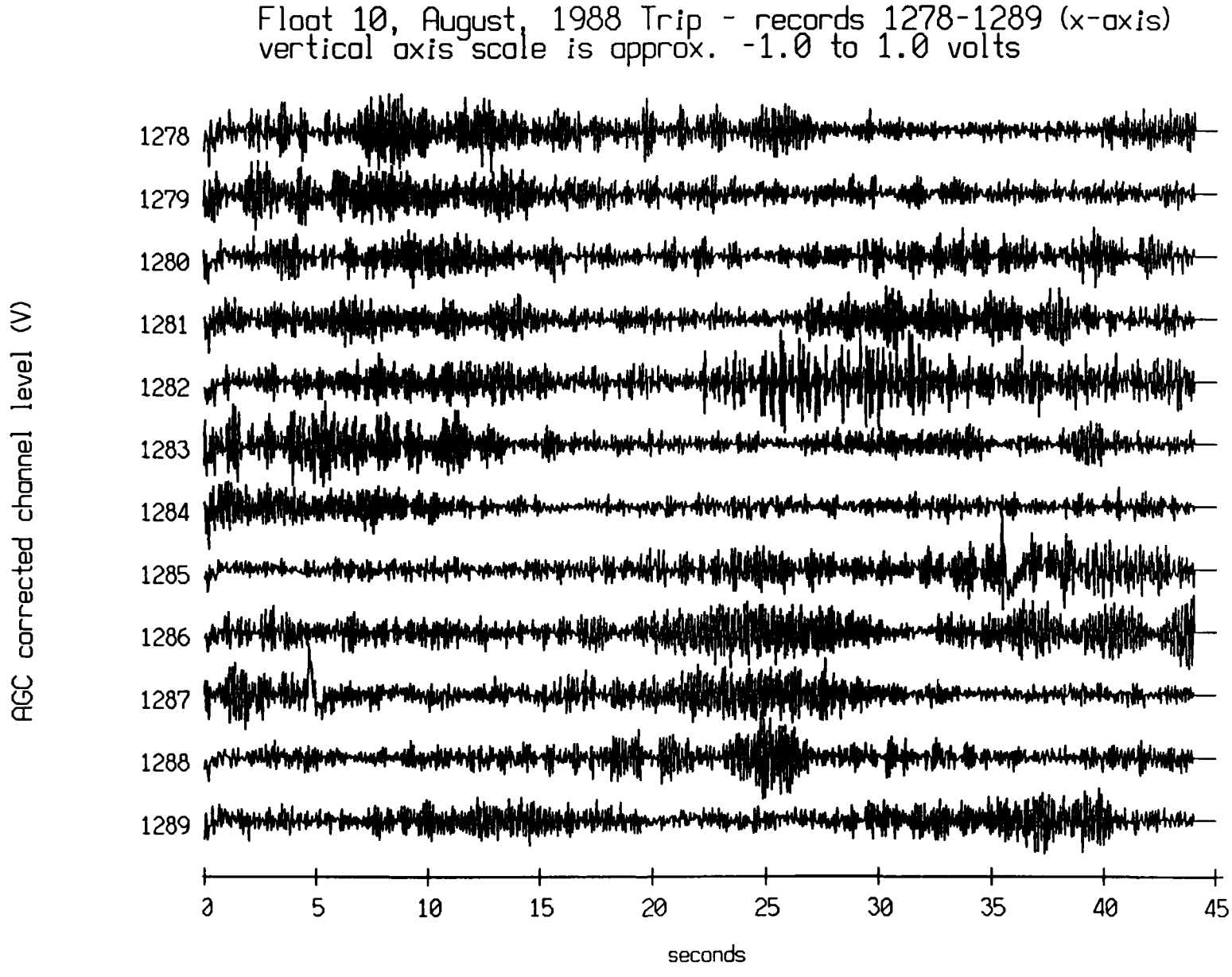


Figure XI.38a

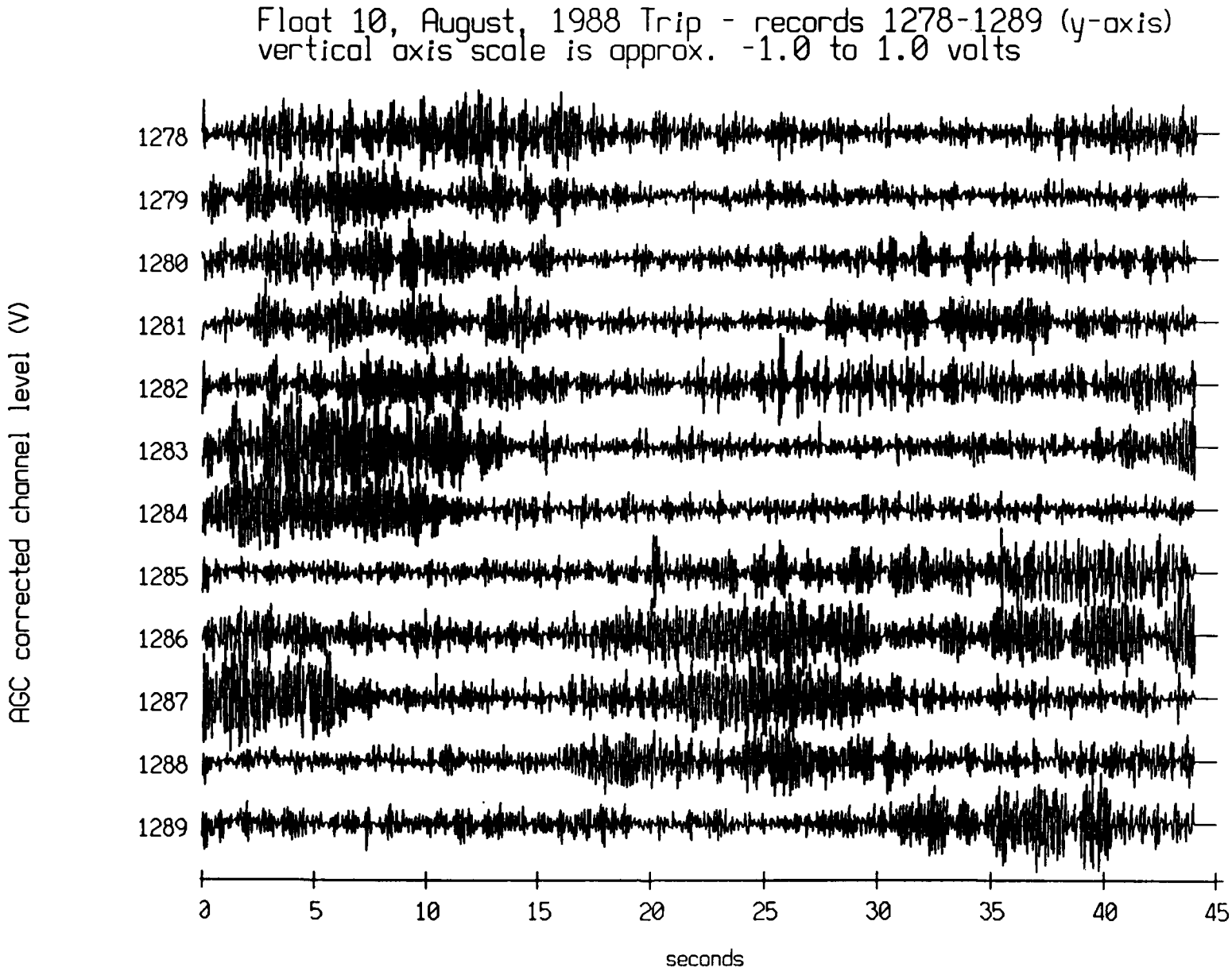


Figure XI.38b

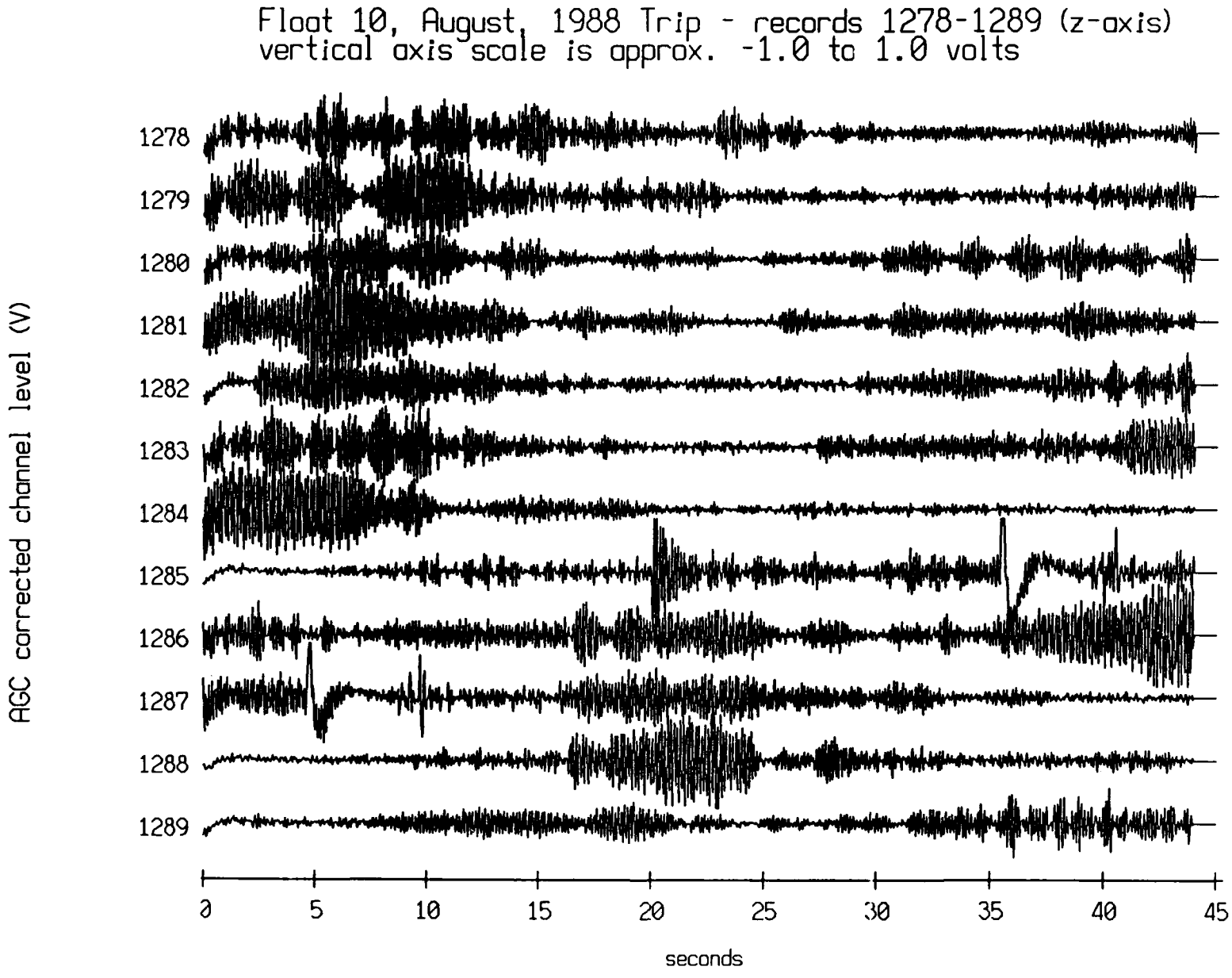


Figure XI.38c

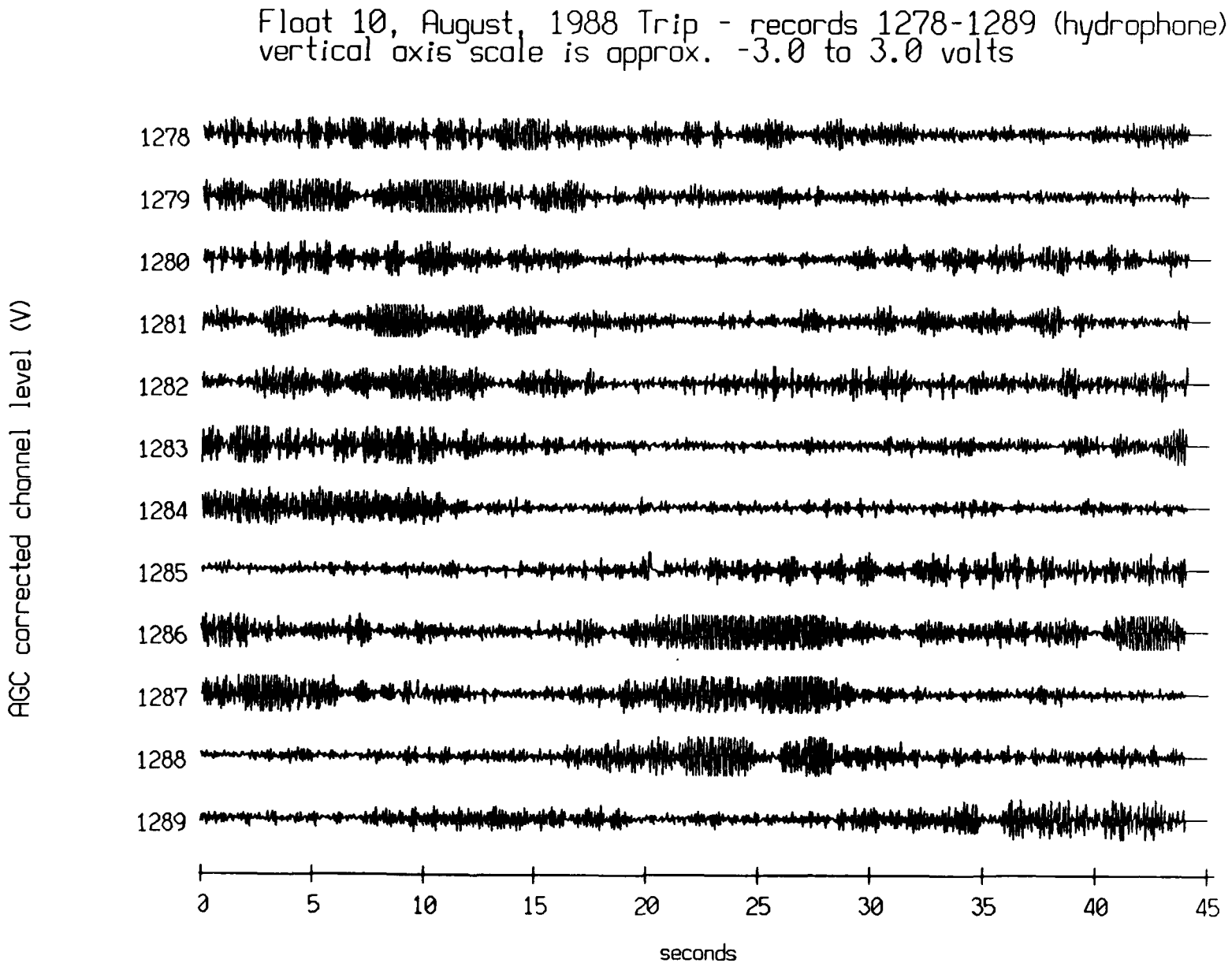


Figure XI.38d

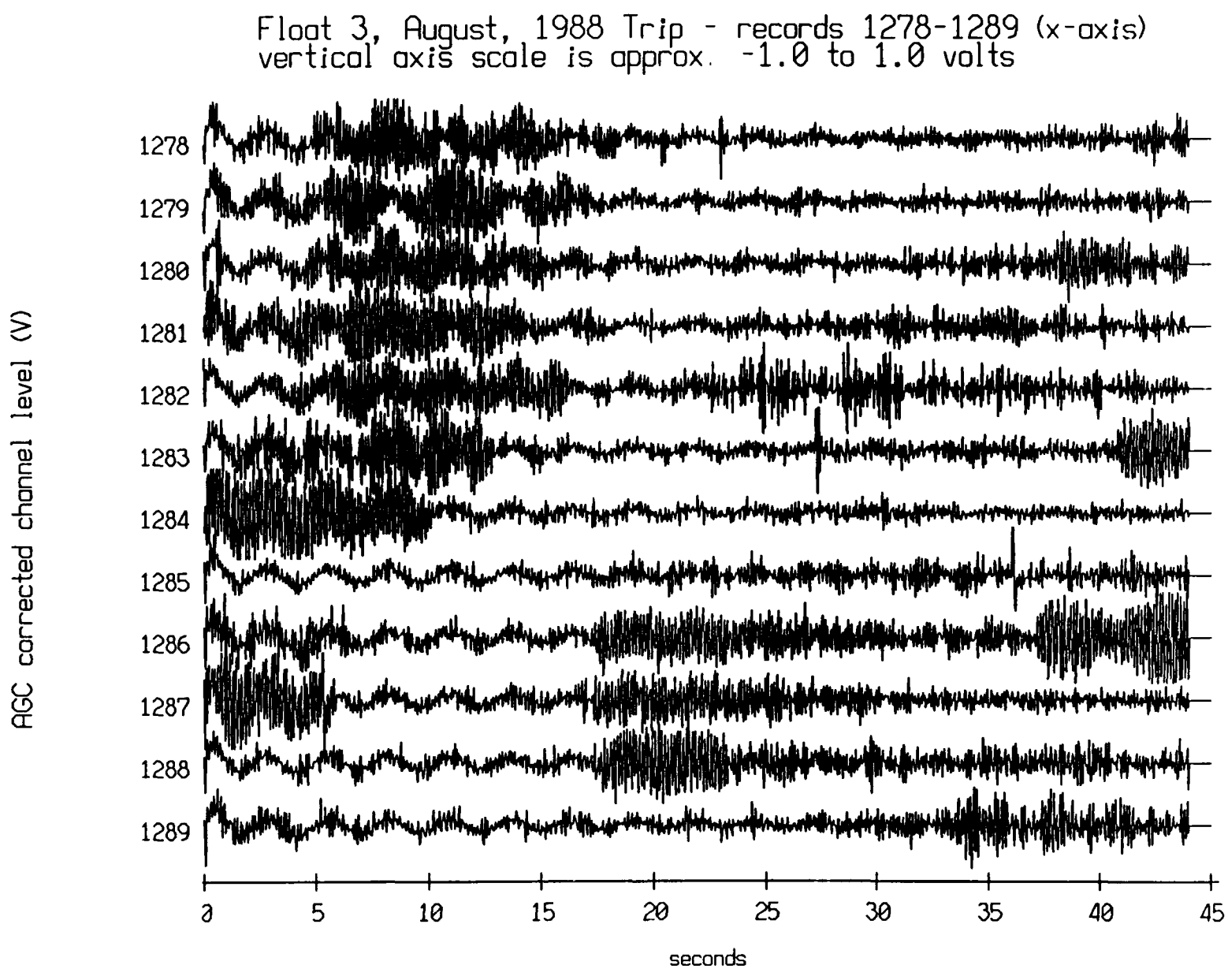


Figure XI.39a

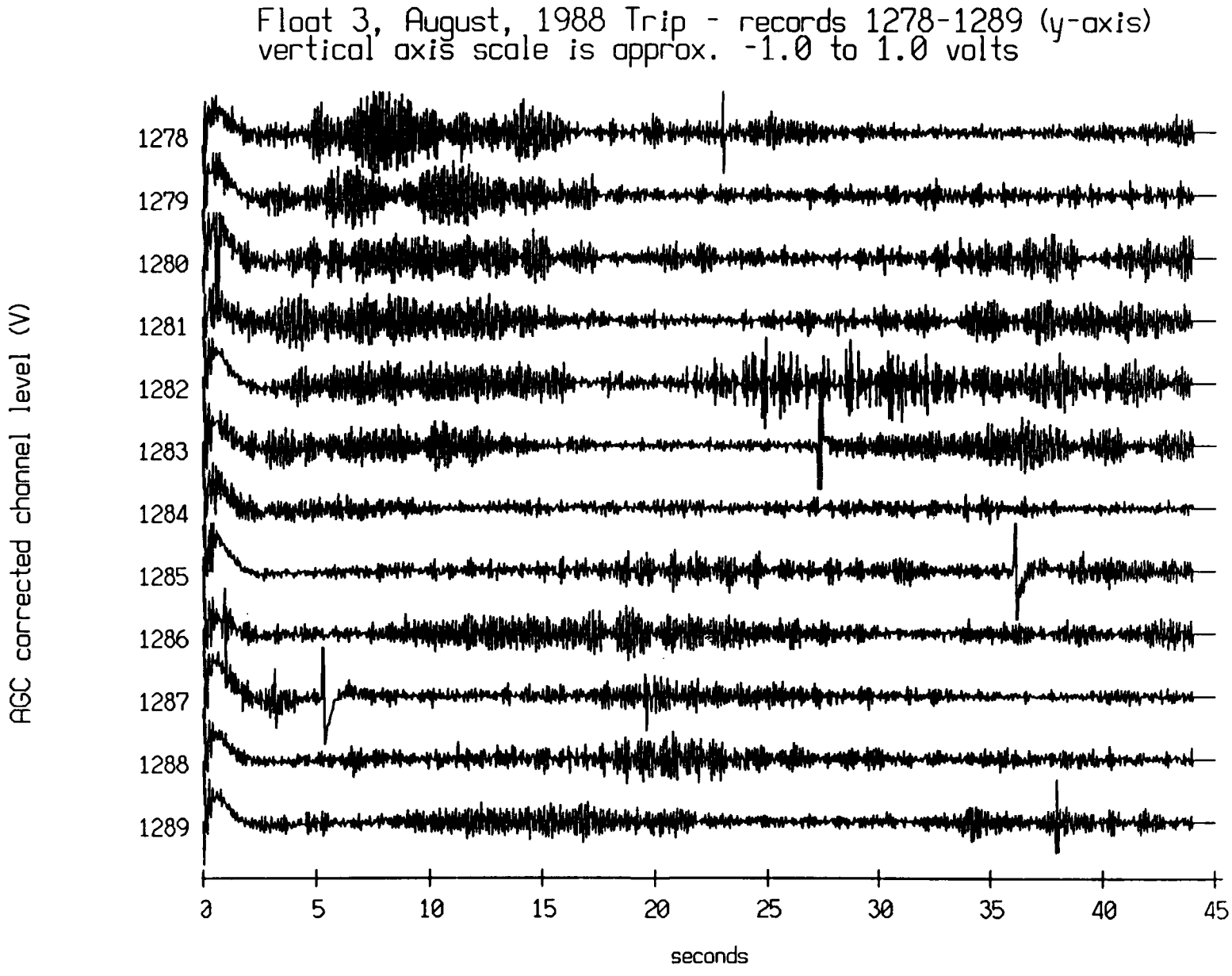


Figure XI.30b

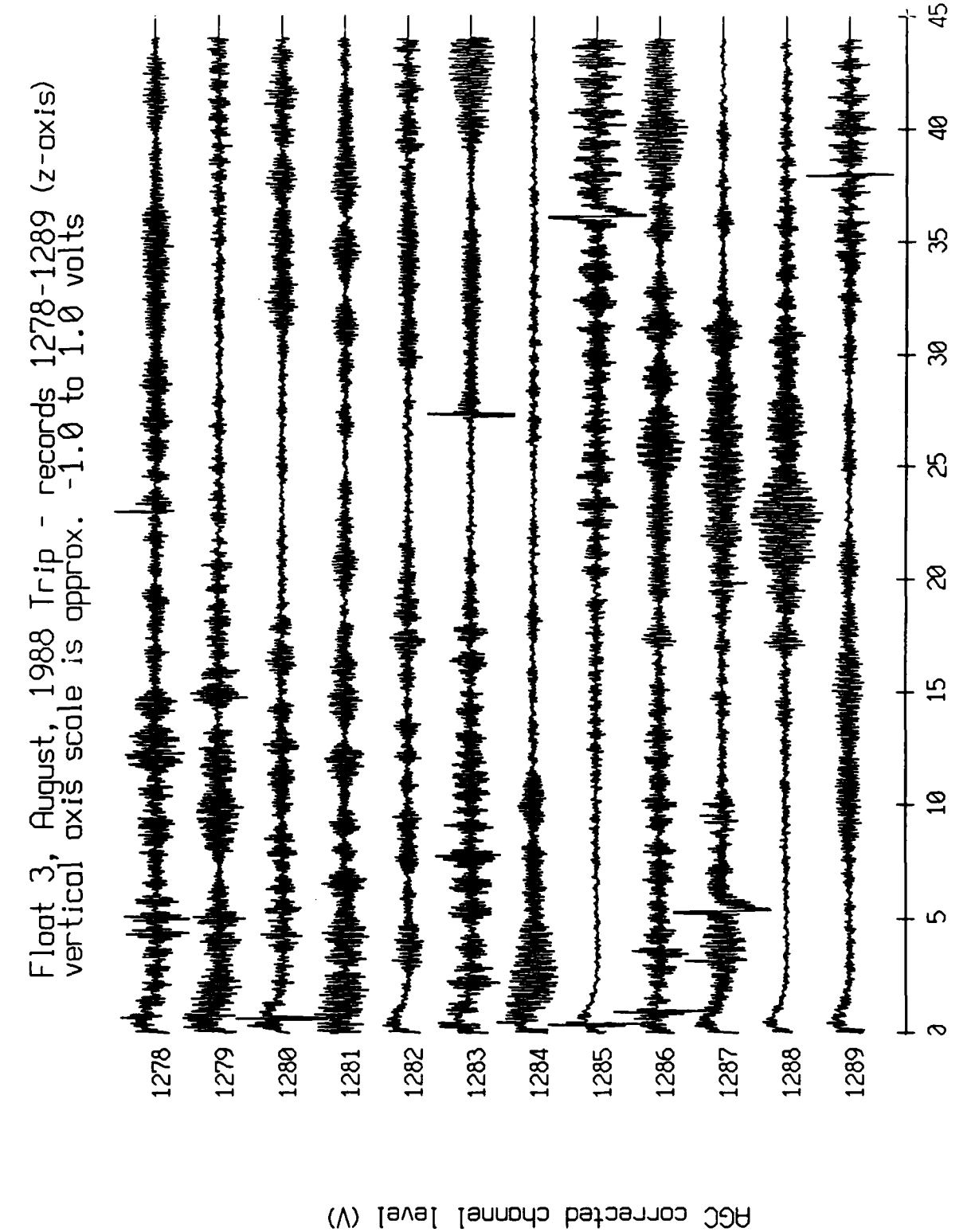


Figure XI.39c

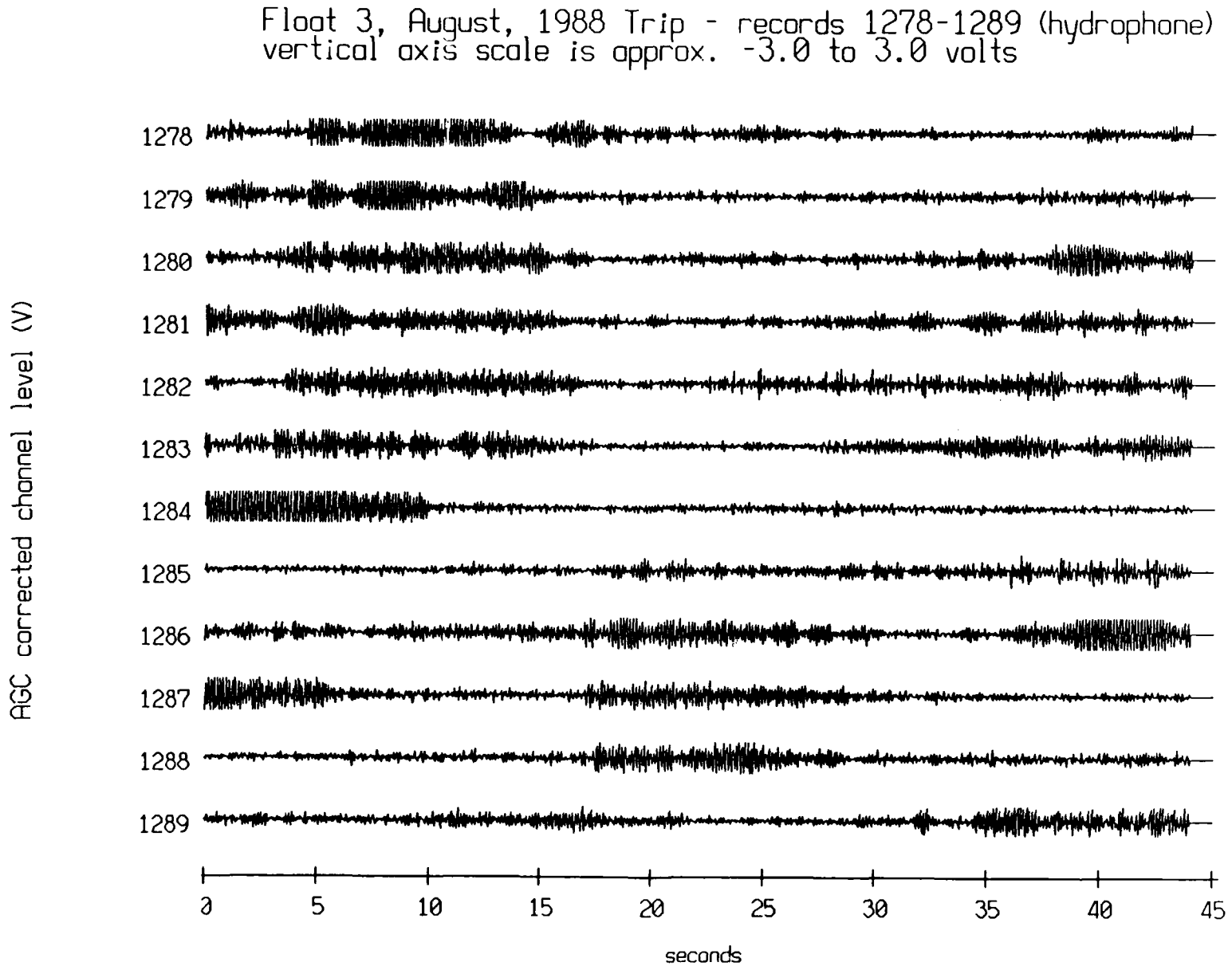


Figure XI.30d

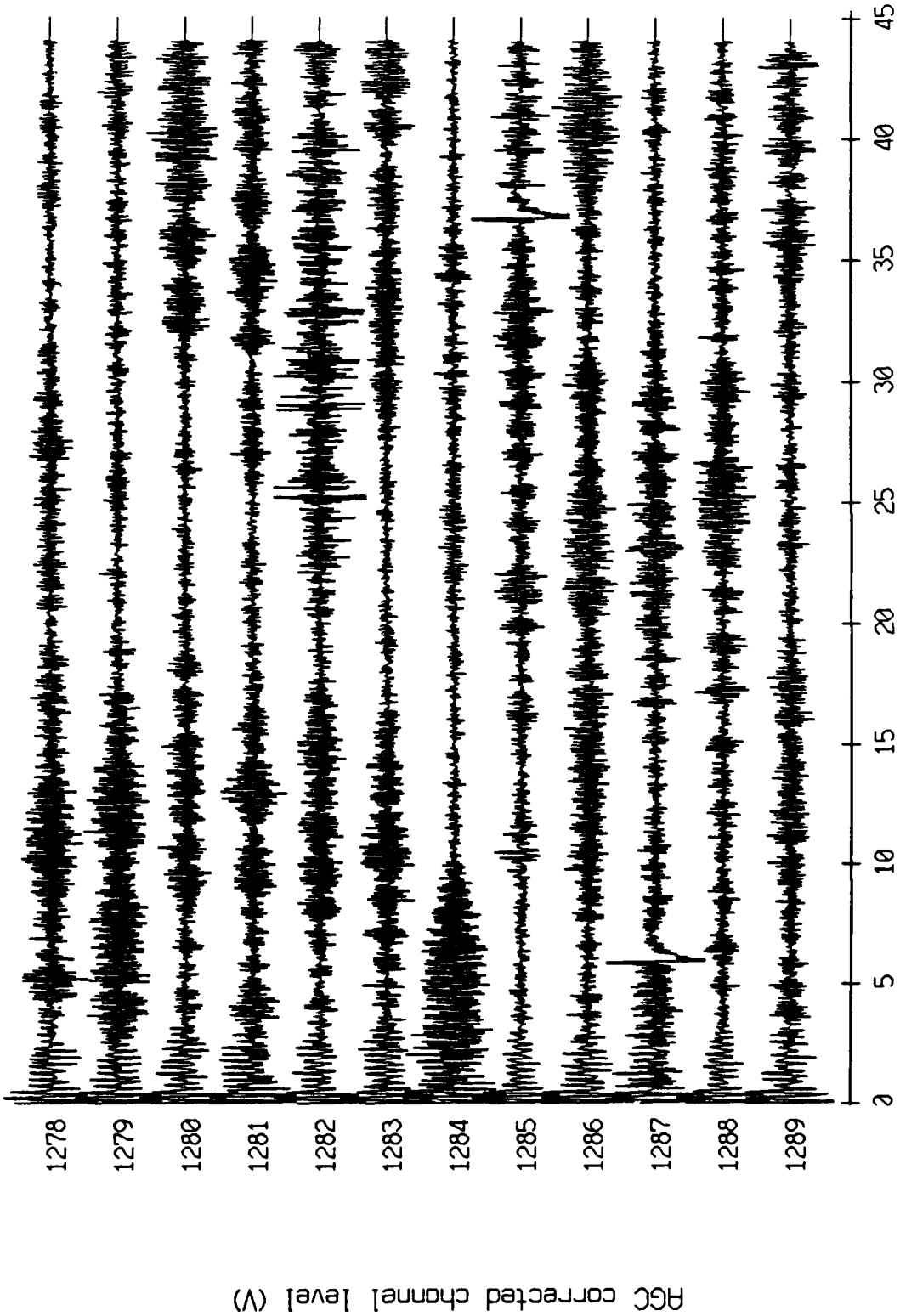


Figure XI.40a

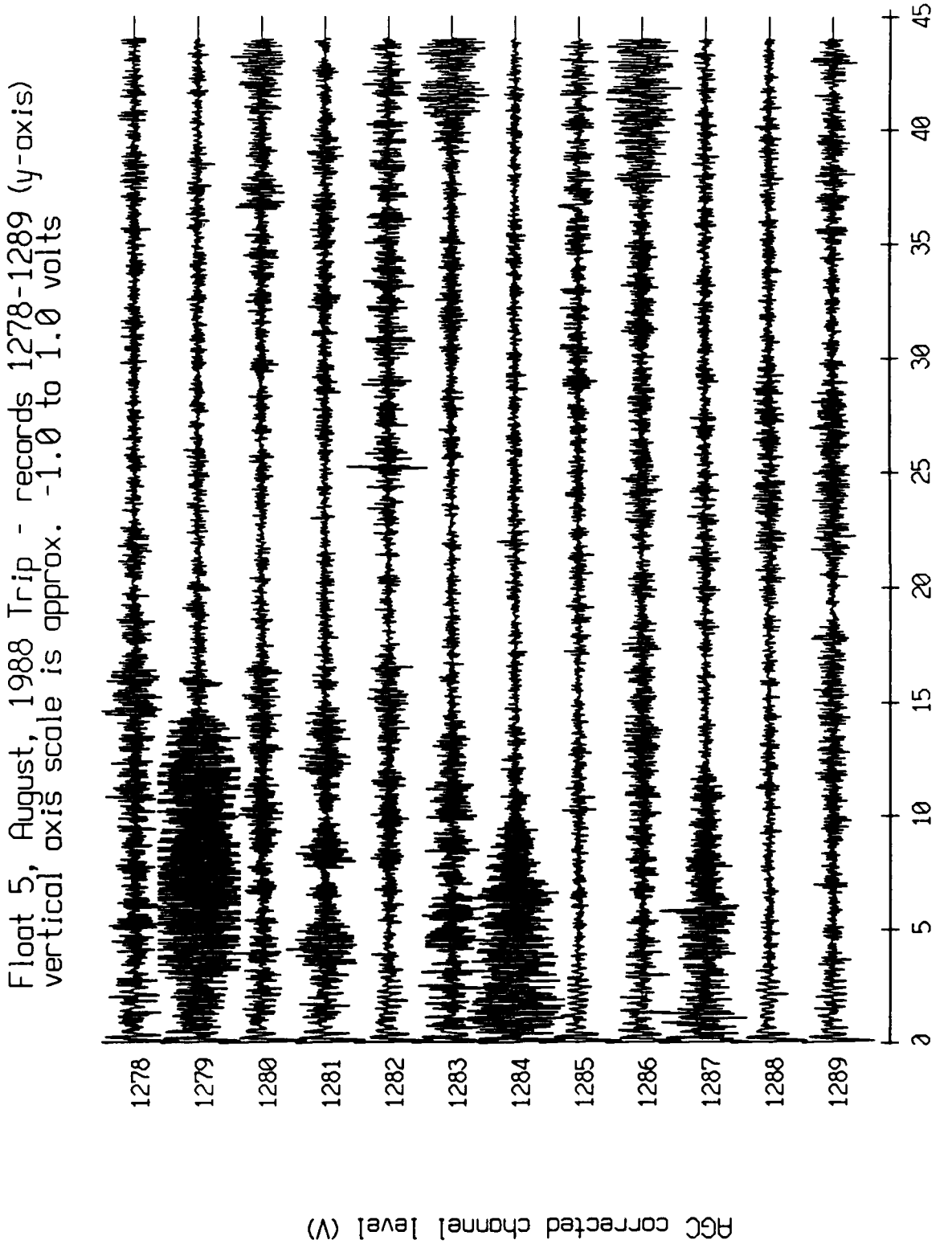


Figure XI.40b

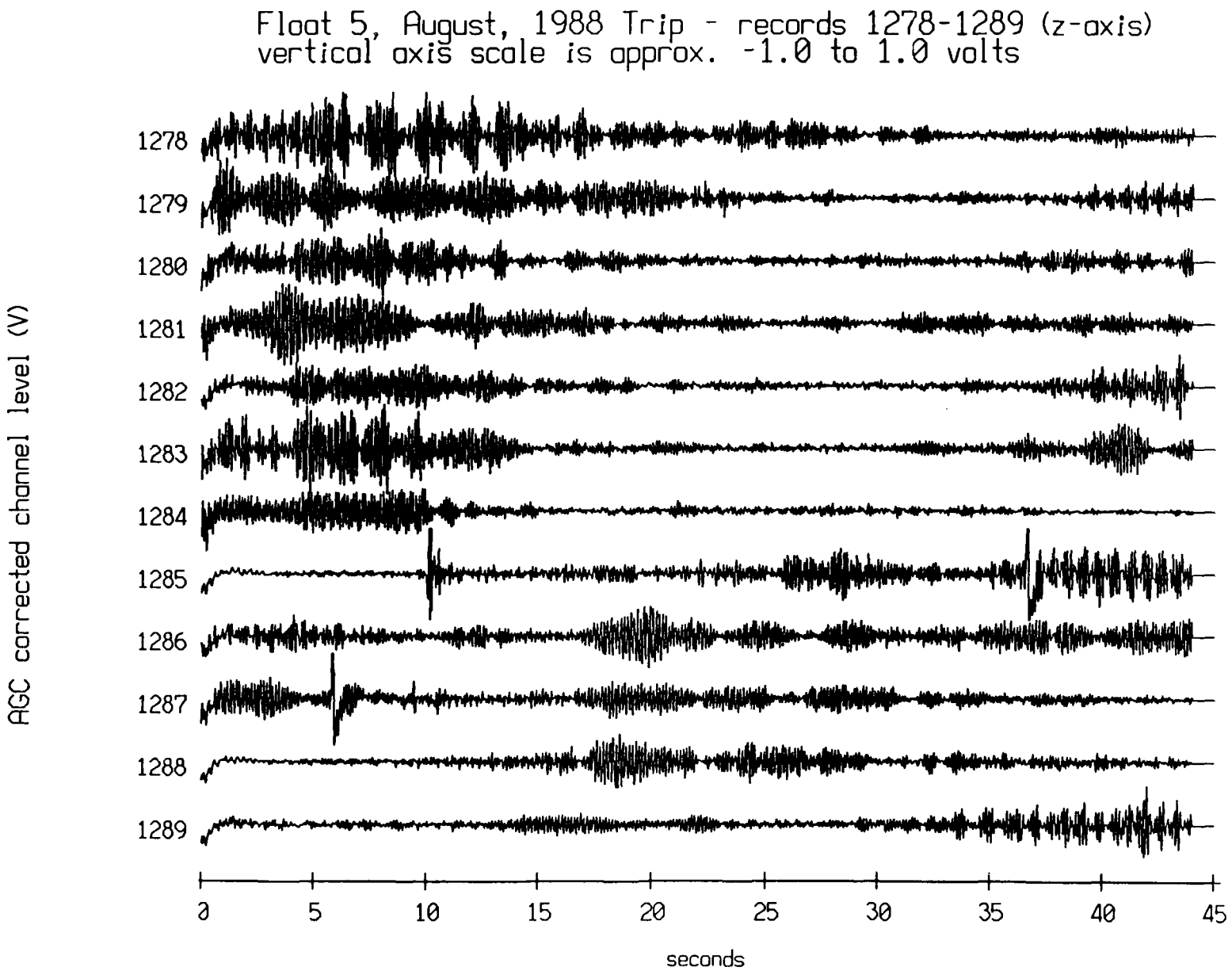


Figure XI-40c

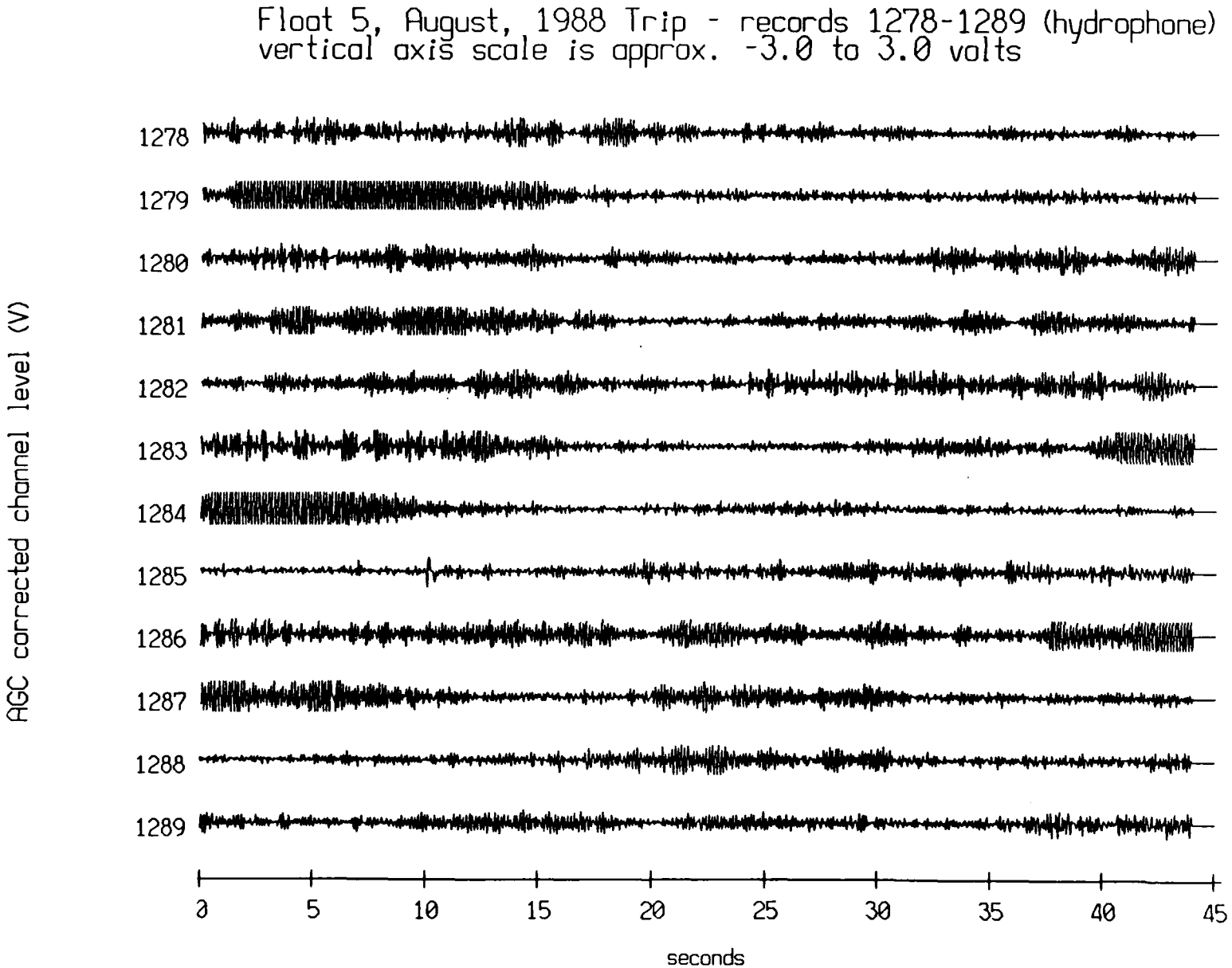


Figure XI.40d

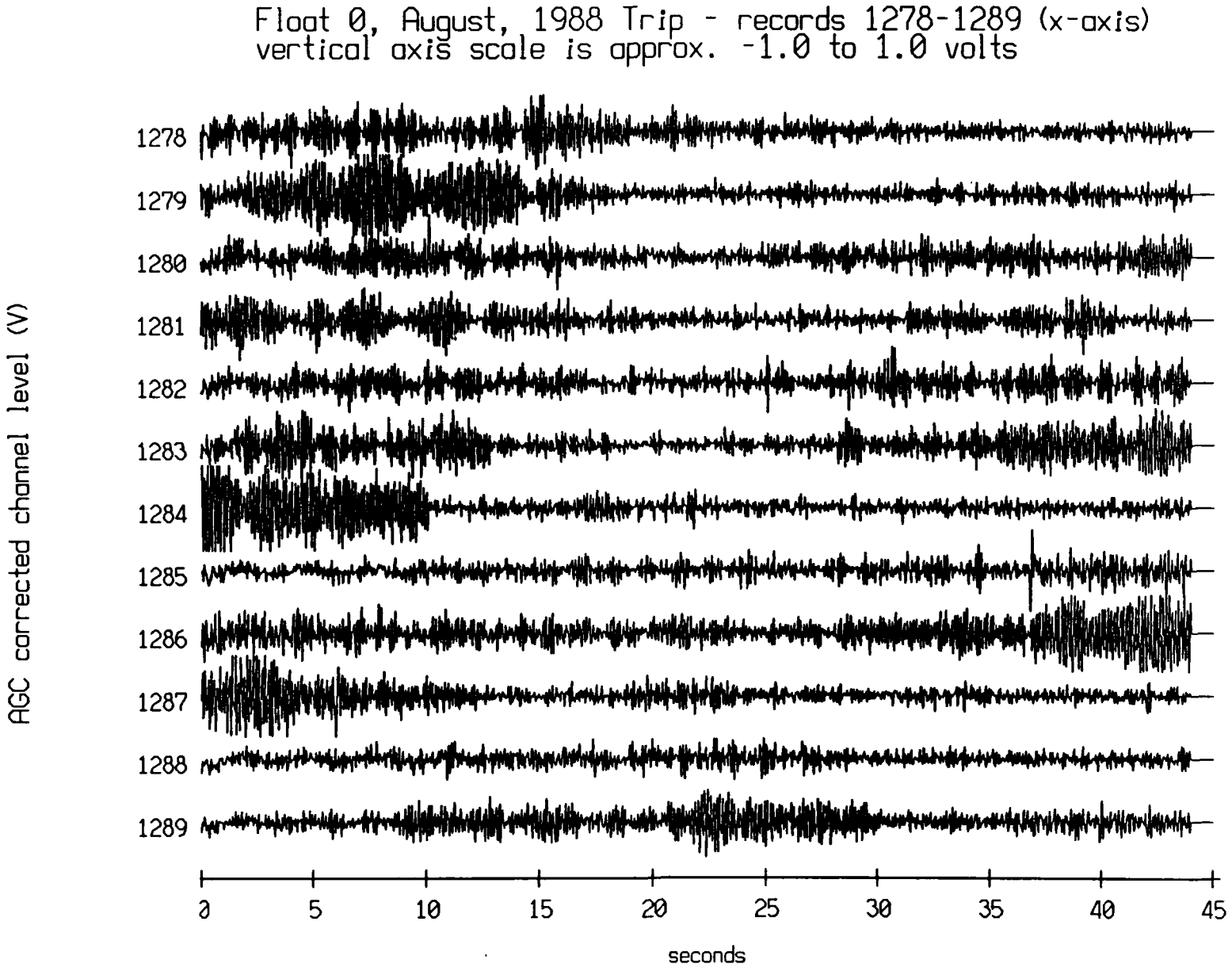


Figure XI.41a

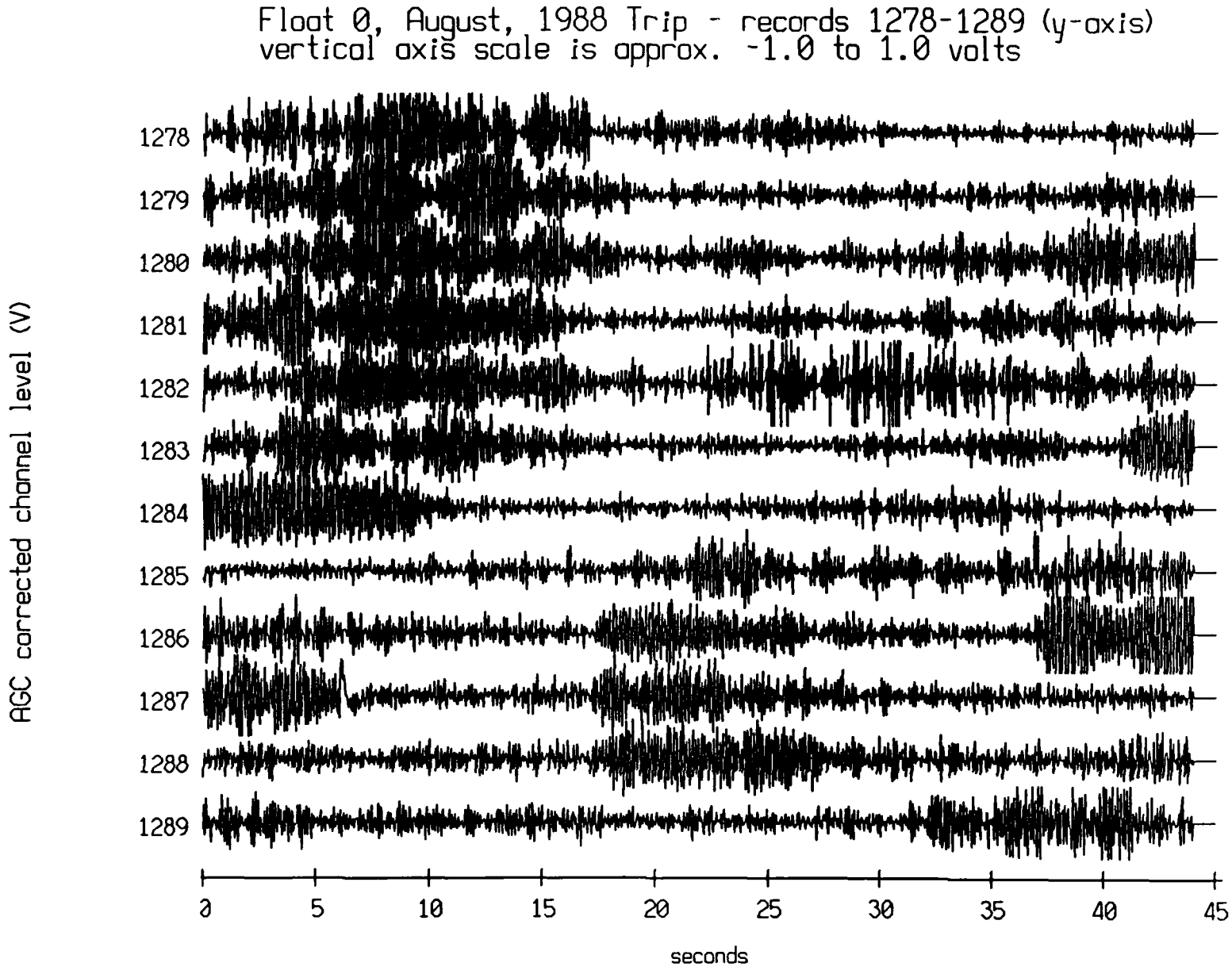


Figure XI.41b

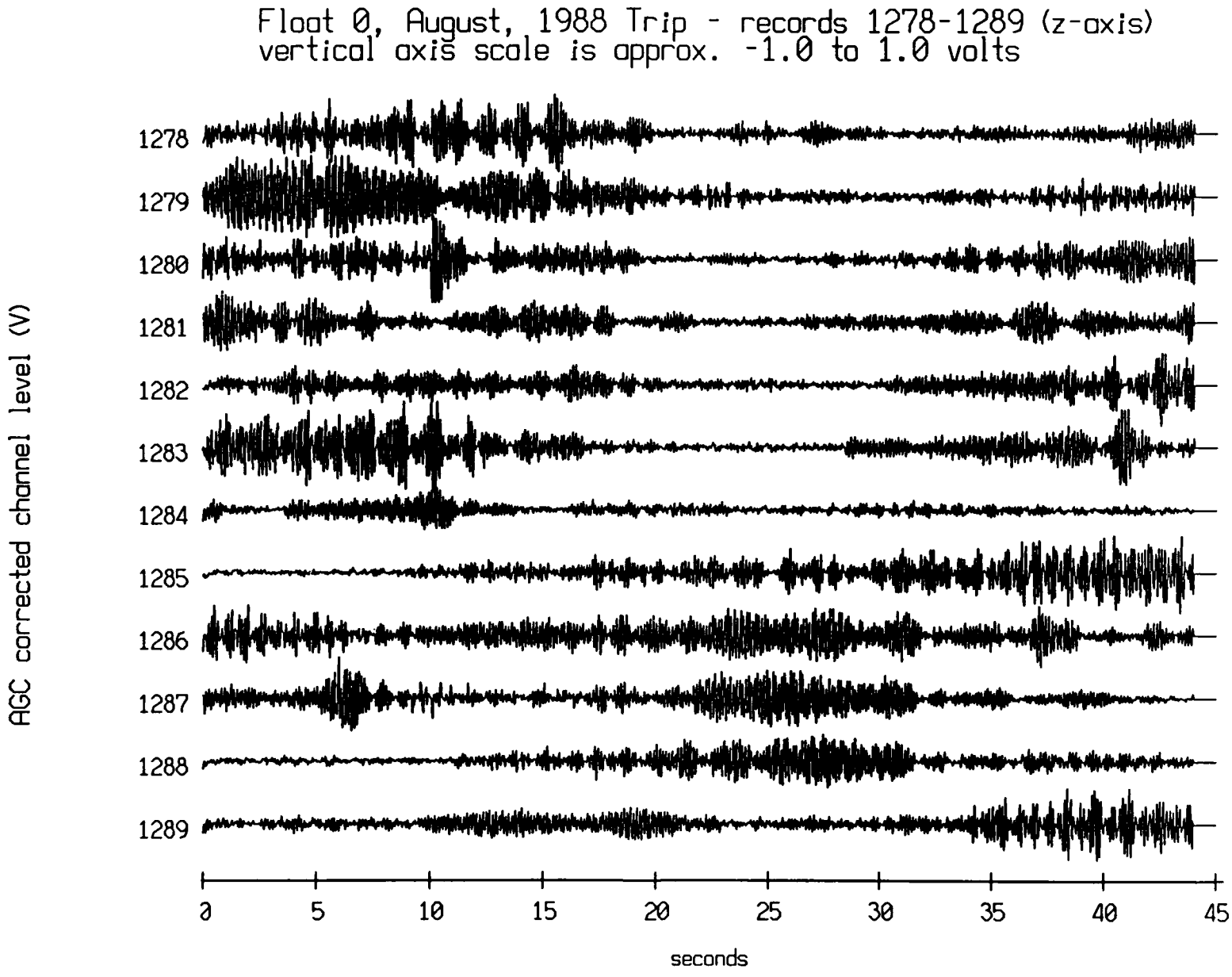


Figure XI.41c

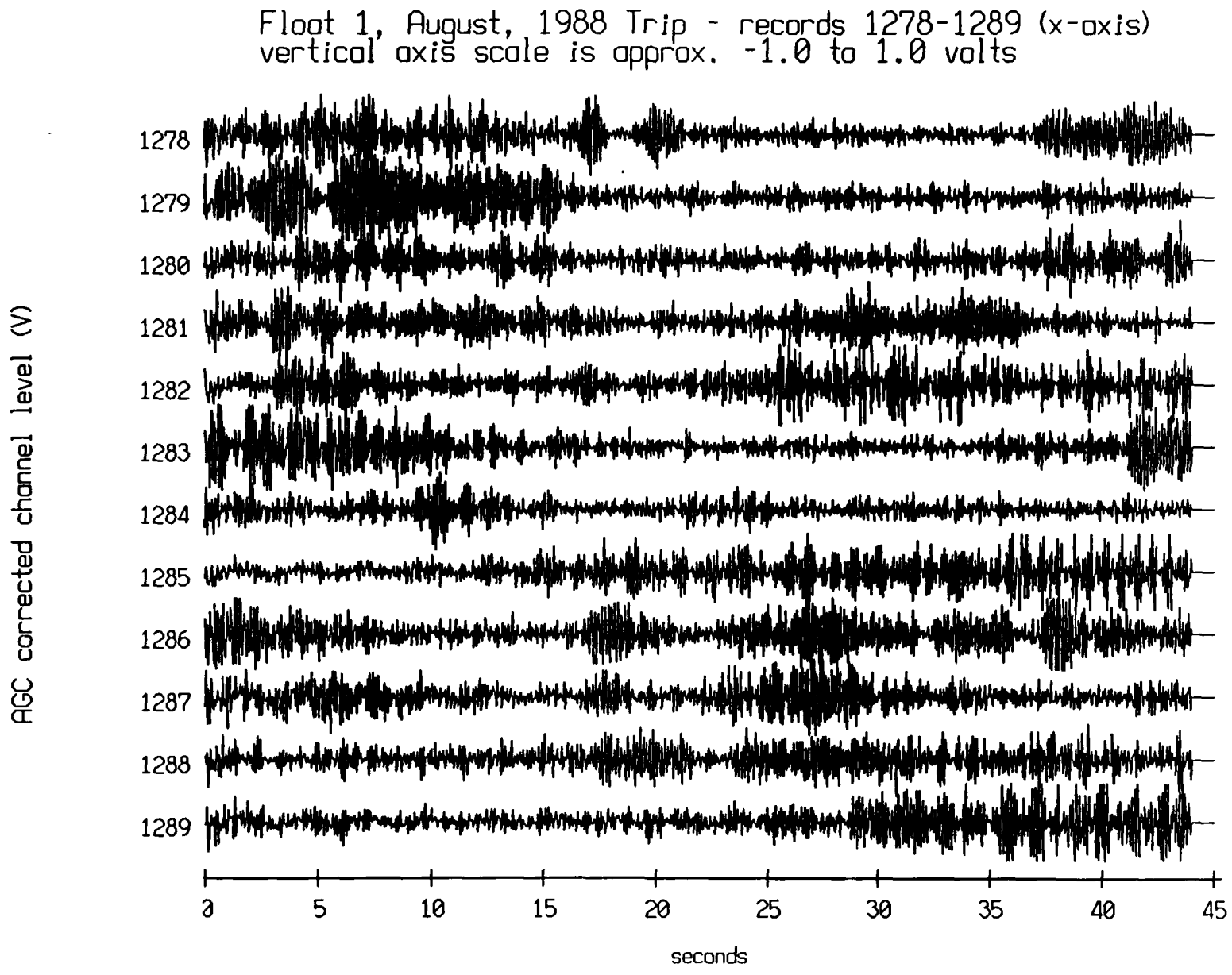


Figure XI.42a

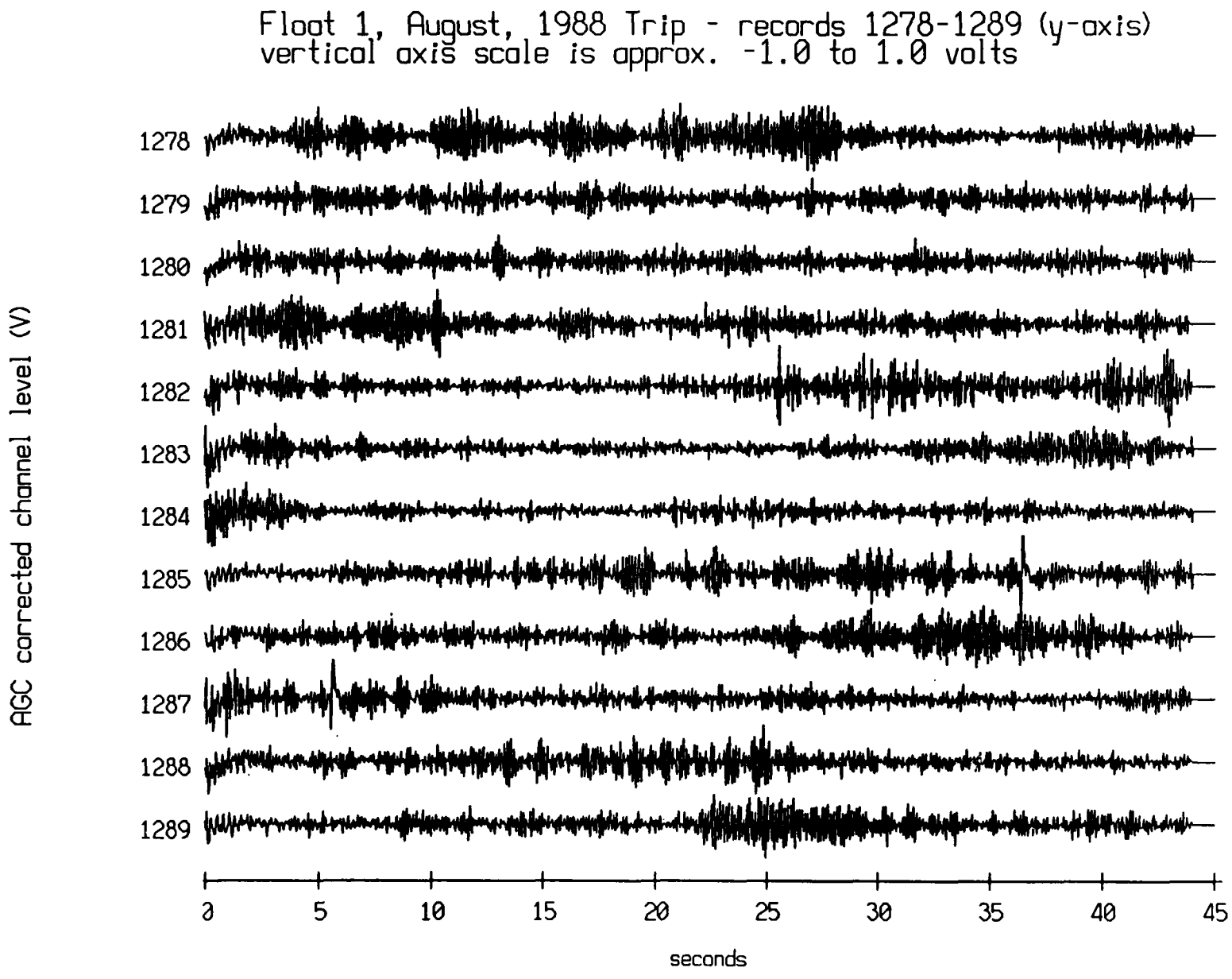


Figure XI.42b

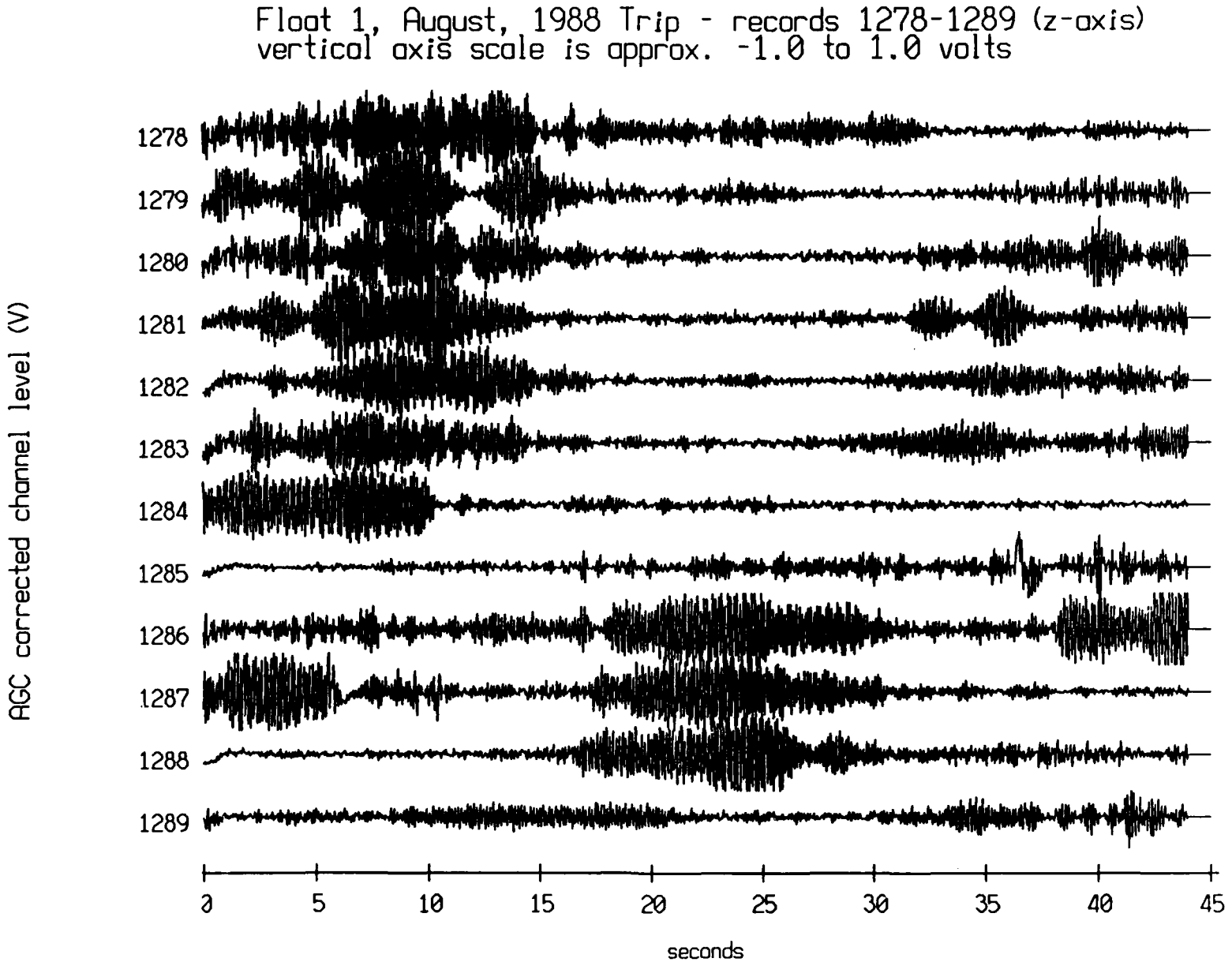


Figure XI.42c

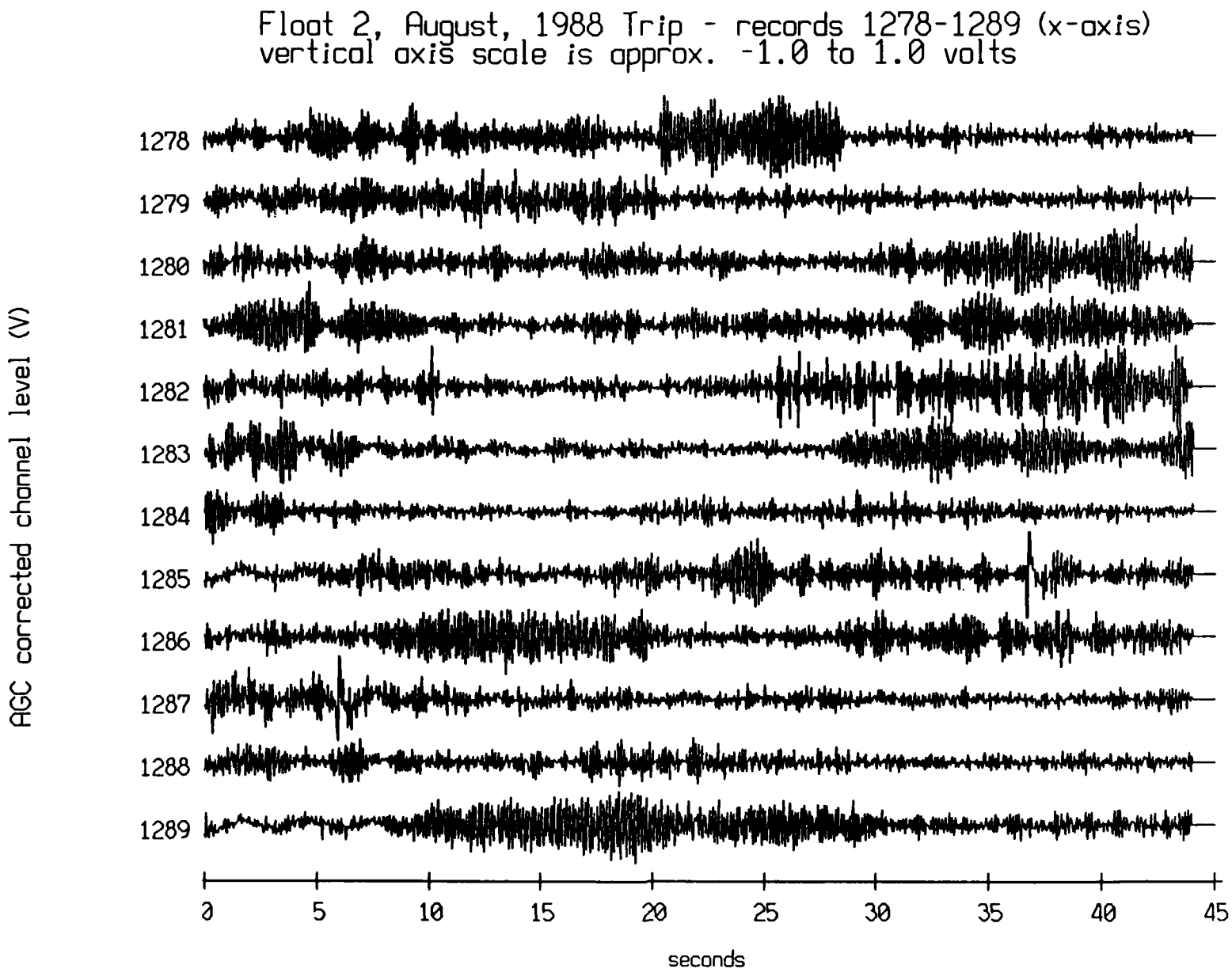


Figure XI.43a

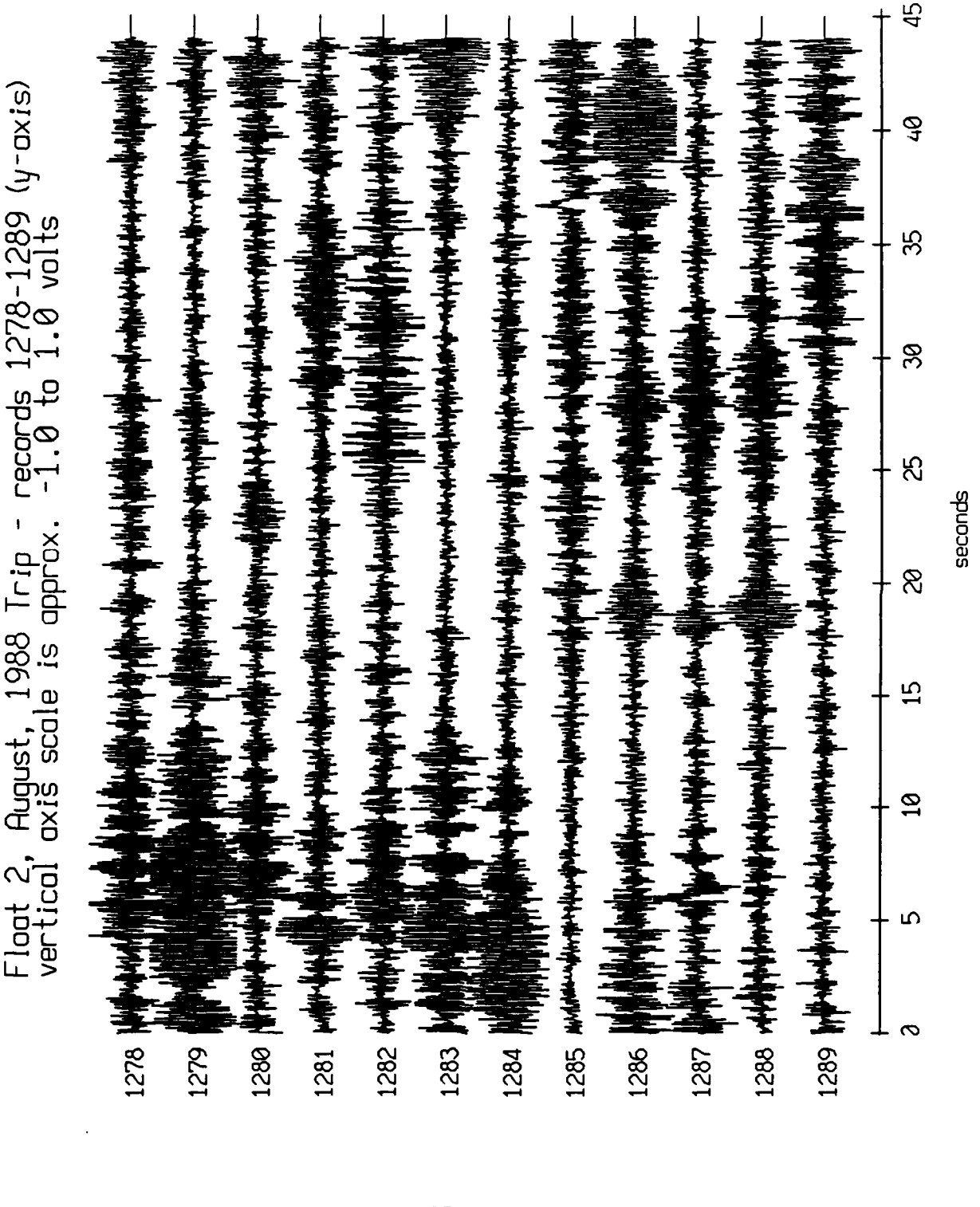


Figure XI.43b

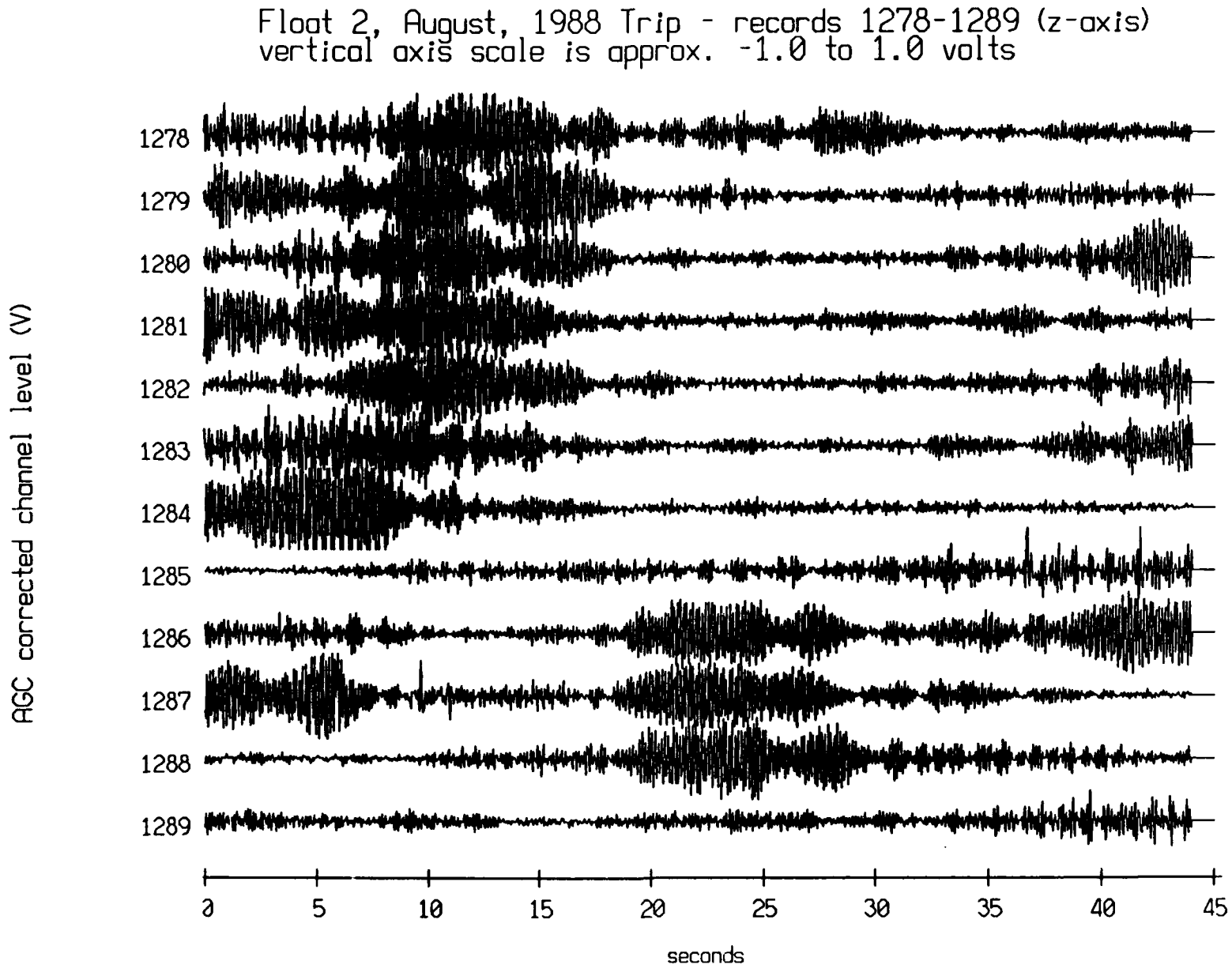


Figure XI.43c

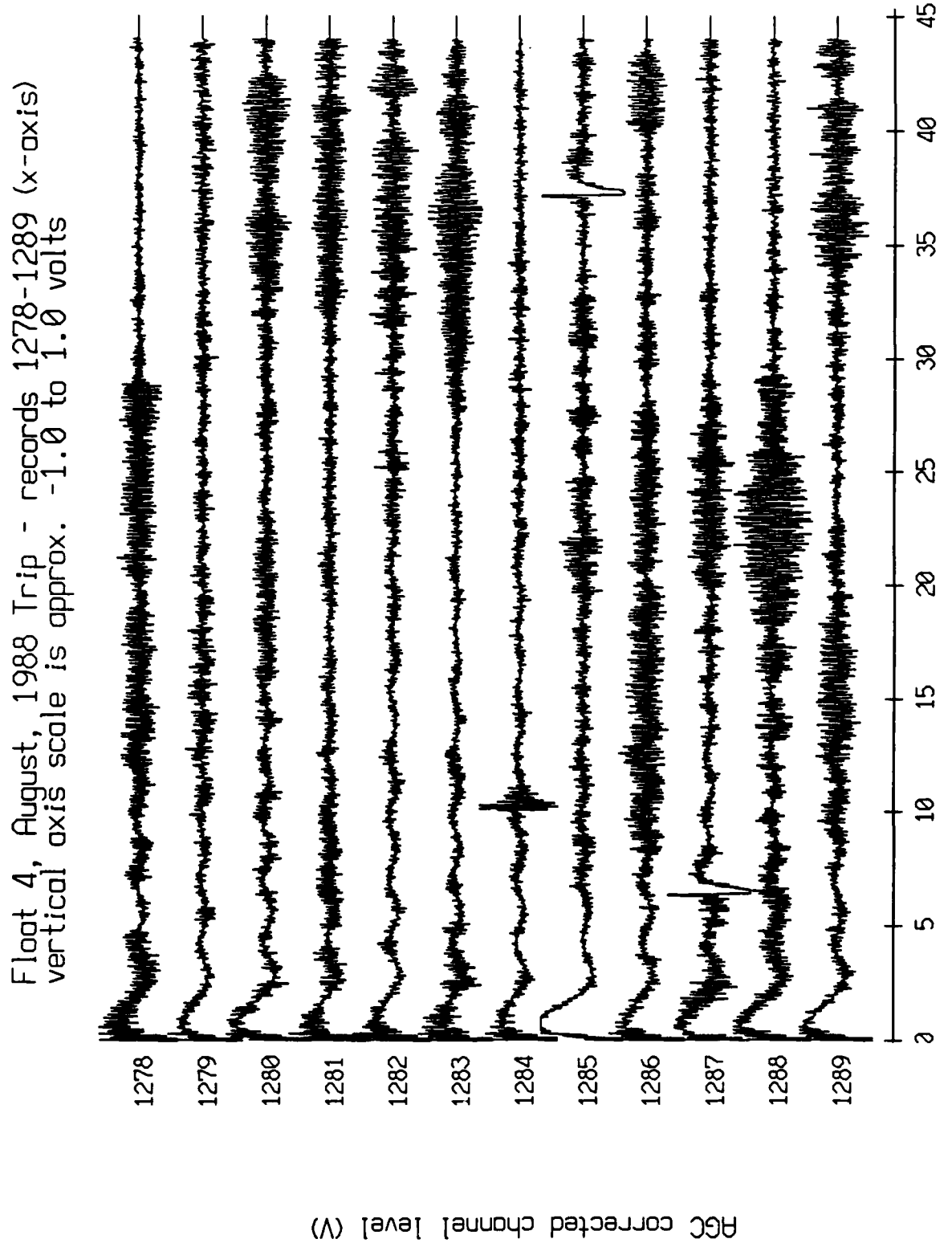


Figure XI.44a

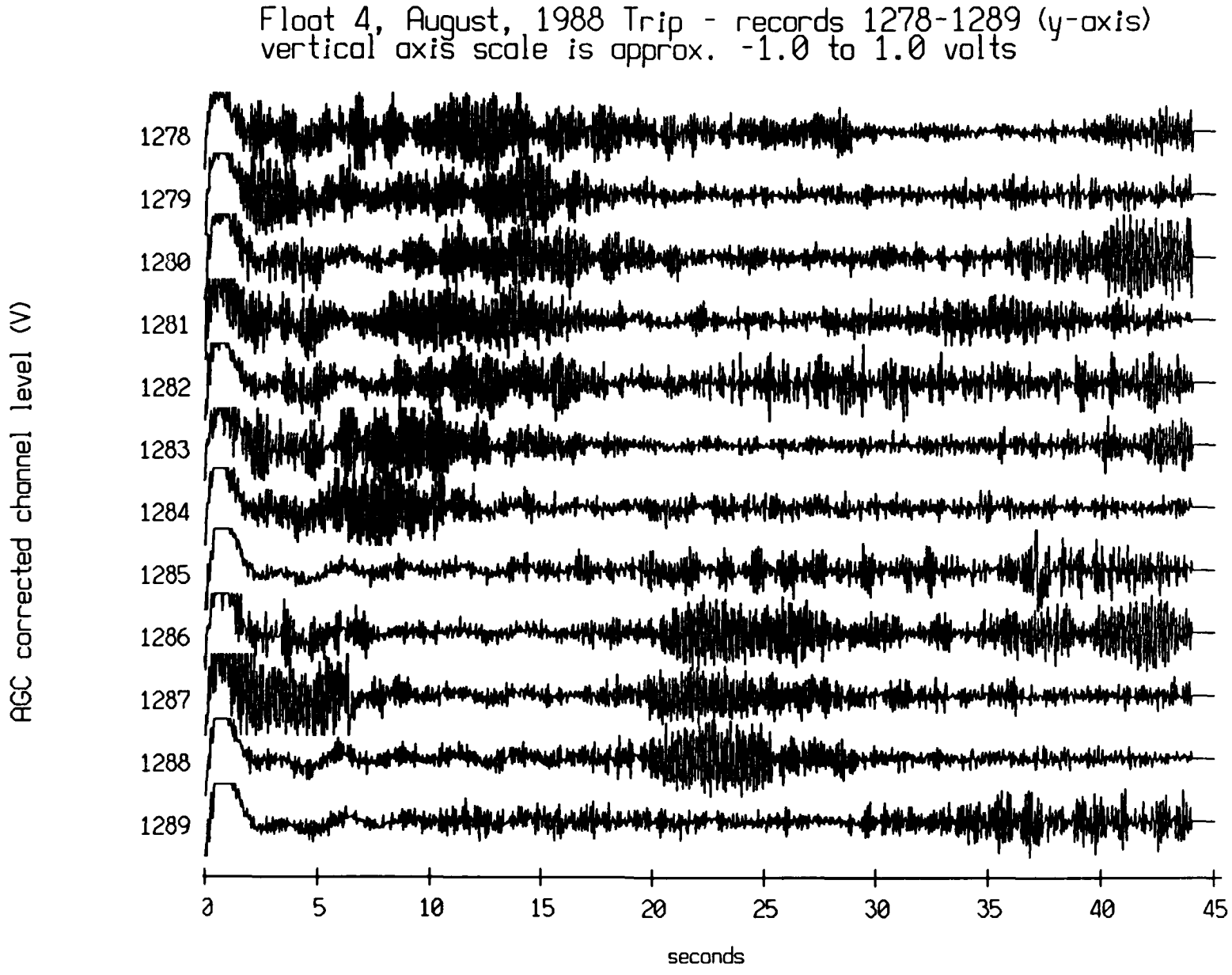


Figure XI.44b

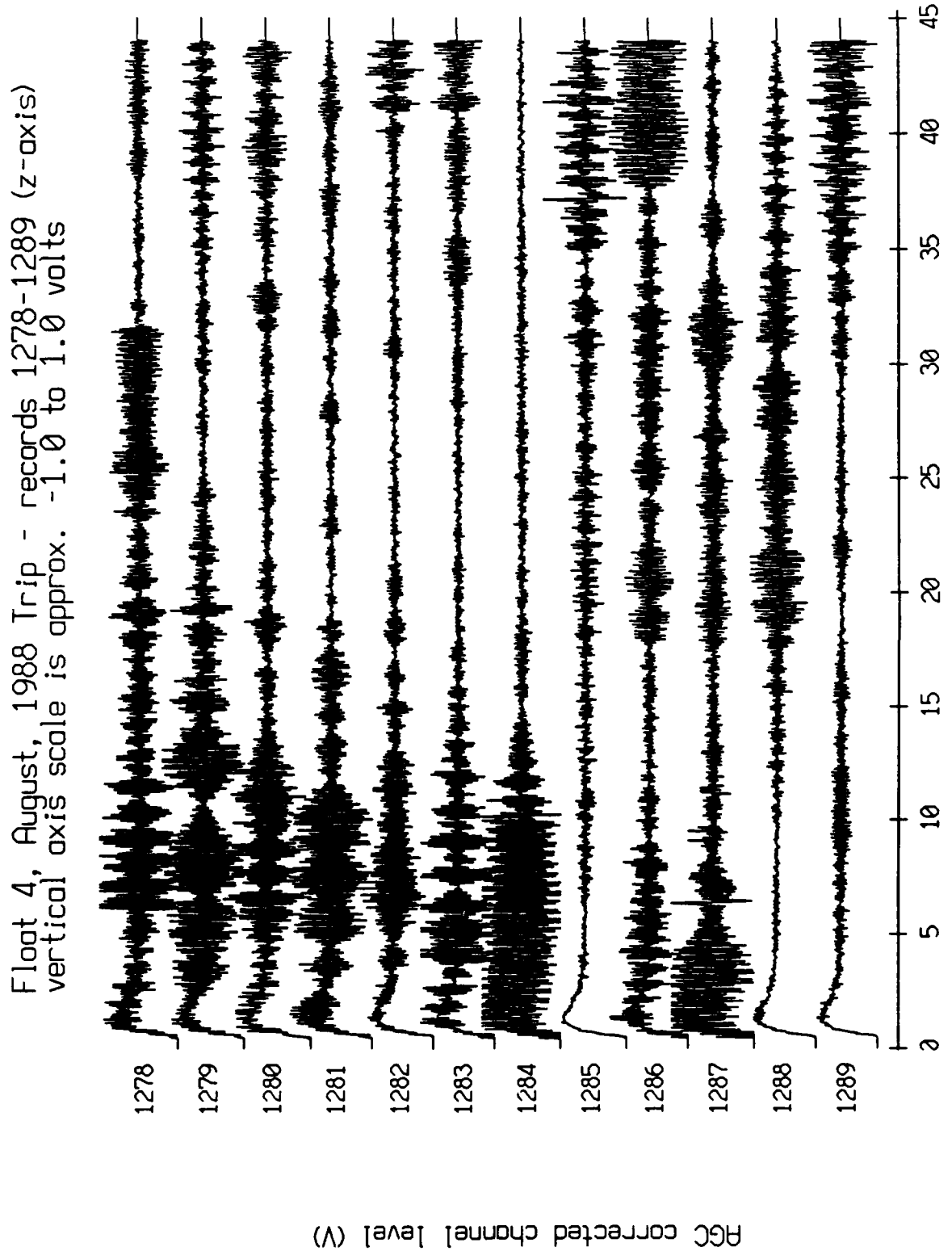


Figure XI.44c

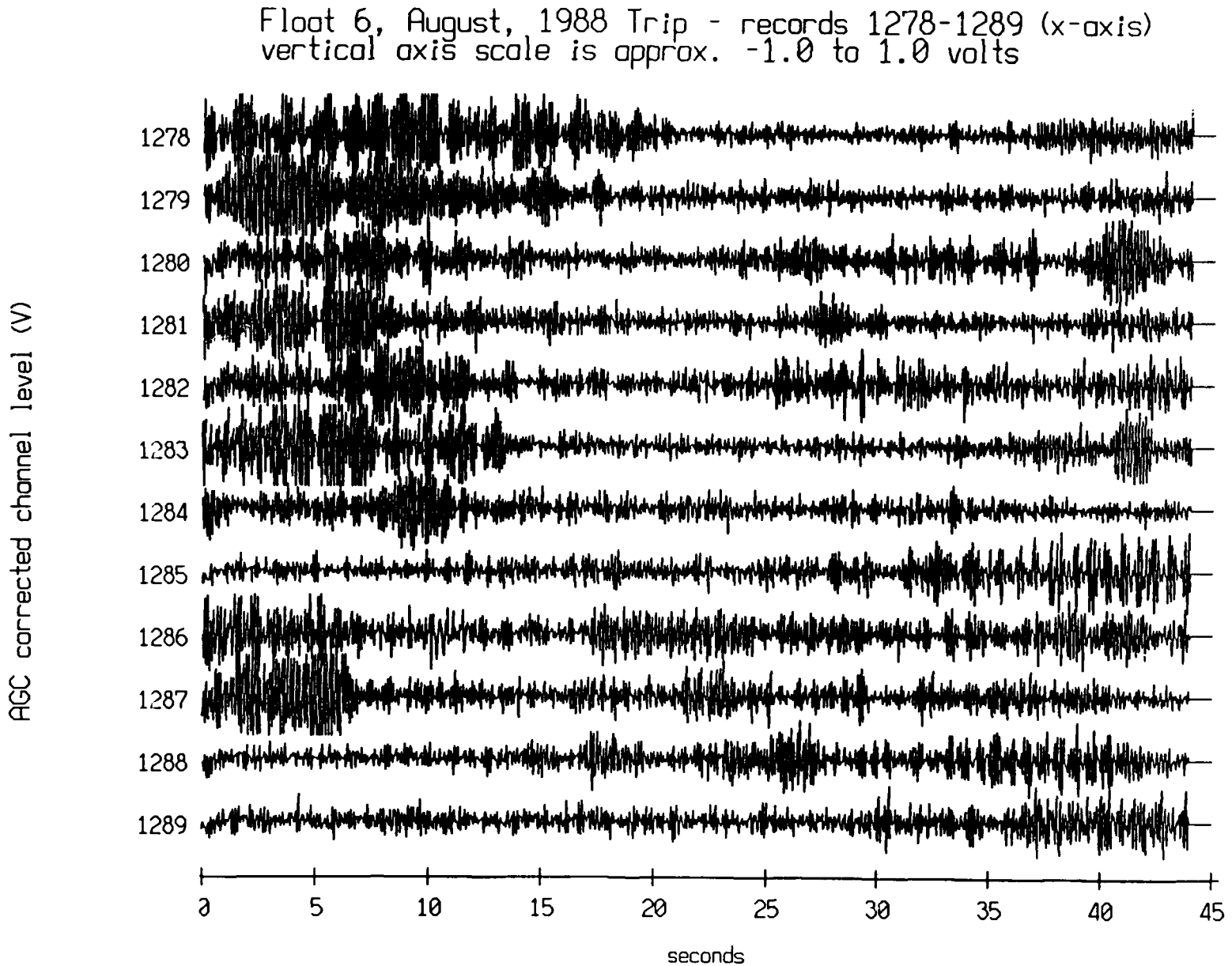


Figure XI.45a

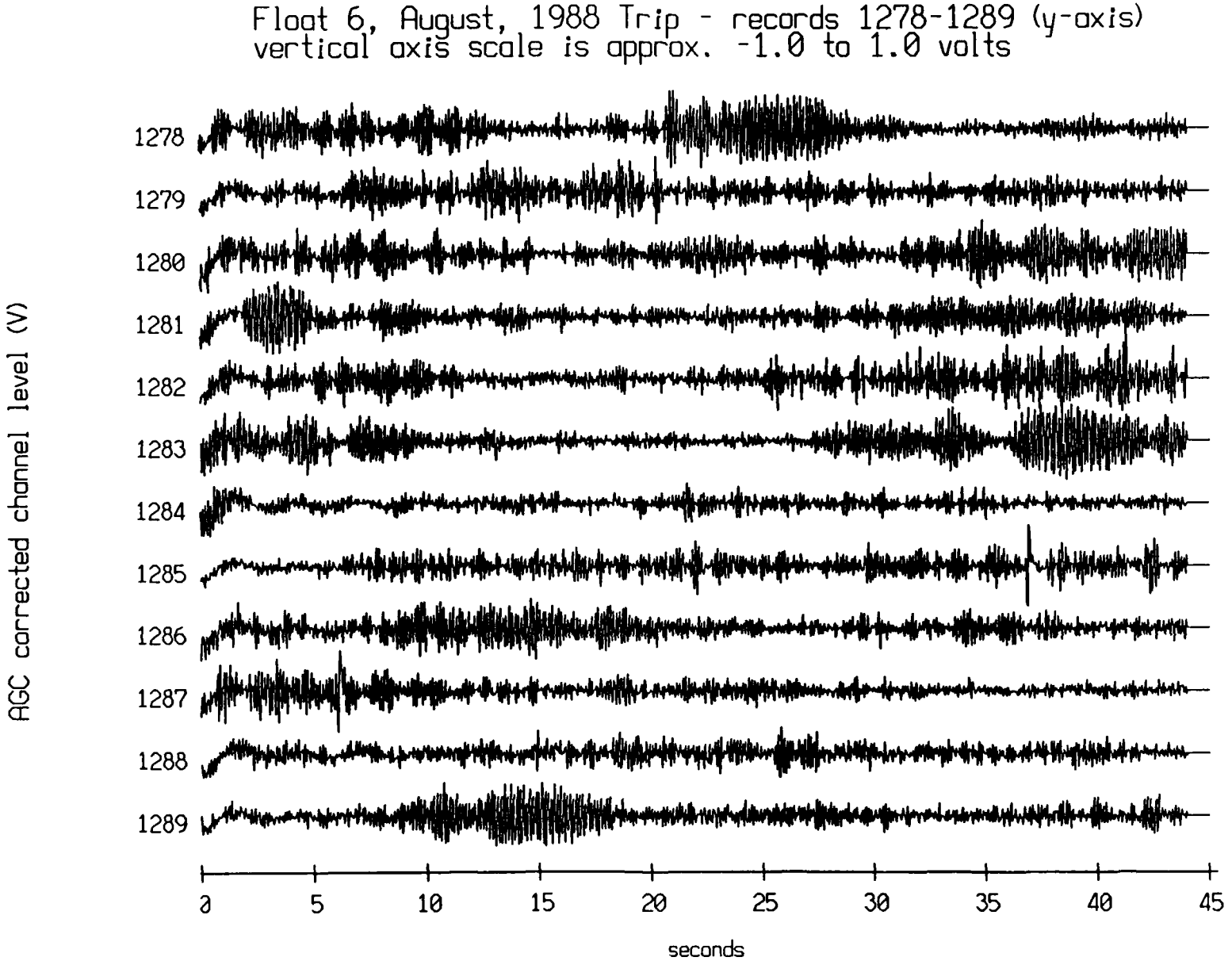


Figure XI.45b

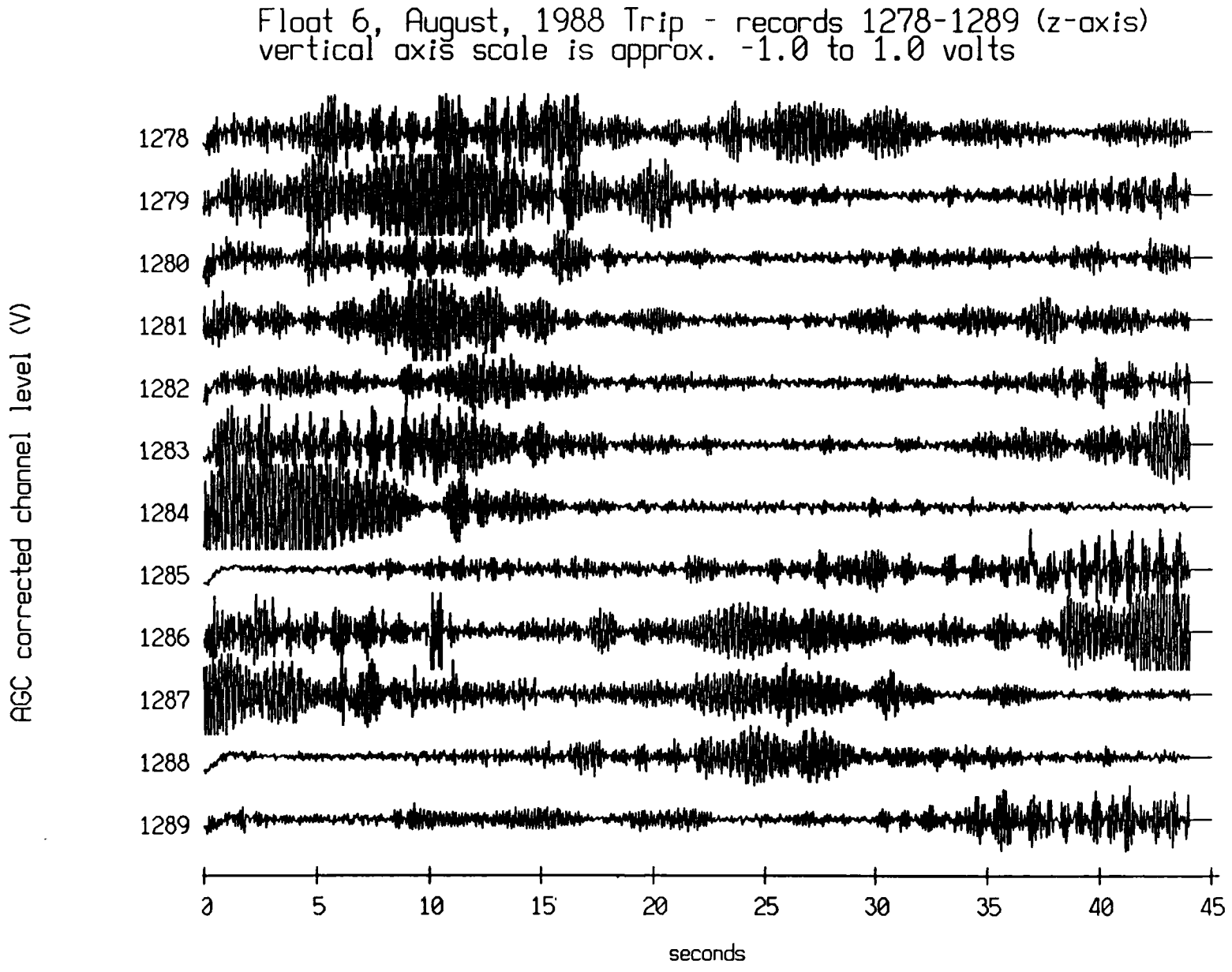


Figure XI.45c

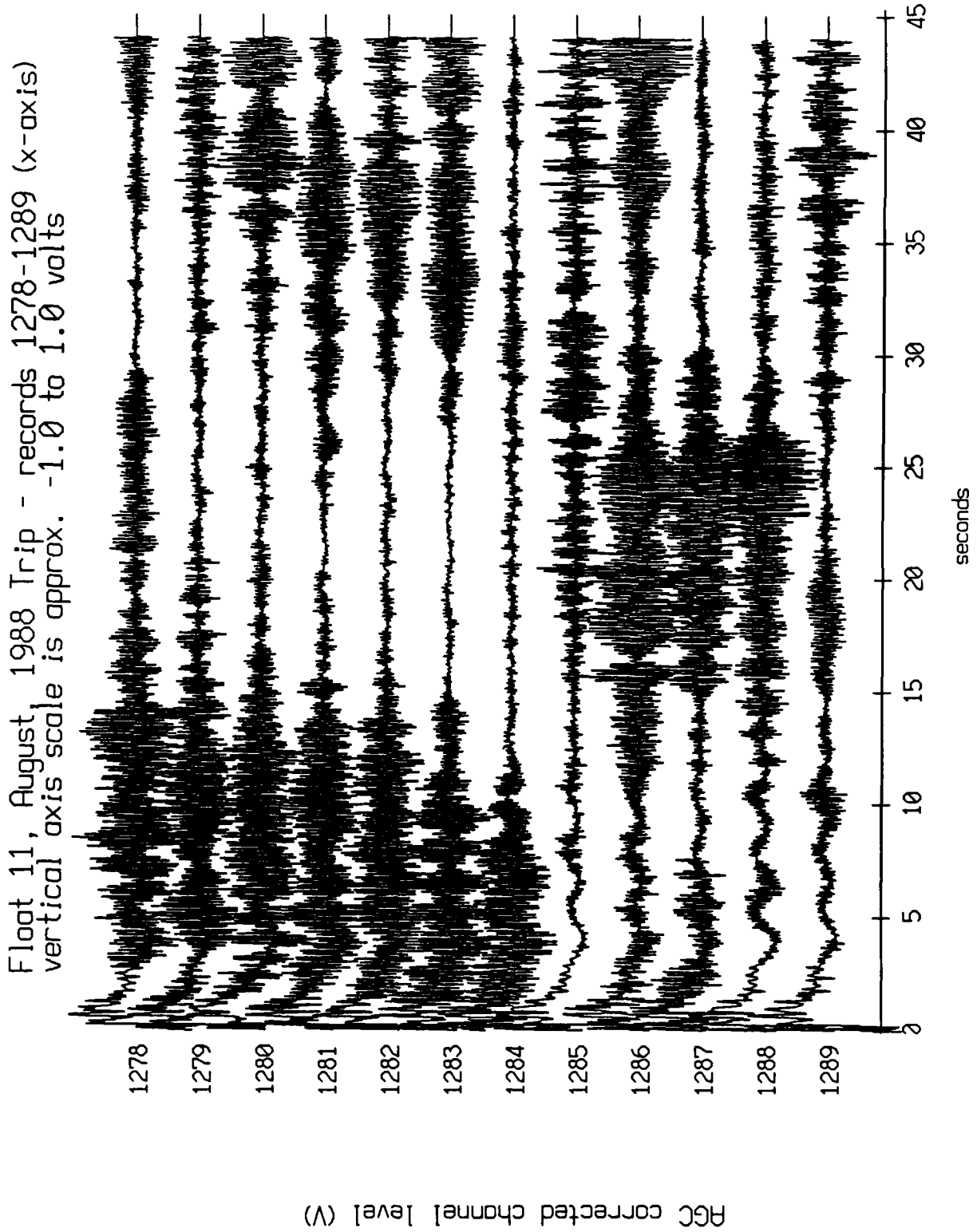


Figure XI.46a

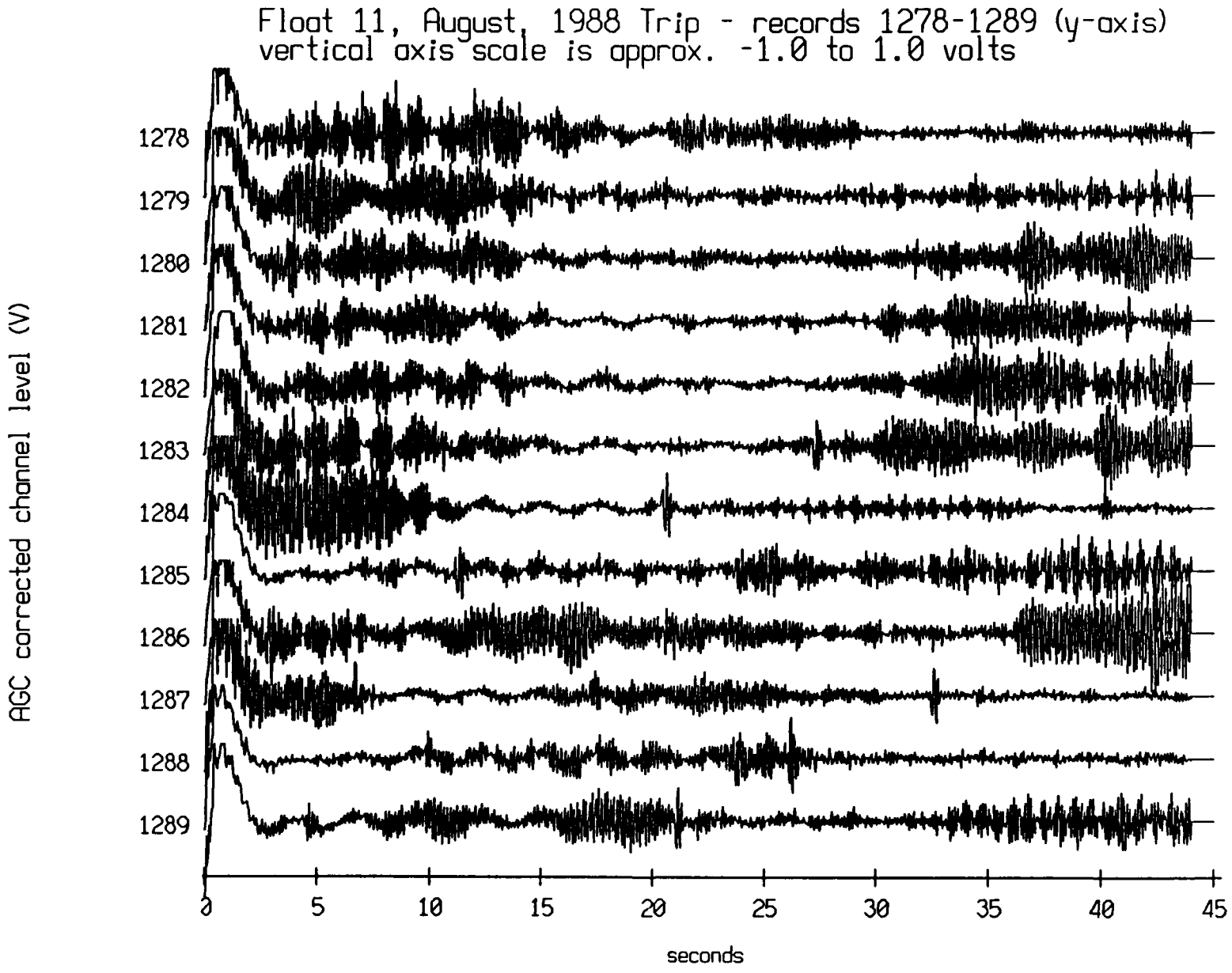


Figure XI.46b

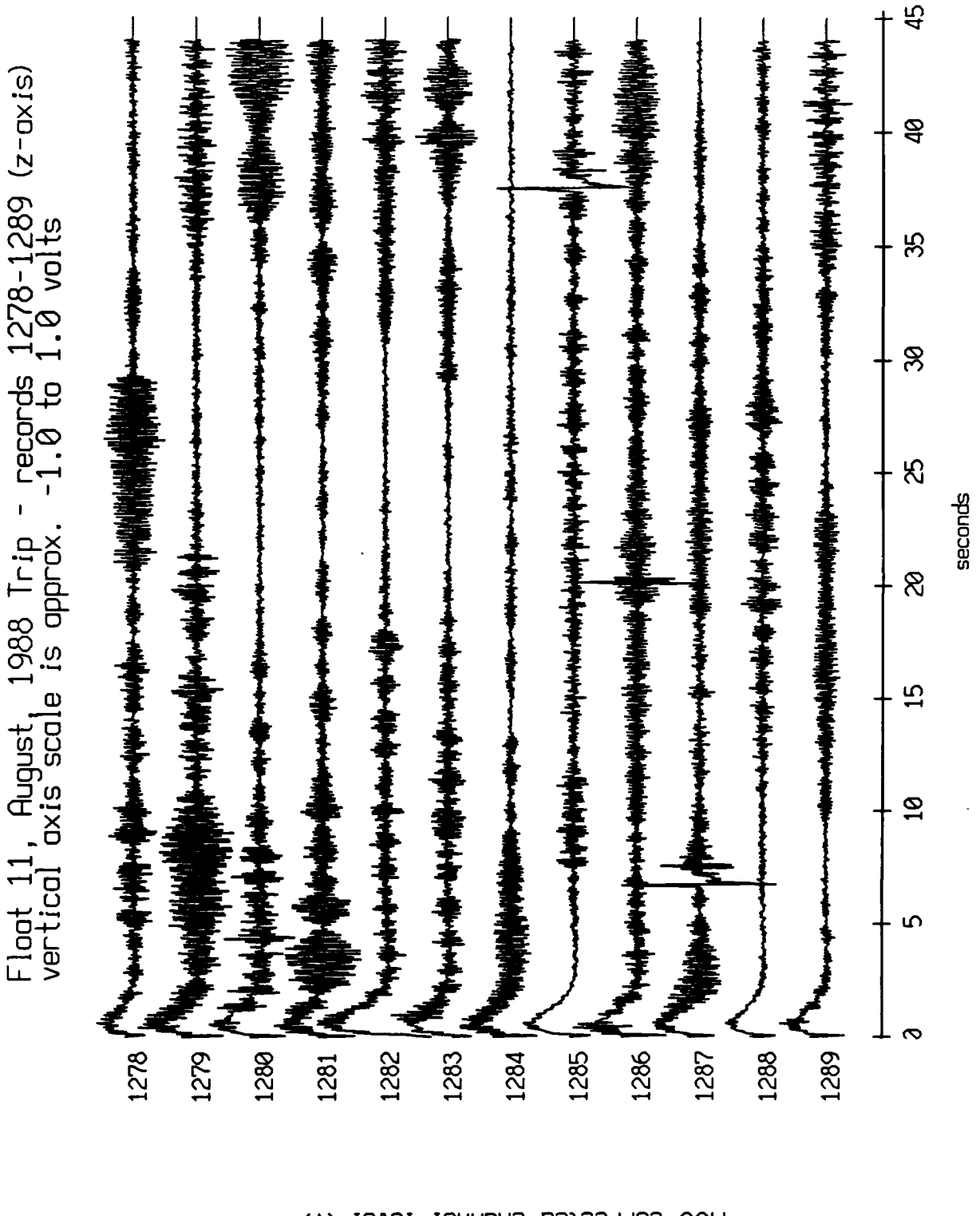


Figure XI.46c

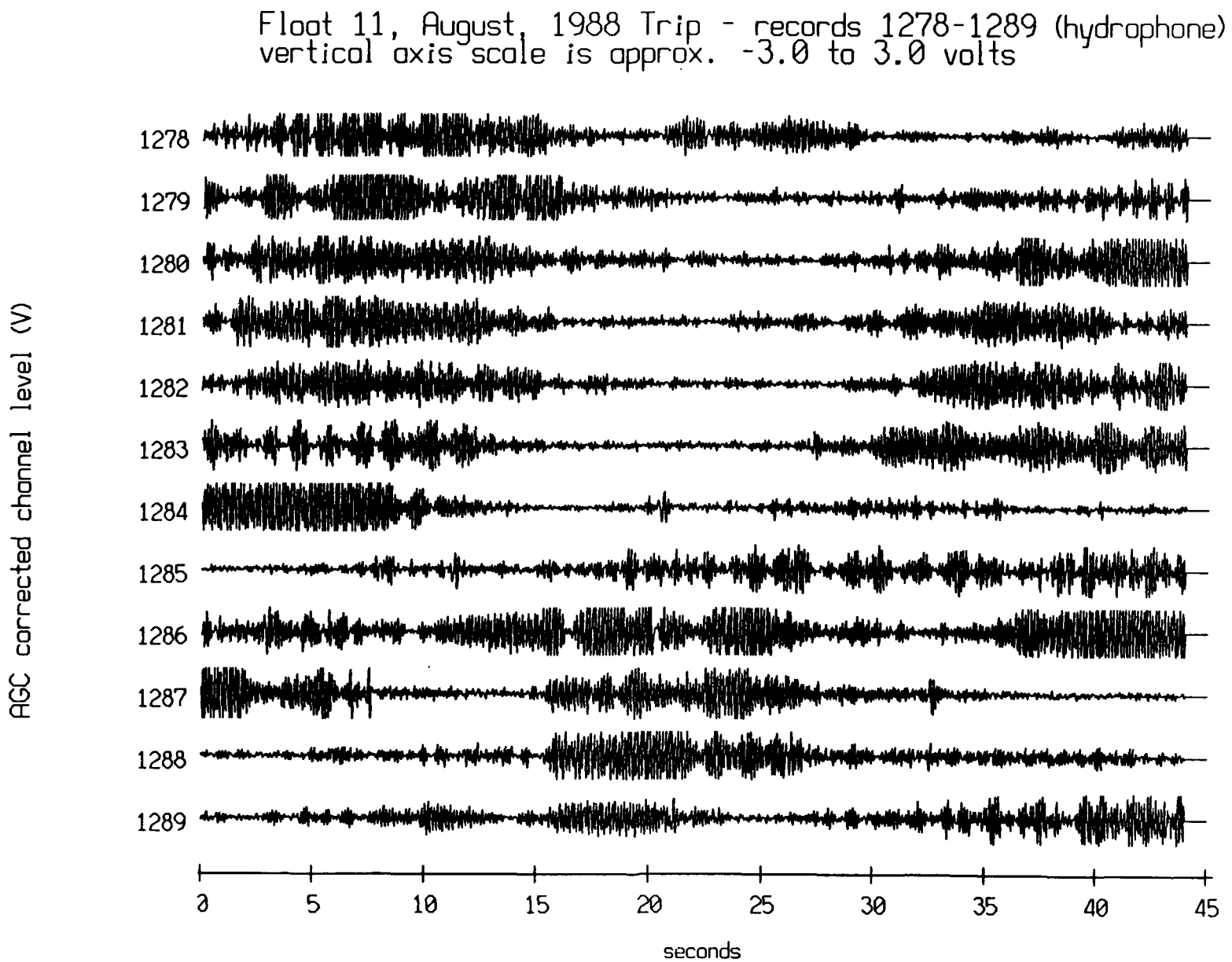


Figure XI.46d

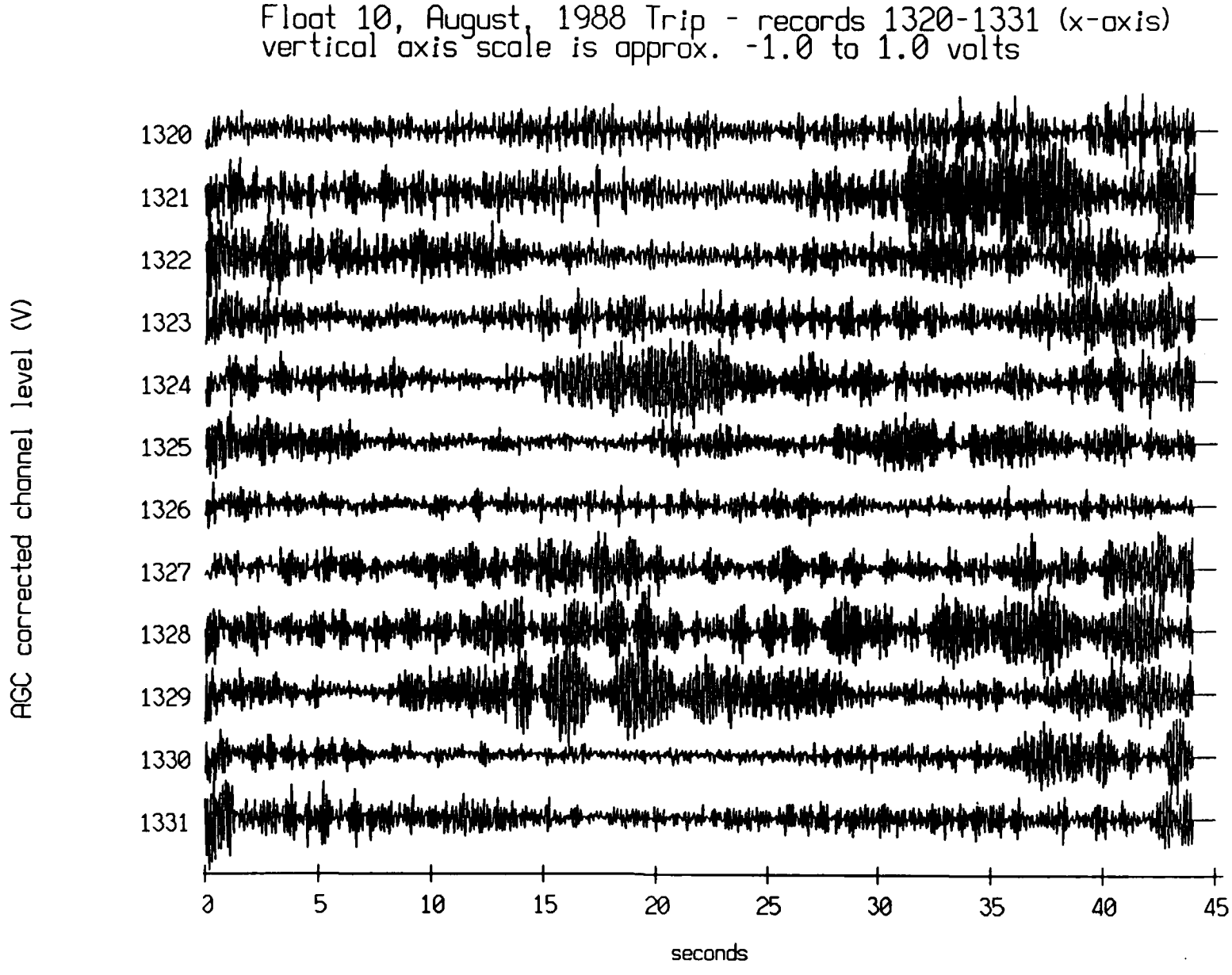


Figure XI.47a

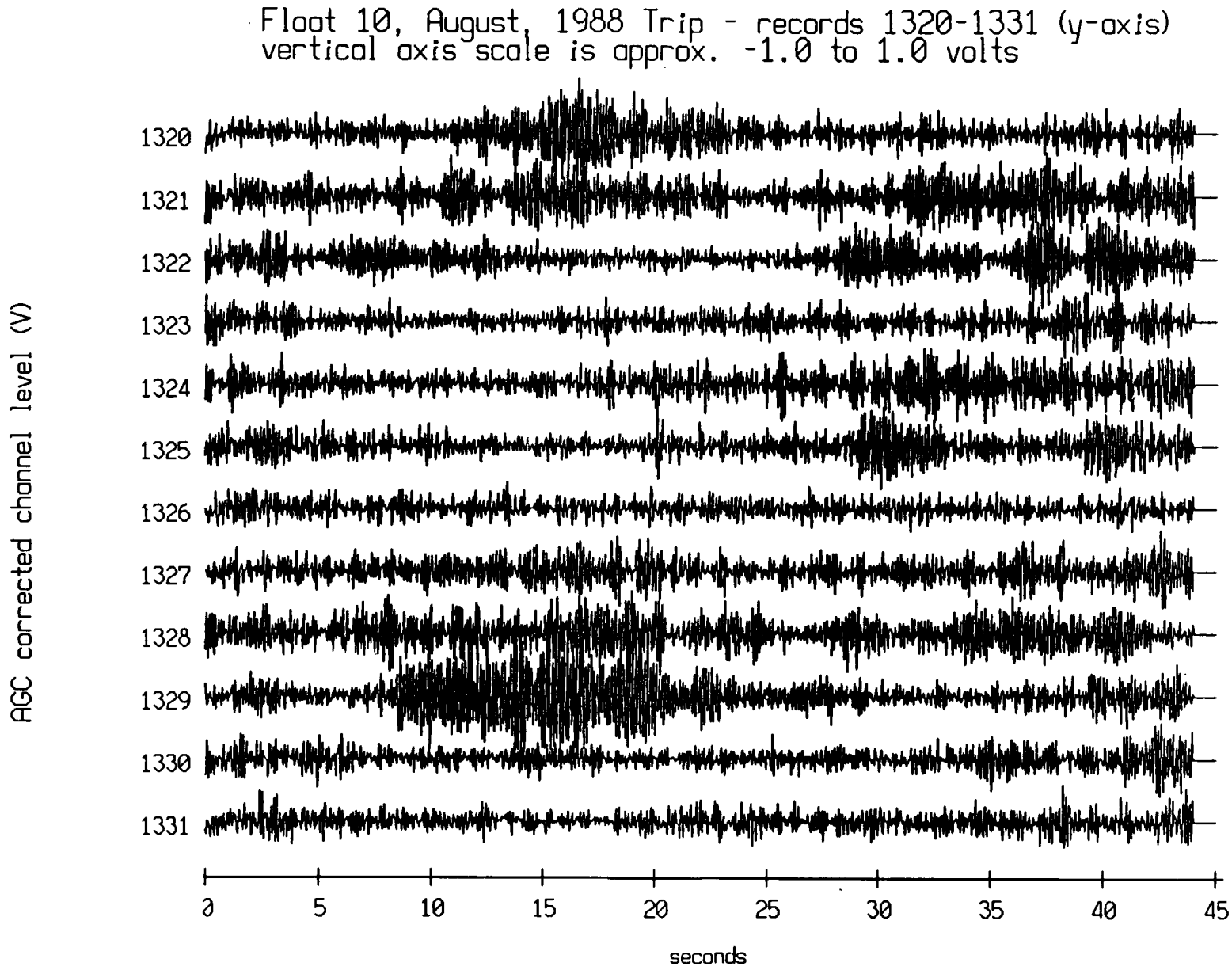


Figure XI.47b

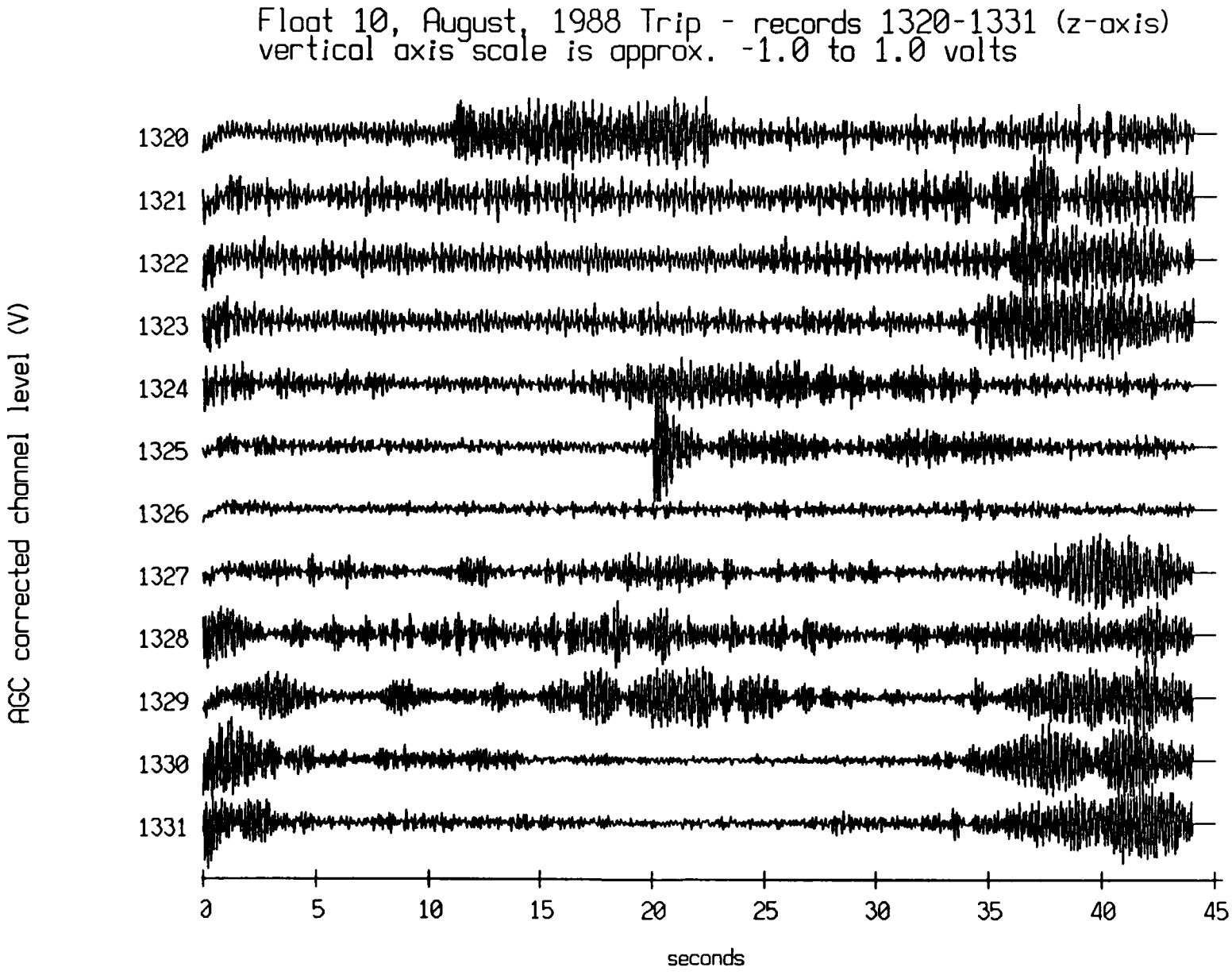


Figure XI.47c

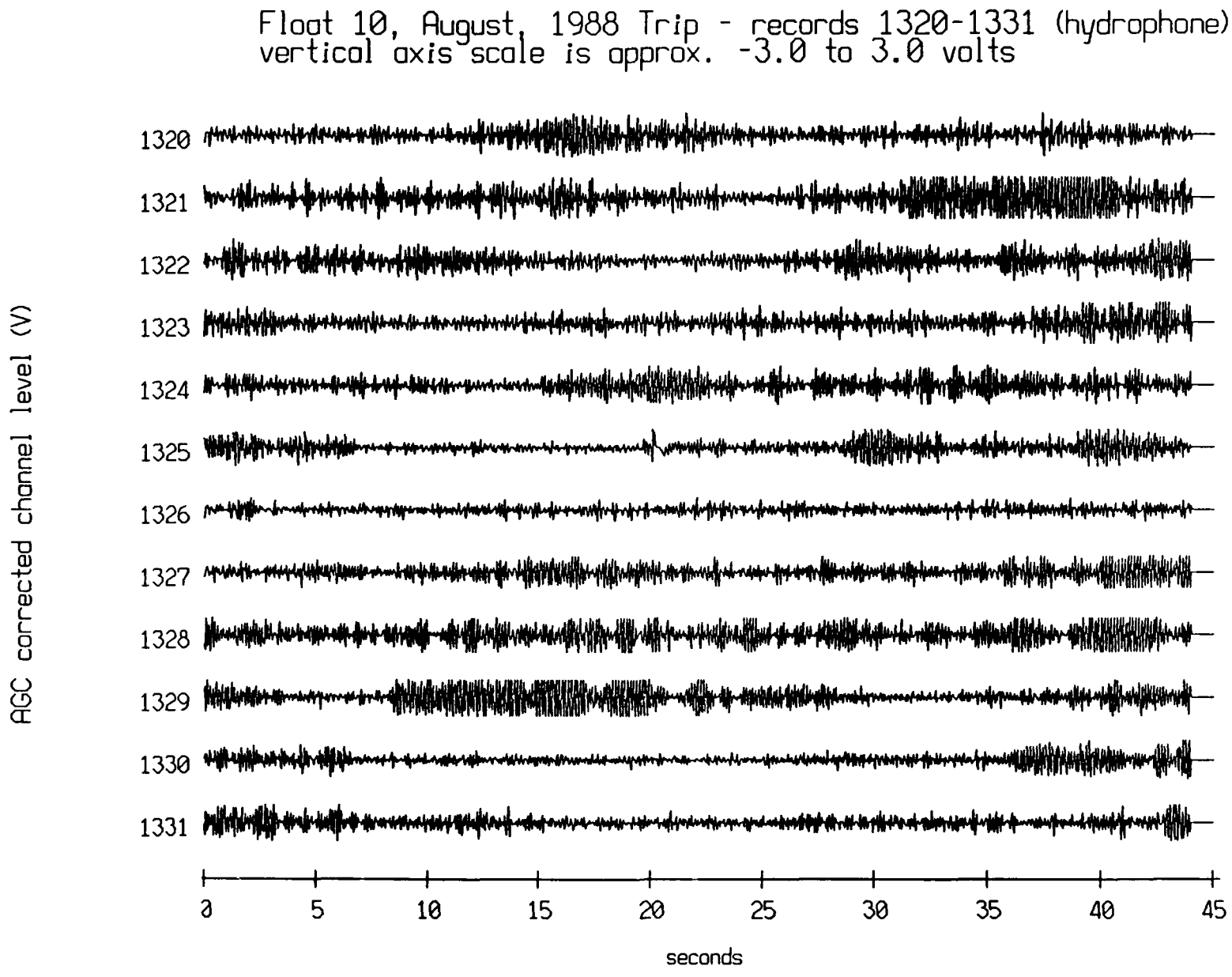


Figure XI.47d

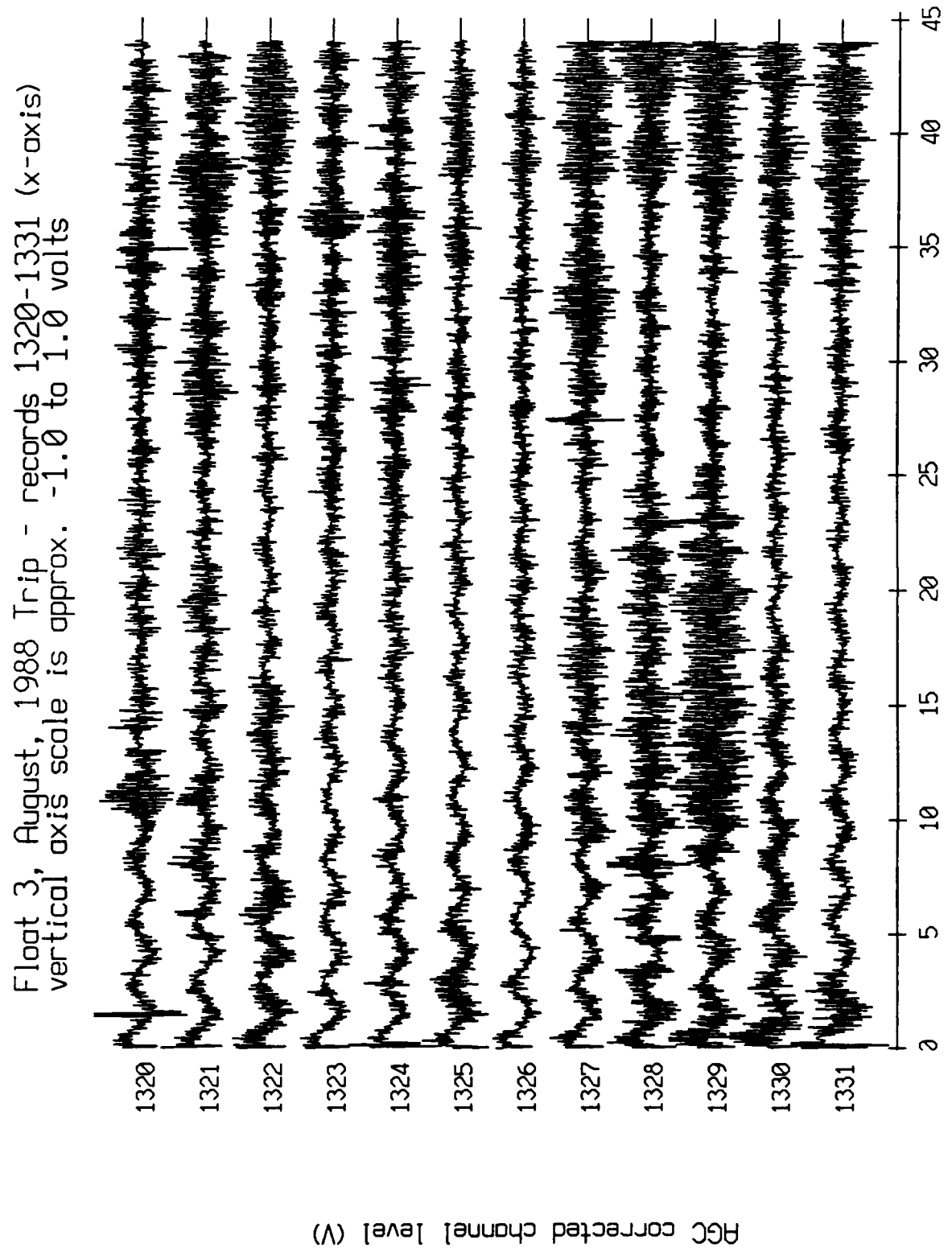


Figure XI.48a

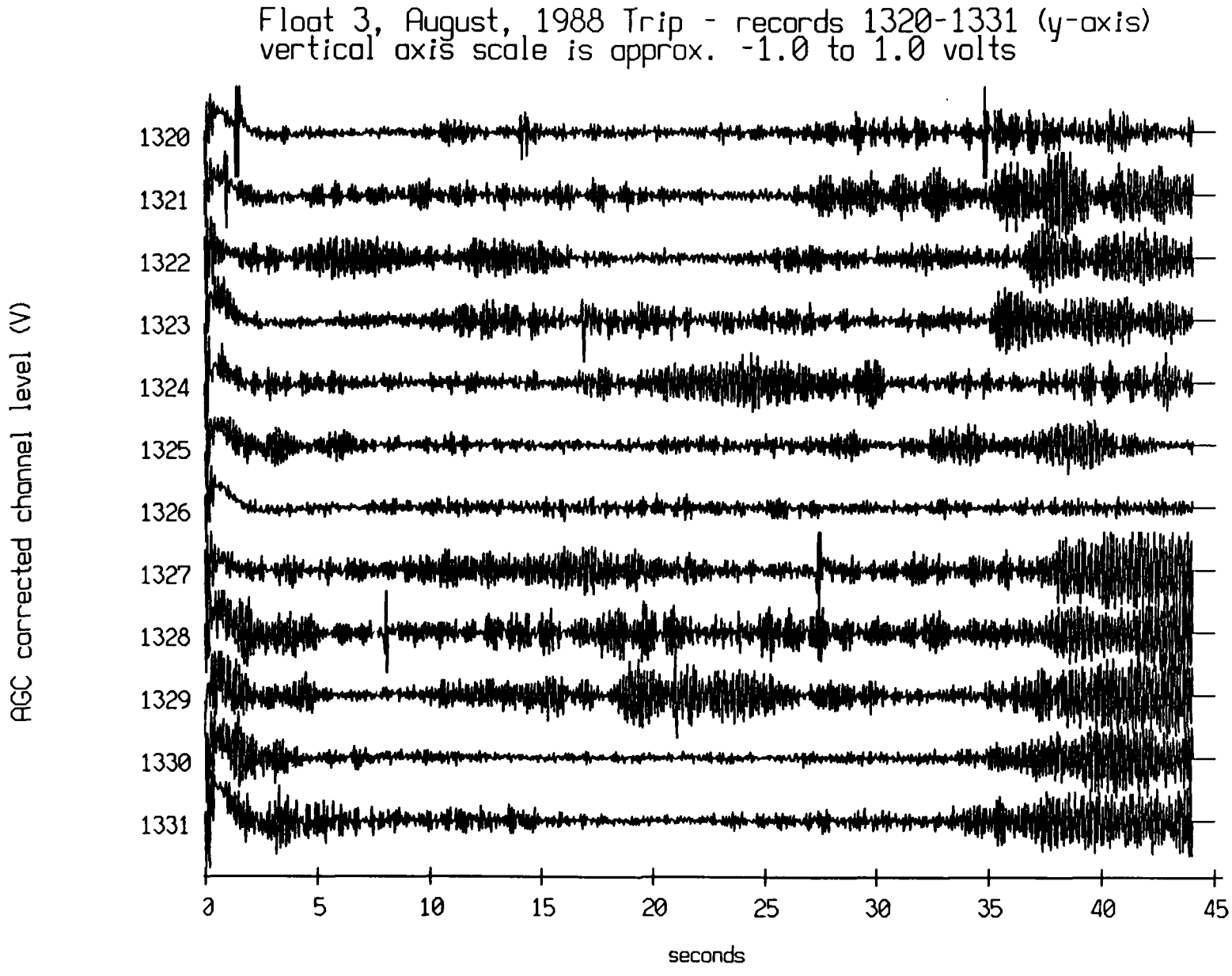


Figure XI.48b

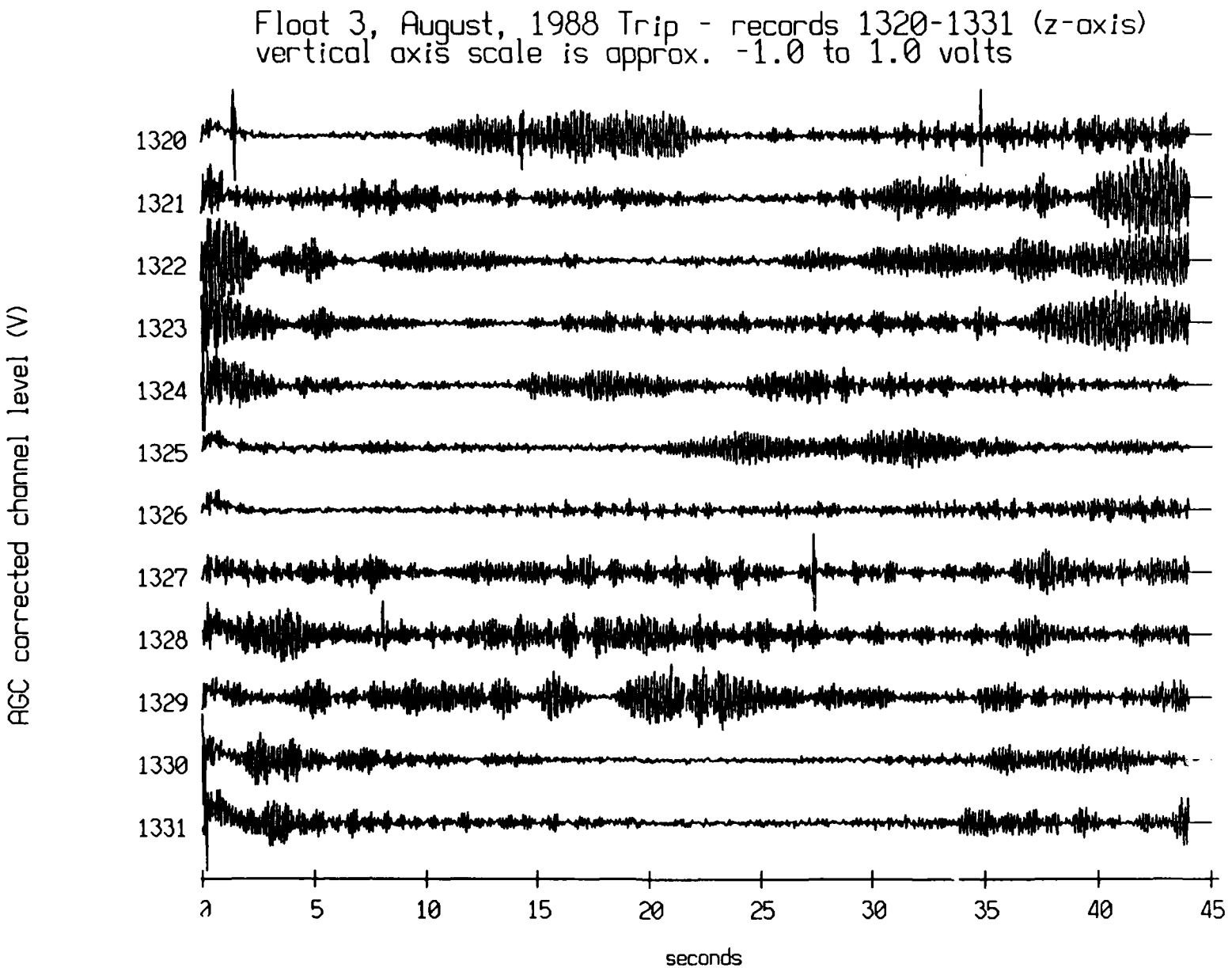


Figure XI.48c

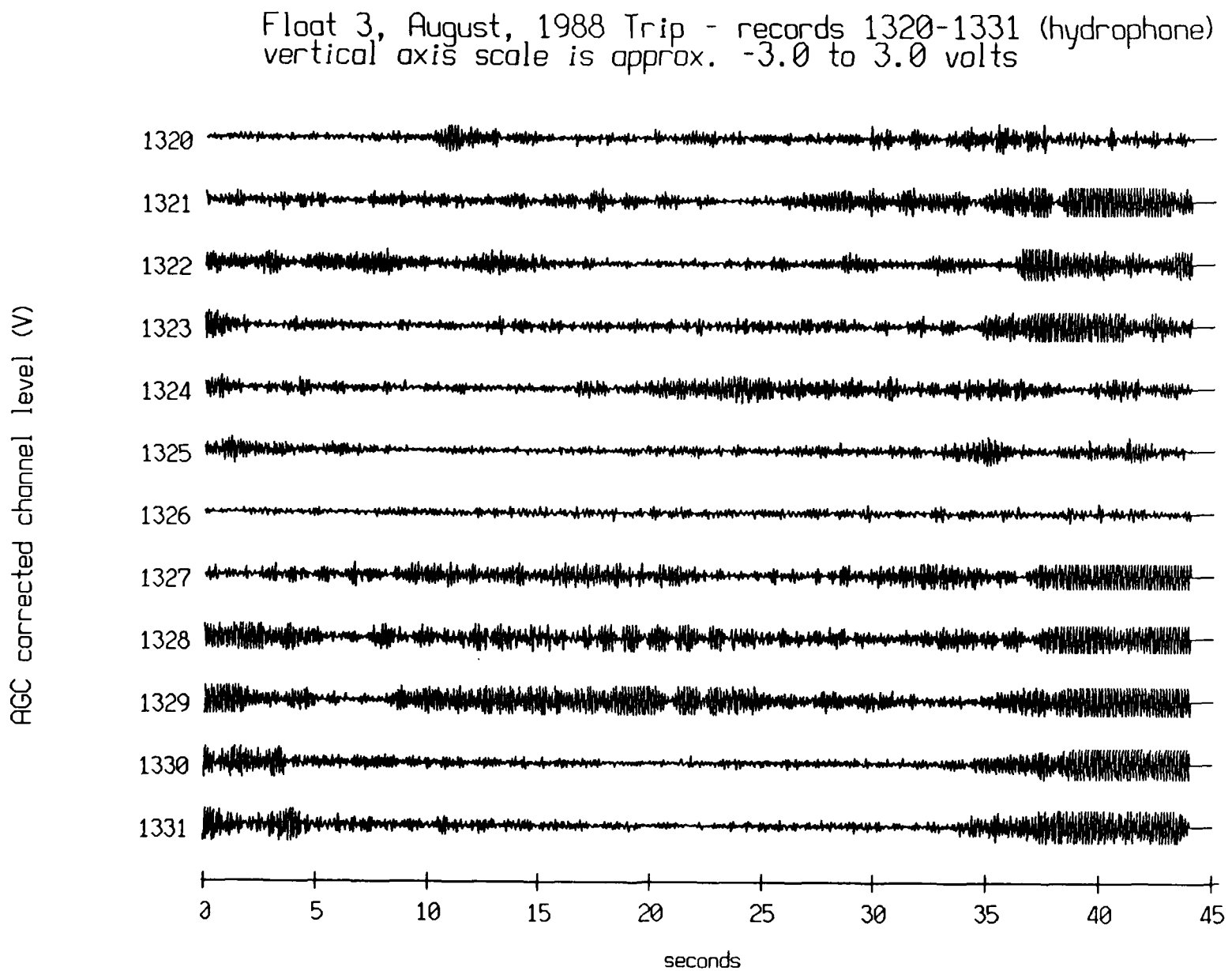


Figure XI.48d

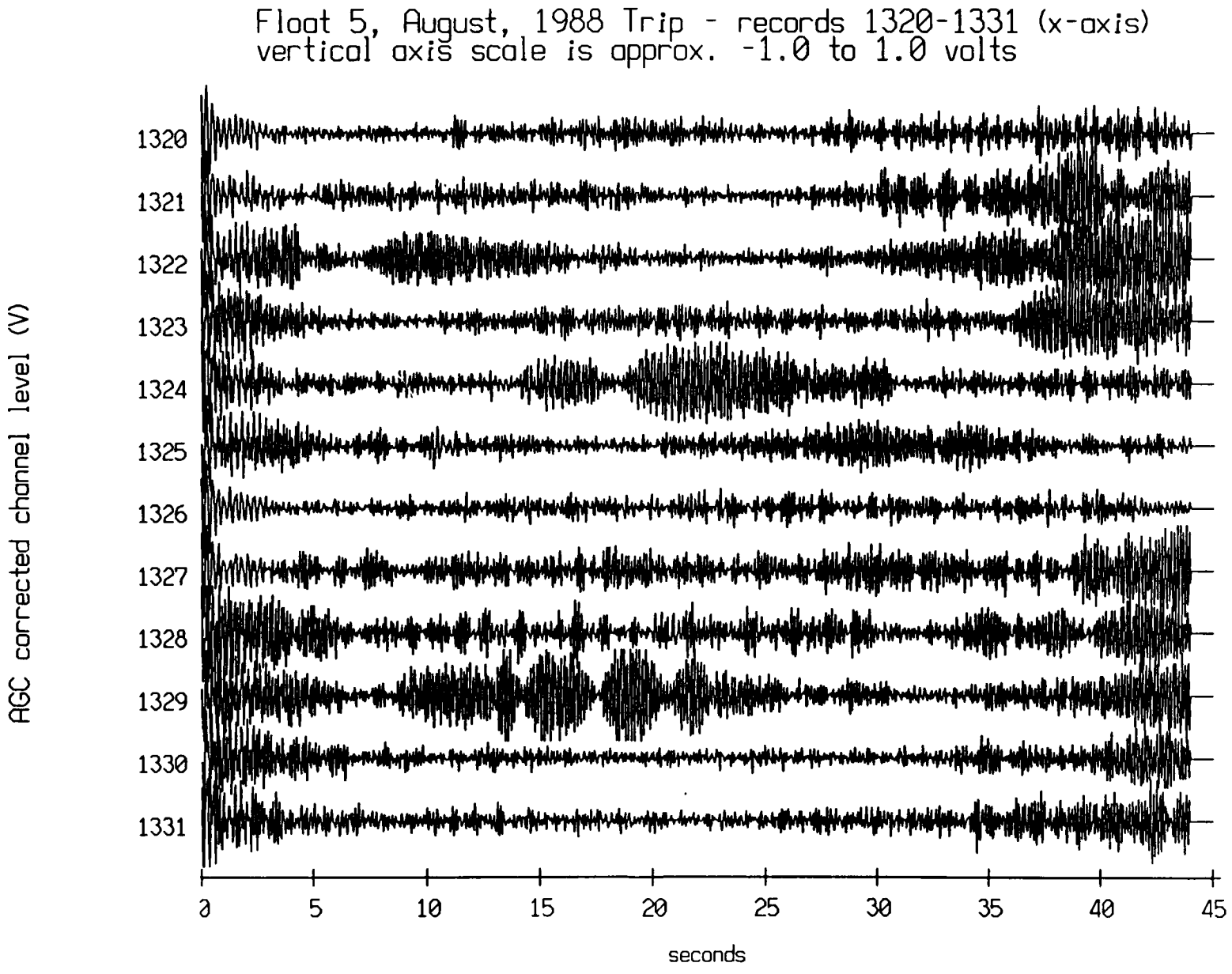


Figure XI.49a

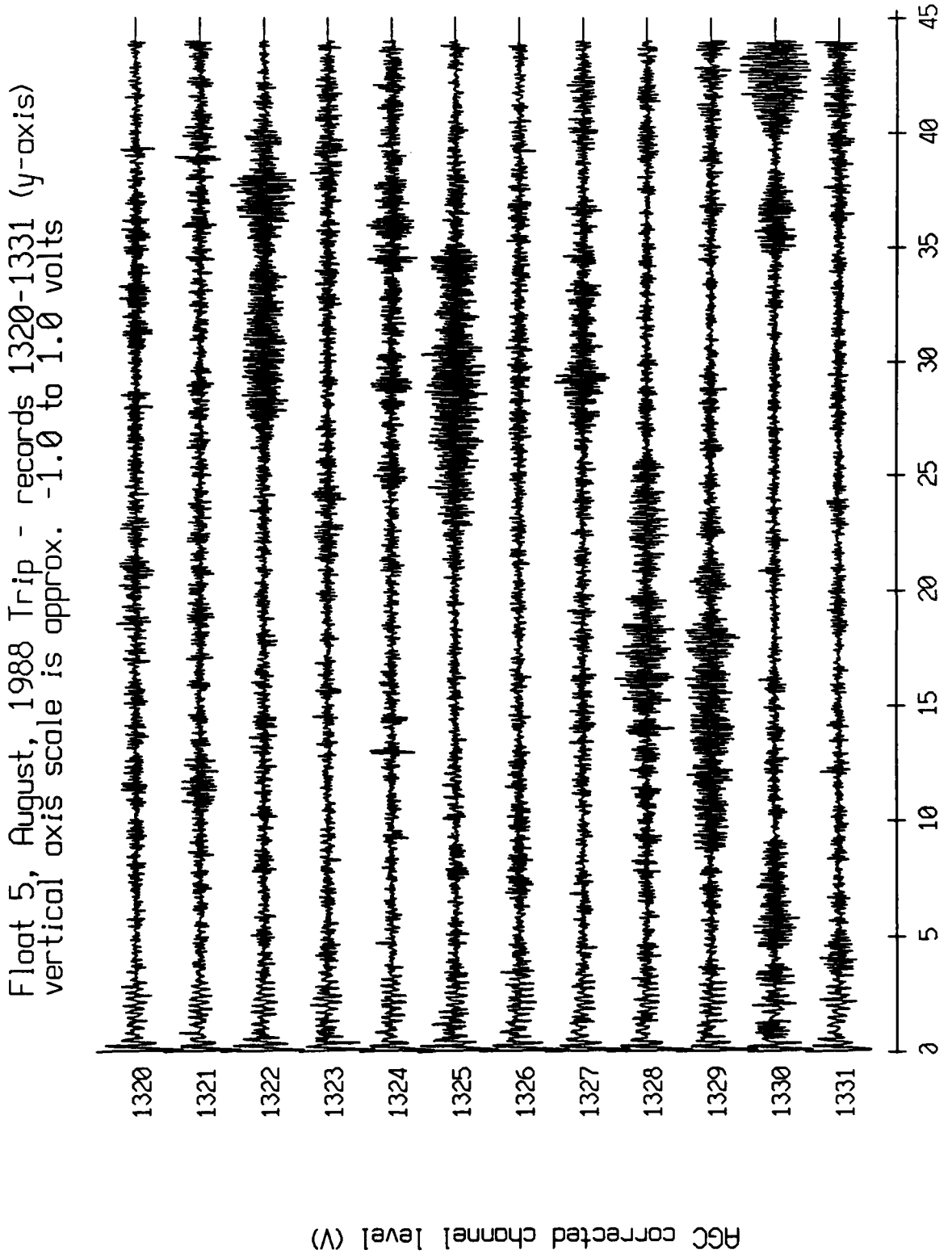


Figure XI.49b

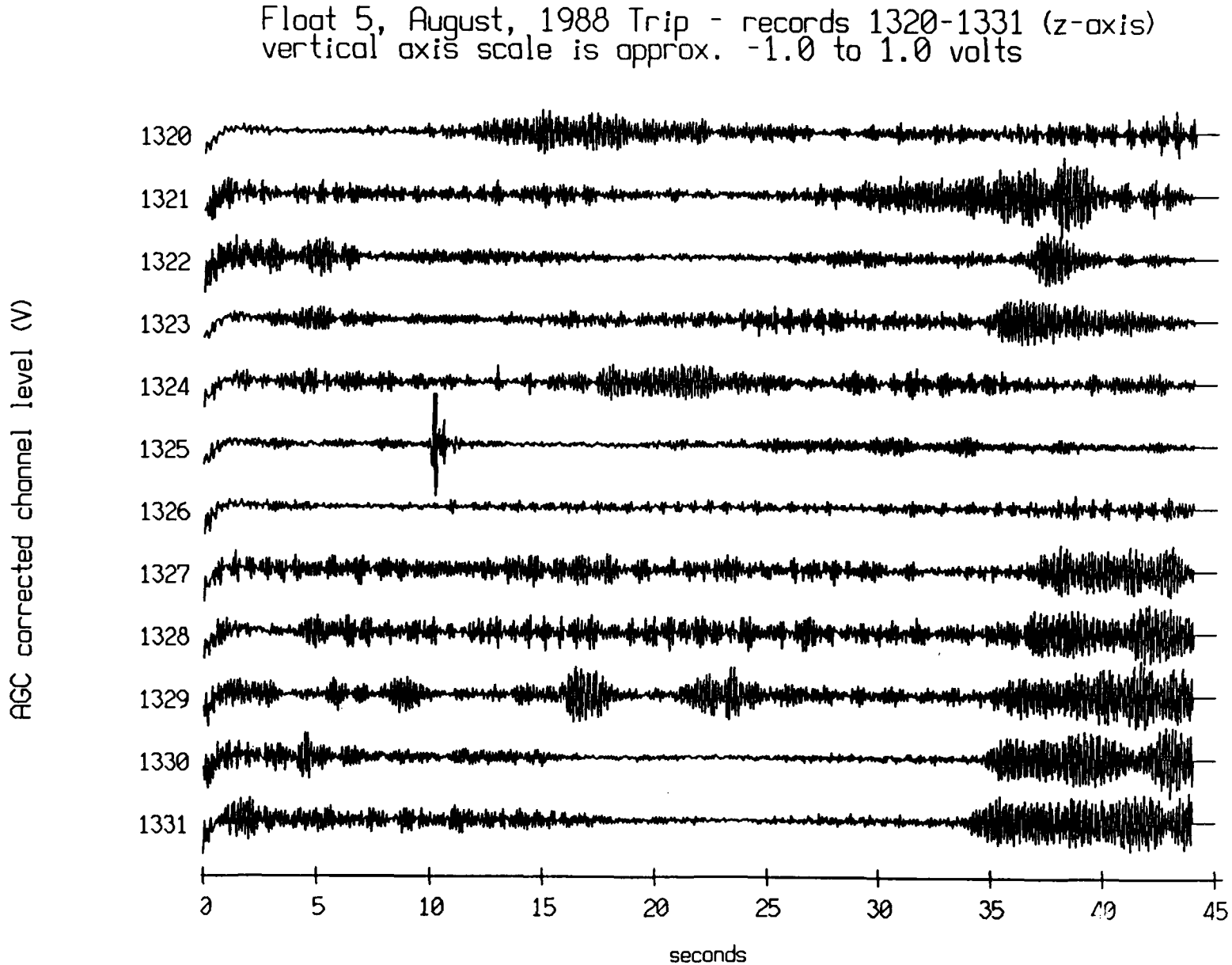


Figure XI.49c

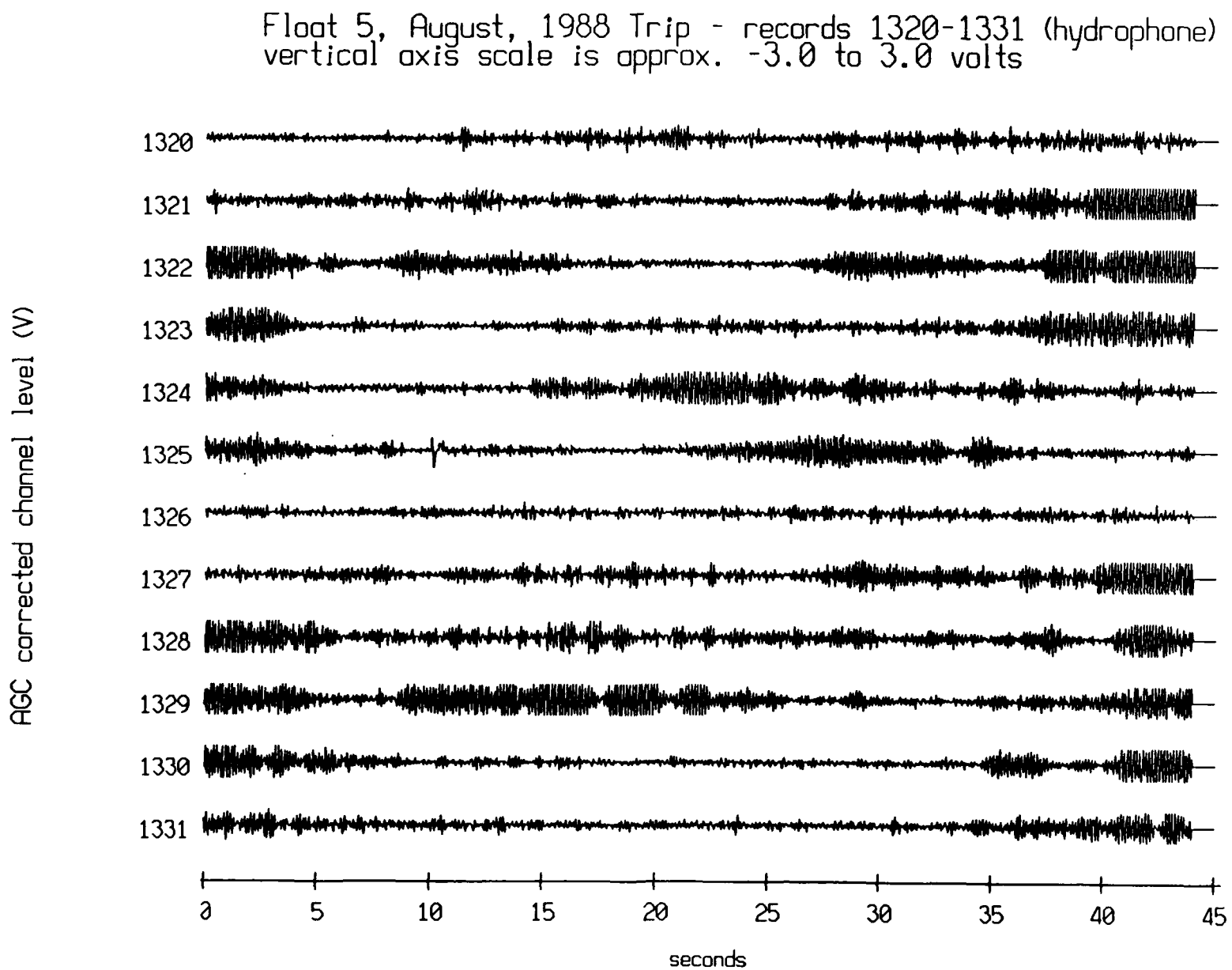


Figure XI.49d

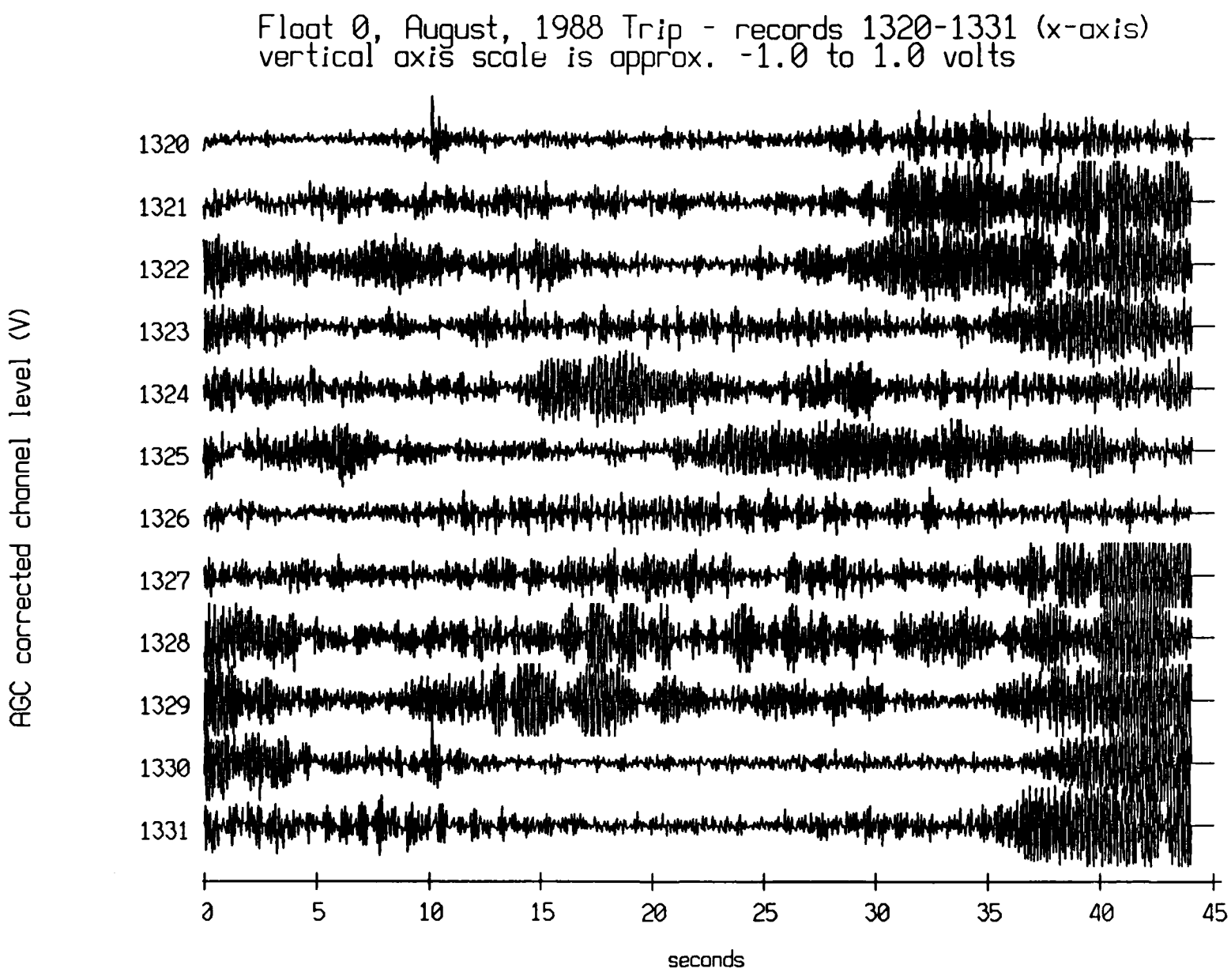


Figure XI.50a

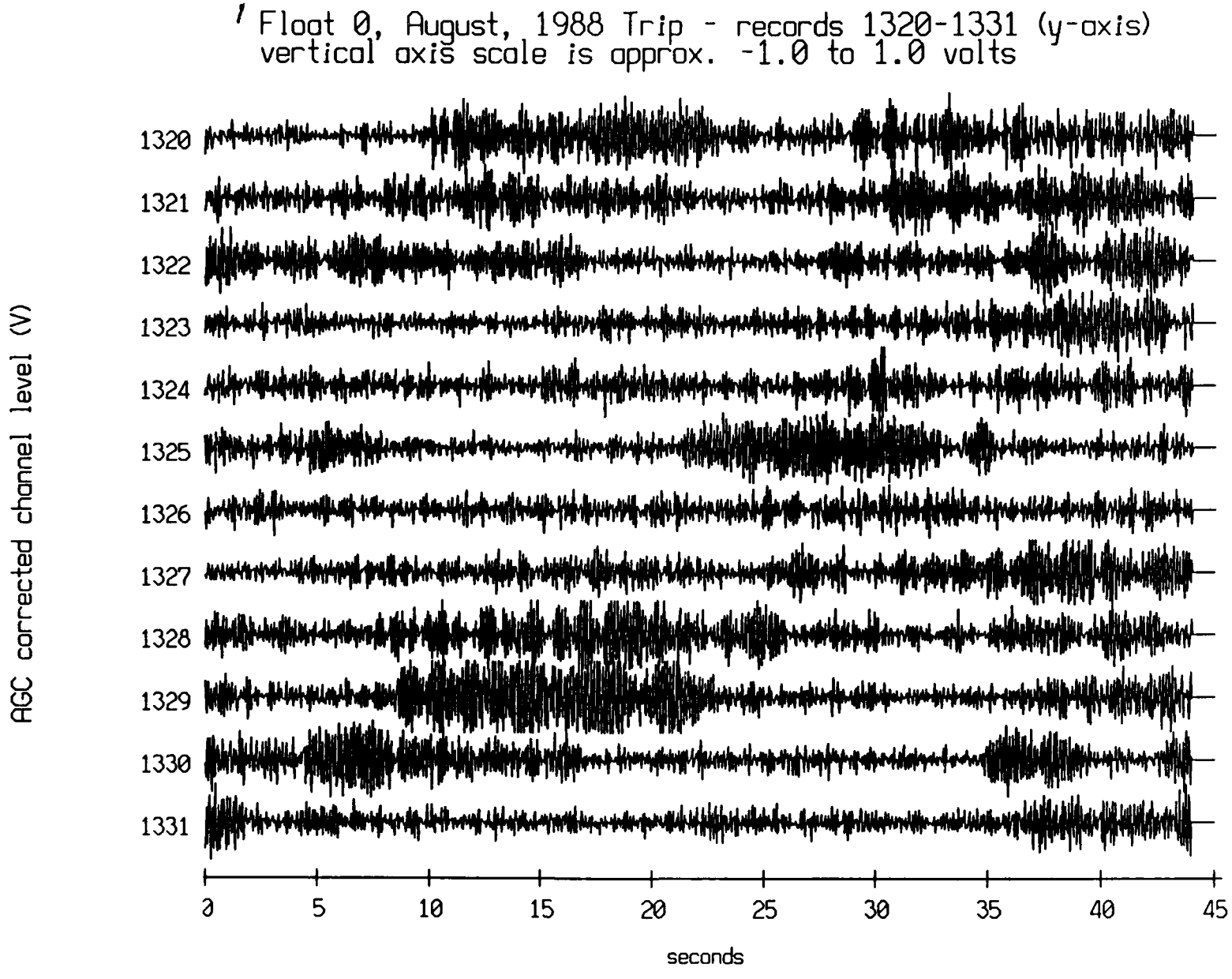


Figure XI.50b

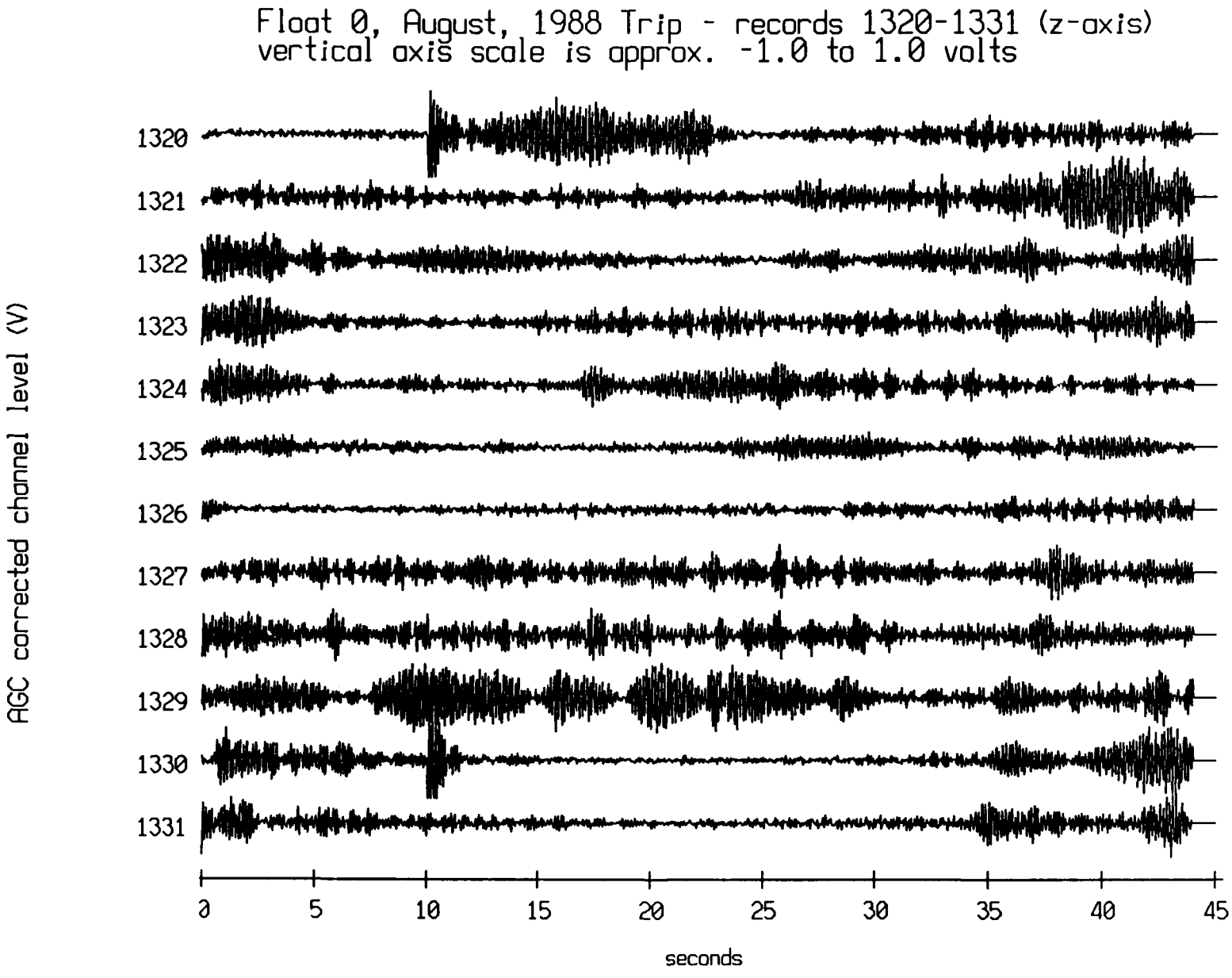


Figure XI.50c

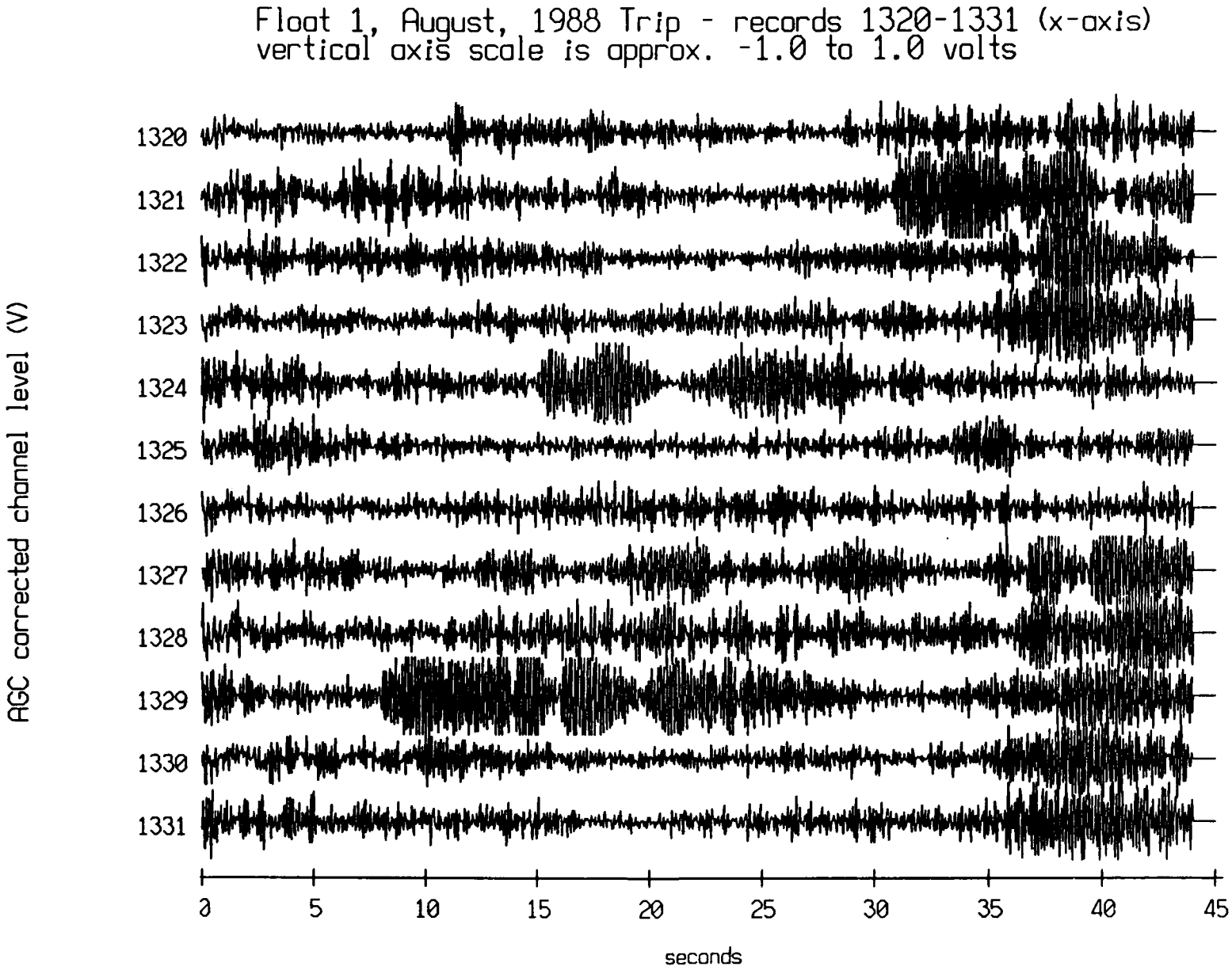


Figure XI.51a

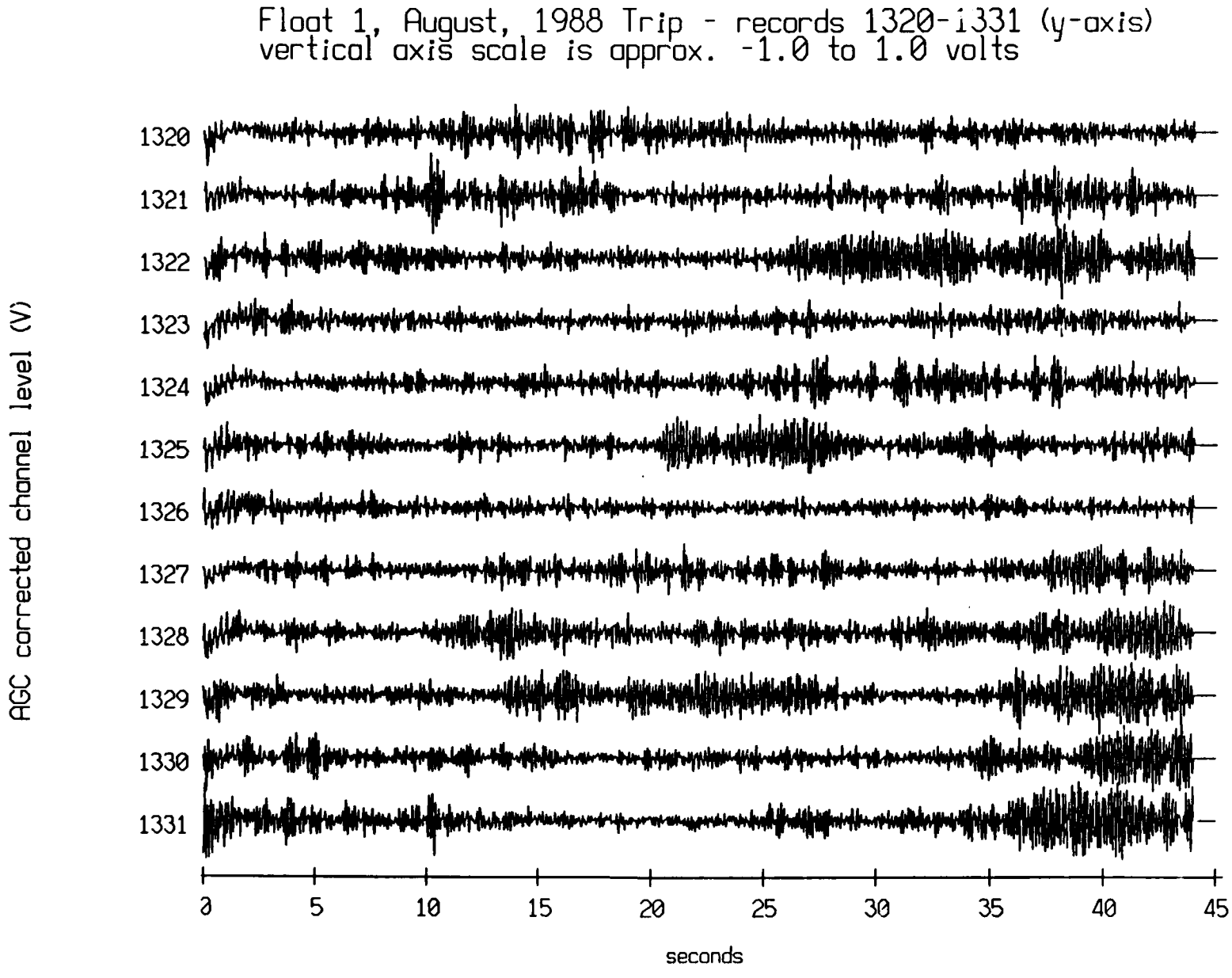


Figure XI.51b

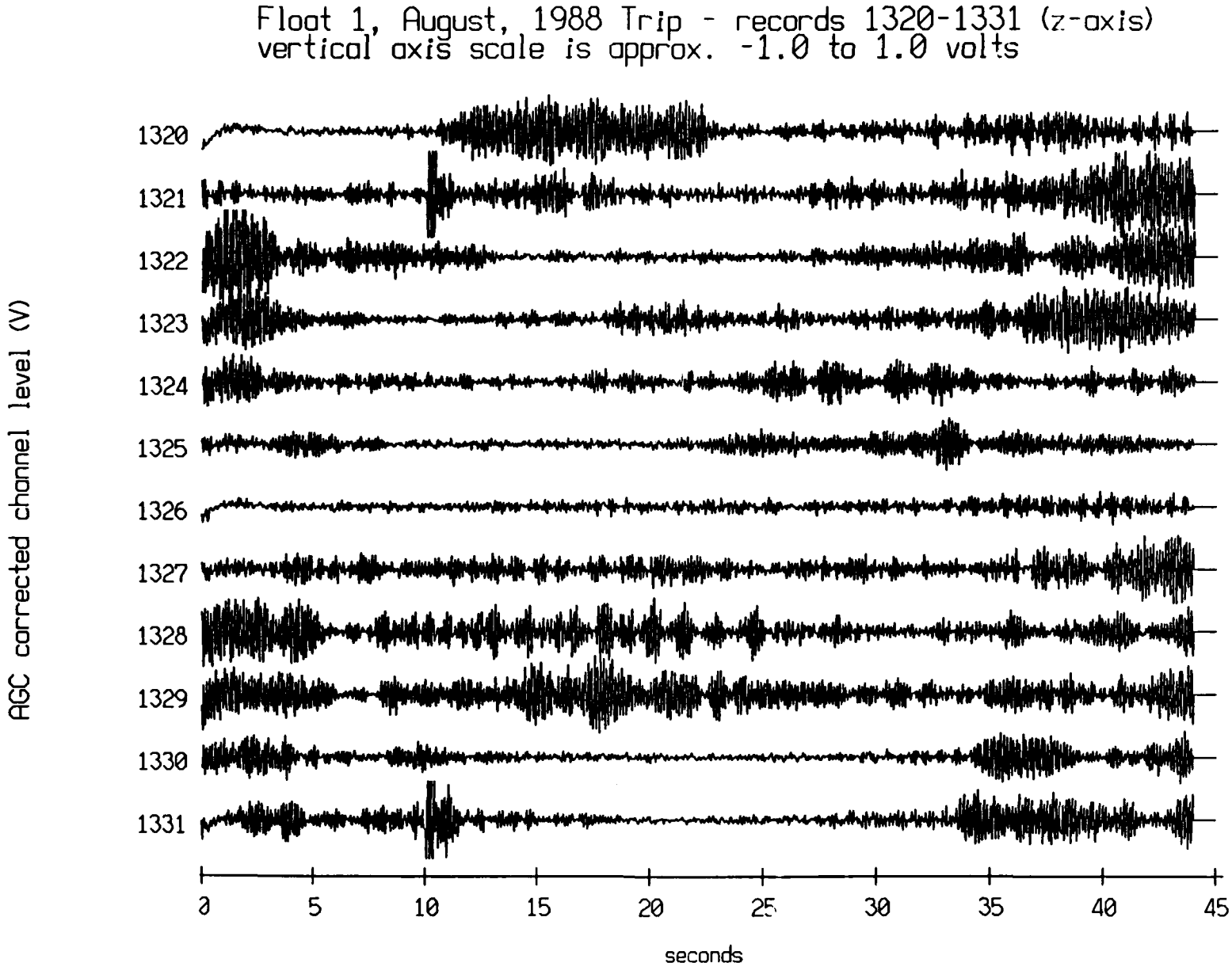


Figure XI.51c

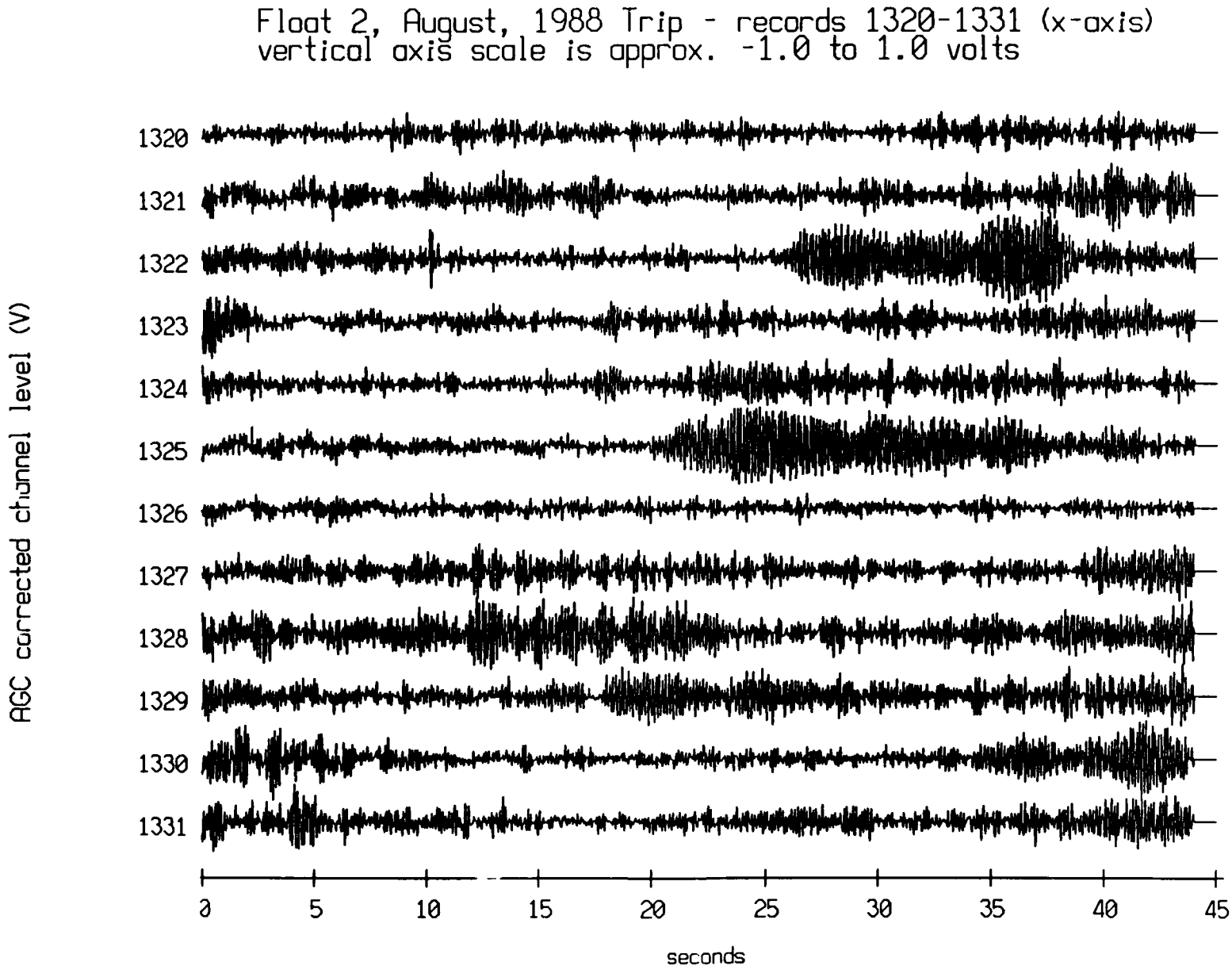


Figure XI.52a

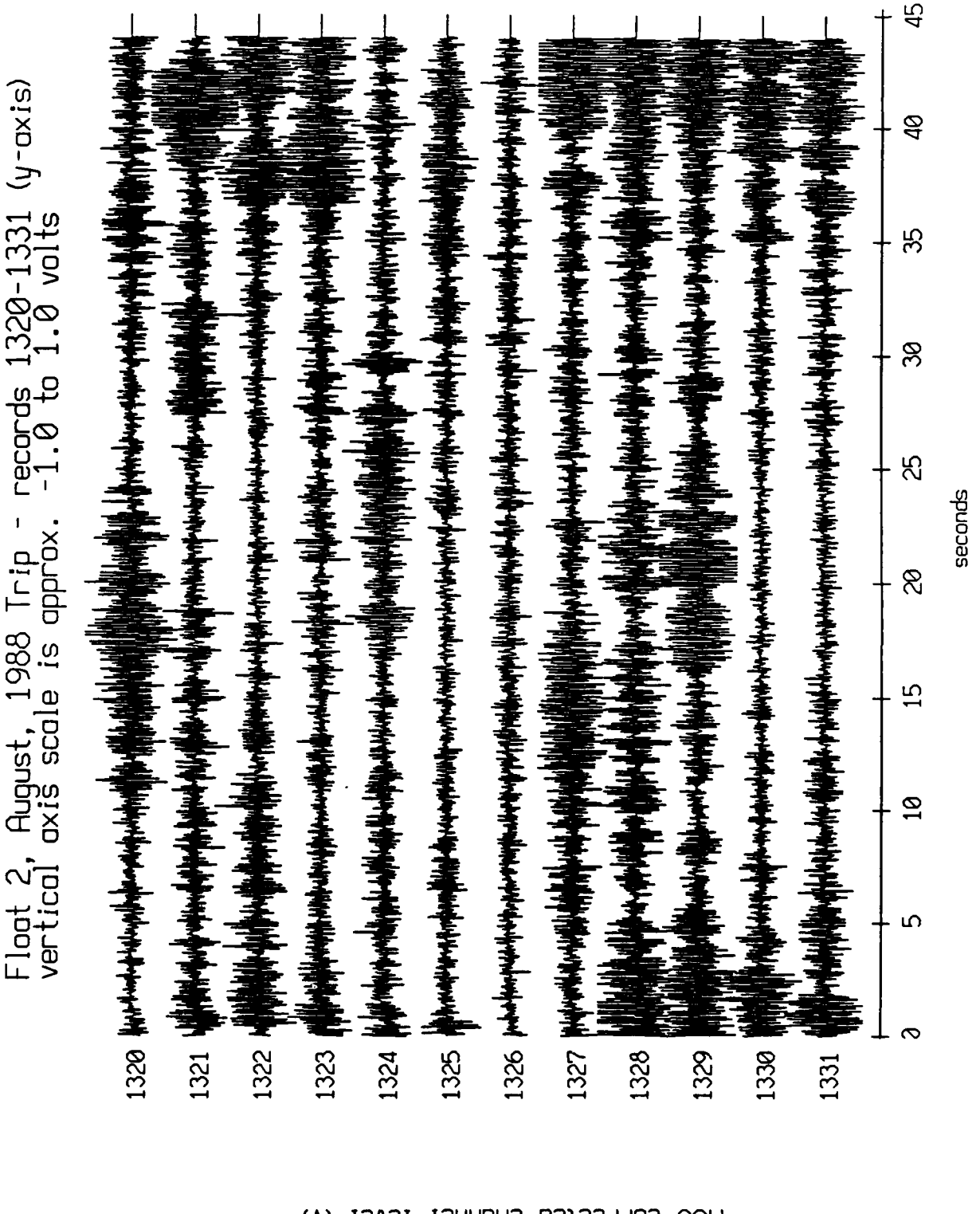


Figure XI.52b

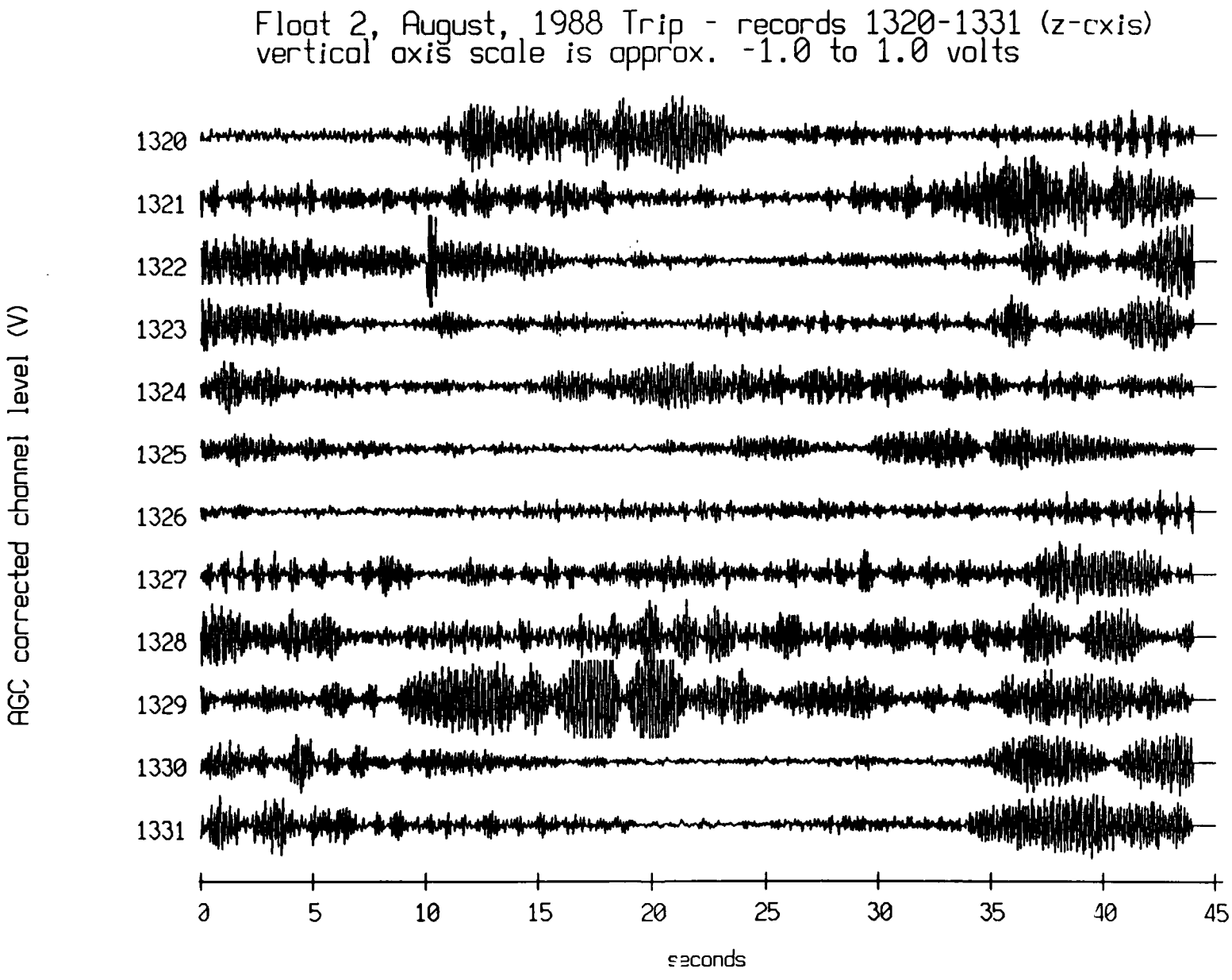


Figure XI.52c

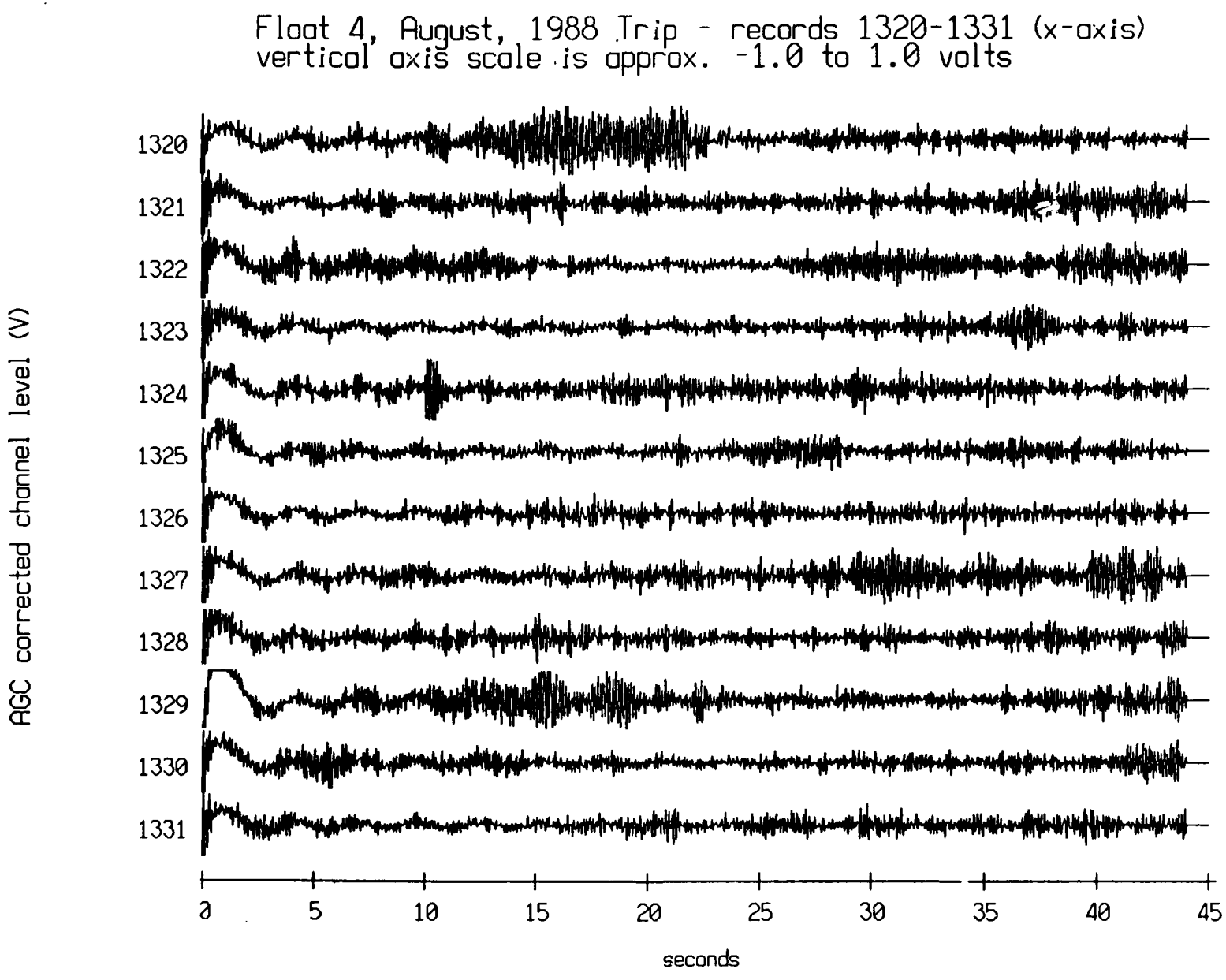


Figure XI.53a

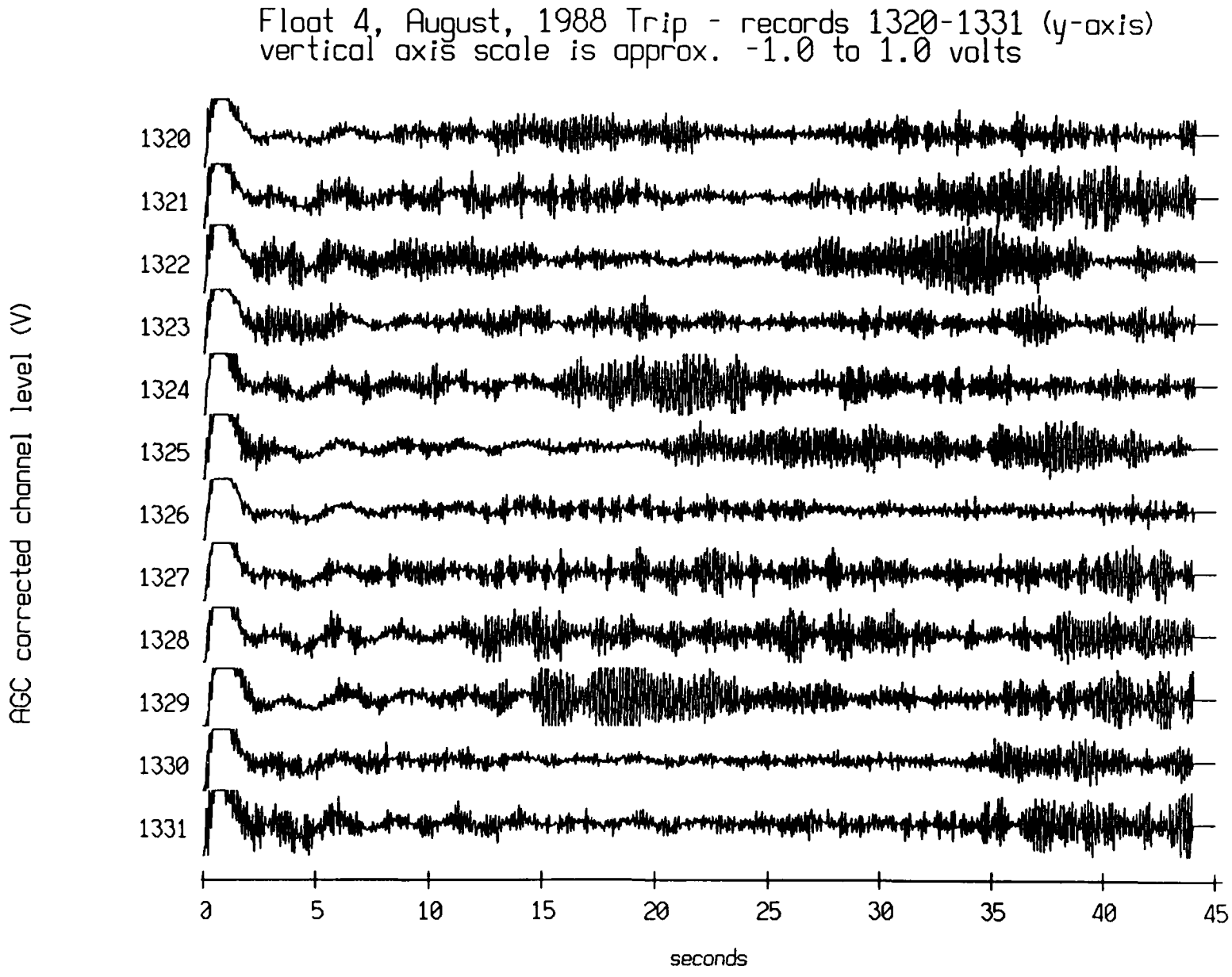


Figure XI.53b

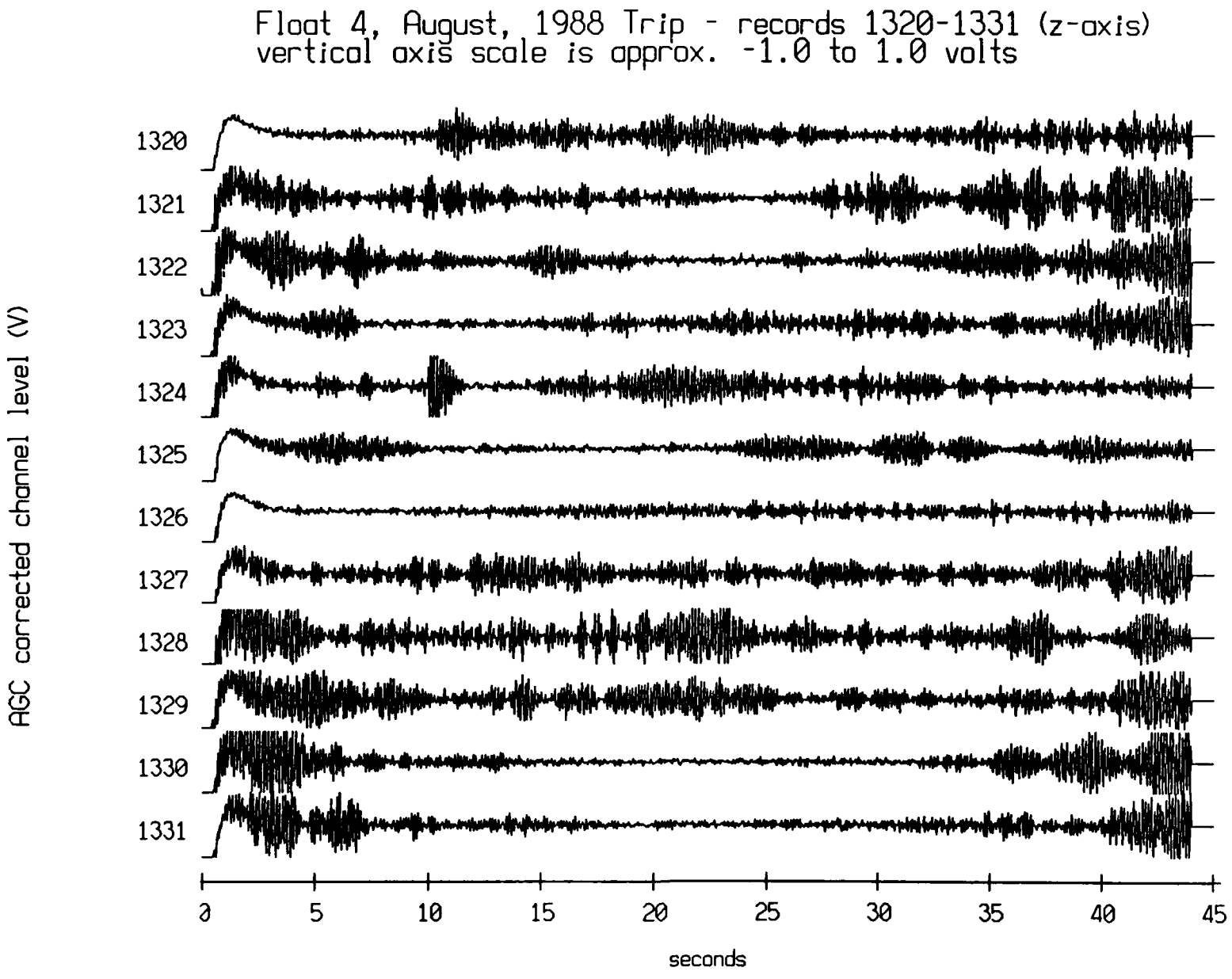


Figure XI.53c

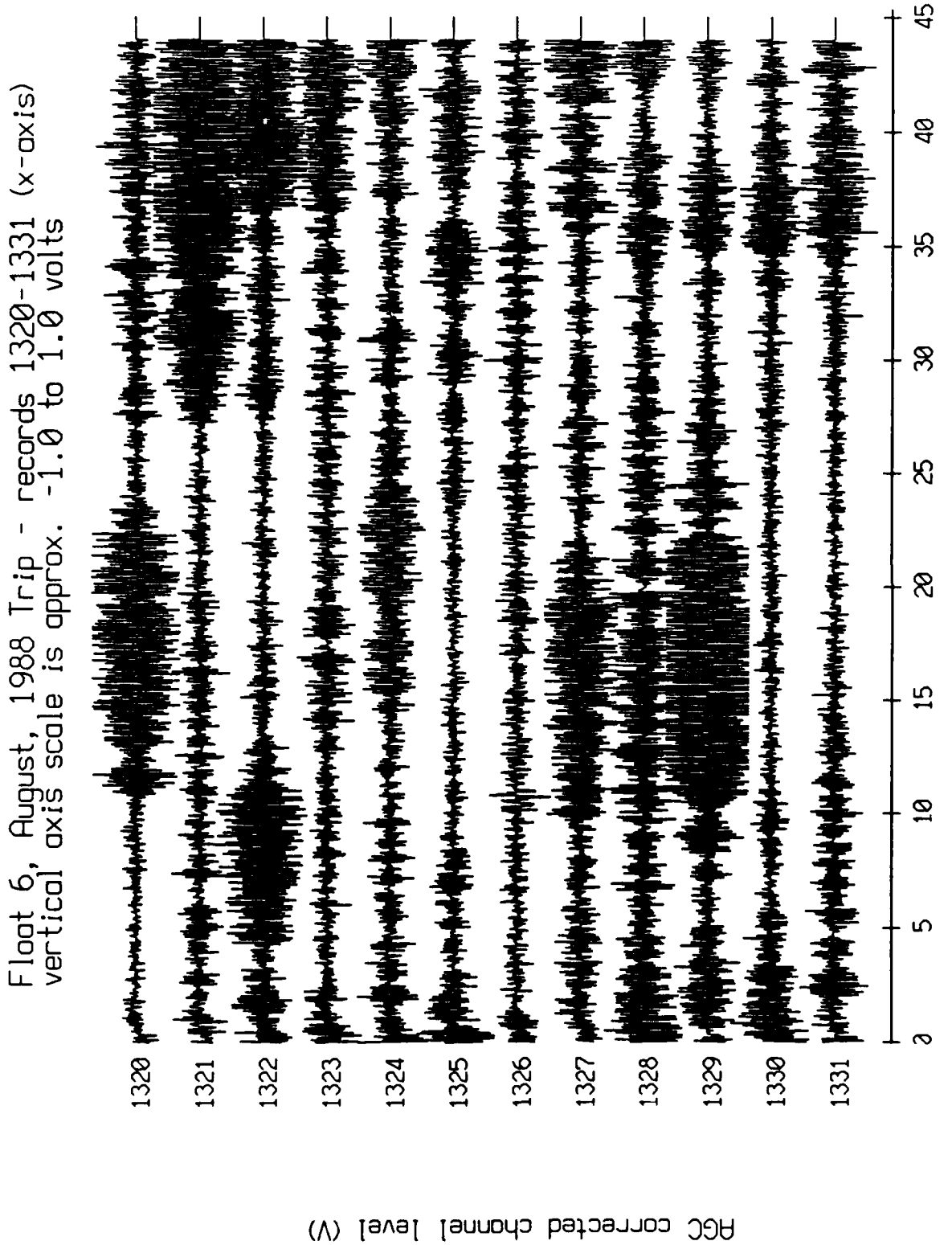


Figure XI.54a

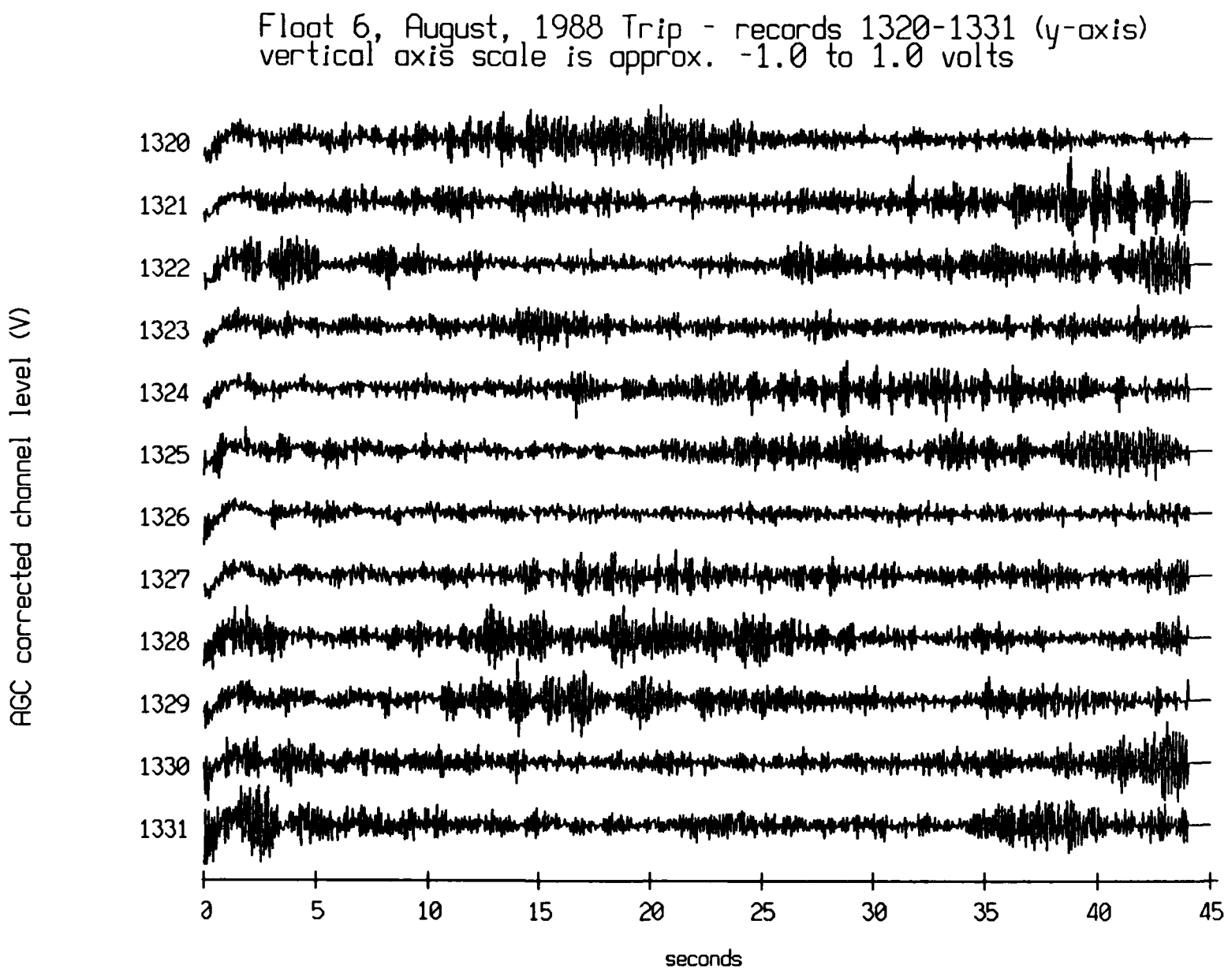


Figure XI.5-1b

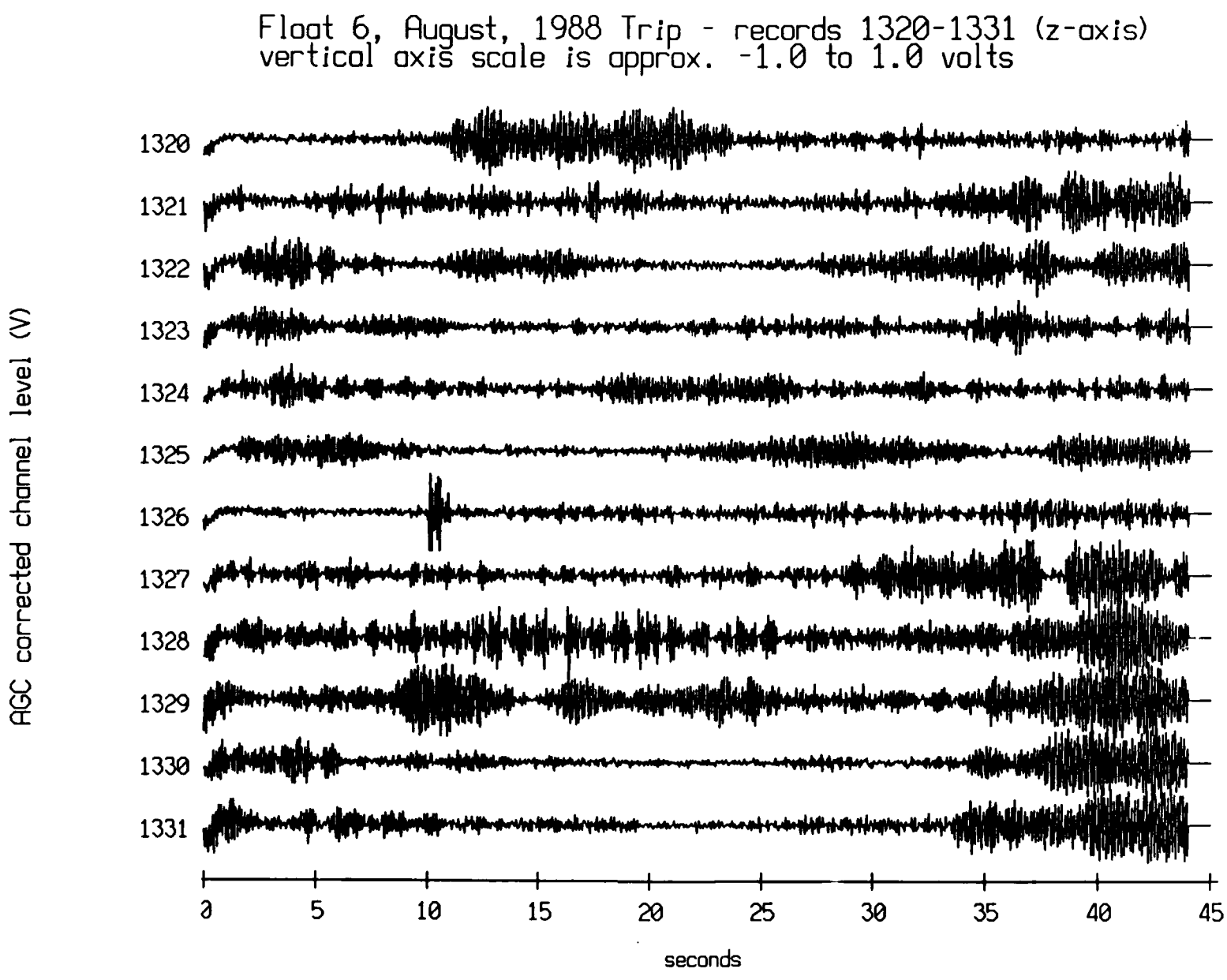


Figure XI.54c

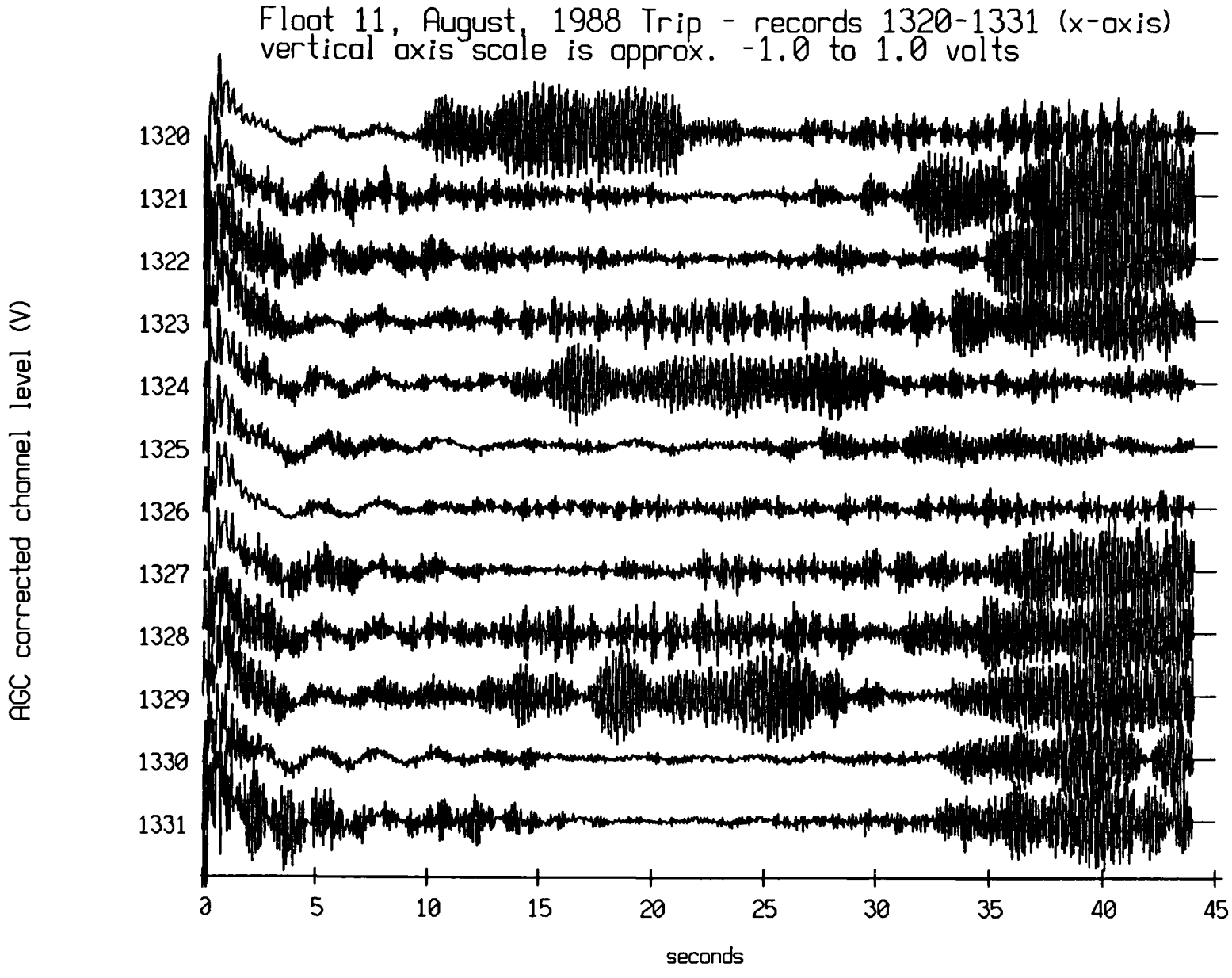


Figure XI.55a

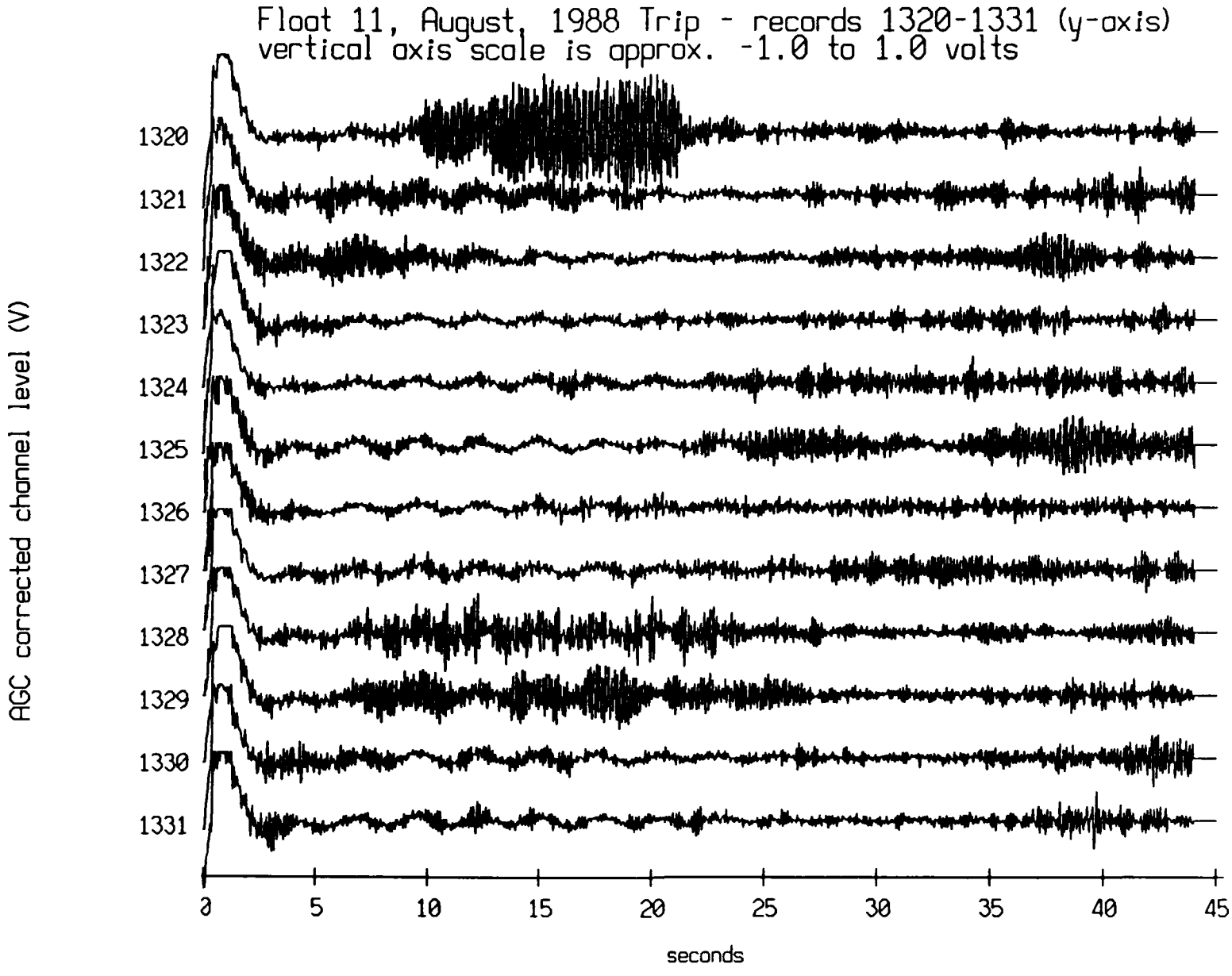


Figure XI.55b

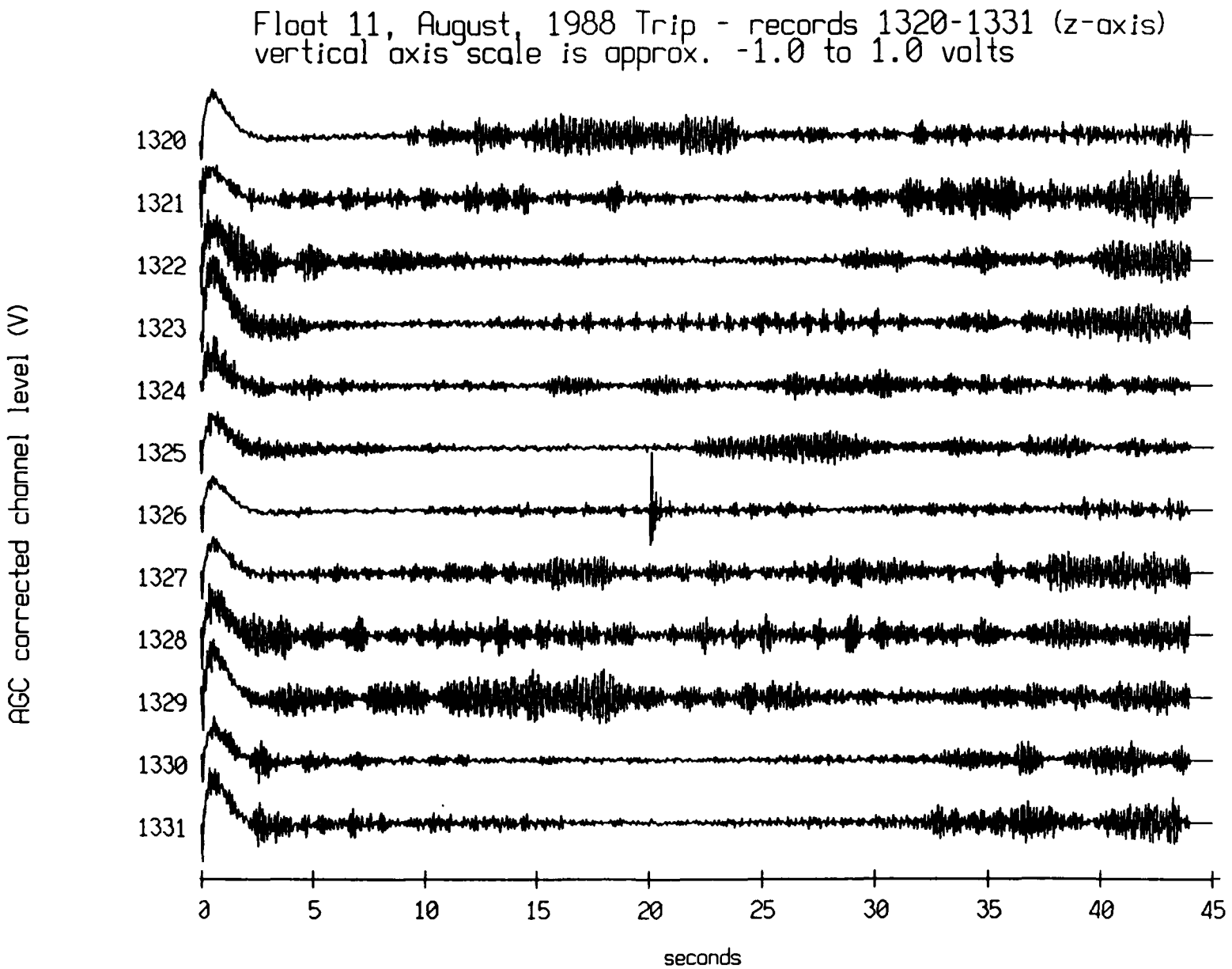


Figure XI.55c

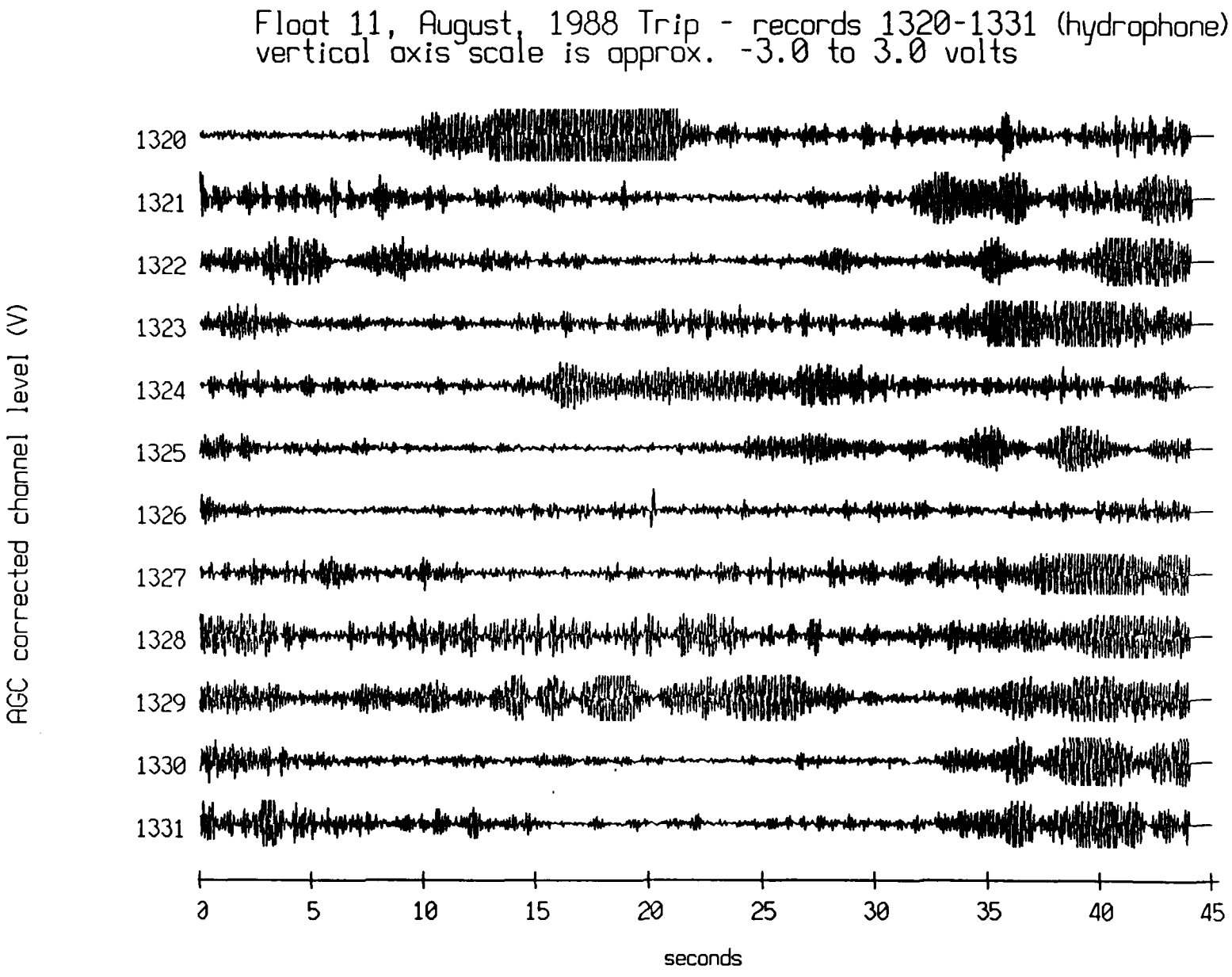


Figure XI.55d

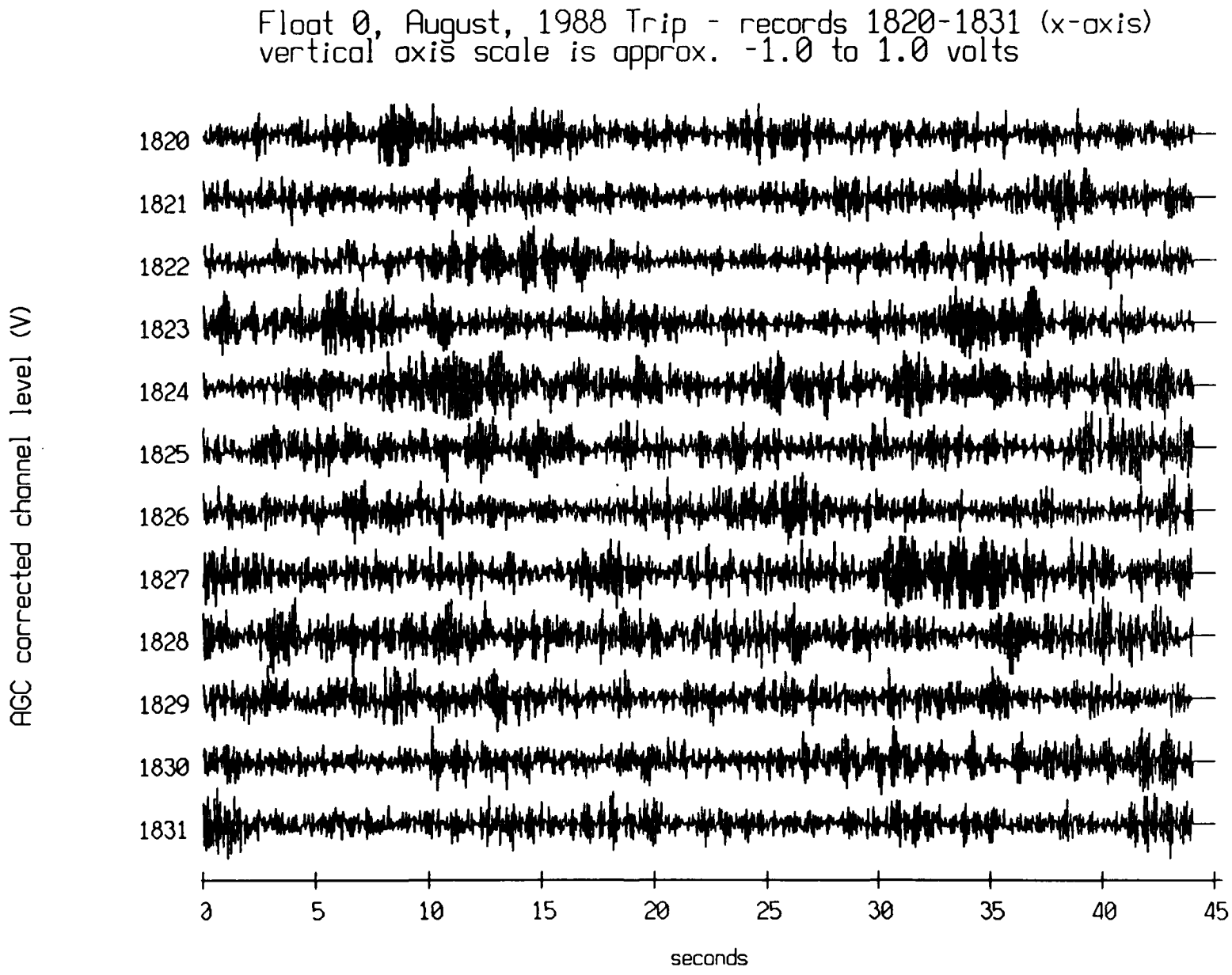


Figure XI.56a

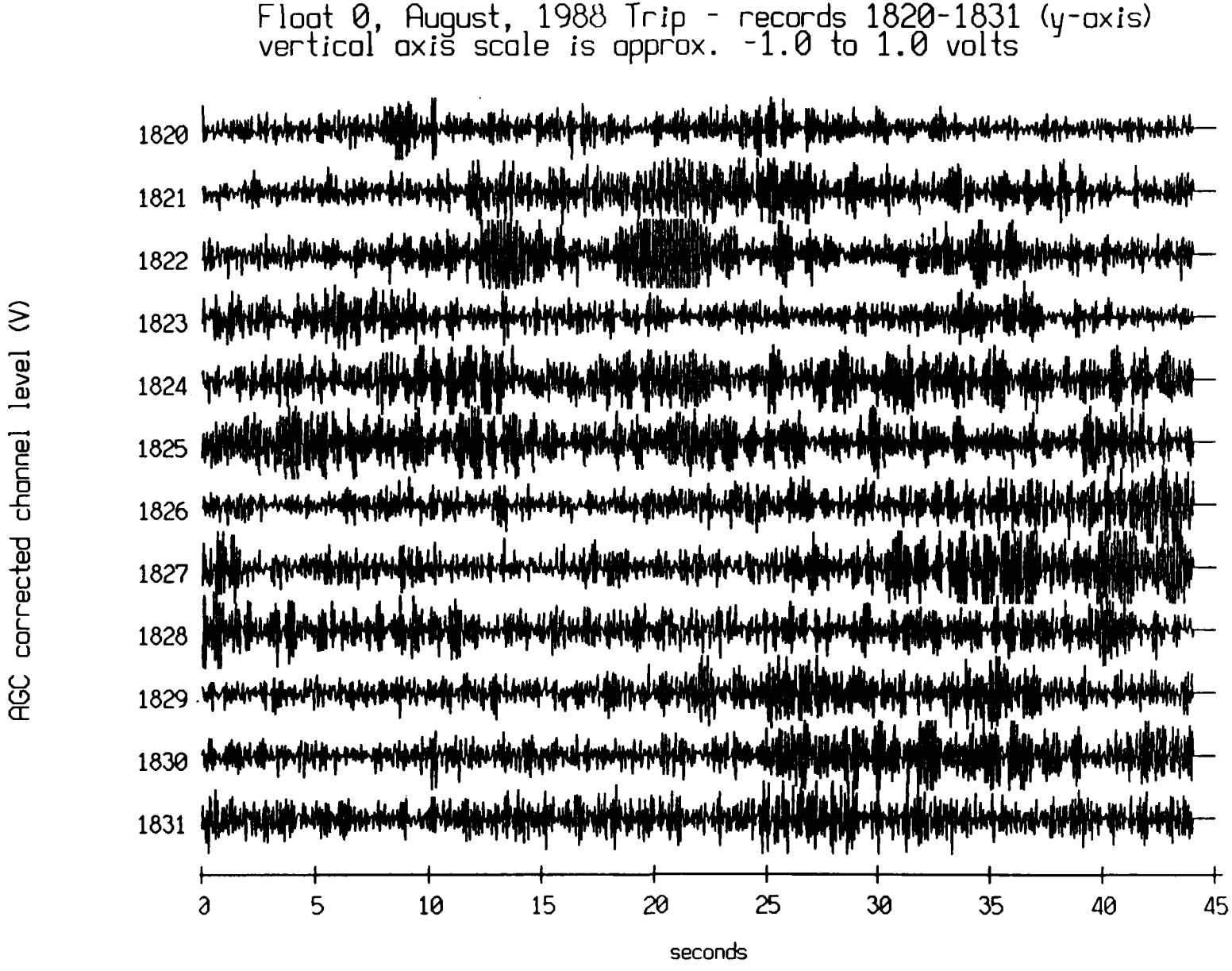


Figure XI.56b

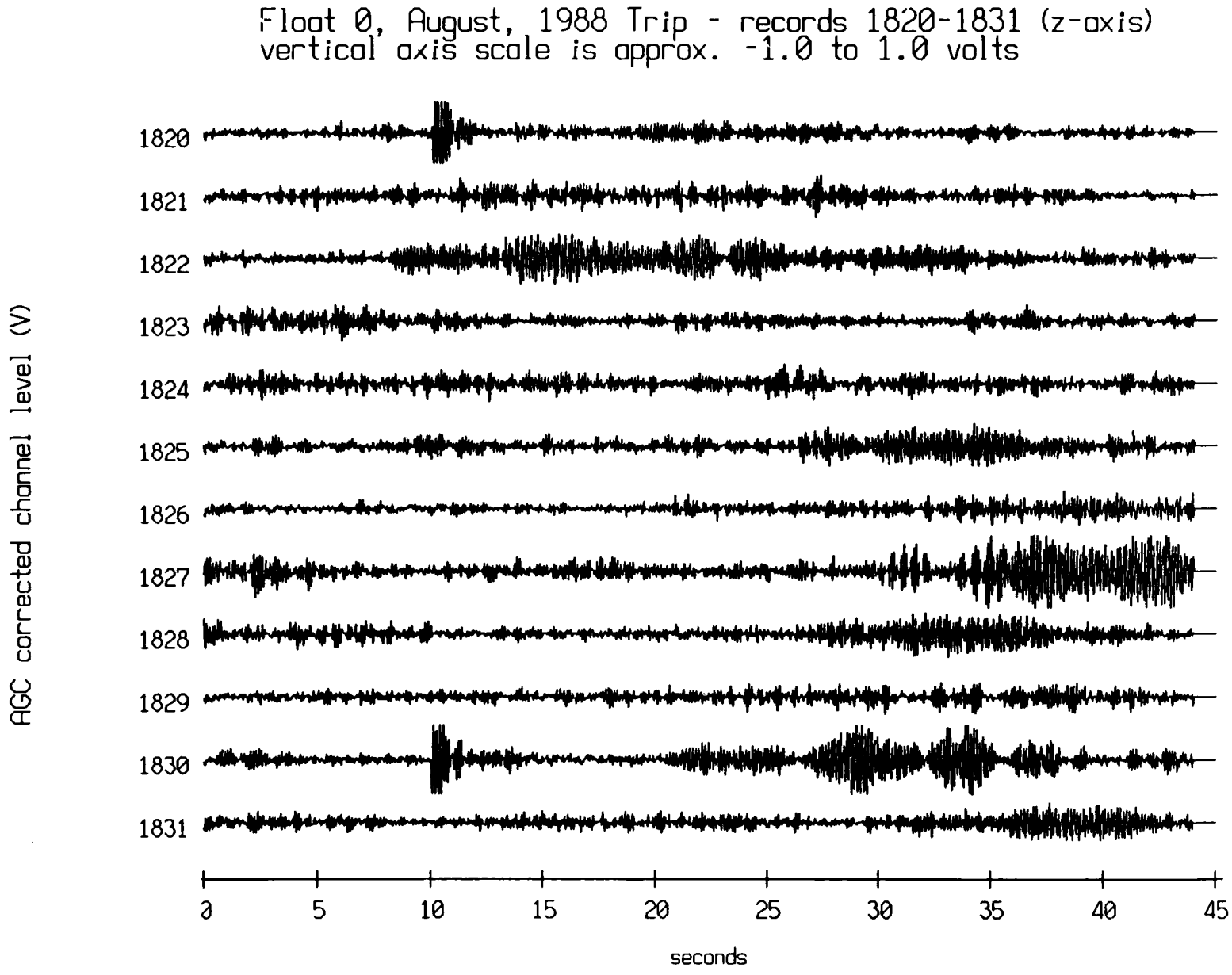


Figure XI.56c

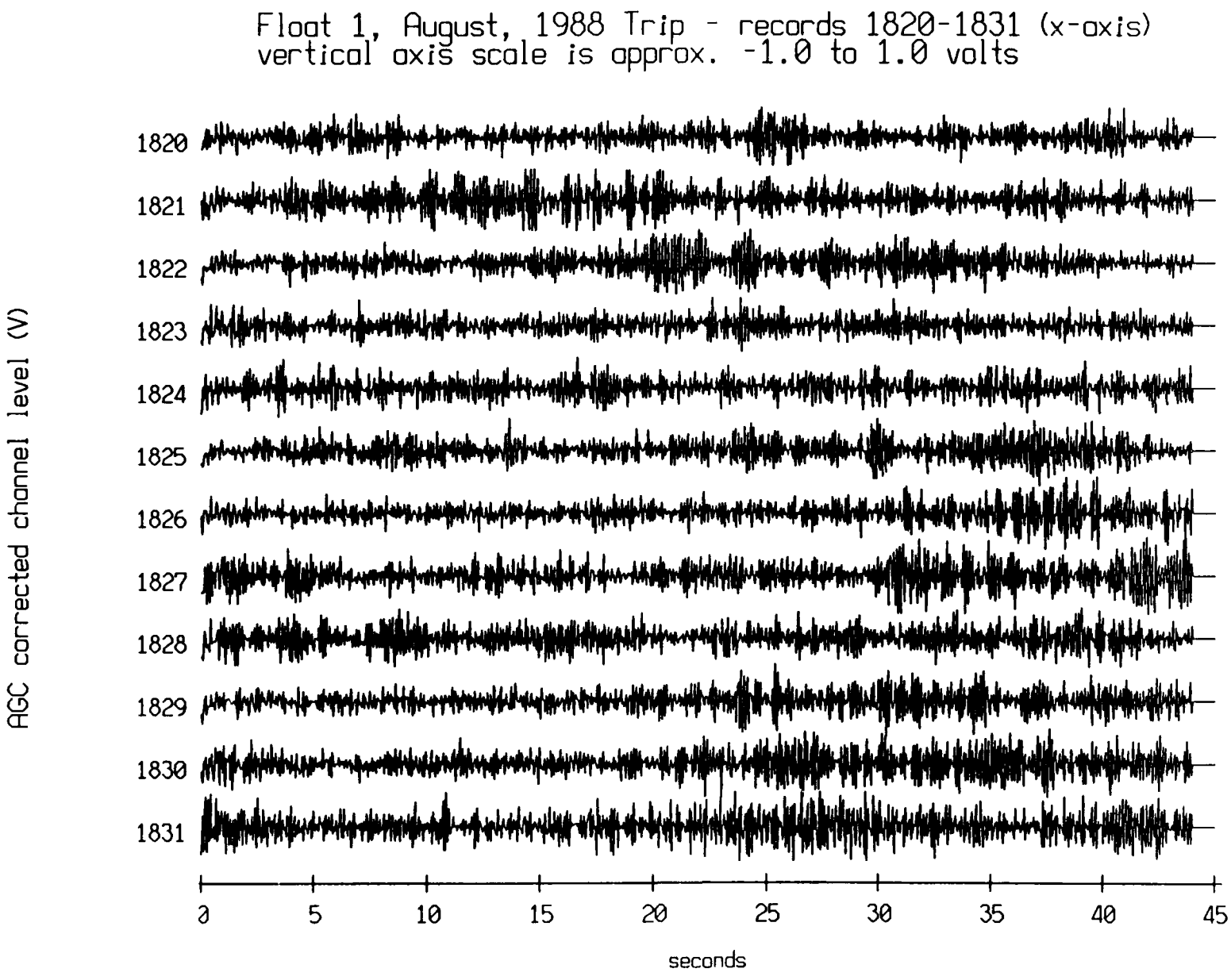


Figure XI.57a

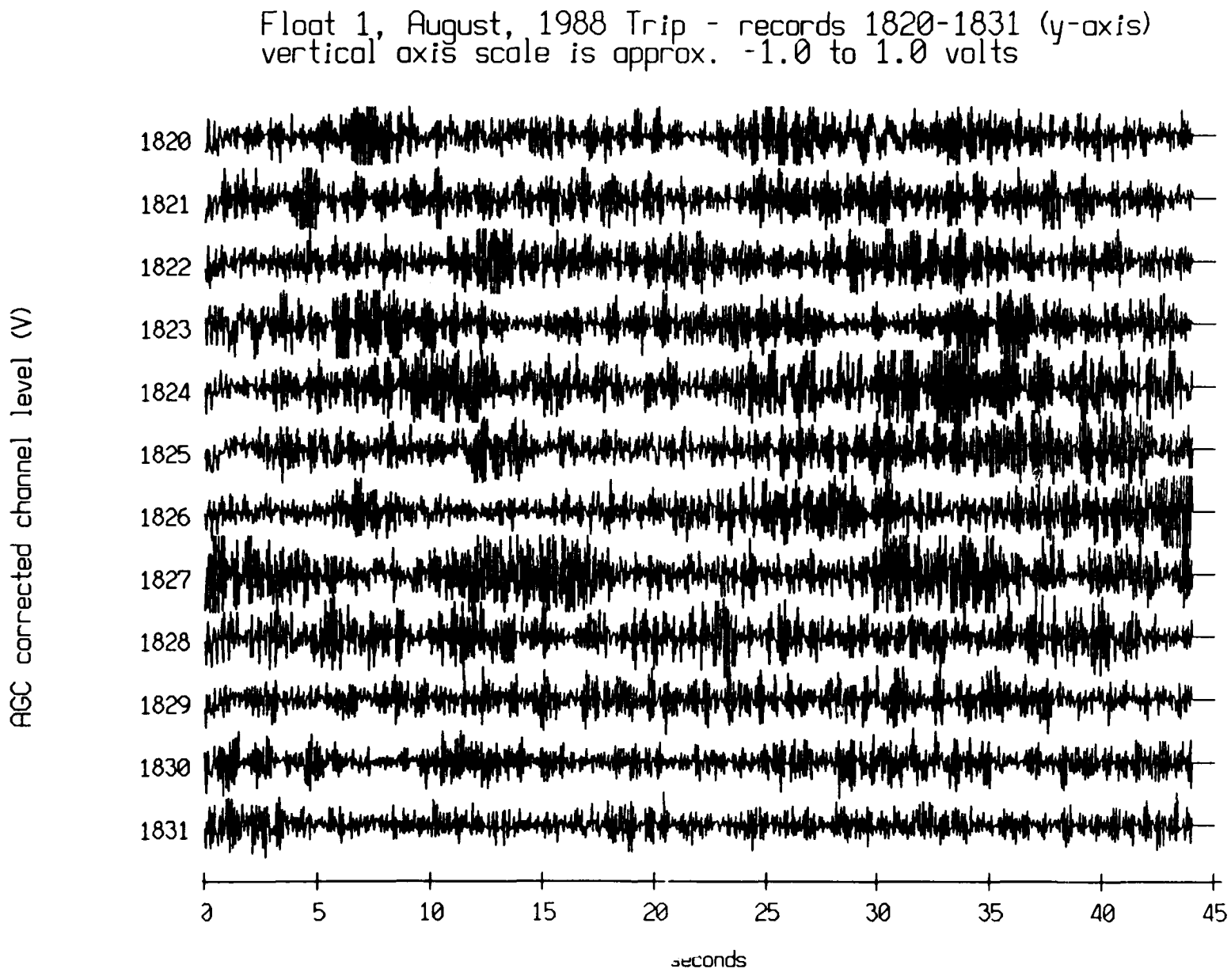


Figure XI.57b

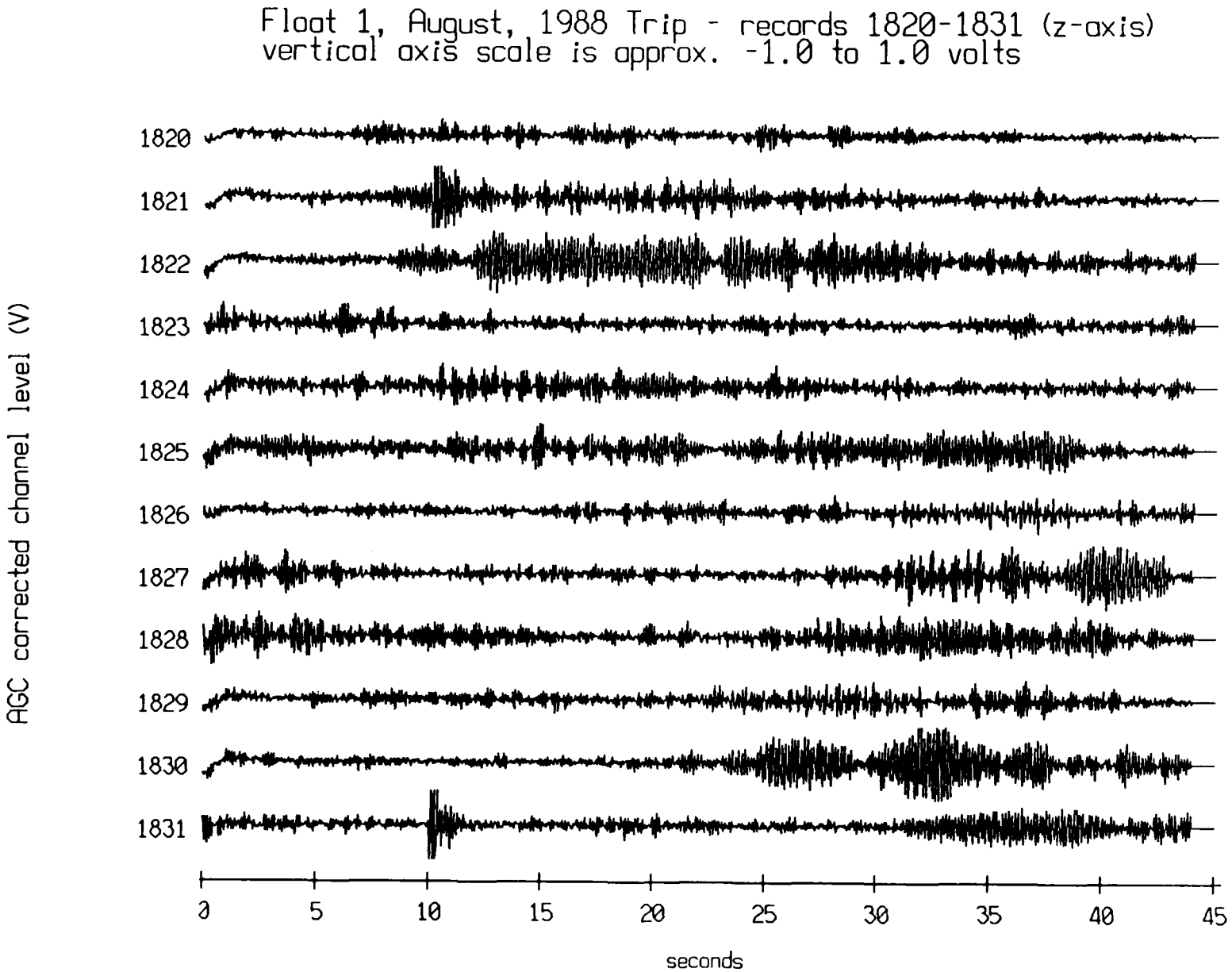


Figure XI.57c

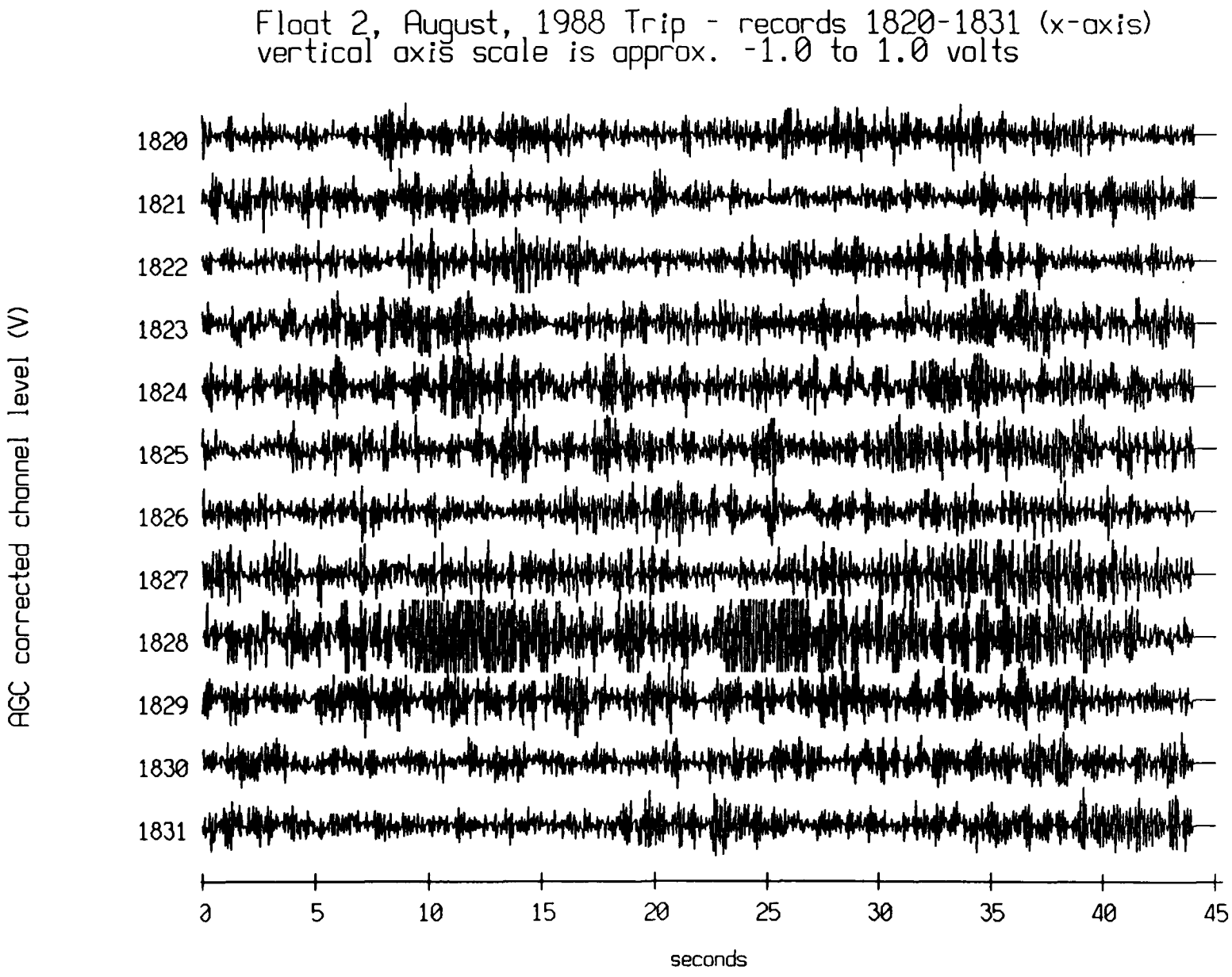


Figure XI.58a

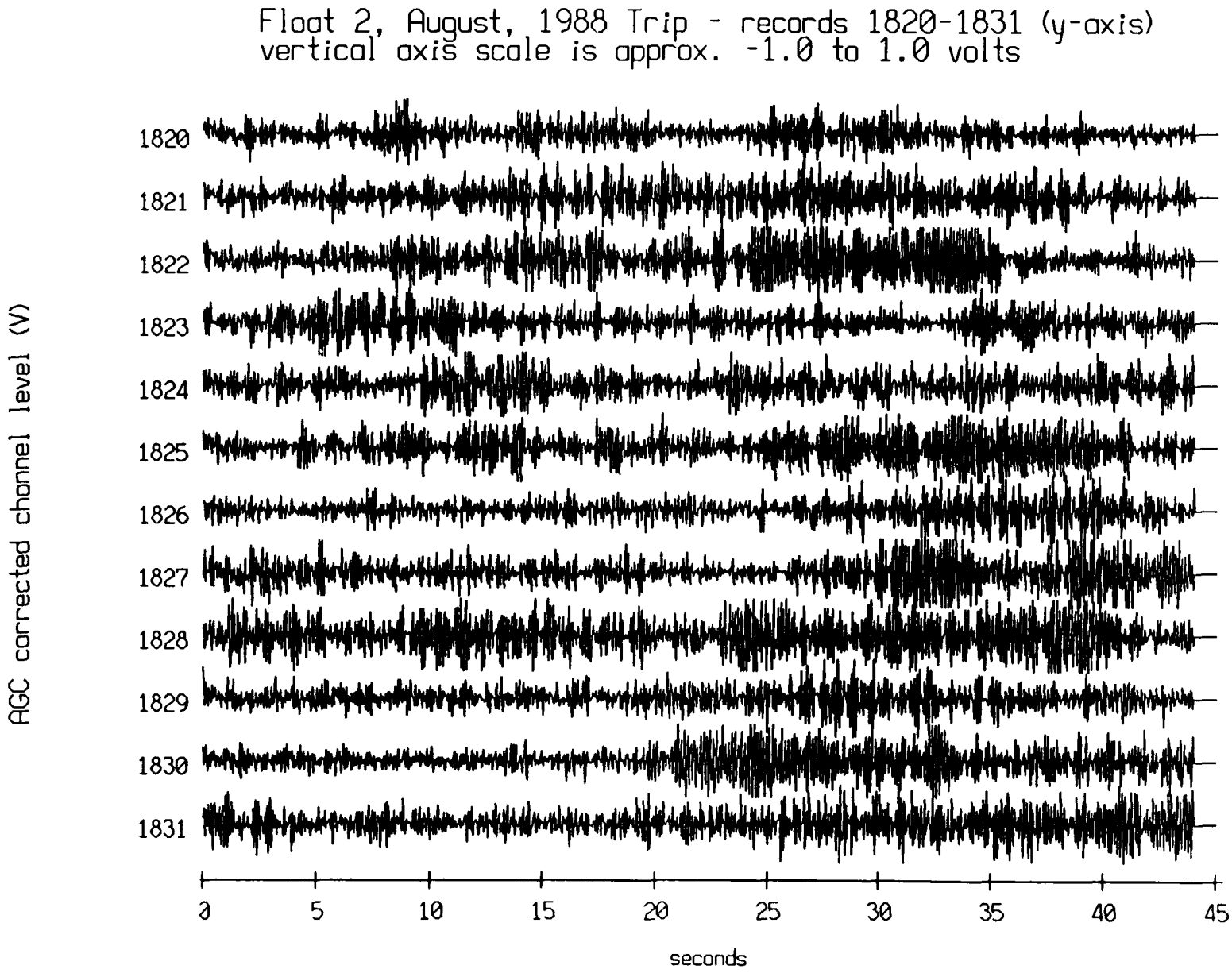


Figure XI.58b

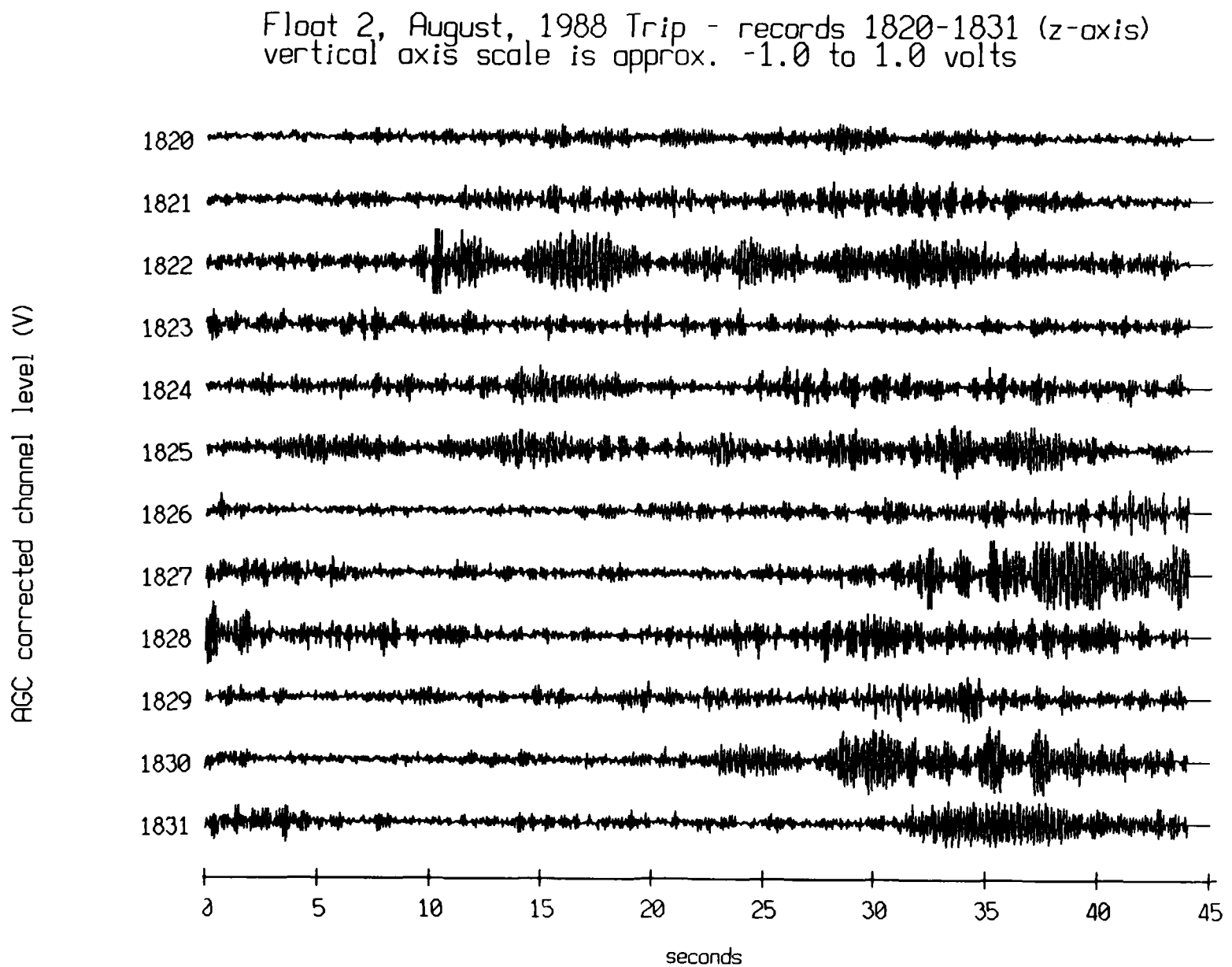


Figure XI.58c

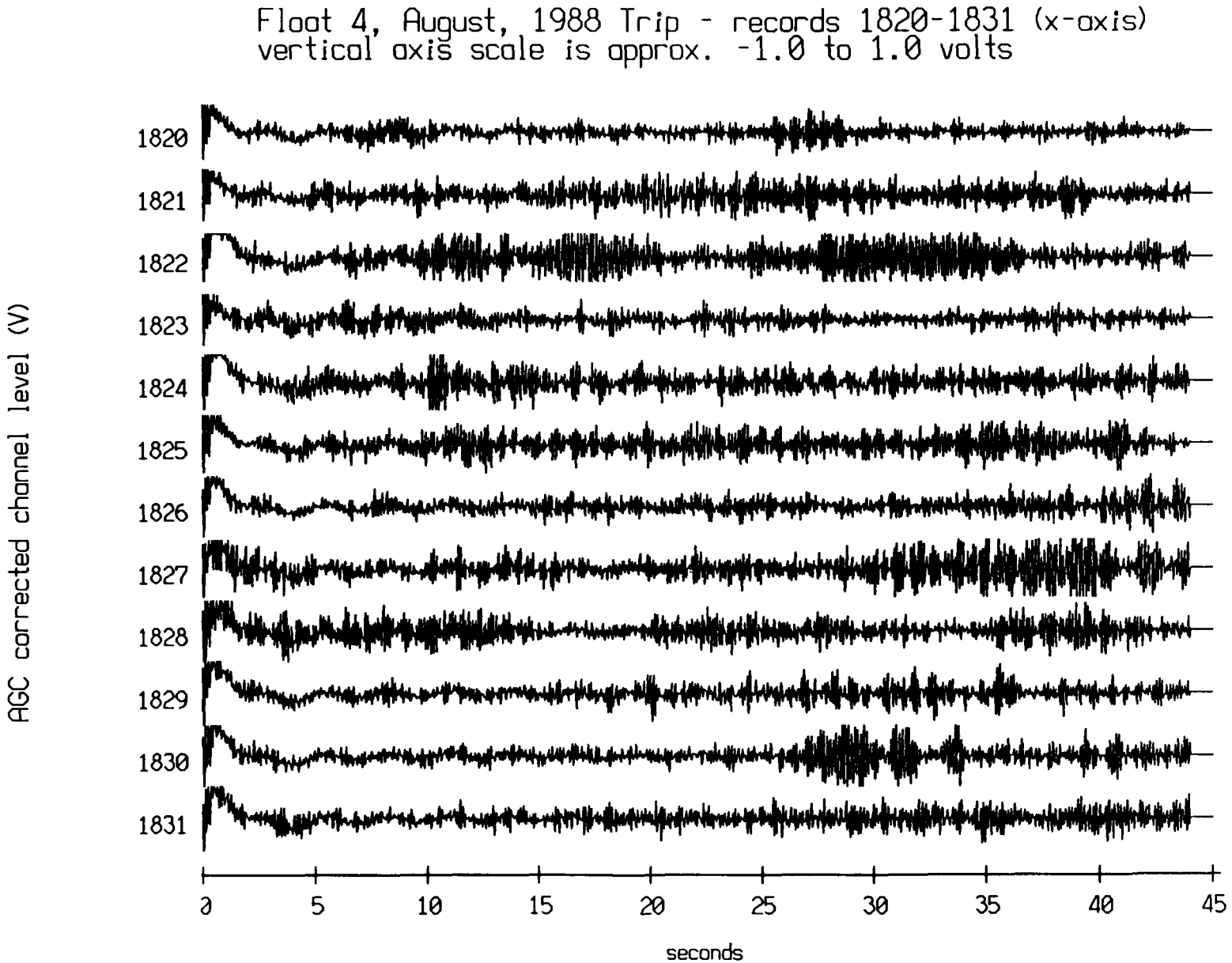


Figure XI.50a

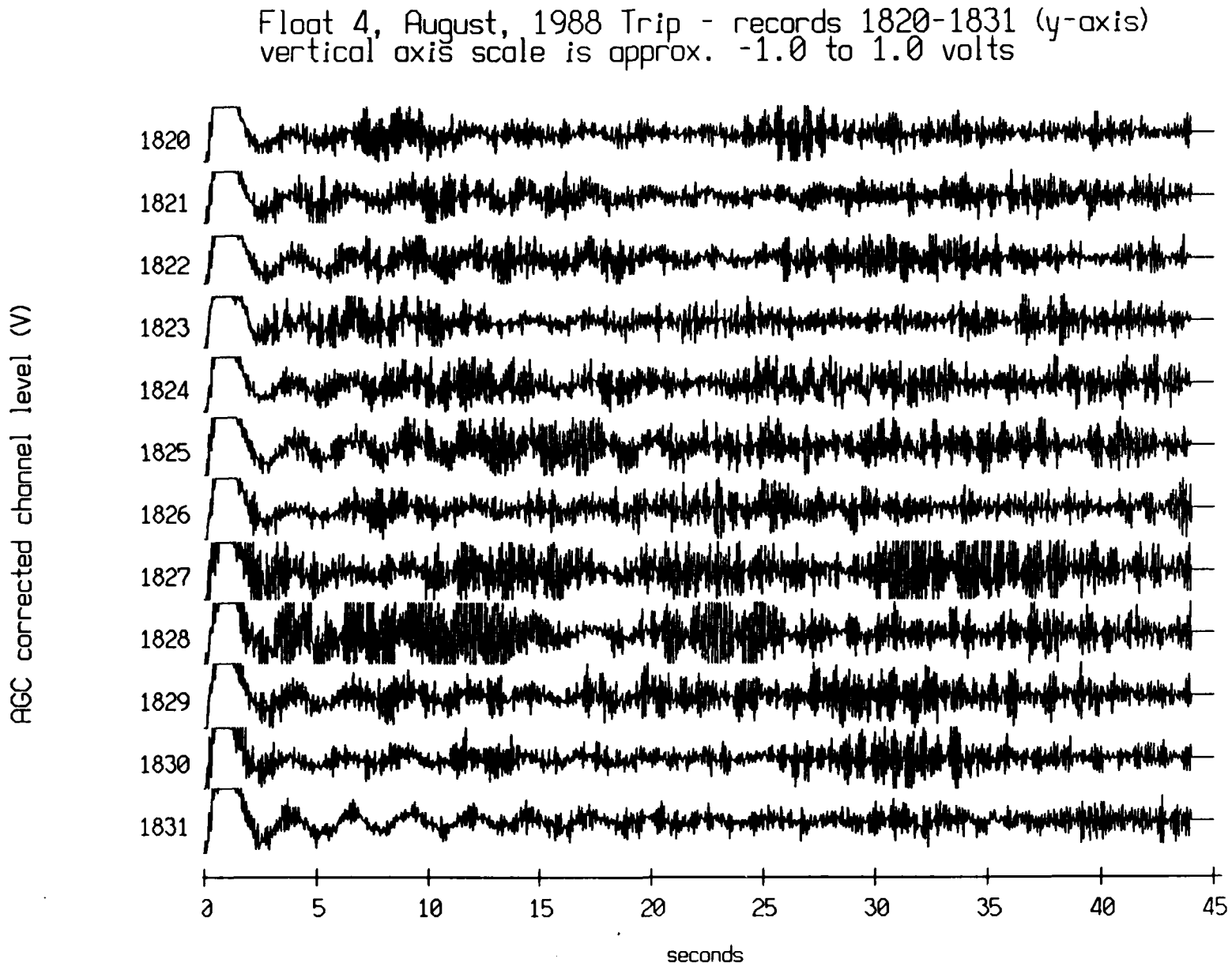


Figure XI.59b

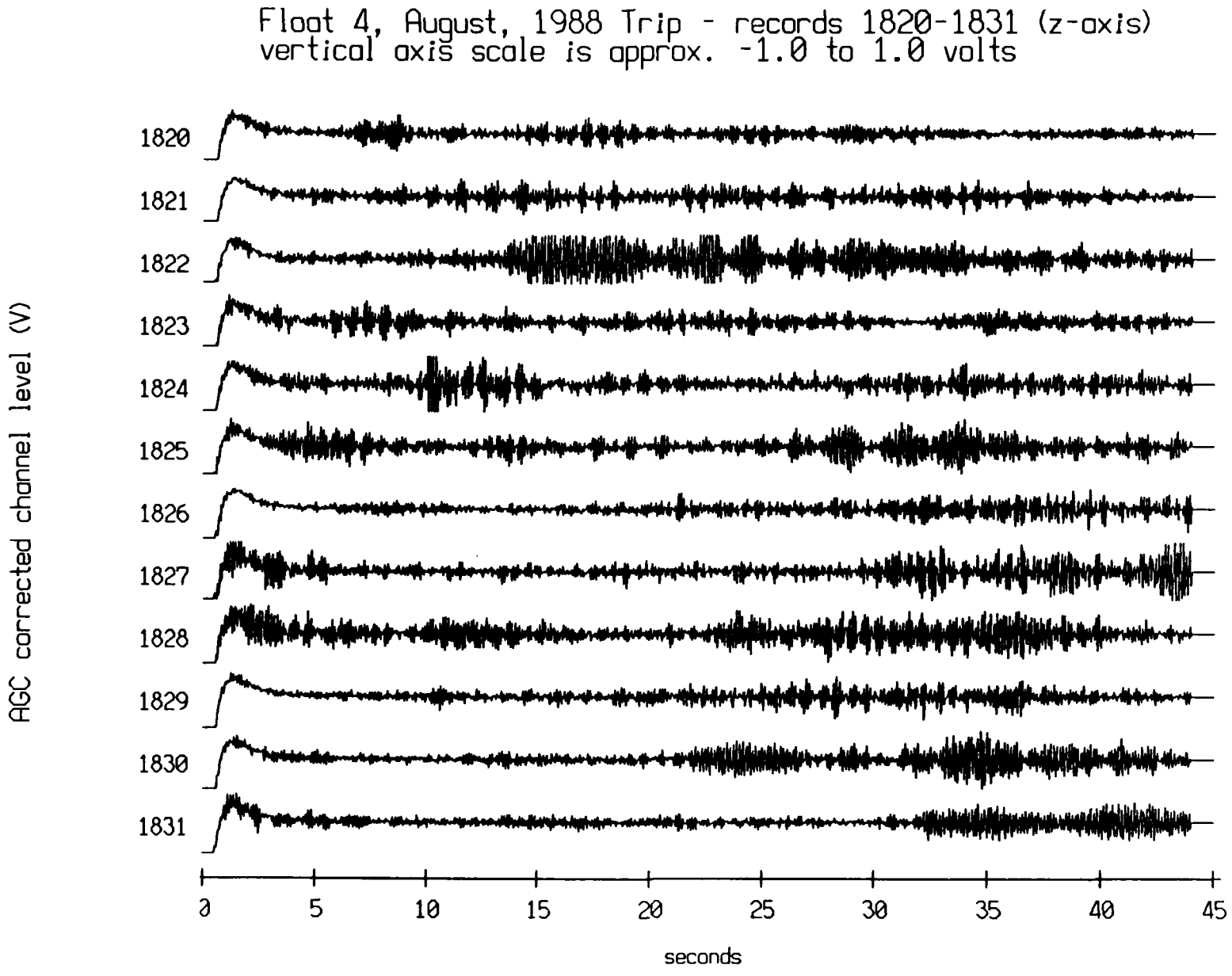


Figure XI.59c

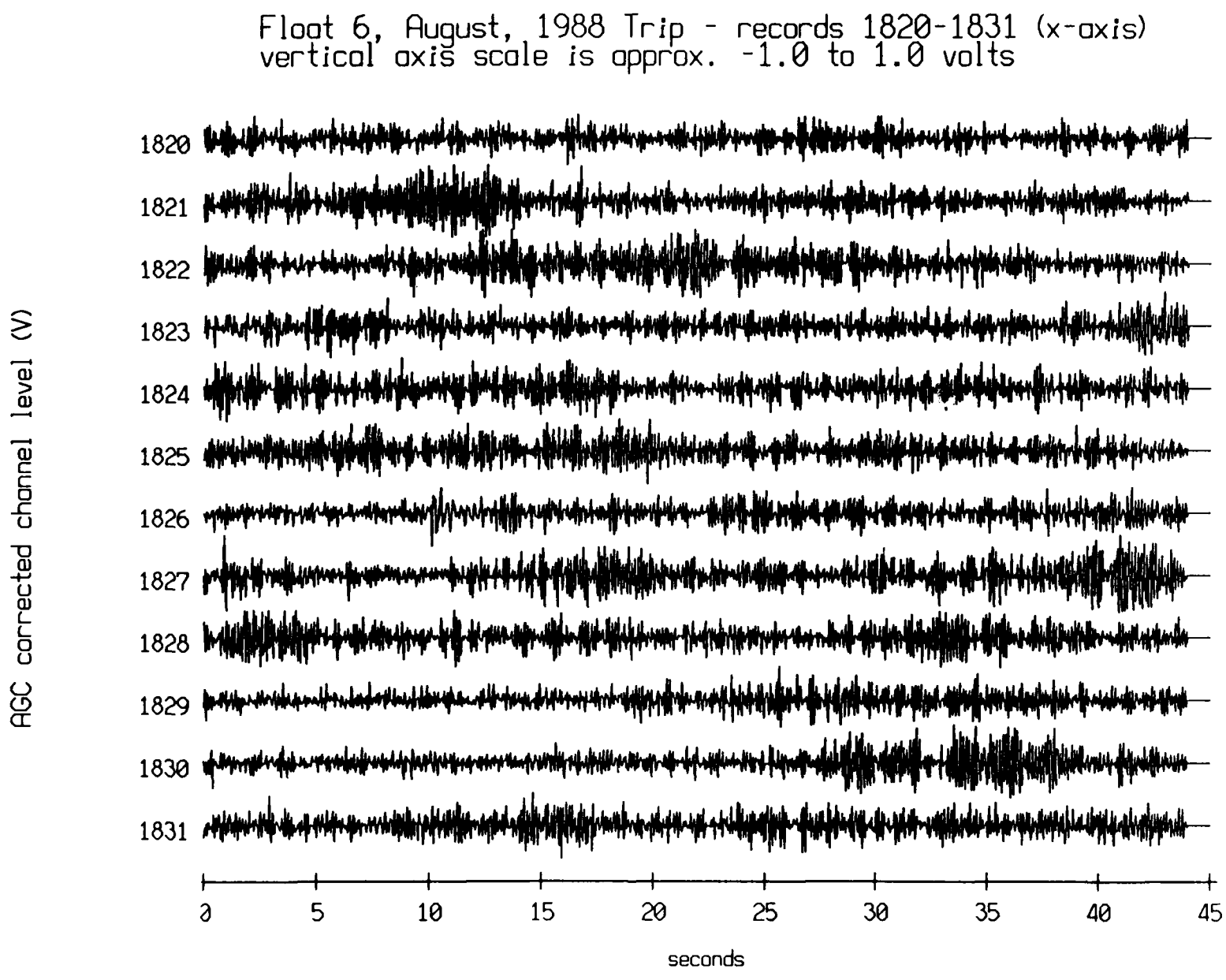


Figure XI.60a

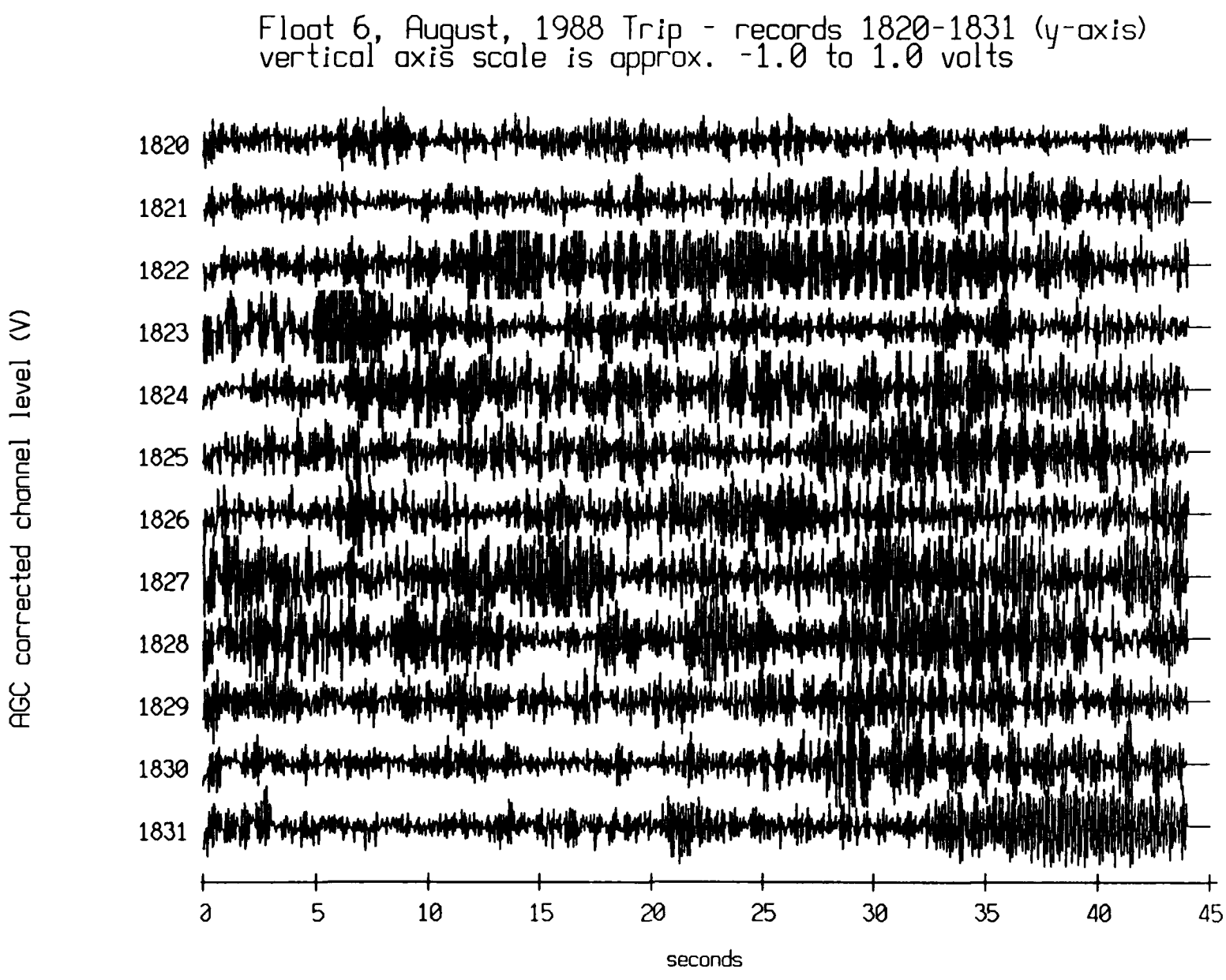


Figure XI.60b

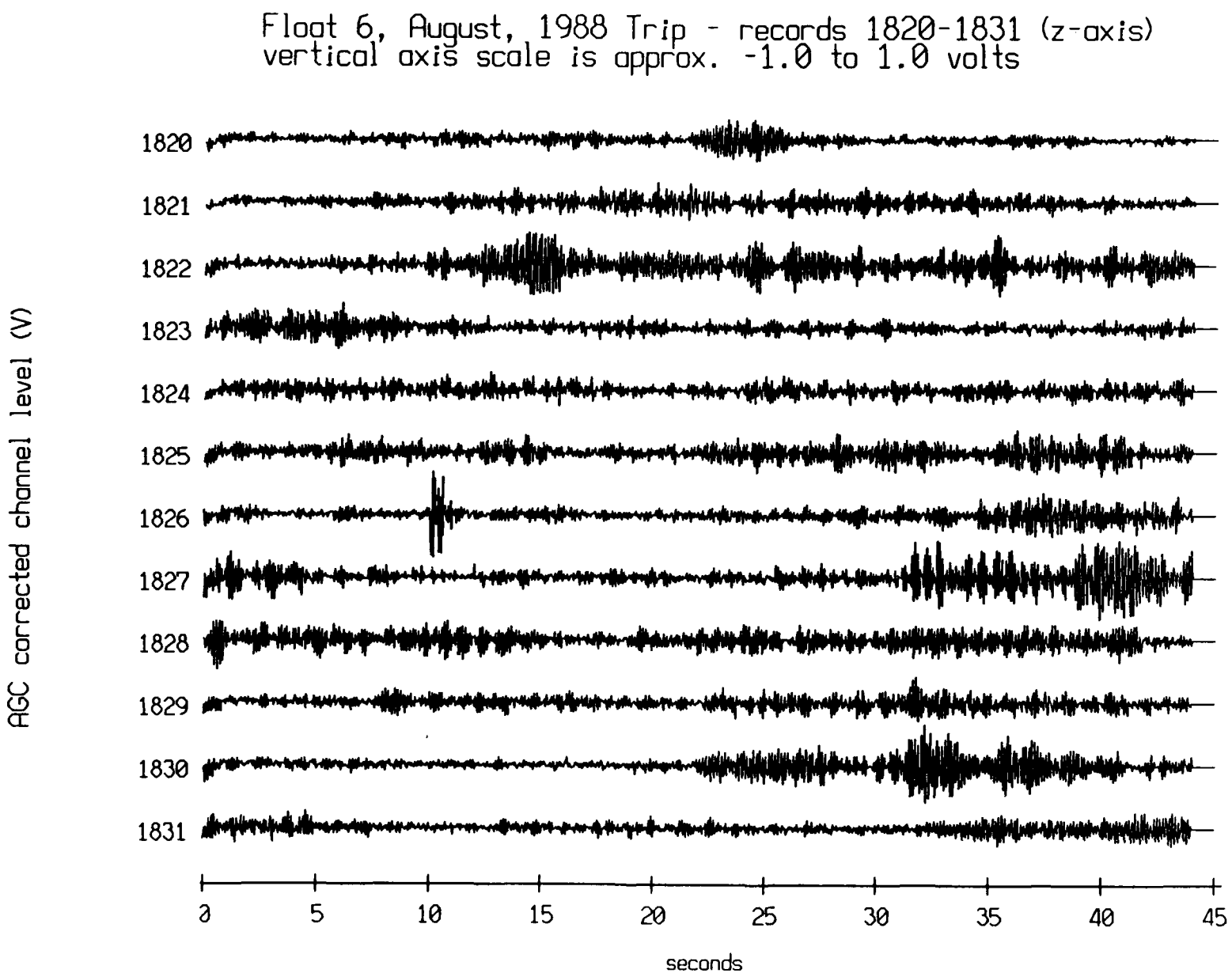


Figure XI.60c

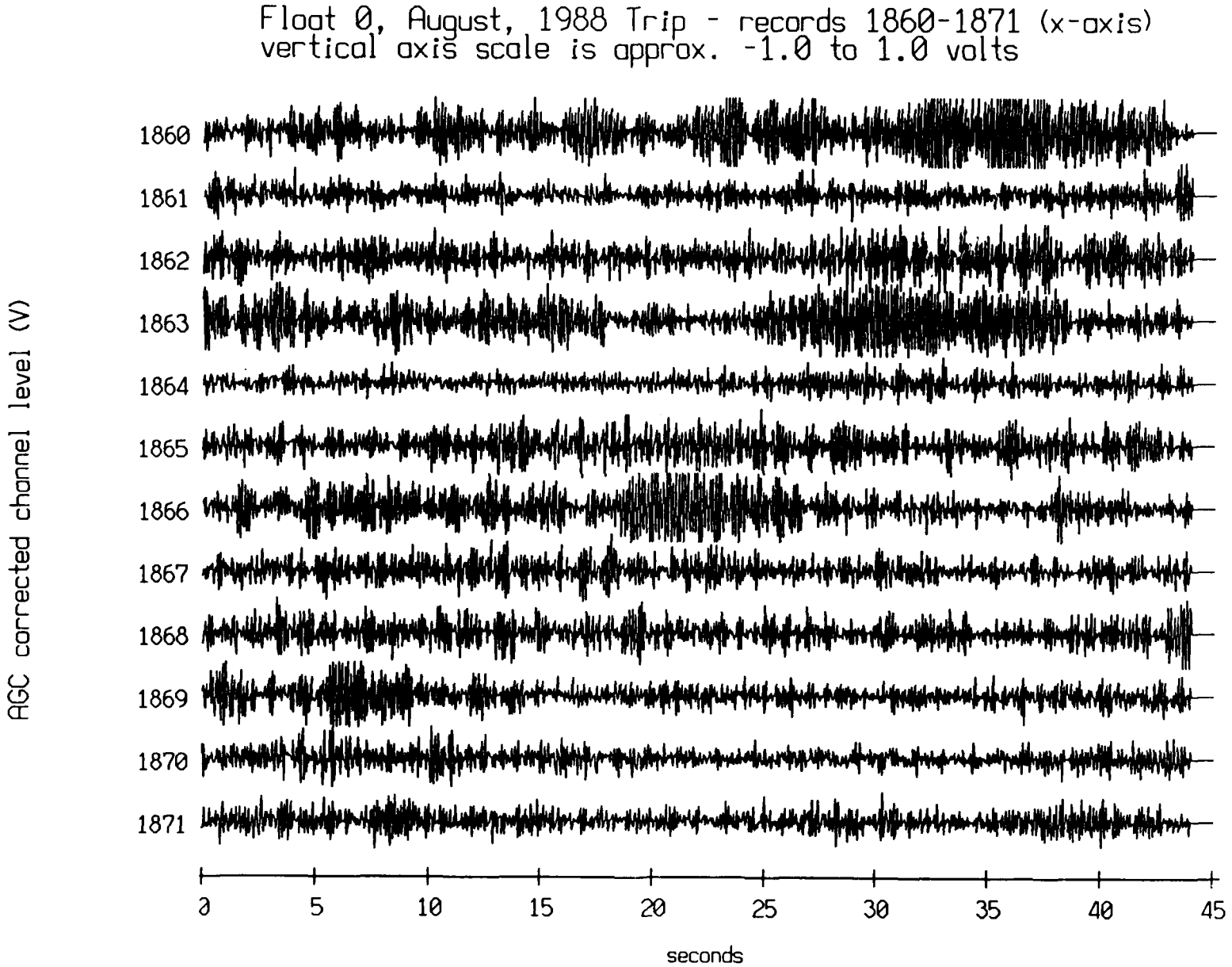


Figure XI.61a

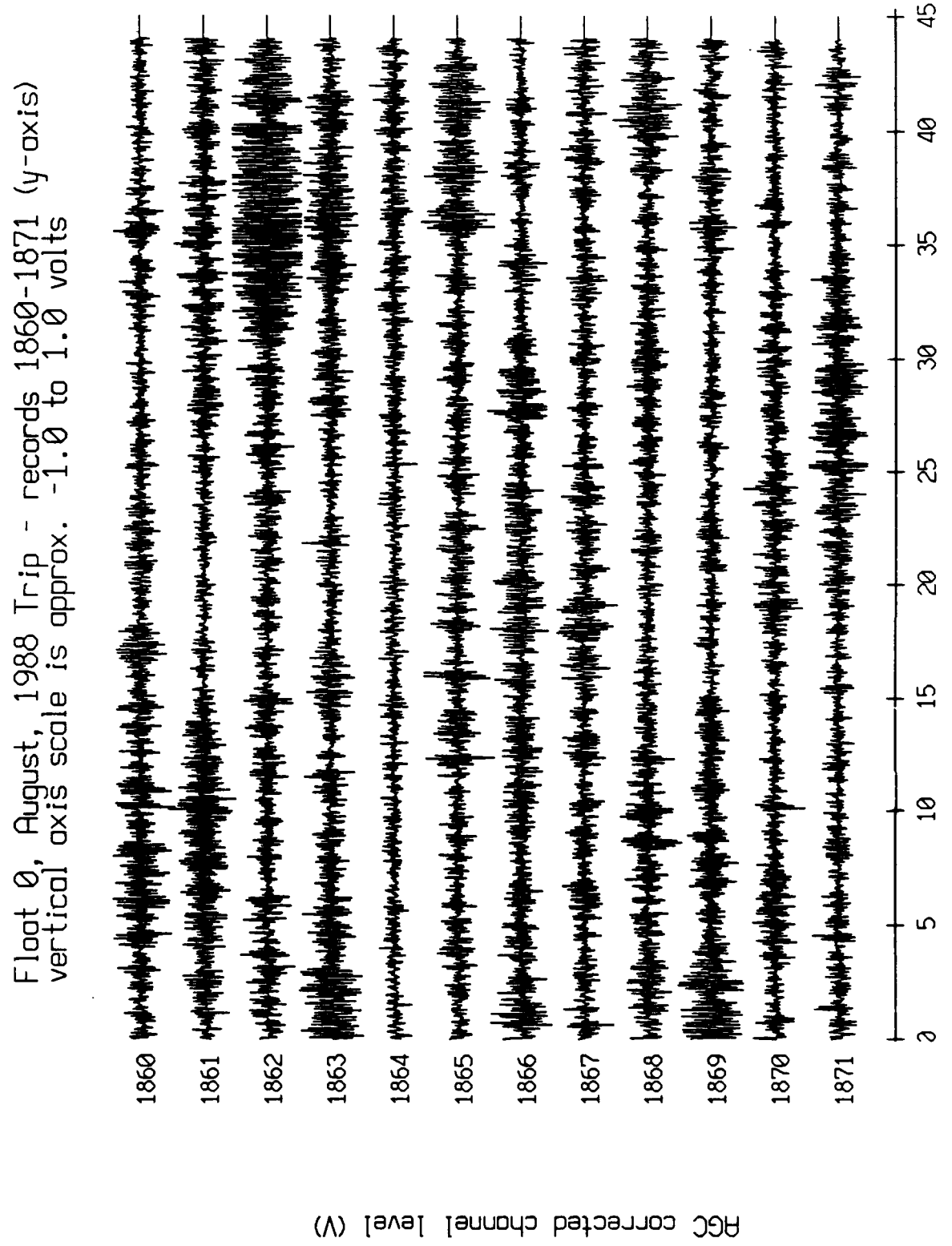


Figure XI.61b

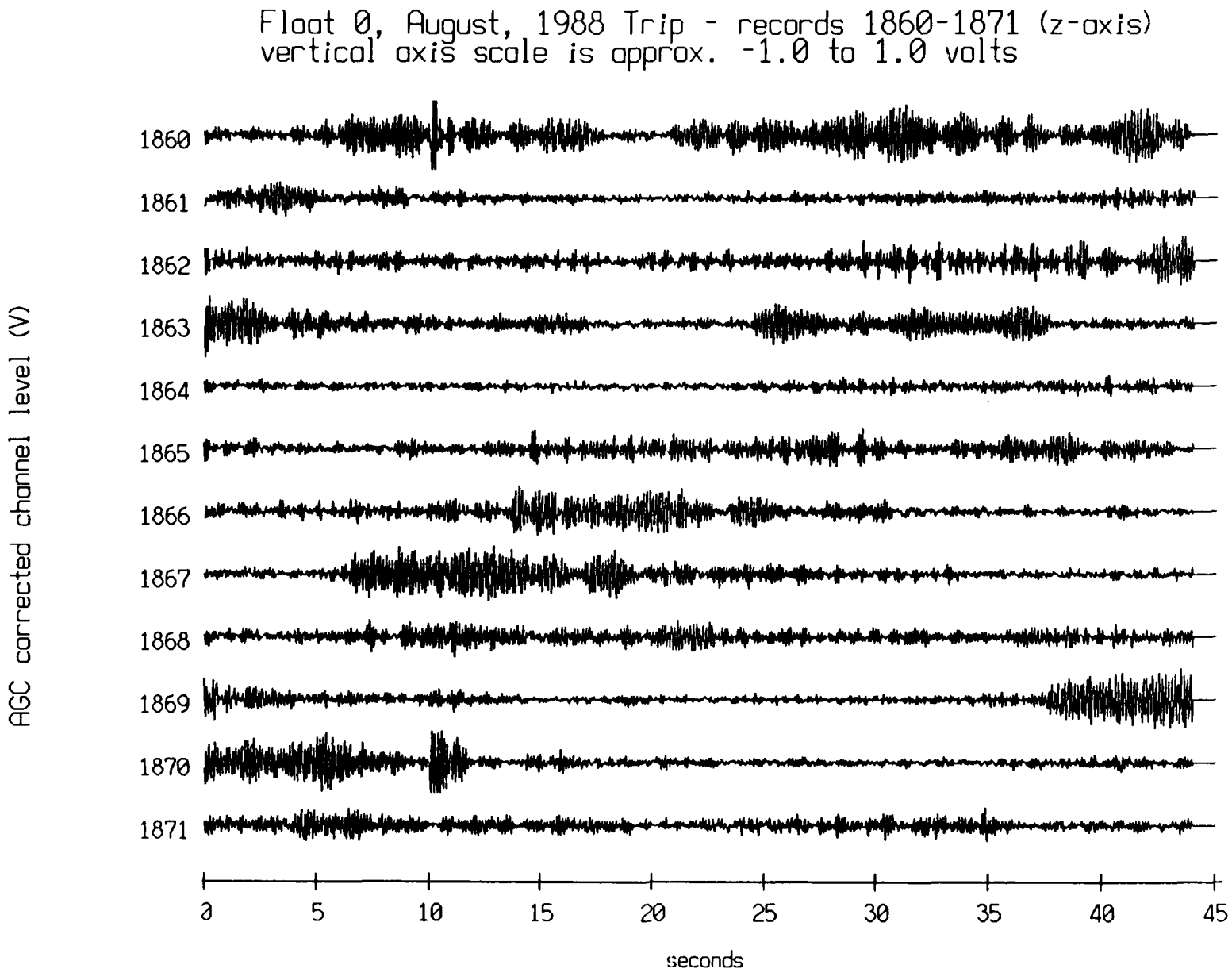


Figure XI.61c

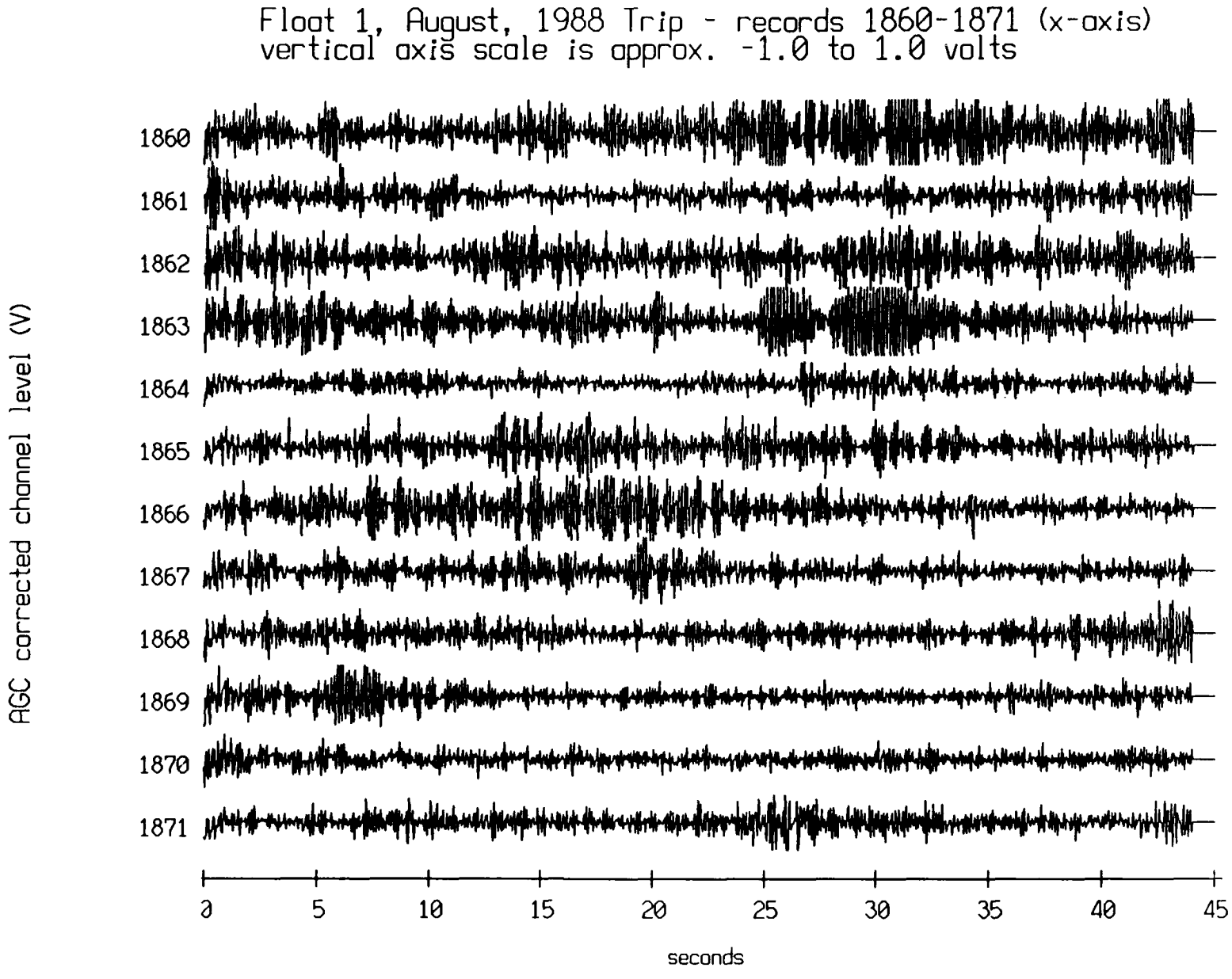


Figure XI.62a

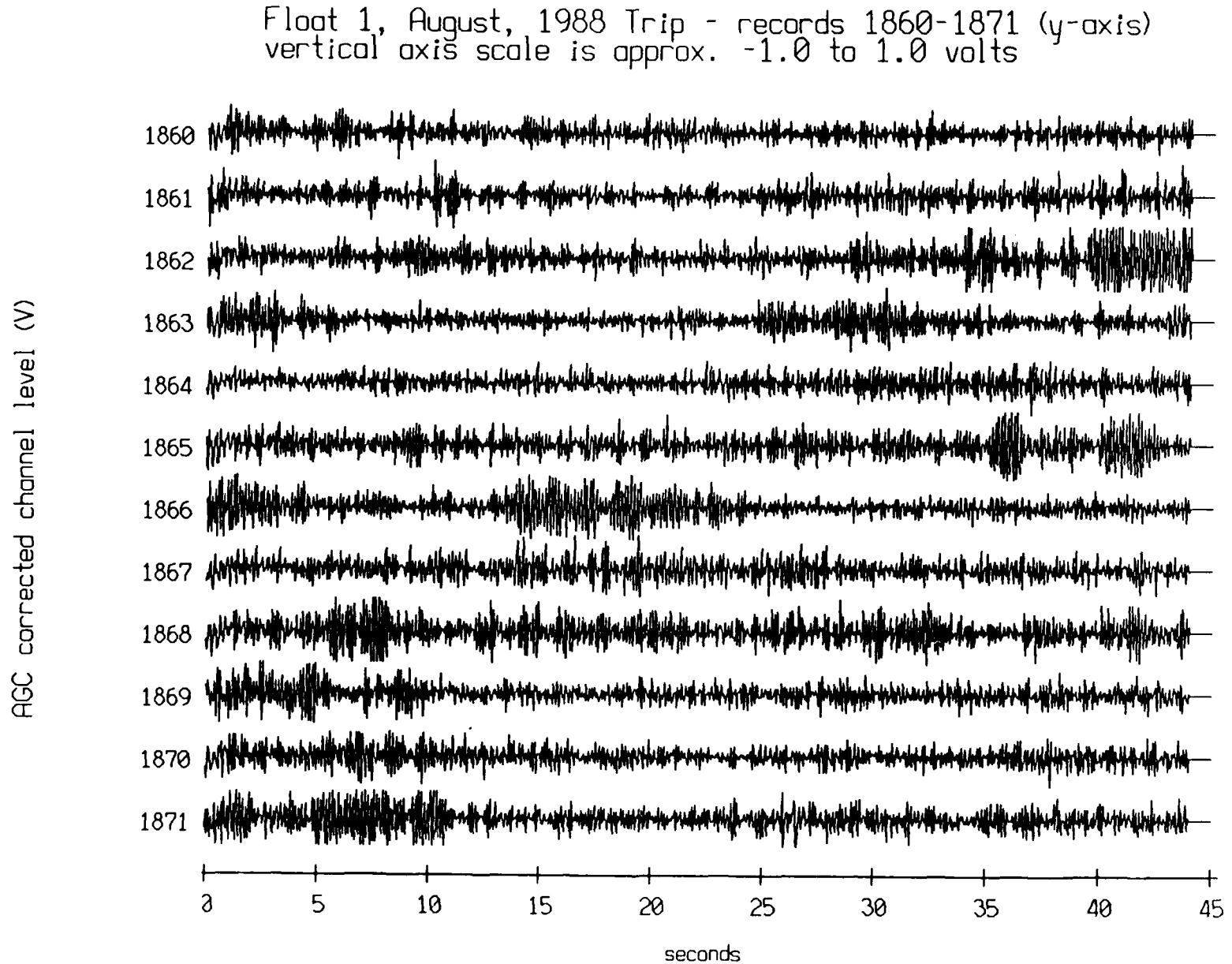

Float 1, August, 1988 Trip - records 1860-1871 (y-axis)
vertical axis scale is approx. -1.0 to 1.0 volts
AGC corrected channel level (V)
1860
1861
1862
1863
1864
1865
1866
1867
1868
1869
1870
1871
0
5
10
15
20
25
30
35
40
45
seconds

Figure XI.6b

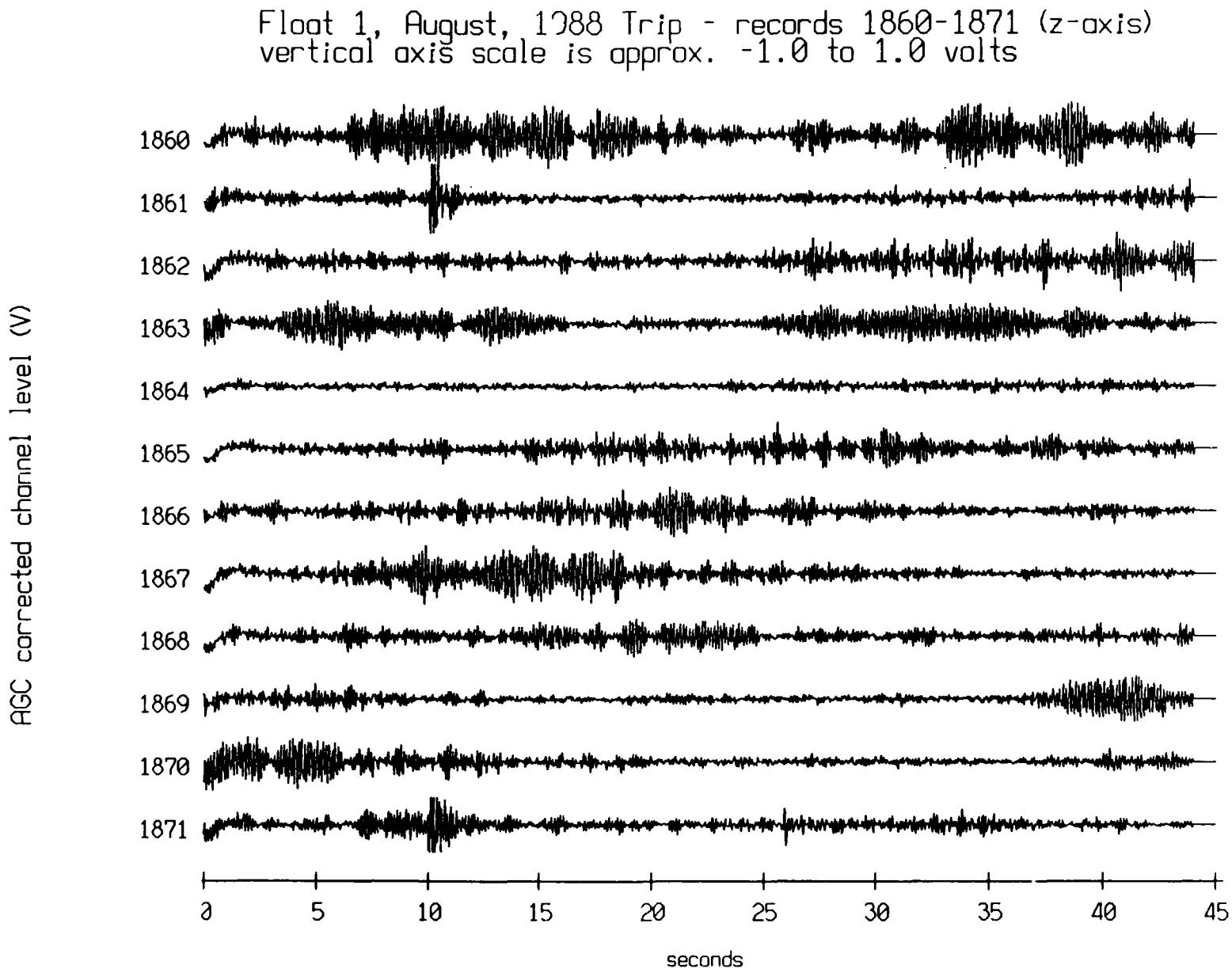


Figure XI.62c

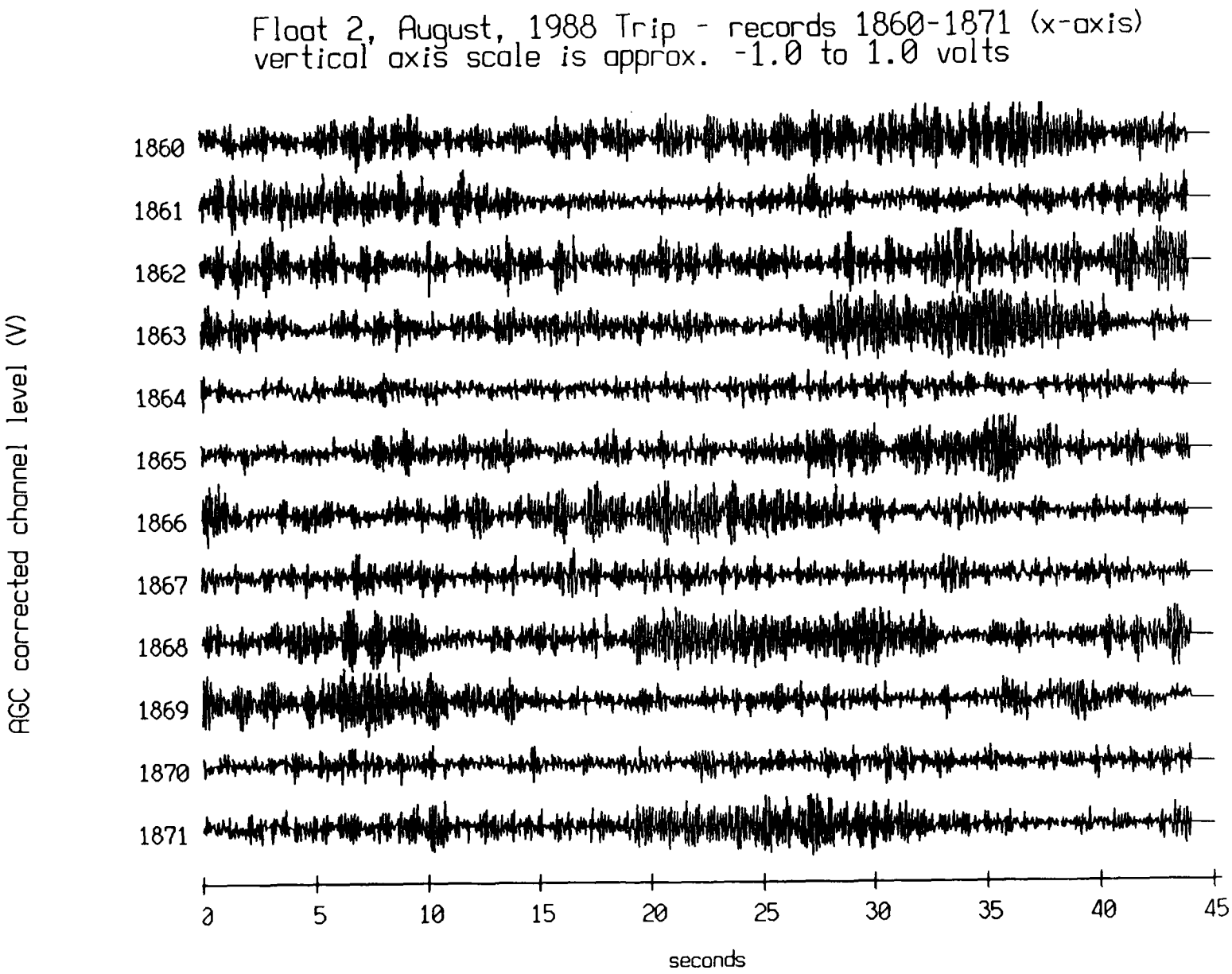


Figure XI.63a

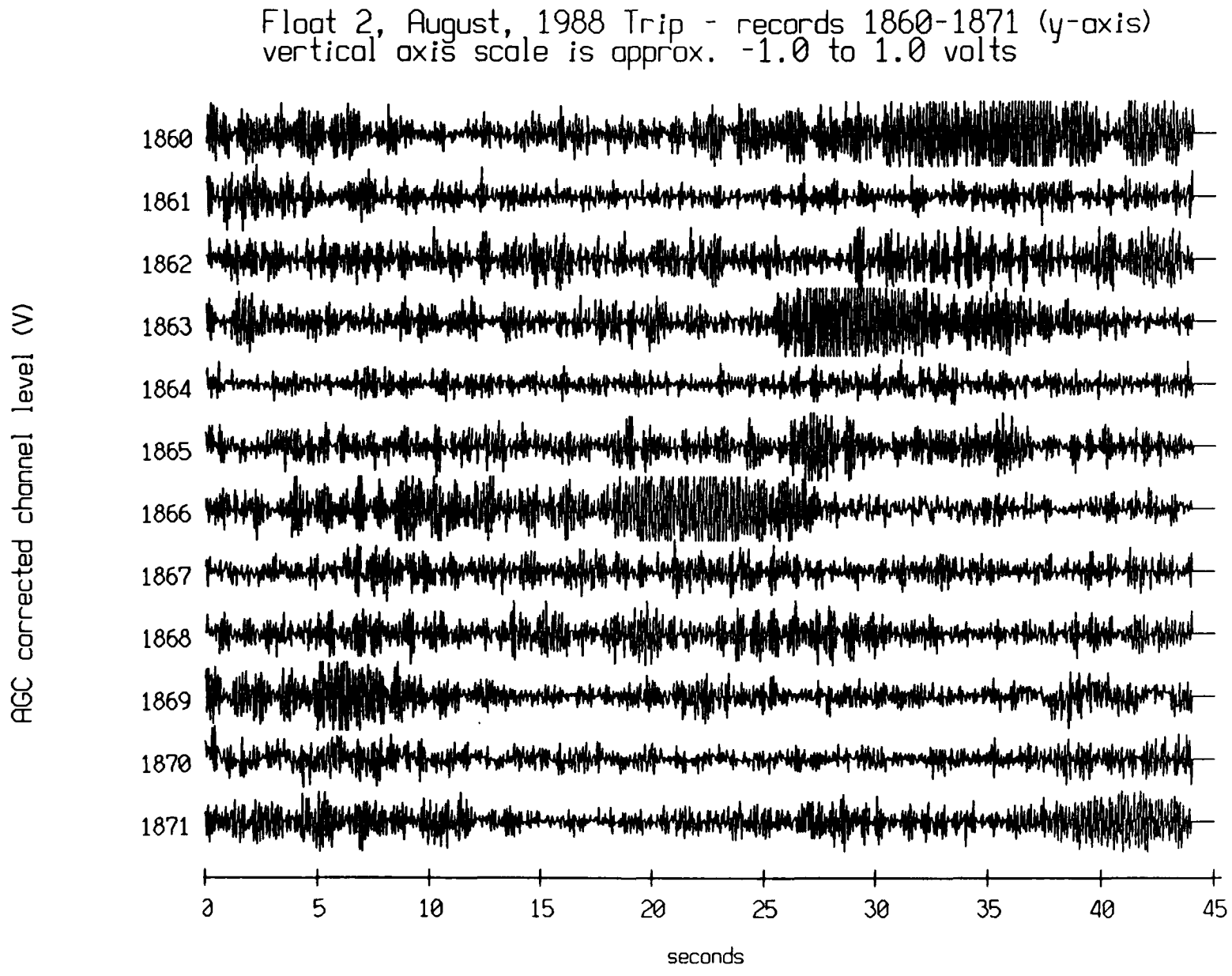


Figure XI.63b

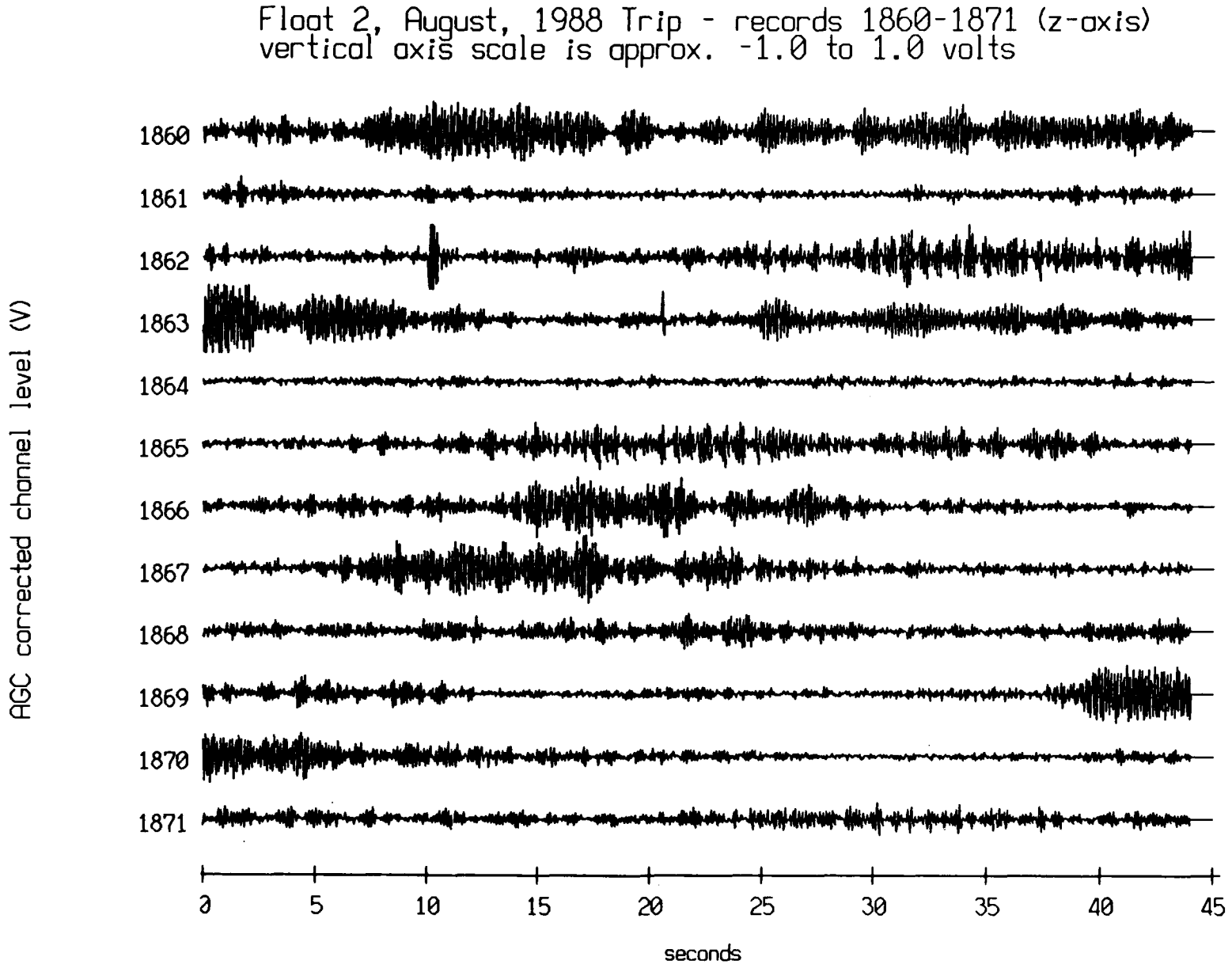


Figure XI.63c

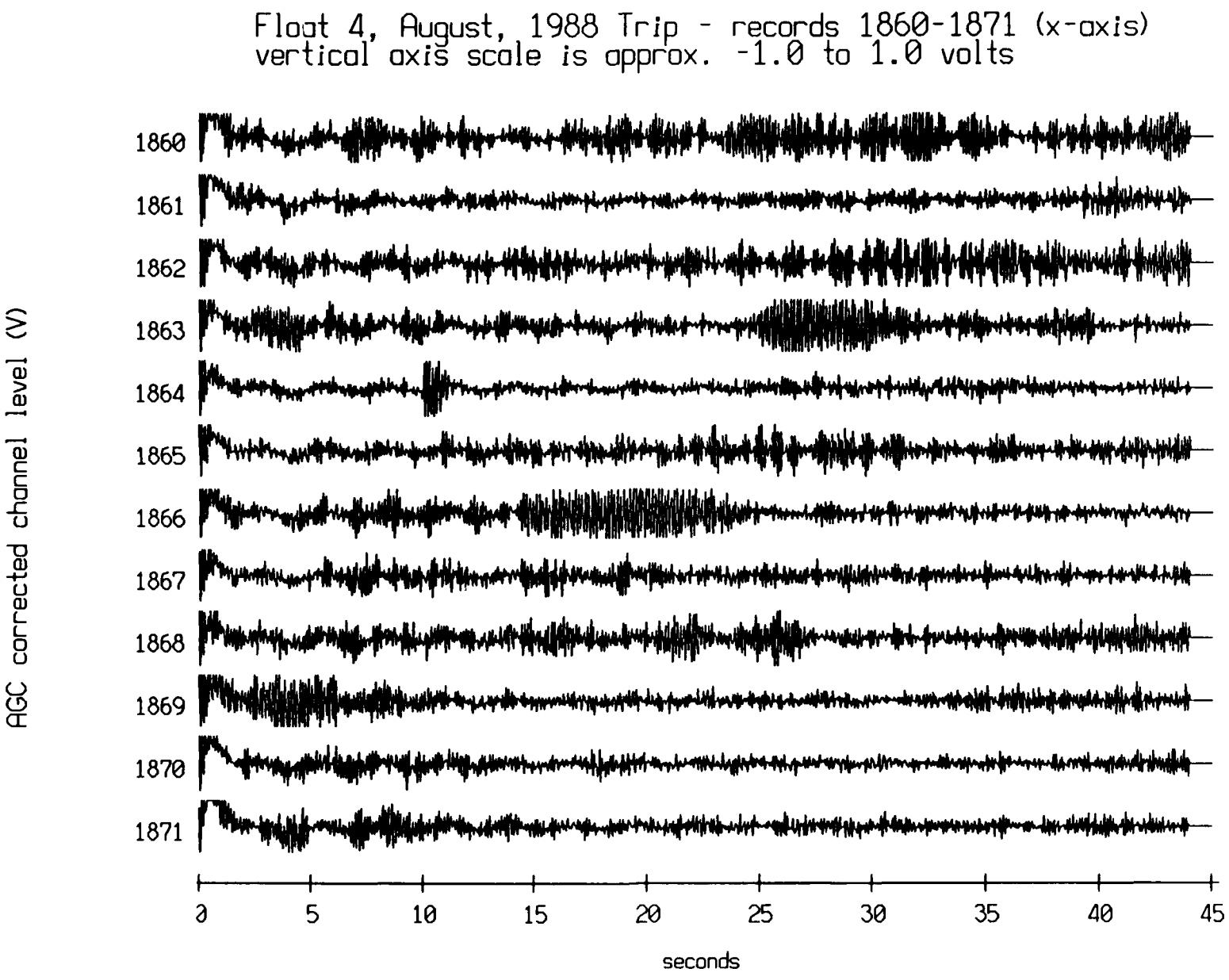


Figure XI.64a

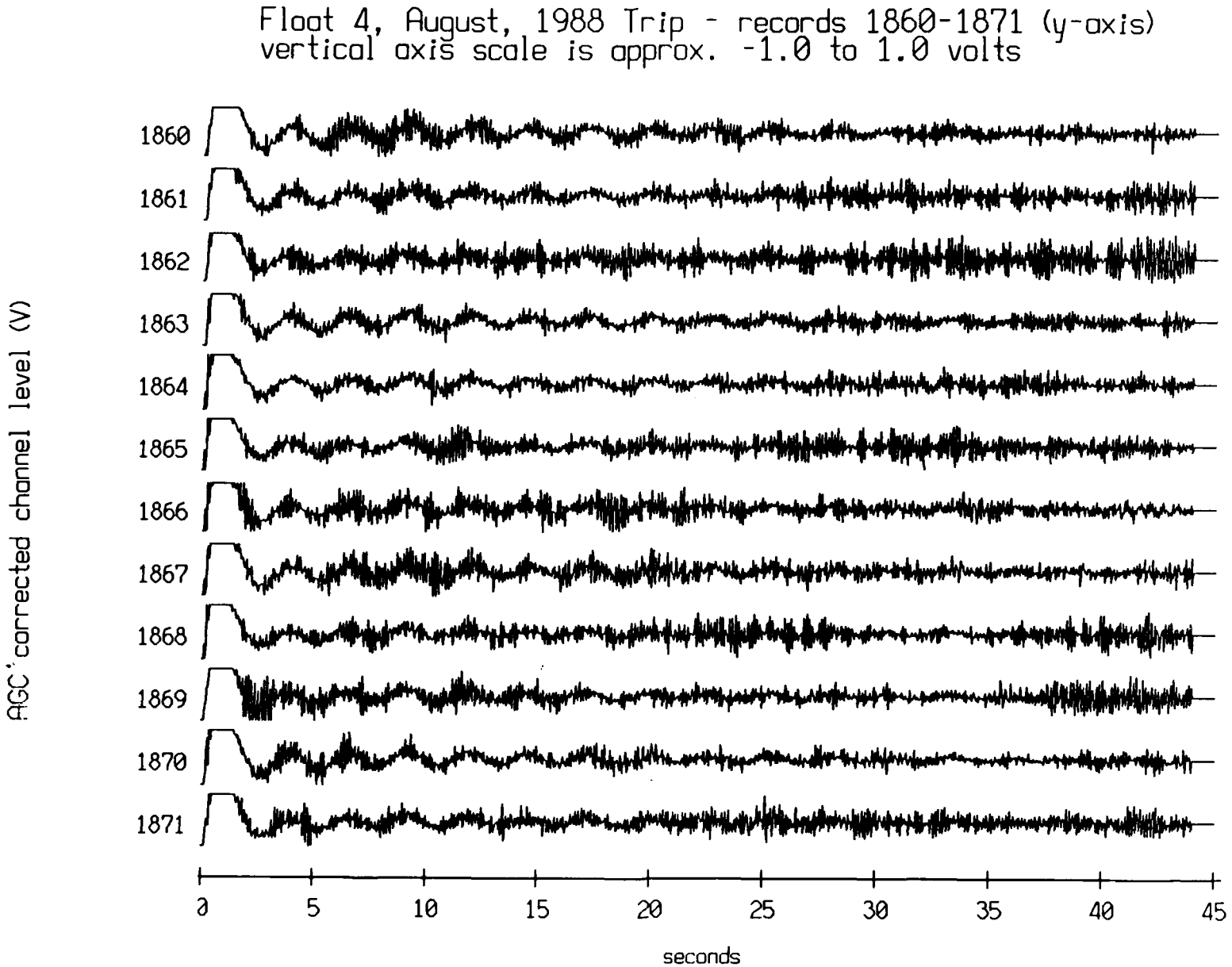


Figure XI.64b

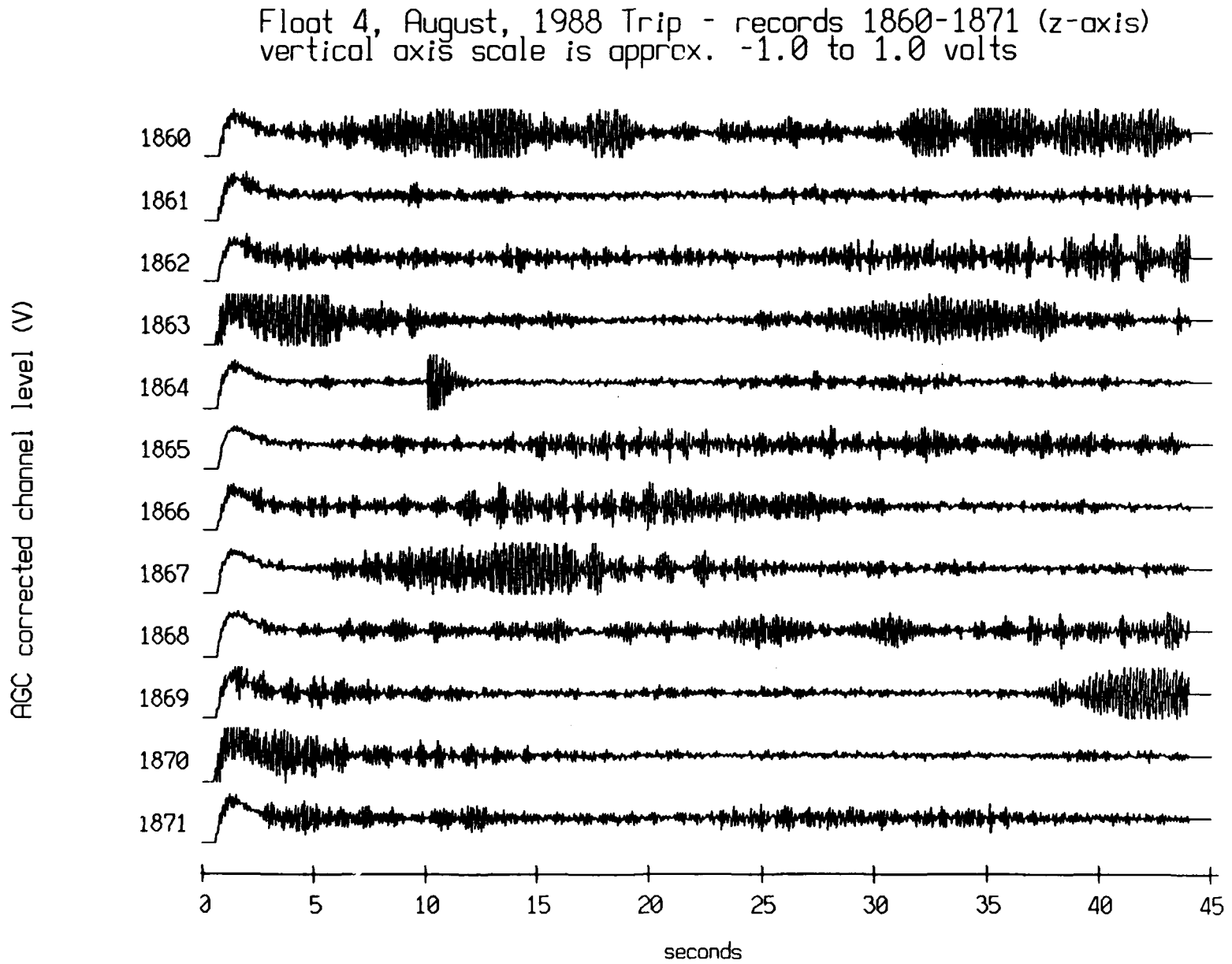


Figure XI 64c

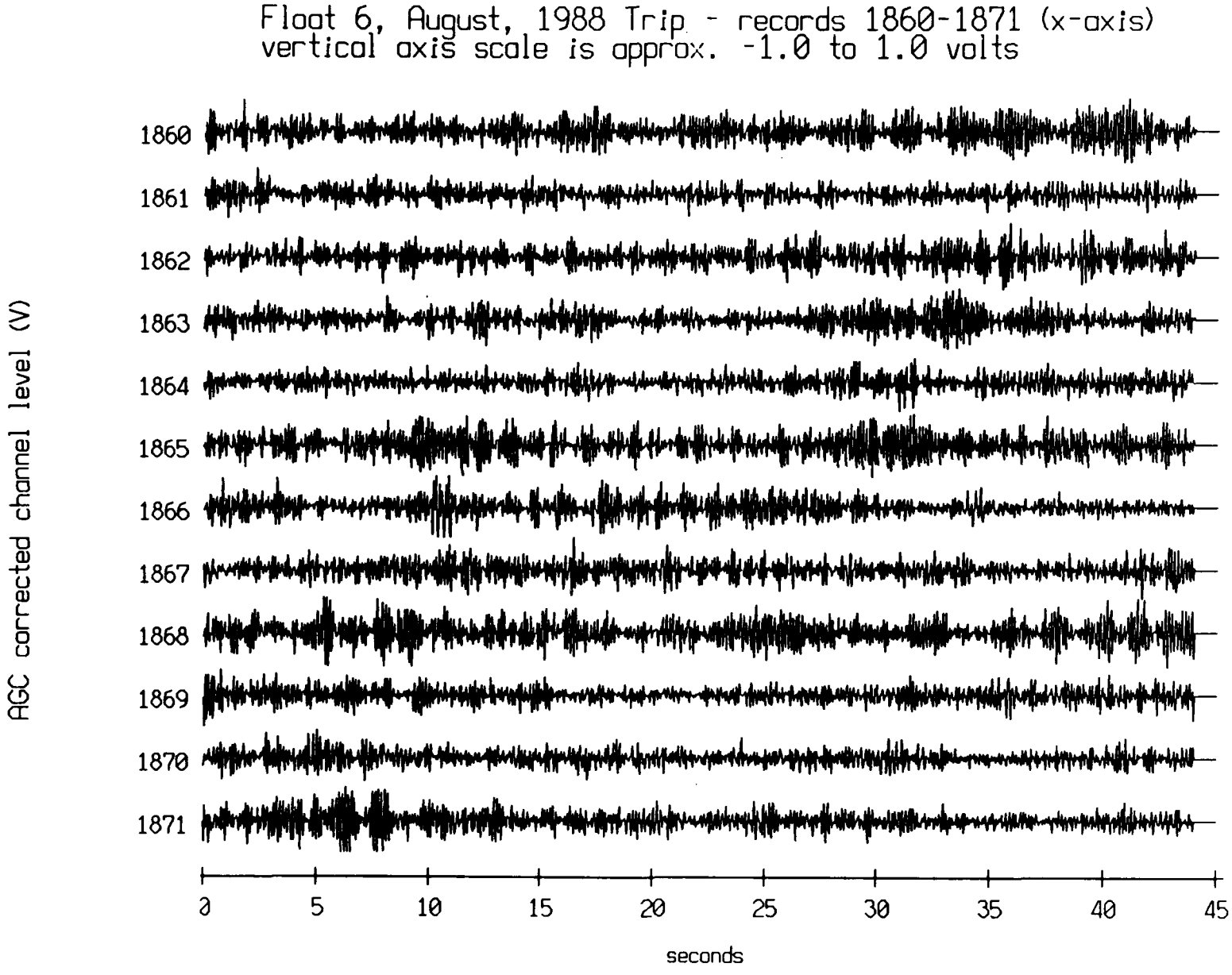


Figure XI.65a

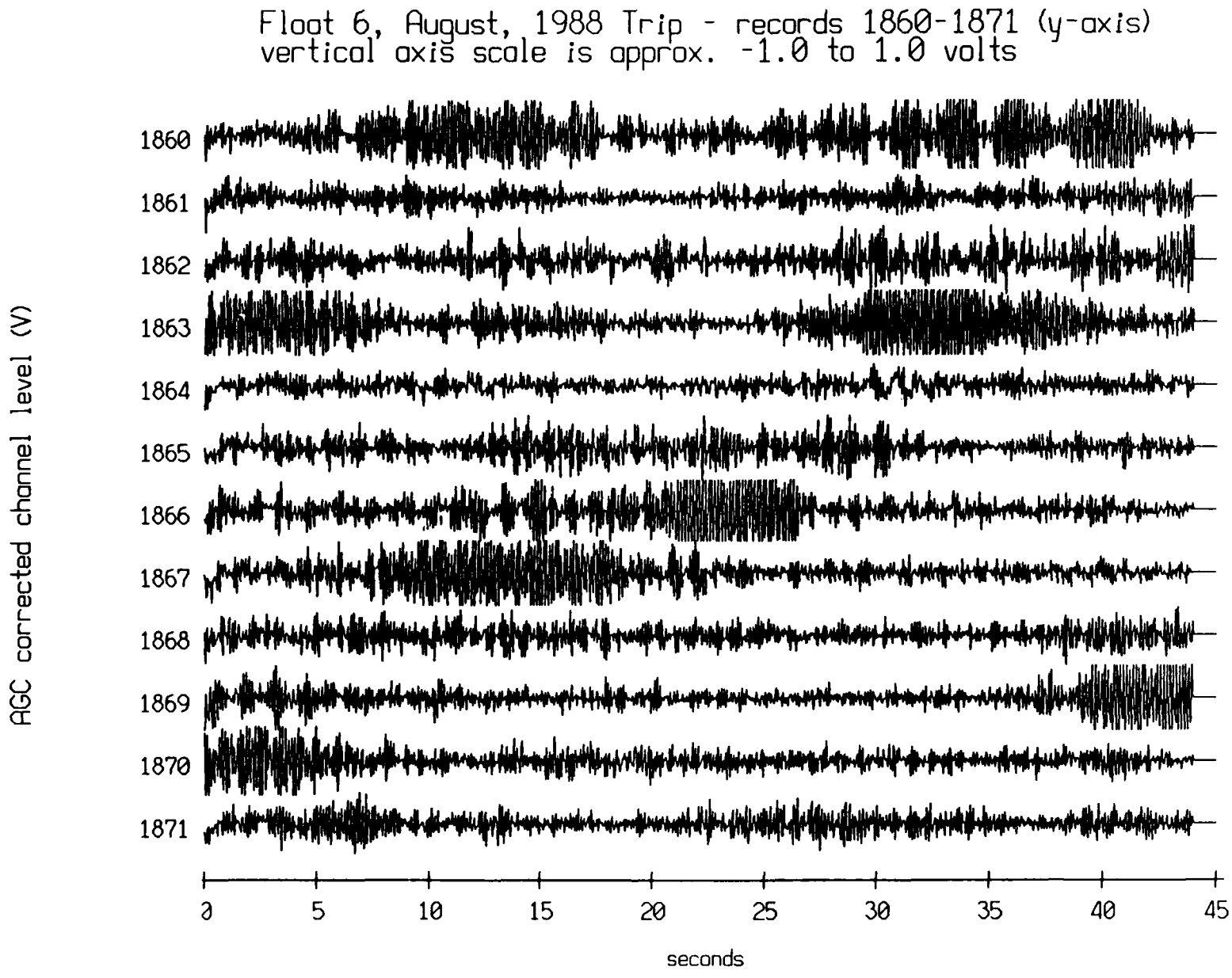


Figure XI.65b

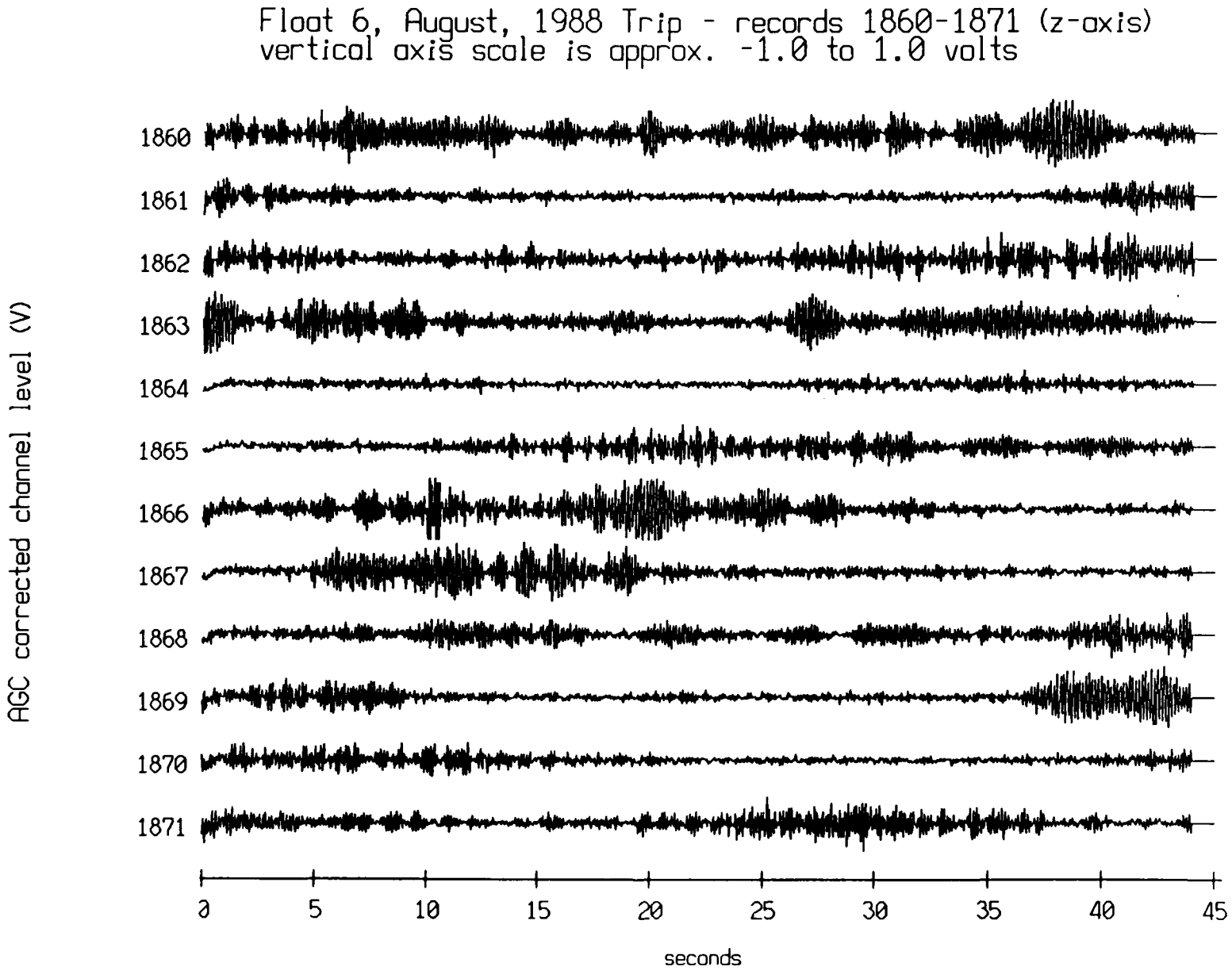


Figure XI.65c

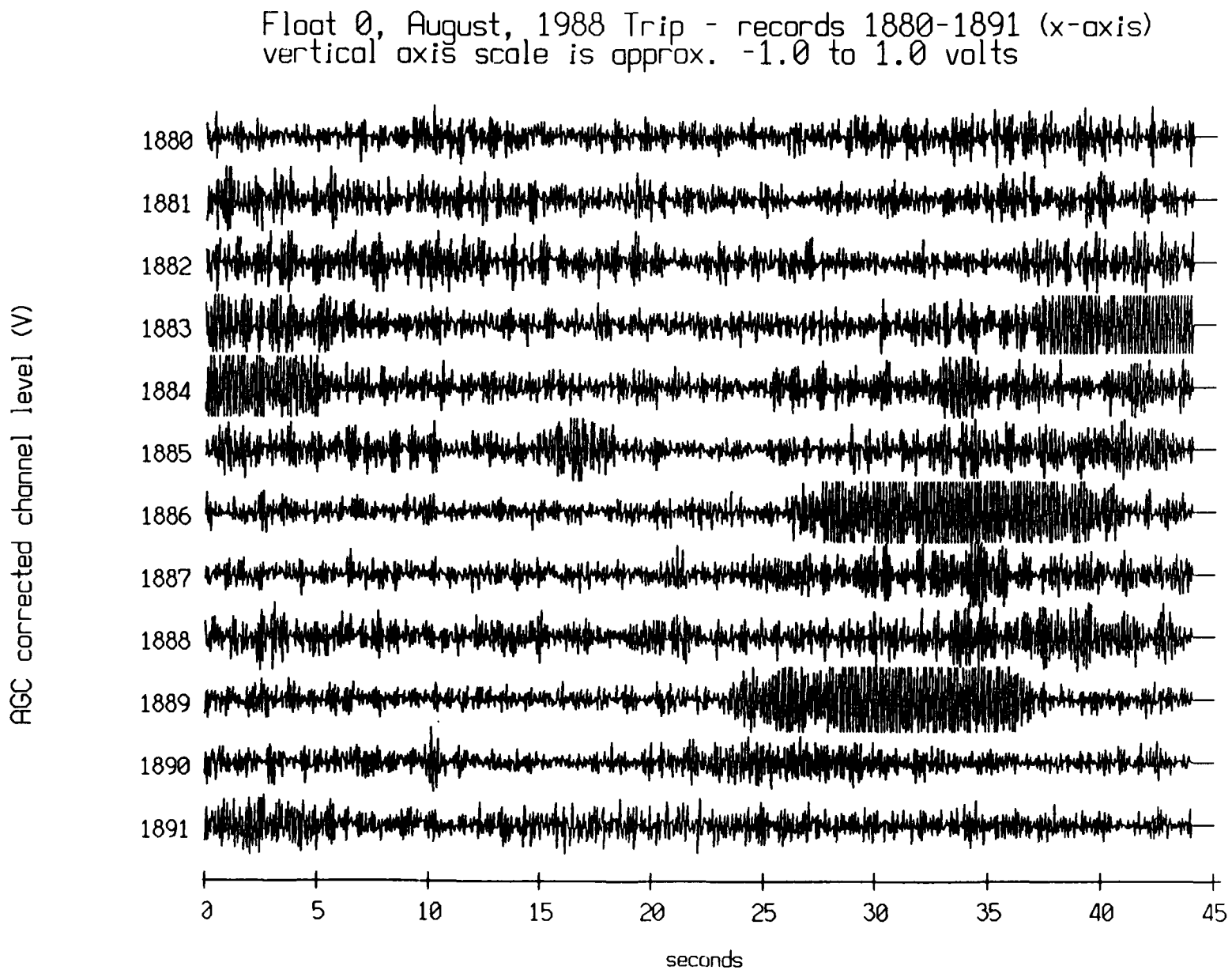

Float 0, August, 1988 Trip - records 1880-1891 (x-axis)
vertical axis scale is approx. -1.0 to 1.0 volts
AGC corrected channel level (V)
1880
1881
1882
1883
1884
1885
1886
1887
1888
1889
1890
1891
0
5
10
15
20
25
30
35
40
45
seconds

Figure XI.6a

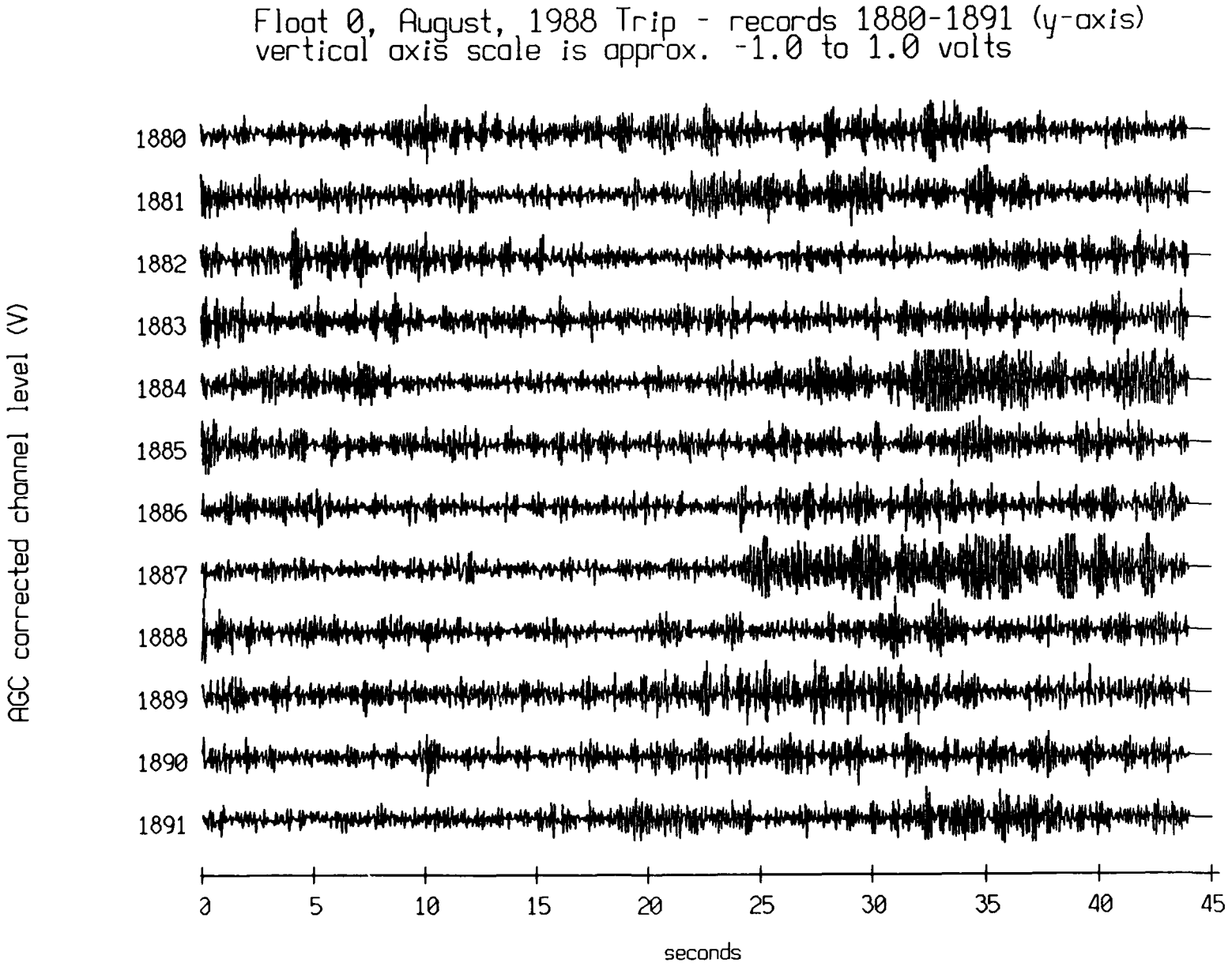


Figure XI.66b

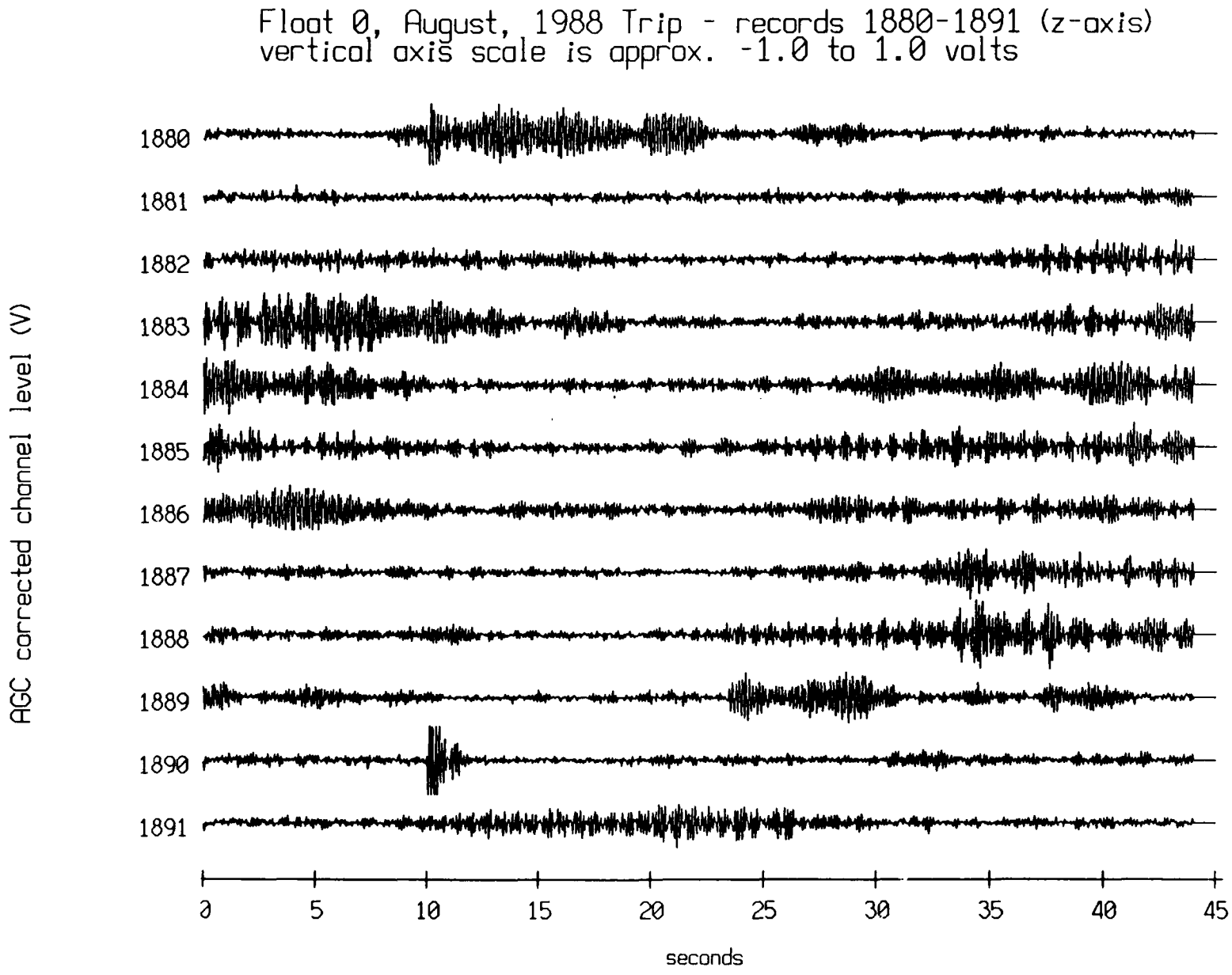


Figure XI.66c

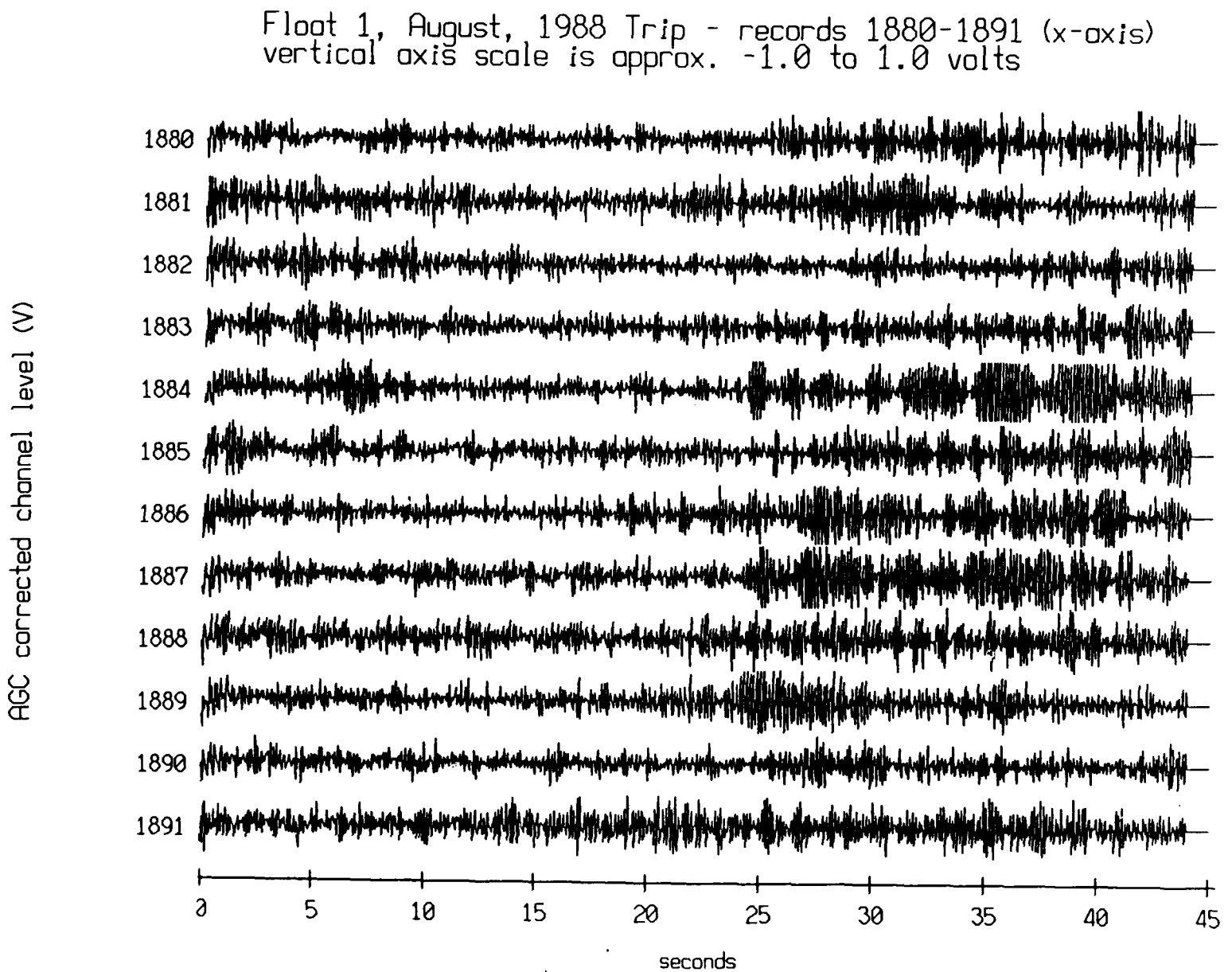


Figure XI.67a

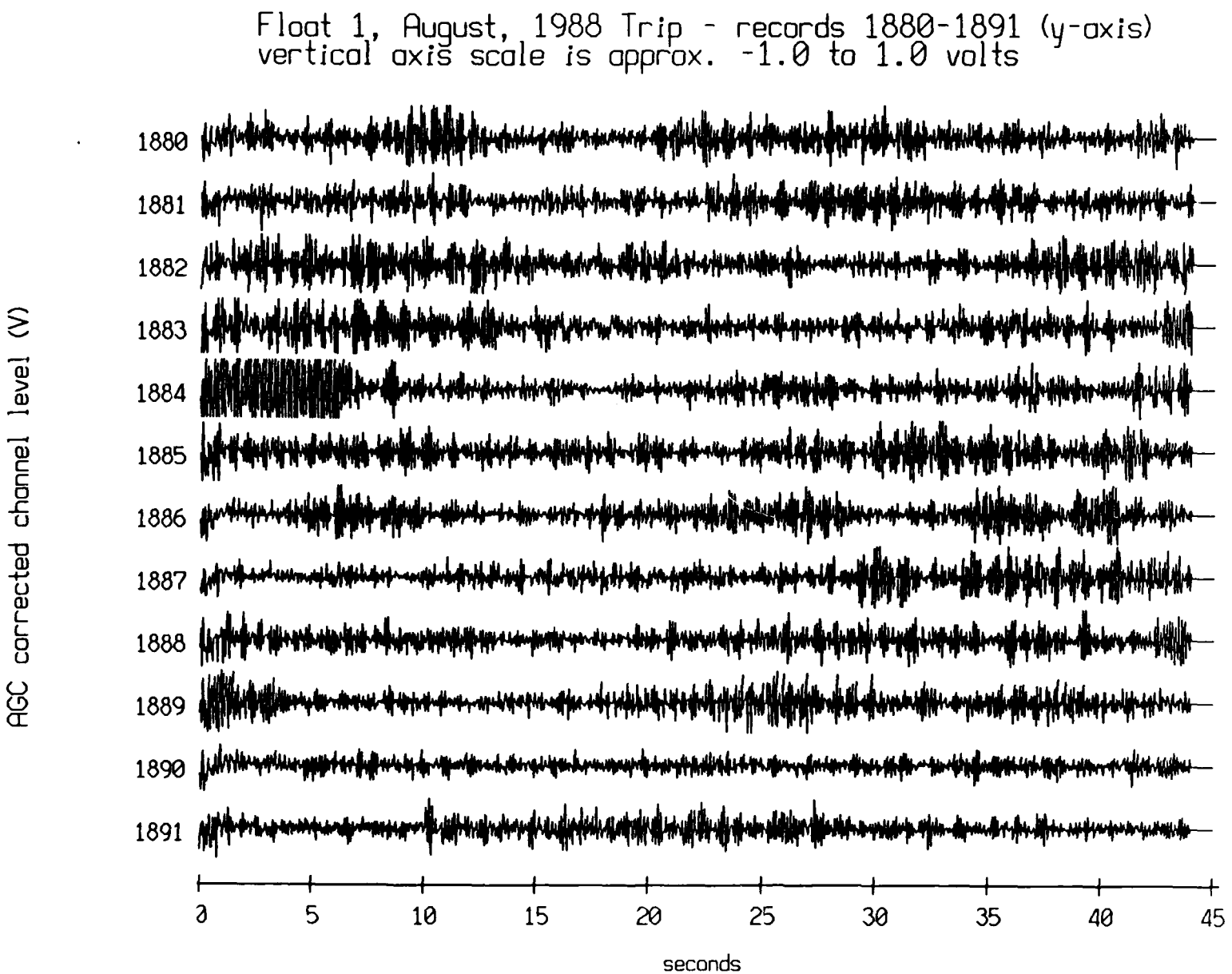


Figure XI.67b

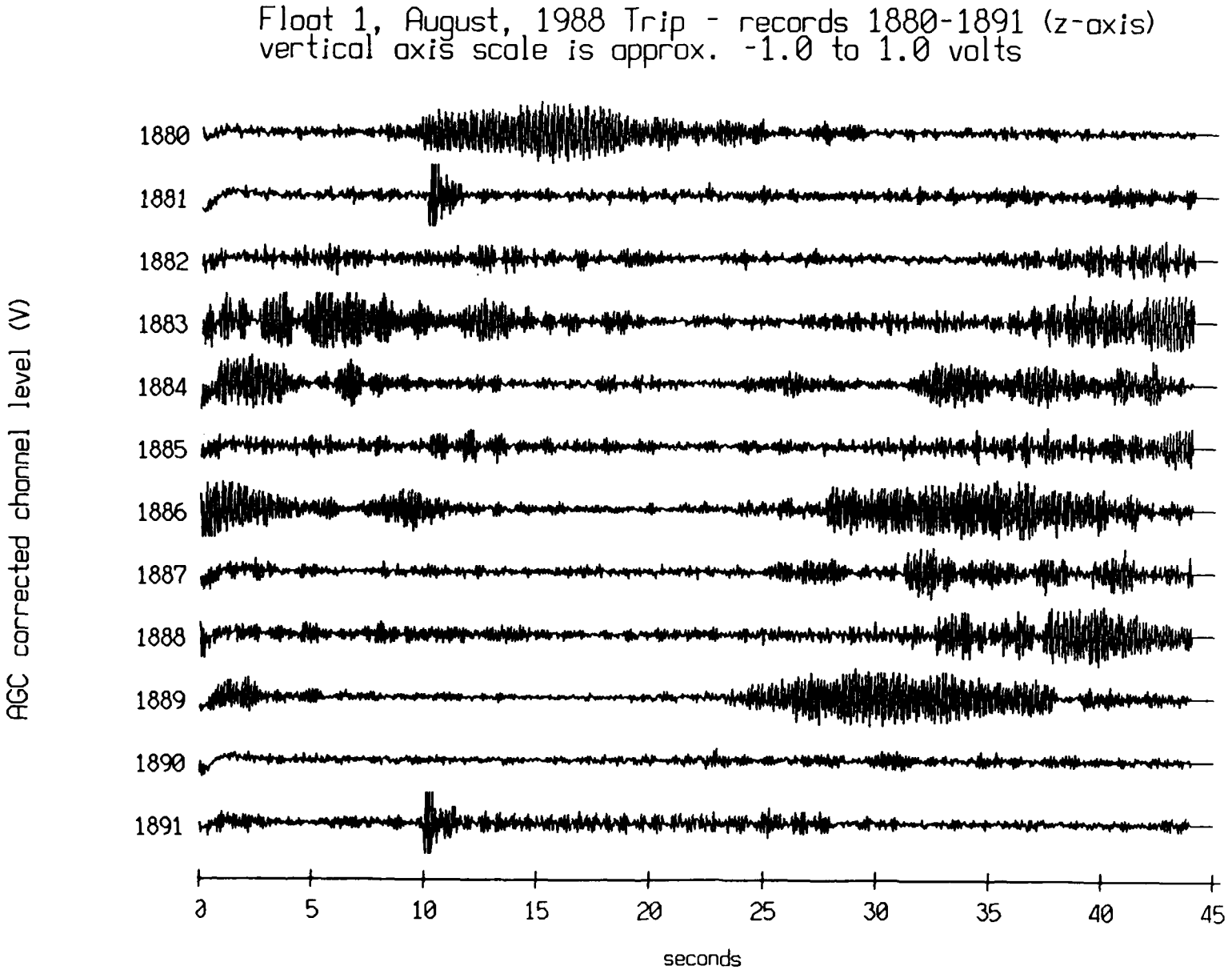


Figure XI.67c

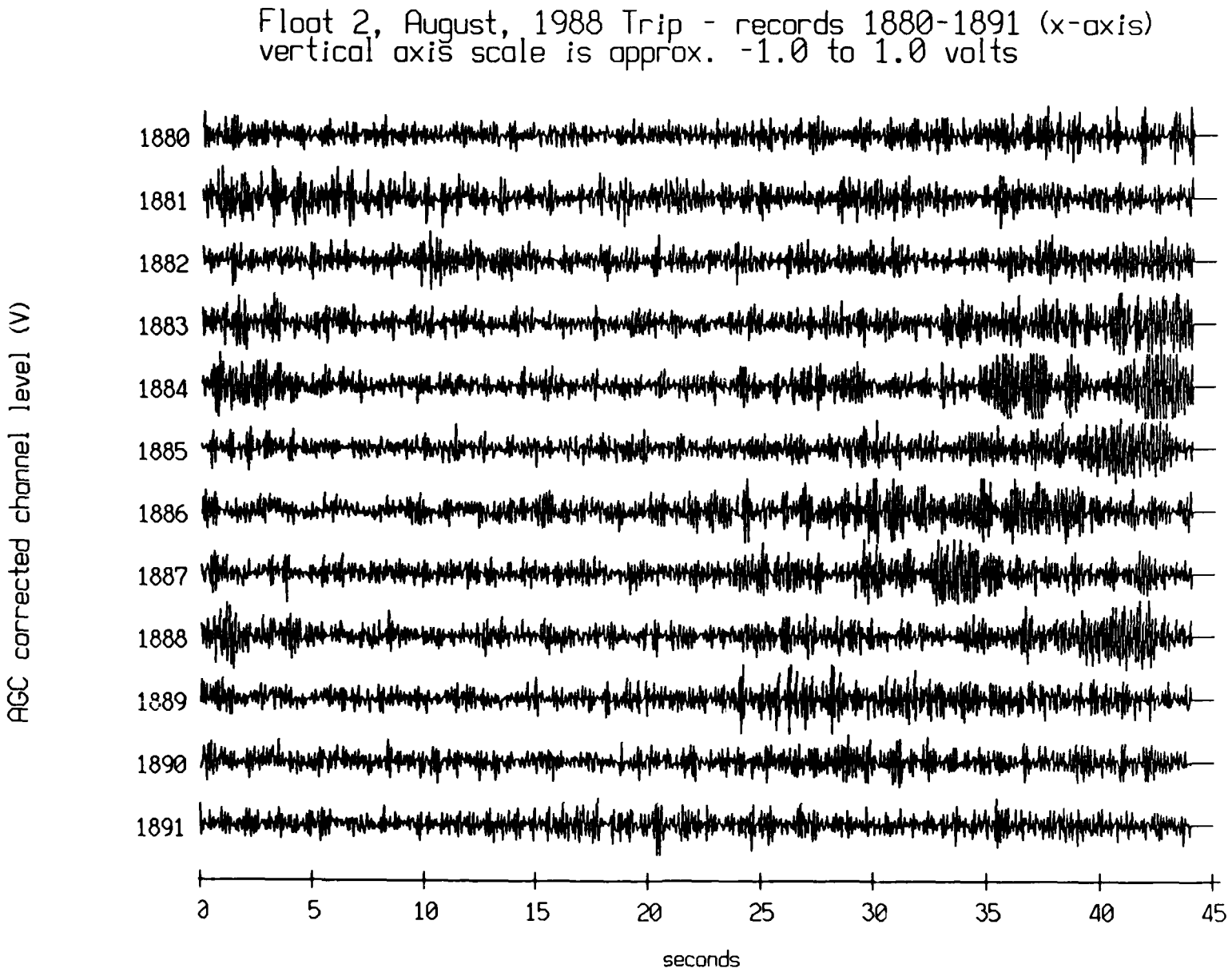


Figure XI.68a

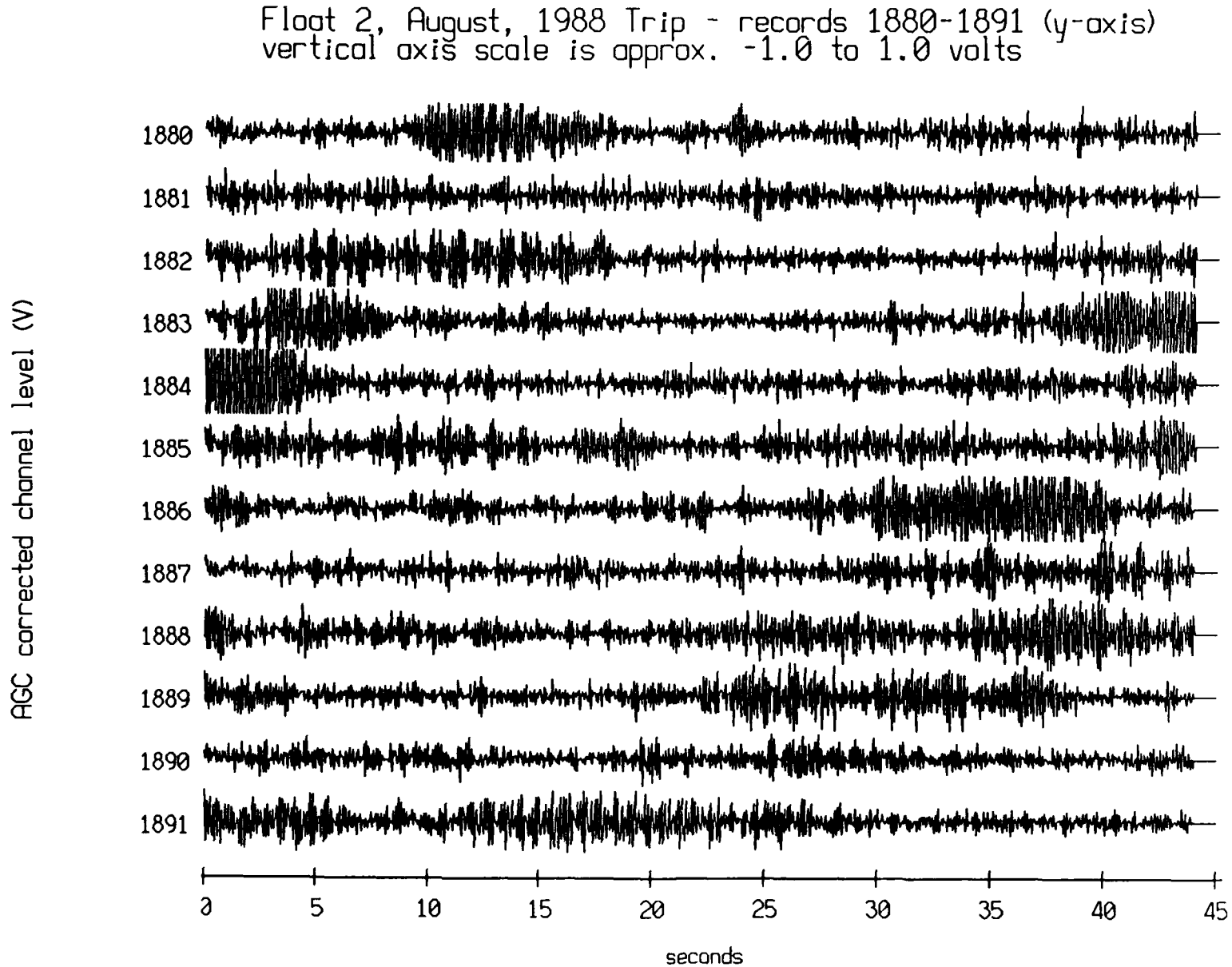


Figure XI.68b

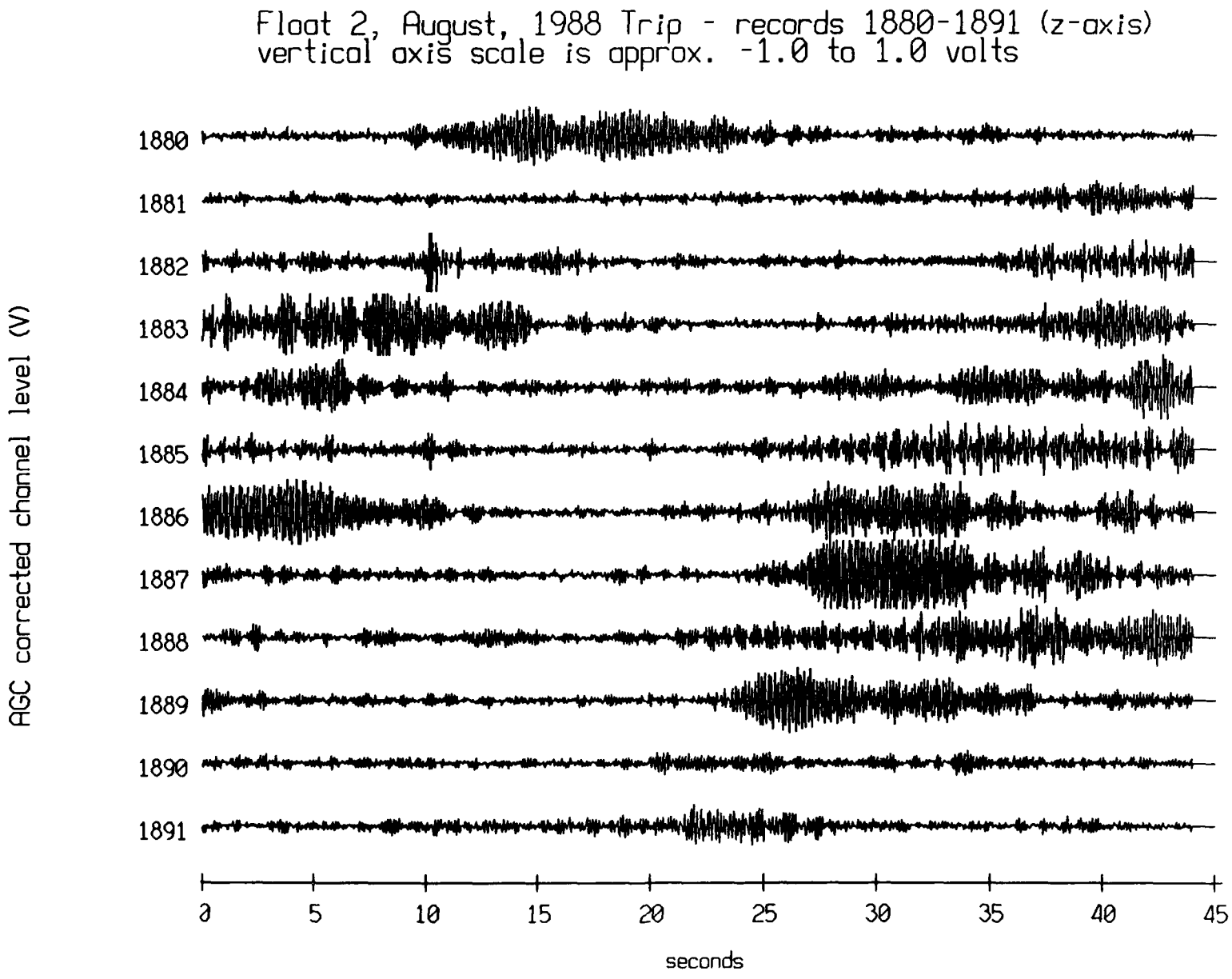


Figure XI.68c

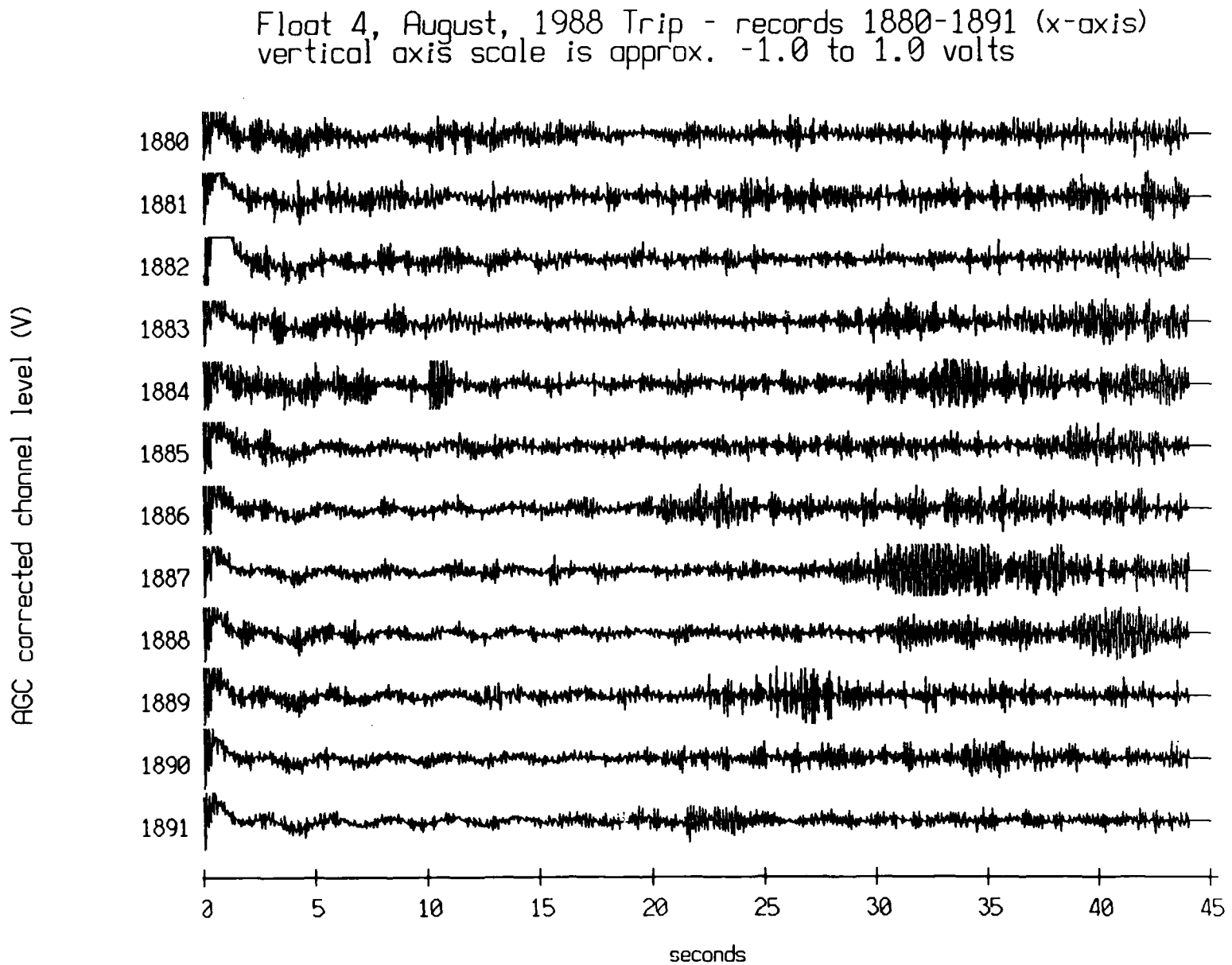


Figure XI.69a

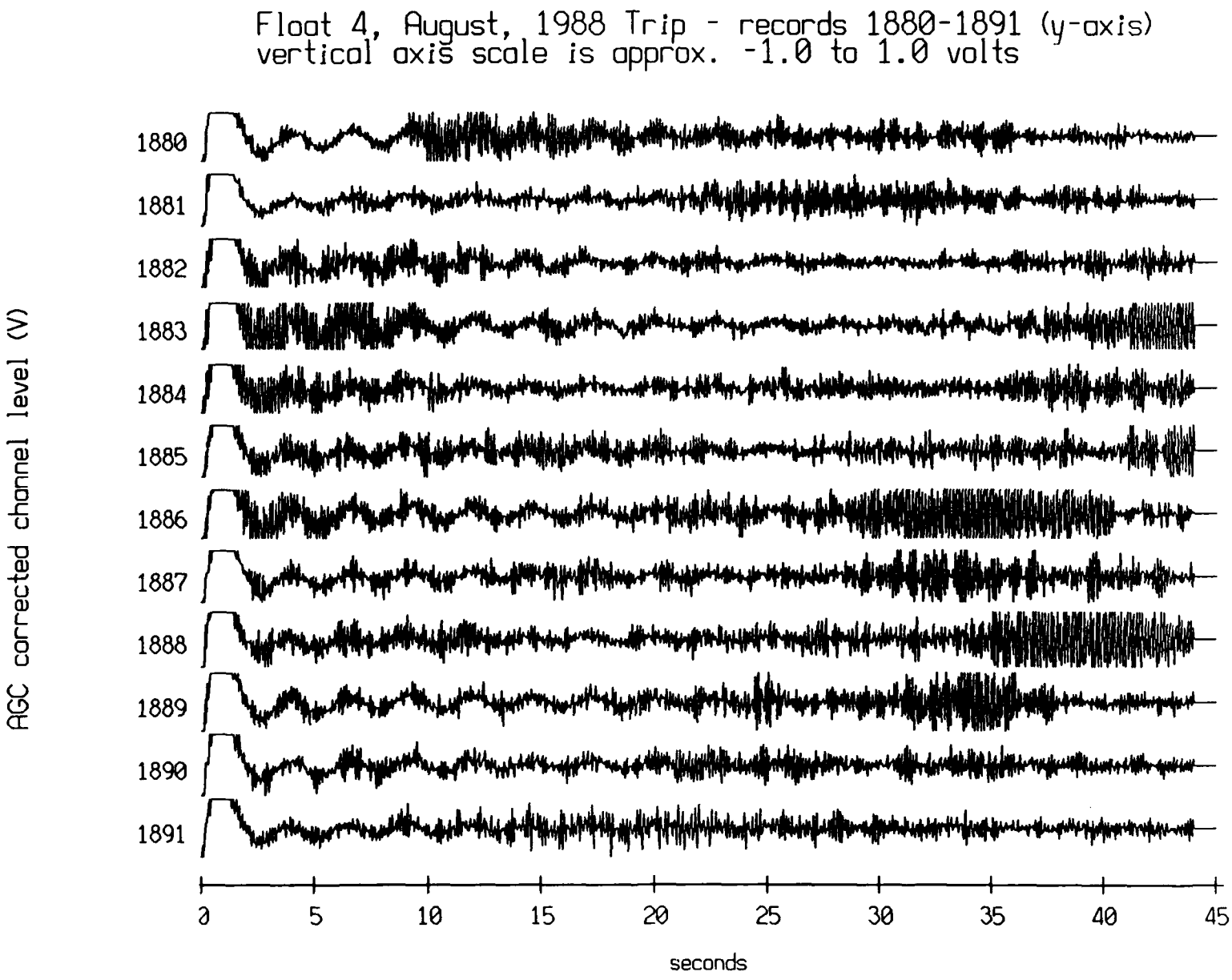


Figure XI.69b

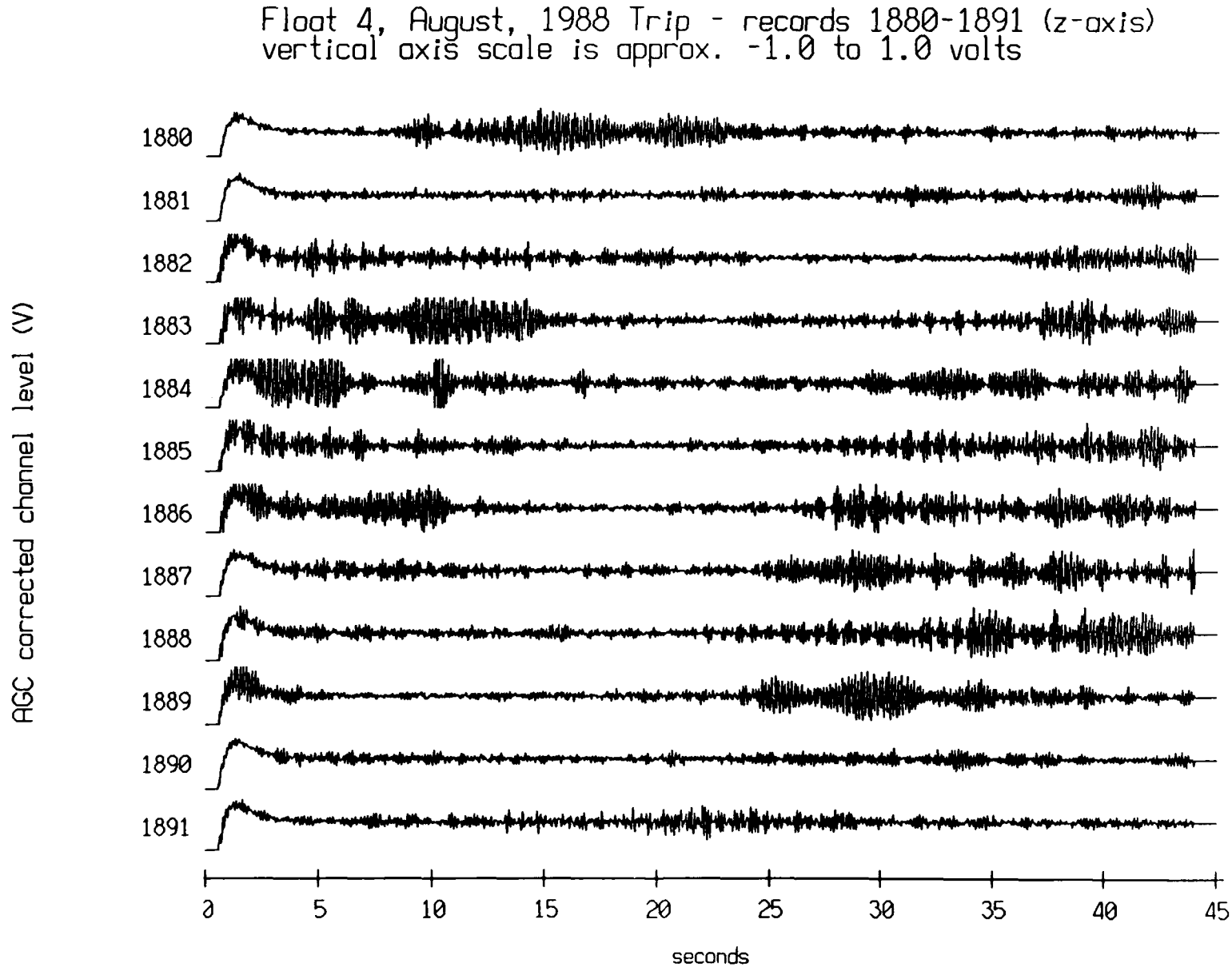


Figure XI.69c

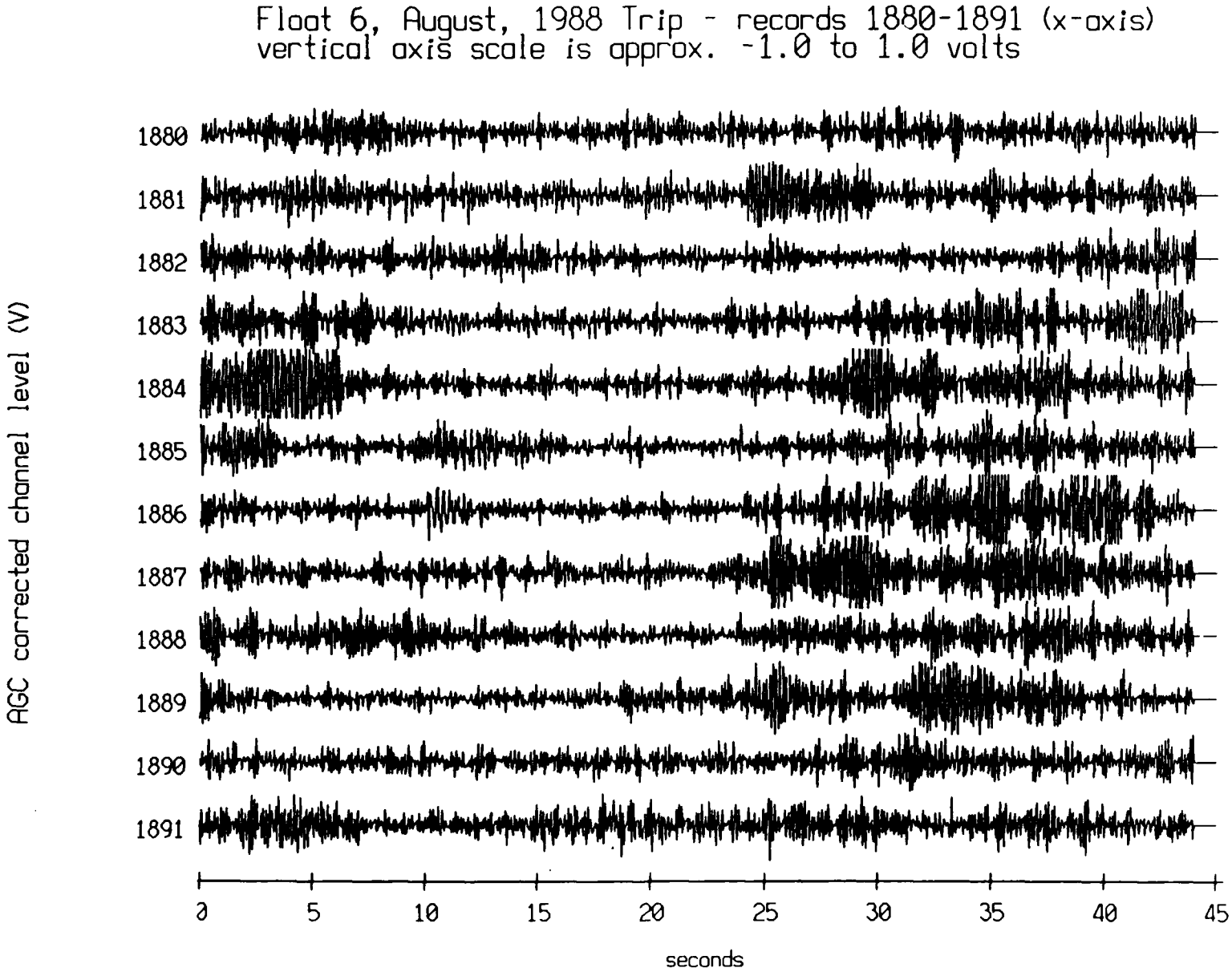


Figure XI.70a

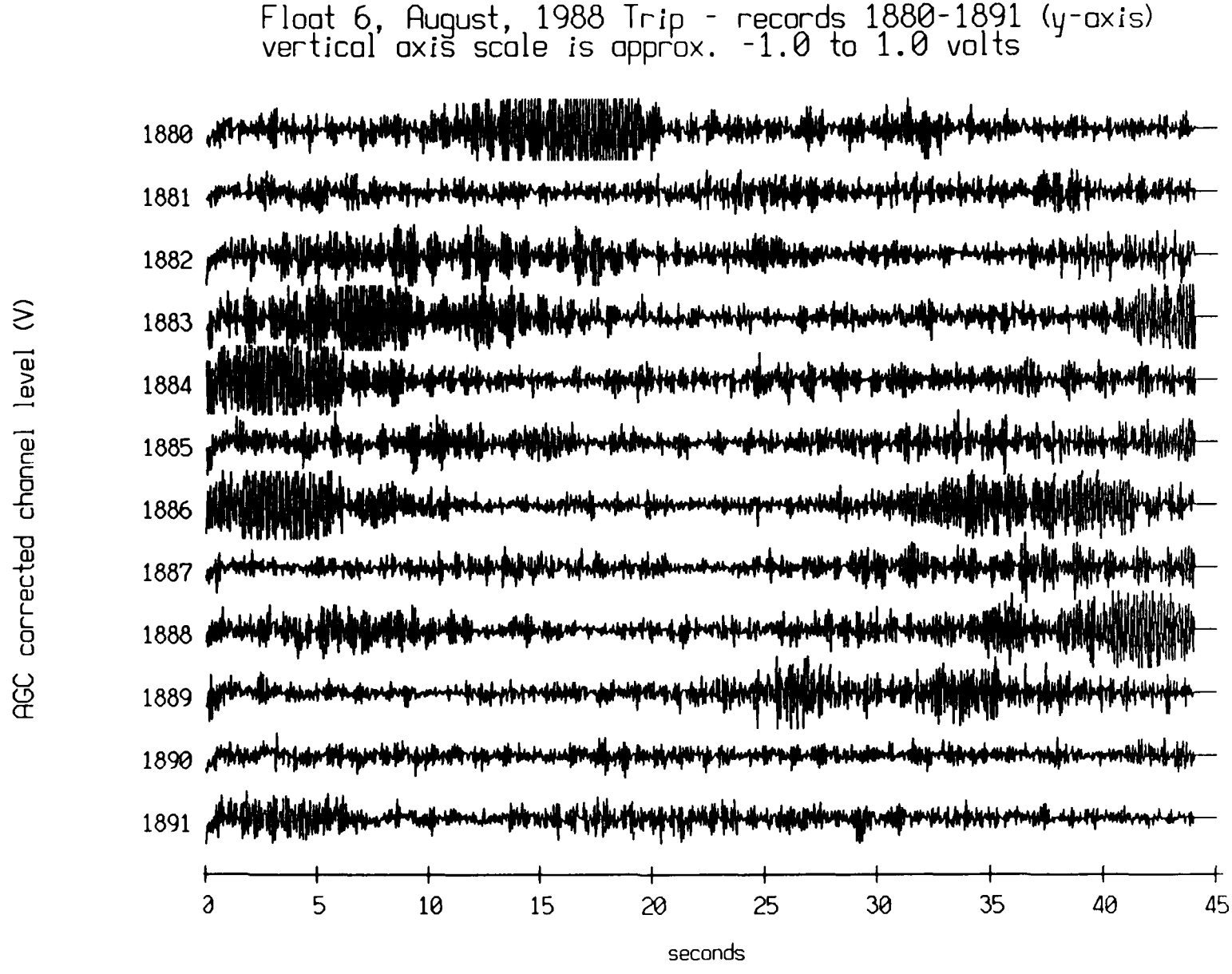


Figure XI.7ob

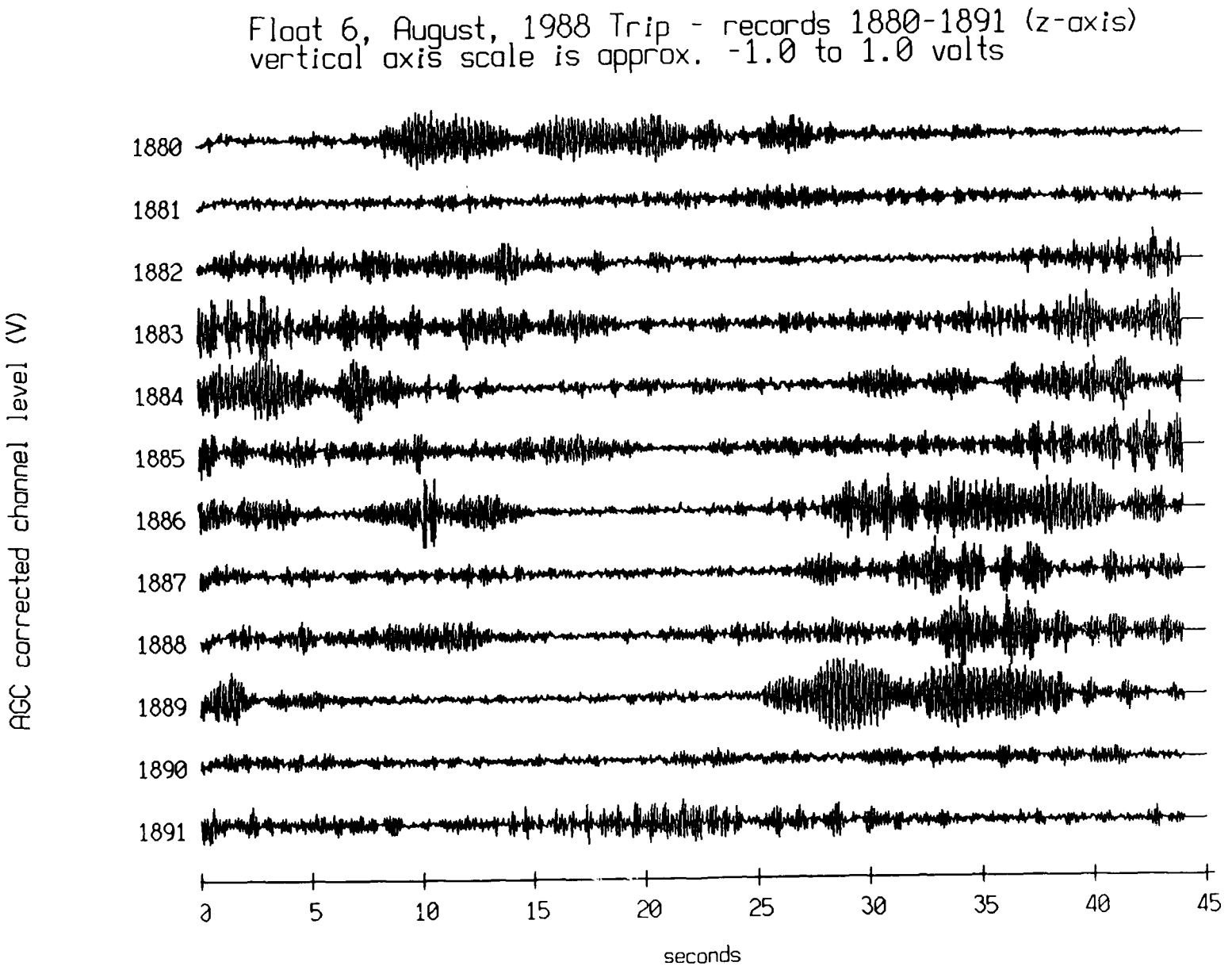


Figure XI.70c

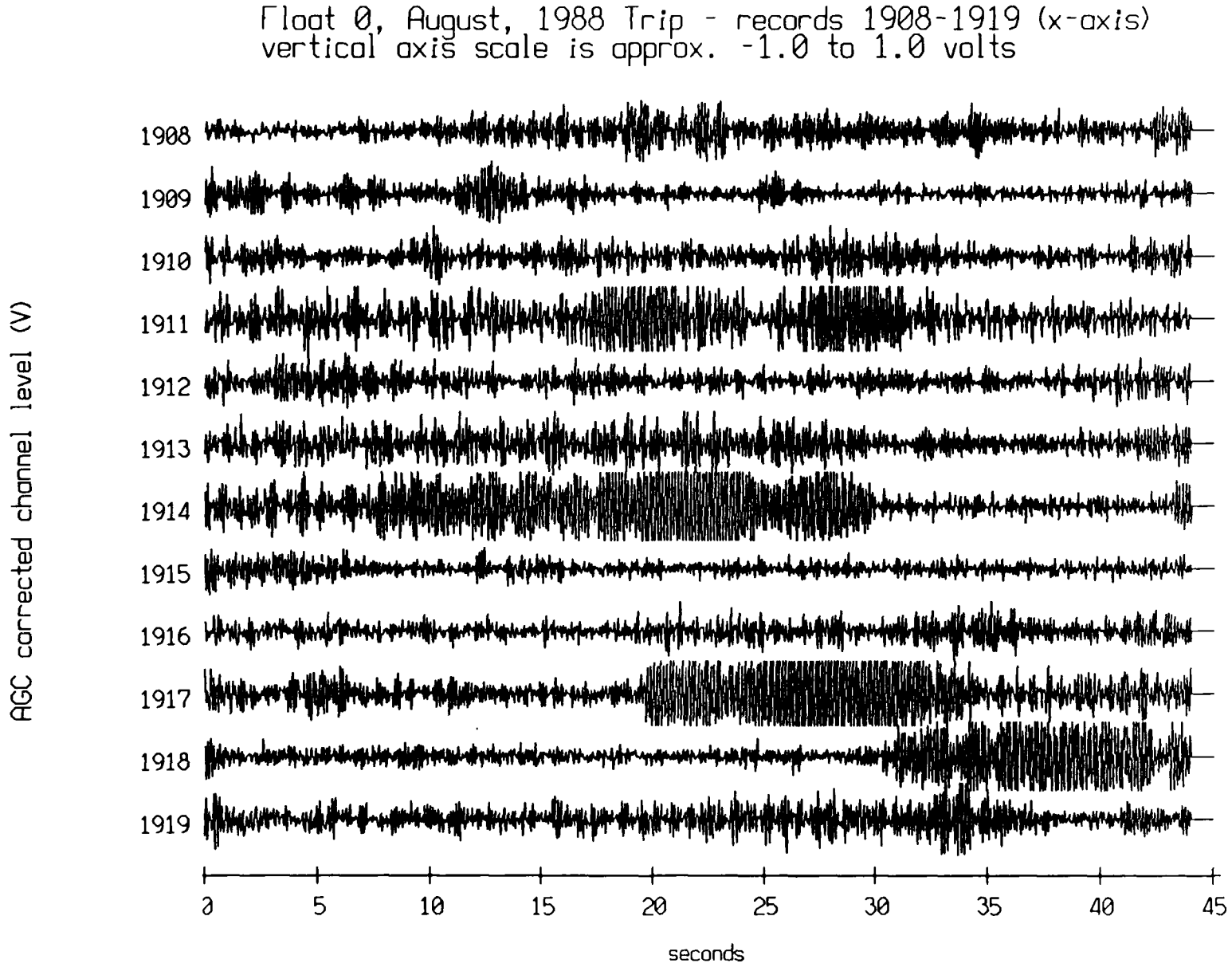


Figure XI.71a

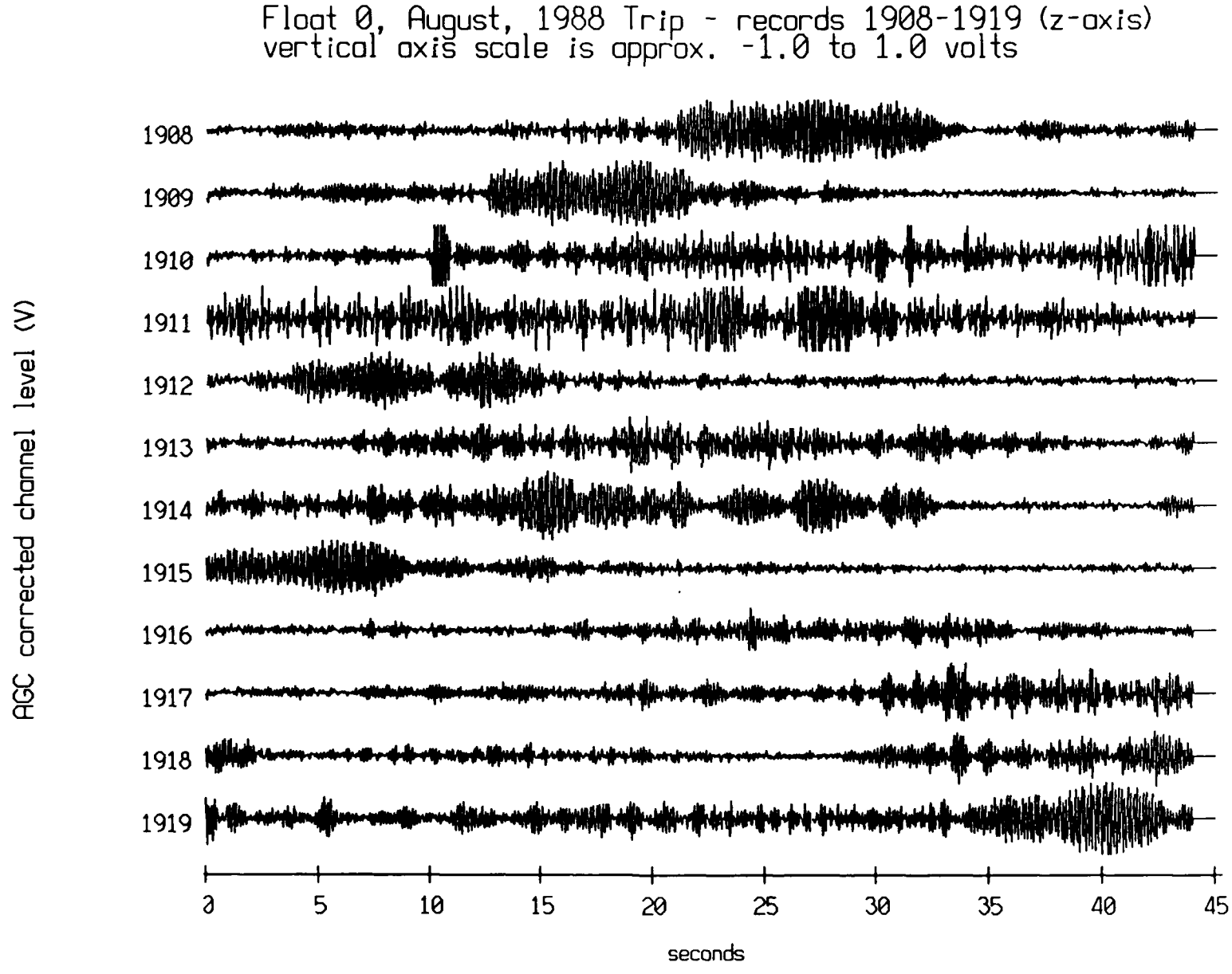


Figure XI.71c

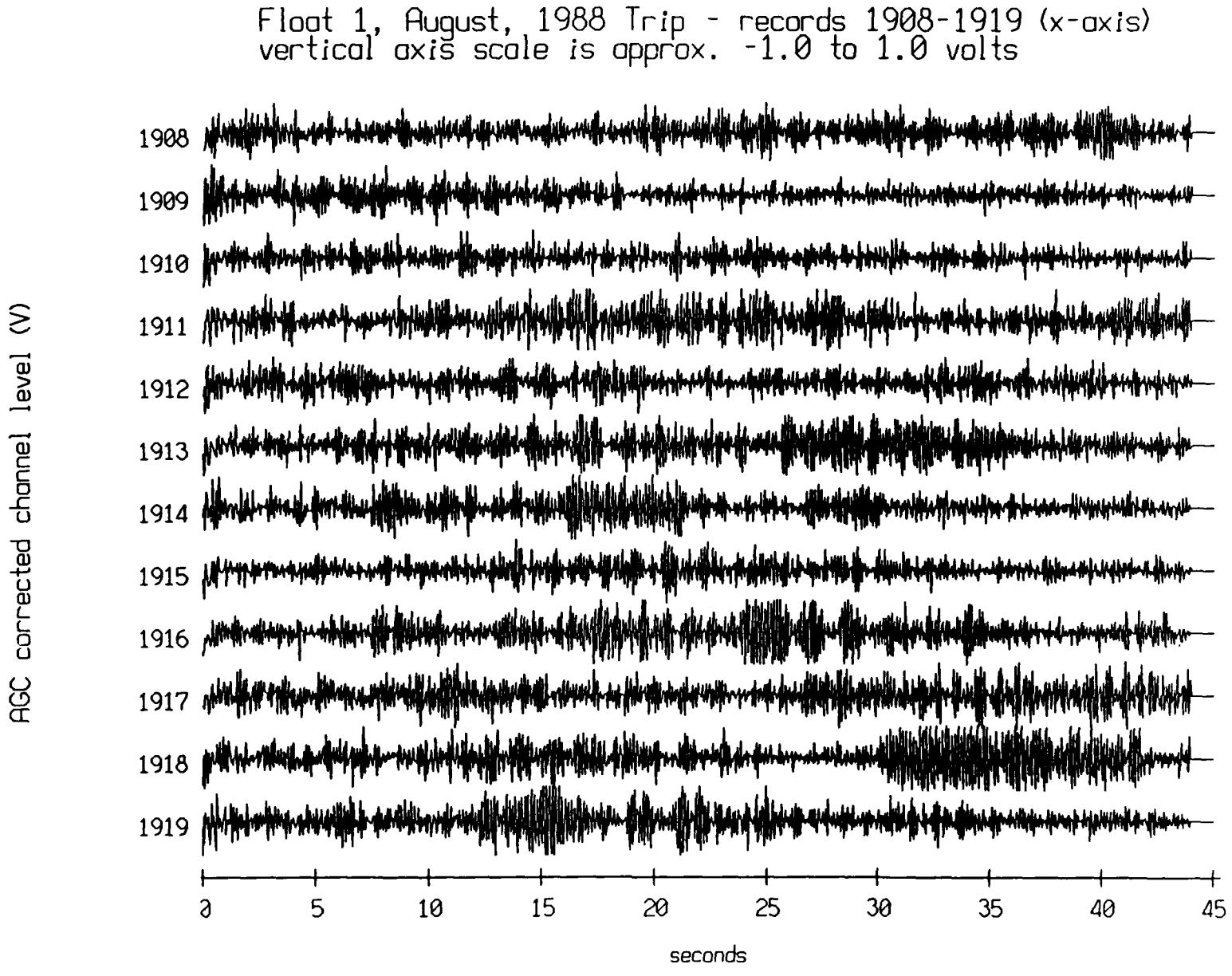


Figure XI.72a

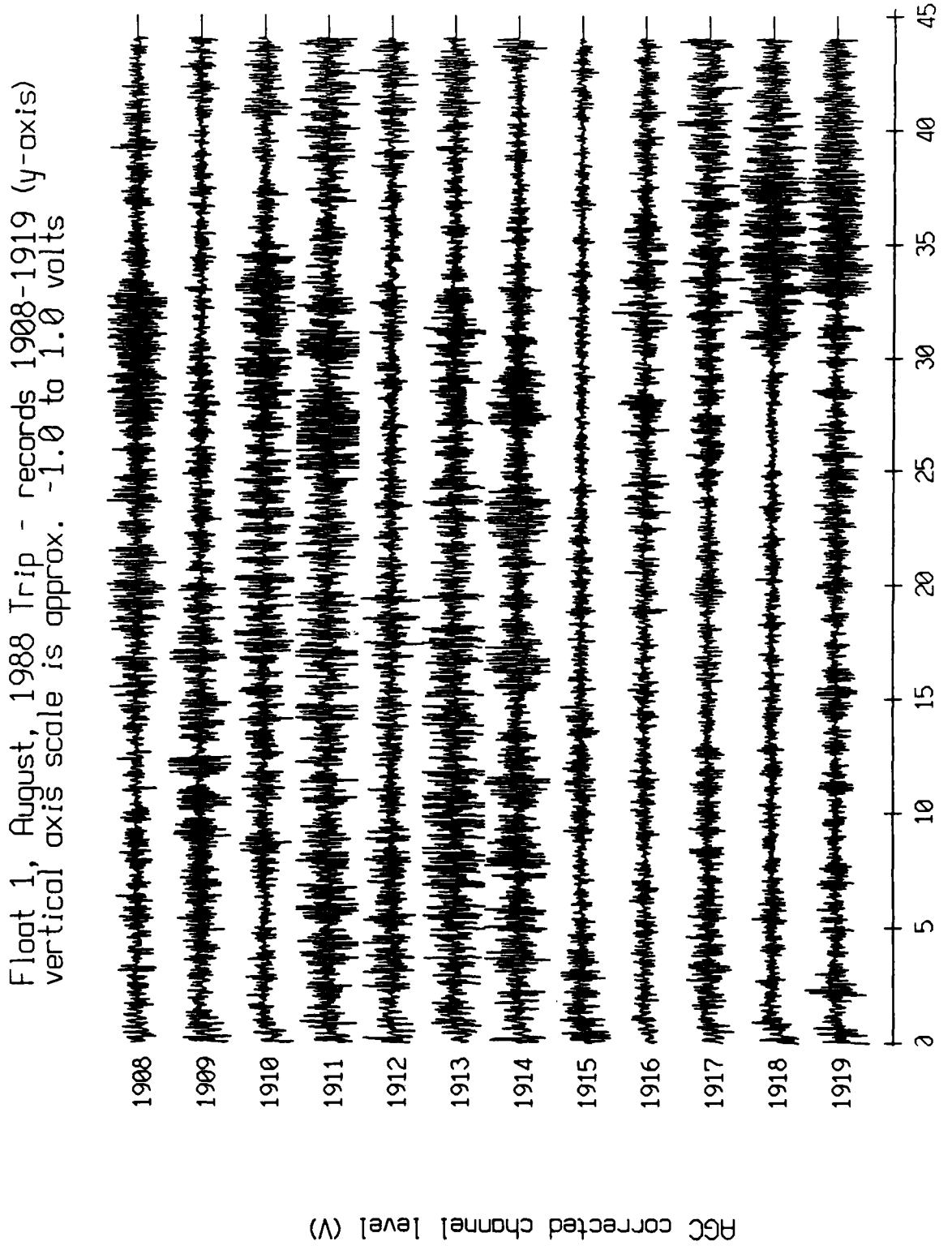


Figure XI.72b

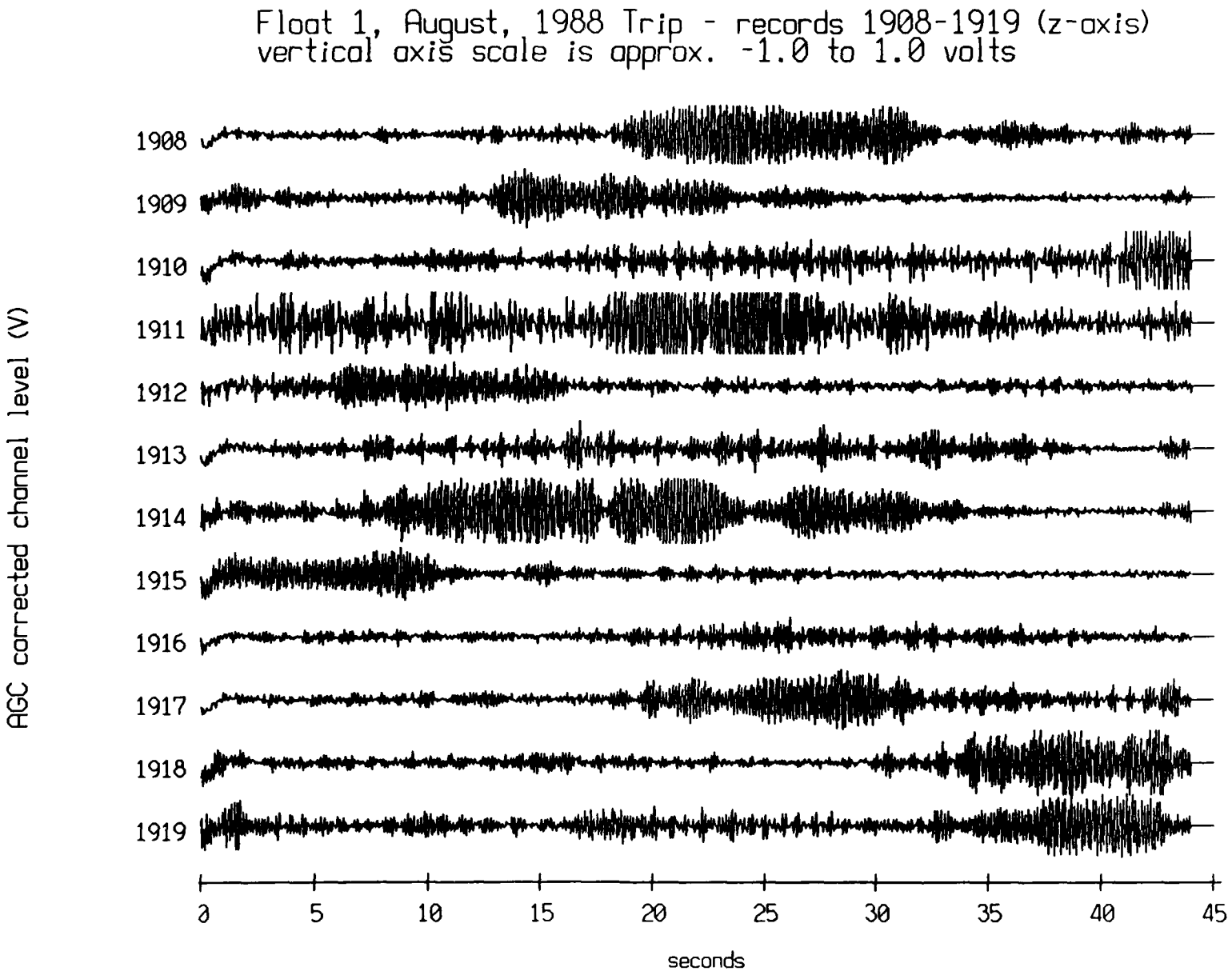


Figure XI.72c

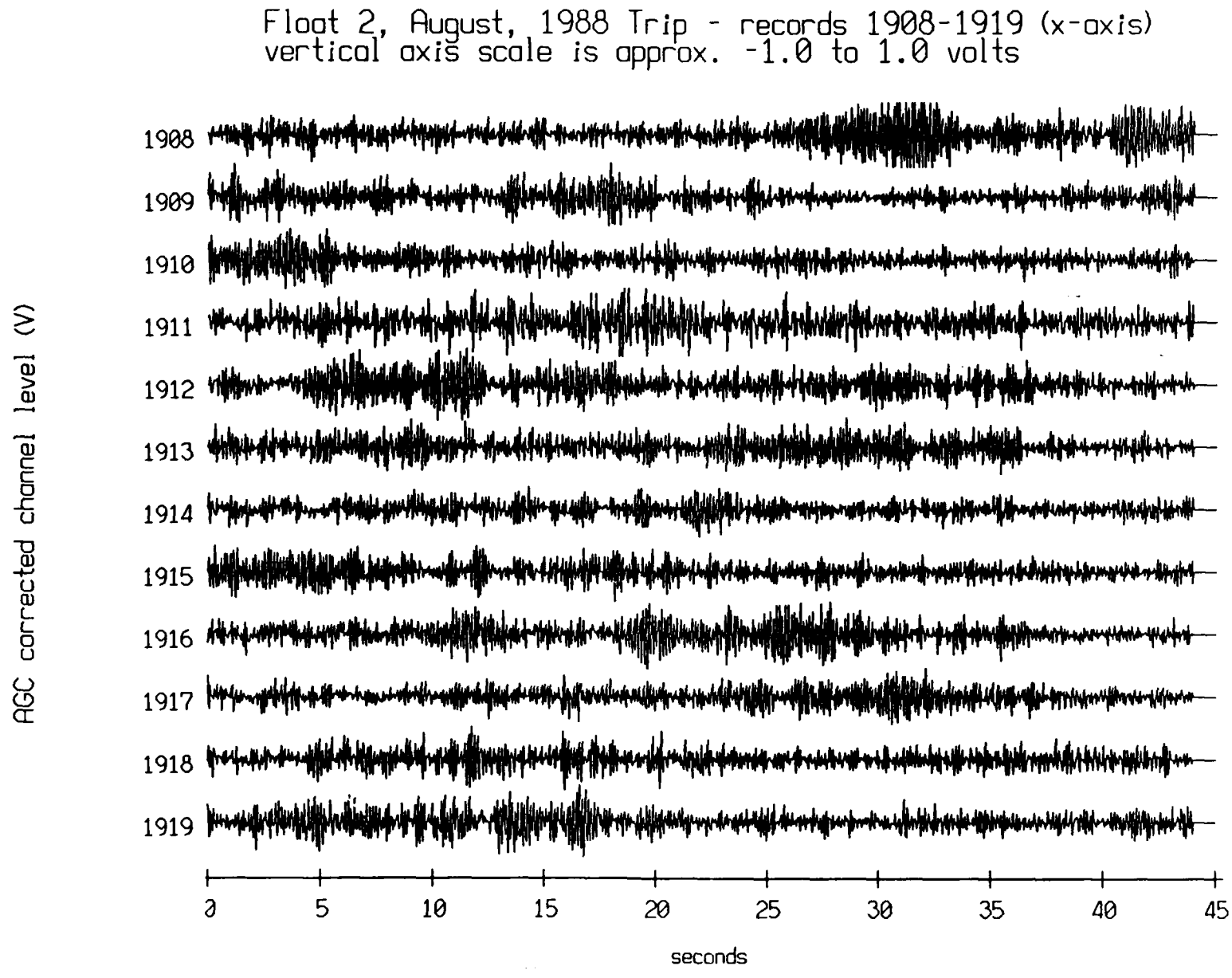


Figure XI.73a

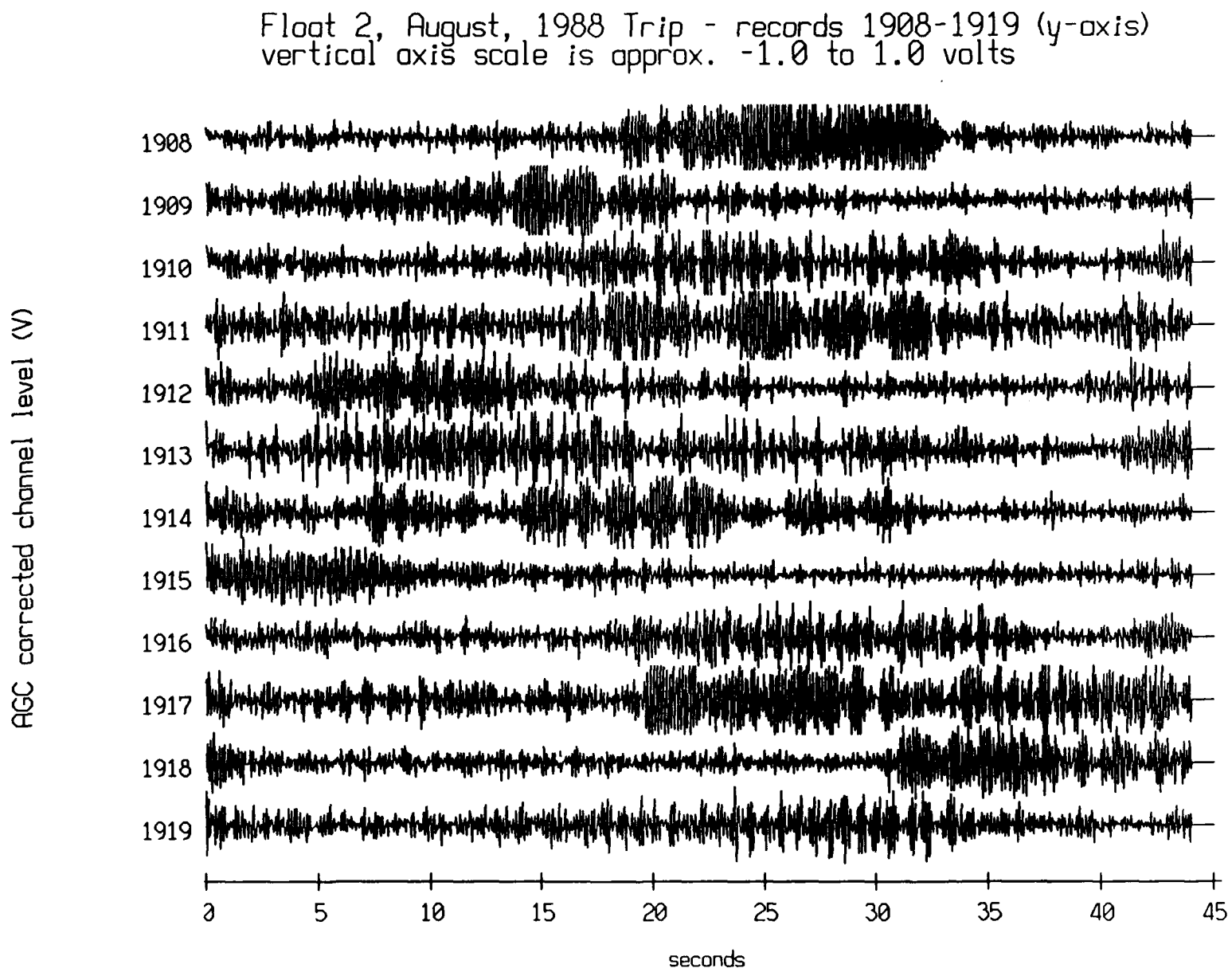


Figure XI.73b

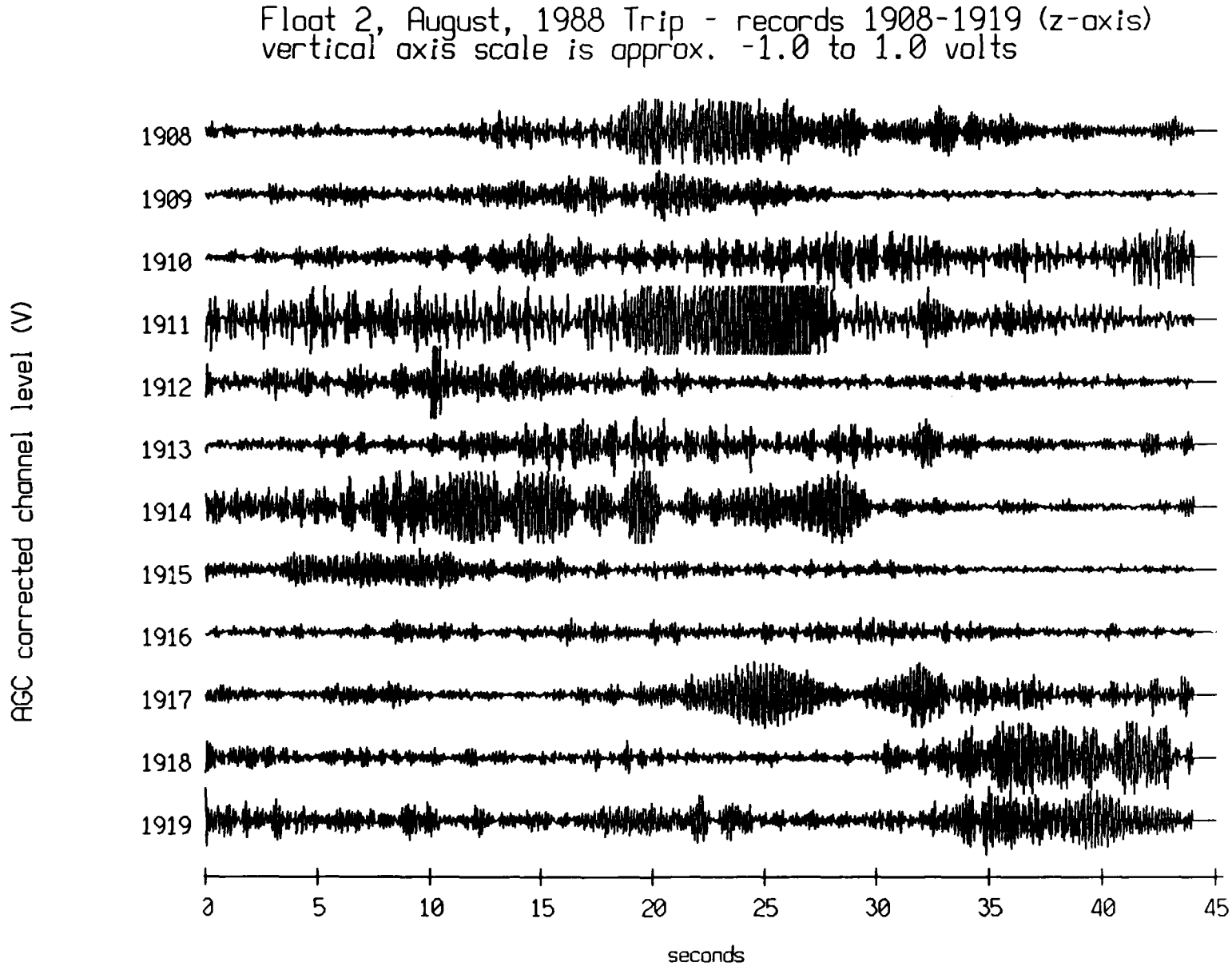


Figure XI.73c

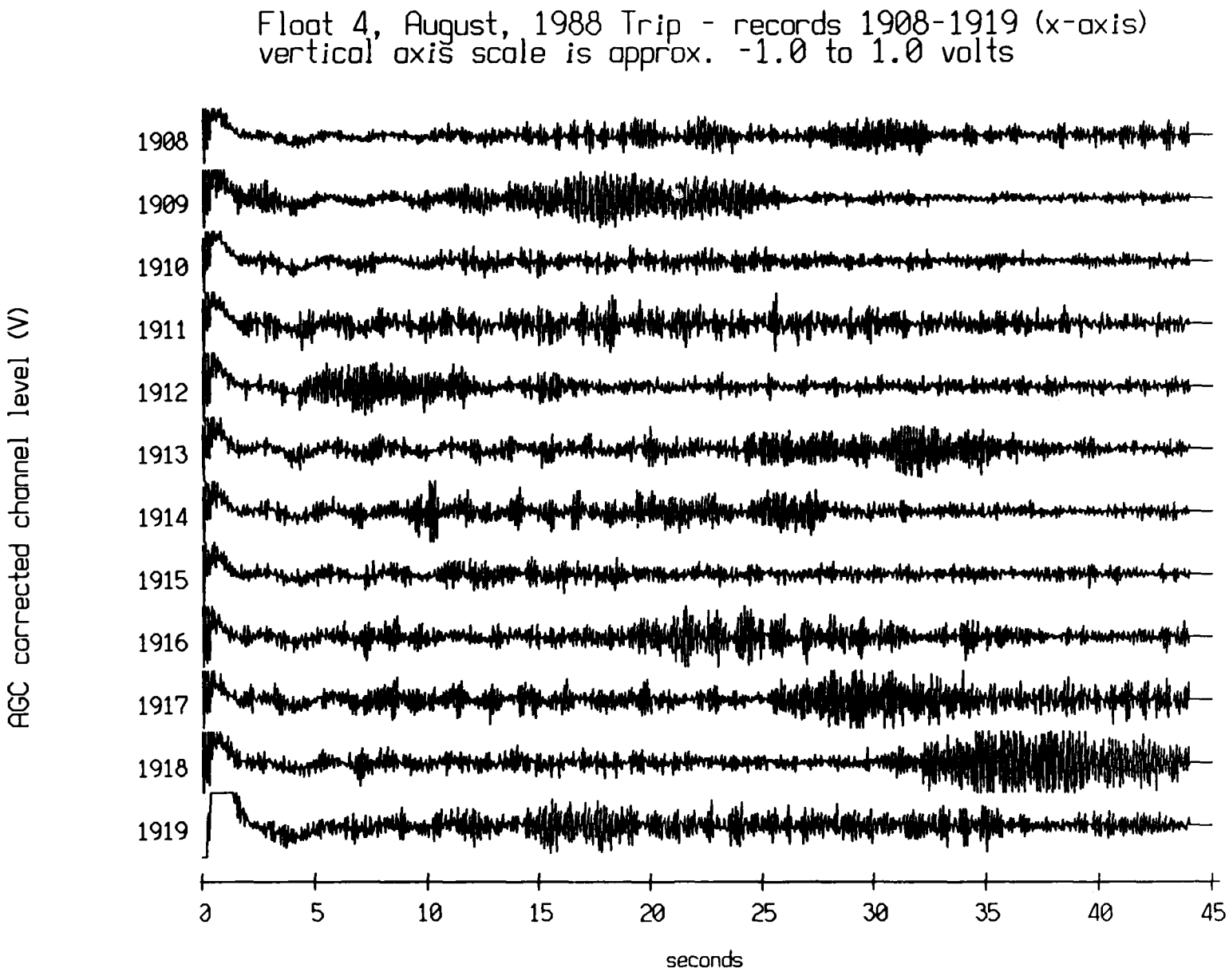


Figure XI.74a

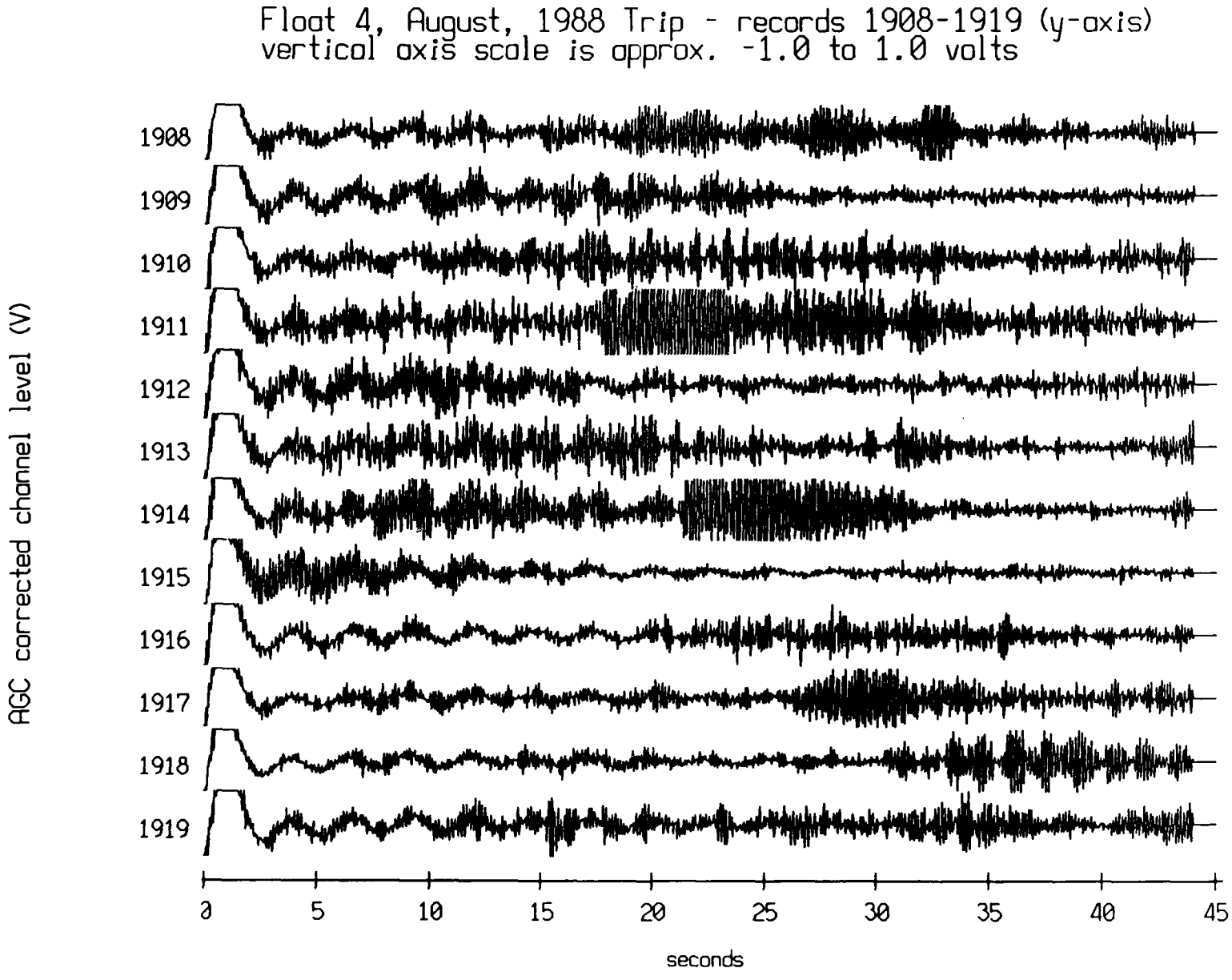


Figure XI.74b

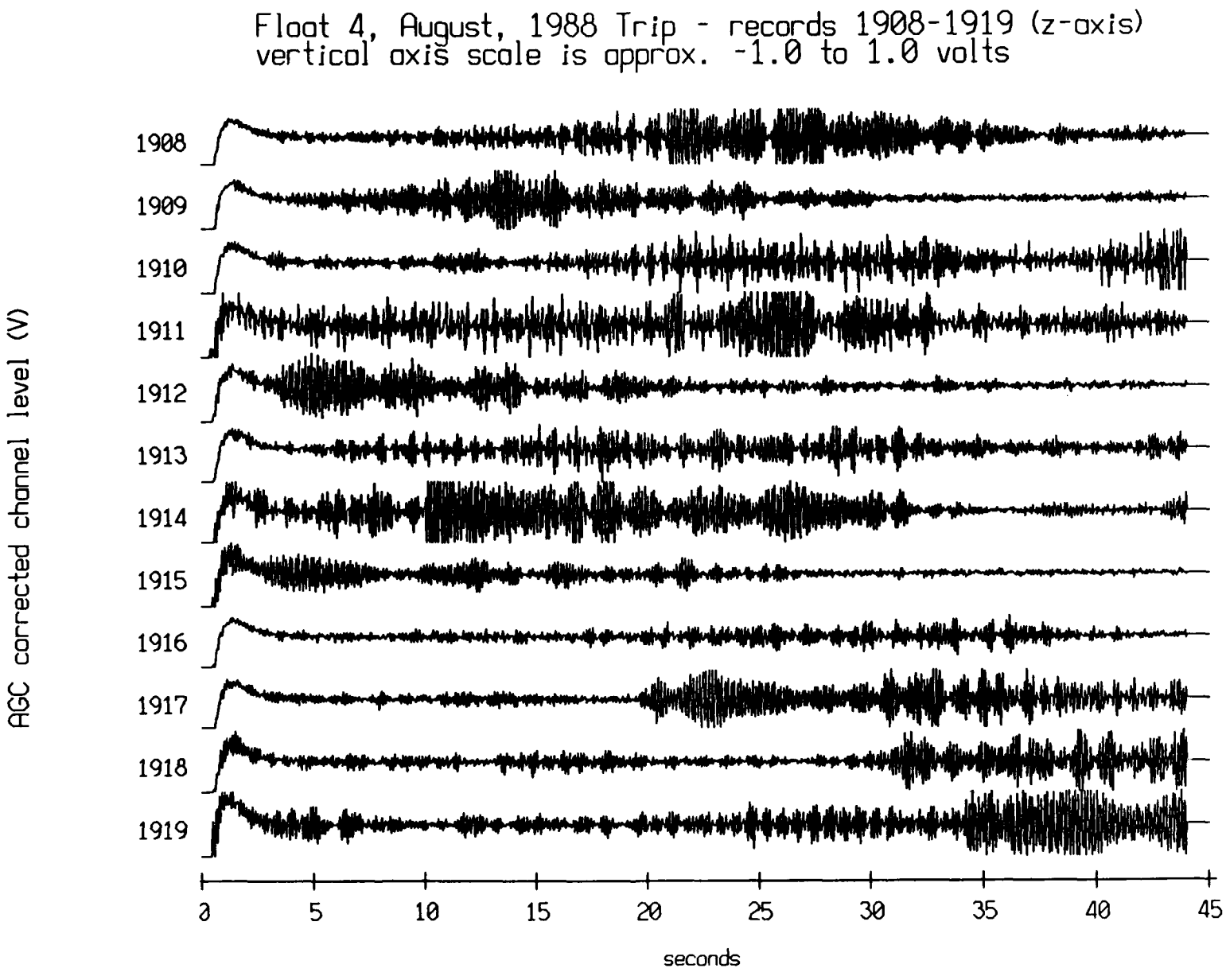


Figure XI.74c

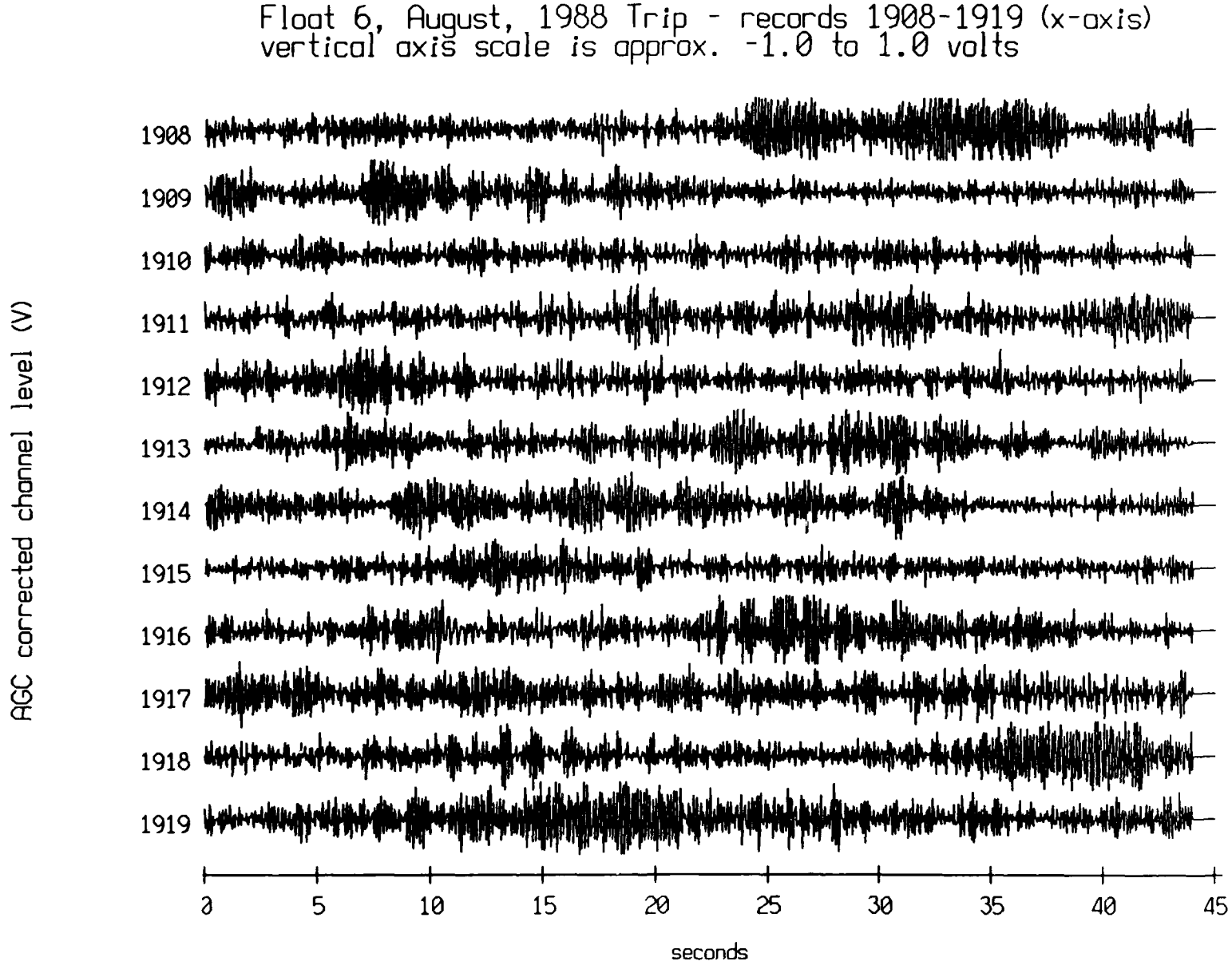


Figure XI.75a

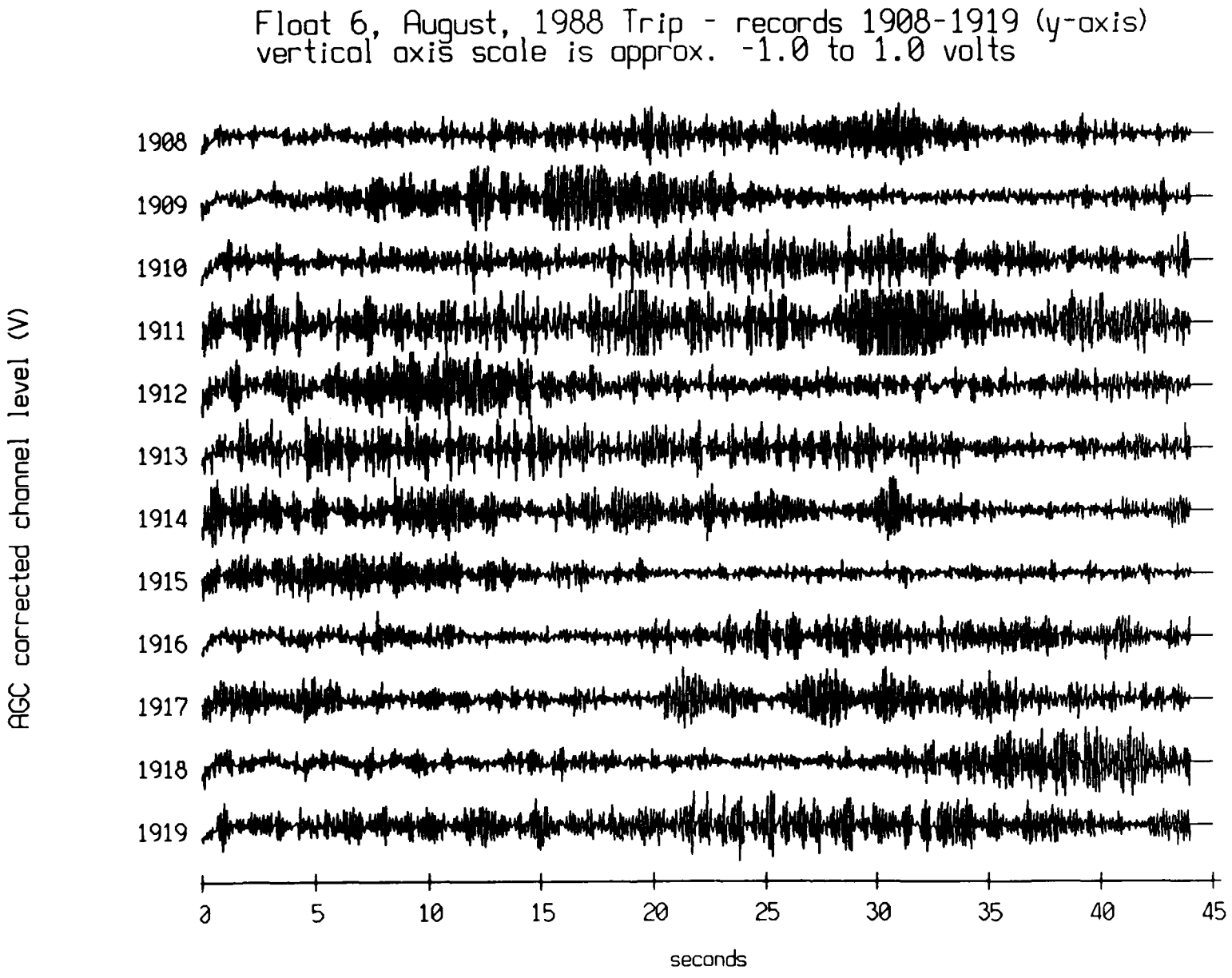


Figure XI.75b

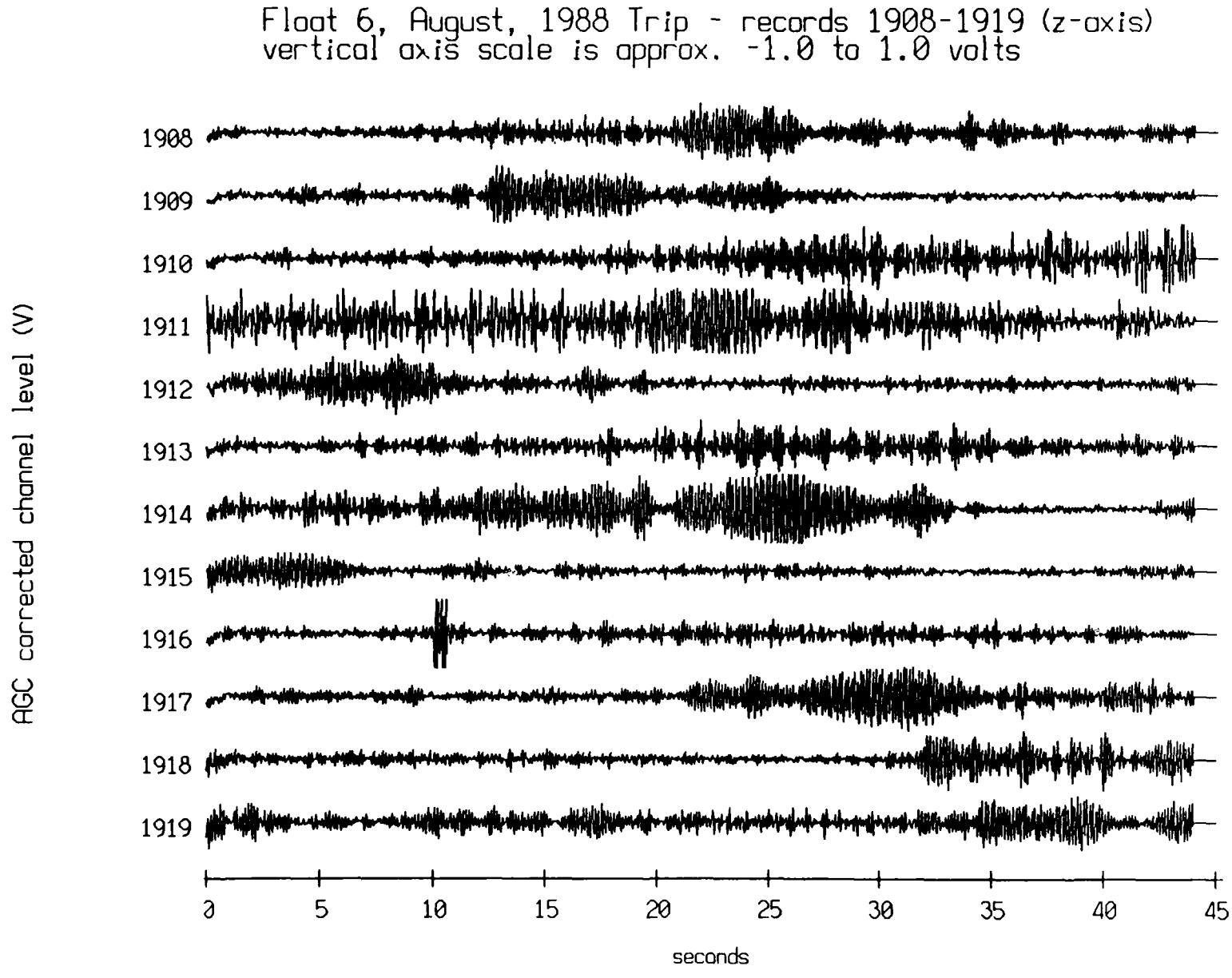

Float 6, August, 1988 Trip - records 1908-1919 (z-axis)
vertical axis scale is approx. -1.0 to 1.0 volts
AGC corrected channel level (V)
1908
1909
1910
1911
1912
1913
1914
1915
1916
1917
1918
1919
0
5
10
15
20
25
30
35
40
45
seconds

Figure XI.5c

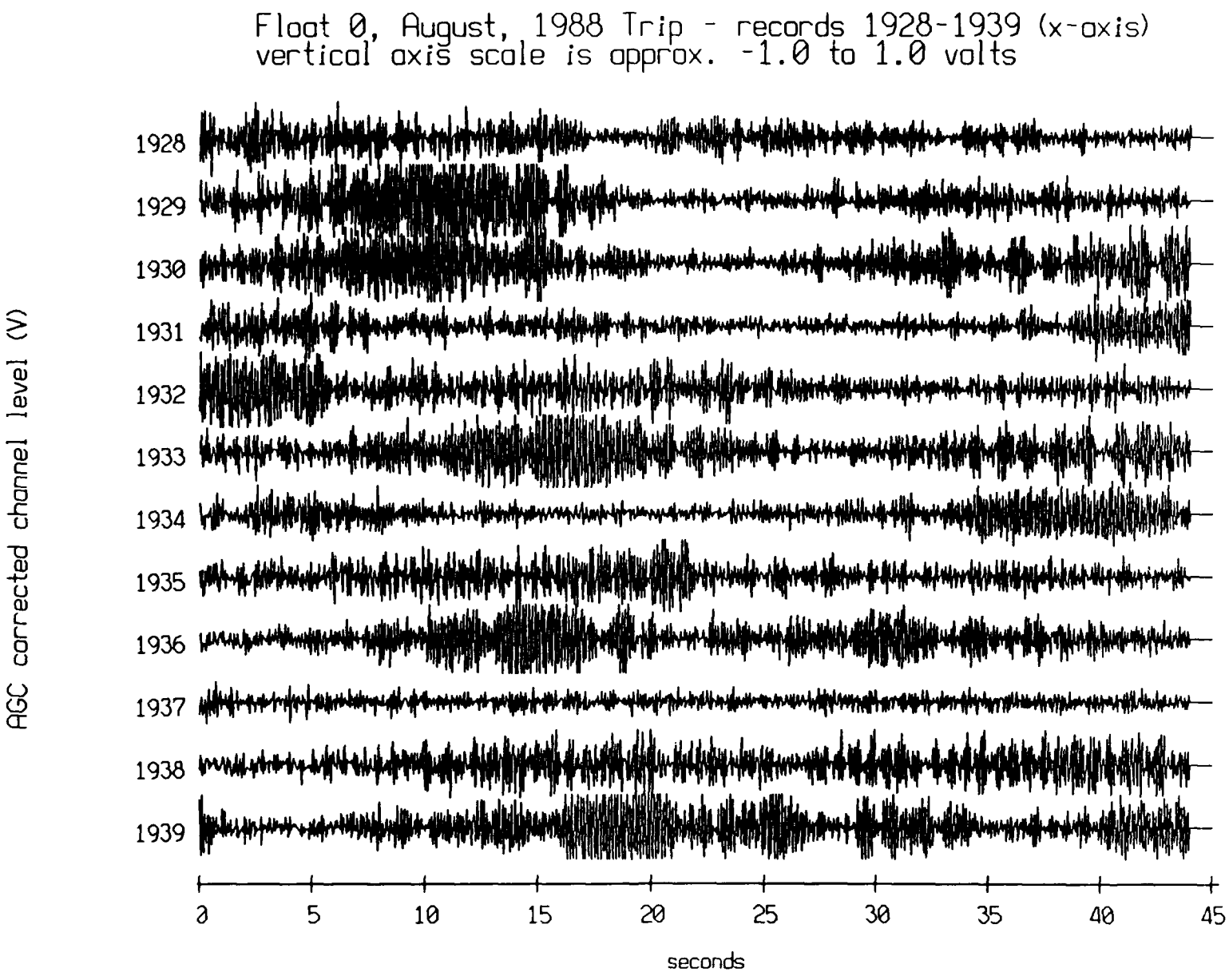


Figure XI.76a

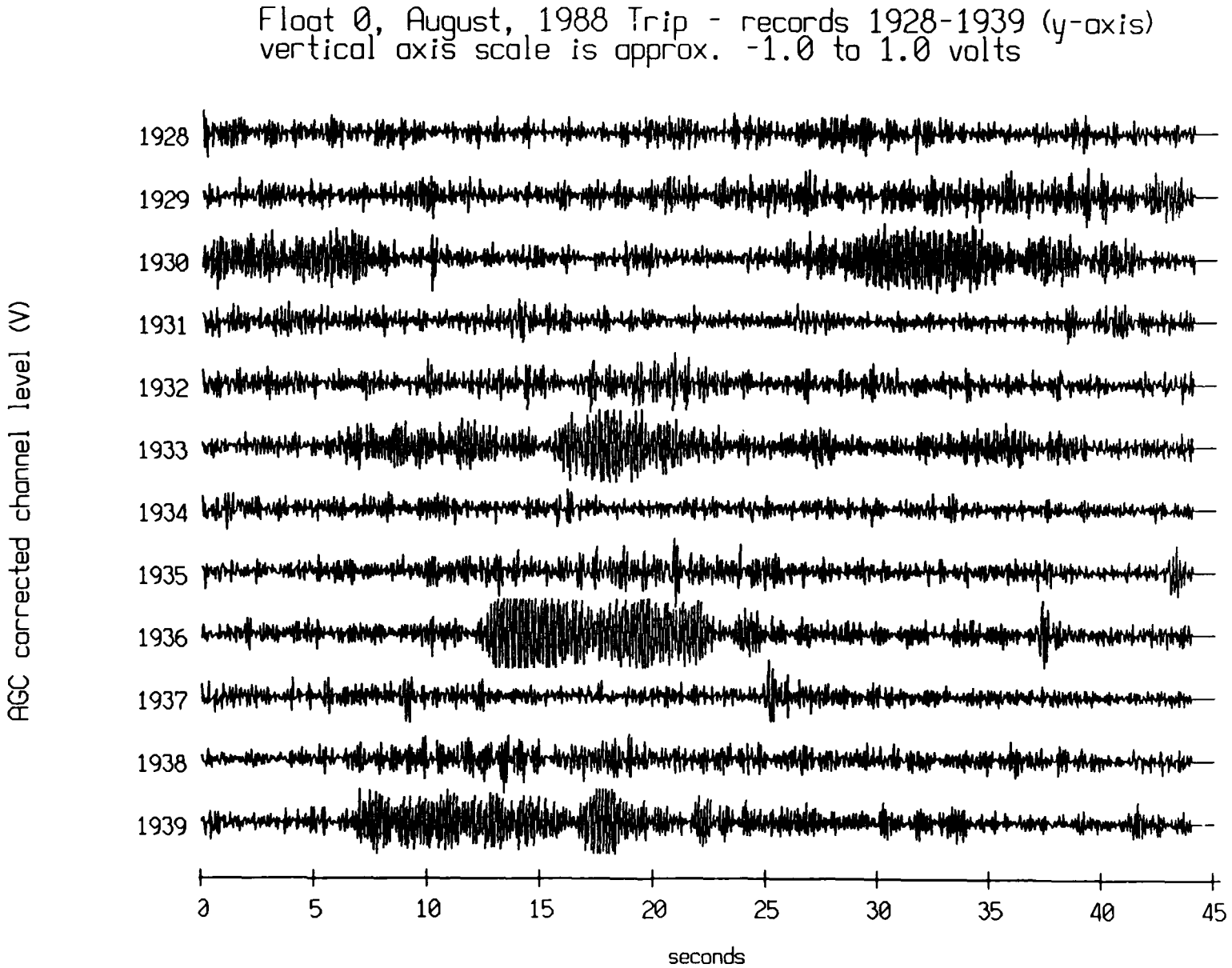


Figure XI.76b

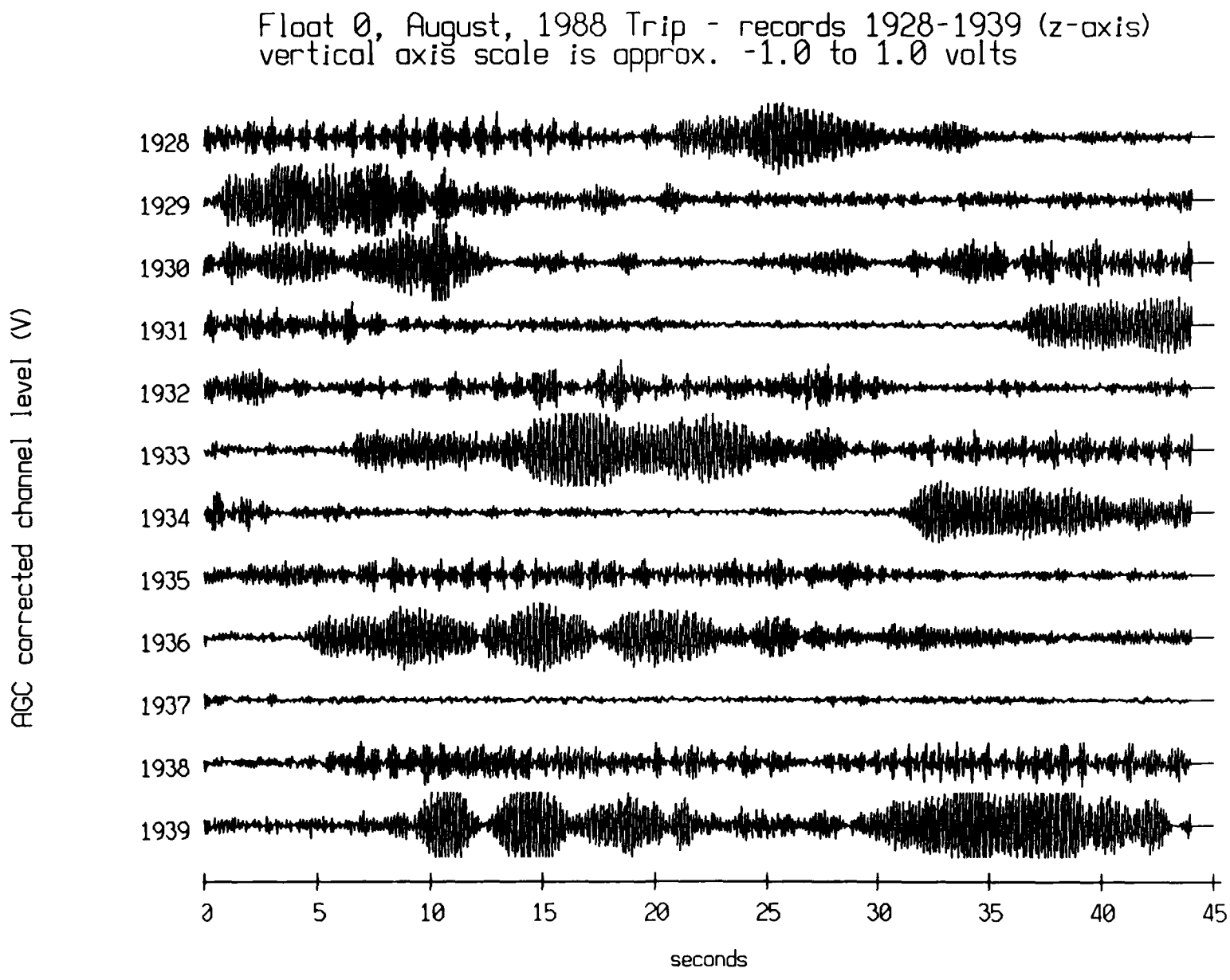


Figure XI.76c

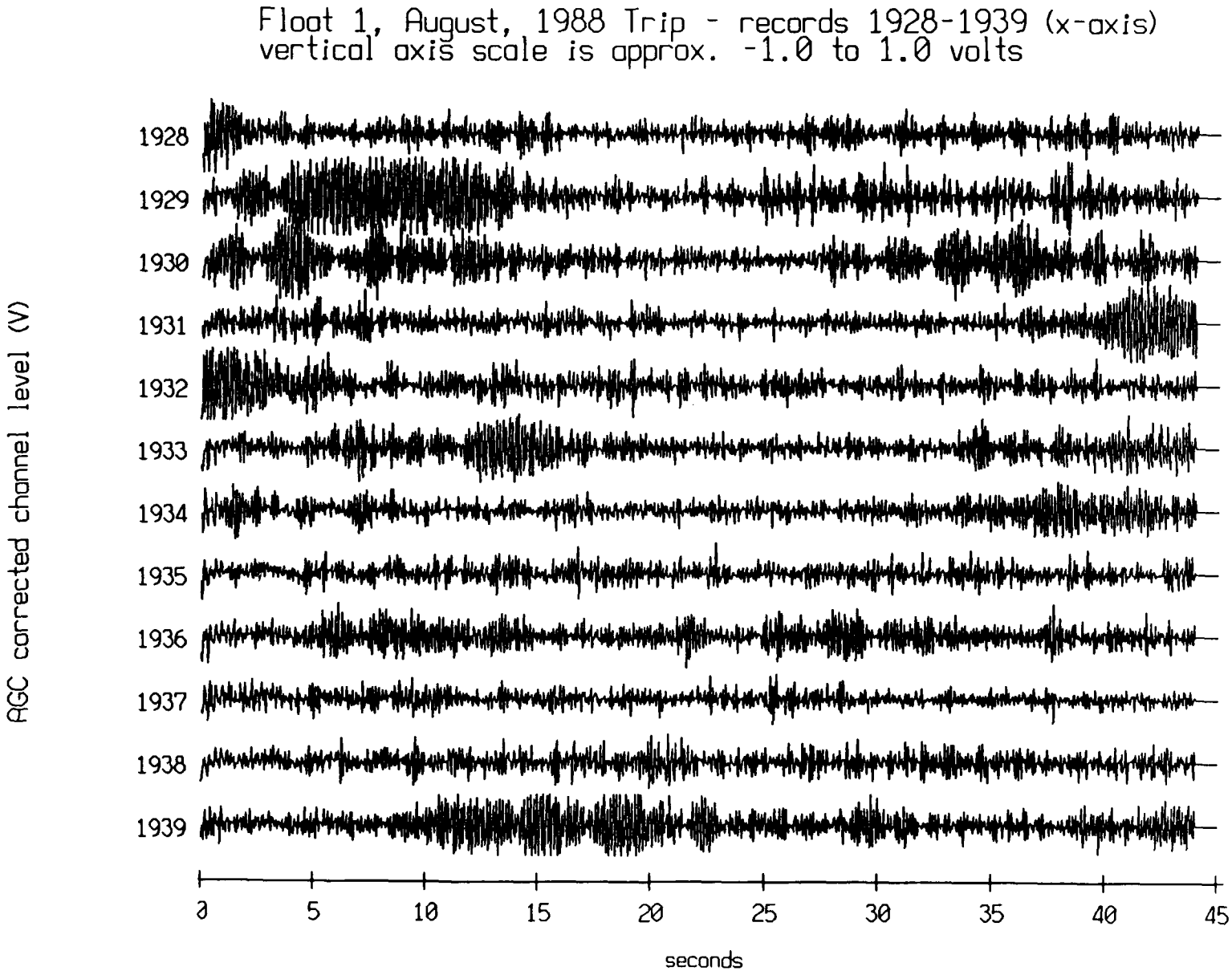


Figure XI.77a

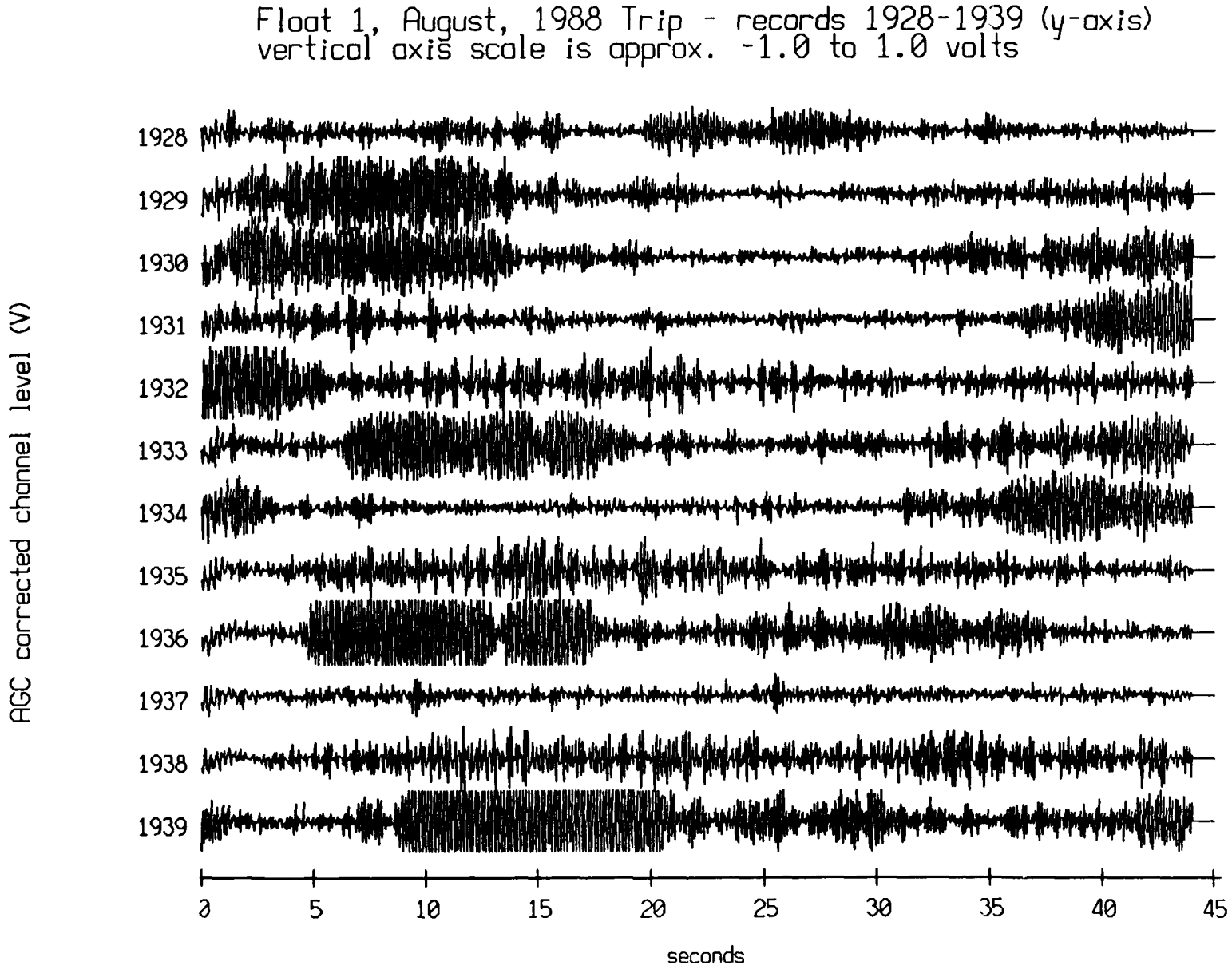


Figure XI.77b

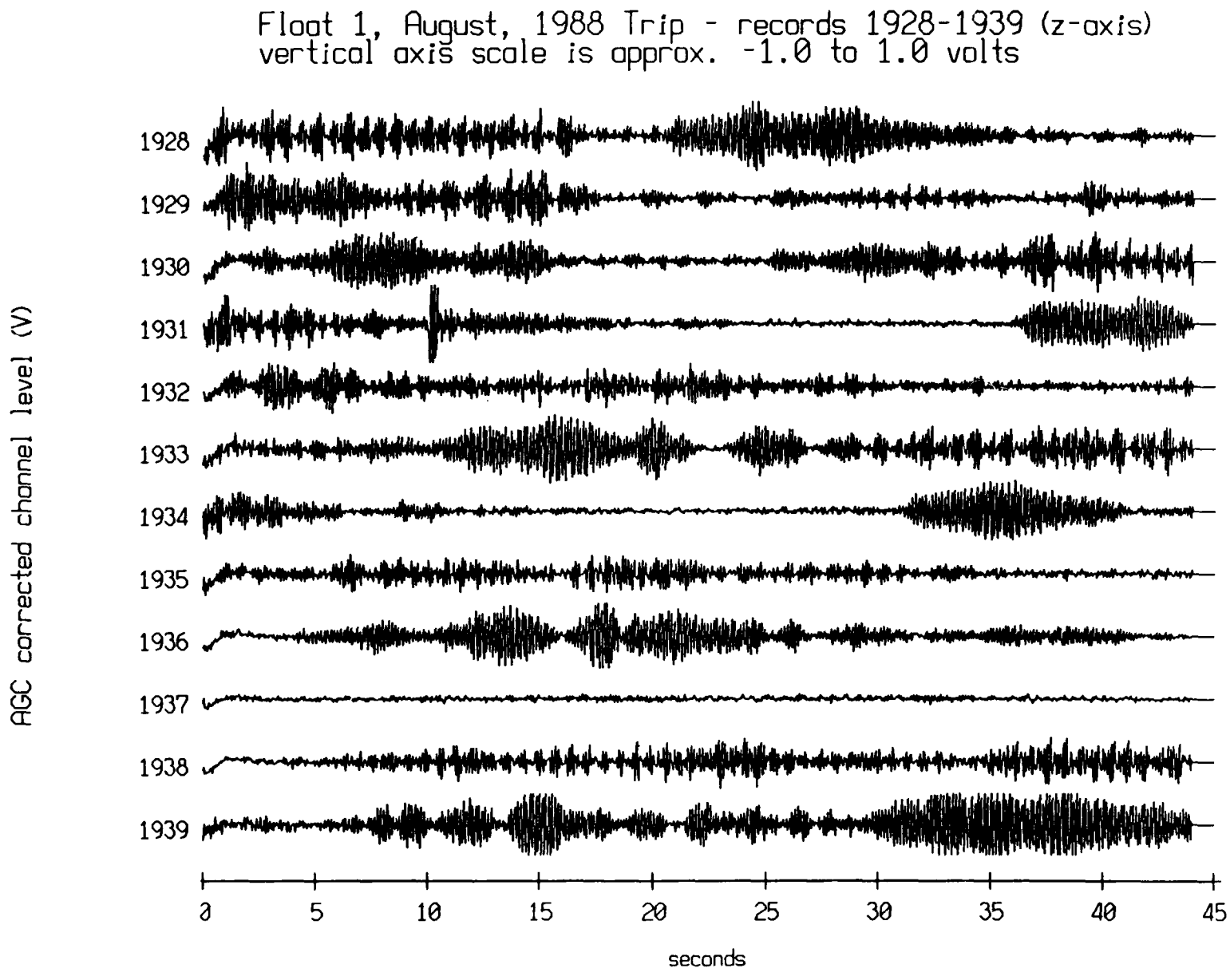

Float 1, August, 1988 Trip - records 1928-1939 (z-axis)
vertical axis scale is approx. -1.0 to 1.0 volts
AGC corrected channel level (V)
1928
1929
1930
1931
1932
1933
1934
1935
1936
1937
1938
1939
0
5
10
15
20
25
30
35
40
45
seconds

Figure XI.7c

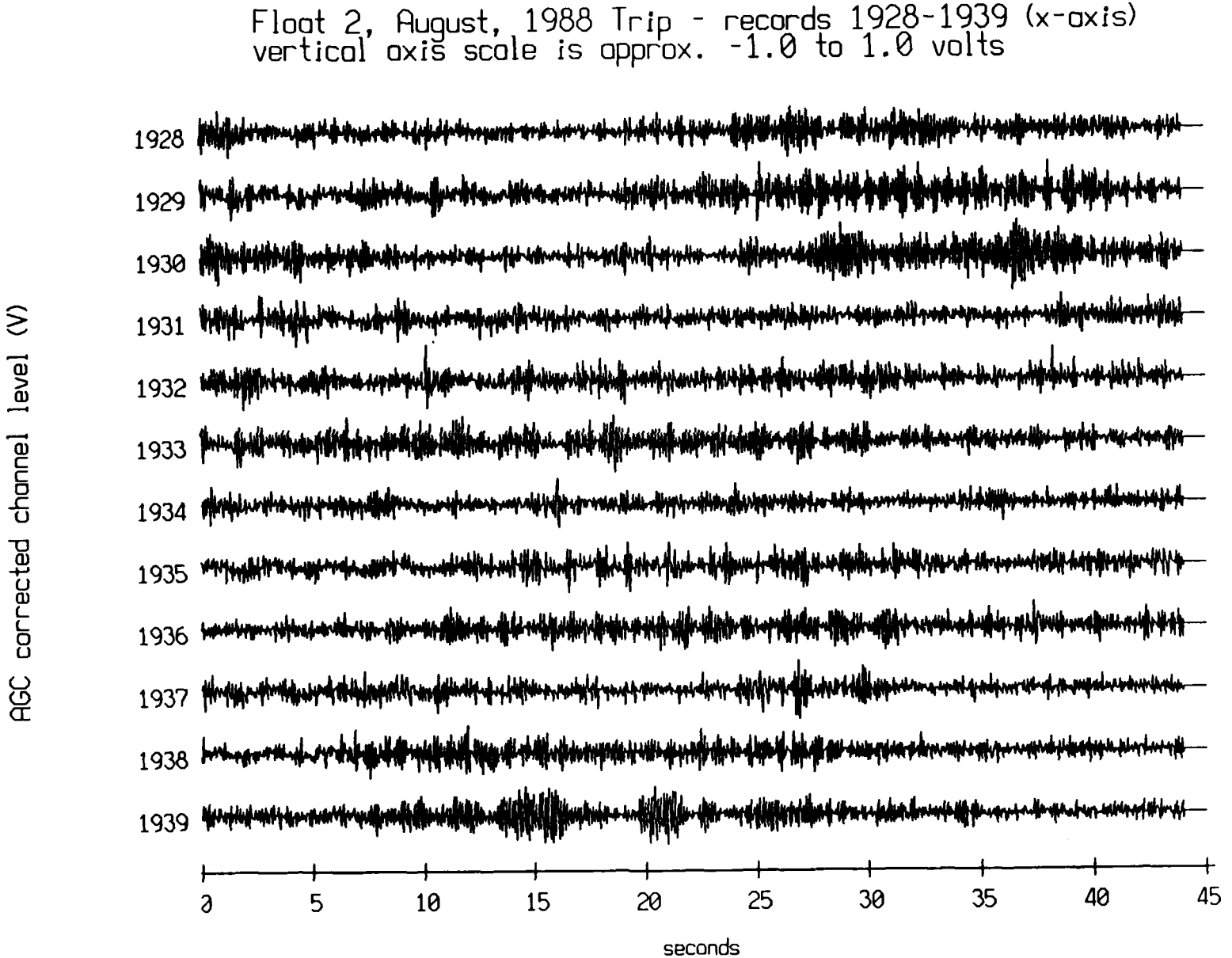


Figure XI.78a

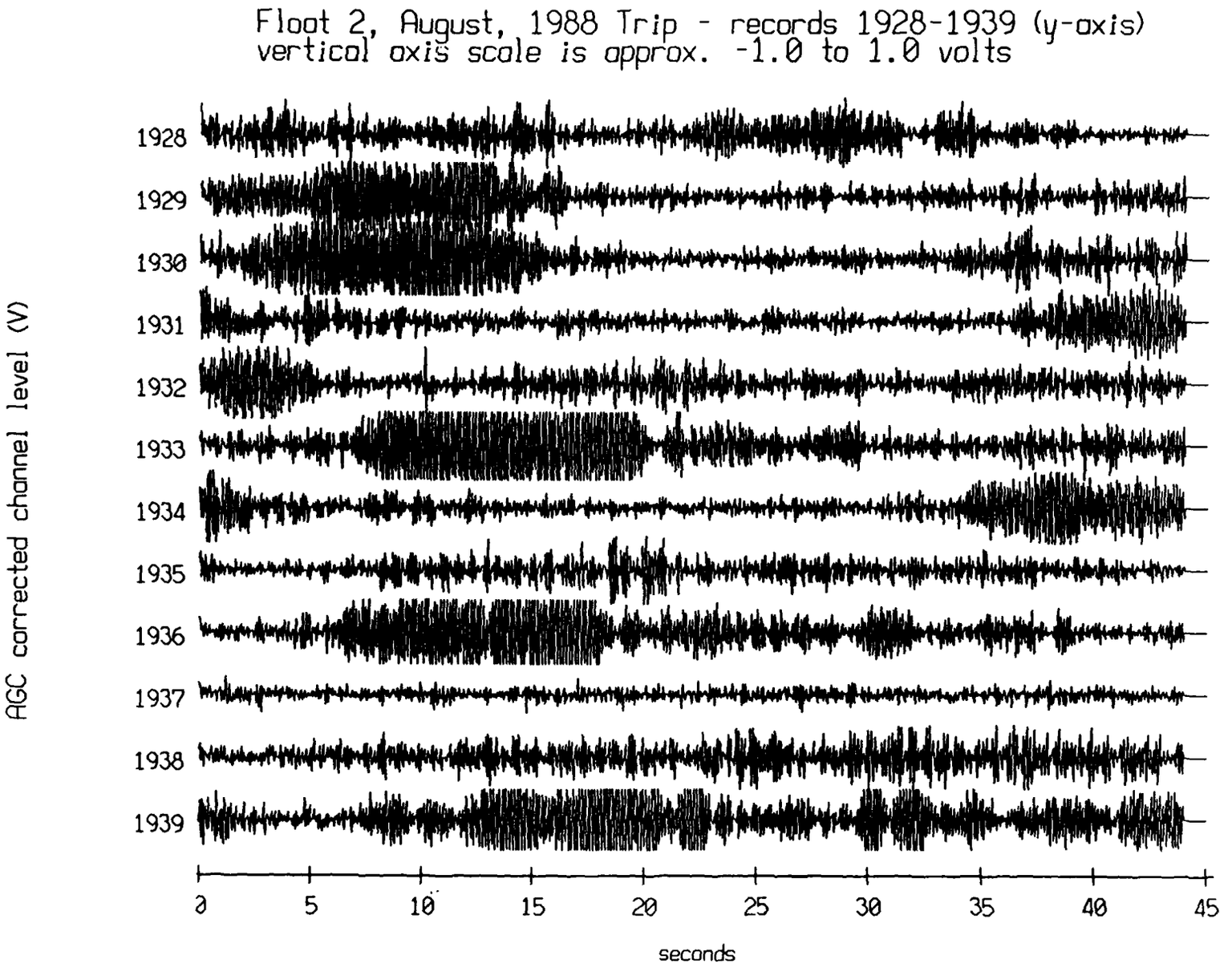


Figure XI.78b

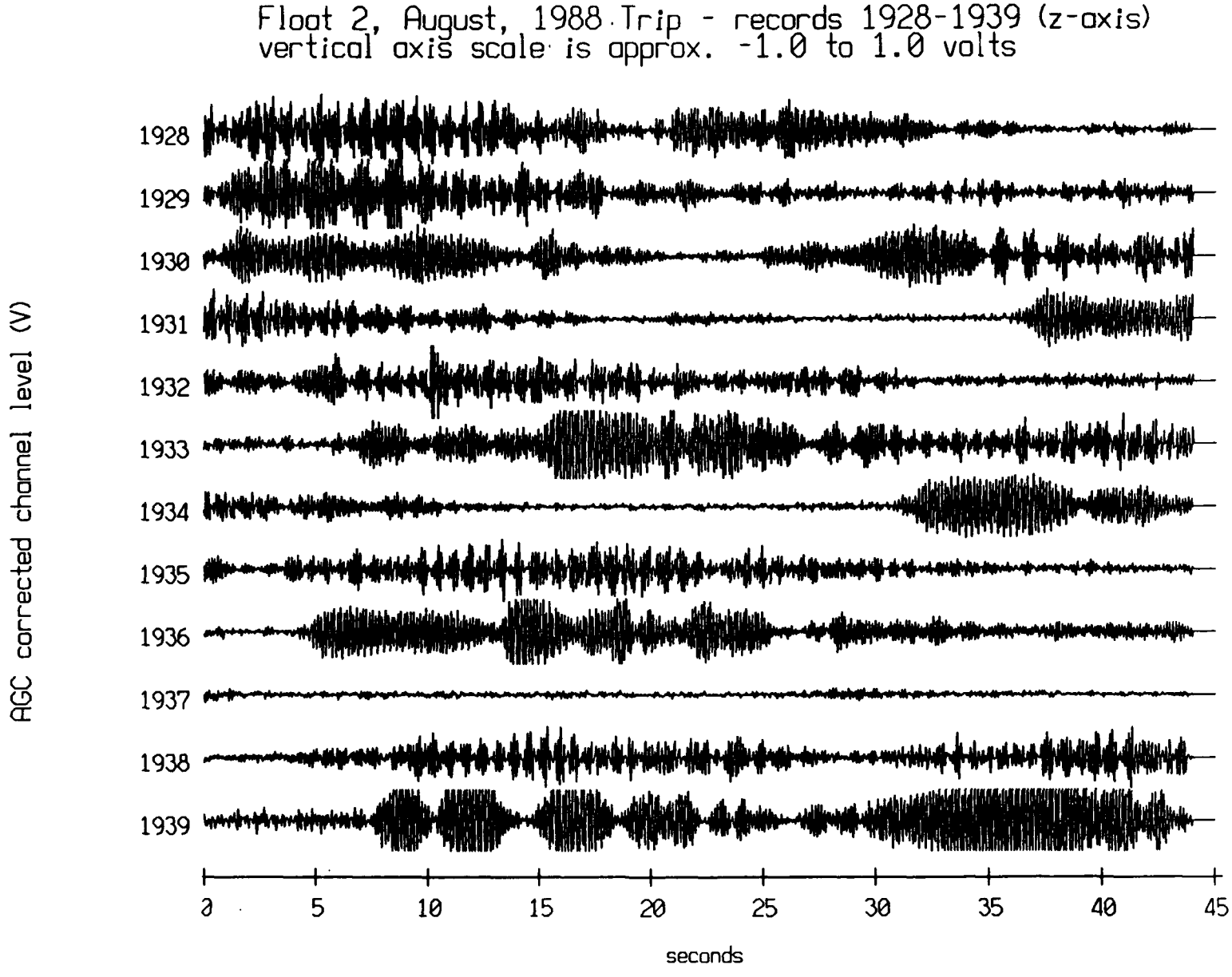


Figure XI.78c

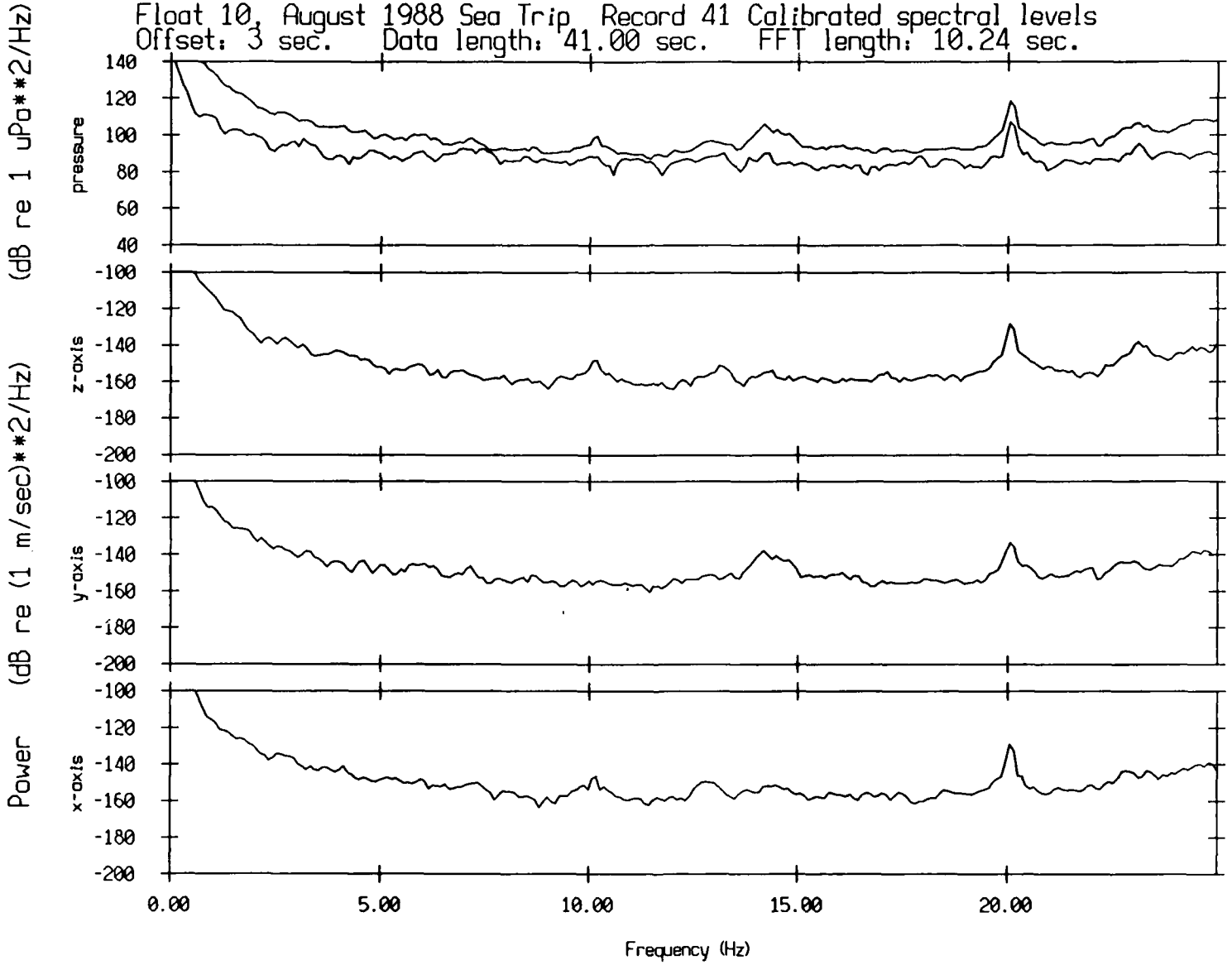


Figure XII.1a

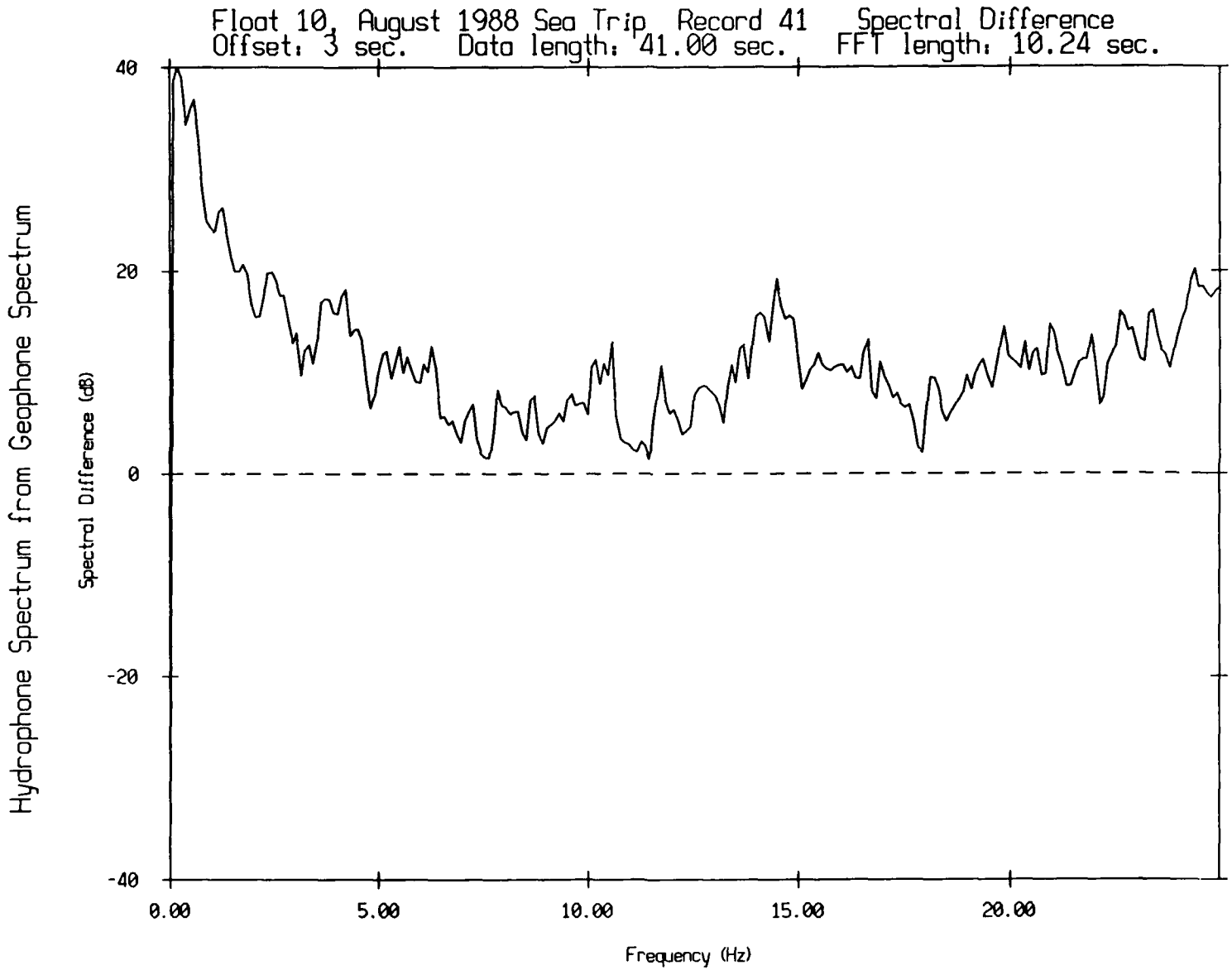


Figure XII.1b

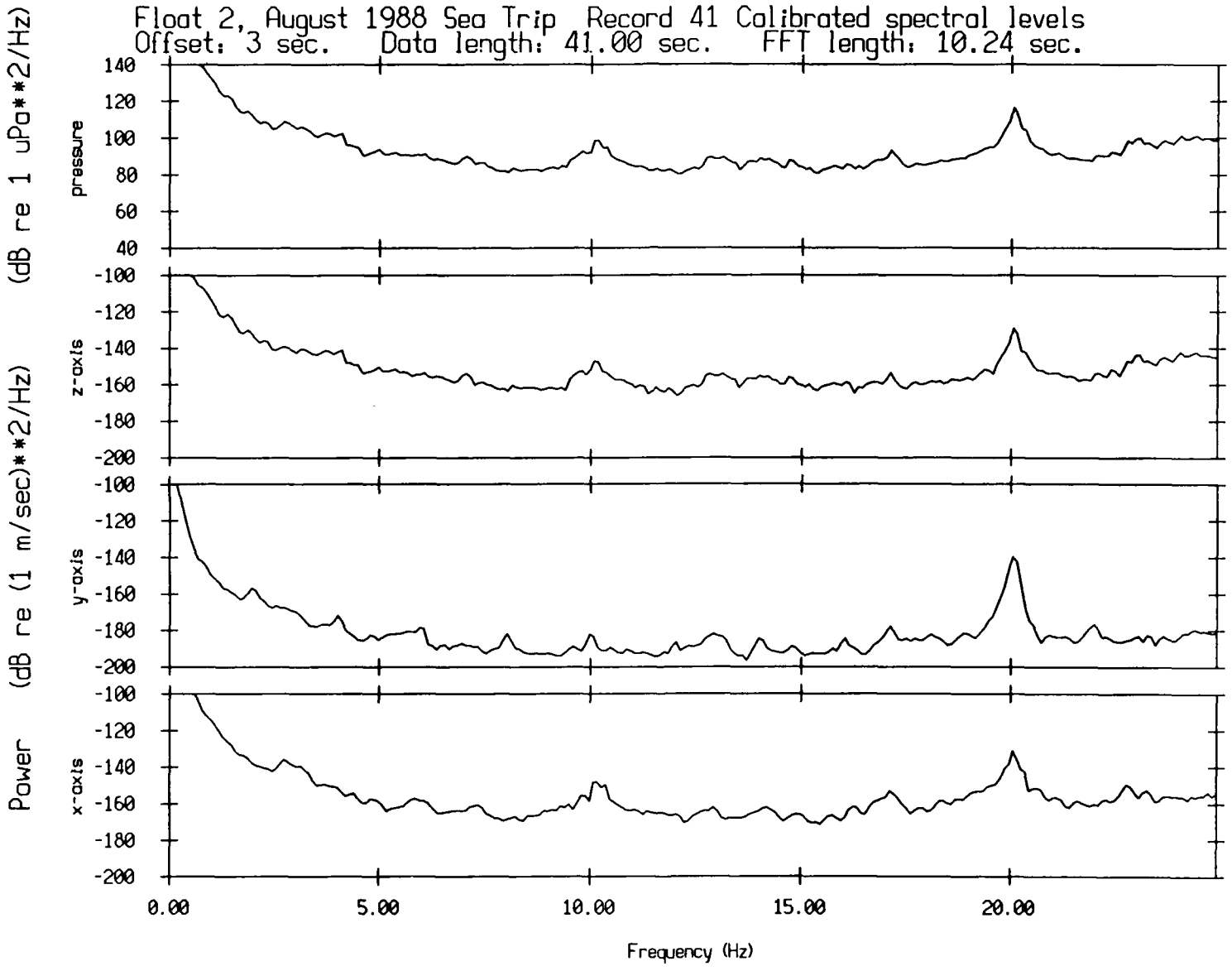

Float 2, August 1988 Sea Trip Record 41 Calibrated spectral levels
Offset: 3 sec. Data length: 41.00 sec. FFT length: 10.24 sec.
Power (dB re (1 m/sec)**2/Hz) (dB re 1 uPa**2/Hz)
pressure
z-axis
y-axis
x-axis
140
120
100
80
60
40
-100
-120
-140
-160
-180
-200
0.00
5.00
10.00
15.00
20.00
Frequency (Hz)

Figure XII.2

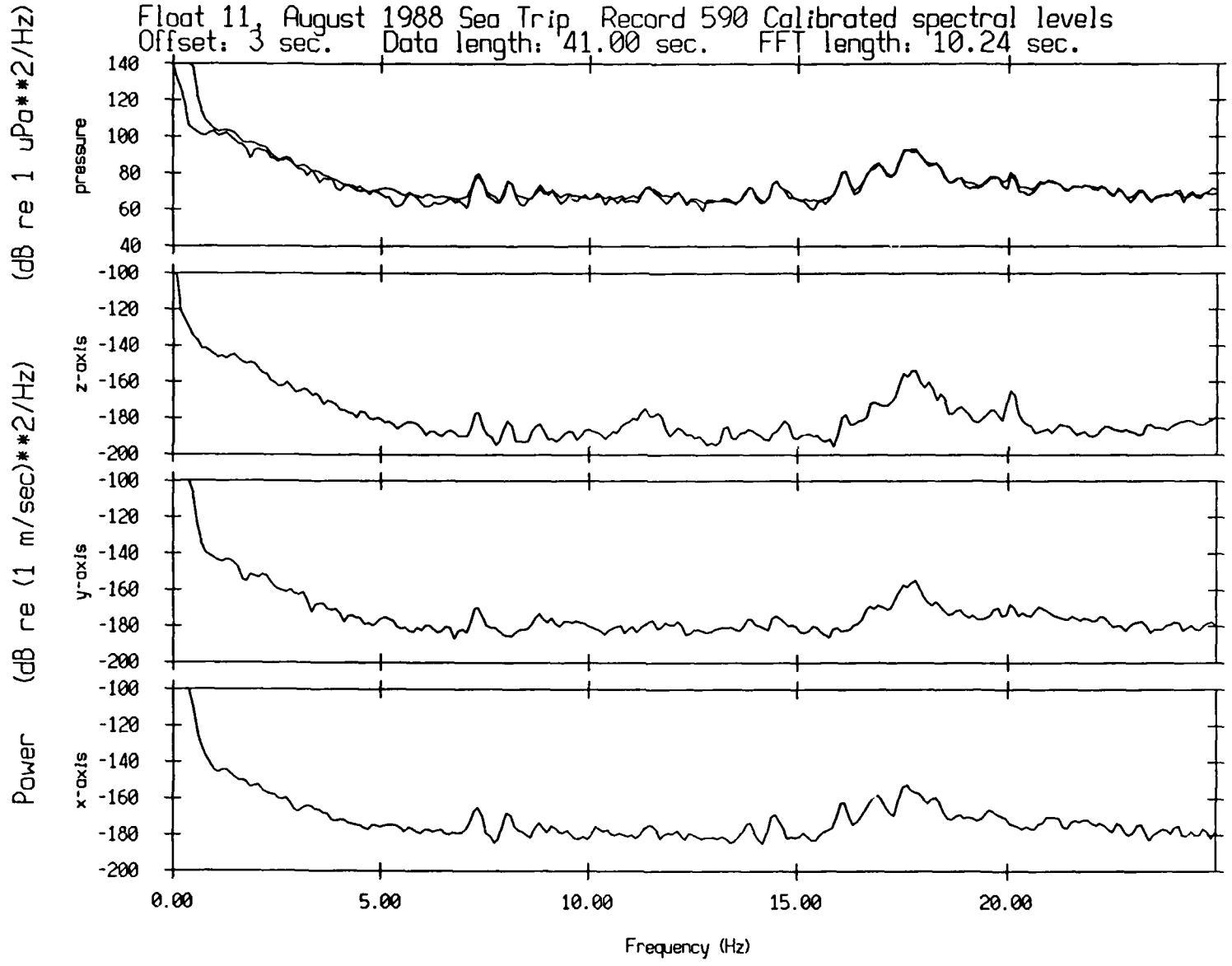

Float 11, August 1988 Sea Trip Record 590 Calibrated spectral levels
Offset: 3 sec. Data length: 41.00 sec. FFT length: 10.24 sec.
Power (dB re (1 m/sec)**2/Hz) (dB re 1 uPa**2/Hz)
pressure
z-axis
y-axis
x-axis
140
120
100
80
60
40
-100
-120
-140
-160
-180
-200
0.00
5.00
10.00
15.00
20.00
Frequency (Hz)

Figure XII.3

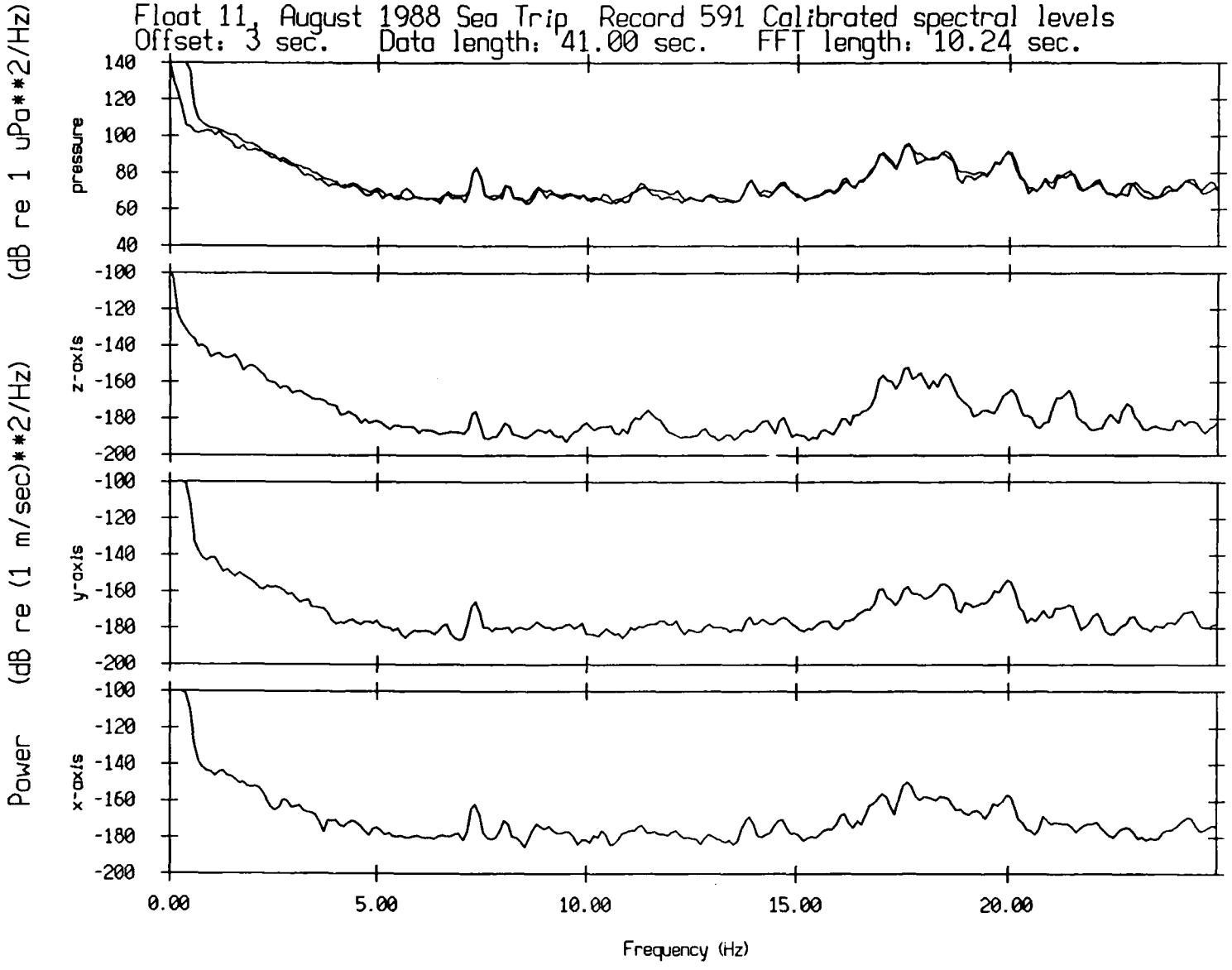

Float 11, August 1988 Sea Trip Record 591 Calibrated spectral levels
Offset: 3 sec. Data length: 41.00 sec. FFT length: 10.24 sec.
Power (dB re (1 m/sec)**2/Hz) (dB re 1 uPa**2/Hz)
pressure
z-axis
y-axis
x-axis
140
120
100
80
60
40
-100
-120
-140
-160
-180
-200
0.00
5.00
10.00
15.00
20.00
Frequency (Hz)

Figure XII.4

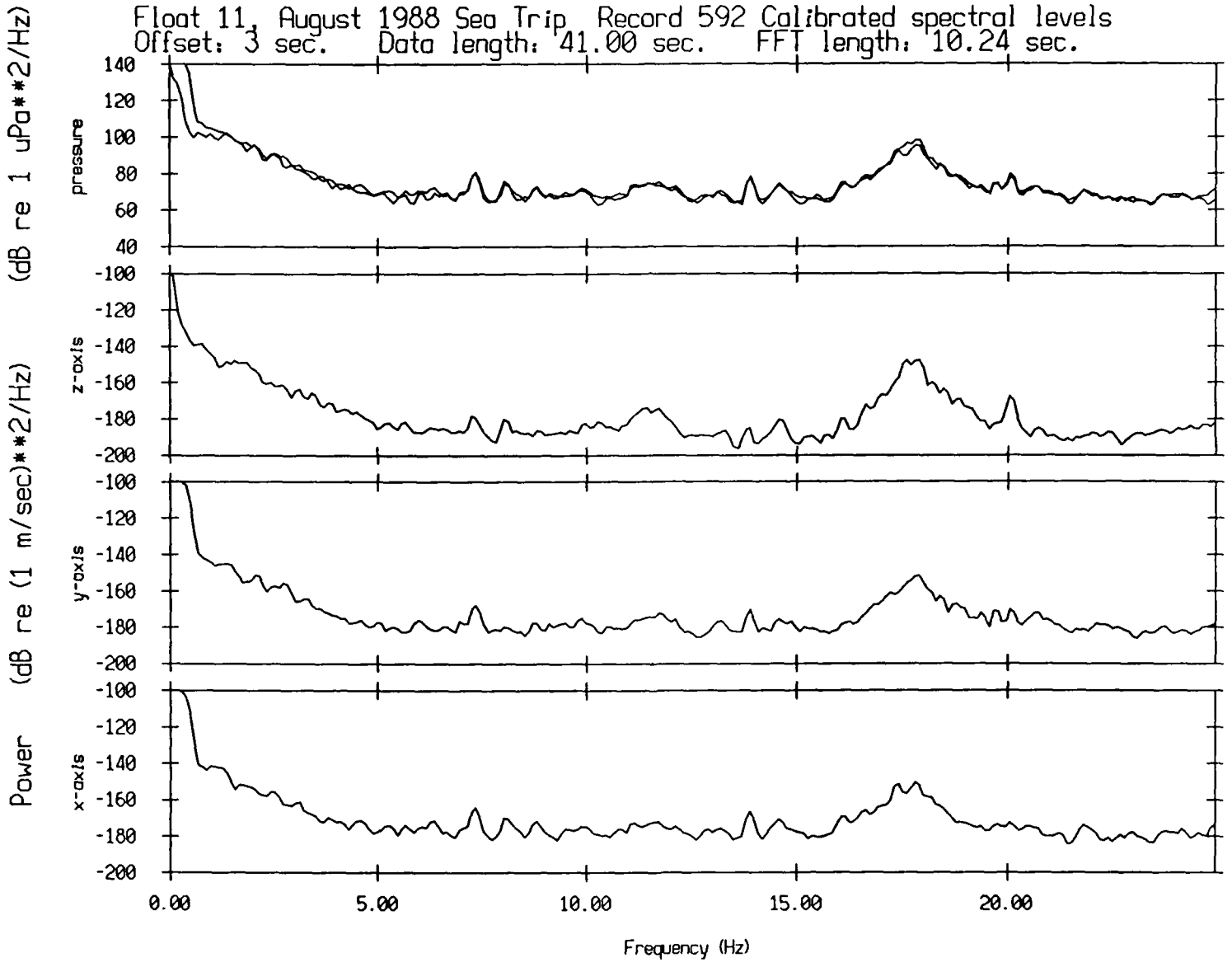

Float 11, August 1988 Sea Trip Record 592 Calibrated spectral levels
Offset: 3 sec. Data length: 41.00 sec. FFT length: 10.24 sec.
Power (dB re (1 m/sec)**2/Hz) (dB re 1 uPa**2/Hz)
pressure
z-axis
y-axis
x-axis
140
120
100
80
60
40
-100
-120
-140
-160
-180
-200
0.00
5.00
10.00
15.00
20.00
Frequency (Hz)

Figure XII.5

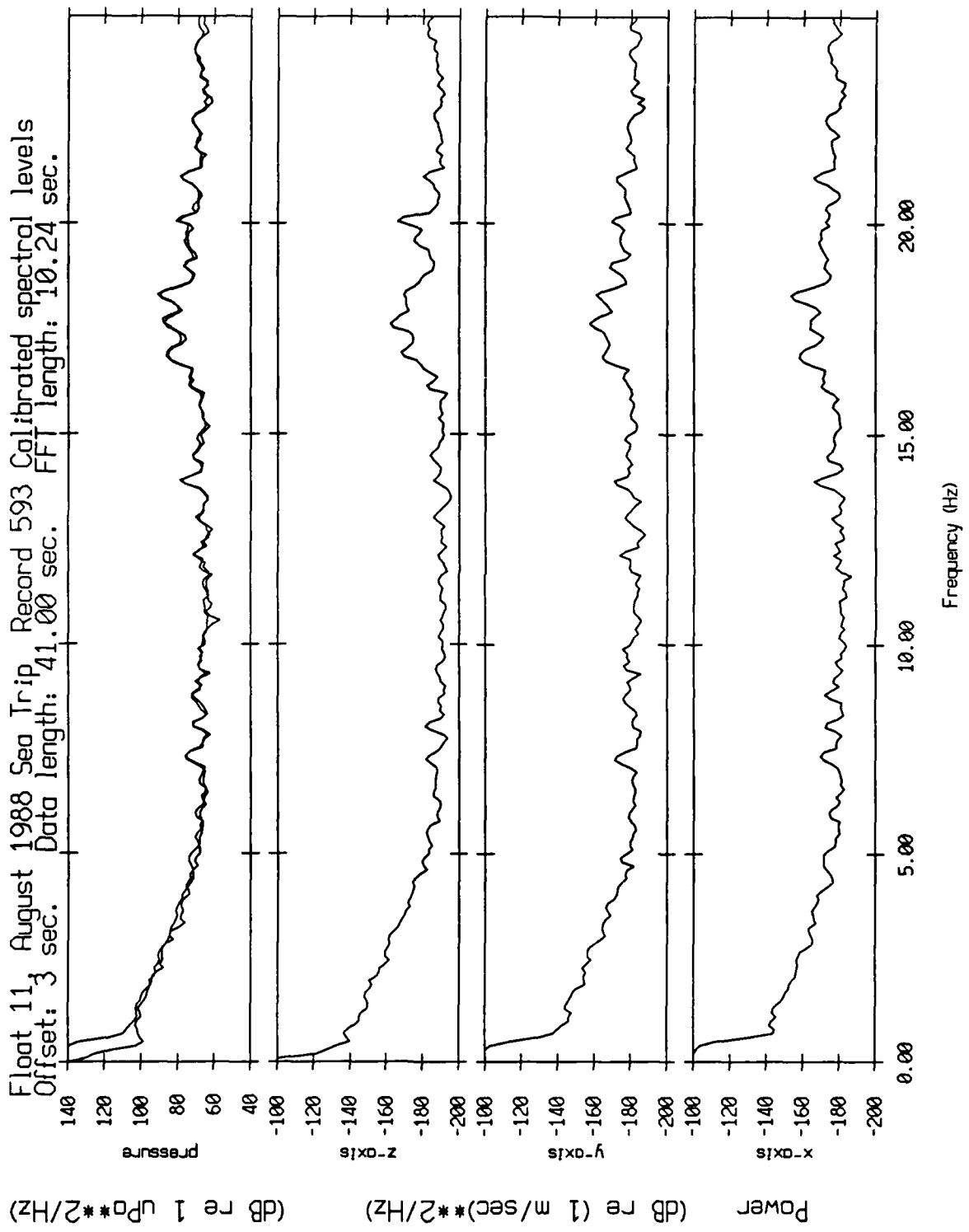

Float 11 August 1988 Sea Trip Record 593 Calibrated spectral levels
Offset: 3 sec. Data length: 41.00 sec. FFT length: 10.24 sec.
pressure
z-axis
y-axis
x-axis
Power (dB re (1 m/sec)**2/Hz)
(dB re 1 uPa**2/Hz)
Frequency (Hz)
0.00
5.00
10.00
15.00
20.00

Figure XII.6

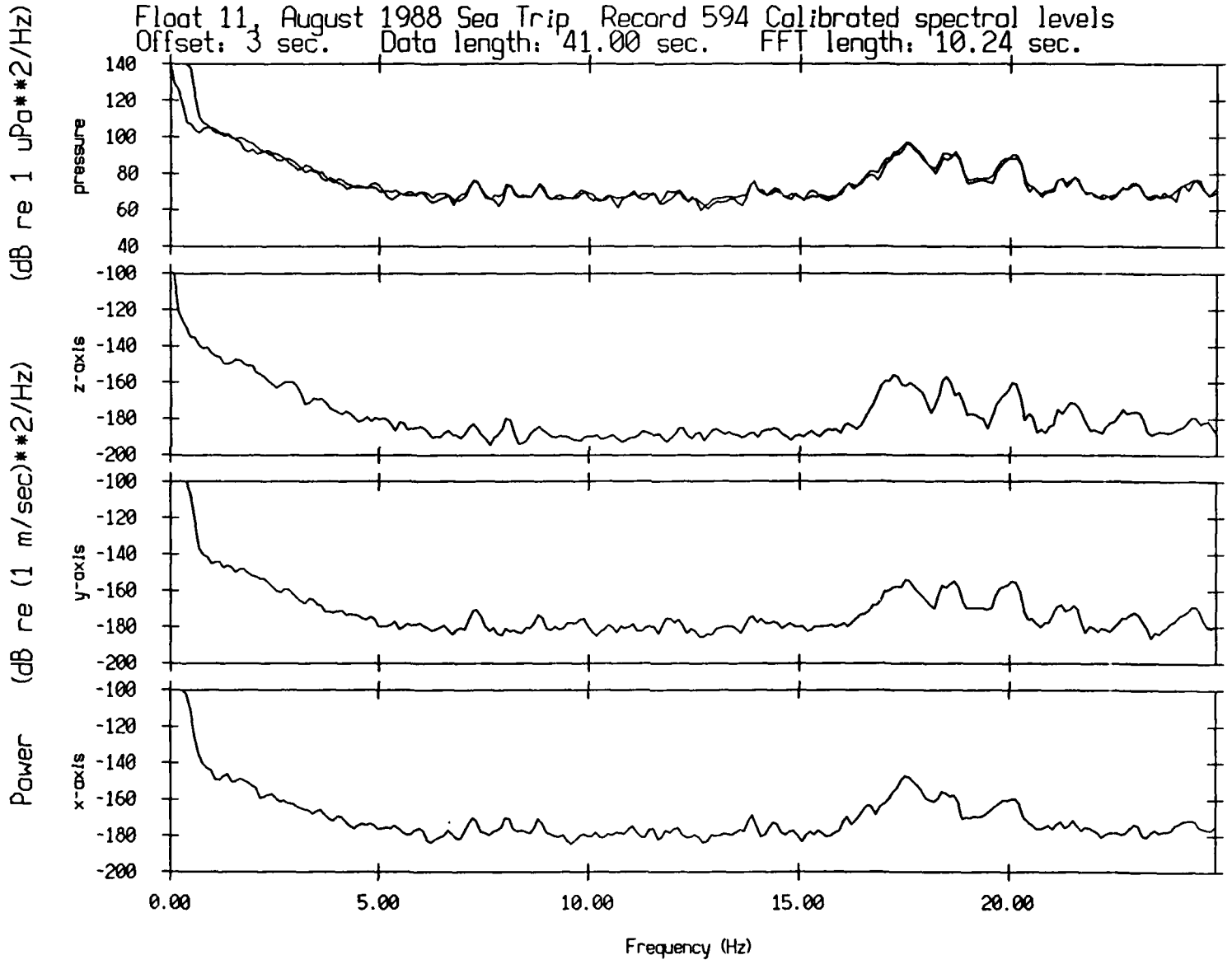

Float 11, August 1988 Sea Trip Record 594 Calibrated spectral levels
Offset: 3 sec. Data length: 41.00 sec. FFT length: 10.24 sec.
Power (dB re (1 m/sec)**2/Hz) (dB re 1 uPa**2/Hz)
pressure
z-axis
y-axis
x-axis
140
120
100
80
60
40
-100
-120
-140
-160
-180
-200
0.00
5.00
10.00
15.00
20.00
Frequency (Hz)

Figure XII.7

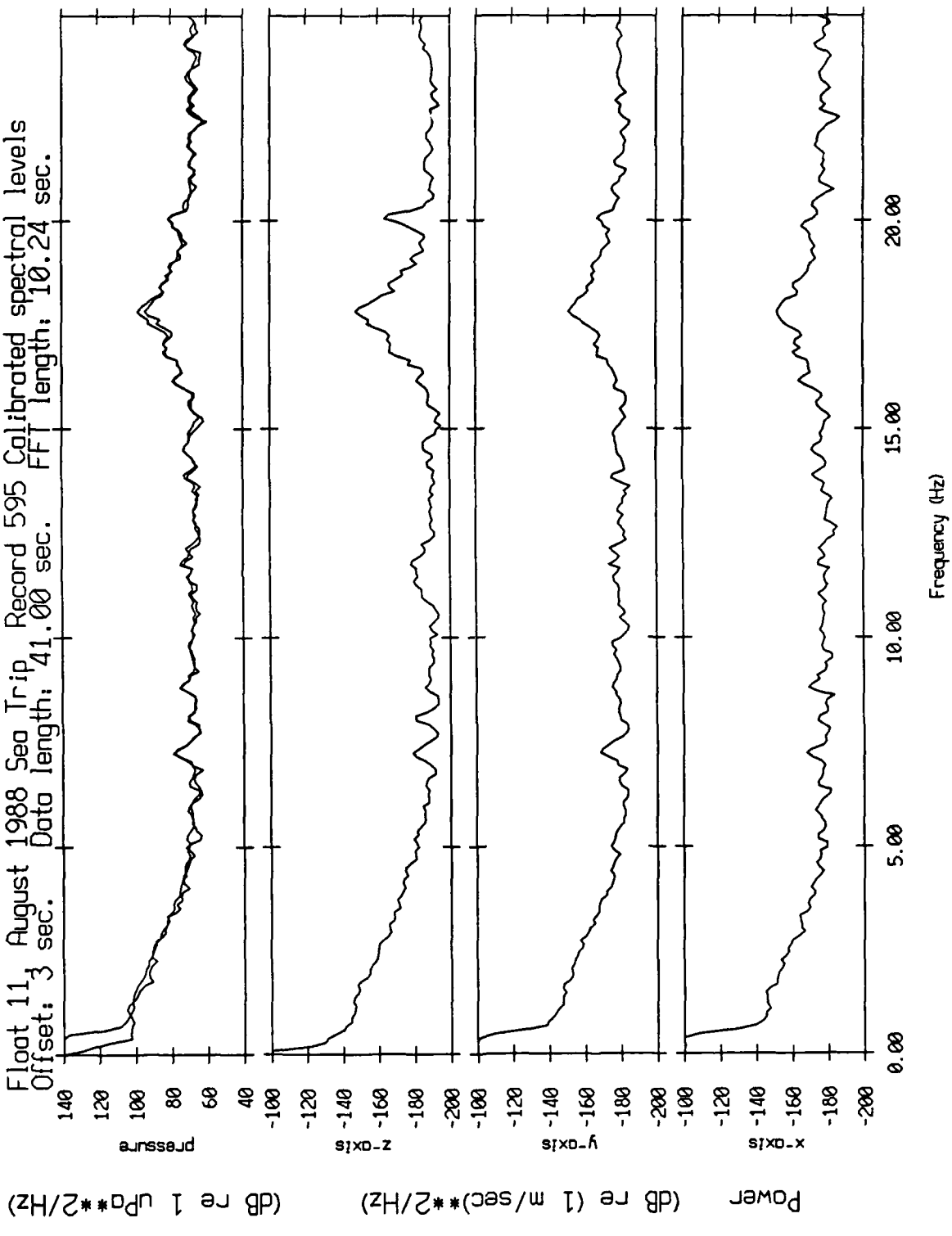

Float 11, August 1988 Sea Trip, Record 595 Calibrated spectral levels
Offset: 3 sec. Data length: 41.00 sec. FFT length: 10.24 sec.
pressure
z-axis
y-axis
x-axis
(dB re 1 uPa**2/Hz)
(dB re (1 m/sec)**2/Hz)
Power
Frequency (Hz)
0.00
5.00
10.00
15.00
20.00

Figure XII.8

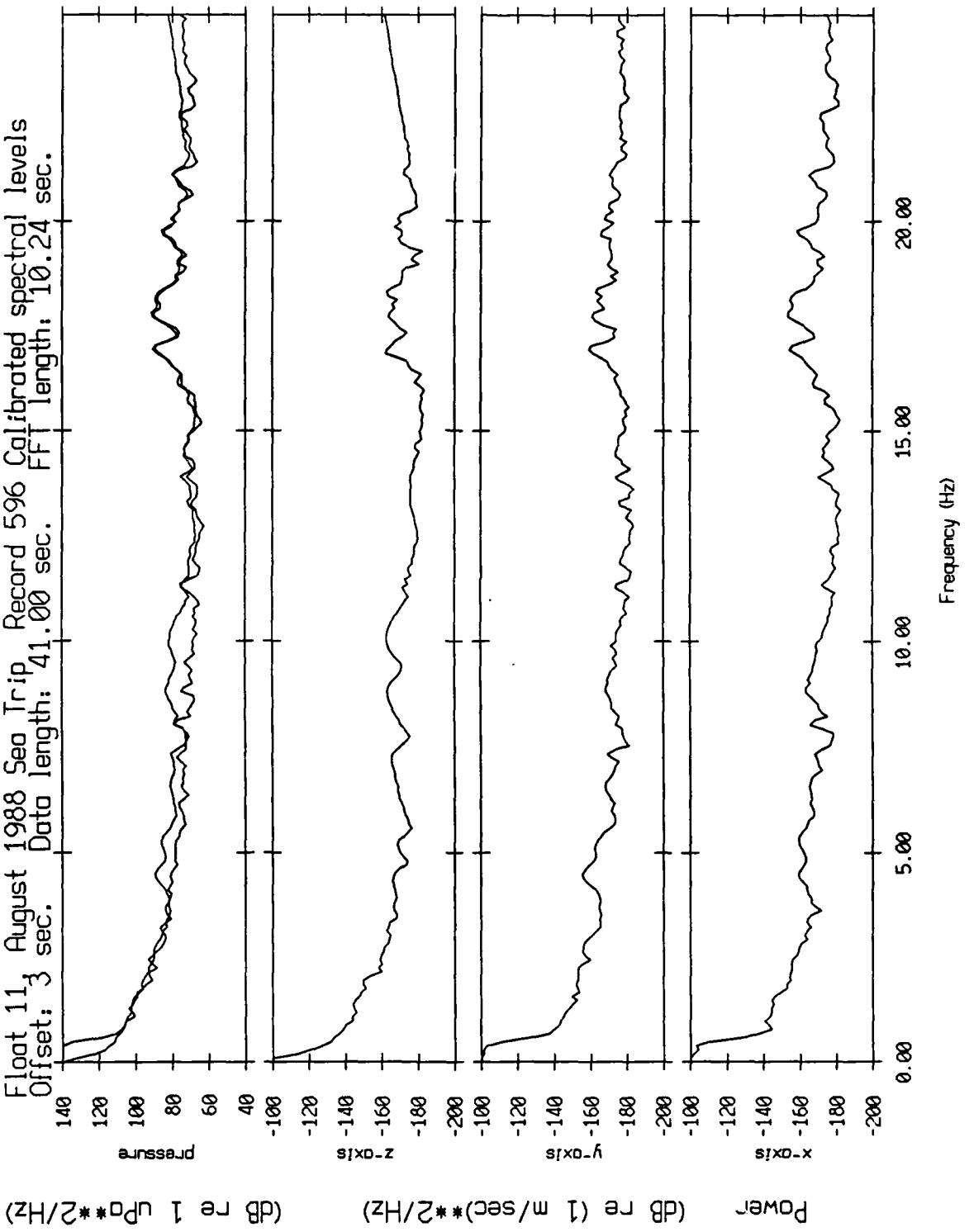

Float 11, August 1988 Sea Trip, Record 596 Calibrated spectral levels
Offset: 3 sec. Data length: 41.00 sec. FFT length: 10.24 sec.
pressure
z-axis
y-axis
x-axis
Power (dB re (1 m/sec)**2/Hz)
(dB re 1 uPa**2/Hz)
140
120
100
80
60
40
-100
-120
-140
-160
-180
-200
0.00
5.00
10.00
15.00
20.00
Frequency (Hz)

Figure XII.9

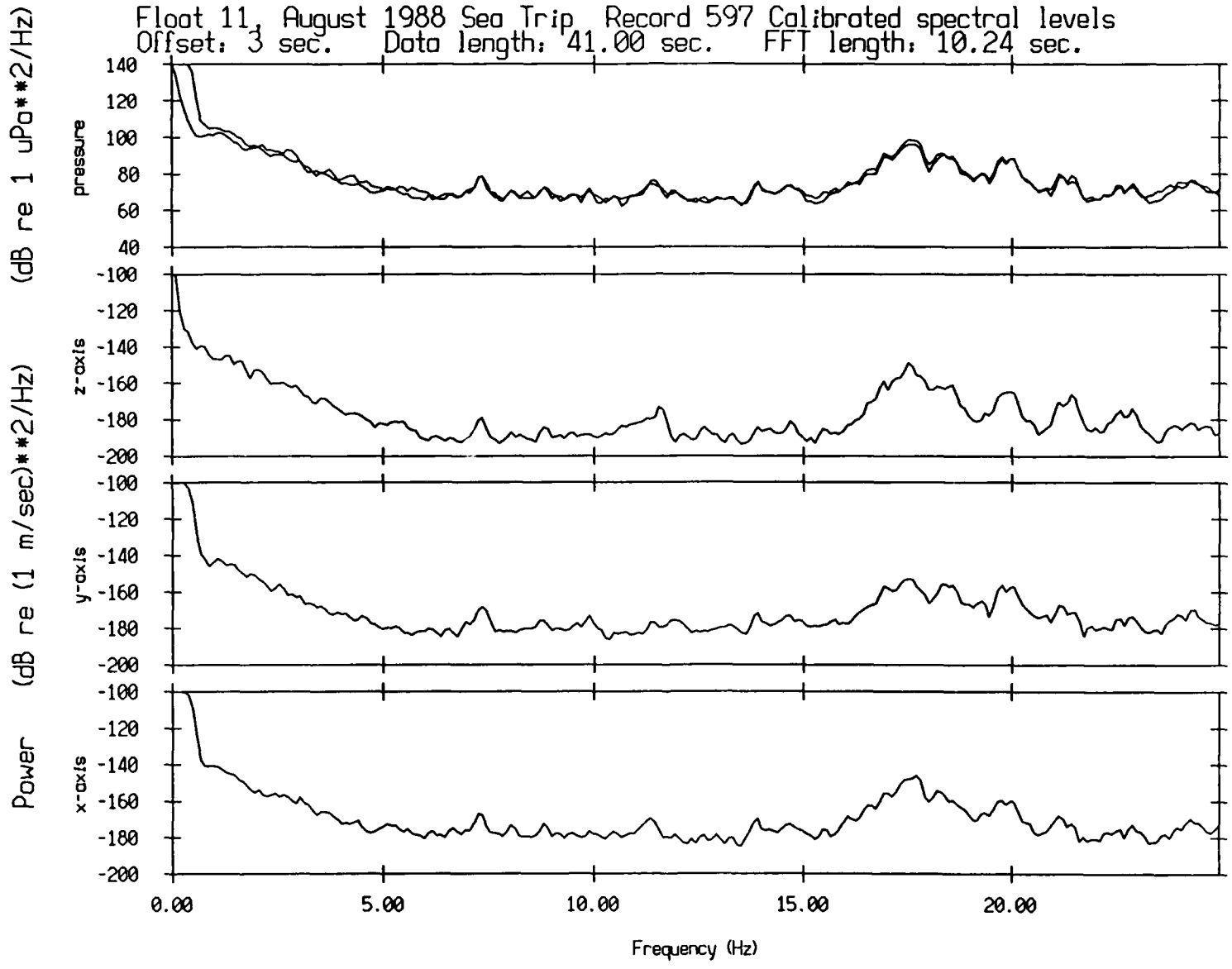


Figure XII.10

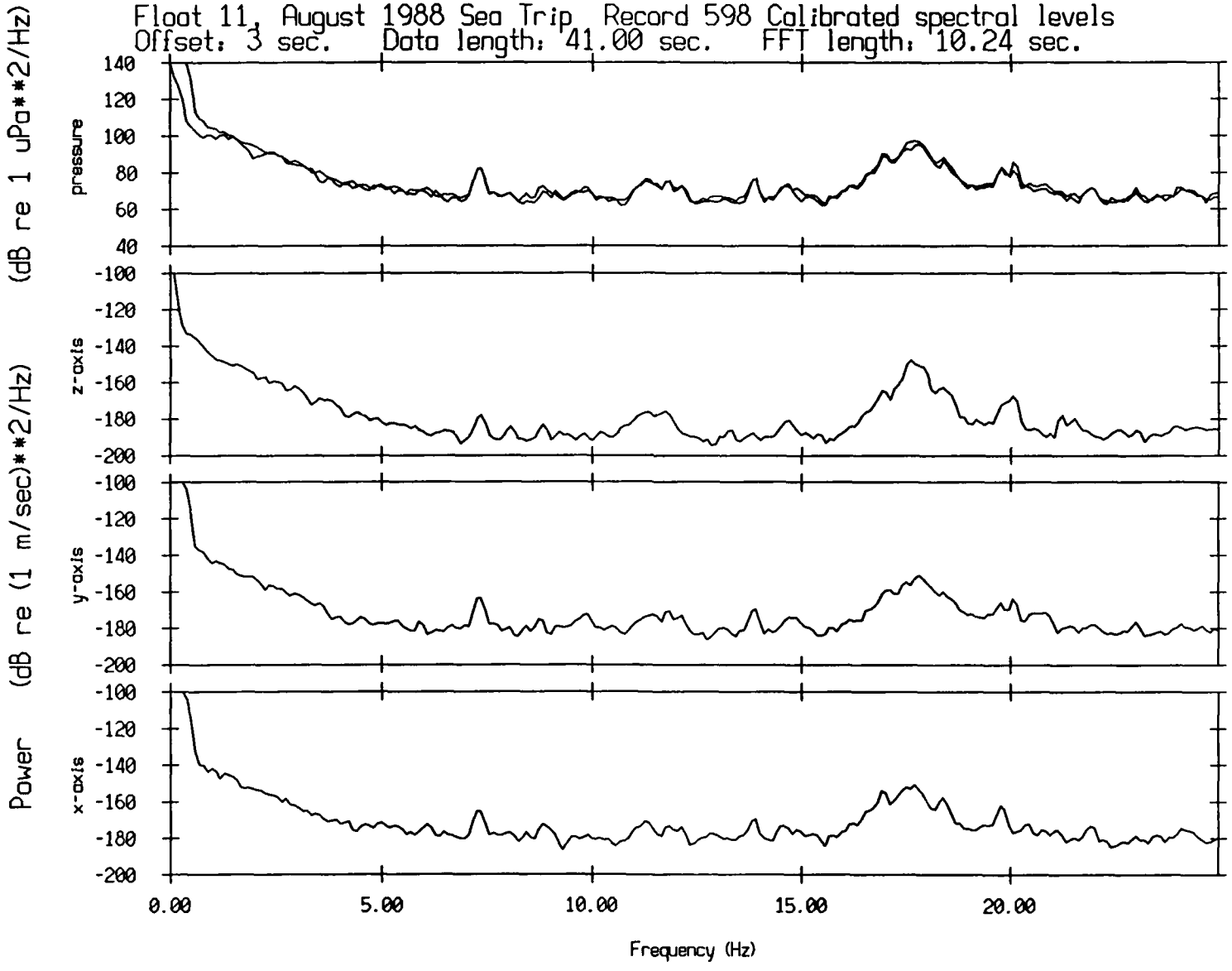


Figure XII.11

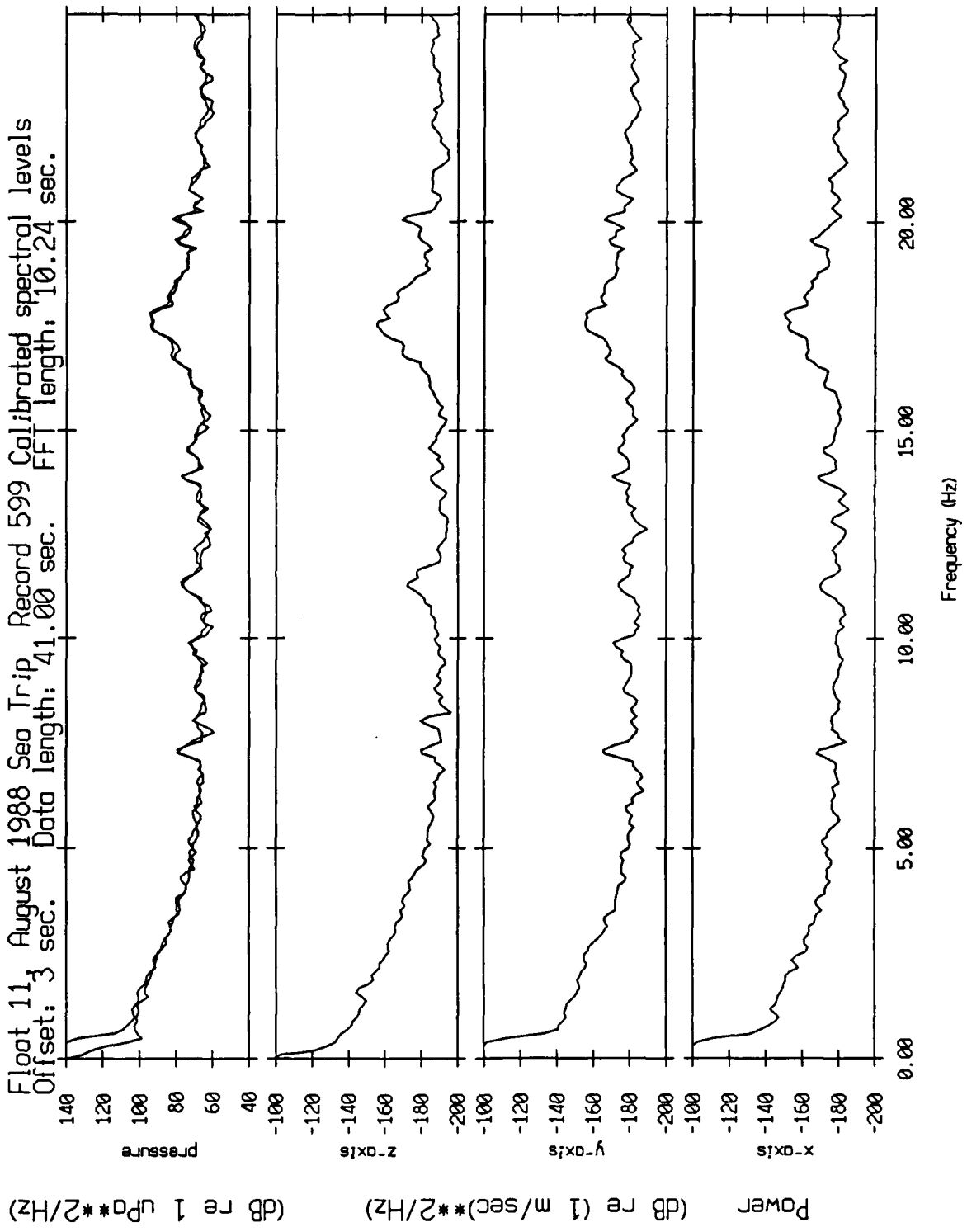


Figure XII.12

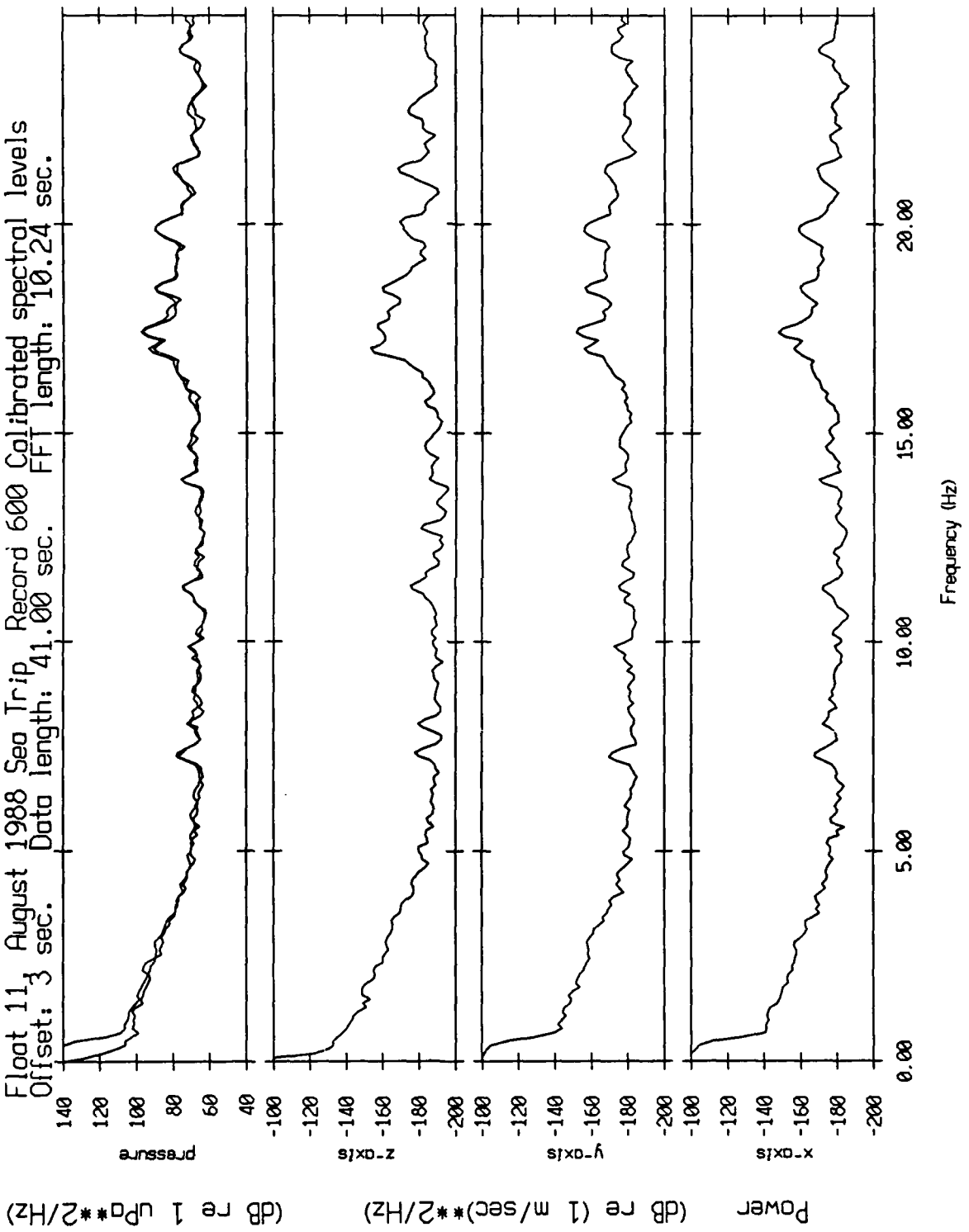


Figure XII.13

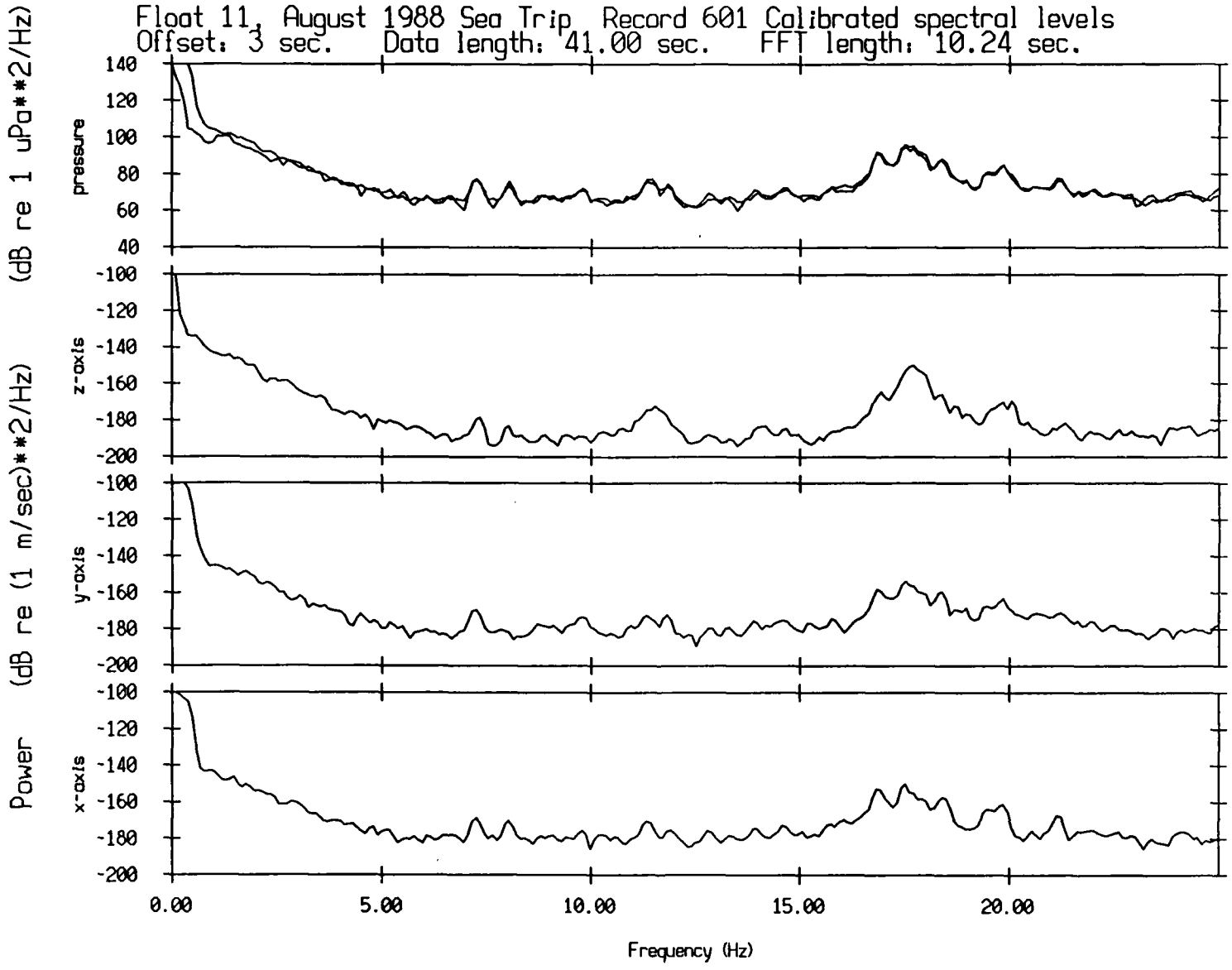


Figure XII.14

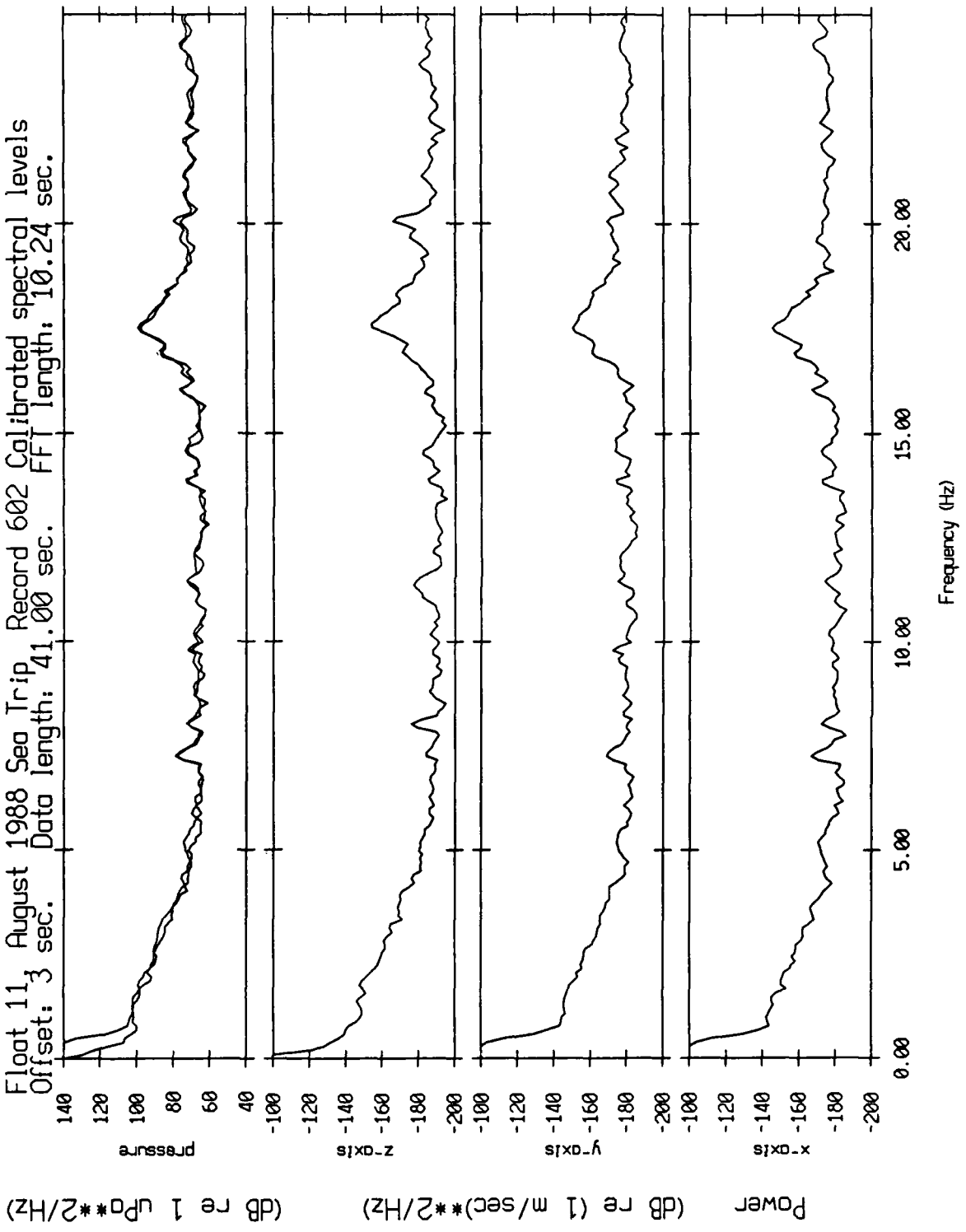


Figure XII.15

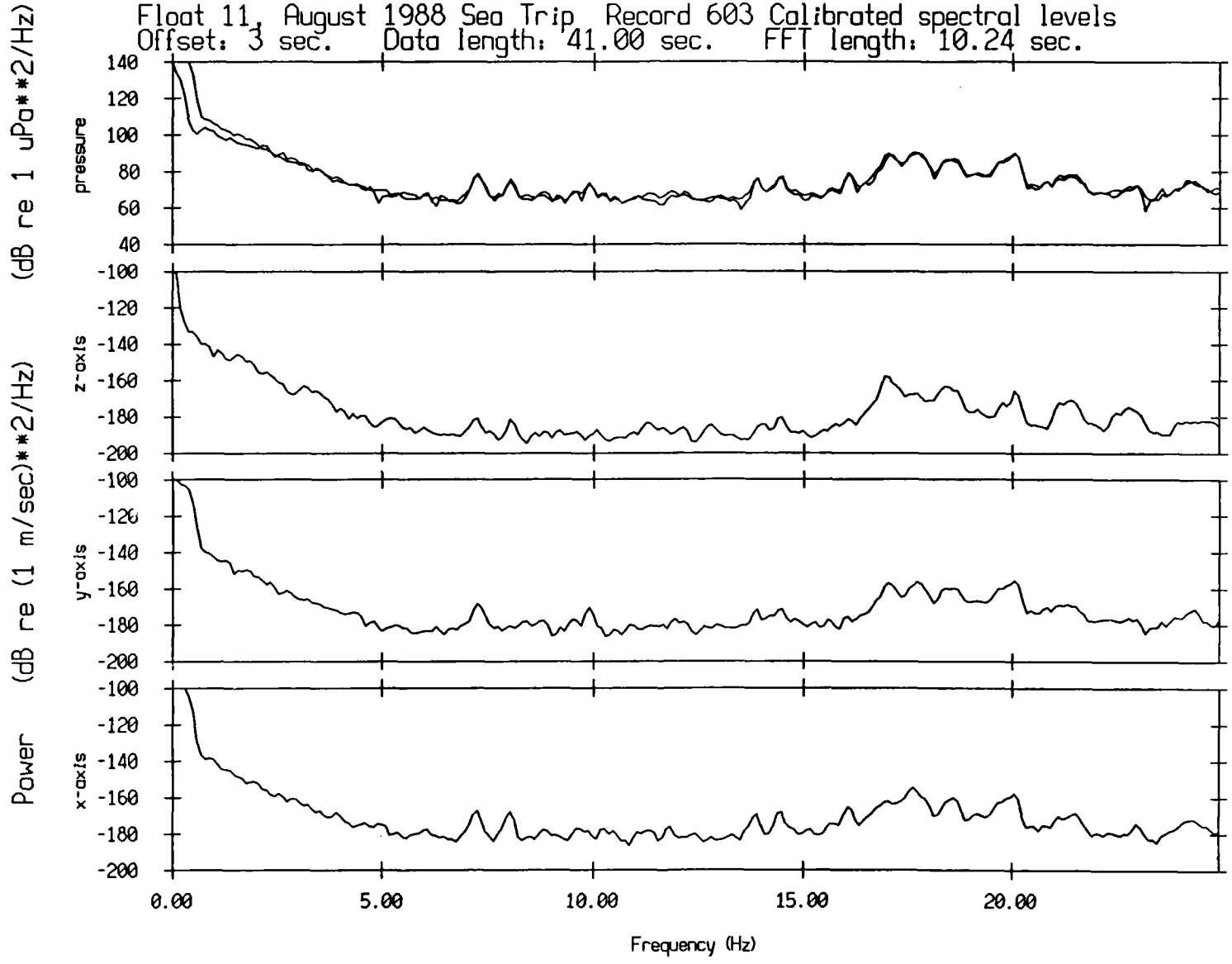


Figure XII.16

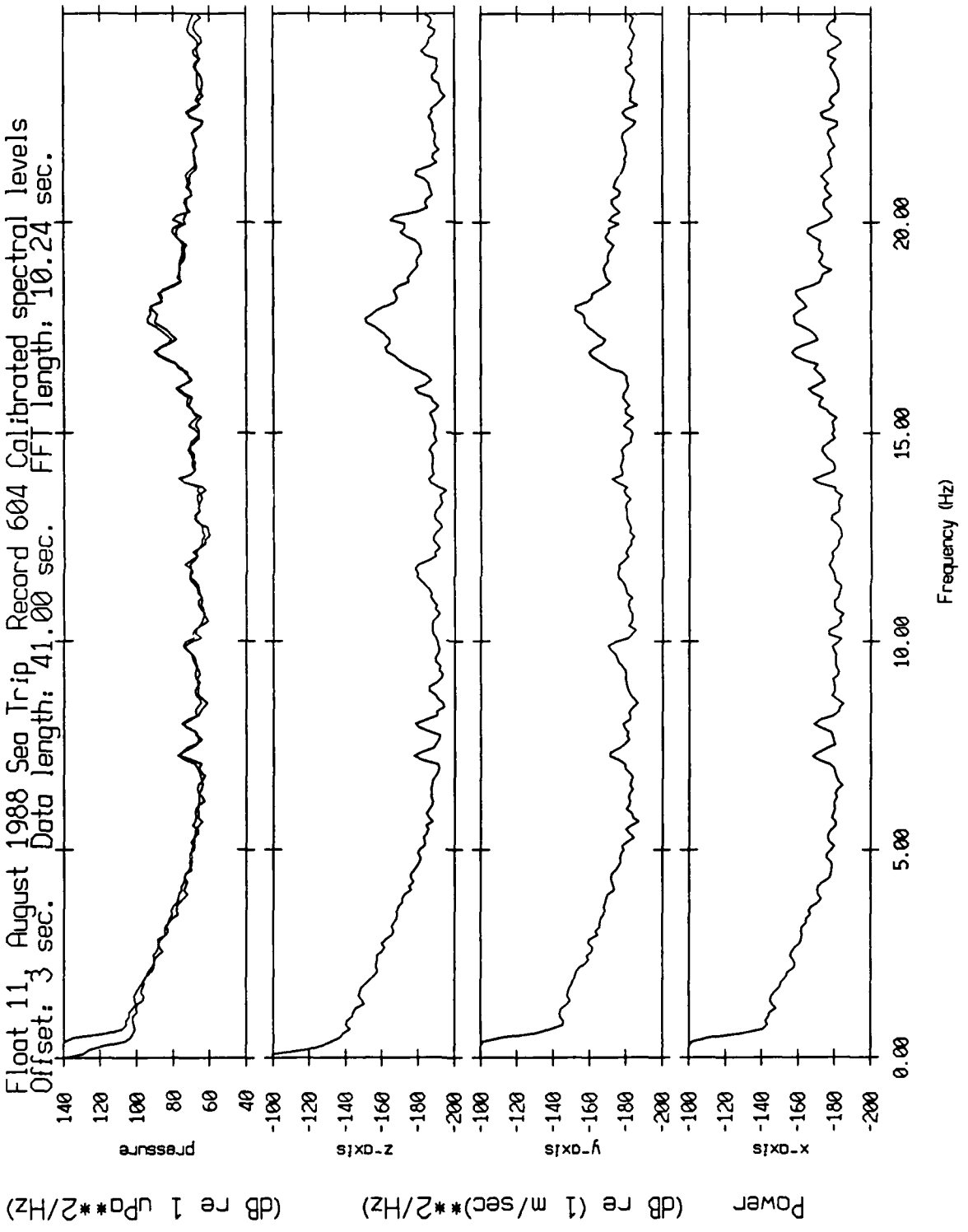


Figure XII.17

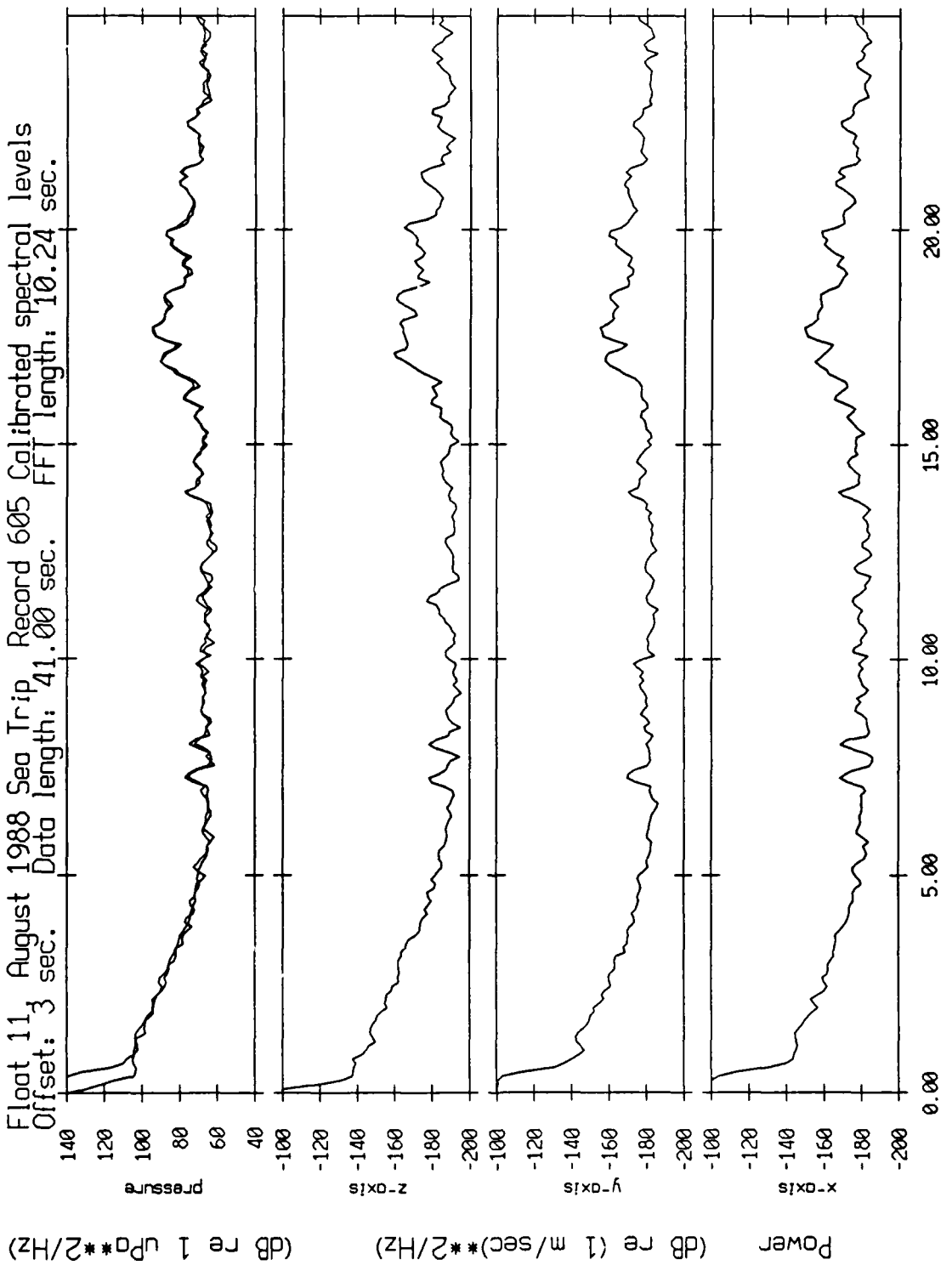


Figure XII.18

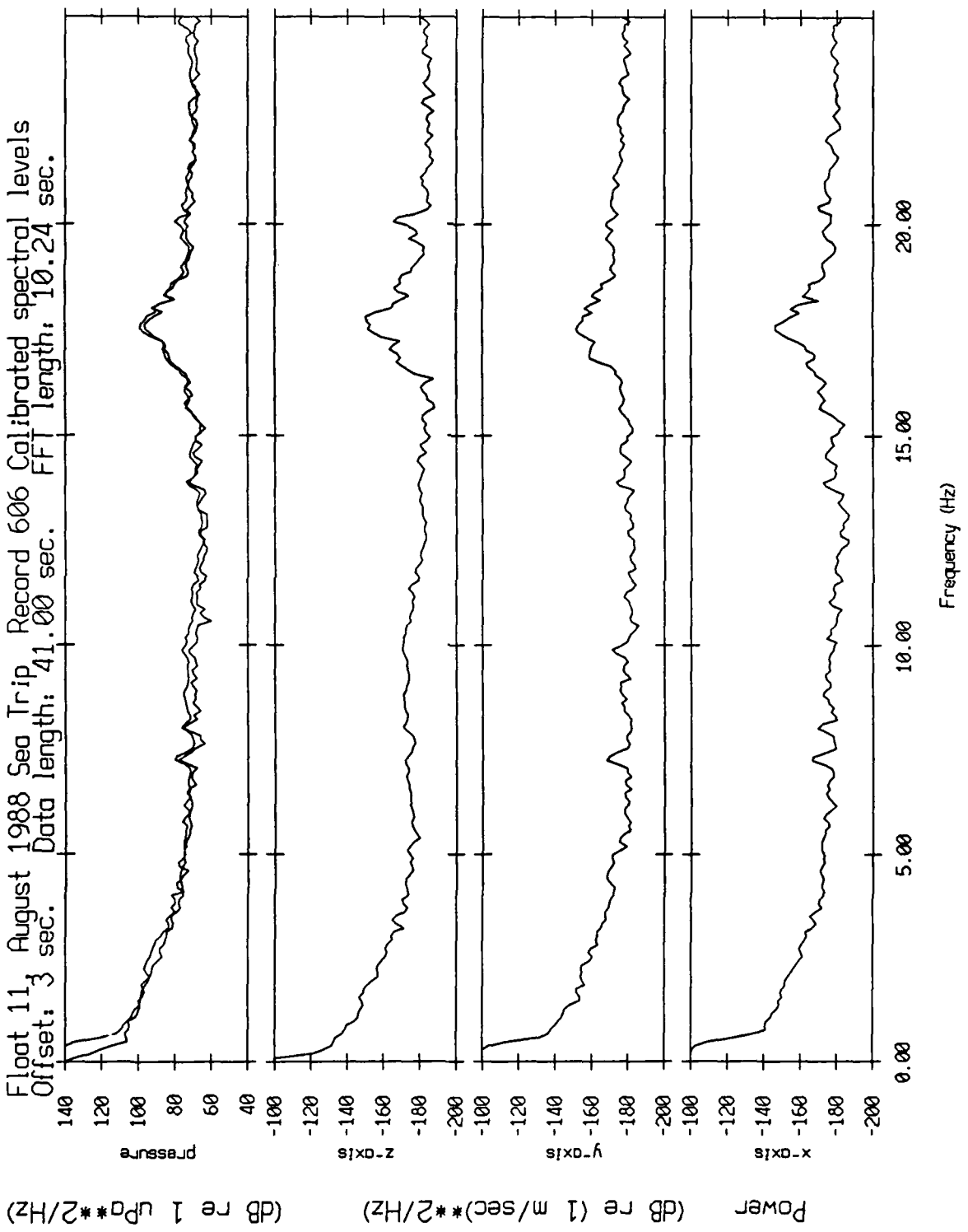


Figure XII.19

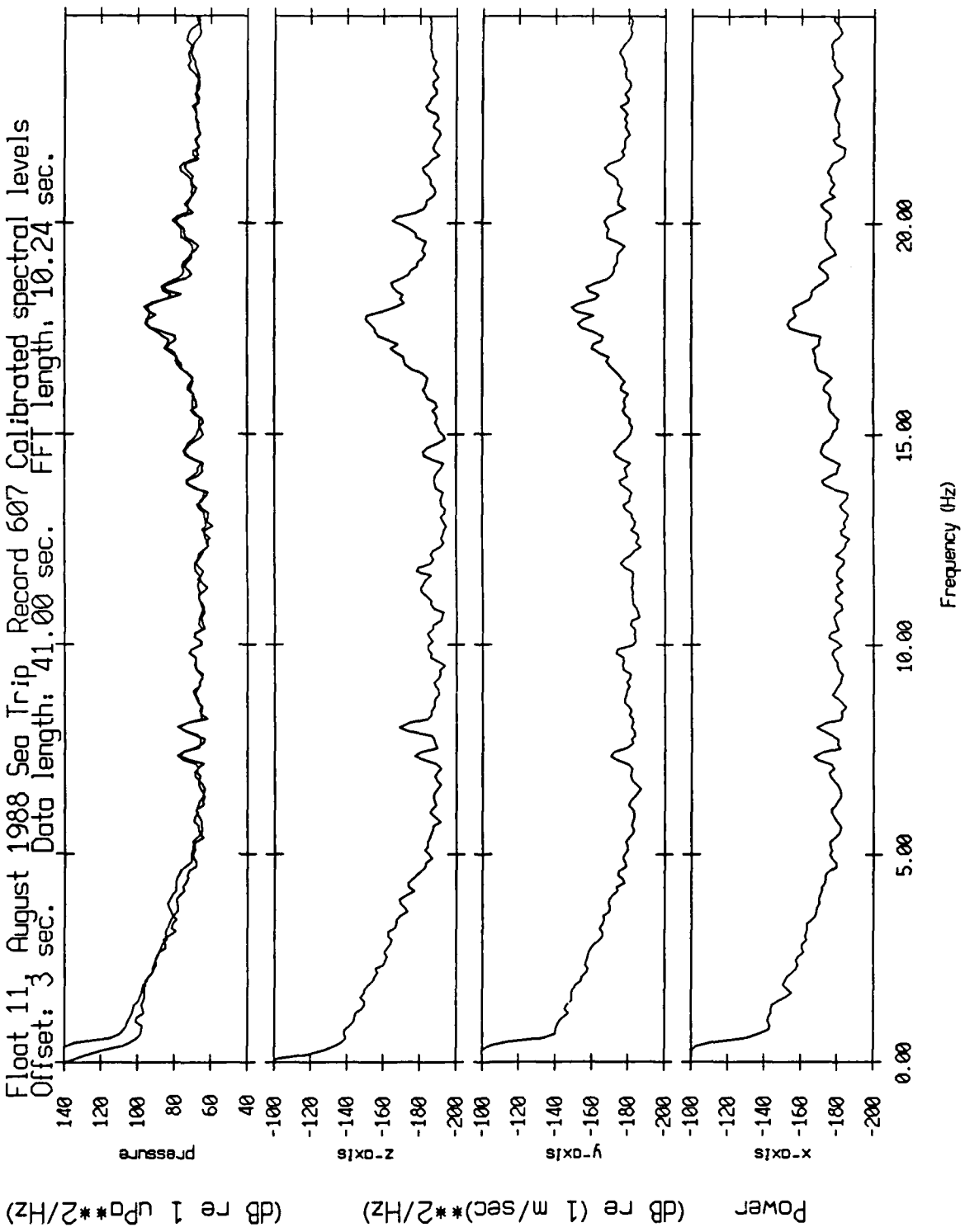


Figure XII.20

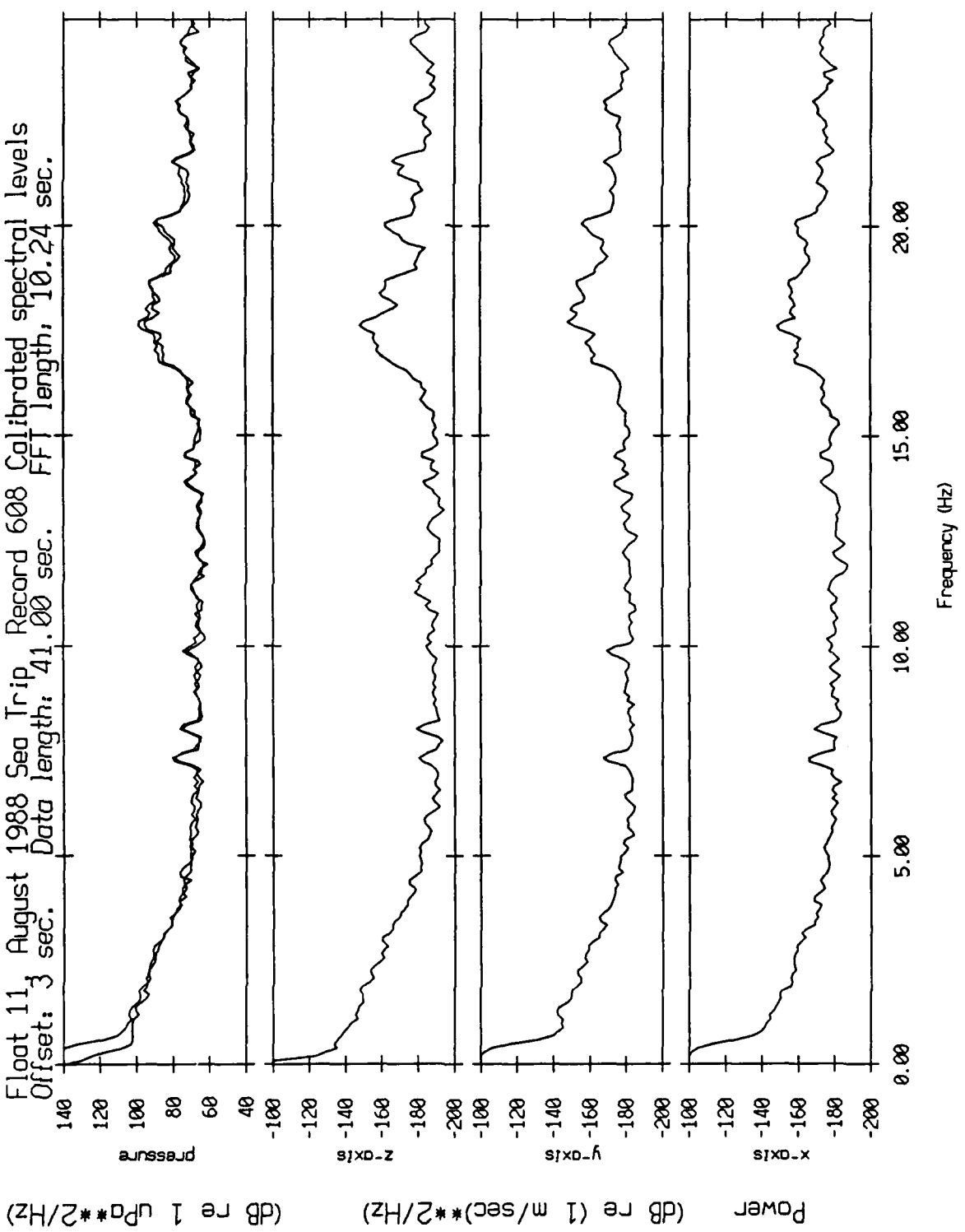


Figure XII.21

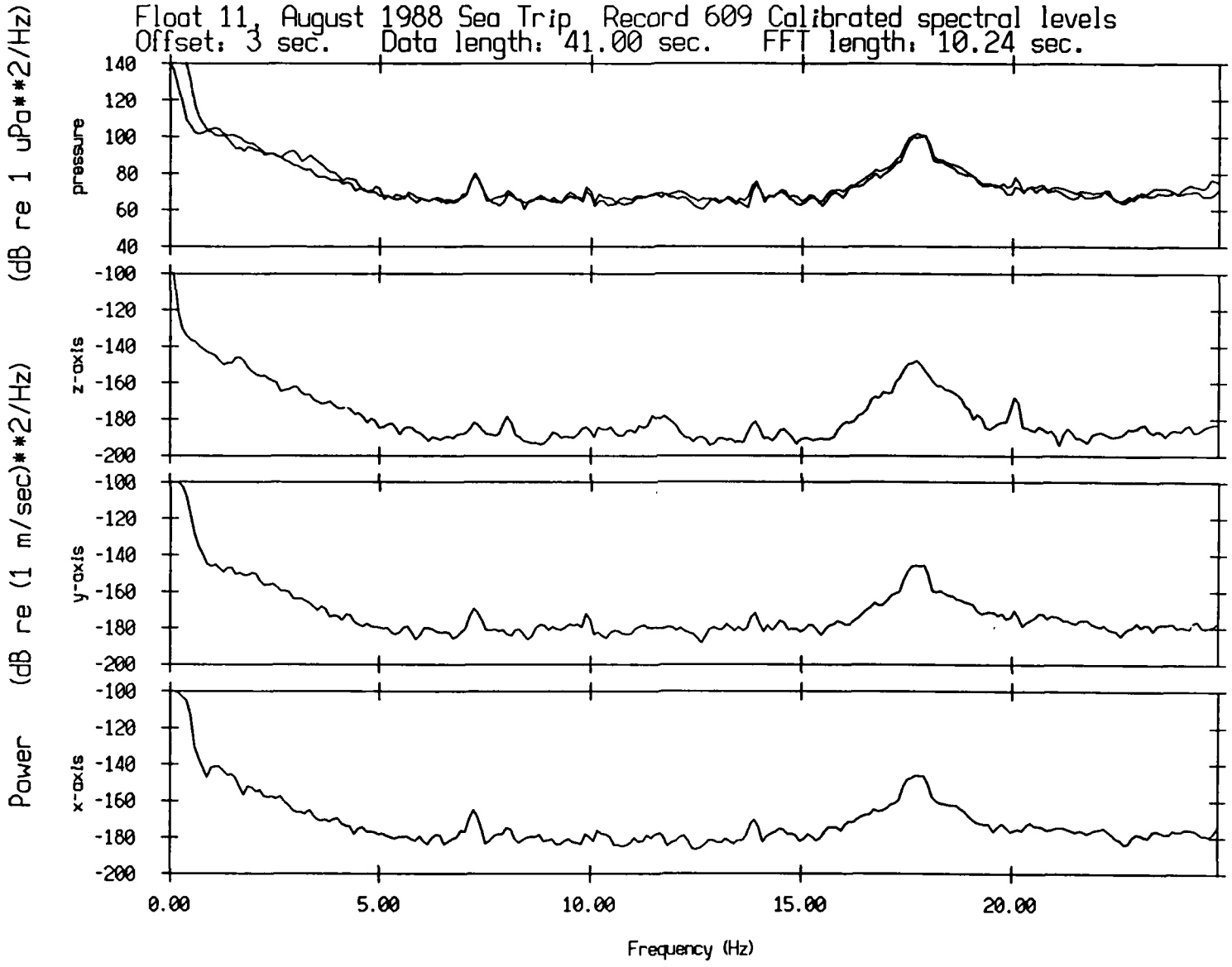


Figure XII.22

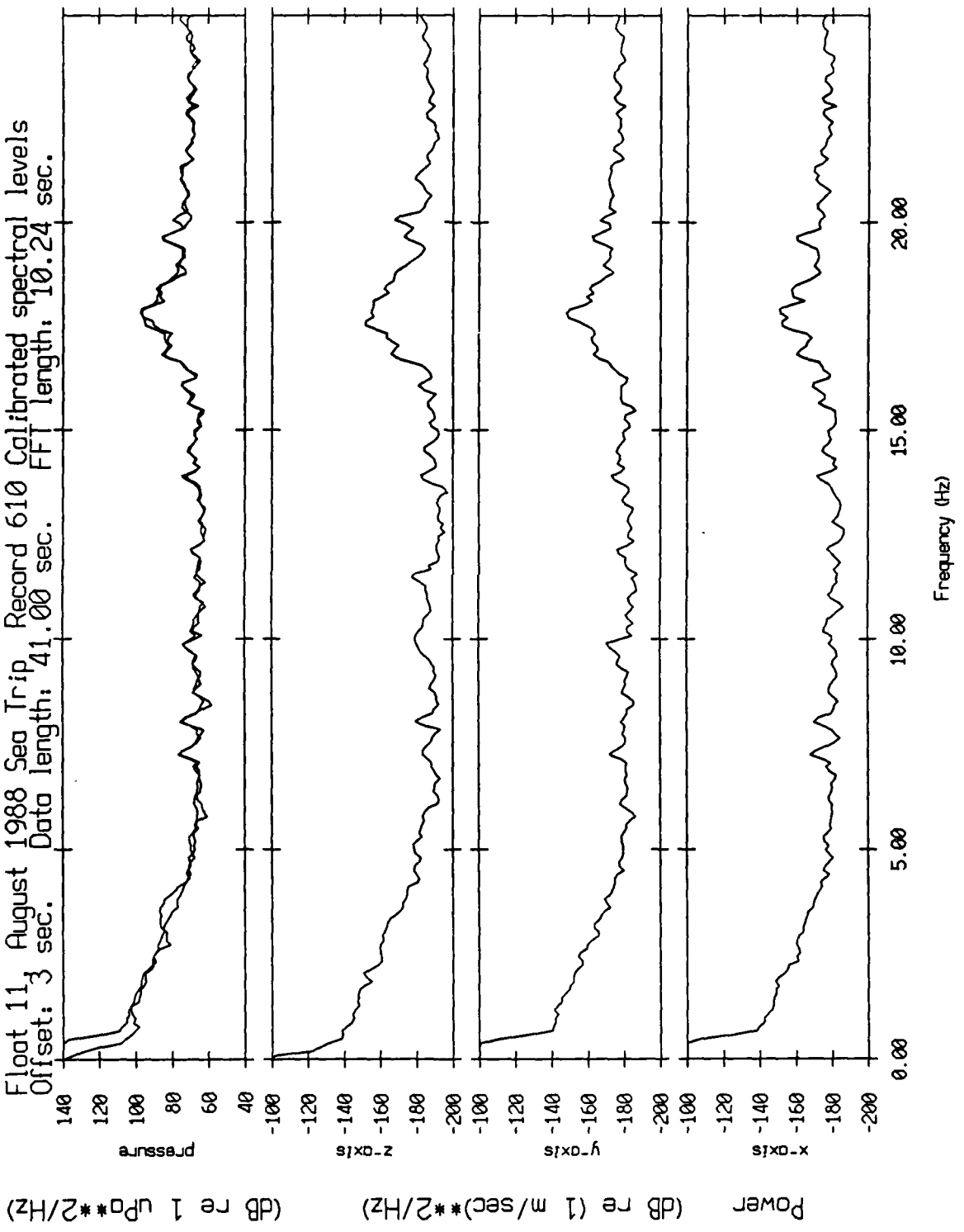


Figure XII.23

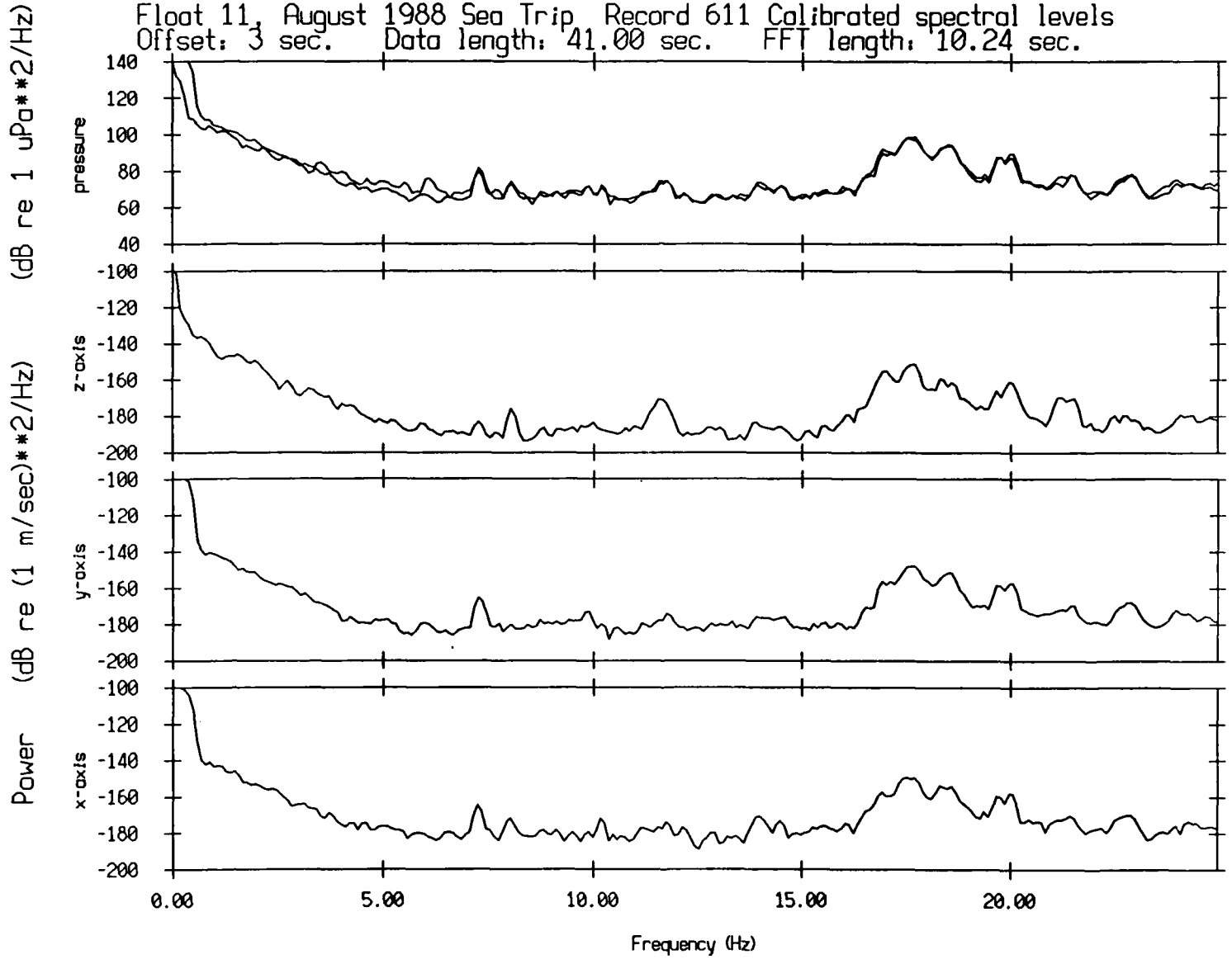


Figure XII.24

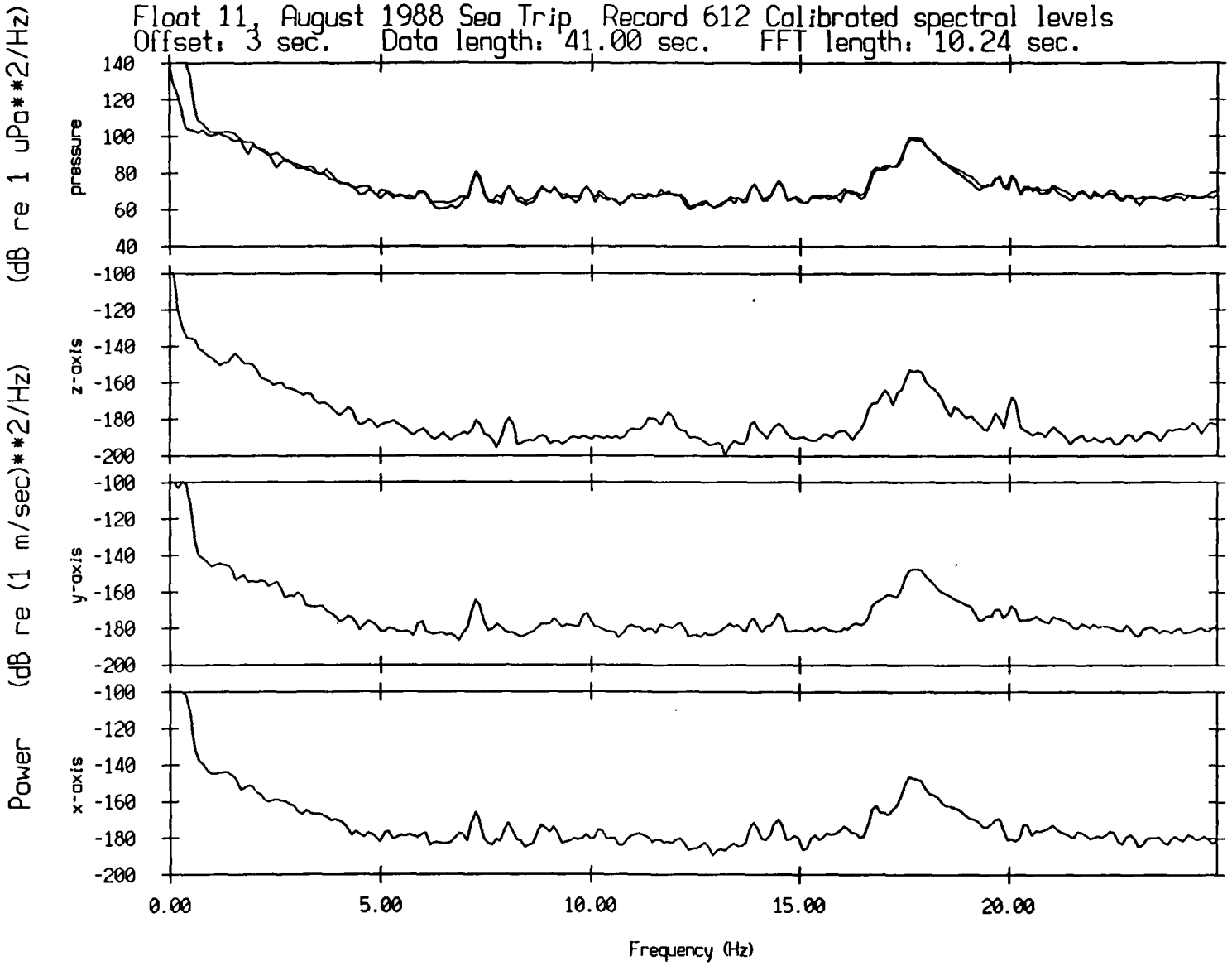


Figure XII.25

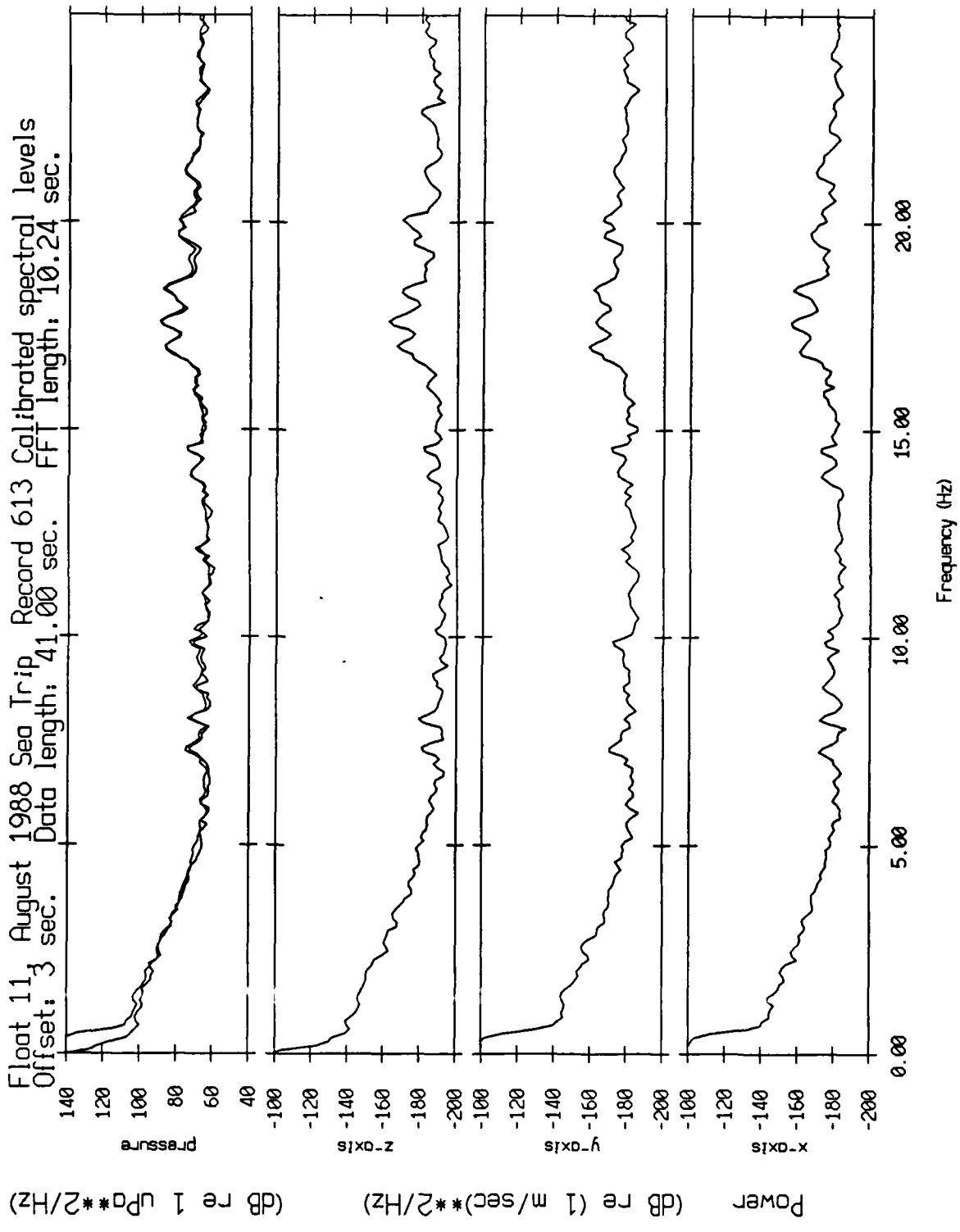


Figure XII.26

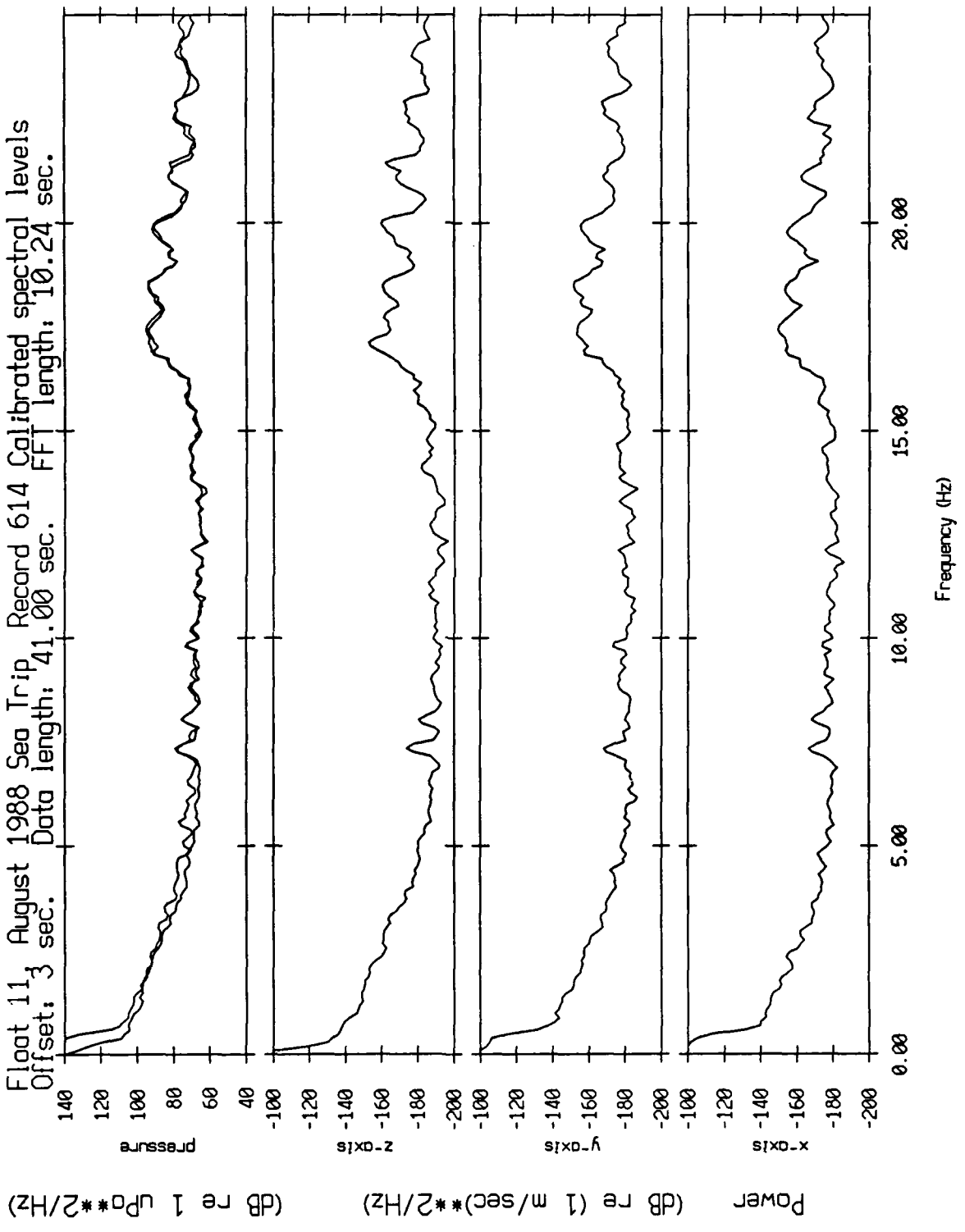


Figure XII.27

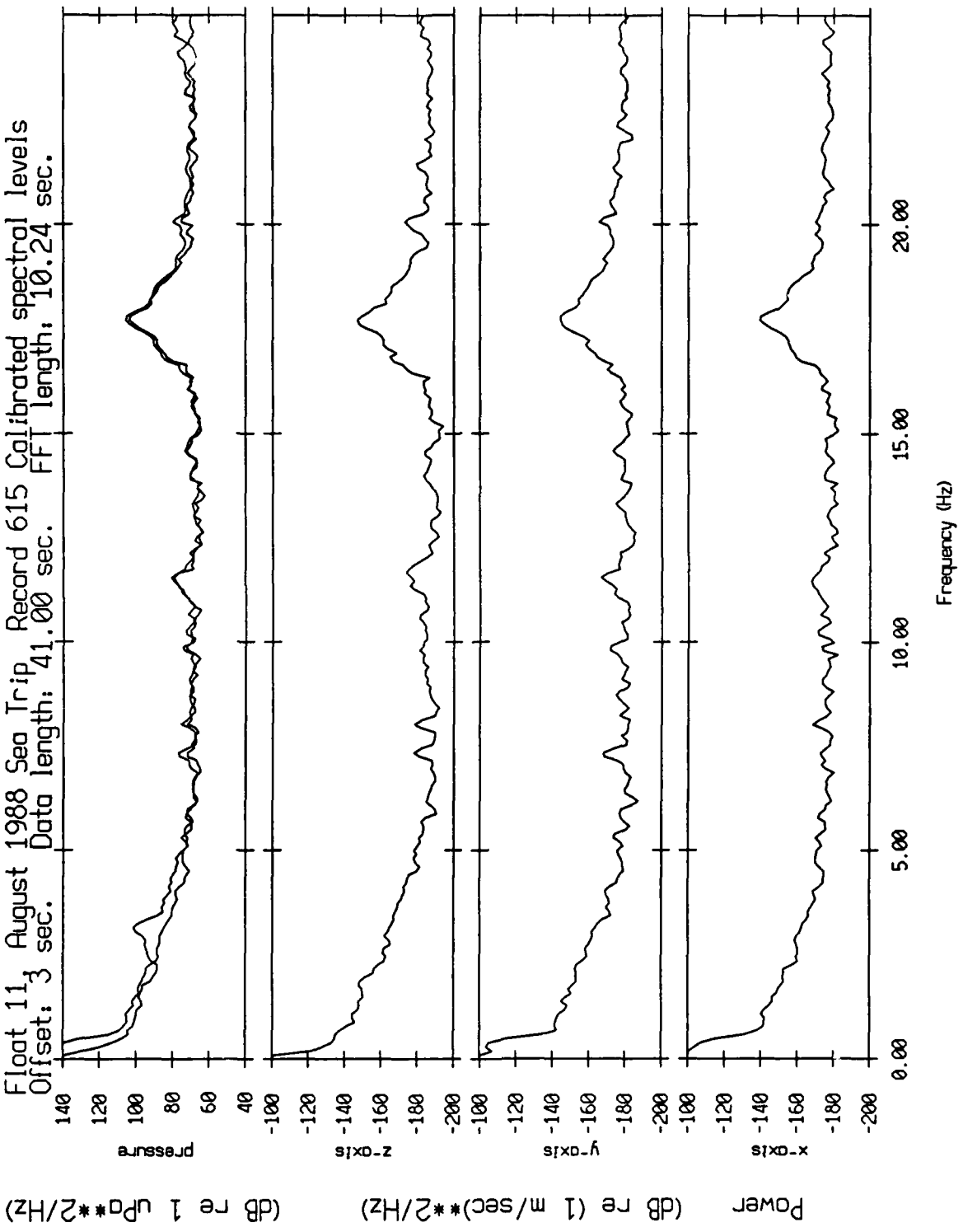


Figure XII.28

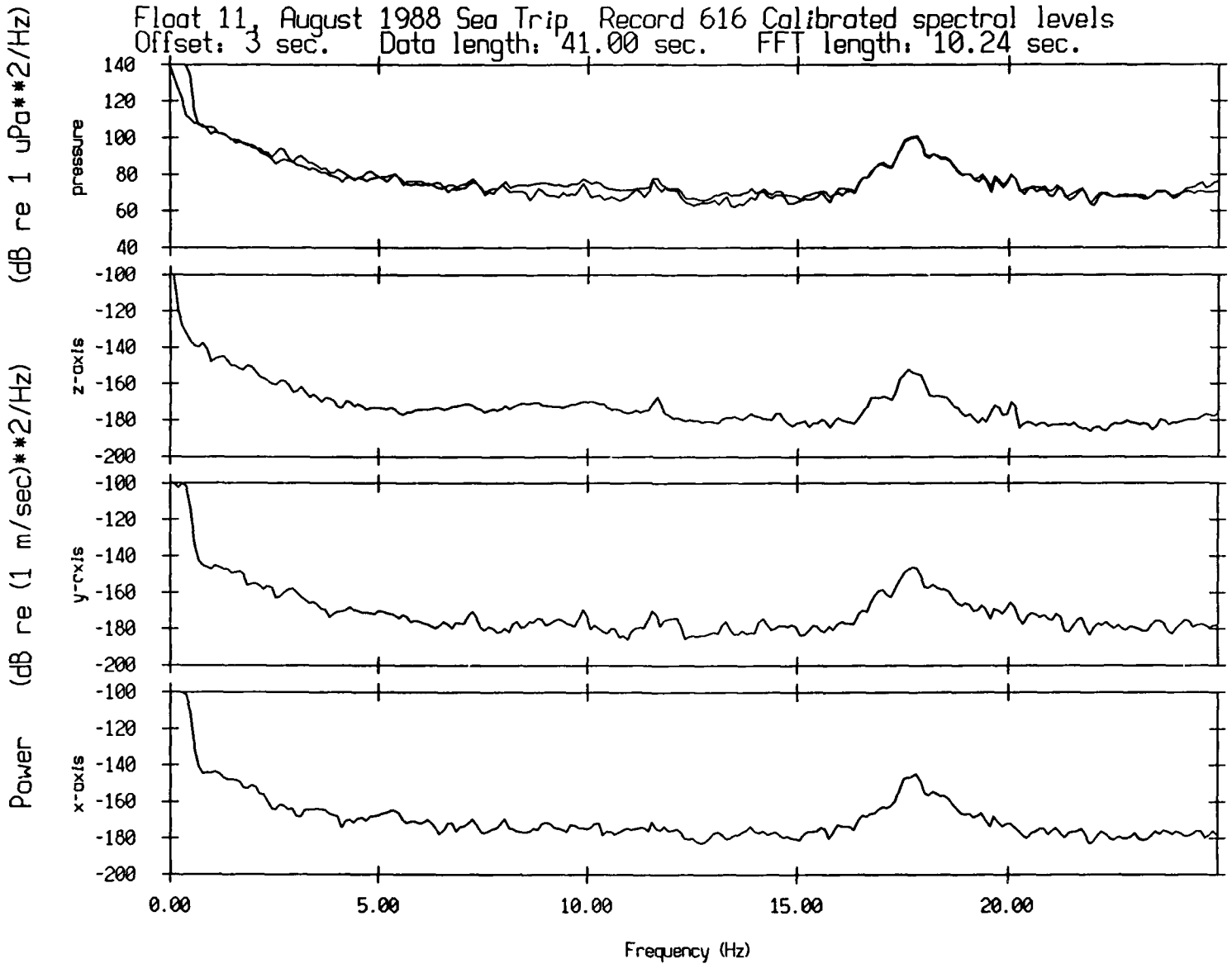


Figure XII.29

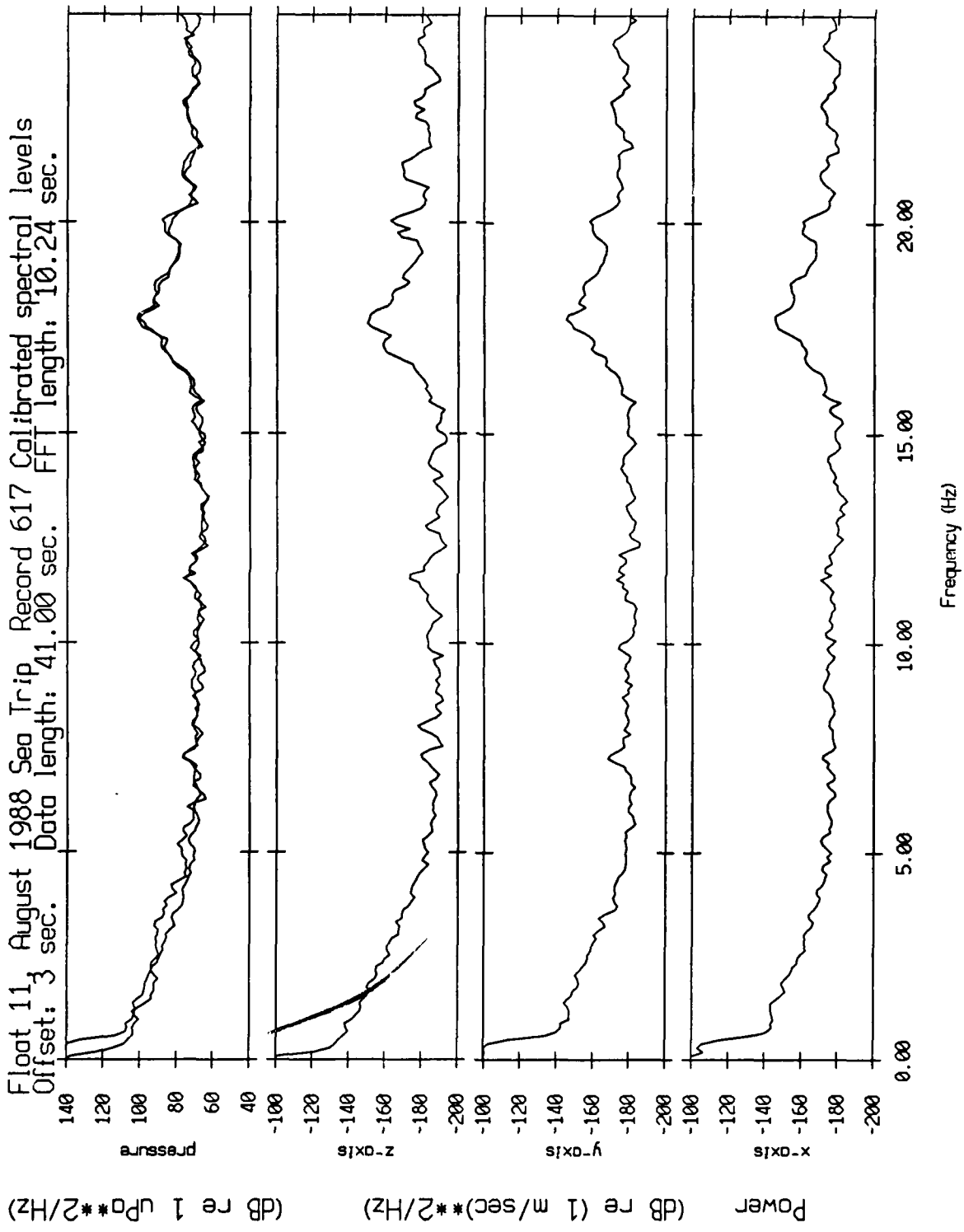


Figure XII.30

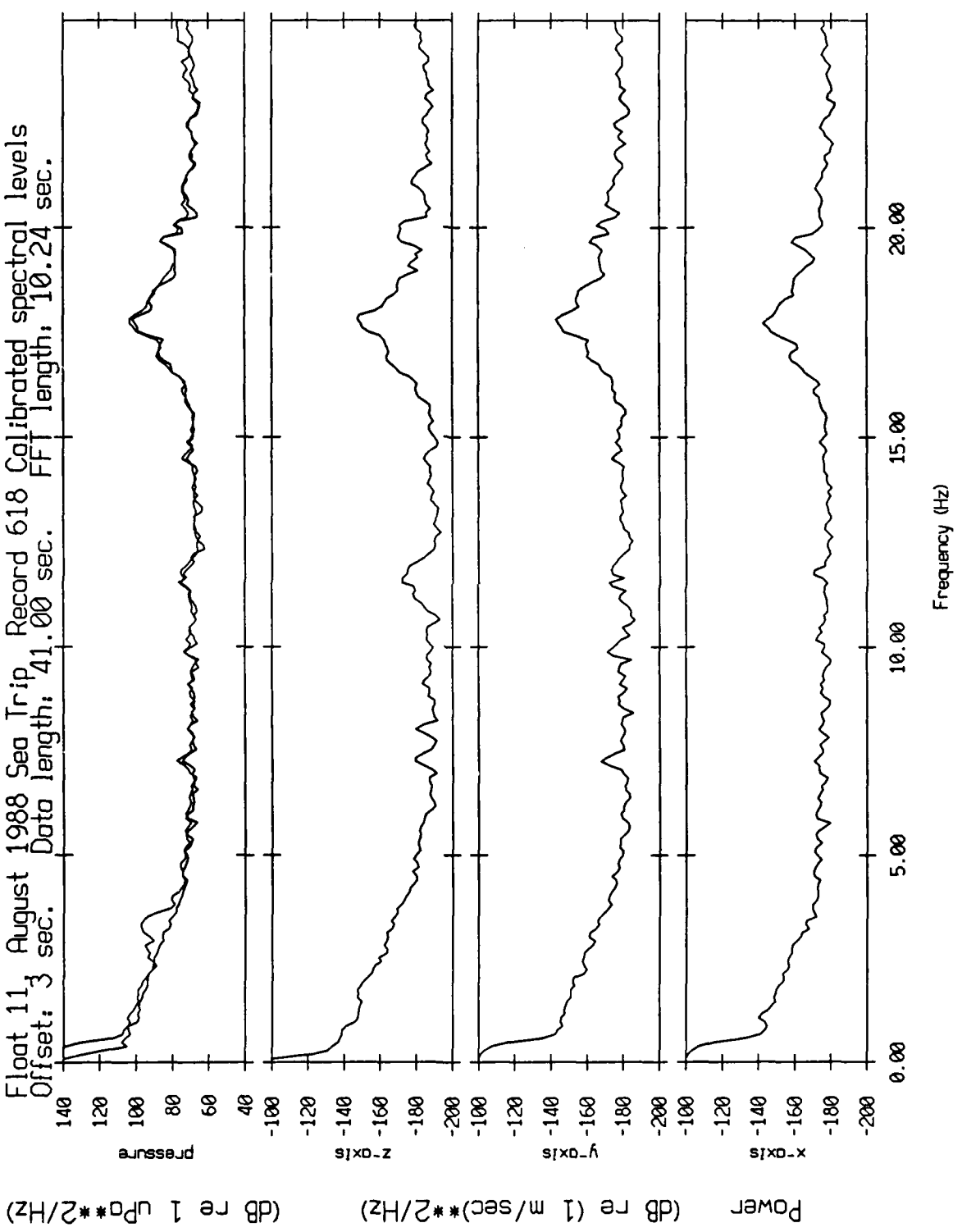


Figure XII.31

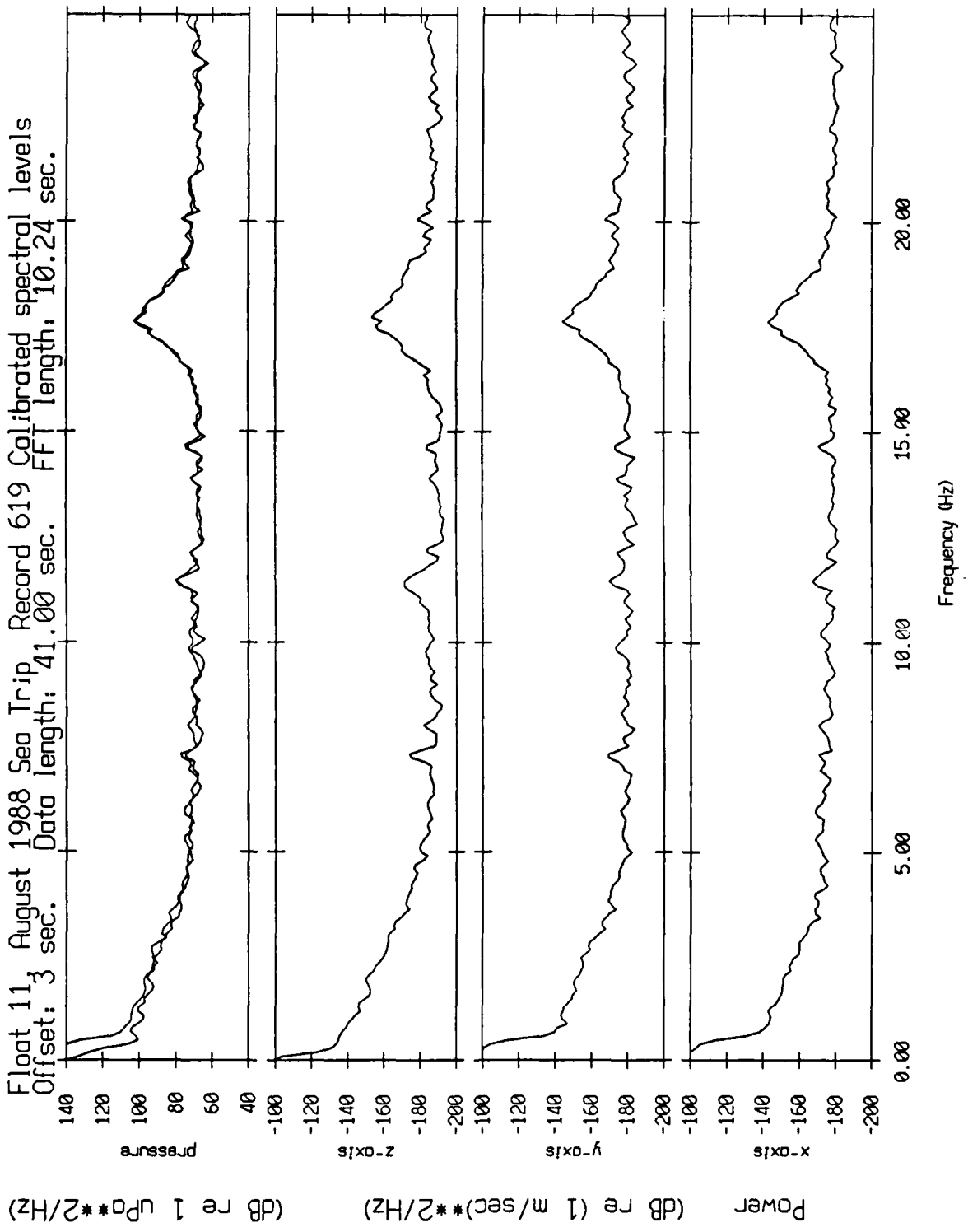


Figure XII.32

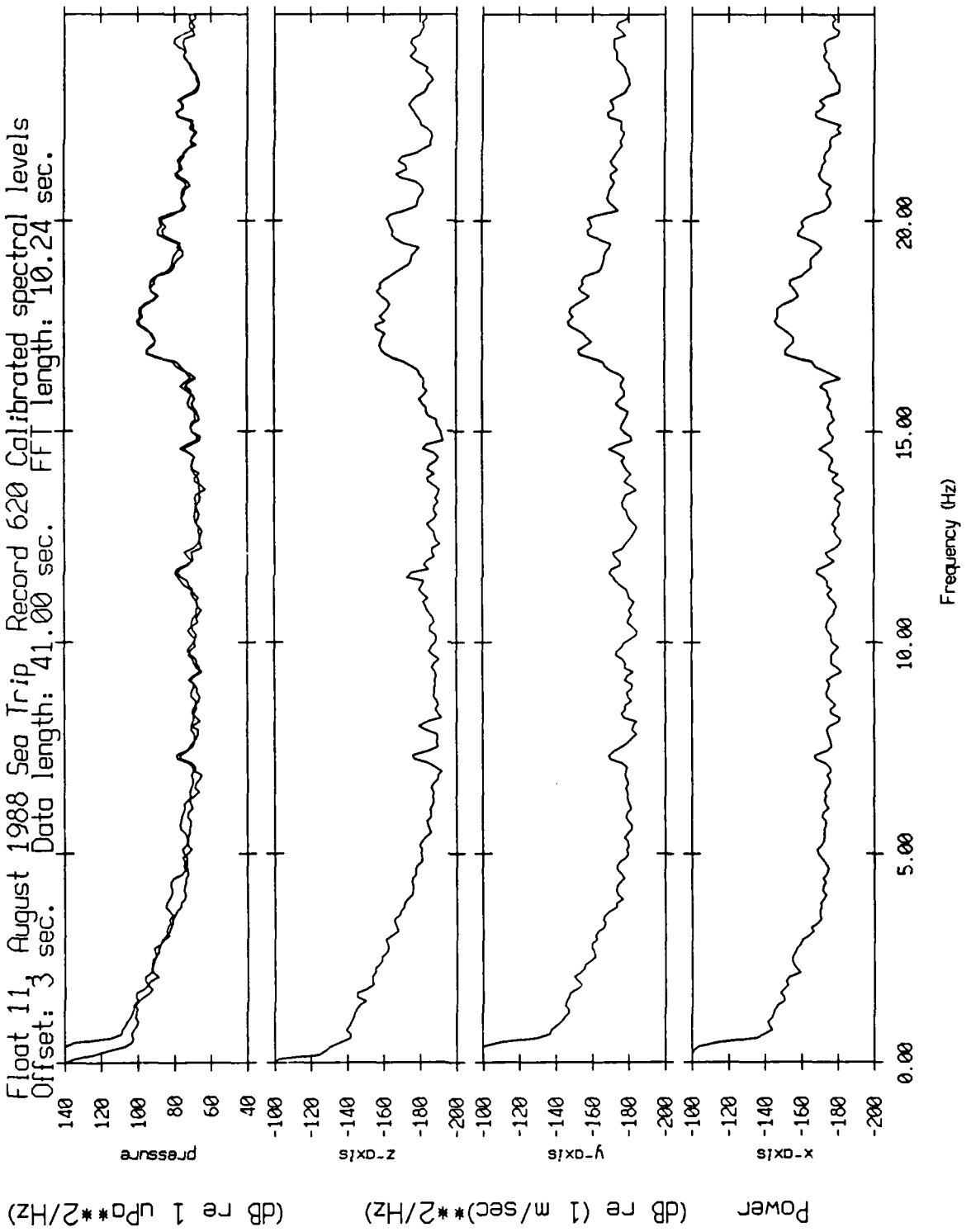


Figure XII.33

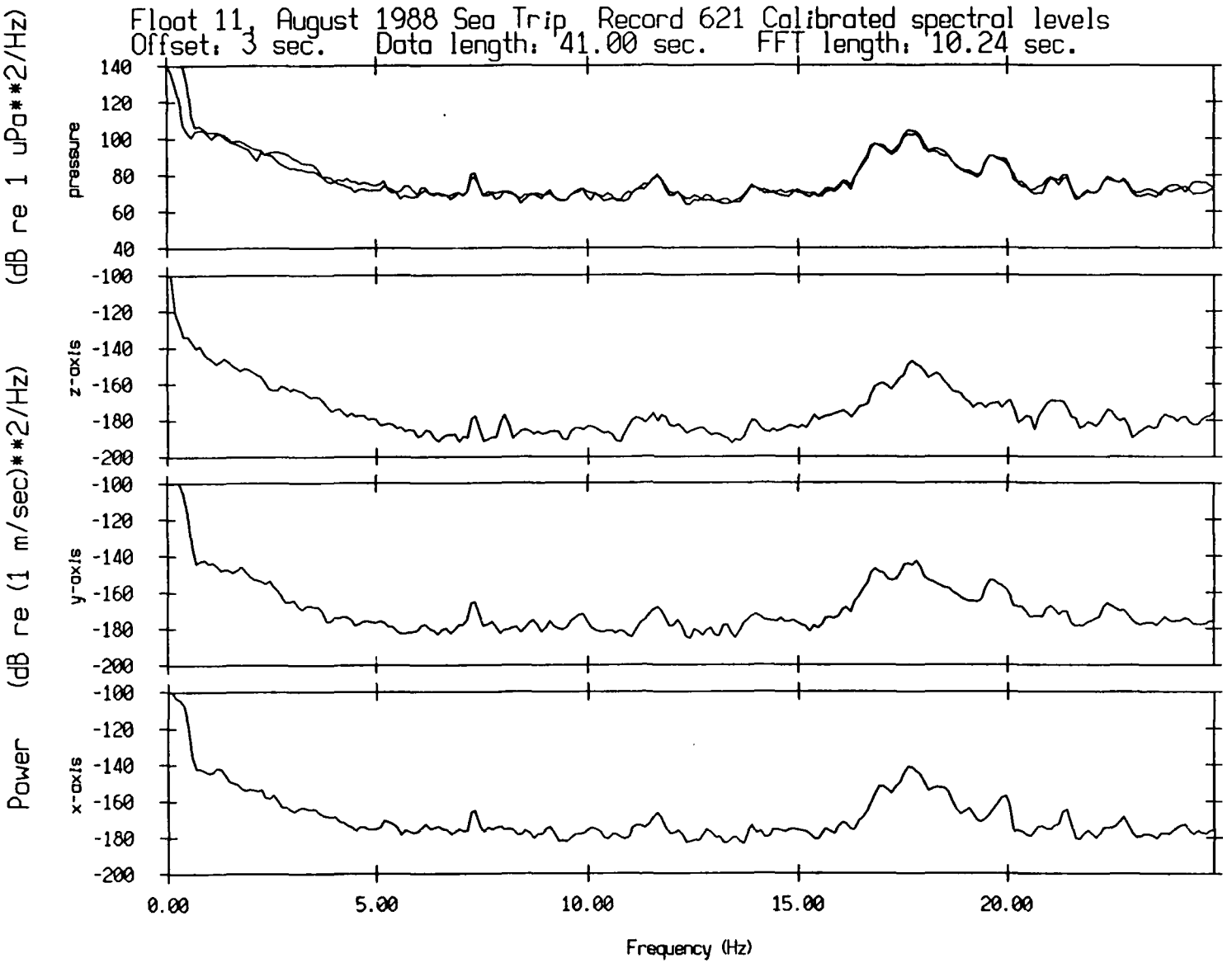


Figure XII.34

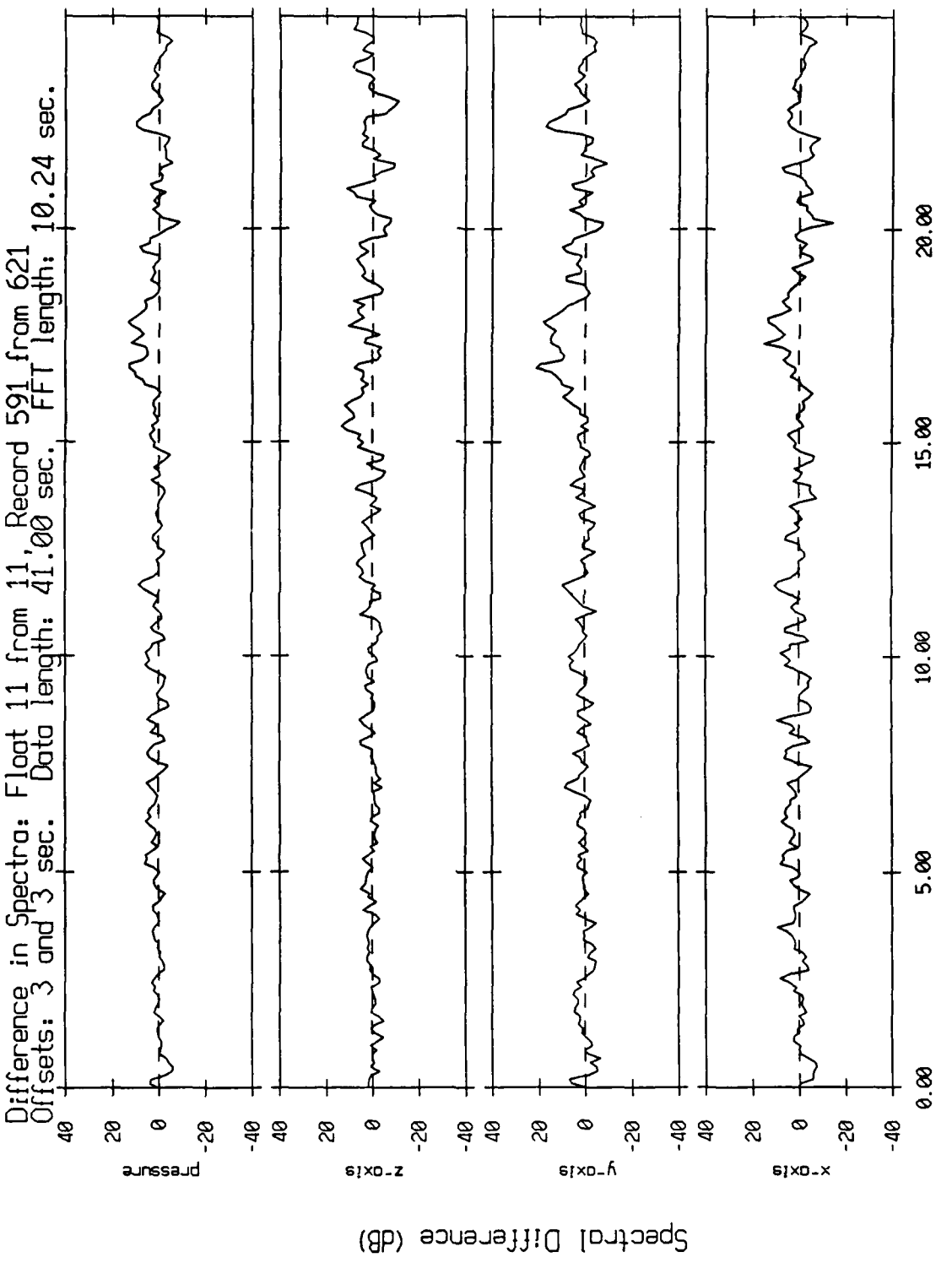


Figure XII.35

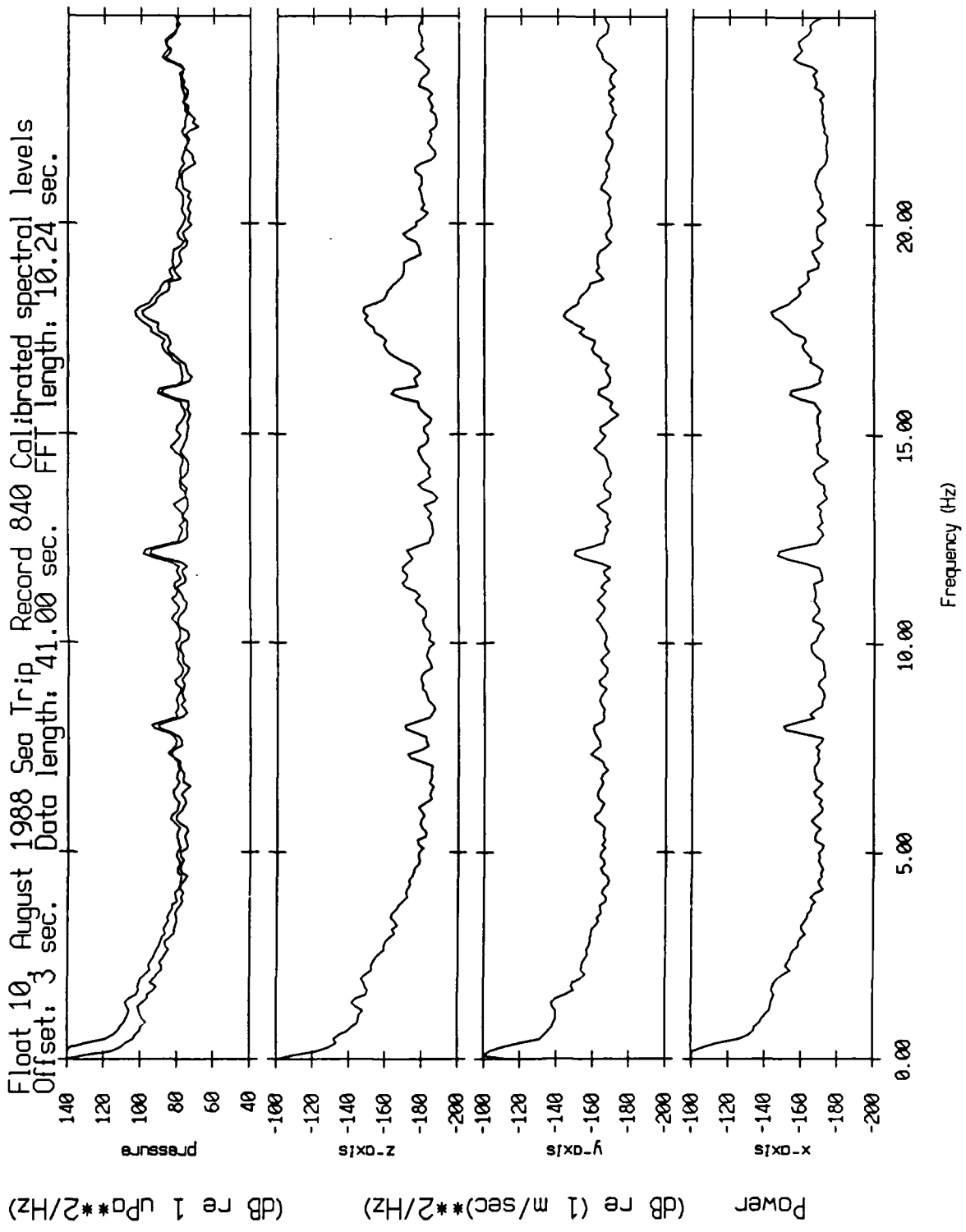


Figure XII.36a

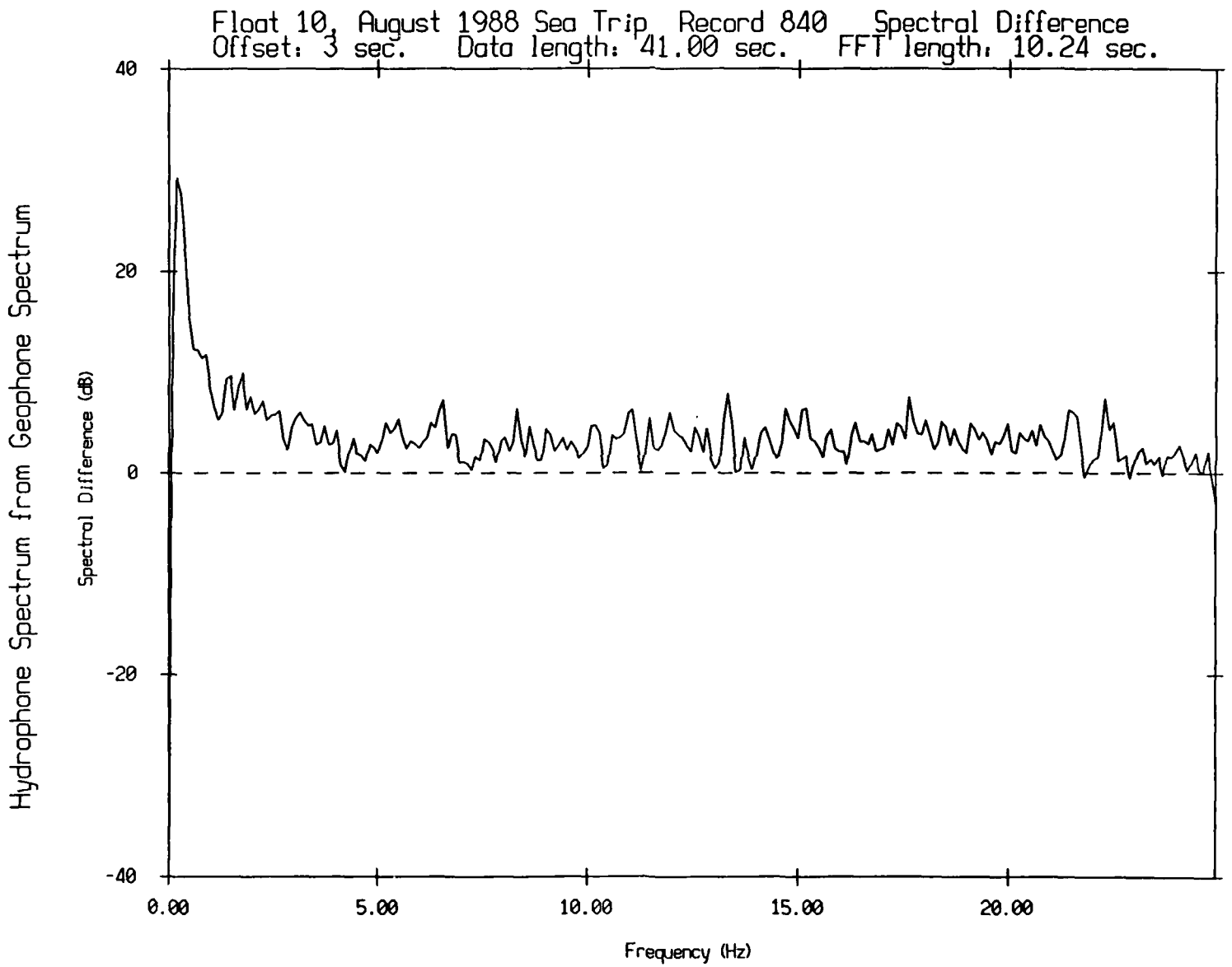


Figure XII.36b

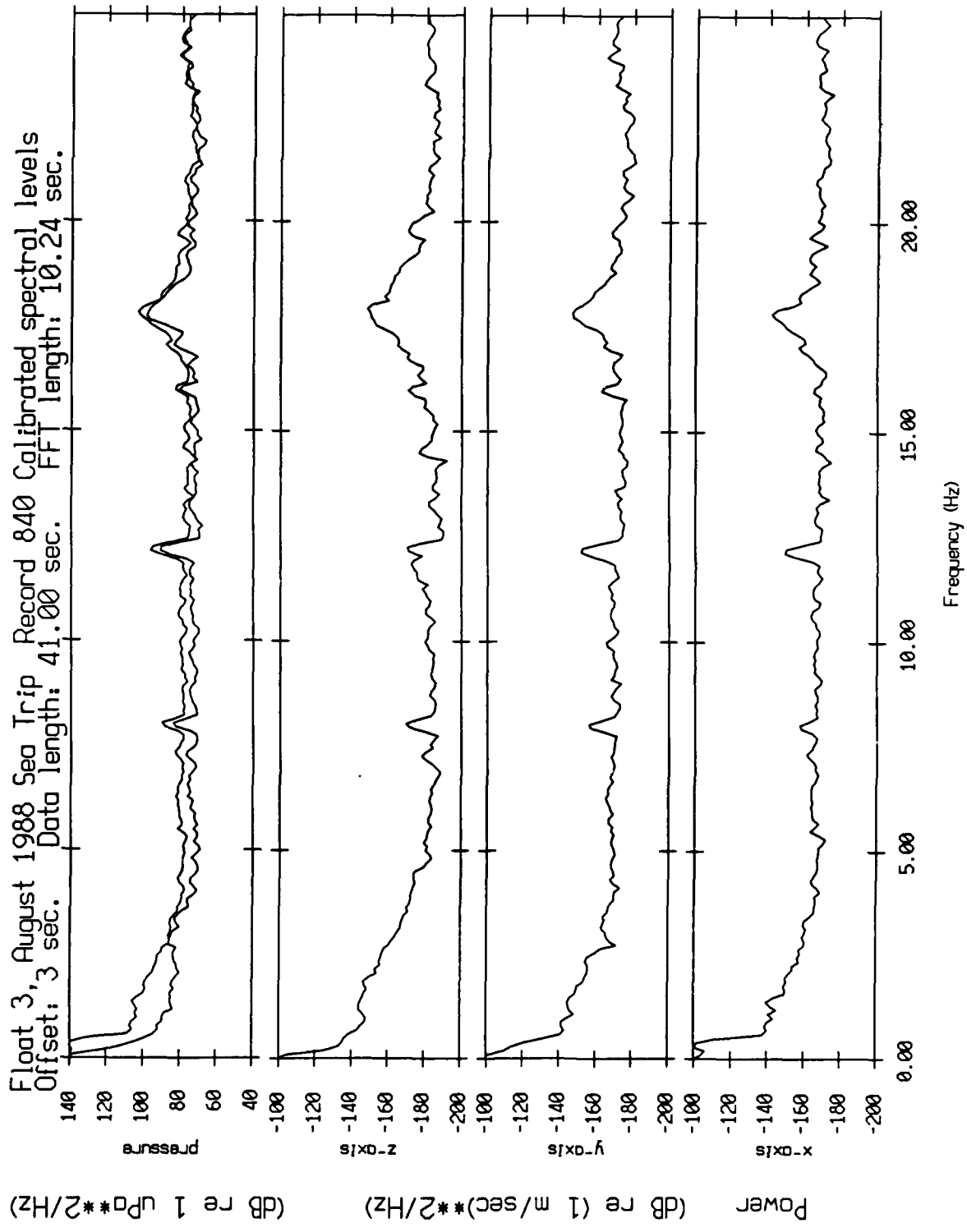


Figure XII.37a

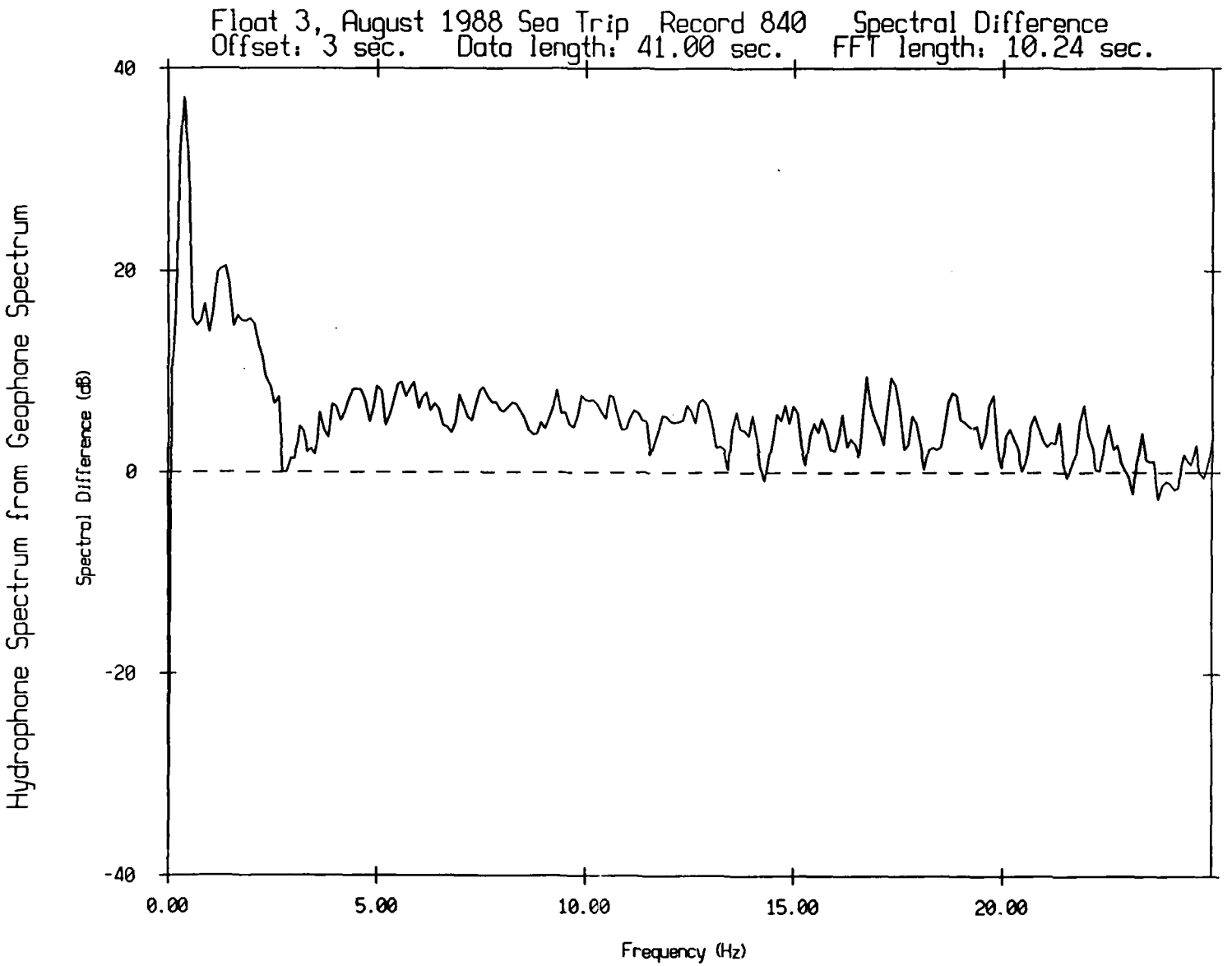


Figure XII.37b

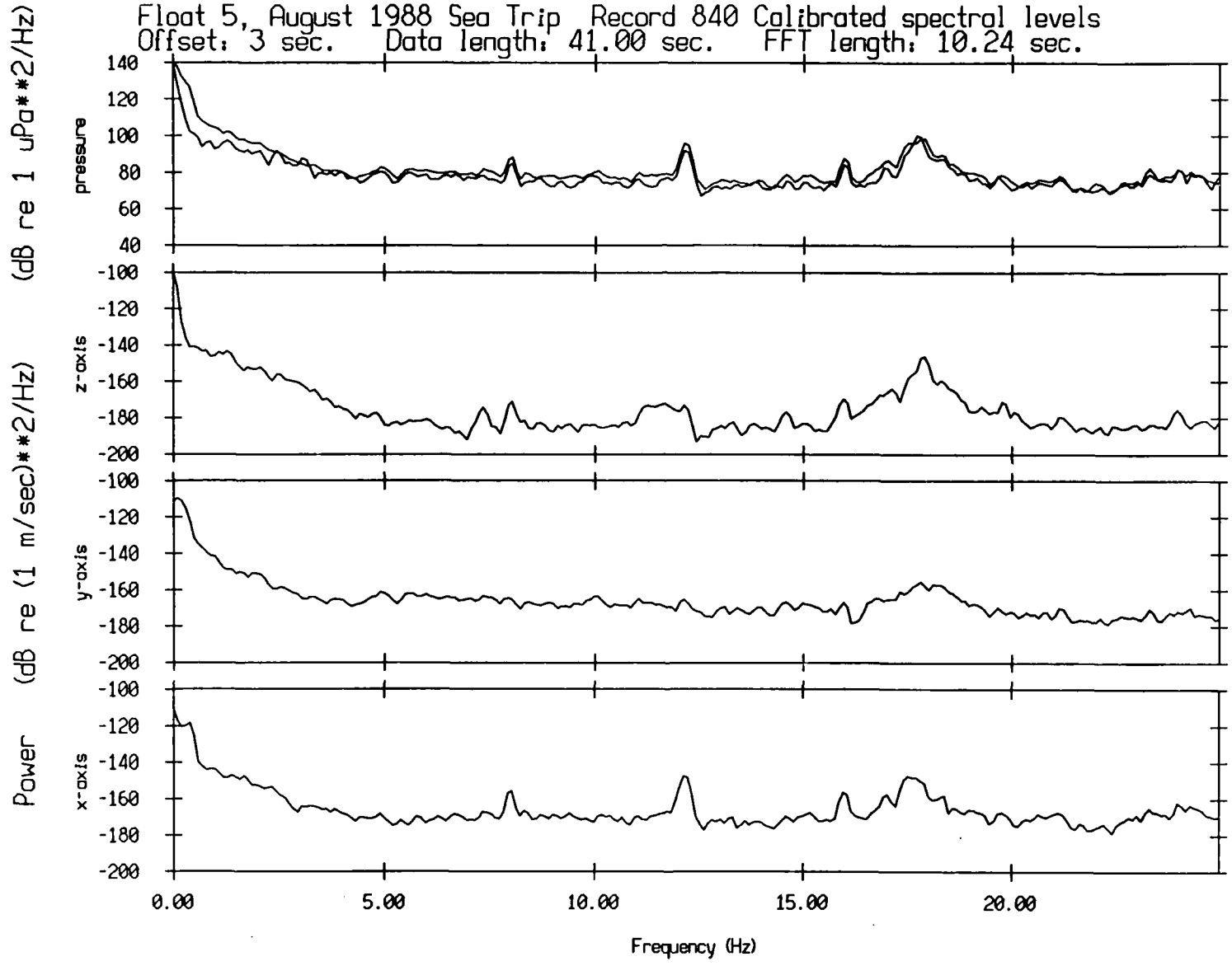


Figure XII.38a

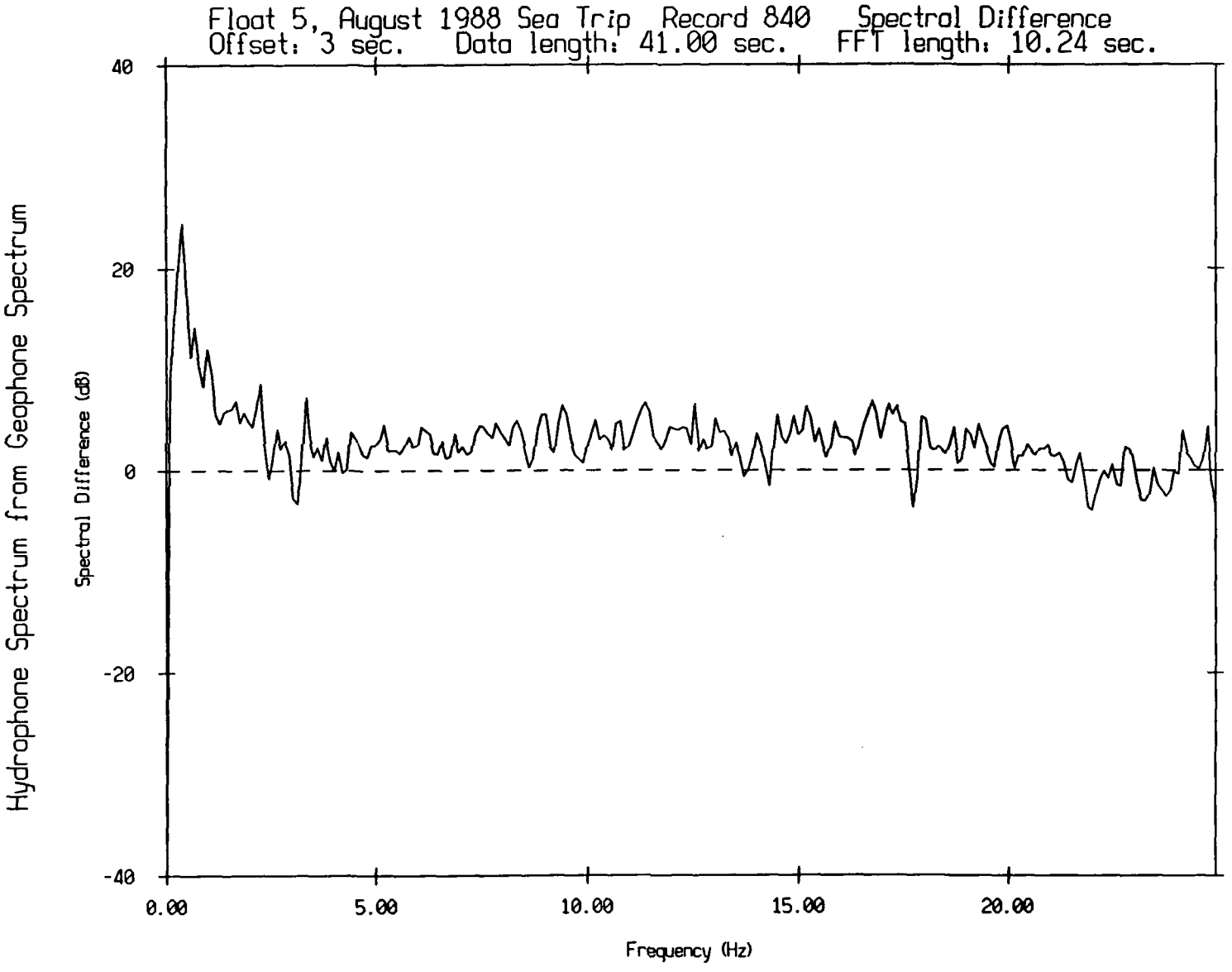


Figure XII.38b

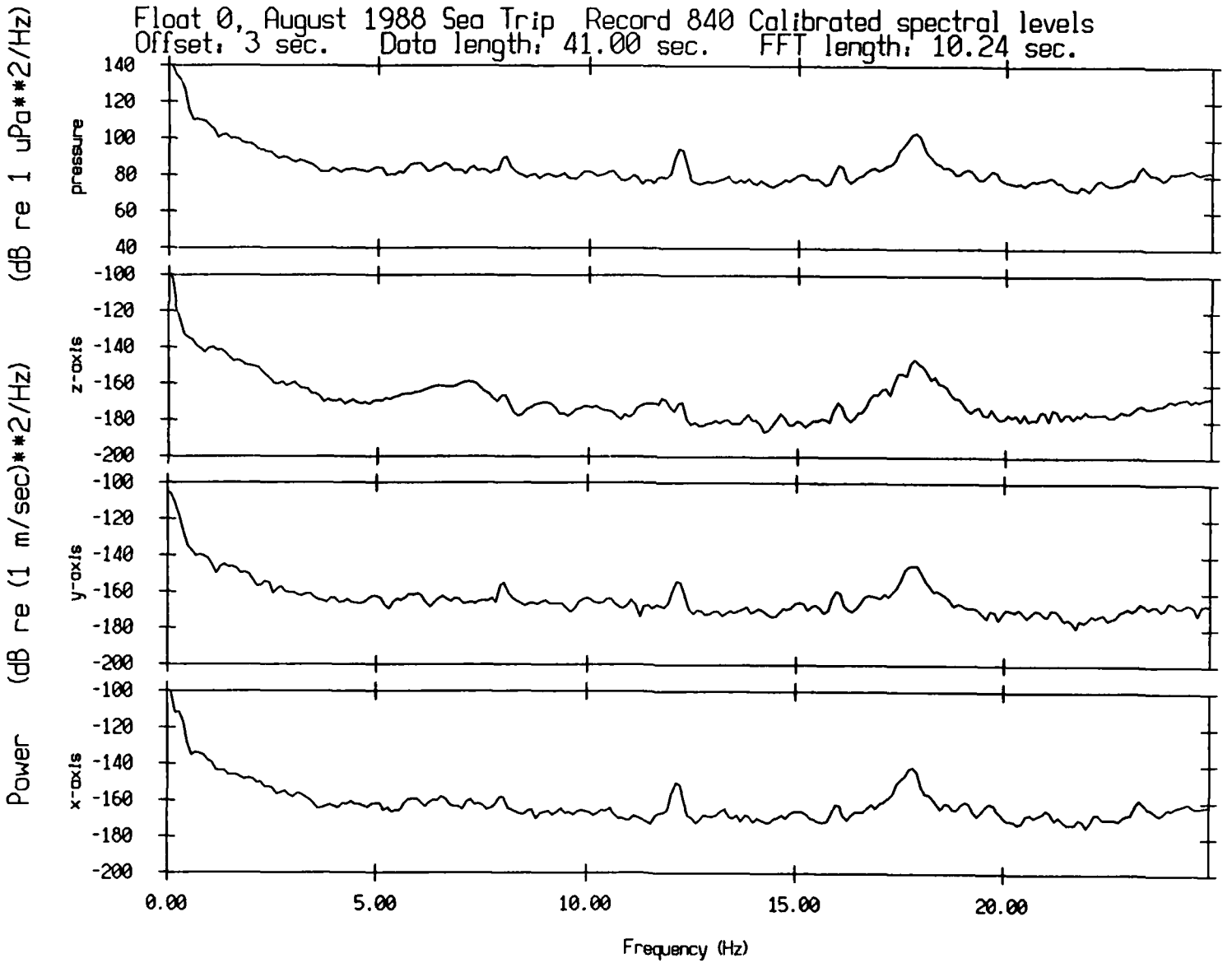


Figure XII.39

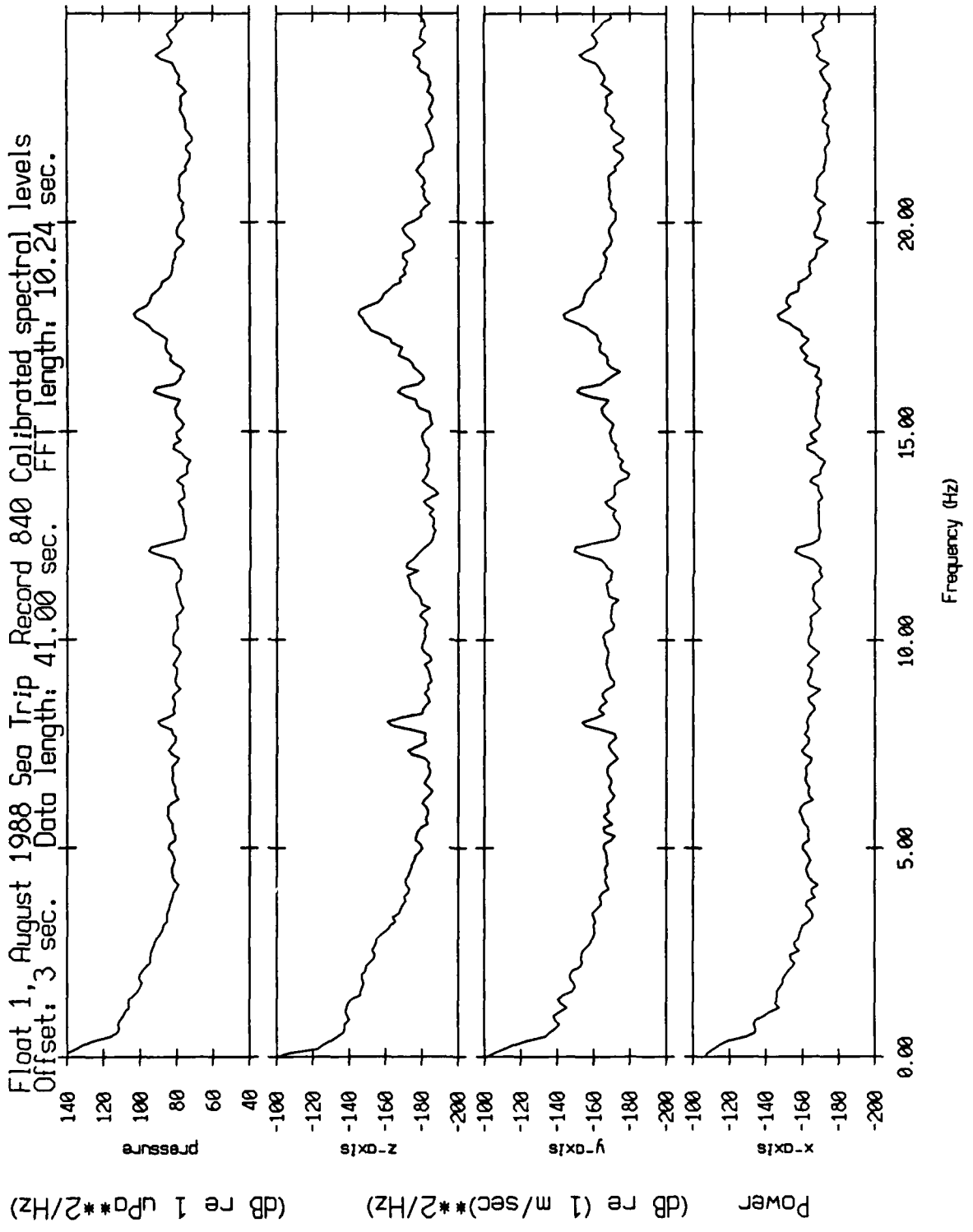


Figure XII.40

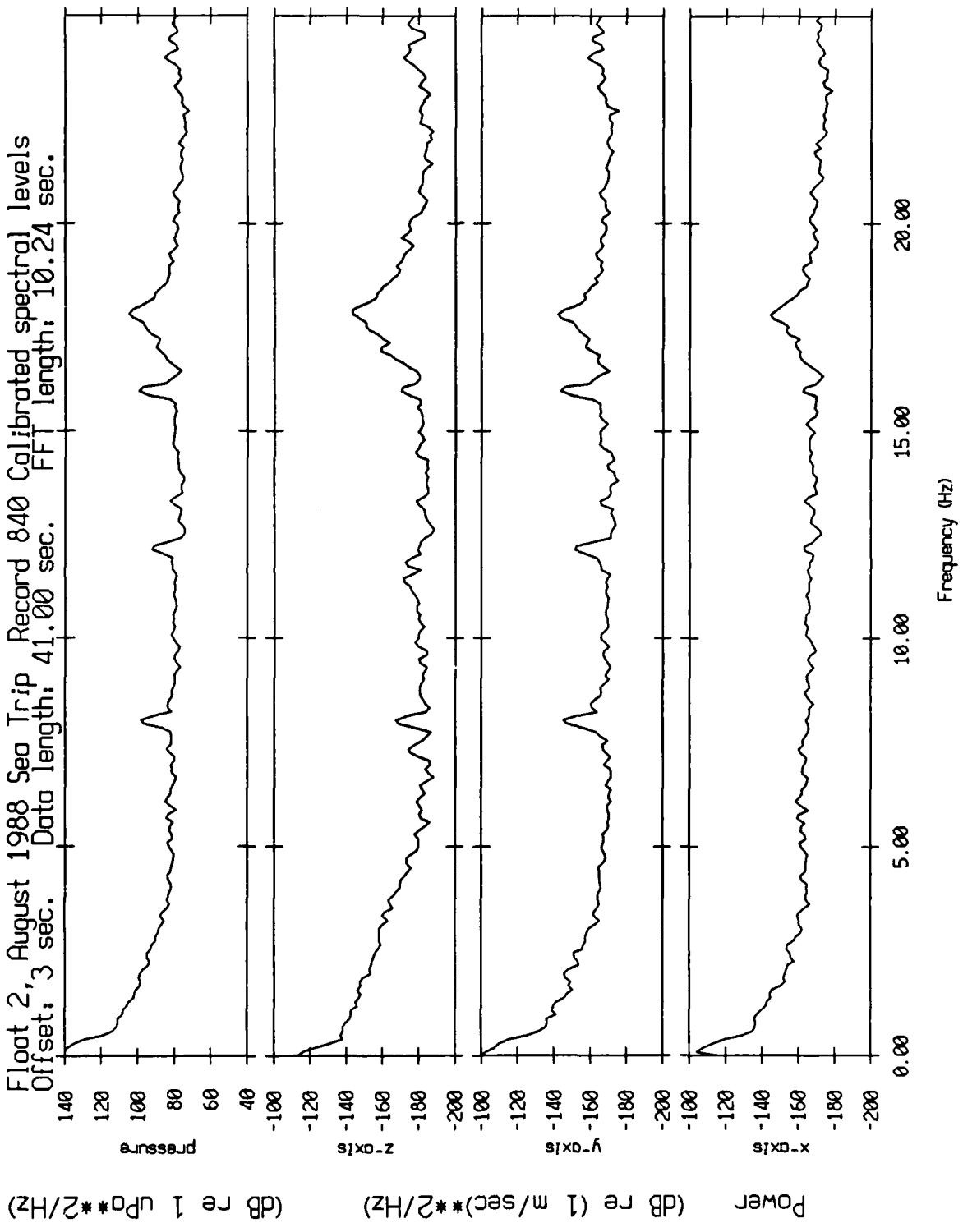


Figure XII.41

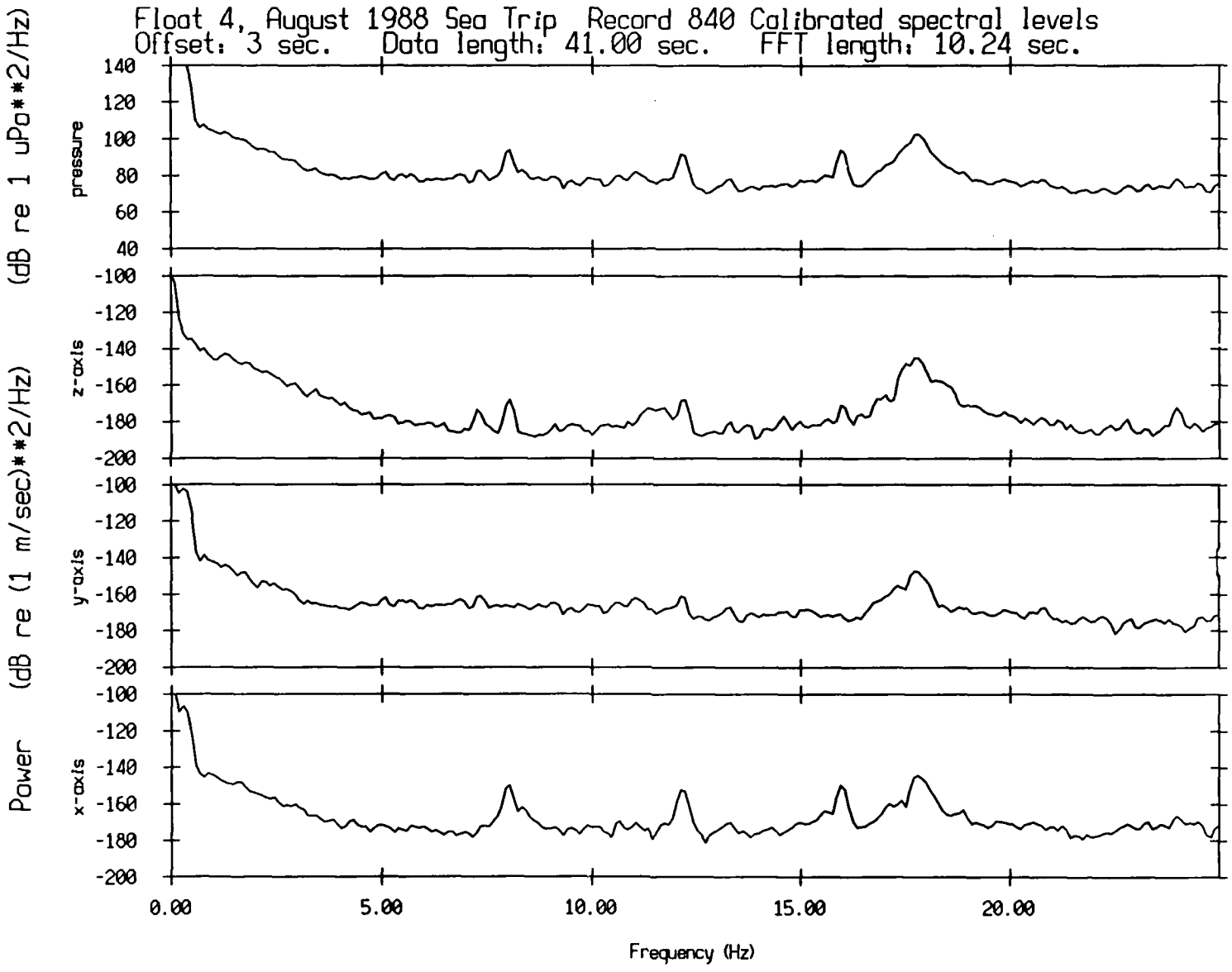


Figure XII.12

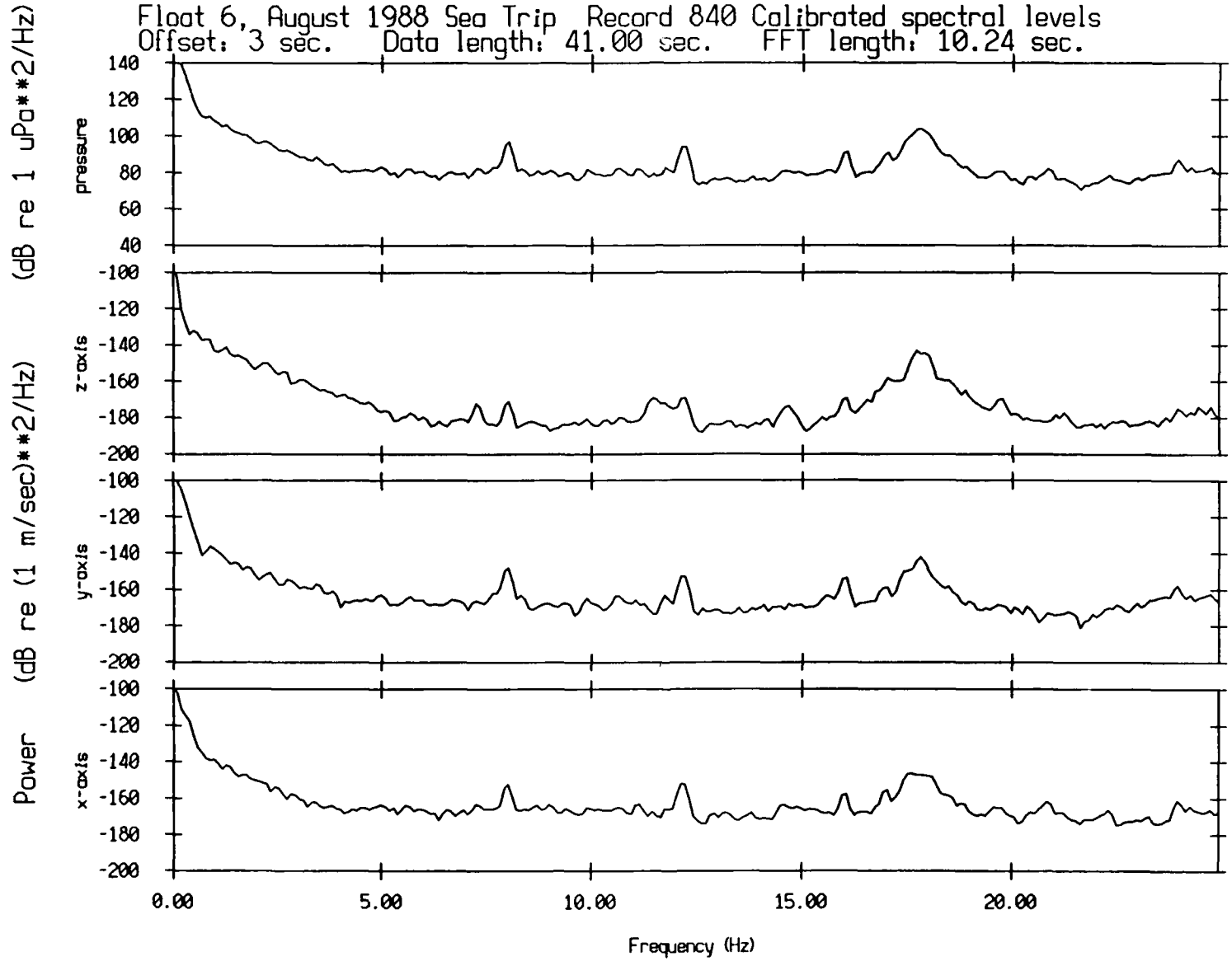


Figure XII.13

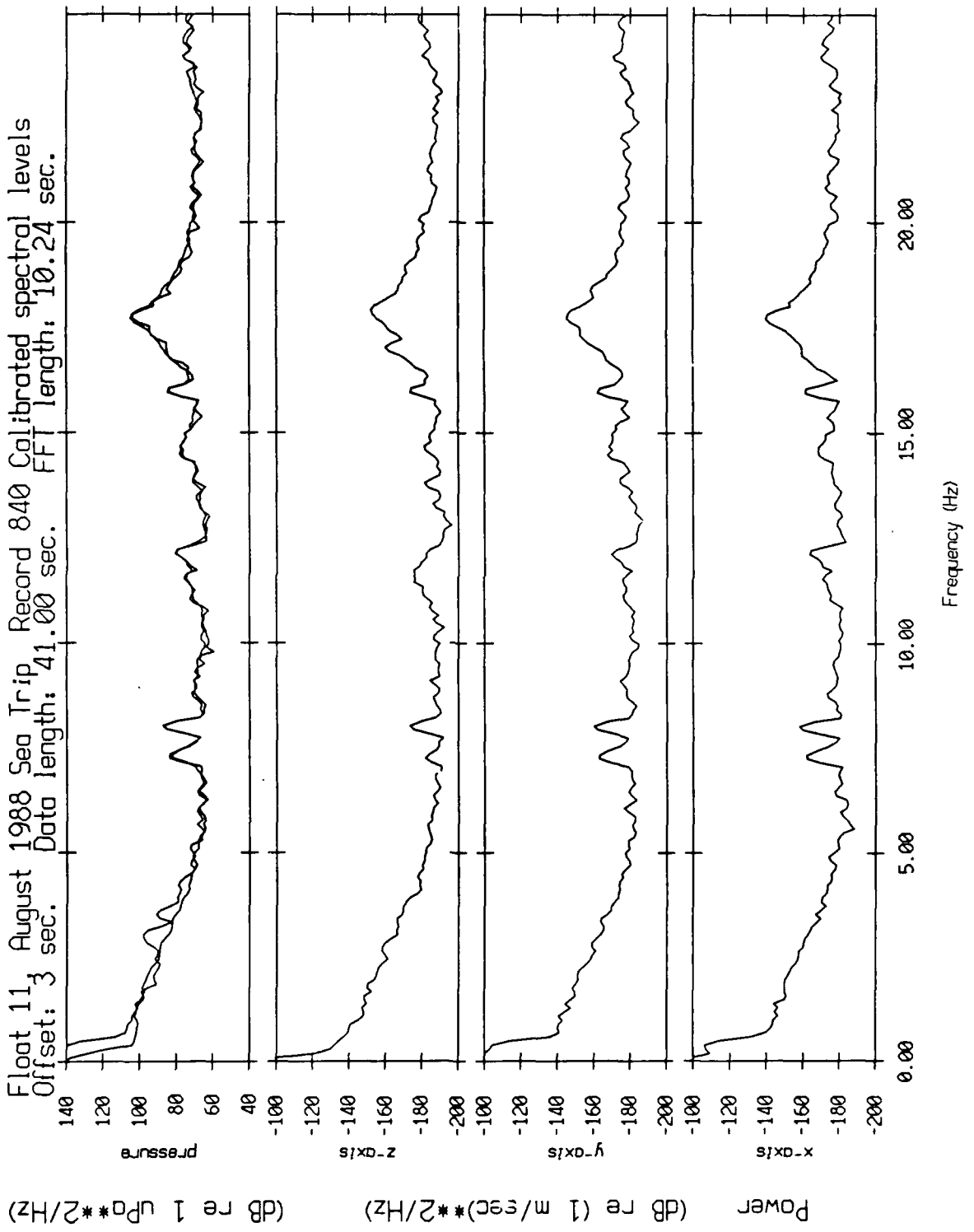


Figure XII.44a

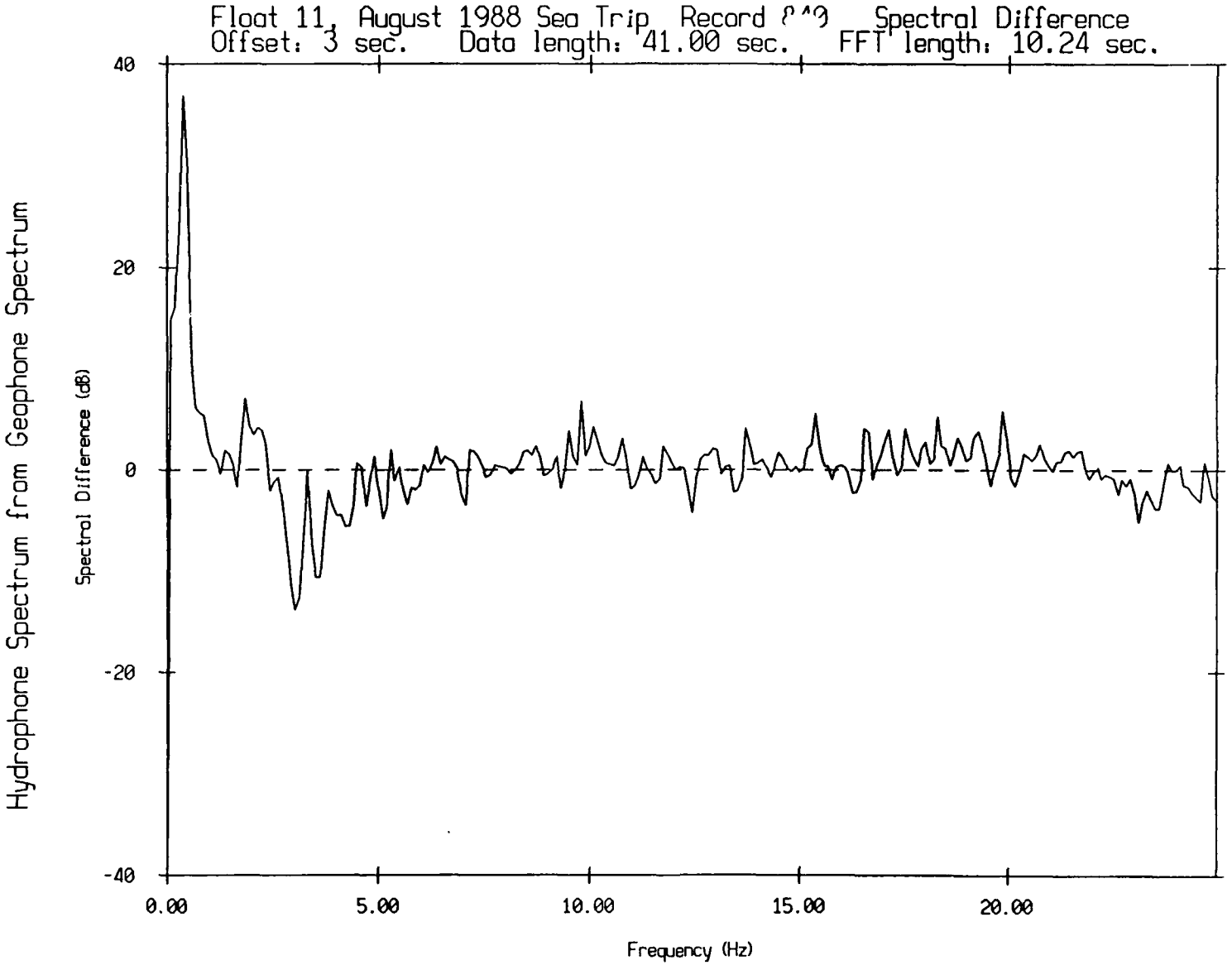


Figure XII.41b

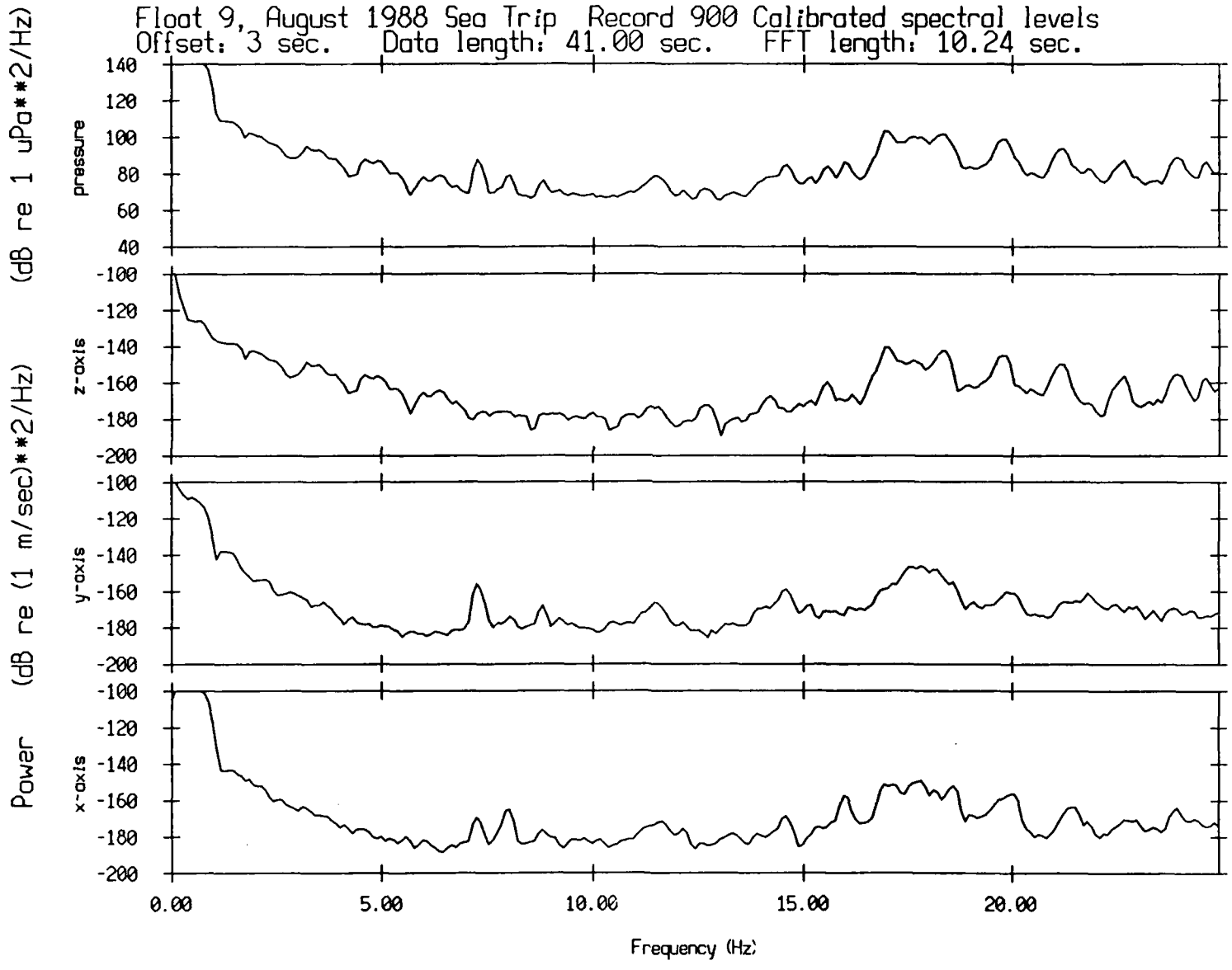


Figure XII.45

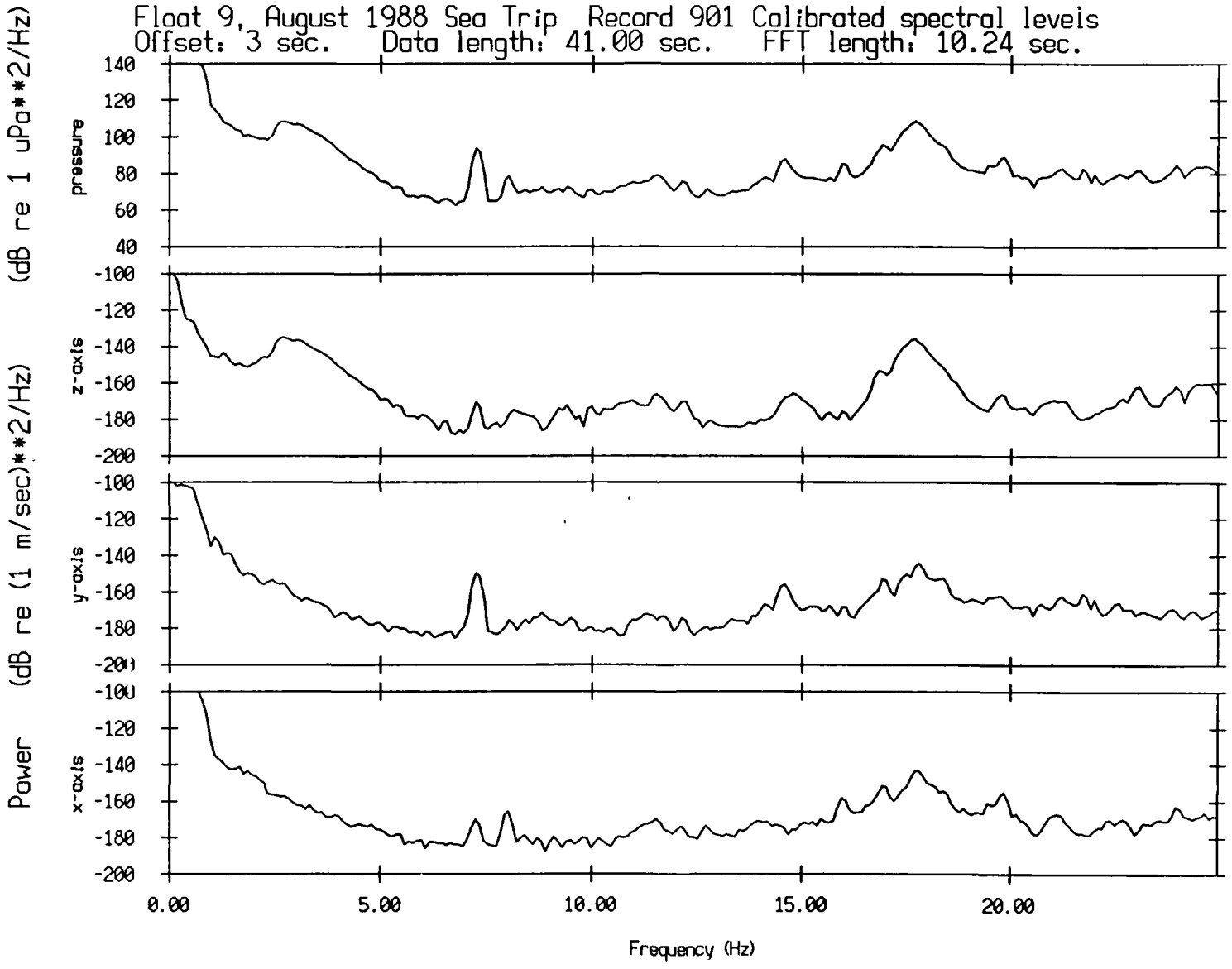


Figure XII.46

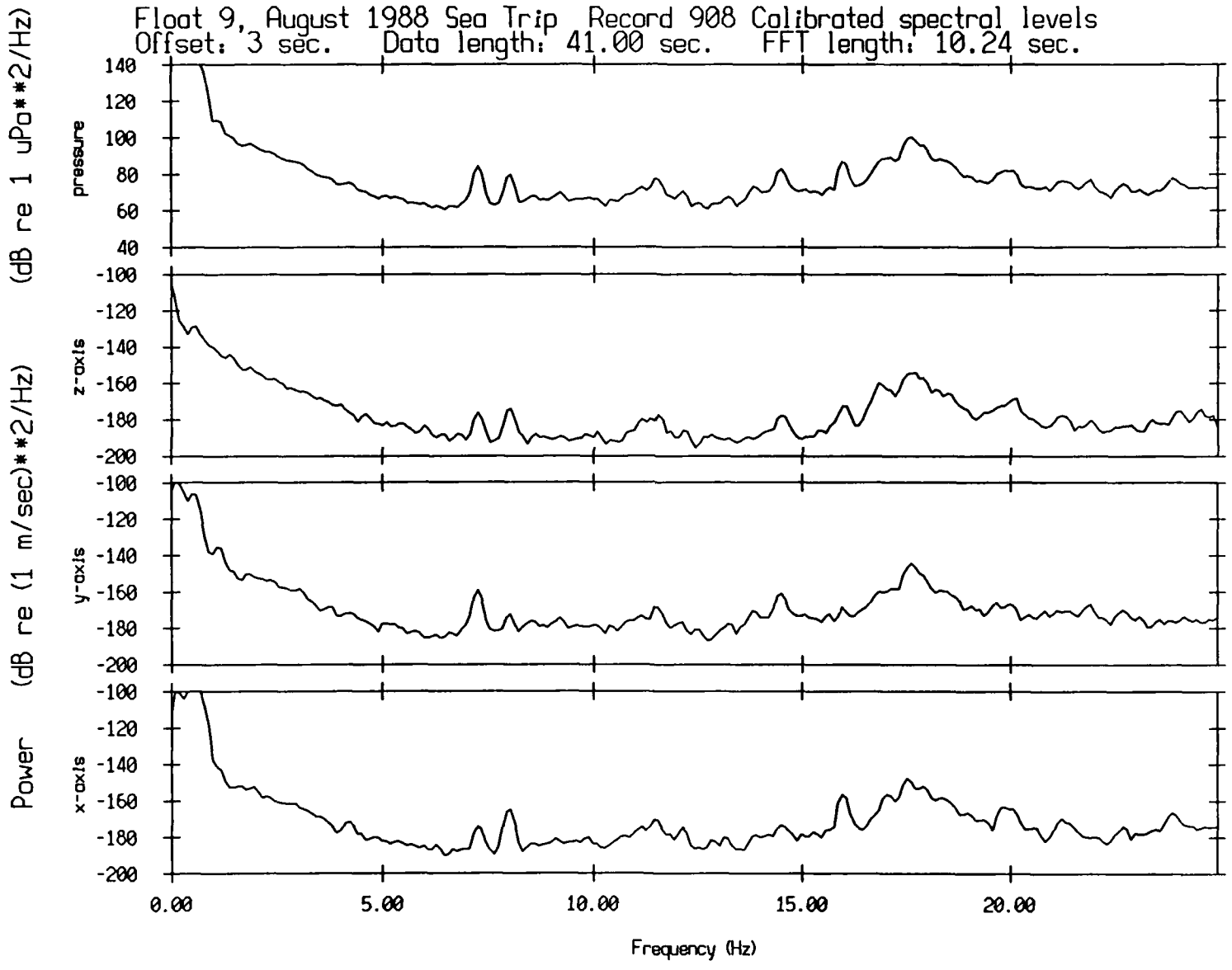


Figure XII.17

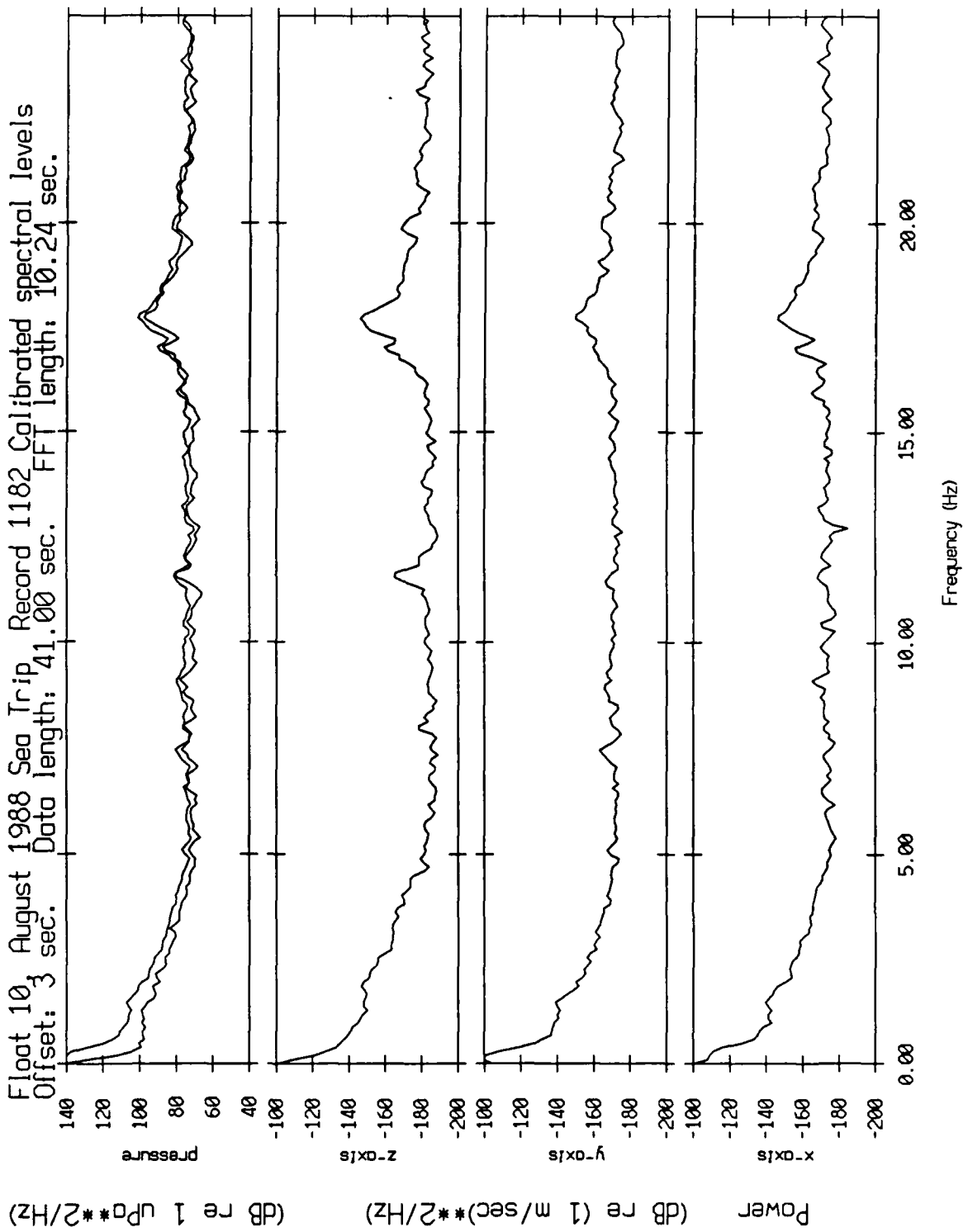


Figure XII.48a

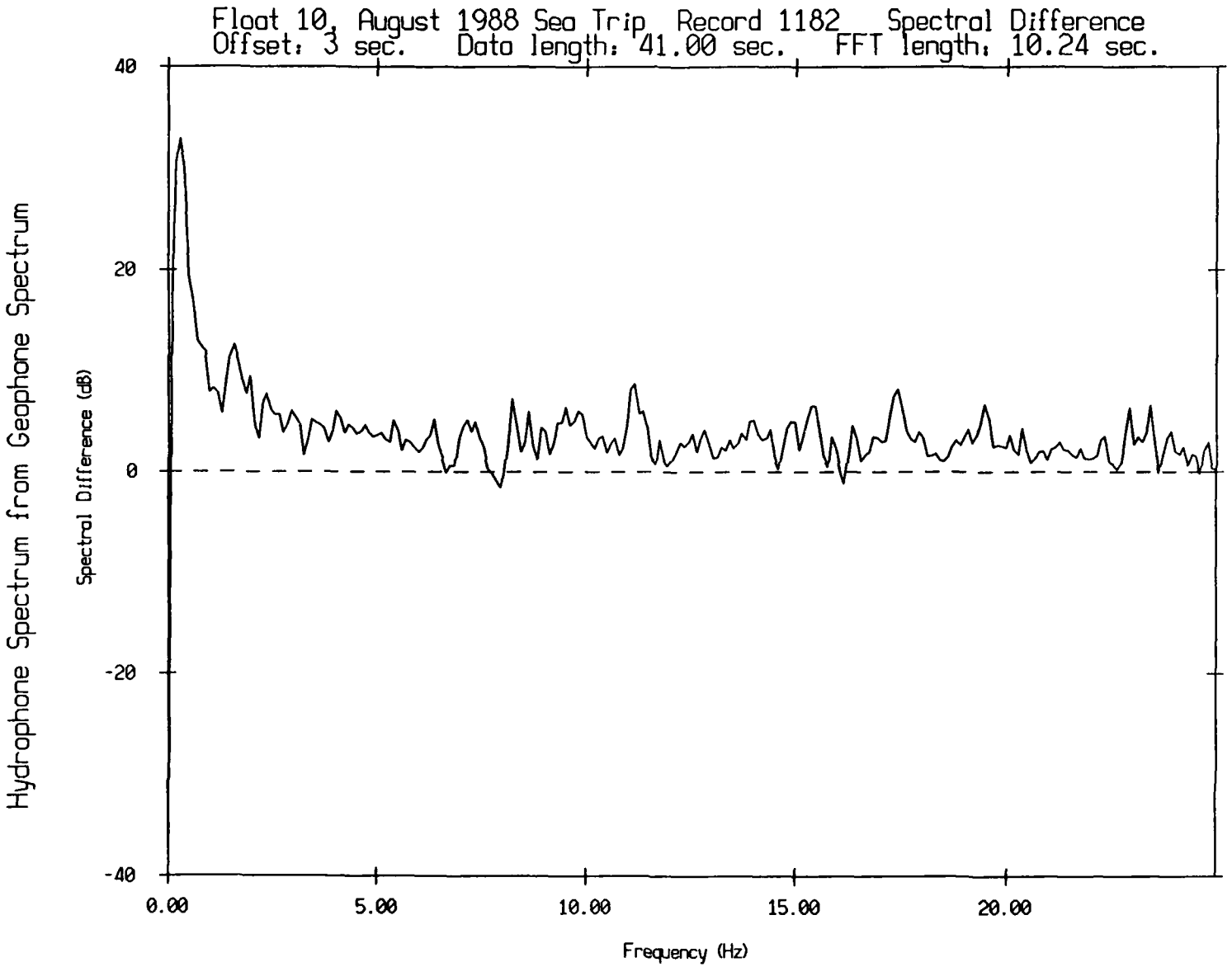


Figure XII.48b

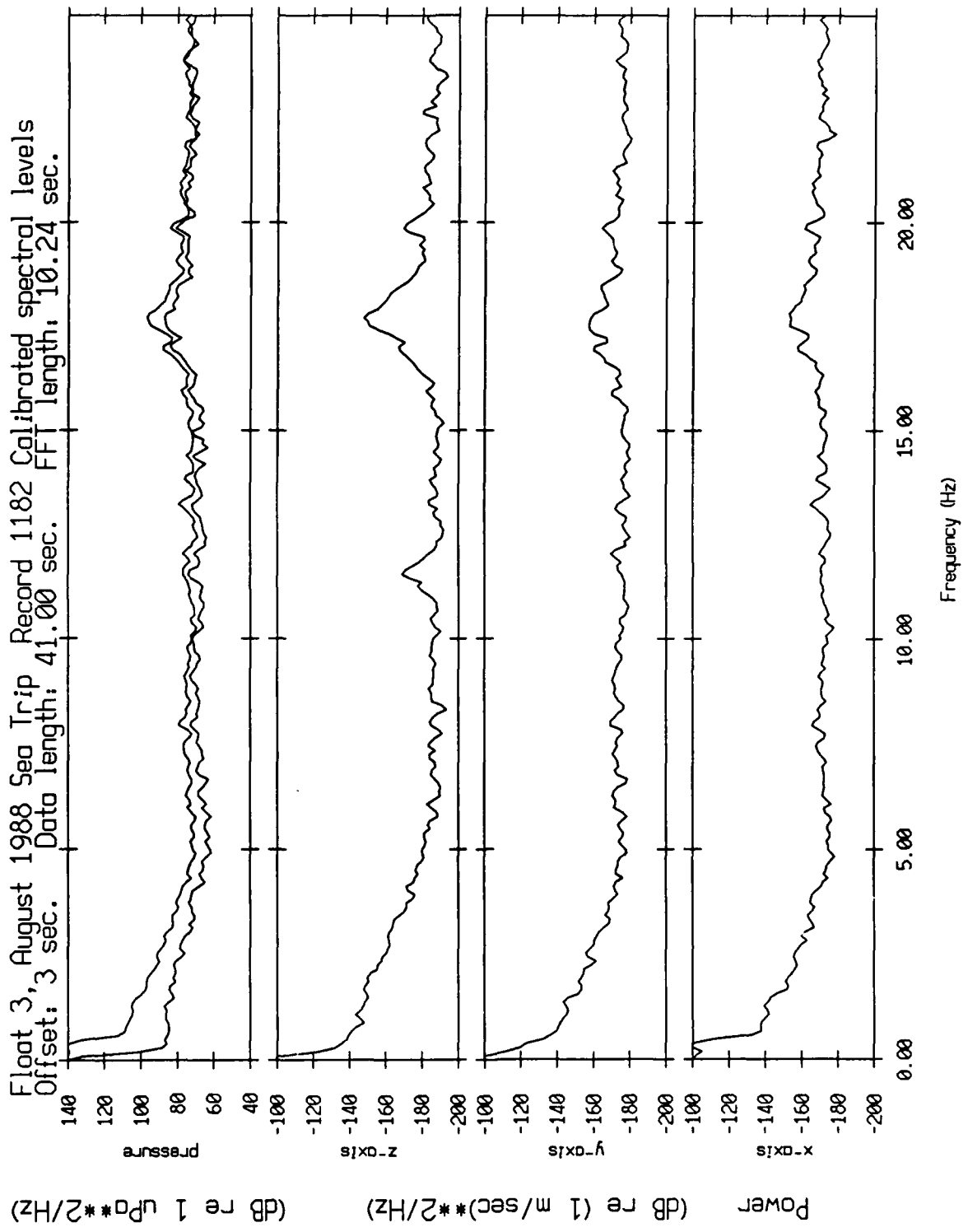


Figure XII.49a

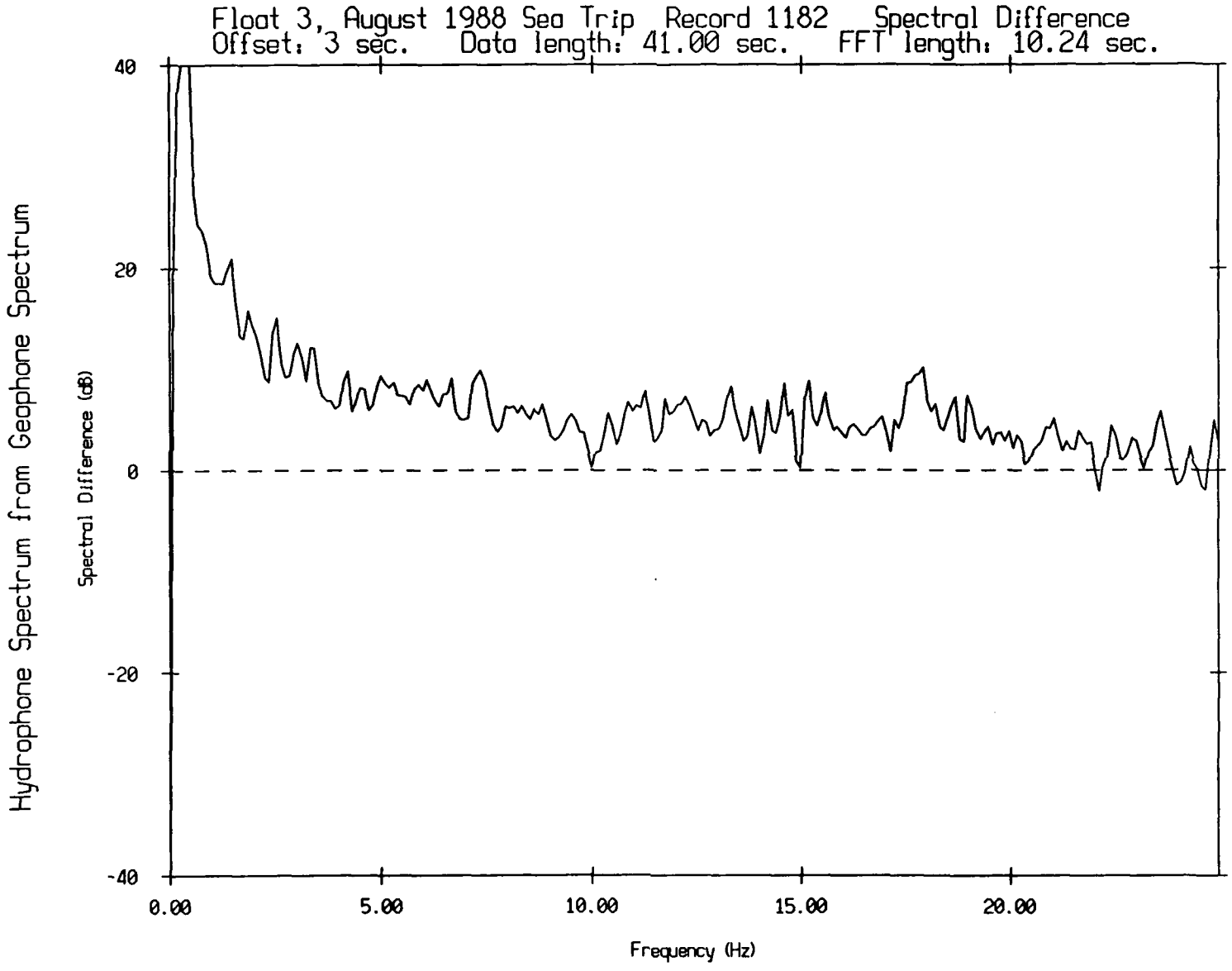


Figure XII 49b

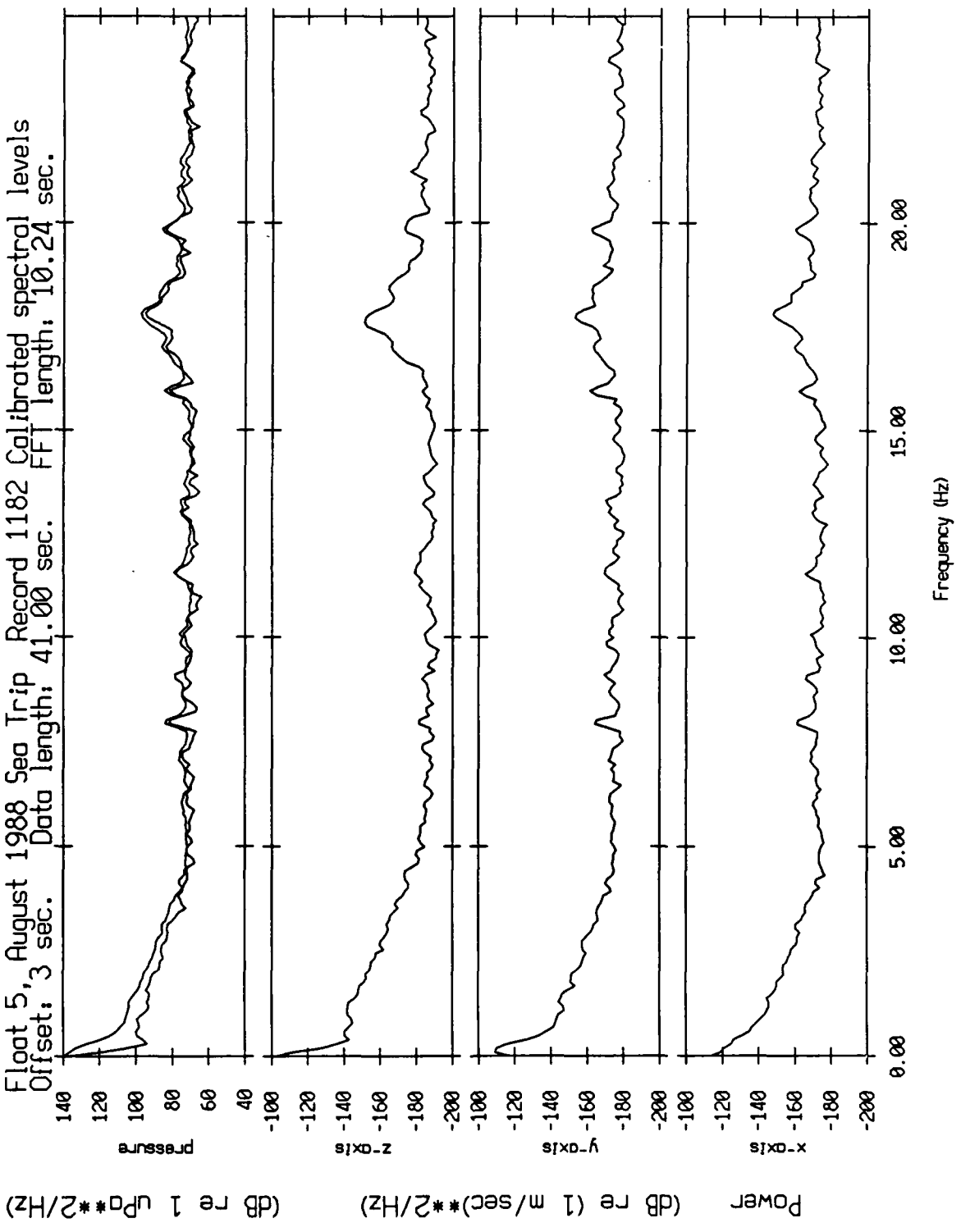


Figure XII.50a

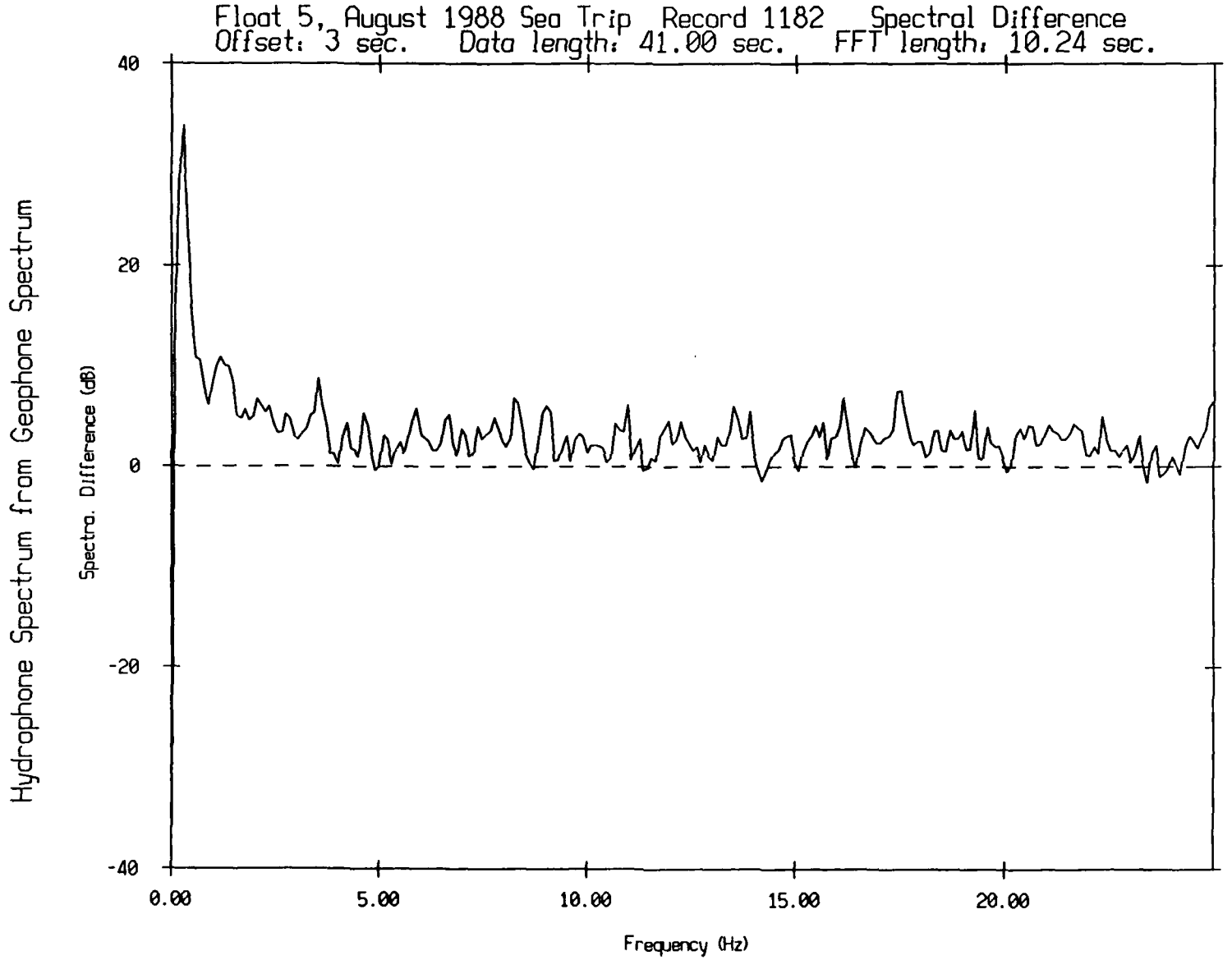


Figure XII.50b

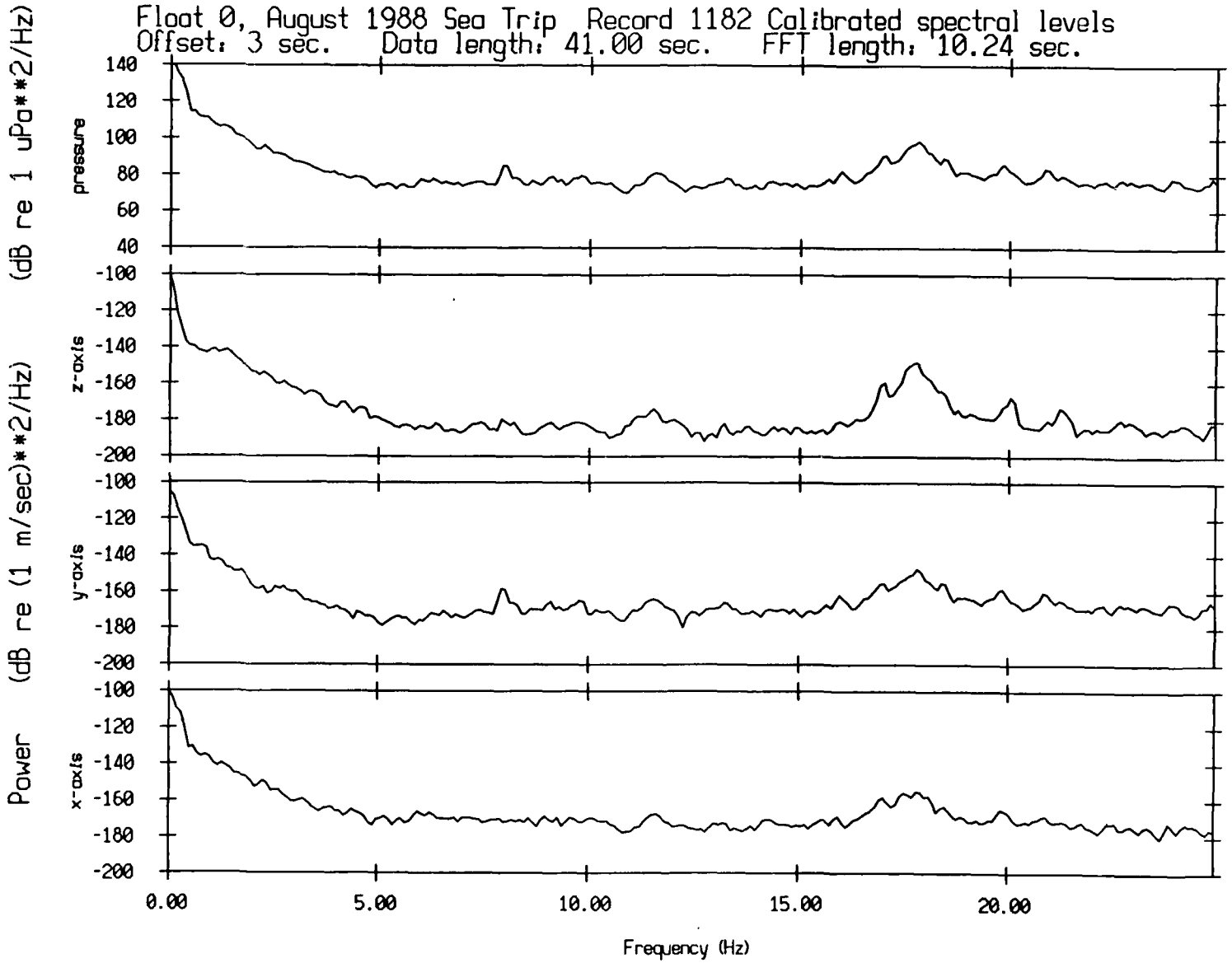


Figure XII.51

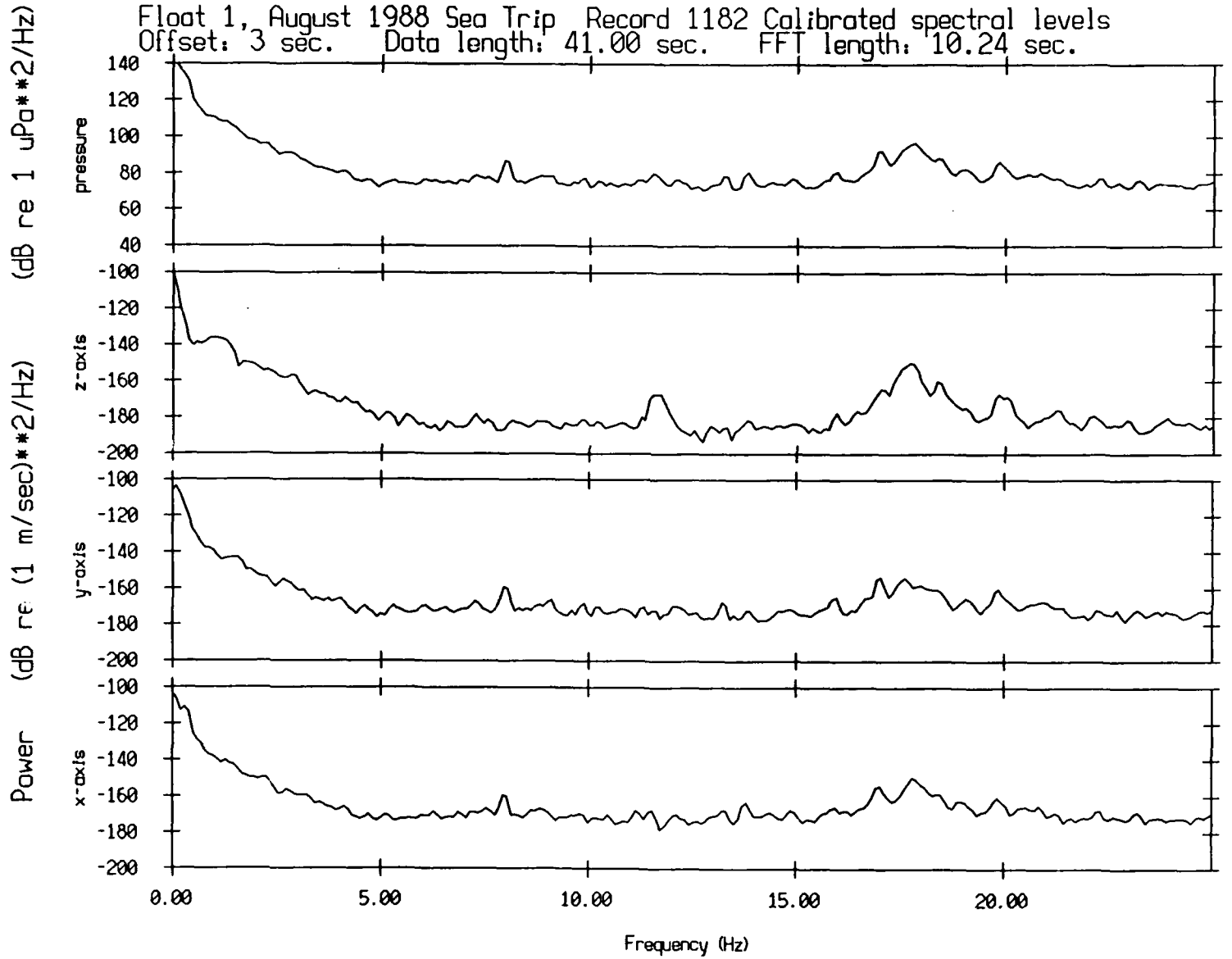


Figure XII.52

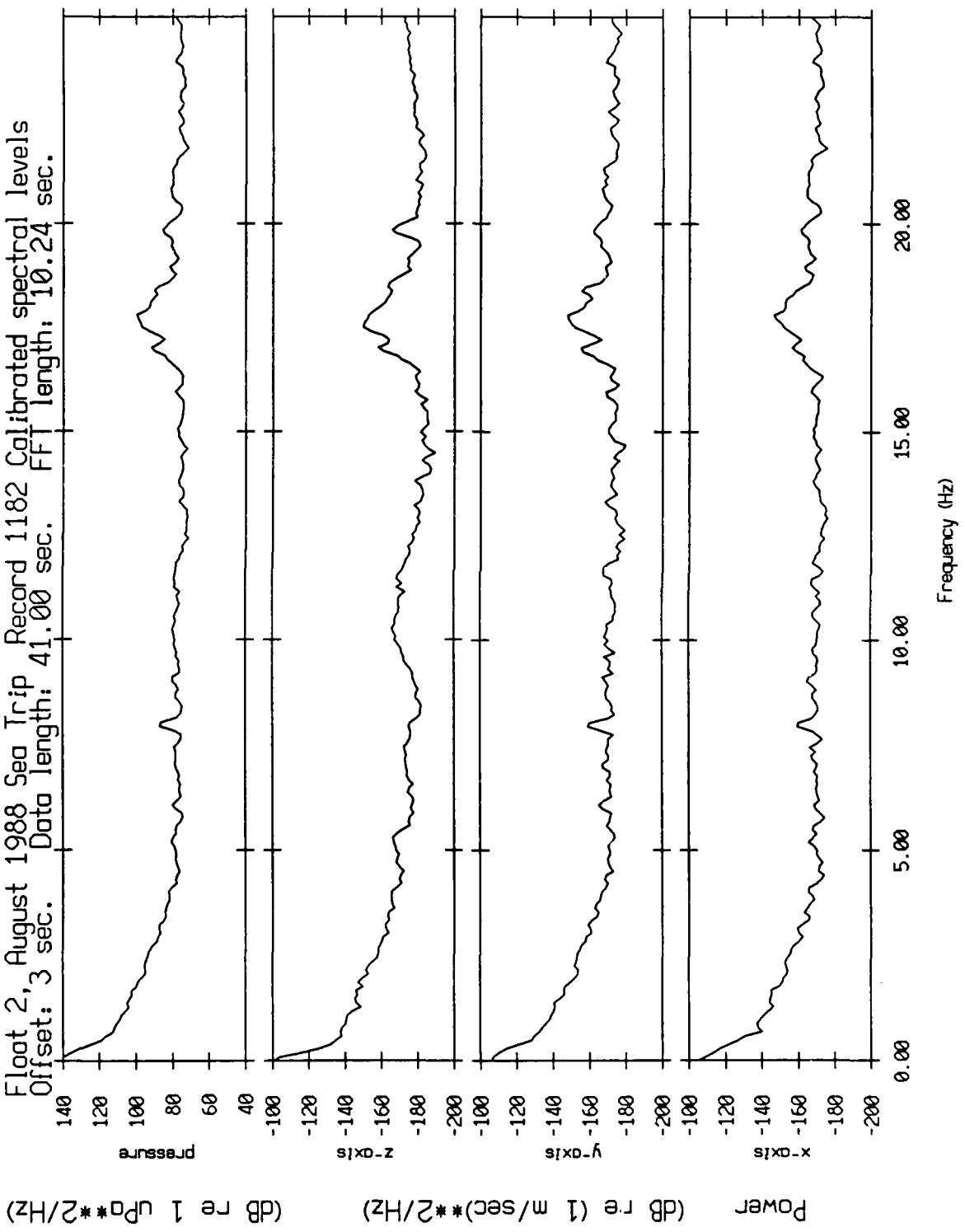


Figure XII.53

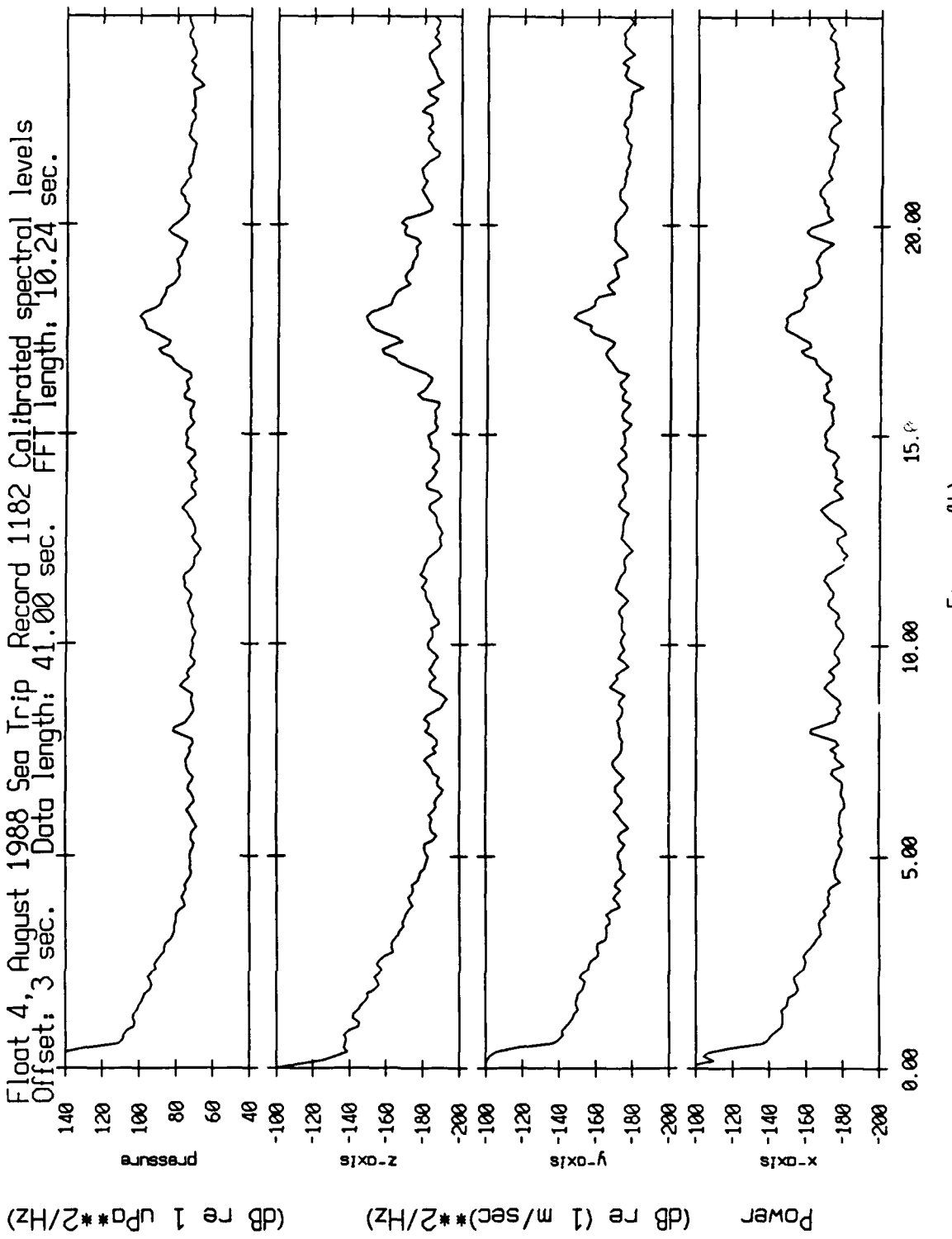


Figure XII.54

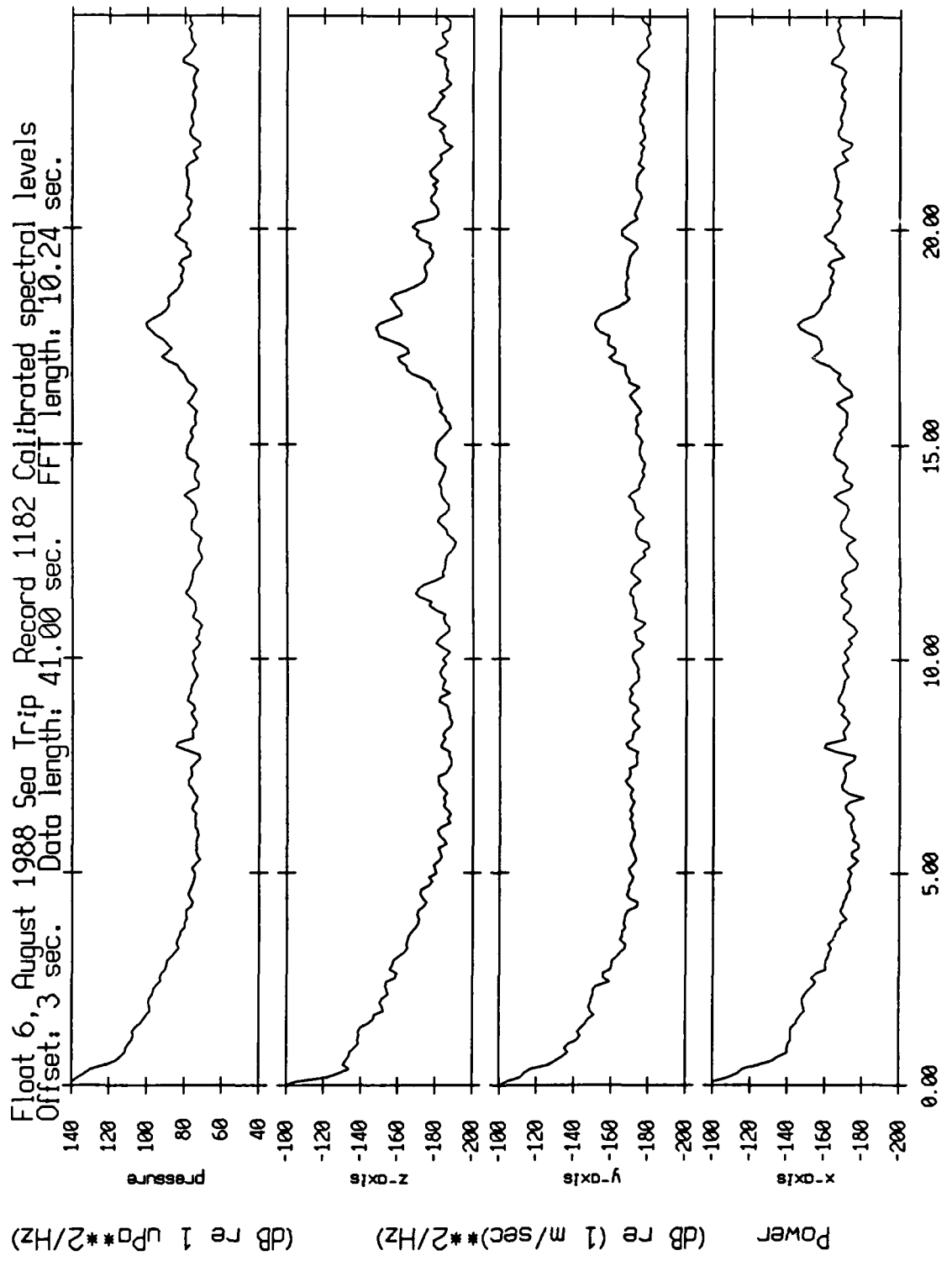


Figure XII.55

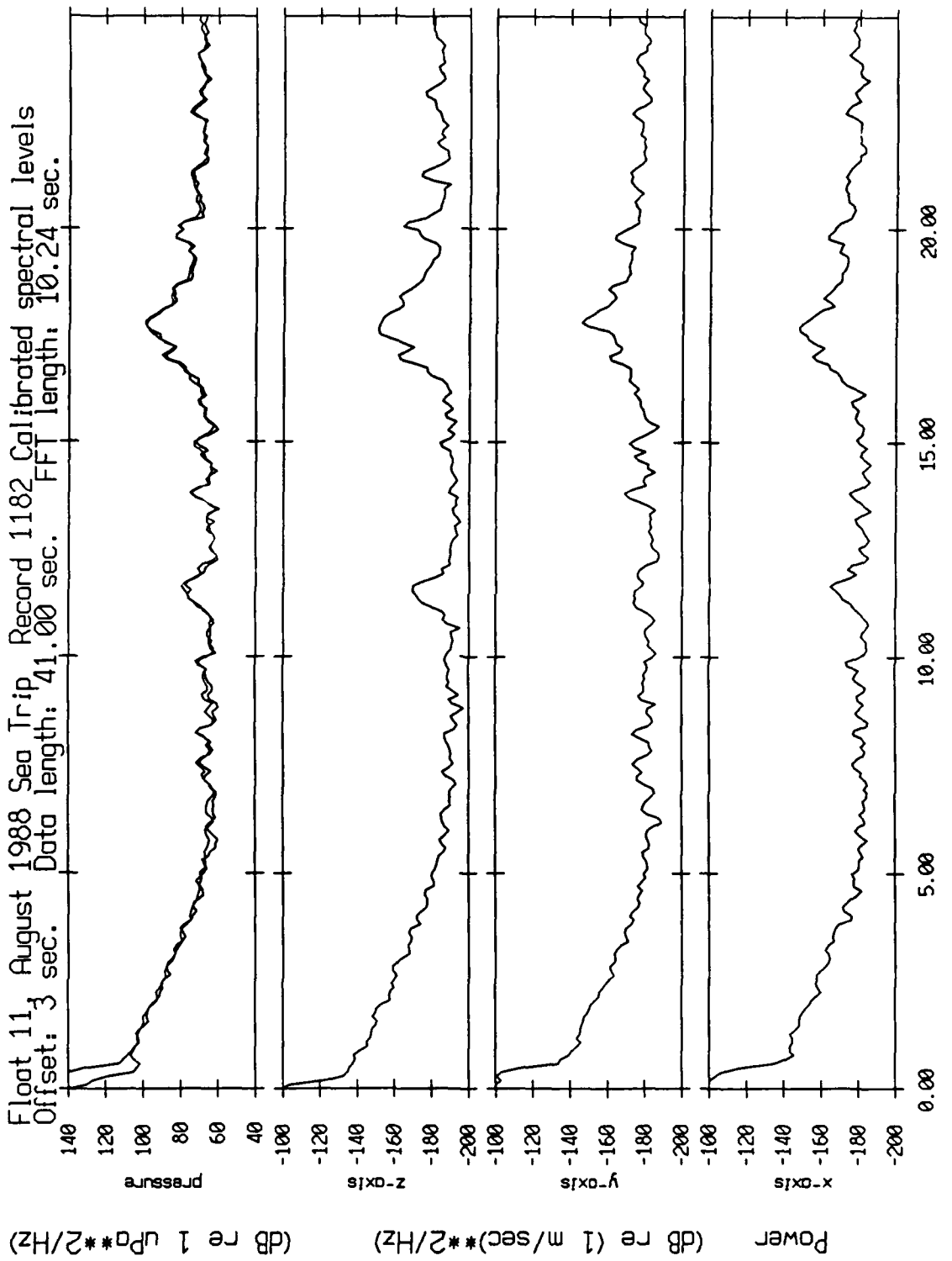


Figure XII.56a

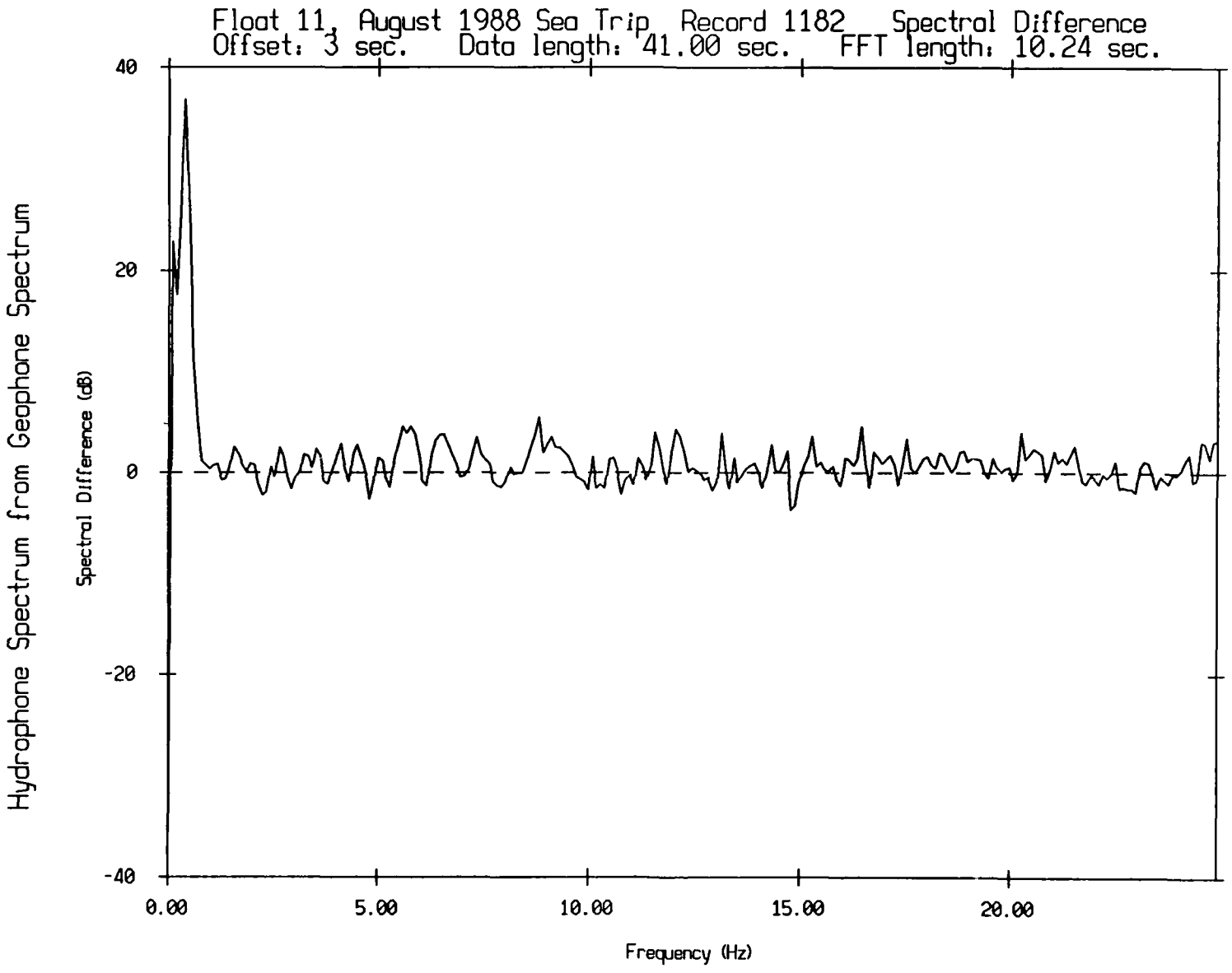


Figure XII.56b

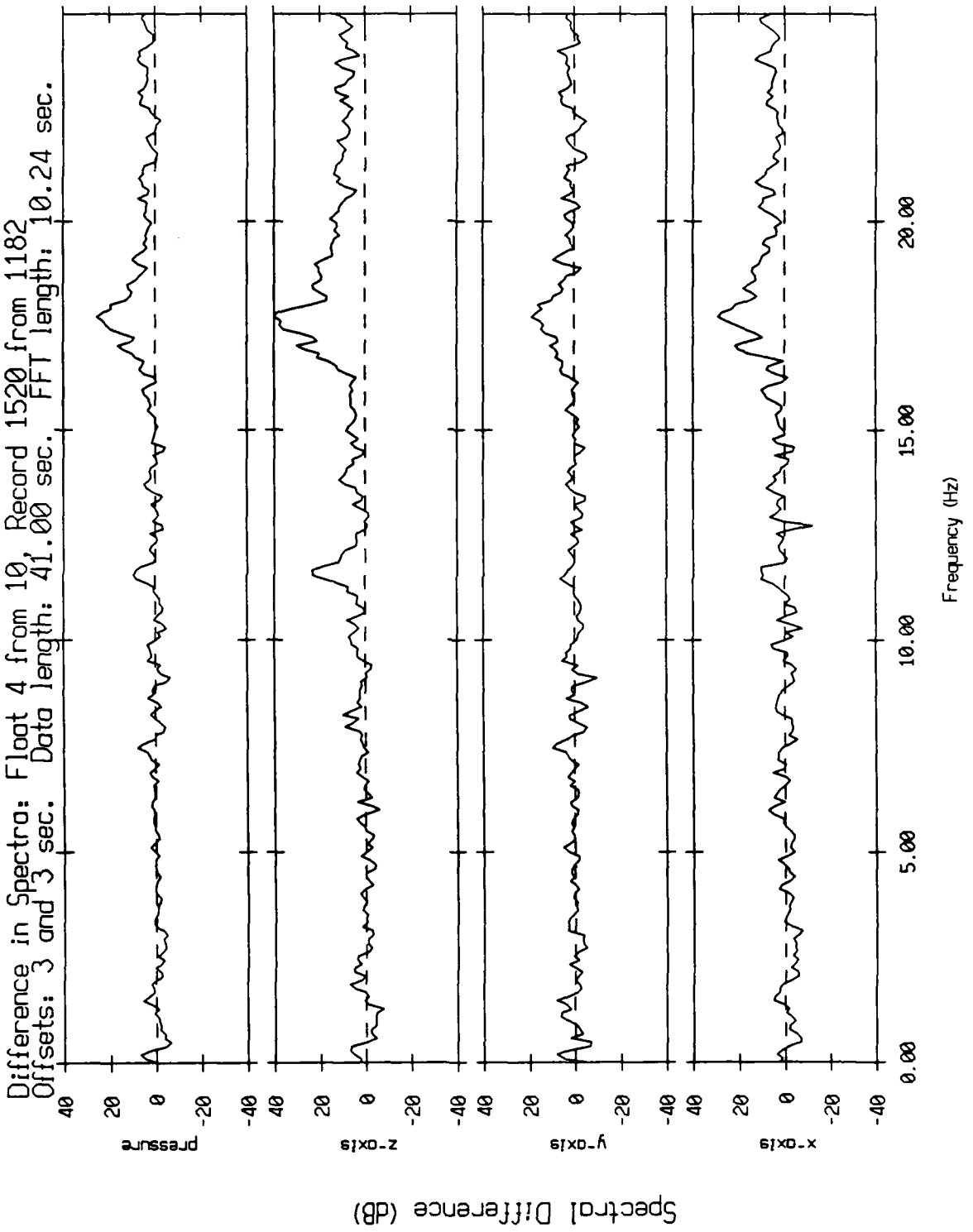


Figure XII.57

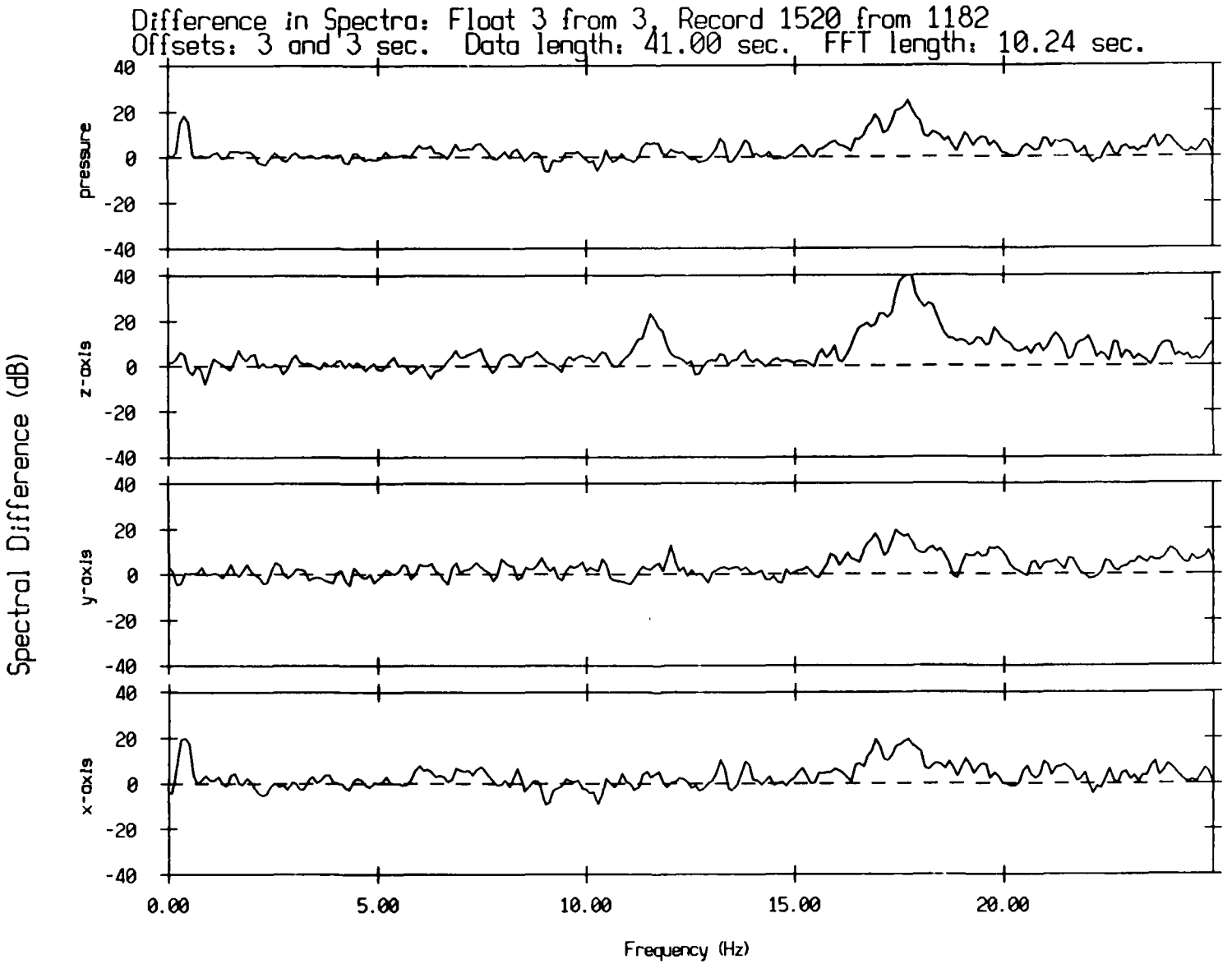


Figure XII.58

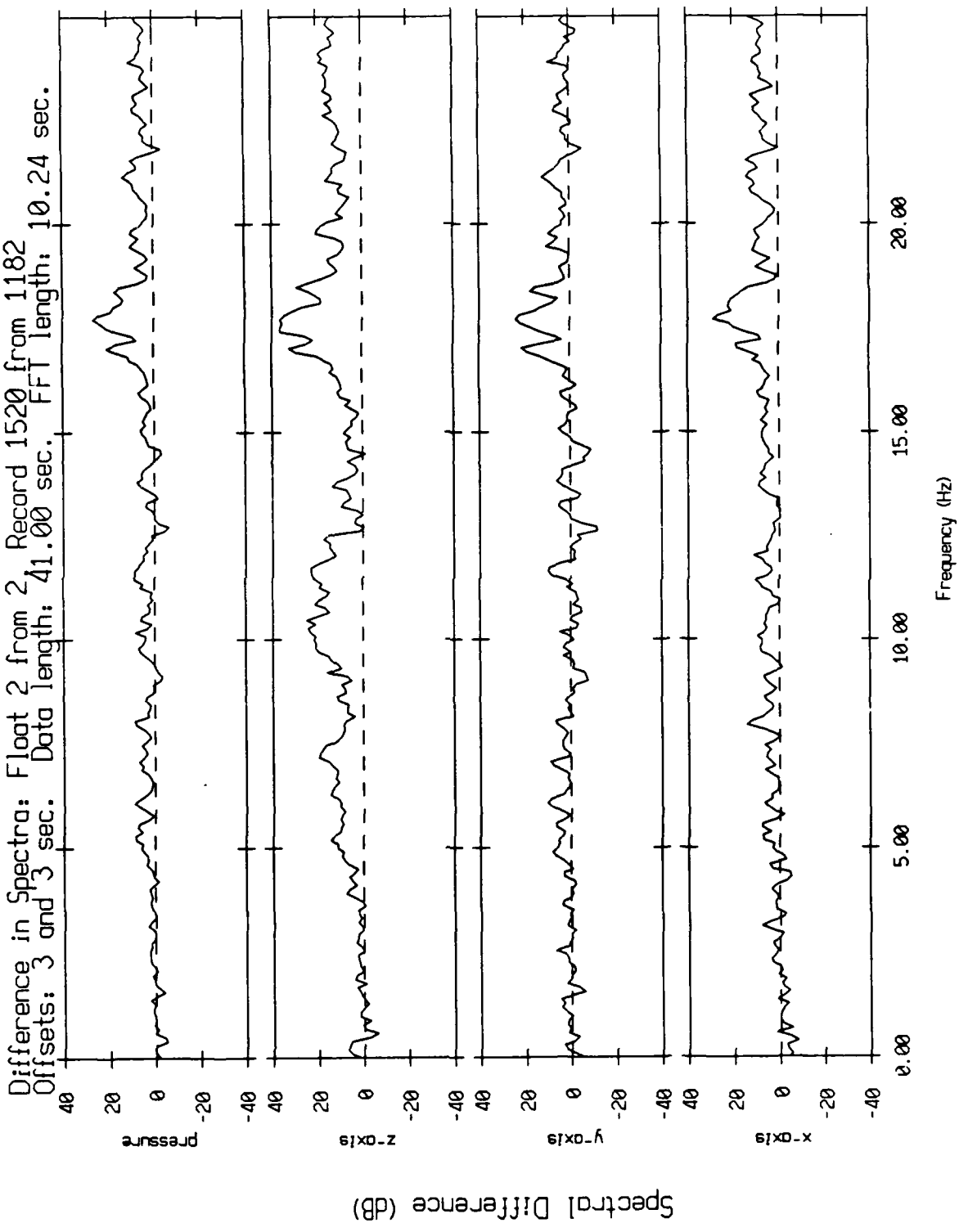


Figure XII.59

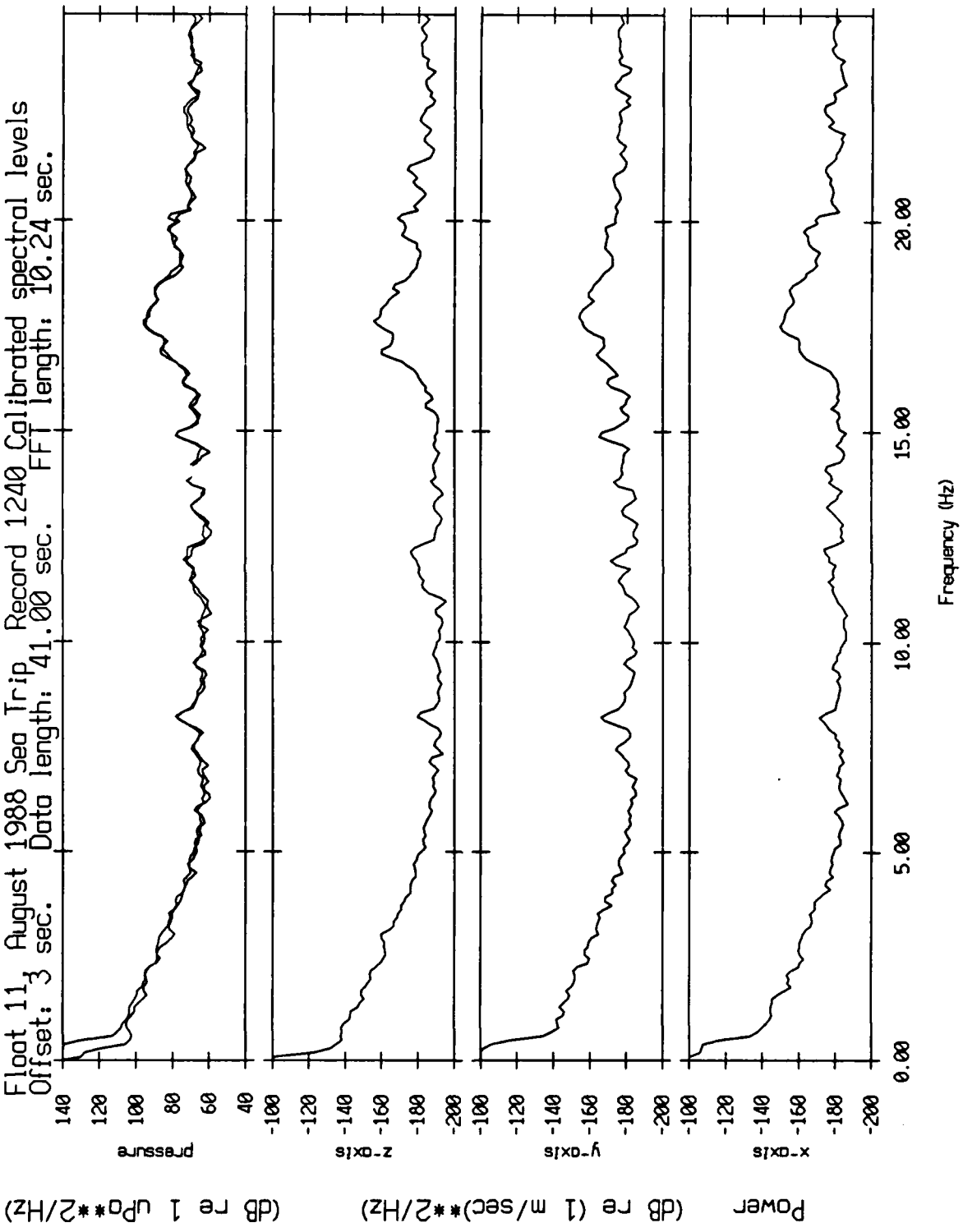


Figure XII.60a

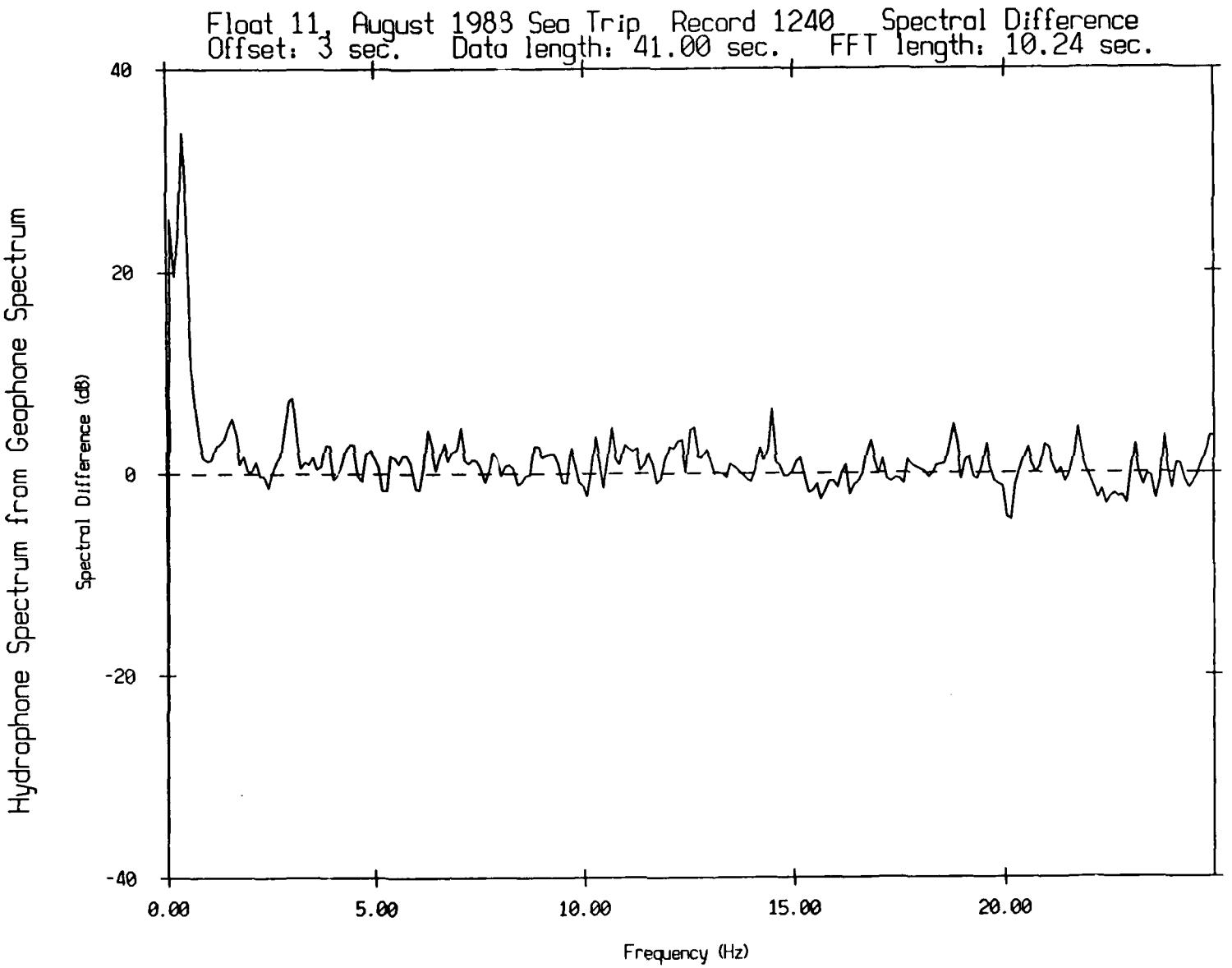


Figure XII.00b

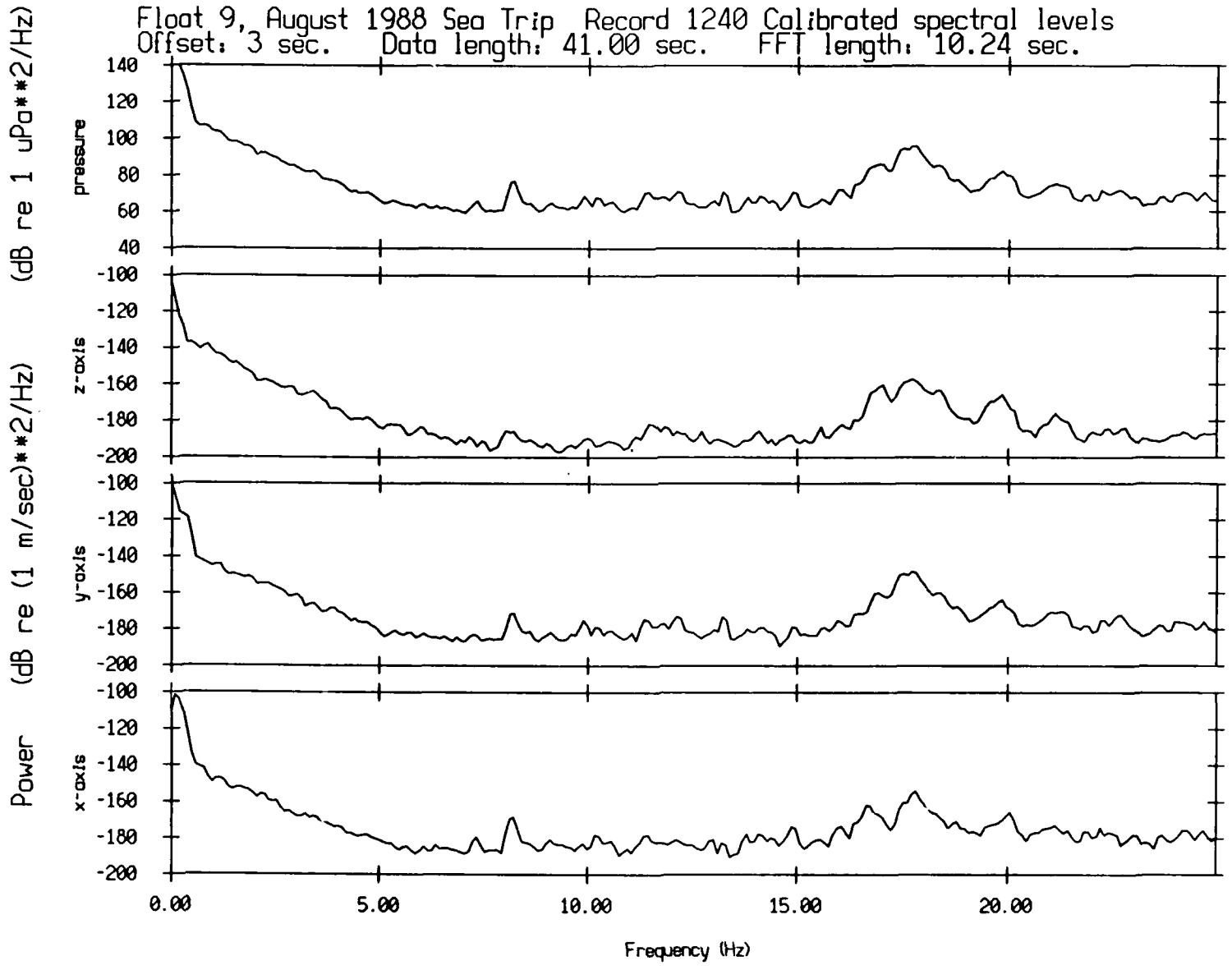


Figure XII.61

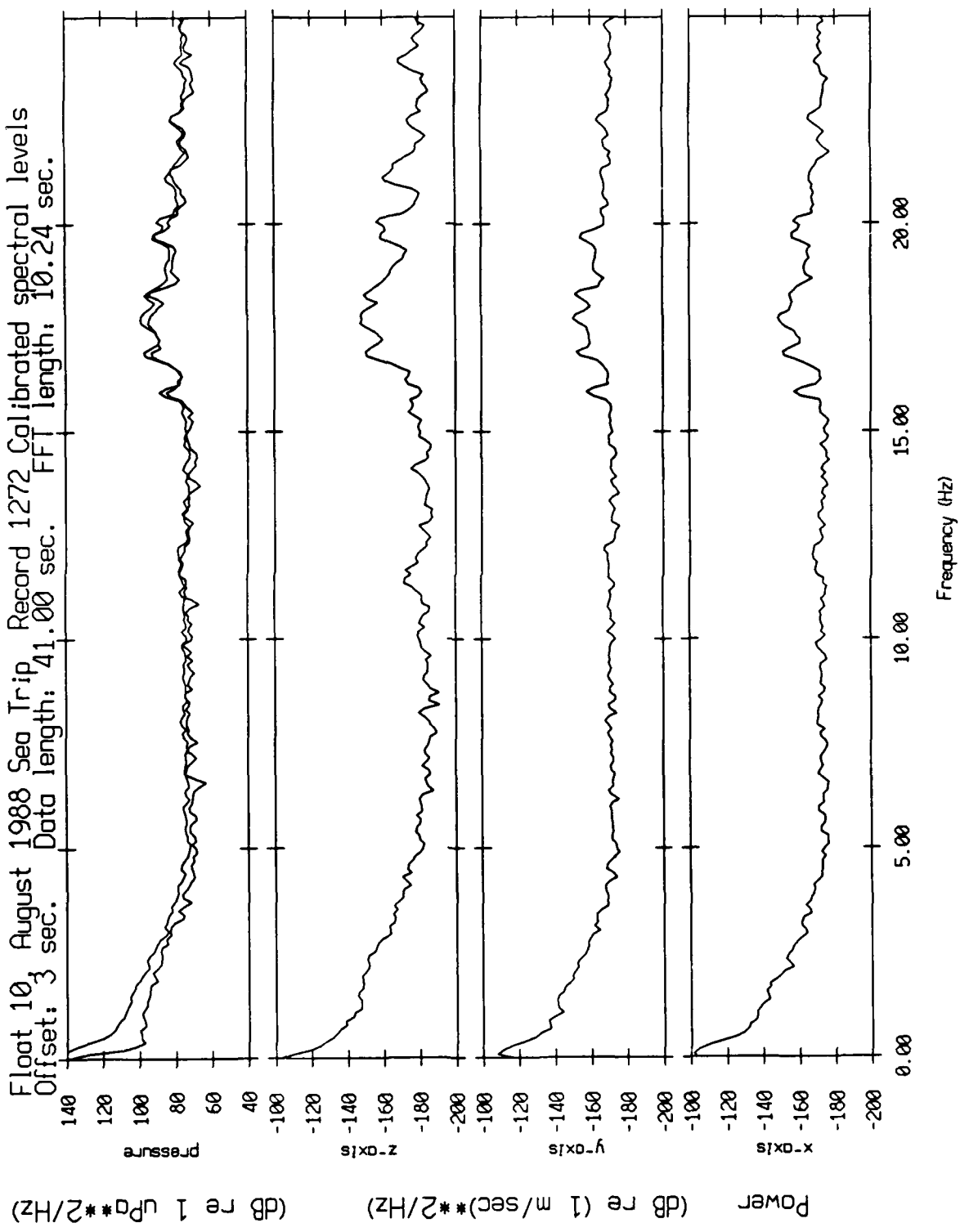


Figure XII.62a

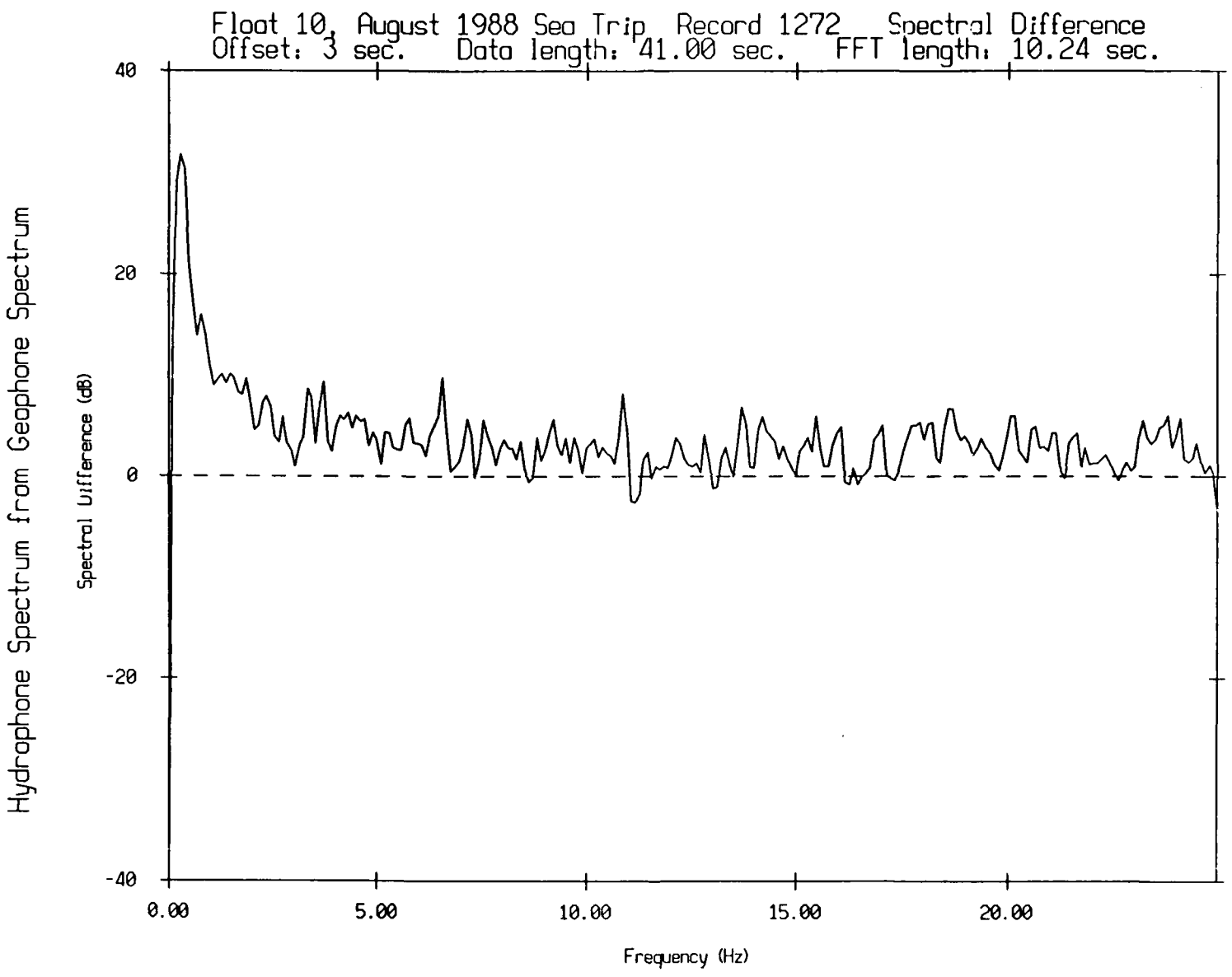


Figure XII.62b

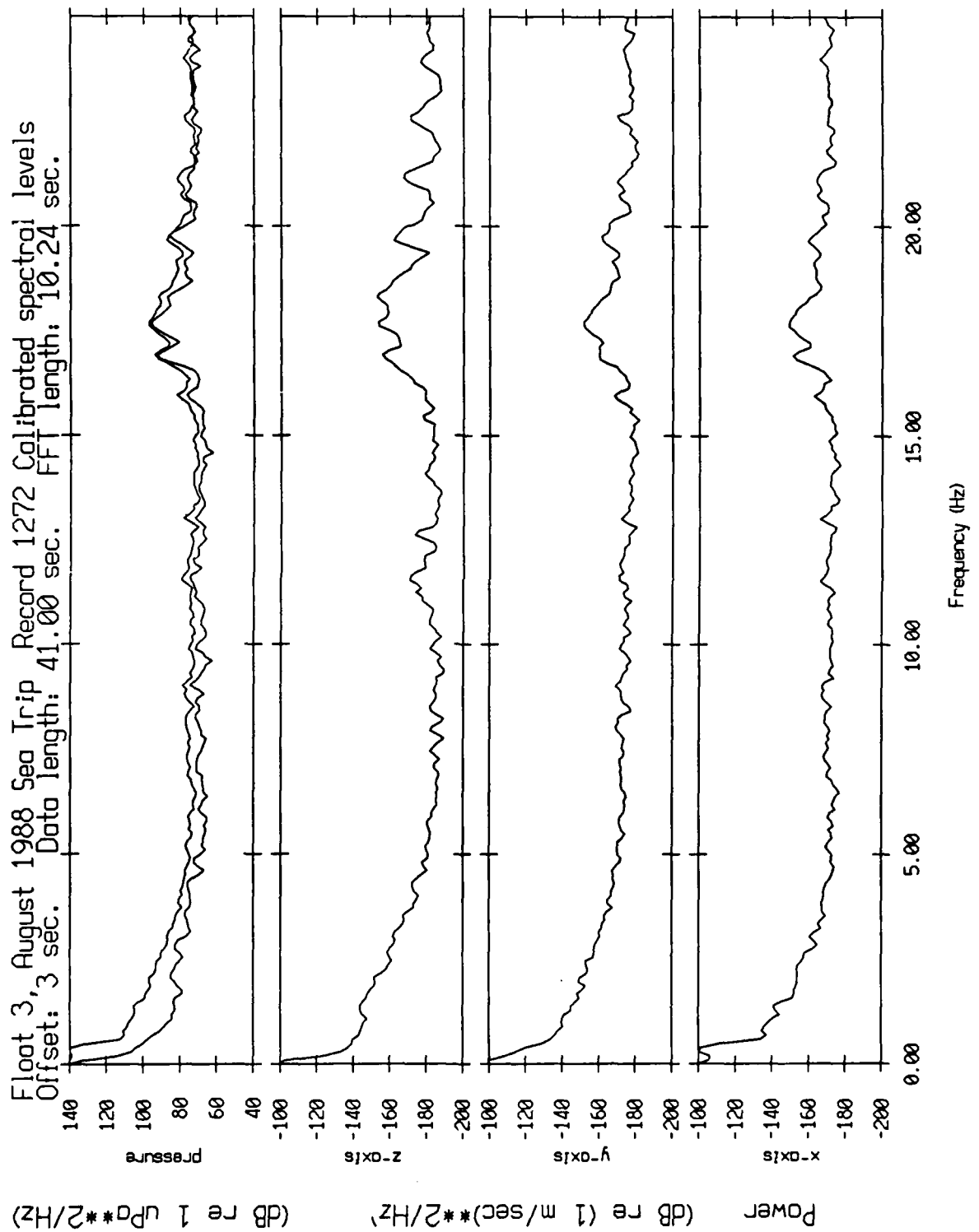


Figure XII.63a

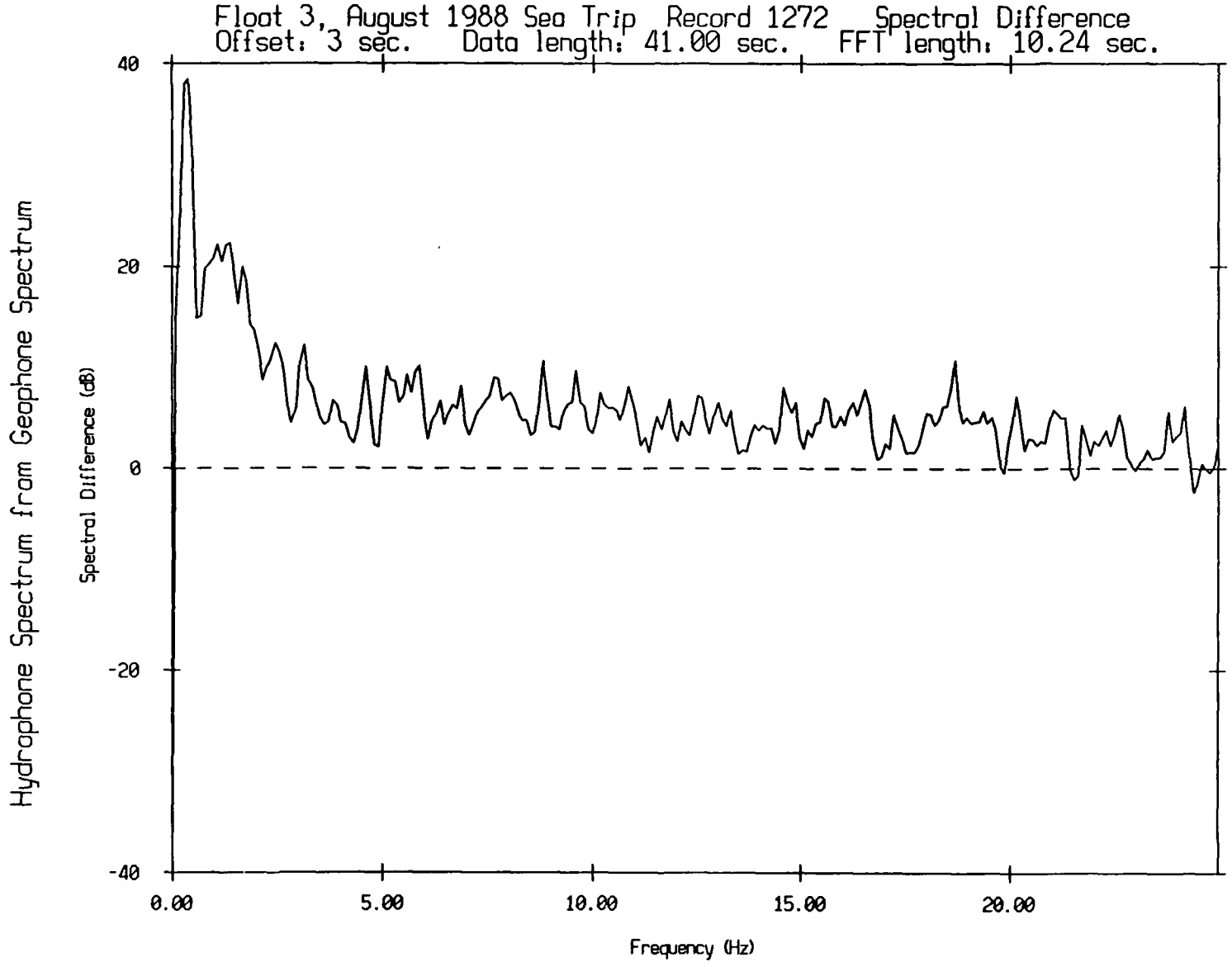


Figure XII.63b

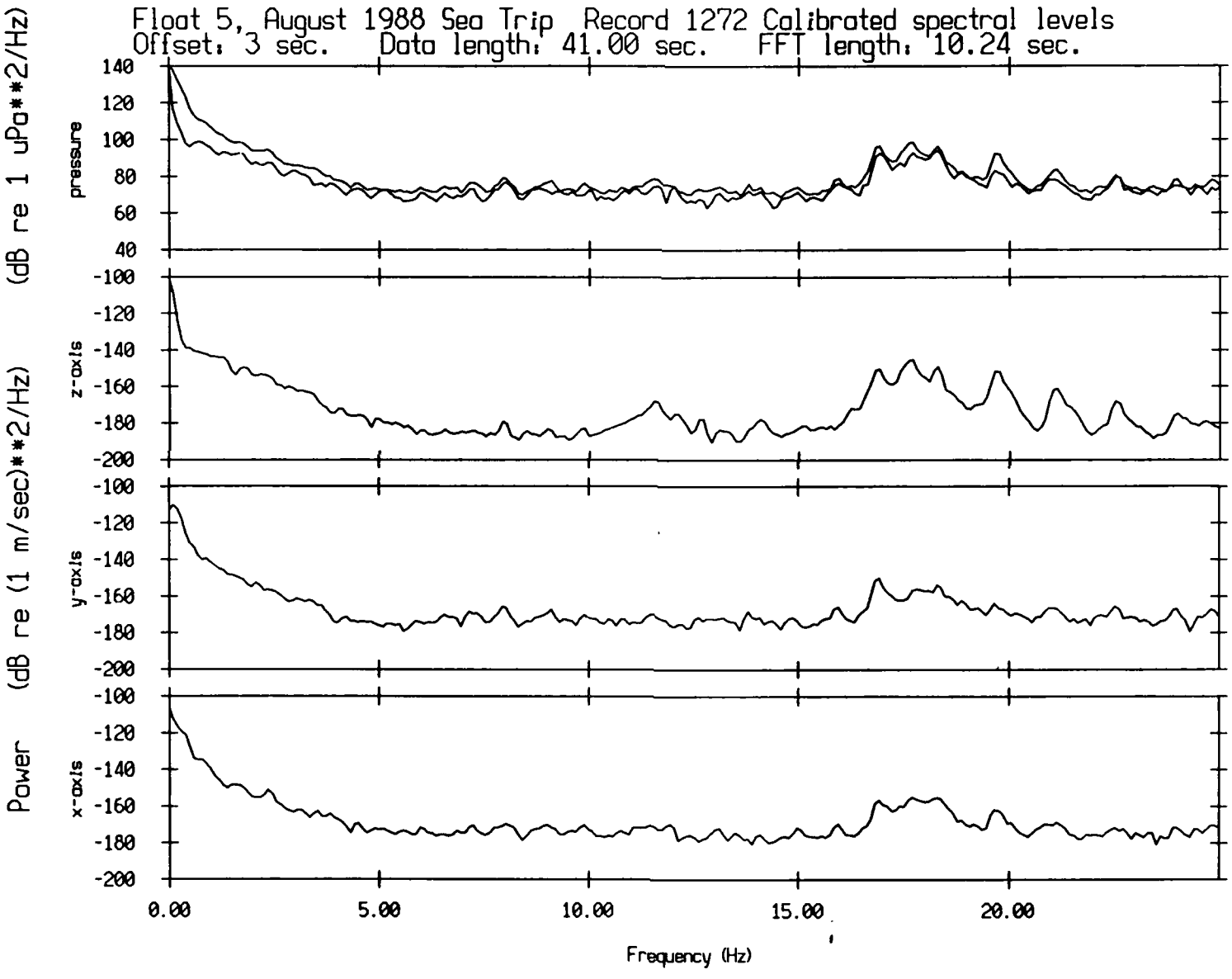


Figure XII.61a

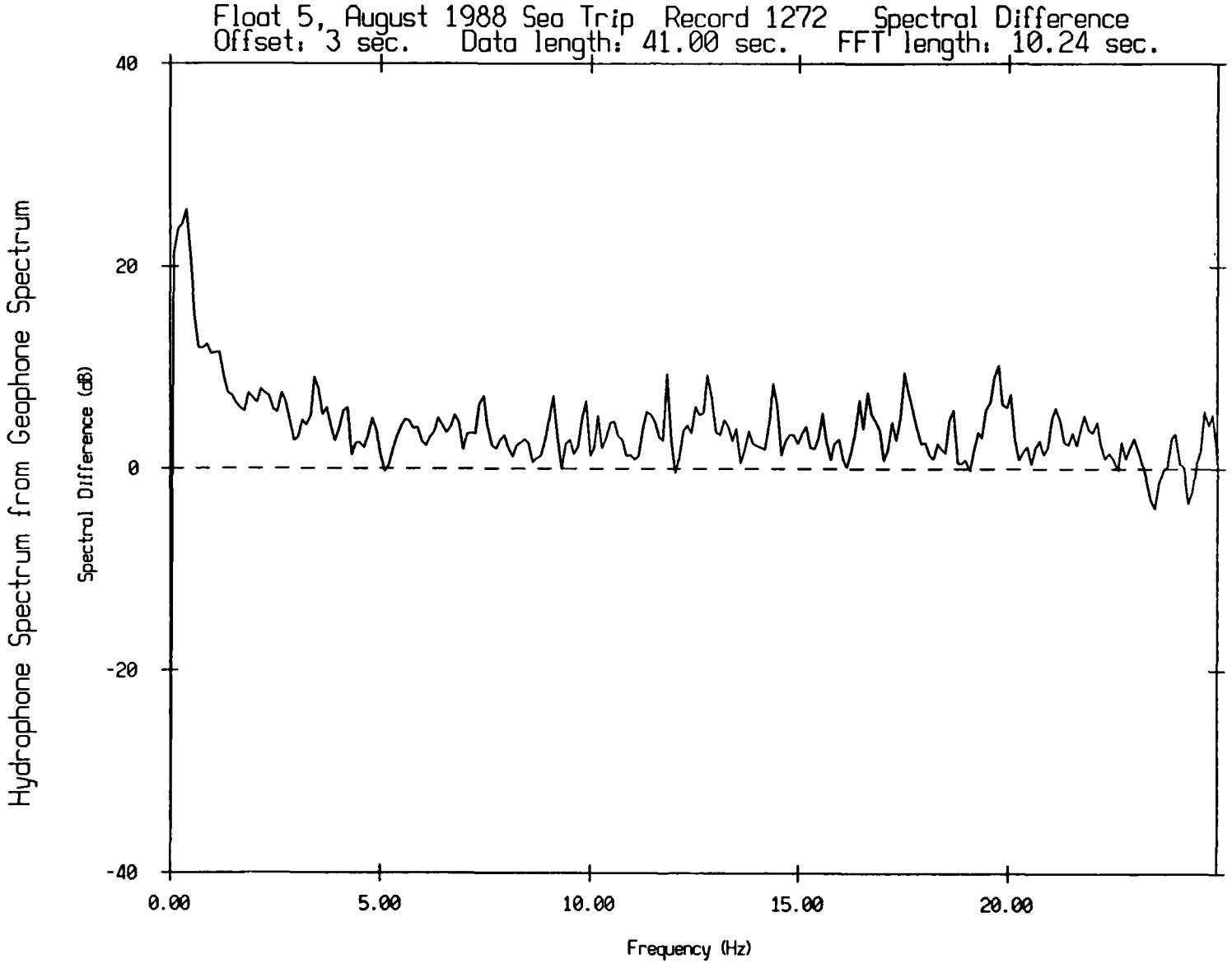


Figure XII.64b

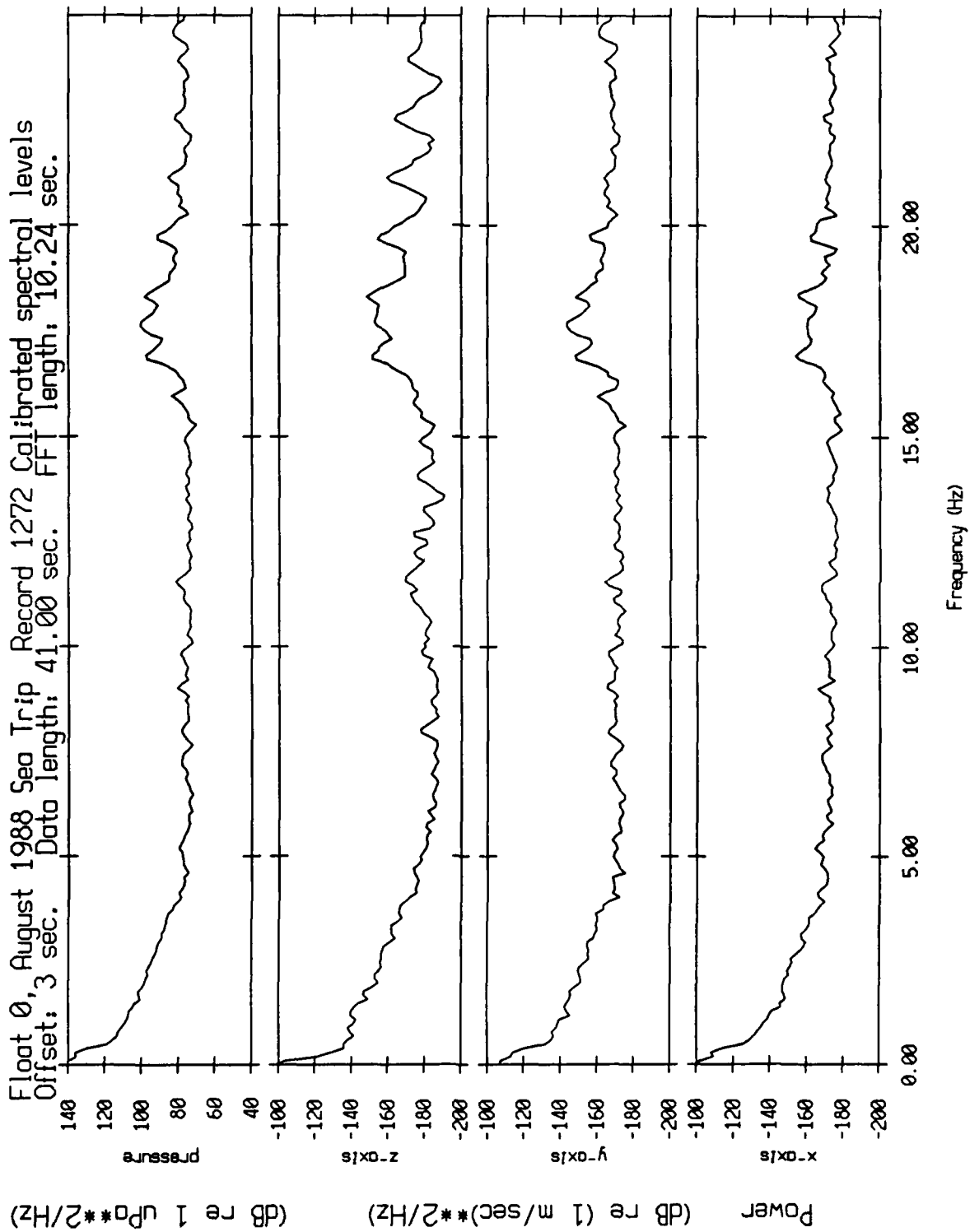


Figure XII.65

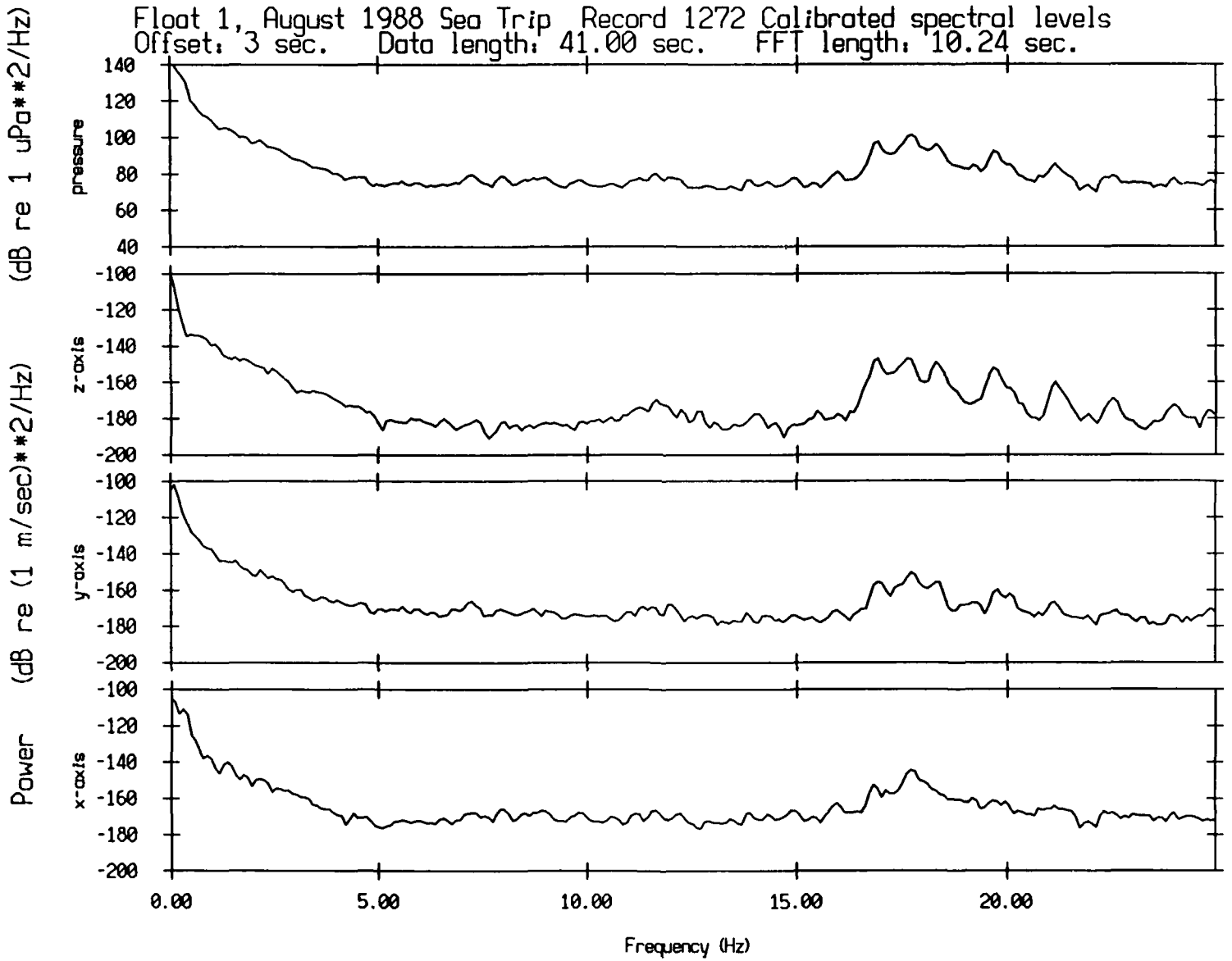


Figure XII.66

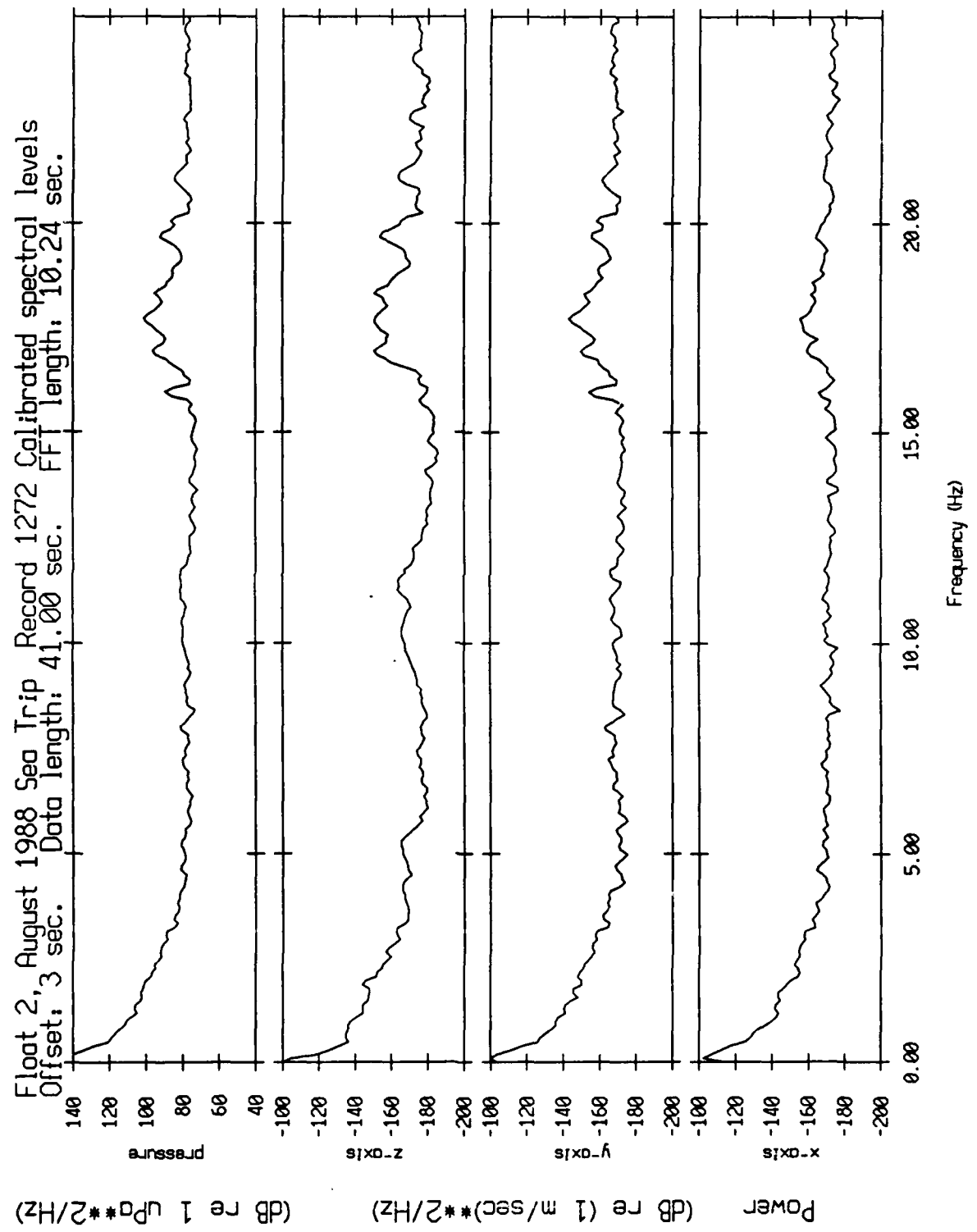


Figure XII.67

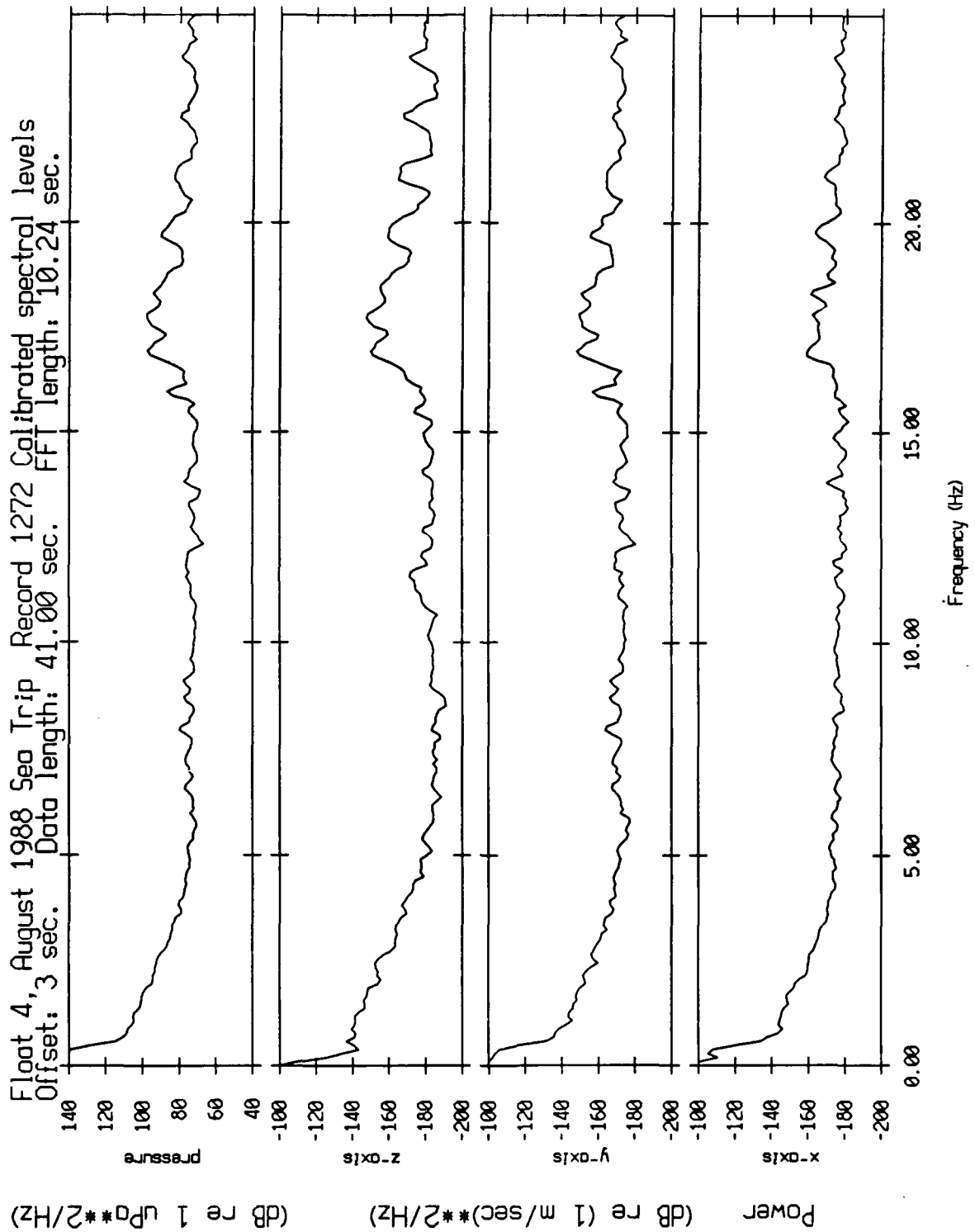


Figure XII.68

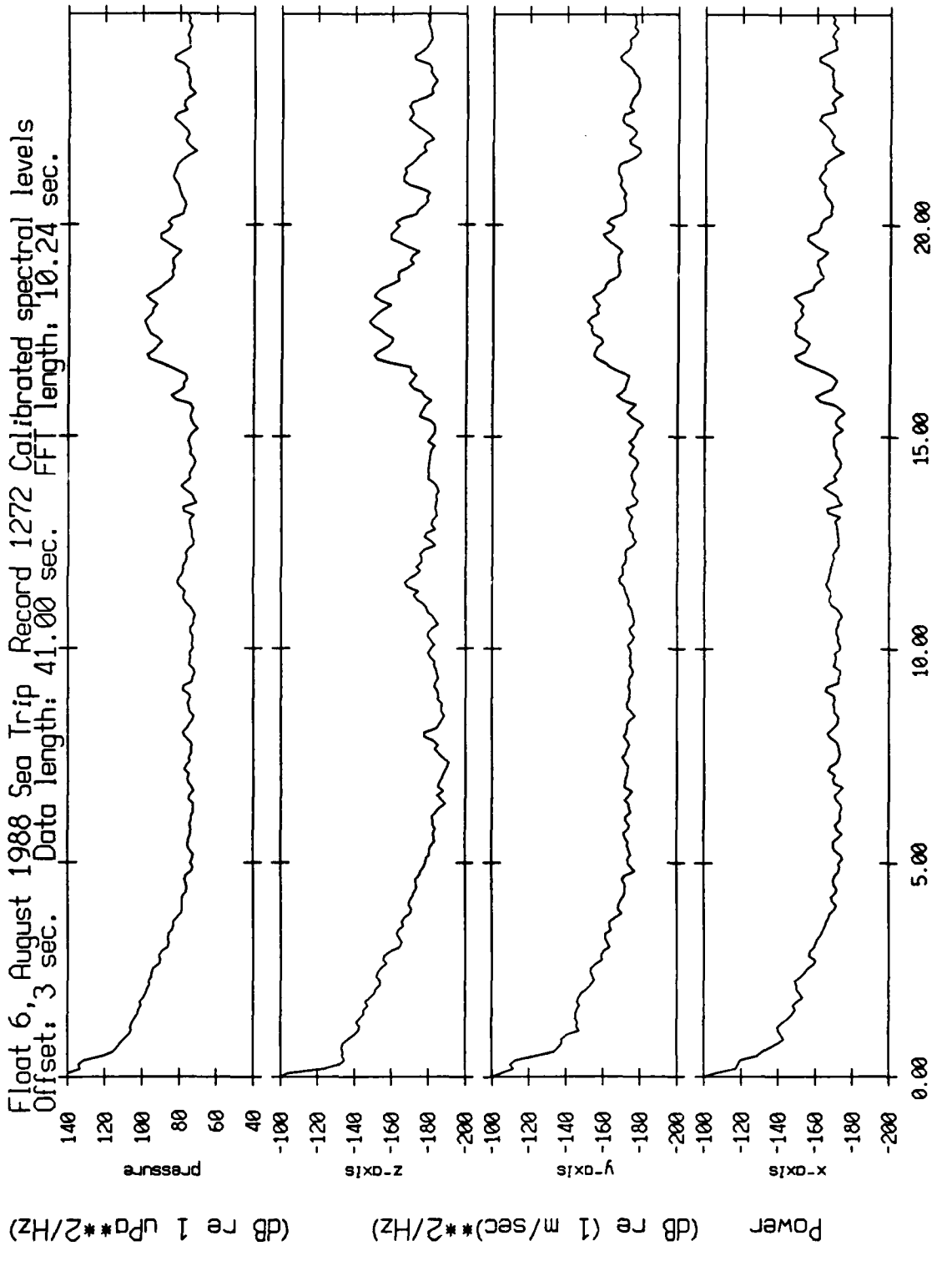


Figure XII.69

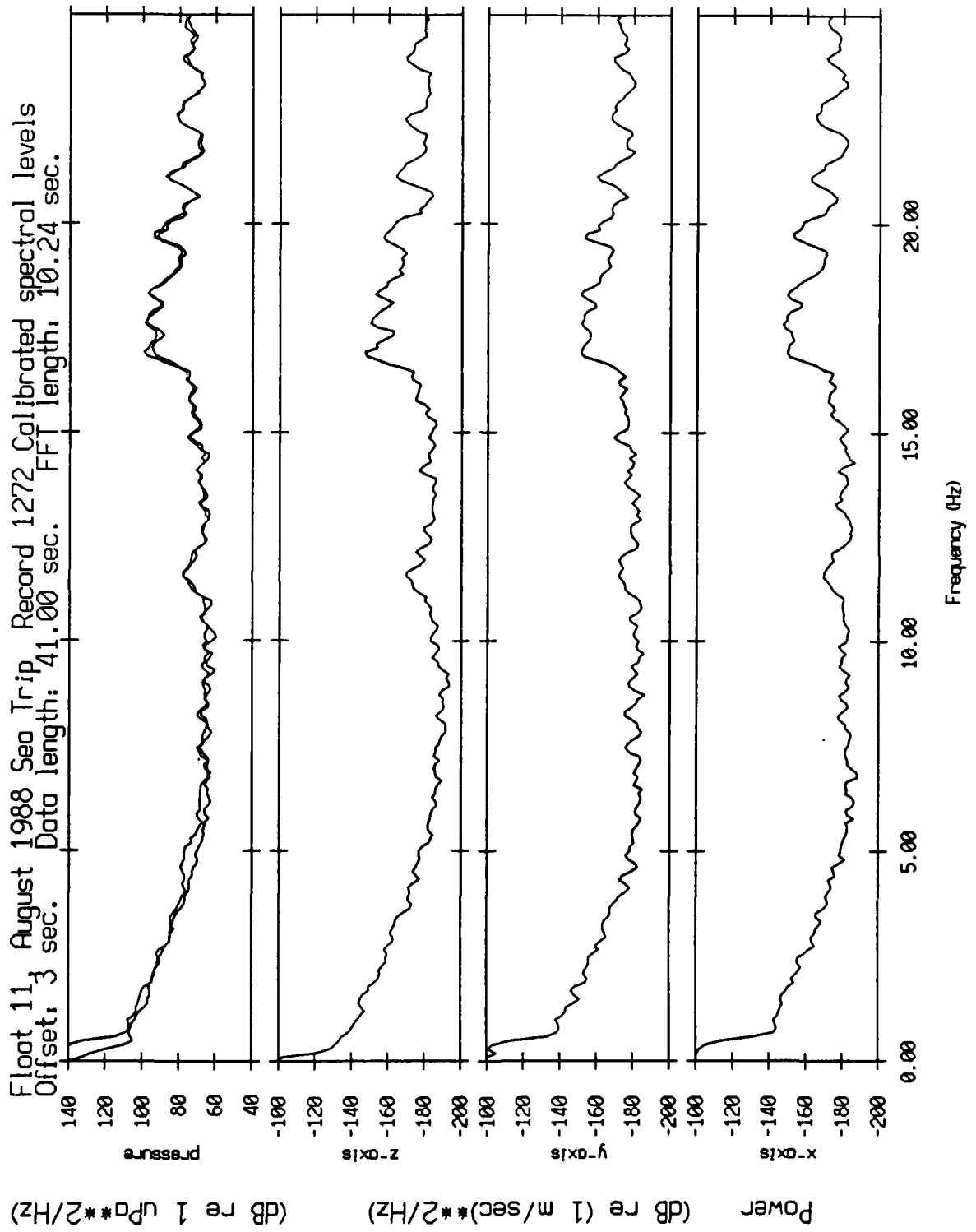


Figure XII.70a

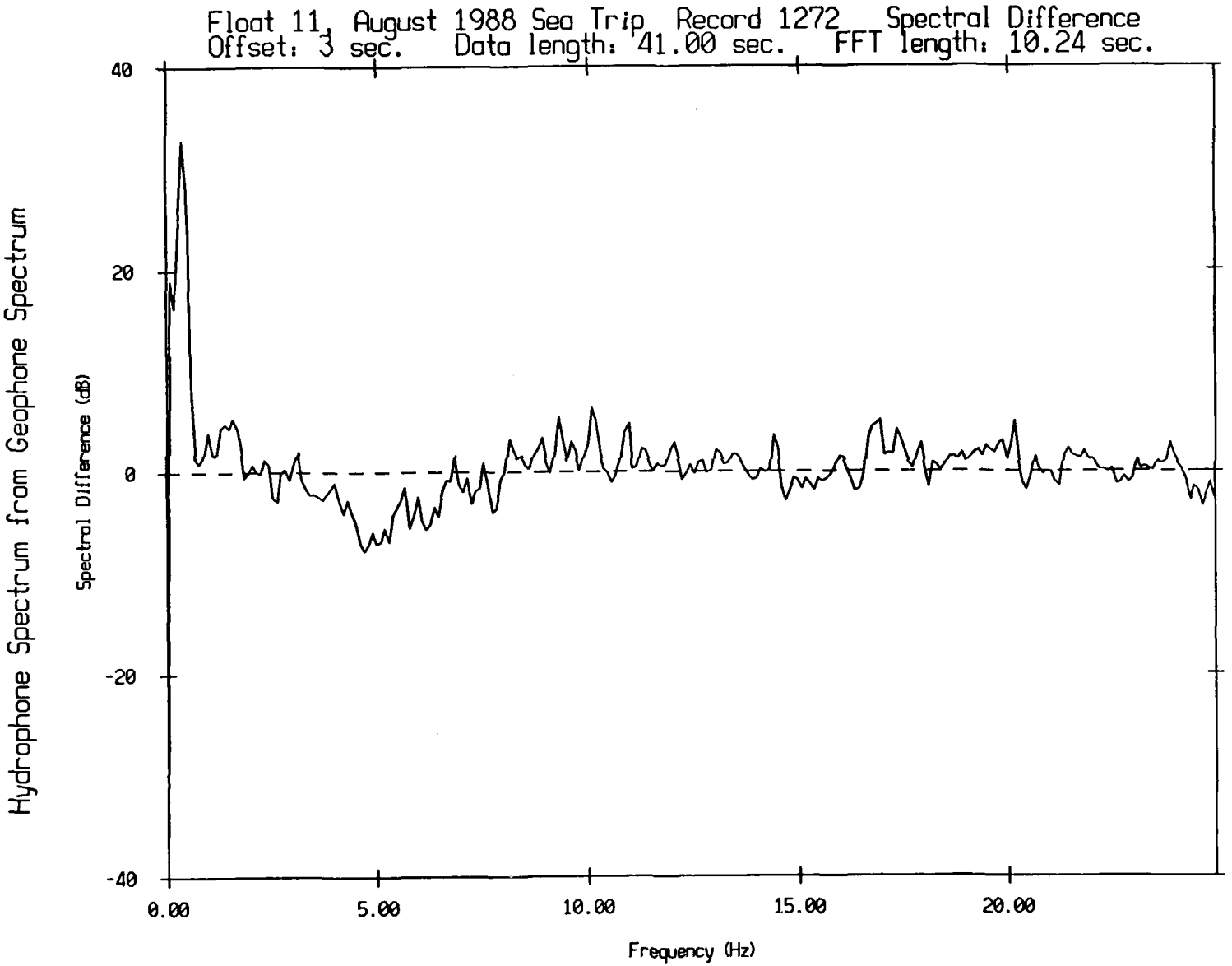


Figure XII.70b

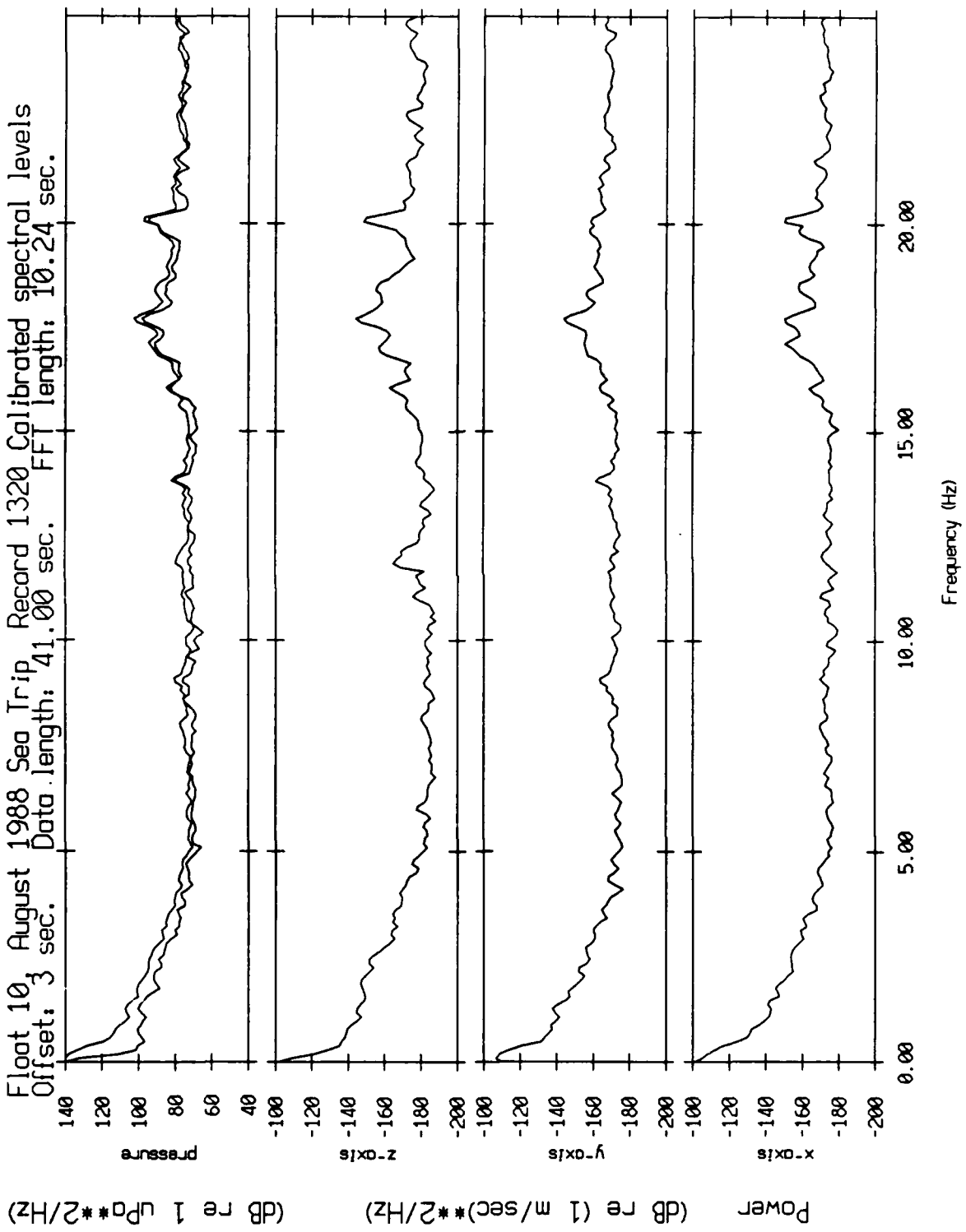


Figure XII.71a

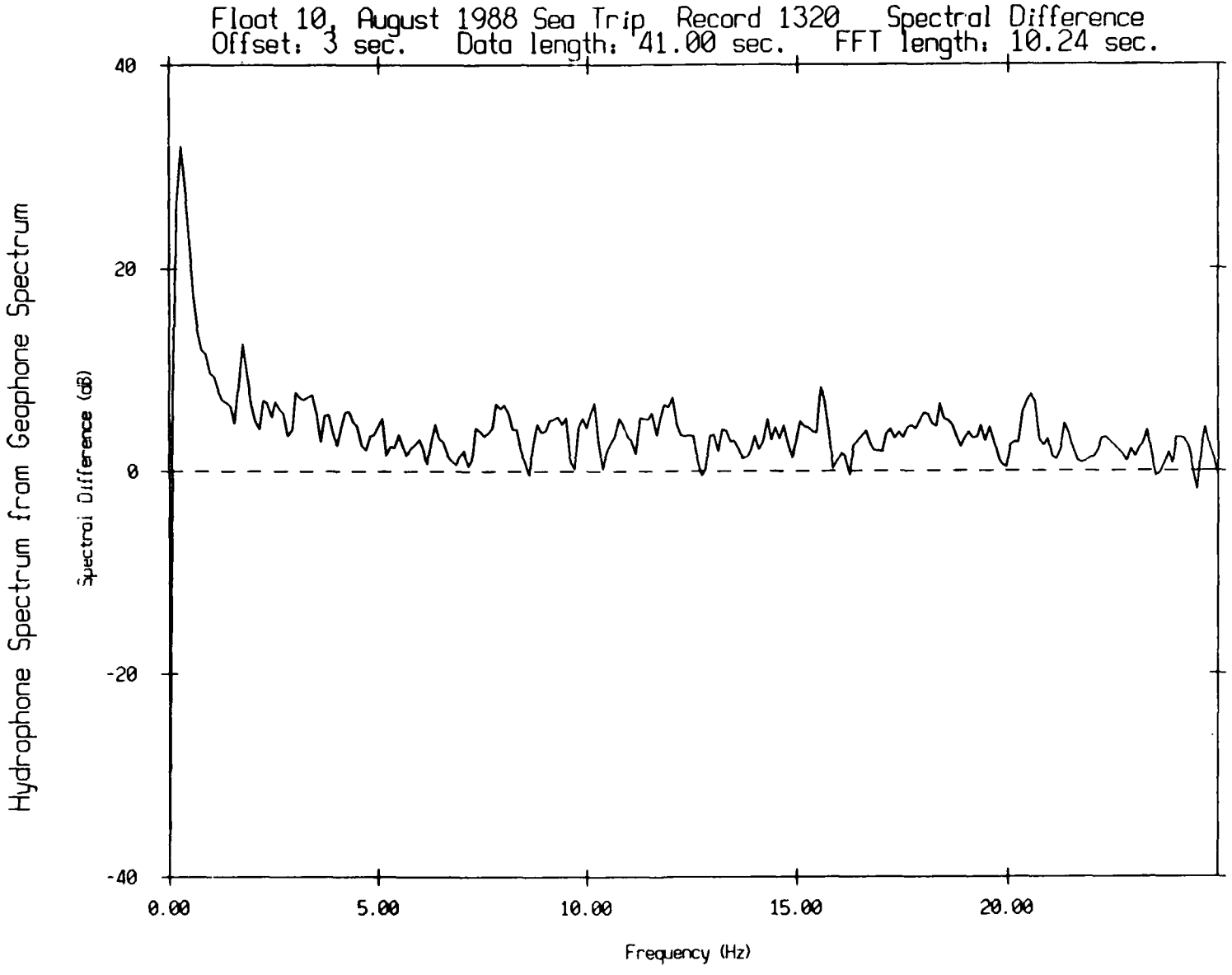


Figure XII.71b

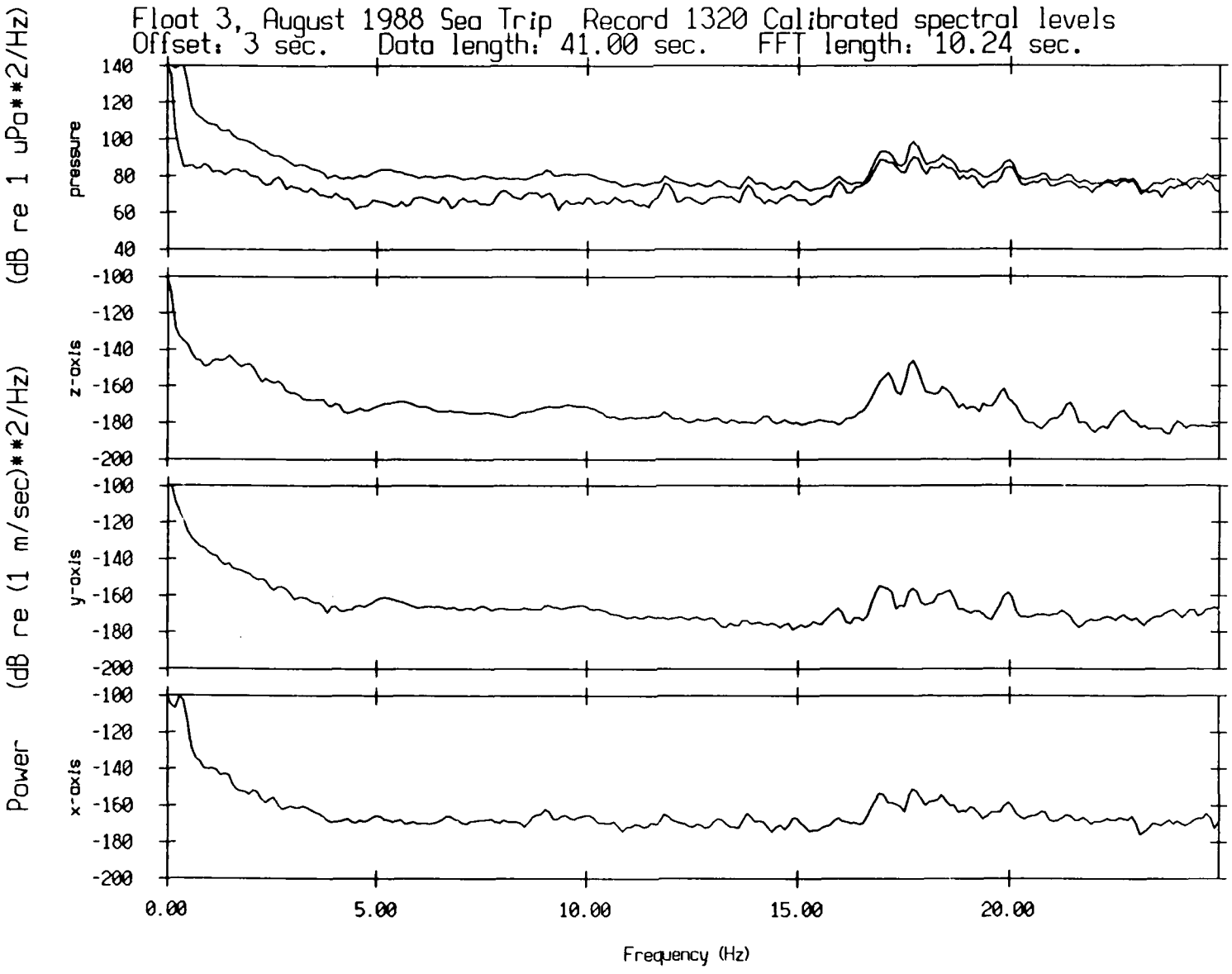


Figure XII.72a

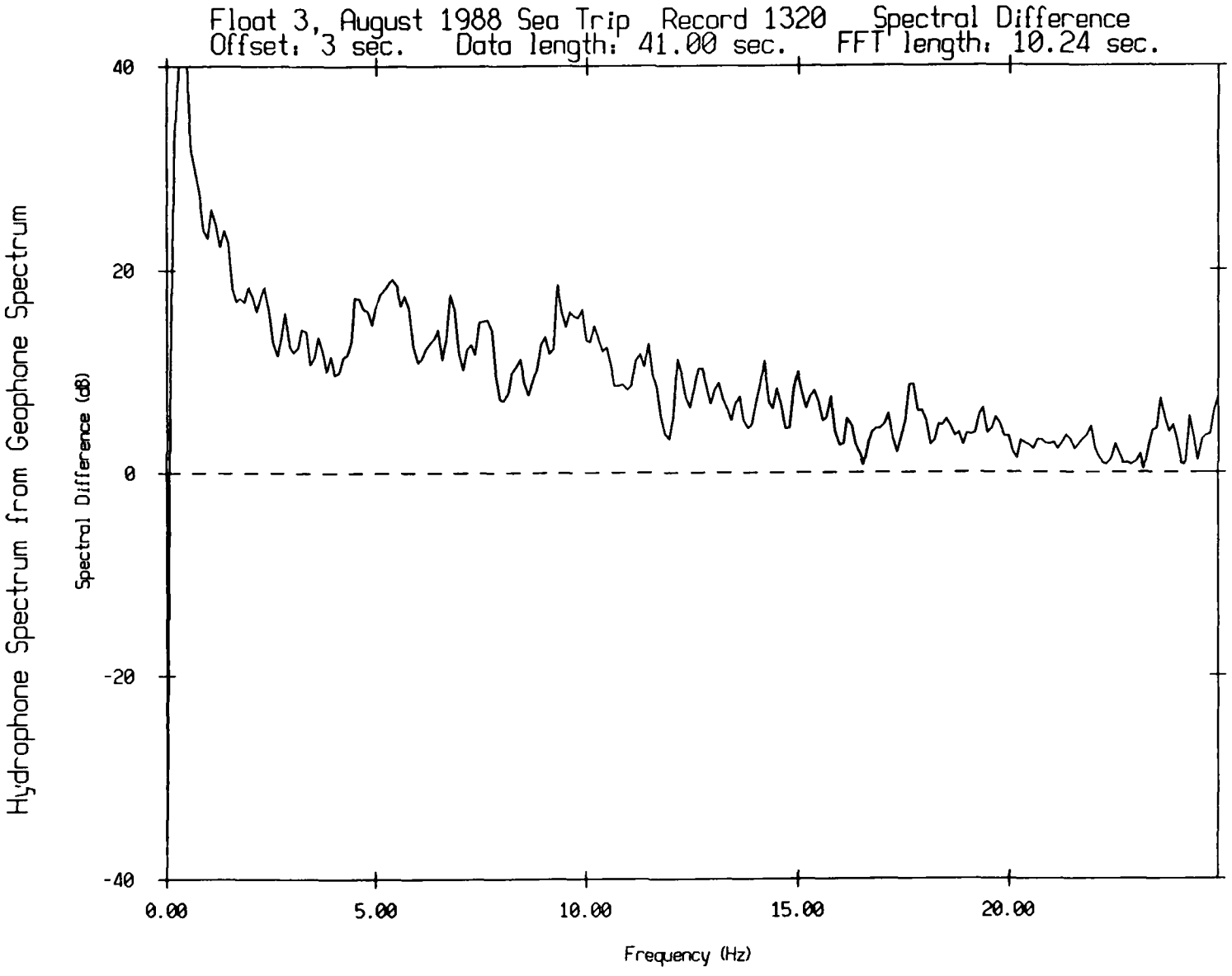


Figure XII.72b

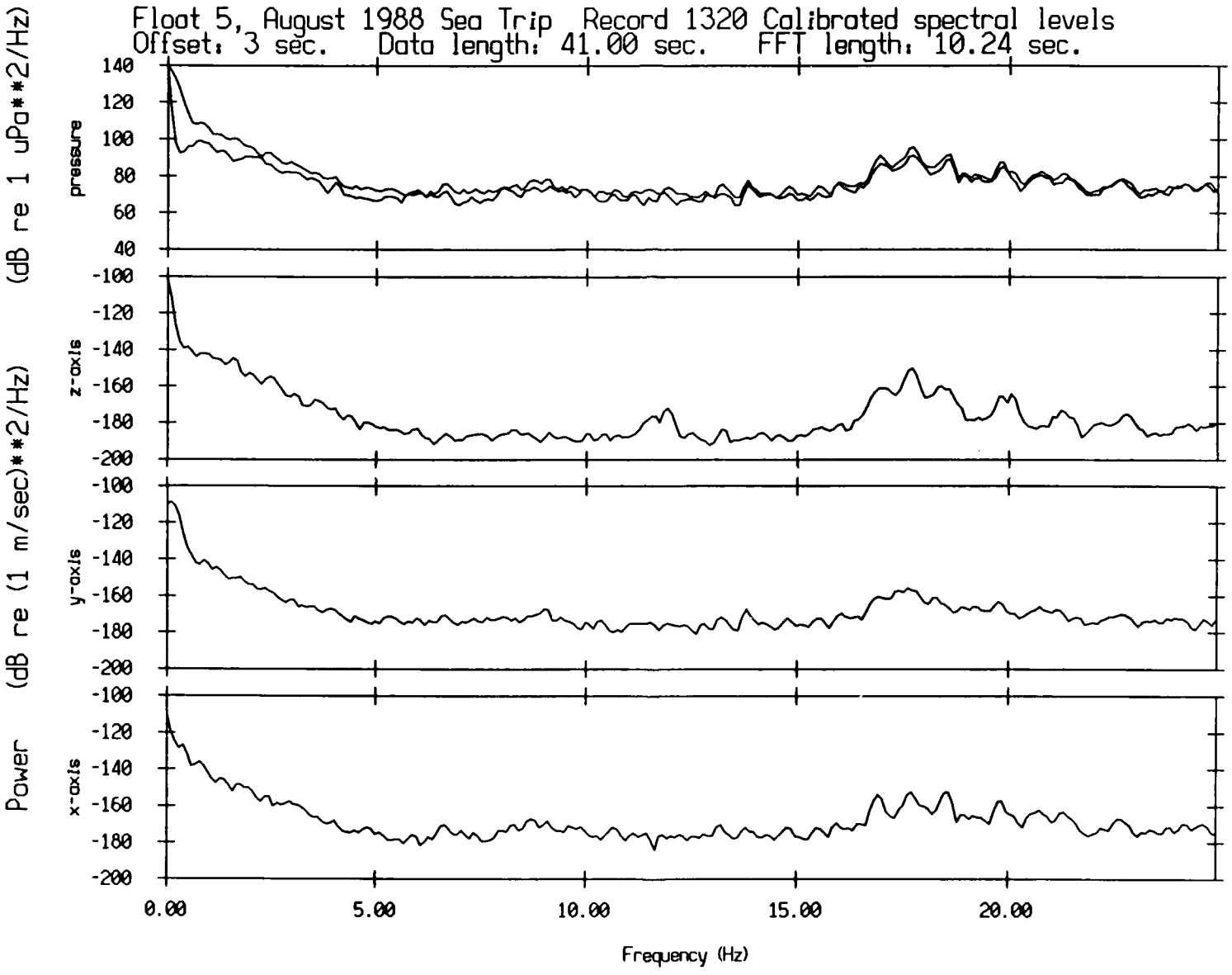


Figure XII.73a

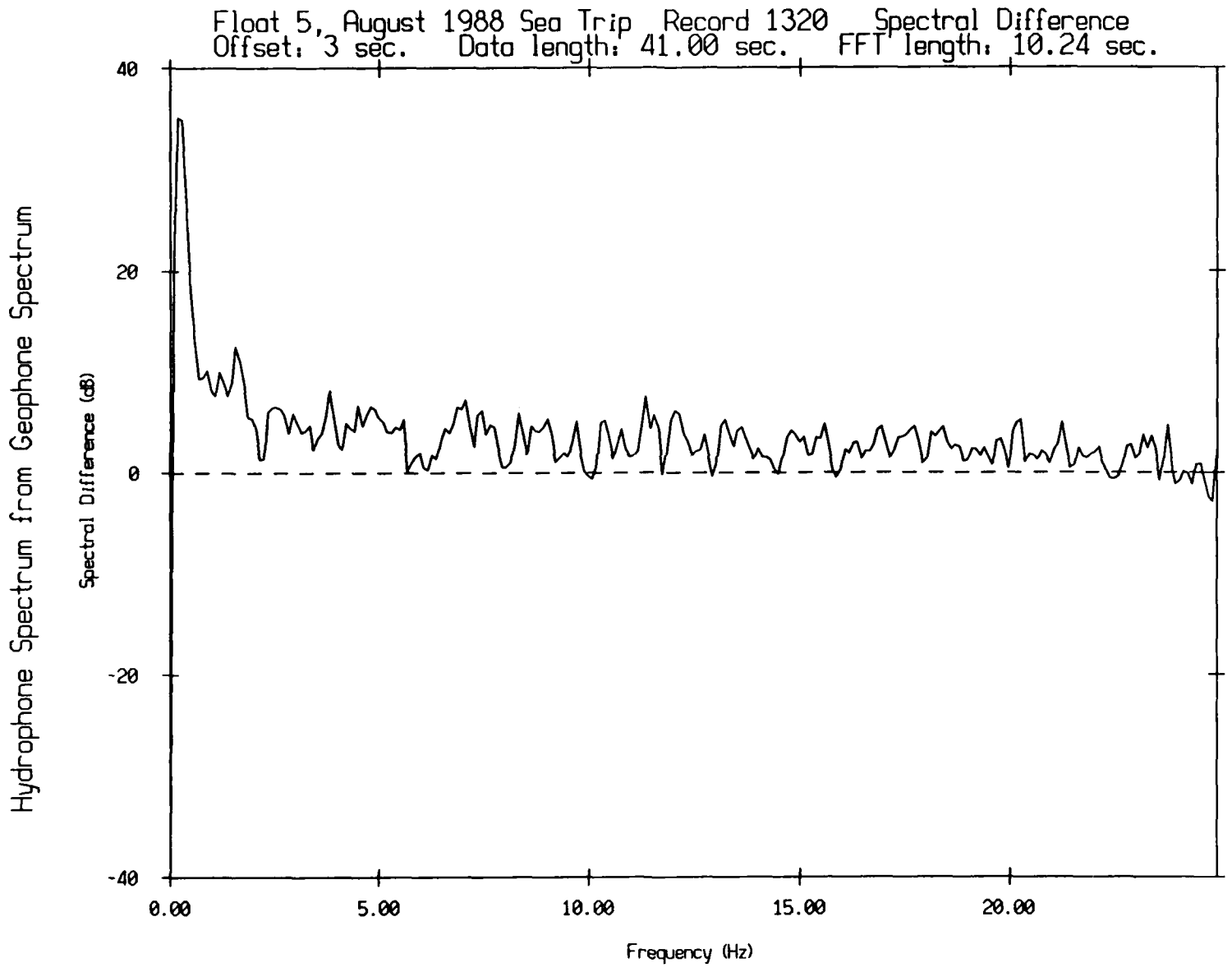


Figure XII.73b

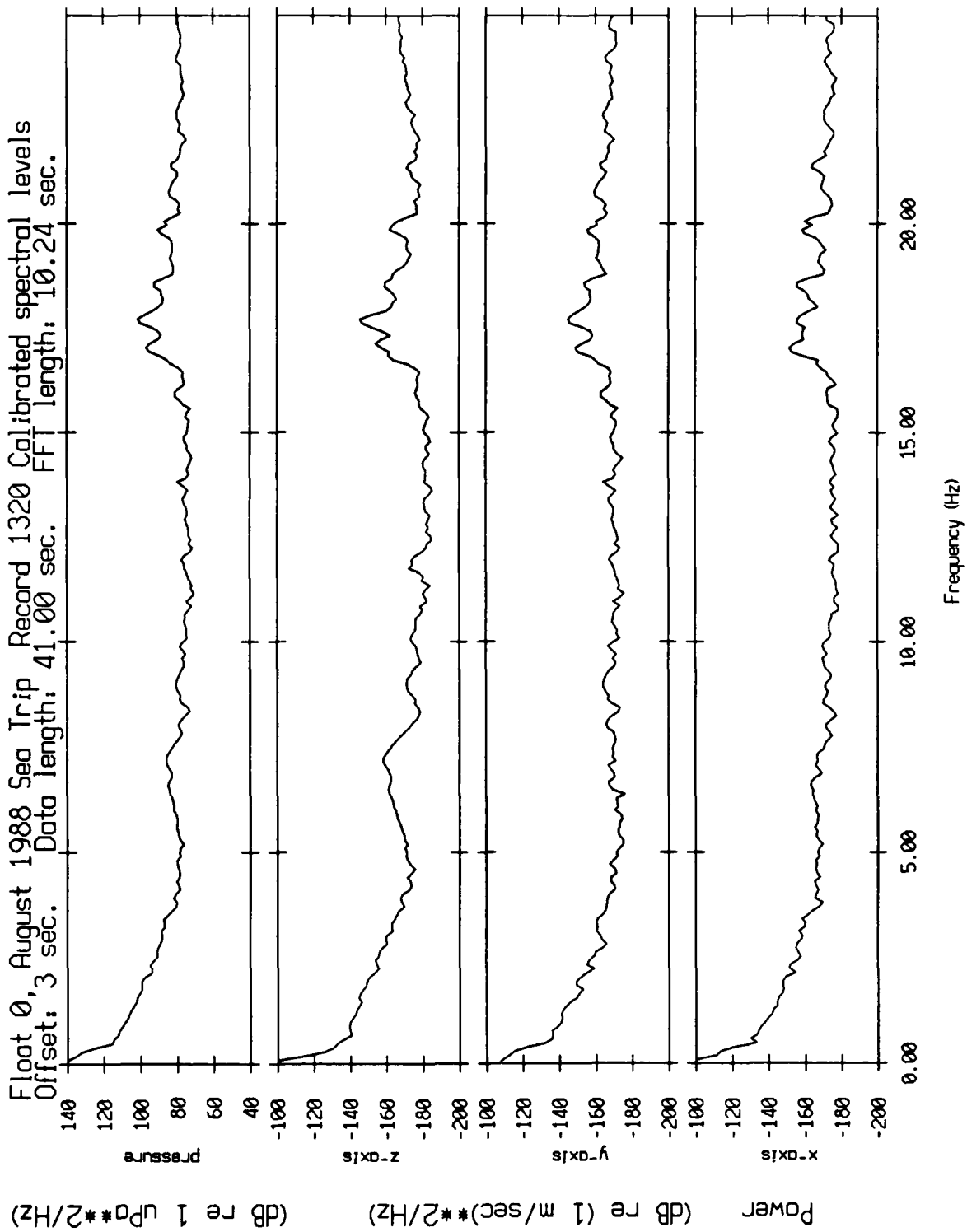


Figure XII.74

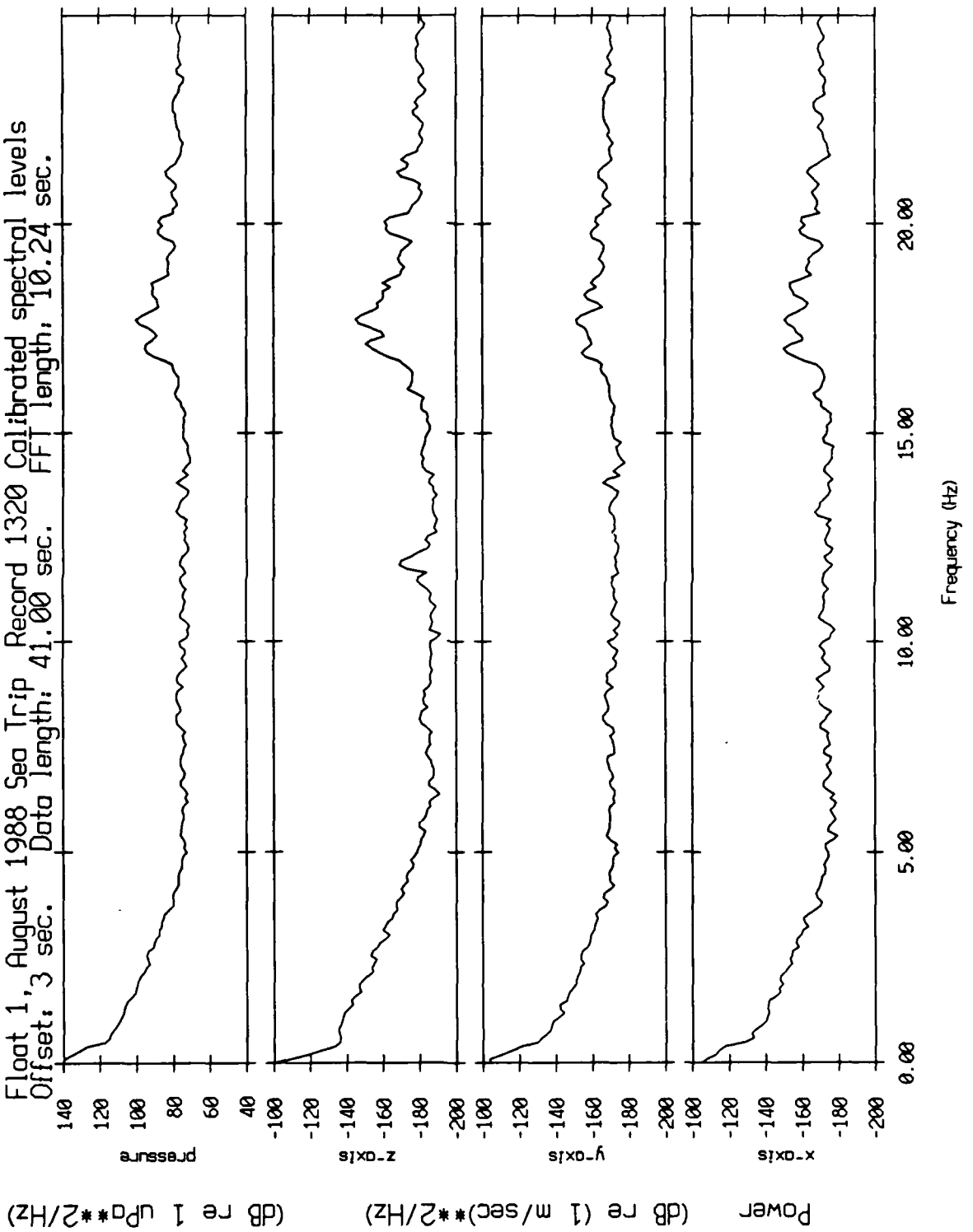


Figure XII.75

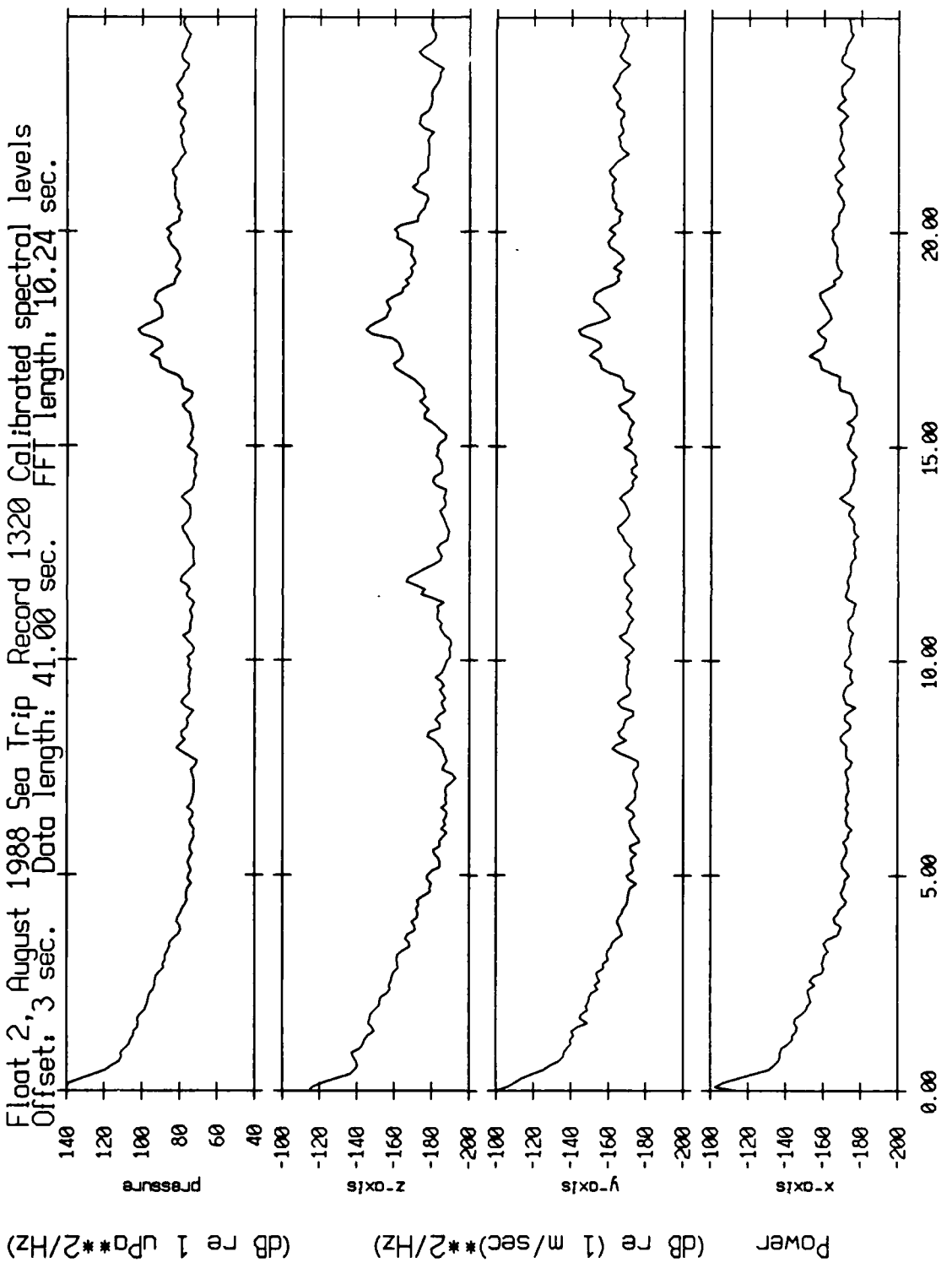


Figure XII.76

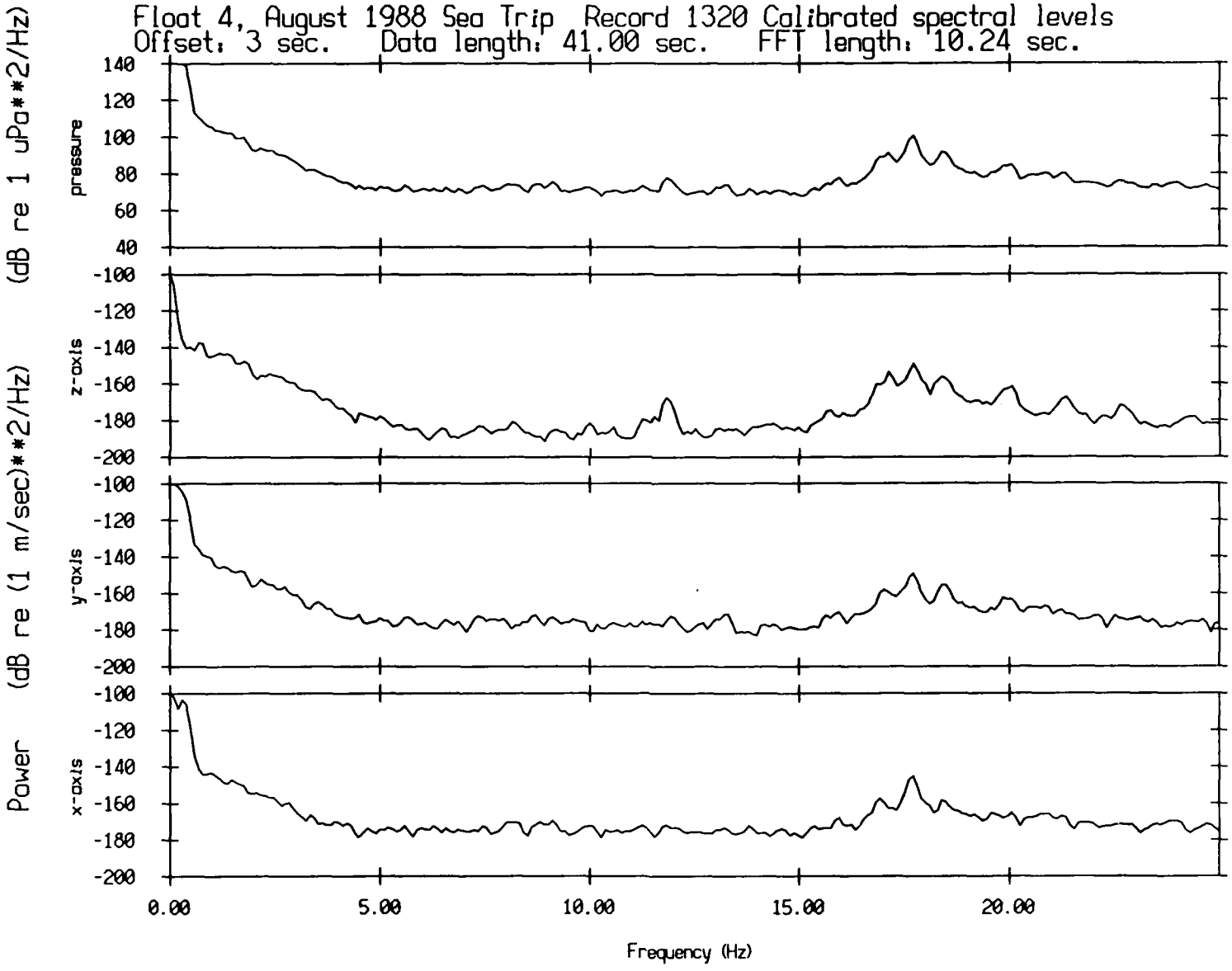

Float 4, August 1988 Sea Trip Record 1320 Calibrated spectral levels
Offset: 3 sec. Data length: 41.00 sec. FFT length: 10.24 sec.
Power (dB re (1 m/sec)**2/Hz) (dB re 1 uPa**2/Hz)
pressure
z-axis
y-axis
x-axis
140
120
100
80
60
40
-100
-120
-140
-160
-180
-200
0.00
5.00
10.00
15.00
20.00
Frequency (Hz)

Figure XII.7

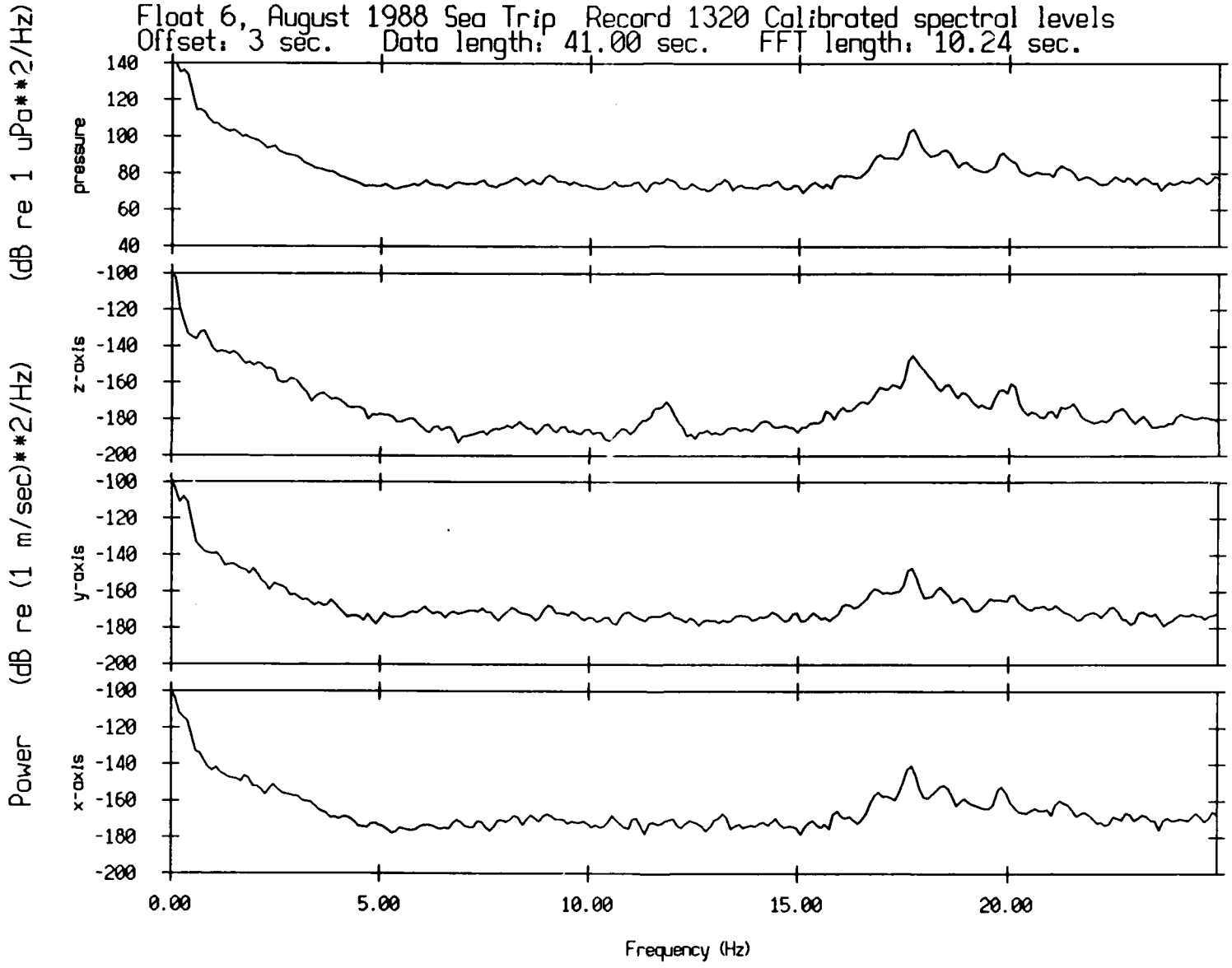

Float 6, August 1988 Sea Trip Record 1320 Calibrated spectral levels
Offset: 3 sec. Data length: 41.00 sec. FFT length: 10.24 sec.
Power (dB re (1 m/sec)**2/Hz) (dB re 1 uPa**2/Hz)
pressure
z-axis
y-axis
x-axis
140
120
100
80
60
40
-100
-120
-140
-160
-180
-200
0.00
5.00
10.00
15.00
20.00
Frequency (Hz)

Figure XII.8

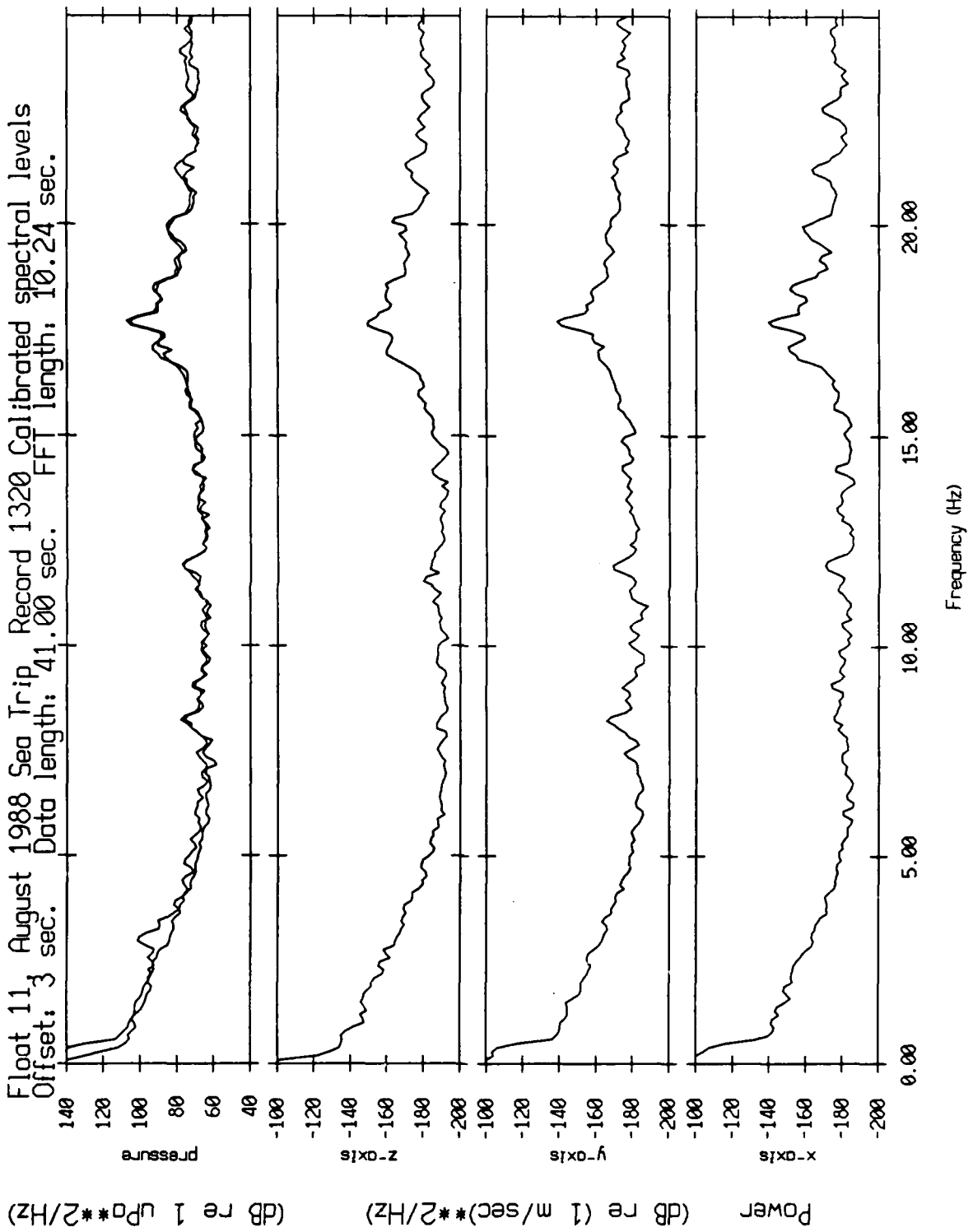


Figure XII.79a

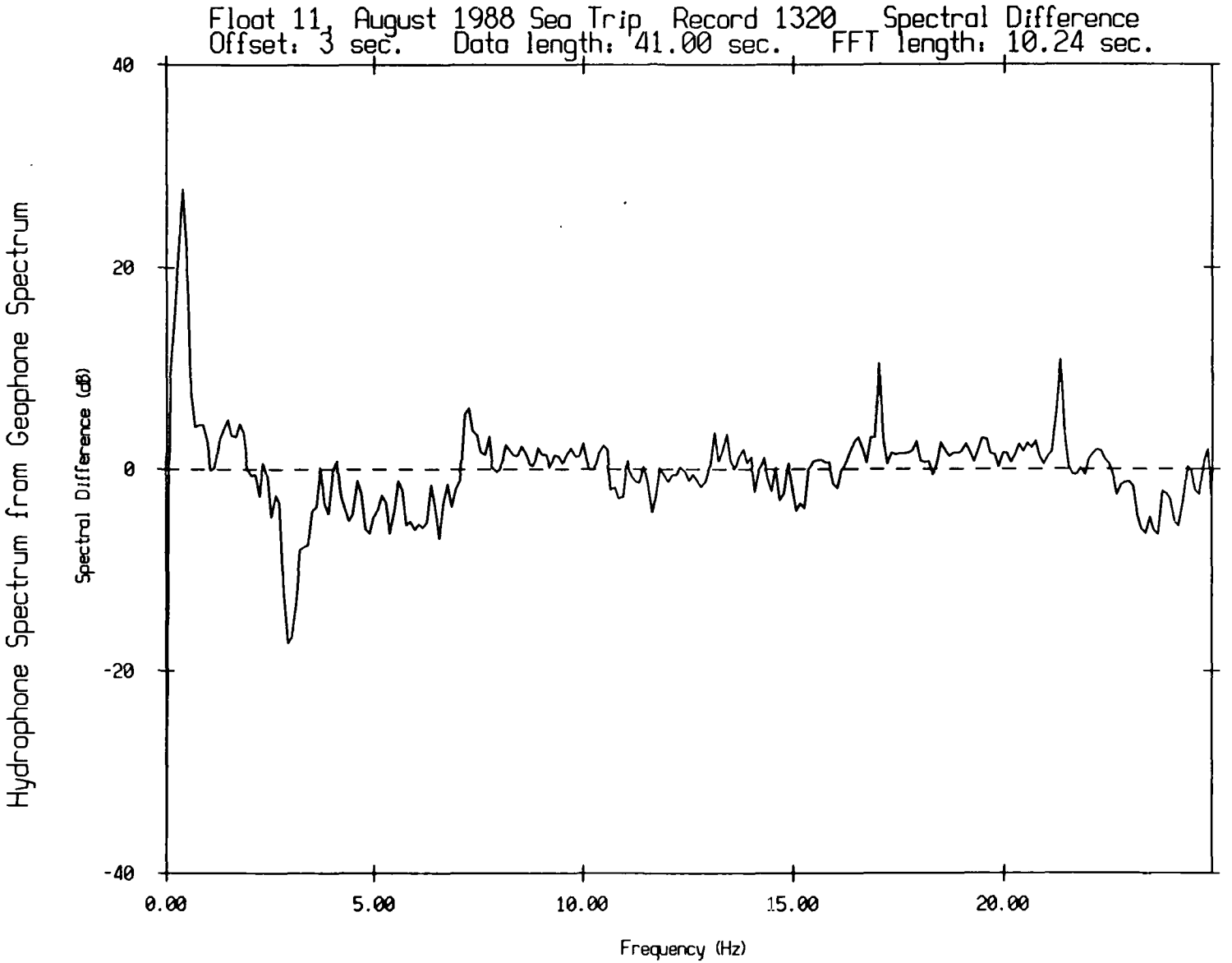


Figure XII.70b

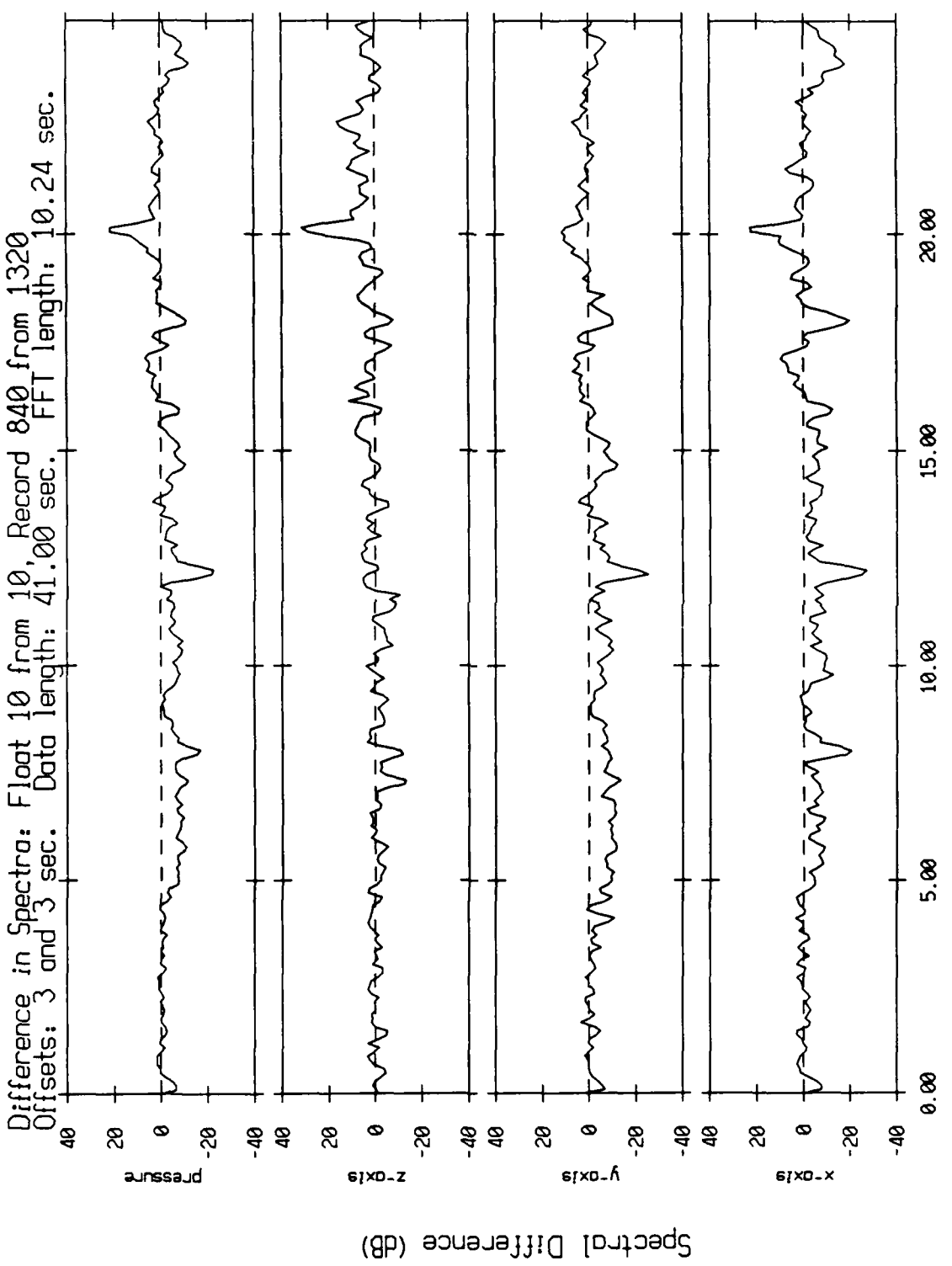


Figure XII.80

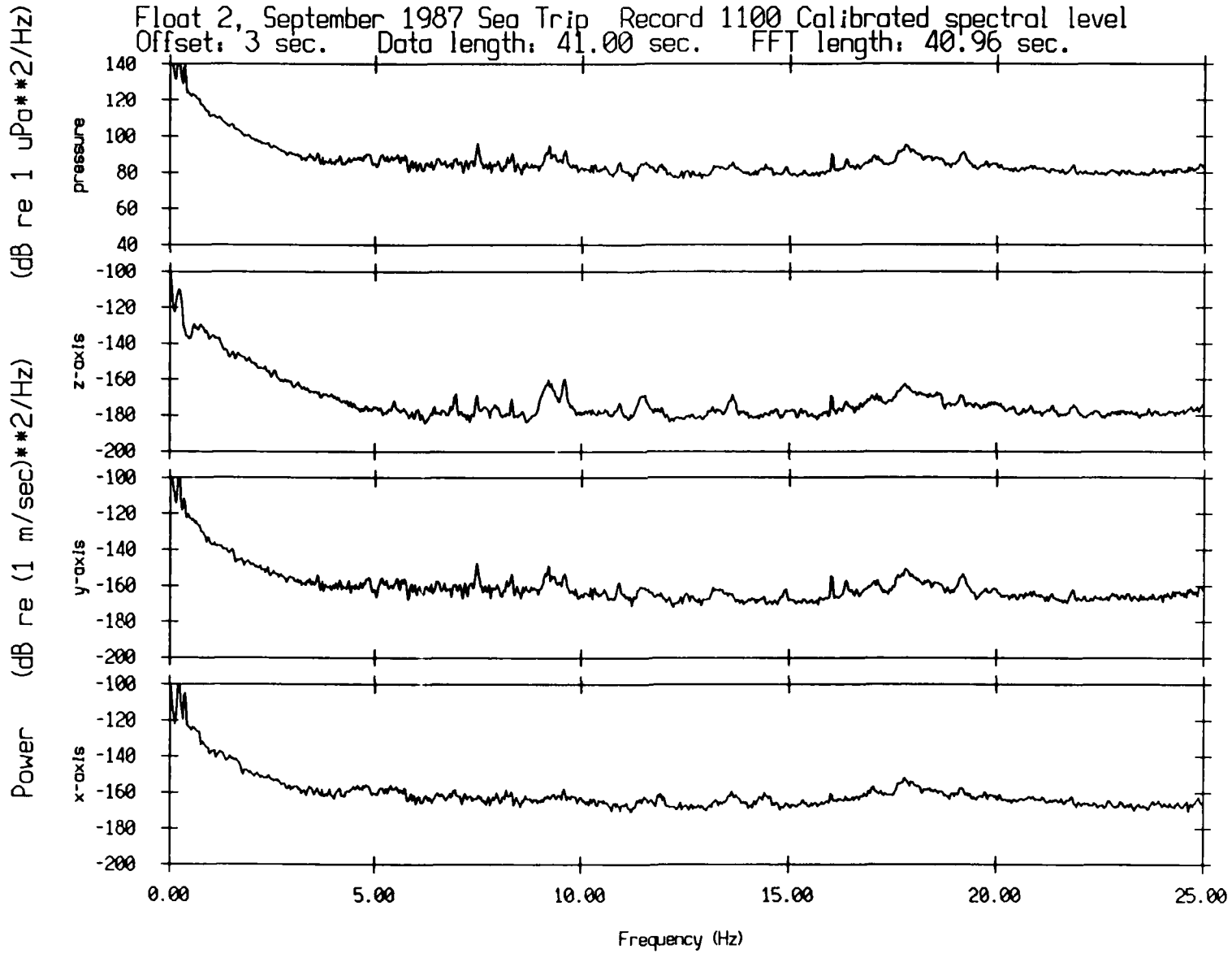


Figure XII.81

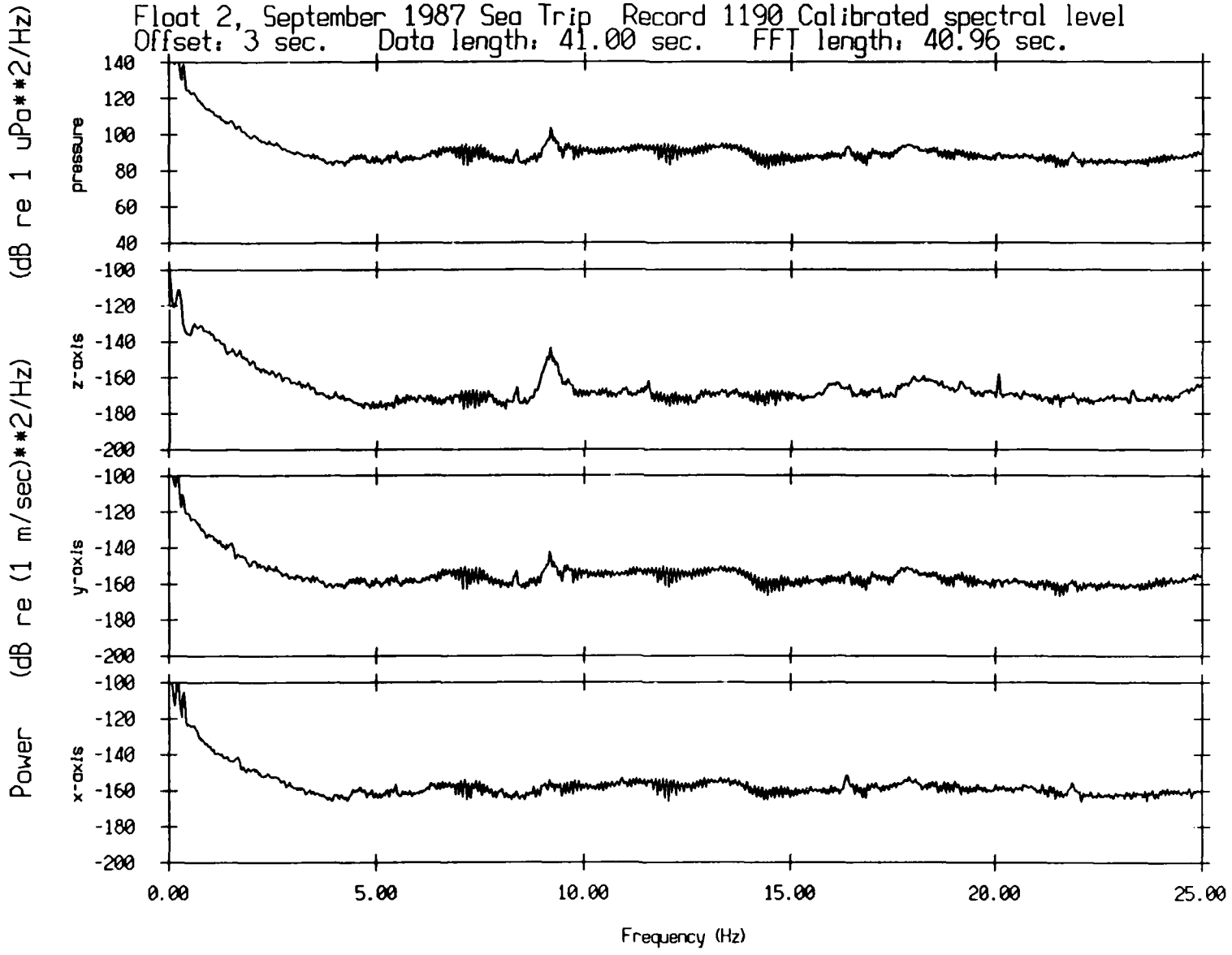


Figure XII.82

SWALLOW FLOAT VLF DATA ACQUISITION SYSTEM

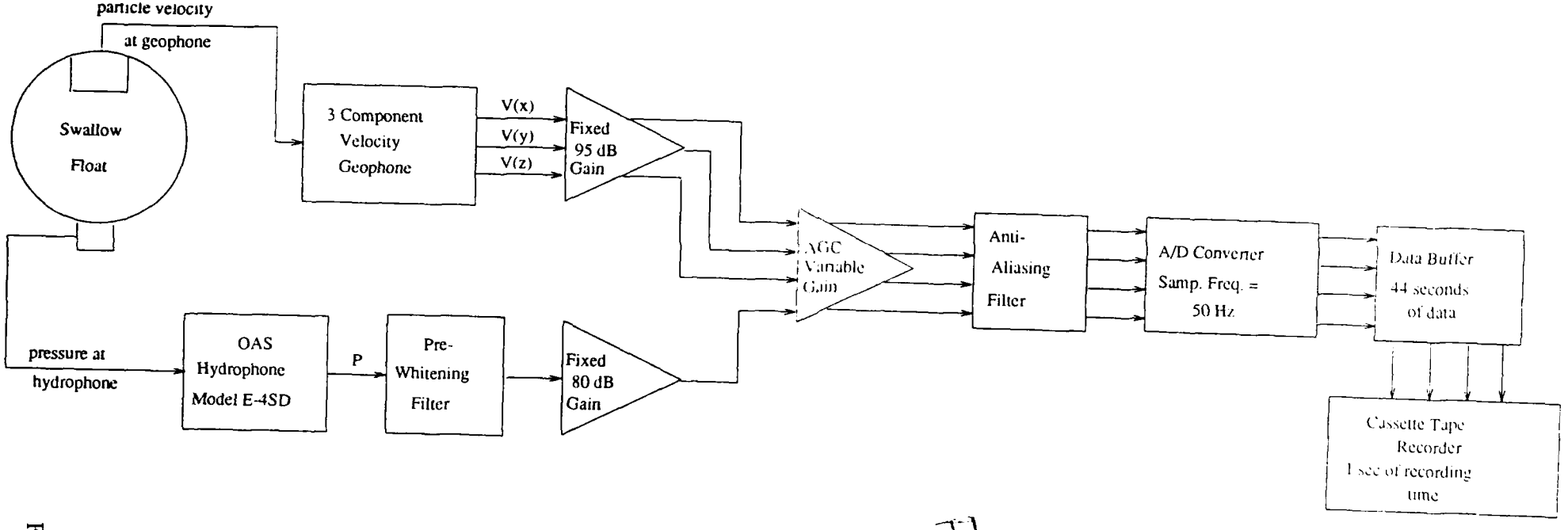


Figure A1.1

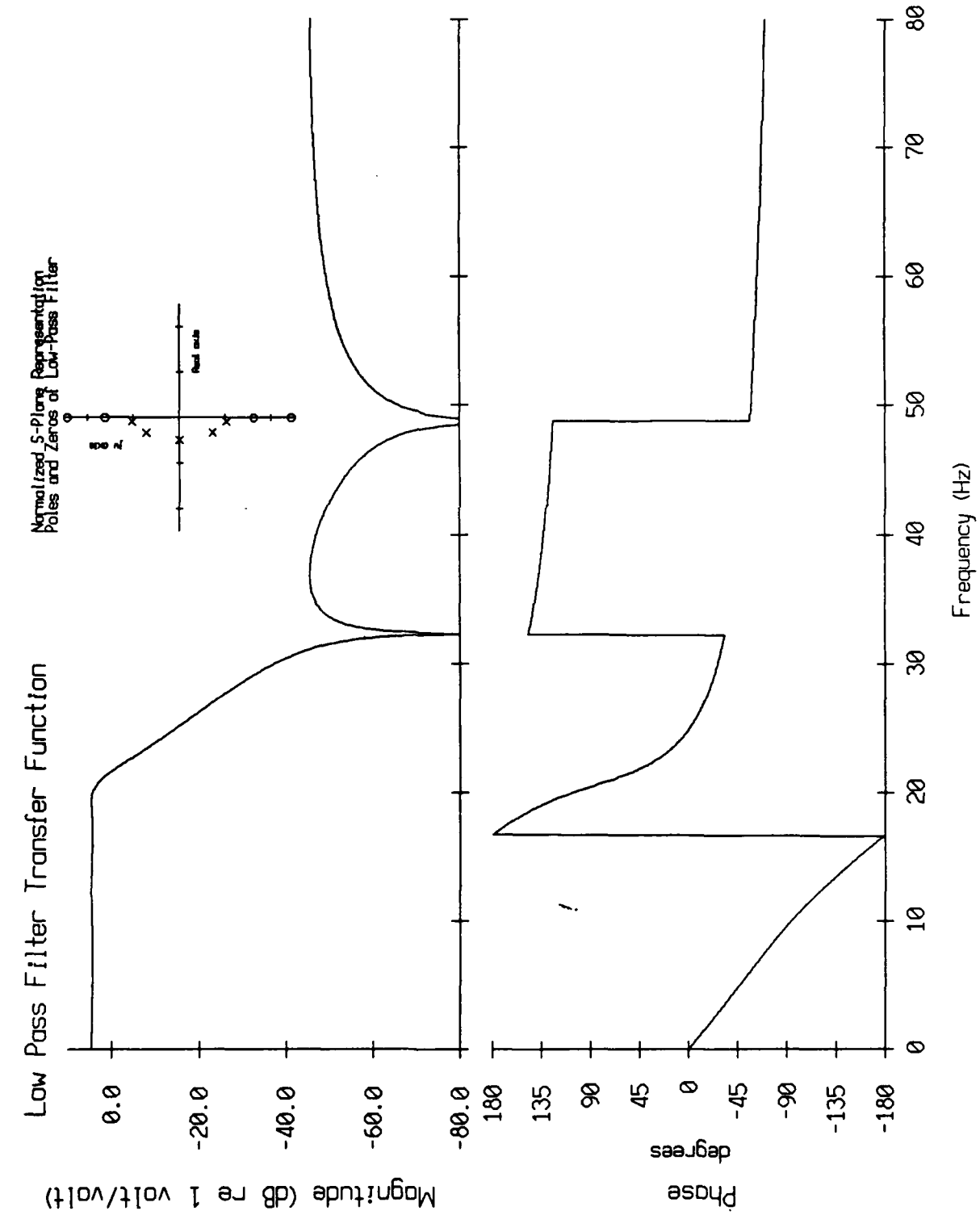

Low Pass Filter Transfer Function
Normalized S-Plane Representation
Poles and Zeros of Low-Pass Filter
Magnitude (dB re 1 volt/volt)
0.0
-20.0
-40.0
-60.0
-80.0
Phase
degrees
180
135
90
45
0
-45
-90
-135
-180
0
10
20
30
40
50
60
70
80
Frequency (Hz)

Figure A1.2

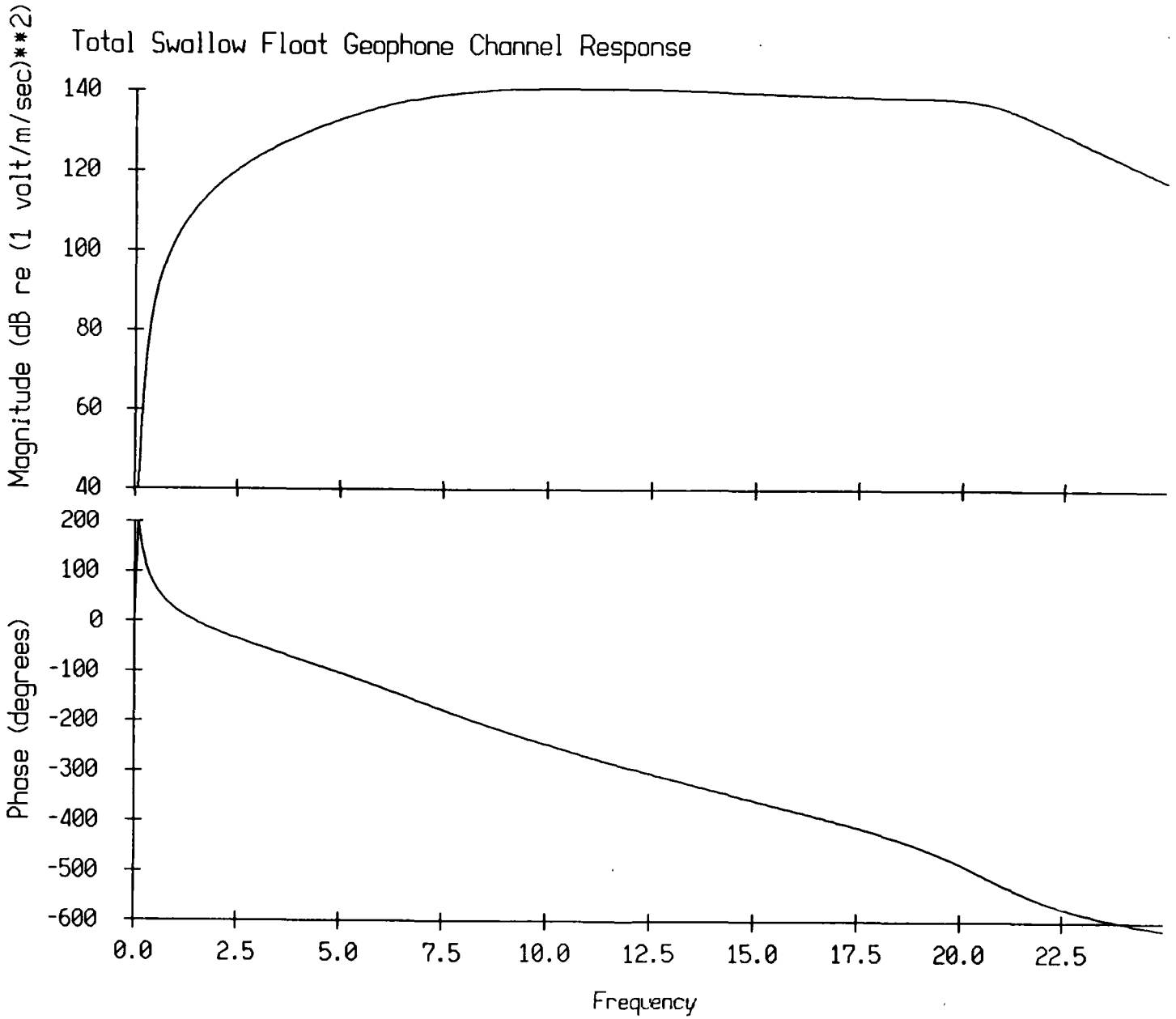

Total Swallow Float Geophone Channel Response
Magnitude (dB re (1 volt/m/sec)**2)
140
120
100
80
60
40
Phase (degrees)
200
100
0
-100
-200
-300
-400
-500
-600
0.0
2.5
5.0
7.5
10.0
12.5
15.0
17.5
20.0
22.5
Frequency

Figure A1.3

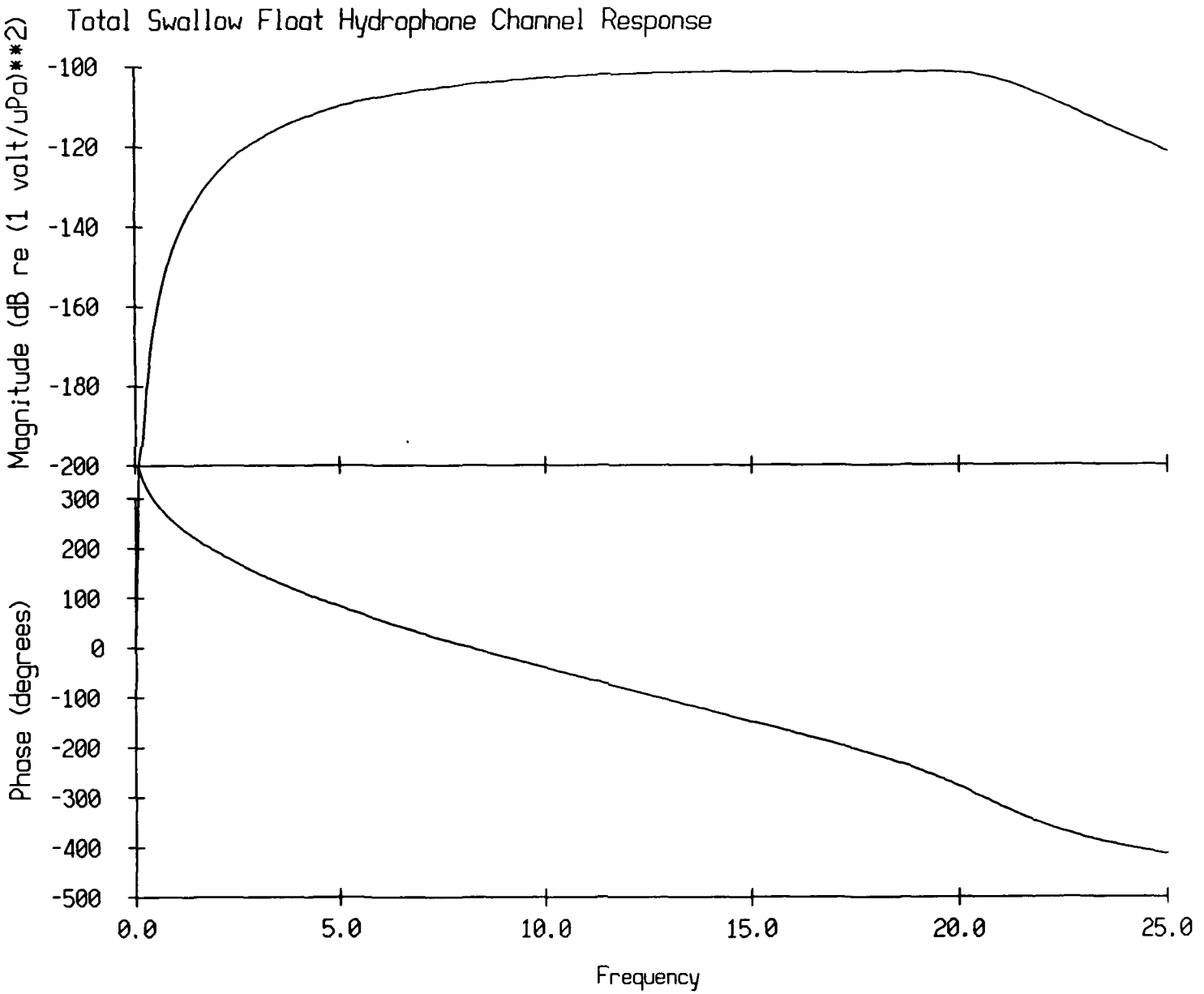

Total Swallow Float Hydrophone Channel Response
Magnitude (dB re (1 volt/uPa)**2)
-100
-120
-140
-160
-180
-200
Phase (degrees)
300
200
100
0
-100
-200
-300
-400
-500
0.0
5.0
10.0
15.0
20.0
25.0
Frequency

Figure A1.4

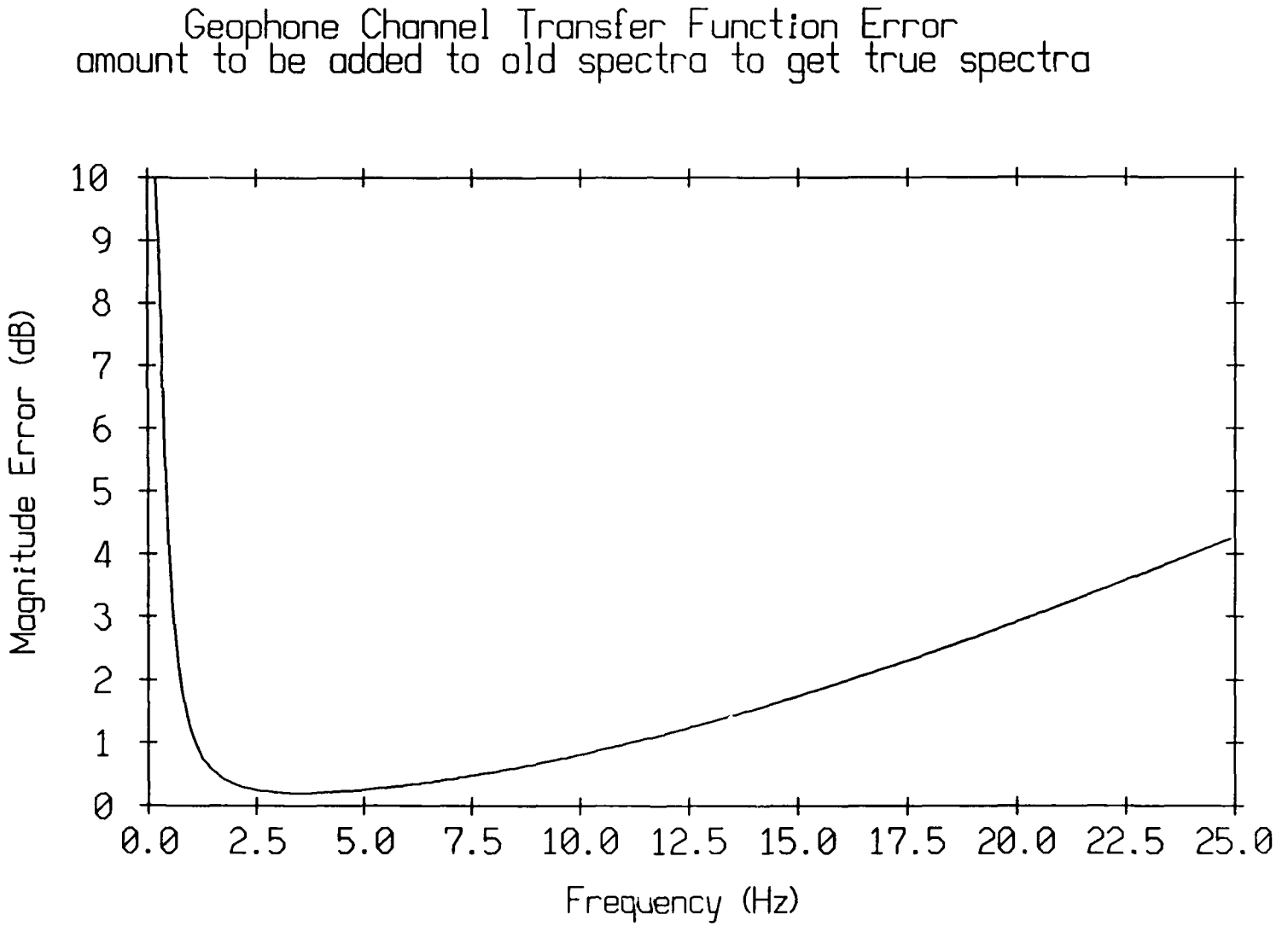

Geophone Channel Transfer Function Error
amount to be added to old spectra to get true spectra
Magnitude Error (dB)
10
9
8
7
6
5
4
3
2
1
0
0.0
2.5
5.0
7.5
10.0
12.5
15.0
17.5
20.0
22.5
25.0
Frequency (Hz)

Figure A1.5

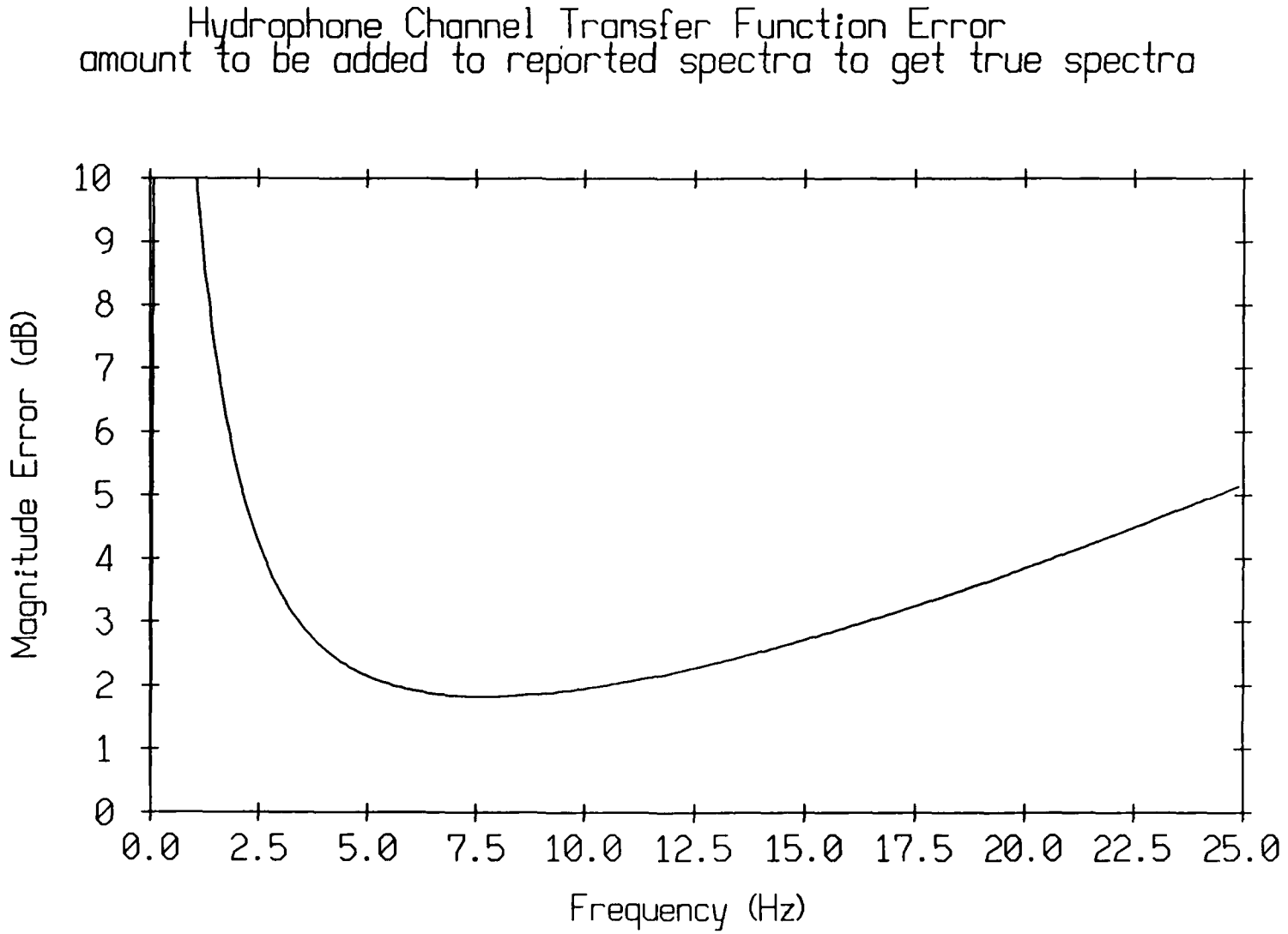

Hydrophone Channel Transfer Function Error
amount to be added to reported spectra to get true spectra
Magnitude Error (dB)
10
9
8
7
6
5
4
3
2
1
0
0.0
2.5
5.0
7.5
10.0
12.5
15.0
17.5
20.0
22.5
25.0
Frequency (Hz)

Figure A1.6

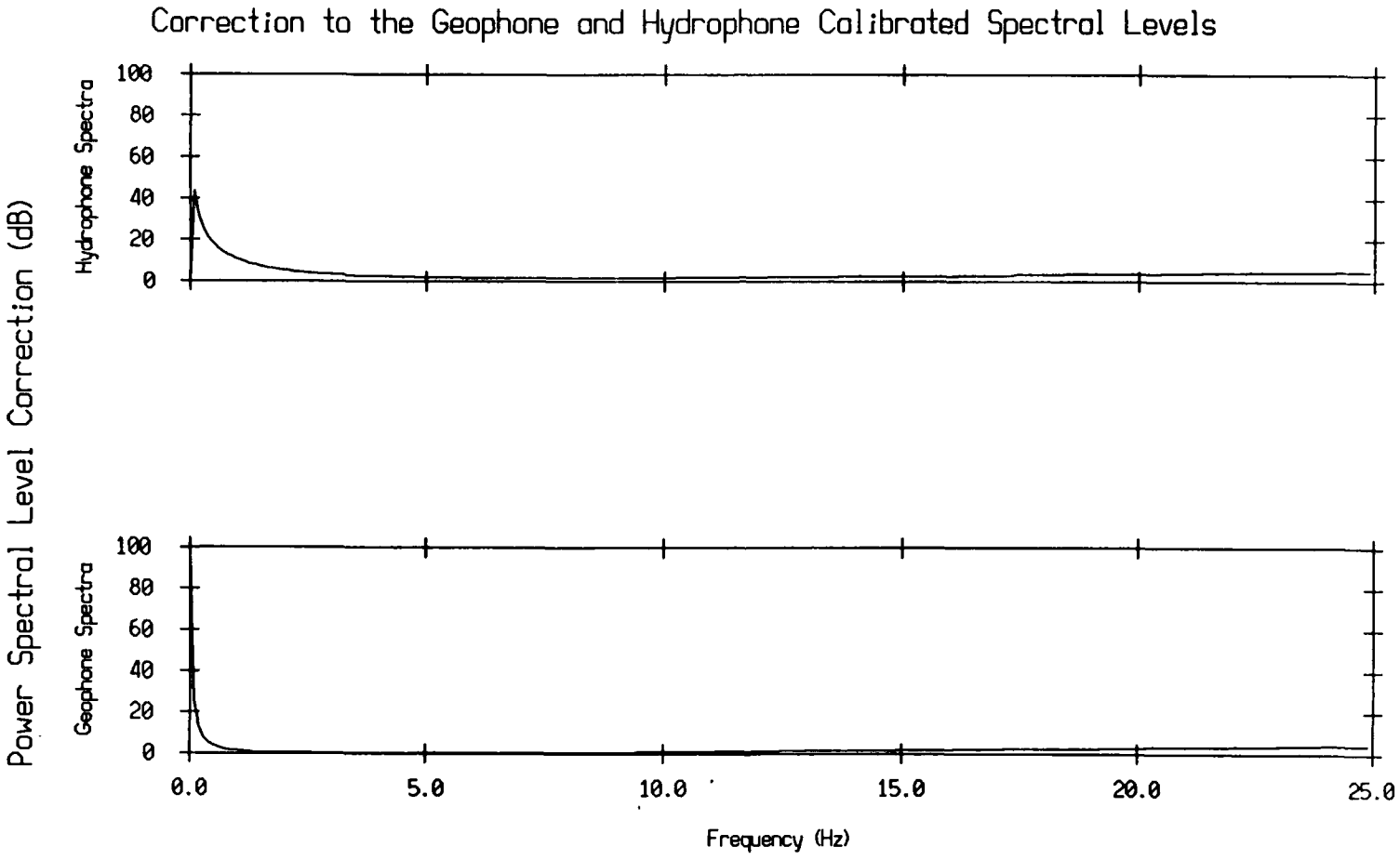

Correction to the Geophone and Hydrophone Calibrated Spectral Levels
Power Spectral Level Correction (dB)
Hydrophone Spectra
Geophone Spectra
100
80
60
40
20
0
0.0
5.0
10.0
15.0
20.0
25.0
Frequency (Hz)

Figure A1.7

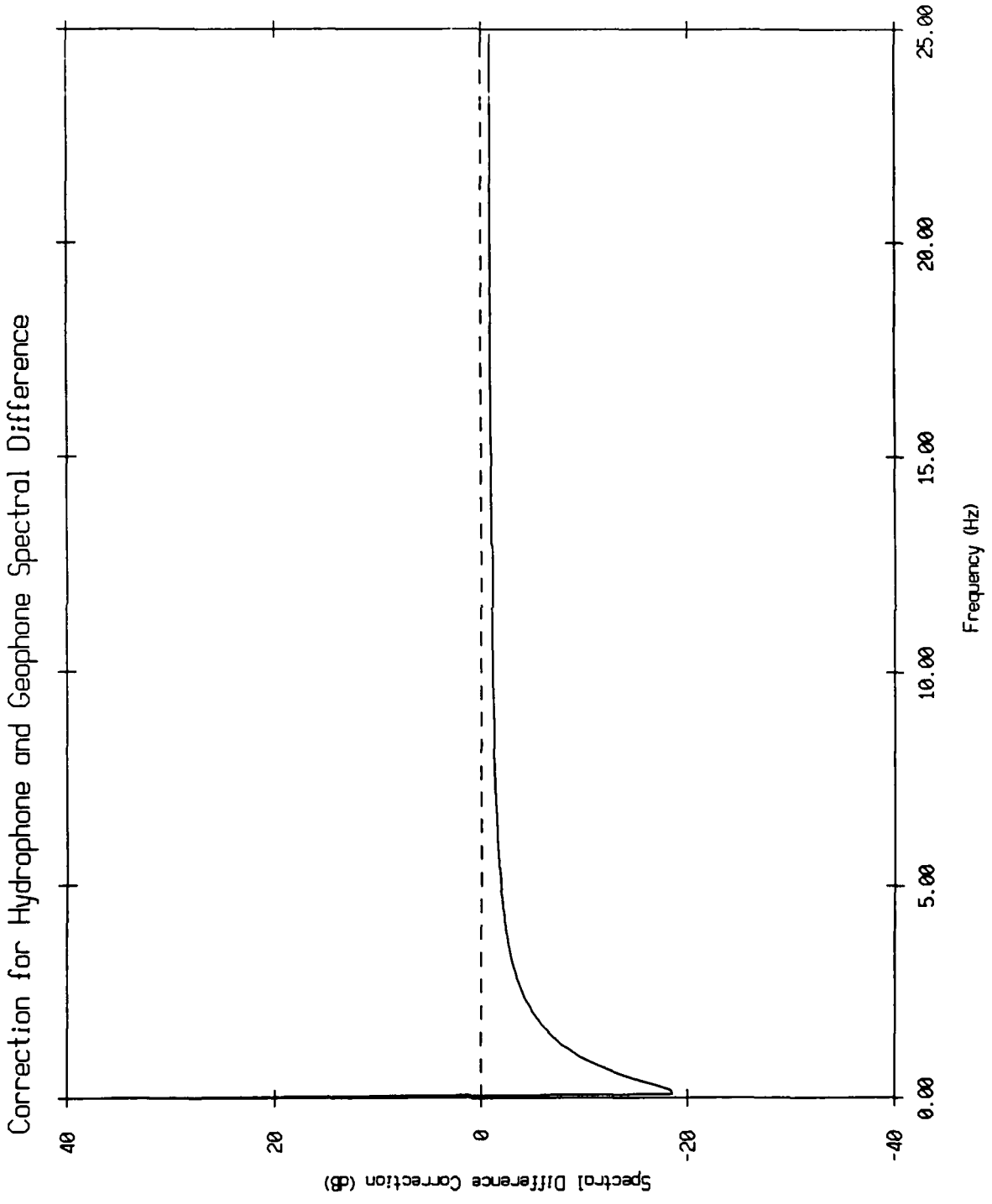

Correction for Hydrophone and Geophone Spectral Difference
Spectral Difference Correction (dB)
40
20
0
-20
-40
0.00
5.00
10.00
15.00
20.00
25.00
Frequency (Hz)

Figure A1.8

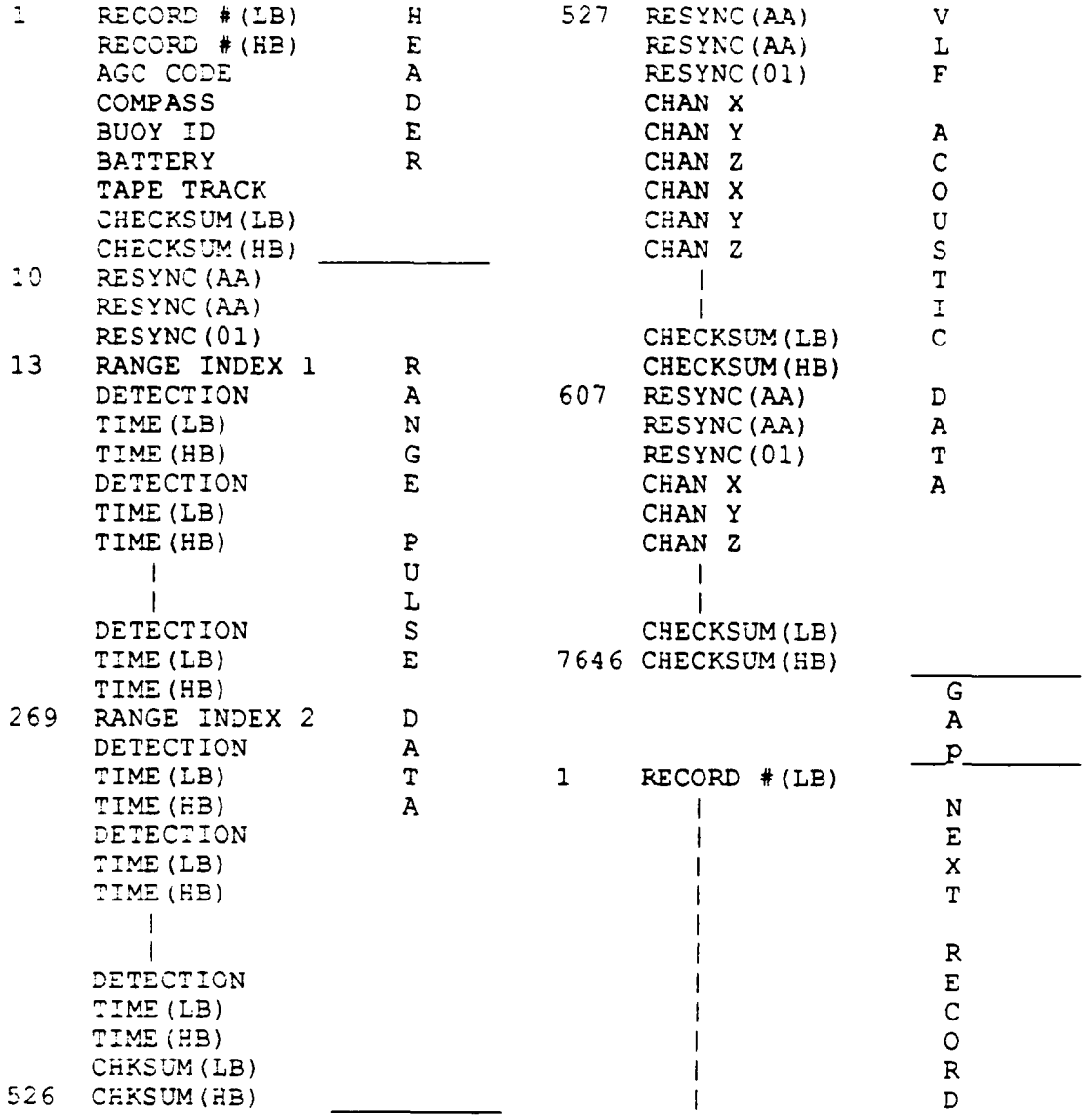


FIG. SWALLOW DATA RECORD FORMAT

Figure A1.9

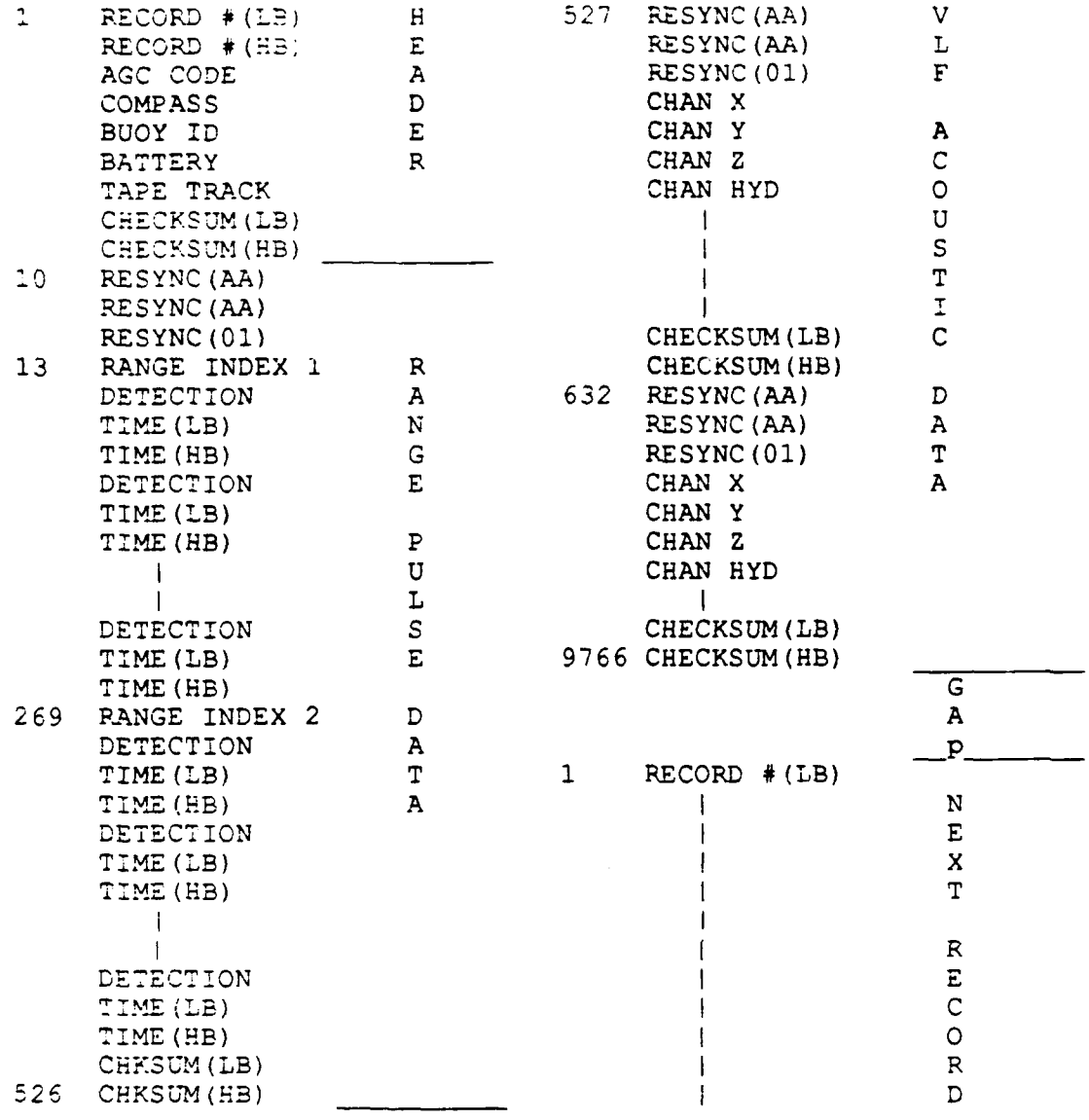
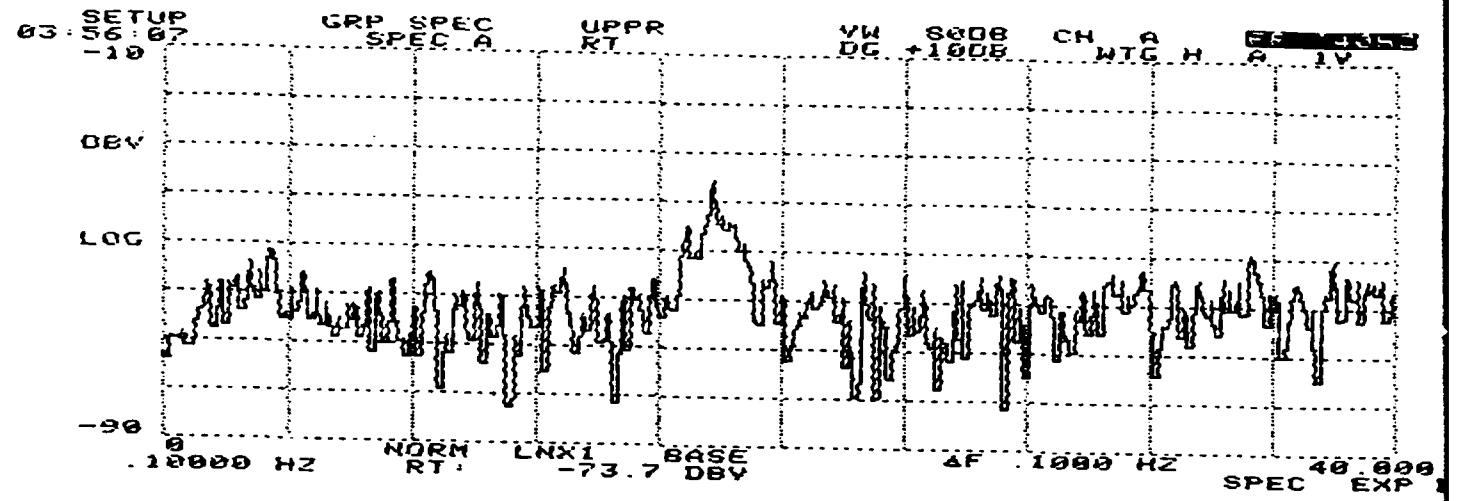
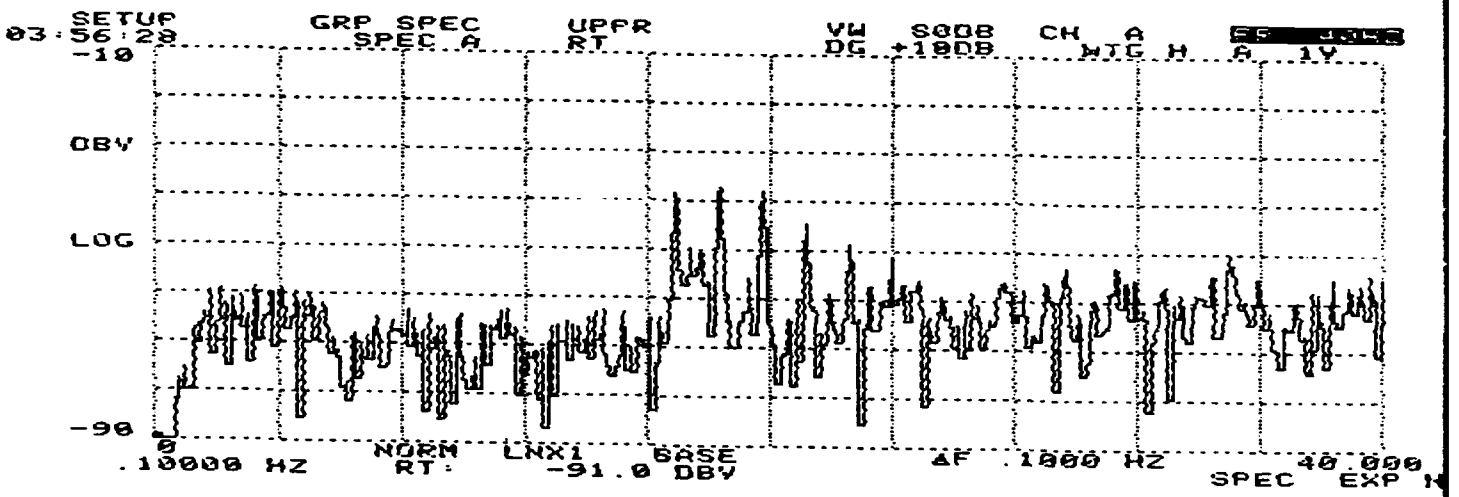


FIG. SWALLOW DATA RECORD FORMAT WITH HYDROPHONE

Figure A1.10


SETUP
03:56:07
GRP SPEC
SPEC A
UPPR
RT
VW S00B CH A
DG +100B WTG H A 1V
-10
DBV
LOG
-90
0
.10000 HZ
NORM LNX1 BASE
RT: -73.7 DBV
ΔF .1000 HZ
40.000
SPEC EXP


SETUP
03:56:28
GRP SPEC
SPEC A
UPPR
RT
VW S00B CH A
DG +100B WTG H A 1V
-10
DBV
LOG
-90
0
.10000 HZ
NORM LNX1 BASE
RT: -91.0 DBV
ΔF .1000 HZ
40.000
SPEC EXP

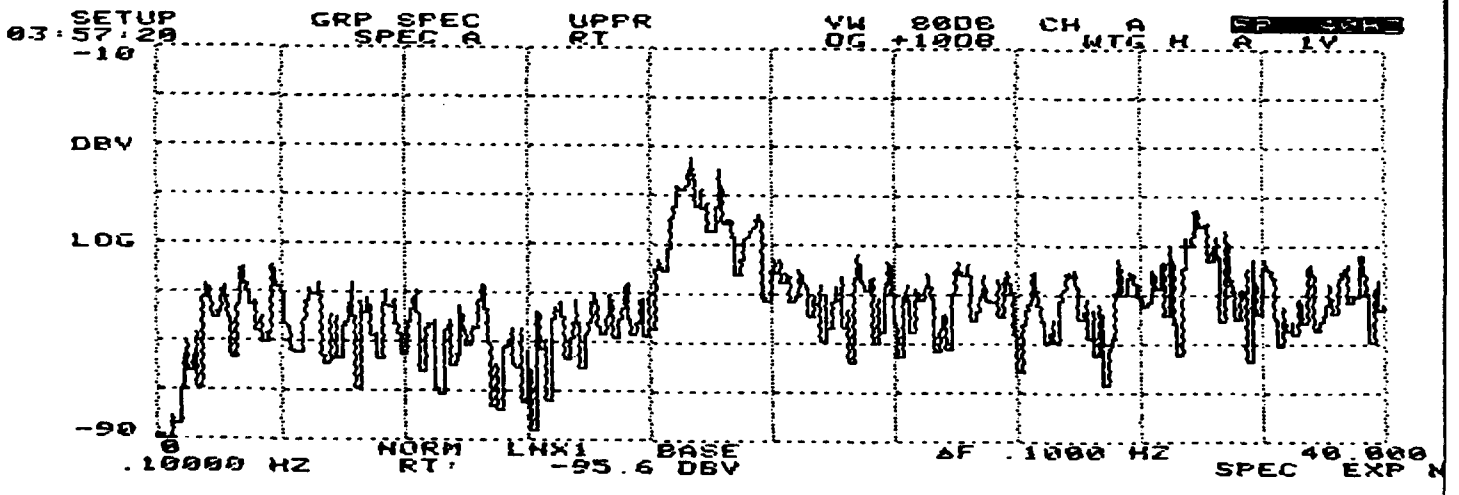
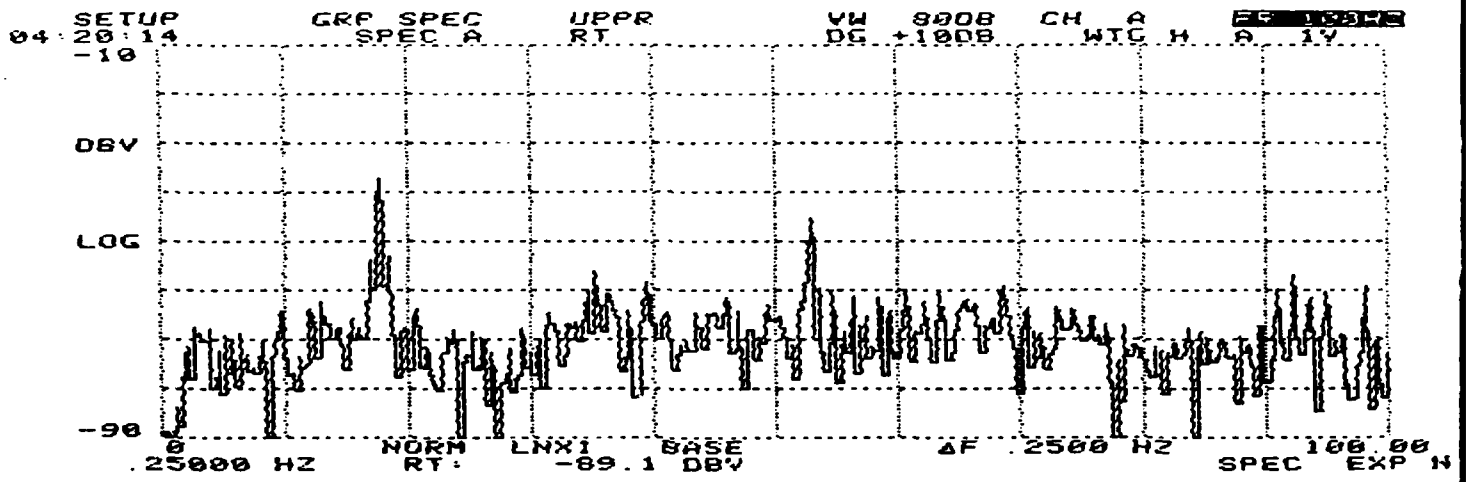

SETUP
03:57:29
GRP SPEC
SPEC A
UPPR
RT
VW S00B CH A
DG +100B WTG H A 1V
-10
DBV
LOG
-90
0
.10000 HZ
NORM LNX1 BASE
RT: -95.6 DBV
ΔF .1000 HZ
40.000
SPEC EXP

Figure A3.1


SETUP
04:20:14
GRP SPEC
SPEC A
UPPR
RT
VW 8008
DG +10DB
CH A
WTG H
A 1V
-10
DBV
LOG
-90
0
.25000 HZ
NORM
RT:
LNX1
-89.1
BASE
DBV
ΔF .2500 HZ
100.00
SPEC
EXP

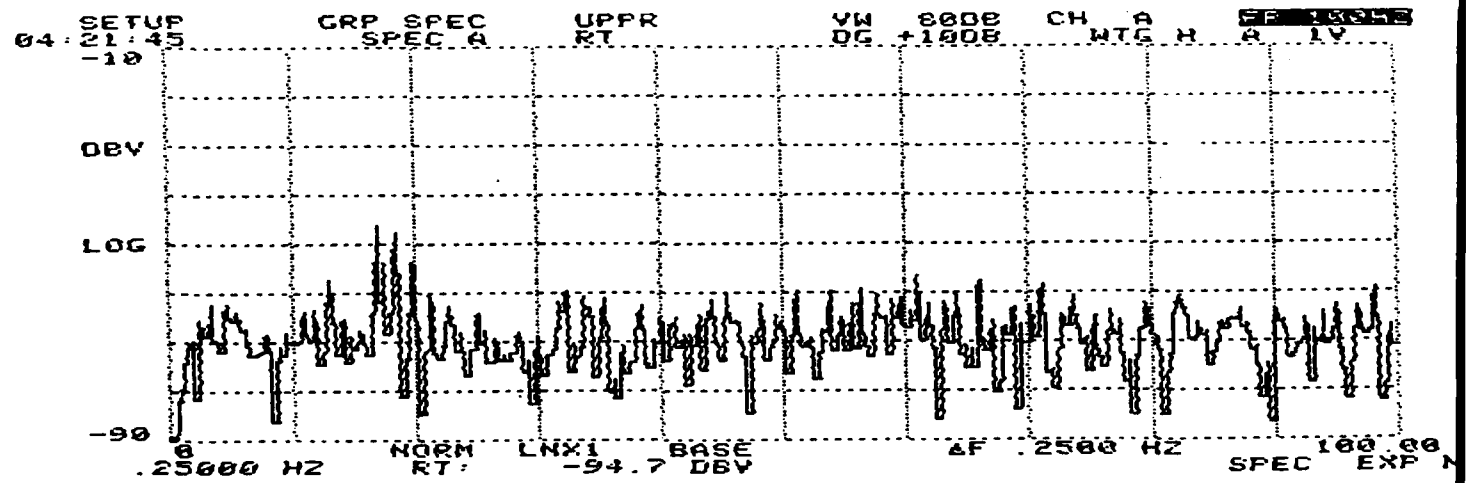

SETUP
04:21:45
GRP SPEC
SPEC A
UPPR
RT
VW 8008
DG +10DB
CH A
WTG H
A 1V
-10
DBV
LOG
-90
0
.25000 HZ
NORM
RT:
LNX1
-94.7
BASE
DBV
ΔF .2500 HZ
100.00
SPEC
EXP

Figure A3.2

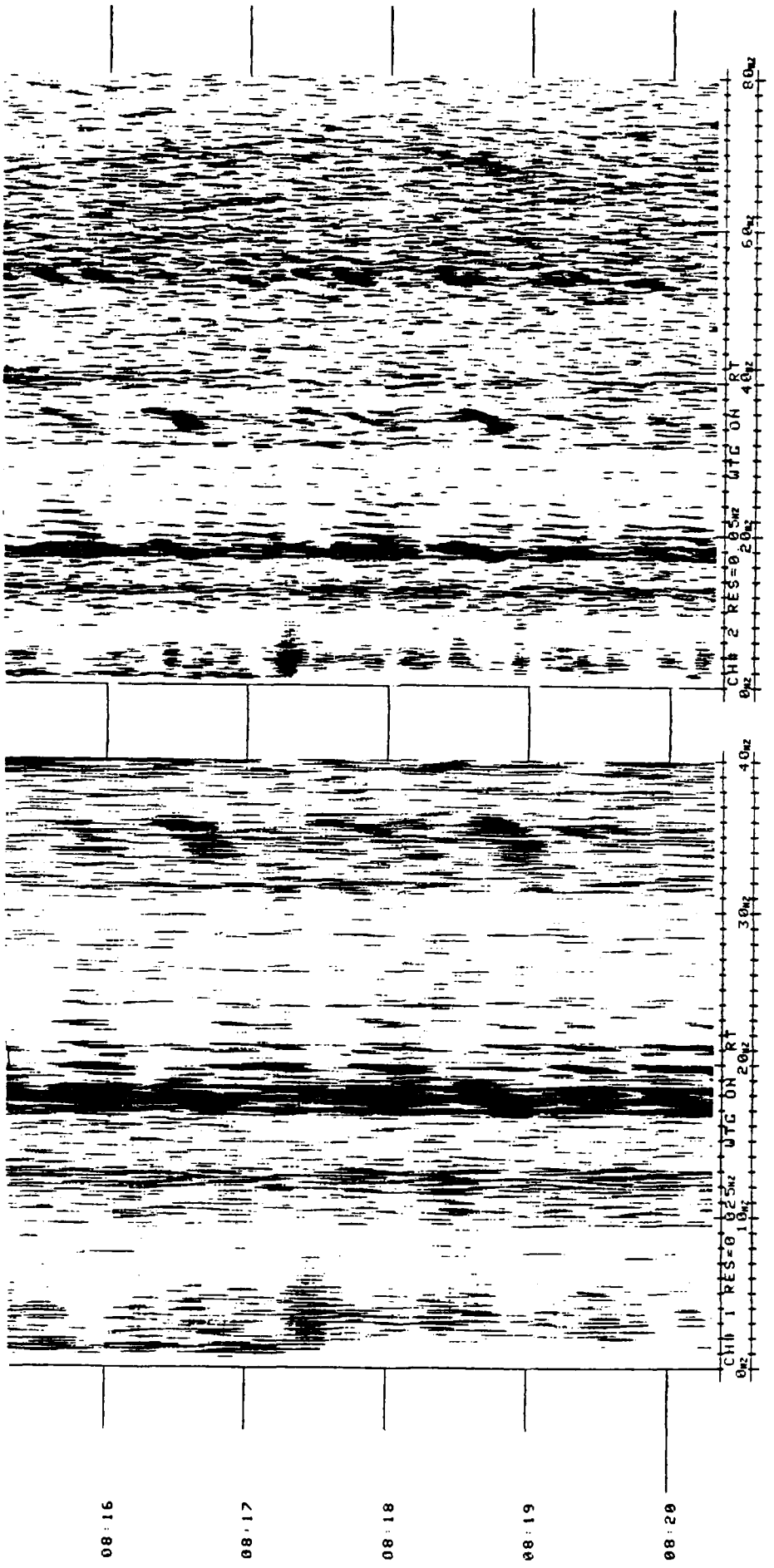

08:16
08:17
08:18
08:19
08:20
CH# 1 RES=0 0.25Hz UTC ON RT
0Hz
10Hz
20Hz
30Hz
40Hz
CH# 2 RES=0 0.5Hz UTC ON RT
0Hz
20Hz
40Hz
60Hz
80Hz

Figure A3.3